

アンメット・メディカル・ニーズに応える 創薬基盤研究の推進および臨床応用への展開

平成 27 年度～平成 31 年度
私立大学戦略的研究基盤形成支援事業
研究成果報告書

令和 2 年 5 月

学校法人名 東北医科薬科大学

大 学 名 東北医科薬科大学

研究組織名 大学院薬学研究科

研究代表者 丹野 孝一

(東北医科薬科大学大学院薬学研究科 教授)

— 目 次 —

1. はしがき	1
2. 研究成果報告書概要	3
3. 研究発表状況（主要論文）	
研究テーマ 1	
新規がん分子標的治療薬の創製	55
研究テーマ 2	
老年性神経系疾患（老人性認知症、高齢者うつ病）改善薬の開発 ---	295
研究テーマ 3	
難治性疼痛に対する緩和医療法の確立	419

平成 27 年度～平成 31 年度「私立大学戦略的研究基盤形成支援事業」
(創薬研究) 研究成果報告書発刊にあたって

研究代表者 丹野 孝一

アンメット・メディカル・ニーズ (いまだ有効な治療薬/治療法のない医療ニーズ) に応える治療薬/治療法の開発は最も社会的要請の強い研究課題の一つとなっています。本学ではハイテク・リサーチ・センター整備事業「生体内分子標的理論にもとづく創薬とその臨床治療への応用 (平成 17～21 年度)」および私立大学戦略的研究基盤形成支援事業「癌および加齢性疾患の制御と QOL 向上を目指す創薬 (平成 22～26 年度)」を実施し、創薬基礎研究に関する顕著な成果を上げてきました。本プロジェクト「アンメット・メディカル・ニーズに応える創薬基盤研究の推進および臨床応用への展開」では、これまで培ってきた知識・経験・技術をもとに、アンメット・メディカル・ニーズに応える治療薬の開発を目指した創薬基盤研究を推進するとともに、東北地方における創薬研究の拠点としての役割を果たすことを目的に企画しました。

本プロジェクトは、①制がん化合物やホルモン受容体制御化合物の分子設計、合成法の開発と機能解析、②化学物質の毒性評価および③神経精神疾患、難治性疼痛や気管支喘息の発症メカニズムの解明などにおいて独創的で先駆的な成果を上げている 7 つの研究室 (創薬化学、分子薬化学、医薬合成化学、環境衛生学、薬理学、機能形態学、病態生理学) で組織されています。本プロジェクトでは、これまで本学が醸成してきた基礎薬学研究を 3 つのテーマ、すなわち、「1. 新規がん分子標的治療薬の創製」、「2. 老年性神経系疾患 (老人性認知症、高齢者うつ病) 改善薬の開発」および「3. 難治性疼痛に対する緩和医療法の確立」に集結し、研究の進展を図ってきました。

本プロジェクトにおいて①抗腫瘍性天然物とそれらの類縁化合物ならびに新規抗腫瘍性ヌクレオシドの合成、②各種 P450 活性の評価スクリーニング系の樹立と応用、③新規選択的エストロゲン受容体モジュレーターの合成ならびに抗うつ作用・認知障害改善作用とそれらの作用機序の解明、④難治性疼痛治療薬のターゲットとなる特異的受容体の発見、および⑤ μ オピオイド受容体遺伝子の一塩基変異が気管支喘息の増悪因子となる可能性を明らかにするなど、それぞれの研究テーマにおいて優れた研究成果を上げることができました。本研究プロジェクトの研究成果がアンメット・メディカル・ニーズに応える治療薬の開発に繋がることを期待しております。

法人番号	041004
プロジェクト番号	S1511001L

平成 27 年度～平成 31 年度「私立大学戦略的研究基盤形成支援事業」 研究成果報告書概要

1 学校法人名 東北医科薬科大学 2 大学名 東北医科薬科大学

3 研究組織名 東北医科薬科大学大学院薬学研究科

4 プロジェクト所在地 宮城県仙台市青葉区小松島 4-4-1

5 研究プロジェクト名 アンメット・メディカル・ニーズに応える創薬基盤研究の推進および臨床
応用への展開

6 研究観点 研究拠点を形成する研究

7 研究代表者

研究代表者名	所属部局名	職名
丹野 孝一	大学院薬学研究科	教授

8 プロジェクト参加研究者数 73 名

9 該当審査区分 理工・情報 生物・医歯 人文・社会

10 研究プロジェクトに参加する主な研究者

研究者名	所属・職名	プロジェクトでの研究課題	プロジェクトでの役割
丹野 孝一	薬理学教室・教授	老年性精神系疾患の発症メカニ ズムの解明と治療薬の開発	老年性精神疾患改善薬の開 発(研究代表者)
吉村 祐一	分子薬化学教室・教授	抗腫瘍性ヌクレオシド誘導体の 設計と合成	新規ヌクレオシド系抗腫瘍薬 の探索
永田 清	環境衛生学教室・教授	毒性発現および薬物相互作用の 評価とスクリーニング系の構築	毒性および薬物相互作用の 評価
遠藤 泰之	創薬化学教室・教授	エストロゲン受容体制御にもとづく 神経系疾患改善薬および新規抗 がん活性化化合物の探索	老年性精神疾患改善薬およ びがん分子標的薬の開発
溝口 広一	機能形態学教室・教授	難治性疼痛の発症メカニズムの 解明と特異的鎮痛薬の開発	難治性疼痛治療薬の創製
高橋 知子	病態生理学教室・教授	オピオイド受容体遺伝子多型の 解析および個別化医療への応用	難治性疼痛緩和療法の確立
大野 勲	医学教育推進センター・ 教授	オピオイド受容体遺伝子多型の 解析および個別化医療への応用	難治性疼痛緩和療法の確立

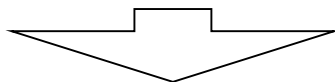
法人番号	041004
プロジェクト番号	S1511001L

<研究者の変更状況(研究代表者を含む)>

旧

プロジェクトでの研究課題	所属・職名	研究者氏名	プロジェクトでの役割
研究テーマ1・新規がん分子標的治療薬の創製」抗腫瘍性天然物および類縁化合物の合成と構造活性相関研究	大学院薬学研究科・医薬合成化学教室・教授	加藤 正	研究代表者

(変更の時期:平成 29 年 1 月 6 日)



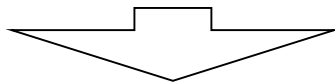
新

変更前の所属・職名	変更(就任)後の所属・職名	研究者氏名	プロジェクトでの役割
大学院薬学研究科・環境衛生学教室・教授	大学院薬学研究科・環境衛生学教室・教授	永田 清	研究代表者

旧

プロジェクトでの研究課題	所属・職名	研究者氏名	プロジェクトでの役割
研究テーマ1・新規がん分子標的治療薬の創製」抗腫瘍性天然物および類縁化合物の合成と構造活性相関研究	大学院薬学研究科・環境衛生学教室・教授	永田 清	研究代表者

(変更の時期:平成 29 年 4 月 1 日)



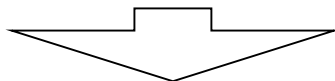
新

変更前の所属・職名	変更(就任)後の所属・職名	研究者氏名	プロジェクトでの役割
大学院薬学研究科・医薬合成化学教室・教授	創薬研究センター・教授	加藤 正	研究代表者

旧

プロジェクトでの研究課題	所属・職名	研究者氏名	プロジェクトでの役割
難治性疼痛の発症メカニズムの解明と特異的鎮痛薬の開発	大学院薬学研究科・機能形態学教室・特任教授	櫻田 忍	難治性疼痛治療薬の創製

(変更の時期:平成 29 年 4 月 1 日)



新

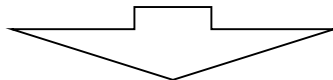
変更前の所属・職名	変更(就任)後の所属・職名	研究者氏名	プロジェクトでの役割
大学院薬学研究科・機能形態学教室・准教授	大学院薬学研究科・機能形態学教室・教授	溝口 広一	難治性疼痛治療薬の創製

法人番号	041004
プロジェクト番号	S1511001L

旧

プロジェクトでの研究課題	所属・職名	研究者氏名	プロジェクトでの役割
研究テーマ1・新規がん分子標的治療薬の創製」抗腫瘍性天然物および類縁化合物の合成と構造活性相関研究	大学院薬学研究科・医薬合成化学教室・教授	加藤 正	研究代表者

(変更の時期:平成 31 年 4 月 1 日)



新

変更前の所属・職名	変更(就任)後の所属・職名	研究者氏名	プロジェクトでの役割
大学院薬学研究科 薬理学教室・教授	大学院薬学研究科 薬理学教室・教授	丹野 孝一	研究代表者

11 研究の概要(※ 項目全体を10枚以内で作成)

(1) 研究プロジェクトの目的・意義及び計画の概要

アンメット・メディカル・ニーズ(いまだ有効な治療薬/治療法のない医療ニーズ)に応える治療薬/治療法の開発は、最も社会的要請の強い研究課題の一つである。本学では、ハイテク・リサーチ・センター整備事業として「生体内分子標的理論にもとづく創薬とその臨床治療への応用(平成 17～21 年度)」、および私立大学戦略的研究基盤形成支援事業として「癌および加齢性疾患の制御とQOL向上を目指す創薬(平成 22～26 年度)」を実施し、創薬基礎研究に関する優れた成果をあげてきた。本プロジェクトでは、これまで蓄積してきた基礎研究成果を集約し、アンメット・メディカル・ニーズの高い疾患領域、すなわち、①がん、②老年性神経系疾患(老人性認知症、高齢者うつ病)および③難治性疼痛に対する創薬研究の推進を図り、東北地方における創薬研究拠点としての役割を果たすことを目的として企画した。本研究プロジェクトの目指す最終ゴールは、非臨床・臨床試験に進める有望な候補化合物を創出し、アカデミア発/日本発の画期的新薬として臨床応用研究(実用化研究)へと結び付けることである。具体的には以下の 3 つの研究テーマを実施する。

「研究テーマ 1. 新規がん分子標的治療薬の創製」

- (1) 抗腫瘍性天然物および類縁化合物の合成と構造活性相関研究
- (2) 新規抗腫瘍性ヌクレオシド誘導体の設計と合成
- (3) 薬効/毒性発現および薬物相互作用の評価とそのスクリーニング系の構築

「研究テーマ 2. 老年性神経系疾患(老人性認知症、高齢者うつ病)改善薬の開発」

- (1) エストロゲン受容体制御にもとづく老年性神経系疾患改善薬の設計と合成
- (2) 精神疾患モデル動物を用いた老年性神経系疾患改善薬の評価および作用メカニズムの解明

「研究テーマ 3. 難治性疼痛に対する緩和医療法の確立」

- (1) 難治性疼痛の発症メカニズムの解明および特異的疼痛治療薬の創製
- (2) μ オピオイド受容体遺伝子多型の解析および個別化医療への応用

本研究プロジェクトで計画している疾患ターゲットやメカニズムの解明、疾患に対するタンパクなどに作用する新規化合物の探索・同定、疾患モデル動物の作製、薬効/副作用の予測法の樹立、リード化合物からリード化合物さらには開発候補化合物への展開などの創薬方法論の開発は、学術的にも実践的にも大きな波及効果が期待できる。

法人番号	041004
プロジェクト番号	S1511001L

(2) 研究組織

本研究組織は東北医科薬科大学大学院薬学研究科の 7 教室 30 名の教員によって構成されており、新規化合物を設計・合成する有機化学・創薬化学系研究室と機能解析や動物試験を行う生化学・薬理系研究室を本プロジェクトの 3 つの研究テーマに組織化できるように配置している。研究代表者は全体の統括、調整を行うとともに、各研究室間の連携を促進するため本プロジェクトの運営会議、成果公表の取り纏め、成果発表会(創薬研究センターシンポジウム)の企画を行い、プロジェクトの充実に努めている。それぞれの研究テーマ組織は以下の通りである。

「研究テーマ1. 新規がん分子標的治療薬の創製」

吉村教授を責任者とし、医薬合成化学教室、分子薬化学教室および環境衛生学教室の 3 教室で組織し、教員 13 名、ポスドク 2 名、大学院博士課程学生 2 名および修士課程学生 18 名で研究を行っている。

「研究テーマ2. 老年性神経系疾患(老人性認知症、高齢者うつ病)改善薬の開発」

遠藤教授を責任者とし、創薬化学教室および薬理学教室の 2 教室で組織し、教員 7 名、大学院博士課程学生 5 名および修士課程学生 7 名で研究を行っている。

「研究テーマ3. 難治性疼痛に対する緩和医療法の確立」

溝口教授を責任者とし、機能形態学教室および病態生理学教室の 2 教室で組織し、教員 10 名、大学院博士課程学生 4 名および修士課程学生 5 名で研究を行っている。

研究者以外に技術系職員 2 名と事務系職員 1 名が担当するなど、大学が積極的に支援を行っている。

(3) 研究施設・設備等

総研究施設面積は 2108m²であり、7 つの研究室が参画し、教員 30 名、ポスドク 2 名、大学院博士課程学生 11 名および修士課程学生 30 名の総勢 73 名の研究者が、本プロジェクトを推進している。

本プロジェクトで設置した以下の研究設備(装置)は、多くの研究者に有効に活用されている(括弧内は平成 27～31 年度の 5 年間の稼働時間を表す)。

- ・リアルタイム細胞アナライザー (1950 時間)
- ・超高感度等温滴定型カロリーメーター (93 時間)
- ・正立型共焦点レーザー顕微鏡システム (1580 時間)
- ・擦過行動リアルタイム定量化システム (434 時間)
- ・全自動磁気細胞分離装置 (438 時間)

(4) 研究成果の概要 ※下記、13及び14に対応する成果には下線及び*を付すこと。

研究テーマごとに研究成果の概要を記載する。

「研究テーマ1. 新規がん分子標的治療薬の創製」

「抗腫瘍性天然物および類縁化合物の合成と構造活性相関研究」では、医薬合成化学教室で創製した候補化合物「FK-A11」[ヒストン脱アセチル化酵素(HDAC)/ホスファチジルイノシトール 3-キナーゼ(PI3K)二重阻害薬]の臨床応用に向けた大量合成法の確立、HDAC 阻害薬のリード化合物の創製、新しい分子標的抗がん薬のシード天然物であるナキジノール B(脳腫瘍細胞増殖抑制活性物質)、リファガール[PI3K阻害活性物質]、および TAN-1813[ファルネシル基転移酵素(FTase)阻害活性物質]の合成法の確立と構造活性相関の解明による新規リード化合物/候補化合物の創製を目的に研究を遂行した。その結果、①「FK-A11」の工業的製造法を確立するとともに(特許*2)、新規合成法(改良法)の開発に成功し(従来法:全 24 工程、総収率 3.5%; 改良法:全 15 工程、総収率 10%)、工業的製造法への道を拓いた(特許*2)。②スピルコスタチンおよび FK228 の類縁体合成を行い、アイソフォーム選択的 HDAC 阻害薬の創出に成功した(論文*31)。③脳腫瘍の抗がん剤シードであるナキジノール B の全合成を世界に先駆けて達成した(論文*11)。④リファガール類縁体の合成と活性評価を行った結果、リファガールの生合成前駆体と考えられるシホノディクチアール B が優れたキナーゼ阻害活性を示すことを見出した(特許*1、論文*33)。⑤抗がん活性を有するマクロラクトン天然物 マンデラリド A およびイソマンデラリド A の全合成を達成した(論文*34)。⑥抗がん活性を有する 9-デオキシキセニアラクトール C の合成研究では、ラクトール環を有する 9 員環部の立体選択的な構築法を開発した(学会*1, 12, 30, 35)。

法人番号	041004
プロジェクト番号	S1511001L

「新規抗腫瘍性ヌクレオシド誘導体の設計と合成」では、新規骨格を有するヌクレオシド系分子標的抗がん薬の創製を目指し、そのデザイン、合成、および生物活性評価を行った。始めに、含硫黄誘導体を疑似糖部とする 4'-チオヌクレオシド誘導体の探索を行った。Vorbrüggen 法を用い、各種核酸塩基を導入した 3'-デオキシ-4'-チオヌクレオシド誘導体の合成を達成した(学会*96)。また、Pummerer 型チオグリコシル化反応を用い、4'-置換 4'-チオリボヌクレオシド誘導体の合成も達成した(学会*18)。さらに、ジヒドロチオピラン環ヌクレオシド誘導体の構造活性相関研究のため新たな合成法の開発に取り組んだ(学会*32)。

これまでに蓄積された種々の修飾ヌクレオシド合成法を核酸医薬の開発へと展開させることを検討した。はじめに、2'-5' 連結型環状ジヌクレオチドの合成を検討した(学会*44, 76)。また、前述の 4'-置換 4'-チオリボヌクレオシド誘導体の合成における合成中間体を用いた糖部立体構造を固定化したヌクレオシド誘導体の合成を行った。

4'位に置換基をもつスタブジン誘導体の構造活性相関研究とその鏡像異性体間における薬理活性への影響を解明することを目指し検討を行った。当研究室によって開発された酸化グリコシル化反応を利用することで、4'-置換スタブジン誘導体の合成を達成した(学会*64, 97)。この合成における中間体を基質とするリパーゼを用いた光学分割を検討し、高い光学純度で両鏡像異性体を得ることに成功した(学会*16)。得られた光学活性なヌクレオシド誘導体の絶対構造を決定し、リパーゼを用いた光学分割における立体選択性について新たな知見を得た(学会*7)。

生体分子を基本骨格とする有機分子触媒のデザインと合成を行い、不斉反応に応用可能な新規有機分子触媒の開発を目指し検討を行った。2'位にアミノ基をもつウリジン誘導体の合成を行い、得られた各誘導体を不斉有機触媒として用いた Diels-Alder 反応への適応を試みた(論文*1)。ペプチド構造をもつ有機分子触媒を設計、合成し、不斉反応への適応について検討した(学会*65, 73)。

立体選択的なイミノ糖誘導体の合成を検討すると共に、得られた化合物の生物活性を評価した。グルコシダーゼ阻害活性を持つ化合物の立体選択的合成法を確立し、本方法を用いた構造活性相関研究により、これまでに無い強い活性を持つ化合物を見いだすことに成功した(論文*7, 学会*67, 94)。

新たな合成法開発の一環として、各種新反応の開拓を行った。超原子価ヨウ素とジフェニルジセレンドを用いた環化反応を検討し、分子内エーテル環化反応の開発(学会*72)、及び含窒素複素環化合物の合成へと展開させた(学会*8, 17, 20, 33)。パラジウム触媒による位置選択的炭素炭素結合形成反応を開発した(論文*26, 学会*34, 43, 74, 95)。ルテニウム触媒を用いた閉環メタセシスによる種々の複素環化合物の合成を行った(論文*14, 学会*6, 19, 66)。

「薬効/毒性発現および薬物相互作用の評価とそのスクリーニング系の構築」では、薬効あるいは副作用に最も大きく寄与する要因は、投与薬物の血中濃度であり、その濃度には薬物代謝酵素 P450 (CYP) 活性が大きく関わっているため、薬物、食品成分を含む化学物質による薬効、毒性あるいは薬物相互作用発症を予測するために CYP 活性変動を正確に評価可能な複数のスクリーニング系を樹立した。まず、CYP 活性阻害は、アデノウイルスを用いて、複数の CYP を同時に発現させ、カクテル基質と LC/MS/MS を用いることで、一度に 5 種の CYP 活性を調べることができる評価系を樹立した(論文*29, 48, 学会*77, 79, 99, 105)。また、薬物動態関連遺伝子の解析を行い、新規誘導機序を明らかにし(論文*28, 39, 学会*50, 54, 80, 82, 84)、特に薬物相互作用で問題となっている CYP3A4 と CYP1A2 については、これらの遺伝子とレポーター遺伝子の組み替えを行い、レポーター活性を測定することで簡便に薬物代謝酵素誘導の評価可能なシステムの構築を行った(論文*40, 47, 学会*100)。これらの評価系を用いて薬物のみならず健康食品の網羅的解析を行い、健康食品の約 20~30% に活性阻害や誘導を引き起こす可能性があることを明らかにした(論文*41, 49, 学会*26, 49, 平成 30 年度および平成 31 年度創薬研究センターシンポジウム)。また、CYP3A4 を強く誘導した健康食品については、CYP3A4 と酵素誘導に関与する核内受容体をヒト化したマウスを用いて、実際に *in vivo* で CYP3A4 が誘導され、薬物の効果が低下するかについて調べ、誘導の強かったフォルスコリンはヒトで薬物相互作用を引き起こす可能性を明らかにした(学会*23)。さらに、薬物、食品成分を含む化学物質による毒性発現は培養細胞に CYP を発現させ、リアルタイム細胞アナライザーによって評価し、健康食品製品の中には細胞毒性をしたものが幾つか見出された。一方、医薬品としても用いられているビタミンAによる催奇形性の発症が問題となっている。ビタミンAの活性体のレチノイン酸を

法人番号	041004
プロジェクト番号	S1511001L

代謝する CYP26 は、レチノイン酸の濃度が上昇すると誘導されてくる。この CYP26 遺伝子を用いて、組織内のごく微量のレチノイン酸濃度を測定可能な *in vitro* スクリーニング系の樹立に成功し(学会*45, 46, 51, 83, 101)、これを用いてアゾール系の農薬が催奇形性を発症するか予測した。一方で、Human Induced Pluripotent Stem Cells (hiPSCs) 細胞から肝細胞への分化は、現在まである程度の薬物代謝酵素活性を得ることに成功したが、成熟肝細胞が示す薬物代謝酵素活性を示すまでには至っていない。当研究室を含め、現在までに報告されている分化肝細胞における肝薬物代謝酵素群の発現比率は胎児肝細胞に類似している。特に、代表的な P450 である CYP3A においては、胎児型 P450 と呼ばれる CYP3A7 の発現量は高く、成人型 P450 である CYP3A4 の発現量が低い。これらから、当研究室で分化させた hiPSCs 由来肝細胞は胎児肝様細胞にまでは分化していると考えている。そして、肝臓が成熟する過程で起きる胎児型 CYP3A7 から成人型 CYP3A4 への発現量の入れ替わり(スイッチ)の分子機序を解明することが、hiPSCs の成熟肝細胞への分化に重要な役割を担う因子の探索の足がかりになると予想し、この機序の解明を試みた。現在のところ、肝臓特異的発現に関わっている転写因子の中で HNF3 β が CYP3A7 発現を強く抑制していることを見出した(学会*24)。

「研究テーマ2. 老年性神経系疾患(老人性認知症、高齢者うつ病)改善薬の開発」

「エストロゲン受容体制御にもとづく老年性神経系疾患改善薬の設計と合成」では、新しい疎水性構造を用いた核内受容体制御を基盤として方向性を絞って研究を展開した。エストロゲン受容体 β が神経系作用に関与する可能性を考え、 α β サブタイプ選択性を一つの課題とした。分子設計・合成により、高い β 選択的及び α 選択的化合物を見出し、受容体構造との関係性を明らかにした(論文*56, 77, 96, 学会*157)。エストロゲン受容体のアゴニスト/アンタゴニスト制御をもう一つの課題とし、ジフェニルメタン型化合物の系統合成により、疎水性構造の変化による制御法への重要な情報を見出した(論文*94)。また、新しい疎水性構造を用いた新規細胞増殖阻害薬の創製への展開も行い、がん細胞パネルスクリーニングを含む細胞増殖試験で有効な抗がん化合物を見出した(論文*55, 75, 76, 82)。薬理学教室との共同研究では、我々が開発した新規選択的エストロゲン受容体モジュレーター (SERM) である「BE360」の抗うつ、抗認知症効果を確立した(論文*84)。

「精神疾患モデル動物を用いた老年性神経系疾患改善薬の評価および作用メカニズムの解明」では、創薬化学教室で開発した「BE360」がうつ病や認知症のモデル動物として用いられている嗅球摘出マウスのうつ様行動および認知障害の両方を改善することを見出した。「BE360」の改善メカニズムは海馬の転写因子 CREB のリン酸化を介した脳由来神経栄養因子(BDNF)増加により、海馬歯状回での神経細胞増殖促進が関与していることを明らかにした(論文*84, 学会*203)。なお、AMP 活性化プロテインキナーゼ活性化薬(論文*61)やアルツハイマー型認知症治療薬であるメマンチン(論文*71)も「BE360」と同様なメカニズムで抗うつ作用を発現することを見出している。さらに、女性の更年期障害である閉経後のうつ病に対する「BE360」の効果を検討するため、メスマウスの卵巣摘出およびストレスを負荷した閉経後うつ病モデル動物を作製した。女性の更年期障害モデルのうつ様行動に対しても「BE360」が改善作用を示し、そのメカニズムとしては、上記の作用メカニズムに加え海馬において神経保護因子である Bcl-2 を増加し神経保護作用を示した(学会*148, 163, 201)。このモデル動物における子宮重量の低下は、エストラジオールまたはタモキシフェン投与によって増加するのに対して「BE360」は、子宮重量に影響を与えなかった。以上のことから、「BE360」は、生殖器に影響のない高齢期に観察されるうつ病および認知障害といった精神疾患の治療薬に成り得る可能性を示唆した(学会*148, 163, 201)。また、更年期障害は、女性のみならず男性においても認知されるようになってきた。しかしながら、男性における更年期の気分変動を検討するための動物モデルはほとんど見当たらなかった。上記で示した女性の更年期障害モデルを参考にし、精巣摘出マウスにストレスを負荷し、行動解析を行なった。この男性更年期障害モデル動物において衝動性様の行動を示すことを明らかにした(平成 31 年度創薬研究センターシンポジウム)。今後このモデルを用いて更なる検討を行うことにより更年期の男性に認められる衝動性に関連する病態の解明および治療薬の開発に繋がることが示唆された。

統合失調症は閉経後にも小さな発症のピークがあり、エストロゲンレベルの低下と相関している。我々

法人番号	041004
プロジェクト番号	S1511001L

は、「BE360」の統合失調症に対する作用を検討するためモデル動物の作製を試みている(論文*54, 62)。神経新生抑制薬(メチルアゾキシメタノール)を胎生期に投与することにより簡便な神経発達障害仮説に基づいた統合失調症モデルマウス作製に成功した(論文*62、学会*120, 130, 141, 178)。

高齢者における咀嚼や口腔機能低下と脳の機能または糖代謝系との関連性を解明するため、長期間粉末食でマウスを飼育し、その影響を検討した。その結果、粉末食飼育マウスは多動や低不安行動を発現し、その異常行動発現にはカテコールアミン系、GABA 系および前頭皮質のドパミン D₄ 受容体の変化が関与する可能性を示した(論文*65, 92、学会*121, 135, 156, 214)。さらに、粉末食飼育マウスでは、低不安行動の他、血清コルチコステロン濃度の増加、海馬グルコルチコイド受容体発現量の減少が認められ、これらの変化は、粉末食から固形食に切り替えて飼育することで改善することが判明した。従って、咀嚼や口腔機能の低下に起因する脳機能や糖代謝系の変化には、視床下部—下垂体—副腎皮質系が関与している可能性も示した(学会*173)。

潰瘍性大腸炎は 20-30 歳までの若い年齢層に多く発症する疾患と考えられてきたが、近年では 40 歳代から 60 歳代の発症例も増えてきている。症状として血便を伴う下痢や腹痛などの消化器症状の他に抑うつや不安などの精神症状も多く現れてくるが、そのメカニズムについては不明である。このような背景の下、我々は消化性大腸炎に伴うつ病モデルマウスの作製に成功し、そのメカニズムとして大腸の炎症性サイトカイン産生増加を介した海馬歯状回の神経新生の抑制に起因することを明らかにした(論文*60)。

「研究テーマ3. 難治性疼痛に対する緩和医療法の確立」

「難治性疼痛の発症メカニズムの解明および特異的疼痛治療薬の創製」では、dermorphin (μ オピオイド受容体アゴニスト)誘導体の「amidino-TAPA」をプロトタイプ化合物として、各種難治性疼痛(神経損傷性神経障害性疼痛、炎症性疼痛、神経絞扼性がん性疼痛、多発性硬化症疼痛)に有効かつ、依存性のない新規鎮痛薬を開発すると共に、難治性疼痛治療のターゲットとなる μ オピオイド受容体スプライスバリエーションの特定を目的に研究を遂行した。その結果、各種難治性疼痛に有効な新規鎮痛薬として、「amidino-TAPA」およびその誘導体「ADAMB」を見出した(学会*288, 289)。また、既存の麻薬性鎮痛薬である oxycodone と methadone も、特定の難治性疼痛に対して有効であることを発見した(学会*225, 228, 237, 238, 239, 286, 290, 301, 314)。これら難治性疼痛に有効な鎮痛薬は、共通した特定の薬理作用を持つことを発見し、難治性疼痛治療薬のターゲットとなる特異的受容体を見出した(学会*288, 289)。本研究結果は、難治性疼痛に対する特異的治療薬の開発において、従来とは大きく異なる新たな方向性を示した。

「 μ オピオイド受容体遺伝子多型の解析および個別化医療への応用」では、 μ オピオイド受容体遺伝子多型と疼痛治療薬の免疫応答に及ぼす影響の関連性を解析するとともに、得られた解析結果から、疼痛治療薬によるアレルギー疾患や感染症の発症・悪化の感受性増大リスクを軽減するための情報基盤を確立し、個別化療法への応用に向けた新規疼痛治療薬の創製を目的に研究を遂行した。その結果、 μ オピオイド受容体を起点とする神経/内分泌/免疫ネットワークを介した気管支喘息の発症(論文*112, 114)および増悪機序が明らかとなり(論文*105, 117, 123, 124, 130, 133, 134)、性が神経/内分泌/免疫ネットワークを介した免疫応答制御に深く関与していることが示唆された(論文*110, 132)。特に、CD103⁺ 樹状細胞や CD8⁺ T 細胞は末梢免疫応答の修飾における責任細胞の一つであることが明らかとなった(論文*111, 115)。さらに、 μ オピオイド受容体遺伝子(OPRM1)の一塩基変異(A118G SNP, rs1799971)は、本邦の気管支喘息患者の 64%に認められ、遺伝子型 GG は気管支喘息の増悪因子となる可能性が示された(学会*254, 260)。日常生活環境において遺伝子型 GG は、リガンドの存在下で末梢組織に発現する μ オピオイド受容体の機能変化を誘導し、Th2 細胞分化を促進させる可能性が明らかとなった(学会*251)。受容体遺伝子多型や性、生活習慣に関するこれらの結果は、 μ オピオイド受容体を標的とする難治性疼痛制御において、安全性と個別化療法の確立のために重要な基盤情報となり得ることを示した。

<優れた成果が上がった点>

「研究テーマ1. 新規がん分子標的治療薬の創製」

天然物をシードとする創薬研究では、「FK-A11」(HDAC/PI3K 二重阻害薬)の新規合成法(改良法)の開

法人番号	041004
プロジェクト番号	S1511001L

発に成功し(従来法:全 24 工程、総収率 3.5%; 改良法:全 15 工程、総収率 10%)、工業的製造法への道を拓いた(特許*2)。また、リファガール類縁体の合成と活性評価を行った結果、リファガールの生合成前駆体と考えられるシホノディクチアールBが優れたキナーゼ阻害活性を示すことを見出した(特許*1, 論文*33)。

ヌクレオシド誘導体の設計と合成研究では、①核酸塩基としてチミン、シトシンを導入した 3'-デオキシ-4'-チオヌクレオシド誘導体の合成を達成した。さらに、核酸塩基としてウラシル、チミン、シトシンを導入した 4'-置換 4'-チオリボヌクレオシド誘導体の合成も達成した。本チオヌクレオシドに関して、糖部の立体構造を固定化した誘導体の合成法を確立することが出来た。②抗 HIV 活性が認められなかったものの、4'-フルオロメチルスタブジンの合成を達成した。さらに 4'位に置換基を持つスタブジン誘導体の光学分割に成功した。また、その絶対構造を決定し、リパーゼを用いた光学分割における立体選択性について新たな知見を得ることが出来た。③グルコシダーゼ阻害活性を持つ化合物の立体選択的合成法を確立することが出来た。また、本方法によりこれまでに無い強い活性を持つ化合物を見いだすことが出来た。④遷移金属触媒を用いた位置選択的炭素炭素結合形成反応を開発することが出来た。

薬効/毒性発現および薬物相互作用の評価とそのスクリーニング系の構築では、①正確な薬物相互作用評価を可能するために、薬物動態関連遺伝子誘導の新規分子機構を 2 種明らかとした。また、これを基に薬物代謝酵素活性誘導および阻害評価系の構築に成功した。②薬物代謝酵素活性誘導および阻害評価系を用いて薬物のみならず健康食品の網羅的解析を行い、健康食品の約 20~30%に活性阻害や誘導を引き起こす可能性があることを明らかとした。③レチノイン酸の低濃度(数 nM)検出可能な手法を開発し、化学物質によるレチノイン酸濃度変動による催奇形性発症予測可能な *in vitro* スクリーニング系を樹立した。④hiPSCs 細胞から肝細胞への分化は、胎児肝様細胞にまで達し、ある程度の薬物代謝酵素活性を得ることに成功した。また、肝臓特異的発現に関わっている転写因子の中で HNF3 α が CYP3A7 発現を強く抑制していることを見出した。

「研究テーマ2. 老年性神経系疾患(老人性認知症、高齢者うつ病)改善薬の開発」

エストロゲン受容体制御にもとづく老年性神経系疾患改善薬の設計と合成では、①エストロゲン受容体 β 選択性及び α 選択性が高い化合物を見出し、受容体構造との関係性を明らかにした(論文*56, 77, 96、学会*157)。②エストロゲン受容体のアゴニスト/アンタゴニスト制御をもう一つの課題とし、ジフェニルメタン型化合物の系統合成により、疎水性構造の変化による制御法への重要な情報を見出した(論文*94)。③新しい疎水性構造を用いた新規細胞増殖阻害薬の創製への展開も行い、がん細胞パネルスクリーニングを含む細胞増殖試験で有効な抗がん化合物を見出した(論文*55, 75, 76, 82)。④薬理学教室との共同研究では、我々が開発した新規選択的エストロゲン受容体モジュレーター (SERM) である BE360 の抗うつ、抗認知症効果を確立した(論文*84)。

精神疾患モデル動物を用いた老年性神経系疾患改善薬の評価および作用メカニズムの解明では、①「BE360」選択的エストロゲン受容体モジュレーターが精神疾患モデル動物(嗅球摘出マウス、卵巣摘出+ストレス負荷マウス)において海馬歯状回の神経細胞の増殖を促進し、抗うつ作用および認知障害改善作用を示すことを明らかにした(論文*84、学会*148, 163, 201, 203)。さらに、②ホルモン補充療法により乳がんや子宮体がんが認められていたが「BE360」は生殖器に影響を及ぼさないことも見出した(学会*148, 163, 201)。また、③従来詳細に検討されていなかった男性の更年期障害モデル動物の作製(平成 31 年度創薬研究センターシンポジウム)および神経発達障害仮説に基づいた簡便な統合失調症モデル動物の作製(論文*62、学会*120, 130, 141, 178)にも成功した。

「研究テーマ3. 難治性疼痛に対する緩和医療法の確立」

難治性疼痛の発症メカニズムの解明および特異的疼痛治療薬の創製では、①神経損傷性神経障害性疼痛、炎症性疼痛、多発性硬化症疼痛、神経絞扼性がん性疼痛などの各種難治性疼痛に有効な新規鎮痛薬として、「amidino-TAPA」およびその誘導体「ADAMB」を見出した(学会*288, 289)。また、②既存の麻薬性鎮痛薬である oxycodone と methadone も、特定の難治性疼痛に対して有効であることを発見した(学会*225, 228, 237, 238, 239, 286, 290, 301, 314)。③これら難治性疼痛に有効な鎮痛薬は、共通した特定の

法人番号	041004
プロジェクト番号	S1511001L

薬理作用を持つことを発見し、難治性疼痛治療薬のターゲットとなる特異的受容体を見出した(学会*288, 289)。

μ オピオイド受容体遺伝子多型の解析および個別化医療への応用では、① μ オピオイド受容体を起点とする神経/内分泌/免疫ネットワークを介した気管支喘息の発症(論文*112, 114)および増悪機序が明らかとなり(論文*105, 117, 123, 124, 130, 133, 134)、性が神経/内分泌/免疫ネットワークを介した免疫応答制御に深く関与していることが示唆された(論文*110, 132)。特に、CD103⁺ 樹状細胞や CD8⁺ T 細胞は末梢免疫応答の修飾における責任細胞の一つであることが明らかとなった(論文*111, 115)。さらに、② μ オピオイド受容体遺伝子 (*OPRM1*) の一塩基変異 (A118G SNP, rs1799971) は、本邦の気管支喘息患者の 64% に認められ、遺伝子型 GG は気管支喘息の増悪因子となる可能性が示された(学会*254, 260)。③日常生活環境において遺伝子型 GG は、リガンドの存在下で末梢組織に発現する μ オピオイド受容体の機能変化を誘導し、Th2 細胞分化を促進させる可能性が明らかとなった(学会*251)。

<課題となった点>

「研究テーマ1. 新規がん分子標的治療薬の創製」

「FK-A11」の改良合成法は、工程数の削減および総収率の向上に繋がったものの、光学分割法を用いているため、望まない立体化学を有する副生成物が得られてしまう。そのため、副生成物を有効に利用する方法や副生成物を生じない不斉反応への展開が必要であるが、まだその目的を達成していない。一方、抗がん活性を有する 9 員環キセニアジテルペノイドである 9-デオキシキセニアラクトール C の合成研究では、ラクトール環上への側鎖導入が困難であり大きな課題であったが、現在合成経路を見直し、カルボニル基を足掛かりとした新しい合成法を検討しており、今後の全合成および類縁化合物の系統的な合成への展開が期待される。さらに、スクアレン合成酵素阻害剤であるビスボスクアール A の合成研究では、望む立体配置を有する四環性骨格の構築法および側鎖導入法が課題であるが、現在、光学活性体を用いて検討中である。

4'-置換 4'-チオスクレオシド誘導体の合成において、縮環反応とアルドール反応を組み合わせたワンポット反応の再現性に問題があったが、塩基の当量をコントロールすることでその問題を解決した。糖部の立体構造を固定化した誘導体の合成に際し、位置選択的な保護基の導入が非常に困難であったが、塩基部を利用した選択的保護を試みたところ、予想外にも望みの化合物が一段階で合成出来た。4'位に置換基を持つスタブジン誘導体の光学分割において、当初立体選択性が非常に低いものであった。中間体の構造を最適化することにより、高い光学純度で両鏡像異性体を得ることが出来た。

CYP3A4 を強く誘導した健康食品については、CYP3A4 と酵素誘導に関与する核内受容体をヒト化したマウスを用いて、酵素誘導により薬物相互作用を実際に引き起こすか検討し、フォルスコリンはヒトで薬物相互作用を引き起こすことが示唆されたが、野生型マウスでは薬物相互作用が認められたが、必ずしもヒト化マウスの *in vivo* で CYP3A4 誘導を示さず、CYP3A4 以外のマウス CYP の関与が予測され、今後、新たな評価系の構築の検討が課題となった。

iPS 細胞から成熟肝細胞への分化は、まだ成功の報告例はない。我々は胎児型発現と成熟型発現を示す肝臓が成熟する過程で起きる胎児型 CYP3A7 から成人型 CYP3A4 への発現量の入れ替わり(スイッチ)の分子機序を解明することが、hiPSCs の成熟肝細胞への分化に重要と考えている。そのために、現在、CYP3A7 発現を強く抑制する HNF3 β の役割の解明を行っている。

「研究テーマ2. 老年性神経系疾患(老人性認知症、高齢者うつ病)改善薬の開発」

新規疎水性構造カルボランの反応性に関する知見が少なく、環への求電子試薬の導入反応の収率や再現性に問題があったが、溶媒や反応濃度などの条件検討により、その改善を行い、合成法を確立した。受容体 α β サブタイプのリガンド結合領域はアミノ酸 2 個の違いしかなく、その選択性の一般化は困難であったが、分子動力学の専門家との共同研究により、選択性の条件の検討が進展している(論文*56, 67, 94, 96、学会*108)。

「BE360」の抗うつ作用および認知障害改善作用は、エストロゲン受容体に結合して発現していることを見出した。しかしながら、エストロゲン受容体のどちらのサブタイプ(α , β)を介しているか選択的なアンタ

法人番号	041004
プロジェクト番号	S1511001L

ゴニストが少なく同定できていない。さらに、エストロゲン受容体は膜や核に存在することが知られているが「BE360」が膜および／または核に結合して作用を発現しているか不明である為、「BE360」に蛍光プローブ標識等を結合した化合物を合成し局在を評価する必要がある。また、簡便な統合失調症モデルマウス作製に関する論文に時間を費やし「BE360」の有効性について評価ができていないため今後検討する。

「研究テーマ3. 難治性疼痛に対する緩和医療法の確立」

本研究課題において、従来から使用している各種難治性疼痛(神経損傷性神経障害性疼痛、炎症性疼痛、多発性硬化症疼痛、神経絞扼性がん性疼痛)の実験動物モデルの他に、新たな難治性疼痛モデルとして脳腫瘍誘発疼痛の実験動物モデルの確立を試みた。しかし、有用かつ汎用性の高い実験動物モデルを確立することは出来なかった。

疼痛治療薬によるアレルギー疾患の発症・悪化の感受性増大リスクを軽減するための基盤研究において、IL-4 存在下で活性化した T 細胞に発現する μ オピオイド受容体における遺伝子一塩基多型が、免疫応答制御に特に重要な役割を果たしている可能性が示された(学会*251)。このことは、我々が目的とする難治性疼痛新規治療薬の有効性と安全性の評価において、薬物の分布および動態に加えて患者の免疫状態との相互作用を解析する必要性を示唆するものである。さらに、 μ オピオイド受容体の遺伝子多型による Th2 型免疫応答の亢進は、環境要因である性によって影響されることが明らかとなり、遺伝的背景と環境要因の相互作用から新規疼痛治療薬の有効性と安全性を評価する必要がある。

<自己評価の実施結果と対応状況>

毎年6月に学内において「創薬研究センターシンポジウム」を開催し、各研究室からの成果報告を行い、進捗状況と研究方針について確認と議論を行っている。また、本シンポジウムでは、学外から関連分野の第一線で活躍されている研究者(3名)を講演者として招聘しており、その先生方からも貴重な助言を頂いている。有効な研究費運用の維持に関しては創薬研究センター運営委員会で各年度の予算執行について討議している。平成29年度終了時(中間報告書作成時)における研究成果を研究費配分に反映させる予定であったが、計画遂行がいずれも順調であったため従来の配分を維持した。なお、本研究プロジェクト終了時に本学自己評価委員会により詳細な審査に基づき厳正な評価が実施される予定である。

<外部(第三者)評価の実施結果と対応状況>

本プロジェクトを終了するにあたり、2名の外部評価者に「計画の達成度」、「得られた研究成果」、「研究教育拠点形成」および「プロジェクト全体の評価(総合評価)」に関しての評価およびコメントを依頼した。その結果、いずれの項目とも高い評価を頂いた。また、平成28年度に設置された医学部との緊密な連携体制を強化することで地域医療ならびにアンメット・メディカル・ニーズに応える先導的研究拠点としての役割を担えるように発展して欲しいとのコメントを頂いた。この点に関しては本プロジェクトの研究成果を基盤に、これまで以上に医薬連携体制を強化し、本学が地域医療ならびに創薬研究の拠点になれるよう邁進していきたい。

<研究期間終了後の展望>

今後も本研究プロジェクトに参画した研究室が連携を取りながら、がん、老年性神経系疾患および難治性疼痛に対する新規医薬品のシードとなる化合物の創製を目指して研究を継続していきたいと考えている。それぞれの研究テーマについての今後の研究方針を以下に記述する。

「研究テーマ1. 新規がん分子標的治療薬の創製」

抗がん活性を有する9-デオキシキセニアラクトール C の合成研究に関しては、側鎖導入法を検討した後、全合成およびその類縁体を合成し、構造活性相関研究に発展させたいと考えている。さらに、本合成法は、同様な基本骨格を有するクリスタキセニシン A およびその縮環体であるブルミスクレリン A の全合成研究に応用したいと考えている。一方、マンデラリド A の全合成研究で用いた銀触媒による光学活性なフラン環およびピラン環の新規合成法は、ピペリジンやピロリジンなどの含窒素複素環の合成に応用し、

法人番号	041004
プロジェクト番号	S1511001L

それらを含む天然物群の系統的な合成に活用したいと考えている。また、FTase 阻害薬「TAN-1813」の合成研究においては、モデル化合物での検討結果より、二つの重要中間体をカップリングさせるために必要な新知見を得ている。この方法論を用いて「TAN-1813」の完全化学合成を世界に先駆けて達成する。

各種グリコシル化によるチオヌクレオシド誘導体の合成を展開させると共に、新たなグリコシル化反応の開発へと展開させていく。種々の4'-置換ヌクレオシド誘導体の合成を行うと共に、光学活性なヌクレオシド誘導体を合成し、生物活性評価を行う。エナンチオマー間での活性の違いを評価することで、生物活性における立体化学の一般性を確立出来るものと考えられる。一方、チオヌクレオシド誘導体の構造活性相関研究が、高い抗腫瘍活性、もしくは抗 HIV 活性を有する誘導体の創製に繋がる事が期待される。特に、糖部立体構造を固定化した誘導体の合成が可能になったことから、選択的な薬理活性を発現させる核酸医薬の発展に貢献できるに違いない。また、今回開発した炭素炭素結合形成反応は更なる結合形成反応へと展開が可能であり、種々の化合物合成へと応用できると考えられる。

肝障害発症には薬物代謝酵素活性阻害および誘導が強く関わっていることから、本研究で構築した薬物代謝酵素活性誘導および阻害評価系の有効性が証明されたので、これらの系を活用し、薬物肝障害発症リスク評価系を新たに構築する。CYP3A4 を誘導および活性阻害を強く示すことが判明した健康食品は、ヒト化マウスを用いて、ヒトにおける薬物相互作用の予測を行って行く必要がある。また、iPS 細胞の成熟肝細胞分化の研究については、分化薬物代謝活性が CYP 発現の違いの原因を解明し、新たな分化の手法の開発を目指す。現在共同研究者等はヒト小腸上皮細胞と同等な薬物代謝活性を示す分化に成功しており、その分化手法を改良することで成熟肝細胞と同等な薬物代謝活性を有する分化を目指す。

「研究テーマ2. 老年性神経系疾患(老人性認知症、高齢者うつ病)改善薬の開発」

本研究で見出したエストロゲン関連化合物の *in vivo* での構造活性相関により、神経薬理学的知見と、分子論的作用機構の間を埋める結果が得られることを期待している。また、本研究で見出した新しい細胞増殖阻害化合物は新しい作用機構をもつ抗がん薬の端緒となる可能性がある。

神経系への作用が期待されているエストロゲン受容体βに選択的に作用する化合物が設計および合成されている。したがって、「BE360」の抗うつ作用および認知障害改善作用メカニズムにおけるエストロゲン受容体サブタイプの同定後、精神疾患モデル動物を用いて選択性のある化合物の有効性について検討する。さらに、簡便な統合失調症モデル動物を用いて「BE360」の効果およびその機序を行動薬理学的並びに分子生物学的手法により解明する。

「研究テーマ3. 難治性疼痛に対する緩和医療法の確立」

「Amidino-TAPA」や methadone の構造を基に、類似構造を持ちかつそれぞれの特許に抵触しない新規化合物を、現在合成中である。合成した新規化合物の各種難治性疼痛に対する有効性を検討し、またメカニズムを解明する予定である。また、「amidino-TAPA」は精神依存性を示さないこと(論文*106、学会*271, 274, 304, 315)、methadone も著しく精神依存性が弱い麻薬性鎮痛薬であることから、新規化合物の精神依存性の有無を検討し、新規化合物を依存性の無い難治性疼痛の特異的治療薬として開発する予定である。

μ オピオイド受容体遺伝子 (*OPRM1*) の一塩基変異 (A118G SNP, rs1799971) と同様の多型を有するマウス (*Oprm1* SNP A112G) を用いて、内因性 μ オピオイド受容体アゴニストによる末梢免疫応答の変化をさらに多面的に解析する。特に Th1 型免疫応答が主体となる感染免疫応答や、Th17 型免疫応答が主体となる一部の喘息病態や創病変の動物モデルを用いて、神経/内分泌/免疫ネットワークの観点から感染症や創傷の発症と悪化の感受性増大リスクを評価する。加えて、 μ オピオイド受容体一塩基多型と新規疼痛治療薬の作用(疼痛緩和効果、リガンドとの親和性、細胞内シグナル伝達の差異等)を解明し、臨床試験へと発展させる。

<研究成果の副次的効果>

「研究テーマ1. 新規がん分子標的治療薬の創製」

抗がん活性を有するマンデラリド A の全合成では、合成終盤のマクロラクトン化反応において、想定し

法人番号	041004
プロジェクト番号	S1511001L

ていない水酸基の位置で環化したイソマンデラリド A が得られた。本化合物の抗がん活性を評価したところ、ターゲット天然物であるマンデラリド A よりも強い生物活性を有していることが判明した(論文*34)。さらに、マンデラリド A の構造中に含まれる光学活性なピラン環およびフラン環の構築法では、金触媒を用いる方法が一般的であったが、これを銀触媒に代替える方法論を開発し、合成コストの削減に成功した(論文*35)。また、「FK-A11」の工業的製造法の開発により(特許*2)、臨床応用に向けた動物実験や非臨床試験などの研究が推進されることが期待できる。また、リファガールおよび関連化合物の新たな生物活性を見出したことより(特許*1)、これら天然物をシードした創薬研究を進展させることができる。

各種グリコシル化反応により様々なヌクレオシド誘導体の合成法を確立することが出来た。今後、これらのグリコシル化を適応させることで、望みの官能基を有する種々の誘導体が合成可能となることが期待され、抗腫瘍活性、もしくは抗 HIV 活性をもつ新たな化合物の創製に貢献できるものと考えられる。4'-置換 4'-チオヌクレオシド誘導体の合成において、糖部の立体構造を容易に固定化可能となったことから、核酸医薬の構成素子となる新たなヌクレオシドユニットの供給が容易となり、アンチセンス法に有用な人工核酸の開発に寄与できるものと考えられる。一方、選択的なグルコシダーゼ阻害活性を持つ化合物の立体選択的合成法を確立することが出来た。未だ多くの課題を残しているものの、将来的には糖尿病治療における薬物選択肢の幅を広げることに貢献できるものと考えられる。

CYP3A4 の肝臓および腸管における誘導評価を行った 2 種の *in vitro* スクリーニング系から得られたデータを比較したところ、CYP3A4 には従来から考えられていたものとは異なる分子機序を見出した。その一つに CYP3A4 は核内受容体である PXR に結合することで誘導されることが知られていたが、本研究の過程でプロテインキナーゼの活性化により誘導されることを明らかにした。また、hiPSCs の成熟肝細胞への分化に重要な役割を担う因子の探索を行ってきた課程で、肝臓が成熟する過程で起きる胎児型 CYP3A7 から成人型 CYP3A4 への発現量の入れ替わり(スイッチ)の分子機序に肝特異的転写因子が関与していることを見出した。特にその転写因子の一つである HNF3 β は CYP3A7 の発現を強く抑制するが、その発現は胎児肝臓で低く、成熟に伴って上昇することが分かっている。従って、胎児型 CYP3A7 から成人型 CYP3A4 への発現スイッチは、この転写因子の成熟に伴う上昇によって CYP3A7 発現が抑制されていることが示唆された。

「研究テーマ2. 老年性神経系疾患(老人性認知症、高齢者うつ病)改善薬の開発」

本研究での構造の基礎となる新規疎水性構造の医薬分子設計への応用の方法論は、第 16 回国際ホウ素化学会議での招待講演、日本薬学会の会報での解説など、普及に努めている(図書*2、論文*50、学会*158)。また、新規疎水性骨格としてのホウ素クラスターの計算科学的解析が、本プロジェクトを通じて生体分子とのドッキング研究を通じて発展した(論文*56, 67, 94, 96、学会*108)。本研究の新規リガンドが生物学的ツールとして生物科学研究に用いられてきている(論文*81)。特に、本研究との関連性もある神経細胞分化の研究にも用いられ、進展している(論文*95)。

候補化合物「BE360」はうつ病、認知症、骨粗鬆症のモデル動物に対して有効であった。さらに、この化合物を評価する際用いた精神疾患モデル動物については、生体機能と創薬シンポジウム 2016 および第 16 回生物化学若手研究者セミナー(いずれも招待講演)で発表(学会*178, 203)し、臨床を反映したモデルであることが評価され産学連携に発展し精神疾患に対する治療薬・サプリメント開発および病態解明に繋げることができた。この「BE360」については、老化に伴い生じる気分障害、記憶力低下および寝たきりにつながる骨粗鬆症による骨折といった高齢者の QOL 低下に福音をもたらす可能性を示した。

「研究テーマ3. 難治性疼痛に対する緩和医療法の確立」

難治性疼痛治療薬のターゲットとなりうる特異的受容体に関して、用途特許の申請が可能か検討中である。また、新規化合物に難治性疼痛に対する有効性を見出した場合、ならびに新規化合物に精神依存性が無いことを見出した場合は、それぞれ「難治性疼痛治療薬」ならびに「依存性の無い鎮痛薬」として、特許申請を行う予定である。

OPRM1A118G SNP, rs1799971 はアジア人において多い遺伝子多型であり受容体機能を変調させる多型であることから、オピオイドネットワークを介した免疫応答制御の解析において用いた *Oprm1* SNP

法人番号	041004
プロジェクト番号	S1511001L

A112G マウスは、 μ オピオイド受容体を標的とする種々の新規化合物の有効性評価において有用なモデル動物の作製に寄与できる可能性が明らかとなった。

12 キーワード(当該研究内容をよく表していると思われるものを8項目以内で記載してください。)

- | | | |
|---------------------|----------------------|-----------------------|
| (1) <u>創薬</u> | (2) <u>分子標的抗がん薬</u> | (3) <u>ヌクレオシド誘導体</u> |
| (4) <u>毒性発現予測</u> | (5) <u>エストロゲン受容体</u> | (6) <u>老年性精神疾患治療薬</u> |
| (7) <u>難治性疼痛治療薬</u> | (8) <u>受容体遺伝子多型</u> | |

13 研究発表の状況(研究論文等公表状況。印刷中も含む。)

上記、11(4)に記載した研究成果に対応するものには*を、本報告書に全文を掲載した主要論文には文献番号に二重線を付した。

<雑誌論文>

「研究テーマ1. 新規がん分子標的治療薬の創製」

- *1. Synthesis of 2'-Aminouridine Derivatives as an Organocatalyst for Diels-Alder Reaction, Wakamatsu, H.; Itoh, M.; Natori, Y.; Yoshimura, Y. *Nucleosides Nucleotides Nucleic Acids*, in press (査読有).
- 2. UDP-Glucuronosyltransferase (UGT) -Mediated Attenuations of Cytochrome P450 3A4 Activity: UGT Isoform-Dependent Mechanism of Suppression, Miyauchi, Y.; Tanaka, Y.; Nagata, K.; Yamazoe, Y.; Mackenzie, P.I.; Yamada, H.; Ishii, Y. *British J. Pharmacol.* **2020**, *177*, 1077-1089 (査読有).
- 3. A Novel Approach to Oxazole-Containing Diterpenoid Synthesis from Plant Roots: Salviamines E and F, Narita, K.; Fujisaki, N.; Sakuma, Y.; Katoh, T. *Org. Biomol. Chem.* **2019**, *17*, 655-663 (査読有).
- 4. A Concise Approach for Producing Optically Pure Carboxylic Acid Segments for the Synthesis of Bicyclic Dipeptide Histone Deacetylase Inhibitors, Narita, K.; Sayar, N.; Saijo, K.; Ishioka, C.; Katoh, T. *Synthesis*, **2019**, *51*, 1408-1418 (査読有).
- 5. Facile Total Synthesis of Thailandepsins D-F: Novel Bicyclic Dipeptide Histone Deacetylase Inhibitors Isolated from a Microorganism, Sayar, N.; Narita, K.; Katoh, T. *Synthesis*, **2019**, *51*, 1419-1426 (査読有).
- 6. In Vitro and In Vivo Antitumor Activity and the Mechanism of Siphonodictyal B in Human Colon Cancer Cells, Chikamatsu, S.; Saijo, K.; Imai, H.; Narita, K.; Kawamura, Y.; Katoh, T.; Ishioka, C. *Cancer Medicine*, **2019**, *8*, 5662-5672 (査読有).
- *7. Catalytic Asymmetric Synthesis of Stereoisomers of 1-C-n-butyl-LABs for the SAR Study of α -Glucosidase Inhibition, Natori, Y.; Sakuma, T.; Watanabe, H.; Wakamatsu, H.; Kato, A.; Adachi, I.; Takahata, T.; Yoshimura, Y. *Tetrahedron* **2019**, *75(20)*, 2866-2876 (査読有).
- 8. Conjugate Vaccine Produces Long-Lasting Attenuation of Fentanyl vs. Food Choice and Blocks Expression of Opioid Withdrawal-Induced Increases in Fentanyl Choice in Rats, Townsend, A.; Blake, S.; Faunce, K. E.; Hwang, C. S.; Natori, Y.; Zhou, B.; Bremer, P. T.; Janda, K. D.; Bank, M. L. *Neuropsychopharmacology* **2019**, *44*, 1681-1689 (査読有).
- 9. A Chemically Contiguous Hapten Approach for a Heroin-Fentanyl Vaccine, Natori, Y.; Hwang, C. S.; Lin, L.; Smith, L. C.; Zhou, B.; Janda, K. D. *Beilstein J. Org. Chem.* **2019**, *15*, 1020-1031 (査読有).
- 10. Phosphorylation-Deficient Mutant of Retinoid X Receptor α at Thr167 Alters Fasting Response and Energy Metabolism in Mice, Sueyoshi, T.; Sakuma, T.; Shindo, S.; Fashe, M.; Kanayama, T.; Ray, M.; Moore, R.; Negishi, M. A. *Lab. Invest.* **2019**, *99*, 1470-1483 (査読有).
- *11. A Novel Approach to Sesquiterpenoid Benzoxazole Synthesis from Marine Sponges: Nakijinols A, B and E-G, Takeda, Y.; Nakai, K.; Narita, K.; Katoh, T. *Org. Biomol. Chem.*, **2018**, *16*, 3639-3647 (査読有).
- 12. Total Syntheses of Liphagal: A Potent and Selective Phosphoinositide 3-Kinase α (PI3K α) Inhibitor from the Marine Sponge *Aka Coralliphaga*, Narita, K.; Katoh, T. *Heterocycles*, **2018**, *96*, 3-41 (査読有).

法人番号	041004
プロジェクト番号	S1511001L

13. Improved Admixture Vaccine of Fentanyl and Heroin Hapten Immunoconjugates: Antinociceptive Evaluation of Fentanyl-Contaminated Heroin, Hwang, C. S.; Smith, L. C.; Natori, Y.; Ellis, B.; Zhou, B.; Janda, K. D. *ACS Omega* **2018**, *3*, 11537–11543 (査読有).
- *14. Synthesis of Various Heterocycles Having Dienamide Moiety by Ring-Closing Metathesis of Ene-ynamides, Wakamatsu, H.; Sasaki, Y.; Kawahata, M.; Yamaguchi, K.; Yoshimura, Y. *Synthesis* **2018**, *50(17)*, 3467–3486 (査読有).
15. Glycosylation Reactions Mediated by Hypervalent Iodine: Application to the Synthesis of Nucleosides and Carbohydrates, Yoshimura, Y.; Wakamatsu, H.; Natori, Y.; Saito, Y.; Minakawa, N. *Beilstein J. Org. Chem.* **2018**, *14*, 1595–1618 (査読有).
16. Synthesis of 4'-Thionucleosides as Antitumor and Antiviral Agents, Yoshimura, Y.; Saito, Y.; Natori, Y.; Wakamatsu, H. *Chem. Pharm. Bull.* **2018**, *66*, 139–146 (査読有).
17. Efficient Syntheses of Cocaine Vaccines and Their in Vivo Evaluation, Kimishima, A.; Olson, M. E.; Natori, Y.; Janda, K. D. *ACS Med. Chem. Lett.* **2018**, *9*, 411–416 (査読有).
18. Efficacious Vaccine against Heroin Contaminated with Fentanyl, Hwang, C. S.; Smith, L. C.; Natori, Y.; Ellis, B.; Zhou, B.; Janda, K. D. *ACS Chem. Neurosci.* **2018**, *9*, 1269–1275 (査読有).
19. Practical Synthesis of 4'-Thioribonucleosides from L-Arabinose via Novel Reductive Ring-Contraction Reaction and Pummerer-Type Thioglycosylation, Wakamatsu, H.; Nitta, K.; Shoji, N.; Natori, Y.; Saito, Y.; Yoshimura, Y. *Curr. Protoc. Nucleic Acid Chem.* **2018**, *71*, 1.43.1–1.43.12 (査読有).
20. Sulfotransferase 4A1 Increases its Expression in Mouse Neurons as they Mature, Hashiguchi, T.; Shindo, S.; Chen, S. H.; Hong, J. S.; Negishi, M. *Drug Metab Dispos.* **2018**, *46*, 860–864 (査読有).
21. Synthetic Study toward Total Synthesis of Marine Diterpenoid Cristaxenicin A: Synthesis of δ -Unsaturated Lactone Bearing α -Bulky Substituent, Nakai K.; Sayar, N.; Yoshimura, Y.; Watanabe, K. *Journal of Tohoku Medical and Pharmaceutical University*, **2017**, *64*, 57–63.
22. Unified Synthesis of the Marine Sesquiterpene Quinones (+)-Smenoqualone, (-)-Ilimaquinone, (+)-Smenospongine, and (+)-Isospongiaquinone, Katoh, T.; Atsumi, S.; Saito, R.; Narita, K.; Katoh, T. *Eur. J. Org. Chem.*, **2017**, 3837–3849 (査読有).
23. Antitumor Activity and Pharmacologic Characterization of the Depsipeptide Analog as a Novel Histone Deacetylase/Phosphatidylinositol 3-Kinase Dual Inhibitor, Saijo, K.; Imai, H.; Chikamatsu, S.; Narita, K.; Katoh, T.; Ishioka, C. *Cancer Sci.*, **2017**, *108*, 1469–1475 (査読有).
24. Total Synthesis of Marine Sesquiterpene Quinones (+)-Cyclosporgiaquinone-1 and (-)-Dehydrocyclosporgiaquinone-1 with a Tetracyclic Benzo[a]xanthene Skeleton, Takeda, T.; Narita, K.; Katoh, T. *Eur. J. Org. Chem.*, **2017**, 901–907 (査読有).
25. Development of a Glycosylation Reaction: A Key to Accessing Structurally Unique Nucleosides, Yoshimura, Y. *Heterocycles* **2017**, *94*, 1625–1651 (査読有).
- *26. Palladium-Catalyzed Regioselective Hydroarylation of Ynamides with Aryl Iodides: Easy Synthesis of Various Substituted Enamides Containing Stilbene Derivatives, Wakamatsu, H.; Yanagisawa, R.; Kimura, S.; Osawa, N.; Natori, Y.; Yoshimura, Y. *Synlett* **2017**, *28*, 2135–2138 (査読有).
27. Activated Brain-Derived Neurotrophic Factor/TrkB Signaling in Rat Dorsal and Ventral Hippocampi Following 10-Day Electroconvulsive Seizure Treatment, Enomoto, S.; Shimizu, K.; Nibuya, M.; Suzuki, E.; Nagata, K.; Kondo, T. *Neurosci. Lett.*, **2017**, *660*, 45–50 (査読有).
- *28. CYP3A4 Induction Mechanism of Polycyclic Aromatic Hydrocarbons Differs from that of Rifampicin in PXR Binding Element, Aratsu, Y.; Odagiri, R.; Shoji, R.; Watanabe, K.; Kumagai, T.; Shindo, S.; Sasaki, T.; Nagata, K. *Fundam. Toxicol. Sci.*, **2017**, *4*, 229–239 (査読有).
- *29. Effect of Health Foods on Cytochrome P450-Mediated Drug Metabolism, Sasaki, T.; Sato, Y.; Kumagai, T.; Yoshinari, K.; Nagata, K. *J. Pharm. Health Care Sci.*, **2017**, *3*, 14 (査読有).
30. Total Synthesis of the Depsipeptide FR901375 and Preliminary Evaluation of Its Biological Activity, Narita, K.; Katoh, Y.; Ojima, K.; Dan, S.; Yamori, T.; Ito, A.; Yoshida, M.; Katoh, T. *Eur. J. Org. Chem.*, **2016**, 5667–5677 (査読有).
- *31. Synthesis and Biological Evaluation of Novel FK228 Analogues as Potential Isoform Selective HDAC Inhibitors, Narita, K.; Matsuhara, K.; Itoh, J.; Akiyama, Y.; Dan, S.; Yamori, T.; Ito, A.; Yoshida, M.;

法人番号	041004
プロジェクト番号	S1511001L

- Katoh, T. *Eur. J. Med. Chem.*, **2016**, *121*, 592–609 (査読有).
32. Low-Dose Spiruchostatin-B, a Potent Histone Deacetylase Inhibitor Enhances Radiation-Induced Apoptosis in Human Lymphoma U937 Cells via Modulation of Redox Signaling, Rehman, M. U.; Jawaid, P.; Zhao, Q. L.; Li, P.; Narita, K.; Katoh, T.; Shimizu, T.; Kondo, T. *Free Radic. Res.*, **2016**, *50*, 596–610 (査読有).
- *33. Enantioselective Total Synthesis of (–)-Siphonodictyal B and (+)-8-*epi*-Siphonodictyal B with Phosphatidylinositol 3-Kinase Inhibitory Activity, Kikuchi, T.; Narita, K.; Saijo, K.; Ishioka, C.; Katoh, T. *Eur. J. Org. Chem.*, **2016**, 5659–5666 (査読有).
- *34. Enantioselective Total Synthesis of Mandelalide A and Isomandelalide A: Discovery of a Cytotoxic Ring-Expanded Isomer, Veerasamy, N.; Ghosh, A.; Li, J.; Watanabe, K.; Serrill, D. J.; Ishmael, E. J.; McPhail, L. K.; Carter, G. R. *J. Am. Chem. Soc.*, **2016**, *138*, 770–773 (査読有).
- *35. Stereoselective, Ag-Catalyzed Cyclizations To Access Polysubstituted Pyran Ring Systems: Synthesis of C₁–C₁₂ Subunit of Madeirolide A, Watanabe, K.; Li, J.; Veerasamy, N.; Ghosh, A.; Carter, G. R. *Org. Lett.*, **2016**, *18*, 1744–1747 (査読有).
36. Total Synthesis of Thailandepsin B, a Potent HDAC Inhibitor Isolated from a Microorganism, Narita, K.; Katoh, T. *Chem. Pharm. Bull.*, **2016**, *64*, 913–917 (査読有).
37. Docking Study and Biological Evaluation of Pyrrolidine-based Iminosugars as Pharmacological Chaperones for Gaucher Disease, Kato, A.; Nakagome, I.; Sato, K.; Yamamoto, A.; Adachi, I.; Nash, R. J.; Fleet, G. W. J.; Natori, Y.; Watanabe, Y.; Imahori, I.; Yoshimura, Y.; Takahata, H.; Hirono, S. *Org. Biomol. Chem.* **2016**, *14*, 1039–1048 (査読有).
38. Development of Stereoselective Synthesis of Biologically Active Nitrogen-heterocyclic Compounds: Applications for Syntheses of Natural Product and Organocatalyst, Natori, Y.; Imahori, T.; Yoshimura, Y. *J. Synth. Org. Chem. Jpn.* **2016**, *74*, 335–349 (査読有).
- *39. Activation of p38 Mitogen-Activated Protein Kinase by Clotrimazole Induces Multidrug Resistance-Associated Protein 3 Activation through a Novel Transcriptional Element, Sasaki, T.; Inami, K.; Numata, Y.; Funakoshi, K.; Yoshida, M.; Kumagai, T.; Kanno, S.; Matsui, S.; Toriyabe, T.; Yamazoe, Y.; Yoshinari, K.; Nagata, K. *J. Pharmacol. Exp. Ther.*, **2016**, *359*, 102–109 (査読有).
- *40. レポーター遺伝子導入培養細胞を用いた健康食品による CYP1A1/1A2 誘導の網羅的評価、熊谷 健佐々木崇光、永田 清、*医療薬学*, **2016**, *42*, 701–708 (査読有).
- *41. Indirubin, a Component of Ban-Lan-Gen, Activates CYP3A4 Gene Transcription through the Human Pregnane X Receptor, Kumagai, T.; Aratsu, Y.; Sugawara, R.; Sasaki, T.; Miyairi, S.; Nagata, K. *Drug Metab. Pharmacokinet.*, **2016**, *31*, 139–145 (査読有).
42. Directed Synthesis of 2-Spiroindolines from Indole Derivatives by Formic Acid-Induced *N*-Acyliminium Ion-Conjugated Diene Spirocyclization, Abe, H.; Miyagawa, N.; Hasegawa, S.; Kobayashi, T.; Aoyagi, S.; Kibayashi, C.; Katoh, T.; Ito, H. *Tetrahedron Lett.*, **2015**, *56*, 921–924 (査読有).
43. Biochemical, Biological and Structural Properties of Romidepsin (FK228) and Its Analogs as Novel HDAC/PI3K Dual Inhibitors, Saijo, K.; Imamura, J.; Narita, K.; Oda, A.; Shimodaira, H.; Katoh, T.; Ishioka, C. *Cancer Sci.*, **2015**, *106*, 208–215 (査読有).
44. Catalytic Asymmetric Synthesis of (–)-*E*- δ -Viniferin via an Intramolecular C–H Insertion of Diaryldiazomethane using Rh₂(S-TFPTTL)₄, Natori, Y.; Ito, M.; Anada, M.; Nambu, H.; Hashimoto, S. *Tetrahedron Lett.* **2015**, *56*, 4324–4327 (査読有).
45. Construction of an Isonucleoside on a 2,6-Dioxobicyclo[3.2.0]-heptane Skeleton, Yoshimura, Y.; Kobayashi, S.; Kaneko, H.; Suzuki, T.; Imamichi, T. *Molecules* **2015**, *20*, 4623–4634 (査読有).
46. Suppression of Cytochrome P450 3A4 Function by UDP-Glucuronosyltransferase 2B7 through a Protein-Protein Interaction: Cooperative Roles of the Cytosolic Carboxyl-Terminal Domain and the Luminal Anchoring Region, Miyauchi, Y.; Nagata, K.; Yamazoe, Y.; Mackenzie, P. I.; Yamada, H.; Ishii, Y. *Mol. Pharmacol.*, **2015**, *88*, 800–812 (査読有).
- *47. Simultaneous Evaluation of Human CYP3A4 and ABCB1 Induction by Reporter Assay in LS174T Cells, Stably Expressing their Reporter Genes, Inami, K.; Sasaki, T.; Kumagai, T.; Nagata, K. *Biopharm. Drug Dispos.*, **2015**, *36*, 139–147, 2015 (査読有).

法人番号	041004
プロジェクト番号	S1511001L

- *48. Development of a Highly Reproducible System to Evaluate Inhibition of Cytochrome P450 3A4 Activity by Natural Medicines, Sato, Y.; Sasaki, T.; Takahashi, S.; Kumagai, T.; Nagata, K. *J. Pharm. Pharm. Sci.*, **2015**, *18*, 316–327 (査読有).
- *49. 培養細胞を用いた健康食品と医薬品との薬物相互作用の網羅的調査 熊谷 健、佐々木崇光、佐藤 裕、高橋昌悟、細川正清、頭金正博、松永民秀、大森 栄、永田 清、東京都病院薬剤師会雑誌 (THPA), **2015**, *64*, 14–22 (査読無).
- 「研究テーマ2. 老年性神経系疾患(老人性認知症、高齢者うつ病)改善薬の開発」
- *50. ホウ素クラスターの形状と疎水性を利用した創薬 遠藤泰之、ファルマシア, **2020**, *56*, (査読有)
51. Liver Hydrolysate Improves Depressive-Like Behavior in Olfactory Bulbectomized Mice: Involvement of Hippocampal Neurogenesis through the AMPK/BDNF/CREB Pathway, Nakagawasai, O.; Yamada, K.; Odaira, T.; Takahashi, K.; Nemoto, W.; Sakuma, W.; Wakou, M.; Lin, J.R.; Tan-No, K. *J. Pharmacol. Sci.*, in press (査読有).
52. Downregulation of Spinal Angiotensin Converting Enzyme 2 is Involved in Neuropathic Pain Associated with Type 2 Diabetes Mellitus in Mice, Yamagata, R.; Nemoto, W.; Nakagawasai, O.; Takahashi, K.; Tan-No, K. *Biochem. Pharmacol.*, **2020**, *174*, 113825 (査読有).
53. Effect of Spinal Angiotensin-Converting Enzyme 2 Activation on the Formalin-Induced Nociceptive Response in Mice, Nemoto, W.; Yamagata, R.; Nakagawasai, O.; Nakagawa, K.; Hung, W.Y.; Fujita, M.; Tadano, T.; Tan-No, K. *Eur. J. Pharmacol.*, **2020**, *872*, 172950 (査読有).
- *54. Role of Prefrontal Cortical 5-HT_{2A} Receptors and Serotonin Transporter in the Behavioral Deficits in Post-Pubertal Rats Following Neonatal Lesion of the Ventral Hippocampus, Mitazaki, S.; Nakagawasai, O.; Onogi, H.; Watanabe, K.; Takahashi, K.; Tan-No, K.; Quirion, R.; Srivastava, L.K.; Tadano, T. *Behav. Brain Res.*, **2020**, *377*, 112226 (査読有).
- *55. Anti-Cancer Activity of *m*-Carborane-Containing Trimethoxyphenyl Derivatives through Tubulin Polymerization Inhibition, Kaise, A.; Endo, Y.; Ohta, K. *Bioorg. Med. Chem.*, **2019**, *27*, 1139–1144 (査読有).
- *56. ER Subtype Selectivity of *m*-Carborane Containing Phenols: *G*-Alkyl Groups on the *m*-Carborane Cage Enhance ER α Selectivity, Ohta, K.; Ogawa, T.; Kato, K.; Oda, A.; Endo, Y. *Bioorg. Med. Chem. Lett.*, **2019**, *29*, 2290–2293 (査読有).
57. Design and Synthesis of Novel Breast Cancer Therapeutic Drug Candidates Based upon the Hydrophobic Feedback Approach of Antiestrogens, Ohta, K.; Kaise, A.; Taguchi, F.; Aoto, S.; Ogawa, T.; Endo, Y. *Molecules*, **2019**, *24*, 3966 (査読有).
58. Benzolactam-Related Compounds Promote Apoptosis of HIV-Infected Human Cells via Protein Kinase C-Induced HIV Latency Reversal, Matsuda, K.; Kobayakawa, T.; Tsuchiya, K.; Hattori, S.; Nomura, W.; Gatanaga, H.; Yoshimura, K.; Oka, S.; Endo, Y.; Tamamura, H.; Mitsuya, H.; Maeda, K. *J. Biol. Chem.*, **2019**, *294*, 116–129 (査読有).
59. An Automated Microliter-Scale High-Throughput Screening System (MSHTS) for Real-Time Monitoring of Protein Aggregation Using Quantum-Dot Nanoprobes, Sasaki, R.; Tainaka, R.; Ando, Y.; Hashi, Y.; Deepak, H. V.; Suga, Y.; Murai, Y.; Anetai, M.; Monde, K.; Ohta, K.; Ito, I.; Kikuchi, H.; Oshima, Y.; Endo, Y.; Nakao, H.; Sakono, M.; Uwai, K.; Tokuraku, K. *Scientific Reports*, **2019**, *9*, 1–9 (査読有).
- *60. Effect of *Enterococcus Faecalis* 2001 on Colitis and Depressive-Like Behavior in Dextran Sulfate Sodium-Treated Mice: Involvement of the Brain-Gut Axis, Takahashi, K.; Nakagawasai, O.; Nemoto, W.; Odaira, T.; Sakuma, W.; Onogi, H.; Nishijima, H.; Furihata, R.; Nemoto, Y.; Iwasa, H.; Tan-No, K.; Tadano, T. *J. Neuroinflammation*, **2019**, *16*, 201 (査読有).
- *61. Mechanisms Underpinning AMP-Activated Protein Kinase-Related Effects on Behavior and Hippocampal Neurogenesis in an Animal Model of Depression, Odaira, T.; Nakagawasai, O.; Takahashi, K.; Nemoto, W.; Sakuma, W.; Lin, J.L.; Tan-No, K. *Neuropharmacology*, **2019**, *150*, 121–133 (査読有).
- *62. Prenatal Treatment with Methylazoxymethanol Acetate as a Neurodevelopmental Disruption Model of Schizophrenia in Mice, Takahashi, K.; Nakagawasai, O.; Sakuma, W.; Nemoto, W.; Odaira, T.; Lin, J.L.; Onogi, H.; Srivastava, L.K.; Tan-No, K. *Neuropharmacology*, **2019**, *150*, 1–14 (査読有).

法人番号	041004
プロジェクト番号	S1511001L

63. Anti-Hypersensitive Effect of Angiotensin (1-7) on Streptozotocin-Induced Diabetic Neuropathic Pain in Mice, Ogata, Y.; Nemoto, W.; Yamagata, R.; Nakagawasai, O.; Shimoyama, S.; Furukawa, T.; Ueno, S.; Tan-No, K. *Eur. J. Pain*, **2019**, *23*, 739-749 (査読有).
64. Etidronate Attenuates Tactile Allodynia by Spinal ATP Release Inhibition in Mice with Partial Sciatic Nerve Ligation, Yamagata, R.; Nemoto, W.; Nakagawasai, O.; Hung, W.Y.; Shima, K.; Endo, Y.; Tan-No, K. *Naunyn Schmiedebergs Arch. Pharmacol.*, **2019**, *392*, 349-357 (査読有).
- *65. Involvement of Catecholaminergic and GABAergic Mediations in the Anxiety-Related Behavior in Long-Term Powdered Diet-Fed Mice, Yaoita, F.; Tsuchiya, M.; Arai, Y.; Tadano, T.; Tan-No, K. *Neurochem. Int.*, **2019**, *124*, 1-9 (査読有).
66. Synthesis, Structure-Activity Relationships, and Mechanistic Studies of 5-Arylazo-Tropolone Derivatives as Novel Xanthine Oxidase (XO) Inhibitors, Sato, D.; Kisen, T.; Kumagai, M.; Ohta, K. *Bioorg. Med. Chem.*, **2018**, *26*, 536-542 (査読有).
- *67. Novel Androgen Receptor Full Antagonists: Design, Synthesis, and a Docking Study of a Glycerol and Aminoglycerol Derivatives that Contain p-Carborane Cages, Kaise, A.; Ohta, K.; Fujii, S.; Oda, A.; Goto, T.; Endo, Y. *Bioorg. Med. Chem.*, **2018**, *26*, 3805-3811(査読有).
68. Behavioral and Molecular Pharmacological Study of the Role of Angiotensin II in Spinal Pain Transmission, Nemoto, W., *Yakugaku Zasshi*, **2018**, *138*, 1235-1240 (査読有).
69. Effect of Repeated Oral Administration of Chondroitin Sulfate on Neuropathic Pain Induced by Partial Sciatic Nerve Ligation in Mice, Nemoto, W.; Yamada, K.; Nakagawasai, O.; Ogata, Y.; Chiba, M.; Yamagata, R.; Sakurai, H.; Tan-No, K. *J. Pharmacol. Sci.*, **2018**, *137*, 403-406 (査読有).
70. Antidepressant-Like Effect of Aripiprazole via 5-HT_{1A}, D₁, and D₂ Receptors in the Prefrontal Cortex of Olfactory Bulbectomized Mice, Takahashi, K.; Nakagawasai, O.; Nemoto, W.; Odaira, T.; Sakuma, W.; Tan-No, K. *J. Pharmacol. Sci.*, **2018**, *137*, 241-247 (査読有).
- *71. Memantine Ameliorates Depressive-Like Behaviors by Regulating Hippocampal Cell Proliferation and Neuroprotection in Olfactory Bulbectomized Mice, Takahashi, K.; Nakagawasai, O.; Nemoto, W.; Kadota, S.; Isono, J.; Odaira, T.; Sakuma, W.; Arai, Y.; Tadano, T.; Tan-No, K. *Neuropharmacology*, **2018**, *137*, 141-155 (査読有).
72. Kappa Opioid Receptor Agonist Administration in Olfactory Bulbectomized Mice Restores Cognitive Impairment through Cholinergic Neuron Activation, Takahashi, K.; Nakagawasai, O.; Sugawara, M.; Sato, A.; Nemoto, W.; Tadano, T.; Tan-No, K. *Biol. Pharm. Bull.*, **2018**, *41*, 957-960 (査読有).
73. Neutrophils Provide a Favorable IL-1-Mediated Immunometabolic Niche that Primes GLUT4 Translocation and Performance in Skeletal Muscles, Tsuchiya, M.; Sekiai, S.; Hatakeyama, H.; Koide, M.; Chaweewannakorn, C.; Yaoita, F.; Tan-No, K.; Sasaki, K.; Watanabe, M.; Sugawara, S.; Endo, Y.; Itoi, E.; Hagiwara, Y.; Kanzaki, M. *Cell Rep.*, **2018**, *23*, 2354-2364 (査読有).
74. Involvement of Peripheral Alpha2A Adrenoceptor in the Acceleration of Gastrointestinal Transit and Abdominal Visceral Pain Induced by Intermittent Deprivation of REM Sleep, Yaoita, F.; Muto, M.; Murakami, H.; Endo, S.; Kozawa, M.; Tsuchiya, M.; Tadano, T.; Tan-No, K. *Physiol. Behav.*, **2018**, *186*, 52-61 (査読有).
- *75. Design and Synthesis of p-Carborane-Containing Sulfamates as Multitarget Anti-Breast Cancer Agents, Kaise, A.; Ohta, K.; Shirata, C.; Endo, Y. *Bioorg. Med. Chem.*, **2017**, *25*, 6417-6426 (査読有).
- *76. Novel p-Carborane-Containing Multitarget Anticancer Agents Inspired by the Metabolism of 17 β -Estradiol, Kaise, A.; Ohta, K.; Endo, Y. *Bioorg. Med. Chem.*, **2017**, *25*, 6371-6378 (査読有).
- *77. Design and Synthesis of Iodocarborane-Containing Ligands with High Affinity and Selectivity toward ER β , Ohta, K.; Ogawa, T.; Endo, Y. *Bioorg. Med. Chem. Lett.*, **2017**, *27*, 4030-4033 (査読有).
78. Structure Activity Relations of Rosmarinic acid Derivatives for the Amyloid β Aggregation Inhibition and Antioxidant Properties, Taguchi, R.; Hatayama, K.; Takahashi, T.; Hayashi, T.; Sato, Y.; Sato, D.; Ohta, K.; Nakano, H.; Seki, C.; Endo, Y.; Tokuraku, K.; Uwai, K. *Eur. J. Med. Chem.*, **2017**, *138*, 1066-1075 (査読有).
79. Time-Dependent Role of Prefrontal Cortex and Hippocampus on Cognitive Improvement by Aripiprazole in Olfactory Bulbectomized Mice, Takahashi, K.; Nakagawasai, O.; Nemoto, W.; Odaira, T.; Arai, Y.; Hisamitsu, T.; Tan-No, K. *Eur. Neuropsychopharmacol.*, **2017**, *27*, 1000-1010 (査読有).

法人番号	041004
プロジェクト番号	S1511001L

80. Inhibitory Effect of Angiotensin (1-7) on Angiotensin III-Induced Nociceptive Behaviour in Mice, Nemoto, W.; Yamagata, R.; Ogata, Y.; Nakagawasai, O.; Tadano, T.; Tan-No, K. *Neuropeptides*, **2017**, *65*, 71-76 (査読有).
- *81. BA321, a Novel Carborane Analog that Binds to Androgen and Estrogen Receptors, Acts as a New Selective Androgen Receptor Modulator of Bone in Male Mice, Watanabe, K.; Hirata, M.; Tominari, T.; Matsumoto, C.; Endo, Y.; Murphy, G.; Nagase, H.; Inada, M.; Miyaura, C. *Biochem. Biophys. Res. Commun.*, **2016**, *478*, 279-285 (査読有).
- *82. Design, Synthesis, and Anti-Proliferative Activity of 1-(4-Methoxyphenyl)-12-Hydroxymethyl-*p*-Carborane Derivatives, Kaise, A.; Ohta, K.; Endo, Y. *Eur. J. Med. Chem.*, **2016**, *122*, 257-263 (査読有).
83. Symmetric 4,4'-(Piperidin-4-ylidenemethylene)bisphenol Derivatives as Novel Tunable Estrogen Receptor (ER) Modulators, Sato, M.; Ohta, K.; Kaise, A.; Aoto, S.; Endo, Y. *Bioorg. Med. Chem.* **2016**, *24*, 1089-1094 (査読有).
- *84. BE360, a New Selective Estrogen Receptor Modulator, Produces Antidepressant and Antidementia Effects through the Enhancement of Hippocampal Cell Proliferation in Olfactory Bulbectomized Mice, Nakagawasai, O.; Nemoto, W.; Onogi, H.; Moriya, T.; Lin, J.-R. Odaira, T.; Yaoita, F.; Ogawa, T.; Ohta, K.; Endo, Y.; Tan-No, K. *Behav. Brain Res.*, **2016**, *297*, 315-322 (査読有).
85. Alterations in Behavioral Responses to Dopamine Agonists in Olfactory Bulbectomized Mice: Relationship to Changes in the Striatal Dopaminergic System, Takahashi, K.; Nakagawasai, O.; Nemoto, W.; Nakajima, T.; Arai, Y.; Hisamitsu, T.; Tan-No, K. *Psychopharmacology*, **2016**, *233*, 1311-1322 (査読有).
86. The Bisphosphonates Clodronate and Etidronate Exert Analgesic Effects by Acting on Glutamate- and/or ATP-Related Pain Transmission Pathways, Shima, K.; Nemoto, W.; Tsuchiya, M.; Tan-No, K.; Takano-Yamamoto, T.; Sugawara, S.; Endo, Y. *Biol. Pharm. Bull.*, **2016**, *39*, 770-777 (査読有).
87. ERK5 Induces Ankrd1 for Catecholamine Biosynthesis and Homeostasis in Adrenal Medullary Cells, Obara, Y.; Nagasawa, R.; Nemoto, W.; Pellegrino, M.J.; Takahashi, M.; Habecker, B.A.; Stork, P.J.S.; Ichihyanagi, O.; Ito, H.; Tomita, Y.; Ishii, K.; Nakahata, N. *Cell. Signal.*, **2016**, *28*, 177-189 (査読有).
88. Alterations in Behavioral Responses to Dopamine Agonists in Olfactory Bulbectomized Mice: Relationship to Changes in the Striatal Dopaminergic System, Takahashi, K.; Nakagawasai, O.; Nemoto, W.; Nakajima, T.; Arai, Y.; Hisamitsu, T.; Tan-No, K. *Psychopharmacology*, **2016**, *233*, 1311-1322 (査読有).
89. Involvement of Spinal Angiotensin II System in Streptozotocin-Induced Diabetic Neuropathic Pain in Mice, Ogata, Y.; Nemoto, W.; Nakagawasai, O.; Yamagata, R.; Tadano, T.; Tan-No, K. *Mol. Pharmacol.*, **2016**, *90*, 205-213 (査読有).
90. Chondroitin Sulfate Attenuates Formalin-Induced Persistent Tactile Allodynia, Nemoto, W.; Yamada, K.; Ogata, Y.; Nakagawasai, O.; Onodera, K.; Sakurai, H.; Tan-No, K. *J. Pharmacol. Sci.*, **2016**, *131*, 275-278 (査読有).
91. Effects of Methylphenidate on the Impairment of Spontaneous Alternation Behavior in Mice Intermittently Deprived of REM Sleep, Nijima-Yaoita, F.; Nagasawa, Y.; Tsuchiya, M.; Arai, Y.; Tadano, T.; Tan-No, K. *Neurochem. Int.*, **2016**, *100*, 128-137 (査読有).
- *92. 睡眠や食習慣の乱れに起因した精神神経障害動物モデルの作製、八百板富紀枝 *YAKUGAKU ZASSHI*, **2016**, *136*, 895-904 (査読有).
93. 断続的なレム断眠負荷による病態動物モデルの作製、八百板富紀枝 *BIO Clinica*, **2016**, *31*, 993-995 (査読無).
- *94. Estrogenic Activity of Bis(4-hydroxyphenyl)methanes with Cyclic Hydrophobic Structure, Kojima, K.; Ogawa, T.; Kitao, S.; Sato, M.; Oda, A.; Ohta, K.; Endo, Y. *Bioorg. Med. Chem.*, **2015**, *23*, 6900-6911 (査読有).
- *95. Activation of RXR/PPAR γ Underlies Neuroprotection by Bexarotene in Ischemic Stroke, Certo, M.; Endo, Y.; Ohta, K.; Sakurada, S.; Bagetta, G.; Amantea, D. *Pharmacol. Res.*, **2015**, *102*, 298-307 (査読有).
- *96. Design and Synthesis of Carborane-Containing Estrogen Receptor-Beta (ER β)-Selective Ligands,

法人番号	041004
プロジェクト番号	S1511001L

- Ohta, K.; Ogawa, T.; Oda, A.; Kaise, A.; Endo, Y. *Bioorg. Med. Chem. Lett.* **2015**, *25*, 4174–4178 (査読有).
- *97. Synthesis and Biological Evaluation of Novel *m*-Carborane-Containing Estrogen Receptor Partial Agonists as SERM Candidates, Ohta, K.; Ogawa, T.; Kaise, A.; Endo, Y. *Bioorg. Med. Chem. Lett.* **2015**, *25*, 3213–3216 (査読有).
98. Structure–Activity Relationship Study of Diphenylamine–Based Estrogen Receptor (ER) Antagonists, Ohta, K.; Chiba, Y.; Kaise, A.; Endo, Y. *Bioorg. Med. Chem.*, **2015**, *23*, 861–867 (査読有).
99. Involvement of p38 MAPK Activation Mediated through AT1 Receptors on Spinal Astrocytes and Neurons in Angiotensin II– and III–Induced Nociceptive Behavior in Mice, Nemoto, W.; Ogata, Y.; Nakagawasai, O.; Yaoita, F.; Tadano, T.; Tan–No, K. *Neuropharmacology*, **2015**, *99*, 221–231 (査読有).
100. Liver Hydrolysate Attenuates the Sickness Behavior Induced by Concanavalin A in Mice, Nakagawasai, O.; Yamada, K.; Nemoto, W.; Sato, S.; Ogata, Y.; Miya, K.; Sakurai, H.; Tan–No, K. *J. Pharmacol. Sci.*, **2015**, *127*, 489–492 (査読有).
101. The Intrathecal Administration of Losartan, an AT1 Receptor Antagonist, Produces an Antinociceptive Effect through the Inhibition of p38 MAPK Phosphorylation in the Mouse Formalin Test, Nemoto, W.; Ogata, Y.; Nakagawasai, O.; Yaoita, F.; Tadano, T.; Tan–No, K. *Neurosci. Lett.*, **2015**, *585*, 17–22 (査読有).
- 「研究テーマ3. 難治性疼痛に対する緩和医療法の確立」
102. Anxiolytic-like Effects of Bergamot Essential Oil are Insensitive to Flumazenil in Rats, Rombolà, L.; Scuteri, D.; Adornetto, A.; Straface, M.; Sakurada, T.; Sakurada, S.; Mizoguchi, H.; Corasaniti, M.T.; Bagetta, G.; Tonin, P.; Morrone, L.A. *Evid. Based Complement. Alternat. Med.*, **2019**, *Volume 2019*, Article ID 2156873 1–6 (査読有).
103. Neuropharmacology of the Neuropsychiatric Symptoms of Dementia and Role of Pain: Essential Oil of Bergamot as a Novel Therapeutic Approach, Scuteri, D.; Rombolà, L.; Morrone, L.A.; Bagetta, G.; Sakurada, S.; Sakurada, T.; Tonin, P.; Corasaniti, M.T. *Int. J. Mol. Sci.*, **2019**, *20*, E3327 1–13 (査読有).
104. Neuropharmacological Properties of the Essential Oil of Bergamot for the Clinical Management of Pain-related BPSDs, Scuteri, D.; Rombolà, L.; Tridico, L.; Mizoguchi, H.; Watanabe, C.; Sakurada, T.; Sakurada, S.; Corasaniti, M.T.; Bagetta, G.; Morrone, L.A. *Curr. Med. Chem.*, **2019**, *26*, 3764–3774 (査読有).
- *105. 脳と喘息病態～精神的ストレスの受容と気管支喘息の増悪を繋ぐ脳から肺への情報伝達～、宮坂智充、川上佳織、奥山-土橋 佳織、河野資、高橋知子、大野勲、『呼吸』e レポート, 2019, *3*, 1–9 (査読無)
- *106. μ オピオイド受容体の多様性, 溝口広一 東北医科薬科大学研究誌, **2018**, *65*, 1–6 (査読有).
107. Possible Involvement of the Peripheral μ -Opioid System in Antinociception Induced by Bergamot Essential Oil to Allodynia after Peripheral Nerve Injury, Komatsu, T.; Katsuyama, S.; Uezono, Y.; Sakurada, C.; Tsuzuki, M.; Hamamura, K.; Bagetta, G.; Sakurada, S.; Sakurada, T. *Neurosci. Lett.*, **2018**, *686*, 127–132 (査読有).
108. Antinociceptive Effect of Inhalation of the Essential Oil of Bergamot in Mice, Scuteri, D.; Crudo, M.; Rombolà, L.; Watanabe, C.; Mizoguchi, H.; Sakurada, S.; Sakurada, T.; Greco, R.; Corasaniti, M.T.; Morrone, L.A.; Bagetta, G. *Fitoterapia*, **2018**, *129*, 20–24 (査読有).
109. ETosis–Derived DNA Trap Production in Middle Ear Effusion is a Common Feature of Eosinophilic Otitis Media, Ohta, N.; Ueki, S.; Konno, Y.; Hirokawa, M.; Kubota, T.; Tomioka–Matsutani, S.; Suzuki, T.; Ishida, Y.; Kawano, T.; Miyasaka, T.; Takahashi, T.; Suzuki, T.; Ohno, I.; Kakehata, S.; Fujieda, S. *Allergol. Int.*, **2018**, *67*, 414–416 (査読有).
- *110. 女性における喘息重症化メカニズムの解明に向けた基礎研究：樹状細胞の性差、宮坂智充、増田千愛、川上佳織、高橋知子、大野勲、アレルギーの臨床, 2018, *38*, 51(351)–55(355) (査読有).
- *111. 成人女性における喘息重症化病態を基礎研究から考える：性特異的 Th2 型免疫応答を担う CD103+樹状細胞の役割、宮坂智充、増田千愛、川上佳織、高橋知子、大野勲、アレルギーの臨床, 2018, *38*, 55(563)–59(567) (査読有).
- *112. Increased Susceptibility to Allergic Asthma with the Impairment of Respiratory Tolerance Caused by

法人番号	041004
プロジェクト番号	S1511001L

- Psychological Stress, Kawano, T.; Ouchi, R.; Ishigaki, T.; Masuda, C.; Miyasaka, T.; Ohkawara, Y.; Ohta, N.; Takayanagi, M.; Takahashi, T.; Ohno, I. *Int. Arch. Allergy Immunol.*, **2018**, *177*, 1–15 (査読有).
113. The expression of 11 beta hydroxysteroid dehydrogenase in severe allergic rhinitis, Ohta, N.; Noguchi, N.; Takahashi, T.; Suzuki, T.; Kakuta, R.; Suzuki, Y.; Awataguchi, T.; Suzuki, T.; Takahashi, Y.; Shoji, F.; Wada, K.; Kawano, T.; Ohno, I.; Kusano, Y.; Miyasaka, T.; Osafune, H.; Matsutani, S.; Yaginuma, Y.; Ishida, Y.; Saito, Y.; Yamazaki, M.; Ikeda, R. *Otolaryngol. Pol.* **2018**, *73*, 18–22 (査読有).
- *114. Maternal Separation as Early-Life Stress Causes Enhanced Allergic Airway Responses by Inhibiting Respiratory Tolerance in Mice, Ouchi, R.; Kawano, T.; Yoshida, H.; Ishii, M.; Miyasaka, T.; Ohkawara, Y.; Takayanagi, M.; Takahashi, T.; Ohno, I. *Tohoku. J. Exp. Med.* **2018**, *246*, 155–165 (査読有).
- *115. Sex-Based Differences in CD103+ Dendritic Cells Promote Female-Predominant Th2 Cytokine Production During Allergic Asthma, Masuda, C.; Miyasaka, T.; Kawakami, K.; Inokuchi, J.; Kawano, T.; Dobashi-Okuyama K.; Takahashi, T.; Takayanagi, M.; Ohno, I. *Clin. Exp. Allergy*, **2018**, *48*, 379–393 (査読有).
116. Combined Treatment with D-Allose, Docetaxel and Radiation Inhibits the Tumor Growth in an In Vivo Model of Head and Neck Cancer, Hoshikawa, H.; Kamitori, K.; Indo, K.; Mori, T.; Kamata, M.; Takahashi, T.; Tokuda, M. *Oncol. Lett.*, **2018**, *15*, 3422–3428 (査読有).
- *117. The Interplay between Neuroendocrine Activity and Psychological Stress-Induced Exacerbation of Allergic Asthma, Miyasaka, T.; Dobashi-Okuyama, K.; Takahashi, T.; Takayanagi, M.; Ohno, I. *Allergol. Int.*, **2018**, *67*, 32–42 (査読有).
118. Aromatherapy and Aromatic Plants for the Treatment of Behavioural and Psychological Symptoms of Dementia in Patients with Alzheimer's Disease: Clinical Evidence and Possible Mechanisms, Scuteri, D.; Morrone, L.A.; Rombolà, L.; Avato, P.R.; Bilia, A.R.; Corasaniti, M.T.; Sakurada, S.; Sakurada, T.; Bagetta, G. *Evid. Based Complement. Alternat. Med.*, **2017**, *Volume 2017*, Article ID 9416305 1–8 (査読有).
119. Antinociceptive Effect of Tebanicline for Various Noxious Stimuli-Induced Behaviours in Mice, Hayashi, T.; Katsuyama, S.; Orito, T.; Suzuki, T.; Sakurada, S. *Neurosci. Lett.*, **2017**, *638*, 46–50 (査読有).
120. The Involvement of Spinal Release of Histamine on Nociceptive Behaviors Induced by Intrathecally Administered Spermine, Mizoguchi, H.; Watanabe, C.; Hayashi, T.; Iwata, Y.; Watanabe, H.; Katsuyama, S.; Hamamura, K.; Sakurada, T.; Ohtsu, H.; Yanai, K.; Sakurada, S. *Eur. J. Pharmacol.*, **2017**, *800*, 9–15 (査読有).
121. Bergamot Essential Oil Attenuates Anxiety-Like Behaviour in Rats, Rombolà, L.; Tridico, L.; Scuteri, D.; Sakurada, T.; Sakurada, S.; Mizoguchi, H.; Avato, P.; Corasaniti, M.T.; Bagetta, G.; Morrone, L. A. *Molecules*, **2017**, *22*, E614: 1–11 (査読有).
122. Opioids Resistance in Chronic Pain Management, Morrone, L.A.; Scuteri, D.; Rombolà, L.; Mizoguchi, H.; Bagetta, G. *Curr. Neuropharmacol.*, **2017**, *15*, 444–456 (査読有).
- *123. Neuropsychiatry Phenotype in Asthma: Psychological Stress-Induced Alterations of the Neuroendocrine-Immune System in Allergic Airway Inflammation, Ohno, I. *Allergol. Int.*, **2017**, *66*, S2–S8 (査読有).
- *124. The Interrelationship between Asthma and Brain Activities: Psychological Stress-Related Asthma as a New Asthma Phenotype, Ohno, I. *Arerugi*, **2017**, *66*, 153–160 (査読有).
125. Intrathecal Morphine-3-Glucuronide-Induced Nociceptive Behavior via δ_2 Opioid Receptors in the Spinal Cord, Komatsu, T.; Katsuyama, S.; Nagase, H.; Mizoguchi, H.; Sakurada, C.; Tsuzuki, M.; Sakurada, S.; Sakurada, T. *Pharmacol. Biochem. Behav.*, **2016**, *140*, 68–74 (査読有).
126. Involvement of Spinal Glutamate in Nociceptive Behavior Induced by Intrathecal Administration of Hemokinin-1 in Mice, Watanabe, C.; Mizoguchi, H.; Bagetta, G.; Sakurada, S. *Neurosci. Lett.*, **2016**, *617*, 236–239 (査読有).
127. ラベンダーオイルの末梢局所皮下投与によるパクリタキセル誘発性末梢神経障害性疼痛抑制効果の検討、勝山 壮、音羽 亮、武井佐和子、櫻田 忍、倉本敬二、*日本末病システム学会雑誌*, **2016**, *22*, 47–53 (査読有).
128. Analgesic Effects of 1st Generation Anti-histamines in Mice, Takahashi, M.; Shima, K.; Tsuchiya, M.;

法人番号	041004
プロジェクト番号	S1511001L

- Hagiwara, Y.; Mizoguchi, H.; Sakurada, S.; Sugawara, S.; Fujita, T.; Tadano, T.; Watanabe, M.; Fukumoto, S.; Endo, Y. *Biol. Pharm. Bull.*, **2016**, *39*, 620–624 (査読有).
129. Rational Basis for the Use of Bergamot Essential Oil in Complementary Medicine to Treat Chronic Pain, Rombolà, L.; Amantea, D.; Russo, R.; Adornetto, A.; Berliocchi, L.; Tridico, L.; Corasaniti, M.T.; Sakurada, S.; Sakurada, T.; Bagetta, G.; Morrone, L.A. *Mini Rev. Med. Chem.*, **2016**, *16*, 721–728 (査読有).
- *130. The Involvement of Central Nervous System Histamine Receptors in Psychological Stress-Induced Exacerbation of Allergic Airway Inflammation in Mice, Miyasaka, T.; Okuyama-Dobashi, K.; Masuda, C.; Iwami, S.; Sato, M.; Mizoguchi, H.; Kawano, T.; Ohkawara, Y.; Sakurada, S.; Takayanagi, M.; Ohno, I. *Allergol. Int.*, **2016**, *65*, S38–S44 (査読有).
131. Human CD4⁺ CD8⁺ Invariant Natural Killer T Cells Promote IgG Secretion from B Cells Stimulated by Cross-Linking of Their Antigen Receptors, Miyasaka, T.; Watanabe, Y.; Akahori, Y.; Miyamura, N.; Ishii, K.; Kinjo, Y.; Miyazaki, Y.; Liu, T.-Y.; Uemura, Y. and Kawakami, K. *World Journal of Vaccines*, **2016**, *6*, 34–41 (査読有).
- *132. CD8⁺ T Cells Mediate Female-Dominant IL-4 Production and Airway Inflammation in Allergic Asthma, Ito, C.; Okuyama-Dobashi, K.; Miyasaka, T.; Masuda, C.; Sato, M.; Kawano, T.; Ohkawara, Y.; Kikuchi, T.; Takayanagi, M.; Ohno, I. *PLoS One*, **2015**, *10*, e0140808 (査読有).
- *133. ストレスによる喘息増悪の病態、宮坂智充、大野 勲、*喘息*, **2015**, *28*, 133–139 (査読有).
- *134. ストレス喘息；asthma nervosa から新たな喘息フェノタイプへ、大野 勲、宮坂智充、山内広平、中村 豊、*アレルギーの臨床*, **2015**, *35*, 62–65 (査読有).

<図書>

1. 中分子創薬に資するペプチド・核酸・糖鎖の合成技術、「新規グリコシル化反応の開発-Pummerer型チオグリコシル化反応の開発と展開」、若松秀章、名取良浩、斎藤有香子、吉村祐一、シーエムシー出版、2018、2、(p.181–188). (ISBN: 978-4-7813-1320-7)
- *2. Boron-Based Compounds: Potential and Emerging Applications in Medicine, ed.by Vinas, C.; Hey-Hawkins, E. Chapter 1. Carboranes as Hydrophobic Pharmacophores: Applications for Design of Nuclear Receptor Ligands. p.3–19, Endo, Y., Wiley, July 2018. ISBN: 978-1-119-27555-8
3. 基礎有機化学問題集 第2版、渡邊一弘、加藤正、他(共著)、廣川書店、2017
4. トワイクロス先生の緩和ケア処方薬 第2版、溝口広一(武田文和、鈴木 勉 監訳)、医学書院、2017、36 (p.581–593, p.595–617).
5. 疾患薬理学、溝口広一(成田 年 監修)、Neo Medical、2016、13 (p. 19–31).
6. Aromatherapy: Basic Mechanisms and Evidence Based Clinical Use, Watanabe, C.; Mizoguchi, H.; Sakurada, S. (Edited by Bagetta, G.; Cosentino, M.; Sakurada, T.), CRC Press, **2015**, 18 (p.251–268).

<学会発表>

「研究テーマ1. 新規がん分子標的治療薬の創製」

- *1. 抗がん活性を有する 9-デオキシキセニアラクトール C の合成研究、佐藤廣河、成田紘一、吉村祐一、渡邊一弘、日本薬学会第 140 年会、京都、2020 年 3 月。
2. 抗炎症作用を有するクリスタキセニシン A の全合成研究、分銅和香、中居啓陽、Sayar Noel、佐藤廣河、成田紘一、吉村祐一、渡邊一弘、日本薬学会第 140 年会、京都、2020 年 3 月。
3. 抗炎症作用を有するメロテルペン誘導体クリソゲンエステルの合成研究、佐々木里菜、渡邊一弘、佐藤廣河、成田紘一、吉村祐一、日本薬学会第 140 年会、京都、2020 年 3 月。
4. スクアレン合成酵素阻害剤ピサボスクアール A の合成研究、吉田昌太郎、成田紘一、佐藤廣河、渡邊一弘、吉村祐一、日本薬学会第 140 年会、京都、2020 年 3 月。
5. アルキルヒドロキノン天然物ビオラセイド A および C の簡便合成、成田紘一、木村龍平、佐藤廣河、渡邊一弘、吉村祐一、日本薬学会第 140 年会、京都、2020 年 3 月。
- *6. エニナミドを基質とする閉環メタセシスの新たなアプローチと複素環化合物合成への応用、若松秀章、小野賛、高橋将典、吉村祐一、日本薬学会第 140 年会、京都、2020 年 3 月。
- *7. 4'-置換ヌクレオシド誘導体の光学分割、遠藤柚季乃、若松秀章、伊藤恭平、斎藤有香子、名取良

法人番号	041004
プロジェクト番号	S1511001L

- 造、吉村祐一、日本薬学会第 140 年会、京都、2020 年 3 月。
- *8. 超原子価ヨウ素とジフェニルジセレニドを用いた分子間反応による含窒素複素環化合物の合成法の開発、鈴木郁、名取良造、萬浩太、若松秀章、斎藤有香子、吉村祐一、日本薬学会第 140 年会、京都、2020 年 3 月。
9. 4'-置換 4'-チオリボシルチミン誘導体の合成、前田璃音、若松秀章、庄子希望、名取良造、吉村祐一、日本薬学会第 140 年会、京都、2020 年 3 月。
10. GM3 セラミド部の類似体である長鎖脂肪酸の合成研究、名取良造、若松秀章、伊藤瑛将、褰地陽太、金野美里、斎藤有香子、井ノ口仁一、吉村祐一、日本薬学会第 140 年会、京都、2020 年 3 月。
11. スクアレン合成酵素阻害剤 ビザボスクアール A の合成研究、吉田昌太郎、成田紘一、渡邊一弘、吉村祐一、日本薬学会第 139 年会、千葉、2019 年 3 月。
- *12. 抗がん活性を有する 9-デオキシキセニアラクトール C の合成研究、佐々木里菜、佐藤廣河、成田紘一、渡邊一弘、吉村祐一、創業懇話会 2019 in 秋保、仙台、2019 年 6 月。
13. スクアレン合成酵素阻害剤 ビザボスクアール A の合成研究、吉田昌太郎、成田紘一、佐藤廣河、渡邊一弘、吉村祐一、第 58 回日本薬学会東北支部大会、仙台、2019 年 10 月。
14. アルキルヒドロキノン天然物 ビオラセイド A の簡便合成、成田紘一、木村龍平、佐藤廣河、渡邊一弘、吉村祐一、第 58 回日本薬学会東北支部大会、仙台、2019 年 10 月。
15. フェンタニルが混入したヘロインに対するワクチンの開発研究、名取良造、Candy S. Hwang、Lauren C. Smith、Beverly Ellis、Bin Zhou、Kim D. Janda、第 58 回日本薬学会東北支部大会、仙台、2019 年 10 月。
- *16. 4'-置換ヌクレオシド誘導体の光学分割、遠藤柚季乃、若松秀章、伊藤恭平、斎藤有香子、名取良造、吉村祐一、第 58 回日本薬学会東北支部大会、仙台、2019 年 10 月。
- *17. 超原子価ヨウ素とジフェニルジセレニドを用いた含窒素複素環化合物の合成法の開発、鈴木郁、名取良造、萬浩太、若松秀章、斎藤有香子、吉村祐一、創業懇話会 2019 in 秋保、仙台、2019 年 6 月。
- *18. 縮環/アルドールタンデム反応を利用した 4'-置換 4'-チオヌクレオシドの合成、前田璃音、若松秀章、庄子希望、名取良造、吉村祐一、日本薬学会第 139 年会、千葉、2019 年 3 月。
- *19. エニナミドの閉環メタセシスによる様々な複素環化合物の合成、若松秀章、佐々木好美、川幡正俊、山口健太郎、吉村祐一、日本薬学会第 139 年会、千葉、2019 年 3 月。
- *20. 超原子価ヨウ素とジフェニルジセレニドを用いた分子内環化反応による含窒素複素環化合物の合成法の開発、名取良造、鈴木郁、萬浩太、須玉夏海、若松秀章、斎藤有香子、吉村祐一、日本薬学会第 139 年会、千葉、2019 年 3 月。
21. CYP26A1 レポーター遺伝子を用いたレチノイン酸の低濃度測定法の開発、永田 清、第 1 回 内外環境応答研究会、富山、2019 年 10 月。
22. 非リン酸化 ER α (S216A) 導入マウスを用いたエストロゲン受容体の新規機能の解析、進藤佐和子、第 1 回 内外環境応答研究会、富山、2019 年 10 月。
- *23. 健康食品による薬物相互作用解析、熊谷 健、令和元年 内外環境応答・代謝酵素研究会、仙台、2019 年 9 月。
- *24. 肝成熟に伴う CYP3A7 の発現低下に HNF3 β が関与する？ 白井晃太郎 令和元年 内外環境応答・代謝酵素研究会、仙台、2019 年 9 月。
25. UDP-グルクロン酸転移酵素 (UGT) によるシトクロム P450 3A4 活性の抑制: UGT 分子種依存的な抑制機序とラット肝臓を用いた in vivo 解析、宮内 優、永田 清、山添 康、Peter MACKENZIE、田中 嘉孝、石井祐次、第 46 回日本毒性学会学術年会、徳島、2019 年 6 月。
- *26. プロポリス含有健康食品による CYP 誘導評価と薬物相互作用、熊谷 健、星 利香、長田大輝、渡邊夢実、進藤佐和子、永田 清、第 46 回日本毒性学会学術年会、徳島、2019 年 6 月。
27. ベンゾオキサゾール骨格を有するセスキテルペン ナキジノール A 及び B の合成、武田由貴、加藤 武、熱海 秀、成田紘一、加藤 正、日本薬学会第 138 年会、金沢、2018 年 3 月。
28. 海洋天然物 Cristaxenicin A および Plumisclerin A の合成研究、Noel Sayar、中井啓陽、吉村祐一、渡邊一弘、日本薬学会第 138 年会、金沢、2018 年 3 月。
29. 海洋由来ジテルペン系天然物 Cristaxenicin A の合成研究、中井啓陽、Noel Sayar、吉村祐一、渡邊一弘、日本薬学会第 138 年会、金沢、2018 年 3 月。

法人番号	041004
プロジェクト番号	S1511001L

- *30. 海洋性ジテルペノイド 9-デオキシキセニアラクトール C の合成研究、渡邊一弘、高橋央宜、吉村祐二、日本薬学会第 138 年会、金沢、2018 年 3 月。
31. フェンタニルで汚染されたヘロインに対するワクチンの開発研究、名取良浩、Candy S. Hwang、Lauren C. Smith、Beverly Ellis、Bin Zhou、Kim D. Janda、第 36 回メディシナルケミストリーシンポジウム、京都、2018 年 11 月。
- *32. ジヒドロチオピラン環ヌクレオシド誘導体の合成研究、斎藤有香子、山崎佳子、高橋江里佳、名取良浩、若松秀章、吉村祐一、第 57 回日本薬学会東北支部大会、仙台、2018 年 10 月。
- *33. 超原子価ヨウ素とジフェニルジセレニドを用いたピペリジン環構築法の開発、名取良浩、萬浩太、鈴木郁、若松秀章、斎藤有香子、吉村祐一、第 57 回日本薬学会東北支部大会、仙台、2018 年 10 月。
- *34. パラジウム触媒を用いたイナミドの位置選択的炭素炭素結合形成反応、若松秀章、池内麻衣、吉村祐一、日本薬学会第 138 年会、金沢、2018 年 3 月。
- *35. 抗がん活性を有する 9-デオキシキセニアラクトール C の合成研究: キセニアラクトール骨格の構築、渡邊一弘、高橋央宜、吉村祐一、加藤 正、第 47 回複素環化学討論会、高知、2017 年 10 月。
36. ベンゾオキサゾール環を有するセスキテルペン ナキジノール B の合成研究、武田由貴、加藤武、熱海 秀、成田紘一、渡邊一弘、吉村祐一、加藤 正、第 56 回日本薬学会東北支部大会、青森、2017 年 10 月。
37. 海洋由来ジテルペノイド系天然物 Cristaxenicin A の合成研究、中井啓陽、Noel Sayar、吉村祐一、渡邊一弘、第 56 回日本薬学会東北支部大会、青森、2017 年 10 月。
38. 多標的キナーゼ阻害薬としてのテルペノイド類化合物の同定とその特徴、近松園子、西條 憲、今井 源、成田紘一、加藤 正、石岡千加史、第 76 回日本癌学会学術総会、横浜、2017 年 9 月。
39. 多標的キナーゼ阻害薬としてのテルペノイド類化合物の同定、近松園子、西條 憲、成田紘一、加藤 正、石岡千加史、第 21 回日本がん分子標的治療学会学術集会、福岡、2017 年 6 月。
40. 5-ヒドロキシナフトオキサゾール天然物 サルビアミン E および F の全合成、成田紘一、藤崎成美、佐久間裕太、加藤 正、日本薬学会第 137 年会、仙台、2017 年 3 月。
41. カンナビノイド受容体アゴニスト活性を有するフェルギネン B の全合成、加藤友哉、成田紘一、加藤 正、日本薬学会第 137 年会、仙台、2017 年 3 月。
42. セスキテルペンベンゾオキサゾール骨格を有するナキジノール A の合成研究、武田由貴、加藤武、熱海 秀、成田紘一、加藤 正、日本薬学会第 137 年会、仙台、2017 年 3 月。
- *43. イナミドを基質としたパラジウム触媒による炭素炭素結合形成反応、若松秀章、石井彩香、菊池洋平、高橋彩乃、柳澤里佳、木村 翔、大澤直央、名取良浩、吉村祐一、第 64 回有機金属化学討論会、仙台、2017 年 9 月。
- *44. 2'-5'結合を有する環状ジヌクレオチドの合成研究、若生有未、名取良浩、若松秀章、吉村祐一、日本薬学会第 137 年会、仙台、2017 年 3 月。
- *45. レチノイン酸類似化合物同時測定系の構築、鈴木裕之、森 謙太、進藤佐和子、熊谷 健、永田 清、中村 仁、第 57 回日本薬学会東北支部大会、仙台、2017 年 10 月。
- *46. アゾール構造を含む農薬によるヒト CYP 代謝活性阻害、手賀 要、鈴木裕之、進藤佐和子、熊谷 健、永田 清、第 57 回日本薬学会東北支部大会、仙台、2017 年 10 月。
47. PAHs によるシトクロム P450 遺伝子発現変動のメカニズムの解析、及川和憲、渡辺孝樹、進藤佐和子、熊谷 健、永田 清、第 57 回日本薬学会東北支部大会、仙台、2017 年 10 月。
48. UGT1A 分子種発現の各種細胞間比較と誘導剤による影響、緒方龍也、森本麻友、進藤佐和子、熊谷 健、永田 清、第 57 回日本薬学会東北支部大会、仙台、2017 年 10 月。
- *49. CYP 遺伝子発現作用に及ぼす健康食品の影響、渡邊夢実、熊谷 健、佐々木崇光、永田 清、フォーラム 2017 衛生薬学・環境トキシコロジー、仙台、2017 年 9 月。
- *50. CYP3A4 遺伝子の新規転写活性化について、渡辺孝樹、小田桐玲生、荒津祐輔、佐々木崇光、進藤佐和子、熊谷 健、永田 清、フォーラム 2017 衛生薬学・環境トキシコロジー、仙台、2017 年 9 月。
- *51. レチノイン酸の低濃度測定可能な CYP26A1 遺伝子レポーターアッセイ系の構築、森 謙太、鈴木裕之、塩谷安奈里、佐々木崇光、進藤佐和子、熊谷 健、永田 清、フォーラム 2017 衛生薬学・環境トキシコロジー、仙台、2017 年 9 月。
52. 薬と健康食品との相互作用、永田 清、フォーラム 2017 衛生薬学・環境トキシコロジー、仙台、2017 年 9 月。
53. PXR が関わるおかしな P450 誘導、永田 清、平成 29 年度内外環境応答・代謝酵素研究会、福岡、

法人番号	041004
プロジェクト番号	S1511001L

2017 年 9 月.

- *54. 同一 PXR 結合配列を介した異なる CYP3A4 誘導機序について、荒津祐輔、小田桐玲生、渡辺孝樹、佐々木崇光、熊谷 健、永田 清、第 56 回日本薬学会東北支部大会、青森、2017 年 10 月.
- 55. HDAC/PI3K 二重阻害剤デブシペプチド類化合物のヒト軟部肉腫細胞に対する抗腫瘍効果の評価、西條 憲、成田紘一、加藤 正、石岡千加史、第 75 回日本癌学会学術総会、横浜、2016 年 10 月.
- 56. 海洋天然物シクロスポンジアキノン-1 及び類縁物質の全合成、武田由貴、成田紘一、加藤 正、第 55 回日本薬学会東北支部大会、郡山、2016 年 9 月.
- 57. ナフトオキサゾール骨格を有するサルビアミン F の全合成、成田紘一、藤崎成美、佐久間裕太、加藤 正、第 55 回日本薬学会東北支部大会、郡山、2016 年 9 月.
- 58. ヒト軟部肉腫細胞に対する HDAC/PI3K 二重阻害剤としてのデブシペプチド類化合物の抗腫瘍効果の検討、西條 憲、成田紘一、加藤 正、石岡千加史、第 20 回日本がん分子標的治療学会、別府、2016 年 5 月.
- 59. Total Synthesis of Bicyclic Depsipeptide Natural Products and Evaluation of Their Biological Activity, Koichi Narita, Tadashi Katoh, French-Japanese Symposium on Medicinal and Fine Chemistry (FJS 2016), Tokyo, Japan, May, 2016.
- 60. ヒストン脱アセチル化酵素(HDAC)阻害剤 FK228 類縁体合成、成田紘一、松原圭介、加藤 正、日本薬学会第 136 年会、横浜、2016 年 3 月.
- 61. 大環状デブシペプチド類天然物 FR-901375 の全合成、加藤友哉、成田紘一、加藤 正、日本薬学会第 136 年会、横浜、2016 年 3 月.
- 62. 生合成仮説を基軸とした(+)-リファガールの全合成、渡辺拓実、神島堯明、菊地拓也、成田紘一、加藤 正、日本薬学会第 136 年会、横浜、2016 年 3 月.
- 63. 抗腫瘍活性を有するシクロスポンジアキノン-1 の全合成、武田由貴、成田紘一、加藤 正、日本薬学会第 136 年会、横浜、2016 年 3 月.
- *64. 4'-フルオロメチルスタブジンの合成研究、伊藤恭平、名取良浩、菅野裕也、齋藤華子、若松秀章、齋藤有香子、吉村祐一、第 34 回メディシナルケミストリーシンポジウム、つくば、2016 年 11 月-12 月.
- *65. ペプチド構造を有する有機分子触媒を用いた不斉反応の開発、阿部美保、若松秀章、名取良浩、吉村祐一、第 42 回反応と合成の進歩シンポジウム、静岡、2016 年 11 月.
- *66. エニナミドを基質とする閉環メタセシスの新たなアプローチ、若松秀章、高橋将典、諏訪純一、小椋玲奈、吉村祐一、第 46 回複素環化学討論会、金沢、2016 年 9 月.
- *67. イミノ糖を含む複素環化合物の合成とその生物活性評価、名取良浩、第 15 回化学系若手研究者セミナー、仙台、2016 年 10 月.
- 68. 2-デオキシ-2-フルオロフコースの合成研究、名取良浩、草野宏光、顧 建国、吉村祐一、第 55 回日本薬学会東北支部大会、郡山、2016 年 9 月.
- 69. イリジウム触媒を用いた含窒素複素環の構築法の開発、名取良浩、菊地俊輔、長岡杏花、曾雌歩実、吉村祐一、第 55 回日本薬学会東北支部大会、郡山、2016 年 9 月.
- 70. 極長鎖 GM3 分子種による慢性炎症惹起メカニズム、狩野裕考、郷 慎司、新田昇大、ヴェイロン ルーカス、カタニオ アンナ、レティツァ マリレナ、名取良浩、吉村祐一、安藤弘宗、石田秀治、樺山一哉、下山敦史、深瀬浩一、チャンパ マリア、マウリ ラウラ、プリネッティ アレッサンドロ、ソニーノ サンドロ、鈴木明身、井ノ口仁一、第 89 回 日本生化学会、仙台、2016 年 9 月.
- 71. 内因性リガンドとしての極長鎖 GM3 ガングリオシドによる慢性炎症惹起機構、狩野裕考、郷 慎司、新田昇大、ヴェイロン ルーカス、カタニオ アンナ、レティツァ マリレナ、名取良浩、吉村祐一、安藤弘宗、石田秀治、樺山一哉、下山敦史、深瀬浩一、チャンパ マリア、マウリ ラウラ、プリネッティ アレッサンドロ、ソニーノ サンドロ、鈴木明身、井ノ口仁一、第 58 回日本脂質生化学会、秋田、2016 年 6 月.
- *72. 超原子価ヨウ素とジフェニルジセレニドを用いた分子内エーテル環化反応、須玉夏海、齋藤有香子、名取良浩、吉村祐一、日本薬学会第 136 年会、横浜、2016 年 3 月.
- *73. 二元機能型トリペプチド有機分子触媒を用いた不斉ディールスアルダー反応、阿部美保、若松秀章、吉村祐一、日本薬学会第 136 年会、横浜、2016 年 3 月.
- *74. イナミドを基質とした Mizoroki-Heck 型反応、若松秀章、柳澤里佳、木村 翔、大澤直央、名取良浩、吉村祐一、日本薬学会第 136 年会、横浜、2016 年 3 月.

法人番号	041004
プロジェクト番号	S1511001L

75. ピロリジン型イミノ糖を基盤とした新規 GCase 高親和性リガンドのデザインとファーマコロジカルシャペロン効果について、加藤 敦、山本亜里紗、友原啓介、足立伊佐雄、渡邊靖香、名取良浩、吉村祐一、中込 泉、広野修一、日本薬学会第 136 年会、横浜、2016 年 3 月。
- *76. 2'-5'連結型環状ジヌクレオチドの合成研究、若生有未、名取良浩、若松秀章、吉村祐一、日本薬学会第 136 年会、横浜、2016 年 3 月。
- *77. ヒト肝 P450 発現模倣細胞 (Ad-P450 細胞) を利用した薬物代謝評価、佐々木 崇光、佐藤 裕、熊谷 健、吉成 浩一、永田 清、第 23 回 HAB 研究機構 学術年会、つくば、2016 年 5 月。
78. ACTIVATION OF P38 MAPK BY CLOTRIMAZOLE ENHANCES THE TRANSCRIPTION OF HUMAN MRP3 THROUGH A NOVEL TRANSCRIPTIONAL ELEMENT, Takamitsu Sasaki, Keita Inami, Takeshi Kumagai, Kouichi Yoshinari, Kiyoshi Nagata, 11TH International ISSX meeting, Busan, Korea, 2016, June.
- *79. 健康食品による薬物代謝 P450 活性阻害の網羅的評価、永田 清、佐藤 裕、熊谷 健、佐々木崇光、フォーラム 2016 衛生薬学・環境トキシコロジー、東京、2016 年 9 月。
- *80. 多環芳香族炭化水素による CYP2D6 発現誘導機構の解析、稲見敬太、佐々木崇光、熊谷 健、吉成浩一、永田 清、H28 度内外環境応答・代謝酵素研究会、静岡、2016 年 9 月。
- *81. CYP26A1 レポーター遺伝子発現ウイルスを用いた低濃度下におけるレチノイン酸合成・代謝酵素活性阻害評価系の検討、塩谷安奈里、渡邊美智子、渡辺郁実、角田駿哉、若生俊也、佐々木崇光、熊谷 健、永田 清、H28 度内外環境応答・代謝酵素研究会、静岡、2016 年 9 月。
- *82. CYP3A4 遺伝子の基本的転写活性化に関わる新規シスエレメントの探索、小田桐玲生、佐々木崇光、熊谷 健、永田 清、H28 度内外環境応答・代謝酵素研究会、静岡、2016 年 9 月。
- *83. CYP26A1 レポーター遺伝子発現ウイルスを用いたレチノイン酸の誘導評価、塩谷安奈里、渡邊美智子、渡辺郁実、角田駿哉、若生俊也、佐々木崇光、熊谷 健、永田 清、第 55 回日本薬学会東北支部大会、福島、2016 年 9 月。
- *84. CYP3A4 遺伝子転写活性化に関わる新規シスエレメントの探索、小田桐玲生、佐々木崇光、熊谷 健、永田 清、第 55 回日本薬学会東北支部大会、福島、2016 年 9 月。
85. デプシペプチド類天然物の全合成および生物活性評価、成田紘一、加藤友哉、加藤 正、第 33 回メディシナルケミストリーシンポジウム、千葉、2015 年、11 月。
86. 選択的 PI3K α 阻害活性物質(+)-リファガールの全合成、菊地拓也、神島堯明、成田紘一、加藤 正、第 41 回反応と合成の進歩シンポジウム、大阪、2015 年 10 月。
87. 有機化学教育(講義、実習、研究)の活性化に向けての大学の取組み—東北薬科大学を例にして—、加藤 正、第 10 回有機化学系教科担当教員会議(薬学教育協議会主催)、大阪、2015 年 10 月。
88. デプシペプチド類縁体の PI3K 阻害剤としての特性に関する検討、西條 憲、成田紘一、下平秀樹、加藤 正、石岡千加史、第 74 回日本癌学会学術総会、名古屋、2015 年 10 月。
89. 生合成仮説を基軸とした(+)-リファガールの全合成研究、渡辺拓実、神島堯明、菊地拓也、成田紘一、加藤 正、第 54 回日本薬学会東北支部大会、矢巾町、2015 年 9 月。
90. 大環状デプシペプチド類天然物 FR-901375 の全合成、加藤友哉、成田紘一、加藤 正、第 54 回日本薬学会東北支部大会、矢巾町、2015 年 9 月。
91. 抗がん活性天然物マンデラリド A の全合成に向けて: Ag(I) 触媒による cis-2,5-DHF および 3,6-DHP の合成、渡邊一弘、日本薬学会東北支部 第 13 回化学系若手研究者セミナー、2015 年 9 月。
92. デプシペプチド類縁体の PI3K 阻害活性についての検討、李 仁、西條 憲、下平秀樹、成田紘一、加藤 正、石岡千加史、第 19 回日本がん分子標的治療学会、松山、2015 年 6 月。
93. PTP1B 阻害活性を有するダイシダバロン A, B および C の全合成、成田紘一、福井友理恵、佐藤江里、安達剛史、加藤 正、第 26 回万有仙台シンポジウム、仙台、2015 年 6 月。
- *94. 1-*O*-*n*-ブチル-L-イミノフラノース誘導体の触媒的不斉合成と酵素阻害活性評価、佐久間俊嘉、名取良浩、中川進平、加藤 敦、足立伊佐雄、吉村祐一、第 33 回メディシナルケミストリーシンポジウム、千葉、2015 年 11 月。
- *95. イナミドを基質とした Mizoroki-Heck 型反応とスチルベン誘導体の合成、若松秀章、大澤直央、柳澤里佳、木村 翔、名取良浩、吉村祐一、第 41 回反応と合成の進歩シンポジウム、大阪、2015 年 10 月。
- *96. 4'位に硫黄が置換した 3'-デオキシヌクレオシドの合成研究、安達桃子、伊藤文、名取良浩、若松秀

法人番号	041004
プロジェクト番号	S1511001L

- 章、吉村祐一、第 54 回日本薬学会東北支部大会、盛岡、2015 年 9 月。
- *97. スタブジン誘導体の合成研究、伊藤恭平、菅野裕也、齋藤華子、若松秀章、名取良浩、齋藤有香子、吉村祐一、第 54 回日本薬学会東北支部大会、盛岡、2015 年 9 月。
98. サイクリン依存性キナーゼ 1 (Cdk1) が CYP2D6 及び CYP3A4 遺伝子発現に及ぼす影響の解析、稲見敬太、佐々木崇光、中島菜月、小野 緑、熊谷 健、永田 清、H27 度内外環境応答・代謝酵素研究会、旭川、2015 年 7 月。
- *99. 薬物代謝酵素発現細胞及び誘導評価細胞を用いた薬物性肝障害研究について、佐々木崇光、熊谷 健、永田 清、第 42 回日本毒性学会学術年会、金沢、2015 年 6 月。
- *100. レポーター遺伝子導入細胞株を用いた健康食品による CYP1A1/1A2 誘導の網羅的評価、永田 清、佐々木崇光、熊谷 健、フォーラム 2015 衛生薬学・環境トキシコロジー、神戸、2015 年 9 月。
- *101. レチノイン酸代謝酵素 CYP26 の活性阻害評価系構築、新井 悠、佐々木崇光、稲見敬太、佐藤 裕、熊谷 健、吉成浩一、永田 清、第 54 回日本薬学会東北支部大会、岩手、2015 年 9 月。
102. Profiles of Immune Cells and Reproduction of Immune-Mediated Drug-Induced Injury, Yasuyuki Fujisaka, Yasuteru Kondo, Takamitsu Sasaki, Takayuki Kogure, Jun Inoue, Yu Nakagome, Yuuta Wakui, Tomoaki Iwata, Tatsuki Morosawa, Teruyuki Umetu, Hiroyuki Suzuki, Hiroaki Yamaguchi, Nariyasu Mano, Kiyoshi Nagata, Tooru Shimosegawa, American College of Gastroenterology 2015 annual scientific meeting, Honolulu, Hawaii, 2015, October.
103. Profiles of Immune in Peripheral Blood and Reproduction of Immune-Mediated Drug-Induced Injury *In Vitro*, Yasuyuki Fujisaka, Yasuteru Kondo, Takayuki Kogure, Jun Inoue, Yu Nakagome, Tomoaki Iwata, Tatsuki Morosawa, Teruyuki Umetu, Hiroyuki Suzuki, Hiroaki Yamaguchi, Takamitsu Sasaki, Nariyasu Mano, Kiyoshi Nagata, Tooru Shimosegawa, 第 19 回日本肝臓学会、東京、2015 年 10 月。
104. シトクロム P450 3A4 と UDP-グルクロン酸転移酵素 1A7 の生細胞内でのタンパク質相互作用：機能的相互作用および蛍光共鳴移動 (FRET) 解析、江越菜月、木下亨佑、古葉弘樹、生城真一、永田 清、山添 康、Peter I Mackenzie、山田英之、石井祐次、日本薬物動態学会第 30 回年会、東京、2015 年 11 月。
- *105. ヒト肝細胞における P450 活性を模倣した細胞評価系の構築、佐藤 裕、佐々木崇光、新井 悠、熊谷 健、永田 清、日本薬物動態学会第 30 回年会、東京、2015 年 11 月。
- 「研究テーマ2. 老年性神経系疾患(老人性認知症、高齢者うつ病)改善薬の開発」
106. キサンチンオキシダーゼ阻害作用を有するトロポロン誘導体の探索、太田公規、佐藤 輔、皆瀬麻子、遠藤 泰之、日本薬学会第 140 年会、京都、2020 年 3 月。
107. 抗腫瘍活性を示す m-カルボラン含有トリメトキシフェニル誘導体、皆瀬麻子、太田公規、遠藤泰之、日本薬学会第 140 年会、京都、2020 年 3 月。
- *108. アンドロゲン受容体とカルボラン誘導体との複合体の分子動力学シミュレーション、金井 涼、加藤 紘一、仲吉朝希、太田公規、遠藤泰之、栗本英治、小田彰史、日本薬学会第 140 年会、京都、2020 年 3 月。
109. 潰瘍性大腸炎に起因するうつ様症状に対する肝臓水解物の効果、小平貴代、中川西修、山田耕太郎、佐久間若菜、高橋浩平、根本 互、石澤大輔、高橋成弥、穂積智香子、櫻井英知、丹野孝一、日本薬学会第 140 年会、京都、2020 年 3 月。
110. 酵素分解サバペプチドの抗疲労メカニズム、中川西修、佐久間若菜、根本 互、松本 聡、只野 武、丹野孝一、日本薬学会第 140 年会、京都、2020 年 3 月。
111. 断続的断眠誘発性衝動性様行動における海馬 α 2A 受容体の関与、八百板富紀枝、名村幸大、柴田 楓、菅原 彩、土谷昌広、只野 武、丹野孝一、第 93 回日本薬理学会年会、横浜、2020 年 3 月。
112. 嗅球摘出マウスの海馬 AMPK の役割、小平貴代、中川西修、根本 互、高橋浩平、佐久間若菜、丹野孝一、第 93 回日本薬理学会年会、横浜、2020 年 3 月。
113. 球状ホウ素クラスターを基盤とする新規エストロゲン受容体リガンドの設計と合成、皆瀬麻子、大山美優、吉見友弘、太田公規、遠藤泰之、第 37 回メディシナルケミストリーシンポジウム、東京、2019 年 11 月。
114. キサンチンオキシダーゼ阻害作用を示すトロポロン誘導体の探索、太田公規、佐藤大輔、皆瀬麻子、遠藤泰之、第 37 回メディシナルケミストリーシンポジウム、東京、2019 年 11 月。

法人番号	041004
プロジェクト番号	S1511001L

115. 新規 5-アリールアゾトロポロン誘導体の細胞増殖抑制活性と活性メカニズム、皆瀬麻子、氣仙拓也、畠山瑞季、太田公規、佐藤大輔、今野茉歩、遠藤泰之、日本薬学会第 139 年会、千葉、2019 年 3 月。
116. Liver Hydrolysate Improves Depressive-Like Behavior in Olfactory Bulbectomized Mice: Involvement of Hippocampal Neurogenesis Through AMPK/BDNF/CREB Pathway, Kotaro Yamada, Osamu Nakagawasai, Takayo Odaira, Kohei Takahashi, Wataru Nemoto, Wakana Sakuma, Jia-Rong Lin, Hidetomo Sakurai, Koichi Tan-No, ICoFF/ISNFF, 京都, 2019 年 12 月。
117. レプチン欠損マウスの接触性痛覚過敏に対するアンジオテンシン (1-7) の抑制効果、山縣涼太、根本 互、中川西修、丹野孝一、第 58 回日本薬学会東北支部大会、仙台、2019 年 10 月。
118. 長期粉末食飼育誘発性低不安行動におけるヒスタミン神経系の関与、八百板富紀枝、長谷山咲子、宮澤将之、野田芙優、土谷昌広、丹野孝一、第 58 回日本薬学会東北支部大会、仙台、2019 年 10 月。
119. Captopril の海馬 Angiotensin(1-7)/Mas 受容体系の活性化を介した抗うつ効果、小平貴代、中川西修、小野涼太郎、根本 互、高橋浩平、佐久間若菜、丹野孝一、第 58 回日本薬学会東北支部大会、仙台、2019 年 10 月。
- *120. Schizophrenia-Like Symptoms in the Offspring of Methylazoxymethanol-Treated Mice, Kohei Takahashi, Osamu Nakagawasai, Wakana Sakuma, Wataru Nemoto, Takayo Odaira, Jia-Rong Lin, Hiroshi Onogi, Lalit K. Srivastava, Minoru Tsuji, Hiroshi Takeda, Koichi Tan-No, 6th Congress of Asian College of Neuropsychopharmacology, 福岡, 2019 年 10 月。
- *121. Involvement of Catecholaminergic and GABAergic Mediations in the Anxiety-Related Behavior Induced by Long-Term Powdered Food Feeding, Fukie Yaoita, Masahiro Tsuchiya, Yuichiro Arai, Takeshi Tadano, Koichi Tan-No, 6th Congress of Asian College of Neuropsychopharmacology, 福岡, 2019 年 10 月。
122. 長期粉末食飼育マウスにおける結腸機能と免疫細胞の関連性、八百板富紀枝、宮澤将之、土谷昌広、土谷 忍、神崎 展、只野 武、丹野孝一、第 70 回日本薬理学会北部会、札幌、2019 年 8 月。
123. レプチン欠損マウスの神経障害性疼痛に対するアンジオテンシン (1-7) の効果、山縣涼太、根本 互、中川西修、丹野孝一、第 70 回日本薬理学会北部会、札幌、2019 年 9 月。
124. 絞扼性神経損傷マウスにおける diminazene aceturate の抗痛覚過敏作用、洪 琬貽、根本 互、中川西修、丹野孝一、第 70 回日本薬理学会北部会、札幌、2019 年 9 月。
125. Angiotensin 変換酵素阻害薬 Captopril の抗うつ作用は Angiotensin (1-7)/Mas 受容体を介する、小平貴代、中川西修、小野涼太郎、根本 互、高橋浩平、佐久間若菜、荒井裕一郎、只野武、丹野孝一、第 23 回活性アミンに関するワークショップ、東京、2019 年 8 月。
126. 2 型糖尿病マウスの神経障害性疼痛における脊髄アンジオテンシン系の関与、根本 互、山縣涼太、丹野孝一、生体機能と創薬シンポジウム 2019、東京、2019 年 8 月。
127. 糖尿病性神経障害性疼痛における脊髄アンジオテンシン系の関与の解明—新たな治療戦略を目指して—、丹野孝一、小湊佳輝、山縣涼太、根本 互、生体機能と創薬シンポジウム 2019、東京、2019 年 8 月。
128. p-Hydroxyamphetamine Causes Prepulse Inhibition Disruptions in Mice: Contribution of Catecholamine and Serotonin Neurotransmission, Hiroshi Onogi, Osamu Nakagawasai, Wataru Nemoto, Satoru Mitazaki, Koichi Tan-No, Takeshi Tadano, 2019 International Society for Neurochemistry Meeting, Montreal, 2019 年 8 月。
129. Antinociceptive Effect of Diminazene Aceturate, an Angiotensin-Converting Enzyme 2 Activator, in the Mouse Formalin Test, Wataru Nemoto, Ryota Yamagata, Osamu Nakagawasai, Shota Michimata, Koharu Nakagawa, Koichi Tan-No, 2019 International Society for Neurochemistry Meeting, Montreal, 2019 年 8 月。
- *130. Behavioral, Cytoarchitectural, and Neurochemical Changes in the Offspring of Methylazoxymethanol Treated in Mice, Osamu Nakagawasai, Kohei Takahashi, Wakana Sakuma, Wataru Nemoto, Takayo Odaira, Lin Jia-Rong, Hiroshi Onogi, Lalit K Srivastava, Koichi Tan-No, 2019 International Society for Neurochemistry Meeting, Montreal, 2019 年 8 月。
131. AMPK 活性化は嗅球摘出マウスにおいて海馬 PKC ζ /NF- κ B/BDNF/CREB を介して抗うつ効果を示す、小平貴代、中川西修、高橋浩平、根本 互、佐久間若菜、丹野孝一、日本薬学会第 139 年

法人番号	041004
プロジェクト番号	S1511001L

- 会, 千葉, 2019 年 3 月.
132. デキストラン硫酸ナトリウム誘発性潰瘍性大腸炎モデルマウスのうつ様症状に対する肝臓水解物の効果、中川西修、山田耕太郎、小平貴代、佐久間若菜、高橋浩平、根本 互、石澤大輔、大沼健太郎、高橋成弥、大久保未佑、西村優希、穂積智香子、櫻井英知、只野 武、丹野孝一、日本薬学会第 139 年会、千葉、2019 年 3 月.
 133. 海馬 AMPK シグナリングの活性化は嗅球摘出マウスのうつ様行動を改善する、小平貴代、中川西修、根本互、高橋浩平、佐久間若菜、丹野孝一、第 92 回日本薬理学会年会、大阪、2019 年 3 月.
 134. 坐骨神経部分結紮マウスにおけるエチドロン酸の抗痛覚過敏作用について、根本 互、山縣涼太、中川西修、洪 琬貽、島 和弘、遠藤康男、丹野孝一、第 92 回日本薬理学会年会、大阪、2019 年 3 月.
 - *135. 長期粉末食飼育誘発性不安関連行動におけるノルアドレナリンおよびドパミン神経系の、八百板富紀枝、土谷昌広、荒井裕一朗、只野 武、丹野孝一、第 92 回日本薬理学会年会、大阪、2019 年 3 月.
 136. マルチターゲット型抗腫瘍活性を示す新規カルボラン誘導体の創製、皆瀬麻子、太田公規、白田智七美、遠藤泰之、第 36 回メディシナルケミストリーシンポジウム、京都、2018 年 11 月.
 137. ホウ素クラスターの医薬活性化化合物における基礎骨格としての可能性、皆瀬麻子、氣仙拓也、佐藤大輔、太田公規、遠藤泰之、第 17 回化学系若手研究者セミナー、仙台、2018 年 9 月.
 138. ホウ素クラスター誘導体の抗腫瘍活性とそのメカニズムについて、皆瀬麻子、白田智七美、太田公規、遠藤泰之、日本薬学会第 138 年会、金沢、2018 年 3 月.
 139. 過敏性腸症候群モデルマウスにおけるエキセナチドの効果、八百板富紀枝、川浪啓豪、今泉宏紀、丹野孝一、第 57 回日本薬学会東北支部大会、仙台、2018 年 10 月.
 140. 断眠ストレス負荷誘発性異常行動におけるヒスタミン神経系の関与、今泉宏紀、八百板富紀枝、川浪啓豪、長谷山咲子、丹野孝一、第 57 回日本薬学会東北支部大会、仙台、2018 年 10 月.
 - *141. 胎生期 Methylazoxymethanol 投与マウスの統合失調症モデル動物としての妥当性、高橋浩平、中川西修、小野木弘志、根本 互、小平貴代、佐久間若菜、丹野孝一、第 57 回日本薬学会東北支部大会、仙台、2018 年 10 月.
 142. Angiotensin (1-7) Prevents Streptozotocin-Induced Diabetic Neuropathic Pain in Mice, Wataru Nemoto, Yoshiki Ogata, Ryota Yamagata, Osamu Nakagawasai, Koichi Tan-No, 31th European College of Neuropsychopharmacology Congress, Barcelona, 2018 年 10 月.
 143. Memantine Produces Antidepressant Effect Through the Enhancement of Hippocampal Neurogenesis in Olfactory Bulbectomized Mice, Osamu Nakagawasai, Kohei Takahashi, Wataru Nemoto, Takayo Odaira, Wakana Sakuma, Yuichiro Arai, Takeshi Tadano, Koichi Tan-No, 31th European College of Neuropsychopharmacology Congress, Barcelona, 2018 年 10 月.
 144. 断続的断眠ストレス負荷誘発性低不安行動におけるヒスタミン神経系の関与、八百板富紀枝、今泉 宏紀、川浪啓豪、土谷昌広、只野 武、丹野孝一、第 69 回日本薬理学会北部会、富山、2018 年 9 月.
 145. 2 型糖尿病モデルマウスにおけるアンジオテンシン(1-7)の抗痛覚過敏作用、山縣涼太、根本 互、中川西修、丹野孝一、第 69 回日本薬理学会北部会、富山、2018 年 9 月.
 146. メマンチンの海馬ドパミン神経系を介した抗うつ効果、高橋浩平、中川西修、根本 互、小平貴代、佐久間若菜、荒井裕一朗、只野 武、丹野孝一、第 22 回活性アミンに関するワークショップ、徳島、2018 年 7 月.
 147. Hippocampal AMPK Activation Suppresses Depressive-Like Behavior in Olfactory Bulbectomized Mice, Takayo Odaira, Osamu Nakagawasai, Wataru Nemoto, Kohei Takahashi, Wakana Sakuma, Ryotaro Ono, Koichi Tan-No, 18th World Congress of Basic and Clinical Pharmacology, 京都, 2018 年 7 月.
 - *148. Antidepressant Effect of BE360, a New Selective Estrogen Receptor Modulator, and Its Mechanism in Ovariectomized Mice, Wakana Sakuma, Osamu Nakagawasai, Wataru Nemoto, Takayo Odaira, Takumi Ogawa, Kiminori Ohta, Yasuyuki Endo, Koichi Tan-No, 18th World Congress of Basic and Clinical Pharmacology, 京都, 2018 年 7 月.
 149. Liver Hydrolysate Produces Antidepressant and Antidementia Effects in Olfactory Bulbectomized Mice, Osamu Nakagawasai, Kotaro Yamada, Takayo Odaira, Wakana Sakuma, Wataru Nemoto,

法人番号	041004
プロジェクト番号	S1511001L

- Hidetomo Sakurai, Koichi Tan-No, 18th World Congress of Basic and Clinical Pharmacology, 京都, 2018 年 7 月.
150. Involvement of Peripheral Alpha2A Adrenoceptor in the Acceleration of Gastrointestinal Transit and Abdominal Pain induced by Intermittent Sleep Deprivation, Fukie Yaoita, Keigo Kawanami, Hiroki Imaizumi, Takeshi Tadano, Koichi Tan-No, 18th World Congress of Basic and Clinical Pharmacology, 京都, 2018 年 7 月.
151. Anti-Allodynic Effect of Angiotensin (1-7) on Streptozotocin-Induced Diabetic Neuropathic Pain, Ryota Yamagata, Wataru Nemoto, Yoshiki Ogata, Osamu Nakagawasai, Koichi Tan-No, 18th World Congress of Basic and Clinical Pharmacology, 京都, 2018 年 7 月.
152. Inhibitory Effect of Repeated Oral Administration of Chondroitin Sulfate on the Formalin-Induced Tactile Allodynia in Mice, Wataru Nemoto, Kotaro Yamada, Osamu Nakagawasai, Yoshiki Ogata, Hidetomo Sakurai, Koichi Tan-No, 18th World Congress of Basic and Clinical Pharmacology, 京都, 2018 年 7 月.
153. 身体疲労モデルマウスにおける酵素分解サバペプチドの効果、中川西修、佐久間若菜、石澤大輔、根本 互、松本 聡、只野 武、丹野 孝一、日本薬学会第 138 年会、金沢、2018 年 3 月.
154. 神経障害性疼痛に対するコンドロイチン硫酸の抑制効果、根本 互、山田耕太郎、中川西修、小湯佳輝、千葉聖斗、山縣涼太、櫻井英知、丹野孝一、日本薬学会第 138 年会、金沢、2018 年 3 月.
155. 嗅球摘出マウスにおけるメマンチンの抗うつ効果とその作用機序、高橋浩平、中川西修、根本 互、小平貴代、佐久間若菜、丹野孝一、日本薬学会第 138 年会、金沢、2018 年 3 月.
- *156. 長期粉末食飼育がマウスの情動発達に及ぼす影響について、八百板富紀枝、今泉宏紀、川浪啓豪、土谷昌広、只野 武、丹野孝一、日本薬学会第 138 年会、金沢、2018 年 3 月.
- *157. Structural Differences of the Ligand Binding Pockets between Estrogen Receptor-Alpha and Beta, Koichi Kato, Kenichiro Fujii, Tomoki Nakayoshi, Yurie Watanabe, Shuichi Fukuyoshi, Kiminori Ohta, Yasuyuki Endo, Noriyuki Yamaotsu, Shuichi Hirono, Eiji Kurimoto, Akifumi Oda, XXIX IUPAP Conference on Computational Physics, CCP2017, Paris, 2017 年 7 月.
- *158. Hydrophobicity and Electronic Effects of Carborane for Application in Medicinal Drug Design (invited lecture), Yasuyuki Endo, Keisuke Yamamoto, Kiminori Ohta, Hiroto Yamazaki, Asako Kaise, 16th International Meeting on Boron Chemistry (IMEBORON XVI), Hong Kong, 2017 年 7 月.
159. カルボラン含有非ステロイド型 2-methoxyestradiol 誘導体の抗腫瘍活性、皆瀬麻子、太田公規、遠藤泰之、日本ケミカルバイオロジー学会第 12 回年会、札幌、2017 年 6 月.
160. フェニルアゾトロポロン誘導体のキサンチンオキシダーゼ阻害活性とそのメカニズム解析、佐藤 大輔、氣仙拓也、太田公規、遠藤泰之、日本薬学会第 137 年会、仙台、2017 年 3 月.
161. Wieland-Miescher ケトン誘導体の加溶媒分解条件下における協奏的骨格転位反応、猪股浩平、遠藤泰之、日本薬学会第 137 年会、仙台、2017 年 3 月.
162. 新規 SERD 化合物の探索:カルボラン含有 ER リガンドによる ER ダウンレギュレーション、皆瀬麻子、吉見友弘、太田公規、遠藤泰之、日本薬学会第 137 年会、仙台、2017 年 3 月.
- *163. 卵巣摘出マウスのうつ様行動に対する新規選択的エストロゲン受容体モジュレーターBE360 の効果、佐久間若菜、中川西修、根本 互、小平貴代、小川卓巳、太田公規、遠藤泰之、只野 武、丹野孝一、第 21 回活性アミンに関するワークショップ、京都、2017 年 8 月.
164. Structural Differences of the Ligand Binding Pockets between Estrogen Receptor-Alpha and Beta, Koichi Kato, Kenichiro Fujii, Tomoki Nakayoshi, Yurie Watanabe, Shuichi Fukuyoshi, Kiminori Ohta, Yasuyuki Endo, Noriyuki Yamaotsu, Shuichi Hirono, Eiji Kurimoto, Akifumi Oda, XXIX IUPAP Conference on Computational Physics, CCP2017, Paris, 2017 年 7 月.
165. Hydrophobicity and Electronic Effects of Carborane for Application in Medicinal Drug Design (invited lecture), Yasuyuki Endo, Keisuke Yamamoto, Kiminori Ohta, Hiroto Yamazaki, Asako Kaise, 16th International Meeting on Boron Chemistry (IMEBORON XVI), Hong Kong, 2017 年 7 月.
166. カルボラン含有非ステロイド型 2-methoxyestradiol 誘導体の抗腫瘍活性、皆瀬麻子、太田公規、遠藤泰之、日本ケミカルバイオロジー学会第 12 回年会、札幌、2017 年 6 月.
167. フェニルアゾトロポロン誘導体のキサンチンオキシダーゼ阻害活性とそのメカニズム解析、佐藤 大輔、氣仙拓也、太田公規、遠藤泰之、日本薬学会第 137 年会、仙台、2017 年 3 月.
168. Wieland-Miescher ケトン誘導体の加溶媒分解条件下における協奏的骨格転位反応、猪股浩平、遠

法人番号	041004
プロジェクト番号	S1511001L

- 藤泰之、日本薬学会第 137 年会、仙台、2017 年 3 月。
169. 新規 SERD 化合物の探索:カルボラン含有 ER リガンドによる ER ダウンレギュレーション、皆瀬麻子、吉見友弘、太田公規、遠藤泰之、日本薬学会第 137 年会、仙台、2017 年 3 月。
170. 脊髄疼痛伝達機構における Angiotensin II の役割に関する行動および分子薬理学的研究、根本 互、第 39 回東北薬学セミナー、仙台、2017 年 12 月。
171. 断続的レム断眠ストレス負荷誘発性衝動性様症状における海馬ノルアドレナリン神経系の関与、八百板富紀枝、川浪啓豪、今泉宏紀、柴田 楓、菅原 彩、只野 武、丹野孝一、第 56 回日本薬学会東北支部大会、青森、2017 年 10 月。
172. 嗅球摘出マウスにおけるメマンチンの海馬 CREB-BDNF 系を介する抗うつ効果、高橋浩平、中川西修、根本 互、小平貴代、丹野孝一、第 68 回日本薬理学会北部会、山形、2017 年 9 月。
- *173. 長期粉末食飼育誘発性低不安行動におけるグルココルチコイド受容体およびノルアドレナリン神経系の関与、八百板富紀枝、小澤美芙由、遠藤汐里、土谷昌広、荒井裕一朗、只野 武、丹野孝一、第 68 回日本薬理学会北部会、山形、2017 年 9 月。
174. スレプトゾトシン誘発性 1 型糖尿病マウスにおけるアンジオテンシン (1-7) の抗アロディニア作用、山縣涼太、根本 互、小湊佳輝、中川西修、丹野孝一、第 68 回日本薬理学会北部会、山形、2017 年 9 月。
175. Activation of AMP-Activated Protein Kinase Induces Anti-Depressant Like Effect in Olfactory Bulbectomized Mice, Takayo Odaira, Osamu Nakagawasai, Wataru Nemoto, Kohei Takahashi, Wakana Sakuma, Ryotaro Ono, Koichi Tan-No, 第 60 回日本神経化学会、仙台、2017 年 9 月。
176. 海馬 AMPK 活性化による抗うつ作用メカニズムについて、小平貴代、中川西修、根本 互、高橋浩平、佐久間若菜、小野涼太郎、丹野孝一、生体機能と創薬シンポジウム 2017、京都、2017 年 8 月。
177. 1 型糖尿病モデルマウスにおける神経障害性疼痛に対するアンジオテンシン (1-7) の抑制効果、山縣涼太、根本 互、小湊佳輝、中川西修、丹野孝一、生体機能と創薬シンポジウム 2017、京都、2017 年 8 月。
- *178. 神経発達障害仮説に基づいた統合失調症モデル動物作製の試み、中川西修、第 16 回生物化学若手研究者セミナー、仙台、2017 年 7 月。
179. 嗅球摘出マウスのうつ様行動に対するメマンチンの効果、高橋浩平、中川西修、根本 互、小平貴代、丹野孝一、日本薬学会第 137 年会、仙台、2017 年 3 月。
180. 断続的レム断眠負荷誘発性交替率低下に対するメチルフェニデートの効果、八百板富紀枝、永澤佑佳、土谷昌広、荒井裕一朗、只野 武、丹野孝一、日本薬学会第 137 年会、仙台、2017 年 3 月。
181. 嗅球摘出マウスの精神機能障害に対する肝臓水解物の効果:海馬 AMP 活性化プロテインキナーゼの関与について、中川西修、山田耕太郎、小平貴代、佐久間若菜、根本 互、櫻井英知、丹野孝一、日本薬学会第 137 年会、仙台、2017 年 3 月。
182. AMPK 活性化剤である AICAR は抗うつ作用をもたらす、小平貴代、中川西修、根本 互、佐久間若菜、丹野孝一、第 90 回日本薬理学会年会、長崎、2017 年 3 月。
183. 嗅球摘出マウスの認知機能障害に対するアリピプラゾールの効果、高橋浩平、中川西修、根本 互、小平貴代、荒井裕一朗、久光 正、丹野孝一、第 90 回日本薬理学会年会、長崎、2017 年 3 月。
184. アンジオテンシン (1-7) は糖尿病性神経障害性疼痛を抑制する、小湊佳輝、根本 互、中川西修、丹野孝一、第 90 回日本薬理学会年会、長崎、2017 年 3 月。
185. アンジオテンシン III 誘発性侵害刺激行動に対するアンジオテンシン (1-7) の抑制作用について、根本 互、中川西修、丹野孝一、第 90 回日本薬理学会年会、長崎、2017 年 3 月。
186. 嗅球摘出マウスのうつ様行動に対する Angiotensin 変換酵素阻害薬 Captopril の効果、小野涼太郎、中川西修、小平貴代、佐久間若菜、根本 互、丹野孝一、第 26 回神経行動薬理若手研究者の集い、福岡、2017 年 3 月。
187. フェニルアゾトロポロン誘導体のキサンチンオキシダーゼ阻害活性、佐藤大輔、氣仙拓也、太田公規、遠藤泰之、第 34 回メディシナルケミストリーシンポジウム、つくば、2016 年 11 月。
188. メカニズムに着目したカフェイン酸誘導体のアミロイド β 凝集阻害活性評価、田口莉帆、高橋倫人、畑山晃輝、太田公規、橋友理香、関 千草、中野博人、遠藤泰之、徳樂清孝、上井幸司、第 34 回メディシナルケミストリーシンポジウム、つくば、2016 年 11 月。
189. ホウ素クラスターを中心骨格とする新規選択的エストロゲン受容体抑制薬 (SERD) の開発、皆瀬麻子、吉見友弘、太田公規、遠藤泰之、第 34 回メディシナルケミストリーシンポジウム、つくば、2016 年

法人番号	041004
プロジェクト番号	S1511001L

- 11月.
190. ランダムスクリーニングから見出されたトロポロン誘導体の多様な生物活性、太田公規、佐藤友紀、皆瀬麻子、遠藤泰之、第55回日本薬学会東北支部大会、郡山、2016年9月.
 191. キサンチンオキシダーゼ阻害活性を示すフェニルアゾトロポロン誘導体の探索、佐藤大輔、氣仙拓也、太田公規、遠藤泰之、第55回日本薬学会東北支部大会、郡山、2016年9月.
 192. 新規 XO 阻害剤の定量的構造活性相関と結合様式の解析、太田公規、佐藤 匠、石井康博、遠藤泰之、日本薬学会第 136 年会、横浜、2016 年 3 月.
 193. カルボラン含有グリセロール誘導体の抗アンドロゲン活性、皆瀬麻子、太田公規、小田彰史、遠藤泰之、日本薬学会第 136 年会、横浜、2016 年 3 月.
 194. 7員環含有 Wieland-Miescher ケトン誘導体における新規骨格転位反応、猪股浩平、遠藤泰之、日本薬学会第136年会、横浜、2016年3月.
 195. Long-Term Feeding on Powdered Food Causes Hyperglycemia and Signs of Systemic Illness in Mice, Hiroyuki Yoneda, Masahiro Tsuchiya, Fukie Nijima-Yaoita, Shinobu Tsuchiya, Yoshihiro Hagiwara, Keiichi Sasaki, Shunji Sugawara, Yasuo Endo, Koichi Tan-No, Makoto Watanabe, International Conference on Food for Health in Niigata 2016, 新潟、2016 年 11 月.
 196. ニューロン新生マーカー・BrdU の脳内分布における拡散型ヌクレオシドトランスポーター1 の役割の解明、木村準也、吉田寛伸、竹生田淳、Bastos Gilmar、鈴木登紀子、吉川雄朗、根本 互、中川西修、丹野孝一、谷内一彦、平沢典保、守屋孝洋、第 67 回日本薬理学会北部会、札幌、2016 年 9 月.
 197. 断続的断眠ストレス負荷誘発性交替行動障害における海馬誘導型一酸化窒素合成酵素の関与、八百板富紀枝、永澤佑佳、土谷昌広、荒井裕一朗、只野 武、丹野孝一、第 67 回日本薬理学会北部会、札幌、2016 年 9 月.
 198. 嗅球摘出マウスにおける線条体 Dopamine 受容体機能変化とそれに及ぼす抗うつ薬の影響、高橋浩平、中川西修、根本 互、菊地恵理、佐久間若菜、小平貴代、丹野孝一、第 67 回日本薬理学会北部会、札幌、2016 年 9 月.
 199. 過敏性腸症候群モデルの消化器症状におけるアドレナリン $\alpha 2$ 受容体サブタイプの関与、八百板富紀枝、村上裕樹、柴田 楓、菅原 彩、只野 武、丹野孝一、第 55 回日本薬学会東北支部大会、郡山、2016 年 9 月.
 200. 1 型糖尿病モデルマウスの機械的アロディニアにおける脊髄内アンジオテンシン II 系の関与、山縣涼太、根本 互、小湊佳輝、中川西修、八百板富紀枝、丹野孝一、生体機能と創薬シンポジウム 2016、仙台、2016 年 8 月.
 - *201. 更年期障害モデルマウスのうつ状態に対する新規選択的エストロゲン受容体モジュレーターBE360 の効果、佐久間若菜、中川西修、根本 互、小湊佳輝、八百板富紀枝、小川卓巳、太田公規、遠藤泰之、丹野孝一、生体機能と創薬シンポジウム 2016、仙台、2016 年 8 月.
 202. 脊髄疼痛伝達機構におけるアンジオテンシン II の役割、根本 互、小湊佳輝、丹野孝一、生体機能と創薬シンポジウム 2016、仙台、2016 年 8 月.
 - *203. 精神疾患モデル動物作製とその発現機序の解明、中川西修、生体機能と創薬シンポジウム 2016、仙台、2016 年 8 月.
 204. スカブロニン G-メチルエステルの認知障害改善作用とその機序について、小平貴代、中川西修、林嘉蓉、根本 互、佐久間若菜、小原祐太郎、小早川優、中田雅久、丹野孝一、次世代を担う創薬・医療薬理シンポジウム 2016、仙台、2016 年 8 月.
 205. うつ病モデルマウスの脳内ドパミン神経機能変化について、中川西修、高橋浩平、根本 互、菊地恵理、佐久間若菜、八百板富紀枝、荒井裕一朗、只野 武、丹野孝一、第 20 回活性アミンに関するワークショップ、筑波、2016 年 8 月.
 206. カルボラン含有2-methoxyestradiol誘導体の細胞増殖抑制作用とメカニズム解析、皆瀬麻子、太田公規、遠藤泰之、第33回メディシナルケミストリーシンポジウム、千葉、2015年11月.
 207. 新規チオフェン含有エストロゲン受容体制御化合物の開発、青砥沙也加、田口 史、皆瀬麻子、太田公規、遠藤泰之、第33回メディシナルケミストリーシンポジウム、千葉、2015年11月.
 208. トリアジン構造を有する新規キサンチンオキシダーゼ阻害剤の創製、太田公規、佐藤 匠、石井康博、遠藤泰之、第33回メディシナルケミストリーシンポジウム、千葉、2015年11月.
 209. 新規カルボラン含有医薬化合物創製への挑戦、皆瀬麻子、太田公規、遠藤泰之、第54回日本薬学会東北支部大会、盛岡、2015年9月.

法人番号	041004
プロジェクト番号	S1511001L

210. バナナ型構造を持つエストロゲン受容体リガンドにおけるアゴニスト-アンタゴニストバランスの制御、太田公規、皆瀬麻子、遠藤泰之、日本ケミカルバイオロジー学会 第10回年会、仙台、2015年6月。
211. エストロゲン代謝物を基にデザインした球状ホウ素クラスター含有新規抗腫瘍性化合物の開発とメカニズム解析、皆瀬麻子、太田公規、遠藤泰之、日本ケミカルバイオロジー学会 第10回年会、仙台、2015 年6月。
212. ホルマリン誘発性アロディニアに対するコンドロイチン硫酸の効果、根本 互、山田耕太郎、中川西修、小野寺甲仁、小湊佳輝、櫻井英知、丹野孝一、日本薬学会第 136 年会、横浜、2016 年 3 月。
213. アンジオテンシン II が関わる病態とその治療薬の薬理、丹野孝一、第 28 回東北薬科大学生涯教育講演会、仙台、2015 年 10 月。
- *214. 長期粉末食飼育誘発性マウス異常行動に対するメチルフェニデートの効果、藤巻玲香、八百板富紀枝、佐々木貴史、土谷昌広、荒井裕一朗、根本 互、中川西修、只野 武、丹野孝一、第 54 回日本薬学会東北支部大会、盛岡、2015 年 9 月。
215. 過敏性腸症候群モデルの消化器症状における腸管 $\alpha 2c$ アドレナリン受容体の関与、武藤正通、八百板富紀枝、村上裕樹、根本 互、中川西修、只野 武、丹野孝一、第 54 回日本薬学会東北支部大会、盛岡、2015 年 9 月。
216. 断続的断眠ストレス負荷誘発性情動行動障害に対する ADHD 治療薬の効果、八百板富紀枝、永澤佑佳、土谷昌広、荒井裕一朗、根本 互、中川西修、只野 武、丹野孝一、第 66 回日本薬理学会北部会、富山、2015 年 9 月。
217. 脊髄疼痛伝達機構におけるアンジオテンシン III の役割、根本 互、小湊佳輝、中川西修、八百板富紀枝、只野 武、丹野孝一、第 66 回日本薬理学会北部会、富山、2015 年 9 月。
218. 有痛性糖尿病性ニューロパチーにおける脊髄アンジオテンシン系の関与、小湊佳輝、根本 互、中川西修、八百板富紀枝、只野 武、丹野孝一、第 66 回日本薬理学会北部会、富山、2015 年 9 月。
219. 有痛性糖尿病性神経障害における脊髄アンジオテンシン II の関与、小湊佳輝、根本 互、中川西修、八百板富紀枝、只野 武、丹野孝一、生体機能と創薬シンポジウム 2015、船橋、2015 年 8 月。
220. スカブロニン G メチルエステルは認知障害やうつ様症状を海馬の神経新生促進作用により改善する、林嘉蓉、中川西修、根本 互、小原祐太郎、八百板富紀枝、荒井裕一朗、只野 武、小早川優、中田雅久、丹野孝一、第 19 回活性アミンに関するワークショップ、いわき、2015 年 8 月。
221. The Effects of Liver Hydrolysate on Physical Fatigue and Sickness Behavior, Kotaro Yamada, Osamu Nakagawasai, Wataru Nemoto, Hidetomo Sakurai, Koichi Tan-No, 12th Asian Congress of Nutrition, 横浜、2015 年 5 月。
- 「研究テーマ3. 難治性疼痛に対する緩和医療法の確立」
222. Mechanism of Bilateral Pain under the Inflammatory State、渡辺千寿子、善積克、櫻田忍、溝口広一、第 93 回日本薬理学会年会、横浜、2020 年 3 月。
223. Inhibitory Effect of Gabapentin for Interstitial Cystitis/Bladder Pain Syndrome in Rats、善積克、渡辺千寿子、溝口広一、第 93 回日本薬理学会年会、横浜、2020 年 3 月。
224. モルヒネ非感受性 μ オピオイド受容体プライスバリエーション選択的作動薬を志向したモルヒナン誘導体の合成、丹羽淳一、本城綾香、米澤佑、平山重人、唐木文霞、伊藤謙之介、溝口広一、藤井秀明、第 11 回北里化学シンポジウム、東京、2019 年 12 月。
- *225. モルヒネ抵抗性炎症性疼痛の制御、溝口広一、第 11 回仙台痛みフォーラム、仙台、2019 年 12 月。
226. The Development of Bilateral Pain under the Inflammatory State, Chizuko Watanabe, Masaru Yoshizumi, Takafumi Hayashi, Shinobu Sakurada, Hirokazu Mizoguchi, Novel Pain Therapeutics: From Basic Research to Clinical Translation and Rehabilitation, Rende (Cosenza), Italy, October 2019.
227. Possible Involvement of Histamine on Nociceptive Behaviors Induced by Intrathecally Administered CCK-8, Shinobu Sakurada, Takafumi Hayashi, Chizuko Watanabe, Sou Katsuyama, Tsuneyoshi Suzuki, Tsukasa Sakurada, Novel Pain Therapeutics: From Basic Research to Clinical Translation and Rehabilitation, Rende (Cosenza), Italy, October 2019.
- *228. Management of Morphine-Resistant Inflammatory Pain, Hirokazu Mizoguchi, Chizuko Watanabe, Masaru Yoshizumi, Yuta Aoki, Asami Komiyama, Shinobu Sakurada, Novel Pain Therapeutics: From Basic Research to Clinical Translation and Rehabilitation, Rende (Cosenza), Italy, October 2019.

法人番号	041004
プロジェクト番号	S1511001L

229. LPS 誘発性間質性膀胱炎モデルラットに対するガバペンチンの効果、善積克、渡辺千寿子、溝口広二、第 58 回日本薬学会東北支部大会、仙台、2019 年 10 月。
230. 炎症性疼痛下における対側性疼痛発現機構の解明、渡辺千寿子、善積克、櫻田忍、溝口広一、第 58 回日本薬学会東北支部大会、仙台、2019 年 10 月。
231. I 型糖尿病モデルマウスにおけるアロディニアの発現機序の解明、林貴史、勝山壮、渡辺千寿子、櫻田司、鈴木常義、櫻田忍、第 70 回日本薬理学会北部会、札幌、2019 年 9 月。
232. 間質性膀胱炎モデルラットに対するガバペンチンの薬効評価、善積克、渡辺千寿子、溝口広一、第 70 回日本薬理学会北部会、札幌、2019 年 9 月。
233. 間質性膀胱炎モデルラットにおけるガバペンチンの有効性、善積克、渡辺千寿子、溝口広一、第 39 回鎮痛薬・オピオイドペプチドシンポジウム、東京、2019 年 8 月。
234. 非天然型モルフィナン骨格を有する MRGPRX2 リガンドの創出、飯尾啓太、沓村憲樹、南雲康行、斉藤毅、山本直司、岩間美佐都、溝口広一、長瀬博、第 39 回鎮痛薬・オピオイドペプチドシンポジウム、東京、2019 年 8 月。
235. 難治性痒みに有効な新規低分子ペプチドの創成、石田宗一郎、櫻田忍、溝口広一、関千草、上井幸司、中野博人、日本化学会北海道支部 2019 年夏季研究発表会、苫小牧、2019 年 7 月。
236. 抗搔痒作用をもつ新規低分子ペプチドの創成、石田宗一郎、櫻田忍、溝口広一、関千草、上井幸司、中野博人、日本化学会北海道支部 2019 年夏季研究発表会、苫小牧、2019 年 7 月。
- *237. 炎症性疼痛制御における methadone の特異的作用、渡辺千寿子、込山麻美、善積克、櫻田忍、溝口広一、第 13 回日本緩和医療薬学会、千葉、2019 年 6 月。
- *238. 炎症性疼痛下における morphine の鎮痛作用減弱機構、溝口広一、青木祐太、渡辺千寿子、善積克、櫻田忍、第 13 回日本緩和医療薬学会、千葉、2019 年 6 月。
- *239. 神経障害性疼痛に対する methadone の脊髄鎮痛作用、善積克、角貴祐、渡辺千寿子、櫻田忍、溝口広一、第 13 回日本緩和医療薬学会、千葉、2019 年 6 月。
240. Development of Agonists Toward Morphine-Insensitive μ Opioid Receptor Variants, Hideaki Fujii, Ayaka Honjo, Yu Yonezawa, Ayano Miyota, Shigeto Hirayama, Fumika Karaki, Kennosuke Itoh, Hirokazu Mizoguchi, 20th Tetrahedron Symposium, Bangkok, Thailand, June 2019.
241. Design and Synthesis of Novel MRGPRX2 Ligands with Unnatural Morphinan Skeleton, Keita Ito, Noriki Kutsumura, Yasuyuki Nagumo, Tsuyoshi Saitoh, Naoshi Yamamoto, Misato Iwama, Hirokazu Mizoguchi, Hiroshi Nagase, The 27th French-Japanese Symposium on Medicinal and Fine Chemistry, Fukuoka, May 2019.
242. Gabapentin Differently Modulates Pre-Synaptic GABA Release in the Spinal Dorsal Horn and Locus Coeruleus of Rat after Nerve Injury, Masaru Yoshizumi, Ken-ichiro Hayashida, James C. Eisenach, Chizuko Watanabe, Hirokazu Mizoguchi, 7th International Congress on Neuropathic Pain, London, UK, May 2019.
243. Mirror image pain 発現機構における NMDA 受容体の関与、渡辺千寿子、善積克、川瀬涼音、櫻田忍、溝口広一、第 92 回日本薬理学会年会、大阪、2019 年 3 月。
244. 培養アストロサイトからのグルタミン酸誘発性グルタミン酸遊離におけるガバペンチンの促進効果、善積克、林田健一郎、James C. Eisenach、河谷正仁、渡辺千寿子、溝口広一、第 92 回日本薬理学会年会、大阪、2019 年 3 月。
245. Sex-based difference in CD86 expression on CD103+ dendritic cells promotes female-predominant Th2 cytokine production during allergic asthma. Tomomitsu Miyasaka, Chiaki Masuda, Kaori Kawakami, Jin-ichi Inokuchi, Tasuku Kawano, Kaori Dobashi-Okuyama, Motoaki Takayanagi, Tomoko Takahashi, Isao Ohno. 17th International Congress of Immunology, Beijing, 2019, October.
246. Involvement of airway epithelial cells in dendritic cell activation leading to female-predominant Th2 cytokine production in allergic asthma. Kaori Kawakami, Tomomitsu Miyasaka, Chiaki Masuda, Tasuku Kawano, Tomoko Takahashi, Motoaki Takayanagi, Isao Ohno. 17th International Congress of Immunology, Beijing, 2019, October.
247. 真菌オリゴ DNA による気管支喘息の制御とその免疫機序、鈴木柊伍、平田大実、宮坂智充、佐藤光、笠松純、石井恵子、川上佳織、高橋知子、大野勲、川上和義、アレルギー・好酸球研究会 2019、東京、2019 年 10 月。
248. 女性優位な Th2 サイトカイン産生を担う樹状細胞の活性化に関与する気道上皮細胞の役割、宮坂

法人番号	041004
プロジェクト番号	S1511001L

- 智充、川上佳織、増田千愛、河野資、高橋知子、高柳元明、大野勲、アレルギー・好酸球研究会 2019、東京、2019 年 10 月。
249. 気管支喘息増悪における好酸球数の増加に関与する μ オピオイド受容体遺伝子一塩基多型、川上佳織、宮坂智充、中村豊、宮田敏、佐藤美希、目時弘仁、曾良一郎、山内広平、河野資、下川宏明、高柳元明、高橋知子、大野勲、アレルギー・好酸球研究会 2019、東京、2019 年 10 月。
250. 喘息モデルマウスに対する気管支肺胞上皮幹細胞を用いた治療効果についての検討、石井聖人、河野資、滝口迪瑠、高橋稜、木村諒、宮坂智充、松尾平、大野勲、高橋知子、第 58 回日本薬学会東北支部大会、仙台、2019 年 10 月。
- *251. オピオイド受容体遺伝子一塩基多型が喘息病態に及ぼす影響の解析、原田真裕美、宮坂智充、川上佳織、中村豊、宮田敏、佐藤美希、目時弘仁、曾良一郎、山内広平、河野資、下川宏明、高柳元明、高橋知子、大野勲、第 58 回日本薬学会東北支部大会、仙台、2019 年 10 月。
252. 好中球・好酸球混合型喘息における精神的ストレスの関与～精神的ストレスによる免疫寛容の抑制と Th17 細胞の分化誘導～、河野資、石井聖人、宮坂智充、大河原雄一、高柳元明、高橋知子、大野勲、第 53 回東北アレルギー懇話会、仙台、2019 年 7 月。
253. 真菌より見出したオリゴ DNA による Th2 免疫抑制を介した気管支喘息の制御、鈴木柊伍、平田大実、宮坂智充、佐藤光、笠松純、石井恵子、川上佳織、高橋知子、大野勲、川上和義、第 68 回日本アレルギー学会学術大会、東京、2019 年 6 月。
- *254. 気管支喘息増悪におけるヒト μ オピオイド受容体遺伝子一塩基多型の関与、川上佳織、宮坂智充、中村豊、宮田敏、佐藤美希、目時弘仁、曾良一郎、山内広平、河野資、下川宏明、高柳元明、高橋知子、大野勲、第 68 回日本アレルギー学会学術大会、東京、2019 年 6 月。
255. 精神的ストレスが免疫寛容に及ぼす影響と喘息発症、河野資、大内竜介、石井聖人、宮坂智充、大河原雄一、高柳元明、高橋知子、大野勲、第 68 回日本アレルギー学会学術大会、東京、2019 年 6 月。
256. 喘息気道炎症における樹状細胞の活性化に関与する気道上皮細胞の性差、川上佳織、宮坂智充、増田千愛、立崎史歩、中村豊、河野資、山内広平、高柳元明、高橋知子、大野勲、第 59 回日本呼吸器学会学術講演会、東京、2019 年 4 月。
257. 気管支喘息における樹状細胞の活性化の性差に関与する気道上皮細胞の役割、川上佳織、宮坂智充、増田千愛、河野資、高柳元明、高橋知子、大野勲、日本薬学会第 139 年会、千葉、2019 年 3 月。
258. 気管支喘息モデルマウスにおける気管支肺胞上皮幹細胞(Bronchioalveolar stem cells (BASCs))の治療効果の検討、石井聖人、河野資、滝口迪瑠、柏原若奈、平泉花菜、鈴木涼平、佐藤美菜香、宮坂智充、松尾平、高柳元明、大野勲、高橋知子、日本薬学会第 139 年会、千葉、2019 年 3 月。
259. 気管支喘息における樹状細胞活性化の性差に関与する気道上皮細胞の役割、宮坂智充、川上佳織、増田千愛、鹿野さくら、河野資、高柳元明、高橋知子、大野勲、第 1 回日本アレルギー学会東北地方会、仙台、2019 年 2 月。
- *260. 気管支喘息の増悪におけるオピオイド受容体遺伝子一塩基多型の関与、川上佳織、宮坂智充、中村豊、宮田敏、佐藤美希、目時弘仁、鹿野さくら、曾良一郎、山内広平、河野資、下川宏明、高柳元明、高橋知子、大野勲、第 1 回日本アレルギー学会東北地方会、仙台、2019 年 2 月。
261. 気管支肺胞上皮幹細胞 (Bronchioalveolar stem cells (BASCs)) の気管支喘息モデルマウスに対する効果の検討、石井聖人、河野資、滝口迪瑠、柏原若奈、平泉花菜、鈴木涼平、佐藤美菜香、宮坂智充、松尾平、高柳元明、大野勲、高橋知子、第 1 回日本アレルギー学会東北地方会、仙台、2019 年 2 月。
262. 幼少期ストレスによる免疫寛容の抑制を介した喘息発症モデル、大内竜介、河野資、宮坂智充、大河原雄一、高柳元明、高橋知子、大野勲、第 1 回日本アレルギー学会東北地方会、仙台、2019 年 2 月。
263. New Tripeptide for Antipruritic Agent, Soichiro Ishida, Shinobu Sakurada, Hirokazu Mizoguchi, Chigusa Seki, Koji Uwai, Yuko Okuyama, Hiroto Nakano, 10th International Peptide Symposium, Kyoto, December 2018.
264. 鎮痛作用を有する新規かご型オピオイドペプチド化合物の合成研究、岸里涼太、櫻田忍、溝口広二、林貴史、関千草、上井幸司、奥山祐子、中野博人、第 36 回メディシナルケミストリーシンポジウム、京都、2018 年 11 月。

法人番号	041004
プロジェクト番号	S1511001L

265. モルヒネ非感受性 μ オピオイド受容体スプライスバリエーション選択的作動薬を志向したモルヒナン誘導体の合成、本城綾香、米澤佑、御代田彩乃、平山重人、唐木文霞、伊藤謙之介、溝口広一、藤井秀明、第 36 回メディシナルケミストリーシンポジウム、京都、2018 年 11 月。
266. モルヒネ非感受性 μ オピオイド受容体選択的作動薬を志向したモルヒナン誘導体の合成、本城綾香、御代田彩乃、平山重人、唐木文霞、伊藤謙之介、溝口広一、藤井秀明、第 44 回反応と合成の進歩シンポジウム、熊本、2018 年 11 月。
267. 神経障害性疼痛における抗てんかん薬バルプロ酸の鎮痛機構、善積克、林田健一郎、渡辺千寿子、河谷正仁、James C. Eisenach、溝口広一、第 57 回日本薬学会東北支部大会、仙台、2018 年 10 月。
268. Mirror image pain 発現機構の解明、川瀬涼音、渡辺千寿子、大野澤歩美、善積克、櫻田忍、溝口広一、第 57 回日本薬学会東北支部大会、仙台、2018 年 10 月。
269. μ 受容体作動薬の末梢性抗搔痒作用、岩間美佐都、竹田詩織、福原直也、渡辺千寿子、善積克、櫻田忍、溝口広一、第 57 回日本薬学会東北支部大会、仙台、2018 年 10 月。
270. Involvement of the Spinal Release of Histamine on Nociceptive Behaviors Induced by Spermine. Hirokazu Mizoguchi, Chizuko Watanabe, Takafumi Hayashi, Yoko Namioka, Hiroyuki Watanabe, Toru Orito, Masaru Yoshizumi, Kenji Onodera, Shinobu Sakurada, World Histamine Symposium 2018, Kobe, July 2018.
- *271. Identification of the μ -Opioid Receptor Splice Variants Involved in the Lack of Rewarding Effect for Amidino-TAPA, Hirokazu Mizoguchi, Maya Yoshioka, Chizuko Watanabe, Akira Otowa, Shinobu Sakurada, The 18th World Congress of Basic and Clinical Pharmacology, Kyoto, July 2018.
272. The Development of Mirror Image Pain in a Mouse Model of Inflammatory Pain, Chizuko Watanabe, Takafumi Sato, Akira Otowa, Tsukasa Sakurada, Shinobu Sakurada, Hirokazu Mizoguchi, The 18th World Congress of Basic and Clinical Pharmacology, Kyoto, July 2018.
273. 天然由来成分の抗かゆみ活性、芦部文一朗、松見繁、丸山徹也、溝口広一、櫻田忍、日本薬学会第 138 年会、金沢、2018 年 3 月。
- *274. 依存性のない新規鎮痛薬の探索、溝口広一、第 2 回仙台痛みフォーラム、仙台、2018 年 2 月。
275. クリプトコックスから見出したオリゴ DNA による気管支喘息の発症抑制効果、宮坂智充、川上和義、石井恵子、奥山(土橋)香織、川上佳織、増田千愛、河野資、高柳元明、高橋知子、大野勲、第 2 回東北医真菌研究会、仙台、2018 年 12 月。
276. 気管支肺上皮幹細胞を用いた急性好酸球性気道炎症の治療効果の検討、石井聖人、河野資、柏原若奈、平泉花菜、鈴木涼平、佐藤美菜香、宮坂智充、松尾平、高柳元明、大野勲、高橋知子、第 57 回日本薬学会東北支部大会、仙台、2018 年 10 月。
277. 喘息病態の性差に関与する樹状細胞サブセットの解析、鹿野さくら、宮坂智充、増田千愛、川上佳織、河野資、井ノ口仁一、高柳元明、高橋知子、大野勲、第 57 回日本薬学会東北支部大会、仙台、2018 年 10 月。
278. 新規 Toll-like receptor 9 アゴニストによる喘息気道炎症抑制効果の検討、宮坂智充、川上和義、石井恵子、奥山香織、佐藤光、川上佳織、増田千愛、佐藤佑樹、塩田哲也、野村俊樹、渡邊祐里絵、宮原杏奈、松本郁美、菅野恵美、丹野寛大、河野資、高柳元明、高橋知子、大野勲、アレルギー・好酸球研究会 2018、東京、2018 年 9 月。
279. 免疫寛容誘導に対する精神的ストレスの影響と喘息発症、河野資、大内竜介、宮坂智充、大河原雄一、高柳元明、高橋知子、大野勲、アレルギー・好酸球研究会 2018、東京、2018 年 9 月。
280. 女性喘息患者における Th2 型免疫応答の亢進に関与する Estradiol の役割、川上佳織、宮坂智充、増田千愛、河野資、高橋知子、高柳元明、大野勲、第 67 回日本アレルギー学会学術大会、千葉、2018 年 6 月。
281. 幼少期ストレスによる喘息発症モデル—幼少期ストレスと免疫寛容の抑制—、大内竜介、河野資、宮坂智充、大河原雄一、高柳元明、高橋知子、大野勲、第 67 回日本アレルギー学会学術大会、千葉、2018 年 6 月。
282. 女性ホルモン依存的 IL-5 産生の亢進に関与する CD103+ 樹状細胞の役割、宮坂智充、増田千愛、川上佳織、河野資、井ノ口仁一、高柳元明、高橋知子、大野勲、第 58 回日本呼吸器学会学術講演会、大阪、2018 年 4 月。
283. 幼少期ストレスによる喘息発症モデル—幼少期ストレスによる免疫寛容の抑制—、河野資、大内竜

法人番号	041004
プロジェクト番号	S1511001L

- 介、宮坂智充、大河原雄一、高柳元明、高橋知子、大野勲、第 58 回日本呼吸器学会学術講演会、大阪、2018 年 4 月。
284. 気管支喘息重症化の性差に關与する氣道上皮細胞の Estradiol 依存的機能変化、川上佳織、宮坂智充、増田千愛、河野資、高柳元明、高橋知子、大野勲、日本薬学会第 138 年会、金沢、2018 年 3 月。
285. 喘息病態における女性優位な Th2 型免疫応答を誘導する CD103+ 樹状細胞の機能亢進に關与する 17β -estradiol の役割、増田千愛、宮坂智充、川上佳織、河野資、高柳元明、高橋知子、大野勲、日本薬学会第 138 年会、金沢、2018 年 3 月。
- *286. 炎症性疼痛制御における methadone の特異的作用、込山麻美、渡辺千寿子、音羽 亮、櫻田 忍、溝口広一、第 68 回日本薬理学会北部会、山形、2017 年 9 月。
287. 難治性掻痒症治療薬 nalfurafine の末梢性抗掻痒作用、音羽 亮、渡辺千寿子、長瀬 博、櫻田 忍、溝口広一、第 68 回日本薬理学会北部会、山形、2017 年 9 月。
- *288. Effectiveness of amidino-TAPA against morphine-resistant neuropathic pain、溝口広一、渡辺千寿子、音羽 亮、櫻田 忍、第 60 回日本神経化学学会大会、仙台、2017 年 9 月。
- *289. Amidino-TAPA の神経障害性疼痛に対する有効性、溝口広一、渡辺千寿子、音羽 亮、櫻田 忍、第 4 回包括的緩和医療科学学術研究会・第 5 回 Tokyo 疼痛緩和次世代研究会合同研究会、東京、2017 年 8 月。
- *290. 炎症性疼痛下における各種麻薬性鎮痛薬における鎮痛効果とその耐性形成能、込山麻美、溝口広一、渡辺千寿子、音羽 亮、櫻田 忍、第 90 回日本薬理学会年会、長崎、2017 年 3 月。
291. Possible involvement of CD103+ dendritic cells in female-predominant Th2 priming in asthma. MIYASAKA Tomomitsu, MASUDA Chiaki, KAWAKAMI Kaori, INOKUCHI Jin-ichi, KAWANO Tasuku, TAKAYANAGI Motoaki, TAKAHASHI Tomoko, OHNO Isao、第 46 回日本免疫学会学術集会、仙台、2017 年 12 月。
292. Influence of sex-related difference in dendritic cells on female-predominant Th2 cytokine production in asthma. Tomomitsu Miyasaka, Chiaki Masuda, Kaori Kawakami, Tasuku Kawano, Jin-ichi Inokuchi, Tomoko Takahashi, Motoaki Takayanagi, Isao Ohno. The 27th Congress of Interasma Japan / North Asia, Kumamoto, 2017, October.
293. Early life stress increased the risk of adult-onset asthma through the inhibition of the development of respiratory tolerance in a murine model. Tasuku Kawano, Ryusuke Ouchi, Tomomitsu Miyasaka, Yuichi Ohkawara, Motoaki Takayanagi, Tomoko Takahashi, Isao Ohno. The 27th Congress of Interasma Japan / North Asia, Kumamoto, 2017, October.
294. Involvement of sex-related functions of dendritic cells in female-predominant allergic inflammation in asthma. Chiaki Masuda, Tomomitsu Miyasaka, Kaori Dobashi-Okuyama, Tasuku Kawano, Inokuchi Jin-ichi, Tomoko Takahashi, Motoaki Takayanagi, Isao Ohno. The 11th International Conference on Allergy, Asthma & Clinical Immunology, Edinburgh, 2017, September.
295. Male-dominant suppressive activity of CD8+ T cells on CD4+ T cells: assessing female-dominant allergic airway inflammation, Tomomitsu Miyasaka, Chihiro Ito, Kaori Dobashi-Okuyama, Chiaki Masuda, Toshiaki Kikuchi, Tasuku Kawano, Tomoko Takahashi, Motoaki Takayanagi, Isao Ohno. The 11th International Conference on Allergy, Asthma & Clinical Immunology, Edinburgh, 2017, September.
296. Sex-related differences in allergic asthma: possible involvement of CD103+ dendritic cells in enhanced Th2 cytokine production in females. Tomomitsu Miyasaka, Chiaki Masuda, Kaori Kawakami, Jin-ichi Inokuchi, Tasuku Kawano, Motoaki Takayanagi, Tomoko Takahashi, Isao Ohno. The 8th Congress of the International Society for Gender Medicine, Sendai, 2017, September.
297. The increased susceptibility to adult-onset asthma through the inhibition of the development of respiratory tolerance by early life stress. Tasuku Kawano, Ryusuke Ouchi, Tomomitsu Miyasaka, Yuichi Ohkawara, Tomoko Takahashi, Motoaki Takayanagi, Isao Ohno. The 11th International Conference on Allergy, Asthma & Clinical Immunology, Edinburgh, 2017, September.
298. 精神的ストレスによる喘息発症モデル-精神的ストレスによる免疫寛容の抑制-、河野 資、大内竜介、宮坂智充、大河原雄一、高柳元明、高橋知子、大野 勲、第 66 回日本アレルギー学会学術大会、東京、2017 年 6 月。

法人番号	041004
プロジェクト番号	S1511001L

299. 肥満という表現型は必ずしも喘息増悪と関係しない—マウス喘息モデルを用いた検討—、大河原雄二、宮坂智充、河野 資、高橋知子、大野 勲、第 66 回日本アレルギー学会学術大会、東京、2017 年 6 月。
300. 幼少期ストレスによる成人喘息発症モデル—幼少期ストレスによる免疫寛容の抑制—、河野 資、大内竜介、宮坂智充、大河原雄一、高柳元明、高橋知子、大野 勲、第 57 回呼吸器学会学術講演会、東京、2017 年 4 月。
- *301. 炎症性疼痛下における各種麻薬性鎮痛薬の鎮痛効果とその耐性形成能、込山麻美、溝口広一、渡辺千寿子、音羽 亮、櫻田 忍、第 67 回日本薬理学会北部会、札幌、2016 年 9 月。
302. Nalfurafine の末梢性抗搔痒作用、音羽 亮、溝口広一、渡辺千寿子、長瀬 博、櫻田 忍、第 89 日本薬理学会年会、横浜、2016 年 3 月。
303. Hemokinin-1 誘発性疼痛関連行動の発現機構、渡辺千寿子、溝口広一、音羽 亮、櫻田 忍、第 89 回日本薬理学会年会、横浜、2016 年 3 月。
- *304. Amidino-TAPA の非依存性に関わる μ オピオイド受容体スプライスバリエーションの探索、溝口広一、渡辺千寿子、音羽 亮、吉岡麻也、櫻田 忍、第 89 回日本薬理学会年会、横浜、2016 年 3 月。
305. Early life stress increased the risk of adult-onset asthma through the inhibition of the development of respiratory tolerance in murine model. OUCHI Ryusuke, KAWANO Tasuku, MIYASAKA Tomomitsu, OHKAWARA Yuichi, TAKAYANAGI Motoaki, TAKAHASHI Tomoko, OHNO Isao, 第 45 回日本免疫学会学術集会、宜野湾市、2016 年 12 月。
306. A novel Toll-like receptor 9 agonist derived from *Cryptococcus neoformans* attenuates asthmatic airway responses. MIYASAKA Tomomitsu, KAWAKAMI Kazuyoshi, ISHII Keiko, DOBASHI-OKUYAMA Kaori, NOMURA Toshiki, MASUDA Chiaki, WATANABE Yurie, MIYAHARA Anna, MATSUMOTO Ikumi, TAKAYANAGI Motoaki, TAKAHASHI Tomoko, OHNO Isao, 第 45 回日本免疫学会学術集会、宜野湾市、2016 年 12 月。
307. Sex-related differences in the interaction of CD4⁺ T cells with CD8⁺ T cells lead to female-dominant allergic airway inflammation. Tomomitsu Miyasaka, Chihiro Ito, Kaori Dobashi-Okuyama, Chiaki Masuda, Tasuku Kawano, Yuichi Ohkawara, Toshiaki Kikuchi, Motoaki Takayanagi, Isao Ohno, International Congress of Immunology, Melbourne, 2016, August.
308. 喘息増悪における μ オピオイド受容体遺伝子多型と臨床病態との相関、大野 勲、宮坂智充、中村 豊、宮田 敏、佐藤美希、高柳元明、下川宏明、山内広平、第 65 回日本アレルギー学会学術大会、東京、2016 年 6 月。
309. 精神的ストレスによる免疫寛容の抑制と喘息発症の感受性増大の機序、河野 資、大内竜介、吉田 仁美、宮坂智充、大河原雄一、高柳元明、大野 勲、第 65 回日本アレルギー学会学術大会、東京、2016 年 6 月。
310. 幼少期ストレスによる免疫寛容の抑制と喘息発症リスクの増大、大内竜介、河野 資、吉田 仁美、新田典秀、宮坂智充、大河原雄一、高柳元明、大野 勲、第 56 回呼吸器学会学術講演会、京都、2016 年 4 月。
311. 重症喘息における精神的ストレスの関与～精神的ストレスによる免疫寛容の抑制と Th17 細胞の分化誘導～、河野 資、下田奈々、加羽香澄、大内竜介、新田典秀、宮坂智充、大河原雄一、高柳元明、高橋知子、大野 勲、第 55 回日本薬学会東北支部会、郡山、2016 年 9 月。
312. ラベンダーオイルの末梢局所投与によるパクリタキセル誘発性末梢神経障害性疼痛抑制効果の検討、勝山 壮、音羽 亮、倉本敬二、櫻田 忍、第 22 回日本未病システム学会学術総会、札幌、2015 年 10 月。
313. 当院における入院患者を対象としたアロマトリートメント(精油成分)による疼痛緩和作用の検討<第一報>、真井健吾、椎崎正秀、前間邦生、楠直子、池末いづみ、桑波田日香里、勝山 壮、小松 生明、櫻田 司、櫻田 忍、第 9 回日本緩和医療薬学会年会、横浜、2015 年 10 月。
- *314. 多発性硬化症疼痛に対するオピオイド性鎮痛薬の効果、溝口広一、渡辺千寿子、音羽 亮、長瀬 博、櫻田 忍、第 9 回日本緩和医療薬学会年会、横浜、2015 年 10 月。
- *315. Amidino-TAPA の非依存性に関わる μ オピオイド受容体スプライスバリエーションの探索、溝口広一、渡辺千寿子、音羽 亮、吉岡麻也、櫻田 忍、第 45 回日本神経精神薬理学会・第 37 回日本生物学的精神医学会合同年会、東京、2015 年 9 月。
316. 難治性搔痒症治療薬 nalfurafine の末梢性抗搔痒作用、音羽 亮、小笠原蓉子、新井田隆宏、溝口

法人番号	041004
プロジェクト番号	S1511001L

<p><u>広一、渡辺千寿子、勝山 壮、長瀬 博、櫻田 忍</u>、第 66 回日本薬理学会北部会、富山、2015 年 9 月。</p> <p>317. Psychological stress increases susceptibility to the development of asthma through inhibiting respiratory tolerance. <u>KAWANO Tasuku</u>, <u>ISHIGAKI Takahiro</u>, <u>Nitta Norihide</u>, <u>MIYASAKA Tomomitsu</u>, <u>OHKAWARA Yuichi</u>, <u>TAKAYANAGI Motoaki</u>, <u>OHNO Isao</u>. 第 44 回日本免疫学会総会、札幌、2015 年 11 月。</p> <p>318. 気管支喘息における μ オピオイド受容体一塩基多型と臨床病態との相関、<u>大野 勲</u>、<u>宮坂智充</u>、<u>中村 豊</u>、<u>宮田 敏</u>、<u>佐藤美希</u>、<u>森 拓夢</u>、<u>川島祐里佳</u>、<u>高柳元明</u>、<u>下川宏明</u>、<u>山内広平</u>、第 101 回日本呼吸器学会東北地方会、福島、2015 年 10 月。</p> <p>319. 気管支喘息における μ オピオイド受容体一塩基多型と臨床病態との相関、<u>大野 勲</u>、<u>宮坂智充</u>、<u>中村 豊</u>、<u>宮田 敏</u>、<u>佐藤美希</u>、<u>森 拓夢</u>、<u>川島祐里佳</u>、<u>高柳元明</u>、<u>川島宏明</u>、<u>山内広平</u>、第 101 回日本呼吸器学会東北地方会、福島市、2015 年 10 月。</p> <p>320. 幼少期ストレスによる免疫寛容の抑制を介した喘息発症の機序、<u>新田典秀</u>、<u>河野 資</u>、<u>宮坂智充</u>、<u>大河原雄一</u>、<u>高柳元明</u>、<u>大野 勲</u>、第 54 回日本薬学会東北支部大会、矢巾、2015 年 9 月。</p> <p>321. 精神的ストレスによる免疫寛容の抑制と喘息発症の感受性増大の機序—ストレス誘導性グルココルチコイドの役割—、<u>河野 資</u>、<u>石垣貴裕</u>、<u>新田典秀</u>、<u>吉田仁美</u>、<u>宮坂智充</u>、<u>大河原雄一</u>、<u>高柳元明</u>、<u>大野 勲</u>、第 42 回日本神経内分泌学会、仙台、2015 年 9 月。</p> <p>322. 肥満による気管支喘息増悪と内臓脂肪組織の免疫代謝調節機構の変化、<u>大河原雄一</u>、<u>岩田敏信</u>、<u>宮坂智充</u>、<u>河野 資</u>、<u>石垣貴裕</u>、<u>伊藤ひろ</u>、<u>佐藤美希</u>、<u>増田千愛</u>、<u>高柳元明</u>、<u>大野 勲</u>、第 64 回日本アレルギー学会学術大会、東京、2015 年 5 月。</p> <p>323. 精神的ストレスによる免疫寛容の抑制と喘息発症の感受性増大の機序、<u>河野 資</u>、<u>石垣貴裕</u>、<u>新田典秀</u>、<u>宮坂智充</u>、<u>大河原雄一</u>、<u>高柳元明</u>、<u>大野 勲</u>、第 64 回日本アレルギー学会学術大会、東京、2015 年 5 月。</p> <p>324. 精神的ストレスによる免疫寛容の抑制と喘息発症の感受性の増大、<u>河野 資</u>、<u>石垣貴裕</u>、<u>宮坂智充</u>、<u>大河原雄一</u>、<u>菊地利明</u>、<u>高柳元明</u>、<u>大野 勲</u>、第 55 回呼吸器学会学術講演会、東京、2015 年 4 月。</p>

<研究成果の公開状況> (上記以外)

シンポジウム・学会等の実施状況、インターネットでの公開状況等
<既に実施しているもの>

《平成 31 年度 創薬研究センターシンポジウム》開催日：平成 31 年 6 月 22 日(土)

研究成果発表(口頭7題)

1. 麻薬類に対するワクチンの開発研究
(名取 良浩、Candy S. Hwang、君嶋 敦、Lauren C. Smith、Margaret E. Olson、Beverly Ellis、Bin Zhou、吉村 祐一、Kim D. Janda)
2. 抗原虫活性を有するクリスタキセニシン A の全合成研究
(分銅 和香、中井 啓陽、Sayar Noel、成田 紘一、吉村 祐一、渡邊 一弘)
3. 新規三次元疎水性構造単位を用いた医薬分子設計のコンセプトとその実証
(遠藤 泰之、太田 公規、皆瀬 麻子)
4. プロポリス含有健康食品による薬物相互作用解析
(熊谷 健、星 利香、長田 大輝、渡邊 夢実、進藤 佐和子、永田 清)
5. 間質性膀胱炎モデルラットの確立とガバペンチンの有効性(善積 克、渡辺 千寿子、溝口 広一)
6. 好中球・好酸球混合型喘息における精神的ストレスの関与
～精神的ストレスによる免疫寛容の抑制とT細胞分化誘導～
(河野 資、石井 聖人、萩庭 幹太、山口 祐式、佐藤 伸輔、宮坂 智充、大河原 雄一、高柳 元明、高橋 知子、大野 勲)
7. 脊髄 Angiotensin 系の不均衡が糖尿病性神経障害性疼痛に寄与する
(山縣 涼太、根本 互、小湊 佳輝、中川西 修、八百板 富紀枝、丹野 孝一)

研究成果発表(ポスター7題)

1. 4'置換スクレオシド誘導体の合成と光学分割の検討

法人番号	041004
プロジェクト番号	S1511001L

- (遠藤 柚季乃、若松 秀章、伊藤 恭平、斎藤 有香子、名取 良浩、吉村 祐一)
- スクアレン合成酵素阻害剤 ビサボスクアール A の合成研究
(吉田 昌太郎、成田 紘一、渡邊 一弘、吉村 祐一)
 - m-カルボラン含有トリメトキシフェニル誘導体の抗腫瘍活性(皆瀬 麻子、太田 公規、遠藤 泰之)
 - リン酸化エストロゲン受容体の免疫細胞における役割の探索
(進藤 佐和子、熊谷 健、永田 清、根岸 正彦)
 - 炎症性疼痛下における TRPV1 チャネルの機能的変化
(渡辺 千寿子、佐藤 駿文、善積 克、櫻田 忍、溝口 広一)
 - 気管支喘息の増悪における μ オピオイド受容体の一塩基多型の関与
(川上 佳織、宮坂 智充、菊池 かなみ、千丸 正尊、原田 真裕美、竹内 圭亮、杉本 大幸、佐藤 美希、河野 資、曾良 一郎、中村 豊、目時 弘仁、高柳 元明、高橋 知子、大野 勲)
 - 加齢性男性性腺機能低下症候群動物モデルの作製
(佐久間 若菜、中川西 修、根本 互、小平 貴代、八百板 富紀枝、丹野 孝一)

特別講演3題

- オレキシン受容体選択的リガンドの設計・合成とその薬理作用
(筑波大学睡眠研究機構・長瀬 博 特命教授)
- 末梢性神経障害性疼痛治療薬としてのニコチン受容体作動薬の可能性
(和歌山県立医科大学医学部・岸岡 史郎 特別顧問)
- 薬物作用を本質的に紐解くための技術革新とその応用
(星薬科大学 薬理研究室・成田 年 主任教授)

《平成30年度 創薬研究センターシンポジウム》開催日：平成30年6月23日(土)

研究成果発表(口頭7題)

- 4'-置換 4'-チオリボヌクレオシド誘導体の合成研究
(前田璃音、若松秀章、庄子希望、名取良浩、吉村祐一)
- ベンゾオキサゾール骨格を有するセスキテルペン ナキジノール類の合成
(武田由貴、中井啓陽、成田紘一、加藤 正)
- 化学酵素的手法による Swaminathan-Narayanan ケトン型キラル合成素子の創製
(猪股 浩平、成田 沙奈美、庄子 佳穂、三浦 亜里沙、野田 貴子、遠藤 泰之)
- Mirror image pain発現機構におけるNMDA受容体の関与
(渡辺千寿子、田代 隆、大野澤歩美、音羽 亮、善積 克、櫻田 忍、溝口広一)
- 嗅球摘出マウスにおけるAMP-Activated Protein Kinase (AMPK) の活性化を介した抗うつ効果
(小平 貴代、中川西 修、根本 互、高橋 浩平、佐久間 若菜、八百板 富紀枝、丹野 孝一)
- 生体内におけるリン酸化エストロゲン受容体の脳内における新規機能の探索
(進藤 佐和子、Hao Hu、熊谷 健、永田 清、根岸 正彦)
- 気管支喘息における臨床病態の増悪に関与する μ オピオイド受容体の一塩基多型
(宮坂智充、佐藤美希、中村豊、宮田敏、目時弘仁、川上佳織、河野資、下川宏明、高柳元明、山内広平、高橋知子、大野勲)

研究成果発表(ポスター7題)

- 2-デオキシ-2-フルオロフコース誘導体の合成研究
(名取良浩、草野宏光、相原瞳、斎藤有香子、若松秀章、吉村祐一)
- クリスタキセニンAの全合成に向けたOxy-Cope環化前駆体の合成研究
(渡邊 一弘、中井 啓陽、Sayar Noel、成田 紘一、吉村 祐一)
- 新規フェニルアゾトロポロン誘導体の細胞増殖抑制活性とメカニズム解析
(皆瀬麻子、氣仙拓也、佐藤大輔、太田公規、遠藤泰之)
- 神経障害性疼痛モデルラットにおけるバルプロ酸の鎮痛機構—脊髄グルタミン酸放出の調節—
(善積克、林田健一郎、James C. Eisenach、渡辺千寿子、溝口広一)
- 断続的レム断眠ストレス負荷誘発性衝動性様症状における海馬アドレナリン α 2A受容体の関与
(八百板富紀枝、川浪啓豪、今泉宏紀、根本互、中川西修、丹野孝一)
- CYP遺伝子発現誘導を引き起こす健康食品の検討(熊谷 健、渡邊夢実、進藤佐和子、永田 清)
- 急性好酸球性気道炎症に対する気管支肺胞上皮幹細胞の抗炎症効果の検討

法人番号	041004
プロジェクト番号	S1511001L

(石井聖人、河野資、柏原若奈、平泉花菜、鈴木涼平、佐藤美菜香、宮坂智充、高柳元明、大野勲、高橋知子)

特別講演3題

1. アジア圏海洋生物由来生物活性物質を創薬シードとする化学的研究
(明治薬科大学薬学部・薬化学・齋藤 直樹 教授)
2. ペプチドミメティックを基盤とした中分子創薬研究
(東京医科歯科大学・生体材料工学研究所・玉村 啓和 教授)
3. 環状デブシペプチド天然物の全合成、類縁体合成、活性評価、および三次元構造解析
(東北大学大学院薬学研究科・反応制御化学・土井 隆行 教授)

《平成29年度 創薬研究センターシンポジウム》開催日：平成29年6月17日(土)

研究成果発表(口頭7題)

1. トロポロン骨格を有する新規キサンチンオキシダーゼ阻害剤の探索とそのメカニズム解析
(佐藤大輔、氣仙拓也、太田公規、遠藤泰之)
2. エニナミドの閉環メタセシスによる複素環化合物の合成
(若松秀章、高橋将典、小椋玲奈、諏訪純一、吉村祐一)
3. カンナビノイド受容体に親和性を有するフェルギネン B の全合成
(成田紘一、加藤友哉、吉村祐一、加藤 正)
4. 免疫細胞におけるリン酸化エストロゲン受容体の機能的役割の解析 (進藤佐和子、根岸正彦)
5. 脊髄 Angiotensin 系は糖尿病性神経障害性疼痛の治療標的になり得るか？
(根本 互、小湊佳輝、山縣涼太、中川西修、八百板富紀枝、丹野孝一)
6. 多発性硬化症疼痛に対する麻薬性鎮痛薬の効果 (溝口広一、渡辺千寿子、音羽 亮、櫻田 忍)
7. 幼少期ストレスによる喘息発症モデル～幼少期ストレスによる免疫寛容の抑制～
(大内竜介、河野 資、宮坂智充、大河原雄一、高柳元明、高橋知子、大野 勲)

研究成果発表(ポスター8題)

1. カルボラン含有新規選択的エストロゲン受容体抑制薬(SERD)化合物の探索
(皆瀬麻子、吉見友弘、太田公規、遠藤泰之)
2. 3'-デオキシ-4'-チオヌクレオシド誘導体の合成
(安達桃子、若松秀章、伊藤 文、齋藤有香子、名取良浩、吉村祐一)
3. キセニアラクトール骨格構築法の開発 (渡邊一弘、高橋央宜、吉村祐一、加藤 正)
4. 健康食品による CYP 遺伝子発現作用の *in vivo* 評価 (熊谷 健、佐々木崇光、永田 清)
5. 更年期うつ病モデルマウスにおける新規選択的エストロゲン受容体モジュレーター BE360 の抗うつ効果 (佐久間若菜、中川西修、根本 互、小平貴代、八百板富紀枝、小川卓巳、太田公規、遠藤泰之、丹野孝一)
6. 糖尿病性神経障害性疼痛に対するアンジオテンシン(1-7)の抑制効果
(山縣涼太、根本 互、小湊佳輝、中川西修、八百板富紀枝、丹野孝一)
7. 炎症性疼痛下における麻薬性鎮痛薬の鎮痛効果ならびに鎮痛耐性形成
(込山麻美、渡辺千寿子、音羽 亮、櫻田 忍、溝口広一)
8. 精神的ストレスによるアレルギー性気道炎症の増悪における中枢性ヒスタミン受容体の関与
(岩見俊哉、宮坂智充、増田千愛、河野 資、川上佳織、高柳元明、高橋知子、大野 勲)

特別講演3題

1. オートファジー欠損マウスからわかったこと (新潟大学大学院医歯学総合研究科・小松雅明 教授)
2. サイアタンジテルペノイドの不斉全合成と生物活性 (早稲田大学理工学術院・中田雅久 教授)
3. 痛みメモリーを消去するLPAシグナル制御創薬研究
(長崎大学大学院医歯薬学総合研究科・植田弘師 教授)

《平成28年度 創薬研究センターシンポジウム》開催日：平成28年6月18日(土)

研究成果発表(口頭7題)

1. 気管支喘息における Th2 サイトカイン産生の性差に関与する樹状細胞の役割
(増田千愛、宮坂智充、岩見俊哉、河野 資、大河原雄一、井ノ口仁一、高柳元明、高橋知子、大野 勲)
2. 神経障害性疼痛に対する麻薬性鎮痛薬ならびに新規鎮痛薬の効果

法人番号	041004
プロジェクト番号	S1511001L

(溝口広一、渡辺千寿子、音羽 亮、櫻田 忍)

3. 嗅球摘出マウスにおける脳内ドパミン神経機能の変化に対する三環系抗うつ薬 Imipramine の影響 (高橋浩平、中川西修、根本 互、菊地恵理、佐久間若菜、八百板富紀枝、丹野孝一)
4. 健康食品の CYP 活性に対する網羅的評価 (熊谷 健、佐藤 裕、佐々木崇光、永田 清)
5. 3'-デオキシ-4'-チオヌクレオシドの立体選択的合成 (安達桃子、伊藤 文、名取良浩、若松秀章、吉村祐一)
6. 変異 AR に対するカルボラン含有グリセロール誘導体の活性評価 (皆瀬麻子、阿部孝俊、太田公規、小田彰史、遠藤泰之)
7. ジスルフィド結合を有する大環状デプシペプチド FR901375 の全合成 (加藤友哉、成田紘一、加藤 正)

研究成果発表(ポスター8題)

1. 幼少期ストレスによる喘息発症リスクの増大—ストレスによる免疫寛容の抑制— (大内竜介、河野 資、新田典秀、宮坂智充、大河原雄一、高柳元明、高橋知子、大野勲)
2. 炎症性疼痛下における各種麻薬性鎮痛薬の鎮痛効果とその耐性形成能 (込山麻美、溝口広一、渡辺千寿子、音羽 亮、櫻田 忍)
3. 長期粉末食飼育誘発性マウス異常行動に対する ADHD 治療薬の効果 (八百板富紀枝、柴田 楓、菅原 彩、土谷昌広、荒井裕一朗、根本 互、中川西修、只野 武、丹野孝一)
4. レチノイン酸レセプター、RAR/RXR を介した CYP26A1 遺伝子発現誘導評価系の構築 (塩谷安奈里、渡邊美智子、角田駿哉、若生俊也、佐々木崇光、熊谷 健、永田 清)
5. CYP3A4 遺伝子転写活性化の新規分子機構の解明 (小田桐玲生、佐々木崇光、熊谷 健、永田 清)
6. スタブジン誘導体の合成研究 (伊藤恭平、菅野裕也、齋藤華子、若松秀章、名取良浩、齋藤有香子、吉村祐一)
7. 高尿酸血症改善へ向けた新規 XO 阻害剤の創製 (太田公規、石井康博、佐藤 匠、遠藤泰之)
8. 生合成仮説を基軸とした(+)-リファガールの全合成 (渡辺拓実、神島堯明、菊地拓也、成田紘一、加藤 正)

特別講演(3題)

1. 二重活性化型触媒の創製を基盤とする新規分子骨格構築反応の開発 (大阪大学産業科学研究所・笹井宏明 教授)
2. 新しい天然物を獲る—休眠遺伝子を活用する天然物の創出— (東北大学大学院薬学研究科・大島吉輝 教授)
3. 核酸系医薬におけるフッ素置換基の役割 (北海道大学大学院薬学研究院・松田 彰 教授)

《共催講演会等》

1. セミナー(平成31年3月4日) 井上 誠 准教授 (University of Illinois at Urbana-Champaign) 状況に応じた免疫システム変調と中枢神経機能変調—多発性硬化症研究をもとに
2. 特別講演会(平成29年1月13日) 今道友純 主任研究員 (Frederick National Laboratory for Cancer Research) IL-27のHIV抑制機構とDNA刺激によるIFN- λ 1の産生
3. 特別講演会(平成28年11月7日) 藤井秀明 教授 (北里大学薬学部) δ オピオイド受容体逆作動薬における窒素置換基に関する構造活性相関研究
4. 特別講演会(平成28年10月21日) 渡邊廣行 研究員 (Uppsala University) 脊髄オピオイド系が外傷性脳損傷後の姿勢非対称性に関与する可能性
5. 特別講演会(平成28年10月18日) 濱村賢吾 助教 (第一薬科大学) “生体リズム”および“血清中エクソソーム”に着目した神経障害性疼痛の病態解明
6. 特別講演会(平成27年10月21日) Prof. David R. Williams (Indiana University)

《インターネットでの公開状況》

本研究プロジェクトの目的・研究計画概要 (<http://www.tohoku-mpu.ac.jp/about/a20/>) および平成27-29年度の「研究進捗状況報告書の概要」 (<http://www.tohoku-mpu.ac.jp/wp/wp-content/uploads/2019/05/b7cbd27efd694b40bd87cdb185aa7dd7.pdf>) を公開している。

<これから実施する予定のもの>

本研究プロジェクトの「研究成果報告書」を公開する予定である。

法人番号	041004
プロジェクト番号	S1511001L

14 その他の研究成果等

《特許出願》

- *1. 発明の名称: リファガールの類縁体、及びリファガール又はその類縁体を含む多標的キナーゼ阻害剤
 発明者: 石岡千加史、西條 憲、加藤 正、成田紘一 (出願人: 国立大学法人 東北大学)
 特許出願番号: 特願 2017-091712 (出願日 平成 29 年 5 月 2 日)
 特許公開番号: 現時点では未公開
- *2. 発明の名称: デプシペプチド類化合物の製造中間体及びその製造方法(Method for Producing Depsipeptide Compounds and Synthetic Intermediates Therefor)
 発明者: 石岡千加史、西條 憲、加藤 正、成田紘一 (出願人: 国立大学法人 東北大学)
 国際特許出願番号: PCT/JP2017/001140 (出願日 2017 年 01 月 13 日)
 国際特許公開番号: WO2017/122822 (公開日 2017 年 7 月 20 日).

《企業からの依頼講演》

- 3. 抗ウイルス剤探索を目的としたヌクレオシド誘導体合成法の開発、吉村祐一、富士フィルム富山事業所社内ゼミ、富山、2017 年 8 月 22 日.

15 「選定時」及び「中間評価時」に付された留意事項及び対応

<「選定時」に付された留意事項>

アゴニスト/アンタゴニストバランスなどの問題は、分子動力学専門家と共同で効率的な解決を模索して欲しい。

<「選定時」に付された留意事項への対応>

分子動力学の専門家である小田彰史教授(名城大学薬学部)との共同研究を開始し、エストロゲン受容体 β 選択性やアゴニスト/アンタゴニスト制御に関して、設計・合成した化合物と受容体のドッキングシミュレーションを含む結果を本研究期間中に論文および学会発表するなど(論文*56, 67, 94, 96, 97、学会*164)、協力体制を作り、効率的に研究を推進している。

<「中間評価時」に付された留意事項>

該当なし

<「中間評価時」に付された留意事項への対応>

留意事項としての指摘はなかったが、評価コメントの中で①若手研究員・大学院生のテニュアトラック制度導入や②AMED(日本医療研究開発機構)の積極的な活用と連携を視野に入れた研究の展開に期待が示されていた。テニュアトラック制度の導入に関しては本研究プロジェクトのプログラム中に取り入れることができなかったが、今後全学上げて取り組むべき課題であると認識している。また、本研究プロジェクトで非常に優れた化合物を見出したので、今後は AMED 等と連携しながらアンメット・メディカル・ニーズに応えられる医薬品の創出を目指していきたい。

法人番号	041004
プロジェクト番号	S1511001L

16 施設・装置・設備・研究費の支出状況(実績概要)

(千円)

年度・区分		支出額	内 訳						備 考
			法 人 負 担	私 学 助 成	共同研 究機関 負担	受託 研究等	寄付金	その他()	
平成 27 年度	施 設	0							
	装 置	0							
	設 備	81,206	27,071	54,135					
	研究費	21,000	11,179	9,821					
平成 28 年度	施 設	0							
	装 置	0							
	設 備	0							
	研究費	24,799	15,918	8,881					
平成 29 年度	施 設	0							
	装 置	0							
	設 備	0							
	研究費	29,041	19,041	10,000					
平成 30 年度	施 設	0							
	装 置	0							
	設 備	0							
	研究費	21,000	11,750	9,250					
平成 31 年度	施 設	0							
	装 置	0							
	設 備	0							
	研究費	21,000	16,106	4,894					
総 額	施 設	0	0	0	0	0	0	0	
	装 置	0	0	0	0	0	0	0	
	設 備	81,206	27,071	54,135	0	0	0	0	
	研究費	116,840	73,994	42,846	0	0	0	0	
総 計		198,046	101,065	96,981	0	0	0	0	

法人番号

041004

17 施設・装置・設備の整備状況（私学助成を受けたものはすべて記載してください。）

《施設》（私学助成を受けていないものも含め、使用している施設をすべて記載してください。）（千円）

施設名称	整備年度	研究施設面積	研究室等数	使用者数	事業経費	補助金額	補助主体
創薬研究センター	H18	2,108㎡	7教室	73名			

※ 私学助成による補助事業として行った新增築により、整備前と比較して増加した面積

㎡

《装置・設備》（私学助成を受けていないものは、主なもののみを記載してください。）

（千円）

装置・設備の名称	整備年度	型番	台数	稼働時間数	事業経費	補助金額	補助主体
（研究設備） リアルタイム細胞アナライザー	H27	xCELLigence RTCA SPシステム	1式	1950 h h h	13,413	8,942	私学助成
超高感度等温適定型 カロリメーター	H27	Affinity ITC Auto LV オートサンプリングシステム	1式	93 h h	32,821	21,880	私学助成
正立型共焦点レーザー 顕微鏡システム	H27	Ni-E,C2+	1式	1580 h h h	20,552	13,701	私学助成
擦過行動リアルタイム 定量化システム	H27	SCLABA-Realシステム	1式	434 h h	8,916	5,943	私学助成
全自動磁気細胞分離装置	H27	130-092-545	1式	438 h h	5,504	3,669	私学助成

18 研究費の支出状況

【テーマ1】

（千円）

年 度	平成 27 年度			
小 科 目	支 出 額	積 算 内 訳		
		主 な 使 途	金 額	主 な 内 容
教 育 研 究 経 費 支 出				
消 耗 品 費	5,518	薬品・実験材料・その他	5,518	試薬・研究試料・実験用品・文房具・OA用品
光 熱 水 費	0		0	
通信運搬費	9	郵便・運搬	9	サンプル等配送 等
印刷製本費	35	論文等印刷	35	論文印刷、文献複写
旅費交通費	777	学会・研究発表	777	学会参加、研究打合せ
報酬・委託料	261	委託・支払報酬	261	分析・検査、英文校正、講演料等
(賃借料)	5	設備賃借費	5	容器使用料
(修繕費)	106	設備修繕	106	機器修理、メンテナンス
計	6,711		6,711	
ア ル バ イ ト 関 係 支 出				
人件費支出 (兼務職員)				
教育研究経費支出				
計	0			
設 備 関 係 支 出(1個又は1組の価格が500万円未満のもの)				
教育研究用機器備品	2,289	機械器具	2,289	有機溶媒精製装置 他
図 書				
計	2,289		2,289	
研 究 ス タ ッ フ 関 係 支 出				
リサーチ・アシスタント				
ポスト・ドクター				
研究支援推進経費				
計	0		0	

法人番号

041004

【テーマ1】

(千円)

年 度	平成 28 年度			
小 科 目	支 出 額	積 算 内 訳		
		主 な 使 途	金 額	主 な 内 容
教 育 研 究 経 費 支 出				
消 耗 品 費	6,077	薬品・実験材料・その他	6,077	試薬・研究試料・実験用品・文房具・OA用品
光 熱 水 費	0		0	
通信運搬費	4	郵便・運搬	4	サンプル等配送 等
印刷製本費	120	論文等印刷	120	論文印刷・文献複写
旅費交通費	380	学会・研究発表	380	学会参加・研究打合せ
報酬・委託料	463	委託・支払報酬	463	分析・検査、英文校正、講演料等
(賃借料)	5	設備賃借費	5	容器使用料
(修繕費)	570	設備修繕	570	機器修理、メンテナンス
計	7,619		7,619	
ア ル バ イ ト 関 係 支 出				
人件費支出 (兼務職員)				
教育研究経費支出				
計	0		0	
設 備 関 係 支 出(1個又は1組の価格が500万円未満のもの)				
教育研究用機器備品	1,381	機械器具	1,381	スターラー付低温恒温槽 他
図 書				
計	1,381		1,381	
研 究 ス タ ッ フ 関 係 支 出				
リサーチ・アシスタント				
ポスト・ドクター	3,799	研究補助	3,799	学内1人
研究支援推進経費				
計	3,799		3,799	

【テーマ1】

(千円)

年 度	平成 29 年度	積 算 内 訳		
小 科 目	支 出 額	主 な 内 容		
		主 な 使 途	金 額	
教 育 研 究 経 費 支 出				
消 耗 品 費	6,718	薬品・実験材料・その他	6,718	試薬・研究試料・実験用品・文房具・OA用品
光 熱 水 費	0		0	
通信運搬費	3	郵便・運搬	3	サンプル等配送 等
印刷製本費	112	論文等印刷	112	論文印刷・文献複写
旅費交通費	619	学会・研究発表	619	学会参加・研究打合せ
報酬・委託料	209	委託	209	分析・検査、英文校正
(賃借料)	1	設備賃借費	1	容器使用料
(修繕費)	21	設備修繕	21	機器修理、メンテナンス
計	7,683		7,683	
ア ル バ イ ト 関 係 支 出				
人件費支出 (兼務職員)				
教育研究経費支出				
計	0		0	
設 備 関 係 支 出(1個又は1組の価格が500万円未満のもの)				
教育研究用機器備品	1,317	機械器具	1,317	薬用冷蔵ショーケース 他
図 書				
計	1,317		1,317	
研 究 ス タ ッ フ 関 係 支 出				
リサーチ・アシスタント				
ポスト・ドクター	8,041	研究補助	8,041	学内2人
研究支援推進経費				
計	8,041		8,041	

法人番号

041004

【テーマ1】

(千円)

年 度	平成 30 年度			
小 科 目	支 出 額	積 算 内 訳		
		主 な 使 途	金 額	主 な 内 容
教 育 研 究 経 費 支 出				
消 耗 品 費	6,880	薬品・実験材料・その他	6,880	試薬・研究試料・実験用品・文房具・OA用品
光 熱 水 費	0		0	
通信運搬費	2	郵便・運搬	2	サンプル等配送 等
印刷製本費	0		0	
旅費交通費	91	学会・研究発表	91	学会参加・研究打合せ
報酬・委託料	71	委託	71	分析・検査、英文校正
(賃借料)	4	設備賃借費	4	容器使用料
(修繕費)	528	設備修繕	528	機器修理、メンテナンス
計	7,576		7,576	
ア ル バ イ ト 関 係 支 出				
人件費支出 (兼務職員)				
教育研究経費支出				
計	0		0	
設 備 関 係 支 出(1個又は1組の価格が500万円未満のもの)				
教育研究用機器備品	1,424	機械器具	1,424	低温循環水槽クールマンパル 他
図 書				
計	1,424		1,424	
研 究 ス タ ッ フ 関 係 支 出				
リサーチ・アシスタント				
ポスト・ドクター				
研究支援推進経費				
計	0		0	

【テーマ1】

(千円)

年 度	平成 31 年度			
小 科 目	支 出 額	積 算 内 訳		
		主 な 使 途	金 額	主 な 内 容
教 育 研 究 経 費 支 出				
消 耗 品 費	8,802	薬品・実験材料・その他	8,801	試薬・研究試料・実験用品・文房具・OA用品
光 熱 水 費	0		0	
通信運搬費	3	郵便・運搬	3	サンプル等配送 等
印刷製本費	0		0	
旅費交通費	0		0	
報酬・委託料	18	委託	18	分析・検査、英文校正
(賃借料)	3	設備賃借費	3	容器使用料
(修繕費)	174	設備修繕	174	機器修理、メンテナンス
計	9,000		8,999	
ア ル バ イ ト 関 係 支 出				
人件費支出 (兼務職員)				
教育研究経費支出	0		0	
計	0		0	
設 備 関 係 支 出(1個又は1組の価格が500万円未満のもの)				
教育研究用機器備品	0		0	
図 書	0		0	
計	0		0	
研 究 ス タ ッ フ 関 係 支 出				
リサーチ・アシスタント	0		0	
ポスト・ドクター	0		0	
研究支援推進経費	0		0	
計	0		0	

(様式2)

法人番号

041004

【テーマ2】

(千円)

年 度	平成 27 年度			
小 科 目	支 出 額	積 算 内 訳		
		主 な 使 途	金 額	主 な 内 容
教 育 研 究 経 費 支 出				
消 耗 品 費	4,670	薬品・実験材料・その他	4,670	試薬・研究試料・実験用品・文房具・OA用品
光 熱 水 費	0		0	
通信運搬費	2	郵便・運搬	2	サンプル等配送 等
印刷製本費	65	論文等印刷	65	論文印刷・文献複写
旅費交通費	0		0	
報酬・委託料	196	委託・支払報酬	196	分析・検査、英文校正、講演料等
(賃借料)	0		0	
(修繕費)	13	設備修繕	13	機器修理、メンテナンス
計	4,946		4,946	
ア ル バ イ ト 関 係 支 出				
人件費支出 (兼務職員)				
教育研究経費支出	0		0	
計	0		0	
設 備 関 係 支 出(1個又は1組の価格が500万円未満のもの)				
教育研究用機器備品	1,054	機械器具	1,054	ダイヤフラム型真空ポンプ 他
図 書				
計	1,054		1,054	
研 究 ス タ ッ フ 関 係 支 出				
リサーチ・アシスタント				
ポスト・ドクター				
研究支援推進経費				
計	0		0	

【テーマ2】

(千円)

年 度	平成 28 年度			
小 科 目	支 出 額	積 算 内 訳		
		主 な 使 途	金 額	主 な 内 容
教 育 研 究 経 費 支 出				
消 耗 品 費	5,684	薬品・実験材料・その他	5,684	試薬・研究試料・実験用品・文房具・OA用品
光 熱 水 費	0		0	
通信運搬費	0		0	
印刷製本費	79	論文等印刷	79	論文印刷・文献複写
旅費交通費	0		0	
報酬・委託料	124	委託・支払報酬	124	分析・検査、英文校正、講演料等
(賃借料)	0		0	
(修繕費)	113	設備修繕	113	機器修理、メンテナンス
計	6,000		6,000	
ア ル バ イ ト 関 係 支 出				
人件費支出 (兼務職員)				
教育研究経費支出				
計	0		0	
設 備 関 係 支 出(1個又は1組の価格が500万円未満のもの)				
教育研究用機器備品				
図 書				
計	0		0	
研 究 ス タ ッ フ 関 係 支 出				
リサーチ・アシスタント				
ポスト・ドクター				
研究支援推進経費				
計	0		0	

【テーマ2】

(千円)

年 度	平成 29 年度			
小 科 目	支 出 額	積 算 内 訳		
		主 な 使 途	金 額	主 な 内 容
教 育 研 究 経 費 支 出				
消 耗 品 費	5,482	薬品・実験材料・その他	5,482	試薬・研究試料・実験用品・文房具・OA用品
光 熱 水 費	0		0	
通信運搬費	2	郵便・運搬	2	サンプル等配送 等
印刷製本費	59	論文等印刷	59	論文印刷・文献複写
旅費交通費	0		0	
報酬・委託料	423	委託・支払報酬	423	分析・検査、英文校正、振込手数料
(賃借料)	0		0	
(修繕費)	34	設備修繕	34	機器修理、メンテナンス
計	6,000		6,000	
ア ル バ イ ト 関 係 支 出				
人件費支出 (兼務職員)				
教育研究経費支出				
計	0		0	
設 備 関 係 支 出(1個又は1組の価格が500万円未満のもの)				
教育研究用機器備品				
図 書				
計	0		0	
研 究 ス タ ッ フ 関 係 支 出				
リサーチ・アシスタント				
ポスト・ドクター				
研究支援推進経費				
計	0		0	

【テーマ2】

(千円)

年 度	平成 30 年度			
小 科 目	支 出 額	積 算 内 訳		
		主 な 使 途	金 額	主 な 内 容
教 育 研 究 経 費 支 出				
消 耗 品 費	4,662	薬品・実験材料・その他	4,662	試薬・研究試料・実験用品・文房具・OA用品
光 熱 水 費	0		0	
通信運搬費	0		0	
印刷製本費	0		0	
旅費交通費	0		0	
報酬・委託料	3	委託	3	分析・検査、英文校正
(賃借料)	0		0	
(修繕費)	135	設備修繕	135	機器修理、メンテナンス
計	4,800		4,800	
ア ル バ イ ト 関 係 支 出				
人件費支出 (兼務職員)				
教育研究経費支出				
計	0		0	
設 備 関 係 支 出(1個又は1組の価格が500万円未満のもの)				
教育研究用機器備品	1,200	機械器具	1,200	小型冷却遠心機 他
図 書				
計	1,200		1,200	
研 究 ス タ ッ フ 関 係 支 出				
リサーチ・アシスタント				
ポスト・ドクター				
研究支援推進経費				
計	0		0	

法人番号

041004

【テーマ2】

(千円)

年 度	平成 31 年度			
小 科 目	支 出 額	積 算 内 訳		
		主 な 使 途	金 額	主 な 内 容
教 育 研 究 経 費 支 出				
消 耗 品 費	5,508	薬品・実験材料・その他	5,508	試薬・研究試料・実験用品・文房具・OA用品
光 熱 水 費	0		0	
通信運搬費	3	郵便・運搬	3	サンプル等配送 等
印刷製本費	56	論文等印刷	56	論文印刷・文献複写
旅費交通費	185	学会・研究発表	185	学会参加・研究打合せ
報酬・委託料	59	委託	59	分析・検査、英文校正
(賃借料)	30	設備賃借費	30	容器使用料
(修繕費)	0		0	
計	5,841		5,841	
ア ル バ イ ト 関 係 支 出				
人件費支出 (兼務職員)				
教育研究経費支出				
計	0		0	
設 備 関 係 支 出(1個又は1組の価格が500万円未満のもの)				
教育研究用機器備品	159	機械器具	159	冷却保存容器
図 書				
計	159		159	
研 究 ス タ ッ フ 関 係 支 出				
リサーチ・アシスタント				
ポスト・ドクター				
研究支援推進経費				
計	0		0	

【テーマ3】

(千円)

年 度	平成 27 年度			
小 科 目	支 出 額	積 算 内 訳		
		主 な 使 途	金 額	主 な 内 容
教 育 研 究 経 費 支 出				
消 耗 品 費	5,281	薬品・実験材料・その他	5,281	試薬・研究試料・実験用品
光 熱 水 費	0		0	
通信運搬費	0		0	
印刷製本費	294	論文等印刷	294	論文印刷・文献複写
旅費交通費	355	学会・研究発表	355	学会参加・研究打合せ
報酬・委託料	70	委託	70	分析・検査、英文校正
(賃借料)	0		0	
(修繕費)	0		0	
計	6,000		6,000	
ア ル バ イ ト 関 係 支 出				
人件費支出 (兼務職員)				
教育研究経費支出				
計	0		0	
設 備 関 係 支 出(1個又は1組の価格が500万円未満のもの)				
教育研究用機器備品				
図 書				
計	0		0	
研 究 ス タ ッ フ 関 係 支 出				
リサーチ・アシスタント				
ポスト・ドクター				
研究支援推進経費				
計	0		0	

法人番号

041004

【テーマ3】

(千円)

年 度	平成 28 年度			
小 科 目	支 出 額	積 算 内 訳		
		主 な 使 途	金 額	主 な 内 容
教 育 研 究 経 費 支 出				
消 耗 品 費	5,687	薬品・実験材料・その他	5,687	試薬・研究試料・実験用品・文房具・OA用品
光 熱 水 費	0		0	
通信運搬費	2	郵便・運搬	2	サンプル等配送 等
印刷製本費	29	論文等印刷	29	論文印刷・文献複写
旅費交通費	177	学会・研究発表	177	学会参加・研究打合せ
報酬・委託料	105	支払報酬	105	講演料等
(賃借料)	0		0	
(修繕費)	0		0	
計	6,000		6,000	
ア ル バ イ ト 関 係 支 出				
人件費支出 (兼務職員)				
教育研究経費支出				
計	0		0	
設 備 関 係 支 出(1個又は1組の価格が500万円未満のもの)				
教育研究用機器備品				
図 書				
計	0		0	
研 究 ス タ ッ フ 関 係 支 出				
リサーチ・アシスタント				
ポスト・ドクター				
研究支援推進経費				
計	0		0	

【テーマ3】

(千円)

年 度	平成 29 年度			
小 科 目	支 出 額	積 算 内 訳		
		主 な 使 途	金 額	主 な 内 容
教 育 研 究 経 費 支 出				
消 耗 品 費	5,054	薬品・実験材料・その他	5,054	試薬・研究試料・実験用品・文房具・OA用品
光 熱 水 費	0		0	
通信運搬費	0		0	
印刷製本費	0		0	
旅費交通費	316	学会・研究発表	316	学会参加・研究打合せ
報酬・委託料	630	委託	630	分析・検査、英文校正
(賃借料)	0		0	
(修繕費)	0		0	
計	6,000		6,000	
ア ル バ イ ト 関 係 支 出				
人件費支出 (兼務職員)				
教育研究経費支出				
計	0		0	
設 備 関 係 支 出(1個又は1組の価格が500万円未満のもの)				
教育研究用機器備品				
図 書				
計	0		0	
研 究 ス タ ッ フ 関 係 支 出				
リサーチ・アシスタント				
ポスト・ドクター				
研究支援推進経費				
計	0		0	

法人番号

041004

【テーマ3】

(千円)

年 度	平成 30 年度	積 算 内 訳		
小 科 目	支 出 額	主 な 内 容		
		主 な 使 途	金 額	
教 育 研 究 経 費 支 出				
消 耗 品 費	5,346	薬品・実験材料・その他	5,346	試薬・研究試料・実験用品・文房具・OA用品
光 熱 水 費	0		0	
通信運搬費	0		0	
印刷製本費	1	論文等印刷	1	論文印刷・文献複写
旅費交通費	653	学会・研究発表	653	学会参加・研究打合せ
報酬・委託料	0		0	
(賃借料)	0		0	
(修繕費)	0		0	
計	6,000		6,000	
ア ル バ イ ト 関 係 支 出				
人件費支出 (兼務職員)				
教育研究経費支出				
計	0		0	
設 備 関 係 支 出(1個又は1組の価格が500万円未満のもの)				
教育研究用機器備品				
図 書				
計	0		0	
研 究 ス タ ッ フ 関 係 支 出				
リサーチ・アシスタント				
ポスト・ドクター				
研究支援推進経費				
計	0		0	

【テーマ3】

(千円)

年 度	平成 31 年度	積 算 内 訳		
小 科 目	支 出 額	主 な 内 容		
		主 な 使 途	金 額	
教 育 研 究 経 費 支 出				
消 耗 品 費	5,902	薬品・実験材料・その他	5,902	試薬・研究試料・実験用品・文房具・OA用品
光 熱 水 費	0		0	
通信運搬費	0		0	
印刷製本費	0		0	
旅費交通費	98	学会・研究発表	98	学会参加・研究打合せ
報酬・委託料	0		0	
(賃借料)	0		0	
(修繕費)	0		0	
計	6,000		6,000	
ア ル バ イ ト 関 係 支 出				
人件費支出 (兼務職員)				
教育研究経費支出				
計	0		0	
設 備 関 係 支 出(1個又は1組の価格が500万円未満のもの)				
教育研究用機器備品				
図 書				
計	0		0	
研 究 ス タ ッ フ 関 係 支 出				
リサーチ・アシスタント				
ポスト・ドクター				
研究支援推進経費				
計	0		0	

研究テーマ 1

新規がん分子標的治療薬の創製

RESEARCH PAPER

UDP-Glucuronosyltransferase (UGT)-mediated attenuations of cytochrome P450 3A4 activity: UGT isoform-dependent mechanism of suppression

Yuu Miyauchi^{1,2} | Yoshitaka Tanaka² | Kiyoshi Nagata³ | Yasushi Yamazoe⁴ |
Peter I. Mackenzie⁵ | Hideyuki Yamada^{1†} | Yuji Ishii¹ 

¹Laboratory of Molecular Life Sciences,
Graduate School of Pharmaceutical Sciences,
Kyushu University, Fukuoka, Japan

²Division of Pharmaceutical Cell Biology,
Graduate School of Pharmaceutical Sciences,
Kyushu University, Fukuoka, Japan

³Department of Environmental and Health
Science, School of Pharmaceutical Sciences,
Tohoku Medical and Pharmaceutical
University, Sendai, Japan

⁴Food Safety Commission, Cabinet Office,
Government of Japan, Tokyo, Japan

⁵Department of Clinical Pharmacology,
Flinders Medical Centre and Flinders
University, Adelaide, SA, Australia

Correspondence

Yuji Ishii, Laboratory of Molecular Life
Sciences, Graduate School of Pharmaceutical
Sciences, Kyushu University, 3-1-1 Maidashi,
Higashi-ku, Fukuoka 812-8582, Japan.
Email: ishii@phar.kyushu-u.ac.jp

Funding information

Japan Society for the Promotion of Science,
Grant/Award Number: 25293039; Ministry of
Education, Culture, Sports, Science and
Technology, Grant/Award Number: 19590147;
Japan Research Foundation for Clinical
Pharmacology

Background and Purpose: Cytochrome P450 (CYP, P450) 3A4 is involved in the metabolism of 50% of drugs and its catalytic activity *in vivo* is not explained only by hepatic expression levels. We previously demonstrated that UDP-glucuronosyltransferase (UGT) 2B7 suppressed CYP3A4 activity through an interaction. In the present study, we target UGT1A9 as another candidate modulator of CYP3A4.

Experimental Approach: We prepared co-expressed enzymes using the baculovirus-insect cell expression system and compared CYP3A4 activity in the presence and absence of UGT1A9. Wistar rats were treated with dexamethasone and liver microsomes were used to elucidate the role of CYP3A-UGT1A interactions.

Key Results: UGT1A9 and UGT2B7 interacted with and suppressed CYP3A4. Kinetic analyses showed that both of the UGTs significantly reduced V_{\max} of CYP3A4 activity. In addition, C-terminal truncated mutants of UGT1A9 and UGT2B7 still retained the suppressive capacity. Dexamethasone treatment induced hepatic CYP3As and UGT1As at different magnitudes. Turnover of CYP3A was enhanced about twofold by this treatment.

Conclusion and Implications: The changes of kinetic parameters suggested that UGT1A9 suppressed CYP3A4 activity with almost the same mechanism as UGT2B7. The luminal domain of UGTs contains the suppressive interaction site(s), whereas the C-terminal domain may contribute to modulating suppression in a UGT isoform-specific manner. CYP3A-UGT1A interaction seemed to be disturbed by dexamethasone treatment and the suppression was partially cancelled. CYP3A4-UGT interactions would help to better understand the causes of inter/intra-individual differences in CYP3A4 activity.

Abbreviations: CNX, calnexin; CPR, NADPH-cytochrome P450 reductase; CYP and P450, cytochrome P450; DDI, drug-drug interactions; HLM, human liver microsomes; SNP, single-nucleotide polymorphism; UGT, UDP-glucuronosyltransferase.

[†]Deceased

1 | INTRODUCTION

Cytochrome P450 (CYP, P450) 3A4 is involved in the metabolism of 30–50% of drugs clinically used (Thummel & Wilkinson, 1998; Zanger & Schwab, 2013). Thus, it is very important to understand the causes of inter-individual differences of CYP3A4 activities, especially as there is a large discrepancy between the difference in its expression level and in CYP3A4-mediated drug clearance. Hepatic expression levels of CYP3A4 differ up to 40-fold, but the variance in CYP3A4-mediated drug clearance is only as much as 10-fold (Lamba, Lin, Schuetz, & Thummel, 2002; Shimada, Yamazaki, Mimura, Inui, & Guengerich, 1994). In other P450 isoforms, single-nucleotide polymorphisms (SNPs) clearly explain discrepancies between expression levels and clearance; CYP2C9*2 and CYP2D*18 show lower catalytic activities because the SNPs attenuate their enzymatic functions. In contrast, however, CYP3A4 SNPs which can affect activity without changing expression levels are very rare. Thus, SNPs cannot account for this discrepancy in the case of CYP3A4 (Johansson & Ingelman-Sundberg, 2011; Zanger & Schwab, 2013).

To address this issue, we focused on protein–protein interactions between CYP3A4 and UDP-glucuronosyltransferase (UGT) as a post-translational mode of regulation of CYP3A4 activity. Interactions of P450 with NADPH-cytochrome P450 reductase (CPR) and cytochrome b5 were well examined (Hildebrandt & Estabrook, 1971; Lu, Junk, & Coon, 1969). P450–P450 and UGT–UGT oligomerization were also reported and protein interactions were shown to control their activities (Backes & Kelley, 2003; Ishii, Takeda, & Yamada, 2010). However, although P450 and UGT both localize to the endoplasmic reticulum membrane, they had been thought to work separately because of differences in their membrane topologies. P450 faces the cytosol whereas the majority of the UGT protein is oriented to the lumen. With UGT, only the C-terminal region is predicted to form a transmembrane helix followed by a cytosolic tail, the region composed of about 20 residues extruding to the cytosol (Black, 1992; Radomska-Pandya, Czernik, Little, Battaglia, & Mackenzie, 1999). Despite such a large topological difference, however, it is reasonable that P450 and UGT interact with each other because some chemicals are hydroxylated by P450 and sequentially glucuronidated by UGT. To validate our hypothesis, we have detected P450–UGT complexes by several biochemical methods and reported that P450 could modulate UGT function (Ishii et al., 2007; Ishii et al., 2014; Nakamura et al., 2016; Takeda et al., 2005; Takeda et al., 2009; Taura et al., 2000). Other groups also supported our reports (Fremont, Wang, & King, 2005; Fujiwara & Itoh, 2014; Rouleau, Audet-Delage, Desjardins, Girard-Bock, & Guillemette, 2017). In our last study, we confirmed the reverse effect; UGT2B7 suppressed CYP3A4 activity by inhibiting substrate binding to the P450. In addition, we also determined interaction sites of UGT2B7 with CYP3A4. Hydrophobic regions in the C-terminal region and luminal membrane anchoring region were necessary for CYP3A4–UGT2B7 interaction. These two sites work cooperatively in the suppression (Miyachi et al., 2015).

Although we reported that UGT2B7 could suppress CYP3A4, the mechanism of the suppression and whether other UGT isoforms also

What is already known

- Two drug-metabolizing enzymes, cytochrome P450 (CYP) and UDP-glucuronosyltransferase (UGT) form complexes.
- UGT2B7 interacts with and suppresses CYP3A4 activity by inhibiting substrate binding.

What does this study add

- Another UGT isoform, UGT1A9 also suppresses CYP3A4 in a UGT isoform-dependent fashion.
- Dexamethasone affected and partially abrogated the CYP3A–UGT1A interactions in rat liver.

What is the clinical significance

- CYP–UGT interactions contribute to our understanding of the causes of drug–drug interactions.
- These interactions also result in the large differences in hepatic enzyme level between individuals.

modulate CYP3A4 function remain unclear. To address this issue, in the present study, we focused on UGT1A9, another major human isoform and performed a comparative study with UGT2B7.

2 | METHODS

2.1 | Construction of recombinant baculovirus and mammalian expression vectors

Bac-to-Bac[®] Baculovirus Expression System (Life Technologies, Carlsbad, CA) was used to prepare recombinant baculovirus. The recombinant baculoviruses coding CYP3A4, human P450 reductase (CPR), UGT2B7 wild-type (WT) and its truncated mutant lacking transmembrane followed by cytoplasmic domain (Δ TM or Δ 493–529) were prepared as described previously (Miyachi et al., 2015). The open reading frame of UGT1A9 was amplified using pIRES-UGT1A9 (Uchaipichat et al., 2004) as a template, KOD-Plus-Neo DNA Polymerase (Toyobo Life Science, Osaka, Japan), and the following primers: sense, 5'-CGGGATCCGTGATGGCTTGCACAGGGTG-3' (primer A); anti-sense, 5'-CGGGATCCCACTTCTCAATGGGTCTTGG-3' (underline, *Bam*HI site). Thermal cycling condition was as follows: initial denaturation, 94°C, 2 min; 40 cycling step, 98°C, 10 s; 52°C, 30 s; 68°C, 1 min; hold, 4°C. The PCR products were digested with *Bam*HI and inserted into pFastBac1 cleaved with the same enzyme. To generate the truncated mutant of UGT1A9 (Δ 488–530) which lacks the transmembrane and cytoplasmic domains, we performed PCR with primer A as sense primer and the following anti-sense one: 5'-CGGGATCCGTGATGGCTTGCACAGGGTG-3' (underline, *Bam*HI site).

The recombinant pFastBac1 vectors were transfected into the competent *Escherichia coli* DH10Bac™ strain (Life Technology). After positive clones were selected by blue white selection, recombinant bacmids, baculoviral DNAs for producing recombinant virus, were prepared according to the user's manual. In addition, we subcloned UGT1A9 cDNA into the pcDNA3.1/hygro (–) vector for experiments with mammalian cells. An HA-tag was added to its C-terminus to improve detection in pull-down assays. The introduction of an HA-tag was performed by two rounds of PCR. A forward part of the HA-tag was introduced in the first round, and the latter part followed by a restriction site was introduced in the second round using pairs of primers below: the first round sense, primer A; the first round anti-sense, 5'-ATCTGGAACATCGTATGGGTAATGGGCTTGGATTGTGGG-3' (bold, forward part of HA-tag); the second round sense, primer A; the second round anti-sense, 5'-CGGGATCCTCAAGCGTAATCTGG AACATCGTATGGGTAAT-3' (underline, *Bam*HI site; bold, coding HA-tag). In the second round, PCR products of the first round were used as the template. PCR was carried out as described above. Δ488-530-HA construct was generated by QuickChange site-directed mutagenesis with pcDNA3.1_WT-HA as a template using the following primers: sense, 5'-CAGTACCATTCTTGGACTACCCATACGATG TTCCA-3'; anti-sense, 5'-TGGAACATCGTATGGGTAGTCCAAGGAAT GGTACTG-3'. The primers were designed using Agilent QuikChange Primer Design Program (<https://www.genomics.agilent.com/primerDesignProgram.jsp>). Hexa-histidine conjugated CYP3A4 has been cloned into bacmid for Ni²⁺ pull-down assay (Miyauchi et al., 2015). We amplified the cDNA of CYP3A4-6 × His with the following primers: sense, 5'-ATAAGAATGCGGCCGCGTATGGCTCTCATCCC AGA-3'; anti-sense, 5'-CCGCTCGAGTCAGTGATGGTGATGGT GATGGGCTCCACTTAC-3' (underline, *Not*I and *Xho*I site, respectively; bold, coding hexa-histidine). All of the sequences of the constructs were confirmed by an ABI 3130xl Genetic analyser, using a BigDye® Terminator v3.1 Cycle Sequencing Kit (Life Technologies).

2.2 | Culture of insect cells and preparation of homogenates

All the cellular experiments were carried out and analysed by a single investigator, so no blinding was undertaken. Sf9 (RRID: CVCL_0549) insect cells were cultured according to our previous study (Miyauchi et al., 2015). We prepared cell homogenates from infected cells for the CYP3A4 assay. For preparation of cell homogenates, 2.0×10^6 cells were seeded in 35-mm dish 24 hr prior to viral infection. Following medium exchange, baculoviruses were transfected. Twenty-four hours after the infection, hemin-BSA was supplied to the cells (final concentration of $1 \mu\text{g}\cdot\text{ml}^{-1}$ of hemin). Forty-eight hours after hemin supply, cells were harvested in homogenization buffer, 10-mM Tris-HCl (pH 7.5) containing 0.25-M sucrose, 10% glycerol, and 1× protease inhibitor cocktail (Nacalai Tesque, Kyoto, Japan), and homogenates were prepared by sonication for 30 s with a Ultrasonic Cleaner UT-51N (SHARP, Osaka, Japan).

2.3 | Culture of COS-1 cells and transfection of mammalian expression vector

COS-1 cells (RRID:CVCL_0223) were cultured in DMEM containing high glucose (Wako Pure Chemical Industries, Osaka, Japan) supplied with 10% FBS. Cells were seeded to 35-mm dishes and transfected with 2-μg pcDNA3.1 vectors by Lipofectamine 3000 (Life Technologies). Cells were harvested with lysis buffer, 20-mM Tris-HCl (pH 7.4) containing 150-mM NaCl, 1% Triton X-100, 10% glycerol, and sonicated to prepare whole cell lysate. When we use the lysates for pull-down assay, those were sequentially centrifuged, and supernatants were collected.

2.4 | Pull-down assay

Whole cell lysate (600 μg) was mixed with 15 μl of magnetic agarose beads conjugated with Ni-nitrilotriacetic acid (Qiagen, Hilden, Germany) equilibrated with lysis buffer. To avoid non-specific binding, we added another 200-mM sodium chloride, 40-mM imidazole, 0.05% Emulgen 911 and 0.2% BSA to the mixture. Protein binding to the beads was conducted at 4°C for 4 hr. The beads were washed three times with 20-mM Tris-HCl (pH 7.4 at 4°C) containing 200-mM sodium chloride, 40-mM imidazole, 20% glycerol and 0.05% Emulgen 911. Then binding proteins were eluted from the beads with 20 μl of 10-mM sodium phosphate (pH 7.4) containing 300-mM sodium chloride, 250-mM imidazole, 20% glycerol and 0.05% Emulgen 911. Samples were stored until analysis by immunoblotting.

2.5 | Immunoblotting

The immuno-related procedures used comply with the recommendations made by the *British Journal of Pharmacology* (Alexander et al., 2018). Proteins were separated by SDS-PAGE and electroblotted onto a PVDF membrane (Immobilon-P; Millipore, Bedford, MA; Cat# IPVH00010). The blotted membrane was washed with TBS-T, 20-mM Tris-HCl (pH 7.5) containing 150-mM NaCl, and 0.1% Tween 20 and blocked with 2% skim milk in TBS-T at room temperature for 30 min. For detection of targets, the following primary antibodies and detection kit were utilized: rabbit polyclonal anti-UGT1A antibody (H-300, Cat# sc-25847, RRID:AB_2241481), mouse monoclonal anti-CPR antibody (F-10, Cat# sc-25270, RRID:AB_627391; Santa Cruz Biotechnology, Dallas, TX), goat polyclonal anti-CYP3A2 serum (Daiichi Pure Chemicals, Tokyo, Japan; Cat# 877), rabbit polyclonal anti-UGT2B7 antibody, rabbit polyclonal anti-GAPDH antibody (Proteintech, Rosemont, IL; respective Cat# 16661-1-AP and 10494-1-AP, respective RRID:AB_2214249 and AB_2263076), rabbit polyclonal anti-calnexin (CNX) antibody (GeneTex, Irvine, CA; Cat# GTX112886, RRID:AB_1949822), rabbit polyclonal anti-6-His antibody (Bethyl Laboratories, Montgomery, TX; Cat# A190-114A, RRID: AB_67321), rabbit polyclonal anti-hemagglutinin (HA) antibody (Sigma-Aldrich, St. Louis, MO; Cat# H6908, RRID:AB_260070), and

WB-MAB-3A Human CYP3A Western Blotting Kit (Corning Gentest, Woburn, MA; Cat# 458254, RRID:AB_712943). The primary antibodies were diluted 2,000-fold with TBS-T containing 2% skim milk. The membranes were incubated with the diluted primary antibody at 4°C overnight. The diluted primary antibodies were collected, stored at 4°C and reused up to 10 times. Immunochemical detection was performed with HRP-conjugated secondary antibody, HRP-rabbit anti-goat IgG (MP Biomedicals, Santa Ana, CA; Cat# 59301), HRP-donkey anti-rabbit IgG, or HRP-sheep anti-mouse IgG (GE Healthcare, Little Chalfont, UK; respective Cat# NA934V and NA931V). After the first antibody treatment, the membranes were extensively washed with TBS-T and incubated with the secondary antibody diluted 10,000-fold with TBS-T containing 2% skim milk at room temperature for 1 hr. Then the membranes were washed extensively again. EzWestLumi plus (ATTO, Tokyo, Japan) was utilized as a substrate of HRP, and the signals were visualized and quantified with a ChemiDoc MP System (Bio-Rad, Hercules, CA). For detection of another target on the same membrane, antibodies were stripped after detection. All the stripping processes were carried out at room temperature. Used membrane was incubated with stripping buffer, 25-mM glycine-HCl (pH 2.0) containing 1% sodium dodecylsulphate for 30 min. After that, the membrane was neutralized by washing three times for 5 min in TBS-T, reblocked with TBS-T containing 2% skim milk for 30 min and used in an incubation with another primary antibody.

2.6 | Assay of CYP3A4 activity

CYP3A4 activity was measured with P450-Glo CYP3A4 Assay System (Luciferin-PFBE: Promega, Madison, WI). CYP3A4 activity was determined by measuring chemiluminescence according to the manufacturer's protocol with insect cell homogenates (20 µg in each well) as enzyme source. NADPH was used instead of regenerating system because its oxidized form (NADP⁺) was reported to inhibit UGT function (Nishimura et al., 2007). In kinetic experiments, the substrate concentration varied from 6.25 to 150 µM. Data were fitted to the Michaelis–Menten model defined by the equation below:

$$V = V_{\max} \times S / (K_M + S),$$

where V is the reaction rate, S is the substrate concentration, V_{\max} is the maximum enzyme velocity and K_M is the Michaelis constant, which is equal to the concentration of substrate for half-maximal velocity.

2.7 | Preparation of microsomes from dexamethasone-treated rats

Animal experiments in this study were approved by the Institutional Animal Care and Experiment Committee of Kyushu University (application approval number: A19-084). Animal studies are reported in compliance with the ARRIVE guidelines (Kilkenny, Browne, Cuthill, Emerson, & Altman, 2010) and with the recommendations made by the *British Journal of Pharmacology*. Male Wistar rats (5 weeks old, $N =$

5 in each group, 150–164 g of body weight) were purchased from CLEA Japan (Tokyo, Japan), randomly divided into two groups, and maintained for 1 week. They were treated with dexamethasone 21-phosphate intraperitoneally at a dose of 80 mg·kg^{−1} in saline every day for 4 days. Control rats were injected with the same amount of saline. The day following the last treatment, livers were removed and perfused with ice-cold saline and microsomes were prepared individually from the liver homogenates by differential centrifugation as described elsewhere (Oguri et al., 1996). Collected microsomes were resuspended in 0.25-M sucrose, snap-frozen in liquid nitrogen and stored at −80°C prior to use. To determine relative protein levels of CYP3A, UGT1A, and CPR in the rat liver microsomes by immunoblotting, CNX was selected as a loading control and each band was standardized to the corresponding CNX band. CNX is an ER marker protein and a previous report suggested that dexamethasone treatment does not affect CNX protein level (Fujii et al., 2006). Intensities of CYP3A were quite different between control and dexamethasone-treated groups. Thus, we utilized 10- and 1-µg microsomes of control and dexamethasone-treated rats, respectively, in order to detect the CYP3A bands at the same range. In kinetic analyses, assays were conducted with 20-µg microsomes and luciferin-PFBE as enzyme source and substrate, respectively, and CYP3A activity was calculated with relative expression levels of CYP3A explained above in each sample. Animal treatment/sample preparation and the later analysis were conducted in a blinded manner.

2.8 | Other methods

Protein concentrations of rat liver microsomes were determined by the method of Lowry, Rosebrough, Farr, and Randall (1951), and those of lysates prepared from COS-1 cells and homogenates from insect cells were by Protein Assay CBB Solution (Nacalai Tesque) with BSA as a standard.

2.9 | Data and statistical analysis

Results are presented as the means ± SD of measurements obtained from six batches of cells or five rats in each group per experiment. Statistical analysis was undertaken only for studies where each group size was at least $N = 5$ with GraphPad Prism 5.04 software (GraphPad software, La Jolla, CA; RRID:SCR_002798). Statistical significance in comparison among the three groups was determined by ANOVA followed by Dunnett's test only when the former F value was significant and there was no significant variance in homogeneity. The statistical significance between the two groups was determined by Student's t test (unpaired, two tailed), and we also confirmed that there was no significant variance in homogeneity between the two groups. A P value less than 0.05 was considered statistically significant. Protein expression levels of rat liver CYP3A, UGT1A, and CPR relative to CNX were further normalized to each mean value of controls to adjust for unwanted sources of variation and to show the clear effects of dexamethasone on their protein levels. The data and

statistical analysis comply with the recommendations on experimental design and analysis in pharmacology (Curtis et al., 2018).

2.10 | Materials

Synthetic oligonucleotides were purchased from Life Technologies. Restriction enzymes, bacterial alkaline phosphatase, and T4 DNA ligase were from Takara Bio (Shiga, Japan). Human liver microsomes (HLM) 50 donors pooled were from Corning® Gentest. NADPH was from Oriental Yeast (Tokyo, Japan). All other reagents were of the highest grade commercially available.

2.11 | Nomenclature of targets and ligands

Key protein targets and ligands in this article are hyperlinked to corresponding entries in <http://www.guidetopharmacology.org>, the common portal for data from the IUPHAR/BPS Guide to PHARMACOLOGY (Harding et al., 2018), and are permanently archived in the Concise Guide to PHARMACOLOGY 2019/20 (Alexander et al., 2019).

3 | RESULTS

3.1 | Confirmation of CYP3A4, UGTs and CRP expression in insect microsomes

The drug-metabolizing enzymes were transiently expressed in insect cells and their presence was confirmed in prepared homogenates by

immunoblotting. With every enzyme, specific bands were observed with the same MW as those in positive controls, HLM, and/or their standards, and insect GAPDH was detected as loading control (Figure 1). In UGT detection, HLM showed broad bands and different migrations from those of the recombinant ones. The primary antibody we used can react with several human UGT isoforms, which resulted in the difference. As the results indicated the suitability of the expression system, we next prepared homogenates from cells that co-expressed the drug-metabolizing enzymes of interest.

3.2 | Suppression of CYP3A4 activity by UGT1A9 and UGT2B7

We estimated the effect of each UGT on CYP3A4 activity using Sf9 homogenates as enzyme sources. The effect of UGTs on CYP3A4 function was examined by comparing CYP3A4 activity between P450/CPR doubly expressing homogenates and P450/CPR/UGT ternary expressing ones (none, UGT1A9, and UGT2B7 in Figure 2, respectively). It is well known that P450 activity highly depends on CPR (Lu et al., 1969; Miwa & Lu, 1984). To avoid misestimating the effect of UGTs, we quantified the enzymes by immunoblotting (Figure S1). Although expression levels of CYP3A4 and CPR were markedly different among the three groups, their P450/CPR ratios were comparable (Table S1). Co-expression of UGT1A9/2B7 significantly suppressed CYP3A4 activity (Figure 2a), which was consistent with our last study reporting UGT2B7-mediated suppression of CYP3A4 (Miyauchi et al., 2015). Further, we performed kinetic analysis to characterize UGT isoform-dependent differences in the

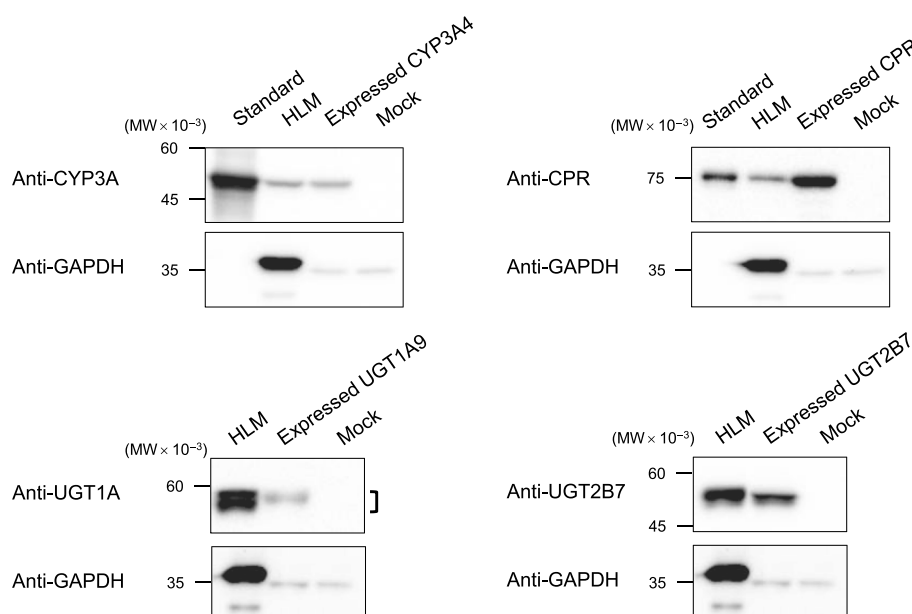


FIGURE 1 Immunoblotting to confirm the expression of the recombinant enzymes, CYP3A4, CPR, UGT1A9, and UGT2B7. Antibodies against human-CYP3A, human-CPR, human-UGT1A, human-UGT2B7, and human-GAPDH were used as primary antibodies. HLM and recombinant enzymes were positive controls. The protein amounts loaded were as follows: HLM, 10 µg; Supersomes (as a CYP3A4 standard), 5 pmol of CYP3A4; purified CPR, 100 ng; and the Sf9 homogenates (as denoted), 20 µg, respectively. Mock represents homogenates prepared from Sf9 cells infected with control virus

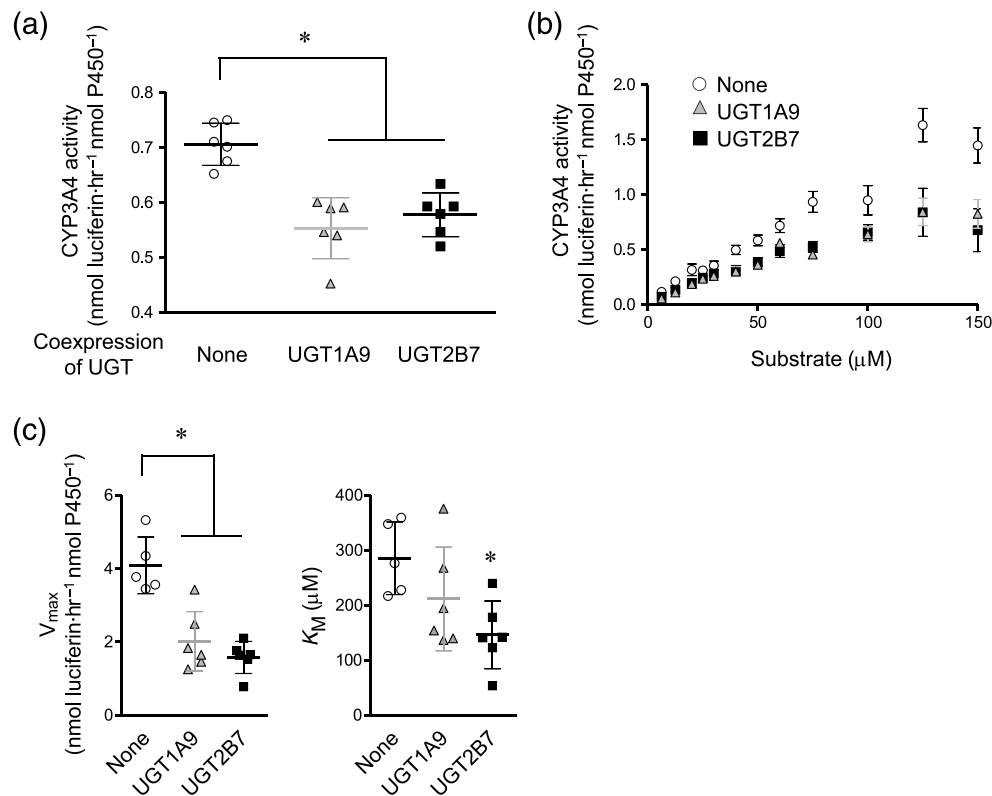


FIGURE 2 Comparison of CYP3A4 activity in the absence and presence of UGT1A9/2B7. Sf9 cells were seeded in 35-mm dishes and independently infected with recombinant baculoviruses. CYP3A4 activity was measured with Sf9 homogenates (20-μg protein) as enzyme source and luciferin-PFBE (50 μM) as a substrate. The mean ± SD of CYP3A4 activities are shown ($N = 6$). The result of quantitative immunoblotting is shown in Figure S1, and protein levels of expressed enzymes are summarized in Table S1 (a). Kinetic analysis to estimate the effect of coexpression of UGT1A9 and UGT2B7 on CYP3A4 activity. Using Sf9 homogenates as enzyme source, CYP3A4 activity was compared between CYP3A4/CPR homogenates (none, open circle) and CYP3A4/CPR/UGT homogenates (UGT1A9, grey triangle; UGT2B7, closed square). Data were fitted to the Michaelis–Menten model. Each plot represents the mean ± SD of six different samples (b). Calculated V_{\max} and K_M values were compared. The kinetic parameters were determined in each sample, to obtain six sets of V_{\max} and K_M values in each group. The mean ± SD of six sets of parameters are shown, and the values are listed in Table 1 (c). Statistical significance was determined by ANOVA followed by Dunnett's test only when the former F value was significant and there was no significant variance in homogeneity (vs. none)

suppression of CYP3A4 activity. We used the same homogenates in kinetic analysis as an enzyme source. The data were fitted to the Michaelis–Menten model (Figure 2b). We conducted curve fitting in every sample to obtain six sets of V_{\max} and K_M in each group. The calculated parameters are presented in Figure 2c, and the mean ± SD of

the parameters are listed in Table 1. Both of the UGTs significantly reduced V_{\max} of CYP3A4 activity, but only UGT2B7 decreased K_M (Figure 2c and Table 1).

TABLE 1 Effect of coexpression of UGT1A9 and UGT2B7 on CYP3A4 activity

Construct	Kinetic parameter	
	V_{\max} (nmol·hr ⁻¹ ·nmol P450 ⁻¹)	K_M (μM)
None	3.94 ± 0.77	269.2 ± 71.37
UGT1A9	2.02 ± 0.81*	211.4 ± 94.23
UGT2B7	1.58 ± 0.44*	146.2 ± 61.61*

Note. The mean ± SD of calculated parameters in Figure 2c ($N = 6$ in each group) are listed.

Abbreviations: P450, cytochrome P450; UGT, UDP-glucuronosyltransferase.

* $P < .05$ versus none.

TABLE 2 Carboxyl-terminal sequences of deletion mutants of UGT1A9 and UGT2B7

Protein	Sequence
UGT1A9	D ₄₈₇ <u>VIGFLLAVVLTVA</u> ITFK ₅₀₅ CCAYGYRKCLGKKGRVKKAHKSKTH ₅₃₀
UGT1A9 ΔTM	D ₄₈₇
UGT2B7	D ₄₉₃ <u>VIGFLLVCVATVIV</u> ITK ₅₁₀ CCLFCFWKFAKAKKGKND ₅₂₉
UGT2B7 ΔTM	D ₄₉₃

Note. Truncated mutants of UGT1A9 and UGT2B7 lacking the C-terminal region were constructed. The postulated transmembrane regions of UGT are underlined (Mackenzie, 1986; Radominska-Pandya et al., 1999) and proceed the cytosolic tail. The subscript numbers represent the location of the residues of each UGT counted from the N-terminal methionine of the mature form.

Abbreviation: UGT, UDP-glucuronosyltransferase.

3.3 | Role of carboxyl-terminal region of UGT1A9 in the suppression of CYP3A4 activity

We previously indicated that both the C-terminal region and luminal membrane binding domains were necessary for UGT2B7 to suppress

CYP3A4 activity (Miyachi et al., 2015). However, it remains unclear which domain is more critical for the suppression caused by UGT1A9 (Figure 2). To address this issue, we generated a UGT1A9 truncated mutant that lacks the C-terminal region, containing the transmembrane helix and following cytosolic tail (Δ TM, Table 2). First, we

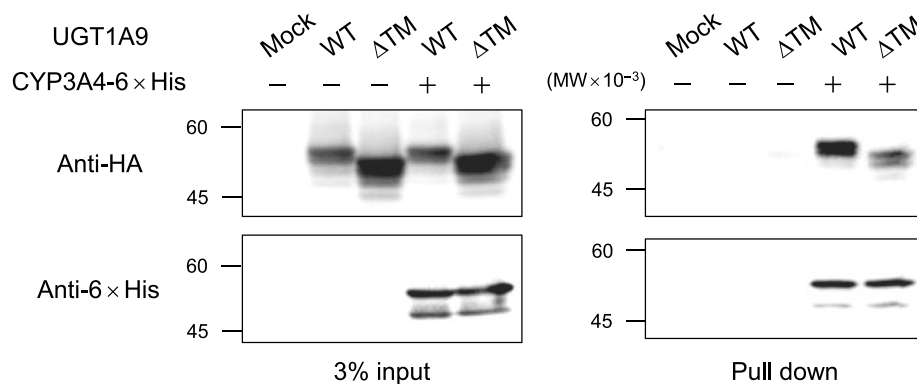


FIGURE 3 Pull-down assay to detect protein–protein interactions between CYP3A4 and UGT1A9 WT/ Δ TM. CYP3A4-6 \times His and UGT1A9-HA were transiently expressed in COS-1 cells, and lysates were prepared. Pull-down assay was performed by mixing Ni-nitrilotriacetic acid magnetic beads and 600 μ g of lysate. Bound proteins were eluted by buffer containing a high level of imidazole. Pull-down samples and 20- μ g lysates (3% input) were analysed by immunoblotting

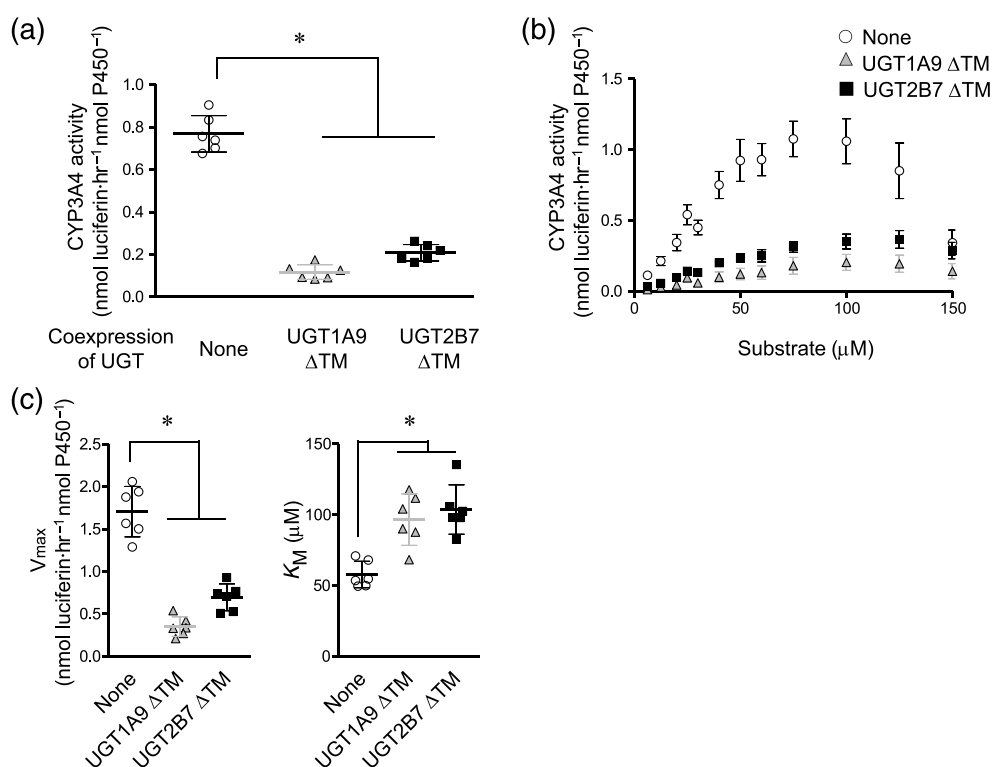


FIGURE 4 Effect of C-terminal truncated mutants of UGT1A9 and UGT2B7 on CYP3A4 activity. CYP3A4 activity was measured with Sf9 homogenates (20- μ g protein) as enzyme source and luciferin-PFBE (50 μ M) as a substrate. The mean \pm SD of CYP3A4 activities are shown ($N = 6$). The result of quantitative immunoblotting is shown in Figure S2, and protein levels of expressed enzymes are summarized in Table S2 (a). Kinetic analysis showing the effect of UGT truncated mutants. The homogenates mentioned above were used as enzyme sources, and CYP3A4 activity was compared between CYP3A4/CPR homogenates (none, open circle) and CYP3A4/CPR/UGT homogenates (UGT1A9 Δ TM, grey triangle; UGT2B7 Δ TM, closed square). Data were fitted to the Michaelis–Menten model. Each plot represents the mean \pm SD of the six samples (b). Calculated V_{\max} and K_M values were compared. The kinetic parameters were determined in each sample, so we obtained six pairs of V_{\max} and K_M values in each group. The mean \pm SD of six calculated parameters are shown, and the values are listed in Table 3 (c). Statistical significance was determined by ANOVA followed by Dunnett's test only when the former F value was significant and there was no significant variance in homogeneity (vs. none)

examined the role of this region in the interaction with CYP3A4 by pull-down assay. To mimic physiological conditions, we used mammalian cells (COS-1) instead of insect cells in this assay. An HA-tag was conjugated to the C-terminus of UGT1A9 to improve sensitivity of

detection. We have already ascertained that the epitope tag did not inhibit P450–UGT interactions (Nakamura et al., 2016). Both WT and Δ TM UGT1A9 forms were co-precipitated with CYP3A4-6 \times His (Figure 3), which suggested that UGT1A9 could interact with CYP3A4

TABLE 3 Effect of C-terminal deletion mutants (Δ TM) of UGT1A9 and UGT2B7 on CYP3A4 activity

Construct	Kinetic parameter	
	V_{\max} (nmol·hr ^{−1} ·nmol P450 ^{−1})	K_M (μ M)
None	1.71 \pm 0.30	57.9 \pm 9.3
UGT1A9	0.35 \pm 0.12*	96.7 \pm 18.2*
UGT2B7	0.70 \pm 0.16*	103.8 \pm 17.4*

Note. The mean \pm SD of calculated parameters in Figure 4c (N = 6 in each group) are listed.
Abbreviations: P450, cytochrome P450; UGT, UDP-glucuronosyltransferase.
*P < .05 versus none.

TABLE 4 Effect of dexamethasone treatment on hepatic CYP3A activity in Wistar rat

Treatment	Kinetic parameter	
	V_{\max} (pmol·min ^{−1} relative CYP3A ^{−1})	K_M (μ M)
Control	0.167 \pm 0.040	81.2 \pm 17.7
Dexamethasone	0.244 \pm 0.059*	47.7 \pm 6.5*

Note. Assays were conducted with rat liver microsomes and luciferin derivative as enzyme sources and substrate, respectively. The mean \pm SD value of the calculated parameters shown in Figure 5c (N = 5 in each group) are listed.
*P < .05 versus control.

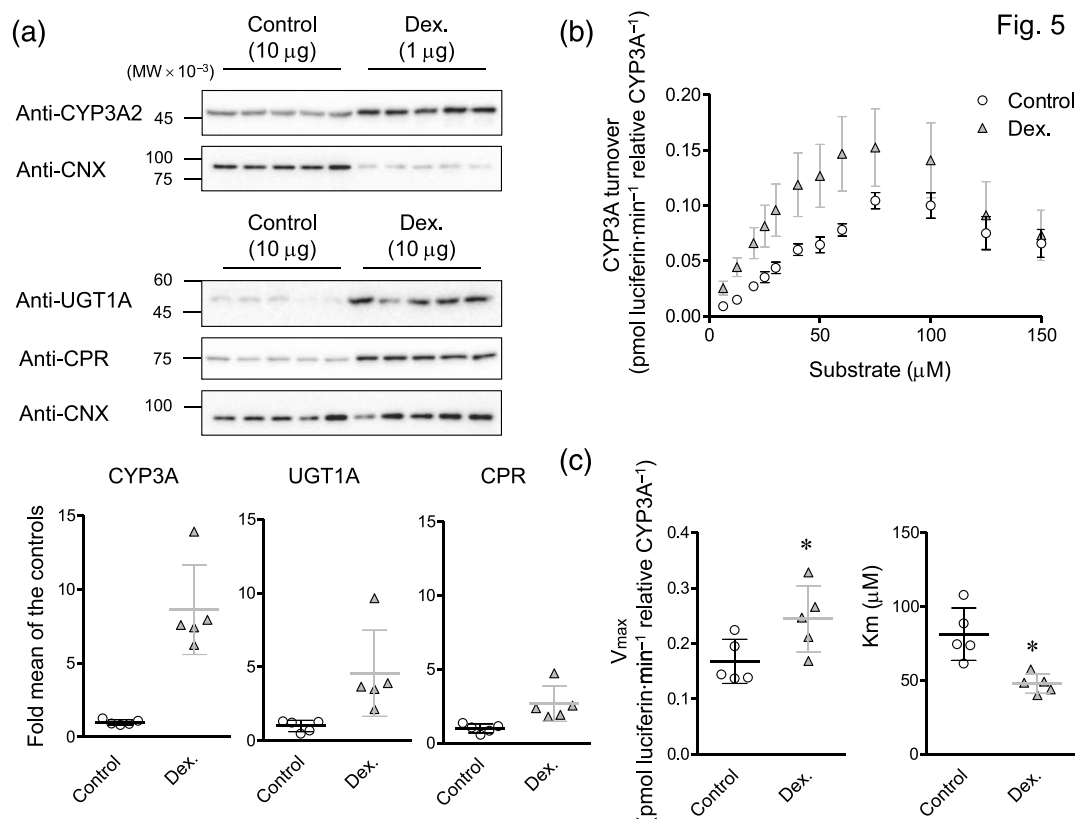


FIGURE 5 Effect of dexamethasone treatment on CYP3A–UGT1A interaction in rat liver. Induction ranges of CYP3As, UGT1As, and CPR were determined by immunoblotting. Wistar rats (male, 5 weeks old, N = 5 in each group) were treated with dexamethasone in saline at a dose of 80 mg·kg^{−1} in a day for 4 days. The control group was treated with the same amount of saline. One day after the last treatment, liver microsomes were prepared and analysed individually. Dex represents dexamethasone-treated rats. Calnexin (CNX), an ER marker protein, was also detected as a loading control. Relative protein levels (control mean = 1.0) are shown as the mean \pm SD. The amount of microsomes utilized in the immunoblotting was 10 μ g except for detection of CYP3As in dexamethasone-treated rats (1 μ g) (a). CYP3A turnovers are shown as the mean \pm SD (N = 5) for each substrate concentration. Kinetic analysis with individual rat liver microsomes. Data were fitted to the Michaelis–Menten model. Values of the y axis represent turnover of CYP3A, an activity related to CYP3A levels as determined by immunoblotting shown in Figure 5a, not an activity per microsomal protein (b). Five sets of V_{\max} and K_M for each group were calculated. These are shown as the mean \pm SD. Statistical significance was determined by Student's *t* test (unpaired, two tailed) (c)

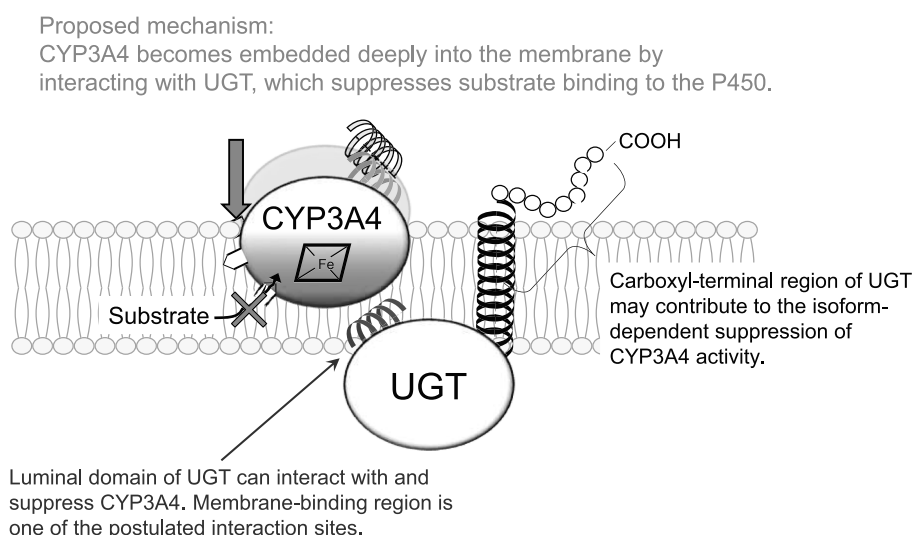


FIGURE 6 Postulated mechanism of UGT-mediated suppression of CYP3A4 activity

without the C-terminal region. We then determined whether the mutant could suppress CYP3A4 activity to the same extent as UGT1A9 WT. We prepared coexpressed homogenates using the baculovirus-insect cell system, containing unconjugated CYP3A4 and UGT1A9 or UGT2B7 Δ TM. Both of the truncated mutants still functioned as a suppressor of CYP3A4 activity (Figure 4a; and the results of quantitative immunoblotting are shown in Figure S2 and summarized in Table S2). Further, kinetic analysis indicated that they significantly reduced V_{\max} of CYP3A4 activity as shown for their WT counterparts (Figure 4b,c and Table 3). In contrast, the effects of the Δ TM mutants on K_M of CYP3A4 activity were far different from those observed in their WT: Both of the Δ TM mutants significantly increased K_M (Figure 2c and Table 1). Therefore, it is suggested that the C-terminal region of UGT1A9 and UGT2B7 has a unique modifying role in the suppression of CYP3A4 activity. Nevertheless, the luminal domain of both UGT1A9 and UGT2B7 is crucial to modulating CYP3A4 function.

3.4 | Dexamethasone treatment cancelled UGT1A-dependent suppression of CYP3A in rat liver

For further evaluation of the role of CYP3A–UGT1A interactions, we focused on dexamethasone, a strong inducer of hepatic CYP3A1, CYP3A2, UGT1A1, and 1A6 in rat (De Martin et al., 2014; Ghosal, Sadrieh, Reik, Levin, & Thomas, 1996; Jemnitz, Veres, Monostory, & Vereczkey, 2000). The UGT-mediated suppression of CYP3As should be affected if dexamethasone treatment induces CYP3As and UGT1As to different extents. To confirm that, we calculated CYP3A turnover (activity per relative CYP3A levels, but not the activity per microsomal protein), with the luciferin derivative as a substrate. We determined the impact of dexamethasone treatment on hepatic CYP3A–UGT1A interactions by using liver microsomes ($N = 5$ in each group). The results of quantitative immunoblotting are shown in

Figure 5a. CNX, an ER marker protein, was used as a loading control, and signals of CYP3A, UGT1A, and CPR were standardized to that of CNX to calculate relative expression levels (Figure 5b). Fold inductions, the value of expression levels after dexamethasone treatment divided by those of control, are also presented. First, CYP3A levels were compared with anti-CYP3A2 antibody which can cross-react with CYP3A1. Almost the same levels of CYP3As were detected in 10 μ g of microsomes from control rats and 1 μ g of those from dexamethasone-treated rats, suggesting that the treatment induces CYP3As at about 10-fold (in detail, 8.7-fold). UGT1As were also induced by dexamethasone, but induction rates were lower than those of CYP3A, 4.6-fold, while the treatment had little effect on CPR, 2.7-fold (Figure 5a). The result of kinetic analysis is shown in Figure 5b, calculated parameters are shown in Figure 5c, and the values are listed in Table 4. Dexamethasone treatment significantly increased V_{\max} and reduced K_M of CYP3A activity.

4 | DISCUSSION AND CONCLUSIONS

This study demonstrates that UGT1A9, like UGT2B7, alters CYP3A4 activity. We have reported UGT2B7-mediated suppression of CYP3A4, so this is the second study supporting our hypothesis that P450 and UGT work cooperatively through protein–protein interactions. Both UGT1A9 and UGT2B7 suppressed CYP3A4 activity (Figure 2a), mainly by a significant reduction in V_{\max} . There were also effects on K_M which were slightly different between the UGT isoforms (Tables 1 and 3). UGT2B7 markedly decreased the K_M of CYP3A4 activity, which was not observed in our last study (Miyachi et al., 2015). In that study, microsomes were utilized as enzyme source while homogenates were used in this study, so the presence of the other cellular components may have affected the results. In our previous study, we tried to determine the step(s) in the P450 catalytic cycle at which UGT2B7 suppresses P450 function. UGT2B7 down-

regulated CYP3A4 function not only at the substrate oxidation step but also during NADPH consumption, H_2O_2 generation and substrate oxidation driven by cumene hydroperoxide (Shunt pathway). Based on these data, we suspected that UGT2B7 suppresses substrate binding to P450, the start point of catalytic cycle, and proved that by comparing substrate-binding difference spectra in the presence and absence of the UGT (Miyachi et al., 2015). The present study revealed that UGT1A9 also suppressed CYP3A4 and the suppressive effect was equal or more significant than UGT2B7 (Figures 2 and 4). Given that, it is reasonable to consider that UGT1A9, like UGT2B7, inhibits substrate binding to P450. However, we cannot judge which UGT is a better suppressor of CYP3A4 because their expression levels were quantified by immunoblotting with different primary antibodies. Further, it is difficult to determine the percentage of UGT interacting with CYP3A4 in our co-expression system. Both UGTs may contribute to the reduction of toxic H_2O_2 by inhibiting substrate binding to CYP3A4 in order to reduce oxidative stress elicited by the P450 under physiological conditions.

The C-terminal region of UGT is believed to be involved in UGT localization (Iyanagi et al., 1986; Meech & Mackenzie, 1997). In addition to its role as a targeting signal, this region was also reported to be important for maintaining catalytic function in UGT1A6 (Ouzzine, Magdalou, Burchell, & Fournel-Gigleux, 1999). In the case of UGT1A9, however, the hexa-His-tag fused C-terminal truncated mutant could be purified in the baculovirus-insect cell system, with reduced but measurable activity (Kurkela, Morsky, Hirvonen, Kostainen, & Finel, 2004). Thus, the role of this region in glucuronidation activity seems somehow different among UGT isoforms in addition to suppression of CYP3A4 activity, as observed in the effects on K_M (Tables 1 and 3). Currently, splice variants of UGT1A and 2B7 have been reported in several human tissues. These variants have shorter C-terminal regions than WT as they lack the transmembrane and cytoplasmic domains. Although the variants themselves exhibit no marked activity, they play a role as suppressors of WT UGT function through protein–protein interaction (Bellemare, Rouleau, Harvey, & Guillemette, 2010; Guillemette, Levesque, & Rouleau, 2014; Menard et al., 2011). Our results with truncated mutants of UGTs raise the possibility that the UGT variants also interact with and suppress CYP3A4 under physiological conditions.

It has been proposed that UGT has another membrane-associating region in its luminal domain (Laakkonen & Finel, 2010; Meech & Mackenzie, 1998; Ouzzine et al., 1999). In P450, similarly, the FG loop is also predicted to be associated with membrane (Brown & Black, 1989; Szczesna-Skorupa, Ahn, Chen, Doray, & Kemper, 1995). Given this, it is reasonable to predict that P450 and UGT interact with each other through the membrane. This study indicated that UGT1A9 also interacted with and suppressed CYP3A4 in the absence of its C-terminal region (Figures 3 and 4), which led to our current model of UGT-mediated suppression of CYP3A4 (Figure 6). The main interaction site of UGT is the luminal membrane binding domain and this domain may interact with the FG loop of CYP3A4. Interaction with UGT could drag CYP3A4 more deeply into the ER membrane. From a recent computer simulation, influx of

substrate to P450 can be altered by the depth of P450 in the membrane (Berka, Hendrychova, Anzenbacher, & Otyepka, 2011; Berka, Paloncova, Anzenbacher, & Otyepka, 2013). Another group also reported that the lipid content of the membrane could change the degree of P450 insertion, thereby affecting P450 activity, especially with CYP3A4 (Ahn, Guengerich, & Yun, 1998; Kim, Ahn, & Yun, 2003). Thus, the change of P450 location in the membrane could elicit suppression of CYP3A4 activity.

A key question is whether the CYP3A4–UGT interaction occurs and regulates CYP3A4 under physiological conditions. We have confirmed the interaction with several biochemical methods: CYP1A1-conjugated affinity chromatography (Taura et al., 2004), GST-overlay assay (Ishii et al., 2014; Takeda et al., 2005), chemical crosslinking (Takeda et al., 2009) and co-immunoprecipitation/pull-down assay (Ishii et al., 2007; Miyachi et al., 2015; Nakamura et al., 2016). In addition, other groups also detected P450–UGT interactions by MS using human tissue samples (Fujiwara & Itoh, 2014; Rouleau et al., 2017). We have demonstrated that rat CYP3As form a metabolosome with several UGT isoforms evidenced by co-immunoprecipitation using anti-CYP3A2 antibody (Ishii et al., 2007). Further, UGTs in the CYP3A–UGT complex of the co-immunoprecipitate are also catalytically active (Ishii et al., 2007). It is conceivable that there is physiological significance for the metabolosome, CYP3A–UGT complex. In the present study, we suggest that dexamethasone treatment could partially cancel UGT1A-mediated CYP3A suppression by higher inductions of CYP3A compared to UGTs. We have reported that rat P450 interacts with and regulates UGT as well as human P450, and CYP3A4 regulates activities of human UGT1A1 and UGT1A6 through protein–protein interaction (Ishii et al., 2007; Ishii et al., 2014; Nakamura et al., 2016). Given the results, it is reasonable to postulate that rat UGT1A1 and 1A6 suppress CYP3A, like human UGT1A9. Dexamethasone treatment up-regulated CYP3A turnover and significantly increased V_{\max} and reduced K_M of CYP3A activity, suggesting that a portion of CYP3A showed higher catalytic activity in livers of dexamethasone-treated rats (Figure 5 and Table 4). This result suggested that dexamethasone treatment increased the amount of CYP3A that is not complexed to UGT1A, resulting in the increase of CYP3A affinity to the substrate and higher catalytic activity. This implies that CYP3A–UGT interactions regulate P450 activity under physiological conditions and this regulation is partly ablated when the molecular ratios of P450 and UGT are markedly altered by chemical-elicited inductions. Mismatch between CYP3A4 protein level and its catalytic activity in HLM also supported the presence of the interaction *in vivo*. Wandel and his colleagues (1998) utilized several batches of HLM and examined the relationship between CYP3A4 protein levels and activity using midazolam, one representative CYP3A substrate and reported that this relationship was weak ($r^2 = .31$). In that study, HLM from patient #13 had a high CYP3A4 content but failed to show a corresponding high catalytic activity. The hepatic expression level of UGTs in this patient might be higher than that in other patients, although those remain to be established. Further, Kummer, Hamann, Haschke, and Krahenbuhl (2016) reported interesting

clinical data about the care of Crigler-Najjar syndrome type II patients. Phenobarbital is utilized to up-regulate expression of UGT1A1 in these patients. However, they demonstrated that St. John's Wort, a strong inducer of CYP3A4 but not UGT1A1, also reduced total serum bilirubin and worked as an alternative drug to phenobarbital. We previously showed that CYP3A4 increased UGT1A1 activity through protein-protein interaction, an effect that would well explain the clinical report (Ishii et al., 2014). Hence, *in vivo* evidence supports the existence of P450-UGT interactions under physiological conditions.

Some drugs like phenobarbital and rifampicin can induce P450s through activation of nuclear receptors and cause drug-drug interactions (DDI), an important issue for clinical therapeutics (Fuhr, 2000; Harmsen, Meijerman, Beijnen, & Schellens, 2007). Induction of hepatic expression levels of P450 has been the main focus as a trigger of such DDI, but drugs could also affect P450-UGT complexes as shown with dexamethasone, thereby altering P450 activity (Figure 5). To date, the effect on P450-UGT interactions is indistinguishable from that of P450 induction in altering P450 activity. Thus, we have to establish methods to quantify P450-UGT complexation and comprehensively assess the effects on P450 activity in order to minimize the risk of DDI.

In conclusion, we demonstrate for the first time that UGT1A9, a major UGT isoform, can suppress CYP3A4 activity through protein-protein interaction. Further, we conclude that the molecular mechanism underlying UGT1A9-mediated suppression of CYP3A4 activity is very similar to that of UGT2B7. However, there are 22 UGT isoforms in human (Rowland, Miners, & Mackenzie, 2013), and their effects on CYP3A4 may be different. Thus, further studies are necessary to estimate their effects comprehensively. CYP3A4-UGT interactions are one aspect of the post-translational regulation of CYP3A4 activity, which may lead to a better understanding of the causes of the large inter-individual differences in P450 activities.

ACKNOWLEDGEMENTS

The authors thank Mr. Ken-ichi Yamada for constructing the UGT1A9-HA in pcDNA3.1/hygro (–) vector. The authors also thank the Research Support Center, Graduate School of Medical Sciences, Kyushu University, for technical support. This study was supported in part by the Japan Research Foundation for Clinical Pharmacology; the Grant-in-Aid for Scientific Research (B)(25293039) from Japan Society for the Promotion of Science; and the Grant-in-Aid for Scientific Research (C)(19590147) from the Ministry of Education, Culture, Sports, Science and Technology to Y.I.

CONFLICT OF INTEREST

The authors declare no conflict of interest.

AUTHOR CONTRIBUTIONS

All the authors participated in the research design. Y.M. and Y.I. performed the experiments and analysed the data. Y.M., Y.T., P.I.M., and Y.I. wrote the manuscript.

DECLARATION OF TRANSPARENCY AND SCIENTIFIC RIGOUR

This declaration acknowledges that this paper adheres to the principles for transparent reporting and scientific rigour of preclinical research as stated in the *BJP* guidelines for Design & Analysis, Immunoblotting and Immunochemistry, and Animal Experimentation, and as recommended by funding agencies, publishers, and other organizations engaged with supporting research.

MEETINGS IN WHICH A PART OF DATA WERE PRESENTED

18th Microsomes and Drug Oxidation (MDO)–12th European Regional Meeting of International Society for the Study of Xenobiotics (ISSX; 2012), 28th Japanese Society of the Study of Xenobiotics (JSSX; 2013), 134th Annual meeting of Japanese Society of Pharmaceutical Sciences (2014), 19th North American Regional Meeting of ISSX–29th JSSX (2014; Miyauchi et al.), and 20th MDO (2014; Ishii et al.).

ORCID

Yuji Ishii  <https://orcid.org/0000-0002-2069-0219>

REFERENCES

- Ahn, T., Guengerich, F. P., & Yun, C. H. (1998). Membrane insertion of cytochrome P450 1A2 promoted by anionic phospholipids. *Biochemistry*, 37(37), 12860–12866. <https://doi.org/10.1021/bi980804f>
- Alexander, S. P., Kelly, E., Marrion, N. V., Mathie, A., Peters, J. A., Veale, E. L., ... Collaborators, GTP (2019). The concise guide to PHARMACOLOGY 2019/20: Introduction and Other Protein Targets. *British Journal of Pharmacology*, 176, S1–S120. <https://doi.org/10.1111/bph.14747>
- Alexander, S. P. H., Roberts, R. E., Broughton, B. R. S., Sobey, C. G., George, C. H., Stanford, S. C., ... Ahluwalia, A. (2018). Goals and practicalities of immunoblotting and immunohistochemistry: A guide for submission to the British Journal of Pharmacology. *British Journal of Pharmacology*, 175(3), 407–411.
- Backes, W. L., & Kelley, R. W. (2003). Organization of multiple cytochrome P450s with NADPH-cytochrome P450 reductase in membranes. *Pharmacology & Therapeutics*, 98(2), 221–233.
- Bellemare, J., Rouleau, M., Harvey, M., & Guillemette, C. (2010). Modulation of the human glucuronosyltransferase UGT1A pathway by splice isoform polypeptides is mediated through protein-protein interactions. *The Journal of Biological Chemistry*, 285(6), 3600–3607.
- Berka, K., Hendrychova, T., Anzenbacher, P., & Otyepka, M. (2011). Membrane position of ibuprofen agrees with suggested access path entrance to cytochrome P450 2C9 active site. *The Journal of Physical Chemistry*, 115(41), 11248–11255. <https://doi.org/10.1021/jp204488j>
- Berka, K., Paloncova, M., Anzenbacher, P., & Otyepka, M. (2013). Behavior of human cytochromes P450 on lipid membranes. *The Journal of Physical Chemistry*, 117(39), 11556–11564. <https://doi.org/10.1021/jp4059559>
- Black, S. D. (1992). Membrane topology of the mammalian P450 cytochromes. *The FASEB Journal*, 6(2), 680–685. <https://doi.org/10.1096/fasebj.6.2.1537456>
- Brown, C. A., & Black, S. D. (1989). Membrane topology of mammalian cytochromes P-450 from liver endoplasmic reticulum. Determination by trypsinolysis of phenobarbital-treated microsomes. *The Journal of Biological Chemistry*, 264(8), 4442–4449.

- Curtis, M. J., Alexander, S., Cirino, G., Docherty, J. R., George, C. H., ... Ahluwalia, A. (2018). Experimental design and analysis and their reporting II: Updated and simplified guidance for authors and peer reviewers. *British Journal of Pharmacology*, 175(7), 987–993.
- De Martin, S., Gabbia, D., Albertin, G., Sfriso, M. M., Mescoli, C., ... Palatini, P. (2014). Differential effect of liver cirrhosis on the pregnane X receptor-mediated induction of CYP3A1 and 3A2 in the rat. *Drug Metabolism and Disposition*, 42(10), 1617–1626.
- Fremont, J. J., Wang, R. W., & King, C. D. (2005). Coimmunoprecipitation of UDP-glucuronosyltransferase isoforms and cytochrome P450 3A4. *Molecular Pharmacology*, 67(1), 260–262.
- Fuhr, U. (2000). Induction of drug metabolising enzymes: Pharmacokinetic and toxicological consequences in humans. *Clinical Pharmacokinetics*, 38(6), 493–504. <https://doi.org/10.2165/00003088-200038060-00003>
- Fujii, Y., Khoshnoodi, J., Takenaka, H., Hosoyamada, M., Nakajo, A., Bessho, F., ... Yan, K. (2006). The effect of dexamethasone on defective nephrin transport caused by ER stress: A potential mechanism for the therapeutic action of glucocorticoids in the acquired glomerular diseases. *Kidney International*, 69(8), 1350–1359. <https://doi.org/10.1038/sj.ki.5000317>
- Fujiwara, R., & Itoh, T. (2014). Extensive protein-protein interactions involving UDP-glucuronosyltransferase (UGT) 2B7 in human liver microsomes. *Drug Metabolism and Pharmacokinetics*, 29(3), 259–265.
- Ghosal, A., Sadrieh, N., Reik, L., Levin, W., & Thomas, P. E. (1996). Induction of the male-specific cytochrome P450 3A2 in female rats by phenytoin. *Archives of Biochemistry and Biophysics*, 332(1), 153–162. <https://doi.org/10.1006/abbi.1996.0327>
- Guillemette, C., Levesque, E., & Rouleau, M. (2014). Pharmacogenomics of human uridine diphospho-glucuronosyltransferases and clinical implications. *Clinical Pharmacology and Therapeutics*, 96(3), 324–339.
- Harding, S. D., Sharman, J. L., Faccenda, E., Southan, C., Pawson, A. J., Ireland, S., ... Davies, J. A. (2018). The IUPHAR/BPS Guide to PHARMACOLOGY in 2018: Updates and expansion to encompass the new guide to IMMUNOPHARMACOLOGY. *Nucleic Acids Research*, 46(D1), D1091–D1106. <https://doi.org/10.1093/nar/gkx1121>
- Harmsen, S., Meijerman, I., Beijnen, J. H., & Schellens, J. H. (2007). The role of nuclear receptors in pharmacokinetic drug-drug interactions in oncology. *Cancer Treatment Reviews*, 33(4), 369–380. <https://doi.org/10.1016/j.ctrv.2007.02.003>
- Hildebrandt, A., & Estabrook, R. W. (1971). Evidence for the participation of cytochrome b₅ in hepatic microsomal mixed-function oxidation reactions. *Archives of Biochemistry and Biophysics*, 143(1), 66–79. [https://doi.org/10.1016/0003-9861\(71\)90186-x](https://doi.org/10.1016/0003-9861(71)90186-x)
- Ishii, Y., Iwanaga, M., Nishimura, Y., Takeda, S., Ikushiro, S., ... Yamada, H. (2007). Protein-protein interactions between rat hepatic cytochromes P450 (P450s) and UDP-glucuronosyltransferases (UGTs): Evidence for the functionally active UGT in P450-UGT complex. *Drug Metabolism and Pharmacokinetics*, 22(5), 367–376.
- Ishii, Y., Koba, H., Kinoshita, K., Oizaki, T., Iwamoto, Y., Takeda, S., ... Yamada, H. (2014). Alteration of the function of the UDP-glucuronosyltransferase 1A subfamily by cytochrome P450 3A4: Different susceptibility for UGT isoforms and UGT1A1/7 variants. *Drug Metabolism and Disposition*, 42(2), 229–238. <https://doi.org/10.1124/dmd.113.054833>
- Ishii, Y., Takeda, S., & Yamada, H. (2010). Modulation of UDP-glucuronosyltransferase activity by protein-protein association. *Drug Metabolism Reviews*, 42(1), 145–158.
- Iyanagi, T., Haniu, M., Sogawa, K., Fujii-Kuriyama, Y., Watanabe, S., Shively, J. E., & Anan, K. F. (1986). Cloning and characterization of cDNA encoding 3-methylcholanthrene inducible rat mRNA for UDP-glucuronosyltransferase. *The Journal of Biological Chemistry*, 261(33), 15607–15614.
- Jemnitz, K., Veres, Z., Monostory, K., & Vereczkey, L. (2000). Glucuronidation of thyroxine in primary monolayer cultures of rat hepatocytes: in vitro induction of UDP-glucuronosyltransferases by methylcholanthrene, clofibrate, and dexamethasone alone and in combination. *Drug Metabolism and Disposition*, 28(1), 34–37.
- Johansson, I., & Ingelman-Sundberg, M. (2011). Genetic polymorphism and toxicology-with emphasis on cytochrome p450. *Toxicological Sciences*, 120(1), 1–13. <https://doi.org/10.1093/toxsci/kfq374>
- Kilkenny, C., Browne, W., Cuthill, I. C., Emerson, M., & Altman, D. G. (2010). Animal research: Reporting in vivo experiments: The ARRIVE guidelines. *British Journal of Pharmacology*, 160, 1577–1579.
- Kim, K. H., Ahn, T., & Yun, C. H. (2003). Membrane properties induced by anionic phospholipids and phosphatidylethanolamine are critical for the membrane binding and catalytic activity of human cytochrome P450 3A4. *Biochemistry*, 42(51), 15377–15387.
- Kummer, O., Hammann, F., Haschke, M., & Krahenbuhl, S. (2016). Reduction of hyperbilirubinemia with hypericum extract (St. John's Wort) in a patient with Crigler-Najjar syndrome type II. *British Journal of Clinical Pharmacology*, 81(5), 1002–1004.
- Kurkela, M., Morsky, S., Hirvonen, J., Kostinen, R., & Finel, M. (2004). An active and water-soluble truncation mutant of the human UDP-glucuronosyltransferase 1A9. *Molecular Pharmacology*, 65(4), 826–831. <https://doi.org/10.1124/mol.65.4.826>
- Laakkonen, L., & Finel, M. (2010). A molecular model of the human UDP-glucuronosyltransferase 1A1, its membrane orientation, and the interactions between different parts of the enzyme. *Molecular Pharmacology*, 77(6), 931–939. <https://doi.org/10.1124/mol.109.063289>
- Lamba, J. K., Lin, Y. S., Schuetz, E. G., & Thummel, K. E. (2002). Genetic contribution to variable human CYP3A-mediated metabolism. *Advanced Drug Delivery Reviews*, 54(10), 1271–1294.
- Lowry, O. H., Rosebrough, N. J., Farr, A. L., & Randall, R. J. (1951). Protein measurement with the Folin phenol reagent. *The Journal of Biological Chemistry*, 193(1), 265–275.
- Lu, A. Y., Junk, K. W., & Coon, M. J. (1969). Resolution of the cytochrome P-450-containing ω -hydroxylation system of liver microsomes into three components. *The Journal of Biological Chemistry*, 244(13), 3714–3721.
- Mackenzie, P. I. (1986). Rat liver UDP-glucuronosyltransferase. cDNA sequence and expression of a form glucuronidating 3-hydroxyandrogens. *The Journal of Biological Chemistry*, 261(30), 14112–14117.
- Meech, R., & Mackenzie, P. I. (1997). Structure and function of uridine diphosphate glucuronosyltransferases. *Clinical and Experimental Pharmacology & Physiology*, 24(12), 907–915. <https://doi.org/10.1111/j.1440-1681.1997.tb02718.x>
- Meech, R., & Mackenzie, P. I. (1998). Determinants of UDP glucuronosyltransferase membrane association and residency in the endoplasmic reticulum. *Archives of Biochemistry and Biophysics*, 356(1), 77–85.
- Menard, V., Eap, O., Roberge, J., Harvey, M., Levesque, E., & Guillemette, C. (2011). Transcriptional diversity at the UGT2B7 locus is dictated by extensive pre-mRNA splicing mechanisms that give rise to multiple mRNA splice variants. *Pharmacogenetics and Genomics*, 21(10), 631–641.
- Miwa, G. T., & Lu, A. Y. (1984). The association of cytochrome P-450 and NADPH-cytochrome P-450 reductase in phospholipid membranes. *Archives of Biochemistry and Biophysics*, 234(1), 161–166.
- Miyauchi, Y., Nagata, K., Yamazoe, Y., Mackenzie, P. I., Yamada, H., & Ishii, Y. (2015). Suppression of cytochrome P450 3A4 function by UDP-glucuronosyltransferase 2B7 through a protein-protein interaction: Cooperative roles of the cytosolic carboxyl-terminal domain and the luminal anchoring region. *Molecular Pharmacology*, 88(4), 800–812. <https://doi.org/10.1124/mol.115.098582>
- Nakamura, T., Yamaguchi, N., Miyauchi, Y., Takeda, T., Yamazoe, Y., ... Ishii, Y. (2016). Introduction of an N-glycosylation site into UDP-glucuronosyltransferase 2B3 alters its sensitivity to cytochrome P450

- 3A1-dependent modulation. *Frontiers in Pharmacology*, 7:427. eCollection 2016 <https://doi.org/10.3389/fphar.2016.00427>
- Nishimura, Y., Maeda, S., Ikushiro, S., Mackenzie, P. I., Ishii, Y., & Yamada, H. (2007). Inhibitory effects of adenine nucleotides and related substances on UDP-glucuronosyltransferase: Structure-effect relationships and evidence for an allosteric mechanism. *Biochimica et Biophysica Acta*, 1770(11), 1557–1566. <https://doi.org/10.1016/j.bbagen.2007.07.011>
- Oguri, K., Kurogi, A., Yamabe, K., Tanaka, M., Yoshisue, K., ... Yoshimura, H. (1996). Purification of a phenobarbital-inducible UDP-glucuronosyltransferase isoform from dog liver which catalyzes morphine and testosterone glucuronidation. *Archives of Biochemistry and Biophysics*, 325(2), 159–166.
- Ouzzine, M., Magdalou, J., Burchell, B., & Fournel-Gigleux, S. (1999). An internal signal sequence mediates the targeting and retention of the human UDP-glucuronosyltransferase 1A6 to the endoplasmic reticulum. *The Journal of Biological Chemistry*, 274(44), 31401–31409. <https://doi.org/10.1074/jbc.274.44.31401>
- Radomska-Pandya, A., Czernik, P. J., Little, J. M., Battaglia, E., & Mackenzie, P. I. (1999). Structural and functional studies of UDP-glucuronosyltransferases. *Drug Metabolism Reviews*, 31(4), 817–899.
- Rouleau, M., Audet-Delage, Y., Desjardins, S., Girard-Bock, C., & Guillemette, C. (2017). Endogenous protein interactome of human UDP-glucuronosyltransferases exposed by untargeted proteomics. *Frontiers in Pharmacology*, 8:23. eCollection 2017. <https://doi.org/10.3389/fphar.2017.00023>
- Rowland, A., Miners, J. O., & Mackenzie, P. I. (2013). The UDP-glucuronosyltransferases: Their role in drug metabolism and detoxification. *The International Journal of Biochemistry & Cell Biology*, 45(6), 1121–1132. <https://doi.org/10.1016/j.biocel.2013.02.019>
- Shimada, T., Yamazaki, H., Mimura, M., Inui, Y., & Guengerich, F. P. (1994). Interindividual variations in human liver cytochrome P-450 enzymes involved in the oxidation of drugs, carcinogens and toxic chemicals: Studies with liver microsomes of 30 Japanese and 30 Caucasians. *The Journal of Pharmacology and Experimental Therapeutics*, 270(1), 414–423.
- Szczesna-Skorupa, E., Ahn, K., Chen, C. D., Doray, B., & Kemper, B. (1995). The cytoplasmic and N-terminal transmembrane domains of cytochrome P450 contain independent signals for retention in the endoplasmic reticulum. *The Journal of Biological Chemistry*, 270(41), 24327–24333. <https://doi.org/10.1074/jbc.270.41.24327>
- Takeda, S., Ishii, Y., Iwanaga, M., Mackenzie, P. I., Nagata, K., Yamazoe, Y., ... Yamada, H. (2005). Modulation of UDP-glucuronosyltransferase function by cytochrome P450: Evidence for the alteration of UGT2B7-catalyzed glucuronidation of morphine by CYP3A4. *Molecular Pharmacology*, 67(3), 665–672. <https://doi.org/10.1124/mol.104.007641>
- Takeda, S., Ishii, Y., Iwanaga, M., Nurrochmad, A., Ito, Y., Mackenzie, P. I., ... Yamada, H. (2009). Interaction of cytochrome P450 3A4 and UDP-glucuronosyltransferase 2B7: Evidence for protein-protein association and possible involvement of CYP3A4 J-helix in the interaction. *Molecular Pharmacology*, 75(4), 956–964. <https://doi.org/10.1124/mol.108.052001>
- Taura, K., Naito, E., Ishii, Y., Mori, M. A., Oguri, K., & Yamada, H. (2004). Cytochrome P450 1A1 (CYP1A1) inhibitor α -naphthoflavone interferes with UDP-glucuronosyltransferase (UGT) activity in intact but not in permeabilized hepatic microsomes from 3-methylcholanthrene-treated rats: Possible involvement of UGT-P450 interactions. *Biological & Pharmaceutical Bulletin*, 27(1), 56–60.
- Taura, K. I., Yamada, H., Hagino, Y., Ishii, Y., Mori, M. A., & Oguri, K. (2000). Interaction between cytochrome P450 and other drug-metabolizing enzymes: Evidence for an association of CYP1A1 with microsomal epoxide hydrolase and UDP-glucuronosyltransferase. *Biochemical and Biophysical Research Communications*, 273(3), 1048–1052. <https://doi.org/10.1006/bbrc.2000.3076>
- Thummel, K. E., & Wilkinson, G. R. (1998). In vitro and in vivo drug interactions involving human CYP3A. *Annual Review of Pharmacology and Toxicology*, 38, 389–430. <https://doi.org/10.1146/annurev.pharmtox.38.1.389>
- Uchaipichat, V., Mackenzie, P. I., Guo, X. H., Gardner-Stephen, D., Galetin, A., Houston, J. B., & Miners, J. O. (2004). Human UDP-glucuronosyltransferases: Isoform selectivity and kinetics of 4-methylumbelliferone and 1-naphthol glucuronidation, effects of organic solvents, and inhibition by diclofenac and probenecid. *Drug Metabolism and Disposition*, 32(4), 413–423. <https://doi.org/10.1124/dmd.32.4.413>
- Wandel, C., Bocker, R. H., Bohrer, H., deVries, J. X., Hofmann, W., ... Martin, E. (1998). Relationship between hepatic cytochrome P450 3A content and activity and the disposition of midazolam administered orally. *Drug Metabolism and Disposition*, 26(2), 110–114.
- Zanger, U. M., & Schwab, M. (2013). Cytochrome P450 enzymes in drug metabolism: Regulation of gene expression, enzyme activities, and impact of genetic variation. *Pharmacology & Therapeutics*, 138(1), 103–141.

SUPPORTING INFORMATION

Additional supporting information may be found online in the Supporting Information section at the end of this article.

How to cite this article: Miyauchi Y, Tanaka Y, Nagata K, et al. UDP-Glucuronosyltransferase (UGT)-mediated attenuations of cytochrome P450 3A4 activity: UGT isoform-dependent mechanism of suppression. *Br J Pharmacol*. 2020;1–13. <https://doi.org/10.1111/bph.14900>

In Vitro and in Vivo antitumor activity and the mechanism of siphonodictyal B in human colon cancer cells

Sonoko Chikamatsu¹  | Ken Saijo^{1,2}  | Hiroo Imai^{1,2} | Koichi Narita³ | Yoshifumi Kawamura¹ | Tadashi Katoh⁴ | Chikashi Ishioka^{1,2}

¹Department of Clinical Oncology, Institute of Development, Aging and Cancer, Tohoku University, Sendai, Japan

²Department of Medical Oncology, Tohoku University Hospital, Sendai, Japan

³Laboratory of Synthetic and Medicinal Chemistry, Faculty of Pharmaceutical Sciences, Tohoku Medical and Pharmaceutical University, Sendai, Japan

⁴Faculty of Pharmaceutical Sciences, Research Center for Drug Discovery, Tohoku Medical and Pharmaceutical University, Sendai, Japan

Correspondence

Chikashi Ishioka, Department of Clinical Oncology, Institute of Development, Aging and Cancer, Tohoku University, 4-1, Seiryomachi, Aoba-ku, Sendai, Japan.
Email: chikashi@tohoku.ac.jp

Abstract

Liphagal, isolated from the marine sponge *Aka coralliphaga*, exhibits phosphatidylinositol 3-kinase alpha (PI3K α) inhibitory activity and cytotoxic effects in human cancer cells. Siphonodictyal B, the biogenetic precursor of liphagal, also has PI3K inhibitory activity. However, its cytotoxic or antitumor activities have not been evaluated. In this study, we demonstrated that siphonodictyal B inhibits several kinases such as CDK4/6, CDK7, and PIM2 in addition to PI3K in vitro and that siphonodictyal B exhibits more potent cytotoxic effects than liphagal against human colon cancer cell lines. Furthermore, treatment with siphonodictyal B resulted in increased PARP cleavage, a larger sub-G1 fraction, and a larger annexin V-positive cell population, all of which are indicative of apoptosis induction. As a mechanism of apoptosis induction, we found that siphonodictyal B activates the p38 MAPK pathway, leading the upregulation of proapoptotic factors. Moreover, siphonodictyal B increased ROS levels, thus promoting p38 MAPK pathway activation. NAC, an ROS scavenger, almost completely reversed both the cytotoxic and p38 MAPK pathway-activating effects of siphonodictyal B. These results indicate that the p38 MAPK pathway might be involved downstream of ROS signaling as part of the mechanism of siphonodictyal B-induced apoptosis. Finally, siphonodictyal B displayed antitumor effects in a human colon cancer xenograft mouse model and increased p38 phosphorylation in tumor tissue. These results suggest that siphonodictyal B could serve as the basis of a novel anticancer drug.

KEYWORDS

liphagal, p38 MAPK pathway, reactive oxygen species, siphonodictyal B, terpenoid

1 | INTRODUCTION

Compounds isolated from natural products have attracted attention, as some possess unique chemical structures and biological activities that can lead to the development of novel anticancer drugs.¹⁻³ Terpenoids are the most widespread

group of natural products with a chemically characteristic structure of five-carbon isoprene units.^{1,2} Liphagal and siphonodictyal B are meroterpenoids that were isolated from the marine sponge *Aka coralliphaga*^{4,5} (Figure 1). Generally, it is difficult to obtain sufficient samples of natural products for biological assays or developing pharmaceutical products

This is an open access article under the terms of the Creative Commons Attribution License, which permits use, distribution and reproduction in any medium, provided the original work is properly cited.

© 2019 The Authors. *Cancer Medicine* published by John Wiley & Sons Ltd.

because of their scarcity. Meanwhile, the total synthesis of such natural compounds has been pursued with great enthusiasm. Concerning liphagal and siphonodictyal B, efficient and successful total synthetic methods have been reported.⁵ In the synthetic process, siphonodictyal B corresponds to the biogenetic precursor of liphagal.⁵

Furthermore, both liphagal and siphonodictyal B have been reported to exert inhibitory activity against phosphatidylinositol 3-kinase (PI3K),^{4,6} a lipid kinase that converts phosphatidylinositol 4,5-bisphosphate to phosphatidylinositol 3,4,5-triphosphate (PIP3). PIP3 in turn activates protein kinase B (AKT) and downstream molecules, leading to the promotion of cell growth, proliferation, and survival.⁷ In many types of cancer cells, the PI3K-AKT pathway is frequently activated through gain-of-function mutations in PIK3CA, which encodes p110 α , the catalytic subunit of PI3K.⁸ Therefore, PI3K is considered a potential drug target for cancer therapy.^{9,10} Although liphagal was reported to exhibit cytotoxic effects in human colon cancer cells,⁴ the effects of siphonodictyal B on human cancer cell have never been evaluated. In the present study, we illustrated that siphonodictyal B induced apoptosis more potently than liphagal in human colon cancer cells. Then, we focused on siphonodictyal B and analyzed the mechanism by which siphonodictyal B induces apoptosis. Furthermore, we confirmed the *in vivo* antitumor activity of siphonodictyal B in a human colon cancer cell xenograft mouse model.

2 | MATERIALS AND METHODS

2.1 | Reagents

Liphagal and siphonodictyal B were synthesized chemically and provided by Tadashi Katoh at Tohoku Medical and Pharmaceutical University (Sendai, Japan). GDC0941 was purchased from Abcam (Cambridge, UK). Palbociclib was purchased from ChemoScene (Monmouth Junction, NJ, USA). SB203580 was purchased from Cayman Chemical Company (Ann Arbor, MI, USA). N-acetyl-L-cysteine (NAC) was purchased from Sigma-Aldrich (St. Louis, MO, USA).

2.2 | Cell lines and cell culture

The human colon cancer cell lines HCT 116 and SW480 were purchased from American Type Culture Collection (ATCC, Manassas, VA, USA). HT-29 was a gift from Dr John M. Mariandason at Ludwig Institute for Cancer Research, Austin Hospital (Heidelberg, VIC, Australia). Early passage aliquots were frozen. Cells used in this study were replenished from the frozen stocks. All cell lines were cultured in RPMI-1640 medium supplemented 10% fetal bovine serum at 37°C in an atmosphere of 5%CO₂.

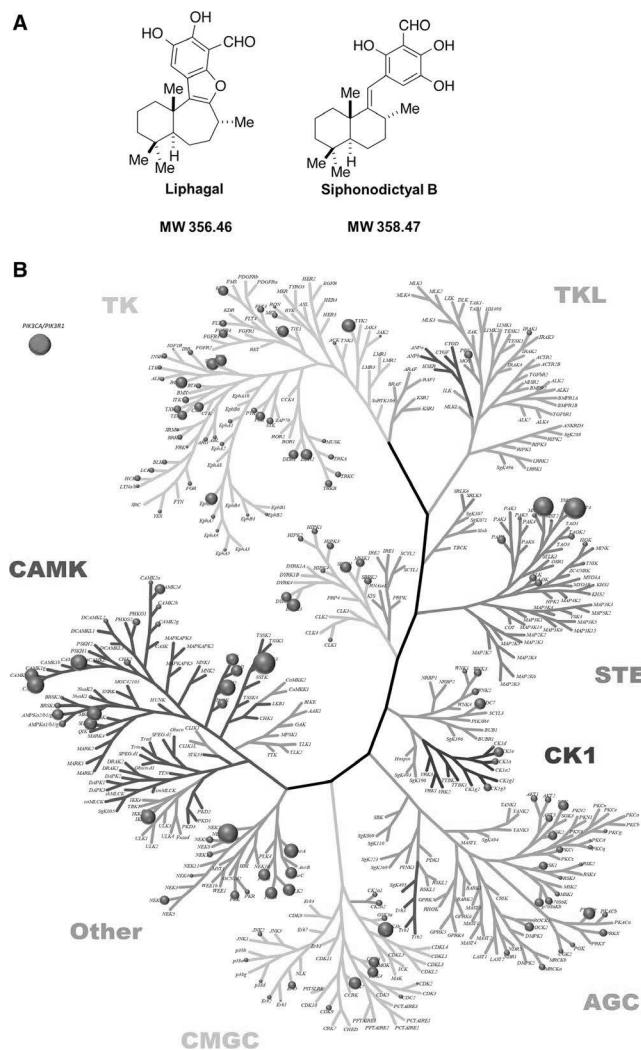


FIGURE 1 Chemical structure and kinome inhibition plot. A, Chemical structure of liphagal and siphonodictyal B. B, Plot of kinome inhibition by siphonodictyal B. The inhibition of 313 protein kinases by siphonodictyal B at 10 μ mol/L was evaluated using the off-chip mobility shift assay or immobilized metal ion affinity-based fluorescence polarization assay. The strengths of the inhibitory activities against kinases are illustrated by the sizes of the circles. PI3K was not included in the tree because of its lipid kinase features. Therefore, the circle was written in a separate frame

2.3 | Enzyme assay in cell-free system

Cellular kinase activities were evaluated using nonradioisotopic methods such as the off-chip mobility shift assay or IMAP (Carna Biosciences, Kobe, Japan).¹¹ A kinase inhibition profiling panel was produced on the basis of the kinase inhibition rates. In off-chip mobility shift assay, compound solution was prepared in assay buffer (20 mmol/L HEPES, 0.01% Triton X-100, 2 mmol/L DTT, pH 7.5) and incubated in a 384-well plate at room temperature. The reaction was stopped by adding Termination Buffer (QuickScout Screening Assist MSA; Carna Biosciences, Kobe, Japan).

Kinase	CDK4/ Cyclin D3	CDK6/ Cyclin D3	CDK7/Cyclin H/		PIK3CA/ PIK3R1 ^a
			MAT1	PIM2	
Liphalgal	19.9	6.78	1.27	5.31	4.12
Siphonodictyal B	32.9	69.1	13.7	6.99	2.62

Kinase inhibitory activities were measured by the off-chip mobility shift assay. IC₅₀ (μmol/L) value was shown.

^aKikuchi T, Narita K, Saijo K, Ishioka C, Katoh T. Enantioselective Total Synthesis of (–)-Siphonodictyal B and (+)-8-epi-Siphonodictyal B with Phosphatidylinositol 3-Kinase α (PI3Kα) Inhibitory Activity. 2016;2016(34):5659–66.

TABLE 1 Evaluation of kinases inhibitory activities of liphalgal or siphonodictyal B

The substrate peptide and the phosphorylated peptide in the reaction solution were separated and quantified by LabChip system (Perkin Elmer, MA, USA). In IMAP assay, compound solution was prepared in assay buffer (20 mmol/L HEPES, 0.01% Tween-20, 2 mmol/L DTT, pH 7.4) and incubated in a 384-well black plate at room temperature. IMAP binding reagent (IMAP Screening Express kit; Molecular Devices, CA, USA) was added and incubated for 30 minutes. The kinase reaction was evaluated at the fluorescence polarization.

2.4 | Cell proliferation assay

Cells were seeded in 96-well plates at 4000 cells/well and incubated for 24 hours, then treated with each concentration of siphonodictyal B. In experiments with SB203580 or NAC, cells were further preincubated for 24 or 1 hour before application of siphonodictyal B, respectively. Cells were incubated with Cell Counting Kit-8 (Dojindo Molecular Technologies, Kumamoto, Japan) for 1.5 hours. Then, the absorbance of each well was measured using SpectraMaxM2e (Molecular Devices, CA, USA). The ratios of surviving cells to control cells treated with 0.1% DMSO were calculated.

2.5 | Cell cycle analysis

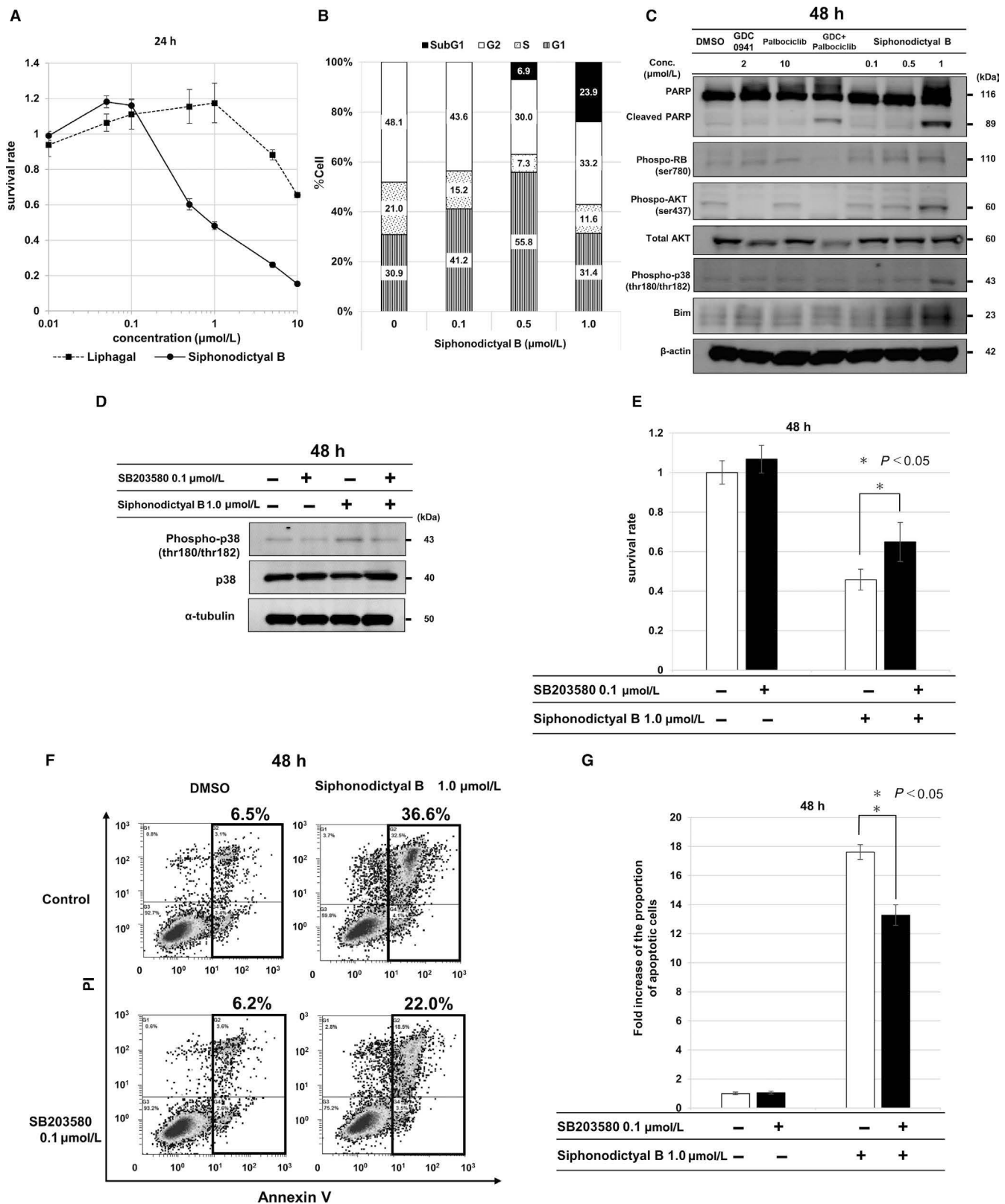
A total of 1×10^6 HCT 116 cells were seeded and incubated for 24 hours. Cells were treated with each concentration of siphonodictyal B for 24 hours. Cells were harvested, washed in PBS, and fixed with 70% ethanol overnight at 4°C. After that, cells were incubated with RNase and propidium iodide (PI). The measurement was performed using FC-500 (Beckman Coulter, CA, USA).

2.6 | Western blot analysis

HCT 116 cells were seeded in six-well plates at 2×10^5 cells/well and incubated for 24 hours. Cells were treated with each concentration of siphonodictyal B, GDC0941, palbociclib, or a combination of GDC0941 and palbociclib for 48 hours. Cells were harvested and lysed using RIPA buffer. The proteins were separated on an SDS-PAGE and transferred to PVDF membranes. Then, the membranes were blocked for 1 hour and incubated with primary antibodies overnight at 4°C. The membranes were washed and incubated with secondary antibodies for 1 hour at room temperature. Next, the resultant bands were detected using an Odyssey Infrared Imaging system

FIGURE 2 Effects by siphonodictyal B on cell proliferation, the cell cycle, and apoptosis. A, The antiproliferative effects of liphalgal and siphonodictyal B. HCT 116 cells were treated with liphalgal or siphonodictyal B at a concentration of 0.01, 0.05, 0.1, 0.5, 1, 5, or 10 μmol/L for 24 h. The ratios of surviving cells to control cells treated with 0.1% DMSO were calculated. Data are the means ± SD of three independent experiments performed triplicate. B, Flow cytometric analysis of the cell cycle. The G1, S, G2/M, and sub-G1 phase populations are shown. HCT 116 cells were treated with siphonodictyal B at a concentration of 0.1, 0.5, or 1.0 μmol/L for 24 h. Siphonodictyal B induced G1 arrest and increased the sub-G1 population. C, Western blot analysis of cells treated with 2 μmol/L GDC0941, 10 μmol/L palbociclib, a combination of 2 μmol/L GDC0941 and 10 μmol/L palbociclib (GDC + palbociclib), or siphonodictyal B (0.1, 0.5, or 1 μmol/L) for 48 h. Cleaved PARP, phospho-AKT, phospho-RB, phospho-p38, and Bim were analyzed. D, Western blot analysis of phospho-p38 expression in cells treated with siphonodictyal B with or without SB203580 for 48 h. E, Antiproliferative effects of siphonodictyal B with or without SB203580 for 48 h. The ratios of surviving cells to control cells were calculated. Data are the means ± SD of three independent experiments performed triplicate. **P* < 0.05 compared with cells treated with siphonodictyal B alone. F, Flow cytometric analyses of apoptosis using annexin V and PI double staining in HCT 116 cells. HCT 116 cells were treated with siphonodictyal B with or without SB203580 for 48 h. The percentages of apoptotic cells are shown. G, The bar charts representing the proportion of apoptotic cells expressed as the fold increase vs that for untreated cells. Data are the means ± SD of three independent experiments. **P* < 0.05 compared with cells treated with siphonodictyal B alone

(LI-COR, NB, USA). Antibodies against phospho-RB (Ser780), AKT, phospho-AKT (Ser437), PARP, phospho-p38 MAPK (Thr180/Tyr182), p38 MAPK, and Bim were purchased from Cell Signaling Technology (Danvers, MA, USA). Antibodies against β -actin and α -tubulin were purchased from Sigma-Aldrich.



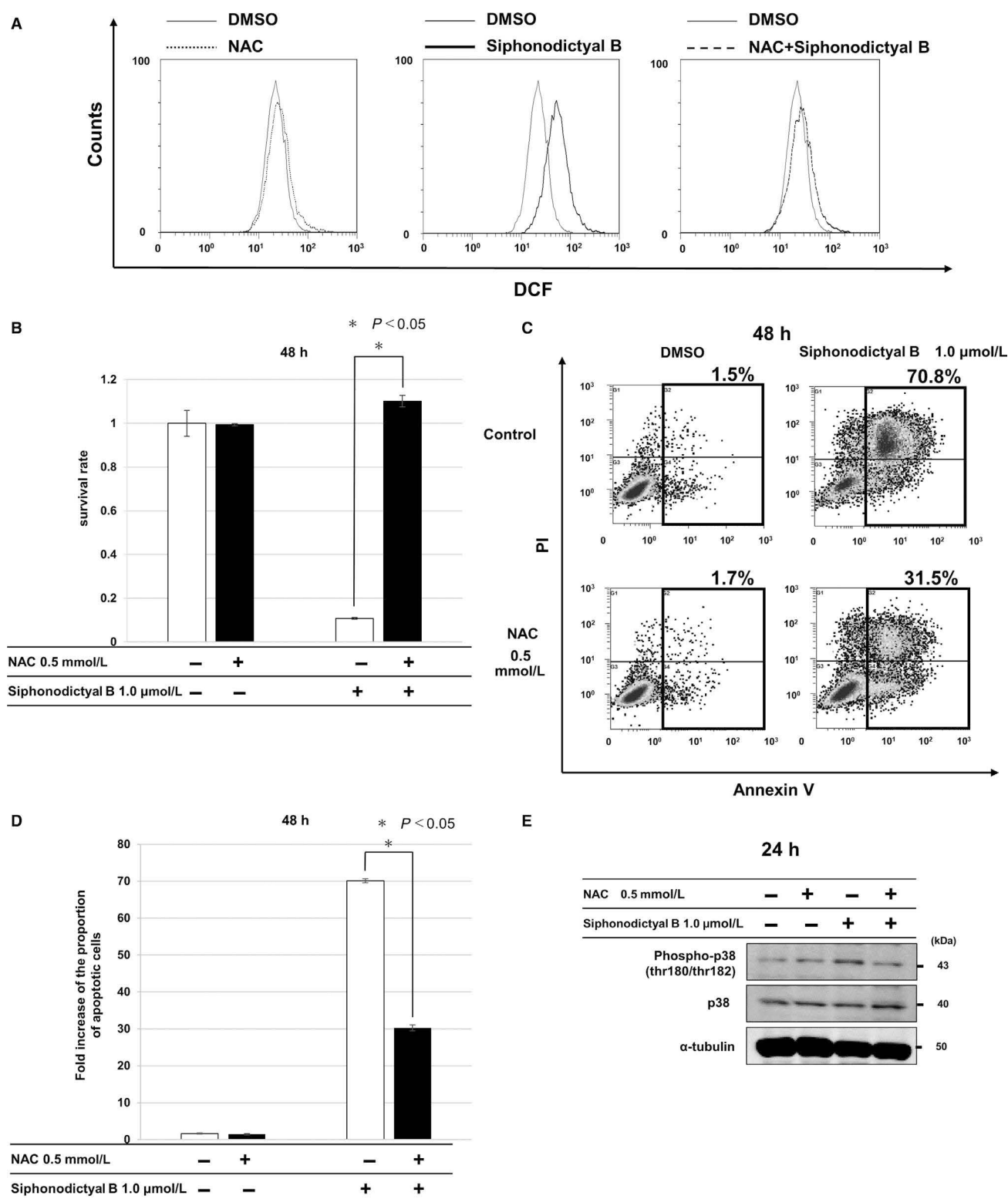


FIGURE 3 Elevation of intracellular ROS levels by siphonodictyal B. A, Flow cytometry of intracellular ROS levels using DCFDA staining in HCT 116 cells. HCT 116 cells were treated with siphonodictyal B with or without NAC for 2 h. B, Antiproliferative effects of siphonodictyal B with or without NAC for 24 h. The ratios of surviving cells to control cells were calculated. Data are the means \pm SD of three independent experiments performed triplicate. * $P < 0.05$ compared with cells treated with siphonodictyal B alone. C, Flow cytometry of apoptosis using Annexin V and PI double staining in HCT 116 cells. HCT 116 cells were treated with siphonodictyal B with or without NAC for 24 h. The percentages of apoptotic cells are shown. D, The bar charts express the proportion of apoptotic cells as fold increases vs the number of cells treated with 0.1% DMSO. Data are the means \pm SD of three independent experiments. * $P < 0.05$ compared with cells treated with siphonodictyal B alone. E, Western blotting of phospho-p38 in cells treated with siphonodictyal B with or without NAC for 24 h

2.7 | siRNA transfection

HCT 116 cells were seeded in 24-well plates at 2.5×10^4 cells/well and incubated for 24 hours. Cells were transfected with 6 pmol/well siRNA against p38 or negative control siRNA using Lipofectamine 2000 Transfection Reagent (Thermo Fisher Scientific, Waltham, MA, USA). All siRNAs were purchased from Thermo Fisher Scientific.

2.8 | Annexin V-PI double staining

HCT 116 cells were seeded in six-well plates at 2×10^5 cells/well and incubated for 24 hours. In experiments with SB203580 or NAC, cells were further preincubated for 24 or 1 hour before application of siphonodictyal B, respectively. Cells were washed with PBS and stained using an Annexin V-FITC Apoptosis Detection Kit (Nacalai Tesque, Kyoto, Japan). The measurement was performed using FC-500.

2.9 | Reactive oxygen species (ROS) detection

HCT 116 cells were treated with each drug for 2 hours and stained using a DCFDA/H2DCFDA—Cellular Reactive Oxygen Species Detection Assay Kit (Abcam). The measurement was performed using FC-500.

2.10 | Xenograft mouse model

All animal experiments were performed according to the Regulations for Animal Experiments and Related Activities at Tohoku University. Six-week-old female Balb/c nude mice were purchased from Charles River Laboratories (Wilmington, MA, USA). HCT 116 cells (5×10^6) were implanted subcutaneously into the right flanks of nude mice. After tumor formation was confirmed, mice were assigned to treatment with 20 mg/kg siphonodictyal B or vehicle (four mice per group) administered intraperitoneally every 3 days. Siphonodictyal B was dissolved in saline with 2.5% CremophorEL[®] and 2.5% ethanol. Tumor volumes were calculated on the basis of tumor mass using the formula $\text{length} \times \text{width} \times \text{width}/2$ (mm^3). The body weights of mice were also measured every 3 days.

2.11 | Immunohistochemistry

Tumor tissues were collected from mice, fixed in 10% formalin, and embedded in paraffin. Tumor sections on slides were dewaxed, rehydrated, and incubated with a specific antibody against phospho-p38.

2.12 | Statistical analysis

All data were presented as the mean \pm standard deviation. Statistical analysis was performed using JMP Pro 12 software (SAS, Cary, NC, USA). Unless otherwise noted, the significance of differences was examined using Student's *t* tests. $P < 0.05$ indicated a statistically significant difference.

3 | RESULTS

3.1 | Evaluation of the kinase inhibitory activities of liphagal and siphonodictyal B in cell-free system

Although liphagal and siphonodictyal B were reported to have PI3K (p110 α /p85 α) inhibitory activity with IC₅₀ values of 4.1 and 2.6 $\mu\text{mol/L}$, respectively,⁶ their inhibitory activities against other kinases have not been evaluated. Therefore, we evaluated the inhibitory activities of liphagal and siphonodictyal B against 313 kinases using a kinase panel assay. As shown in Figure S1 and Figure 1B, liphagal and siphonodictyal B had inhibitory activities against several kinases. In particular, liphagal and siphonodictyal B strongly inhibited activities against cyclin-dependent kinase 4 (CDK4), CDK6, CDK7, and proto-oncogene proviral integration site for murine leukemia virus-2 (PIM-2). The IC₅₀ values of liphagal and siphonodictyal B against CDK4, CDK6, CDK7, and PIM2 are shown in Table 1.

3.2 | Cytotoxic effects of liphagal and siphonodictyal B against human colon cancer cell lines

We performed cell proliferation assays to evaluate the cytotoxic effects of liphagal and siphonodictyal B on human colon cancer cell lines. Siphonodictyal B exhibited more potent cytotoxic effects than liphagal in HCT 116 cells (Figure 2A). Similar results were also shown in HT-29 and SW480 cells (Figure S2). Based on these results, we focused on siphonodictyal B in subsequent experiments.

3.3 | The effects of siphonodictyal B on the cell cycle in HCT 116 cells

We performed FACS analyses to evaluate the effects of siphonodictyal B on the cell cycle. As shown in Figure 2B, both the G1 and sub-G1 populations were slightly increased by treatment with 0.5 $\mu\text{mol/L}$ siphonodictyal B. Moreover, the sub-G1 phase was clearly increased by treatment with 1.0 $\mu\text{mol/L}$ siphonodictyal B. These results revealed that

siphonodictyal B induces apoptosis at higher concentrations in HCT 116 cells.

3.4 | Siphonodictyal B induces apoptosis in HCT 116 via the induction of Bim

We performed Western blotting to investigate the molecular mechanism of apoptosis induced by siphonodictyal B. As shown in Figure 2C, treatment with 0.5 or 1.0 $\mu\text{mol/L}$ of siphonodictyal B increased the levels of the apoptosis-promoting protein Bim concentration dependently in HCT 116 cells. Treatment with 1.0 $\mu\text{mol/L}$ siphonodictyal B also induced PARP cleavage. These results suggested that apoptosis induced by siphonodictyal B is attributable to the induction of Bim. Although siphonodictyal B has PI3K and CDK4/6 inhibitory activity, it did not inhibit AKT phosphorylation at Ser473 or RB phosphorylation at Ser780 in HCT 116 cells. By contrast, the PI3K inhibitor GDC0941 inhibited AKT phosphorylation. The CDK4 inhibitor palbociclib inhibited RB phosphorylation. Moreover, the combination of GDC0941 and palbociclib increased PARP cleavage. From these results, it was assumed that inhibitory activities against PI3K and CDK4/6 did not contribute to apoptosis induced by siphonodictyal B.

3.5 | Siphonodictyal B induces apoptosis through p38 phosphorylation

It was previously reported that apoptosis is induced through activation of the p38 MAPK pathway in HCT 116 cells.^{12,13} Therefore, we performed Western blotting to evaluate the effects of siphonodictyal B on the p38 MAPK pathway. As shown in Figure 2C, treatment with 1.0 $\mu\text{mol/L}$ siphonodictyal B for 48 hour clearly induced p38 phosphorylation. Addition of the p38-specific inhibitor SB203580 to siphonodictyal B resulted in reduced p38 phosphorylation (Figure 2D). In the cell proliferation assay, the addition of SB203580 partially canceled the cytotoxic effect of siphonodictyal B (Figure 2E). Likewise, in the annexin V-PI double staining assay, the population of apoptotic cells induced by siphonodictyal B was attenuated by the addition of SB203580 (Figure 2F,G).

Moreover, the contribution of the p38 pathway was further validated via an RNAi approach. The protein level of phosphorylated p38 was significantly lower in cells treated

with p38 siRNA (si#1 and si#2) than in cells treated with control RNA (siScr) (Figure S2A). Depletion of p38 partially reduced the cytotoxic effect of siphonodictyal B (Figure S2B). As expected, the annexin V-PI double staining assay revealed that the induction of apoptosis by siphonodictyal B was lower in cells treated with p38 siRNA than in cells treated with control siRNA (Figure S2C,D). From these results, it was considered that in HCT 116 cells, siphonodictyal B induced apoptosis partially through the induction of p38 phosphorylation.

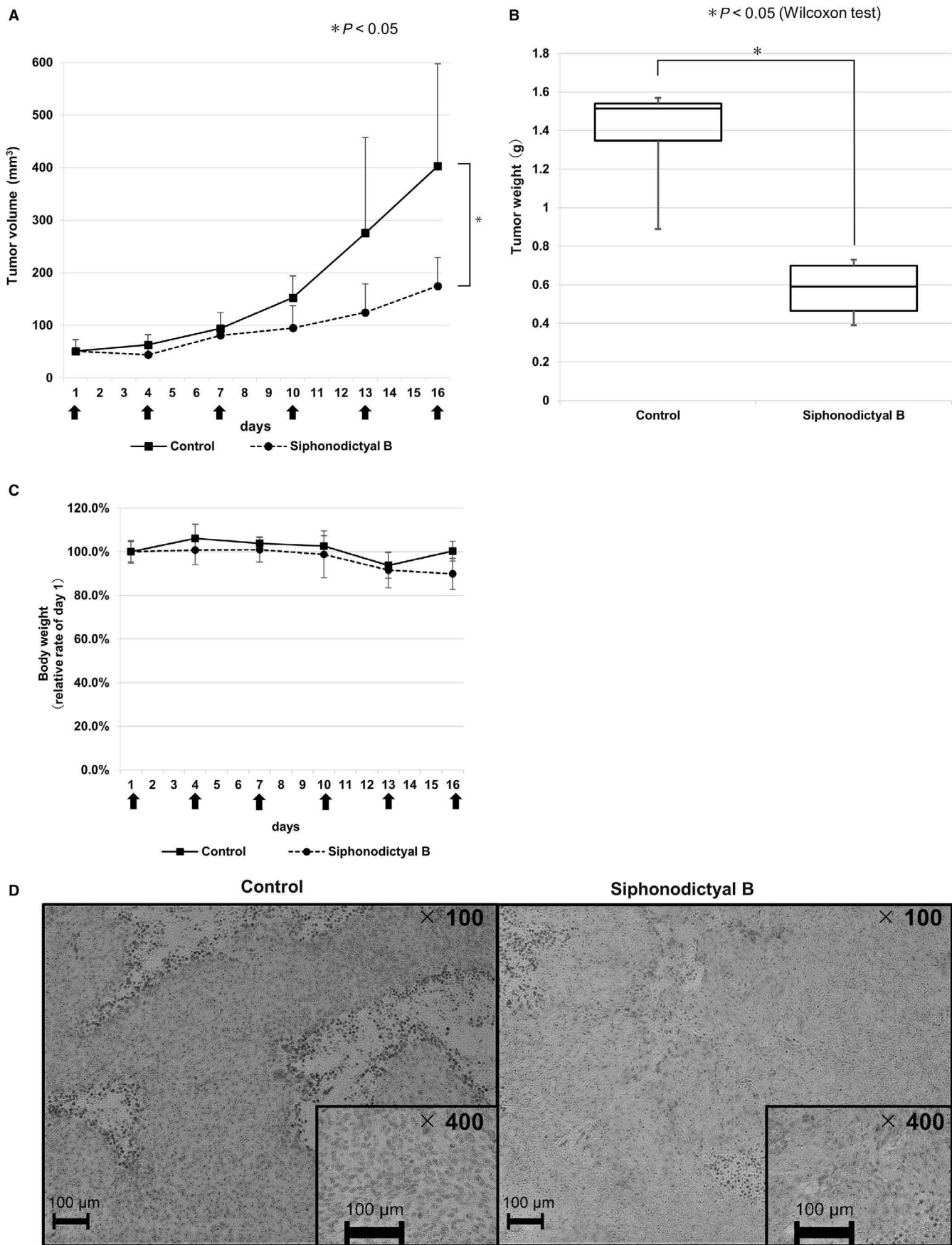
3.6 | Siphonodictyal B induced apoptosis in HCT 116 cells by increasing ROS production

It had been reported that several terpenoids increased ROS levels and subsequently induced apoptosis in cancer cells.^{14–17} We performed 2',7'-dichlorofluorescein diacetate (DCFDA) staining and FACS analysis to evaluate whether apoptosis induction by siphonodictyal B is related to ROS production. As shown in Figure 3A, ROS levels were higher in cells treated with siphonodictyal B than in those treated with DMSO. However, increased ROS production induced by siphonodictyal B was completely canceled by the addition of NAC, a scavenger of ROS (Figure 3A). The cytotoxic effects induced by siphonodictyal B alone were almost completely rescued by the addition of NAC (Figure 3B). Furthermore, the population of apoptotic cells induced by siphonodictyal B was greatly reduced by the addition of NAC (Figure 3C,3). These results indicated that siphonodictyal B induced apoptosis through the induction of ROS production in HCT 116 cells. The upregulation of phosphorylated p38 by siphonodictyal B was reduced by NAC (Figure 3E). These results suggested that siphonodictyal B induced apoptosis through the increase of ROS production and subsequent activation of the p38 MAPK pathway in HCT 116 cells.

3.7 | Evaluation of the in vivo antitumor activity of siphonodictyal B

Antitumor efficacy was evaluated using HCT 116 xenograft mouse models. Mice were divided in two groups (control group: solvent was intraperitoneally administered every 3 days and siphonodictyal B group: 20 mg/kg of siphonodictyal B was intraperitoneally administered every 3 days). As

FIGURE 4 Antitumor activity of siphonodictyal B in vivo. (A–C) HCT116 cells were implanted subcutaneously into the right flanks of mice. Mice were treated with siphonodictyal B (20 mg/kg) or vehicle via intraperitoneal injection every 3 d. Four mice were used for each treatment group. The tumor volumes in mice treated with vehicle or siphonodictyal B. The siphonodictyal B injection times are shown by black arrows. Data are the means \pm SD from four mice. $*P < 0.05$ compared with the control group. Tumor weights were measured and represented by the boxplot. Data are the medians \pm SD from four mice. $*P < 0.05$ compared with the control group. Body weights of mice were measured every 3 days. The relative ratios to the initial weights are shown. The siphonodictyal B injection times are shown by black arrows. Data are the means \pm SD from four mice. Activation of the p38 MAPK pathway induced by siphonodictyal B in vivo. The in vivo biologic activity of siphonodictyal B was evaluated via immunohistochemistry using an antibody against phospho-p38



shown in Figure 4A,B, the tumor volume and weight were both significantly smaller in the siphonodictyal B group than in the control group. Body weights of mice in the siphonodictyal B group were similar to those in control mice (Figure 4C).

To confirm the induction of p38 MAPK pathway activation by siphonodictyal B in tumor tissue, tumors were isolated from mice after all treatments. The status of phosphorylated p38 in tumor tissue was immunohistochemically determined using the specific antibody. As shown in Figure 4D, tumor tissue in the siphonodictyal B group was strongly stained by the phosphorylated p38 antibody compared to the findings in the control group. This result verified the pharmacodynamic effects of siphonodictyal B in vivo, which is consistent with p38 MAPK pathway activation in vitro.

4 | DISCUSSION

In the present study, we demonstrated that the terpenoid siphonodictyal B might induce apoptosis in colon cancer cells via ROS-p38 MAPK pathway activation in vitro and inhibited tumor growth in vivo.

We observed that siphonodictyal B had kinase inhibitory activity against CDK4 and PI3K using the off-chip mobility shift assay. However, siphonodictyal B did not reduce the expression levels of phosphorylated AKT and phosphorylated RB. It is known that mTORC1 and S6K regulate the negative feedback loop that attenuates insulin/IGF receptor signaling. mTORC1/S6K inhibitors suppress this negative feedback loop, thus upregulating the PI3K/AKT and ERK pathways.¹⁸ Similarly, as this example, cell signaling pathways complicatedly interfere with each other. We speculated that the inhibitory effects of siphonodictyal B on individual kinases were masked because the multitarget effects of the compound might influence multiple signaling pathways that interfere with each other, although we did not pursue this issue in this study.

Both liphagal and siphonodictyal B induced cell growth inhibitory activity in a concentration-dependent manner. Although it was already known that liphagal inhibited cell proliferation,⁴ the effect of siphonodictyal B on cell proliferation had not been previously studied as far as we know. We elucidated that siphonodictyal B exhibits more potent cell growth inhibitory activity than liphagal.

5-FU, irinotecan, and oxaliplatin, cetuximab (anti-epidermal growth factor receptor antibody), and aflibercept (vascular endothelial growth factor antagonist) are key drugs for colon cancer chemotherapy.^{19–22} Previous studies reported that mutation of *RAS*, *BRAF*, *TP53*, and *PIK3CA* is involved in resistance to these drugs.^{23–26} HCT 116 (*KRAS* G13D mutant, *BRAF* wild type, *TP53* wild type, and *PIK3CA* H1047R mutant), HT-29 (*KRAS* wild type, *BRAF* V600E mutant, *TP53* R237H mutant, and *PIK3CA*

P499T mutant), and SW480 (*KRAS* G12V mutant, *BRAF* wild type, *TP53* R237H mutant, and *PIK3CA* wild type) cells were used to evaluate the anticell proliferation activity of siphonodictyal B, which was similar in the three cell lines (Figure S2). These results suggest that anticell proliferation effect of siphonodictyal B is independent of these genes, it is expected that siphonodictyal B might overcome these resistances.

In normal cells, apoptosis is strictly regulated to maintain a healthy balance of survival and death.²⁷ Apoptosis occurs via activation of the caspase family through intrinsic and extrinsic apoptotic pathways. The intrinsic pathway controls caspase family activation through the expression of the proapoptotic (eg, Bim, BAK, BAX) and antiapoptotic proteins (eg, BCL-2, MCL-1, XIAP).²⁸ In this study, we found that siphonodictyal B induced apoptosis via upregulation of Bim.

Terpenoids such as echnocystic acid, dehydrocostus lactone, and furanodiene have the ability to induce apoptosis through p38 MAPK pathway activation.²⁹ We found that downregulation of the p38 MAPK pathway at least partially attenuated siphonodictyal B-induced apoptosis in HCT 116 cells. The result showed that siphonodictyal B induces apoptosis at least in part through p38 MAPK pathway activation.

Previous research found that the p38 MAPK pathway was activated by various extracellular or endogenous cellular stimuli. ROS represent a major trigger of the p38 MAPK pathway.³⁰ Moreover, it is known that moderate levels of ROS play an important role in healthy cell proliferation and differentiation.³¹ However, excessive ROS levels reaching the toxic threshold result in irreversible damage to intracellular molecules, such as lipids, proteins, and nucleic acids.³² Therefore, the antioxidant defense system tightly controls ROS generation in normal cells. Conversely, ROS production is upregulated in cancer cells, and elevated ROS levels are associated with abnormal cell proliferation. However, excessive levels of ROS also damage cancer cells. Therefore, if there is a drug that modulates a balance of ROS generation and elimination, it may be a novel anticancer drug with a few side effects that is less toxic to normal cells.³³ In the present study, siphonodictyal B markedly promoted ROS generation and induced apoptosis.

As shown in Figure 4B,E, NAC almost completely reversed both cell growth inhibition and p38 phosphorylation induced by siphonodictyal B. However, when the p38 MAPK pathway was downregulated via p38 inhibition or depletion, the cytotoxic and apoptosis-inducing effects of siphonodictyal B were partially attenuated. These results also suggest that the p38 MAPK pathway is involved downstream of ROS signaling as part of the mechanism of siphonodictyal B-induced apoptosis in HCT 116 cells.

Also, siphonodictyal B significantly suppressed tumor growth in vivo. We preliminarily investigated the antitumor

effects of siphonodictyal Bintraperitoneally administrated at a dosage of 20 mg/kg. The antitumor effect is expected to be further enhanced by optimizing the administration route, frequency, and dosage in the future. We hope that siphonodictyal B might become a promising seed of novel anticancer drug.

CONFLICT OF INTEREST

The authors have no conflicts to disclose in relation to this work.

DATA AVAILABILITY STATEMENT

The data that support the findings of this study are available from the corresponding author upon reasonable request.

ORCID

Sonoko Chikamatsu  <https://orcid.org/0000-0002-5322-0723>

Ken Saijo  <https://orcid.org/0000-0003-0179-3789>

REFERENCES

- Huang M, Lu JJ, Huang MQ, Bao JL, Chen XP, Wang YT. Terpenoids: natural products for cancer therapy. *Expert Opin Investig Drugs*. 2012;21(12):1801-1818.
- Yang H, Dou QP. Targeting apoptosis pathway with natural terpenoids: implications for treatment of breast and prostate cancer. *Curr Drug Targets*. 2010;11(6):733-744.
- Yang L, Yang C, Li C, et al. Recent advances in biosynthesis of bioactive compounds in traditional Chinese medicinal plants. *Sci Bull (Beijing)*. 2016;61:3-17.
- Marion F, Williams DE, Patrick BO, et al. Liphagal, a Selective inhibitor of PI3 kinase alpha isolated from the sponge akacoral-liphaga: structure elucidation and biomimetic synthesis. *Org Lett*. 2006;8(2):321-324.
- Kamishima T, Kikuchi T, Narita K, Katoh T. Biogenetically inspired total synthesis of (+)-Liphagal: a potent and selective phosphoinositide 3-kinase α (PI3K α) inhibitor from the marine sponge Aka coralliphaga. *Eur J Org Chem*. 2014;2014(16):3443-3450.
- Kikuchi T, Narita K, Saijo K, Ishioka C, Katoh T. Enantioselective total synthesis of (–)-siphonodictyal B and (+)-8-epi-siphonodictyal B with phosphatidylinositol 3-kinase α (PI3K α) inhibitory activity. *Eur J Organic Chem*. 2016;2016(34):5659-5666.
- Janku F. Phosphoinositide 3-kinase (PI3K) pathway inhibitors in solid tumors: from laboratory to patients. *Cancer Treat Rev*. 2017;59:93-101.
- Thorpe LM, Yuzugullu H, Zhao JJ. PI3K in cancer: divergent roles of isoforms, modes of activation and therapeutic targeting. *Nat Rev Cancer*. 2015;15(1):7-24.
- Engelman JA. Targeting PI3K signalling in cancer: opportunities, challenges and limitations. *Nat Rev Cancer*. 2009;9(8):550-562.
- Hennessy BT, Smith DL, Ram PT, Lu Y, Mills GB. Exploiting the PI3K/AKT pathway for cancer drug discovery. *Nat Rev Drug Discov*. 2005;4(12):988-1004.
- Kitagawa D, Yokota K, Gouda M, et al. Activity-based kinase profiling of approved tyrosine kinase inhibitors. *Genes Cells*. 2013;18(2):110-122.
- Fung K, Brierley GV, Henderson S, et al. Butyrate-induced apoptosis in HCT116 colorectal cancer cells includes induction of a cell stress response. *J Proteome Res*. 2011;10(4):1860-1869.
- Bragado P, Armesilla A, Silva A, Porras A. Apoptosis by cisplatin requires p53 mediated p38alpha MAPK activation through ROS generation. *Apoptosis*. 2007;12(9):1733-1742.
- Li M, Song L-H, Yue G-L, et al. Bigelovin triggered apoptosis in colorectal cancer in vitro and in vivo via upregulating death receptor 5 and reactive oxidative species. *Sci Rep*. 2017;7:42176.
- Dong Y, Yin S, Song X, et al. Involvement of ROS-p38-H2AX axis in novel curcumin analogues-induced apoptosis in breast cancer cells. *Mol Carcinog*. 2016;55(4):323-334.
- Bayala B, Bassole IH, Scifo R, et al. Anticancer activity of essential oils and their chemical components - a review. *Am J Cancer Res*. 2014;4(6):591-607.
- Fang FQ, Guo HS, Zhang J, Ban LY, Liu JW, Yu PY. Anticancer effects of 2-oxoquinoline derivatives on the HCT116 and LoVo human colon cancer cell lines. *Mol Med Rep*. 2015;12(6):8062-8070.
- Rozengurt E, Soares HP, Sinnet-Smith J. Suppression of feedback loops mediated by PI3K/mTOR induces multiple overactivation of compensatory pathways: an unintended consequence leading to drug resistance. *Mol Cancer Ther*. 2014;13(11):2477-2488.
- Yamazaki K, Nagase M, Tamagawa H, et al. Randomized phase III study of bevacizumab plus FOLFIRI and bevacizumab plus mFOLFOX6 as first-line treatment for patients with metastatic colorectal cancer (WJOG4407G). *Annals Oncol*. 2016;27(8):1539-1546.
- Stintzing S, Modest DP, Rossius L, et al. FOLFIRI plus cetuximab versus FOLFIRI plus bevacizumab for metastatic colorectal cancer (FIRE-3): a post-hoc analysis of tumour dynamics in the final RAS wild-type subgroup of this randomised open-label phase 3 trial. *Lancet Oncol*. 2016;17(10):1426-1434.
- Tabernero J, Van Cutsem E, Lakomy R, et al. Afibercept versus placebo in combination with fluorouracil, leucovorin and irinotecan in the treatment of previously treated metastatic colorectal cancer: Prespecified subgroup analyses from the VELOUR trial. *Eur J Cancer*. 2014;50(2):320-331.
- Bras-Goncalves RA, Rosty C, Laurent-Puig P, Soulie P, Dutrillaux B, Poupon MF. Sensitivity to CPT-11 of xenografted human colorectal cancers as a function of microsatellite instability and p53 status. *Br J Cancer*. 2000;82(4):913-923.
- Lin Y-L, Liao J-Y, Yu S-C, et al. KRAS mutation is a predictor of oxaliplatin sensitivity in colon cancer cells. *PLoS ONE*. 2012;7(11):e50701.
- Boyer J, McLean EG, Aroori S, et al. Characterization of p53 Wild-type and null isogenic colorectal cancer cell lines resistant to 5-fluorouracil, Oxaliplatin, and Irinotecan. *Clin Cancer Res*. 2004;10(6):2158-2167.
- Hsu CP, Kao TY, Chang WL, Nieh S, Wang HL, Chung YC. Clinical significance of tumor suppressor PTEN in colorectal carcinoma. *Eur J Surg Oncol*. 2011;37(2):140-147.

26. Hammond WA, Swaika A, Mody K. Pharmacologic resistance in colorectal cancer: a review. *Ther Adv Med Oncol*. 2016;8(1):57-84.
27. Goldar S, Khaniani MS, Derakhshan SM, Baradaran B. Molecular mechanisms of apoptosis and roles in cancer development and treatment. *Asian Pac J Cancer Prev*. 2015;16(6):2129-2144.
28. Hassan M, Watari H, AbuAlmaaty A, Ohba Y, Sakuragi N. Apoptosis and molecular targeting therapy in cancer. *Biomed Res Int*. 2014;2014:150845.
29. Thoppil RJ, Bishayee A. Terpenoids as potential chemopreventive and therapeutic agents in liver cancer. *World J Hepatol*. 2011;3(9):228-249.
30. Son Y, Cheong YK, Kim NH, Chung HT, Kang DG, Pae HO. Mitogen-activated protein kinases and reactive oxygen species: how can ROS activate MAPK pathways? *J Signal Transduct*. 2011;2011:792639.
31. Trachootham D, Alexandre J, Huang P. Targeting cancer cells by ROS-mediated mechanisms: a radical therapeutic approach? *Nat Rev Drug Discov*. 2009;8(7):579-591.
32. Sreevalsan S, Safe S. Reactive oxygen species and colorectal cancer. *Curr Colorectal Cancer Rep*. 2013;9(4):350-357.
33. Redza-Dutordoir M, Averill-Bates DA. Activation of apoptosis signalling pathways by reactive oxygen species. *Biochim Biophys Acta*. 2016;1863(12):2977-2992.

SUPPORTING INFORMATION

Additional supporting information may be found online in the Supporting Information section at the end of the article.

How to cite this article: Chikamatsu S, Saijo K, Imai H, et al. In Vitro and in Vivo antitumor activity and the mechanism of siphonodictyal B in human colon cancer cells. *Cancer Med*. 2019;8:5662–5672. <https://doi.org/10.1002/cam4.2409>



Catalytic asymmetric synthesis of stereoisomers of 1-C-*n*-butyl-LABs for the SAR study of α -glucosidase inhibition

Yoshihiro Natori ^{a,*}, Toshihiro Sakuma ^a, Haruka Watanabe ^a, Hideaki Wakamatsu ^a,
Atsushi Kato ^b, Isao Adachi ^b, Hiroki Takahata ^{c,1}, Yuichi Yoshimura ^{a,**}

^a Faculty of Pharmaceutical Sciences, Tohoku Medical and Pharmaceutical University, Sendai, 981-8558, Japan

^b Department of Hospital Pharmacy, University of Toyama, Toyama, 930-0194, Japan

^c Faculty of Pharmaceutical Sciences, Tohoku Pharmaceutical University, Sendai, 981-8558, Japan

ARTICLE INFO

Article history:

Received 7 March 2019

Received in revised form

27 March 2019

Accepted 1 April 2019

Available online 5 April 2019

Keywords:

Stereoselective synthesis

Iminosugar

α -Glucosidase inhibitor

ABSTRACT

We achieved synthesis of seven stereoisomers of 1-C-*n*-butyl-L-aminofuranose derivatives using catalytic asymmetric alkylation and Negishi coupling as key reactions. The synthetic strategy based on these key reactions was quite useful, since both α - and β -aminofuranoses could be obtained by switching the chirality of the ligand employed for the AAA reaction. The common intermediates for α - and β -isomers were subjected to further manipulations to install a diol unit at C2 and C3 to give the desired stereoisomers of L-aminofuranose derivatives. We achieved the preparation of all stereoisomers of 1-C-*n*-butyl-L-aminofuranose derivatives, with the exception of β -lyxo type aminofuranose. It is noteworthy that a synthetic route for many stereoisomers of aminofuranose derivatives was developed. Unfortunately, none of the L-aminofuranoses obtained showed inhibitory activity against the α -glucosidases examined—e.g., maltase, sucrase, and isomaltase.

© 2019 Published by Elsevier Ltd.

1. Introduction

Diabetes mellitus is a chronic metabolic disease caused by dysfunction of insulin, and leads to hyperglycemia. It is categorized into two major types, types 1 and 2, as well as several minor types. Patients with type 1 diabetes lack production of insulin due to autoimmune pancreatic β -cell destruction. Thus, injection of insulin is indispensable for their treatment. On the other hand, inadequate insulin secretion and tolerance toward insulin give rise to type 2 diabetes, which is the most common form of diabetes. Indeed, 90% of individuals with diabetes have the type 2 form [1]. WHO reported that diabetes caused 1.5 million deaths in the world in 2012 and 422 million people had diabetes in 2014 [2].

The cause of type 2 diabetes is complicated, but is thought to involve both genetic factors and lifestyle-related factors such as obesity, physical activity, diet and stress. As a consequence of diabetes, many organs are damaged, increasing the risk of heart

disease and stroke, neuropathy in the feet, diabetic retinopathy and kidney failure. Therefore, as the number of patients with diabetes rises, there is a concomitant rise in global health care costs. The initial management of type 2 diabetes consists of exercise and dietary changes to control the blood glucose levels [3]. In patients whose blood glucose levels are not lowered by these approaches, antidiabetic drugs are often used. Antidiabetic drugs are classified into several mechanistic classes, i.e., sulfonylureas, biguanides, meglitinides, thiazolidinediones, DPP IV inhibitors, SGLT2 inhibitors, α -glucosidase inhibitors, and bile acid sequestrants. α -Glucosidase inhibitors, which are oral antidiabetic agents, block the hydrolysis of disaccharides (e.g., maltose and sucrose) and suppress postprandial hyperglycemia [4]. As depicted in Fig. 1, three α -glucosidase inhibitors (acarbose, voglibose, and miglitol) have been approved and used in clinical treatment [5]. Miglitol is an iminosugar derivative that can act as a transition state analogue while binding to an active site of α -glucosidase (Fig. 1) [6].

For some time now, we have been focused on the design and synthesis of novel iminosugar derivatives with potential glycosidase inhibitory actions [7]. Recently, we discovered a new inhibitor, α -1-C-butyl-1,4-dideoxy-1,4-imino-L-arabinitol (α -1-C-butyl-LAB, **1a**), which strongly inhibits several α -glucosidases. The structure-activity relationship (SAR) investigations of LAB were mainly

* Corresponding author.

** Corresponding author.

E-mail addresses: natori-y@tohoku-mpu.ac.jp (Y. Natori), yoshimura@tohoku-mpu.ac.jp (Y. Yoshimura).

¹ Deceased on 1st March, 2014.

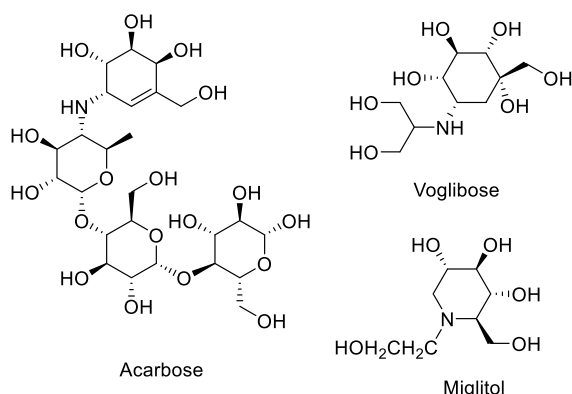


Fig. 1. Structures of approved α -glucosidase inhibitors.

performed on C1 substituents, and revealed that α -glucosidases are able to recognize alkyl substituents at the C1 position. Further support was provided by a docking simulation between an enzyme and 1-C-butyl-LAB, which led us to synthesize 1-C-(aryl)butyl-LAB derivatives that exhibited potent inhibitory activities toward α -glucosidases, including maltase, isomaltase and sucrose. On the other hand, introduction of a second alkyl group into either the C3 or N-position of **1a** strongly diminished their inhibitory activities. In addition, a D-enantiomer of **1a**, α -1-C-butyl-1,4-dideoxy-1,4-imino-D-arabinitol (α -1-C-butyl-DAB), showed only moderate to weak inhibitory activities toward the same enzymes (Fig. 2).

These results prompted us to further investigate the SAR of LABs, focusing on the effects of the stereochemistry of hydroxyl groups on a pyrrolidine ring. Herein we describe our synthesis of the stereoisomers of **1a** (1-C-*n*-butyl-L-iminofuranoses **1**), which proceeds with an asymmetric allylic alkylation reaction as a key step. This synthesis should make an important contribution to the SAR study of iminosugars as potential α -glycosidase inhibitors.

2. Results and discussion

Our original synthesis of α -1-C-butyl-LAB **1a** was achieved by starting from a chiral oxazolidinone **2**. We converted **2** to the key intermediate **6** by means of palladium-catalyzed asymmetric allylic alkylations (AAA) [8,9] and Negishi cross-coupling [10] (Scheme 1). In the former AAA reaction, an (*S,S*)-naphthyl Trost ligand was used to control a newly formed chiral center and obtain (*R*)-2-amino-homoallyl alcohol derivative **4**. After ring closing metathesis and iodination of the primary hydroxyl group, the latter Negishi coupling of **5** allowed us to synthesize many iminosugar derivatives

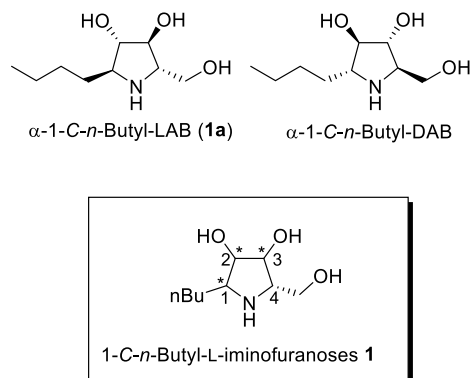
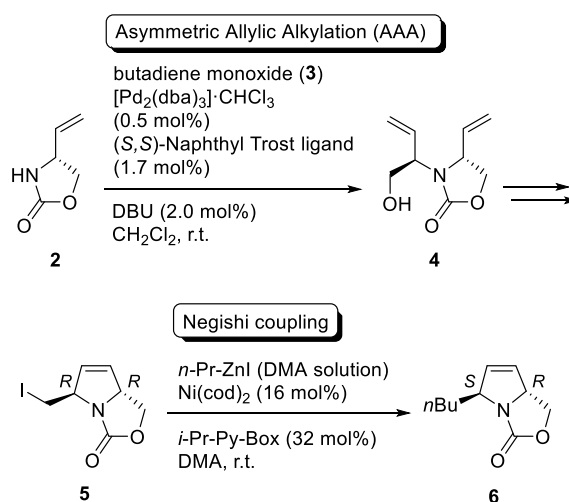


Fig. 2. Structures of 1-C-*n*-butyl-LAB, -DAB and -iminofuranoses **1**.

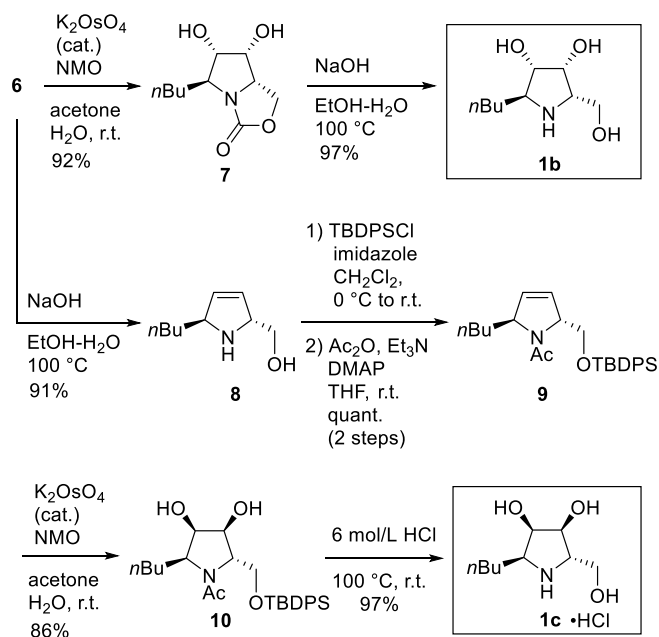


Scheme 1. Preparation of chiral intermediate **6** for synthesizing 1-C-*n*-butyl- α -L-iminofuranose derivatives.

having side chains of various lengths substituted at the C1 position. By tracing the previous method, we prepared the same key intermediate **6** from which the synthesis of 2- and 3-stereoisomers of α -1-C-butyl-LAB **1** was started.

Among the 2- and 3-stereoisomers, iminofuranoses having *lyxo*- and *ribo*-configurations were obtainable by simple *cis*-dihydroxylation of **6** with osmium tetroxide. In addition, selective formation of *lyxo*- and *ribo*-iminofuranoses would be achieved by restricting the approach of the oxidative agent. We previously reported that epoxidation of **6** proceeded selectively through the β -side, since the α -side was shielded by a bulky *n*-butyl group [7,11]. Thus, the *cis*-dihydroxylation of **6** by treatment with a catalytic amount of K_2OsO_4 and *N*-methylmorpholine *N*-oxide (NMO) selectively gave an iminofuranose derivative **7** in good yield. NOE experiments of **7** clearly showed that it had a *lyxo*-configuration as expected (Fig. 1S in the Supplementary Data). Cleavage of the oxazolidinone ring under basic conditions afforded α -1-C-butyl-*lyxo*-iminofuranose (**1b**) in 97% yield.

On the other hand, to synthesize the *ribo*-iminofuranose derivative, it is necessary to block the β -side and induce α -side oxidation [11]. A simple molecular modeling consideration revealed that the rigid structure of **7** fixed by a fused oxazolidinone ring forced the bulky butyl group to occupy a pseudo-axial position. The resulting disposition of the substituent acted to shield the α -side. Therefore, cleavage of the oxazolidinone ring and introduction of a bulky protecting group at the C5-primary hydroxyl group might efficiently switch the stereoselectivity of oxidation from the β -to α -side. Following this strategy, an oxazolidinone ring of **6** was hydrolyzed by treatment with aqueous NaOH to give a dihydropyrrole derivative **8**. The primary alcohol of **8** was protected by a bulky TBDPS group and the remaining imino group was acetylated to give an *N*-acetyldihydropyrrole **9** quantitatively. As we expected, *cis*-dihydroxylation of **9** under the conditions used for **6** selectively produced a *ribo*-iminofuranose derivative **10**, deprotection of which under acidic conditions gave an HCl salt of α -1-C-butyl-*ribo*-iminofuranose (**1c**), with an excellent yield, as a sole product (Scheme 2). The selectivity of dihydroxylation was affected by an N-protecting group: introduction of an *N*-nosyl group, instead of acetyl, resulted in a slight decrease of selectivity (*ribo*: *lyxo* = 9 : 1; Scheme 1S in the Supplementary Data). The stereochemistry was confirmed by NOE experiments of major dihydroxylated product of nosyl derivative, which was deprotected to afford the same iminosugar as in **1c**.



Scheme 2. Syntheses of 1-C-*n*-butyl- α -L-iminofuranoses **1b** and **1c**.

(Fig. 2S and Scheme 2S in the Supplementary Data).

The fact that epoxidation of **6** and the subsequent oxirane ring cleavage gave only the *arabino*-iminofuranose derivative, as reported previously [7], implied the difficulty of synthesizing the *xylo*-derivative by this synthetic route. As an alternative approach, we intended to synthesize the *xylo*-derivative from *lyxo*-iminofuranose **1b** by epimerizing C2-carbon after selective protection of the C3- and C5-hydroxyl groups.

After N-acetylation of **1b** by successive acylation and selective deacylation steps, the resulting product was treated with 2,2-dimethoxypropane (2,2-DMP) in the presence of 10-camphorsulfonic acid (CSA) to give a ketal **11** with a yield of 58% in 3 steps. Although many attempts were made to invert the stereochemistry at C2 of the ketal **11** by S_N2 reactions, including the Mitsunobu reaction, none of the reactions gave a desired product having a *xylo*-configuration (data not shown). Next, we tried to obtain the *xylo*-iminofuranose derivative by using oxidation and a hydride reduction sequence for epimerization at the C2 position. The oxidation of **11** was performed by treatment with CrO_3 -pyridine- Ac_2O in dichloromethane to give a ketone **12** in 52% yield. Among the hydride reductions of ketone **12** examined with various hydride sources, the reaction with LiBH_4 showed the best result (Table 1S in the Supplementary Data). Treatment of **12** with LiBH_4 in EtOH at room temperature gave an inseparable mixture of *lyxo*- and *xylo*-iminofuranose derivatives **11** and **13** (**11** : **13** = 3 : 2) in 66% yield. To separate the diastereomeric mixture, secondary hydroxyl groups of **11** and **13** were once protected by a *p*-anisoyl group and the resulting mixture was separated by a silica gel column to give *p*-anisoylates **14a** and **14b** in 43% and 29% yield, respectively. Finally, all protecting groups of **14b** were deprotected at once by treatment with refluxing aqueous HCl to give α -1-C-butyl-*xylo*-iminofuranose (**1d**) as an HCl salt (Scheme 3).

Having completed the synthesis of α -1-C-butyl-iminofuranoses, we proceeded to synthesize a series of β -C-*n*-butyl derivatives. A common intermediate for β -C-*n*-butyl-iminofuranoses was prepared along with that for the α -C-*n*-butyl derivatives mentioned above. A chiral oxazolidinone **2** was subjected to an AAA reaction using an (*R,R*)-naphthyl Trost ligand in place of the (*S,S*)-ligand, giving the (*S*)-2-amino-homoallyl alcohol derivative **15a** and its

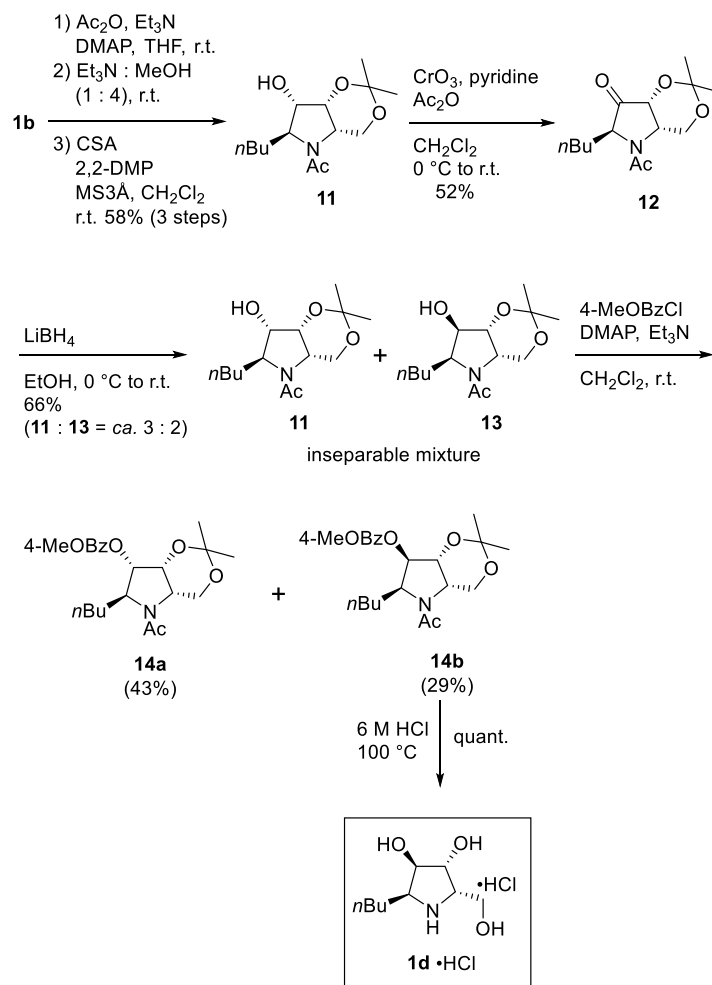
epimer **15b**, after protection of primary hydroxyl groups with a TBDPS, in 61% and 6% yield, respectively. RCM reaction of **15a** in the presence of Grubbs' 1st catalyst, followed by desilylation, gave a dihydropyrrole **17**. Iodination of **17** with I_2 and triphenylphosphine gave **18**, which was subjected to the Negishi cross-coupling reaction with *n*-propyl zinc iodide to give the common intermediate **19** for synthesizing β -C-*n*-butyl-iminofuranoses (Scheme 4).

cis-Dihydroxylation of **19** by treatment with K_2OsO_4 and NMO as in the case of **6** and **9** gave a diol **20** as a sole product because of steric hindrance around the C1 and C4 substituents. Hydrolysis of **20** under acidic conditions cleaved an oxazolidinone ring to give 1-C-*n*-butyl- β -L-*ribo*-iminofuranose (**1g**) as an HCl salt (Scheme 5). Epoxidation of **19**, on the other hand, by a dioxirane derivative generated from trifluoroacetone and Oxone[®] gave a mixture of diastereomers (12 : 1) in 88% yield. The structure of the major product was expected to be **21a**. It is considered that the epoxidation from the α -side [11] proceeded with the same stereo-selectivity as the dihydroxylation from **19** to **20**.

As described above, a bulky butyl group at C1 of **6** strongly shielded an α -side of the C2 position of iminosugar to limit the reaction—e.g., to limit epoxidation and dihydroxylation—only from the β -side [11] or to restrict cleavage of epoxide only from the C3-side. This steric effect no longer existed in the intermediate **21a** since a butyl group occupied a β -position, resulting in a loss of reaction bias around the C2 position. Thus, cleavage of the epoxide ring of **21a** was expected to occur on either the C2 or C3 side. This suggested that both *xylo*- and *arabino*-derivatives could be obtained from one intermediate in the case of the β -isomer. Indeed, treatment of **21a** under acidic conditions efficiently cleaved its epoxide ring to give the desired *xylo*- and *arabino*-iminosugar derivatives **22a,b** as an inseparable mixture. To separate the mixture of diastereomers, we intended to use selective acetal formation between the C4 and C5 hydroxyl groups of the *xylo*-iminosugar, which could not be allowed for the *arabino*-derivative. The oxazolidinone ring of **22a,b** was opened by NaOH under refluxing conditions and the resulting products were further converted to *N*-acetyl derivatives **23a,b** in 2 steps. Treatment of **23a,b** with 2,2-dimethoxypropane (2,2-DMP) and CSA resulted in the formation of acetal **24** and triol **23b**, which were easily separated by silica gel column chromatography, in 54% and 29% yield, respectively. Deprotection of **24** by treatment with 6 mol/L HCl under reflux conditions gave 1-C-*n*-butyl- β -L-*xylo*-iminofuranose (**1h**) as a HCl salt. Similarly, 1-C-*n*-butyl- β -L-*arabino*-iminofuranose (**1e**) was obtained from **25** quantitatively. The NOE experiments of **1h** clearly showed that it had a *xylo* configuration (Fig. 3S in the Supplementary Data). Since **1e** was obtained from the common epoxide **21a**, which produced **1h**, the results also suggested that **1e** had an *arabino* configuration.

To achieve synthesis of the 1-C-*n*-butyl- β -L-*lyxo*-iminofuranose (**1f**), we tried to epimerize stereochemistry at C2 of acetal **24** by the Mitsunobu reaction. However, the reaction to obtain *p*-nitrobenzoate **25** did not proceed under the Mitsunobu conditions (*p*-nitrobenzoic acid, triphenylphosphine and DEAD or Bis(2-methoxyethyl) azodicarboxylate [12] in THF). As mentioned above, in the case of the *xylo*-iminofuranose derivative, the oxidation and hydride reduction sequence gave a desired epimerized product. However, the method failed to yield either *lyxo*-iminofuranose derivative (Scheme 3S in the Supplementary Data).

With the seven stereoisomers of L-iminofuranoses (**1a-e**, **1g, h**) in hand, we next evaluated the inhibitory activities of the stereoisomers against rat intestinal α -glycosidases including maltase, sucrase, and isomaltase [13]. The results are summarized in Table 1. Among the tested compounds, the original α -*arabino* derivative **1a** was only active against all α -glycosidases. Its 2'-epimer α -*lyxo*-iminofuranose **1b** showed moderate inhibitory activity against

Scheme 3. Synthesis of 1-C-n-butyl- α -L-iminofuranose **2d**.

sucrase and weak activity against maltase. The other stereoisomers did not show any inhibition toward α -glycosidases. Our previous docking study demonstrated that a long aliphatic substituent at C1 of **1a** was required to fit a hydrophobic pocket existing in a catalytic domain of rat maltase.

The fact that the obtained β -isomers (**1e**, **g**, **h**) exhibited diminished inhibitory activities in comparison with that of **1a** was in accordance with the results of the docking simulations. Together with the finding that D-iminofuranoses did not inhibit activity toward α -glycosidases, the results also revealed that the specific placement of all three hydroxyl groups on iminofuranose was highly important for their binding to the enzyme. On the other hand, the result that the *lyxo* derivatives showed weak inhibition suggests that a SAR study on C2 substitution of iminosugar might also yield new inhibitors, since the reduction of inhibitory activity by this substitution was less than those for the C3 and C4 substituents.

3. Conclusion

We achieved the synthesis of seven stereoisomers of 1-C-n-butyl-L-iminofuranose derivatives by using AAA and Negishi coupling as key reactions. The synthetic strategy based on these key reactions is quite attractive because both α - and β -iminofuranoses can be obtained by changing a chiral ligand of the palladium catalyst for the AAA reaction. The common intermediates for α - and

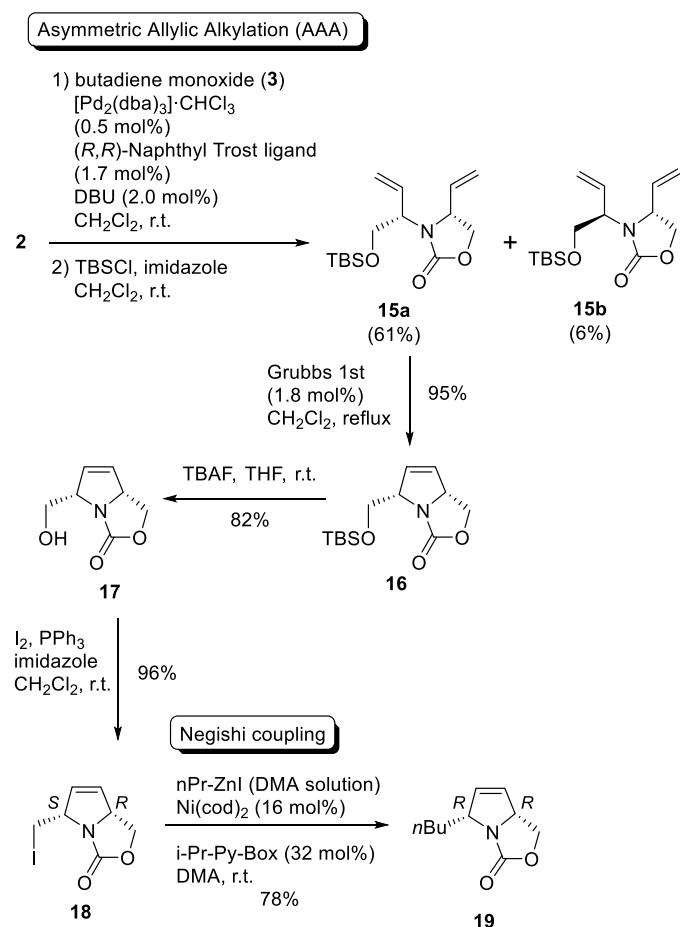
β -isomers obtained were converted to the desired iminofuranose derivatives by stepwise introduction of diol units. Although a β -L-*lyxo* type iminofuranose having all *cis*-substituted groups could not be synthesized, it is worth noting that a synthetic route for many stereoisomers of iminofuranose derivatives was developed. Unfortunately, none of the L-iminofuranoses except the L-*arabino* derivative showed inhibitory activity against α -glycosidases. Attempts to synthesize new iminosugar derivatives based on this strategy are ongoing in our laboratories, and the results, including further SAR studies of iminosugars, will be reported in the future.

4. Experimental section

4.1. General experimental procedures

All reactions were run under an atmosphere of argon unless otherwise indicated. Infrared (IR) spectra were recorded on a Perkin-Elmer 1600 series FT-IR spectrometer. Mass spectra were recorded on a JEOL JMN-DX 303/JMA-DA 5000 spectrometer. Microanalyses were performed on a Perkin-Elmer CHN 2400 elemental analyzer. Optical rotations were measured with a JASCO DIP-360 or JASCO P-1020 digital polarimeter at the sodium D line (589 nm) with the solvent and concentration indicated.

Proton nuclear magnetic resonance (^1H NMR) spectra were recorded on a JEOL JNM-EX 270 (270 MHz), JEOL JNM-AL 400 (400 MHz), Varian Unity-500 (500 MHz), or JNM-LA (600 MHz)



Scheme 4. Preparation of chiral intermediate **19** for synthesizing 1-*C*-*n*-butyl- β -L-iminofuranose derivatives.

spectrometer using tetramethylsilane as the internal standard. Chemical shifts are reported relative to the internal standard (tetramethylsilane, δ_{H} 0.00; CDCl_3 , δ_{H} 7.26; CD_3OD , δ_{H} 3.31; D_2O , δ_{H} 4.79). The following abbreviations are used: s = singlet, d = doublet, t = triplet, q = quartet, m = multiplet, br = broad. Carbon-13 nuclear magnetic resonance (^{13}C NMR) spectra were recorded using a JEOL JNM-AL 400 (100 MHz) or Varian Unity-500 (125 MHz). The following internal references were used: CDCl_3 (δ 77.0) or CD_3OD (δ 49.0). Acetone was used as an internal standard in ^{13}C NMR in D_2O . Column chromatography was carried out on silica gel 60N (40–50 μm) for flash chromatography purchased from Kanto Chemical. Dichloromethane (CH_2Cl_2), tetrahydrofuran (THF), and *N,N*-dimethylacetamide (DMA) were dehydrated grade and purchased from Kanto Chemical.

4.2. Synthesis

Compounds **2**, **4**, **5**, **6** were prepared according to the reported procedures [7,8].

4.2.1. (5*S*,6*S*,7*R*,7*aS*)-5-Butyl-6,7-dihydroxytetrahydropyrrolo[1,2-*c*]oxazol-3(1*H*)-one (**7**)

4-Methylmorpholine *N*-oxide (1.76 mL, 8.42 mmol) and potassium osmate dihydrate (97.3 mg, 0.38 mmol) were added to a solution of compound **6** (347 mg, 1.91 mmol) in acetone/ H_2O (2:1, 54 mL). After the mixture was stirred at room temperature for 5 h, the solvents were removed under reduced pressure. Traces of water

were removed from the mixture by azeotropic distillations with toluene (2 \times 5 mL) under reduced pressure and the residue was purified by silica gel column chromatography (hexane/EtOAc = 3/1) to give diol **7** (398 mg, 97%) as brown oil; $[\alpha]_{\text{D}}^{25} = +25.7$ (c 0.10, CH_3OH). ^1H NMR (400 MHz, CD_3OD) δ : 0.94 (t, $J = 7.2$ Hz, 3H), 1.34–1.57 (m, 5H), 1.67–1.76 (m, 1H), 3.41–3.46 (m, 1H), 3.84 (t, $J = 3.4$ Hz, 1H), 3.97 (dd, $J = 3.4, 7.2$ Hz, 1H), 4.02–4.05 (m, 1H), 4.40 (t, $J = 8.7$ Hz, 1H), 4.49 (dd, $J = 3.4, 8.7$ Hz, 1H). ^{13}C NMR (100 MHz, CD_3OD) δ : 14.40, 23.67, 29.68, 34.95, 62.28, 63.76, 64.46, 73.10, 81.29, 164.99. IR (NaCl) cm^{-1} : 3445, 2932, 1731. EI-MS (m/z): 215 (M^+). HRMS Calcd for $\text{C}_{10}\text{H}_{17}\text{NO}_4$: 215.1158; Found: 215.1149.

4.2.2. α -1-*C*-Butyl-*L*-lyxo-iminofuranose (**1b**)

NaOH (761 mg, 19.0 mmol) was added to a solution of diol **7** (394 mg, 1.83 mmol) in EtOH/ H_2O (2:1, 27 mL), and the mixture was refluxed for 5 h. The reaction mixture was cooled to room temperature and concentrated. The residue was purified by silica gel column ($\text{Et}_2\text{O}/\text{CH}_3\text{OH}/28\% \text{NH}_3 \text{ aq.} = 80:20:1$) to yield **1b** (339 mg, 98%) as a white solid; $[\alpha]_{\text{D}}^{25} = -42.0$ (c 0.50, CH_3OH). ^1H NMR (400 MHz, CD_3OD) δ : 0.94 (t, $J = 7.0$ Hz, 3H), 1.29–1.49 (m, 5H), 1.66–1.70 (m, 1H), 3.01–3.06 (m, 1H), 3.25–3.30 (m, 1H), 3.65–3.71 (m, 2H), 3.78 (dd, $J = 6.3, 11.2$ Hz, 1H), 4.07 (t, $J = 4.4$ Hz, 1H). ^{13}C NMR (100 MHz, CD_3OD) δ : 14.34, 23.86, 30.20, 34.79, 61.72, 61.89, 62.04, 73.43, 79.08. IR (KBr) cm^{-1} : 3438, 3264, 2955, 2871. EI-MS (m/z): 189 (M^+). HRMS Calcd for $\text{C}_9\text{H}_{19}\text{NO}_3$: 189.1365; Found: 189.1370.

4.2.3. {(2*R*,5*S*)-5-Butyl-2,5-dihydro-1*H*-pyrrol-2-yl}methanol (**8**)

NaOH (830 mg, 20.7 mmol) was added to a solution of compound **6** (394 mg, 1.83 mmol) in EtOH/ H_2O (2:1, 24 mL), and the mixture was refluxed for 1 h. The reaction mixture was cooled to room temperature and concentrated. The residue was passed through a short pad of silica gel (eluting with $\text{CH}_3\text{OH}/28\% \text{NH}_3 \text{ aq.} = 100:1$). The filtrate was then concentrated, and the residue was purified by silica gel chromatography ($\text{CH}_2\text{Cl}_2/\text{CH}_3\text{OH}/28\% \text{NH}_3 \text{ aq.} = 90:9:1$) to provide alcohol **8** (275 mg, 89%) as a colorless oil. $[\alpha]_{\text{D}}^{23} = +366$ (c 0.81, CH_3OH). ^1H NMR (400 MHz, CD_3OD) δ : 0.93 (t, $J = 7.0$ Hz, 3H), 1.31–1.44 (m, 4H), 1.45–1.57 (m, 2H), 3.49 (d, $J = 5.8$ Hz, 2H), 3.93–3.98 (m, 1H), 4.00–4.05 (m, 1H), 5.79–5.81 (m, 1H), 5.87–5.90 (m, 1H). ^{13}C NMR (100 MHz, CD_3OD) δ : 14.37, 23.87, 29.77, 37.31, 65.95, 66.04, 67.82, 129.80, 134.66. IR (NaCl) cm^{-1} : 3306, 2926, 1643. EI-MS (m/z): 155 (M^+); HRMS Calcd for $\text{C}_9\text{H}_{17}\text{NO}$: 155.1310; Found: 155.1308.

4.2.4. 1-[(2*S*,5*R*)-2-Butyl-5-[(*tert*-butyldiphenylsilyl)oxy]methyl]-2,5-dihydro-1*H*-pyrrol-1-yl]ethanone (**9**)

tert-Butylchlorodiphenylsilane (251 μL , 0.97 mmol) was added to a solution of alcohol **8** (100 mg, 0.64 mmol) and imidazole (87.7 mg, 1.29 mmol) in CH_2Cl_2 (3.0 mL) at 0 $^\circ\text{C}$. The reaction mixture was stirred at room temperature for 1 h. The reaction was quenched with sat. $\text{NaHCO}_3 \text{ aq.}$ (5 mL), and the whole mixture was extracted with CH_2Cl_2 (5 mL \times 2). The combined organic layers were washed with sat. NaCl aq. (10 mL) and dried over anhydrous Na_2SO_4 . Filtration and evaporation *in vacuo* furnished the crude product, which was purified by silica gel chromatography (hexane: ethylacetate = 20:1 \rightarrow 10:1) to provide TBDPS ether (214 mg, 84%) as a pale yellow oil; $[\alpha]_{\text{D}}^{23} = +151$ (c 0.98, CHCl_3); ^1H NMR (400 MHz, CDCl_3) δ : 0.90 (t, $J = 6.8$ Hz, 3H), 1.05 (s, 9H), 1.21–1.50 (m, 6H), 3.59 (d, $J = 6.1$ Hz, 2H), 3.93 (dd, $J = 6.1, 10.9$ Hz, 1H), 4.10–4.14 (m, 1H), 5.75 (td, $J = 1.8, 3.9$ Hz, 1H), 5.81 (td, $J = 1.8, 3.9$ Hz, 1H), 7.35–7.44 (m, 6H), 7.65 (dt, $J = 2.1, 7.9$ Hz, 4H); ^{13}C NMR (100 MHz, CDCl_3) δ : 14.07, 19.25, 22.84, 26.87, 28.68, 37.15, 64.67, 66.59, 67.35, 127.63, 129.13, 129.61, 133.70, 133.94, 135.58, 135.61; IR (NaCl) cm^{-1} : 3070, 2998, 2957, 2929, 2857; EI-MS (m/z): 393 (M^+); HRMS Calcd for $\text{C}_{25}\text{H}_{35}\text{NOSi}$: 393.2488; Found: 393.2506.

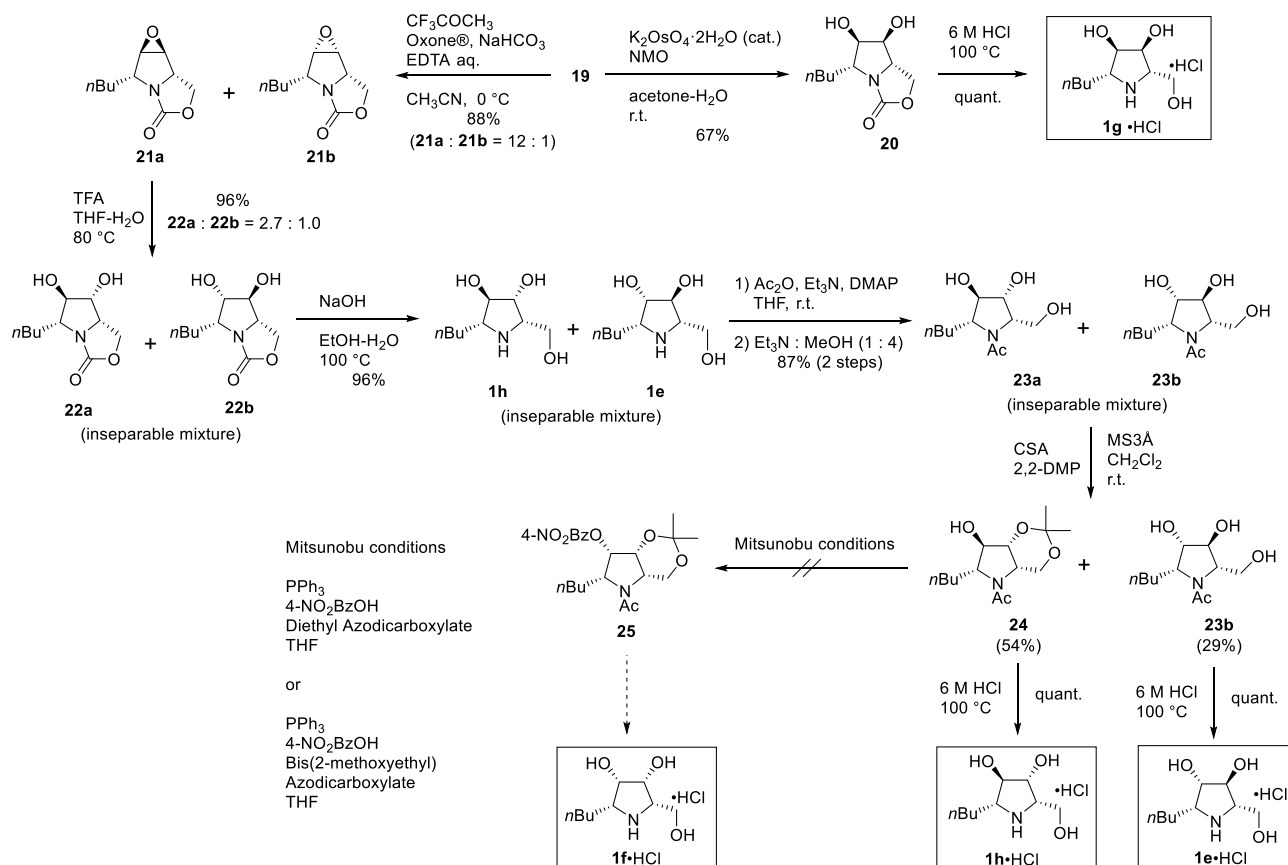
Scheme 5. Synthesis of 1-C-n-butyl-β-L-iminofuranose derivatives **1e**, **g**, **h**.

Table 1
 IC₅₀ (μM) values of 1-C-n-butyl-L-iminofuranoses for rat intestinal α-glycosidases.

Comp	Config	α-Glycosidases		
		Maltase	Sucrase	Isomaltase
1a	α-arabino	0.13	0.032	4.7
1b	α-lyxo	350.9	22.5	NI
1c	α-ribo	NI	NI	NI
1d	α-xylo	NI	NI	NI
1e	β-arabino	NI	423	NI
1g	β-ribo	NI	NI	NI
1h	β-xylo	NI	331	NI

NI: no inhibition (less than 50% inhibition at 1000 μM).

NEt₃ (49.3 μL, 0.35 mmol), DMAP (2.7 mg, 0.02 mmol) and acetic anhydride (25.0 μL, 0.27 mmol) were added to a solution of the obtained TBDPS ether in THF (4.0 mL). After stirring at room temperature for 3 h, the reaction was quenched with sat. NH₄Cl aq. (10 mL). The whole mixture was extracted with ethylacetate (10 mL × 2), and the combined organic layers were washed with sat. NaCl aq. (10 mL) and dried over anhydrous Na₂SO₄. Filtration and evaporation *in vacuo* furnished the crude product, which was purified by silica gel column chromatography (hexane/EtOAc = 20:1 → 10:1) to provide compound **9** (88.4 mg, 91%) as a colorless oil; [α]_D²⁷ = +174 (c 0.57, CHCl₃). ¹H NMR (400 MHz, CDCl₃, ca 1.4 : 1.0 mixture of amide rotamers) (major) δ: 0.85–0.91 (m, 3H), 1.02 (s, 9H), 1.17–1.26 (m, 4H), 1.68–1.72 (m, 1H), 1.88–1.92 (m, 1H), 2.08 (s, 3H), 3.98 (dd, *J* = 2.3, 9.8 Hz, 1H), 4.07–4.13 (m, 1H), 4.58–4.63 (m, 1H), 4.75–4.79 (m, 1H), 5.77 (td, *J* = 2.3, 4.3 Hz, 1H), 5.81–5.88 (m, 1H), 7.34–7.46 (m, 6H), 7.60–7.65 (m, 4H); (minor) δ: 0.85–0.91 (m, 3H), 1.04 (s, 9H), 1.17–1.26 (m, 5H), 1.68–1.72 (m,

1H), 1.82 (s, 3H), 3.57 (dd, *J* = 6.6, 10.1 Hz, 1H), 3.79 (dd, *J* = 3.4, 10.1 Hz, 1H), 4.49–4.54 (m, 1H), 4.71–4.75 (m, 1H), 5.81–5.88 (m, 2H), 7.34–7.46 (m, 6H), 7.60–7.65 (m, 4H). ¹³C NMR (100 MHz, CDCl₃) δ: 13.97, 14.07, 19.10, 19.25, 22.31, 22.59, 22.65, 22.66, 25.74, 26.27, 26.72, 26.75, 30.92, 34.71, 62.19, 65.56, 65.63, 66.09, 66.72, 66.85, 127.16, 127.53, 127.75, 127.77, 128.52, 129.52, 129.86, 132.87, 133.06, 133.68, 135.48, 135.52, 168.93, 169.28. IR (NaCl) cm⁻¹: 3071, 3049, 3014, 2998, 2957, 2930, 2858, 1651, 1630, 1589. EI-MS (*m/z*): 435 (M⁺); HRMS Calcd for C₂₇H₃₇NO₂Si: 435.2594; Found: 435.2586.

4.2.5. 1-((2*S*,3*R*,4*S*,5*S*)-2-Butyl-5-[(*tert*-butyldiphenylsilyl)oxy]methyl)-3,4-dihydropyrrolidin-1-yl)ethanone (**10**)

4-methylmorpholine *N*-oxide (357 μL, 1.7 mmol) and potassium osmate dihydrate (19.8 mg, 0.08 mmol) were added to a solution of alkene **9** in acetone/H₂O (1.6:1, 4.7 mL). After stirring at room temperature for 20 h, the solvents were removed under reduced pressure. Traces of water were removed from the mixture by azeotropic distillations with toluene (5 mL × 2) under reduced pressure. The residue was purified by silica gel column chromatography (hexane/ethylacetate = 20/1) to give diol **10** (182 mg, 83%) as a yellow amorphous solid; [α]_D²⁶ = +20.3 (c 1.74, CHCl₃). ¹H NMR (400 MHz, CDCl₃, mixture of amide rotamers) δ: 0.85–0.94 (m, 3H), 1.03–1.07 (m, 9H), 1.32–1.56 (m, 5H), 1.79 (brs, 1H), 2.04 and 2.08 (s, 3H), 2.92–3.08 (m, 1H), 3.40–3.84 (m, 2H), 3.88–4.21 (m, 2H), 4.29–4.37 (m, 1H), 4.51–4.63 (m, 1H), 7.34–7.49 (m, 6H), 7.54–7.67 (m, 4H). ¹³C NMR (100 MHz, CDCl₃, mixture of amide rotamers) δ: 13.89, 13.97, 19.20, 21.95, 22.03, 22.47, 22.89, 26.68, 26.80, 26.88, 28.75, 29.96, 30.17, 32.15, 34.30, 59.03, 59.06, 61.23, 61.71, 65.08, 66.21, 70.31, 70.40, 71.59, 74.36, 74.54, 127.72, 127.75, 127.86, 127.95,

128.10, 128.21, 129.80, 130.09, 130.21, 131.52, 131.78, 132.99, 133.11, 135.45, 135.49, 135.51, 135.71, 170.39, 170.54. IR (KBr) cm^{-1} : 3375, 3072, 3052, 2958, 2932, 2859, 1615, 1464, 1428. EI-MS (m/z): 469 (M^+). HRMS Calcd for $\text{C}_{27}\text{H}_{39}\text{NO}_4\text{Si}$: 469.2648; Found: 469.2648.

4.2.6. α -1-C-Butyl-L-ribo-iminofuranose (**1c**) hydrochloride

A solution of **10** (34.6 mg, 0.07 mmol) in 6 mol/L HCl (1.0 mL) was stirred at 100 °C for 12 h. The whole mixture was transferred into a separate funnel and washed with CH_2Cl_2 (3 mL \times 2). The water layer was evaporated to obtain imino sugar **1c** hydrochloride (18.1 mg, quant.) as a white solid; mp > 143 °C (decomp.). $[\alpha]_D^{25} = -30.9$ (c 0.71, CH_3OH). ^1H NMR (400 MHz, CD_3OD) δ : 0.96 (t, $J = 7.0$ Hz, 3H), 1.35–1.48 (m, 4H), 1.68–1.72 (m, 1H), 1.85–1.95 (m, 1H), 3.44–3.50 (m, 2H), 3.77 (dd, $J = 5.6, 12.0$ Hz, 1H), 3.89 (dd, $J = 3.0, 12.0$ Hz, 1H), 4.08 (t, $J = 3.0$ Hz, 1H), 4.16–4.19 (m, 1H). ^{13}C NMR (100 MHz, CD_3OD) δ : 14.11, 23.55, 27.45, 29.13, 59.70, 63.23, 63.81, 71.98, 73.30. IR (KBr) cm^{-1} : 3363, 2945, 2537, 1618. EI-MS (m/z): 189 (M^+). HRMS Calcd for $\text{C}_9\text{H}_{19}\text{NO}_3$: 189.1365; Found: 189.1358.

4.2.7. 1-((4aS,6S,7S,7aR)-6-Butyl-7-hydroxy-2,2-dimethyltetrahydro-[1,3]dioxino[5,4-b]pyrrol-5(6H)-yl)ethanone (**11**)

NEt_3 (710 μL , 5.06 mmol), DMAP (61.8 mg, 0.51 mmol) and acetic anhydride (478 μL , 5.06 mmol) were added to a solution of compound **1b** (319 mg, 1.69 mmol) in THF (20 mL). After stirring at room temperature for 4 h, the mixture was evaporated. The residue was solved in $\text{NEt}_3/\text{CH}_3\text{OH}$ (NEt_3 : $\text{CH}_3\text{OH} = 1 : 4$, 20 mL). After stirring at room temperature for 48 h, the mixture was evaporated to afford the residue, which was purified by silica gel column chromatography (Et_2O : $\text{CH}_3\text{OH} = 10 : 1 \rightarrow 5 : 1$) to provide the *N*-Ac-triol (291 mg, 75%) as a colorless oil; $[\alpha]_D^{27} = +19.4$ (c 4.57, CH_3OH). ^1H NMR (400 MHz, CD_3OD , ca 1.5:1.0 mixture of amide rotamers) δ : 0.91–0.97 (m, 3H), 1.14–1.61 (m, 6H), 2.08 and 2.14 (s, 3H), 3.64–3.68 (m, 1H), 3.79–3.95 (m, 2H), 4.03–4.17 (m, 2H), 4.48–4.53 (m, 1H). ^{13}C NMR (100 MHz, CD_3OD , mixture of amide rotamers) δ : 14.33, 14.34, 21.94, 23.00, 23.39, 23.49, 29.76, 29.82, 32.14, 35.00, 49.85, 57.30, 58.91, 61.94, 62.56, 67.04, 67.92, 70.57, 71.43, 74.46, 75.22, 172.87, 173.29. IR (NaCl) cm^{-1} : 3270, 2933, 1614. EI-MS (m/z): 231 (M^+). HRMS Calcd for $\text{C}_{11}\text{H}_{21}\text{NO}_4$: 231.1471; Found: 231.1480.

Activated MS3A (molecular sieve 3 Å) (120 mg) was added to a solution of the obtained triol (289 mg, 0.27 mmol) in CH_2Cl_2 (3 mL). 2,2-dimethoxy propane (306 μL , 2.50 mmol) and CSA (10-camphorsulfonic acid) (87.0 mg, 0.38 mmol) were added to the suspension. After stirring at room temperature for 12 h, the reaction mixture was filtered with a pad of celite eluting with EtOAc. The solvents were evaporated to furnish the residue, which was purified by silica gel column chromatography (hexane: ethyl acetate = 4 : 1 \rightarrow 0 : 1) to provide compound **11** (140 mg, 67%) as a colorless oil; $[\alpha]_D^{25} = +5.47$ (c 0.79, CH_3OH). ^1H NMR (400 MHz, CDCl_3 , mixture of amide rotamers) δ : 0.87–0.95 (m, 3H), 1.25–1.59 (m, 6H), 1.39 (s, 3H), 1.42 (s, 3H), 2.07 (s, 3H), 3.11 (d, $J = 2.9$ Hz, 1H), 3.61–3.63 (m, 1H), 3.73–3.88 (m, 1H), 3.98–4.09 (m, 1H), 4.15–4.24 (m, 1H), 4.29–4.38 (m, 1H), 4.38–4.50 (m, 1H). ^{13}C NMR (100 MHz, CDCl_3) δ : 14.05, 22.69, 22.75, 24.45, 26.22, 27.80, 32.41, 55.58, 60.72, 65.31, 69.11, 74.29, 99.90, 170.65. IR (NaCl) cm^{-1} : 3428, 2987, 2934, 2873, 1737, 1634. EI-MS (m/z): 271 (M^+). HRMS Calcd for $\text{C}_{14}\text{H}_{25}\text{NO}_4$: 271.1784; Found: 271.1776.

4.2.8. (4aS,6S,7aR)-5-Acetyl-6-butyl-2,2-dimethyltetrahydro-[1,3]dioxino[5,4-b]pyrrol-7-(7aH)-one (**12**)

CrO_3 (68.9 mg, 0.689 mmol) was added to a solution of pyridine (111 μL , 1.38 mmol) and acetic anhydride (65.1 μL , 0.689 mmol) in CH_2Cl_2 (5.0 mL), then the mixture was cooled in an ice bath. A solution of compound **11** (62.3 mg, 0.23 mmol) in CH_2Cl_2 (1.0 mL) was

added to the CrO_3 -pyridine-acetic anhydride complex at 0 °C. After stirring at room temperature for 6 h, the reaction was quenched with 2-propanol (53 μL , 0.69 mmol). After stirring at room temperature for 2 h, the mixture was filtered with a pad of celite eluting with EtOAc. The solvents were evaporated to furnish the residue, which was purified by silica gel column chromatography (hexane: ethyl acetate = 5 : 1 \rightarrow 2 : 1) to provide ketone **12** (32.4 mg, 52%) as a colorless oil; $[\alpha]_D^{26} = +26.9$ (c 1.31, CHCl_3). ^1H NMR (400 MHz, CDCl_3 , mixture of amide rotamers) δ : 0.84–0.95 (m, 3H), 0.96–1.54 (m, 4H), 1.37 (s, 3H), 1.40 (s, 3H), 1.74–2.09 (m, 2H), 2.11 and 2.13 (s, 3H), 3.63–3.73 (m, 1H), 4.10–4.17 (m, 1H), 4.24–4.33 (m, 1H), 4.37–4.42 (m, 1H), 4.45–4.50 (m, 1H). ^{13}C NMR (100 MHz, CDCl_3 , mixture of amide rotamers) δ : 13.67, 13.77, 22.03, 22.35, 22.40, 22.59, 25.50, 25.55, 26.20, 26.35, 30.10, 33.10, 53.00, 54.57, 60.73, 61.61, 61.73, 62.65, 70.39, 72.51, 100.82, 101.26, 170.03, 170.41, 209.26, 210.06. IR (NaCl) cm^{-1} : 3428, 2924, 2859, 1770, 1634. EI-MS (m/z): 269 (M^+). HRMS Calcd for $\text{C}_{14}\text{H}_{23}\text{NO}_4$: 269.1627; Found: 269.1629.

4.2.9. 1-((4aS,6S,7S,7aR)-6-Butyl-7-hydroxy-2,2-dimethyltetrahydro-[1,3]dioxino[5,4-b]pyrrol-5(6H)-yl)ethanone (**11**), 1-((4aS,6S,7R,7aR)-6-Butyl-7-hydroxy-2,2-dimethyltetrahydro-[1,3]dioxino[5,4-b]pyrrol-5(6H)-yl)ethanone (**13**)

LiBH_4 (15.3 mg, 0.70 mmol) was added to a solution of ketone **12** (37.9 mg 0.141 mmol) in EtOH (2.0 mL) at 0 °C. After stirring at room temperature for 12 h, the reaction was quenched by addition of sat. NH_4Cl aq. (5.0 mL). The whole mixture was extracted with CH_2Cl_2 (5 mL \times 2) and the combined organic layers were washed with sat. NaCl aq. (5 mL). The organic layer was dried over anhydrous Na_2SO_4 . Filtration and evaporation *in vacuo* furnished the crude product, which was purified by silica gel column chromatography (hexane/EtOAc = 5 : 1 \rightarrow 1 : 1) to provide an inseparable mixture of **11** and **13** (**11** : **13** = 3 : 2, 25.2 mg, 66%). The diastereomer ratio was determined by HPLC analysis [Inertsil® CN-3 column (30 : 1 hexane/*i*PrOH; 1.0 mL/min): **11** t_R 3.89 min; **13** t_R 6.57 min]; $[\alpha]_D^{20} = +19.4$ (c 2.32, CHCl_3). ^1H NMR (400 MHz, CDCl_3 , mixture of amide rotamers) (mixture of **11** and **13**) δ : 0.88–0.94 (m, 3H), 1.25–1.58 (m, 12H), 2.03 and 2.07 (s, 3H), 2.76 (brs, 0.3H), 3.11 (d, $J = 2.9$ Hz, 0.5H), 3.61–3.80 (m, 2H), 3.91–4.19 (m, 3H), 4.36–4.50 (m, 2H). ^{13}C NMR (100 MHz, CDCl_3) δ : 13.80, 13.88, 13.92, 13.97, 22.40, 22.49, 22.62, 22.90, 23.22, 23.36, 23.48, 24.17, 24.39, 24.46, 25.82, 26.00, 26.29, 27.13, 27.51, 28.01, 28.54, 29.47, 29.59, 31.78, 32.14, 55.15, 55.36, 56.12, 57.12, 59.90, 60.40, 60.60, 60.77, 61.37, 61.59, 63.41, 65.03, 65.72, 68.88, 69.88, 73.10, 74.00, 74.41, 74.79, 75.77, 99.15, 99.65, 99.79, 169.57, 170.53, 170.69. IR (NaCl) cm^{-1} : 3391, 2933, 2873, 1622, 1416. EI-MS (m/z): 271 (M^+). HRMS Calcd for $\text{C}_{14}\text{H}_{25}\text{NO}_4$: 271.1784; Found: 271.1773.

4.2.10. (4aS,6S,7S,7aR)-5-Acetyl-6-butyl-2,2-dimethylhexahydro-[1,3]dioxino[5,4-b]pyrrol-7-yl 4-methoxybenzoate (**14a**), (4aS,6S,7R,7aR)-5-Acetyl-6-butyl-2,2-dimethylhexahydro-[1,3]dioxino[5,4-b]pyrrol-7-yl 4-methoxybenzoate (**14b**)

A mixture of **11** and **13** (**11** : **13** = 3 : 2, 27.0 mg, 0.10 mmol) was dissolved in CH_2Cl_2 (1.0 mL) and the solution was cooled in an ice bath. NEt_3 (42.1 μL , 0.30 mmol), DMAP (2.4 mg, 0.02 mmol) and *p*-methoxybenzoyl chloride (20.3 μL , 0.15 mmol) were added to a solution at 0 °C. After stirring at room temperature for 52 h, the reaction was quenched by addition of sat. NaHCO_3 aq. (3.0 mL). The whole mixture was extracted with CH_2Cl_2 (5 mL \times 2) and the combined organic layers were washed with sat. NaCl aq. (5 mL). The organic layer was dried over anhydrous Na_2SO_4 . Filtration and evaporation *in vacuo* furnished the crude product, which was purified by silica gel column chromatography (hexane/EtOAc = 10 : 1) to afford the mixture of **14a** and **14b**. The mixture of **14a** and **14b**

was purified by preparative TLC (TLC 20 × 20 cm², Et₂O/hexane = 4 : 1) to afford ester **14a** (16.2 mg, 43%) as a colorless oil and ester **14b** (11.0 mg, 29%) as a colorless oil. **14a**: [α]_D²⁵ = −13.6 (c 0.90, CHCl₃). ¹H NMR (400 MHz, CDCl₃, mixture of amide rotamers) δ : 0.87–0.93 (m, 3H), 1.20 (s, 3H), 1.24–1.66 (m, 6H), 1.34 (s, 3H), 2.04 and 2.10 (s, 3H), 3.73–3.80 (m, 1H), 3.87 (s, 3H), 3.99–4.05 (m, 1H), 4.08–4.16 (m, 1H), 4.28–4.50 (m, 1H), 4.61–4.73 (m, 1H), 5.40–5.46 (m, 1H), 6.92–6.95 (m, 2H), 7.98–8.02 (m, 2H). ¹³C NMR (100 MHz, CDCl₃, mixture of amide rotamers) δ : 13.88, 13.95, 22.54, 22.56, 22.61, 23.10, 24.13, 24.61, 26.23, 26.25, 27.42, 30.29, 32.94, 55.46, 55.72, 56.10, 60.35, 61.45, 61.54, 62.75, 68.32, 69.22, 74.55, 75.74, 99.46, 99.61, 113.70, 113.73, 122.07, 131.71, 131.75, 163.63, 165.59, 170.15. IR (NaCl) cm^{−1}: 2935, 1715, 1645, 1606, 1513. EI-MS (*m/z*): 405 (M⁺). HRMS Calcd for C₂₂H₃₁NO₃: 405.2151; Found: 405.2160.

14b: [α]_D²⁵ = +8.96 (c 0.81, CHCl₃). ¹H NMR (400 MHz, CDCl₃, mixture of amide rotamers) δ : 0.77–0.82 (m, 3H), 1.14–1.32 (m, 4H), 1.35 (s, 3H), 1.39 (s, 3H), 1.50–1.56 (m, 1H), 1.63–1.71 (m, 1H), 2.06 and 2.12 (s, 3H), 3.64–3.83 (m, 1H), 3.88 (s, 3H), 4.04–4.21 (m, 1H), 4.29–4.45 (m, 3H), 5.41–5.48 (m, 1H), 6.93–6.97 (d, *J* = 8.8 Hz, 2H), 7.97–8.02 (m, 2H). ¹³C NMR (100 MHz, CDCl₃, mixture of amide rotamers) δ : 13.78, 13.88, 22.78, 22.84, 23.13, 23.26, 23.30, 26.20, 26.57, 28.03, 28.08, 28.29, 29.68, 29.83, 55.21, 55.49, 58.88, 59.93, 60.86, 61.49, 72.42, 72.48, 75.63, 77.40, 99.51, 99.89, 113.83, 121.49, 123.75, 131.76, 131.84, 163.79, 163.88, 165.19, 165.47, 170.08, 170.67. IR (NaCl) cm^{−1}: 3473, 2934, 2873, 1715, 1651, 1606, 1581, 1512. EI-MS (*m/z*): 405 (M⁺). HRMS Calcd for C₂₂H₃₁NO₆: 405.2151; Found: 405.2151.

4.2.11. α -1-C-1-Butyl-L-xylo-iminofuranose (**1d**) hydrochloride

A solution of **14b** (12.0 mg, 0.03 mmol) in 6 mol/L HCl (1.0 mL) was stirred at 100 °C for 12 h. The whole mixture was transferred into a separate funnel and washed with CH₂Cl₂ (3 mL × 3). The water layer was evaporated to obtain **1d** hydrochloride (5.0 mg, 69%) as a white solid; mp > 142 °C (decomp.). [α]_D²¹ = +4.74 (c 0.49, CH₃OH). ¹H NMR (400 MHz, CD₃OD) δ : 0.97 (t, *J* = 7.0 Hz, 3H), 1.36–1.47 (m, 4H), 1.71–1.77 (m, 1H), 1.79–1.88 (m, 1H), 3.70 (td, *J* = 2.9, 7.5 Hz, 1H), 3.79–3.94 (m, 3H), 4.04–4.05 (m, 1H), 4.18 (*J* = 1.4 Hz, 1H). ¹³C NMR (100 MHz, CD₃OD) δ : 14.17, 23.63, 27.00, 29.71, 59.41, 63.39, 64.76, 76.16, 76.41. IR (KBr) cm^{−1}: 3392, 2961, 2497, 1601. EI-MS (*m/z*): 189 (M⁺). HRMS Calcd for C₉H₁₉NO₃: 189.1365; Found: 189.1361.

4.2.12. (R)-3-[(S)-1-[(tert-Butyldimethylsilyl)oxy]but-3-en-2-yl]-4-vinylloxazolidin-2-one (**15a**)

Butadiene monoxide (3.15 mL, 39.1 mmol) was added to a solution of oxazolidinone **2** (2.95 g, 26.1 mmol), (R,R)-Naphthyl Trost ligand (619 mg, 3.0 mol%), Tris(dibenzylideneacetone) dipalladium(0)-chloroform adduct (270 mg, 1.0 mol%) and DBU (390 μ L, 10 mol%) in CH₂Cl₂. After stirring at room temperature for 72 h, the mixture was evaporated to afford the residue, which was purified by silica gel column chromatography (hexane: ethylacetate = 2 : 1) to provide the alcohol (4.62 g) as a colorless oil. The alcohol was dissolved in CH₂Cl₂ (84 mL) and the solution was cooled to 0 °C. Imidazole (3.44 g, 50.5 mmol) and *tert*-butyldimethylsilyl chloride (4.57 g, 30.3 mmol) were added to the solution. After stirring at room temperature for 1 h, the reaction was quenched by addition of H₂O (30 mL). The whole mixture was extracted with EtOAc (100 mL × 2) and the combined organic layers were washed with sat. NaCl aq. (50 mL). The organic layer was dried over anhydrous Na₂SO₄. Filtration and evaporation *in vacuo* furnished the crude product, which was purified by twice silica gel column chromatography (1st column; hexane: ethylacetate = 20 : 1 → 1 : 1, 2nd column; CH₂Cl₂: hexane = 1 : 1 → CH₂Cl₂: CH₃OH = 5 : 1) to give **15a** (2.94 g, 63%) as a colorless oil; [α]_D²³ = +3.94 (c 0.93, CH₂Cl₂). ¹H NMR (400 MHz, CDCl₃) δ : 0.04 (s,

3H), 0.05 (s, 3H), 0.86 (s, 9H), 3.65 (dd, *J* = 4.8, 9.2 Hz, 1H), 3.88–4.12 (m, 3H), 4.37–4.41 (m, 2H), 5.19–5.23 (m, 2H), 5.27–5.35 (m, 2H), 5.72–5.79 (m, 1H), 5.96–6.05 (m, 1H). ¹³C NMR (100 MHz, CDCl₃) δ : 5.56, 18.05, 25.73, 58.61, 60.99, 62.89, 67.26, 118.53, 120.41, 132.75, 135.94, 157.16. IR (NaCl) cm^{−1}: 3499, 3080, 2934, 1753, 1405.

EI-MS (*m/z*): 297 (M⁺). HRMS Calcd for C₁₅H₂₇NO₃Si: 297.1760; Found: 297.1749.

4.2.13. (5S,7aR)-5-[(tert-Butyldimethylsilyl)oxy]methyl]-1,7a-dihydropyrrolo[1,2-c]oxazol-3(5H)-one (**16**)

A solution of diene **15a** (4.76 g, 16.0 mmol) in CH₂Cl₂ (115 mL) was degassed with argon for 30 min and then heated to 40 °C. Four portions of Grubbs 1st catalyst (each 71 mg, 0.863 mmol) were added after 0 h, 10.5 h, 24 h and 65 h. The reaction was stirred an additional 7 h for a total reaction time of 72 h, then cooled to room temperature and concentrated. The residue was purified by silica gel column chromatography (hexane: ethylacetate = 9 : 1 → 1 : 1) to yield compound **16** (3.84 g, 89%) as a white gum; [α]_D²⁶ = +3.20 (c 0.95, CH₂Cl₂). ¹H NMR (400 MHz, CDCl₃) δ : 0.04 (s, 3H), 0.05 (s, 3H), 0.86 (s, 9H), 3.83 (dd, *J* = 1.7, 10.4 Hz, 1H), 4.01 (dd, *J* = 7.8, 10.4 Hz, 1H), 4.30–4.33 (m, 1H), 4.36 (dd, *J* = 4.1, 10.4 Hz, 1H), 4.47 (t, *J* = 7.8 Hz, 1H), 4.95–4.98 (m, 1H), 5.82 (m, 2H). ¹³C NMR (100 MHz, CDCl₃) δ : 5.74, 18.25, 25.73, 58.43, 66.07, 67.08, 69.63, 126.47, 133.55, 158.94. IR (NaCl) cm^{−1}: 2956, 1758. EI-MS (*m/z*): 269 (M⁺). HRMS Calcd for C₁₃H₂₃NO₃Si: 269.1447; Found: 269.1439.

4.2.14. (5S,7aR)-5-(Hydroxymethyl)-1,7a-dihydropyrrolo[1,2-c]oxazol-3(5H)-one (**17**)

A solution of tetra-*n*-butylammonium fluoride (1.0 M solution in THF, 25 mL, 25 mmol) was added to a solution of compound **16** in THF (53 mL) and the reaction mixture was stirred at room temperature for 1 h. The reaction mixture was concentrated and purified by silica gel column chromatography (hexane: ethylacetate = 1 : 1 → 0 : 1) to yield alcohol **17** (1.31 g, 73%) as a white solid; mp 97–99 °C. [α]_D²⁶ = +3.35 (c 1.20, CH₂Cl₂). ¹H NMR (400 MHz, CDCl₃) δ : 3.83–3.89 (m, 1H), 4.02 (dd, *J* = 3.4, 10.6 Hz, 1H), 4.10–4.18 (m, 2H), 4.43 (brs, 1H), 4.60 (t, *J* = 8.7 Hz, 1H), 4.97–4.98 (m, 1H), 5.82 (d, *J* = 5.8 Hz, 1H), 5.96 (d, *J* = 5.8 Hz, 1H). ¹³C NMR (100 MHz, CDCl₃) δ : 61.96, 66.48, 68.10, 69.44, 129.14, 132.13, 160.21. IR (NaCl) cm^{−1}: 3393, 1723. EI-MS (*m/z*): 155 (M⁺). HRMS Calcd for C₇H₉NO₃: 155.0582; Found: 155.0580.

4.2.15. (5S,7aR)-5-(Iodomethyl)-1,7a-dihydropyrrolo[1,2-c]oxazol-3(5H)-one (**18**)

Alcohol **17** (1.25 g, 8.06 mmol), imidazole (1.37 g, 20.2 mmol) and triphenyl phosphine (5.29 g, 20.6 mmol) were dissolved in CH₂Cl₂ (37 mL) and the solution was cooled to 0 °C. Iodine chips (4.09 g, 16.1 mmol) were added to a solution at 0 °C, and then the reaction was stirred for 10 min. The reaction was quenched by addition of sodium thiosulfate aq. (1.0 M, 10 mL), changing the brown reaction mixture to a colorless one. The whole mixture was extracted with CH₂Cl₂ (30 mL × 3) and the combined organic layers were dried over anhydrous Na₂SO₄. Filtration and evaporation *in vacuo* furnished the crude product, which was purified by silica gel column chromatography (hexane: ethylacetate = 4 : 1) to give **18** (1.75 g 82%) as a pale yellow solid; mp 80–82 °C. [α]_D²⁶ = +3.31 (c 1.09, CHCl₃). ¹H NMR (400 MHz, CDCl₃) δ : 3.73 (dd, *J* = 2.7, 10.7 Hz, 1H), 4.09 (dd, *J* = 4.8, 10.7 Hz, 1H), 4.26–4.30 (m, 2H), 4.55 (t, *J* = 8.0 Hz, 1H), 5.01–5.03 (m, 1H), 5.80 (d, *J* = 6.3 Hz, 1H), 6.00 (d, *J* = 6.3 Hz, 1H). ¹³C NMR (100 MHz, CDCl₃) δ : 7.64, 62.63, 66.93, 69.10, 127.40, 135.33, 157.37. IR (KBr) cm^{−1}: 1732. EI-MS (*m/z*): 264 (M⁺). HRMS Calcd for C₇H₈INO₂: 264.9600; Found: 264.9603; Anal. Calcd for C₇H₈INO₂: C, 31.72; H, 3.04; N, 5.28. Found: C, 31.72; H, 3.01; N, 5.22.

4.2.16. (5*R*,7*aR*)-5-Butyl-1,7*a*-dihydropyrrolo[1,2-*c*]oxazol-3(5*H*)-one (**19**)

Preparation of a solution of *n*-propylzinc iodide in *N,N*-dimethylacetamide; Iodine chips (173 mg, 0.68 mmol) were added to a suspension of dried zinc powder (1.34 g, 20.5 mmol) in *N,N*-dimethylacetamide (13 mL). The mixture was stirred for 30 min at room temperature, changing the brown suspension to a colorless one. 1-Iodopropane (1.34 mL, 13.7 mmol) was added to the suspension. After stirring for 3 h at room temperature, the suspension was used as a solution of *n*-propylzinc iodide in *N,N*-dimethylacetamide.

Negishi Coupling; Yellow bis(1,5-cyclooctadiene)nickel(0) (132 mg, 0.480 mmol, 16 mol%) and (*R,R*)-2,6-bis(4-isopropyl-2-oxazolin-2-yl)pyridine (291 mg, 0.966 mmol, 32 mol%) were added to *N,N*-dimethylacetamide (19 mL), and the resulting mixture was stirred for 30 min at room temperature. The resulting deep-blue solution was added to a mixture of compound **18** (800 mg, 3.02 mmol) and pre-prepared *n*-propylzinc iodide solution (13 mL). After stirring for 20 h at room temperature, the reaction was quenched by addition of iodine chips (400 mg, 3.15 mmol). After additional stirring for 10 min, the dark-brown mixture was purified by silica gel column chromatography (hexane: ethylacetate = 4 : 1) to give compound **19** (279 mg, 51%) as a colorless oil; $[\alpha]_D^{25} = -1.91$ (c 0.93, CHCl₃). ¹H NMR (400 MHz, CDCl₃) δ : 0.91 (t, *J* = 7.2 Hz, 3H), 1.24–1.40 (m, 4H), 1.79–1.83 (m, 1H), 2.27–2.31 (m, 1H), 3.98 (dd, *J* = 7.7, 9.7 Hz, 1H), 4.27–4.30 (m, 1H), 4.49 (t, *J* = 7.7 Hz, 1H), 4.93–5.00 (m, 1H), 5.84 (dt, *J* = 1.9, 6.3 Hz, 1H), 5.94 (dt, *J* = 1.9, 6.3 Hz, 1H). ¹³C NMR (100 MHz, CDCl₃) δ : 13.95, 22.60, 27.59, 29.07, 64.29, 66.76, 69.16, 126.22, 135.43, 157.82. IR (NaCl) cm⁻¹: 2927, 2861, 1748. EI-MS (*m/z*): 181 (M⁺). HRMS Calcd for C₁₀H₁₅NO₂: 181.1103; Found: 181.1099.

4.2.17. (5*R*,6*R*,7*S*,7*aS*)-5-Butyl-6,7-dihydroxytetrahydropyrrolo[1,2-*c*]oxazol-3(1*H*)-one (**20**)

4-Methylmorpholine *N*-oxide (151 μ L, 0.73 mmol) and potassium osmate dihydrate (8.4 mg, 0.03 mmol) were added to a solution of compound **19** in acetone/H₂O (2 : 1, 3 mL). After stirring at room temperature for 47 h, the solvents were removed under reduced pressure. Traces of water were removed from the mixture by azeotropic distillations with toluene (1 mL \times 2) under reduced pressure. The residue was purified by silica gel column chromatography (hexane: ethylacetate = 4 : 1 \rightarrow 1 : 1) to give diol **20** (24.0 mg, 67%) as a brown oil; $[\alpha]_D^{25} = -0.42$ (c 1.18, CHCl₃). ¹H NMR (400 MHz, CDCl₃) δ : 0.93 (t, *J* = 7.0 Hz, 3H), 1.32–1.54 (m, 4H), 1.83–1.90 (m, 1H), 2.24–2.33 (m, 1H), 3.20–3.25 (m, 1H), 3.98–4.03 (m, 1H), 4.17 (t, *J* = 3.3 Hz, 1H), 4.23 (t, *J* = 5.7 Hz, 1H), 4.28 (t, *J* = 8.7 Hz, 1H), 4.50 (dd, *J* = 5.7, 8.7 Hz, 1H). ¹³C NMR (100 MHz, CDCl₃) δ : 13.99, 22.71, 24.29, 29.73, 60.72, 62.38, 63.26, 70.57, 73.15, 160.29. IR (NaCl) cm⁻¹: 3371, 2930, 2872, 1731. EI-MS (*m/z*): 215 (M⁺). HRMS Calcd for C₁₀H₁₇NO₄: 215.1158; Found: 215.1158.

4.2.18. β -1-*C*-Butyl-*L*-ribo-iminofuranose (**1g**) hydrochloride

A solution of **20** (15.0 mg, 0.07 mmol) in 6 mol/L HCl (2.0 mL) was stirred at 100 °C for 12 h. The whole mixture was transferred into a separate funnel and washed with CH₂Cl₂ (2 mL \times 3). The water layer was evaporated to obtain iminosugar **1g** hydrochloride (13.4 mg, 88%) as a colorless oil; $[\alpha]_D^{25} = -0.65$ (c 0.73, CH₃OH). ¹H NMR (400 MHz, D₂O) δ : 0.88 (t, *J* = 6.8 Hz, 3H), 1.33–1.41 (m, 4H), 1.71–1.75 (m, 1H), 1.81–1.85 (m, 1H), 3.52 (brs, 1H), 3.75–3.80 (m, 1H), 3.81–3.87 (m, 1H), 3.93 (dd, *J* = 3.9, 11.8 Hz, 1H), 4.32 (m, 1H), 4.52 (dd, *J* = 3.9, 7.0 Hz, 1H). ¹³C NMR (100 MHz, D₂O) δ : 13.65, 22.36, 26.19, 28.22, 58.73, 61.44, 61.49, 70.63, 71.01. IR (NaCl) cm⁻¹: 3351, 2930, 1572. EI-MS (*m/z*): 189 (M⁺+1). HRMS Calcd for C₉H₂₀NO₃: 190.1443; Found: 190.1439.

4.2.19. (1*aS*,1*bS*,6*R*,6*aR*)-6-Butyltetrahydrooxireno[2',3':3,4]pyrrolo[1,2-*c*]oxazol-4(1*aH*)-one (**21a**), (1*aR*,1*bS*,6*R*,6*aS*)-6-Butyltetrahydrooxireno[2',3':3,4]pyrrolo[1,2-*c*]oxazol-4(1*aH*)-one (**21b**)

To a vial with **19** (180 mg, 0.910 mmol) were added CH₃CN (7 mL) and 4 \times 10⁻⁴ M aqueous solution of ethylenediaminetetraacetic acid (4.5 mL). The solution was cooled to 0 °C, and 1,1,1-trifluoroacetone (814 μ L, 9.12 mmol) was added. A mixture of solid Oxone[®] (2.80 g, 4.56 mmol) and NaHCO₃ (574 mg, 6.84 mmol) was added in four portions over 2 h. The reaction was stirred for 2 h at 0 °C, then diluted with 5 mL of H₂O, and extracted with CH₂Cl₂ (3 \times 20 mL). The organic layers were combined and dried over anhydrous Na₂SO₄. Filtration and evaporation *in vacuo* furnished the crude product, which was purified by silica gel column chromatography (Et₂O) to provide epoxide **21a** (145 mg, 81%) as a colorless oil and epoxide **21b** (14.0 mg, 8%) as a colorless oil.

21a: $[\alpha]_D^{25} = -0.06$ (c 0.64, CHCl₃). ¹H NMR (400 MHz, CDCl₃) δ : 0.95 (t, *J* = 7.0 Hz, 3H), 1.38–1.54 (m, 4H), 1.72–1.82 (m, 1H), 2.50–2.59 (m, 1H), 3.52 (dd, *J* = 4.8, 9.7 Hz, 1H), 3.56 (d, *J* = 2.9 Hz, 1H), 3.68 (d, *J* = 2.9 Hz, 1H), 4.14–4.18 (m, 1H), 4.31 (dd, *J* = 6.8, 8.7 Hz, 1H), 4.41 (t, *J* = 8.7 Hz, 1H). ¹³C NMR (100 MHz, CDCl₃) δ : 14.01, 22.70, 25.26, 29.51, 53.89, 58.77, 59.89, 60.10, 63.30, 158.14. IR (NaCl) cm⁻¹: 3494, 2959, 2872, 1747. EI-MS (*m/z*): 197 (M⁺). HRMS Calcd for C₁₀H₁₅NO₃: 197.1052; Found: 197.1043.

21b: $[\alpha]_D^{25} = +6.41$ (c 0.50, CHCl₃). ¹H NMR (400 MHz, CDCl₃) δ : 0.94 (t, *J* = 9.3 Hz, 3H), 1.32–1.50 (m, 4H), 1.73–1.82 (m, 1H), 2.28–2.36 (m, 1H), 3.64 (d, *J* = 2.9 Hz, 1H), 3.70 (dd, *J* = 2.9, 8.8 Hz, 1H), 3.80 (d, *J* = 2.9 Hz, 1H), 4.03 (dd, *J* = 8.3, 11.2 Hz, 1H), 4.35 (dd, *J* = 8.3, 11.2 Hz, 1H), 4.49 (t, *J* = 8.3 Hz, 1H). ¹³C NMR (100 MHz, CDCl₃) δ : 13.92, 22.65, 26.61, 27.59, 57.45, 59.40, 61.40, 64.56, 65.46, 157.58. IR (NaCl) cm⁻¹: 2926, 1747. EI-MS (*m/z*): 197 (M⁺). HRMS Calcd for C₁₀H₁₅NO₃: 197.1052; Found: 197.1046.

4.2.20. (5*R*,6*R*,7*R*,7*aS*)-5-Butyl-6,7-dihydroxytetrahydropyrrolo[1,2-*c*]oxazol-3(1*H*)-one (**22a**), (5*R*,6*S*,7*S*,7*aS*)-5-Butyl-6,7-dihydroxytetrahydropyrrolo[1,2-*c*]oxazol-3(1*H*)-one (**22b**)

Trifluoroacetic acid (416 μ L, 5.44 mmol) was added to a solution of the epoxide **21a** (91.0 mg, 0.46 mmol) in THF/H₂O (3/2, 9.5 mL). After being stirred at 80 °C for 72 h, the reaction mixture was cooled to room temperature and concentrated. The product was purified by silica gel column chromatography (Et₂O only \rightarrow Et₂O: CH₃OH = 20 : 1) to yield an inseparable mixture of **22a** and **22b** (**22a**: **22b** = 2.5 : 1.0, 82.0 mg, 83%) as a colorless oil; $[\alpha]_D^{20} = +5.47$ (c 1.02, CH₃OH). ¹H NMR (400 MHz, CD₃OD, mixture of **22a** and **22b**) δ : 0.93–0.97 (m, 3H), 1.29–1.63 (m, 5H), 1.80–1.89 (m, 1H), 2.18–2.26 (m, 1H), 2.44–2.52 (m, 0.7H), 3.23 (ddd, *J* = 1.5, 4.4, 10.2 Hz, 0.7H), 3.45–3.49 (m, 0.3H), 3.57 (brs, 0.3H), 3.79 (brs, 0.7H), 3.87–3.91 (m, 1H), 4.06 (brs, 0.7H), 4.13–4.18 (m, 0.3H), 4.39 (s, 2H), 4.56 t, *J* = 9.3 Hz, 0.3H). ¹³C NMR (100 MHz, CD₃OD, mixture of **22a** and **22b**) δ : 14.32, 23.70, 23.82, 24.94, 28.68, 30.13, 30.28, 30.91, 63.69, 64.36, 64.91, 66.77, 68.31, 68.81, 75.15, 79.91, 81.48, 84.69, 159.54, 162.41. IR (NaCl) cm⁻¹: 3382, 2925, 1715. EI-MS (*m/z*): 215 (M⁺). HRMS Calcd for C₁₀H₁₇NO₄: 215.1158; Found: 215.1158.

4.2.21. β -1-*C*-Butyl-*L*-xylo-iminofuranose (**1h**), β -1-*C*-Butyl-*L*-arabino-iminofuranose (**1e**)

A mixture of **22a** and **22b** (**22a**: **22b** = 2.5 : 1.0, 43.0 mg, 0.200 mmol) was dissolved in EtOH/H₂O (2:1, 3 mL) and NaOH (761 mg, 19.0 mmol) was added to the solution. The mixture was refluxed for 1 h, then cooled to room temperature and concentrated. The residue was purified by a silica gel column (Et₂O: CH₃OH: 28% NH₃ aq. = 80 : 20 : 1 \rightarrow Et₂O: CH₃OH: 28% NH₃ aq. = 0 : 100 : 2) to yield an inseparable mixture of **1h** and **1e** (**1h**: **1e** = 2.3 : 1, 36.0 mg, 97%) as a colorless oil; $[\alpha]_D^{25} = +0.79$ (c 3.26, CH₃OH); ¹H NMR (400 MHz, CD₃OD, mixture of **1h** and **1e**) δ : 0.95 (t, *J* = 7.0 Hz,

3H), 1.33–1.49 (m, 4H), 1.55–1.74 (m, 2H), 2.81–2.86 (m, 0.7H), 3.00–3.04 (m, 0.3H), 3.13–3.18 (m, 0.3H), 3.21–3.26 (m, 0.7H), 3.63–3.86 (m, 3H), 3.98–4.00 (m, 1H); ^{13}C NMR (100 MHz, CD_3OD , mixture of **1h** and **1e**) δ : 14.28, 23.66, 23.87, 28.10, 30.14, 30.19, 34.26, 60.60, 62.70, 63.35, 63.78, 67.08, 69.31, 78.24, 78.83, 80.12, 83.34. IR (NaCl) cm^{-1} : 3320, 2934, 1682. EI-MS (m/z): 189 (M^+). HRMS Calcd for $\text{C}_9\text{H}_{19}\text{NO}_3$: 189.1365; Found: 189.1368.

4.2.22. 1-((2R,3R,4R,5S)-2-Butyl-3,4-dihydroxy-5-(hydroxymethyl)pyrrolidin-1-yl)ethanone (23a**), 1-((2R,3S,4S,5S)-2-Butyl-3,4-dihydroxy-5-(hydroxymethyl)pyrrolidin-1-yl)ethanone (**23b**)**

A mixture of **1h** and **1e** (136 mg, 0.720 mmol) was dissolved in THF (5 mL), and then NEt_3 (220 μL , 1.58 mmol), DMAP (8.77 mg, 0.07 mmol) and acetic anhydride (122 μL , 1.45 mmol) were added to the solution. After stirring at room temperature for 4 h, the mixture was evaporated. The residue was solved in $\text{NEt}_3/\text{CH}_3\text{OH}$ (NEt_3 : CH_3OH = 1 : 4, 10 mL). After stirring at room temperature for 48 h, the mixture was evaporated to afford the residue, which was purified by silica gel column chromatography (Et_2O : CH_3OH = 10 : 1 \rightarrow 5 : 1) to provide an inseparable mixture of **23a** and **23b** (145 mg, 87%) as a colorless oil; $[\alpha]_D^{23}$ = +14.4 (c 0.26, CH_3OH). ^1H NMR (400 MHz, CD_3OD , mixture of amide rotamers) (mixture of **23a** and **23b**) δ : 0.90–0.97 (m, 3H), 1.36–2.05 (m, 6H), 2.09–2.13 (m, 3H), 3.59–4.20 (m, 6H). ^{13}C NMR (100 MHz, CD_3OD , mixture of amide rotamers) (mixture of **23a** and **23b**) δ : 14.37, 14.43, 22.12, 22.24, 23.66, 23.84, 24.01, 24.04, 28.18, 28.89, 29.70, 29.80, 30.27, 31.17, 33.72, 34.36, 62.00, 62.14, 62.23, 62.86, 63.71, 63.77, 63.83, 66.34, 68.75, 69.38, 77.23, 77.78, 78.06, 79.72, 81.23, 173.29, 174.11. IR (NaCl) cm^{-1} : 3343, 2925, 1731, 1600. EI-MS (m/z): 231 (M^+). HRMS Calcd for $\text{C}_{11}\text{H}_{21}\text{NO}_4$: 231.1471; Found: 231.1468.

4.2.23. 1-((4aS,6R,7R,7aR)-6-Butyl-7-hydroxy-2,2-dimethyltetrahydro-[1,3]dioxino[5,4-b]pyrrol-5(6H)-yl)ethanone (24**), 1-((2R,3S,4S,5S)-2-Butyl-3,4-dihydroxy-5-(hydroxymethyl)pyrrolidin-1-yl)ethanone (**23b**)**

Activated MS3A (120 mg) was added to a solution of triols **23a** and **23b** (62.8 mg, 0.270 mmol) in CH_2Cl_2 (6 mL). 2,2-dimethoxy propane (306 μL , 2.50 mmol) and CSA (18.9 mg, 0.08 mmol) were added to the suspension. After stirring at room temperature for 12 h, the reaction mixture was filtered with a pad of celite eluting with CH_3OH . The solvents were evaporated to furnish the residue, which was purified by silica gel column chromatography (CH_2Cl_2 : CH_3OH = 20 : 1 \rightarrow 10 : 1) to provide compound **24** (27.7 mg, 38%) as a colorless oil and **23b** (9.5 mg, 15%) as a colorless oil.

24: $[\alpha]_D^{26}$ = +0.85 (c 2.03, CHCl_3). ^1H NMR (400 MHz, CDCl_3 , ca 2.0 : 1.0 mixture of amide rotamers) (major) δ : 0.90–0.95 (m, 3H), 1.33–1.45 (m, 10H), 1.63–1.69 (m, 1H), 1.90 (brs, 1H), 2.02 and 2.07 (s, 3H), 3.40 (brs, 1H), 3.48–3.78 (m, 2H), 4.00–4.29 (m, 4H). ^{13}C NMR (100 MHz, CDCl_3 , mixture of amide rotamers) δ : 13.92, 21.51, 21.76, 22.57, 22.62, 24.48, 25.94, 28.89, 28.91, 31.52, 32.74, 55.69, 57.97, 60.95, 61.62, 67.03, 68.80, 75.51, 76.05, 76.88, 98.73, 99.83, 170.13, 170.92. IR (NaCl) cm^{-1} : 3362, 2933, 1728, 1621. EI-MS (m/z): 271 (M^+). HRMS Calcd for $\text{C}_{14}\text{H}_{25}\text{NO}_4$: 271.1784; Found: 271.1786.

23b: $[\alpha]_D^{25}$ = +1.65 (c 1.81, CH_3OH). ^1H NMR (400 MHz, CD_3OD , mixture of amide rotamers) δ : 0.90–0.96 (m, 3H), 1.29–1.66 (m, 5H), 1.83 (brs, 1H), 2.10 and 2.12 (s, 3H), 3.63–3.83 (m, 3H), 3.87–4.13 (m, 3H). ^{13}C NMR (100 MHz, CD_3OD , mixture of amide rotamers) δ : 14.35, 14.45, 21.98, 22.47, 24.00, 24.03, 29.04, 29.80, 30.27, 31.17, 62.23, 62.26, 62.87, 63.18, 66.36, 69.38, 76.55, 76.74, 77.23, 79.03, 173.88, 173.91. IR (NaCl) cm^{-1} : 3334, 2958, 1614. EI-MS (m/z): 231 (M^+). HRMS Calcd for $\text{C}_{11}\text{H}_{21}\text{NO}_4$: 231.1471; Found: 231.1476.

4.2.24. β -1-C-Butyl-L-xylo-iminofuranose (1h**) hydrochloride**

A solution of **24** (15.0 mg, 0.07 mmol) in 6 mol/L HCl (2.0 mL)

was stirred at 100 °C for 12 h. The whole mixture was transferred into a separate funnel and washed with CH_2Cl_2 (2 mL \times 3). The water layer was evaporated to obtain **1h-HCl** (24.2 mg, quant) as a brown oil; $[\alpha]_D^{23}$ = +1.93 (c 0.97, CH_3OH). ^1H NMR (400 MHz, D_2O) δ : 0.88 (t, J = 6.8 Hz, 3H), 1.32–1.42 (m, 4H), 1.78–1.88 (m, 2H), 3.40 (brs, 1H), 3.81 (t, J = 4.1 Hz, 1H), 3.87–3.92 (m, 1H), 3.98 (dd, J = 4.1, 11.8 Hz, 1H), 4.05 (d, J = 1.7 Hz, 1H), 4.23 (d, J = 1.7 Hz, 1H). ^{13}C NMR (100 MHz, D_2O) δ : 13.62, 22.17, 28.54, 31.28, 57.65, 63.66, 66.67, 75.43, 79.79. IR (NaCl) cm^{-1} : 3365, 2928, 1585. EI-MS (m/z): 189 (M^+). HRMS Calcd for $\text{C}_9\text{H}_{19}\text{NO}_3$: 189.1365; Found: 189.1370.

4.2.25. β -1-C-Butyl-L-arabino-iminofuranose (1e**) hydrochloride**

A solution of **23b** (15.0 mg, 0.07 mmol) in 6 mol/L HCl (2.0 mL) was stirred at 100 °C for 12 h. The whole mixture was transferred into a separate funnel and washed with CH_2Cl_2 (2 mL \times 3). The water layer was evaporated to obtain **1e-HCl** (5.0 mg, 79%) as a brown oil. $[\alpha]_D^{23}$ = +2.88 (c 0.77, CH_3OH). ^1H NMR (400 MHz, D_2O) δ : 0.89 (t, J = 6.5 Hz, 3H), 1.38 (brs, 4H), 1.74–1.84 (m, 2H), 3.56 (brs, 1H), 3.73 (t, J = 6.5 Hz, 1H), 3.80 (t, J = 11.3 Hz, 1H), 3.94 (dd, J = 4.8, 11.3 Hz, 1H), 4.07 (brs, 1H), 4.16 (brs, 1H). ^{13}C NMR (100 MHz, D_2O) δ : 13.66, 22.44, 25.29, 28.39, 60.35, 63.51, 68.15, 75.82, 76.73. IR (NaCl) cm^{-1} : 3401, 3307, 3051, 2954, 1562. EI-MS (m/z): 189 (M^+). HRMS Calcd for $\text{C}_9\text{H}_{19}\text{NO}_3$: 189.1365; Found: 189.1366.

4.3. Biological evaluation

Brush border membranes were prepared from the rat small intestine according to our previous method and were assayed at pH 5.8 for rat intestinal maltase, sucrase, and isomaltase using the appropriate disaccharides as substrates [13]. For rat intestinal α -glucosidase activities, the reaction mixture contained 25 mM substrate and the appropriate amount of enzyme, and the incubations were performed for 10–30 min at 37 °C. The reaction was stopped by heating at 100 °C for 3 min. After centrifugation (600 g; 10 min), the resulting reaction mixture was subjected to a Glucose CII-test Wako (Wako Pure Chemical Industries, Osaka, Japan). The absorbance at 505 nm was measured to determine the amount of D-glucose released.

Acknowledgements

This work was supported by JSPS KAKENHI Grant Number 18K06553. This work was supported by a grant from the Strategic Research Foundation Grant-aided Project for Private Universities from the Ministry of Education, Culture, Sport, Science, and Technology, Japan (MEXT).

Appendix A. Supplementary data

Supplementary data to this article can be found online at <https://doi.org/10.1016/j.tet.2019.04.003>.

References

- [1] S. Smyth, A. Heron, *Nat. Med.* 12 (2006) 75–80.
- [2] World Health Organization. Global Report on Diabetes. Available online: <http://www.who.int>. (Accessed 7 January 2019).
- [3] (a) S.E. Kahn, M.E. Cooper, S. Del Prato, *Lancet* 383 (2014) 1068–1083; (b) A.A. Tahrani, C.J. Bailey, S. Del Prato, A.H. Barnett, *Lancet* 378 (2011) 182–197.
- [4] U. Ghani, *Eur. J. Med. Chem.* 103 (2015) 133–162.
- [5] (a) P. Compain, O.R. Martin, *Iminosugars—From Synthesis to Therapeutic Applications*, John Wiley & Sons, Ltd., West Sussex, England, 2007; (b) N. Asano, K. Oseki, E. Tomioka, H. Kizu, K. Matsui, *Carbohydr. Res.* 259 (1994) 243–255; (c) R.J. Nash, A. Kato, C.-Y. Yu, G.W. Fleet, *J. Future Med. Chem.* 3 (2011) 1513–1521; (d) G. Horne, F.X. Wilson, *Prog. Med. Chem.* 50 (2011) 135–176.

- [6] (a) P.H. Joubert, H.L. Venter, G.N. Foukaridis, Br. J. Clin. Pharmacol. 30 (1990) 391–396;
(b) H. Bischoff, Eur. J. Clin. Invest. 24 (1994) 3–10;
(c) N. Kuboyama, I. Hayashi, T. Yamaguchi, Folia Pharmacol. Jpn. 127 (2006) 223–232.
- [7] (a) A. Kato, I. Nakagome, K. Sato, A. Yamamoto, I. Adachi, R.J. Nash, G.W.J. Fleet, Y. Natori, Y. Watanabe, T. Imahori, Y. Yoshimura, H. Takahata, S. Hirono, Org. Biomol. Chem. 14 (2016) 1039–1048;
(b) Y. Natori, T. Imahori, Y. Yoshimura, J. Synth. Org. Chem., Jpn. 74 (2016) 335–349;
(c) Y. Natori, T. Sakuma, Y. Yoshimura, K. Kinami, Y. Hirokami, K. Sato, I. Adachi, A. Kato, H. Takahata, Bioorg. Med. Chem. Lett. 24 (2014) 3298–3301;
(d) A. Kato, E. Hayashi, S. Miyauchi, I. Adachi, T. Imahori, Y. Natori, Y. Yoshimura, R.J. Nash, H. Shimaoka, I. Nakagome, J. Koseki, S. Hirono, H. Takahara, J. Med. Chem. 55 (2012) 10347–10362;
(e) Y. Natori, S. Kikuchi, Y. Yoshimura, A. Kato, I. Adachi, H. Takahata, Heterocycles 86 (2012) 1401–1417;
(f) Y. Natori, T. Imahori, K. Murakami, Y. Yoshimura, S. Nakagawa, A. Kato, I. Adachi, H. Takahata, Bioorg. Med. Chem. Lett. 21 (2011) 738–741.
- [8] B.M. Trost, D.B. Horne, M.J. Woltering, Chem. Eur. J. 12 (2006) 6607–6620.
- [9] R.L. Grange, E.A. Clizbe, P.A. Evans, Synthesis 48 (2016) 2911–2968.
- [10] (a) J.S. Zhou, G.C. Fu, J. Am. Chem. Soc. 125 (2003) 14726–14727;
(b) V.B. Phapale, E. Buñuel, M. García-Iglesias, D.J. Cárdenas, Angew. Chem. Int. Ed. 46 (2007) 8790–8795.
- [11] In this manuscript, the words “ α -side” and “ β -side” were used according to the definition of carbohydrate nomenclature. The same side as the hydroxymethyl group or the equivalent was “ β -side”, and the opposite side was the “ α -side”
- [12] T. Sugimura, K. Hagiya, Chem. Lett. 36 (2007) 566–567.
- [13] M. Kessler, O. Acuto, C. Storelli, H. Murer, M. Müller, G. Semenza, Biochim. Biophys. Acta 506 (1978) 136–154.



Cite this: *Org. Biomol. Chem.*, 2018, **16**, 3639

Received 26th March 2018,

Accepted 21st April 2018

DOI: 10.1039/c8ob00721g

rsc.li/obc

A novel approach to sesquiterpenoid benzoxazole synthesis from marine sponges: nakijinols A, B and E–G†

Yuki Takeda, Keiyo Nakai, Koichi Narita and Tadashi Katoh *

Nakijinols A, B and analogues E through G, which are structurally unique and biologically significant sesquiterpenoid benzoxazoles, can be efficiently obtained in a highly unified manner from the sesquiterpenoid quinone, smenospongine. The starting material is accessible from the (+)-5-methyl Wieland–Miescher ketone. The synthetic method features strategic construction of the requisite dihydroxylated benzoxazole substructure *via* the ring closure of the *N*-(2-hydroxyphenyl)-formamide or -acetamide moiety. The synthesis of nakijinols is reported here for the first time. The absolute configurations of nakijinols A and E were also established.

Introduction

In 1995, Kobayashi *et al.*¹ reported the isolation and structural elucidation of a novel sesquiterpenoid benzoxazole,² nakijinol A (**1**, Fig. 1) from an Okinawan marine sponge belonging to the Spongiidae family. Even though the constitutional structure and relative stereochemistry of **1** have been both determined *via* extensive spectroscopic studies and 2D NMR experiments, its absolute configuration remains to be assigned.¹ It is well established that this marine natural product has a *trans*-fused decalin ring connected to a dihydroxylated benzoxazole ring through a methylene linkage; the decalin unit contains four contiguous asymmetric carbon centres (C-5, C-8, C-9 and C-10) and an *endo*-olefinic double bond (C-3–C-4 linkage).¹ Remarkably, **1** was the first example of naturally occurring sesquiterpenoids that contained a benzoxazole ring. However, the biological activity of **1** has not been established.¹ Nakijinol B (**2**) was originally isolated by Motti *et al.*³ in 2011 from the marine sponge *Dactylospongia elegans*, and its structure was assigned as the C-4 *exo*-olefinic isomer of **1**. Nakijinol B has shown anti-proliferative activity against several human cancer cell lines in the micromolar range.³ In 2014, nakijinol C (**3**), wherein the dihydroxybenzoxazole unit of **1** has been replaced by a methyl trihydroxybenzoate unit, was isolated by Kobayashi *et al.*⁴ from the same sponge in which **1** had been detected. It has been reported that **3** exhibits antimicrobial

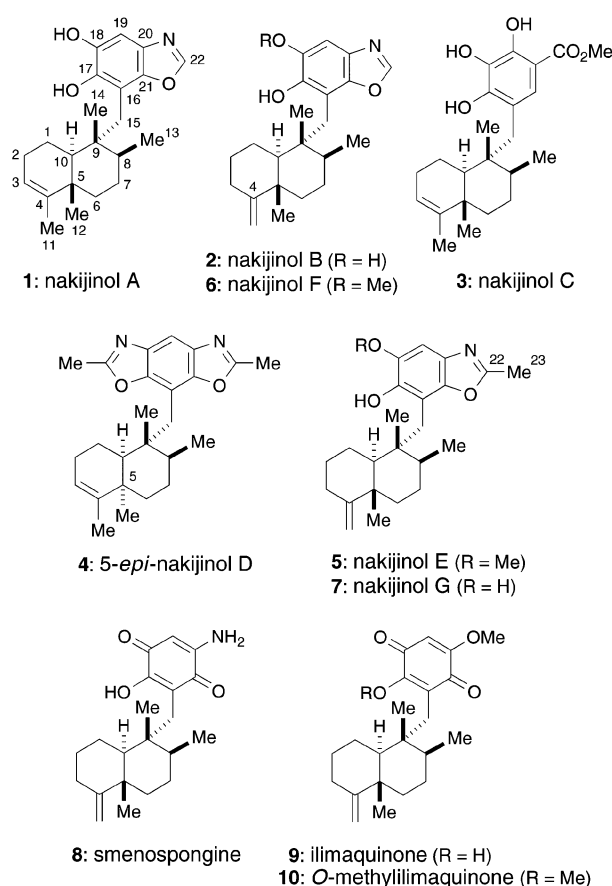


Fig. 1 Structures of nakijinols A–C (**1**–**3**), E–G (**5**–**7**), 5-*epi*-nakijinol D (**4**), smenospongine (**8**), ilimaquinone (**9**) and O-methylilimaquinone (**10**).

Faculty of Pharmaceutical Sciences, Tohoku Medical and Pharmaceutical University, 4-4-1 Komatsushima, Aoba-ku, Sendai, 981-8558, Japan.

E-mail: katoh@tohoku-mpu.ac.jp

† Electronic supplementary information (ESI) available: Copies of ¹H and ¹³C NMR spectra for all new compounds. See DOI: 10.1039/c8ob00721g

activity against several types of bacteria and fungi.⁴ In the same year, 5-*epi*-nakijinol D (4)⁵ was isolated by Proksch *et al.*⁶ from the sponge *Dactylospongia metachromia*. The structure of 4 contains a unique 2,6-dimethylbenzodioxazole unit.⁶

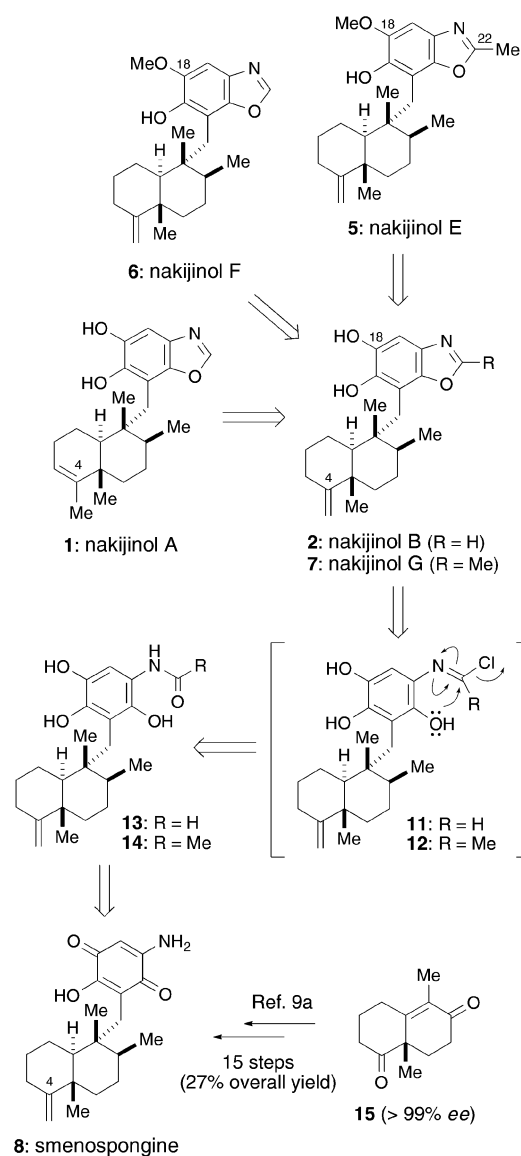
Nakijinol E (5), which incorporates a methyl group at C-22 on the benzoxazole ring, was obtained from *Smenospongia* sponges by Hamann *et al.*⁷ in 2015. It has been shown that 5 has the potential to exert antiproliferative activity *via* the inhibition of β -catenin expression.⁷ More recently, Lin *et al.*⁸ reported the isolation and characterisation of novel nakijinols F (6) and G (7), along with known nakijinols 2 and 5, from a different species of the marine sponge, namely *Hyrtios* sp. The absolute configurations of nakijinols B, F and G have been assigned as depicted in structures 2, 6 and 7, respectively. This was done using a combination of single-crystal X-ray diffraction and electronic circular dichroism analyses.⁸ Nakijinol G has been reported to exhibit protein tyrosine phosphatase 1B inhibitory activity at a low micromolar level.⁸ To the best of our knowledge, these are the only members of the nakijinol family that have been isolated so far.

Results and discussion

Synthetic plan for 1, 2 and 5–7

Retrosynthetic analysis of nakijinols A (1), B (2) and E–G (5–7) is outlined in Scheme 1. The key element of this plan was the strategic construction of the doubly hydroxy-substituted benzoxazole ring system. Thus, we envisioned that the requisite benzoxazole moiety could be established through ring closure of the appropriately functionalised form- and acet-imidoyl chloride intermediates **11** and **12** *via* intramolecular substitution (*i.e.* a nucleophilic addition–elimination sequence) of the chlorine atom by the phenolic hydroxy group in the *ortho* position (*i.e.* **11** \rightarrow **2**; **12** \rightarrow **7**). Therefore, intermediates **11** and **12** could be obtained *via* imidoyl chloride formation of the corresponding *N*-phenyl-formamide **13** and -acetamide **14**, respectively, both of which were accessible from smenospongine (**8**) *via* formylation or acetylation of the amino group, followed by reduction of the quinone moiety. Starting material **8** was prepared from an enantiomerically pure sample of **15** (>99% ee) according to the method previously reported^{9a} (27% overall yield in 15 steps). The cyclized product **2** (*i.e.* nakijinol B) was converted into nakijinol A (**1**) *via* isomerization at the C-4 olefinic double bond. In addition, site-selective *O*-methylation of the C-18 hydroxy group in **2** provided nakijinol F (6). Similarly, nakijinol E (5), which possessed the C-22 methyl group, was derived from the other cyclized product **7** (*i.e.* nakijinol G) by site-selective *O*-methylation of the C-18 hydroxy group.

There are several reports regarding the synthesis of benzoxazoles from the corresponding *N*-acylaminophenols.¹⁰ However, to the best of our knowledge, the method for synthesizing dihydroxy-substituted benzoxazoles (*e.g.* **2** and **7**) from aminohydroxyquinone derivatives (*e.g.* **8**) was previously unheard of.¹¹ Thus, this approach posed a challenge from a

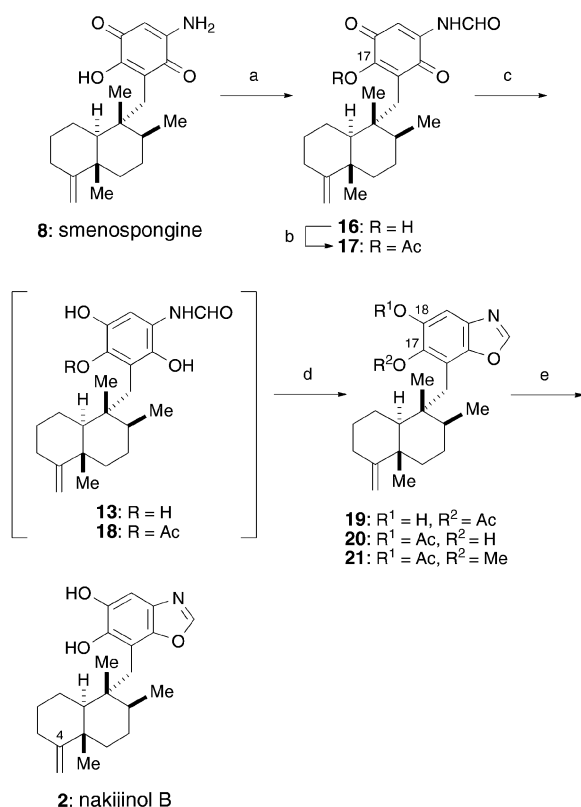


Scheme 1 Plan for the synthesis of nakijinols A (1), B (2) and E–G (5–7).

synthesis viewpoint. Furthermore, another hurdle was choosing mild reaction conditions that would have no impact on the acid-labile *exo*-olefin functionality at C-4, especially during the synthesis of **2** and **7** from **8**.

Synthesis of Nakijinol B (2)

Nakijinol B (**2**) was made as shown in Scheme 2. The synthesis commenced with formylation of the amino group in smenospongine (**8**),^{9a} which afforded the corresponding formamide **16** in 73% yield. There were initial attempts to directly convert **16** into the *N*-(trihydroxyphenyl)formamide **13**, a hypothetical substrate for the key benzoxazole ring formation (Scheme 1), through reduction of the quinone moiety under several conditions [(i) $\text{Na}_2\text{S}_2\text{O}_4$, MeCN/ H_2O , MeOH/ H_2O , or EtOAc/ H_2O , 0 °C to room temperature;¹² (ii) Zn, AcOH, room tempera-



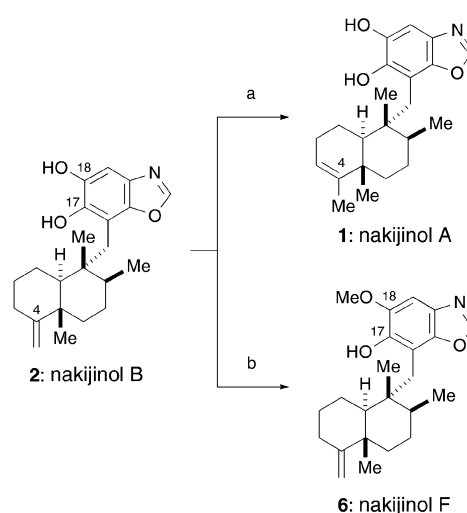
Scheme 2 Synthesis of nakijinols B (2). (a) HCO_2H , Ac_2O , 60 °C, 2 h; then **8**, room temp., 2 h, 73%; (b) Ac_2O , DMAP, THF, 0 °C to room temp., 81%; (c) $\text{Na}_2\text{S}_2\text{O}_4$, $\text{MeCN}/\text{H}_2\text{O}$ (1 : 1), room temp., 30 min; (d) PPh_3 , CCl_4 , MeCN , 50 °C, 2 h, 98% (2 steps, **19/20** ca.1 : 3); (e) NH_3 (2.5% aq.), MeOH , 0 °C, 10 min, 92%. Ac = acetyl, DMAP = 4-(dimethylamino) pyridine.

ture;¹³ (iii) NaBH_4 , MeOH or EtOH , 0 °C to temperature¹⁴]. All of these experiments were unsuccessful and resulted in decomposition of the products. This was likely due to the presence of the sensitive hydroxy group at C-17 in the substrate **16**. Given this, it was decided that masking the reactive hydroxy group as an acetate would be the best way to improve our results. Acetylation of the hydroxy group in **16** provided the corresponding acetate **17** in 81% yield. Subsequent reduction of the quinone moiety in **17** with $\text{Na}_2\text{S}_2\text{O}_4$ ¹⁵ in $\text{MeCN}/\text{H}_2\text{O}$ (1 : 1) at room temperature furnished the requisite hydroquinone **18**. However, since the product was unstable and easily susceptible to oxidation in air, it was used immediately for subsequent reactions without further purification. The crucial benzoxazole ring formation was efficiently achieved by treating the crude product **18** with triphenylphosphine (PPh_3) and carbon tetrachloride (CCl_4)^{10e} in MeCN at 50 °C for 2 h. The benzoxazole products **19** and **20** (the *O*-acetyl-migration product of **19**) were obtained as an inseparable mixture in 98% yield over two steps. Using 400 MHz ^1H NMR spectroscopic analysis, the ratio of products **19** and **20** was estimated to be approximately 1 : 3. We believe that this ring-closing reaction proceeded *via* the reactive imidoyl chloride species as depicted

in structure **11** (Scheme 1). Interestingly, a mixture of **19** and **20** could be converted to the sole product **20** in quantitative yields when this mixture was exposed to triethylamine in MeCN at room temperature.¹⁶ This indicated that the C-18 acetate **20** was thermodynamically more stable than the C-17 acetate **19**. The structure of **20** was assigned based on analysis of the heteronuclear multiple bond correlation (HMBC) spectrum of the C-17 *O*-methylated product **21** (see ESI†), which had been derived from **20**. To advance the synthesis, deprotection of the *O*-acetyl group in a mixture of **19** and **20** was conducted using 2.5% aqueous ammonia in MeOH at 0 °C to afford the first target compound, nakijinol B (**2**), in 92% yield. The spectroscopic properties of **2** (IR, MS and both ^1H and ^{13}C NMR spectroscopy) were identical to those of natural **2**.^{3,8} The optical rotation of synthetic **2** was in agreement with that of natural **2**.

Synthesis of nakijinols A (1) and F (6)

After obtaining the first target compound, nakijinol B (**2**), we next approached the synthesis of the second and third target compounds, nakijinols A (**1**) and F (**6**), as shown in Scheme 3. Acid-induced isomerization of the C-4 *exo*-olefin moiety in **2** was efficiently achieved through treatment with *p*-toluenesulfonic acid in CH_2Cl_2 at room temperature to provide nakijinol A (**1**) in good yield (86%). It is worth noting that the sensitive dihydroxylated benzoxazole moiety present in **2** remained intact during acid-induced olefin isomerization. On the other hand, site-selective *O*-methylation of the C-18 hydroxy group in **2** was successfully achieved using Me_2SO_4 in the presence of Cs_2CO_3 ¹⁷ in acetone at room temperature. This produced nakijinol F (**6**) in 82% yield. Note that no formation of the C-17 *O*-methylated product was observed in this reaction, probably owing to steric crowding around the C-17 hydroxy group in substrate **2**. The spectroscopic properties of **1** and **6** were identical



Scheme 3 Synthesis of nakijinols A (**1**) and F (**6**). (a) $p\text{TsOH} \cdot \text{H}_2\text{O}$, CH_2Cl_2 , room temp., 1 h, 86%; (b) Me_2SO_4 , Cs_2CO_3 , acetone, room temp., 30 min, 82%. $p\text{TsOH}$ = *p*-toluenesulfonic acid.

tical to those obtained for natural **1**¹ and **6**,⁸ respectively. The optical rotations of synthetic **1** and **6** were consistent with those reported for natural **1** and **6**, respectively. The synthesis of **1** also led to the confirmation of its absolute configuration.

Synthesis of nakijinols E (5) and G (7)

Having successfully developed a novel method for constructing the key dihydroxybenzoxazole ring system, we next focused on synthesizing the final two target compounds, nakijinols E (5) and G (7). Both of these compounds have a methyl group at C-22 on the benzoxazole ring, as shown in Scheme 4. Starting from **8**, the synthesis was performed in a manner similar to that described for nakijinols B (2) (Scheme 2) and F (6) (Scheme 3). Twofold acetylation of the amino and the hydroxy groups in **8** afforded the corresponding *N,O*-diacetylated quinone **22** in 80% yield. Subsequent reduction of the quinone moiety in **22** using Na₂S₂O₄ provided hydroquinone **23**, which was immediately utilized without further purification due to its unstable nature. The crucial benzoxazole ring formation of **23** proceeded smoothly and cleanly under the aforementioned conditions (*cf.* **18** → **19** + **20** in Scheme 2), leading to the formation of the requisite benzoxazole products **24** and **25** (*ca.* 2:3)¹⁸ as an inseparable mixture in excellent

yield (98%). Removal of the *O*-acetyl group from a mixture of **24** and **25** furnished the fourth target compound, nakijinol G (7), in a quantitative yield of 99%. Finally, site-selective *O*-methylation of the C-18 hydroxy group in **7** provided the final target compound, nakijinol E (5), in 89% yield. The spectroscopic properties of **7** and **5** were identical to those of natural **7**⁸ and **5**.^{7,8} Optical rotation values for synthetic **7** and **5** matched those reported for natural **7** and **5**, respectively. The synthesis of **5** reported here led to confirmation of its absolute configuration.

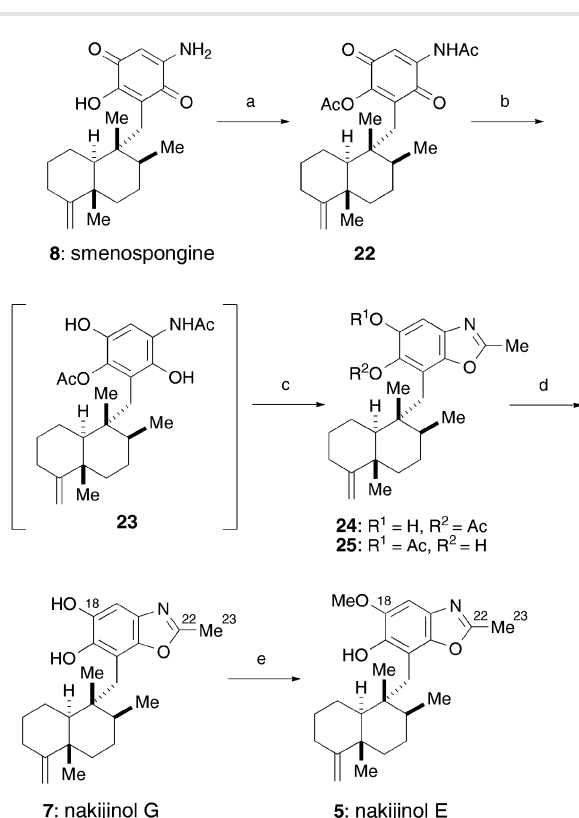
Conclusions

We have achieved the highly efficient synthesis of nakijinols A (1), B (2) and E–G (5–7) for the first time starting from smenospongine (**8**) (1: 45.8% overall yield over six steps; 2: 53.3% overall yield over five steps; 5: 69.0% overall yield over five steps; 6: 43.7% overall yield over six steps and 7: 77.6% overall yield over four steps). The key step of the synthesis was oxazole-ring formation *via* ring closure of the *N*-(2-hydroxyphenyl)-formamide or -acetamide moiety. This was undertaken by PPh₃/CCl₄ in MeCN at 50 °C and provided the requisite dihydroxylated benzoxazole ring substructure in excellent yield (98%) [*cf.* **18** → **19** + **20** in Scheme 2; **23** → **24** + **25** in Scheme 4]. Importantly, this general and flexible synthesis can potentially produce additional analogues of nakijinols in enantiomerically pure forms (*e.g.* analogues possessing various alkyl substituents at C-22 on the benzoxazole ring) in order to explore their structure–activity relationships. Further investigations to identify the mode of action of nakijinols using the synthetic samples are currently in progress.

Experimental section

General experimental procedures

All reactions involving air- and moisture-sensitive reagents were carried out using oven dried glassware and standard syringe-septum cap techniques. Routine monitorings of reaction were carried out using glass-supported Merck silica gel 60 F254 TLC plates. Flash column chromatography was performed on Kanto Chemical Silica Gel 60N (spherical, neutral 40–50 nm) with the solvents indicated. All solvents and reagents were used as supplied with following exceptions. Tetrahydrofuran (THF) was freshly distilled from Na metal/benzophenone under argon. CH₂Cl₂ was distilled from calcium hydride under argon. Measurements of optical rotations were performed with an Anton Paar MCP-100 automatic digital polarimeter. ¹H and ¹³C NMR spectroscopic data were recorded with JEOL AL-400 (400 MHz) and JEOL AL-600 (600 MHz) spectrometers. Chemical shifts were expressed in ppm using Me₄Si (δ = 0) as an internal standard. Infrared (IR) spectral measurements were carried out with a JASCO FT/IR-4100 spectrometer. Low- and High-resolution mass (HRMS)



Scheme 4 Synthesis of nakijinols E (5) and G (7). (a) Ac₂O, DMAP, THF, 60 °C, 2 h, 80%; (b) Na₂S₂O₄, MeCM/H₂O (5:1), room temp., 10 min; (c) PPh₃, CCl₄, MeCN, 50 °C, 2 h, 98% (2 steps, **24/25** *ca.* 2:3); (d) NH₃ (2.5% aq.), MeOH, 0 °C, 10 min, 99%; (e) Me₂SO₄, Cs₂CO₃, acetone, room temp., 45 min, 89%.

spectra were measured on a JEOL JMS-700 high-resolution mass spectrometer.

N-{4-Hydroxy-3,6-dioxo-5-[[[(1R,2S,4aS,8aS)-1,2,4a-trimethyl-5-methylenedecahydronaphthalen-1-yl]methyl]cyclohexa-1,4-dienyl]formamide (16). Acetic anhydride (5.50 mL, 5.8 mmol) was added dropwise to a stirred solution of formic acid (2.50 mL, 6.1 mmol) at 0 °C under argon, and the reaction mixture was stirred at 60 °C for 2 h. A solution of mixed acid anhydride (AcOCHO) prepared above was added dropwise to a stirred powder of smenospongine (**8**)^{9a} (200 mg, 0.58 mmol) at room temperature. After 2 h, the reaction was quenched with water (20 mL) at 0 °C, and the resulting mixture was extracted with EtOAc (3 × 30 mL). The combined extracts were washed with brine (2 × 30 mL), then dried with Na₂SO₄. The mixture was concentrated *in vacuo*, and the residue was purified by column chromatography (hexane/EtOAc, 3:1) to give **16** (158 mg, 73%) as an orange solid. Recrystallization from hexane/EtOAc (2:1) gave an analytical sample of **16** as orange prisms. M.p. 235.0–236.5 °C. [α]_D²⁵ = + 6.0 (*c* = 0.10, CHCl₃). ¹H NMR (400 MHz, CDCl₃): δ = 0.74 (dd, *J* = 11.7, 2.0 Hz, 1H), 0.85 (s, 3H), 0.96 (d, *J* = 6.3 Hz, 3H), 1.04 (s, 3H), 1.10–1.17 (m, 2H), 1.33–1.42 (m, 3H), 1.47 (dd, *J* = 12.1, 3.4 Hz, 1H), 1.50–1.54 (m, 1H), 1.84–1.89 (m, 1H), 2.05–2.09 (m, 2H), 2.33 (td, *J* = 13.8, 5.0 Hz, 1H), 2.45 (d, *J* = 13.7 Hz, 1H), 2.55 (d, *J* = 13.7 Hz, 1H), 4.44 (s, 1H), 4.45 (s, 1H), 7.50 (brs, 1H), 7.64 (s, 1H), 8.53 (br s, 1H), 8.63 (s, 1H) ppm. ¹³C NMR (100 MHz, CDCl₃): δ = 17.3 (q), 17.9 (q), 20.5 (q), 23.3 (t), 28.0 (t), 29.7 (t), 32.6 (t), 32.9 (t), 36.6 (t), 38.2 (d), 40.5 (s), 43.4 (s), 50.3 (d), 102.8 (t), 115.2 (d), 116.5 (s), 131.9 (s), 154.2 (s), 159.5 (s), 160.0 (d), 160.1 (s), 182.7 (s) ppm. IR (neat): ν = 3853, 3734, 3648, 3291, 2924, 2359, 1717, 1636, 1540, 1489, 1373, 1193, 891, 772, 668 cm⁻¹. HRMS (EI): calcd for C₂₂H₂₉NO₄ [M]⁺ 371.2097; found 371.2084.

4-Formamido-3,6-dioxo-2-[[[(1R,2S,4aS,8aS)-1,2,4a-trimethyl-5-methylenedecahydronaphthalen-1-yl]methyl]cyclohexa-1,4-dienyl acetate (17). Acetic anhydride (42.9 μ L, 0.45 mmol) and 4-(dimethylamino)pyridine (3.10 mg, 25 μ mol) were added to a stirred solution of **16** (46.9 mg, 0.13 mmol) in THF (4.0 mL) at 0 °C under argon, and the mixture was stirred at room temperature for 1 h. The reaction was quenched with saturated aqueous NaHCO₃ (5 mL) at 0 °C, and the resulting mixture was extracted with EtOAc (2 × 20 mL). The combined extracts were washed with brine (2 × 10 mL), then dried with Na₂SO₄. The mixture was concentrated *in vacuo*, and the residue was purified by column chromatography (hexane/EtOAc, 4:1) to give **17** (42.2 mg, 81%) as a yellow amorphous powder. [α]_D²⁵ = + 4.2 (*c* = 1.00, CHCl₃). ¹H NMR (400 MHz, CDCl₃): δ = 0.70 (d, *J* = 11.2 Hz, 1H), 0.85 (s, 3H), 0.92 (d, *J* = 6.3 Hz, 3H), 1.05 (s, 3H), 1.20–1.26 (m, 1H), 1.35–1.38 (m, 2H), 1.40 (m, 1H), 1.44 (m, 1H), 1.48–1.55 (m, 2H), 1.86–1.93 (m, 2H), 2.05–2.10 (m, 1H), 2.25–2.34 (m, 1H), 2.34 (s, 3H), 2.41 (d, *J* = 13.2 Hz, 1H), 2.55 (d, *J* = 13.2 Hz, 1H), 4.46 (s, 1H), 4.48 (s, 1H), 7.56 (s, 1H), 8.30 (br s, 1H), 8.60 (s, 1H) ppm. ¹³C NMR (100 MHz, CDCl₃): δ = 17.1 (q), 18.1 (q), 20.5 (q), 20.5 (q), 23.5 (t), 27.8 (t), 28.6 (t), 32.8 (t), 33.7 (t), 36.4 (t), 40.5 (s), 44.0 (s), 50.9 (s), 103.4 (t), 114.3 (d), 133.0 (s), 137.5 (s), 152.0 (s), 159.3 (d), 159.4 (s), 167.7 (s), 179.8 (s), 183.0 (s) ppm. FTIR (neat) ν = 3734, 3648,

2929, 2357, 1780, 1715, 1667, 1612, 1507, 1312, 1219, 1150, 884, 772, 670, 638 cm⁻¹. HRMS (EI): calcd for C₂₄H₃₁NO₅ [M]⁺ 413.2202; found 413.2189.

Mixture of 5-hydroxy-7-[[[(1R,2S,4aS,8aS)-1,2,4a-trimethyl-5-methylenedecahydronaphthalen-1-yl]methyl]benzo[d]oxazol-6-yl acetate (19) and 6-hydroxy-7-[[[(1R,2S,4aS,8aS)-1,2,4a-trimethyl-5-methylenedecahydronaphthalen-1-yl]methyl]benzo[d]oxazol-5-yl acetate (20). A solution of sodium hydrosulfite (846 mg, 4.9 mmol) in water (6.0 mL) was added dropwise to a stirred solution of **17** (50.0 mg, 0.12 mmol) in acetonitrile (6.0 mL) at room temperature. After 30 min, the reaction mixture was poured into water (20 mL), and the resulting mixture was extracted with EtOAc (3 × 20 mL). The combined extracts were washed with brine (2 × 15 mL), then dried with Na₂SO₄. Concentration *in vacuo* gave 4-formamido-3,6-dihydroxy-2-[[[(1R,2S,4aS,8aS)-1,2,4a-trimethyl-5-methylenedecahydronaphthalen-1-yl]methyl]phenyl acetate (**18**) (60.7 mg). This product was used for the next reaction without further purification.

Triphenylphosphine (255 mg, 0.97 mmol) and carbon tetrachloride (47.3 μ L, 0.49 mmol) was added to a stirred solution of the crude product **18** (60.7 mg) in acetonitrile (6.0 mL) at room temperature, and the reaction mixture was further stirred at 50 °C for 2 h. After cooling to room temperature, the reaction mixture was poured into 5% aqueous NaHCO₃ (20 mL), and the resulting mixture was extracted with EtOAc (3 × 20 mL). The combined extracts were washed with brine (2 × 20 mL), then dried with Na₂SO₄. The mixture was concentrated *in vacuo*, and the residue was purified by column chromatography (hexane/EtOAc, 2:1) to give an inseparable mixture of **19** and **20** (*ca.* 1:3) (47.2 mg, 98%, 2 steps). ¹H NMR (400 MHz, CDCl₃): δ = 0.87 (dd, *J* = 12.2, 2.4 Hz, 1/4H), 0.91 (dd, *J* = 12.2, 2.4 Hz, 3/4H), 0.92 (s, 3/4H), 0.94 (s, 9/4H), 0.99 (d, *J* = 5.4 Hz, 3/4H), 1.03 (d, *J* = 5.9 Hz, 9/4H), 1.06 (s, 3/4H), 1.06 (s, 9/4H), 1.19–1.28 (m, 2/4H), 1.19–1.28 (m, 4/6H), 1.40–1.60 (m, 5/4H), 1.40–1.60 (m, 15/4H), 1.89–1.92 (m, 1/4H), 1.89–1.92 (m, 3/4H), 2.20–2.23 (m, 1/4H), 2.20–2.23 (m, 3/4H), 2.30–2.36 (m, 1/4H), 2.30–2.36 (m, 3/4H), 2.38 (s, 3/4H), 2.39 (s, 9/4H), 2.74 (d, *J* = 13.2 Hz, 1/4H), 2.80 (d, *J* = 13.2 Hz, 1/4H), 2.87 (d, *J* = 14.1 Hz, 3/4H), 2.96 (d, *J* = 14.1 Hz, 3/4H), 4.35 (s, 1/4H), 4.35 (s, 3/4H), 4.39 (s, 1/4H), 4.39 (s, 3/4H), 5.53 (s, 3/4H), 6.27 (br s, 1/4H), 7.23 (s, 1/4H), 7.98 (s, 3/4H), 8.02 (s, 1/4H) ppm. ¹³C NMR (100 MHz, CDCl₃): δ = 17.2 (q, 1/4C), 17.3 (q, 3/4C), 18.2 (q, 3/4C), 18.5 (q, 1/4C), 20.4 (q, 1/4C), 20.5 (q, 3/4C), 20.8 (q, 1/4C), 21.1 (q, 3/4C), 23.3 (t, 3/4C), 23.5 (t, 1/4C), 28.0 (t, 1/4C), 28.1 (t, 3/4C), 28.7 (t, 1C), 32.8 (t, 1/4C), 32.9 (t, 3/4C), 35.0 (t, 3/4C), 35.9 (t, 1/4C), 36.3 (t, 1C), 37.5 (d, 1/4C), 37.6 (d, 3/4C), 40.4 (s, 1C), 43.0 (s, 1/4C), 43.1 (s, 3/4C), 49.7 (d, 3/4C), 49.9 (d, 1/4C), 102.8 (t, 3/4C), 103.0 (t, 1/4C), 105.4 (d, 1/4C), 111.2 (d, 3/4C), 112.0 (s, 3/4C), 117.8 (s, 1/4C), 131.8 (s, 3/4C), 136.6 (s, 3/4C), 136.8 (s, 1/4C), 137.9 (s, 1/4C), 144.9 (s, 1/4C), 145.4 (s, 3/4C), 145.6 (s, 1/4C), 151.9 (s, 3/4C), 152.8 (s, 1/4C), 159.6 (s, 1/4C), 159.9 (s, 3/4C), 168.9 (s, 3/4C), 169.1 (s, 1/4C) ppm.

Conversion of a mixture of 19 and 20 to single compound 20. Triethylamine (0.13 mL, 0.92 mmol) was added to a stirred

solution of a mixture of **19** and **20** (ca. 1 : 3, 18.7 mg) in acetonitrile (1.0 mL) at room temperature. After 5 min, the reaction mixture was concentrated *in vacuo* to give a single product of **20** (18.7 mg, 100%) as a pale yellow amorphous solid; $[\alpha]_{\text{D}}^{25} = -46.4$ ($c = 0.11$, CHCl_3). ^1H NMR (400 MHz, CDCl_3): $\delta = 0.88$ – 0.93 (m, 1H), 0.94 (s, 3H), 1.04 (d, $J = 4.8$ Hz, 3H), 1.06 (s, 3H), 1.19 – 1.26 (m, 2H), 1.39 – 1.42 (m, 3H), 1.44 – 1.48 (m, 1H), 1.57 (td, $J = 11.6$, 4.0 Hz, 1H), 1.89 – 1.93 (m, 1H), 2.05 (dd, $J = 13.5$, 3.9 Hz, 1H), 2.22 (br d, $J = 13.0$, 1H), 2.34 (td, $J = 14.5$, 4.7 Hz, 1H), 2.87 (d, $J = 14.0$ Hz, 1H), 2.96 (d, $J = 14.0$ Hz, 1H), 4.35 (s, 1H), 4.40 (s, 1H), 7.46 (s, 1H), 7.98 (s, 1H) ppm. ^{13}C NMR (100 MHz, CDCl_3): $\delta = 17.3$ (q), 18.2 (q), 20.5 (q), 21.1 (q), 23.3 (t), 28.1 (t), 28.7 (t), 32.9 (t), 35.0 (t), 36.3 (t), 37.6 (d), 40.4 (s), 43.1 (s), 49.7 (d), 102.8 (t), 111.2 (d), 112.0 (s), 131.8 (s), 136.6 (s), 145.4 (s), 148.7 (s), 151.9 (d), 159.9 (s), 168.9 (s) ppm. FTIR (neat): $\nu = 3648$, 3566 , 2925 , 2359 , 1771 , 1635 , 1521 , 1457 , 1219 , 772 , 674 cm^{-1} . HRMS (EI): calcd for $\text{C}_{24}\text{H}_{31}\text{NO}_4$ $[\text{M}]^+$ 397.2253; found 397.2236.

6-Methoxy-7-[(1R,2S,4aS,8aS)-1,2,4a-trimethyl-5-methylenedecahydronaphthalen-1-yl]methyl]benzo[d]oxazol-5-yl acetate (21). Cesium carbonate (7.89 mg, 24 μmol) and dimethyl sulfate (9.53 μL , 0.10 mmol) were added to a stirred solution of **20** (8.0 mg, 20 μmol) in acetone (2.0 mL) at room temperature. After 1 h, the reaction was quenched with saturated aqueous NH_4Cl (10 mL), and the resulting mixture was extracted with CHCl_3 (3×10 mL). The combined extracts were washed with brine (2×10 mL), then dried with Na_2SO_4 . The mixture was concentrated *in vacuo*, and the residue was purified by column chromatography (hexane/EtOAc, 3 : 1) to give **21** (5.8 mg, 70%) as a colourless viscous liquid. $[\alpha]_{\text{D}}^{25} = -27.3$ ($c = 0.11$, CH_3OH). ^1H NMR (400 MHz, CDCl_3): $\delta = 0.88$ (dd, $J = 11.7$, 2.0 Hz, 1H), 0.93 (s, 3H), 0.97 (d, $J = 4.9$ Hz, 1H), 1.05 (s, 3H), 1.21 (m, 3H), 1.34 – 1.46 (m, 4H), 1.47 – 1.58 (m, 2H), 1.85 – 1.91 (m, 1H), 2.05 (m, 2H), 2.28 – 2.33 (m, 1H), 2.36 (s, 3H), 2.84 (d, $J = 13.7$ Hz, 1H), 2.90 (d, $J = 13.7$ Hz, 1H), 3.73 (s, 3H), 4.35 (s, 1H), 4.39 (s, 1H), 7.39 (s, 1H), 8.03 (s, 1H) ppm. ^{13}C NMR (100 MHz, CDCl_3): $\delta = 17.3$ (q), 18.2 (q), 20.5 (q), 20.9 (q), 23.4 (t), 28.0 (t), 28.5 (t), 32.9 (t), 35.3 (t), 36.3 (d), 37.6 (s), 40.4 (s), 43.2 (d), 49.7 (t), 61.1 (t), 102.9 (t), 112.6 (d), 118.4 (s), 134.8 (s), 141.9 (s), 148.3 (s), 150.0 (d), 159.8 (s), 169.1 (s) ppm. FTIR (neat) $\nu = 2923$, 2359 , 1771 , 1540 , 1507 , 1457 , 1220 , 894 , 772 , 694 , 683 , 635 , 617 , 606 cm^{-1} . HRMS (EI): calcd for $\text{C}_{25}\text{H}_{33}\text{NO}_4$ $[\text{M}]^+$ 411.2410; found 411.2407.

Nakijinol B (2)

2.5% Aqueous ammonia (40.0 μL , 58 μmol) was added to a stirred solution of a mixture of **19** and **20** (ca. 1 : 3) (18.7 mg, 47 μmol) in MeOH (3.0 mL) at 0°C . After 10 min, the reaction was quenched with saturated aqueous NH_4Cl (15 mL) at 0°C , and the resulting mixture was extracted with EtOAc (3×20 mL). The combined extracts were washed with brine (2×15 mL), then dried with Na_2SO_4 . The mixture was concentrated *in vacuo*, and the residue was purified by column chromatography (hexane/EtOAc, 1 : 1) to give **2** (15.3 mg, 92%) as a pale pink solid. Recrystallization from MeOH gave an analytical sample of **2** as colourless prisms. M.p. 259.5 – 260.5°C {lit.⁸

M.p. 213 – 218°C }. $[\alpha]_{\text{D}}^{25} = -29.3$ ($c = 0.08$, MeOH) {ref.⁸ $[\alpha]_{\text{D}}^{25} = -27.3$ ($c = 0.11$, MeOH); ref.³ $[\alpha]_{\text{D}}^{25} = -6.7$ ($c = 0.075$, MeOH)}. The ^1H and ^{13}C NMR, IR, and MS spectra (see below) are identical to those of natural nakijinol B (**2**).^{3,8} ^1H NMR (400 MHz, CD_3OD): $\delta = 0.93$ – 0.96 (m, 1H), 0.95 (s, 3H), 1.07 (s, 3H), 1.08 (d, $J = 5.9$ Hz, 3H), 1.28 (m, 1H), 1.38 – 1.43 (m, 3H), 1.45 – 1.47 (m, 2H), 1.55 (m, 1H), 1.86 – 1.91 (m, 1H), 2.01 – 2.05 (m, 1H), 2.31 – 2.35 (m, 1H), 2.35 – 2.39 (m, 1H), 2.86 (d, $J = 14.1$ Hz, 1H), 2.94 (d, $J = 14.1$ Hz, 1H), 4.32 (s, 1H), 4.35 (s, 1H), 6.97 (s, 1H), 8.20 (s, 1H) ppm. ^{13}C NMR (400 MHz, $\text{DMSO}-d_6$): $\delta = 0.83$ (1H, dd, $J = 11.7$, 2.0 Hz), 0.87 (3H, s), 0.99 (3H, s), 1.00 (3H, d, $J = 4.9$ Hz), 1.05 – 1.10 (1H, m), 1.13 – 1.24 (1H, m), 1.34 – 1.38 (4H, m), 1.45 (1H, m), 1.81 (1H, m), 1.98 (1H, dd, $J = 13.3$, 3.7 Hz), 2.21 (1H, d, $J = 13.3$ Hz), 2.27 (1H, td, $J = 13.7$, 5.4 Hz), 2.74 (1H, d, $J = 14.1$), 2.81 (1H, d, $J = 14.1$), 4.28 (1H, s), 4.34 (1H, s), 6.94 (1H, s), 8.36 (1H, s) ppm. ^{13}C NMR (100 MHz, CD_3OD): $\delta = 17.9$ (q), 18.9 (q), 21.0 (q), 24.4 (t), 29.2 (t), 29.9 (t), 34.0 (t), 35.5 (t), 37.8 (t), 38.7 (d), 41.6 (s), 44.0 (s), 50.8 (d), 102.2 (d), 103.1 (t), 110.8 (s), 131.3 (s), 144.6 (s), 146.3 (s), 146.4 (s), 152.8 (d), 161.4 (s) ppm. ^{13}C NMR (100 MHz, $\text{DMSO}-d_6$): $\delta = 17.2$ (q), 18.2 (q), 20.1 (q), 22.7 (t), 27.5 (t), 27.9 (t), 32.3 (t), 34.4 (t), 36.1 (t), 37.0 (d), 39.8 (s), 42.2 (s), 48.9 (d), 102.2 (d), 102.8 (t), 109.2 (s), 130.2 (s), 143.1 (s), 144.2 (s), 144.4 (s), 151.7 (d), 159.3 (s) ppm. FTIR (neat): $\nu = 3679$, 2972 , 2865 , 2844 , 1456 , 1321 , 1055 , 1033 , 1013 cm^{-1} . HRMS (EI): calcd for $\text{C}_{22}\text{H}_{29}\text{NO}_3$ $[\text{M}]^+$ 355.2147; found 355.2155.

Nakijinol A (1)

p-Toluenesulfonic acid monohydrate (17.2 mg, 0.10 mmol) was added to a stirred solution of **2** (18.0 mg, 51 μmol) in CH_2Cl_2 (3.0 mL) at room temperature. After 1 h, the reaction was quenched with saturated aqueous NaHCO_3 (5 mL) at 0°C , and the reaction mixture was extracted with EtOAc (3×10 mL). The combined extracts were washed with brine (2×10 mL), then dried with Na_2SO_4 . The mixture was concentrated *in vacuo*, and the residue was purified by column chromatography (hexane/EtOAc, 1 : 1) to give **1** (15.4 mg, 86%) as a colorless solid. Recrystallization from MeOH gave an analytical sample of **1** as colourless prisms. M.p. 245.5 – 247.0°C . $[\alpha]_{\text{D}}^{20} = -29.3$ ($c = 0.15$, MeOH) {lit.¹ $[\alpha]_{\text{D}}^{20} = -172$ ($c = 0.03$, MeOH)}. The ^1H and ^{13}C NMR, IR, and MS spectra (see below) are identical to those of natural nakijinol A (**1**).¹ ^1H NMR (600 MHz, CDCl_3): $\delta = 0.95$ (s, 3H), 0.94 – 0.96 (m, 1H), 1.03 (s, 3H), 1.06 (d, $J = 6.6$ Hz, 3H), 1.17 (dd, $J = 12.3$, 1.6 Hz, 1H), 1.38 – 1.41 (m, 2H), 1.45 – 1.50 (m, 1H), 1.51 (br s, 3H), 1.58 – 1.62 (m, 2H), 1.93 – 1.97 (m, 1H), 1.97 – 2.07 (m, 1H), 2.17 – 2.21 (m, 1H), 2.89 (d, $J = 14.3$ Hz, 1H), 3.01 (d, $J = 14.3$ Hz, 1H), 5.09 (br s, 1H), 5.65 (br s, 1H), 5.73 (s, 1H), 7.14 (s, 1H), 7.95 (s, 1H) ppm. ^1H NMR (600 MHz, CD_3OD): $\delta = 0.89$ – 0.94 (1H, m), 0.95 (3H, s), 1.03 (3H, s), 1.06 (3H, d, $J = 6.2$ Hz), 1.17 (1H, m), 1.36 – 1.40 (2H, m), 1.47 (3H, brs), 1.51 – 1.56 (1H, m), 1.58 – 1.61 (2H, m), 1.98 (2H, m), 2.24 – 2.27 (2H, m), 2.91 (1H, d, $J = 13.9$ Hz), 3.01 (1H, d, $J = 13.9$ Hz), 5.06 (1H, br s), 6.97 (1H, s), 8.22 (1H, s) ppm. ^{13}C NMR (150 MHz, CDCl_3): $\delta = 17.3$ (q), 18.0 (q), 18.2 (q), 20.0 (t), 20.2 (q), 27.0 (t), 28.0 (t), 34.7 (t), 35.7 (t), 37.4 (d), 38.4 (s), 42.8 (s), 47.1 (d), 103.4 (d), 110.4 (s), 120.6 (d), 131.3 (s), 141.0

(s), 143.4 (s), 144.1 (s), 145.8 (s), 151.3 (d) ppm. ^{13}C NMR (150 MHz, CD_3OD): δ = 17.9 (q), 18.4 (q), 18.6 (q), 20.7 (q), 21.1 (q), 28.0 (t), 29.3 (t), 35.6 (t), 37.3 (d), 38.8 (d), 39.6 (s), 43.8 (s), 49.6 (d), 102.6 (d), 111.1 (s), 121.7 (d), 131.4 (s), 145.0 (s), 146.3 (s), 146.3 (s), 144.8 (s), 152.8 (d) ppm. FTIR (neat): ν = 3679, 2972, 2865, 2844, 1456, 1321, 1055, 1033, 1013 cm^{-1} . HRMS (EI): calcd for $\text{C}_{22}\text{H}_{29}\text{NO}_3$ $[\text{M}]^+$ 355.2147; found 355.2143.

Nakijinol F (6)

Cesium carbonate (14.9 mg, 46 μmol) and dimethyl sulfate (4.34 μL , 46 μmol) were added to a stirred solution of **2** (14.8 mg, 42 μmol) in acetone (2.0 mL) at room temperature. After 30 min, the reaction was quenched with saturated aqueous NH_4Cl (10 mL) at 0 $^\circ\text{C}$, and the reaction mixture was extracted with EtOAc (3 \times 20 mL). The combined extracts were washed with brine (2 \times 10 mL), then dried with Na_2SO_4 . The mixture was concentrated *in vacuo*, and the residue was purified by column chromatography (hexane/EtOAc, 4 : 1) to give **6** (12.6 mg, 82%) as a colourless solid. Recrystallization from hexane/EtOAc (1 : 1) gave an analytical sample of **6** as colourless plates. M.p. 202.5–204.0 $^\circ\text{C}$. $[\alpha]_{\text{D}}^{25}$ = –28.4 (c = 0.13, MeOH) {ref.⁸ $[\alpha]_{\text{D}}^{25}$ = –16.2 (c = 0.11, MeOH)}. The ^1H and ^{13}C NMR, IR, and MS spectra (see below) are identical to those of natural nakijinol F (**6**).⁸ ^1H NMR (400 MHz, CDCl_3): δ = 0.94 (dd, J = 11.7, 2.0 Hz, 1H), 0.94 (s, 3H), 1.06 (d, J = 6.0 Hz, 3H), 1.06 (s, 3H), 1.19–1.24 (m, 1H), 1.24–1.28 (m, 1H), 1.37–1.43 (m, 2H), 1.37–1.43 (m, 2H), 1.43–1.47 (m, 1H), 1.46–1.58 (m, 1H), 1.90–1.96 (m, 1H), 2.03–2.06 (m, 1H), 2.26–2.30 (m, 1H), 2.30–2.35 (m, 1H), 2.85 (d, J = 13.6 Hz, 1H), 2.95 (d, J = 13.6 Hz, 1H), 3.95 (s, 3H), 4.33 (s, 1H), 4.37 (s, 1H), 5.99 (s, 1H), 7.11 (s, 1H), 7.92 (s, 1H) ppm. ^{13}C NMR (100 MHz, CDCl_3): δ = 17.4 (q), 18.2 (q), 20.5 (q), 23.3 (t), 28.1 (t), 28.7 (t), 33.0 (t), 34.6 (t), 36.4 (t), 37.5 (d), 40.4 (s), 43.0 (s), 49.5 (d), 56.5 (q), 99.3 (d), 102.5 (t), 109.5 (s), 131.1 (s), 144.4 (s), 145.0 (s), 145.7 (s), 151.9 (d), 160.3 (s) ppm. FTIR (neat): ν = 2928, 2359, 1623, 1523, 1460, 1426, 1362, 1323, 1244, 1219, 1095, 941, 827, 772, 678, 668, 609 cm^{-1} . HRMS (EI): calcd for $\text{C}_{23}\text{H}_{31}\text{NO}_3$ $[\text{M}]^+$ 369.2304; found 369.2292.

4-Acetamido-3,6-dioxo-2-[[[(1R,2S,4aS,8aS)-1,2,4a-trimethyl-5-methylenedecahydronaphthalen-1-yl]methyl]cyclohexa-1,4-dienyl acetate (22). 4-(Dimethylamino)pyridine (7.30 mg, 60 μmol) were added to a stirred solution of **8** (102.9 mg, 0.3 mmol) in acetic anhydride (2.00 mL, 21 mmol) at room temperature, and the mixture was stirred at 60 $^\circ\text{C}$ for 2 h. After cooling to room temperature, the mixture was concentrated *in vacuo*, and the residue was purified by column chromatography (hexane/EtOAc, 4 : 1) to give **22** (102.4 mg, 80%) as an orange amorphous powder. $[\alpha]_{\text{D}}^{25}$ = + 8.00 (c = 0.10, CHCl_3). ^1H NMR (400 MHz, CDCl_3): δ = 0.72 (d, J = 10.8 Hz, 1H), 0.85 (s, 3H), 0.92 (d, J = 6.4 Hz, 1H), 1.05 (s, 3H), 1.15–1.26 (m, 2H), 1.35–1.52 (m, 1H), 1.80–1.90 (m, 2H), 2.08–2.10 (m, 1H), 2.25 (s, 3H), 2.34 (s, 3H), 2.42 (d, J = 13.2 Hz, 1H), 2.52 (d, J = 13.2 Hz, 1H), 4.47 (s, 1H), 4.48 (s, 1H), 7.55 (s, 1H), 8.12 (s, 1H) ppm. ^{13}C NMR (100 MHz, CDCl_3): δ = 17.1 (q), 18.2 (q), 20.5 (q, 2C), 23.6 (q), 25.0 (s), 27.9 (q), 28.7 (t), 32.8 (t), 33.8 (t), 36.4 (t), 38.3 (t), 40.6 (d), 43.9 (d), 50.9 (t), 103.4 (d), 112.9 (s), 132.8 (s),

138.7 (s), 152.1 (s), 159.3 (s), 167.8 (s), 169.1 (s), 180.0 (s), 183.5 (s) ppm. FTIR (neat): ν = 3445, 2926, 2359, 1773, 1663, 1498, 1370, 1312, 1147, 1016 cm^{-1} . HRMS (EI): calcd for $\text{C}_{25}\text{H}_{33}\text{NO}_5$ $[\text{M}]^+$ 427.2359; found 427.2378.

Mixture of 5-hydroxy-2-methyl-7-[[[(1R,2S,4aS,8aS)-1,2,4a-trimethyl-5-methylenedecahydronaphthalen-1-yl]methyl]benzo[d]oxazol-6-yl acetate (24) and 6-hydroxy-2-methyl-7-[[[(1R,2S,4aS,8aS)-1,2,4a-trimethyl-5-methylenedecahydronaphthalen-1-yl]methyl]benzo[d]oxazol-5-yl acetate (25). A solution of sodium hydrosulfite (348 mg, 2.0 mmol) in water (1.0 mL) was added dropwise to a stirred solution of **22** (21.4 mg, 50 μmol) in acetonitrile (5.0 mL) at room temperature. After 5 min, the reaction mixture was poured into water (20 mL), and the resulting mixture was extracted with EtOAc (3 \times 20 mL). The combined extracts were washed with brine (2 \times 15 mL), then dried with Na_2SO_4 . Concentration *in vacuo* gave 4-acetamido-3,6-dihydroxy-2-[[[(1R,2S,4aS,8aS)-1,2,4a-trimethyl-5-methylenedecahydronaphthalen-1-yl]methyl]phenyl acetate (**23**) (30.2 mg). This product was used for the next reaction without further purification.

Triphenylphosphine (52.4 mg, 0.20 mmol) and carbon tetrachloride (9.70 μL , 0.10 mmol) was added to a stirred solution of the crude product **23** (30.2 mg) in acetonitrile (2 mL) at room temperature, and the reaction mixture was further stirred at 65 $^\circ\text{C}$ for 1.5 h. After cooling to room temperature, the reaction mixture was poured into 5% aqueous NaHCO_3 (20 mL), and the resulting mixture was extracted with EtOAc (3 \times 20 mL). The combined extracts were washed with brine (2 \times 10 mL), then dried with Na_2SO_4 . The mixture was concentrated *in vacuo*, and the residue was purified by column chromatography (hexane/EtOAc, 1 : 1) to give an inseparable mixture of **24** and **25** (ca. 2 : 3) (20.2 mg, 98%, 2 steps). ^1H NMR (400 MHz, CDCl_3): δ = 0.87 (dd, J = 11.7, 2.0 Hz, 2/5H), 0.89–0.93 (m, 3/5H), 0.91 (s, 6/5H), 0.93 (s, 9/5H), 1.02 (d, J = 6.8 Hz, 6/5H), 1.03 (d, J = 6.8 Hz, 9/5H), 1.06 (s, 6/5H), 1.06 (s, 9/5H), 1.21–1.58 (m, 14/5H), 1.21–1.58 (m, 21/5H), 1.89 (m, 2/5H), 1.89 (m, 3/5H), 2.02–2.13 (m, 4/5H), 2.02–2.13 (m, 6/5H), 2.27 (s, 6/5H), 2.34 (s, 9/5H), 2.24–2.34 (m, 2/5H), 2.24–2.34 (m, 3/5H), 2.55 (s, 6/5H), 2.56 (s, 9/5H), 2.68 (d, J = 14.1 Hz, 2/5H), 2.77 (d, J = 14.1 Hz, 2/5H), 2.83 (d, J = 14.1 Hz, 3/5H), 2.91 (d, J = 14.1 Hz, 3/5H), 4.35 (s, 2/5H), 4.35 (s, 3/5H), 4.39 (s, 2/5H), 4.39 (s, 3/5H), 6.14 (br s, 2/5H), 7.11 (s, 2/5H), 7.27 (s, 3/5H) ppm. ^{13}C NMR (100 MHz, CDCl_3): δ = 14.4 (q, 1C), 17.3 (q, 1C), 18.3 (q, 3/5C), 18.5 (q, 2/5C), 20.4 (q, 2/5C), 20.5 (q, 3/5C), 20.7 (q, 2/5C), 21.0 (q, 3/5C), 23.3 (t, 3/5C), 23.4 (t, 2/5C), 27.9 (t, 2/5C), 28.0 (t, 3/5C), 28.7 (t, 2/5C), 28.8 (t, 3/5C), 32.8 (t, 2/5C), 32.9 (t, 3/5C), 34.8 (t, 3/5C), 35.5 (t, 2/5C), 36.2 (t, 2/5C, 2/5C), 36.3 (t, 3/5C), 37.1 (d, 2/5C), 37.4 (d, 3/5C), 40.4 (s, 1C), 42.8 (s, 3/5C), 43.0 (s, 2/5C), 49.5 (d, 1C), 102.8 (t, 3/5C), 103.0 (t, 2/5C), 104.1 (d, 2/5C), 110.2 (d, 3/5C), 111.7 (s, 3/5C), 116.9 (s, 2/5C), 132.8 (s, 3/5C), 136.2 (s, 3/5C), 137.2 (s, 2/5C), 137.7 (s, 2/5C), 144.8 (s, 3/5C), 145.3 (s, 2/5C), 145.8 (s, 2/5C), 159.8 (s, 2/5C), 149.6 (s, 3/5C), 159.5 (s, 3/5C), 163.2 (s, 3/5C), 164.1 (s, 2/5C), 169.1 (s, 3/5C), 169.4 (s, 2/5C) ppm. HRMS (EI): calcd for $\text{C}_{25}\text{H}_{33}\text{NO}_4$ $[\text{M}]^+$ 411.2410; found 411.2407.

Nakijinol G (7)

2.5% Aqueous ammonia (0.10 mL, 0.15 mmol) was added to a stirred solution of a mixture of **24** and **25** (ca. 2 : 3) (41.1 mg, 0.10 mmol) in MeOH (5.0 mL) at room temperature. After 10 min, the reaction was quenched with saturated aqueous NH₄Cl (20 mL) at 0 °C, and the resulting mixture was extracted with CHCl₃ (3 × 20 mL). The combined extracts were washed with brine (2 × 15 mL), then dried with Na₂SO₄. The mixture was concentrated *in vacuo*, and the residue was purified by column chromatography (hexane/EtOAc, 1 : 1) to give **7** (36.4 mg, 99%) as a colourless solid. Recrystallization from CHCl₃ gave an analytical sample of **7** as colourless prisms. M.p. 266.0–266.5 °C. [α]_D²⁵ = –42.0 (*c* = 0.10, MeOH) {ref.⁸ [α]_D²⁵ = –18.4 (*c* = 0.10, MeOH)}. The ¹H and ¹³C NMR, IR, and MS spectra (see below) are identical to those of natural nakijinol G (**7**).⁸ ¹H NMR (400 MHz, DMSO-*d*₆): δ = 0.82 (d, *J* = 10.1 Hz, 1H), 0.87 (s, 3H), 1.08–1.12 (m, 2H), 1.01 (s, 3H), 1.02 (d, *J* = 4.9 Hz, 3H), 1.14–1.17 (m, 2H), 1.30–1.38 (m, 5H), 1.40–1.44 (m, 1H), 1.79–1.88 (m, 1H), 1.98–2.00 (m, 1H), 2.22–2.26 (m, 1H), 2.25–2.28 (m, 1H), 2.45 (s, 3H), 2.71 (d, *J* = 14.4 Hz, 1H), 2.78 (d, *J* = 14.4 Hz, 1H), 4.29 (s, 1H), 4.35 (s, 1H), 6.83 (s, 1H) ppm. ¹³C NMR (100 MHz, DMSO-*d*₆): δ = 14.0 (q), 17.4 (q), 18.3 (q), 20.2 (q), 22.8 (t), 27.5 (t), 28.1 (t), 32.4 (t), 34.2 (t), 36.2 (t), 36.7 (d), 39.5 (s), 42.2 (d), 48.7 (d), 101.9 (d), 102.8 (d), 108.8 (s), 131.5 (s), 142.5 (s), 143.4 (s), 145.1 (s), 159.3 (s), 160.8 (s) ppm. FTIR (neat): ν = 2922, 1731, 1456, 1382, 1321, 1054, 1032, 1011, 975, 880, 741, 690, 651, 639, 624 cm^{–1}. HRMS (EI): calcd for C₂₃H₃₁NO₃ [M]⁺ 369.2304; found 369.2292.

Nakijinol E (5)

Cesium carbonate (11.7 mg, 36 μ mol) and dimethyl sulfate (3.10 μ L, 33 μ mol) were added to a stirred solution of **7** (11.1 mg, 30 μ mol) in acetone (2.0 mL) at room temperature. After 10 min, the reaction was quenched with saturated aqueous NH₄Cl (10 mL) at 0 °C, and the reaction mixture was extracted with EtOAc (3 × 20 mL). The combined extracts were washed with brine (2 × 10 mL), then dried with Na₂SO₄. The mixture was concentrated *in vacuo*, and the residue was purified by column chromatography (CH₂Cl₂/EtOAc, 9 : 1) to give **5** (10.2 mg, 89%) as a colourless amorphous solid. [α]_D²⁵ = –23.6 (*c* = 0.11, MeOH) {ref.⁷ [α]_D²⁵ = –29.0 (*c* = 0.10, MeOH)}. The ¹H and ¹³C NMR, IR, and MS spectra (see below) are identical to those of natural nakijinol E (**5**).⁷ ¹H NMR (400 MHz, CDCl₃): δ = 0.93 (dd, *J* = 11.9, 2.3 Hz, 1H), 0.93 (s, 3H), 1.06 (s, 3H), 1.07 (d, *J* = 5.9 Hz, 3H), 1.15–1.23 (m, 1H), 1.21–1.26 (m, 3H), 1.30–1.38 (m, 1H), 1.38–1.46 (m, 3H), 1.50–1.53 (m, 1H), 1.86–1.90 (m, 1H), 2.00–2.03 (m, 1H), 2.26–2.38 (m, 1H), 2.28–2.38 (m, 1H), 2.55 (s, 3H), 2.82 (d, *J* = 14.2 Hz, 1H), 2.91 (d, *J* = 14.2 Hz, 1H), 3.92 (s, 3H), 4.34 (s, 1H), 4.38 (s, 1H), 5.91 (s, 1H), 6.98 (s, 1H) ppm. ¹³C NMR (100 MHz, CDCl₃): δ = 14.5 (q), 17.5 (q), 18.3 (q), 20.5 (q), 23.2 (t), 28.0 (t), 28.7 (t), 33.0 (t), 34.4 (t), 36.3 (t), 37.1 (d), 40.4 (s), 42.8 (s), 49.1 (d), 56.4 (q), 98.7 (d), 102.4 (t), 109.0 (s), 132.3 (s), 143.4 (s), 144.3 (s), 146.3 (s), 160.3 (s), 161.8 (s) ppm. FTIR (neat): ν = 3527, 3083, 2925, 2857, 1729, 1633, 1584, 1459, 1431, 1382, 1324, 1281, 1242,

1213, 1192, 1168, 1130, 1070, 1050, 1007, 991, 941, 889, 829, 756 cm^{–1}. HRMS (EI): calcd for C₂₄H₃₃NO₃ [M]⁺ 383.2460; found 383.2462.

Conflicts of interest

There are no conflicts to declare.

Acknowledgements

This study was financially supported by a JSPS KAKENHI (Grant Number JP15K07865) and a Grant-in-Aid for the Strategic Research Foundation Program at Private Universities (Grant Number S15110010L) from MEXT.

Notes and references

- 1 J. Kobayashi, T. Madona and H. Shigemori, *Tetrahedron Lett.*, 1995, **31**, 5589–5590.
- 2 For a recent review on the pharmacologically active benzoxazole compounds, see: S. Singh, G. Veeraswamy, D. Bhattarai, J. Goo, K. Lee and Y. Choi, *Asian J. Org. Chem.*, 2015, **4**, 1338–1361.
- 3 S. P. B. Ovenden, J. L. Nielson, C. H. Liptrot, R. H. Willis, D. M. Tapiolas, A. D. Wright and C. A. Motti, *J. Nat. Prod.*, 2011, **74**, 65–68.
- 4 H. Suzuki, T. Kubota, A. Takahashi-Nakaguchi, J. Fromont, T. Gono and J. Kobayashi, *Chem. Pharm. Bull.*, 2014, **62**, 209–212.
- 5 The *epi*-nomenclature was conveniently used for the new compound **4** to indicate its *cis*-fused decalin ring moiety, even though the corresponding *trans*-fused isomer (i.e. nakijinol D) has not been reported yet. See: ref. 6.
- 6 G. Daletos, N. J. de Voogd, W. E. G. Müller, V. Wray, W. Lin, D. Feger, M. Kubbutat, A. H. Aly and P. Proksch, *J. Nat. Prod.*, 2014, **77**, 218–226.
- 7 I. H. Hwang, J. Oh, W. Zhou, S. Park, J.-H. Kim, A. G. Chittiboyina, D. Ferreira, G. Y. Song, S. Oh, M. Na and M. Hamann, *J. Nat. Prod.*, 2015, **78**, 453–461.
- 8 J. Wang, F.-R. Mu, W.-H. Jiao, J. Huang, L.-L. Hong, F. Yang, Y. Xu, S.-P. Wang, F. Sun and H.-W. Lin, *J. Nat. Prod.*, 2017, **80**, 2509–2514.
- 9 (a) T. Katoh, S. Atsumi, R. Saito, K. Narita and T. Katoh, *Eur. J. Org. Chem.*, 2017, 3837–3849; (b) Y. Takeda, K. Narita and T. Katoh, *Eur. J. Org. Chem.*, 2017, 901–907; (c) T. Kikuchi, K. Narita, K. Saijo, C. Ishioka and T. Katoh, *Eur. J. Org. Chem.*, 2016, 5659–5666; (d) T. Kamishima, K. Kikuchi, K. Narita and T. Katoh, *Eur. J. Org. Chem.*, 2014, 3443–3450; (e) Y. Fukui, K. Narita and T. Katoh, *Chem. – Eur. J.*, 2014, **20**, 2436–2439; (f) T. Kamishima, T. Kikuchi and T. Katoh, *Eur. J. Org. Chem.*, 2013, 4558–4563; (g) J. Sakurai, K. Watanabe, H. Abe, S. Kanno, M. Ishikawa and T. Katoh, *Chem. – Eur. J.*, 2008, **14**, 829–837.

- 10 (a) J. Hou, Z. Li, Q. Fang, C. Feng, H. Zhang, W. Guo, H. Wang, G. Gu, Y. Tian, P. Liu, R. Liu, J. Lin, Y. Shi, Z. Yin, J. Shen and P. G. Wang, *J. Med. Chem.*, 2012, **55**, 3066–3075; (b) X. Quancai, L. Zhengning and C. Huiying, *Chin. J. Chem.*, 2011, **29**, 925–932; (c) K.-L. Li, Z.-B. Du, C.-C. Guo and Q.-Y. Chen, *J. Org. Chem.*, 2009, **74**, 3286–3292; (d) S. P. Marsden, J. T. Steer and B. S. Orlek, *Tetrahedron*, 2009, **65**, 5503–5512; (e) Y.-H. Yang and M. Shi, *Tetrahedron*, 2006, **62**, 2420–2427; (f) D. Kumar, M. R. Jacob, M. B. Reynolds and S. M. Kerwin, *Bioorg. Med. Chem.*, 2002, **10**, 3997–4004.
- 11 There have been several reports on the synthesis of mono-hydroxy-substituted benzoxazoles from suitably functionalised hydroquinone or quinone derivatives under various reaction conditions, see: (a) X. Li, J. Bian, N. Wang, X. Qian, J. Gu, T. Mu, J. Fan, X. Yang, S. Li, T. Yang, H. Sun, Q. You and X. Zhang, *Bioorg. Med. Chem.*, 2016, **24**, 1006–1013; (b) J. McCabe and A. J. Phillips, *Tetrahedron*, 2013, **69**, 5710–5714; (c) R. J. Bergeron, S. Singh and N. Bharti, *Tetrahedron*, 2011, **67**, 3163–3169; (d) K. Matsumoto and S. A. Kozmin, *Adv. Synth. Catal.*, 2008, **350**, 557–560; (e) S. Fujita, *J. Org. Chem.*, 1983, **48**, 177–183; (f) S. Fujita, K. Koyama and Y. Inagaki, *Synthesis*, 1982, 68–69.
- 12 (a) K. M. Schmid, L. Jensen and S. T. Phillips, *J. Org. Chem.*, 2012, **77**, 4363–4374; (b) M. J. Smith, C. C. Nawrat and C. J. Moody, *Org. Lett.*, 2011, **13**, 3396–3398; (c) A. P. Kostikov, N. Malashikhina and V. V. Popik, *J. Org. Chem.*, 2009, **74**, 1802–1804; (d) R. H. Munday, R. M. Denton and J. C. Anderson, *J. Org. Chem.*, 2008, **73**, 8033–8038; (e) N. Kawai, Y. Fujibayashi, S. Kuwabara, K. Takao, Y. Ijuin and S. Kobayashi, *Tetrahedron*, 2000, **56**, 6467–6478; (f) A. T. Watson, K. Park and D. F. Wiemer, *J. Org. Chem.*, 1995, **60**, 5102–5106; (g) N. Harada, T. Sugioka, Y. Ando, H. Uda and T. Kuruki, *J. Am. Chem. Soc.*, 1988, **110**, 8483–8487.
- 13 (a) A. C. Benniston, T. P. L. Winstanley, H. Lemmetyinen, N. V. Tkachenko, R. W. Harrington and C. Wills, *Org. Lett.*, 2012, **14**, 1374–1377; (b) B. J. D. Wright, C. Chan and S. J. Danishefsky, *J. Nat. Prod.*, 2008, **71**, 409–414.
- 14 M. Yoshida, Y. Maeyama and K. Shishido, *Heterocycles*, 2010, **80**, 623–629.
- 15 The reducing reagent Na₂S₂O₄ has been used most widely for the conversion of sesquiterpenoid quinones to the corresponding hydroquinones. See: ref. 11e–g.
- 16 This operation made it possible to carry out the full assignments for the ¹H and ¹³C NMR spectra of the benzoxazole product (*i.e.* **20**) (see ESI†).
- 17 The use of K₂CO₃ instead of Cs₂CO₃ resulted in a lower yield of product **6** (~70%).
- 18 Interestingly, being different from the case of a mixture of **19** and **20** (*cf.* Scheme 2), exposure of a mixture of **24** and **25** to triethylamine in MeCN could not produce **25** as a single product, but only resulted in a change of the composition ratio from appropriately 2 : 3 to 1 : 3.

SYNTHESIS Reviews and Full Papers in Chemical Synthesis

This electronic reprint is provided for non-commercial and personal use only: this reprint may be forwarded to individual colleagues or may be used on the author's homepage. This reprint is not provided for distribution in repositories, including social and scientific networks and platforms.

Publishing House and Copyright:

© 2018 by
Georg Thieme Verlag KG
Rüdigerstraße 14
70469 Stuttgart
ISSN 0039-7881

Any further use
only by permission
of the Publishing House

Synthesis of Various Heterocycles Having a Dienamide Moiety by Ring-Closing Metathesis of Ene-ynamides

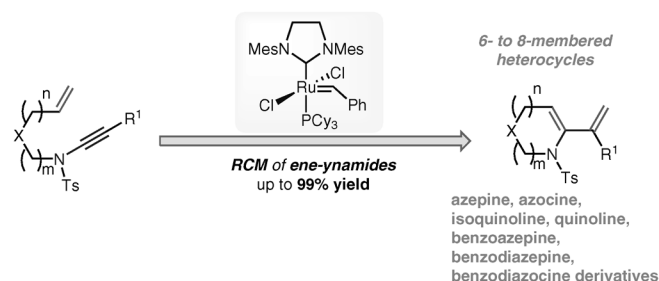
Hideaki Wakamatsu^{*a}Yoshimi Sasaki^aMasatoshi Kawahata^{b,c}Kentaro Yamaguchi^bYuichi Yoshimura^{*a}

^a Faculty of Pharmaceutical Sciences, Tohoku Medical and Pharmaceutical University, 4-4-1 Komatsushima, Aoba-ku, Sendai 981-8558, Japan
hiwaka@tohoku-mpu.ac.jp

yoshimura@tohoku-mpu.ac.jp

^b Kagawa School of Pharmaceutical Sciences, Tokushima Bunri University, 1314-1 Shido, Sanuki, Kagawa 769-2193, Japan

^c Laboratory of Pharmaceutical Sciences and Education, Showa Pharmaceutical University, 3-3165 Higashi-Tamagawagakuen, Machida, Tokyo 194-8543, Japan



Received: 23.03.2018

Accepted after revision: 23.04.2018

Published online: 30.05.2018

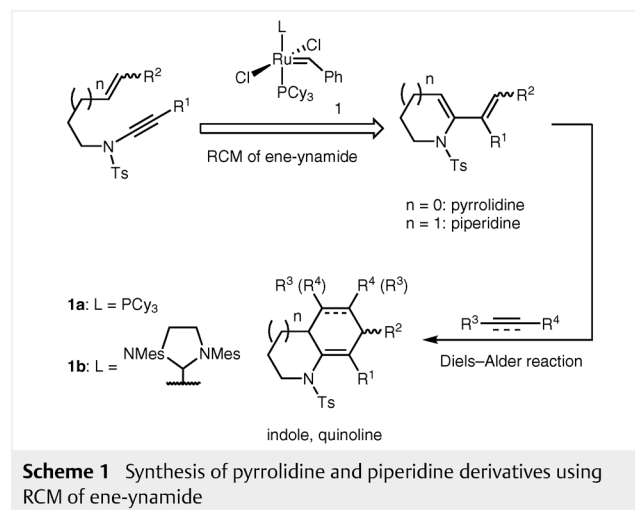
DOI: 10.1055/s-0037-1609857; Art ID: ss-2018-f0202-op

Abstract Ring-closing metathesis (RCM) of ynamides, having alkene substituents of various lengths on the side chain, was demonstrated using the second-generation Grubbs catalyst. When the reaction of ene-ynamides was carried out in the presence of 5 mol% of the catalyst, RCM proceeded smoothly to give quinoline or isoquinoline derivatives having a dienamide unit in good yields. Furthermore, RCM of ene-ynamides, having one more carbon on the side chain, proceeded smoothly to provide seven-membered heterocycles having a dienamide component. Similarly, eight-membered heterocycles, diazocine and benzodiazocine, were also synthesized by RCM of ene-ynamides in good yields.

Key words ruthenium carbene complex, ynamide, ring-closing metathesis, heterocycles, medium-sized ring

Carbon–carbon double bonds have been shown to be useful building blocks in synthetic organic chemistry.¹ Olefin metathesis, which is catalyzed by transition metal complexes, is one of the most powerful tools for the construction of the C=C bonds.² Ring-closing metathesis (RCM) is used as a key reaction for the synthesis of various natural products, and is the essential method for the construction of the carbon framework at this moment. Likewise, ring-closing enyne metathesis (RCEYM) has attracted much interest because various cyclic products having a conjugated diene moiety can be obtained in a single step.³ The distinctive reactivity of ynamides, which have an electron-deficient π -orbital and higher stability relative to ynamines, is attractive for organic chemists.⁴ As useful synthetic methods for the preparation of ynamides have already been reported by Kitamura,⁵ Brückner^{4i,6} and Hsung,⁷ a variety of ynamides can be synthesized at present.

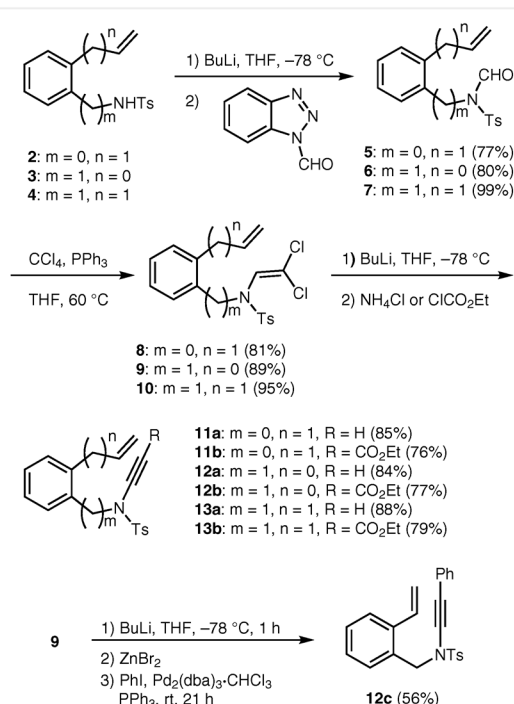
Several kinds of transition-metal-catalyzed reactions of ynamides, including [2+2+1] cycloaddition,^{8g} Pauson–Khand reaction,^{8h} cycloisomerization,⁸ⁱ triazole synthesis,^{8j} [4+2] cycloaddition,^{8k} [2+2] cycloaddition,^{8l} and Sonogashira cross-coupling,^{8m,n} have been reported in recent years.⁸ We have studied RCM of ene-ynamides, which can be applied for the synthesis of pyrrolizidine and piperidine derivatives. Furthermore, the diene derivative, which was obtained by RCM of ene-ynamide, can afford indole and quinoline derivatives by Diels–Alder reaction (Scheme 1).⁹



Scheme 1 Synthesis of pyrrolidine and piperidine derivatives using RCM of ene-ynamide

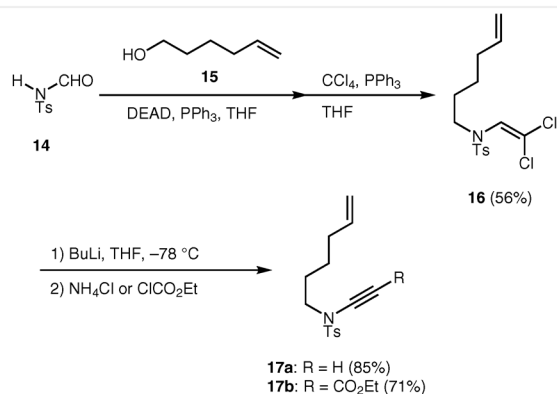
On the basis of the above discussion, we decided to explore the further expansion of the RCM of ene-ynamides. Herein, we wish to report the synthesis of various heterocyclic compounds having a dienamide moiety, especially to establish the efficient synthesis of seven- and eight-membered heterocycles.¹⁰ Ene-ynamide derivatives were prepared by the several synthetic methods, as shown in Schemes 2 through 5.

Tosyl amides **2–4**, which were synthesized by the literature procedure,^{11–13} were treated with butyllithium, followed by treatment with formylbenzotriazole, to provide *N*-formyl derivatives **5–7**. The ynamide unit was constructed by the modified Corey–Fuchs alkyne synthesis^{6,14} to obtain ene-ynamides **11–13**. Ene-ynamide **12c**, having a phenyl group on the alkyne, was obtained from compound **9** by Negishi coupling (Scheme 2).¹⁵



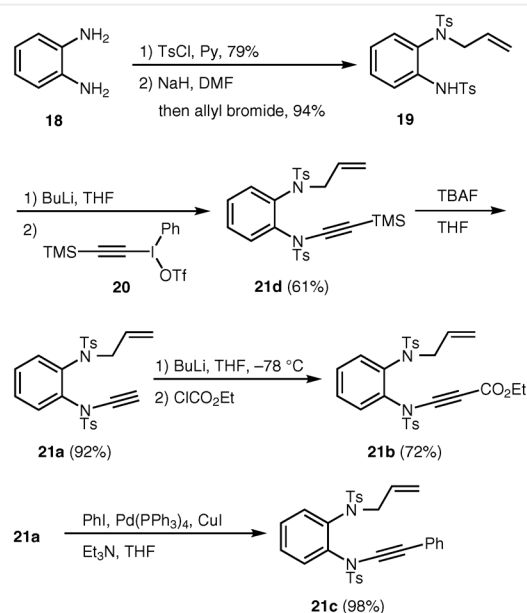
Scheme 2 Preparation of substrate for the synthesis of quinoline, isoquinoline, and benzazepine derivatives

Mitsunobu reaction¹⁶ of **14** and **15**, followed by dichloroolefination, provided **16**, which could be converted into **17** in good yield by treatment with butyllithium (Scheme 3).



Scheme 3 Preparation of substrate for the synthesis of azepine derivative

Allyl tosyl amide **19**, whose synthesis was reported by Stetter,¹⁷ was reacted with butyllithium and iodonium salt **20** to provide **21d** in 61% yield. Ene-ynamide **21a** was obtained from **21d** by the removal of the TMS group on the alkyne. The synthesis of ene-ynamide **21b** and **21c** from **21a** was accomplished by lithiation on the terminal alkyne or Sonogashira cross-coupling¹⁸ (Scheme 4).



Scheme 4 Preparation of substrate for the synthesis of benzodiazepine derivatives

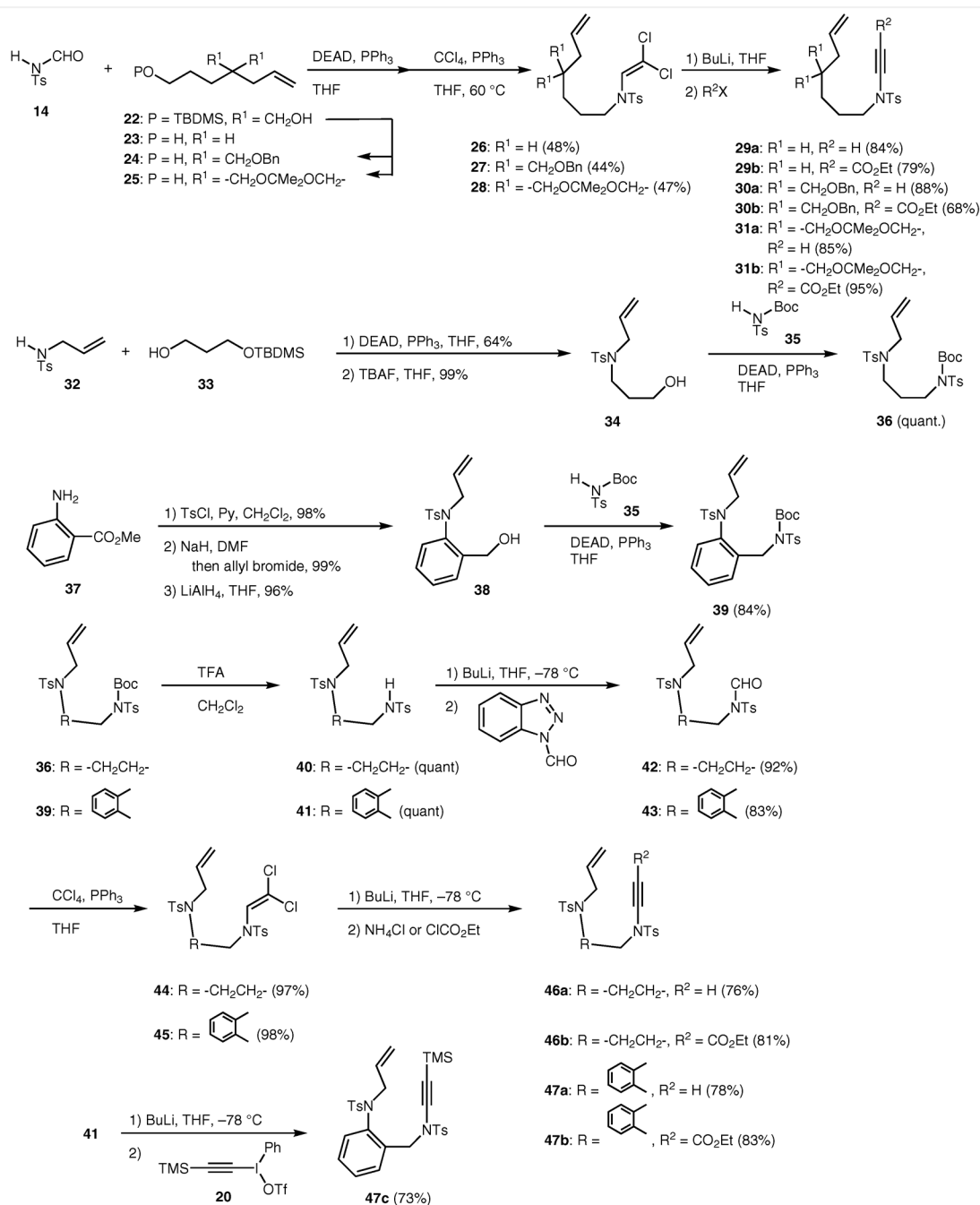
Alcohols **24** and **25** were prepared from **22**¹⁹ by the easy exchange of its protecting group. Mitsunobu reaction of *N*-tosylformamide **14** and alcohol **23–25**, followed by treatment with carbon tetrachloride and triphenylphosphine, provided dichloroolefins **26–28**, which were treated with butyllithium and ammonium chloride or ethyl chlorocarbonate to obtain ene-ynamides **29–31** in good yields (Scheme 5).

The synthetic route for the preparation of compounds **46** and **47** is shown in Scheme 5. *N*-Boc-protected tosylamide derivative **36** was obtained through a stepwise Mitsunobu reaction of propanediol derivative **33** with allyl tosyl amide **32** and *N*-Boc tosylamide **35**, in good yield. On the other hand, the synthesis of another *N*-Boc tosylamide derivative **39** having a phenyl group on the alkyl chain was accomplished by Mitsunobu reaction of **38**, which was synthesized by a literature procedure.²⁰ *N*-Boc deprotection of the compounds **36** and **39** by treatment with trifluoroacetic acid afforded tosylamide derivatives **40** and **41**, which upon formylation, dichloroolefination, and alkylation provided ene-ynamides **46a**, **46b**, and **47a**, **47b**, respectively. TMS-protected ene-ynamide **47c**, on the other hand, was obtained by the reaction of tosylamide **41** with butyllithium and iodonium salt **20**.

The synthesis of quinoline derivative **48** is shown in Table 1. The reaction of **11a** in the presence of 5 mol% of the second-generation Grubbs catalyst **1b** in toluene at 80 °C for 0.5 hour under ethylene atmosphere furnished quinoline derivative **48a** in 93% yield (Table 1, entry 1). The reaction of ene-ynamide having an ethoxycarbonyl group on the alkyne did not give good results (entry 2). However, this

problem was solved by replacing ethylene by argon, leading to the formation of the cyclized product **48b** in 79% yield (entry 3).

Next, Diels–Alder reaction of **48a** with dimethyl acetylenedicarboxylate (DMAD) was examined. It was found that the construction of acridine skeleton was possible, and compound **49** was obtained in 45% yield (Scheme 6).

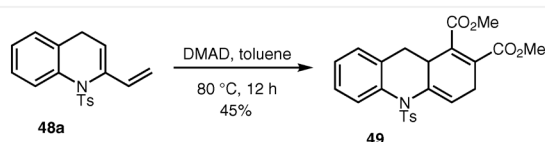


Scheme 5 Preparation of substrate for the synthesis of azocine derivatives

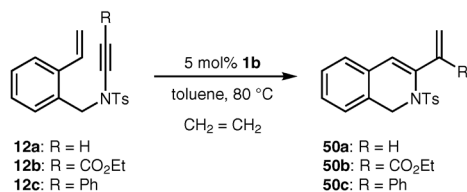
Table 1 Construction of Quinoline Ring

Entry	Substrate	Atmosphere	Time (h)	48	Yield (%)
1	11a	CH ₂ =CH ₂	0.5	48a	93
2	11b	CH ₂ =CH ₂	12	48b	49 ^a
3	11b	Ar	1	48b	79

^a Starting material **11b** was recovered in 11% yield.

**Scheme 6** Synthesis of acridine derivative by Diels–Alder reaction of cyclic dienamides

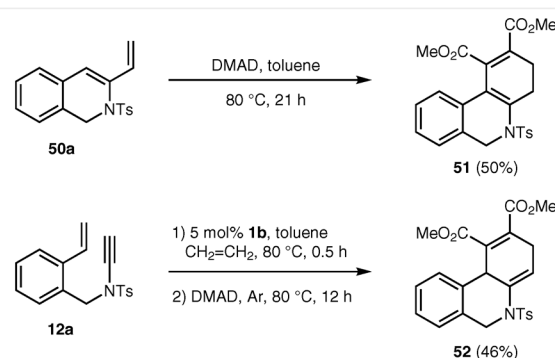
The synthesis of isoquinoline derivatives was examined as further application of the construction of 6+6 ring system. The reaction of ene-ynamide **12a** with 5 mol% of catalyst **1b** under an identical reaction conditions proceeded smoothly to furnish the cyclized product **50a** in 70% yield, in only 30 minutes (Table 2, entry 1). Substituted alkynes can be used in this isoquinoline synthesis, in contrast to the quinoline synthesis. The cyclized product **50b** was obtained in 78% yield, when the ethoxycarbonyl group was substituted on the alkyne (entry 2). Although a slightly longer reaction time was required in the case of the phenyl-substituted alkyne, the resulting isoquinoline derivative **50c** was obtained in almost identical yield (entry 3).

Table 2 Construction of Isoquinoline Ring

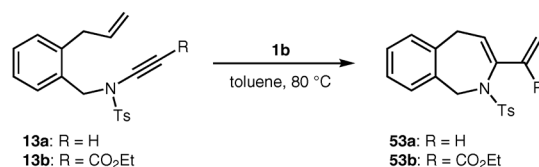
Entry	Substrate	Time (h)	50	Yield (%)
1	12a	0.5	50a	70
2	12b	1	50b	78
3	12c	1.5	50c	77

When a toluene solution of **50a** and DMAD was stirred at 80 °C for 21 hours, the Diels–Alder reaction proceeded smoothly to provide phenanthridine derivative **51** in 50%

yield. However, the double bond of **51** was isomerized to a conjugated position, which was different from the expected position. On the other hand, tricyclic compound **52** was obtained without isomerization of the double bond when the metathesis reaction of **12a** was carried out under identical conditions, followed by the treatment with DMAD under argon atmosphere (Scheme 7).²¹ It is not clear at this stage why the double bond of **52** is not isomerized to a conjugated position. If the lone pair of nitrogen or π electrons is associated to ruthenium center, the double bond isomerization is suppressed.

**Scheme 7** Synthesis of phenanthridine derivatives

The construction of a benzazepine ring was examined next. When a toluene solution of **13a** was stirred with 10 mol% of the catalysts **1b** at 80 °C for 1.5 hours under an ethylene atmosphere, the cyclized product **53a** was obtained in 22% yield (Table 3, entry 1). A corresponding reaction carried out under an argon atmosphere led to an improved yield of **53a** at 49% (entry 2). RCM of **13b**, which was prepared by the introduction of an ethoxycarbonyl group on the alkyne, was attempted next. When the reaction of **13b** was carried out in a manner similar as that used for the synthesis of **53a**, benzazepine derivative **53b** was obtained in 69% yield (entry 3). This yield could be enhanced to 84%

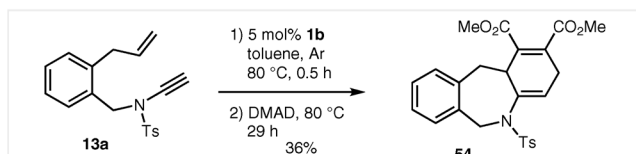
Table 3 Construction of Benzazepine Ring

Entry	Substrate	Atmosphere	1b (mol%)	Time (h)	53	Yield (%) ^a
1	13a	CH ₂ =CH ₂	10	1.5	53a	22
2	13a	Ar	5	0.5	53a	49
3	13b	CH ₂ =CH ₂	10	3.5	53b	69
4	13b	Ar	5	0.5	53b	84

^a Isolated yield.

by performing the reaction under an argon atmosphere (entry 4).

Furthermore, the synthesis of **54** was examined with the aim of constructing the dibenzoazepine skeleton (Scheme 8). Tricyclic heterocycle **54** was obtained in 36% yield when **13a** was exposed to a catalytic amount of **1b** in toluene at 80 °C for 0.5 hour under argon atmosphere, followed by treatment with DMAD at the same temperature.



Scheme 8 Synthesis of dibenzoazepine derivative

Next, RCM of linear α,ω -ene-ynamides was examined. When the reaction of **17a** was carried out in the presence of the catalyst **1b** in toluene at 80 °C for 1 hour, starting material **17a** was recovered in 53% yield (Table 4, entry 1). Replacement of toluene by CH_2Cl_2 led to a better result, and **55a** was obtained in 36% yield after heating for 15 hours, together with 38% of **17a** (entry 2). A similar result was achieved when the reaction was conducted under an argon atmosphere or upon prolonging the reaction time (entries 3 and 4). In the case of **17b**, a substrate having an ethoxycarbonyl group on the alkyne, the yield of the cyclized product **55b** was only 5% when the reaction was carried out in toluene with heating (entry 5). However, a higher yield of **55b** was obtained when the reaction was carried out in CH_2Cl_2 (entry 6).

Table 4 Construction of Azepine Ring

Entry	Substrate	Atmosphere	Time (h)	55	Yield (%) ^a	17	Recovery of 17 (%) ^a
1 ^b	17a	$\text{CH}_2=\text{CH}_2$	1	–	–	17a	53
2	17a	$\text{CH}_2=\text{CH}_2$	15	55a	36	17a	38
3	17a	Ar	26	55a	37	17a	33
4	17a	Ar	48	55a	33	17a	31
5 ^b	17b	$\text{CH}_2=\text{CH}_2$	3	55b	5	17b	74
6	17b	$\text{CH}_2=\text{CH}_2$	1.5	55b	74 ^c	17b	–

^a Yields were determined by ^1H NMR spectroscopy using (*E*)-stilbene as an internal standard.

^b Reaction was carried out in the presence of 5 mol% **1b** in toluene at 80 °C.

^c Isolated yield.

Subsequently, the synthesis of 1,5-benzodiazepine derivatives was also examined. When a solution of **21a** in toluene was exposed to a catalytic amount of **1b** at 80 °C for 1 hour, the starting material **21a** was not consumed, and an inseparable complex mixture consisting of **21a**, cyclized product **56a**, an intermolecular metathesis product with ethylene, and undefined products was obtained (Table 5, entry 1). Replacement of the solvent and a longer reaction time gave a similar result (entry 2). The reaction of the TMS-substituted ene-ynamide **21d** did not proceed and the starting material was recovered (entry 3). Surprisingly, when **21b** was used as the substrate instead of **21a**, benzodiazepine **56b** was obtained in quantitative yield (entry 4). Reduction of the catalyst amount did not affect the yield of **56b** (entry 5). The RCM also proceeded smoothly in CH_2Cl_2 as the solvent, although a longer reaction time was required (entry 6). An excellent yield of **56b** was also observed when the reaction was carried out under an argon atmosphere (entry 7). Likewise, when the phenyl-substituted ene-ynamide **21c** was used as the substrate, benzodiazepine **56c** was obtained in quantitative yield (entry 8).

Table 5 Construction of Benzodiazepine Ring

Entry	Substrate	Solvent	Temp (°C)	Time (h)	56	Yield (%) ^a
1	21a	toluene	80	1	–	–
2	21a	$\text{CH}_2=\text{CH}_2$	reflux	28	–	–
3	21d	toluene	80	5	–	– ^b
4	21b	toluene	80	0.5	56b	99
5 ^c	21b	toluene	80	0.5	56b	99
6	21b	CH_2Cl_2	reflux	15	56b	97
7 ^d	21b	CH_2Cl_2	reflux	20	56b	95
8	21c	toluene	80	1	56c	97

^a Isolated yield.

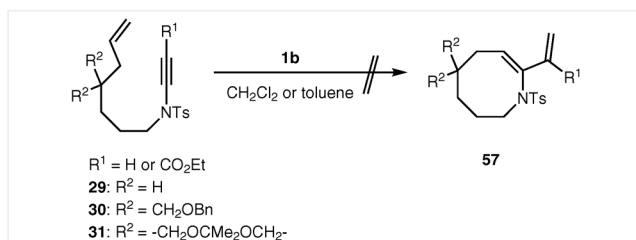
^b Recovered **21d**: 87%.

^c Catalyst **1b** used: 5 mol%.

^d Reaction was carried out under an argon atmosphere.

Encouraged by the successful construction of the six-membered rings and a seven-membered ring, we became interested in the synthesis of eight-membered heterocycles. Initially, various linear ene-ynamides were examined for the synthesis of azocine derivative **57**. However, the desired cyclized product **57** was not obtained in any case, and the

only a trace amount of alkene dimer, formed by the intermolecular reaction of the ene-ynamides was observed in NMR experiment (Scheme 9).



Scheme 9 Construction of azocine ring

Furthermore, RCM of linear ene-ynamide **46**, which contains two tosylamide groups in the chain, was examined. When a CH_2Cl_2 solution of **46a** was heated for 21 hours in the presence of 10 mol% of **1b**, starting material **46a** was recovered in 33% yield (Table 6, entry 1). The introduction of an ethoxycarbonyl group on the alkyne promoted the formation of an eight-membered ring, and diazocine **58b** was obtained in 15% yield (entry 2). Improved yield was achieved when the reaction was performed under an argon atmosphere (entry 3). Higher recovery of starting material **46b** was observed when toluene was used as the solvent (entry 4). However, an encouraging result was observed in the construction of an eight-membered ring, and **58b** was obtained in 78% yield when the reaction was conducted under high-dilution conditions (entry 5).

Table 6 Construction of Diazocine Ring

46a: $R = \text{H}$
46b: $R = \text{CO}_2\text{Et}$
58a: $R = \text{H}$
58b: $R = \text{CO}_2\text{Et}$

Entry	Substrate	Atmosphere	Time (h)	58	Yield (%) ^a	46	Recovery of 46 (%) ^a
1	46a	$\text{CH}_2=\text{CH}_2$	21	–	–	46a	33
2	46b	$\text{CH}_2=\text{CH}_2$	21	58b	15	46b	49
3	46b	Ar	21	58b	33	46b	25
4 ^b	46b	$\text{CH}_2=\text{CH}_2$	6	58b	–	46b	68
5 ^c	46b	Ar	24	58b	78 ^d	–	–

^a Yields were determined by ^1H NMR spectrum using (*E*)-stilbene as an internal standard.

^b Reaction was carried out in the presence of 5 mol% **1b** in toluene at 80 °C.

^c Reaction was carried out under low concentration (0.002 M).

^d Isolated yield.

Next, the synthesis of benzodiazocine was examined. The reaction of **47a** with the catalyst **1b** did not proceed, and starting material was recovered (Table 7, entry 1); shortening of the reaction time did not affect the result (en-

try 2). Then, a solution of **47b** in CH_2Cl_2 was heated in the presence of **1b** for 21 hours, and the reaction was monitored by TLC (entry 3). A new spot appeared on the TLC plate, suggesting the formation of **59b**. However, it was difficult to deduce the correct structure of **59b** due to the broad peaks in its ^1H NMR spectrum. This was probably due to the rapid interconversion of several stable conformers under the influence of the benzene ring, at room temperature. The peaks were clearly separated when the ^1H NMR spectrum was recorded at low temperature of –50 °C (Figure 1). We have reported that the dimeric compound was obtained, because the largest m/z value of FAB-MS spectra was observed at 1133 ($M^+ + \text{H}$).¹⁰ However, the structure of the metathesis product was conclusively established by X-ray crystallography (Figure 2), and it was found that the desired eight-membered ring **59b** was obtained in 14% yield.

Table 7 Construction of Benzodiazocine Ring

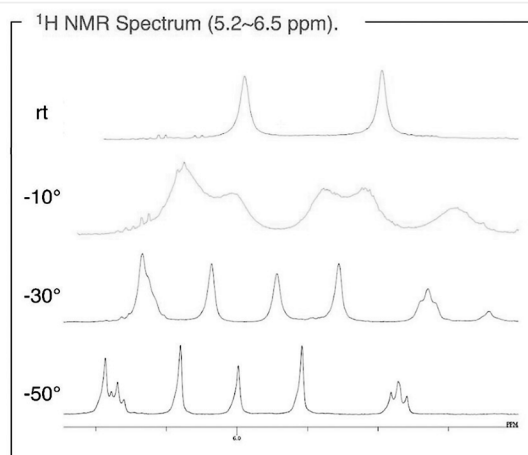
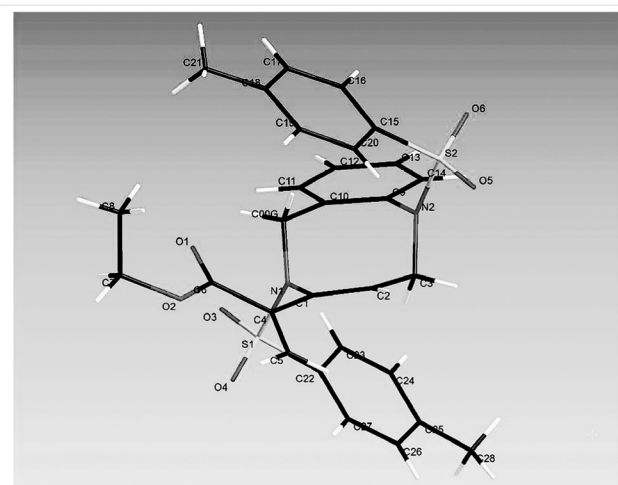
47a: $R = \text{H}$
47b: $R = \text{CO}_2\text{Et}$
47c: $R = \text{Ph}$
59a: $R = \text{H}$
59b: $R = \text{CO}_2\text{Et}$
59c: $R = \text{Ph}$

Entry	Substrate	Atmosphere	Time (h)	59	Yield (%) ^a	47	Recovery of 47 (%) ^a
1	47a	$\text{CH}_2=\text{CH}_2$	21	–	–	47a	58
2 ^b	47a	$\text{CH}_2=\text{CH}_2$	0.5	–	–	47a	53
3	47b	$\text{CH}_2=\text{CH}_2$	21	59b	14	47b	63
4	47b	Ar	21	59b	52	47b	44
5 ^b	47b	$\text{CH}_2=\text{CH}_2$	6	–	–	47b	86
6 ^b	47b	Ar	2	59b	77	–	–
7 ^b	47c	Ar	17	–	–	47c	83
8	47c	Ar	6	–	–	47c	99

^a Isolated yield.

^b Reactions were carried out in the presence of 5 mol% **1b** in toluene at 80 °C.

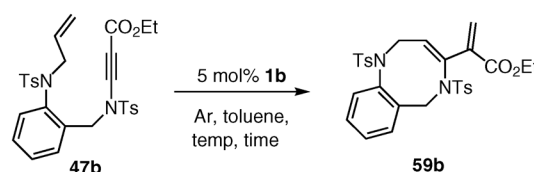
An argon atmosphere was effective for the cyclization of **47b**, and the yield of **59b** was increased to 52% (Table 7, entry 4). Appropriate combination of the solvent and the atmosphere was important for the formation of **59b**. Upon changing the solvent to toluene from CH_2Cl_2 , high recovery of **47b** was observed under an ethylene atmosphere (entry 5) and a higher yield of **59b** was observed under an argon atmosphere (entry 6). Unfortunately, in the case of the phenyl-substituted ene-ynamide **47c**, the formation of the eight-membered heterocycle **59c** was not observed, and the starting material was recovered in high yield (entries 7, 8).

Figure 1 ^1H NMR spectrum of **59b**Figure 2 X-ray crystal structure of **59b**

Furthermore, the effect of temperature on the construction of the eight-membered-ring compounds was examined (Table 8). A lower reaction rate was observed with the decreasing reaction temperature, and **59b** was obtained in 45% yield at room temperature with the recovery of the starting material **47b** in 16% yield (entry 3).

It is thought that this reaction progresses via one of the two pathways described in Scheme 10. In the yne-then-ene pathway (cycle a), the carbene complex **1** first reacts with substrate **A** or ethylene to provide ruthenium carbene complex **I**, which is the active species for the metathesis reaction. Carbene complex **I** then reacts with the alkyne part of **A** to provide ruthenacyclobutene **II**, which is converted to complex **III**. If the ruthenium carbene part of **III** reacts with the alkene part intramolecularly, ruthenacyclobutane **IV** would be obtained, which then converts to product **B**, regenerating ruthenium carbene complex **I**. On the other hand, ruthenium carbene **V** is thought to be formed, when

Table 8 Temperature Effect for the Construction of Eight-Membered Ring



Entry	Temp (°C)	Time (h)	Yield of 59b (%) ^a	Recovery of 47b (%) ^a
1	80	2	77	–
2	50	10	57	4
3	r.t.	42	45	16

^a Isolated yield.

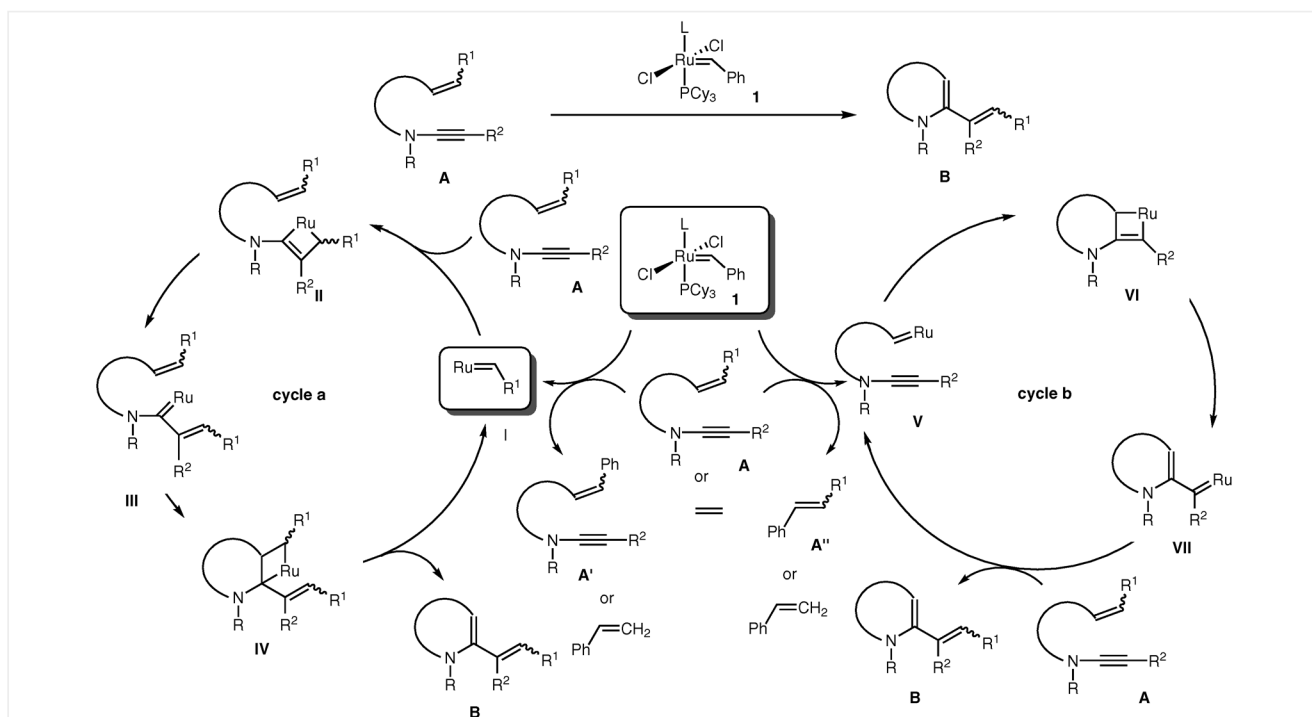
1 reacts with the alkene part of **A** (cycle b, ene-then-yne pathway). The carbene part of complex **V** then reacts with the alkyne part of **V** intramolecularly to provide ruthenacyclobutene **VI**, which converts into complex **VII**. If the carbene part of **VII** reacts with **A** intermolecularly, the desired product **B** would be obtained together with **V**. Two intriguing results were observed in the construction of the seven- and eight-membered ring:

1) The desired product was obtained in high yield when substituents were present on the terminal alkyne, while the yield of the cyclized product was decreased in the case of unsubstituted ene-ynamides.

2) The reaction proceeded under an argon atmosphere to provide the cyclized product in a yield similar to that obtained under an ethylene atmosphere.

The reactivity of the ruthenium complex with the $\text{C}\equiv\text{C}$ bond should increase because of the higher electron density of ynamides. As a result, the yne-then-ene mechanism would predominate (cycle a). On the other hand, it is thought that the reaction of the ruthenium complex and the double bond have an advantage when a substituent exists on the terminal alkyne. The ruthenium carbene should react with the double bond instead of the triple bond, by the introduction of the ethoxycarbonyl group on the alkyne. These effects, which decrease the electron density of ynamides, would favor the predominance of the ene-then-yne mechanism (cycle b).

Taking into consideration the ring-closure factor, it is proposed that the rate of ring closure for medium-sized rings is lower than that for five- or six-membered rings. If the conversion rate from **III** to **IV** decreases, complex **III** would react with the substrate or the other alkene species to provide a variety of alkene compounds. On the other hand, if the conversion rate from **V** to **VI** decreases, complex **V** would react intermolecularly with the alkene part of another substrate to form the alkene dimer. In addition, complex **V** would react only with ethylene in the case of the reaction of **47b** under ethylene atmosphere.



Scheme 10 Proposed reaction mechanism

It is more than evident from the current study that the reaction can proceed by both mechanisms, depending on the substituent on the terminal alkyne, although a recent study strongly supports the predominance of the initial cyclometalation on an alkene over an alkyne.²² It is presumed that the reaction progresses via cycle b in the substrate with the ethoxycarbonyl group on the alkyne. In other words, the construction of medium-sized rings, which is a challenging task in organic chemistry, is achieved by the modification of the substrates suitable for cycle b.

In conclusion, the synthesis of various heterocycles having a dienamide unit was attempted by RCM of ene-ynamides. The reaction proceeded smoothly to provide the products in high yields in the synthesis of quinoline and isoquinoline derivatives, and the argon atmosphere was acceptable for the synthesis of quinoline derivatives. The introduction of an ethoxycarbonyl group on the terminal alkyne of the ene-ynamide was conducive for the construction of the seven-membered ring, although the synthesis of benzodiazepine derivatives from non-substituted ene-ynamides was difficult. Further, the presence of an ethoxycarbonyl group on the terminal alkyne of the ene-ynamides and an argon atmosphere under the given reaction conditions were necessary for the formation of the eight-membered ring. In particular, an eight-membered ring could be constructed under these reaction conditions; thus, this method would serve as a useful strategy for the construction of eight-membered rings, which is a challenging task in organic chemistry.

The metathesis reactions were carried out under an atmosphere of ethylene (1 atm) or an argon atmosphere (1 atm). All other manipulations were carried out under an atmosphere of argon, unless otherwise mentioned. Ru complexes were purchased from Aldrich Chemical Company. All other solvents and reagents were purified when necessary using standard procedure. Column chromatography was performed on silica gel 60 N (spherical, neutral, 40–60 μ m, Kanto Chemical Co.). IR spectra were recorded on PerkinElmer FT-IR 1725X spectrophotometer. ^1H and ^{13}C NMR spectra were recorded on a Jeol JNM-EX400 (^1H : 400 MHz, ^{13}C : 100 MHz) spectrometer. Chemical shift values were reported in ppm (δ) downfield from TMS as an internal standard, or residual solvent peak [^1H NMR, CHCl_3 (7.24); ^{13}C NMR, CHCl_3 (77.0)]. Coupling constants (J) are reported in hertz (Hz). EI mass spectra were recorded on a Jeol JMN-DX 303/JMA-DA 5000 mass spectrometer.

N-(2-Allylphenyl)-*N*-formyl-*p*-toluenesulfonamide (5)

To a solution of **2** (1.37 g, 4.77 mmol) in THF (25 mL) was added BuLi (3.6 mL, 5.72 mmol, 1.58 M hexane solution) slowly at -78°C , and stirred at the same temperature for 1 h. To the resulting mixture was added 1-formylbenzotriazole (1.40 g, 9.53 mmol), and warmed to -30°C for 1 h. Sat. aq. NH_4Cl was added, and the aqueous phase was extracted with EtOAc. The combined organic phases were washed with brine, and dried (MgSO_4). The volatiles were removed under reduced pressure, and the residue was purified by column chromatography on silica gel (hexane/ Et_2O 3:1) to provide **5** (1.15 g, 77%) as a colorless oil.

IR (neat): 1715 (s), 1597 (m), 1361 (s), 1172 (s) cm^{-1} .

^1H NMR (400 MHz, CDCl_3): δ = 9.29 (br, 1 H), 7.61 (d, J = 8.2 Hz, 2 H), 7.40–7.29 (m, 4 H), 7.16 (dt, J = 1.5, 7.7 Hz, 1 H), 6.66 (d, J = 7.7 Hz, 1 H), 5.68 (dddd, J = 6.3, 7.3, 10.1, 16.9 Hz, 1 H), 5.08–5.00 (m, 2 H), 3.19 (dd, J = 7.3, 15.9 Hz, 1 H), 2.99 (dd, J = 6.3, 15.9 Hz, 1 H), 2.47 (s, 3 H).

^{13}C NMR (100 MHz, CDCl_3): δ = 161.1, 145.8, 140.4, 135.3, 134.5, 130.4, 130.2, 130.1, 129.9, 128.2, 127.1, 117.2, 35.1, 21.7.

MS (EI): m/z = 315 (M^+), 287, 160, 132, 117, 91.

HRMS (EI): m/z calcd for $\text{C}_{17}\text{H}_{17}\text{NO}_3\text{S}$ (M^+): 315.0929; found: 315.0926.

***N*-Formyl-*N*-(2-vinylbenzyl)-*p*-toluenesulfonamide (6)**

According to the procedure for the synthesis of **5**, a solution of **3** (1.76 g, 6.12 mmol), BuLi (4.7 mL, 7.35 mmol, 1.58 M hexane solution) and 1-formylbenzotriazole (1.80 g, 12.25 mmol) in THF (30 mL) was stirred at 0 °C for 1 h to afford **6** (1.54 g, 80%) after purification by column chromatography on silica gel (hexane/EtOAc 5:1) as a colorless oil.

IR (neat): 1699 (s), 1597 (m), 1361 (s), 1166 (s) cm^{-1} .

^1H NMR (400 MHz, CDCl_3): δ = 9.21 (s, 1 H), 7.40 (d, J = 8.2 Hz, 2 H), 7.26–7.09 (m, 6 H), 6.85 (dd, J = 11.1, 17.4 Hz, 1 H), 5.36 (dd, J = 1.5, 17.4 Hz, 1 H), 5.25 (dd, J = 1.5, 11.1 Hz, 1 H), 4.87 (s, 2 H), 2.37 (s, 3 H).

^{13}C NMR (100 MHz, CDCl_3): δ = 161.3, 144.9, 137.1, 135.2, 133.9, 131.0, 129.7, 128.9, 128.0, 127.7, 127.1, 126.2, 117.1, 42.9, 21.5.

MS (EI): m/z = 315 (M^+), 160, 133, 115, 91.

HRMS (EI): m/z calcd for $\text{C}_{17}\text{H}_{17}\text{NO}_3\text{S}$ (M^+): 315.0929; found: 315.0922.

***N*-(2-Allylbenzyl)-*N*-formyl-*p*-toluenesulfonamide (7)**

According to the procedure for the synthesis of **5**, a solution of **4** (2.95 g, 9.78 mmol), BuLi (7.4 mL, 11.74 mmol, 1.58 M hexane solution) and 1-formylbenzotriazole (2.88 g, 19.57 mmol) in THF (50 mL) was stirred at 0 °C for 40 min to afford **7** (3.18 g, 99%) after purification by column chromatography on silica gel (hexane/Et₂O 2:1) as a colorless oil.

IR (neat): 1699 (s), 1597 (m), 1361 (s), 1166 (s) cm^{-1} .

^1H NMR (400 MHz, CDCl_3): δ = 9.24 (s, 1 H), 7.50 (d, J = 8.2 Hz, 2 H), 7.20 (d, J = 8.2 Hz, 2 H), 7.14 (d, J = 7.7 Hz, 1 H), 7.06–6.99 (m, 3 H), 5.86 (ddt, J = 10.3, 16.9, 6.0 Hz, 1 H), 5.05 (dd, J = 1.5, 10.3 Hz, 1 H), 4.88 (dd, J = 1.5, 16.9 Hz, 1 H), 4.77 (s, 2 H), 3.35 (d, J = 6.0 Hz, 2 H), 2.29 (s, 3 H).

^{13}C NMR (100 MHz, CDCl_3): δ = 161.0, 144.8, 136.9, 135.9, 134.7, 132.0, 129.5, 129.2, 127.3, 127.2, 126.8, 126.1, 115.7, 42.2, 36.4, 21.0.

MS (EI): m/z = 329 (M^+), 174, 130, 115, 91.

HRMS (EI): m/z calcd for $\text{C}_{18}\text{H}_{19}\text{NO}_3\text{S}$ (M^+): 329.1086; found: 329.1082.

***N*-(2-Allylphenyl)-*N*-(2,2-dichlorovinyl)-*p*-toluenesulfonamide (8)**

To a solution of **5** (1.15 g, 3.65 mmol) and PPh_3 (2.39 g, 9.12 mmol) in THF (24 mL) was added CCl_4 (2.9 mL, 29.90 mmol) in THF (12 mL, total 0.1 M) at 60 °C over 3 h, and stirred at the same temperature for 1 h. After cooling the reaction mixture to r.t., sat. aq. NaHCO_3 was added, and the aqueous phase was extracted with EtOAc. The combined organic phases were washed with brine, and dried (MgSO_4). The volatiles were removed under reduced pressure, and the residue was purified by column chromatography on silica gel (hexane/EtOAc 10:1) to provide **8** (1.12 g, 81%) as a pale red oil.

IR (neat): 1598 (w), 1367 (s), 1170 (s) cm^{-1} .

^1H NMR (400 MHz, CDCl_3): δ = 7.55 (d, J = 8.3 Hz, 2 H), 7.33–7.28 (m, 4 H), 7.10 (s, 1 H), 7.08 (m, 1 H), 6.71 (d, J = 7.8 Hz, 1 H), 5.83 (m, 1 H), 5.15–5.10 (m, 2 H), 3.35 (d, J = 4.9 Hz, 2 H), 2.46 (s, 3 H).

^{13}C NMR (100 MHz, CDCl_3): δ = 144.7, 140.7, 135.6, 135.2, 134.4, 130.0, 129.7, 129.7, 129.0, 127.8, 126.4, 125.9, 116.9, 112.8, 35.4, 21.5.

MS (EI): m/z = 381 (M^+), 285, 226, 191, 150, 130, 115, 91.

HRMS (EI): m/z calcd for $\text{C}_{18}\text{H}_{17}^{35}\text{Cl}_2\text{NO}_2\text{S}$ (M^+): 381.0357; found: 381.0360.

***N*-(2,2-Dichlorovinyl)-*N*-(2-vinylbenzyl)-*p*-toluenesulfonamide (9)**

According to the procedure for the synthesis of **8**, a solution of **6** (1.42 g, 4.50 mmol), PPh_3 (2.95 g, 11.26 mmol) and CCl_4 (3.6 mL, 36.92 mmol) in THF (45 mL) was stirred at 60 °C for 12 h to afford **9** (1.53 g, 89%) as a pale yellow solid after purification by column chromatography on silica gel (hexane/EtOAc 10:1); mp 93 °C.

IR (KBr): 1596 (w), 1356 (m), 1164 (s) cm^{-1} .

^1H NMR (400 MHz, CDCl_3): δ = 7.73 (d, J = 8.2 Hz, 2 H), 7.48 (d, J = 7.7 Hz, 1 H), 7.35 (d, J = 8.2 Hz, 2 H), 7.29 (dd, J = 7.2, 7.7 Hz, 1 H), 7.21 (dd, J = 7.2, 7.7 Hz, 1 H), 7.17 (d, J = 7.7 Hz, 1 H), 7.07 (dd, J = 11.1, 17.4 Hz, 1 H), 6.04 (s, 1 H), 5.63 (dd, J = 1.5, 17.4 Hz, 1 H), 5.35 (dd, J = 1.5, 11.1 Hz, 1 H), 4.53 (s, 2 H), 2.46 (s, 3 H).

^{13}C NMR (100 MHz, CDCl_3): δ = 144.3, 137.7, 135.0, 133.7, 131.4, 130.0, 129.9, 128.6, 128.0, 127.7, 127.5, 126.2, 124.5, 116.9, 50.8, 21.6.

MS (EI): m/z = 381 (M^+), 285, 226, 117, 91.

HRMS (EI): m/z calcd for $\text{C}_{18}\text{H}_{17}^{35}\text{Cl}_2\text{O}_2\text{S}$ (M^+): 381.0357; found: 381.0385.

***N*-(2-Allylbenzyl)-*N*-(2,2-dichlorovinyl)-*p*-toluenesulfonamide (10)**

According to the procedure for the synthesis of **8**, a solution of **7** (2.65 g, 8.05 mmol), PPh_3 (5.28 g, 20.13 mmol) and CCl_4 (6.4 mL, 66.02 mmol) in THF (40 mL) was stirred at 60 °C for 9 h to afford **10** (3.03 g, 95%) as a white solid after purification by column chromatography on silica gel (hexane/Et₂O 2:1); mp 72–73 °C.

IR (KBr): 1598 (w), 1356 (m), 1165 (s) cm^{-1} .

^1H NMR (400 MHz, CDCl_3): δ = 7.73 (d, J = 8.2 Hz, 2 H), 7.36 (d, J = 8.2 Hz, 2 H), 7.27–7.15 (m, 4 H), 6.05 (s, 1 H), 5.94 (ddt, J = 10.1, 16.9, 6.3 Hz, 1 H), 5.08 (ddt, J = 1.9, 10.1, 1.5 Hz, 1 H), 4.97 (ddt, J = 1.9, 16.9, 1.5 Hz, 1 H), 4.46 (s, 2 H), 3.50 (dt, J = 6.3, 1.5 Hz, 2 H), 2.47 (s, 3 H).

^{13}C NMR (100 MHz, CDCl_3): δ = 144.3, 138.6, 136.5, 134.7, 132.4, 130.0, 129.9, 129.8, 128.4, 127.7, 127.4, 126.3, 124.7, 116.0, 50.8, 36.4, 21.5.

MS (EI): m/z = 395 (M^+), 299, 155, 131, 105, 91.

HRMS (EI): m/z calcd for $\text{C}_{19}\text{H}_{19}^{35}\text{Cl}_2\text{NO}_2\text{S}$ (M^+): 395.0514; found: 395.0492.

***N*-(2-Allylphenyl)-*N*-ethynyl-*p*-toluenesulfonamide (11a)**

To a solution of **8** (228.1 mg, 0.60 mmol) in THF (10 mL) was added BuLi (0.85 mL, 1.31 mmol, 1.55 M hexane solution) at –78 °C, and stirred at the same temperature for 0.5 h. Sat. aq. NH_4Cl was added, and the aqueous phase was extracted with EtOAc. The combined organic phases were washed with brine, and dried (MgSO_4). The volatiles were removed under reduced pressure, and the residue was purified by column chromatography on silica gel (hexane/EtOAc 10:1) to provide **11a** (157.5 mg, 85%) as a white solid; mp 87–88 °C.

IR (KBr): 2131 (m), 1597 (w), 1369 (s), 1168 (s) cm^{-1} .

^1H NMR (400 MHz, CDCl_3): δ = 7.71 (d, J = 8.2 Hz, 2 H), 7.36 (d, J = 8.2 Hz, 2 H), 7.32–7.29 (m, 2 H), 7.12 (m, 1 H), 6.82 (d, J = 7.7 Hz, 1 H), 5.91 (ddt, J = 10.6, 16.9, 6.8 Hz, 1 H), 5.15–5.09 (m, 2 H), 3.49 (br, 2 H), 2.76 (s, 1 H), 2.47 (s, 3 H).

^{13}C NMR (100 MHz, CDCl_3): δ = 145.1, 139.6, 136.4, 135.6, 133.6, 130.4, 129.5, 129.5, 128.2, 127.6, 127.0, 116.7, 76.9, 57.7, 35.2, 21.5.

MS (EI): m/z = 311 (M^+), 263, 246, 156, 128, 91.

HRMS (EI): m/z calcd for $\text{C}_{18}\text{H}_{17}\text{NO}_2\text{S}$ (M^+): 311.0980; found: 311.0979.

Ethyl [(2-Allylphenyl)-(p-toluenesulfonyl)amino]propynoate (**11b**)

To a solution of **8** (0.33 g, 0.86 mmol) in THF (17 mL) was added BuLi (1.2 mL, 1.90 mmol, 1.58 M hexane solution) at -78°C , and stirred at the same temperature for 0.5 h. To the resulting mixture was added ethyl chlorocarbonate (0.17 mL, 1.73 mmol) and warmed to -50°C over 0.5 h. Sat. aq. NH_4Cl was added, and the aqueous phase was extracted with EtOAc. The combined organic phases were washed with brine and dried (MgSO_4). The volatiles were removed under reduced pressure, and the residue was purified by column chromatography on silica gel (hexane/EtOAc 10:1) to provide **11b** (0.25 g, 76%) as a pale yellow oil.

IR (neat): 2220 (s), 1706 (s), 1597 (w), 1375 (s), 1177 (s) cm^{-1} .

^1H NMR (400 MHz, CDCl_3): δ = 7.75 (d, J = 8.2 Hz, 2 H), 7.40–7.30 (m, 4 H), 7.16 (ddd, J = 1.9, 6.8, 8.2 Hz, 1 H), 6.83 (dd, J = 1.0, 7.7 Hz, 1 H), 5.87 (ddt, J = 10.6, 17.4, 6.8 Hz, 1 H), 5.14–5.07 (m, 2 H), 4.22 (q, J = 7.3 Hz, 2 H), 3.40 (br, 2 H), 2.49 (s, 3 H), 1.30 (t, J = 7.3 Hz, 3 H).

^{13}C NMR (100 MHz, CDCl_3): δ = 153.9, 145.9, 139.4, 135.3, 135.2, 133.2, 130.6, 130.1, 129.9, 128.4, 127.8, 127.2, 117.1, 82.6, 65.9, 61.4, 35.1, 21.6, 14.0.

MS (EI): m/z = 383 (M^+), 338, 319, 290, 272, 244, 228, 154, 128, 115, 91.

HRMS (EI): m/z calcd for $\text{C}_{21}\text{H}_{21}\text{NO}_4\text{S}$ (M^+): 383.1191; found: 383.1185.

N-Ethynyl-N-(2-vinylbenzyl)-p-toluenesulfonamide (**12a**)

According to the procedure for the synthesis of **11a**, a solution of **9** (305.9 mg, 0.80 mmol) and BuLi (1.1 mL, 1.76 mmol, 1.58 M hexane solution) in THF (16 mL) was stirred at -78°C for 1 h to afford **12a** (209.6 mg, 84%) as a white solid after purification by column chromatography on silica gel (hexane/EtOAc 10:1); mp 88 – 89°C .

IR (KBr): 2141 (m), 1596 (w), 1360 (s), 1174 (s) cm^{-1} .

^1H NMR (400 MHz, CDCl_3): δ = 7.79 (d, J = 8.2 Hz, 2 H), 7.49 (d, J = 7.7 Hz, 1 H), 7.34 (d, J = 8.2 Hz, 2 H), 7.29 (ddd, J = 1.9, 7.3, 7.7 Hz, 1 H), 7.24–7.17 (m, 2 H), 7.01 (dd, J = 11.1, 17.4 Hz, 1 H), 5.62 (dd, J = 1.5, 17.4 Hz, 1 H), 5.32 (dd, J = 1.5, 11.1 Hz, 1 H), 4.52 (s, 2 H), 2.59 (s, 1 H), 2.45 (s, 3 H).

^{13}C NMR (100 MHz, CDCl_3): δ = 144.8, 137.5, 133.9, 133.3, 130.5, 130.3, 129.7, 128.7, 127.6, 127.5, 125.9, 117.0, 75.8, 59.8, 52.4, 21.5.

MS (EI): m/z = 310 ($M^+ - 1$), 156, 129, 117, 91.

HRMS (EI): m/z calcd for $\text{C}_{18}\text{H}_{17}\text{NO}_2\text{S}$ (M^+): 311.0980; found: 311.0992.

Ethyl [(p-Toluenesulfonyl)-(2-vinylbenzyl)amino]propynoate (**12b**)

According to the procedure for the synthesis of **11b**, a solution of **9** (313.3 mg, 0.82 mmol), BuLi (1.2 mL, 1.97 mmol, 1.58 M hexane solution), and ethyl chlorocarbonate (0.16 mL, 1.64 mmol) in THF (16 mL)

was stirred at -50°C for 0.5 h to afford **12b** (240.7 mg, 77%) as a pale yellow oil after purification by column chromatography on silica gel (hexane/benzene 2:3).

IR (neat): 2219 (s), 1702 (s), 1375 (m), 1172 (s) cm^{-1} .

^1H NMR (400 MHz, CDCl_3): δ = 7.75 (d, J = 8.7 Hz, 2 H), 7.47 (d, J = 7.2 Hz, 1 H), 7.34–7.29 (m, 3 H), 7.24–7.21 (m, 2 H), 6.94 (dd, J = 10.9, 17.2 Hz, 1 H), 5.59 (dd, J = 1.2, 17.2 Hz, 1 H), 5.33 (dd, J = 1.2, 10.9 Hz, 1 H), 4.67 (s, 2 H), 4.14 (q, J = 7.2 Hz, 2 H), 2.46 (s, 3 H), 1.25 (t, J = 7.2 Hz, 3 H).

^{13}C NMR (100 MHz, CDCl_3): δ = 153.8, 145.4, 137.7, 133.9, 133.2, 130.3, 130.3, 129.9, 129.1, 127.8, 127.8, 126.3, 117.6, 82.5, 68.1, 61.4, 52.7, 21.6, 14.0.

MS (EI): m/z = 383 (M^+), 228, 182, 154, 129, 117, 91.

HRMS (EI): m/z calcd for $\text{C}_{21}\text{H}_{21}\text{NO}_4\text{S}$ (M^+): 383.1191; found: 383.1194.

N-Phenylethynyl-N-(2-vinylbenzyl)-p-toluenesulfonamide (**12c**)

To a solution of **9** (239.0 mg, 0.63 mmol) in THF (8 mL) was added BuLi (0.87 mL, 1.38 mmol, 1.58 M hexane solution) at -78°C , and stirred at the same temperature for 0.5 h. To the resulting mixture was added ZnBr_2 (168.9 mg, 0.75 mmol) in THF (2 mL), and stirred at r.t. for 0.5 h to provide the crude alkynylzinc solution. This alkynylzinc solution was transferred with THF (3 mL) to the alkylpalladium complex in THF solution (5 mL), which was prepared from PhI (0.08 mL, 0.75 mmol), $\text{Pd}_2(\text{dba})_3\cdot\text{CHCl}_3$ (32.4 mg, 31.26 μmol) and PPh_3 (32.8 mg, 0.13 mmol). The resulting mixture was stirred at r.t. for 21 h. After the volatiles were removed under reduced pressure, brine was added and the aqueous phase was extracted with EtOAc. The combined organic phases were washed with brine, and dried (MgSO_4). The volatiles were removed under reduced pressure, and the residue was purified by column chromatography on silica gel (hexane/EtOAc 10:1) to provide **12c** (134.9 mg, 56%) as a pale yellow oil.

IR (neat): 2238 (s), 1598 (m), 1366 (s), 1170 (s) cm^{-1} .

^1H NMR (400 MHz, CDCl_3): δ = 7.85 (d, J = 8.2 Hz, 2 H), 7.52 (d, J = 7.7 Hz, 1 H), 7.38–7.27 (m, 5 H), 7.25–7.14 (m, 5 H), 7.07 (dd, J = 11.1, 17.4 Hz, 1 H), 5.65 (dd, J = 1.0, 17.4 Hz, 1 H), 5.33 (dd, J = 1.0, 11.1 Hz, 1 H), 4.61 (s, 2 H), 2.46 (s, 3 H).

^{13}C NMR (100 MHz, CDCl_3): δ = 144.7, 137.8, 134.0, 133.4, 130.8, 130.7, 129.7, 128.8, 128.0, 127.7, 127.6, 127.4, 126.8, 126.0, 122.7, 117.0, 82.4, 71.5, 52.8, 21.6.

MS (EI): m/z = 387 (M^+), 248, 232, 217, 155, 117, 91.

HRMS (EI): m/z calcd for $\text{C}_{24}\text{H}_{21}\text{NO}_2\text{S}$ (M^+): 387.1293; found: 387.1291.

N-(2-Allylbenzyl)-N-ethynyl-p-toluenesulfonamide (**13a**)

According to the procedure for the synthesis of **11a**, a solution of **10** (182.5 mg, 0.46 mmol) and BuLi (0.64 mL, 1.01 mmol, 1.58 M hexane solution) in THF (9 mL) was stirred at -78°C for 1 h to afford **13a** (131.5 mg, 88%) as a pale yellow oil after purification by column chromatography on silica gel (hexane/EtOAc 10:1).

IR (neat): 2132 (w), 1597 (w), 1369 (m), 1173 (s) cm^{-1} .

^1H NMR (400 MHz, CDCl_3): δ = 7.80 (d, J = 8.2 Hz, 2 H), 7.36 (d, J = 8.2 Hz, 2 H), 7.30–7.14 (m, 4 H), 5.93 (ddt, J = 10.1, 16.9, 6.0 Hz, 1 H), 5.06 (dd, J = 1.5, 10.1 Hz, 1 H), 4.96 (dd, J = 1.5, 16.9 Hz, 1 H), 4.47 (s, 2 H), 3.45 (d, J = 6.0 Hz, 2 H), 2.60 (s, 1 H), 2.47 (s, 3 H).

^{13}C NMR (100 MHz, CDCl_3): δ = 144.8, 138.7, 136.4, 133.9, 131.7, 130.3, 129.9, 129.7, 128.7, 127.6, 126.3, 116.0, 76.0, 59.7, 52.4, 36.5, 21.5.

MS (EI): m/z = 324 ($M^+ - 1$), 260, 170, 143, 131, 117, 91.

HRMS (EI): m/z calcd for $C_{19}H_{19}NO_2S$ (M^+): 325.1136; found: 325.1143.

Ethyl [(2-Allylbenzyl)-(p-toluenesulfonyl)amino]propynoate (**13b**)

According to the procedure for the synthesis of **11b**, a solution of **10** (179.5 mg, 0.45 mmol), BuLi (0.69 mL, 1.09 mmol, 1.58 M hexane solution), and ethyl chlorocarbonate (0.09 mL, 0.91 mmol) in THF (9 mL) was stirred at -10°C for 2 h to afford **13b** (142.7 mg, 79%) as a pale yellow oil after purification by column chromatography on silica gel (hexane/EtOAc 10:1).

IR (neat): 2218 (s), 1705 (s), 1597 (w), 1375 (s), 1172 (s) cm^{-1} .

^1H NMR (400 MHz, CDCl_3): δ = 7.76 (d, J = 8.2 Hz, 2 H), 7.34 (d, J = 8.2 Hz, 2 H), 7.28 (dt, J = 1.9, 7.2 Hz, 1 H), 7.25–7.14 (m, 3 H), 5.91 (ddt, J = 10.1, 16.9, 5.8 Hz, 1 H), 5.06 (dd, J = 1.5, 10.1 Hz, 1 H), 4.94 (dd, J = 1.5, 16.9 Hz, 1 H), 4.60 (s, 2 H), 4.14 (q, J = 7.2 Hz, 2 H), 3.41 (d, J = 5.8 Hz, 2 H), 2.46 (s, 3 H), 1.25 (t, J = 7.2 Hz, 3 H).

^{13}C NMR (100 MHz, CDCl_3): δ = 14.0, 21.6, 36.6, 52.5, 61.4, 68.0, 82.6, 116.2, 126.6, 127.8, 129.0, 129.9, 130.1, 130.2, 131.1, 133.9, 136.3, 138.6, 145.5, 153.9.

MS (EI): m/z = 398 ($M^+ + 1$), 242, 196, 155, 131, 117, 91.

HRMS (EI): m/z calcd for $C_{22}H_{23}NO_4S$ (M^+): 397.1348; found: 397.1344.

N-(2,2-Dichlorovinyl)-N-hex-5-enyl-p-toluenesulfonamide (**16**)

To a solution of **14** (2.99 g, 15.00 mmol), **15** (2.5 mL, 20.41 mmol), and PPh_3 (5.51 g, 21.01 mmol) in THF (30 mL) was added DEAD (8.9 mL, 19.51 mmol) at 0°C , and the mixture was stirred at r.t. for 4 h. The volatiles were removed under reduced pressure, and the residue passed through a short column of silica gel (eluent: hexane/EtOAc 5:1) to provide the crude alkylated formyltosylamide. To a solution of this crude product and PPh_3 (9.84 g, 37.50 mmol) in THF (30 mL) was added CCl_4 (12 mL, 123.00 mmol) in THF (10 mL) at 60°C over 3 h, and the resulting mixture was stirred at the same temperature for 12 h. Sat. aq NaHCO_3 was added after cooling to r.t., and the aqueous phase was extracted with Et_2O . The combined organic phases were washed with brine, and dried (MgSO_4). The volatiles were removed under reduced pressure, and the residue was purified by column chromatography on silica gel (hexane/EtOAc 10:1) to provide **16** (2.91 g, 56%) as a white solid; mp 90°C .

IR (KBr): 1599 (w), 1356 (s), 1165 (s) cm^{-1} .

^1H NMR (400 MHz, CDCl_3): δ = 7.69 (d, J = 8.2 Hz, 2 H), 7.33 (d, J = 8.2 Hz, 2 H), 6.28 (s, 1 H), 5.76 (ddt, J = 10.2, 16.9, 6.8 Hz, 1 H), 5.02–4.94 (m, 2 H), 3.33 (t, J = 7.2 Hz, 2 H), 2.44 (s, 3 H), 2.05 (dt, J = 6.8, 7.2 Hz, 2 H), 1.56–1.48 (m, 2 H), 1.42–1.36 (m, 2 H).

^{13}C NMR (100 MHz, CDCl_3): δ = 144.1, 138.1, 135.5, 129.8, 127.2, 124.9, 124.3, 114.9, 48.9, 33.1, 27.8, 25.7, 21.6.

MS (EI): m/z = 347 (M^+), 264, 251, 192, 155, 91.

HRMS (EI): m/z calcd for $C_{15}H_{19}^{35}\text{Cl}_2\text{NO}_2\text{S}$ (M^+): 347.0514; found: 347.0522.

N-Ethynyl-N-hex-5-enyl-p-toluenesulfonamide (**17a**)

According to the procedure for the synthesis of **11a**, a solution of **16** (206.2 mg, 0.59 mmol) and BuLi (0.82 mL, 1.30 mmol, 1.58 M hexane solution) in THF (10 mL) was stirred at -78°C for 1 h to afford **17a** (140.0 mg, 85%) as a white solid after purification by column chromatography on silica gel (hexane/EtOAc 10:1); mp 43°C .

IR (KBr): 2133 (m), 1598 (w), 1359 (s), 1169 (s) cm^{-1} .

^1H NMR (400 MHz, CDCl_3): δ = 7.80 (d, J = 8.2 Hz, 2 H), 7.35 (d, J = 8.2 Hz, 2 H), 5.75 (ddt, J = 10.1, 16.9, 6.3 Hz, 1 H), 5.02–4.93 (m, 2 H), 3.31 (t, J = 7.3 Hz, 2 H), 2.73 (s, 1 H), 2.45 (s, 3 H), 2.05 (dt, J = 6.3, 7.3 Hz, 2 H), 1.66 (tt, J = 7.3, 7.7 Hz, 2 H), 1.41 (tt, J = 7.3, 7.7 Hz, 2 H).

^{13}C NMR (100 MHz, CDCl_3): δ = 144.6, 138.0, 134.4, 129.7, 127.5, 114.8, 75.9, 59.0, 50.8, 32.9, 26.9, 25.2, 21.5.

MS (EI): m/z = 276 ($M^+ - 1$), 212, 155, 122, 91.

HRMS (EI): m/z calcd for $C_{15}H_{19}O_2\text{NS}$ (M^+): 277.1136; found: 277.1122.

Ethyl [Hex-5-enyl-(p-toluenesulfonyl)amino]propynoate (**17b**)

According to the procedure for the synthesis of **11b**, a solution of **16** (313.0 mg, 0.90 mmol), BuLi (1.3 mL, 2.16 mmol, 1.63 M hexane solution), and ethyl chlorocarbonate (0.17 mL, 1.80 mmol) in THF (18 mL) was stirred at -20°C for 1.5 h to afford **17b** (223.3 mg, 71%) as a colorless oil after purification by column chromatography on silica gel (hexane/ Et_2O 3:1).

IR (neat): 2219 (s), 1705 (s), 1597 (w), 1376 (s), 1174 (s) cm^{-1} .

^1H NMR (400 MHz, CDCl_3): δ = 7.82 (d, J = 8.2 Hz, 2 H), 7.38 (d, J = 8.2 Hz, 2 H), 5.73 (ddt, J = 10.1, 16.9, 6.3 Hz, 1 H), 5.02–4.93 (m, 2 H), 4.23 (q, J = 7.2 Hz, 2 H), 3.42 (t, J = 7.3 Hz, 2 H), 2.46 (s, 3 H), 2.08–2.01 (m, 2 H), 1.72–1.63 (m, 2 H), 1.42–1.33 (m, 2 H), 1.31 (t, J = 7.2 Hz, 3 H).

^{13}C NMR (100 MHz, CDCl_3): δ = 154.2, 145.4, 137.8, 134.2, 130.0, 127.7, 115.1, 82.4, 67.7, 61.5, 51.2, 32.9, 27.3, 25.2, 21.7, 14.1.

MS (EI): m/z = 348 ($M^+ - 1$), 304, 194, 166, 148, 91.

HRMS (EI): m/z calcd for $C_{18}H_{23}O_4\text{NS}$ (M^+): 349.1348; found: 349.1339.

N-[2-(N-Allyl-N-p-toluenesulfonylamino)phenyl]-N-ethynyl-p-toluenesulfonamide (**21a**)

To a solution of **21d** (243.1 mg, 0.44 mmol) in THF (4 mL) was added TBAF (1.3 mL, 1.32 mmol, 1 M THF solution) at 0°C , and stirred at the same temperature for 5 min. Sat. aq NH_4Cl was added, and the aqueous phase was extracted with EtOAc. The combined organic phases were washed with brine and dried (MgSO_4). The volatiles were removed under reduced pressure, and the residue was purified by column chromatography on silica gel (hexane/EtOAc 2:1) to provide **21a** (194.1 mg, 92%) as a white solid; mp 146°C .

IR (KBr): 2130 (w), 1596 (m), 1372 (m), 1165 (s) cm^{-1} .

^1H NMR (400 MHz, CDCl_3): δ = 7.85 (d, J = 8.2 Hz, 2 H), 7.84 (d, J = 7.7 Hz, 2 H), 7.41–7.25 (m, 6 H), 7.20 (dd, J = 1.5, 7.7 Hz, 1 H), 6.99 (dd, J = 1.5, 7.7 Hz, 1 H), 5.95 (ddt, J = 10.1, 16.9, 6.8 Hz, 1 H), 5.09–5.02 (m, 2 H), 4.22 (d, J = 6.8 Hz, 2 H), 2.72 (s, 1 H), 2.49 (s, 3 H), 2.45 (s, 3 H).

^{13}C NMR (100 MHz, CDCl_3): δ = 145.3, 143.8, 138.3, 137.6, 136.1, 133.5, 133.2, 131.4, 129.8, 129.6, 129.5, 129.1, 129.0, 128.7, 128.5, 119.3, 77.2, 58.1, 54.4, 21.8, 21.6.

MS (EI): m/z = 480 (M^+), 325, 262, 171, 139, 91.

HRMS (EI): m/z calcd for $C_{25}H_{24}N_2O_4\text{S}_2$ (M^+): 480.1177; found: 480.1180.

Ethyl [2-(Allyl-p-toluenesulfonylamino)phenyl]-p-toluenesulfonylamino]propynoate (**21b**)

To a solution of **21a** (305.9 mg, 0.64 mmol) in THF (13 mL) was added BuLi (0.42 mL, 0.70 mmol, 1.65 M hexane solution) at -78°C , and stirred at the same temperature for 0.5 h. To the resulting mixture was added ethyl chlorocarbonate (0.07 mL, 0.76 mmol), and warmed to -15°C for 1.5 h. Sat. aq NH_4Cl solution was added, and the aqueous phase was extracted with EtOAc. The combined organic phases were

washed with brine and dried (MgSO₄). The volatiles were removed under reduced pressure, and the residue was purified by column chromatography on silica gel (hexane/Et₂O Ac 2:1) to provide **21b** (252.2 mg, 72%) as a white solid; mp 48 °C.

IR (KBr): 2221 (s), 1706 (s), 1597 (w), 1374 (m), 1176 (s) cm⁻¹.

¹H NMR (400 MHz, CDCl₃): δ = 7.90 (d, *J* = 8.7 Hz, 2 H), 7.74 (d, *J* = 8.2 Hz, 2 H), 7.41 (d, *J* = 8.7 Hz, 2 H), 7.30 (d, *J* = 8.2 Hz, 2 H), 7.39–7.28 (m, 2 H), 7.13 (dd, *J* = 1.5, 7.7 Hz, 1 H), 7.05 (dd, *J* = 1.9, 7.7 Hz, 1 H), 5.93 (ddt, *J* = 9.7, 16.9, 7.2 Hz, 1 H), 5.09–5.02 (m, 2 H), 4.21–4.15 (m, 4 H), 2.49 (s, 3 H), 2.44 (s, 3 H), 1.26 (t, *J* = 7.2 Hz, 3 H).

¹³C NMR (100 MHz, CDCl₃): δ = 153.9, 146.0, 143.9, 137.8, 136.6, 135.6, 133.0, 132.9, 131.3, 130.0, 129.8, 129.5, 129.2, 129.2, 128.6, 128.6, 119.6, 83.1, 66.5, 61.5, 54.6, 21.8, 21.6, 14.1.

MS (EI): *m/z* = 552 (M⁺), 507, 397, 334, 259, 243, 169, 139, 91.

HRMS (EI): *m/z* calcd for C₂₈H₂₈N₂O₆S₂ (M⁺): 552.1389; found: 552.1385.

***N*-[2-(*N*-Allyl-*N*-*p*-toluenesulfonylamino)phenyl]-*N*-(2-phenylethynyl)-*p*-toluenesulfonamide (21c)**

To a mixture of Pd(PPh₃)₄ (13.4 mg, 11.59 μmol), CuI (2.2 mg, 11.59 μmol), and PhI (0.05 mL, 0.46 mmol) in Et₃N (2 mL) and benzene (1 mL) was added **21a** (111.4 mg, 0.23 mmol) at r.t., and the mixture was stirred at the same temperature for 48 h. The volatiles were removed under reduced pressure, and the residue was purified by column chromatography on silica gel (hexane/EtOAc, 2:1) to provide **21c** (126.4 mg, 98%) as a white solid; mp 53 °C.

IR (KBr): 2241 (w), 1597 (w), 1356 (m), 1168 (s) cm⁻¹.

¹H NMR (400 MHz, CDCl₃): δ = 7.92–7.86 (m, 4 H), 7.41–7.24 (m, 12 H), 7.05 (d, *J* = 8.3 Hz, 1 H), 5.97 (ddt, *J* = 9.8, 16.6, 6.8 Hz, 1 H), 5.10–5.02 (m, 2 H), 4.27 (d, *J* = 6.8 Hz, 2 H), 2.49 (s, 3 H), 2.38 (s, 3 H).

¹³C NMR (100 MHz, CDCl₃): δ = 145.2, 143.7, 138.1, 138.0, 136.5, 133.8, 133.3, 131.9, 131.4, 129.6, 129.6, 129.5, 129.1, 128.9, 128.7, 128.6, 128.2, 127.8, 122.7, 119.4, 83.8, 69.8, 54.4, 21.7, 21.6.

MS (EI): *m/z* = 556 (M⁺), 456, 417, 401, 301, 245, 139, 119, 91.

HRMS (EI): *m/z* calcd for C₃₁H₂₈O₄N₂S₂ (M⁺): 556.1490; found: 556.1497.

***N*-[2-(*N*-Allyl-*N*-*p*-toluenesulfonylamino)phenyl]-*N*-(2-trimethylsilyl)ethynyl)-*p*-toluenesulfonamide (21d)**

To a solution of **19** (811.2 mg, 1.78 mmol) in THF (27 mL) was added BuLi (1.3 mL, 1.95 mmol, 1.55 M hexane solution) at –78 °C, and stirred at the same temperature for 1 h. To the resulting mixture was added phenyl(trimethylsilyl)ethynyl)iodonium triflate (960.0 mg, 2.13 mmol). The mixture was warmed to r.t. over 1 h, and stirred at the same temperature for 18 h. Sat. aq. NH₄Cl was added, and the aqueous phase was extracted with EtOAc. The combined organic phases were washed with brine and dried (MgSO₄). The volatiles were removed under reduced pressure, and the residue was purified by column chromatography on silica gel (hexane/EtOAc 2:1) to provide **21d** (595.4 mg, 61%) as a white solid; mp 35–36 °C.

IR (KBr): 2165 (m), 1597 (w), 1359 (m), 1173 (s) cm⁻¹.

¹H NMR (400 MHz, CDCl₃): δ = 7.94 (d, *J* = 8.3 Hz, 2 H), 7.83 (d, *J* = 8.3 Hz, 2 H), 7.39–7.24 (m, 7 H), 7.01 (dd, *J* = 1.0, 7.3 Hz, 1 H), 5.93 (ddt, *J* = 9.8, 16.6, 6.8 Hz, 1 H), 5.05–4.99 (m, 2 H), 4.17 (d, *J* = 6.8 Hz, 2 H), 2.49 (s, 3 H), 2.45 (s, 3 H), 0.12 (s, 9 H).

¹³C NMR (100 MHz, CDCl₃): δ = 145.1, 143.7, 137.9, 137.4, 136.4, 133.6, 133.2, 131.7, 129.5, 129.4, 129.4, 129.1, 129.0, 128.9, 128.4, 119.4, 95.9, 72.6, 54.1, 21.7, 21.6, –0.1.

MS (EI): *m/z* = 552 (M⁺), 537, 397, 241, 169, 91.

HRMS (EI): *m/z* calcd for C₂₈H₃₂N₂O₄S₂Si (M⁺): 552.1573; found: 552.1567.

***N*-(2,2-Dichlorovinyl)-*N*-hept-6-enyl-*p*-toluenesulfonamide (26)**

To a solution of **14** (3.00 g, 15.06 mmol), **23** (2.7 mL, 20.33 mmol), and PPh₃ (5.53 g, 21.08 mmol) in THF (30 mL) was added DEAD (8.9 mL, 19.58 mmol) at 0 °C, and the mixture was stirred at r.t. for 4 h. The volatiles were removed under reduced pressure, and the residue was passed through a short column of silica gel (eluent: hexane/EtOAc 5:1) to provide the crude alkylated formyltosylamide. To a solution of this crude product and PPh₃ (9.87 g, 37.64 mmol) in THF (30 mL) was added CCl₄ (12 mL, 123.48 mmol) in THF (10 mL) at 60 °C for 3 h, and the resulting mixture was stirred at the same temperature for 7 h. Sat. aq. NaHCO₃ was added after cooling to r.t., and the aqueous phase was extracted with Et₂O. The combined organic phases were washed with brine and dried (MgSO₄). The volatiles were removed under reduced pressure, and the residue was purified by column chromatography on silica gel (hexane/Et₂O 10:1) to provide **26** (2.59 g, 48%) as a white solid; mp 69 °C.

IR (KBr): 1599 (w), 1354 (s), 1165 (s) cm⁻¹.

¹H NMR (400 MHz, CDCl₃): δ = 7.69 (d, *J* = 8.5 Hz, 2 H), 7.33 (d, *J* = 8.5 Hz, 2 H), 6.27 (s, 1 H), 5.78 (ddt, *J* = 10.1, 16.9, 6.8 Hz, 1 H), 5.02–4.92 (m, 2 H), 3.31 (t, *J* = 7.5 Hz, 2 H), 2.44 (s, 3 H), 2.03 (dt, *J* = 6.8, 7.2 Hz, 2 H), 1.56–1.47 (m, 2 H), 1.42–1.26 (m, 4 H).

¹³C NMR (100 MHz, CDCl₃): δ = 144.1, 138.6, 135.5, 129.8, 127.2, 124.9, 124.3, 114.6, 49.0, 33.5, 28.3, 28.2, 26.0, 21.6.

MS (EI): *m/z* = 361 (M⁺), 278, 265, 206, 155, 91.

HRMS (EI): *m/z* calcd for C₁₆H₂₁³⁵Cl₂NO₂S (M⁺): 361.0607; found: 361.0667.

***N*-[4,4-Bis(benzyloxymethyl)hept-6-enyl]-*N*-(2,2-dichlorovinyl)-*p*-toluenesulfonamide (27)**

According to the procedure for the synthesis of **26**, a solution of **14** (0.799 g, 4.01 mmol), **24** (1.09 g, 3.09 mmol), PPh₃ (1.01 g, 3.86 mmol), and DEAD (1.7 mL, 3.70 mmol) in THF (6 mL) was stirred at r.t. for 1 h and then a solution of the crude product obtained, an additional amount of PPh₃ (2.02 g, 7.72 mmol), and CCl₄ (2.4 mL, 25.31 mmol) in THF (9 mL) were stirred at 60 °C for 24 h to afford **27** (811.2 mg, 44%) as a colorless oil after purification by column chromatography on silica gel (hexane/EtOAc 10:1).

IR (neat): 1639 (w), 1598 (w), 1360 (s), 1167 (s) cm⁻¹.

¹H NMR (400 MHz, CDCl₃): δ = 7.66 (d, *J* = 8.7 Hz, 2 H), 7.36–7.25 (m, 12 H), 6.29 (s, 1 H), 5.77–5.65 (m, 1 H), 5.04–4.98 (m, 2 H), 4.45 (s, 4 H), 3.30–3.23 (m, 6 H), 2.42 (s, 3 H), 2.07 (d, *J* = 7.7 Hz, 2 H), 1.54–1.44 (m, 2 H), 1.28–1.22 (m, 2 H).

¹³C NMR (100 MHz, CDCl₃): δ = 143.9, 138.6, 135.3, 133.9, 129.7, 128.1, 128.1, 127.2, 127.0, 124.8, 123.0, 117.5, 73.0, 72.4, 49.5, 41.2, 36.4, 28.9, 22.0, 21.4.

MS (EI): *m/z* = 601 (M⁺), 510, 446, 355, 340, 249, 155, 91.

HRMS (EI): *m/z* calcd for C₃₂H₃₇³⁵Cl₂NO₄S (M⁺): 601.1820; found: 601.1814.

***N*-[3-(5-Allyl-2,2-dimethyl[1,3]dioxan-5-yl)-propyl]-*N*-(2,2-dichlorovinyl)-*p*-toluenesulfonamide (28)**

According to the procedure for the synthesis of **26**, a solution of **14** (784.3 mg, 3.94 mmol), **25** (703.0 mg, 3.28 mmol), PPh₃ (1.205 g, 4.59 mmol), and DEAD (1.9 mL, 4.26 mmol) in THF (15 mL) was stirred at

r.t. for 4 h and then a solution of the crude product obtained, an additional amount of PPh_3 (2.15 g, 8.20 mmol), and CCl_4 (2.6 mL, 26.90 mmol) in THF (15 mL) were stirred at 60 °C for 17 h to afford **28** (707.1 mg, 47%) as a white solid after purification by column chromatography on silica gel (hexane/EtOAc 5:1); 54 °C.

IR (KBr): 1598 (w), 1354 (s), 1167 (s) cm^{-1} .

^1H NMR (400 MHz, CDCl_3): δ = 7.68 (d, J = 8.2 Hz, 2 H), 7.33 (d, J = 8.2 Hz, 2 H), 6.31 (s, 1 H), 5.70 (ddt, J = 10.1, 17.9, 7.2 Hz, 1 H), 5.12–5.05 (m, 2 H), 3.56 (d, J = 11.6 Hz, 2 H), 3.50 (d, J = 11.6 Hz, 2 H), 3.31 (t, J = 7.2 Hz, 2 H), 2.44 (s, 3 H), 2.11 (d, J = 7.2 Hz, 2 H), 1.53–1.43 (m, 2 H), 1.40 (s, 3 H), 1.39 (s, 3 H), 1.34–1.28 (m, 2 H).

^{13}C NMR (100 MHz, CDCl_3): δ = 144.2, 135.5, 133.0, 129.9, 127.3, 124.8, 123.9, 118.4, 98.1, 67.5, 49.6, 36.6, 35.0, 29.2, 23.9, 23.6, 21.9, 21.6.

MS (EI): m/z = 461 (M^+), 446, 306, 277, 248, 155, 91.

HRMS (EI): m/z calcd for $\text{C}_{21}\text{H}_{29}^{35}\text{Cl}_2\text{NO}_4\text{S}$ (M^+): 461.1194; found: 461.1175.

N-Ethynyl-N-hept-6-enyl-*p*-toluenesulfonamide (29a)

According to the procedure for the synthesis of **11a**, a solution of **26** (235.7 mg, 0.65 mmol) and BuLi (0.88 mL, 1.43 mmol, 1.63 M hexane solution) in THF (13 mL) was stirred at –78 °C for 20 min to afford **29a** (158.8 mg, 84%) as a pale yellow oil after purification by column chromatography on silica gel (hexane/EtOAc 10:1).

IR (neat): 2133 (m), 1597 (w), 1366 (s), 1169 (s) cm^{-1} .

^1H NMR (400 MHz, CDCl_3): δ = 7.80 (d, J = 8.2 Hz, 2 H), 7.35 (d, J = 8.2 Hz, 2 H), 5.78 (ddt, J = 10.1, 16.9, 6.8 Hz, 1 H), 5.02–4.91 (m, 2 H), 3.29 (t, J = 7.3 Hz, 2 H), 2.73 (s, 1 H), 2.45 (s, 3 H), 2.02 (dt, J = 6.8, 7.2 Hz, 2 H), 1.69–1.60 (m, 2 H), 1.42–1.27 (m, 4 H).

^{13}C NMR (100 MHz, CDCl_3): δ = 144.6, 138.5, 134.5, 129.7, 127.5, 114.5, 75.9, 59.0, 51.0, 33.4, 28.2, 27.4, 25.5, 21.6.

MS (EI): m/z = 290 ($\text{M}^+ - 1$), 227, 155, 136, 91.

HRMS (EI): m/z calcd for $\text{C}_{16}\text{H}_{21}\text{NO}_2\text{S}$ (M^+): 291.1293; found: 291.1298.

Ethyl [Hept-6-enyl-(*p*-toluenesulfonyl)amino]propynoate (29b)

According to the procedure for the synthesis of **11b**, a solution of **26** (287.3 mg, 0.79 mmol), BuLi (1.1 mL, 1.74 mmol, 1.63 M hexane solution), and ethyl chlorocarbonate (0.11 mL, 1.19 mmol) in THF (16 mL) was stirred at –30 °C for 1 h to afford **29b** (228.6 mg, 79%) as a pale yellow oil after purification by column chromatography on silica gel (hexane/EtOAc 10:1).

IR (neat): 2218 (s), 1705 (s), 1597 (w), 1376 (s), 1174 (s) cm^{-1} .

^1H NMR (400 MHz, CDCl_3): δ = 7.82 (d, J = 8.2 Hz, 2 H), 7.37 (d, J = 8.2 Hz, 2 H), 5.76 (ddt, J = 10.1, 16.9, 6.8 Hz, 1 H), 5.02–4.91 (m, 2 H), 4.23 (q, J = 7.2 Hz, 2 H), 3.41 (t, J = 7.3 Hz, 2 H), 2.46 (s, 3 H), 2.05–1.98 (m, 2 H), 1.71–1.62 (m, 2 H), 1.31 (t, J = 7.2 Hz, 3 H), 1.42–1.24 (m, 4 H).

^{13}C NMR (100 MHz, CDCl_3): δ = 154.0, 145.4, 138.3, 134.1, 129.9, 127.5, 114.5, 82.3, 67.6, 61.4, 51.2, 33.3, 28.0, 27.6, 25.3, 21.5, 14.0.

MS (EI): m/z = 363 (M^+), 318, 208, 162, 155, 91.

HRMS (EI): m/z calcd for $\text{C}_{19}\text{H}_{25}\text{NO}_4\text{S}$ (M^+): 363.1504; found: 363.1489.

N-[4,4-Bis(benzyloxymethyl)hept-6-enyl]-N-ethynyl-*p*-toluenesulfonamide (30a)

According to the procedure for the synthesis of **11a**, a solution of **27** (305.5 mg, 0.51 mmol) and BuLi (0.68 mL, 1.12 mmol, 1.63 M hexane

solution) in THF (10 mL) was stirred at –78 °C for 10 min to afford **30a** (237.3 mg, 88%) as a pale yellow oil after purification by column chromatography on silica gel (hexane/EtOAc 10:1).

IR (neat): 2135 (m), 1639 (w), 1597 (w), 1367 (s), 1169 (s) cm^{-1} .

^1H NMR (400 MHz, CDCl_3): δ = 7.77 (d, J = 8.2 Hz, 2 H), 7.35–7.25 (m, 12 H), 5.71 (m, 1 H), 5.04–4.97 (m, 2 H), 4.44 (s, 4 H), 3.28–3.21 (m, 6 H), 2.68 (s, 1 H), 2.42 (s, 3 H), 2.06 (d, J = 7.7 Hz, 2 H), 1.68–1.58 (m, 2 H), 1.30–1.23 (m, 2 H).

^{13}C NMR (100 MHz, CDCl_3): δ = 144.5, 138.6, 134.4, 133.9, 129.6, 128.1, 127.4, 127.2, 127.2, 117.6, 75.9, 73.0, 72.4, 59.0, 51.7, 41.3, 36.3, 28.5, 21.4, 21.4.

MS (EI): m/z = 530 ($\text{M}^+ - 1$), 440, 376, 270, 91.

HRMS (EI): m/z calcd for $\text{C}_{32}\text{H}_{37}\text{O}_4\text{NS}$ (M^+): 531.2443; found: 531.2467.

Ethyl [[4,4-Bis(benzyloxymethyl)hept-6-enyl](*p*-toluenesulfonyl)amino]propynoate (30b)

According to the procedure for the synthesis of **11b**, a solution of **27** (444.4 mg, 0.74 mmol), BuLi (1.0 mL, 1.62 mmol, 1.63 M hexane solution), and ethyl chlorocarbonate (0.08 mL, 0.88 mmol) in THF (15 mL) was stirred at –30 °C for 1 h to afford **30b** (302.7 mg, 68%) as a pale yellow oil after purification by column chromatography on silica gel (hexane/EtOAc 5:1).

IR (neat): 2218 (s), 1704 (s), 1598 (w), 1376 (s), 1174 (s) cm^{-1} .

^1H NMR (400 MHz, CDCl_3): δ = 7.78 (d, J = 8.7 Hz, 2 H), 7.35–7.25 (m, 12 H), 5.68 (m, 1 H), 5.04–4.97 (m, 2 H), 4.44 (s, 4 H), 4.19 (q, J = 7.3 Hz, 2 H), 3.35 (t, J = 7.3 Hz, 2 H), 3.25 (s, 2 H), 3.24 (s, 2 H), 2.43 (s, 3 H), 2.05 (d, J = 6.8 Hz, 2 H), 1.68–1.59 (m, 2 H), 1.27 (t, J = 7.3 Hz, 3 H), 1.26–1.20 (m, 2 H).

^{13}C NMR (100 MHz, CDCl_3): δ = 153.9, 145.2, 138.5, 134.0, 133.7, 129.8, 128.1, 127.5, 127.2, 127.2, 117.6, 82.3, 73.0, 72.2, 67.7, 61.3, 51.9, 41.2, 36.3, 28.5, 21.7, 21.5, 14.0.

MS (EI): m/z = 603 (M^+), 448, 342, 155, 91.

HRMS (EI): m/z calcd for $\text{C}_{35}\text{H}_{41}\text{NO}_6\text{S}$ (M^+): 603.2655; found: 603.2673.

N-[3-(5-Allyl-2,2-dimethyl[1,3]dioxan-5-yl)propyl]-N-ethynyl-*p*-toluenesulfonamide (31a)

According to the procedure for the synthesis of **11a**, a solution of **28** (225.5 mg, 0.49 mmol) and BuLi (0.69 mL, 1.07 mmol, 1.55 M hexane solution) in THF (10 mL) was stirred at –78 °C for 0.5 h to afford **31a** (161.8 mg, 85%) as a pale yellow oil after purification by column chromatography on silica gel (hexane/EtOAc 3:1).

IR (neat): 2134 (m), 1597 (w), 1372 (s), 1170 (s) cm^{-1} .

^1H NMR (400 MHz, CDCl_3): δ = 7.80 (d, J = 8.2 Hz, 2 H), 7.35 (d, J = 8.2 Hz, 2 H), 5.70 (ddt, J = 11.6, 16.9, 7.7 Hz, 1 H), 5.11–5.05 (m, 2 H), 3.55 (d, J = 11.6 Hz, 2 H), 3.50 (d, J = 11.6 Hz, 2 H), 3.29 (t, J = 7.0 Hz, 2 H), 2.75 (s, 1 H), 2.45 (s, 3 H), 2.12 (d, J = 7.7 Hz, 2 H), 1.66–1.54 (m, 2 H), 1.40 (s, 3 H), 1.38 (s, 3 H), 1.33–1.25 (m, 2 H).

^{13}C NMR (100 MHz, CDCl_3): δ = 144.8, 134.5, 132.9, 129.8, 127.6, 118.4, 98.1, 75.8, 67.4, 59.3, 51.6, 36.4, 35.0, 28.9, 24.1, 23.4, 21.6, 21.1.

MS (EI): m/z = 390 ($\text{M}^+ - 1$), 376, 304, 236, 178, 91.

HRMS (EI): m/z calcd for $\text{C}_{21}\text{H}_{29}\text{NO}_4\text{S}$ (M^+): 391.1817; found: 391.1815.

Ethyl [3-(5-Allyl-2,2-dimethyl[1,3]dioxan-5-yl)propyl]-(*p*-toluenesulfonyl)amino}propynoate (31b**)**

According to the procedure for the synthesis of **11b**, a solution of **28** (212.8 mg, 0.46 mmol), BuLi (0.65 mL, 1.01 mmol, 1.55 M hexane solution), and ethyl chlorocarbonate (0.05 mL, 0.55 mmol) in THF (9 mL) was stirred at -30°C for 1 h to afford **31b** (203.3 mg, 95%) as a pale yellow oil after purification by column chromatography on silica gel (hexane/EtOAc 3:1).

IR (neat): 2218 (s), 1705 (s), 1598 (w), 1374 (s), 1175 (s) cm^{-1} .

^1H NMR (400 MHz, CDCl_3): δ = 7.82 (d, J = 8.2 Hz, 2 H), 7.37 (d, J = 8.2 Hz, 2 H), 5.67 (m, 1 H), 5.12–5.05 (m, 2 H), 4.22 (q, J = 7.2 Hz, 2 H), 3.55 (d, J = 11.6 Hz, 2 H), 3.48 (d, J = 11.6 Hz, 2 H), 3.40 (t, J = 7.0 Hz, 2 H), 2.46 (s, 3 H), 2.10 (d, J = 7.3 Hz, 2 H), 1.68–1.59 (m, 2 H), 1.39 (s, 3 H), 1.38 (s, 3 H), 1.30 (t, J = 7.2 Hz, 3 H), 1.30–1.24 (m, 2 H).

^{13}C NMR (100 MHz, CDCl_3): δ = 154.1, 145.6, 134.2, 132.7, 130.1, 127.8, 118.5, 98.1, 82.1, 67.9, 67.4, 61.6, 51.8, 36.5, 35.0, 28.8, 23.8, 23.7, 21.7, 21.5, 14.2.

MS (EI): m/z = 462 ($M^+ - 1$), 448, 308, 250, 220, 155, 91.

HRMS (EI): m/z calcd for $\text{C}_{24}\text{H}_{33}\text{NO}_6\text{S}$ (M^+): 463.2029; found: 463.2026.

***N*-Allyl-*N*-(3-hydroxypropyl)-*p*-toluenesulfonamide (**34**)**

To a solution of **32** (1.81 g, 8.57 mmol), **33** (1.63 g, 8.57 mmol), and PPh_3 (2.81 g, 10.71 mmol) in THF (20 mL) was added DEAD (4.7 mL, 10.29 mmol) at 0°C , and the mixture was stirred at r.t. for 2 h. The volatiles were removed under reduced pressure, and the residue was purified by column chromatography on silica gel (hexane/EtOAc 5:1) to provide *N*-allyl-*N*-[3-(*tert*-butyldimethylsilyloxy)propyl]-*p*-toluenesulfonamide (2.10 g, 64%) as a pale yellow oil.

IR (neat): 1644 (w), 1599 (m), 1345 (s), 1162 (s) cm^{-1} .

^1H NMR (400 MHz, CDCl_3): δ = 7.70 (d, J = 8.3 Hz, 2 H), 7.29 (d, J = 8.3 Hz, 2 H), 5.65 (ddt, J = 10.2, 16.6, 6.3 Hz, 1 H), 5.20–5.10 (m, 2 H), 3.81 (d, J = 6.3 Hz, 2 H), 3.58 (dd, J = 5.9, 6.3 Hz, 2 H), 3.23–3.18 (m, 2 H), 2.42 (s, 3 H), 1.76–1.68 (m, 2 H), 0.87 (s, 9 H), 0.02 (s, 6 H).

^{13}C NMR (100 MHz, CDCl_3): δ = 142.9, 136.9, 133.1, 129.4, 127.0, 118.5, 60.1, 50.7, 44.4, 31.4, 25.7, 21.3, 18.0, -5.6 .

MS (EI): m/z = 382 ($M^+ - 1$), 368, 326, 228, 91.

HRMS (EI): m/z calcd for $\text{C}_{19}\text{H}_{33}\text{NO}_3\text{SSi}$ (M^+): 383.1950; found: 383.1946.

To a solution of the above coupling product (665.1 mg, 1.73 mmol) in THF (3.5 mL) was added TBAF (5.2 mL, 5.20 mmol, 1 M THF solution) at 0°C , and the resulting mixture was stirred at r.t. for 40 min. Sat. aq. NH_4Cl was added, and the aqueous phase was extracted with EtOAc. The combined organic phases were washed with brine and dried (MgSO_4). The volatiles were removed under reduced pressure, and the residue was purified by column chromatography on silica gel (hexane/EtOAc 1:1) to provide **34** (463.5 mg, 99%) as a colorless oil.

IR (neat): 3534 (m), 1644 (w), 1598 (m), 1337 (s), 1159 (s) cm^{-1} .

^1H NMR (400 MHz, CDCl_3): δ = 7.70 (d, J = 8.2 Hz, 2 H), 7.31 (d, J = 8.2 Hz, 2 H), 5.62 (ddt, J = 10.1, 16.4, 6.3 Hz, 1 H), 5.20–5.11 (m, 2 H), 3.82 (d, J = 6.3 Hz, 2 H), 3.74 (dd, J = 5.3, 5.8 Hz, 2 H), 3.25 (dd, J = 6.3, 6.8 Hz, 2 H), 2.44 (s, 3 H), 2.35 (br, 1 H), 1.76–1.69 (m, 2 H).

^{13}C NMR (100 MHz, CDCl_3): δ = 143.2, 136.3, 132.8, 129.6, 126.8, 118.8, 58.6, 50.8, 43.9, 30.6, 21.3.

MS (EI): m/z = 269 (M^+), 224, 155, 114, 91.

HRMS (EI): m/z calcd for $\text{C}_{13}\text{H}_{19}\text{NO}_3\text{S}$ (M^+): 269.1086; found: 269.1104.

***N*-[3-(*N*-Allyl-*N*-*p*-toluenesulfonyl)aminopropyl]-*N*-*tert*-butoxy-carbonyl-*p*-toluenesulfonamide (**36**)**

To a solution of **34** (304.5 mg, 1.13 mmol), **35** (337.4 mg, 1.24 mmol), and PPh_3 (370.6 mg, 1.41 mmol) in THF (6 mL) was added DEAD (0.62 mL, 1.36 mmol) at 0°C , and the mixture was stirred at r.t. for 20 min. The volatiles were removed under reduced pressure, and the residue was purified by column chromatography on silica gel (hexane/EtOAc 3:1) to provide **36** (590.9 mg, quant) as a colorless oil.

IR (neat): 1728 (s), 1644 (w), 1598 (m), 1350 (s), 1157 (s) cm^{-1} .

^1H NMR (400 MHz, CDCl_3): δ = 7.77 (d, J = 8.2 Hz, 2 H), 7.70 (d, J = 8.2 Hz, 2 H), 7.33–7.28 (m, 4 H), 5.63 (ddt, J = 10.1, 16.9, 6.3 Hz, 1 H), 5.20 (d, J = 16.9 Hz, 1 H), 5.15 (d, J = 10.1 Hz, 1 H), 3.85 (d, J = 6.3 Hz, 2 H), 3.83 (t, J = 7.2 Hz, 2 H), 3.22 (t, J = 7.2 Hz, 2 H), 2.44 (s, 3 H), 2.42 (s, 3 H), 2.05–1.96 (m, 2 H), 1.34 (s, 9 H).

^{13}C NMR (100 MHz, CDCl_3): δ = 150.7, 144.1, 143.2, 137.1, 136.7, 132.7, 129.6, 129.2, 127.6, 127.0, 119.2, 84.2, 50.4, 44.8, 44.6, 28.6, 27.7, 21.5, 21.4.

MS (EI): m/z = 522 (M^+), 465, 449, 421, 267, 224, 155, 91.

HRMS (EI): m/z calcd for $\text{C}_{25}\text{H}_{34}\text{N}_2\text{O}_6\text{S}_2$ (M^+): 522.1858; found: 522.1843.

***N*-[2-(*N*-Allyl-*N*-*p*-toluenesulfonyl)aminobenzyl]-*N*-*tert*-butoxy-carbonyl-*p*-toluenesulfonamide (**39**)**

To a solution of **38** (2.97 g, 9.36 mmol), **35** (2.79 g, 10.29 mmol), and PPh_3 (3.07 mg, 11.70 mmol) in THF (50 mL) was added DEAD (5.1 mL, 11.23 mmol) at 0°C , and the mixture was stirred at r.t. for 0.5 h. The volatiles were removed under reduced pressure, and the residue was purified by column chromatography on silica gel (hexane/EtOAc 4:1) to provide **39** (4.50 g, 84%) as a white solid; mp 65°C .

IR (KBr): 1732 (s), 1598 (w), 1354 (s), 1167 (s) cm^{-1} .

^1H NMR (400 MHz, CDCl_3): δ = 7.80 (d, J = 8.2 Hz, 2 H), 7.56 (d, J = 8.2 Hz, 2 H), 7.40 (d, J = 7.2 Hz, 1 H), 7.34–7.28 (m, 5 H), 7.10 (ddd, J = 1.0, 7.2, 7.7 Hz, 1 H), 6.49 (dd, J = 1.0, 7.2 Hz, 1 H), 5.87 (m, 1 H), 5.42 (d, J = 17.6 Hz, 1 H), 5.26 (d, J = 17.6 Hz, 1 H), 5.07–5.01 (m, 2 H), 4.43 (dd, J = 5.8, 14.0 Hz, 1 H), 3.91 (dd, J = 7.7, 14.0 Hz, 1 H), 2.46 (s, 6 H), 1.35 (s, 9 H).

^{13}C NMR (100 MHz, CDCl_3): δ = 151.1, 144.2, 143.7, 139.5, 137.1, 136.6, 135.1, 132.4, 129.5, 129.2, 128.7, 128.2, 128.1, 127.8, 127.0, 126.9, 119.6, 84.3, 54.9, 47.9, 27.8, 21.6, 21.6.

MS (EI): m/z = 570 (M^+), 497, 415, 315, 144, 91.

HRMS (EI): m/z calcd for $\text{C}_{29}\text{H}_{34}\text{N}_2\text{O}_6\text{S}_2$ (M^+): 570.1858; found: 570.1854.

***N*-Allyl-*N*-[3-(*N*-*p*-toluenesulfonyl)aminopropyl]-*p*-toluenesulfonamide (**40**)**

To a solution of **36** (590.9 mg, 1.13 mmol) in CH_2Cl_2 (5 mL) was added TFA (1 mL) at 0°C , and the mixture was stirred at r.t. for 1 h. The volatiles were removed under reduced pressure, and the residue was purified by column chromatography on silica gel (hexane/EtOAc 2:1) to provide **40** (477.7 mg, quant) as a colorless oil.

IR (neat): 3283 (m), 1644 (w), 1598 (m), 1331 (s), 1159 (s) cm^{-1} .

^1H NMR (400 MHz, CDCl_3): δ = 7.76 (d, J = 8.2 Hz, 2 H), 7.67 (d, J = 8.2 Hz, 2 H), 7.34–7.29 (m, 4 H), 5.53 (ddt, J = 10.1, 16.9, 6.8 Hz, 1 H), 5.21 (t, J = 6.8 Hz, 1 H), 5.16–5.08 (m, 2 H), 3.73 (d, J = 6.8 Hz, 2 H), 3.15 (t, J = 6.3 Hz, 2 H), 3.04 (ddd, J = 5.3, 6.8, 6.8 Hz, 2 H), 2.44 (s, 3 H), 2.43 (s, 3 H), 1.76–1.68 (m, 2 H).

^{13}C NMR (100 MHz, CDCl_3): δ = 143.2, 142.9, 136.7, 135.9, 132.4, 129.5, 129.4, 126.7, 126.6, 118.9, 50.7, 44.2, 39.6, 27.8, 21.1, 21.1.

MS (EI): m/z = 422 (M^+), 267, 224, 155, 91.

HRMS (EI): m/z calcd for $C_{20}H_{26}N_2O_4S_2$ (M^+): 422.1334; found: 422.1316.

***N*-Allyl-*N*-[2-(*N*-*p*-toluenesulfonyl)aminomethylphenyl]-*p*-toluenesulfonamide (41)**

To a solution of **39** (4.43 g, 7.76 mmol) in CH_2Cl_2 (40 mL) was added TFA (8 mL) at 0 °C, and the mixture was stirred at r.t. for 1 h. The volatiles were removed under reduced pressure, and the residue was purified by column chromatography on silica gel (hexane/EtOAc 2:1) to provide **41** (3.65 g, quant) as a white solid; mp 121 °C.

IR (KBr): 1597 (w), 1344 (s), 1160 (s) cm^{-1} .

1H NMR (400 MHz, $CDCl_3$): δ = 7.83 (d, J = 8.2 Hz, 2 H), 7.53 (d, J = 7.7 Hz, 1 H), 7.47 (d, J = 8.2 Hz, 2 H), 7.35 (d, J = 8.7 Hz, 2 H), 7.31–7.25 (m, 3 H), 7.09 (dt, J = 1.0, 7.7 Hz, 1 H), 6.35 (d, J = 7.7 Hz, 1 H), 5.63 (dd, J = 3.9, 8.7 Hz, 1 H), 5.50 (dddd, J = 5.8, 8.2, 10.2, 16.9 Hz, 1 H), 4.95 (d, J = 10.2 Hz, 1 H), 4.88 (d, J = 16.9 Hz, 1 H), 4.39 (dd, J = 5.8, 14.0 Hz, 1 H), 4.23–4.15 (m, 2 H), 3.58 (dd, J = 8.2, 14.0 Hz, 1 H), 2.46 (s, 3 H), 2.45 (s, 3 H).

^{13}C NMR (100 MHz, $CDCl_3$): δ = 144.1, 143.2, 138.1, 137.5, 137.0, 134.3, 131.7, 131.6, 129.7, 129.6, 129.0, 128.4, 128.1, 127.4, 127.2, 120.1, 55.0, 43.0, 21.6, 21.5.

MS (EI): m/z = 470 (M^+), 315, 144, 91.

HRMS (EI): m/z calcd for $C_{24}H_{26}N_2O_4S_2$ (M^+): 470.1334; found: 470.1329.

***N*-[3-(*N*-Allyl-*N*-*p*-toluenesulfonyl)aminopropyl]-*N*-formyl-*p*-toluenesulfonamide (42)**

According to the procedure for the synthesis of **5**, a solution of **40** (2.04 g, 4.84 mmol), BuLi (3.6 mL, 5.80 mmol, 1.63 M hexane solution), and 1-formylbenzotriazole (1.42 g, 9.67 mmol) in THF (25 mL) was stirred at –50 °C for 0.5 h to afford **42** (2.01 g, 92%) as a colorless oil after purification by column chromatography on silica gel (hexane/EtOAc 3:1).

IR (neat): 1699 (s), 1643 (w), 1597 (m), 1357 (s), 1165 (s) cm^{-1} .

1H NMR (400 MHz, $CDCl_3$): δ = 9.07 (s, 1 H), 7.75 (d, J = 8.2 Hz, 2 H), 7.66 (d, J = 8.2 Hz, 2 H), 7.38 (d, J = 8.2 Hz, 2 H), 7.29 (d, J = 8.2 Hz, 2 H), 5.55 (ddt, J = 10.1, 16.9, 6.8 Hz, 1 H), 5.19–5.09 (m, 2 H), 3.79 (d, J = 6.8 Hz, 2 H), 3.49–3.43 (m, 2 H), 3.13 (t, J = 6.8 Hz, 2 H), 2.45 (s, 3 H), 2.41 (s, 3 H), 1.85–1.75 (m, 2 H).

^{13}C NMR (100 MHz, $CDCl_3$): δ = 161.1, 145.5, 143.3, 136.5, 134.5, 132.5, 130.3, 129.6, 127.3, 127.0, 119.3, 50.3, 44.5, 40.2, 26.5, 21.5, 21.4.

MS (EI): m/z = 450 (M^+), 295, 224, 155, 91.

HRMS (EI): m/z calcd for $C_{21}H_{26}N_2O_5S_2$ (M^+): 450.1283; found: 450.1287.

***N*-[2-(*N*-Allyl-*N*-*p*-toluenesulfonyl)aminobenzyl]-*N*-formyl-*p*-toluenesulfonamide (43)**

According to the procedure for the synthesis of **5**, a solution of **41** (3.55 g, 7.65 mmol), BuLi (5.8 mL, 9.05 mmol, 1.55 M hexane solution), and 1-formylbenzotriazole (2.22 g, 15.09 mmol) in THF (40 mL) was stirred at –30 °C for 1 h to afford **43** (3.12 g, 83%) as a white solid after purification by column chromatography on silica gel (hexane/EtOAc 4:1); mp 63 °C.

IR (KBr): 1702 (s), 1598 (w), 1349 (s), 1166 (s) cm^{-1} .

1H NMR (400 MHz, $CDCl_3$): δ = 9.24 (s, 1 H), 7.77 (d, J = 8.2 Hz, 2 H), 7.50 (d, J = 8.2 Hz, 2 H), 7.36 (d, J = 8.2 Hz, 2 H), 7.28 (d, J = 8.2 Hz, 2 H), 7.17–7.26 (m, 2 H), 7.05 (ddd, J = 1.9, 6.8, 8.2 Hz, 1 H), 6.41 (d, J = 7.7 Hz, 1 H), 5.85 (dddd, J = 6.3, 7.7, 10.2, 16.9 Hz, 1 H), 5.02–5.10 (m, 2 H), 5.00 (d, J = 16.9 Hz, 1 H), 4.93 (d, J = 16.9 Hz, 1 H), 4.45 (dd, J = 6.3, 14.0 Hz, 1 H), 3.83 (dd, J = 7.7, 14.0 Hz, 1 H), 2.46 (s, 3 H), 2.45 (s, 3 H).

^{13}C NMR (100 MHz, $CDCl_3$): δ = 161.5, 145.6, 143.9, 137.0, 136.9, 134.8, 134.4, 132.3, 130.3, 129.4, 128.5, 128.2, 127.5, 127.4, 127.3, 127.2, 119.7, 54.8, 42.6, 21.6, 21.6.

MS (EI): m/z = 498 (M^+), 343, 315, 159, 144, 91.

HRMS (EI): m/z calcd for $C_{25}H_{26}N_2O_5S_2$ (M^+): 498.1283; found: 498.1273.

***N*-[3-(*N*-Allyl-*N*-*p*-toluenesulfonyl)aminopropyl]-*N*-(2,2-dichloroethenyl)-*p*-toluenesulfonamide (44)**

According to the procedure for the synthesis of **8**, a solution of **42** (2.01 g, 4.45 mmol), PPh_3 (2.92 g, 11.13 mmol), and CCl_4 (3.5 mL, 36.51 mmol) in THF (15 mL) was stirred at 60 °C for 4.5 h to afford **44** (2.24 g, 97%) as a colorless oil after purification by silica gel column chromatography (hexane/EtOAc 3:1).

IR (neat): 1598 (m), 1345 (s), 1165 (s) cm^{-1} .

1H NMR (400 MHz, $CDCl_3$): δ = 7.70–7.65 (m, 2 H), 7.36–7.29 (m, 4 H), 6.20 (s, 1 H), 5.60 (ddt, J = 10.1, 16.9, 6.8 Hz, 1 H), 5.22–5.13 (m, 2 H), 3.79 (d, J = 6.8 Hz, 2 H), 3.33 (t, J = 7.3 Hz, 2 H), 3.15 (t, J = 7.2 Hz, 2 H), 2.45 (s, 3 H), 2.43 (s, 3 H), 1.85–1.76 (m, 2 H).

^{13}C NMR (100 MHz, $CDCl_3$): δ = 144.0, 143.0, 136.1, 134.4, 132.7, 129.6, 129.4, 126.9, 126.7, 124.8, 124.5, 118.7, 50.8, 46.6, 44.7, 27.0, 21.1, 21.1.

MS (EI): m/z = 516 (M^+), 481, 393, 361, 224, 155, 91.

HRMS (EI): m/z calcd for $C_{22}H_{26}^{35}Cl_2N_2O_4S_2$ (M^+): 516.0711; found: 516.0704.

***N*-[2-(*N*-Allyl-*N*-*p*-toluenesulfonyl)aminobenzyl]-*N*-(2,2-dichlorovinyl)-*p*-toluenesulfonamide (45)**

According to the procedure for the synthesis of **8**, a solution of **43** (2.93 g, 5.88 mmol), PPh_3 (3.85 g, 14.69 mmol), and CCl_4 (4.6 mL, 48.19 mmol) in THF (20 mL) was stirred at 60 °C for 4 h to afford **45** (3.27 g, 98%) as a white solid after purification by column chromatography on silica gel (hexane/EtOAc 4:1); mp 137 °C.

IR (KBr): 1736 (w), 1598 (m), 1351 (s), 1166 (s) cm^{-1} .

1H NMR (400 MHz, $CDCl_3$): δ = 7.72–7.78 (m, 3 H), 7.46 (d, J = 8.2 Hz, 2 H), 7.38 (d, J = 8.2 Hz, 2 H), 7.33 (ddd, J = 1.0, 7.2, 7.7 Hz, 1 H), 7.27 (d, J = 8.2 Hz, 2 H), 7.10 (ddd, J = 1.4, 7.7, 7.7 Hz, 1 H), 6.40 (dd, J = 1.0, 8.2 Hz, 1 H), 6.22 (s, 1 H), 5.63 (dddd, J = 5.8, 7.7, 10.1, 16.9 Hz, 1 H), 5.03 (dd, J = 1.5, 10.1 Hz, 1 H), 4.96 (dd, J = 1.5, 16.9 Hz, 1 H), 4.82 (d, J = 16.4 Hz, 1 H), 4.70 (d, J = 16.4 Hz, 1 H), 4.41 (dd, J = 5.8, 13.5 Hz, 1 H), 3.69 (dd, J = 7.7, 13.5 Hz, 1 H), 2.48 (s, 3 H), 2.45 (s, 3 H).

^{13}C NMR (100 MHz, $CDCl_3$): δ = 144.3, 143.9, 138.0, 137.0, 135.3, 134.4, 131.7, 130.0, 129.5, 129.5, 128.6, 128.1, 127.7, 127.4, 127.1, 126.5, 125.7, 120.1, 54.8, 49.5, 21.6, 21.6.

MS (EI): m/z = 564 (M^+), 529, 441, 409, 300, 144, 91.

HRMS (EI): m/z calcd for $C_{26}H_{26}^{35}Cl_2N_2O_4S_2$ (M^+): 564.0711; found: 564.0712.

***N*-[3-(*N*-Allyl-*N*-*p*-toluenesulfonyl)aminopropyl]-*N*-ethynyl-*p*-toluenesulfonamide (46a)**

According to the procedure for the synthesis of **11a**, a solution of **44** (269.6 mg, 0.52 mmol) and BuLi (0.70 mL, 1.15 mmol, 1.63 M hexane solution) in THF (10 mL) was stirred at -78°C for 10 min to afford **46a** (176.2 mg, 76%) as a colorless oil after purification by column chromatography on silica gel (hexane/EtOAc 3:1).

IR (neat): 2134 (m), 1644 (w), 1598 (m), 1364 (s), 1167 (s) cm^{-1} .

^1H NMR (400 MHz, CDCl_3): δ = 7.79 (d, J = 8.2 Hz, 2 H), 7.68 (d, J = 8.2 Hz, 2 H), 7.36 (d, J = 8.2 Hz, 2 H), 7.31 (d, J = 8.2 Hz, 2 H), 5.60 (ddt, J = 10.1, 16.4, 6.3 Hz, 1 H), 5.22–5.12 (m, 2 H), 3.77 (d, J = 6.3 Hz, 2 H), 3.32 (dd, J = 6.8, 7.3 Hz, 2 H), 3.14 (dd, J = 6.8, 7.7 Hz, 2 H), 2.73 (s, 1 H), 2.46 (s, 3 H), 2.43 (s, 3 H), 1.99–1.91 (m, 2 H).

^{13}C NMR (100 MHz, CDCl_3): δ = 144.8, 143.2, 136.2, 133.8, 132.5, 129.7, 129.6, 127.4, 126.9, 119.2, 75.4, 59.3, 51.0, 48.7, 44.5, 26.6, 21.4, 21.3.

MS (EI): m/z = 445 ($\text{M}^+ - 1$), 381, 317, 291, 224, 155, 135, 91.

HRMS (EI): m/z calcd for $\text{C}_{22}\text{H}_{26}\text{N}_2\text{O}_4\text{S}_2$ (M^+): 446.1334; found: 446.1353.

Ethyl [3-(Allyl-*p*-toluenesulfonylamino)propyl]-(*p*-toluenesulfonyl)amino)propynoate (46b)

According to the procedure for the synthesis of **11b**, a solution of **44** (508.8 mg, 0.98 mmol), BuLi (1.3 mL, 2.16 mmol, 1.63 M hexane solution), and ethyl chlorocarbonate (0.11 mL, 1.18 mmol) in THF (20 mL) was stirred at -20°C for 2 h to afford **46b** (415.2 mg, 81%) as a pale yellow oil after purification by column chromatography on silica gel (hexane/EtOAc 2:1).

IR (neat): 2219 (s), 1705 (s), 1598 (w), 1372 (s), 1174 (s) cm^{-1} .

^1H NMR (400 MHz, CDCl_3): δ = 7.81 (d, J = 8.2 Hz, 2 H), 7.67 (d, J = 8.2 Hz, 2 H), 7.38 (d, J = 7.7 Hz, 2 H), 7.31 (d, J = 7.7 Hz, 2 H), 5.60 (ddt, J = 9.7, 16.4, 6.7 Hz, 1 H), 5.22–5.12 (m, 2 H), 4.23 (q, J = 7.3 Hz, 2 H), 3.76 (d, J = 6.7 Hz, 2 H), 3.45 (dd, J = 6.8, 7.7 Hz, 2 H), 3.13 (dd, J = 6.8, 7.3 Hz, 2 H), 2.47 (s, 3 H), 2.43 (s, 3 H), 2.00–1.91 (m, 2 H), 1.31 (t, J = 7.3 Hz, 3 H).

^{13}C NMR (100 MHz, CDCl_3): δ = 153.8, 145.6, 143.4, 136.2, 133.7, 132.6, 130.1, 129.7, 127.6, 127.0, 119.4, 81.8, 67.7, 61.5, 51.2, 49.0, 44.5, 26.9, 21.6, 21.4, 14.0.

MS (EI): m/z = 518 (M^+), 473, 454, 363, 339, 317, 299, 267, 252, 224, 207, 155.

HRMS (EI): m/z calcd for $\text{C}_{25}\text{H}_{30}\text{N}_2\text{O}_6\text{S}_2$ (M^+): 518.1545; found: 518.1538.

***N*-[2-(*N*-Allyl-*N*-*p*-toluenesulfonyl)aminobenzyl]-*N*-ethynyl-*p*-toluenesulfonamide (47a)**

According to the procedure for the synthesis of **11a**, a solution of **45** (303.8 mg, 0.54 mmol) and BuLi (0.76 mL, 1.18 mmol, 1.55 M hexane solution) in THF (10 mL) was stirred at -78°C for 0.5 h to afford **47a** (208.4 mg, 78%) as a pale yellow oil after purification by column chromatography on silica gel (hexane/EtOAc 3:1).

IR (neat): 2136 (s), 1645 (w), 1597 (s), 1348 (s), 1171 (s) cm^{-1} .

^1H NMR (400 MHz, CDCl_3): δ = 7.84 (d, J = 8.7 Hz, 2 H), 7.62 (d, J = 6.8 Hz, 1 H), 7.48 (d, J = 8.2 Hz, 2 H), 7.39 (d, J = 8.2 Hz, 2 H), 7.34–7.26 (m, 3 H), 7.12 (dt, J = 1.5, 7.7 Hz, 1 H), 6.46 (dd, J = 1.0, 8.2 Hz, 1 H), 5.71 (dddd, J = 5.8, 7.7, 10.6, 16.4 Hz, 1 H), 5.01–4.94 (m, 2 H), 4.86 (d, J = 15.9 Hz, 1 H), 4.72 (d, J = 15.9 Hz, 1 H), 4.38 (dd, J = 5.8, 14.0 Hz, 1 H), 3.77 (dd, J = 7.7, 14.0 Hz, 1 H), 2.63 (s, 1 H), 2.49 (s, 3 H), 2.45 (s, 3 H).

^{13}C NMR (100 MHz, CDCl_3): δ = 144.9, 143.9, 137.1, 137.0, 134.6, 134.5, 131.9, 129.9, 129.5, 129.1, 128.7, 128.1, 127.9, 127.8, 127.5, 119.9, 60.4, 58.8, 54.8, 51.5, 21.7, 21.6.

MS (EI): m/z = 494 (M^+), 339, 183, 144, 91.

HRMS (EI): m/z calcd for $\text{C}_{26}\text{H}_{26}\text{N}_2\text{O}_4\text{S}_2$ (M^+): 494.1334; found: 494.1321.

Ethyl [2-(Allyl-*p*-toluenesulfonylamino)benzyl](*p*-toluenesulfonyl)amino)propynoate (47b)

According to the procedure for the synthesis of **11b**, a solution of **45** (382.3 mg, 0.68 mmol), BuLi (0.96 mL, 1.49 mmol, 1.55 M hexane solution), and ethyl chlorocarbonate (0.08 mL, 0.81 mmol) in THF (10 mL) was stirred at -30°C for 1 h to afford **47b** (318.8 mg, 83%) as a pale yellow oil after purification by column chromatography on silica gel (hexane/EtOAc 3:1).

IR (neat): 2220 (s), 1706 (s), 1598 (m), 1348 (s), 1172 (s) cm^{-1} .

^1H NMR (400 MHz, CDCl_3): δ = 7.86 (d, J = 8.2 Hz, 2 H), 7.53 (d, J = 8.2 Hz, 1 H), 7.47 (d, J = 8.2 Hz, 2 H), 7.40 (d, J = 7.7 Hz, 2 H), 7.34–7.26 (m, 3 H), 7.13 (dt, J = 1.5, 7.7 Hz, 1 H), 6.45 (dd, J = 1.0, 8.2 Hz, 1 H), 5.73 (dddd, J = 5.8, 7.7, 10.2, 16.9 Hz, 1 H), 5.09–4.96 (m, 3 H), 4.81 (d, J = 15.9 Hz, 1 H), 4.41 (dd, J = 5.8, 13.5 Hz, 1 H), 4.16 (q, J = 7.2 Hz, 2 H), 3.76 (dd, J = 7.7, 13.5 Hz, 1 H), 2.49 (s, 3 H), 2.45 (s, 3 H), 1.25 (t, J = 7.2 Hz, 3 H).

^{13}C NMR (100 MHz, CDCl_3): δ = 153.9, 145.6, 144.0, 137.2, 136.4, 134.4, 134.1, 131.7, 130.2, 129.5, 129.0, 128.8, 128.2, 128.1, 127.9, 127.5, 120.4, 83.1, 67.3, 61.4, 54.7, 51.5, 21.7, 21.6, 14.1.

MS (EI): m/z = 566 (M^+), 521, 411, 365, 255, 144, 91.

HRMS (EI): m/z calcd for $\text{C}_{29}\text{H}_{30}\text{N}_2\text{O}_6\text{S}_2$ (M^+): 566.1545; found: 566.1533.

***N*-[2-(*N*-Allyl-*N*-*p*-toluenesulfonyl)aminobenzyl]-*N*-(2-trimethylsilylethynyl)-*p*-toluenesulfonamide (47c)**

According to the procedure for the synthesis of **21d**, a solution of **41** (511.7 mg, 1.09 mmol), BuLi (0.80 mL, 1.20 mmol, 1.55 M hexane solution), and phenyl(trimethylsilylethynyl)iodonium triflate (587.5 mg, 1.30 mmol) in toluene (10 mL) was stirred at r.t. for 18 h to afford **47c** (452.1 mg, 73%) as a pale brownish solid after purification by column chromatography on silica gel (hexane/EtOAc 3:1); mp 105°C .

IR (KBr): 2173 (s), 1647 (w), 1597 (m), 1368 (s), 1165 (s) cm^{-1} .

^1H NMR (400 MHz, CDCl_3): δ = 7.81 (d, J = 8.2 Hz, 2 H), 7.60 (dd, J = 1.0, 7.7 Hz, 1 H), 7.49 (d, J = 8.2 Hz, 2 H), 7.37 (d, J = 8.2 Hz, 2 H), 7.32–7.26 (m, 3 H), 7.12 (dt, J = 1.0, 7.7 Hz, 1 H), 6.46 (dd, J = 1.0, 8.2 Hz, 1 H), 5.70 (m, 1 H), 5.01–4.95 (m, 2 H), 4.87 (d, J = 15.7 Hz, 1 H), 4.65 (d, J = 15.7 Hz, 1 H), 4.35 (dd, J = 5.8, 14.0 Hz, 1 H), 3.82 (dd, J = 7.7, 14.0 Hz, 1 H), 2.48 (s, 3 H), 2.45 (s, 3 H), 0.08 (s, 9 H).

^{13}C NMR (100 MHz, CDCl_3): δ = 144.7, 143.8, 137.2, 137.1, 134.7, 134.4, 132.1, 129.7, 129.5, 129.5, 128.6, 128.1, 127.9, 127.8, 127.6, 119.7, 96.1, 72.8, 54.8, 51.8, 21.7, 21.6, -0.0 .

MS (EI): m/z = 566 (M^+), 551, 411, 255, 144, 91.

HRMS (EI): m/z calcd for $\text{C}_{29}\text{H}_{34}\text{N}_2\text{O}_4\text{S}_2\text{Si}_2$ (M^+): 566.1729; found: 566.1717.

Metathesis Reaction of **11a; 1-(*p*-Toluenesulfonyl)-2-vinyl-1,4-dihydroquinoline (48a); Typical Procedure (Table 1, entry 1)**

To a solution of the ruthenium carbene complex **1b** (17.2 mg, 20.22 μmol , 5 mol%) in toluene (15 mL) was added **11a** (125.9 mg, 0.40 mmol) in toluene (5 mL) at 0°C , and the solution was stirred at 80°C for 0.5 h under an ethylene atmosphere. A few drops of ethyl vinyl

ether was added to the mixture, and the volatiles were removed under reduced pressure. The residue was purified by column chromatography on silica gel (hexane/EtOAc 10:1) to afford **48a** (116.8 mg, 93%) as a pale yellow oil.

IR (neat): 1597 (w), 1354 (s), 1172 (s) cm^{-1} .

^1H NMR (400 MHz, CDCl_3): δ = 7.74 (dd, J = 1.0, 8.2 Hz, 1 H), 7.30 (ddd, J = 1.0, 7.3, 8.2 Hz, 1 H), 7.25 (d, J = 8.2 Hz, 2 H), 7.18 (ddd, J = 1.0, 7.3, 7.7 Hz, 1 H), 7.10 (d, J = 8.2 Hz, 2 H), 6.87 (dd, J = 1.0, 7.7 Hz, 1 H), 6.46 (dd, J = 10.6, 17.4 Hz, 1 H), 5.91 (t, J = 4.8 Hz, 1 H), 5.78 (d, J = 17.4 Hz, 1 H), 5.26 (d, J = 10.6 Hz, 1 H), 2.38 (s, 3 H), 2.43–2.02 (br, 2 H).

^{13}C NMR (100 MHz, CDCl_3): δ = 144.0, 140.1, 137.5, 134.7, 133.8, 133.8, 129.2, 128.0, 127.8, 127.2, 126.9, 126.6, 123.2, 115.5, 27.6, 21.6.

MS (EI): m/z = 311 (M^+), 156, 128.

HRMS (EI): m/z calcd for $\text{C}_{18}\text{H}_{17}\text{NO}_2\text{S}$ (M^+): 311.0980; found: 311.0981.

Ethyl 2-[1-(*p*-Toluenesulfonyl)-1,4-dihydroquinolin-2-yl]acrylate (**48b**)

According to the typical procedure for the metathesis reaction of **11a**, a solution of **11b** (40.3 mg, 0.11 mmol) and **1b** (4.5 mg, 5.25 μmol) in toluene (5.5 mL) was stirred at 80 $^\circ\text{C}$ for 1 h under an argon atmosphere to afford **48b** (31.8 mg, 79%) as a pale yellow oil after purification by column chromatography on silica gel (hexane/EtOAc 10:1).

IR (neat): 1719 (s), 1597 (w), 1351 (m), 1170 (s) cm^{-1} .

^1H NMR (400 MHz, CDCl_3): δ = 7.74 (d, J = 7.7 Hz, 1 H), 7.34–7.28 (m, 3 H), 7.19 (dd, J = 7.2, 7.7 Hz, 1 H), 7.14 (d, J = 7.7 Hz, 2 H), 6.89 (d, J = 7.3 Hz, 1 H), 6.31 (s, 1 H), 6.12 (s, 1 H), 6.11 (t, J = 4.8 Hz, 1 H), 4.29 (q, J = 7.3 Hz, 2 H), 2.39 (s, 3 H), 2.29 (br, 2 H), 1.34 (t, J = 7.3 Hz, 3 H).

^{13}C NMR (100 MHz, CDCl_3): δ = 165.7, 144.1, 138.5, 137.3, 136.7, 134.1, 133.9, 129.2, 127.9, 127.4, 127.2, 127.0, 126.7, 125.9, 125.4, 61.0, 27.7, 21.6, 14.2.

MS (EI): m/z = 383 (M^+), 338, 318, 228, 182, 154, 128, 91.

HRMS (EI): m/z calcd for $\text{C}_{21}\text{H}_{21}\text{NO}_4\text{S}$ (M^+): 383.1191; found: 383.1194.

Dimethyl 10-(*p*-Toluenesulfonyl)-3,9,9a,10-tetrahydroacridine-1,2-dicarboxylate (**49**)

To a solution of **48a** (30.6 mg, 0.10 mmol) in toluene (5 mL) was added DMAD (0.06 mL, 0.49 mmol), and the solution was stirred at 80 $^\circ\text{C}$ for 12 h. The volatiles were removed under reduced pressure, and the residue was purified by column chromatography on silica gel (hexane/EtOAc 2:1) to provide **49** (19.9 mg, 45%) as a pale yellow oil.

IR (neat): 1728 (s), 1361 (m), 1171 (s) cm^{-1} .

^1H NMR (400 MHz, CDCl_3): δ = 7.87 (d, J = 8.3 Hz, 1 H), 7.45 (d, J = 8.3 Hz, 2 H), 7.27–7.18 (m, 3 H), 7.10 (dd, J = 7.3, 7.8 Hz, 1 H), 6.96 (d, J = 7.8 Hz, 1 H), 6.17 (m, 1 H), 3.79 (s, 3 H), 3.75 (s, 3 H), 3.32–3.15 (m, 2 H), 2.80 (dd, J = 5.9, 15.6 Hz, 1 H), 2.67 (m, 1 H), 2.39 (s, 3 H), 2.37 (m, 1 H).

^{13}C NMR (100 MHz, CDCl_3): δ = 167.5, 167.0, 144.2, 137.0, 136.7, 135.4, 132.2, 129.8, 129.6, 129.0, 127.6, 127.6, 127.0, 125.4, 124.9, 121.4, 52.4, 52.3, 33.6, 33.1, 28.2, 21.5.

MS (EI): m/z = 453 (M^+), 422, 389, 330, 266, 238, 194, 179.

HRMS (EI): m/z calcd for $\text{C}_{24}\text{H}_{23}\text{NO}_6\text{S}$ (M^+): 453.1246; found: 453.1263.

2-(*p*-Toluenesulfonyl)-3-vinyl-1,2-dihydroisoquinoline (**50a**)

According to the typical procedure for the metathesis reaction of **11a**, a solution of **12a** (48.9 mg, 0.16 mmol) and **1b** (6.7 mg, 7.85 μmol) in toluene (8.0 mL) was stirred at 80 $^\circ\text{C}$ for 0.5 h under an ethylene atmosphere to afford **50a** (34.4 mg, 70%) as a pale yellow oil after purification by column chromatography on silica gel (hexane/EtOAc 10:1).

IR (neat): 1598 (w), 1349 (s), 1164 (s) cm^{-1} .

^1H NMR (400 MHz, CDCl_3): δ = 7.30 (d, J = 8.2 Hz, 2 H), 7.04 (ddd, J = 1.0, 7.0, 7.2 Hz, 1 H), 6.99–6.92 (m, 2 H), 6.83 (d, J = 8.2 Hz, 2 H), 6.68 (d, J = 7.2 Hz, 1 H), 6.54 (dd, J = 11.1, 17.4 Hz, 1 H), 6.44 (s, 1 H), 5.84 (d, J = 17.4 Hz, 1 H), 5.37 (d, J = 11.1 Hz, 1 H), 4.75 (s, 2 H), 2.18 (s, 3 H).

^{13}C NMR (100 MHz, CDCl_3): δ = 143.1, 138.4, 134.3, 133.9, 131.1, 130.0, 128.3, 127.8, 127.5, 127.2, 125.2, 124.9, 120.4, 117.3, 50.4, 21.2.

MS (EI): m/z = 311 (M^+), 156, 128.

HRMS (EI): m/z calcd for $\text{C}_{18}\text{H}_{17}\text{NO}_2\text{S}$ (M^+): 311.0980; found: 311.0979.

Ethyl 2-[2-(*p*-Toluenesulfonyl)-1,2-dihydroisoquinolin-3-yl]acrylate (**50b**)

According to the typical procedure for the metathesis reaction of **11a**, a solution of **12b** (45.4 mg, 0.12 mmol) and **1b** (5.0 mg, 5.92 μmol) in toluene (6.0 mL) was stirred at 80 $^\circ\text{C}$ for 1 h under an ethylene atmosphere to afford **50b** (35.2 mg, 78%) as a pale yellow oil after purification by column chromatography on silica gel (benzene/EtOAc 30:1).

IR (neat): 1721 (s), 1352 (s), 1165 (s) cm^{-1} .

^1H NMR (400 MHz, CDCl_3): δ = 7.33 (d, J = 8.5 Hz, 2 H), 7.09 (dd, J = 7.2, 7.7 Hz, 1 H), 7.03–6.98 (m, 2 H), 6.87 (d, J = 8.5 Hz, 2 H), 6.76 (d, J = 7.7 Hz, 1 H), 6.58 (s, 1 H), 6.34 (d, J = 1.0 Hz, 1 H), 6.08 (d, J = 1.0 Hz, 1 H), 4.85 (s, 2 H), 4.32 (q, J = 7.2 Hz, 2 H), 2.19 (s, 3 H), 1.37 (t, J = 7.2 Hz, 3 H).

^{13}C NMR (100 MHz, CDCl_3): δ = 165.6, 143.1, 138.9, 135.5, 134.6, 130.7, 130.0, 128.4, 128.2, 127.3, 127.3, 127.0, 125.2, 125.1, 122.9, 61.1, 50.1, 21.3, 14.1.

MS (EI): m/z = 383 (M^+), 228, 182, 154, 128.

HRMS (EI): m/z calcd for $\text{C}_{21}\text{H}_{21}\text{NO}_4\text{S}$ (M^+): 383.1191; found: 383.1194.

3-(1-Phenylvinyl)-2-(*p*-toluenesulfonyl)-1,2-dihydroisoquinoline (**50c**)

According to the typical procedure for the metathesis reaction of **11a**, a solution of **12c** (40.2 mg, 0.10 mmol) and **1b** (4.4 mg, 5.19 μmol) in toluene (5.0 mL) was stirred at 80 $^\circ\text{C}$ for 1.5 h under an ethylene atmosphere to afford **50c** (30.8 mg, 77%) as a pale yellow oil after purification by column chromatography on silica gel (hexane/EtOAc 10:1).

IR (neat): 1598 (w), 1354 (s), 1166 (s) cm^{-1} .

^1H NMR (400 MHz, CDCl_3): δ = 7.47–7.28 (m, 7 H), 7.07 (ddd, J = 1.0, 7.3, 7.8 Hz, 1 H), 7.02–6.95 (m, 2 H), 6.89 (d, J = 8.3 Hz, 2 H), 6.73 (d, J = 7.3 Hz, 1 H), 6.41 (s, 1 H), 5.75 (d, J = 1.0 Hz, 1 H), 5.47 (d, J = 1.0 Hz, 1 H), 4.80 (s, 2 H), 2.21 (s, 3 H).

^{13}C NMR (100 MHz, CDCl_3): δ = 147.1, 143.1, 140.0, 140.0, 135.3, 131.2, 130.3, 128.4, 128.2, 128.1, 128.0, 127.8, 127.5, 127.3, 125.2, 125.1, 122.6, 117.5, 50.5, 21.3.

MS (EI): m/z = 387 (M^+), 230, 217, 202, 154, 117, 91.

HRMS (EI): m/z calcd for $\text{C}_{24}\text{H}_{21}\text{NO}_2\text{S}$ (M^+): 387.1293; found: 387.1293.

Dimethyl 5-(*p*-Toluenesulfonyl)-3,4,5,6-tetrahydrophenanthridine-1,2-dicarboxylate (51)

To a solution of **50a** (48.2 mg, 0.15 mmol) in toluene (3 mL) was added DMAD (0.06 mL, 0.46 mmol) at r.t., and the mixture was stirred at 80 °C for 21 h. The volatiles were removed under reduced pressure, and the residue was purified by column chromatography on silica gel (hexane/EtOAc, 2:1) to provide **51** (34.8 mg, 50%) as a pale yellow oil.

IR (neat): 1732 (s), 1354 (m), 1165 (s) cm⁻¹.

¹H NMR (400 MHz, CDCl₃): δ = 7.29 (d, *J* = 8.4 Hz, 2 H), 7.07 (ddd, *J* = 1.0, 6.8, 7.3 Hz, 1 H), 7.02–6.97 (m, 2 H), 6.88 (d, *J* = 8.4 Hz, 2 H), 6.81 (d, *J* = 7.3 Hz, 1 H), 4.72 (s, 2 H), 3.80 (s, 3 H), 3.66 (s, 3 H), 3.00 (t, *J* = 8.9 Hz, 2 H), 2.61 (t, *J* = 8.9 Hz, 2 H), 2.22 (s, 3 H).

¹³C NMR (100 MHz, CDCl₃): δ = 168.3, 166.7, 143.7, 142.0, 136.8, 135.1, 130.2, 129.5, 128.8, 127.4, 127.4, 126.7, 126.6, 125.6, 123.4, 122.1, 52.3, 52.3, 50.8, 27.0, 23.9, 21.3.

MS (EI): *m/z* = 453 (M⁺), 422, 298, 266, 238, 180.

HRMS (EI): *m/z* calcd for C₂₄H₂₃NO₆S (M⁺): 453.1246; found: 453.1244.

Dimethyl 5-(*p*-Toluenesulfonyl)-3,5,6,10b-tetrahydrophenanthridine-1,2-dicarboxylate (52)

According to the typical procedure for the metathesis reaction of **11a**, a solution of **12a** (43.5 mg, 0.14 mmol) and **1b** (5.9 mg, 6.98 μmol) in toluene (7.0 mL) was stirred at 80 °C for 0.5 h under an ethylene atmosphere. After cooling to r.t., DMAD (0.09 mL, 0.70 mmol) was added and the mixture was stirred at 80 °C for 12 h under an argon atmosphere. The volatiles were removed under reduced pressure, and the residue was purified by column chromatography on silica gel (hexane/EtOAc 2:1) to provide **52** (29.1 mg, 46%) as a pale yellow oil.

IR (neat): 1732 (s), 1354 (m), 1168 (s) cm⁻¹.

¹H NMR (400 MHz, CDCl₃): δ = 7.71 (d, *J* = 8.2 Hz, 2 H), 7.31 (d, *J* = 8.2 Hz, 2 H), 7.24–7.21 (m, 3 H), 6.93 (m, 1 H), 5.93 (t, *J* = 3.6 Hz, 1 H), 4.89 (d, *J* = 13.8 Hz, 1 H), 4.34 (d, *J* = 13.8 Hz, 1 H), 3.86 (s, 3 H), 3.77 (t, *J* = 6.3 Hz, 1 H), 3.69 (s, 3 H), 3.22–3.16 (m, 2 H), 2.42 (s, 3 H).

¹³C NMR (100 MHz, CDCl₃): δ = 168.8, 166.6, 144.2, 138.9, 138.6, 134.8, 132.1, 131.6, 129.8, 128.3, 127.7, 127.4, 126.9, 126.9, 123.3, 110.7, 52.5, 52.4, 49.5, 39.2, 29.5, 21.6.

MS (EI): *m/z* = 453 (M⁺), 422, 389, 330, 298, 266, 238, 180.

HRMS (EI): *m/z* calcd for C₂₄H₂₃NO₆S (M⁺): 453.1246; found: 453.1244.

2-(*p*-Toluenesulfonyl)-3-vinyl-2,5-dihydro-1*H*-benzo[*c*]azepine (53a)

According to the typical procedure for the metathesis reaction of **11a**, a solution of **13a** (33.4 mg, 0.10 mmol) and **1b** (4.4 mg, 5.13 μmol) in toluene (5.1 mL) was stirred at 80 °C for 0.5 h under an argon atmosphere to afford **53a** (16.2 mg, 49%) as a pale yellow oil after purification by column chromatography on silica gel (hexane/EtOAc 10:1).

IR (neat): 1597 (w), 1338 (s), 1159 (s) cm⁻¹.

¹H NMR (400 MHz, CDCl₃): δ = 7.27 (d, *J* = 8.2 Hz, 2 H), 7.19–7.11 (m, 2 H), 7.06 (ddd, *J* = 1.9, 7.3, 7.3 Hz, 1 H), 6.97 (d, *J* = 8.2 Hz, 2 H), 6.73 (d, *J* = 7.7 Hz, 1 H), 6.38 (dd, *J* = 10.6, 16.9 Hz, 1 H), 5.77 (t, *J* = 5.8 Hz, 1 H), 5.43 (d, *J* = 16.9 Hz, 1 H), 5.13 (d, *J* = 10.6 Hz, 1 H), 4.81 (s, 2 H), 3.30 (d, *J* = 5.8 Hz, 2 H), 2.30 (s, 3 H).

¹³C NMR (100 MHz, CDCl₃): δ = 142.6, 141.1, 137.0, 135.3, 135.2, 129.8, 129.6, 129.0, 128.8, 127.4, 127.3, 126.3, 125.0, 115.1, 53.5, 33.9, 21.4.

MS (EI): *m/z* = 325 (M⁺), 260, 170, 117, 91.

HRMS (EI): *m/z* calcd for C₁₉H₁₉NO₂S (M⁺): 325.1136; found: 325.1121.

Ethyl 2-[2-(*p*-Toluenesulfonyl)-2,5-dihydro-1*H*-benzo[*c*]azepin-3-yl]acrylate (53b)

According to the typical procedure for the metathesis reaction of **11a**, a solution of **13b** (35.7 mg, 0.09 mmol) and **1b** (3.8 mg, 4.49 μmol) in toluene (4.5 mL) was stirred at 80 °C for 0.5 h under an argon atmosphere to afford **53b** (29.9 mg, 84%) as a pale yellow oil after purification by column chromatography on silica gel (hexane/EtOAc 3:1).

IR (neat): 1722 (s), 1599 (w), 1349 (s), 1162 (s) cm⁻¹.

¹H NMR (400 MHz, CDCl₃): δ = 7.28 (d, *J* = 7.7 Hz, 1 H), 7.11 (d, *J* = 7.7 Hz, 2 H), 7.20–7.09 (m, 2 H), 6.95 (d, *J* = 7.7 Hz, 2 H), 6.80 (d, *J* = 7.2 Hz, 1 H), 6.12 (d, *J* = 1.4 Hz, 1 H), 5.69 (d, *J* = 1.4 Hz, 1 H), 5.63 (t, *J* = 5.3 Hz, 1 H), 4.95 (s, 2 H), 4.22 (q, *J* = 7.2 Hz, 2 H), 3.48 (d, *J* = 5.3 Hz, 2 H), 2.30 (s, 3 H), 1.33 (t, *J* = 7.2 Hz, 3 H).

¹³C NMR (100 MHz, CDCl₃): δ = 165.7, 142.5, 141.4, 138.4, 136.5, 136.1, 135.9, 129.4, 129.2, 128.7, 127.6, 127.2, 126.5, 125.9, 124.4, 60.9, 54.4, 34.7, 21.4, 14.1.

MS (EI): *m/z* = 397 (M⁺), 352, 242, 196, 168, 117, 91.

HRMS (EI): *m/z* calcd for C₂₂H₂₃NO₄S (M⁺): 397.1348; found: 397.1364.

Dimethyl 5-(*p*-Toluenesulfonyl)-5,6,11,11a-tetrahydro-3*H*-dibenzo[*b,e*]azepine-1,2-dicarboxylate (54)

According to the typical procedure for the metathesis reaction of **11a**, a solution of **13a** (33.4 mg, 0.10 mmol) and **1b** (4.4 mg, 5.13 μmol) in toluene (5.1 mL) was stirred at 80 °C for 0.5 h under an argon atmosphere. After cooling to r.t., DMAD (0.04 mL, 0.31 mmol) was added and the mixture was stirred at 80 °C for 29 h under an argon atmosphere. The volatiles were removed under reduced pressure, and the residue was purified by column chromatography on silica gel (hexane/EtOAc 2:1) to provide **54** (17.1 mg, 36%) as a pale yellow oil.

IR (neat): 1732 (s), 1339 (m), 1160 (s) cm⁻¹.

¹H NMR (400 MHz, CDCl₃): δ = 7.38 (d, *J* = 8.2 Hz, 2 H), 7.32 (m, 1 H), 7.24–7.18 (m, 2 H), 7.09 (d, *J* = 8.2 Hz, 2 H), 7.00 (m, 1 H), 5.85 (dd, *J* = 3.4, 3.9 Hz, 1 H), 5.00 (d, *J* = 15.2 Hz, 1 H), 4.36 (d, *J* = 15.2 Hz, 1 H), 3.79 (s, 3 H), 3.77 (s, 3 H), 3.18–3.00 (m, 2 H), 2.92–2.83 (m, 2 H), 2.70 (dd, *J* = 9.2, 15.0 Hz, 1 H), 2.35 (s, 3 H).

¹³C NMR (100 MHz, CDCl₃): δ = 167.6, 167.4, 143.2, 139.0, 137.0, 136.6, 136.6, 136.2, 130.9, 129.5, 129.3, 129.3, 128.3, 127.3, 126.9, 124.4, 53.9, 52.4, 52.3, 39.7, 39.5, 28.4, 21.4.

MS (EI): *m/z* = 467 (M⁺), 436, 403, 371, 344, 280, 252, 213, 104.

HRMS (EI): *m/z* calcd for C₂₅H₂₅NO₆S (M⁺): 467.1403; found: 467.1378.

1-(*p*-Toluenesulfonyl)-7-vinyl-2,3,4,5-tetrahydro-1*H*-azepine (55a)

According to the typical procedure for the metathesis reaction of **11a**, a solution of **17a** (20.7 mg, 0.07 mmol) and **1b** (6.3 mg, 7.46 μmol) in CH₂Cl₂ (4.0 mL) was stirred at reflux for 26 h under an argon atmosphere to afford **55a** (7.7 mg, 37%) as a pale yellow oil together with **17a** (6.8 mg, 33%).

IR (neat): 1599 (w), 1343 (s), 1158 (s) cm⁻¹.

^1H NMR (400 MHz, CDCl_3): δ = 7.76 (d, J = 8.2 Hz, 2 H), 7.27 (d, J = 8.2 Hz, 2 H), 6.25 (dd, J = 10.6, 17.2 Hz, 1 H), 5.94 (dd, J = 6.8, 7.3 Hz, 1 H), 5.29 (d, J = 17.2 Hz, 1 H), 5.05 (d, J = 10.6 Hz, 1 H), 3.49 (br, 2 H), 2.42 (s, 3 H), 1.90–1.84 (m, 2 H), 1.73–1.66 (m, 2 H), 1.36–1.29 (m, 2 H).

^{13}C NMR (100 MHz, CDCl_3): δ = 143.1, 142.4, 139.1, 134.6, 131.9, 129.4, 127.5, 114.6, 49.1, 29.2, 26.0, 23.6, 21.5.

MS (EI): m/z = 277 (M^+), 212, 155, 122, 91.

HRMS (EI): m/z calcd for $\text{C}_{15}\text{H}_{19}\text{NO}_2\text{S}$ (M^+): 277.1136; found: 277.1134.

Ethyl 2-[1-(*p*-Toluenesulfonyl)-4,5,6,7-tetrahydro-1*H*-azepin-2-yl]acrylate (55b)

According to the typical procedure for the metathesis reaction of **11a**, a solution of **17b** (21.2 mg, 0.06 mmol) and **1b** (5.2 mg, 6.07 μmol) in CH_2Cl_2 (3.0 mL) was stirred at reflux for 1.5 h under an ethylene atmosphere to afford **55b** (15.6 mg, 74%) as a pale yellow oil after purification by column chromatography on silica gel (hexane/ Et_2O 3:2).

IR (neat): 1715 (s), 1599 (w), 1344 (s), 1161 (s) cm^{-1} .

^1H NMR (400 MHz, CDCl_3): δ = 7.65 (d, J = 8.2 Hz, 2 H), 7.23 (d, J = 8.2 Hz, 2 H), 6.14 (d, J = 1.7 Hz, 1 H), 5.87 (t, J = 6.8 Hz, 1 H), 5.86 (d, J = 1.7 Hz, 1 H), 3.92 (q, J = 7.3 Hz, 2 H), 3.69–3.63 (m, 2 H), 2.40 (s, 3 H), 2.11–2.04 (m, 2 H), 1.88–1.81 (m, 2 H), 1.50–1.42 (m, 2 H), 1.16 (t, J = 7.3 Hz, 3 H).

^{13}C NMR (100 MHz, CDCl_3): δ = 165.7, 142.8, 139.8, 139.5, 138.4, 131.4, 129.3, 128.0, 127.2, 60.7, 50.7, 30.5, 27.0, 23.4, 21.5, 14.0.

MS (EI): m/z = 349 (M^+), 304, 194, 166, 148, 120, 91.

HRMS (EI): m/z calcd for $\text{C}_{18}\text{H}_{23}\text{NO}_4\text{S}$ (M^+): 349.1348; found: 349.1339.

Ethyl 2-[1,5-Bis-(*p*-toluenesulfonyl)-4,5-dihydro-1*H*-benzo[*b*][1,4]diazepin-2-yl]acrylate (56b)

According to the typical procedure for the metathesis reaction of **11a**, a solution of **21b** (33.3 mg, 0.06 mmol) and **1b** (5.1 mg, 6.03 μmol) in toluene (3.0 mL) was stirred at 80 °C for 0.5 h under an ethylene atmosphere to afford **56b** (33.2 mg, 99%) as a white solid after purification by column chromatography on silica gel (hexane/ EtOAc 2:1); mp 187–188 °C.

IR (KBr): 1720 (m), 1598 (w), 1355 (s), 1164 (s) cm^{-1} .

^1H NMR (400 MHz, CDCl_3): δ = 7.87 (d, J = 8.2 Hz, 2 H), 7.72 (d, J = 8.2 Hz, 2 H), 7.46 (m, 1 H), 7.36–7.26 (m, 7 H), 6.25 (s, 1 H), 5.88 (s, 1 H), 5.30 (dd, J = 2.9, 3.9 Hz, 1 H), 4.57 (dd, J = 3.9, 18.4 Hz, 1 H), 4.15–4.06 (m, 2 H), 3.73 (dd, J = 2.9, 18.4 Hz, 1 H), 2.44 (s, 3 H), 2.42 (s, 3 H), 1.24 (t, J = 7.2 Hz, 3 H).

^{13}C NMR (100 MHz, CDCl_3): δ = 165.1, 144.0, 143.7, 140.3, 139.4, 137.8, 137.0, 136.9, 136.3, 130.4, 129.9, 129.5, 129.1, 128.4, 128.3, 128.1, 127.5, 125.7, 121.4, 61.0, 49.1, 21.6, 21.6, 14.1.

MS (EI): m/z = 552 (M^+), 507, 397, 242, 169, 139, 91.

HRMS (EI): m/z calcd for $\text{C}_{28}\text{H}_{28}\text{N}_2\text{O}_6\text{S}_2$ (M^+): 552.1389; found: 552.1399.

4-(1-Phenylvinyl)-1,5-bis-(*p*-toluenesulfonyl)-2,5-dihydro-1*H*-benzo[*b*][1,4]diazepine (56c)

According to the typical procedure for the metathesis reaction of **11a**, a solution of **21c** (41.9 mg, 0.08 mmol) and **1b** (6.4 mg, 7.53 μmol) in toluene (3.8 mL) was stirred at 80 °C for 1 h under an ethylene atmosphere to afford **56c** (40.7 mg, 97%) as a pale yellow oil after purification by column chromatography on silica gel (hexane/ EtOAc 2:1).

IR (neat): 1597 (m), 1356 (s), 1166 (s) cm^{-1} .

^1H NMR (400 MHz, CDCl_3): δ = 7.94 (d, J = 8.7 Hz, 2 H), 7.61–7.56 (m, 3 H), 7.38–7.32 (m, 3 H), 7.18 (d, J = 8.2 Hz, 2 H), 7.28–7.17 (m, 6 H), 7.10 (dd, J = 1.5, 7.7 Hz, 1 H), 5.39 (s, 1 H), 5.32 (dd, J = 3.4, 3.9 Hz, 1 H), 5.28 (s, 1 H), 4.54 (dd, J = 3.9, 18.4 Hz, 1 H), 3.79 (dd, J = 3.4, 18.4 Hz, 1 H), 2.44 (s, 3 H), 2.40 (s, 3 H).

^{13}C NMR (100 MHz, CDCl_3): δ = 147.8, 144.2, 143.6, 140.4, 139.2, 138.7, 138.7, 137.3, 136.1, 129.7, 129.6, 129.3, 129.2, 128.6, 128.3, 128.2, 128.0, 127.9, 127.2, 126.5, 122.0, 116.4, 48.8, 21.6, 21.5.

MS (EI): m/z = 556 (M^+), 401, 301, 245, 145, 119, 91.

HRMS (EI): m/z calcd for $\text{C}_{31}\text{H}_{28}\text{N}_2\text{O}_4\text{S}_2$ (M^+): 556.1490; found: 556.1481.

Ethyl 2-[1,5-Bis(toluene-4-sulfonyl)-1,4,5,6,7,8-hexahydro[1,5]diazocin-2-yl]acrylate (58b)

According to the typical procedure for the metathesis reaction of **11a**, a solution of **46b** (34.4 mg, 0.07 mmol) and **1b** (5.6 mg, 6.63 μmol) in CH_2Cl_2 (33 mL) was stirred at reflux for 24 h under an argon atmosphere to afford **58b** (26.8 mg, 78%) as a pale yellow oil after purification by column chromatography on silica gel (hexane/ EtOAc 3:2).

IR (neat): 1717 (s), 1598 (w), 1343 (s), 1161 (s) cm^{-1} .

^1H NMR (400 MHz, CDCl_3): δ = 7.65 (d, J = 8.2 Hz, 2 H), 7.58 (d, J = 8.2 Hz, 2 H), 7.31 (d, J = 7.7 Hz, 2 H), 7.23 (d, J = 7.7 Hz, 2 H), 6.18 (t, J = 8.2 Hz, 1 H), 6.16 (s, 1 H), 5.81 (s, 1 H), 3.90 (q, J = 7.3 Hz, 2 H), 3.85 (d, J = 8.2 Hz, 2 H), 3.63 (t, J = 5.3 Hz, 2 H), 3.47–3.41 (m, 2 H), 2.44 (s, 3 H), 2.40 (s, 3 H), 1.93–1.86 (m, 2 H), 1.15 (t, J = 7.3 Hz, 3 H).

^{13}C NMR (100 MHz, CDCl_3): δ = 165.0, 143.4, 143.4, 139.3, 137.8, 136.7, 136.2, 131.0, 130.5, 129.8, 129.4, 127.4, 127.0, 60.9, 51.8, 48.5, 44.1, 27.9, 21.5, 21.5, 13.9.

MS (EI): m/z = 518 (M^+), 473, 397, 363, 335, 317, 267, 238, 207, 180, 155, 134, 91.

HRMS (EI): m/z calcd for $\text{C}_{25}\text{H}_{30}\text{N}_2\text{O}_6\text{S}_2$ (M^+): 518.1545; found: 518.1538.

Supporting Information

Supporting information for this article is available online at <https://doi.org/10.1055/s-0037-1609857>.

References

- (1) For selected reports, see: (a) Zi, G. *Dalton Trans.* **2009**, 42, 9101. (b) Muniz, K.; Hövelmann, C. H.; Streuff, J.; Campos-Gomez, E. *Pure Appl. Chem.* **2008**, 80, 1089. (c) Geurts, K.; Fletcher, S. P.; van Zijl, A. W.; Minnaard, A. J.; Feringa, B. L. *Pure Appl. Chem.* **2008**, 80, 1025. (d) Kalck, P.; Urrutigoity, M.; Dechy-Cabaret, O. *Top. Organomet. Chem.* **2006**, 18, 97. (e) Netscher, T. *J. Organomet. Chem.* **2006**, 691, 5155. (f) Wipf, P.; Kendall, C. *Top. Organomet. Chem.* **2005**, 8, 1. (g) Grigg, R.; Sridharan, V. *Pure Appl. Chem.* **1998**, 70, 1047. (h) Weber, L. *Angew. Chem., Int. Ed. Engl.* **1996**, 35, 271.
- (2) (a) *Handbook of Metathesis*; Grubbs, R. H., Ed.; Wiley-VCH: Weinheim, **2003**. (b) *Topics in Organometallic Chemistry*; Fürstner, A., Ed.; Springer-Verlag: Berlin, **1998**. For selected general reviews, see: (c) Montgomery, T. P.; Ahmed, T. S.; Grubbs, R. H. *Angew. Chem. Int. Ed.* **2017**, 56, 11024. (d) Higman, C. S.; Lummiss, J. A. M.; Fogg, D. E. *Angew. Chem. Int. Ed.* **2016**, 55, 3552. (e) Fustero, S.; Simon-Fuentes, A.; Barrio, P.; Haufe, G.

- Chem. Rev.* **2015**, *115*, 871. (f) Herbert, M. B.; Grubbs, R. H. *Angew. Chem. Int. Ed.* **2015**, *54*, 5018. (g) Nelson, D. J.; Manzini, S.; Urbina-Blanco, C. A.; Nolan, S. P. *Chem. Commun.* **2014**, *50*, 10355. (h) Kress, S.; Blechert, S. *Chem. Soc. Rev.* **2012**, *41*, 4389. (i) Vougioukalakis, G. C.; Grubbs, R. H. *Chem. Rev.* **2010**, *110*, 1746. (j) Nolan, S. P.; Clavier, H. *Chem. Soc. Rev.* **2010**, *39*, 3305. (k) Chauvin, Y. *Angew. Chem. Int. Ed.* **2006**, *45*, 3740. (l) Schrock, R. R. *Angew. Chem. Int. Ed.* **2006**, *45*, 3748. (m) Grubbs, R. H. *Angew. Chem. Int. Ed.* **2006**, *45*, 3760. (n) Hoveyda, A. H.; Zhugralin, A. R. *Nature* **2007**, *450*, 243. (o) Nicolaou, K. C.; Bulger, P. G.; Sarlah, D. *Angew. Chem. Int. Ed.* **2005**, *44*, 4490. (p) Fürstner, A. *Angew. Chem. Int. Ed.* **2000**, *39*, 3012. (q) Grubbs, R. H.; Chang, S. *Tetrahedron* **1998**, *54*, 4413. (r) Schuster, M.; Blechert, S. *Angew. Chem. Int. Ed.* **1997**, *36*, 2037.
- (3) (a) Mori, M. *Top. Organomet. Chem.* **1998**, *1*, 133. (b) Kotha, S.; Panguluri, N. R.; Ali, R. *Eur. J. Org. Chem.* **2017**, 5316. (c) Li, J.; Lee, D. *Eur. J. Org. Chem.* **2011**, 4269. (d) Kotha, S.; Meshram, M.; Tiwari, A. *Chem. Soc. Rev.* **2009**, *38*, 2065. (e) Hansen, E. C.; Lee, D. *Acc. Chem. Res.* **2006**, *39*, 509. (f) Diver, S. T.; Giessert, A. J. *Chem. Rev.* **2004**, *104*, 1317. (g) Poulsen, C. S.; Madsen, R. *Synthesis* **2003**, *1*. (h) Mori, M.; Sakakibara, N.; Kinoshita, A. *J. Org. Chem.* **1998**, *63*, 6082. (i) Kinoshita, A.; Mori, M. *J. Org. Chem.* **1996**, *61*, 8356.
- (4) For recent reviews on the chemistry of ynamines and ynamides, see: (a) Prabagar, B.; Ghosh, N.; Sahoo, A. K. *Synlett* **2017**, 28, 2539. (b) Duret, G.; Le Fouler, V.; Bissert, P.; Bizet, V.; Blanchard, N. *Eur. J. Org. Chem.* **2017**, 6816. (c) Hu, L.; Zhao, J. *Synlett* **2017**, 28, 1663. (d) Cook, A. M.; Wolf, C. *Tetrahedron Lett.* **2015**, *56*, 2377. (e) Wang, X.-N.; Yeom, H.-S.; Fang, L.-C.; He, S.; Ma, Z.-X.; Kedrowski, B. L.; Hsung, R. P. *Acc. Chem. Res.* **2014**, *47*, 560. (f) Evano, G.; Jouvin, K.; Coste, A. *Synthesis* **2013**, 45, 17. (g) Evano, G.; Coste, A.; Jouvin, K. *Angew. Chem. Int. Ed.* **2010**, *49*, 2840. (h) DeKorver, K. A.; Li, H.; Lohse, A. G.; Hayashi, R.; Lu, Z.; Zhang, Y.; Hsung, R. P. *Chem. Rev.* **2010**, *110*, 5064. (i) Brückner, D. *Tetrahedron* **2006**, *62*, 3809. (j) Zifcsak, C. A.; Mulder, J. A.; Hsung, R. P.; Rameshkumar, C.; Wei, L.-L. *Tetrahedron* **2001**, *57*, 7575.
- (5) Kitamura, T.; Kotani, M.; Fujiwara, Y. *Synthesis* **1998**, 1416.
- (6) Brückner, D. *Synlett* **2000**, 1402.
- (7) Zhang, Y.; Hsung, R. P.; Tracey, M. R.; Kurtz, K. C. M.; Vera, E. L. *Org. Lett.* **2004**, *6*, 1151.
- (8) For recent examples of transition-metal-catalyzed reaction of ynamides, see: (a) Gao, Y.; Wu, G.; Zhou, Q.; Wang, J. *Angew. Chem. Int. Ed.* **2018**, *57*, 2716. (b) Liu, X.; Zhang, Z.-X.; Zhou, B.; Wang, Z.-S.; Zheng, R.-H.; Ye, L.-W. *Org. Biomol. Chem.* **2017**, *15*, 10156. (c) Song, W.; Zheng, N. *Org. Lett.* **2017**, *19*, 6200. (d) Alexander, J. R.; Cook, M. J. *Org. Lett.* **2017**, *19*, 5822. (e) Han, X.-L.; Zhou, C.-J.; Liu, X.-G.; Zhang, S.-S.; Wang, H.; Li, Q. *Org. Lett.* **2017**, *19*, 6108. (f) Giri, S. S.; Liu, R.-S. *Adv. Synth. Catal.* **2017**, *359*, 3311. (g) Witulski, B.; Stengel, T. *Angew. Chem. Int. Ed.* **1998**, *37*, 489. (h) Witulski, B.; Gößmann, M. *Chem. Commun.* **1999**, 1879. (i) Couty, S.; Meyer, C.; Cossy, J. *Angew. Chem. Int. Ed.* **2006**, *45*, 6726. (j) Zhang, X.; Hsung, R. P.; Li, H. *Chem. Commun.* **2007**, 2420. (k) Dunetz, J. R.; Danheiser, R. L. *J. Am. Chem. Soc.* **2005**, *127*, 5776. (l) Riddell, N.; Villeneuve, K.; Tam, W. *Org. Lett.* **2005**, *7*, 3681. (m) Tracey, M. R.; Zhang, Y.; Frederick, M. O.; Mulder, J. A.; Hsung, R. P. *Org. Lett.* **2004**, *6*, 2209. (n) Wakamatsu, H.; Takeshita, M. *Synlett* **2010**, 2322.
- (9) (a) Mori, M.; Wakamatsu, H.; Saito, N.; Sato, Y.; Narita, R.; Sato, Y.; Fujita, R. *Tetrahedron* **2006**, *62*, 3872. (b) Saito, N.; Sato, Y.; Mori, M. *Org. Lett.* **2002**, *4*, 803.
- (10) Wakamatsu, H.; Sakagami, M.; Hanata, M.; Takeshita, M.; Mori, M. *Macromol. Symp.* **2010**, 293, 5.
- (11) Correa, A.; Tellitu, I.; Domínguez, E.; SanMartín, R. *J. Org. Chem.* **2006**, *71*, 8316.
- (12) (a) Sherman, E. S.; Fuller, P. H.; Kasi, D.; Chemler, S. R. *J. Org. Chem.* **2007**, *72*, 3896. (b) Fustero, S.; Moscardó, J.; Jiménez, D.; Pérez-Carrión, M. D.; Sánchez-Roselló, M.; del Pozo, C. *Chem. Eur. J.* **2008**, *14*, 9868.
- (13) Bennasar, M. L.; Roca, T.; Monerris, M.; García-Díaz, D. *J. Org. Chem.* **2006**, *71*, 7028.
- (14) (a) Eymery, F.; Iorga, B.; Savignac, P. *Synthesis* **2000**, 185. (b) Corey, E. J.; Fuchs, P. L. *Tetrahedron Lett.* **1972**, 3769.
- (15) (a) Baba, S.; Negishi, E. *J. Am. Chem. Soc.* **1976**, *98*, 6729. (b) Rodríguez, D.; Castedo, L.; Saá, C. *Synlett* **2004**, 783.
- (16) (a) Mitsunobu, O. *Synthesis* **1981**, *1*. (b) Hughes, D. L. *Org. React.* **1992**, *42*, 335.
- (17) Stetter, H. *Chem. Ber.* **1953**, *86*, 161.
- (18) (a) Sonogashira, K.; Tohda, Y.; Hagihara, N. *Tetrahedron Lett.* **1975**, 4467. (b) Chinchilla, R.; Nájera, C. *Chem. Rev.* **2007**, *107*, 874.
- (19) Nicolaou, K. C.; Jung, J.; Yoon, W. H.; Fong, K. C.; Choi, H.-S.; He, Y.; Zhong, Y.-L.; Baran, P. S. *J. Am. Chem. Soc.* **2002**, *124*, 2183.
- (20) (a) Lovely, C. J.; Mahmud, H. *Tetrahedron Lett.* **1999**, *40*, 2079. (b) Mahmud, H.; Lovely, C. J.; Rasika Dias, H. V. *Tetrahedron* **2001**, *57*, 4095.
- (21) Similar result was also obtained in the previous study, see ref. 9.
- (22) Sohn, J.-H.; Kim, K. H.; Lee, H.-Y.; No, Z. S.; Ihse, H. *J. Am. Chem. Soc.* **2008**, *130*, 16506.



Glycosylation reactions mediated by hypervalent iodine: application to the synthesis of nucleosides and carbohydrates

Yuichi Yoshimura^{*1}, Hideaki Wakamatsu¹, Yoshihiro Natori¹, Yukako Saito¹ and Noriaki Minakawa²

Review

[Open Access](#)

Address:

¹Faculty of Pharmaceutical Sciences, Tohoku Medical and Pharmaceutical University, Komatsushima 4-4-1, Aoba-ku, Sendai, 981-8558, Japan and ²Graduate School of Pharmaceutical Science, Tokushima University, Shomachi 1-78-1, Tokushima, 770-8505, Japan

Email:

Yuichi Yoshimura^{*} - yoshimura@tohoku-mpu.ac.jp

^{*} Corresponding author

Keywords:

glycosylation; hypervalent iodine; Lewis acid; nucleoside; oligosaccharide

Beilstein J. Org. Chem. **2018**, *14*, 1595–1618.

doi:10.3762/bjoc.14.137

Received: 02 February 2018

Accepted: 15 June 2018

Published: 28 June 2018

This article is part of the Thematic Series "Hypervalent iodine chemistry in organic synthesis".

Guest Editor: T. Wirth

© 2018 Yoshimura et al.; licensee Beilstein-Institut.

License and terms: see end of document.

Abstract

To synthesize nucleoside and oligosaccharide derivatives, we often use a glycosylation reaction to form a glycoside bond. Coupling reactions between a nucleobase and a sugar donor in the former case, and the reaction between an acceptor and a sugar donor in the latter are carried out in the presence of an appropriate activator. As an activator of the glycosylation, a combination of a Lewis acid catalyst and a hypervalent iodine was developed for synthesizing 4'-thionucleosides, which could be applied for the synthesis of 4'-selenonucleosides as well. The extension of hypervalent iodine-mediated glycosylation allowed us to couple a nucleobase with cyclic allylsilanes and glycal derivatives to yield carbocyclic nucleosides and 2',3'-unsaturated nucleosides, respectively. In addition, the combination of hypervalent iodine and Lewis acid could be used for the glycosylation of glycals and thioglycosides to produce disaccharides. In this paper, we review the use of hypervalent iodine-mediated glycosylation reactions for the synthesis of nucleosides and oligosaccharide derivatives.

Introduction

Nucleic acids and oligosaccharides are both mandatory polymers for the maintenance of life and cell growth. The former exists in nuclei and codes genetic information, which is transformed into proteins through a transcription process known as the "central dogma" (i.e., DNA makes RNA makes proteins).

The latter make up the cell walls of microorganisms and also play a role in transmitting information on the cell surface, whose interactions with proteins are a starting point for signal transduction into cells [1]. Since both types of polymers are essential for cell viability, their biological synthesis, including

the synthesis of their monomer units, e.g., nucleotides, is highly regulated. Damage to these vital molecules often results in congenital disease with ultimately fatal consequences [2,3]. Accordingly, the study of polymers and their biosynthesis is quite important, and informs the development of new drugs for diseases including cancers and infectious diseases caused by viruses [4–7]. Indeed, many drugs related to nucleic acids and oligosaccharides have been developed and used in clinical fields. Synthetic chemists have contributed to the studies by supplying biological tools for the analyses of these polymers, as well as by synthesizing effective drug candidates for the diseases mentioned above [4,8–14].

To synthesize nucleoside and oligosaccharide derivatives, glycosylation reactions are often used to form a glycoside bond. In the case of nucleoside synthesis, a coupling reaction between a persilylated nucleobase and a sugar donor is typically used [15–17]. On the other hand, the reaction between an acceptor and sugar donor is carried out in the presence of an appropriate activator for oligosaccharide synthesis [18,19]. In both cases, a Lewis acid is generally used as an activator for sugar donors. Our previous review focused on the development of glycosylation reactions and their application to the synthesis of nucleoside derivatives [17]. In this review, we showed our glycosylation reactions under oxidative conditions. These were quite useful and the conceptually similar reactions were widely used for synthesizing nucleoside derivatives. Recently, a combination of a Lewis acid catalyst and hypervalent iodine was developed for synthesizing 4'-thionucleosides, which was based on a Pummerer-type reaction coupled with oxidation. The concept of the oxidative glycosylation reaction was successfully applied to the synthesis of other nucleoside derivatives, including 4'-selenonucleosides and carbocyclic nucleosides. The hypervalent iodine-mediated glycosylation has also been used for oligosaccharide synthesis employing glycals and thioglycosides as sugar donors. In this review, we survey the synthesis of nucleoside and disaccharide derivatives under oxidative conditions mostly based on the hypervalent iodine-mediated glycosylation reactions.

Review

Synthesis of 4'-thionucleosides

Over the last decade, we have steadily pursued the identification of novel antitumor and antiviral nucleoside derivatives [17,20–22]. Matsuda and co-workers reported a 2'-substituted cytidine derivative, DMDC (**1**), with potent antitumor activity [23,24]. In other reports, Walker [25] and Secrist [26] independently described the potent antiherpesvirus activity of 2'-deoxy-4'-thionucleoside **2**, in which sulfur was introduced in place of the sugar ring oxygen of 2'-deoxynucleoside. The results for 2'-substituted nucleosides and 2'-deoxy-4'-thionucleosides strongly suggested that 2'-substituted 4'-thionucleosides would be promising candidates for novel antitumor agents. Thus, we designed a novel 2'-substituted 4'-thiocytidine, 4'-thioDMDC (**3**), as our target molecule for potential antitumor agents [27,28] (Figure 1).

At the time we started our project, there had been no reports regarding the synthesis of even 2-substituted 4-thiosugar derivatives. We thus developed the first synthetic route accessing the 4-thiosugar derivative by way of bicyclic intermediate **8** from diacetoneglucose (**5**). Construction of the bicyclic ring of **8** was achieved by consecutive inter-/intramolecular S_N2 reactions of the dimesylate derivative **7** obtained by manipulations of **5**. After acetal hydrolysis and the subsequent hydride reduction, 4-thioarabinose derivative **9** was obtained in good yield. Introduction of a TBDPS group at the primary hydroxy group of **9**, oxidation and Wittig reaction, followed by deprotection of the benzyl group, gave allyl alcohol **11**.

The most popular method to form a glycosyl bond between the sugar moiety and the base of a nucleoside is a Vorbrüggen reaction [15,16], in which a silylated base and sugar donor, e.g., 1-acetoxy sugar, are condensed by a Lewis acid catalyst. It was clear that this reaction could also be used in the synthesis of 4'-thionucleosides as well as normal “4'-oxy” nucleosides. However, for reasons which will be described later, we decided to develop an alternative method to build the glycosyl bond of 4'-thionucleosides by using a direct coupling of a 4-thiosugar

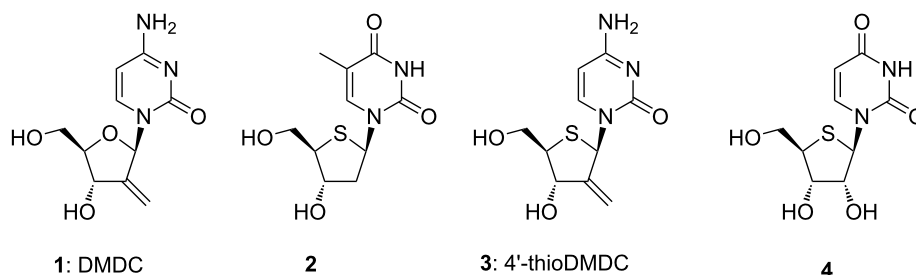


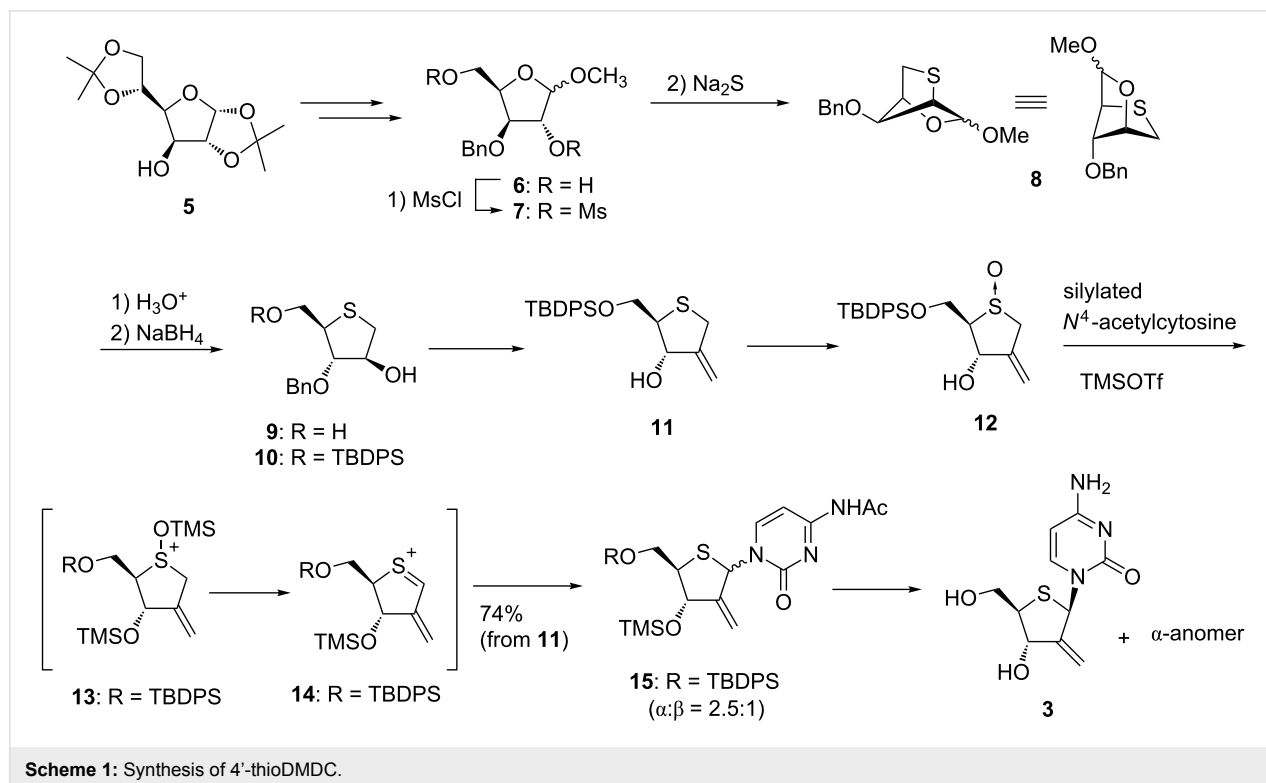
Figure 1: Design of potential antineoplastic nucleosides.

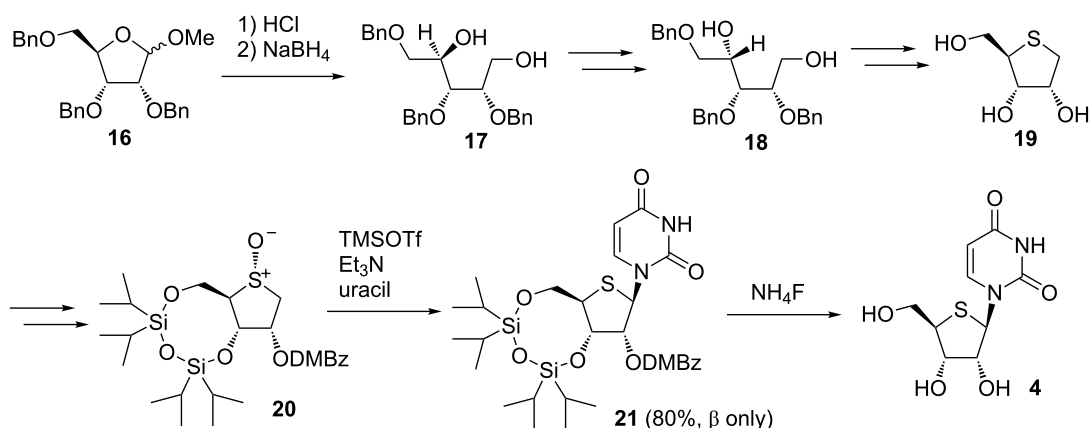
sulfoxide and a silylated base under sila-Pummerer conditions [29,30]. We found that treatment of **12**, obtained by oxidation of **11**, with excess persilylated *N*⁴-acetylcytosine in the presence of TMSOTf as a Lewis acid gave an inseparable mixture of α - and β -anomers of 4'-thioDMDC derivatives **15** in good yield. Based on the study of the sila-Pummerer reaction by Kita, it was plausible that the reaction proceeded via the formation of sulfenium ion **14** which was formed by β -elimination of silylated sulfoxide **13**. The 4'-thioDMDC derivative **15** was deprotected and the resulting anomeric mixture was separated to furnish 4'-thioDMDC (**3**) and its α -anomer [27,28] (Scheme 1).

After we reported the synthesis of 4'-thioDMDC using a Pummerer-type glycosylation reaction, Minakawa and Matsuda applied the reaction to the syntheses of 4'-thioribonucleosides. Applying the synthetic scheme of 2'-deoxy-4'-thionucleoside by Walker to a ribo derivative, 2-dimethoxybenzoate **20** was prepared from tribenzylated ribose **16**. Introduction of a dimethoxybenzoyl (DMBz) group at the 2-position and diastereoselective formation of sulfoxide **20**, favored in Pummerer-type glycosylation reactions and cases where the approach of the nucleophile is restricted, were the key strategies for their synthesis of 4'-thioribonucleosides. Under optimized conditions, the desired 4'-thiouridine derivative **21** was the sole product and it was obtained in excellent yield (Scheme 2). Using the method developed, they succeeded in preparing all four kinds of 4'-thioribonucleosides [31].

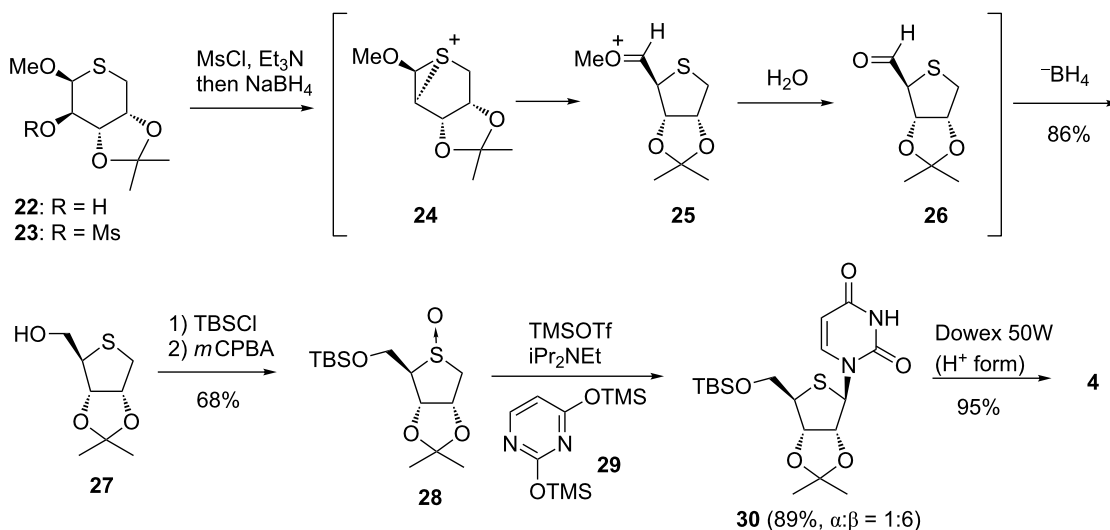
We also synthesized 4'-thioribonucleosides constructing the skeleton of the 4-thioribose via a ring-contraction reaction under reductive conditions [32] from 2-mesylate **23**, which was obtained from **22**. As shown in Scheme 3, the reaction first started to form an episulfonium ion **24** triggered by intramolecular S_N2 reaction at the 5-position by sulfur atom. Secondary, ring contraction from thiopyranose to thiofuranose occurred to produce 5-aldehyde **26**. Finally, hydride reduction of **26** gave the 4-thiofuranose derivative **27**. The Pummerer-type glycosylation reaction of 5-*O*-silylated sulfoxide **28**, by treating with 2,4-bis(trimethylsilyl)uracil (**29**) and excess diisopropylethylamine (DIPEA) in the presence of TMSOTf, gave 4'-thiouridine derivative **30** in a good yield. The reaction stereoselectively proceeded and resulted the predominant formation of the β -anomer due to steric hindrance of the 2,3-di-*O*-isopropylidene group.

Before our reports regarding the Pummerer-type glycosylation, the synthesis of 4'-thionucleosides was based on the known chemistry: typically, a 1-acetoxy-4-thiosugar or its synthetic equivalent was obtained from natural sugars and subjected to the Vorbrüggen reaction as in the case of 2'-deoxy-4'-thionucleosides [25,26]. When synthesizing 4'-thionucleosides by the way of a sulfide derivative **31**, the known chemistry should lead us to use a classical Pummerer reaction to produce 1-acetoxy derivative **33** after converting **31** to the corresponding sulfoxide **32**. Even though this scheme should be promising





Scheme 2: Synthesis of 4'-thioribonucleosides by Minakawa and Matsuda.

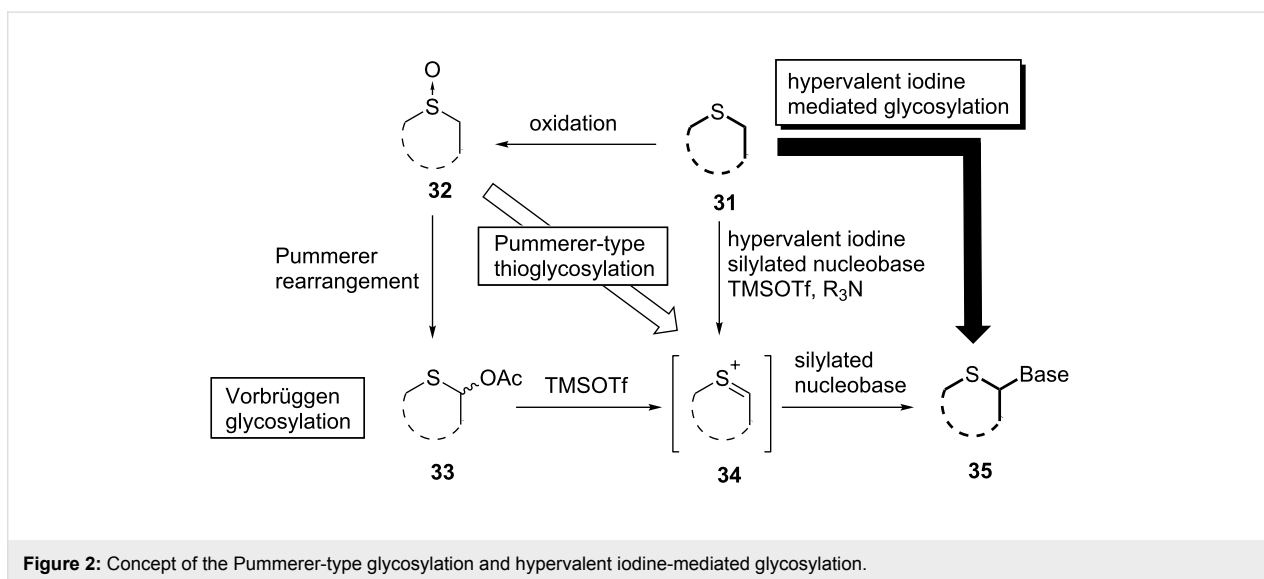


Scheme 3: Synthesis of 4'-thioribonucleosides by Yoshimura.

enough, we intended to introduce an additional synthetic idea based on the fact that both of the reaction intermediate of the Vorbrüggen reaction [15,16] of **33** and the sila-Pummerer reaction developed by Kita [29,30] involving sulfoxide **32** would be the same sulfenium ion **34**. This new glycosylation reaction was unique and attractive since it was capable of skipping a step. In other words, the reaction could directly access sulfenium ion **34** from sulfoxide **32**. Thus we developed the Pummerer-type glycosylation as mentioned above. From these results it can be deduced that the expected sulfenium ion had formed and that the concept of the Pummerer-type glycosylation was actually effective for the formation of the glycosyl bond of 4'-thionucleosides. After we had reported our synthesis of 4'-thioDMDC, the method was widely adopted for the synthesis of 4'-thionucleoside derivatives by other groups and became a standard approach for the glycosylation [33–37]. On the other hand, the

conversion from the sulfide to 4'-thionucleoside using the Pummerer-type glycosylation included an oxidation step. If the oxidation of sulfide **31** and the Pummerer-type glycosylation of the sulfoxide **32** could be performed in the same flask, the reaction could bypass two of the reaction steps and would directly produce 4'-thionucleoside **35** from **31**. Indeed, the utilization of hypervalent iodine would have enabled this short-cut reaction (Figure 2).

Hypervalent iodine reagents have been widely used in organic synthesis [38]. Although originally used as oxidative agents, their use has spread to coupling reactions, including those for the formation of C–C bonds [39–43]. In the case of C–N bond formation, introduction of an azido group using PhI=O and TMSN₃ was reported by Kita and co-workers [44]. Their paper prompted Nishizono et al. to study the glycosylation reaction

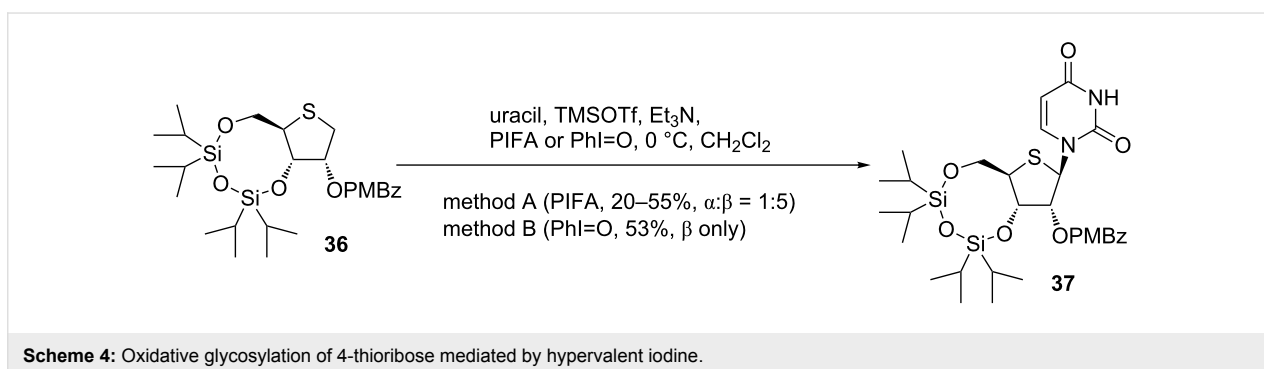


for 4'-thionucleosides using hypervalent iodine reagents. As a 4-thiosugar donor, 2-*p*-methoxybenzoate derivative **36** was prepared following Matsuda's method as shown in Scheme 2, and then was subjected to the Pummerer-type glycosylation mediated by hypervalent iodine. Treatment of **36** with bis(trifluoroacetoxy)iodobenzene (PIFA) and uracil in the presence of trimethylsilyl trifluoromethanesulfonate (TMSOTf) and triethylamine gave a 5:1 mixture of 4'-thiouridine derivative **37** in 55% yield. The reaction of **36** with iodosylbenzene (PhI=O) proceeded stereoselectively and gave only the β -anomer of **37** in 53% yield [45] (Scheme 4).

The mechanism of hypervalent iodine-mediated glycosylation can be expressed as shown in Figure 3. The activated hypervalent iodine reagents in the presence of TMSOTf reacted a sulfur atom of **36** to give **38**, in which elimination of iodobenzene and HX might subsequently occur to generate a sulfenium ion **40** (path a). The nucleophilic attack of the silylated base to the sulfenium ion **40** favored approaching from the β -face to give only the β -anomer **37** as in the case of Minakawa and Matsuda's synthesis described above.

Nishizono considered that the difference between the stereoselectivities of the coupling reactions in methods A and B was caused by the existence of another reaction path of the sulfonium salt (**38** or **39**). In path b, the 4-thiosugar **41** was generated and reacted with a nucleobase, giving a mixture of α - and β -anomers since the reaction might occur by the simple S_N2 reaction. Thus, the reaction proceeded through both paths a and b in method A, but path a was predominant in the reaction of method B [45] (Figure 3).

Nishizono et al. applied the hypervalent iodine-mediated glycosylation to purine 4'-thionucleosides [46]. However, the reaction of **36** with 6-chloropurine resulted in the formation of a regioisomer reacting at the 4-position without any formation of the desired purine 4'-thionucleoside. The result should relate to the acidity of the α hydrogen adjacent to a sulfur atom, which affects the regioselectivity of the reaction. To study the effects of a protecting group on the reaction, the regioselectivity of the reaction was examined using **42** and **43**, which were obtained from **27**. When the 5-hydroxy group was protected with a benzoyl group, the coupling reaction of **42** occurred at the 4-po-



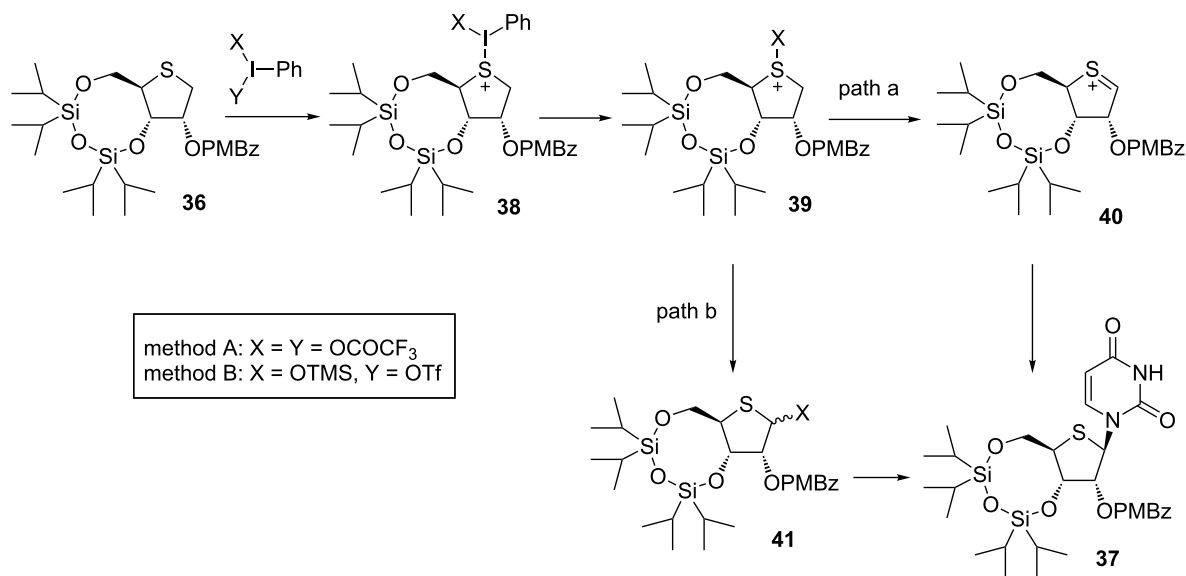
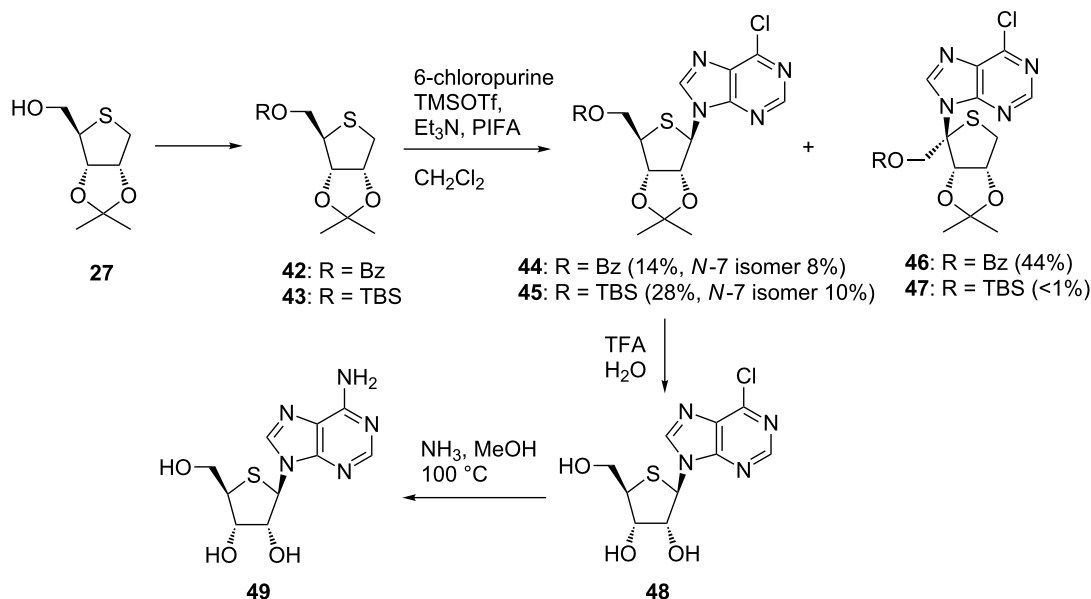


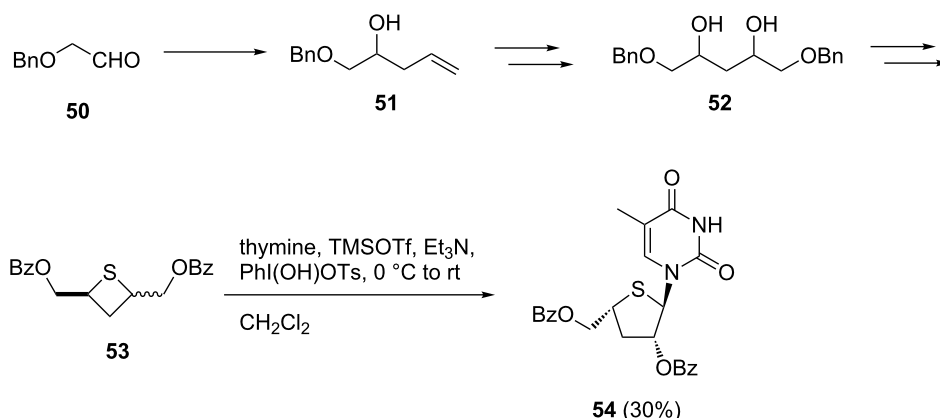
Figure 3: Speculated mechanism of oxidative glycosylation mediated by hypervalent iodine.

sition, as in the case mentioned above, to give **46** in 44% yield along with the desired product and its N7 isomer. In contrast, switching the protecting group of **27** at the 5-position to TBS resulted in the exclusive formation of **45** reacted at the 1-position (28%) along with the N7 stereoisomer (10%). These results support the above-mentioned hypothesis. Finally, 4'-thioadenosine (**49**) was synthesized by treating **45** with TFA followed by methanolic ammonia [46] (Scheme 5).

The same group attempted to apply the oxidative coupling reaction to the synthesis of thietane nucleosides [47]. The substrate of the coupling reaction was prepared as shown in Scheme 6 starting from benzyloxyacetaldehyde (**50**). When a hypervalent iodine reagent was used for glycosylation with a diastereomeric mixture of sulfide **53**, the reaction stereoselectively gave the ring-expanded nucleoside **54** in 30% yield, but did not give the desired thietane nucleoside at all (Scheme 6).



Scheme 5: Synthesis of purine 4'-thioribonucleosides using hypervalent iodine-mediated glycosylation.



Scheme 6: Unexpected glycosylation of a thietanose derivative.

Considered that the ring-expansion occurred in the absence of the hypervalent iodine reagent, the Nishizono and co-workers speculated that the reaction mechanism was as shown in Scheme 7. First, the Lewis acid catalyzed the intramolecular S_N2 reaction of sulfur to form the epi-sulfonium ion **55**, which proceeded only from the *cis*-isomer due to the steric requirement. The subsequent nucleophilic attack leaving the benzoate anion resulted in the formation of a ring-expanded product **56**, which became a substrate of the hypervalent iodine-mediated glycosylation. As a result, 4'-thiofuran nucleoside **54** was stereoselectively obtained with the assistance of the neighboring benzoyl group as in **58**.

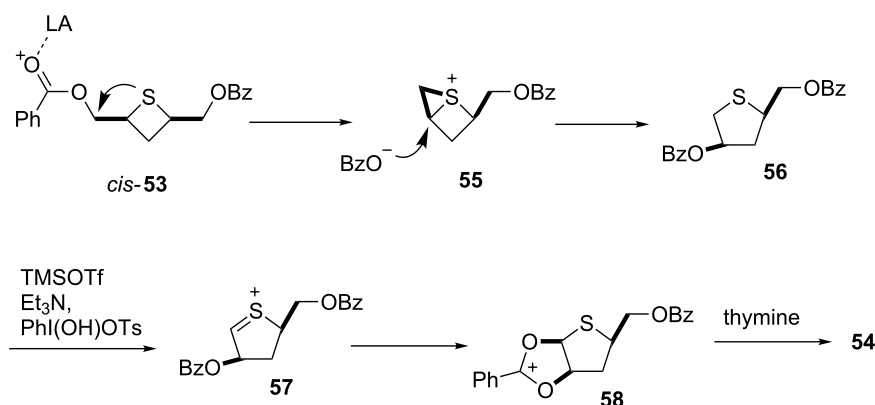
The desired thietanonucleosides **62** and **63** with an anomeric hydroxymethyl group were synthesized by the Pummerer-type glycosylation reaction of *trans*-cyclobutane sulfoxide **59**. The authors concluded that the stereochemistry of the sulfoxide and the nature of the protecting groups had no significant effect on the yield of the Pummerer-type glycosylation [47] (Scheme 8).

Pummerer-type glycosylation, which was developed by our group, improved the synthesis of 4'-thionucleosides. It greatly contributed to search new biological active nucleoside derivatives. The use of hypervalent iodine reagents helped to further improve their synthesis by saving reaction steps to improve synthetic efficiency.

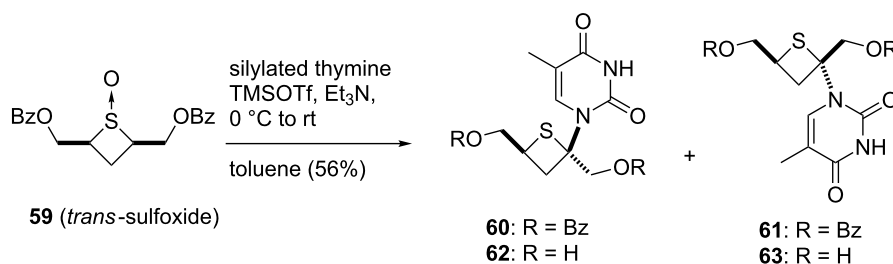
Synthesis of 4'-selenonucleosides

The unique biological activity of 4'-thionucleosides triggered the synthesis of their chalcogen isosters, 4'-selenonucleosides, the activity of which were reported. The first synthesis of 4'-selenonucleosides was reported by Jeong and co-workers in 2008 [48,49].

As in the case of the 4'-thioribonucleoside described in Scheme 3, Jeong et al. chose a 2,3-di-*O*-isopropylidene-protected intermediate as a donor of glycosylation, which was synthesized based on their method developed for 4'-thionucleosides. Starting from compound **64**, which was obtained from



Scheme 7: Speculated mechanism of the ring expansion of a thietanose derivative.



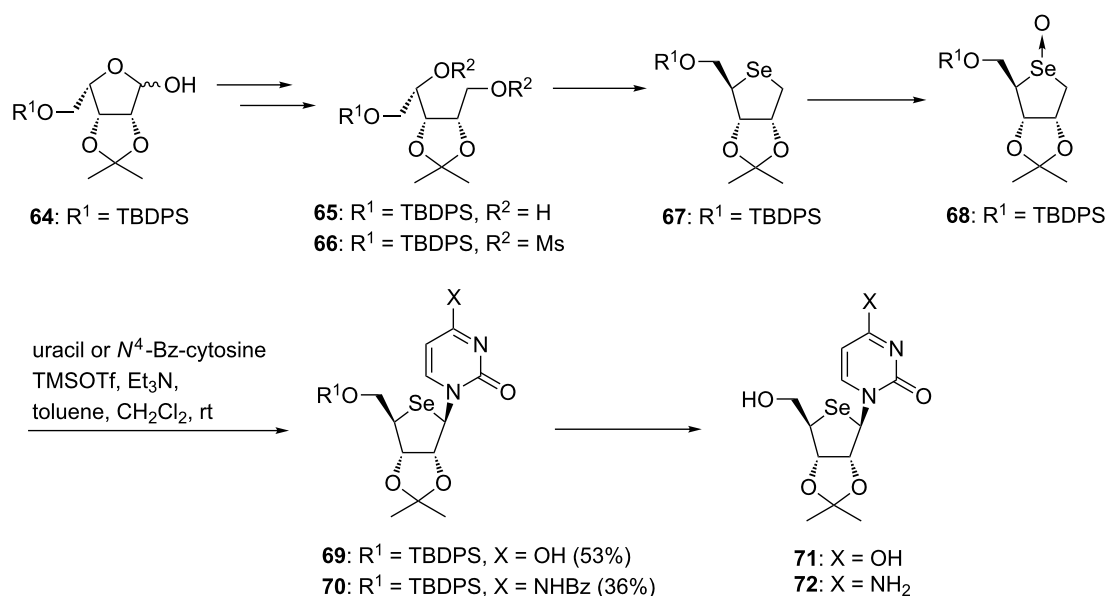
Scheme 8: Synthesis of thietanonucleosides using the Pummerer-type glycosylation.

D-gulonic γ -lactone, dimesylate **66** was prepared. The consecutive inter-/intramolecular S_N2 reactions of **66** by selenide anion gave a 4-seleno sugar **67** in an excellent yield. After converting **67** to the corresponding selenoxide, the resulting **68** was immediately treated with uracil or *N*⁴-benzoylcytosine under the same conditions for Pummerer-type glycosylation to give the desired 4'-selenouridine and 4'-selenocytidine derivatives in moderate yields. Deprotection of the nucleoside derivatives afforded 4'-selenouridine and 4'-selenocytidine, respectively [48] (Scheme 9). In the year in which the first synthesis of 4'-selenonucleoside was reported, Jayakanthan et al. used the same strategy to synthesize 4'-selenonucleosides, including 4'-selenoadenosine [50].

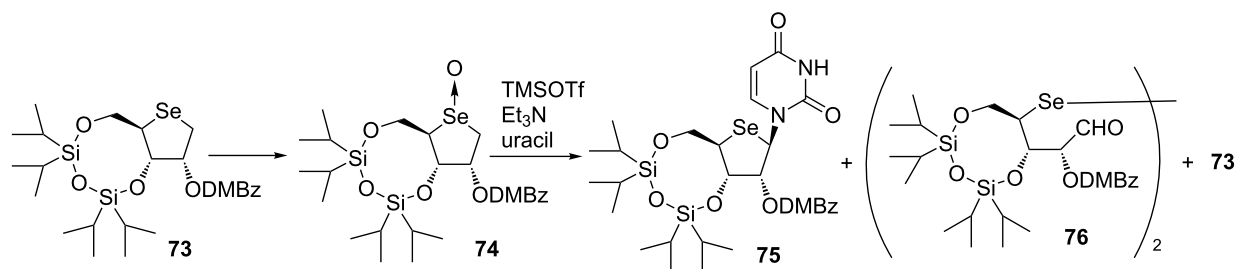
After successful application of the Pummerer-type glycosylation to the synthesis of 4'-selenonucleosides, Jeong's group reported various 4'-selenonucleoside derivatives by using the same method [51–58]. Minakawa and his group attempted to synthesize 4'-selenonucleosides based on their method de-

scribed in Scheme 2 [59]. However, the Pummerer-type glycosylation of selenoxide **74** obtained from **73** gave the desired 4'-selenonucleoside in low yield along with the formation of diselenide **76** and deoxygenated **73** (Scheme 10). One of the reasons for the unsatisfactory result was the instability of selenoxide **74**. Jeong et al. faced the same problem and suppressed decomposition by the immediate reaction after synthesizing the corresponding selenoxide [48].

To overcome these problems, Minakawa decided to use hypervalent iodine for the glycosylation reaction [59] as in Nishizono's synthesis of 4'-thionucleosides [45]. First, they optimized the reaction conditions by examining the reaction of **73** with uracil in the presence of hypervalent iodine reagents. None of the desired pyrimidine nucleoside **75** was formed when the reaction was performed by treatment with iodosylbenzene, TMSOTf and triethylamine in the presence of the silylated uracil (Table 1, entry 1). Instead of trimethylamine, 2,6-lutidine was employed to give **75** in 48% yield together with selenoxide



Scheme 9: First synthesis of 4'-selenonucleosides.



Scheme 10: The Pummerer-type glycosylation of 4-selenoxide **74**.

74 (20%) and starting **73** (8%) (Table 1, entry 2). The use of more reactive hypervalent iodine agents (PIFA and diacetoxyiodobenzene) did not improve the chemical yield of **75** (Table 1, entries 3 and 4). When **73** was treated with iodosylbenzene, TMSOTf, 2,6-lutidine and the silylated uracil in dichloroethane at 50 °C, the reaction gave **75** in 64% yield while suppressing the formation of **74** (Table 1, entry 5).

Minakawa's group attempted to apply the aforementioned reaction to the synthesis of purine derivatives [60]. Based on the reports by Jeong et al., who synthesized 4'-selenoadenosine using the Vorbrüggen reaction [53], they conceived that the hypervalent iodine-mediated reaction of "disarmed" sugar donor **73** bearing an electron-withdrawing group at the 2-position would not readily yield the desired purine derivative. Therefore, they decided to use "armed" seleno sugar **67** as a donor for the hypervalent iodine-mediated glycosylation reaction as in Jeong's synthesis.

The reaction of **67** was performed by treating with silylated 6-chloropurine, iodosylbenzene, TMSOTf and 2,6-lutidine in dichloroethane at 85 °C for 2.5 h to give the desired N9-isomer **78** in 39% yield along with the formation of the N7-isomer **77** (31%) and the α -isomer (8%, N7/N9 mixture). On the other hand, consumption of **67** required longer times and subsequent isomerization to **78** was insufficient at 50 °C, giving **78** in 31% yield with the predominant formation of **77** (40%). The separated N7 isomer **77** was successfully isomerized to the desired N9 isomer **78** in 53% yield upon treatment with TMSOTf in toluene at 90 °C. Under similar conditions, the hypervalent iodine-mediated glycosylation reaction of **67** in the presence of 2,6-dichloropurine was conducted. The coupling reaction proceeded to give an inseparable mixture of N7-isomer **80** and N9-isomer **81** in 64% yield (**80**:**81** = 1:1). To isomerize the undesired N7-isomer to the desired product as in the case of 2,6-dichloropurine, the subsequent treatment of the resulting mixture with TMSOTf in toluene at 90 °C gave rise to exclusive formation of

Table 1: The Pummerer-like glycosylation reaction mediated by hypervalent iodine.

Conditions							Yield (%)	
Entry	Hypervalent iodine (1.2 equiv)	Base (8 equiv)	Solvent	Temp (°C)	Time (h)	75	74	73
1	PhIO	Et ₃ N	CH ₂ Cl ₂	0	4.5	0	0	33
2	PhIO	2,6-lutidine	CH ₂ Cl ₂	rt	17	48	20	8
3	PhI(OCOCF ₃) ₂	2,6-lutidine	CH ₂ Cl ₂	rt	3	38	0	40
4	PhI(OAc) ₂	2,6-lutidine	CH ₂ Cl ₂	rt	5	25	0	20
5	PhIO	2,6-lutidine	ClCH ₂ CH ₂ Cl	50	1.5	64	0	13

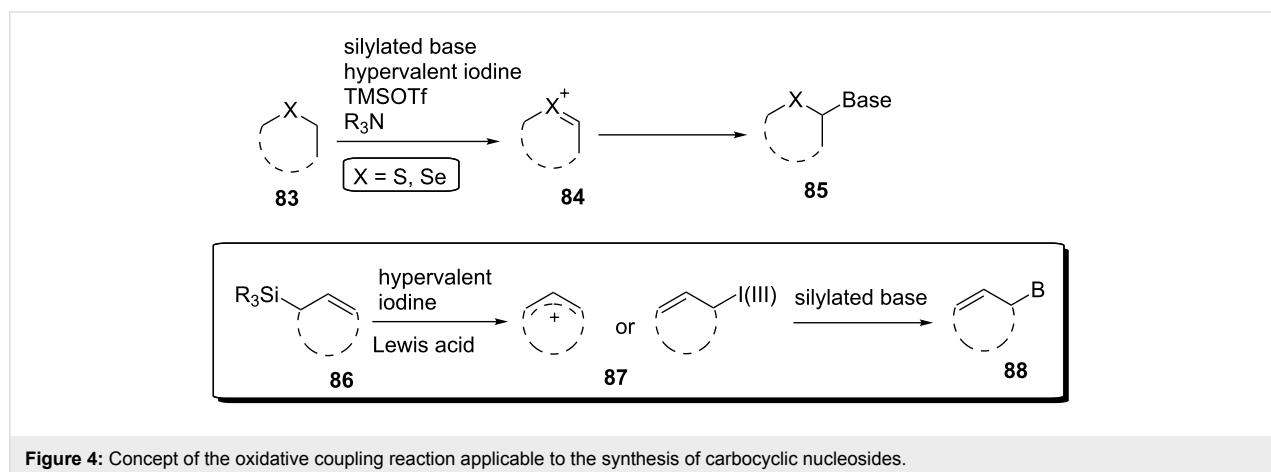
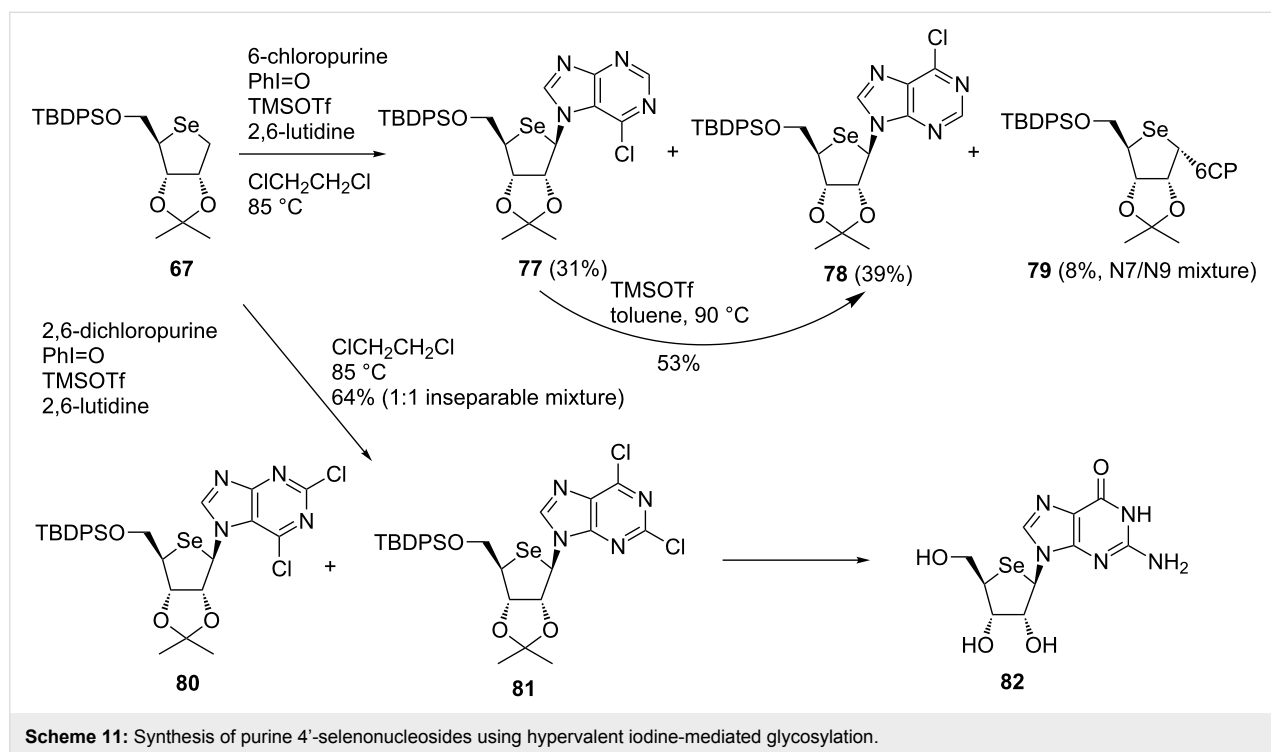
the desired N9-isomer **81** in 62% yield. Finally, **81** was converted to the desired guanosine derivative **82** [60] (Scheme 11).

As in the case of 4'-thionucleosides, the use of hypervalent iodine greatly improved the glycosylation reaction with 4-seleosugars by skipping the preparation of unstable selenoxide derivatives.

Synthesis of carbocyclic nucleosides

As described above, in the hypervalent iodine-mediated glycosylation, a thiosugar donor **83** was oxidized to a cationic intermediate **84** with the assistance of a Lewis acid (TMSOTf) and a base and the subsequent nucleophilic attack of silylated base to

84 gave the desired nucleoside **85**. The success of the hypervalent iodine-mediated glycosylation led us to apply the reaction to the synthesis of carbocyclic nucleosides. In addition, we were also encouraged by the study of Ochiai, who developed the Friedel–Crafts reaction via umpolung of allylsilanes using hypervalent-iodine reagents [61] and the pioneering work on C–N bond formation using hypervalent iodine by Kita [62]. Thus, we envisioned the use of allylsilanes as a pseudosugar donor for the synthesis of carbocyclic nucleosides. We expected to couple a cyclic allylsilane **86**, which could act as a pseudosugar donor for carbocyclic nucleosides **88**, with a persilylated nucleobase by using a combination of hypervalent iodine and an appropriate Lewis acid (Figure 4).



As shown in Scheme 12, an oxidative coupling reaction was examined using a model reaction [63]. Cycloalkenylsilanes **89a,b** and **90a,b** were prepared by hydrosilylation of cyclopentadiene and cyclohexadiene. Using TMSOTf as a Lewis acid, the hypervalent iodine-mediated coupling reaction of **89a,b** and **90a,b** with silylated uracil **29** was examined and the results are summarized in Table 2. Our first attempt to couple triethoxysilanes **89a,b** with **29** in the presence of diacetoxyiodobenzene gave cycloalkenyluracil **91a** and **91b** in 45% and 49% yields respectively (Table 2, entries 1 and 2). On the other hand, the use of trialkylsilanes **90a** and **90b** successfully improved the chemical yield of **91a** and **91b** (Table 2, entries 3 and 4). In contrast, the reactions using PIFA, iodosylbenzene, and [hydroxyl(tosyloxy)iodo]benzene (PhI(OH)OTs) resulted in a decrease of the reaction yield (Table 2, entries 5–7).

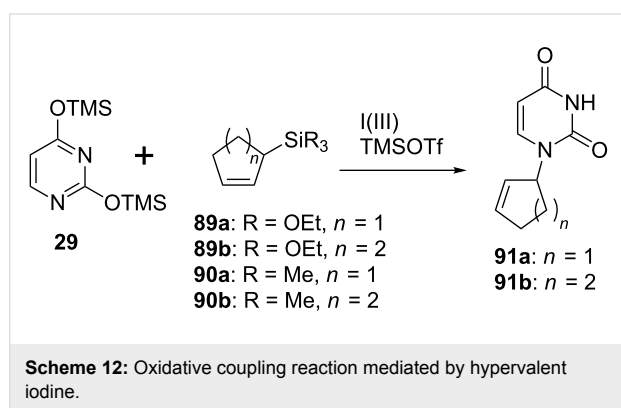


Table 2: Summary of the oxidative coupling reaction using hypervalent iodine.

entry	comp	I(III)	Time (h)	yield (%)
1	89a	PhI(OAc) ₂	15	91a : 45
2	89b	PhI(OAc) ₂	15	91b : 49
3	90a	PhI(OAc) ₂	1	91a : 65
4	90b	PhI(OAc) ₂	1	91b : 65
5	90b	PhI(O ₂ CCF ₃) ₂	1	91b : 55
6	90b	PhIO	1	91b : 57
7	90b	PhI(OH)OTs	1	91b : 29

To prove the usefulness of the oxidative coupling reaction mediated by hypervalent iodine, the reaction was applied to the synthesis of a carbocyclic nucleoside derivative designed as a potential anti-HIV agent.

As a target, cyclohexenylcytosine **99** was designed and was planned to synthesize using the oxidative coupling reaction. To prepare the substrate of the coupling reaction, cyclohexenylsilane **96** was synthesized using the Diels–Alder reaction of

trimethylsilylbutadiene **92** and dimethyl fumarate (**93**), which gave cyclohexene diester **94** (1:1 mixture of diastereomers) [64]. Reduction and subsequent separation by silica gel column chromatography gave diols **95a** and **95b**, the hydroxy groups of which were protected to give di-TBDPS derivatives **96a** and **96b**. The resulting cyclohexenylsilanes **96a** and **96b** were subjected to the oxidative coupling reaction with 2,4-bis(trimethylsilyl)uracil (**29**) using diacetoxyiodobenzene, respectively, and the results are shown in Table 3. The reaction of **96a** gave an inseparable mixture containing 4 stereoisomers of **97a–d** with a ratio of 6:10:2:1.5, which was determined based on the analysis of its ¹H NMR spectrum. The reaction of **96b** also gave a similar result. In both reactions, the formation of cyclohexadiene **98** was observed. These results strongly supported that the reaction proceeded through the carbocation intermediate, as expected and depicted in Figure 4, since **98** was considered to be formed by E1 elimination of the allyl cation intermediate. The fact that **96a** and **96b** showed different reactivities could be explained by the steric interaction between the substituents on the cyclohexene ring and the nucleobase approaching. Compounds **97a–d** were converted to the corresponding cytosine analogues [63]. During the course of conversion, all the stereoisomers were separated. Among them, only the cytosine derivative **99** showed weak anti-HIV activity (Scheme 13 and Table 3).

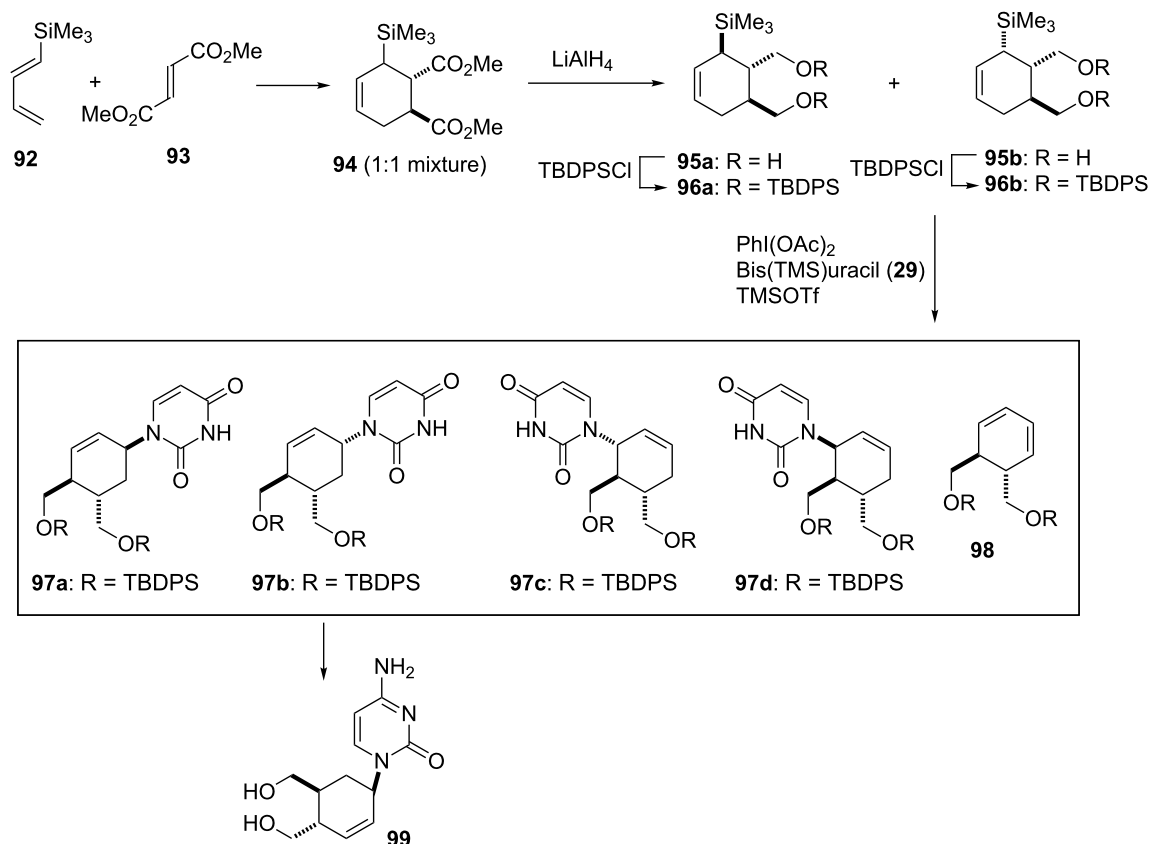
Table 3: Summary of the oxidative coupling reactions of **96a** and **96b**.

comp	time	yield (%)		ratio	
		97a–d	98	recov.	97a:97b:97c:97d
96a	1 h	60	18	0	6:10:2.0:1.5
96b	24 h	50	11	20	3:10:2.5:0.5

An oxidative coupling reaction for synthesizing carbocyclic nucleosides mediated by hypervalent iodine was developed. Since the Friedel–Crafts type reaction involved carbocation intermediate, the reaction always gave a mixture of products. Unfortunately, the reaction was not efficient. However, it is worthy that the oxidative coupling reaction contains a novel type of C–N bond formation and would help to synthesize new carbocyclic nucleosides.

Synthesis of dihydropyranonucleosides

The success of the oxidative coupling reaction for constructing a carbocyclic nucleoside skeleton led us to develop a glycosylation reaction applicable to glycal derivatives. Since an electron-rich enol ether unit of glycal could react with oxidative agents, it was expected to form a cationic intermediate as in the case of allylsilanes described above. A direct coupling of glycals with nucleobases is challenging, since it is formally a C–N bond-



Scheme 13: Synthesis of cyclohexenyl nucleosides using an oxidative coupling reaction.

forming reaction with cleaving of the inactive C–H bond at the γ -position. Actually, the C–N bond-forming reactions using hypervalent iodine agents have attracted much attention [62,65–68]. In the case of the hypervalent iodine-catalyzed coupling reaction with allylsilanes (Figure 5), the reaction involves the following 2 steps: 1) the generation of allyl cation **87** by the oxidation of an allylsilane **86** with PhI(OAc)_2 and TMSOTf, and 2) the subsequent nucleophilic attack of the persilylated base to **87** as shown in Figure 5. Therefore, we expected that subjecting

the electron-rich glycal **100** to the hypervalent iodine-mediated reaction described above would generate an oxocarbenium ion **101** to serve as an intermediate, giving a nucleoside **102**.

First, we attempted model reactions of the oxidative coupling to enol ether using a TMSOTf/PhI(OAc)_2 system. After several attempts, we found that the reaction of 3,4-dihydro-2H-pyran (DHP, **103**) with PhI(OAc)_2 and TMSOTf, starting at -40°C and then gradually raised to room temperature, gave a dihydropyranyluracil derivative **104** in 31% yield [69]. We also found that when Cu(OTf)_2 was used as a catalyst in place of TMSOTf, the reaction gave **104** in 24% yield (Scheme 14).

We speculated that the mechanism of the oxidative coupling reaction was as shown in Scheme 15. DHP (**103**) was reacted with PhI(OAc)_2 to produce an acetoxyiodobenzene derivative **105** with the assistance of TMSOTf. With respect to the pathway from the intermediate **105** to the N1-substituted uracil **104**, there were two plausible routes. In path a, a nucleophilic attack of 2,4-bis(trimethylsilyl)uracil (**29**) occurs prior to an elimination. In path b, on the other hand, an allylic carbocation **110** formed from **108** reacts with **29**. From the result that the reaction of 2,3-dihydrofuran gave side products generated from an

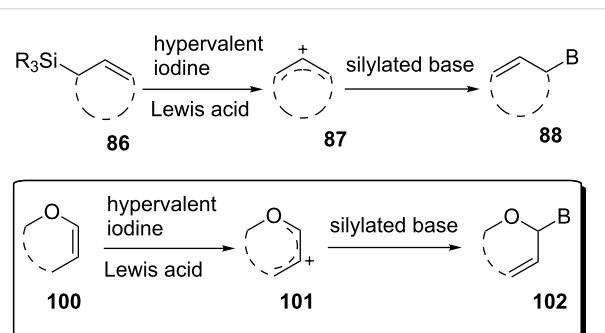
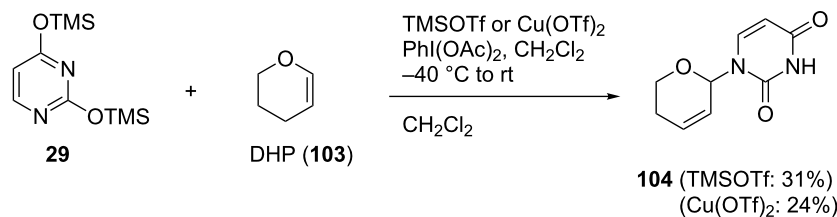


Figure 5: Concept of the oxidative coupling reaction of glycal derivatives.

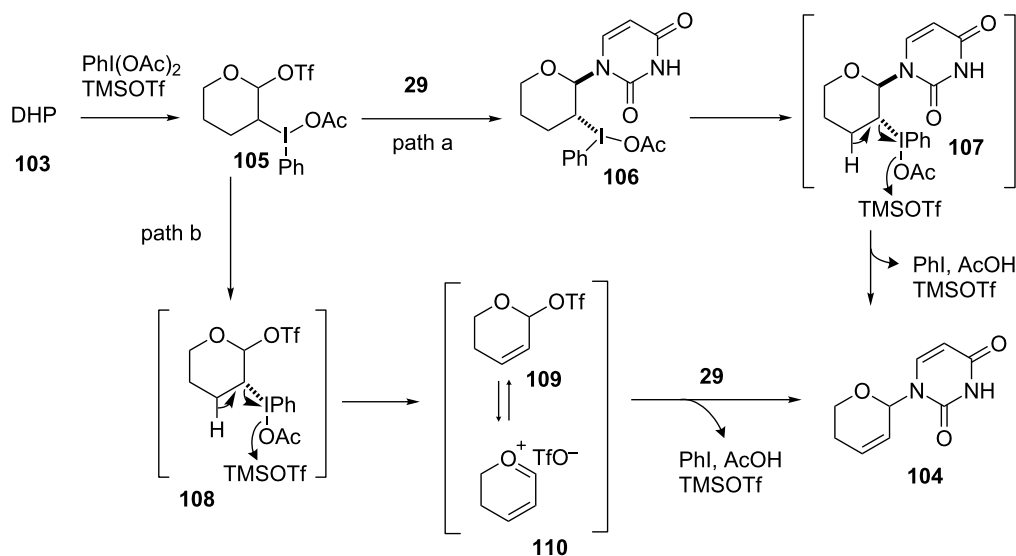


Scheme 14: Oxidative coupling reaction of silylated uracil and DHP using hypervalent iodine.

intermediate resembling **107** (data not shown), it was strongly suggested that the oxidative coupling reaction preferred path a rather than path b (Scheme 15).

Because further optimization of the oxidative coupling reaction was not successful, we decided to examine the effect of adding a co-catalyst. The speculated reaction mechanism depicted in Scheme 15 suggested that the instability of the intermediates **105** and **106** might have caused the low yield of the oxidative coupling. Based on this idea, we intended to use (PhSe)₂ as a co-catalyst, since it might prevent the formation of unstable **105** and **106** and yield **102** in one step (Figure 6).

We examined the effect of (PhSe)₂ as an additive by the reaction of various glycols and their chemical equivalents [69] and the results are summarized in Table 4. The reaction of **103** and **29** was performed by treatment with PhI(OAc)₂ and (PhSe)₂ in the presence of catalytic amounts of TMSOTf to selectively yield a *trans*-isomer of 1-(3-phenylselanyltetrahydropyran-2-yl)uracil (**116**) in 73% yield (Table 4, entry 1). Although this result was unexpected, it was important, since the reaction appeared to be applicable to access various nucleoside derivatives, including 2'-deoxynucleosides. More importantly, we could avoid the use of unstable reagents such as PhSeBr. In other words, the reaction using hypervalent iodine and stable



Scheme 15: Proposed mechanism of the oxidative coupling reaction mediated by hypervalent iodine.

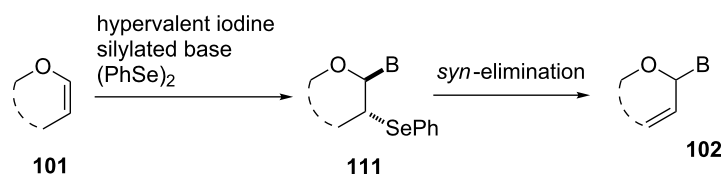


Figure 6: Synthesis of 2',3'-unsaturated nucleosides using hypervalent iodine and a co-catalyst.

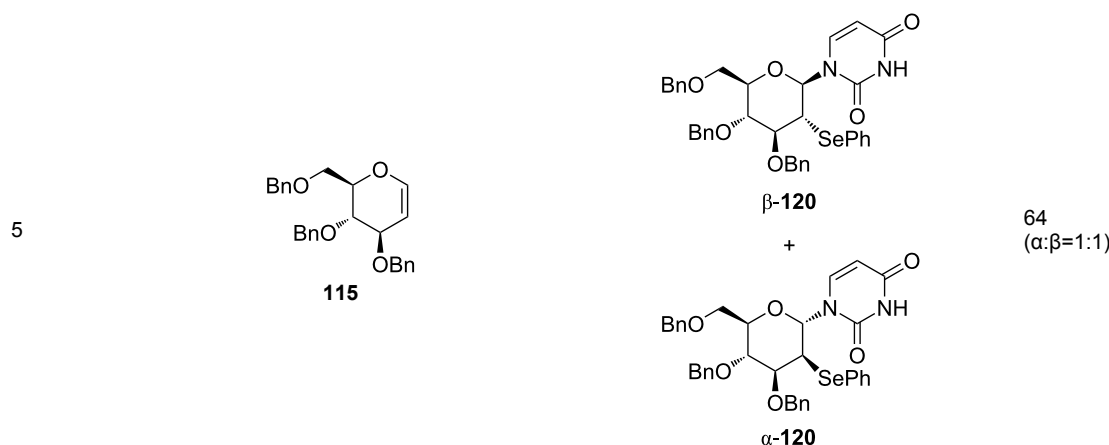
(PhSe)₂ in the presence of a Lewis acid would be expected to yield the same products as the reaction using PhSeBr. The reaction with dihydrofuran (**112**) furnished 1-(3-phenylselanyl-tetrahydrofuran-2-yl)uracil (**117**) in 31% yield (Table 4, entry 2). The reaction of **113** with **29** at –5 °C afforded **118** in 69% yield (Table 4, entry 3). The reaction of **114** gave an anomeric mixture of **119** in 80% yield with the predominant formation of the β-nucleoside (Table 4, entry 4). In contrast, the oxidative glycosylation reaction of D-glucal **115** gave a 1:1 mixture of α-**120** and β-**120** in 64% yield (Table 4, entry 5). From these data, the oxidative coupling reaction mediated by hypervalent iodine of

glycal derivatives can clearly be regarded as a new glycosylation reaction that is applicable to the synthesis of 2'-deoxy- and 2',3'-dideoxydidehydronucleosides, some of which are known to have anti-HIV activity (Table 4).

To reveal the scope of this reaction, we designed a new dihydropyranonucleoside as a potential anti-HIV agent and attempted to synthesize it by using the oxidative coupling reaction [70]. First, the PMB-protected epoxide **121** was converted to diene **122**. The dihydropyran ring of **123** was constructed by RCM of **122** catalyzed by a Grubbs 1st generation catalyst. The

Table 4: Summary of the oxidative coupling reaction of bis(trimethylsilyl)uracil **29** with enol ethers using the TMSOTf/PhI(OAc)₂/(PhSe)₂ system.

<div style="text-align: center;"> </div>			
entry	enol ether	product	yield (%)
1			73
2			31
3			69
4		 β- 119 + α- 119	80 (α:β=1:2)

Table 4: Summary of the oxidative coupling reaction of bis(trimethylsilyl)uracil **29** with enol ethers using the TMSOTf/PhI(OAc)₂/(PhSe)₂ system. (continued)

isomerization of the double bond in **123** by treatment with a Wilkinson catalyst under basic conditions afforded glycal **124** (Scheme 16).

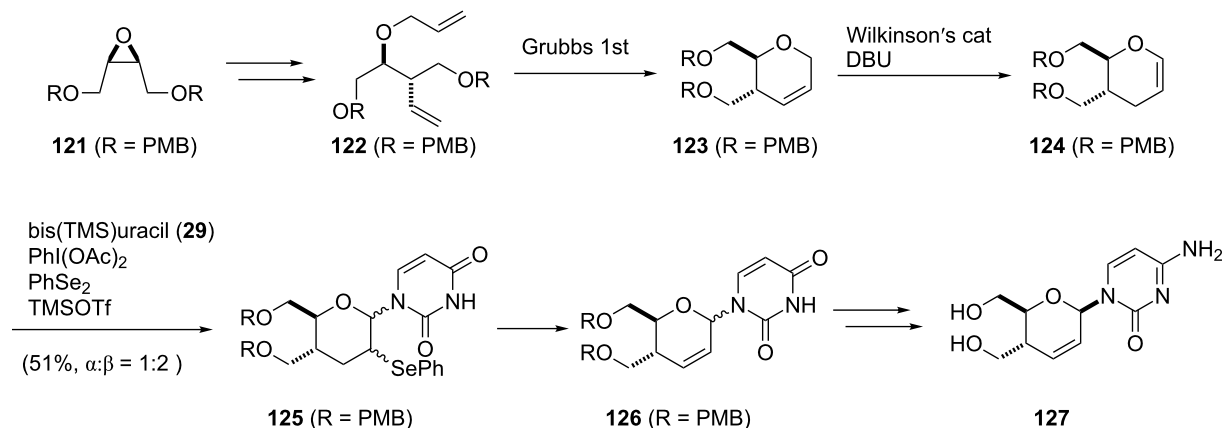
The hypervalent iodine-mediated glycosylation of 2,4-bis(trimethylsilyl)uracil (**29**) with glycal **124** gave an inseparable mixture of α - and β -anomers **125** (α : β = 1:2) in 51% yield as we expected. Compound **125** was then oxidized by treatment with mCPBA, followed by elimination of the resulting selenoxide to give **126**. After the separation of anomers, the major β -anomer was converted into a cytosine derivative **127** [70]. However, **127** did not show any activity against HIV whereas its 5'-thio counterpart did show anti-HIV activity (Scheme 16).

The reaction mediated by hypervalent iodine provides an alternative method for constructing glycosidic bonds of nucleoside derivatives by using a glycal as sugar donor. Its usefulness was

proved by applying the reaction to synthesize new nucleoside derivatives as mentioned above.

Synthesis of acyclic nucleosides

It is known that the oxidative C–C bond cleavage of glycols, epoxides, and olefins takes place by the action of hypervalent iodine [38,71,72]. For example, Havare and Plattner reported the oxidative cleavage of α -aryl aldehydes using iodosylbenzene to give chain-shortened carbonyl compounds and formaldehyde [71]. In the field of carbohydrate chemistry, similar deformylation by action of hypervalent iodine has also been demonstrated: the β -fragmentation reaction of an anomeric alkoxy radical of carbohydrates was mediated by a hypervalent iodine reagent [73]. The reaction results in the formation of carbohydrates with a reduction of one carbon. From the viewpoint of the synthetic method, the reaction would be useful for dehomologation of aldoses and preparation of chiral synthons

**Scheme 16:** Synthesis of dihydropyranonucleoside.

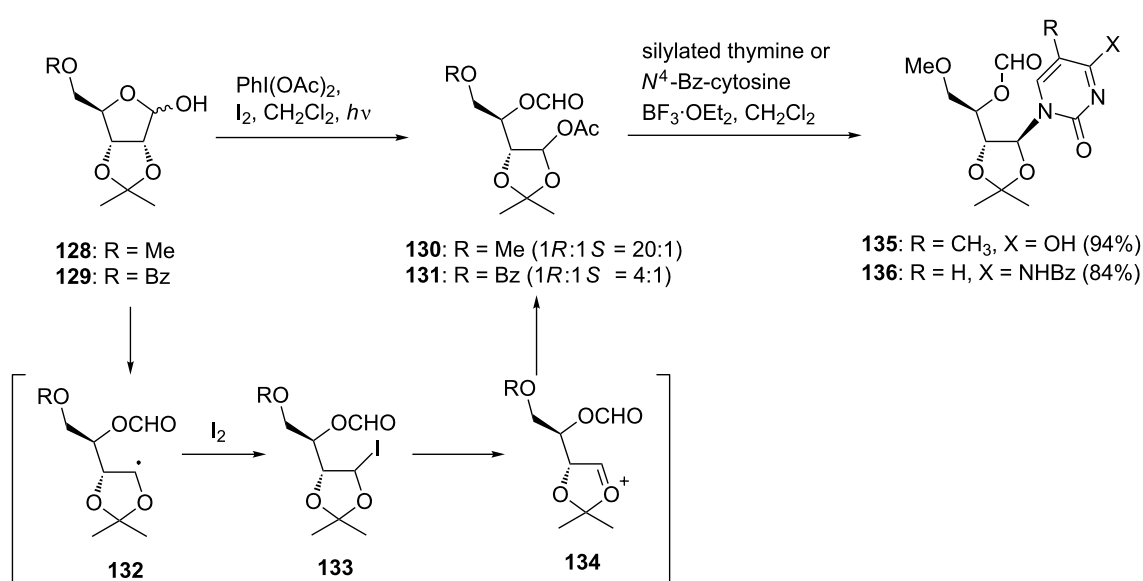
deriving from sugars. The reaction procedure involves the initial formation of an alkoxy anomeric radical by a hypervalent iodine reagent in the presence of iodine, which triggers the β -fragmentation of the C1–C2 bond. As a result, a C2 radical is generated and is further oxidized to a carbocation that is reacted with nucleophilic agents to give the desired products.

Boto et al. applied the reaction to the one-pot synthesis of acyclic nucleosides that belong to an important class of nucleosides with antiviral activity [74]. First, they tried to synthesize acyclic nucleosides in a stepwise manner. The substrates **128** and **129** for the fragmentation reaction were synthesized from ribose in a few steps by the conventional method. The oxidative scission of **128** and **129** was carried out by treatment with diacetoxyiodobenzene and iodine under irradiation with visible light to give acetoxy acetals **130** and **131** in good yields with high stereoselectivities. As shown in Scheme 17, the reaction was expected to proceed via the formation of anomeric alkoxy radicals, which underwent fragmentation to produce radical **132**. The radical **132** could be trapped with iodine, giving iodide **133**. The oxycarbenium ion **134** generated by the extrusion of iodide from **133** reacted with the acetoxy ion to furnish the resulting acetate derivatives. The acetates **130** and **131** were then treated with silylated thymine or *N*⁴-benzoylcytosine in the presence of a Lewis acid to give the desired acyclic nucleosides **135** and **136** in excellent yields. The results revealed that the nucleophilic attack of the nucleobase selectively occurred from the less hindered side of the oxycarbenium ion intermediates, giving 1',2'-*trans* isomers as major products (Scheme 17).

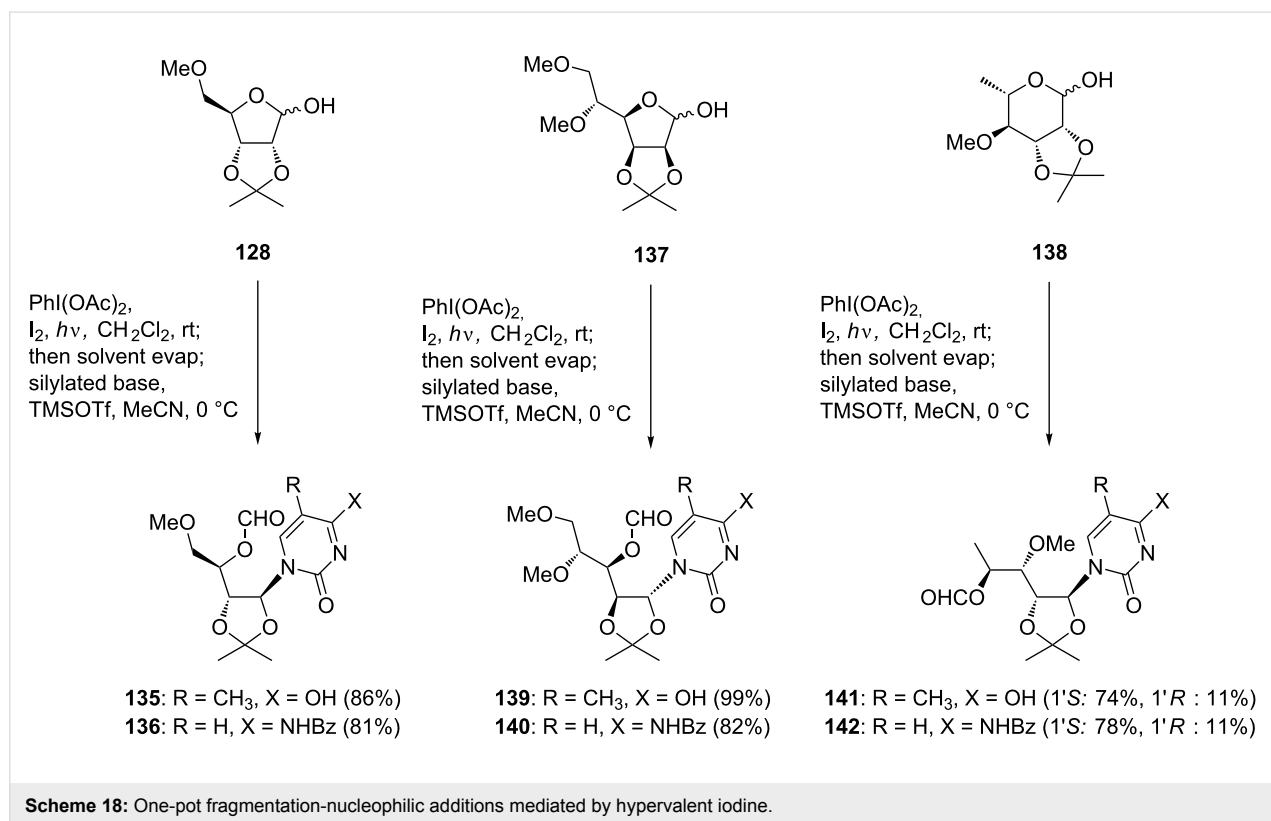
Based on the conditions for the stepwise fragmentation and glycosylation procedure, Boto et al. explored the one-pot version of the reaction [74]. When the β -fragmentation, the first step of oxidative glycosylation, was carried out in CH_2Cl_2 and then the Lewis acid and the silylated base were added, the acyclic nucleosides were obtained in low yields. Boto and co-workers overcame this problem by replacing the solvent before glycosylation. After the fragmentation reaction was finished, the solvent (CH_2Cl_2) was removed and replaced with acetonitrile. The resulting mixture was treated with TMSOTf and the silylated base. Under the optimized conditions, the reactions of ribose derivative **128**, mannose derivative **137**, and rhamnose derivative **138** gave the desired acyclic nucleosides in excellent yields as shown in Scheme 18. It is worth noting that the overall yields for the one-pot process are comparable or superior to those obtained with the two-step procedure (Scheme 18).

Synthesis of disaccharides

Classically, carbohydrates have been considered primarily an energy source for life – as in the cases of glucose, fructose and their oligosaccharides, e.g., starch. However, more recently it has been revealed that oligosaccharides and glycoconjugates also play important roles in various biological processes, as mentioned earlier. As a result, the increasing significance of oligosaccharides in biological events has led to a strong demand for synthetic routes towards oligosaccharides, which would also contribute to the identification and development of drug candidates. For example, cancer immunotherapy based on vaccines



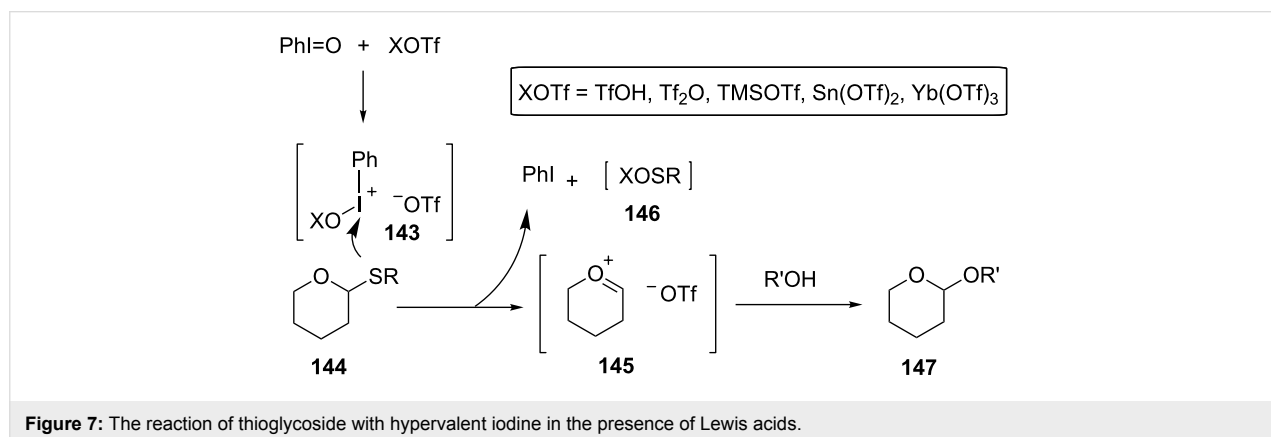
Scheme 17: Synthesis of acetoxyacetals using hypervalent iodine and addition of silylated base.



derived from carbohydrate antigen–adjuvant combinations has received much attention in recent years [75–77]. However, the difficulties associated with the isolation of tumor-associated carbohydrate antigens from natural sources have impeded extensive research. Thus, the most promising approach to the supply of these antigens is to develop a suitable method for their chemical synthesis.

To date, various glycosylation reactions capable of constructing oligosaccharides with high stereoselectivities have been reported [18,19]. Thioglycosides are often used as a sugar donor in these reactions due to their stability under various conditions

and specific activation with thiophilic agents. For example, one of the typical conditions used for the construction of oligosaccharides is the combination of Lewis acids and iodine or its chemical equivalents. Fukase and co-workers reported a glycosylation reaction with thioglycoside using hypervalent iodine reagents in the 1990s [78,79]. The outline and postulated mechanism of the reaction are shown in Figure 7. The reaction of iodosylbenzene and electrophiles, e.g., triflic anhydride or Lewis acids, should generate a potent thiophile **143** that reacts with thioglycoside **144** to form an oxocarbenium ion **145**. The resulting oxocarbenium ion **145** should in turn react with a sugar acceptor to give the glycosylated product **147** (Figure 7).



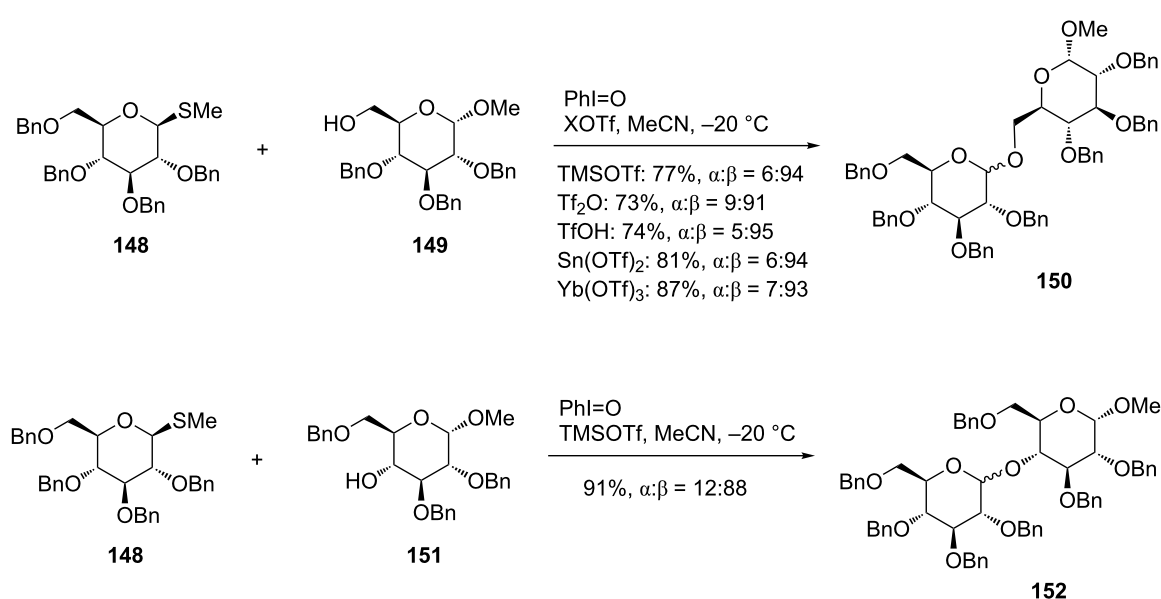
By this reaction, Fukase et al. reported the glycosylation of methyl thioglycoside **148** as a sugar donor to give disaccharides **150** and **152** in high chemical yields as depicted in Scheme 19. As mentioned above, not only triflic anhydride, but various Lewis acids (TMSOTf , $\text{Sn}(\text{OTf})_2$, $\text{Yb}(\text{OTf})_3$) and a Brønsted acid (TfOH) were proven useful as activators, by which the reaction finished in a short time and gave the products with high stereoselectivity [79].

Recently, the reaction was revisited by Kajimoto et al., who sought a glycosylation reaction that could be applied to disarmed thioglycosides using hypervalent iodine reagents [80,81]. One of the reactions they examined was the glycosylation reaction of methyl 2-phthalimidothioglucopyranoside **153** with methyl tribenzylglucopyranoside **149** by PIFA in the presence of various acid catalysts. The results showed that the reaction with PIFA and TfOH afforded the best result, giving disaccharide **154** in 77% yield. On the other hand, the use of bis[cyclohexyl]trifluoromethanesulfonylborane [(cyclo-Hex) $_2\text{BOTf}$] and methanesulfonic acid resulted in a poor yield. The synthesis of disaccharides under the optimized conditions was performed using “odorless” thioglycoside **155** and **149** as the donor and the acceptor [81]. Even with the combination of “disarmed” **155** and “armed” **149**, the reaction gave rise to the desired disaccharide **157** in 87% yield. The same reaction of the corresponding 3-epimer **156** proceeded smoothly to give the disaccharide **158** in good yield (Scheme 20).

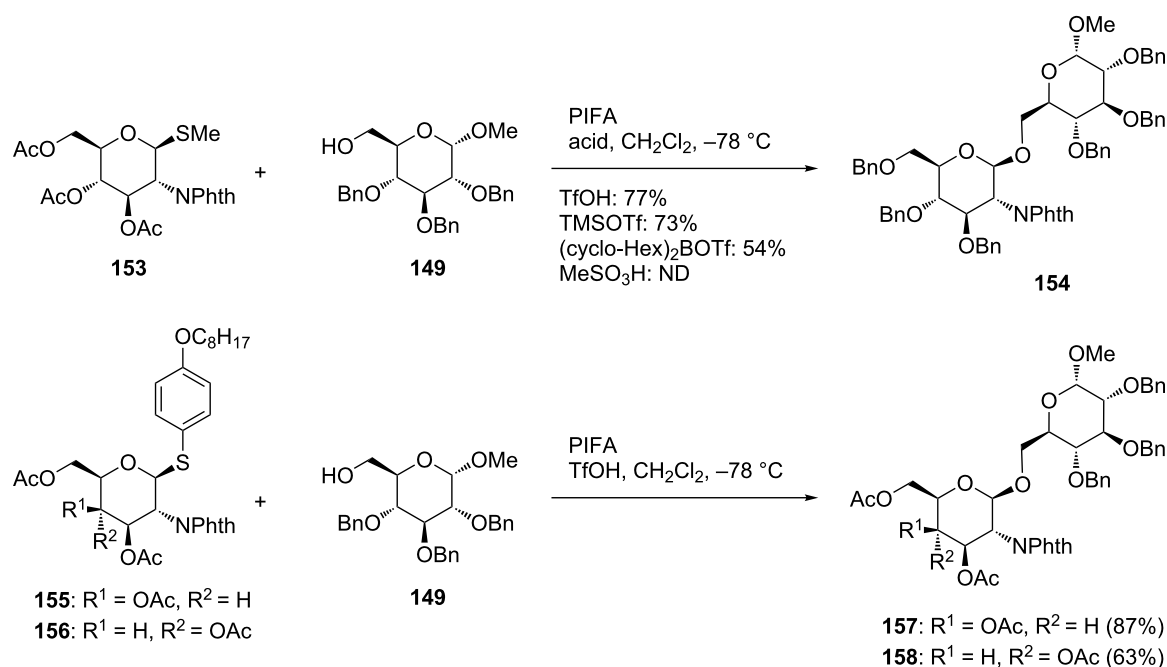
Randolph and Danishefsky reported a glycal assembly strategy to the synthesis of a branched oligosaccharide [82]. Bennett and

co-workers reported that phenyl(trifluoroethyl)iodonium triflimide was a stable promoter for glycosylation reactions using thioglycoside donors [83]. Since the reactions often were unselective in the absence of C2 acetate-directing groups, Bennett et al. investigated the compatibility of the above-mentioned reaction in nitrile solvents documented to have a β -directing effect, with the aim of developing a glycosylation that can be selectively achieved in the absence of directing groups. After preliminary screens, they found that the reaction in the presence of phenyl(trifluoroethyl)iodonium triflimide **160** and the non-nucleophilic base 2,4,6-*tert*-butylpyrimidine (TTBP) at 0 °C with the solvent combination of 2:1 CH_2Cl_2 /pivalonitrile provided the optimal reaction outcome. However, they also encountered a problem: the reduced solubility of substrate in the solvent system resulted in lower yields. They therefore examined mixed nitrile solvents again, and eventually found that a quaternary solvent mixture composed of 6:1:1:1 CH_2Cl_2 /acetonitrile/isobutyronitrile/pivalonitrile greatly improved both the chemical yields and stereoselectivity, as shown in Scheme 21. The results suggested that both the solvent system and iodonium salt promoter are required for selectivity.

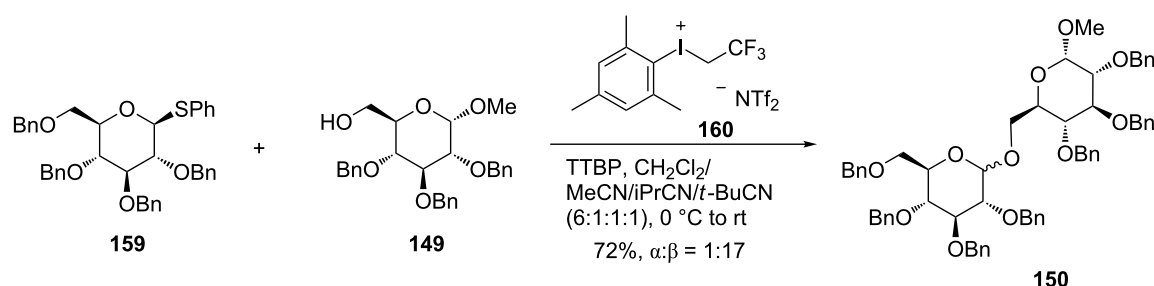
Even though glycals have a π -electron-rich enol ether unit, reports regarding transformations involving glycal oxidation as well as installation of heteroatom substituents at the C2 position were limited. In 2001, Gin's group reported the C2-acycloxyglycosylation procedure based on hypervalent iodine chemistry [84]. In this reaction, the use of a combination of hypervalent iodine and Lewis acid was key, as in the reactions described above. In this procedure, a solution of the glycal



Scheme 19: Synthesis of disaccharides employing thioglycosides under an oxidative coupling reaction mediated by hypervalent iodine.



Scheme 20: Synthesis of disaccharides using disarmed thioglycosides by hypervalent iodine-mediated glycosylation.



Scheme 21: Glycosylation using aryl(trifluoroethyl)iodium triflimide.

donor and a (diacyloxyiodo)benzene reagent was first treated with $\text{BF}_3 \cdot \text{OEt}_2$. Then, the glycosyl acceptor ($\text{R}''\text{OH}$) and a catalytic amount of TfOH were added to the mixture, giving the 1,2-*trans* disubstituted C2-acyloxyglycoside. A plausible mechanism of the reaction is shown in Figure 8. The first step of the reaction between glycal **161** and (diacyloxyiodo)benzene formed the glycosyl ester intermediate **162** bearing a phenyl iodonium(III) functionality at C2, which was transformed to a diacyloxyated product **163**. As evidence in support of this mechanism, they reported that **163** was indeed isolated when the reaction was finished at the first step. In the second step, the resulting diacyloxyated product **163** could effectively glycosylate the appropriate acceptor by the action of TfOH to give the C2-acyloxyglycoside **164** with good selectivity at the anomeric position as a consequence of participation by the neighboring C2 acyloxy group (Figure 8).

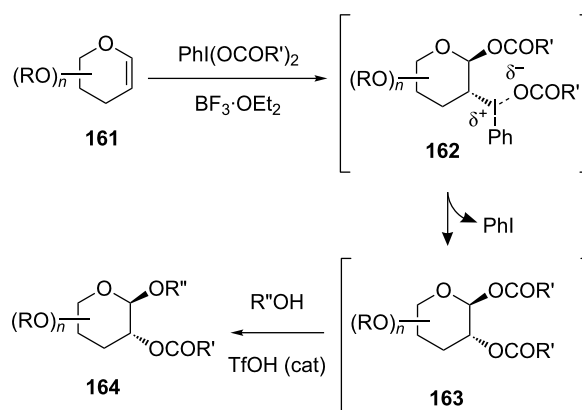
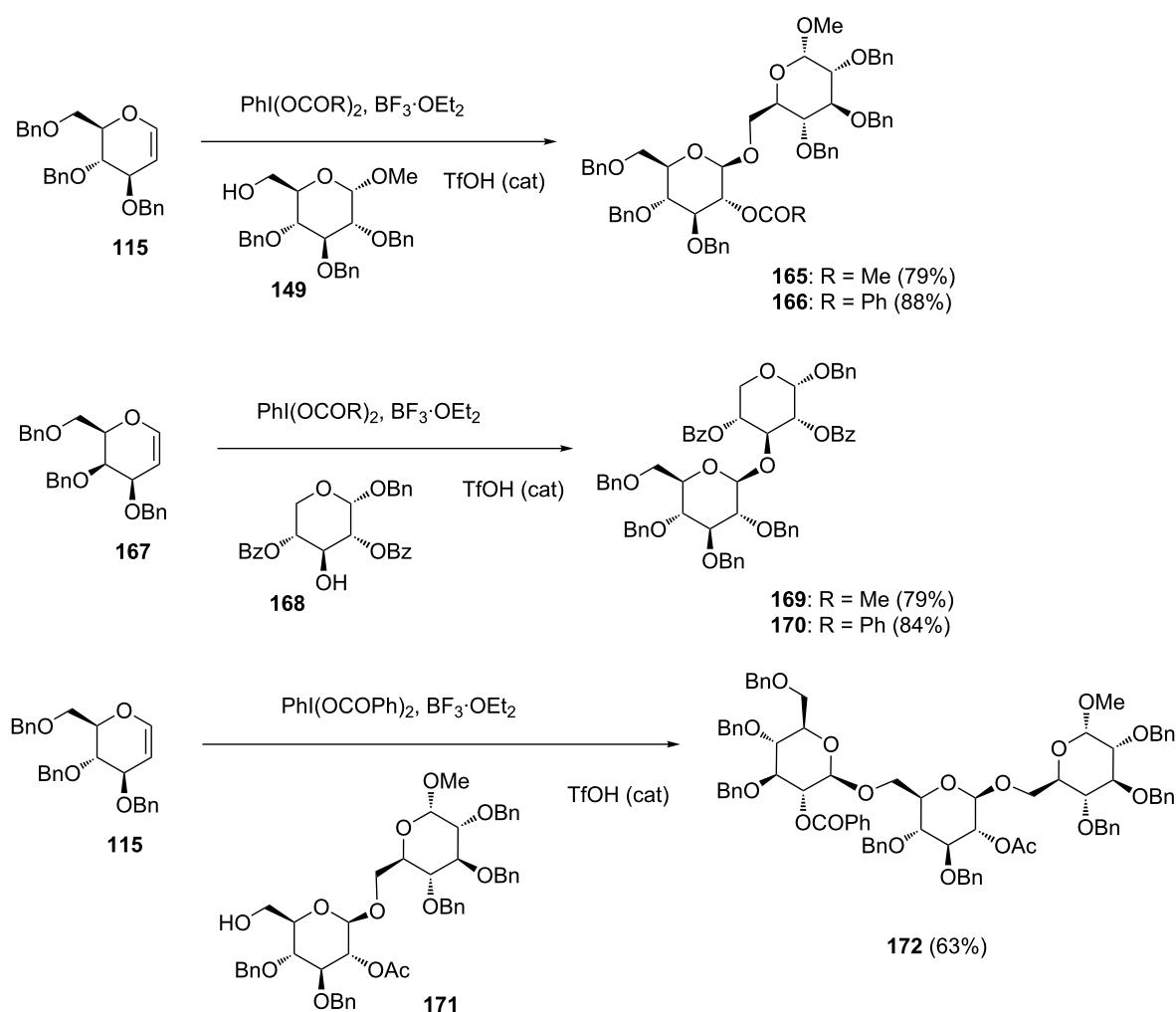


Figure 8: Expected mechanism of hypervalent iodine-mediated glycosylation with glycals.

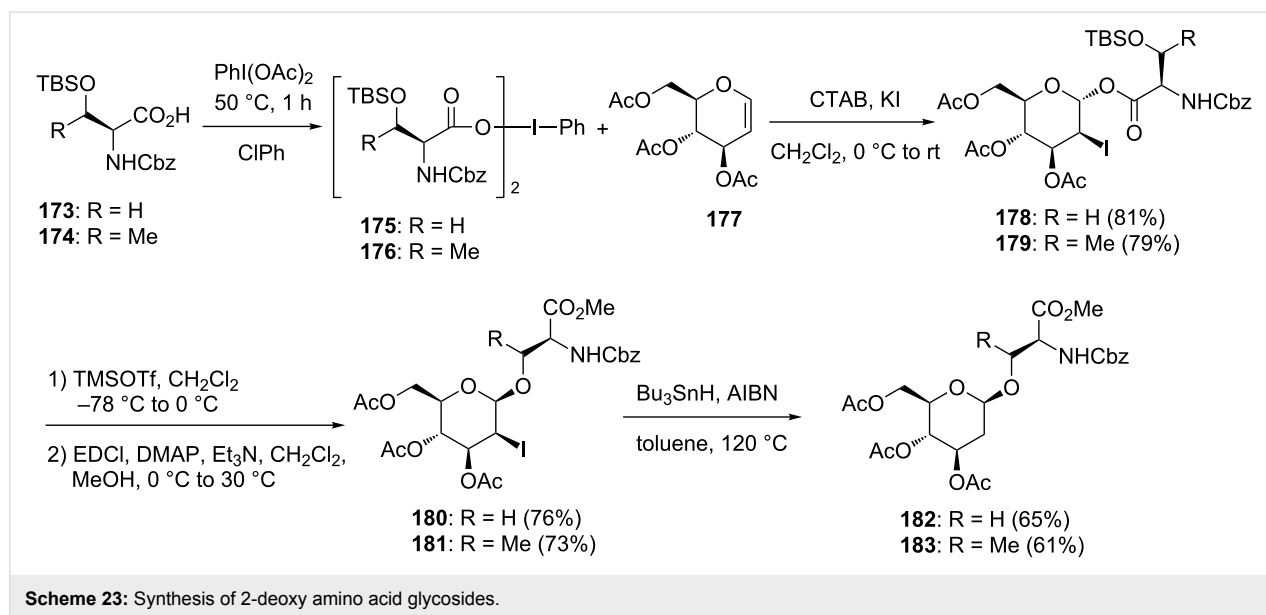
They prepared C2-acyloxy glycosides **165**, **166**, **169**, **170** and **172** using hypervalent iodine-mediated coupling reactions with glycols, and the results are shown in Scheme 22. Either (diacetoxyiodo)benzene or (dibenzoyloxyiodo)benzene could serve as an efficient oxidant, and the reactions utilizing them gave the products installing either the acetate or benzoate functionality, respectively, at the C2-position. Both glucal **115** and galactal **167** were amenable to the oxidative glycosylation reaction to stereoselectively give C2-acyloxylated β -glycosides in good yields [84] (Scheme 22).

Hotha and co-workers utilized the reaction of glycols with hypervalent iodine reagents for the stereoselective synthesis of C2 deoxyglycosides and amino acid glycoconjugates [85]. In their work, they also utilized an important chemical attribute of cetylammmonium bromide (CTAB) – namely, CTAB forms surfactant-assembled lipophilic nanoreactors stable in organic sol-

vents, which could be used for regioselective functionalization of indenes. Therefore, they investigated the regioselective iodination of glycols by using CTAB and hypervalent iodine reagents for the synthesis of 2-deoxy-2-iodoacetates. In the preliminary experiments, the reaction between per-*O*-acetylglucal (**177**) and $\text{PhI}(\text{OAc})_2$ in CTAB and KI gave *trans*-2-iodo α -acetate and its corresponding bromo acetate in a 94:5 ratio. The latter was expected to be formed by halide counter ion exchange between CTAB and KI. Since the reaction occurred as expected, it was applied to the synthesis of amino acid conjugates. Acetyl groups of the (diacetoxyiodo)benzene were exchanged with N- and O-protected amino acids by slow evaporation of a mixture of $\text{PhI}(\text{OAc})_2$ and amino acid **173** and **174** in chlorobenzene to give $\text{PhI}(\text{OCOR})_2$ compounds **175** and **176**. The formation of iodo ester glycosides **178** and **179** from **175** and **176** was achieved in very good yields under the conditions shown in Scheme 23.



Scheme 22: Synthesis of oligosaccharides by hypervalent iodine-mediated glycosylation with glycols.



Notably, the resulting iodo ester glycosides **178** and **179** were considered to have self-assembled structures versatile for the synthesis of serenylated and threonylated glycosides by intramolecular glycosylation. In addition, the access to 2-deoxyglycosides should be easily achievable by subsequent radical deiodination of the products. After several experiments, treatment with a catalytic amount of TMSOTf was found to be suitable for the intramolecular glycosylation, giving the corresponding acid, which was easily converted to the corresponding methyl ester **180** under EDCI/DMAP/MeOH conditions [85]. Similarly, the reaction of the threonine derivative **179** afforded **181** in good yield. Radical deiodination of **180** and **181** using Bu₃SnH and AIBN successfully gave 2-deoxy-β-glycosides **182** and **183**, which were difficult to synthesize from the corresponding 2-deoxy sugar derivative in a stereoselective manner (Scheme 23).

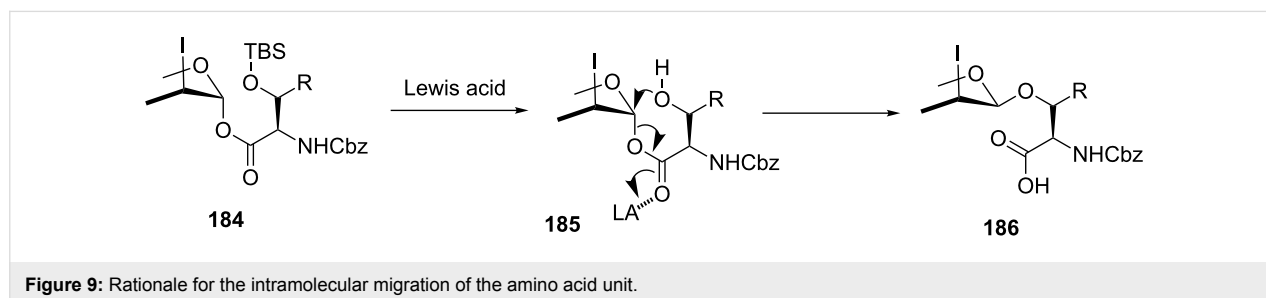
As mentioned above, the iodo ester glycosides were considered to have self-assembled structures suitable for intramolecular glycosylation. As depicted in Figure 9, treatment of **184** with TMSOTf first cleaved the silyl ether to form **185**, which was correctly positioned to undergo intramolecular glycosidation.

As a result, the Lewis acid could also facilitate the departure of the anomeric ester and the resulting **185** gave rise to the intramolecular nucleophilic attack to furnish the corresponding acid **186**.

Glycals and thioglycosides were often used as sugar donors for the glycosylation of oligosaccharides. It is interesting that the hypervalent iodine-mediated oxidative reactions with these derivatives provide a different method to build glycosidic bonds. Diversity in glycoside bond forming reactions would contribute to improve the oligosaccharide synthesis.

Conclusion

The Pummerer-type glycosylation includes oxidation of a sulfide to the corresponding sulfoxide followed by the TMSOTf-mediated coupling reaction. The reaction utilizing hypervalent iodine reagents could bypass one step of the Pummerer-type glycosylation and directly give 4'-thionucleosides from the corresponding sulfide derivative. The reaction could be efficiently applied to the synthesis of 4'-selenonucleosides as well as 4'-thionucleosides. Based on the concept of hypervalent iodine-mediated glycosylation, a reaction applic-



able to the synthesis of carbocyclic nucleosides and a coupling reaction between nucleobase and glycal derivatives were developed. The latter reaction was employed to synthesize dihydropyranonucleosides. Oxidative scission is a characteristic reaction mediated by hypervalent iodine reagents and is typically used for dehomologation of sugars. A one-pot glycosylation using this reaction was also developed for the synthesis of acyclic nucleoside derivatives. In addition to nucleoside synthesis, hypervalent iodine-mediated glycosylation could also be applied to the synthesis of oligosaccharides and glycoconjugates when thioglycosides and glycals were used as sugar donors. There is no doubt that the use of hypervalent iodine reagents greatly improved the efficiency of the synthesis of nucleosides and oligosaccharides. The results of these syntheses demonstrate the power of glycoside bond-forming reactions, and should assist in the future identification or synthesis of biologically active nucleoside and glycoconjugate derivatives.

Acknowledgements

Our work described in this review article was supported in part by a Grant-in-Aid for Scientific Research from JSPS and by a grant from the Strategic Research Foundation Grant-aided Project for Private Universities from the Ministry of Education, Culture, Sport, Science, and Technology, Japan (MEXT).

ORCID® iDs

Hideaki Wakamatsu - <https://orcid.org/0000-0003-4802-6288>

References

- Varki, A. *Glycobiology* **2017**, *27*, 3–49. doi:10.1093/glycob/cww086
- Nyhan, W. L. *Mol. Genet. Metab.* **2005**, *86*, 25–33. doi:10.1016/j.ymgme.2005.07.027
- Muntoni, F.; Brockington, M.; Blake, D. J.; Torelli, S.; Brown, S. C. *Lancet* **2002**, *360*, 1419–1421. doi:10.1016/s0140-6736(02)11397-3
- Jordheim, L. P.; Durantel, D.; Zoulim, F.; Dumontet, C. *Nat. Rev. Drug Discovery* **2013**, *12*, 447–464. doi:10.1038/nrd4010
- Schaefer, L.; Tredup, C.; Gubbiotti, M. A.; Iozzo, R. V. *FEBS J.* **2017**, *284*, 10–26. doi:10.1111/febs.13963
- Maishi, N.; Hida, K. *Cancer Sci.* **2017**, *108*, 1921–1926. doi:10.1111/cas.13336
- Sanderson, R. D.; Elkin, M.; Rapraeger, A. C.; Ilan, N.; Vlodavsky, I. *FEBS J.* **2017**, *284*, 42–55. doi:10.1111/febs.13932
- Meadows, D. C.; Gervay-Hague, J. *ChemMedChem* **2006**, *1*, 16–29. doi:10.1002/cmdc.200500026
- Stutz, A. E., Ed. *Iminosugars as Glycosidase Inhibitors: Nojirimycin and Beyond*; Wiley-VCH: Weinheim, Germany, 1999.
- Asano, N.; Nash, R. J.; Molyneux, R. J.; Fleet, G. W. J. *Tetrahedron: Asymmetry* **2000**, *11*, 1645–1680. doi:10.1016/s0957-4166(00)00113-0
- Saneyoshi, H.; Ito, Y.; Abe, H. *J. Am. Chem. Soc.* **2013**, *135*, 13632–13635. doi:10.1021/ja406724k
- Seo, S.; Onizuka, K.; Nishioka, C.; Takahashi, E.; Tsuneda, S.; Abe, H.; Ito, Y. *Org. Biomol. Chem.* **2015**, *13*, 4589–4595. doi:10.1039/c5ob00199d
- Kato, A.; Hayashi, E.; Miyauchi, S.; Adachi, I.; Imahori, T.; Natori, Y.; Yoshimura, Y.; Nash, R. J.; Shimaoka, H.; Nakagome, I.; Koseki, J.; Hirono, S.; Takahata, H. *J. Med. Chem.* **2012**, *55*, 10347–10362. doi:10.1021/jm301304e
- Kato, A.; Nakagome, I.; Sato, K.; Yamamoto, A.; Adachi, I.; Nash, R. J.; Fleet, G. W. J.; Natori, Y.; Watanabe, Y.; Imahori, T.; Yoshimura, Y.; Takahata, H.; Hirono, S. *Org. Biomol. Chem.* **2016**, *14*, 1039–1048. doi:10.1039/C5OB02223A
- Niedballa, U.; Vorbrüggen, H. *J. Org. Chem.* **1974**, *39*, 3654–3660. doi:10.1021/jo00939a008
- Vorbrüggen, H.; Ruh-Pohlenz, C. *Organic Reactions*; John Wiley & Sons, Inc., 2004. doi:10.1002/0471264180.or055.01
- Yoshimura, Y. *Heterocycles* **2017**, *94*, 1625–1651. doi:10.3987/REV-17-865
- Hanessian, S.; Lou, B. *Chem. Rev.* **2000**, *100*, 4443–4464. doi:10.1021/cr9903454
- Zhu, X.; Schmidt, R. R. *Angew. Chem., Int. Ed.* **2009**, *48*, 1900–1934. doi:10.1002/anie.200802036
- Yoshimura, Y.; Kobayashi, S.; Kaneko, H.; Suzuki, T.; Imamichi, T. *Molecules* **2015**, *20*, 4623–4634. doi:10.3390/molecules20034623
- Kiran, Y. B.; Wakamatsu, H.; Natori, Y.; Takahata, H.; Yoshimura, Y. *Tetrahedron Lett.* **2013**, *54*, 3949–3952. doi:10.1016/j.tetlet.2013.05.062
- Yoshimura, Y.; Asami, K.; Imamichi, T.; Okuda, T.; Shiraki, K.; Takahata, H. *J. Org. Chem.* **2010**, *75*, 4161–4171. doi:10.1021/jo100556u
- Matsuda, A.; Takenuki, K.; Tanaka, M.; Sasaki, T.; Ueda, T. *J. Med. Chem.* **1991**, *34*, 812–819. doi:10.1021/jm00106a049
- Yamagami, K.; Fujii, A.; Arita, M.; Okumoto, T.; Sakata, S.; Matsuda, A.; Ueda, T.; Sasaki, T. *Cancer Res.* **1991**, *51*, 2319–2323.
- Dyson, M. R.; Coe, P. L.; Walker, R. T. *J. Med. Chem.* **1991**, *34*, 2782–2786. doi:10.1021/jm00113a016
- Secrist III, J. A.; Tiwari, K. N.; Riordan, J. M.; Montgomery, J. A. *J. Med. Chem.* **1991**, *34*, 2361–2366. doi:10.1021/jm00112a007
- Yoshimura, Y.; Kitano, K.; Satoh, H.; Watanabe, M.; Miura, S.; Sakata, S.; Sasaki, T.; Matsuda, A. *J. Org. Chem.* **1996**, *61*, 822–823. doi:10.1021/jo9519423
- Yoshimura, Y.; Kitano, K.; Yamada, K.; Satoh, H.; Watanabe, M.; Miura, S.; Sakata, S.; Sasaki, T.; Matsuda, A. *J. Org. Chem.* **1997**, *62*, 3140–3152. doi:10.1021/jo9700540
- Kita, Y.; Yasuda, H.; Tamura, O.; Itoh, F.; Tamura, Y. *Tetrahedron Lett.* **1984**, *25*, 4681–4682. doi:10.1016/s0040-4039(01)91232-8
- Kita, Y.; Tamura, O.; Yasuda, H.; Itoh, F.; Tamura, Y. *Chem. Pharm. Bull.* **1985**, *33*, 4235–4241. doi:10.1248/cpb.33.4235
- Naka, T.; Minakawa, N.; Abe, H.; Kaga, D.; Matsuda, A. *J. Am. Chem. Soc.* **2000**, *122*, 7233–7243. doi:10.1021/ja000541o
- Yoshimura, Y.; Kuze, T.; Ueno, M.; Komiya, F.; Haraguchi, K.; Tanaka, H.; Kano, F.; Yamada, K.; Asami, K.; Kaneko, N.; Takahata, H. *Tetrahedron Lett.* **2006**, *47*, 591–594. doi:10.1016/j.tetlet.2005.11.049
- Jeong, L. S.; Moon, H. R.; Choi, Y. J.; Chun, M. W.; Kim, H. O. *J. Org. Chem.* **1998**, *63*, 4821–4825. doi:10.1021/jo980196+
- Lim, M. H.; Kim, H. O.; Moon, H. R.; Chun, M. W.; Jeong, L. S. *Org. Lett.* **2002**, *4*, 529–531. doi:10.1021/ol017112v
- Jeong, L. S.; Lee, H. W.; Kim, H. O.; Jung, J. Y.; Gao, Z.-G.; Duong, H. T.; Rao, S.; Jacobson, K. A.; Shin, D. H.; Lee, J. A.; Gunaga, P.; Lee, S. K.; Jin, D. Z.; Chun, M. W.; Moon, H. R. *Bioorg. Med. Chem.* **2006**, *14*, 4718–4730. doi:10.1016/j.bmc.2006.03.030

36. Choi, W. J.; Lee, H. W.; Kim, H. O.; Chinn, M.; Gao, Z.-G.; Patel, A.; Jacobson, K. A.; Moon, H. R.; Jung, Y. H.; Jeong, L. S. *Bioorg. Med. Chem.* **2009**, *17*, 8003–8011. doi:10.1016/j.bmc.2009.10.011
37. Qu, S.; Mulamootil, V. A.; Nayak, A.; Ryu, S.; Hou, X.; Song, J.; Yu, J.; Sahu, P. K.; Zhao, L. X.; Choi, S.; Lee, S. K.; Jeong, L. S. *Bioorg. Med. Chem.* **2016**, *24*, 3418–3428. doi:10.1016/j.bmc.2016.05.041
38. Yoshimura, A.; Zhdankin, V. V. *Chem. Rev.* **2016**, *116*, 3328–3435. doi:10.1021/acs.chemrev.5b00547
39. Dohi, T.; Morimoto, K.; Maruyama, A.; Kita, Y. *Org. Lett.* **2006**, *8*, 2007–2010. doi:10.1021/ol060333m
40. Kita, Y.; Morimoto, K.; Ito, M.; Ogawa, C.; Goto, A.; Dohi, T. *J. Am. Chem. Soc.* **2009**, *131*, 1668–1669. doi:10.1021/ja808940n
41. Morimoto, K.; Yamaoka, N.; Ogawa, C.; Nakae, T.; Fujioka, H.; Dohi, T.; Kita, Y. *Org. Lett.* **2010**, *12*, 3804–3807. doi:10.1021/ol101498r
42. Dohi, T.; Ito, M.; Itani, I.; Yamaoka, N.; Morimoto, K.; Fujioka, H.; Kita, Y. *Org. Lett.* **2011**, *13*, 6208–6211. doi:10.1021/ol202632h
43. Ito, M.; Kubo, H.; Itani, I.; Morimoto, K.; Dohi, T.; Kita, Y. *J. Am. Chem. Soc.* **2013**, *135*, 14078–14081. doi:10.1021/ja407944p
44. Tohma, H. *Chem. Commun.* **1998**, 173–174. doi:10.1039/a707727k
45. Nishizono, N.; Baba, R.; Nakamura, C.; Oda, K.; Machida, M. *Org. Biomol. Chem.* **2003**, *1*, 3692–3697. doi:10.1039/B305644A
46. Nishizono, N.; Soma, K.; Baba, R.; Machida, M.; Oda, K. *Heterocycles* **2008**, *75*, 619–634. doi:10.3987/COM-07-11250
47. Nishizono, N.; Akama, Y.; Agata, M.; Sugo, M.; Yamaguchi, Y.; Oda, K. *Tetrahedron* **2011**, *67*, 358–363. doi:10.1016/j.tet.2010.11.038
48. Jeong, L. S.; Tosh, D. K.; Kim, H. O.; Wang, T.; Hou, X.; Yun, H. S.; Kwon, Y.; Lee, S. K.; Choi, J.; Zhao, L. X. *Org. Lett.* **2008**, *10*, 209–212. doi:10.1021/ol7025558
49. Inagaki, Y.; Minakawa, N.; Matsuda, A. *Nucleic Acids Symp. Ser.* **2007**, *51*, 139–140. doi:10.1093/nass/nrm070
50. Jayakanthan, K.; Johnston, B. D.; Pinto, B. M. *Carbohydr. Res.* **2008**, *343*, 1790–1800. doi:10.1016/j.carres.2008.02.014
51. Tosh, D. K.; Choi, W. J.; Kim, H. O.; Lee, Y.; Pal, S.; Hou, X.; Choi, J.; Choi, S.; Jeong, L. S. *J. Org. Chem.* **2008**, *73*, 4259–4262. doi:10.1021/jo8003277
52. Alexander, V.; Choi, W. J.; Chun, J.; Kim, H. O.; Jeon, J. H.; Tosh, D. K.; Lee, H. W.; Chandra, G.; Choi, J.; Jeong, L. S. *Org. Lett.* **2010**, *12*, 2242–2245. doi:10.1021/ol1005906
53. Yu, J.; Kim, J.-H.; Lee, H. W.; Alexander, V.; Ahn, H.-C.; Choi, W. J.; Choi, J.; Jeong, L. S. *Chem. – Eur. J.* **2013**, *19*, 5528–5532. doi:10.1002/chem.201300741
54. Kim, J.-H.; Yu, J.; Alexander, V.; Choi, J. H.; Song, J.; Lee, H. W.; Kim, H. O.; Choi, J.; Lee, S. K.; Jeong, L. S. *Eur. J. Med. Chem.* **2014**, *83*, 208–225. doi:10.1016/j.ejmech.2014.06.031
55. Sahu, P. K.; Kim, G.; Yu, J.; Ahn, J. Y.; Song, J.; Choi, Y.; Jin, X.; Kim, J.-H.; Lee, S. K.; Park, S.; Jeong, L. S. *Org. Lett.* **2014**, *16*, 5796–5799. doi:10.1021/ol502899b
56. Alexander, V.; Song, J.; Yu, J.; Choi, J. H.; Kim, J.-H.; Lee, S. K.; Choi, W. J.; Jeong, L. S. *Arch. Pharmacol. Res.* **2015**, *38*, 966–972. doi:10.1007/s12272-014-0466-6
57. Kim, G.; Choi, Y.; Sahu, P. K.; Yu, J.; Qu, S.; Lee, D.; Jeong, L. S. *Org. Lett.* **2015**, *17*, 4636–4639. doi:10.1021/acs.orglett.5b02393
58. Qu, S.; Kim, G.; Yu, J.; Sahu, P. K.; Choi, Y.; Naik, S. D.; Jeong, L. S. *Asian J. Org. Chem.* **2016**, *5*, 735–741. doi:10.1002/ajoc.201600154
59. Taniike, H.; Inagaki, Y.; Matsuda, A.; Minakawa, N. *Tetrahedron* **2011**, *67*, 7977–7982. doi:10.1016/j.tet.2011.08.020
60. Ishii, K.; Saito-Tarashima, N.; Ota, M.; Yamamoto, S.; Okamoto, Y.; Tanaka, Y.; Minakawa, N. *Tetrahedron* **2016**, *72*, 6589–6594. doi:10.1016/j.tet.2016.08.071
61. Ochiai, M.; Fujita, E.; Arimoto, M.; Yamaguchi, H. *Chem. Pharm. Bull.* **1985**, *33*, 41–47. doi:10.1248/cpb.33.41
62. Dohi, T.; Maruyama, A.; Minamitsuji, Y.; Takenaga, N.; Kita, Y. *Chem. Commun.* **2007**, 1224–1226. doi:10.1039/B616510A
63. Yoshimura, Y.; Ohta, M.; Imahori, T.; Imamichi, T.; Takahata, H. *Org. Lett.* **2008**, *10*, 3449–3452. doi:10.1021/ol8012155
64. Jung, M. E.; Gaede, B. *Tetrahedron* **1979**, *35*, 621–625. doi:10.1016/0040-4020(79)87006-4
65. Ochiai, M.; Miyamoto, K.; Kaneaki, T.; Hayashi, S.; Nakanishi, W. *Science* **2011**, *332*, 448–451. doi:10.1126/science.1201686
66. Cho, S. H.; Yoon, J.; Chang, S. J. *Am. Chem. Soc.* **2011**, *133*, 5996–6005. doi:10.1021/ja111652v
67. Antonchick, A. P.; Samanta, R.; Kulikov, K.; Lategahn, J. *Angew. Chem., Int. Ed.* **2011**, *50*, 8605–8608. doi:10.1002/anie.201102984
68. Souto, J. A.; Zian, D.; Muñoz, K. J. *Am. Chem. Soc.* **2012**, *134*, 7242–7245. doi:10.1021/ja3013193
69. Yoshimura, Y.; Kan-no, H.; Kiran, Y. B.; Natori, Y.; Saito, Y.; Takahata, H. *Synthesis* **2012**, *44*, 1163–1170. doi:10.1055/s-0031-1290749
70. Kan-no, H.; Saito, Y.; Omoto, S.; Minato, S.; Wakamatsu, H.; Natori, Y.; Imamichi, T.; Takahata, H.; Yoshimura, Y. *Synthesis* **2014**, *46*, 879–886. doi:10.1055/s-0033-1340663
71. Havare, N.; Plattner, D. A. *Org. Lett.* **2012**, *14*, 5078–5081. doi:10.1021/ol301675v
72. Miyamoto, K.; Tada, N.; Ochiai, M. J. *Am. Chem. Soc.* **2007**, *129*, 2772–2773. doi:10.1021/ja070179e
73. Francisco, C. G.; Freire, R.; González, C. C.; León, E. I.; Riesco-Fagundo, C.; Suárez, E. J. *Org. Chem.* **2001**, *66*, 1861–1866. doi:10.1021/jo0057452
74. Boto, A.; Hernández, D.; Hernández, R.; Álvarez, E. J. *Org. Chem.* **2007**, *72*, 9523–9532. doi:10.1021/jo701608p
75. Galonić, D. P.; Gin, D. Y. *Nature* **2007**, *446*, 1000–1007. doi:10.1038/nature05813
76. Buskas, T.; Thompson, P.; Boons, G. J. *Chem. Commun.* **2009**, 5335–5349. doi:10.1039/b908664c
77. Fernández-Tejada, A.; Cañada, F. J.; Jiménez-Barbero, J. *Chem. – Eur. J.* **2015**, *21*, 10616–10628. doi:10.1002/chem.201500831
78. Fukase, K.; Aoki, Y.; Kinoshita, I.; Suda, Y.; Kurosawa, M.; Zähringer, U.; Rietschel, E. T.; Kusumoto, S. *Tetrahedron Lett.* **1995**, *36*, 8645–8648. doi:10.1016/0040-4039(95)01863-D
79. Fukase, K.; Kinoshita, I.; Kanoh, T.; Nakai, Y.; Hasuoka, A.; Kusumoto, S. *Tetrahedron* **1996**, *52*, 3897–3904. doi:10.1016/S0040-4020(96)00057-9
80. Kajimoto, T.; Morimoto, K.; Ogawa, R.; Dohi, T.; Kita, Y. *Eur. J. Org. Chem.* **2015**, *2015*, 2138–2142. doi:10.1002/ejoc.201500186
81. Kajimoto, T.; Morimoto, K.; Ogawa, R.; Dohi, T.; Kita, Y. *Chem. Pharm. Bull.* **2016**, *64*, 838–844. doi:10.1248/cpb.c16-00203
82. Randolph, J.; Danishefsky, S. J. *J. Am. Chem. Soc.* **1993**, *115*, 8473–8474. doi:10.1021/ja00071a077
83. Chu, A.-H. A.; Minciunescu, A.; Bennett, C. S. *Org. Lett.* **2015**, *17*, 6262–6265. doi:10.1021/acs.orglett.5b03282
84. Shi, L.; Kim, Y.-J.; Gin, D. Y. *J. Am. Chem. Soc.* **2001**, *123*, 6939–6940. doi:10.1021/ja015991a
85. Islam, M.; Tirukoti, N. D.; Nandi, S.; Hotha, S. J. *Org. Chem.* **2014**, *79*, 4470–4476. doi:10.1021/jo500465m

License and Terms

This is an Open Access article under the terms of the Creative Commons Attribution License (<http://creativecommons.org/licenses/by/4.0>), which permits unrestricted use, distribution, and reproduction in any medium, provided the original work is properly cited.

The license is subject to the *Beilstein Journal of Organic Chemistry* terms and conditions: (<https://www.beilstein-journals.org/bjoc>)

The definitive version of this article is the electronic one which can be found at:
[doi:10.3762/bjoc.14.137](https://doi.org/10.3762/bjoc.14.137)

Medicinal and Bioorganic Chemistry of Nucleosides and Nucleotides

Review

Synthesis of 4'-Thionucleosides as Antitumor and Antiviral Agents

Yuichi Yoshimura,* Yukako Saito, Yoshihiro Natori, and Hideaki Wakamatsu

*Faculty of Pharmaceutical Sciences, Tohoku Medical and Pharmaceutical University;
4-4-1 Komatsushima, Aoba-ku, Sendai 981-8558, Japan.*

Received August 10, 2017

Many attempts have been made to synthesize structurally novel nucleoside derivatives in order to identify effective compounds for the treatment of tumors and virus-caused disease. At our laboratories, as part of our efforts to synthesize 4'-thionucleosides, we have identified and characterized biologically active nucleosides. During the course of our synthetic study, we developed the Pummerer-type thioglycosylation reaction. As a result, we synthesized a potent antineoplastic nucleoside, 1-(2-deoxy-2-fluoro- β -D-4-thio-arabino-furanosyl)cytosine (4'-thioFAC), and several novel 4'-thionucleosides that possess antiherpes virus activities.

Key words nucleoside; antitumor; antiviral; 4'-thionucleoside; antiherpes virus; Pummerer reaction

1. Introduction

To date, many nucleoside antimetabolites have been used as chemotherapeutics for cancers and virus-caused diseases. For example, cytarabine, a cytidine analogue that contains D-arabinose in place of its ribose sugar, is used for treatment of leukemia.^{1,2)} Gemcitabine hydrochloride (2'-deoxy-2'-difluorocytidine) developed by Eli Lilly, is an anticancer drug approved for the treatment of pancreas cancer, and also used clinically for lung cancers and other tumors.^{3,4)} Aciclovir, developed by Wellcome, is a 2',3'-nor derivative (acyclo nucleoside) of guanosine and one of the most successful antiherpes drugs.⁵⁾ Ganciclovir, which also belongs to the category of acyclo nucleosides, is used for treating diseases related to human cytomegalovirus.^{6,7)} 3'-Azido-3'-deoxythymidine (zidovudine, AZT), discovered by Mitsuya of the National Cancer Institute (NCI; Bethesda, MD, U.S.A.), was the first anti-human immunodeficiency virus (HIV) drug approved for the treatment of AIDS, and still plays a significant role in AIDS treatment.⁸⁾ In addition, the recent success of sofosbuvir, an anti-hepatitis C drug developed by Pharmasset (Gilead), has had a huge impact in the field of medicinal chemistry⁹⁾ (Chart 1). The discovery of these important drugs is the fruit of concerted research efforts into the synthesis of nucleoside derivatives. However, the use of nucleoside antimetabolites also has the serious drawback that these agents may acquire drug resistance during clinical use.^{10–12)} To overcome this problem, the synthesis of diverse and structurally novel nucleoside derivatives is urgently needed in order to continue the search for new antitumor and antiviral agents.

2. Development of Pummerer-Type Glycosylation and Its Application to the Synthesis of 4'-Thionucleosides

About 25 years ago, when we started a new project to explore antitumor and antiviral nucleosides, we were intrigued by the reports of Walker and colleagues¹³⁾ and Secrist *et al.*¹⁴⁾ that 2'-deoxy-4'-thionucleosides, in which the ring oxygen

of the 2-deoxyribose constituting 2'-deoxynucleosides was replaced with sulfur, had potent anti-herpes virus activity and, in some cases, cytotoxicity as well. In addition, 2'-substituted cytidine derivatives, *e.g.*, 2'-deoxy-2'-methylenecytidine (DMDC) (2)^{15,16)} and gemcitabine,^{3,4)} were developed and reported to have potent antitumor activity. Most of the nucleoside antimetabolites are prodrugs, which need to be converted to their active form in cells. The corresponding nucleoside mono-, di- and triphosphates are often the active forms that inhibit target enzymes, *e.g.*, DNA polymerase and reverse transcriptase.^{10–12)} Therefore, the nucleoside derivatives must be recognized by intracellular or viral-coded deoxynucleoside kinase as a substrate in order to exert their antitumor or antiviral effects. The above-described results for 4'-thionucleosides and 2'-substituted nucleosides strongly suggest that 2'-substituted 4'-thionucleosides could be recognized by these enzymes and would have promising biological activity. Thus, we chose a novel 2'-substituted 4'-thiocytidine, 4'-thio DMDC (3), as our target molecule for potential antitumor and antiviral agents (Chart 2).

To our knowledge, at the time that we began this project, the only 4'-thionucleosides that had been synthesized were 4'-thioribonucleosides,^{17–19)} 4'-thioarabinonucleosides^{20–22)} and 2'-deoxy-4'-thionucleosides.^{13,14)} The development of a synthetic strategy for 4'-thionucleosides applicable to the synthesis of 2'-substituted derivatives was thus a key to the success of this project. From the viewpoint of the structure–activity relationship, the synthesis should include a glycosylation reaction of nucleobase with 4-thiosugars, since various base-modified analogues could be obtained from a single 4-thiosugar intermediate by the glycosidation strategy. Thus, our first goal was to achieve the synthesis of 4-thiosugars by the method generally applicable to the synthesis of the 2-substituted 4-thiosugar derivatives.

To construct a glycosidic linkage between the base and sugar moiety of the nucleoside skeleton, the Vorbrüggen re-

*To whom correspondence should be addressed. e-mail: yoshimura@tohoku-mpu.ac.jp

action is generally used.²³⁾ It was clear, at the time when we started our project, that the reaction could be used in the synthesis of 4'-thionucleosides as well as normal "4'-oxy" nucleosides. In addition, 1-acetoxy-4-thiosugar **5**, one of the most effective substrates for the Vorbrüggen reaction, could be easily obtained from a corresponding sulfoxide **4** by classical Pummerer rearrangement. On the other hand, we noticed that the Vorbrüggen reaction of 1-acetate **5** generated a sulfenium ion **6** which could also be formed by the sila-Pummerer reaction, developed by Kita *et al.*,^{24,25)} of the sulfoxide **4**. This new type of glycosylation reaction seemed quite attractive since it could bypass one step and achieve direct access to the sulfenium ion **5** from the sulfoxide **4** (Chart 3). Thus, our second goal for the planned synthesis of 4'-thionucleoside was to develop this new "Pummerer-type" thioglycosylation reaction.

Starting from a xylose derivative **8**,²⁶⁾ thiabicyclo sugar **9**

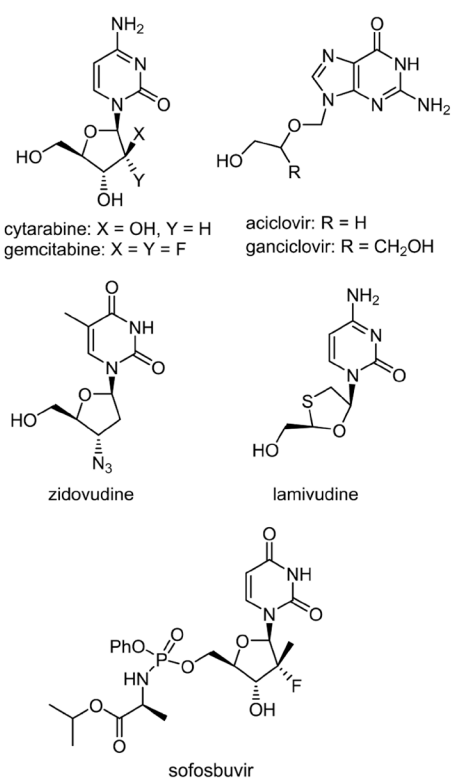


Chart 1

was prepared by methanolysis of the 1,2-isopropylidene group, mesylation of the 2- and 5-hydroxy groups and subsequent inter/intramolecular *S_N2* reaction with sodium sulfide. Hydrolysis of **9** followed by hydride reduction gave a 4-thioarabinose derivative **10** which was protected at the primary hydroxyl group to give **11**. Through the cyclic intermediate **9**, chirality of the 2, 3, and 4 positions of xylose was transferred to the 4, 3, and 2 positions of the 4-thioarabinose derivative **10**, respec-

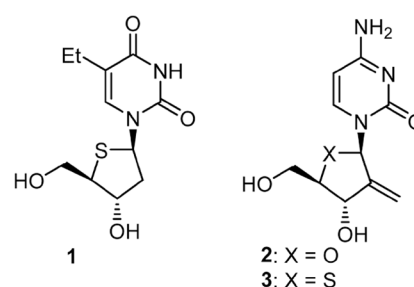


Chart 2

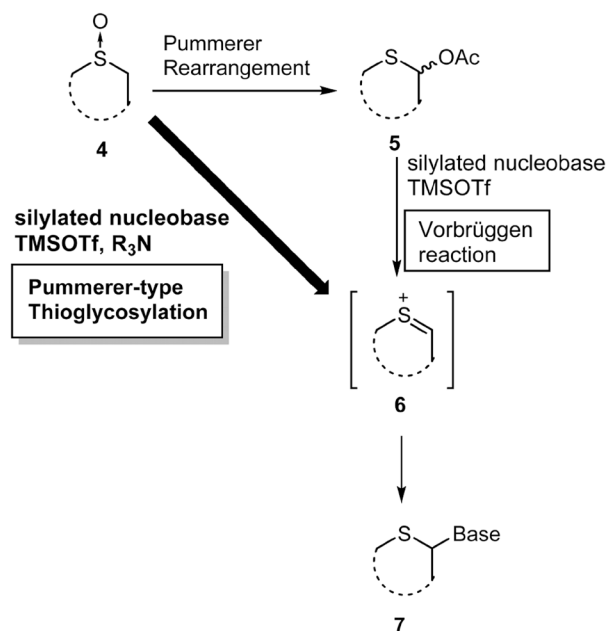


Chart 3

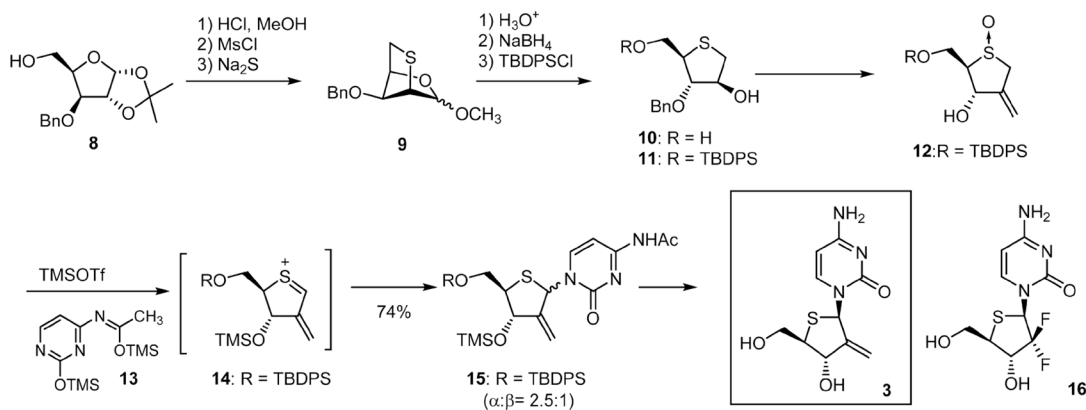


Chart 4

tively. Oxidation of **11** followed by the Wittig reaction gave a methylene derivative which was debenzylated and oxidized to the corresponding sulfoxide to give **12**. Next, we tried the Pummerer-type thioglycosylation of *N*⁴-acetylcytosine with the sulfoxide **12**. Fortunately, we found that the reaction of **12** with excess persilylated *N*⁴-acetylcytosine in the presence of trimethylsilyl trifluoromethanesulfonate (TMSOTf) gave an anomeric mixture of 4'-thioDMDC derivative **15** in good yield. The results suggested that the reaction occurred by forming the expected sulfenium ion **14** and that the concept of the Pummerer-type glycosylation was actually effective for formation of the glycoside bond of 4'-thionucleosides. Deprotection of **15** and the separation of anomers by octadecyl silica (ODS) column chromatography furnished 4'-thioDMDC (**3**) along with its α -anomer.^{27,28} We also synthesized 4'-thiogemcitabine (**16**) from **11** by using a similar synthetic scheme^{27,28} (Chart 4).

As described above, the intermediate for 4'-thioDMDC

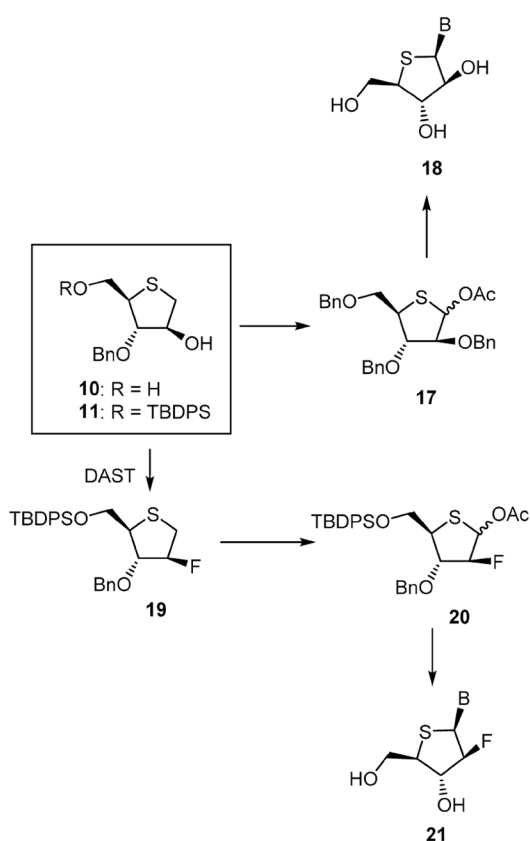


Table 1. Antitumor Activity of 2'-Substituted 4'-Thiocytidine Derivatives

Compound	2'-Substituent	Antineoplastic activities IC ₅₀ (μg/mL)	
		CCRF-HSB-2	KB cells
4'-ThioDMDC (3)	=CH ₂	0.0091	0.12
4'-Thiogemcitabine (16)	F ₂	1.5	17
4'-ThioFAC (21 ; B=Cyt)	F (<i>arabino</i>)	0.051	0.015
Cytarabine	—	0.052	0.26
DMDC (2)	—	0.022	0.44

could also be used for the synthesis of other 4'-thionucleosides. Compound **10** was benzylated at the hydroxyl groups and converted to 1-acetate derivative **17** via Pummerer rearrangement. The Vorbrüggen reaction of **17** with silylated nucleobases in the presence of Lewis acid and the subsequent deprotection gave 4'-thioarabinonucleosides **18**.²⁹ Introduction of a fluoro group at the 2-position was achieved by treatment of **11** with *N,N*-diethylaminosulfur trifluoride (DAST) to give the 2-fluorinated compound **19** with retention of the stereochemistry at the reaction site. Similar results reported by Marquez and colleagues suggested that the reaction proceeded by a neighboring group participation of ring sulfur to form an episulfonium ion prior to the nucleophilic attack of fluoride ion.³⁰ The synthesis of 2'-fluoro-*arabino*-4'-thionucleosides **21** from **19** was achieved by the Vorbrüggen reaction and the subsequent deprotection as in the case of 4'-thioarabinonucleosides^{28,31} (Chart 5).

3. Antitumor Activity of 4'-Thionucleosides

The obtained 2'-substituted 4'-thionucleosides were evaluated for their antitumor and antiviral activities. Among the cytidine derivatives, 4'-thioDMDC (**3**) and 2'-deoxy-2'-fluoro-

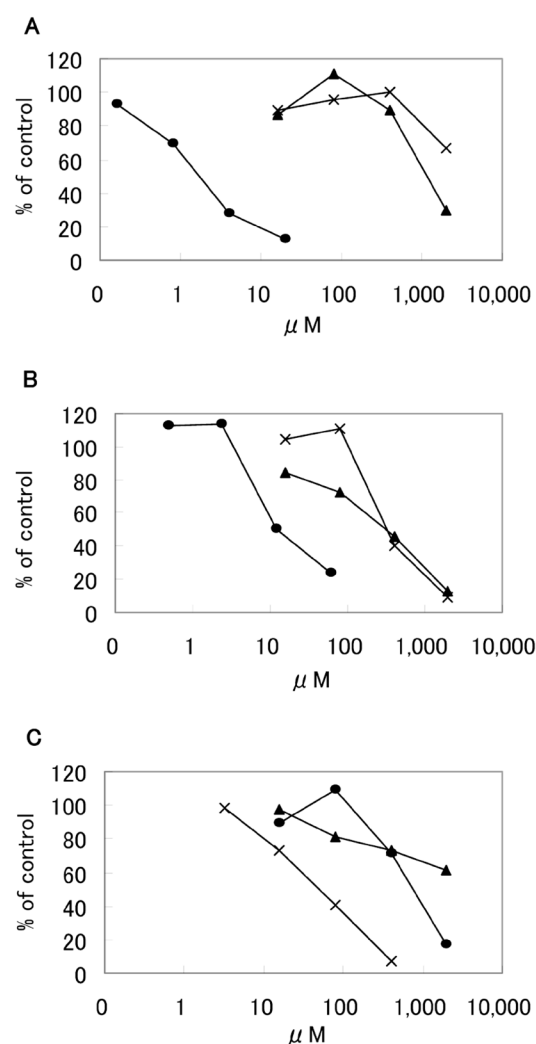


Fig. 1. The Inhibitory Effects of 4'-ThioFACTP, dFdCTP and ddCTP on Mammalian DNA Polymerase α (A), β (B) and γ (C)

●: 4'-thioFACTP; ▲: dFdCTP; ×: ddCTP.

arabino-4'-thiocytidine (4'-thioFAC, **21**; B=cytosine) were shown to have potent cytotoxicities against human T-cell leukemia, CCRF-HSB-2 and solid tumor KB cells comparable to those of cytarabine and the parental DMDC.^{27,28)} On the other hand, 4'-thiogemcitabine (**16**) showed only moderate activity against the same cell lines.^{27,28)} It is worth noting that **21** was 15–30 times more active against KB cells than cytarabine or DMDC (Table 1). Further evaluation of the antitumor activity of **21** revealed it had broad antineoplastic activity against various tumor cell lines including pancreas and colon cancers, and was also active in an *in vivo* assay using nude mice implanted with human tumor cells.^{32–34)}

The mechanism of action of 4'-thioFAC was investigated, revealing that 4'-thioFAC inhibited cellular DNA synthesis, but did not inhibit either RNA or protein synthesis. Potent inhibition against DNA polymerase α by the action of 4'-thioFAC triphosphate (4'-thioFACTP) was observed, whereas 4'-thioFACTP showed moderate to little inhibition against DNA polymerase β and γ (Fig. 1). The kinetic analysis showed that the inhibition mode of 4'-thioFACTP against DNA polymerase α was mixed-type inhibition. The results implied that 4'-thioFACTP inhibited DNA polymerase α in two ways: (a) retarding DNA chain elongation by competing with dCTP at the nucleotide-binding site, (b) acting as a chain terminator after incorporation into DNA.³⁵⁾

The triphosphate of gemcitabine (dFdCTP), on the other hand, did not show potent inhibition against these three DNA polymerases. This result was consistent with the knowledge that the inhibition of ribonucleotide reductase by the diphosphate of gemcitabine was more responsible for its antitumor action.¹²⁾ Since these findings showed that the main target

enzymes of 4'-thioFAC and gemcitabine appeared to be different, the combinatory use of 4'-thioFAC and gemcitabine was expected to have a synergic effect, which was confirmed in an *in vitro* model.³⁵⁾

4. Antiviral Activity of 4'-Thionucleosides

It is well known that 2'-arabinonucleosides³⁶⁾ and 2'-deoxy-2'-fluoroarabinonucleosides³⁷⁾ exhibit antiviral activities, especially against herpesviruses. We therefore evaluated the anti-herpesvirus activities of the 4'-thio counterparts of these nucleosides by culturing them with several viruses, including human herpes simplex virus types 1 and 2 (HSV-1 and -2), varicella zoster virus (VZV), and human cytomegalovirus (HCMV), followed by analysis with a plaque reduction assay.^{29,31,38)} The results are summarized in Tables 2 and 3.

The 5-substituted-4'-thioaraU derivatives (B=5-methyl, 5-ethyl- and 5-iodouracils) showed anti-HSV-1 activity (ED₅₀: 0.43–3.50 $\mu\text{g/mL}$), but moderate to weak inhibitory activity against HSV-2 and VZV. Among the purine derivatives examined, 4'-thioaraG and 2,6-diaminopurine (2,6-DAP) 4'-thioarabinonucleoside (4'-thioaraDAP) showed potent antiviral activity against all of the herpesviruses assayed. It was noteworthy that their antiviral activities were particularly potent against HCMV and were 10 times more active than that of a commercial anti-HCMV drug, ganciclovir (0.010, 0.022 $\mu\text{g/mL}$, respectively, Table 2).

The 2'-fluoroarabinonucleosides showed results similar to those for the 2'-arabino derivatives mentioned above. Based on the comparison of the antiviral activities of 2'-fluoro derivatives with those of arabino derivatives (Tables 2, 3), the antiviral activity was clearly improved by replacing the 2'-substit-

Table 2. Antiviral Activity of 2'-arabino-4'-Thionucleoside **18**

B	Antiviral activities ED ₅₀ ($\mu\text{g/mL}$)				Anti-cell proliferative activity IC ₅₀ ($\mu\text{g/mL}$)
	HSV-1 ^{a,e)}	HSV-2 ^{b,e)}	VZV ^{c,e)}	HCMV ^{d,e)}	CCRF-HSB-2 ^{f)}
5-Me-Ura	0.77	4.6	6.6	44	>100
5-Et-Ura	0.43	6.5	>50	>50	>100
5-I-Ura	3.50	13.6	27.1	>50	>100
Ade	18.4	13.5	1.85	1.36	14.8
2,6-DAP	0.52	0.40	0.11	0.022	0.20
Gua	0.49	0.59	0.11	0.010	0.29
Aciclovir	0.14	0.23	—	—	>100
Ganciclovir	0.016	0.039	3.1	0.21	17

a) VR-3 strain. b) HSV-2 MS strain. c) VZV Oka strain. d) HCMV AD 169 strain. e) Plaque reduction assay. f) MTT assay.

Table 3. Antiviral Activity of 2'-Deoxy-2'-fluoro-arabino-4'-thionucleosides **21**

B	Antiviral activities ED ₅₀ ($\mu\text{g/mL}$)				Antineoplastic activities IC ₅₀ ($\mu\text{g/mL}$)
	HSV-1 ^{a,e)}	HSV-2 ^{b,e)}	VZV ^{c,e)}	HCMV ^{d,e)}	CCRF-HSB-2 ^{f)}
5-Me-Ura	0.43	1.0	24.5	0.088	0.49
5-Et-Ura	0.015	0.073	29.4	>50	>100
5-I-Ura	0.018	0.18	6.8	>50	78
Ade	1.61	3.0	3.0	1.41	54
2,6-DAP	0.0057	0.050	0.101	0.066	2.1
Gua	0.0091	0.063	0.095	0.078	3.6
Aciclovir	0.14	0.23	—	—	>100
Ganciclovir	0.016	0.039	3.1	0.21	17

a) VR-3 strain. b) HSV-2 MS strain. c) VZV Oka strain. d) HCMV AD 169 strain. e) Plaque reduction assay. f) MTT assay.

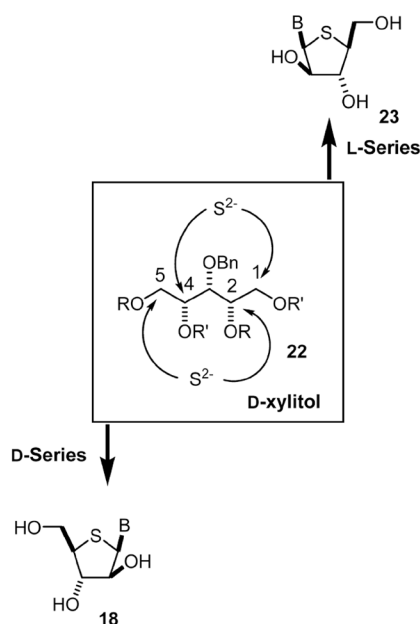


Chart 6

uent from a hydroxyl to a fluoro group on the 4-thioarabinose moiety. In the pyrimidine series, the 5-ethyluracil, 5-iodouracil, and 5-iodouracil derivatives showed potent anti-HSV-1 as well as anti-HSV-2 activities *in vitro* (ED_{50} : 0.015–0.43 $\mu\text{g/mL}$ toward HSV-1, 0.073–1.0 $\mu\text{g/mL}$ toward HSV-2). Among them, the 5-ethyluracil derivative was quite interesting, since it had potent inhibitory activities against both HSV-1 and HSV-2 with lesser cytotoxicity than the 4'-thioarabino counterpart. In the purine series, the guanine and 2,6-diaminopurine derivatives showed broad and prominent antiviral activities. In addition, the cytotoxicity of the purine 2'-fluoro derivatives was slightly improved in comparison to that of the arabino derivatives, but they were still cytotoxic, which impeded further development of these analogues as antiviral drugs.

5. Synthesis of L-Isomers of 4'-Thionucleosides

We achieved the synthesis of 2'-modified 4'-thionucleosides starting from a D-xylose derivative as a chiral synthon. Considering D-xylitol instead of D-xylose as a chiral synthon, we focused on its pseudosymmetrical structure. As described above, during the synthetic scheme adopted, the chirality of the 2, 3, and 4 positions of D-xylitol was transferred to the 4, 3, and 2 positions of the D-4-thioarabinose derivative. The pseudosymmetrical structure of D-xylitol provided a clue that we should shift the carbon units of D-xylitol utilized for 4'-thionucleosides from the 2–5 to the 1–4 positions, which allowed us to synthesize the L-enantiomers of 4'-thioarabinonucleosides (Chart 6). The L-isomers of nucleoside derivatives have garnered much attention as candidates for alternative antiviral agents.³⁹⁾ Indeed, the L-isomer of lamivudine was more potent and less cytotoxic than its D-isomer.^{40–43)} We concluded that our synthetic approach was effective. Adopting a similar synthetic scheme for the D-isomers depicted above, we were able to obtain L-4'-thioarabinonucleosides from D-xylose by shifting the chiral carbons employed. Interestingly, the α -L-cytosine derivative showed moderate anti-HSV-1 activity.⁴⁴⁾

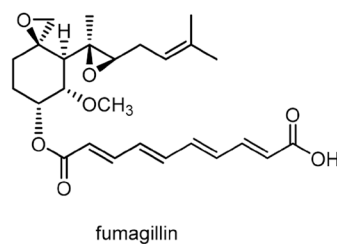
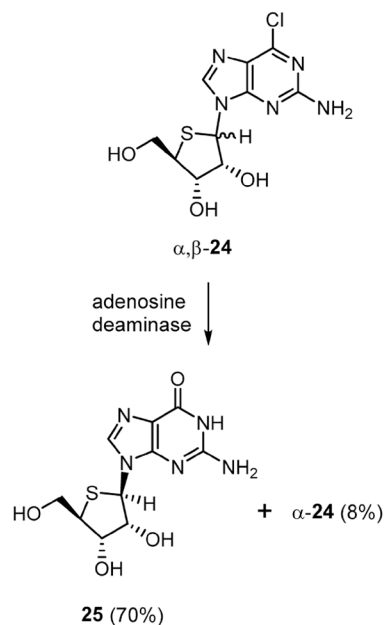


Chart 7

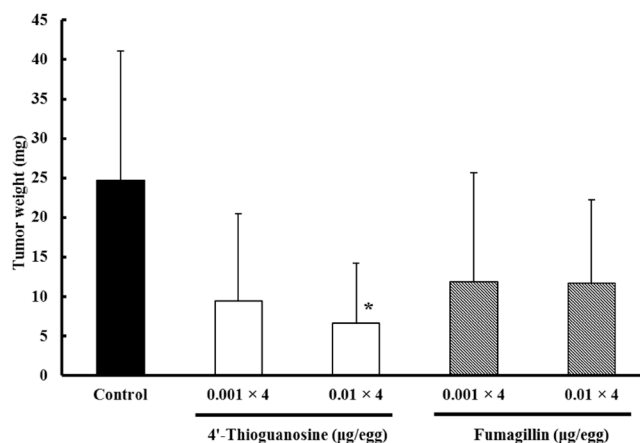


Fig. 2. The Inhibitory Effects of 4'-Thioguanosine on the Growth of an S-180 Tumor Implanted on a Chick Embryo CAM

* $p < 0.05$ vs. Control, Dunnett's multiple comparison test.

6. Synthesis of Purine 4'-Thioribonucleosides as an Inhibitor of Angiogenesis

The synthesis of 4'-thionucleosides was achieved by developing a new synthetic route for the 4-thiosugar portion and combining it with the Pummerer-type glycosylation reaction. To prove the usefulness of the latter Pummerer-type glycosylation, we applied it to the synthesis of 4'-thioribonucleosides.⁴⁵⁾ We then further extended our study to the synthesis

of purine 4'-thioribonucleosides and found that some of the purine 4'-thioribonucleoside derivatives exhibited anti-angiogenesis activity based on our primary screening system.⁴⁶⁾ To obtain several purine analogues, including 4'-thioguanosine, we modified the original synthesis of 4'-thioguanosine.⁴⁷⁾ A mixture of α - and β -anomers of 2-amino-6-chloropurine 4-thioriboside **24** was prepared by the Vorbrüggen reaction of tetraacetyl-4-thioribofuranose. We found that treatment of an inseparable mixture of α,β -**24** with adenosine deaminase gave a pure β -anomer of 4'-thioguanosine (**25**) along with the unreacted α -**24** (Chart 7).

We established a screening system in which the growth of human umbilical vein endothelial cells (HUVECs) was induced by the addition of the conditioned medium of lung carcinoma cell line PC-9. The primary screening using HUVECs resulted in the identification of α,β -**24** and **25** as potent inhibitory compounds. The assay showed that these compounds were more potent than fumagillin (Chart 7), a fungal metabolite which was reported to have anti-angiogenic activity *in vitro* and *in vivo* (Table 4).

To evaluate the *in vivo* anti-angiogenic effect of 4'-thioguanosine, we performed a chick embryo chorioallantoic membrane (CAM) assay. We implanted a murine S-180 tumor onto a CAM that was grown by subcutaneous implantation in mice, and then examined the inhibitory effect of 4'-thioguanosine on the growth of the tumor. The tumor growth was inhibited by the administrations of 0.001–0.01 $\mu\text{g}/\text{d}$ of 4'-thioguanosine (**25**) at 1, 3, 5 and 7 d after implantation. Fumagillin also inhibited the tumor growth at the same doses as 4'-thioguanosine (0.001–0.01 $\mu\text{g}/\text{d}$, Fig. 2). Since **25** was almost inactive against the cancer cell line panel tested (its IC_{50} value was $>50 \mu\text{M}$), **25** was suggested to inhibit the tumor growth by inhibiting the pathway that transmits the angiogenesis signal from certain unidentified growth factors produced by the tumor.⁴⁶⁾

7. Synthesis of 5'-Thiodihydropyranonucleosides

As described above, our first target was 4'-thioDMDC (**3**),

Table 4. The Inhibitory Effects of 4'-Thionucleosides on the Growth of HUVECs Induced by PC-9-Conditioned Medium

	Base	IC_{50} ($\mu\text{g}/\text{mL}$)
4'-Thionucleosides	Guanine (25)	0.021
	2-Amino-6-chloropurine (α,β - 24)	0.027
Fumagillin		2.8

which was synthesized by developing the Pummerer-type thioglycosylation. Following our synthesis of **3**, this new glycosylation method was widely used and became one of the standard methods for constructing a glycosidic bond between a nucleobase and 4-thiosugar unit.^{48–50)} We continued to study the utility of this reaction by applying it to the synthesis of nucleoside derivatives having a 5-thiopyranose system. As a target of potential anti-HIV agents, we designed dihydrothiopyranonucleoside **27**, a ring-expanded analogue of L-4'-thioD4C, which was reported to possess anti-HIV activity⁵¹⁾ (Chart 8). As we mentioned in the context of the synthesis of L-4'-thionucleosides, both the D- and L-isomers of nucleosides were considered to be potentially active against HIV. Therefore, we planned to synthesize the target analogue as a racemate.

To synthesize the substrate of the Pummerer-type thioglycosylation for preparing **27**, diene **29**, prepared from 2-butene-1,4-diol, was subjected to a ring-closing metathesis (RCM) reaction catalyzed by the second generation Grubbs catalyst to give a dihydrothiopyran derivative **30** in excellent yield. After the process of one-carbon deletion, protection at the resulting primary hydroxyl group of **31** and the subsequent oxidation gave a sulfoxide **32**. The Pummerer-type thioglycosylation reaction of sulfoxide **32** by treatment with bis(trimethylsilyl)uracil, TMSOTf, and *N,N*-diisopropylethylamine (DIPEA) gave the dihydrothiopyranyluracil derivative **33** in 45% yield along with the formation of its α -anomer. The results clearly proved that the Pummerer-type thiogly-

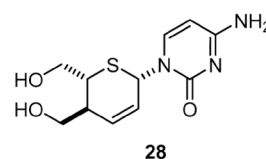
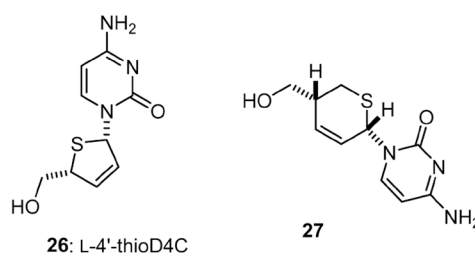


Chart 8

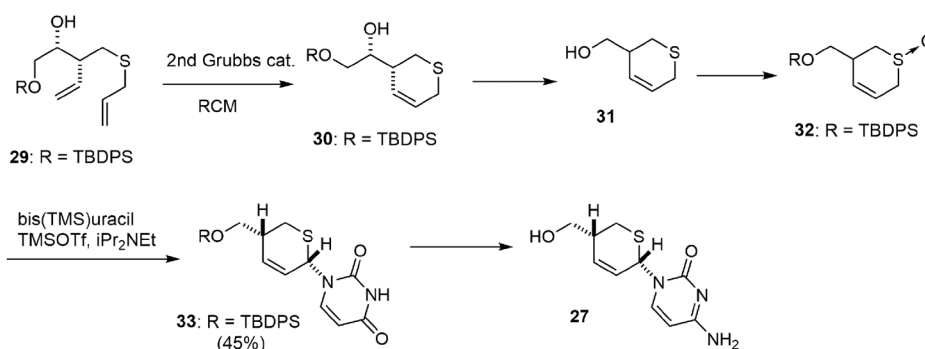


Chart 9

cosylation reaction was effective for the synthesis of 5'-thiopyranonucleoside derivatives as well as 4'-thionucleosides. Finally, conversion of the uracil moiety of **33** to cytosine and desilylation afforded the desired dihydrothiopyranyl cytosine **27**.^{52,53} Although **27** did not show any anti-HIV activity, its bis(hydroxymethyl) analogue **28**, which was obtained by a method similar to that used for synthesis of **27**, was revealed to have anti-HIV activity⁵⁴ (Chart 9).

8. Conclusion

Our early efforts to identify biologically active nucleosides were made to synthesize 4'-thioDMDC and 4'-thiogemcitabine. To achieve their synthesis, we developed the Pummerer-type thioglycosylation. This reaction was successfully applied to synthesize dihydrothiopyranonucleosides as well as 4'-thionucleosides. At present, the reaction has become the standard method for building a glycosidic linkage of 4'-thionucleosides. It is also emphasized that we developed a new synthetic route accessing 4-thiosugar, by which we achieved the synthesis of various 4'-thionucleoside derivatives including L-enantiomers of 4'-thioarabinonucleosides. As a result of these synthetic efforts, we were able to identify many biologically interesting nucleosides that were active against tumors or viruses. In particular, 4'-thioFAC, a 2'-fluoro analogue of 4'-thiocytidine, showed prominent antitumor activity even in an *in vivo* assay. The results unambiguously demonstrated the importance of 4'-thionucleosides for drug development and their promise as drug candidates for antineoplastic and antiviral agents.

Acknowledgments We are thankful to co-workers, whose names are cited in the references, for their intellectual and experimental contributions. This work was supported in part by a Grant-in-Aid for Scientific Research from the Japan Society for the Promotion of Science (JSPS) and by a Grant of the Strategic Research Foundation Grant-in-Aid Project for Private Universities from the Ministry of Education, Culture, Sport, Science and Technology, Japan (MEXT).

Conflict of Interest The authors declare no conflict of interest.

References

- Evans J. S., Musser E. A., Bostwick L., Mengel G. D., *Cancer Res.*, **24**, 1285–1293 (1964).
- Tallman M. S., Gilliland D. G., Rowe J. M., *Blood*, **106**, 1154–1163 (2005).
- Hertel L. W., Boder G. B., Kroin J. S., Rinzel S. M., Poore G. A., Todd G. C., Grindey G. B., *Cancer Res.*, **50**, 4417–4422 (1990).
- Abratt R. P., Bezwoda W. R., Falkson G., Goedhals L., Hacking D., Rugg T. A., *J. Clin. Oncol.*, **12**, 1535–1540 (1994).
- Elion G. B., Furman P. A., Fyfe J. A., de Miranda P., Beauchamp L., Schaeffer H. J., *Proc. Natl. Acad. Sci. U.S.A.*, **74**, 5716–5720 (1977).
- Smith K. O., Galloway K. S., Kennell W. L., Ogilvie K. K., Radatus B. K., *Antimicrob. Agents Chemother.*, **22**, 55–61 (1982).
- Smee D. F., Martin J. C., Verheyden J. P., Matthews T. R., *Antimicrob. Agents Chemother.*, **23**, 676–682 (1983).
- Mitsuya H., Weinhold K. J., Furman P. A., St Clair M. H., Lehrman S. N., Gallo R. C., Bolognesi D., Barry D. W., Broder S., *Proc. Natl. Acad. Sci. U.S.A.*, **82**, 7096–7100 (1985).
- Sofia M. J., Bao D., Chang W., Du J., Nagarathnam D., Rachakonda S., Reddy P. G., Ross B. S., Wang P., Zhang H. R., Bansal S., Espiritu C., Keilman M., Lam A. M., Steuer H. M., Niu C., Otto M. J., Furman P. A., *J. Med. Chem.*, **53**, 7202–7218 (2010).
- Imamichi T., *Curr. Pharm. Des.*, **10**, 4039–4053 (2004).
- Meadows D. C., Gervay-Hague J., *ChemMedChem*, **1**, 16–29 (2006).
- de Sousa Cavalcante L., Monteiro G., *Eur. J. Pharmacol.*, **741**, 8–16 (2014).
- Dyson M. R., Coe P. L., Walker R. T., *J. Med. Chem.*, **34**, 2782–2786 (1991).
- Secrist J. A. 3rd, Tiwari K. N., Riordan J. M., Montgomery J. A., *J. Med. Chem.*, **34**, 2361–2366 (1991).
- Matsuda A., Takenuki K., Tanaka M., Sasaki T., Ueda T., *J. Med. Chem.*, **34**, 812–819 (1991).
- Yamagami K., Fujii A., Arita M., Okumoto T., Sakata S., Matsuda A., Ueda T., Sasaki T., *Cancer Res.*, **51**, 2319–2323 (1991).
- Reist E. J., Gueffroy D. E., Goodman L., *J. Am. Chem. Soc.*, **86**, 5658–5663 (1964).
- Hoffman D. J., Whistler R. L., *Biochemistry*, **9**, 2367–2372 (1970).
- Bellon L., Barascut J. L., Imbach J. L., *Nucleosides Nucleotides*, **11**, 1467–1479 (1992).
- Reist E. J., Fisher L. V., Goodman L., *J. Org. Chem.*, **33**, 189–192 (1968).
- Whistler R. L., Doner L. W., Nayak G. U., *J. Org. Chem.*, **36**, 108–110 (1971).
- Ototani N., Whistler R. L., *J. Med. Chem.*, **17**, 535–537 (1974).
- Niedballa U., Vorbrueggen H., *J. Org. Chem.*, **39**, 3654–3660 (1974).
- Kita Y., Tamura O., Yasuda H., Itoh F., Tamura Y., *Tetrahedron Lett.*, **25**, 4681–4682 (1984).
- Kita Y., Yasuda H., Tamura O., Itoh F., Tamura Y., *Chem. Pharm. Bull.*, **33**, 4235–4241 (1985).
- Nishida A., Hamada T., Yonemitsu O., *Chem. Pharm. Bull.*, **38**, 2977–2980 (1990).
- Yoshimura Y., Kitano K., Satoh H., Watanabe M., Miura S., Sakata S., Sasaki T., Matsuda A., *J. Org. Chem.*, **61**, 822–823 (1996).
- Yoshimura Y., Kitano K., Yamada K., Satoh H., Watanabe M., Miura S., Sakata S., Sasaki T., Matsuda A., *J. Org. Chem.*, **62**, 3140–3152 (1997).
- Yoshimura Y., Watanabe M., Satoh H., Ashida N., Ijichi K., Sakata S., Machida H., Matsuda A., *J. Med. Chem.*, **40**, 2177–2183 (1997).
- Meier C., Knispel T., Marquez V. E., Siddiqui M. A., De Clercq E., Balzarini J., *J. Med. Chem.*, **42**, 1615–1624 (1999).
- Yoshimura Y., Kitano K., Yamada K., Sakata S., Miura S., Ashida N., Machida H., *Bioorg. Med. Chem.*, **8**, 1545–1558 (2000).
- Miura S., Yoshimura Y., Endo M., Machida H., Matsuda A., Tanaka M., Sasaki T., *Cancer Lett.*, **129**, 103–110 (1998).
- Miura S., Yoshimura Y., Endo M., Satoh H., Machida H., Sasaki T., *Cancer Lett.*, **144**, 177–182 (1999).
- Miura S., Endo Y., Yoshimura Y., Endo M., Yonemura Y., Sasaki T., *Oncol. Rep.*, **9**, 1319–1322 (2002).
- Miura S., Yoshimura Y., Satoh H., Izuta S., *Jpn. J. Cancer Res.*, **92**, 562–567 (2001).
- Machida H., Sakata S., “Nucleosides and nucleotides as antitumor and antiviral agents,” ed. by Chu, C. K., Baker, D. C., Plenum, New York and London, 1993, pp. 245–264.
- Watanabe K. A., Reichman U., Hirota K., Lopez C., Fox J. J., *J. Med. Chem.*, **22**, 21–24 (1979).
- Machida H., Ashida N., Miura S., Endo M., Yamada K., Kitano K., Yoshimura Y., Sakata S., Ijichi O., Eizuru Y., *Antiviral Res.*, **39**, 129–137 (1998).
- Mathe C., Gosselin G., *Antiviral Res.*, **71**, 276–281 (2006).
- Coates J. A., Cammack N., Jenkinson H. J., Mutton I. M., Pearson B. A., Storer R., Cameron J. M., Penn C. R., *Antimicrob. Agents Chemother.*, **36**, 202–205 (1992).
- Schinazi R. F., Chu C. K., Peck A., McMillan A., Mathis R., Cannon D., Jeong L. S., Beach J. W., Choi W. B., Yeola S., *Antimicrob. Agents Chemother.*, **36**, 672–676 (1992).
- Coates J. A., Cammack N., Jenkinson H. J., Jowett A. J., Jowett M. I., Pearson B. A., Penn C. R., Rouse P. L., Viner K. C., Cameron J.

- M., *Antimicrob. Agents Chemother.*, **36**, 733–739 (1992).
- 43) Sommadossi J. P., Schinazit R. F., Chu C. K., Xie M. Y., *Biochem. Pharmacol.*, **44**, 1921–1925 (1992).
- 44) Satoh H., Yoshimura Y., Sakata S., Miura S., Machida H., Matsuda A., *Bioorg. Med. Chem. Lett.*, **8**, 989–992 (1998).
- 45) Yoshimura Y., Kuze T., Ueno M., Komiya F., Haraguchi K., Tanaka H., Kano F., Yamada K., Asami K., Kaneko N., Takahata H., *Tetrahedron Lett.*, **47**, 591–594 (2006).
- 46) Miura S., Yamada K., Kano F., Yoshimura Y., *Biol. Pharm. Bull.*, **27**, 520–523 (2004).
- 47) Anisuzzaman A. K. M., Amin M. D., *J. Bangladesh Acad. Sci.*, **2**, 59–64 (1978).
- 48) Kotoulas S. S., Kojic V. V., Bogdanovic G. M., Koumbis A. E., *Bioorg. Med. Chem. Lett.*, **23**, 3364–3367 (2013).
- 49) Kotoulas S. S., Kojic V. V., Bogdanovic G. M., Koumbis A. E., *Tetrahedron*, **71**, 3396–3403 (2015).
- 50) Qu S., Mulamootil V. A., Nayak A., Ryu S., Hou X., Song J., Yu J., Sahu P. K., Zhao L. X., Choi S., Lee S. K., Jeong L. S., *Bioorg. Med. Chem.*, **24**, 3418–3428 (2016).
- 51) Young R. J., Shaw-Ponter S., Thomson J. B., Miller J. A., Cumming J. G., Pugh A. W., Rider P., *Bioorg. Med. Chem. Lett.*, **5**, 2599–2604 (1995).
- 52) Yoshimura Y., Yamazaki Y., Kawahata M., Yamaguchi K., Takahata H., *Tetrahedron Lett.*, **48**, 4519–4522 (2007).
- 53) Yoshimura Y., Yamazaki Y., Saito Y., Takahata H., *Tetrahedron*, **65**, 9091–9102 (2009).
- 54) Yoshimura Y., Yamazaki Y., Saito Y., Natori Y., Imamichi T., Takahata H., *Bioorg. Med. Chem. Lett.*, **21**, 3313–3316 (2011).

HETEROCYCLES, Vol. 94, No. 9, 2017, pp. 1625 - 1651. © 2017 The Japan Institute of Heterocyclic Chemistry
Received, 23rd May, 2017, Accepted, 29th June, 2017, Published online, 13th July, 2017
DOI: 10.3987/REV-17-865

DEVELOPMENT OF A GLYCOSYLATION REACTION: A KEY TO ACCESSING STRUCTURALLY UNIQUE NUCLEOSIDES

Yuichi Yoshimura*

Faculty of Pharmaceutical Sciences, Tohoku Medical and Pharmaceutical University, 4-4-1 Komatsushima, Aoba-ku, Sendai, 981-8558, Japan. E-mail: yoshimura@tohoku-mpu.ac.jp

Abstract – Nucleosides are potential drug candidates for antitumor and antiviral chemotherapies. Thus, the synthesis of structurally diverse nucleosides would contribute to the search for new antitumor and antiviral agents. The use of the glycosylation reaction to synthesize nucleoside derivatives would be a practical way to prepare nucleosides with unnatural sugar moieties. Therefore, we synthesized many nucleoside derivatives by using new glycosylation reactions categorized into three types: 1) a Pummerer-type glycosylation reaction used for constructing 4'-thionucleoside skeletons, 2) a sulfur-assisted Mitsunobu reaction used for isonucleoside syntheses, and 3) an oxidative coupling reaction catalyzed by hypervalent iodine for carbocyclic nucleosides and in the syntheses of dihydropyranonucleosides. In this review, we describe the development of the glycosylation reactions and their application to the synthesis of various structurally unique nucleoside derivatives.

CONTENTS

1. Introduction
2. Development of a Pummerer-type glycosylation reaction toward the synthesis of 4'-thionucleosides
3. Development of a sulfur-assisted Mitsunobu reaction toward the synthesis of isonucleosides
4. Development of an oxidative coupling reaction catalyzed by hypervalent iodine toward the synthesis of carbocyclic nucleosides
5. Application of hypervalent iodine chemistry to the synthesis of dihydropyranonucleosides
6. Conclusion

1. INTRODUCTION

Nucleoside derivatives constitute an important class of compounds because they show antitumor and antiviral activities.¹ To date, many nucleoside antimetabolites have been used as clinical drugs in chemotherapies against cancer and viruses. Idoxuridine, which is a 5-iodo-2'-deoxy derivative of uridine, was the first antiviral agent approved for herpes treatment.² Aciclovir, which is the most popular antiherpes drug developed by Wellcome, is a 2',3'-nor derivative of guanosine.³ The first anti-HIV (Human Immunodeficiency Virus) drug approved for the treatment of AIDS (Acquired Immune Deficiency Syndrome), 3'-azido-3'-deoxythymidine (Zidovudine, AZT), still plays a significant role in AIDS treatment.⁴ Gemcitabine, 2'-deoxy-2'-difluorocytidine, developed by Eli Lilly, is an anticancer drug approved for the treatment of pancreatic cancer and now is being used in chemotherapies against various tumors, including lung cancer.⁵ Sofosbuvir, developed by Pharmasset (Gilead), has had recent success in the treatment of hepatitis C (Figure 1).⁶ These drugs show the importance of studying the synthesis of nucleoside derivatives.

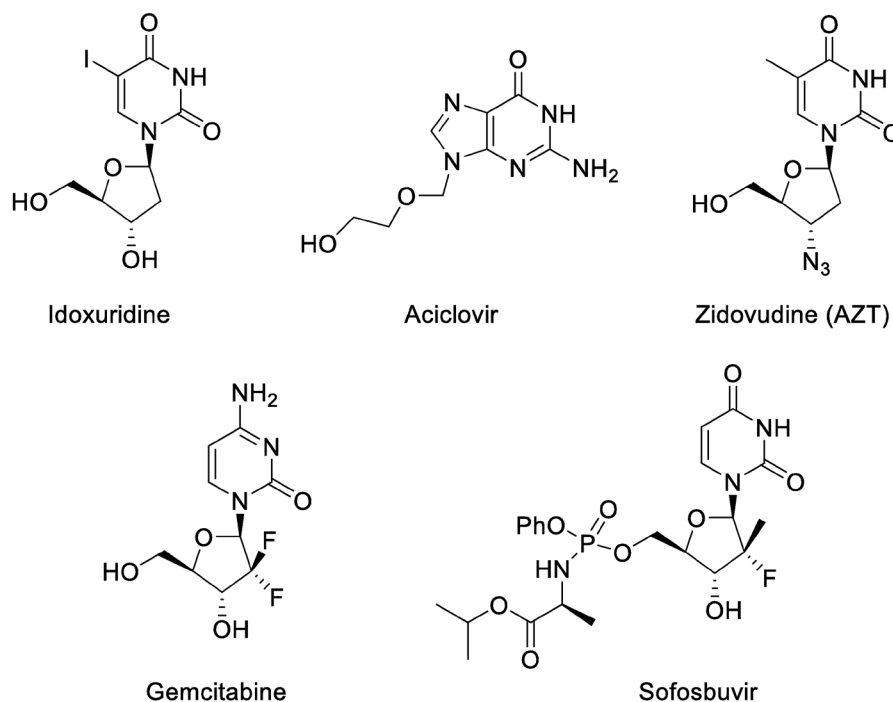


Figure 1. Structures of nucleoside derivatives approved as drugs

Thus, it is necessary to synthesize nucleoside derivatives with structural diversity for discovering new antitumor and antiviral agents. In general, there are three methods used for synthesizing nucleoside derivatives: 1) synthesis starting from a natural nucleoside,⁷ 2) constructing a base moiety on an appropriate sugar portion,⁸ and 3) connecting base and sugar moieties by using glycosylation reactions.⁹ In particular, the third method using a glycosylation reaction is advantageous because various nucleoside

derivatives having different base moieties can be synthesized from one sugar intermediate. To date, we have synthesized many nucleoside derivatives by developing new glycosylation reactions. In this paper, we describe three different glycosylation reactions developed by us: 1) a Pummerer-type glycosylation reaction used for constructing 4'-thionucleoside skeletons, 2) a sulfur-assisted Mitsunobu reaction used for isonucleoside synthesis, and 3) a hypervalent iodine-catalyzed reaction for connecting bases and pseudosugars of carbocyclic nucleosides. In addition, we review the synthesis of nucleoside derivatives with potential biological activities and new structures.

2. DEVELOPMENT OF A PUMMERER-TYPE GLYCOSYLATION REACTION TOWARD THE SYNTHESIS OF 4'-THIONUCLEOSIDES

When we started a new project to explore antitumor and antiviral nucleosides, Walker¹⁰ and Secrist¹¹ independently reported that 2'-deoxy-4'-thionucleosides, in which the ring oxygen of the 2-deoxyribose moiety of 2'-deoxynucleosides was replaced with sulfur, had potent anti-herpesvirus activity and that some of the derivatives had cytotoxicity. Together with their reports, 2'-substituted cytidine derivatives, such as DMDC (**2**)¹² and gemcitabine,⁵ are known to have potent antitumor activity. From these results, we designed 2'-substituted 4'-thiocytidines, 4'-thioDMDC (**3**) and 4'-thiogemcitabine (**4**), as potential antitumor agents (Figure 2). In the synthesis of the target nucleoside derivatives, there were several problems. At the time we started the project, the only 4'-thionucleosides reported were 4'-thioribonucleosides,¹³ 4'-thioarabinonucleosides¹⁴ and 2'-deoxy-4'-thionucleosides.^{10,11} Therefore, we needed to develop a strategy to synthesize 4'-thionucleosides which was also applicable to the synthesis of 2'-substituted derivatives. From structure-activity relationship (SAR) studies, we thought that a synthetic strategy employing a glycosylation reaction with 4-thiosugars was ideal, as mentioned above, since we had obtained various base-modified analogues from one 4-thiosugar intermediate. Thus, the first problem to overcome was the need for a new synthetic route to prepare 4-thiosugars, which can be used to synthesize 2-substituted derivatives.

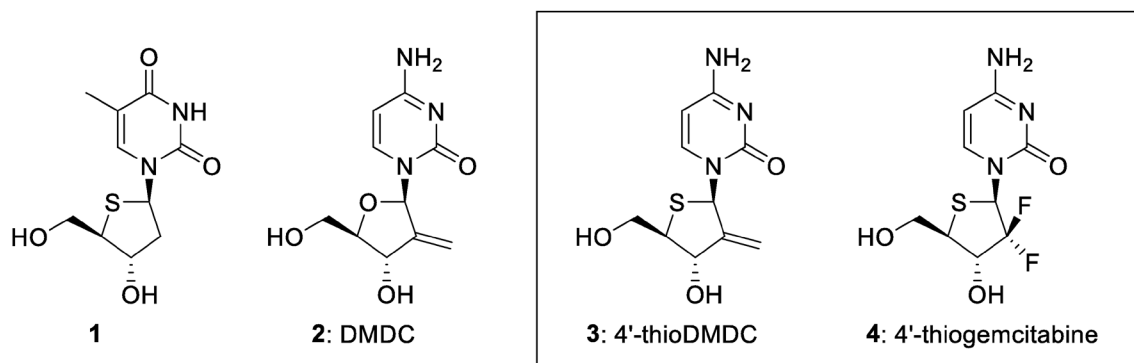
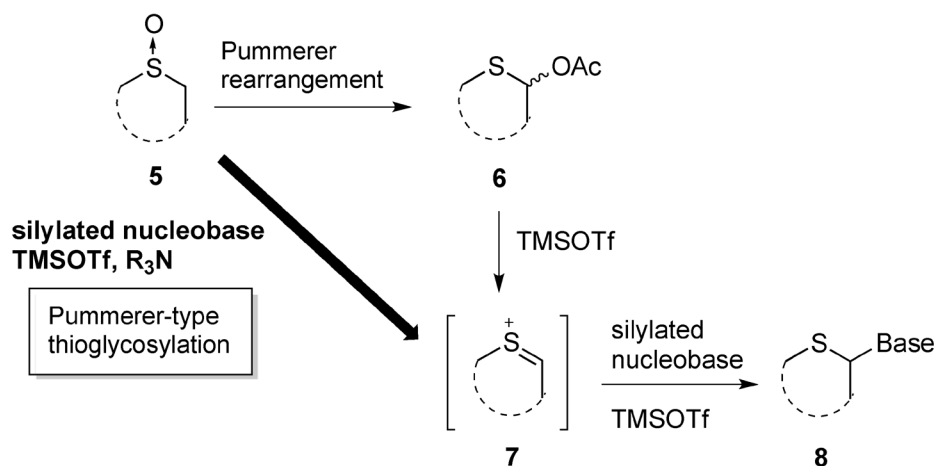


Figure 2. Desired cytotoxic 2'-substituted 4'-thionucleosides

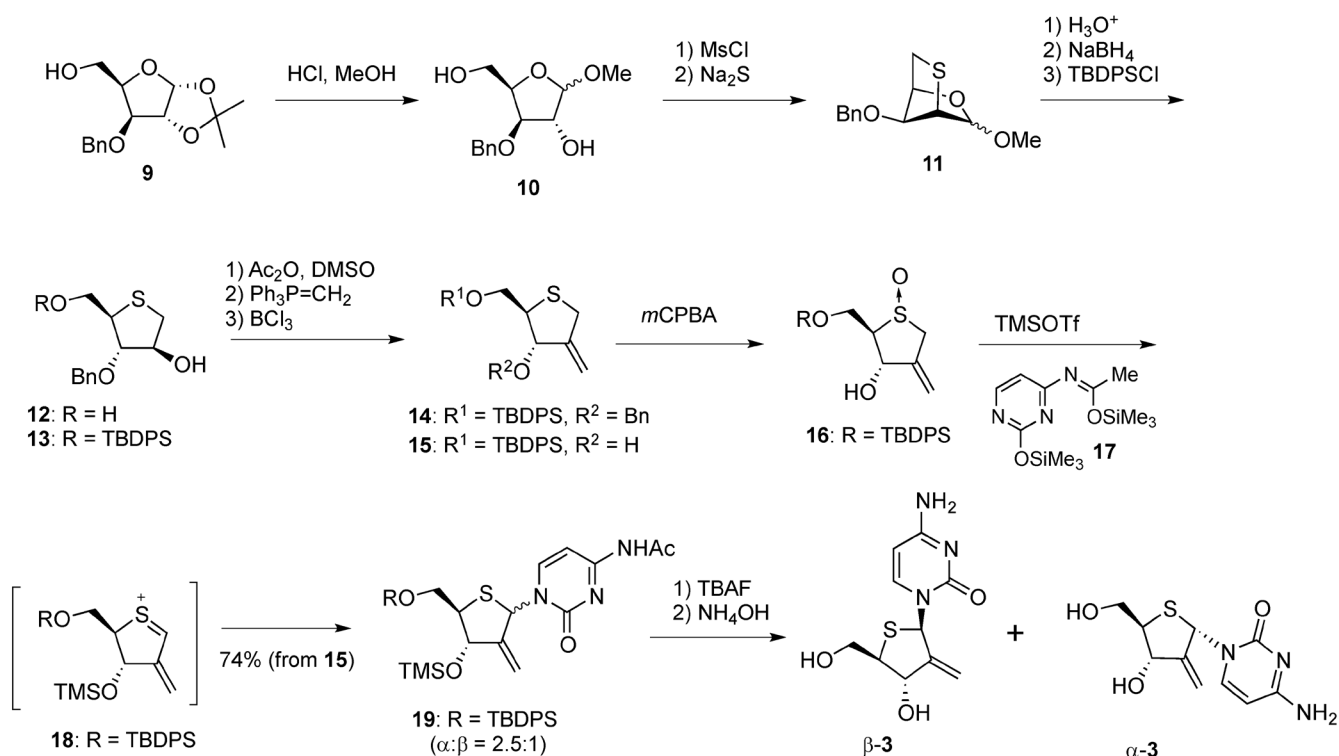
To construct a glycosidic linkage between the base and sugar moiety of nucleoside skeleton **8**, a Vorbrüggen reaction¹⁵ is generally used. As shown by past results,¹⁶ the reaction could be used in the synthesis of 4'-thionucleosides as well as normal "4'-oxy" nucleosides. In addition, we could use original chemistry for sulfur-containing compounds: 1-acetoxy-4-thiosugar **6**, a good substrate for the Vorbrüggen reaction, was easily obtained from the corresponding sulfoxide **5** by using a classical Pummerer rearrangement. Although the scheme mentioned above seemed promising, we introduced an additional synthetic idea. The reaction intermediate of the Vorbrüggen reaction¹⁵ is sulfenium ion **7** which can also be obtained by using a sila-Pummerer reaction, developed by Kita,¹⁷ involving sulfoxide **5**. This new glycosylation reaction is attractive since it skips a step and directly accesses sulfenium ion **7** from sulfoxide **5** (Scheme 1). Thus, our second task for synthesizing 4'-thionucleosides was to develop a Pummerer-type glycosylation reaction.



Scheme 1. Concept for the Pummerer-type glycosylation reaction

First, we developed a synthetic route involving bicyclic intermediate **11** starting from xylose derivative **9**,¹⁸ as shown in Scheme 2. Formation of **11** was performed by consecutive inter-/intramolecular S_N2 reactions of the dimesylate compound obtained from 3-benzylxylose **10**. After acetal hydrolysis of **11**, followed by hydride reduction, 4-thioarabinose derivative **12** was obtained. Through cyclic intermediate **9**, the chiralities of the 2, 3, and 4 positions of the xylose were transferred to the 4, 3, and 2 positions of 4-thioarabinose derivative **12**, respectively. Compound **13**, which was protected at the primary hydroxyl group, was converted to a ketone, and the resulting ketone was subjected to a Wittig reaction to give 3-benzyl-2-methylene derivative **14**. Deprotection of the benzyl group of **14** gave 2-methylene derivative **15**.

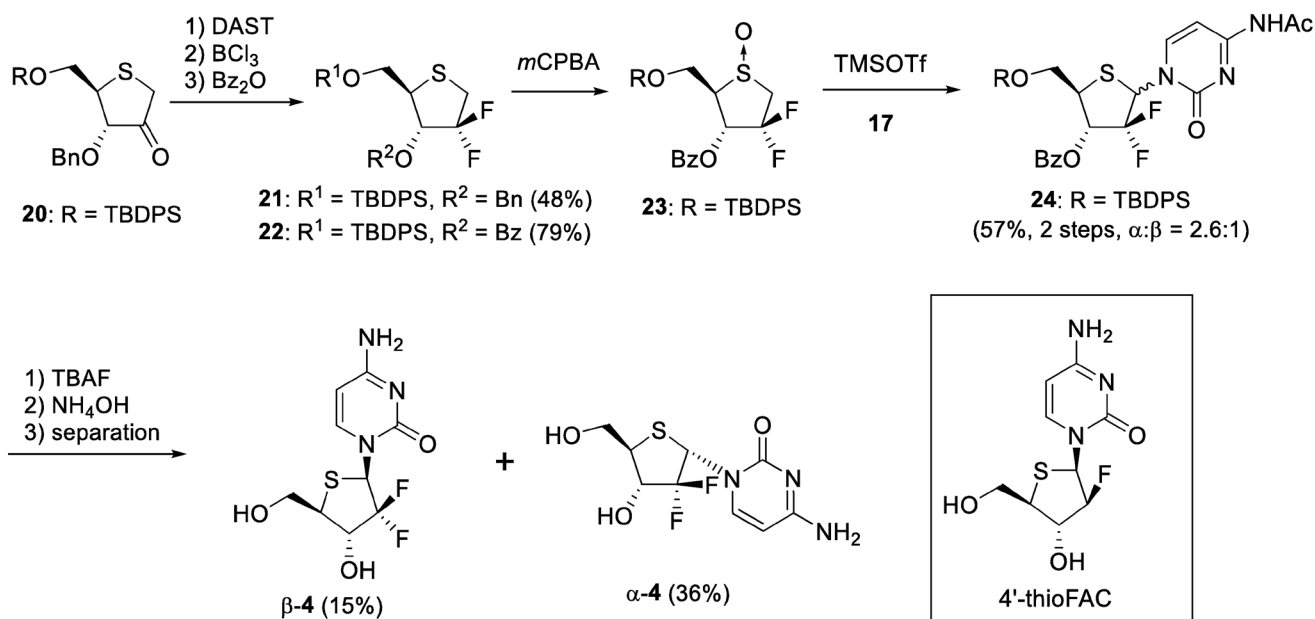
Next, we tried the Pummerer-type glycosylation of *N*⁴-acetylcytosine with sulfoxide **16**, obtained by treatment of **15** with *m*CPBA. We found that simple treatment of **15** with excess persilylated *N*⁴-acetylcytosine in the presence of TMSOTf afforded an anomeric mixture of 4'-thioDMDC derivatives **19** via the formation of sulfenium ion **18** in good yield. Although the ratio of α - and β -anomers was unsatisfactory, the Pummerer-type glycosylation was effective for the formation of the glycoside bond of 4'-thionucleosides. Deprotection of **19** and separation of the anomers afforded 4'-thioDMDC (β -**3**) and its anomer α -**3** (Scheme 2).¹⁹



Scheme 2. Synthesis of 4'-thioDMDC

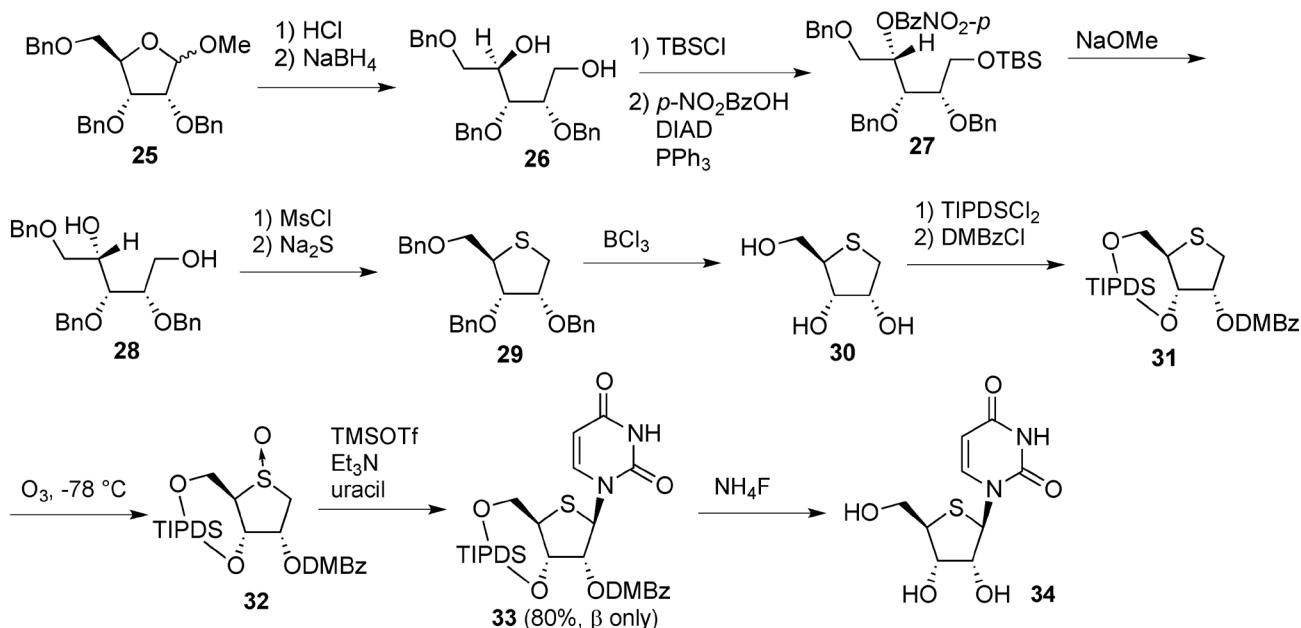
From the common intermediate **20**, described above, we synthesized 4'-thiogemicitabine. The ketone **20** was treated with DAST to give geminal difluoro derivative **21**, which was oxidized to the corresponding sulfoxide to give **23** after conversion of the protecting group. The sulfoxide **23** was subjected to Pummerer-type glycosylation conditions, as in the case of **16**, to give desired 4'-thiogemicitabine derivatives **24** in moderate yield. It is known that 2-fluorosugar derivatives are resistant to hydrolysis and glycosylation due to destabilization of the cationic intermediate by a strong electron-withdrawing fluoro substituent close to the reaction site.²⁰ Thus, the Pummerer-type glycosylation with **23** having difluoro substituents at the 2-position is a suitable method for obtaining the desired nucleoside derivative since the reaction could avoid C-O bond scission at the anomeric center. Deprotection and the subsequent separation of anomers gave α - and β -anomers of 4'-thiogemicitabine¹⁹ (α - and β -**4**, Scheme 3). Among

the synthesized analogues, β -4'-thioDMDC (β -**3**) exhibited potent antitumor activity in comparison to 4'-thiogemcitabine (β -**4**), which showed only moderate activity.^{19,21} On the other hand, the most active 4'-thionucleoside we synthesized was the mono-fluorinated derivative 4'-thioFAC.^{19,22} 4'-ThioFAC showed potent antitumor activity against various tumor cell lines and was active in in vivo assays using nude mouse model-implanted human tumor.²³ Furthermore, we found that a series of 4'-thioFAC analogues had potent antiherpes virus activity.²⁴

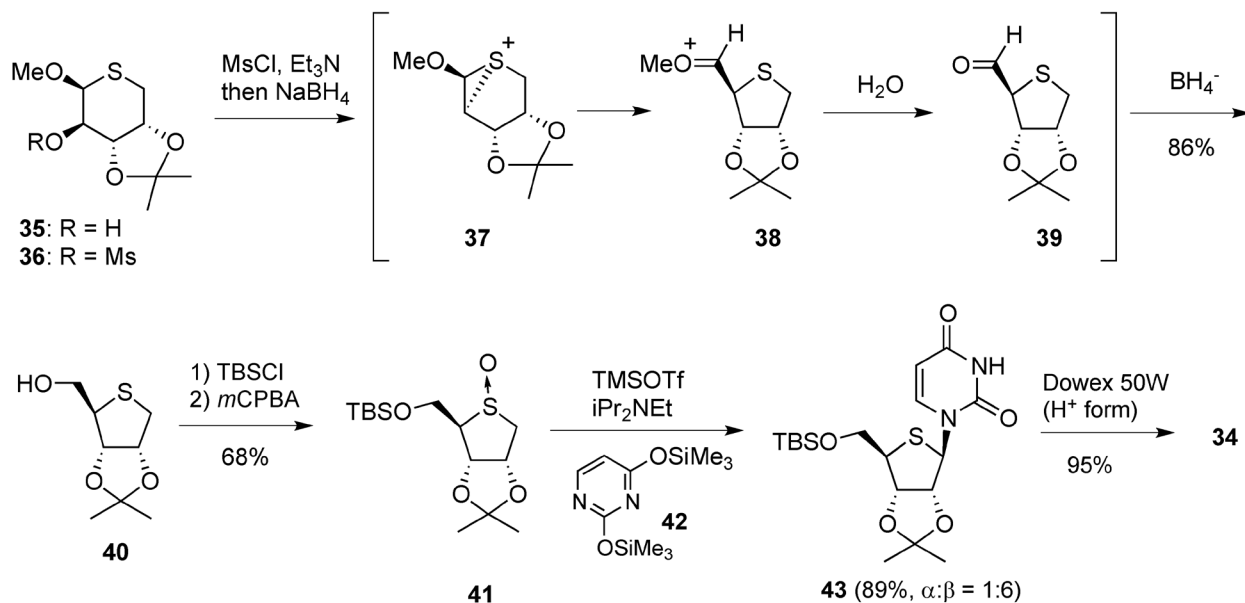


Scheme 3. Synthesis of 4'-thiogemcitabine

After the synthesis of 4'-thioDMDC and 4'-thiogemcitabine using the Pummerer-type glycosylation reaction was reported by us, many other groups reported various 4'-thionucleoside derivatives. Matsuda and co-workers applied the reaction to the syntheses of 4'-thioribonucleosides.²⁵ Diol **26** was synthesized from tri-*O*-benzylated ribose **25**, of which the primary hydroxyl group was protected by the TBS group, and then subjected to the Mitsunobu reaction to give *p*-nitrobenzoate **27**. After deprotection of the *p*-nitrobenzoate moiety, epimerized diol **28** was converted to a 4-thioribose derivative, as in the case of 4'-thioDMDC shown above, to give 4-thioribose derivative **29**. Deprotection of **29** and protection of the 3- and 5-hydroxyl groups by using 1,1,3,3-tetraisopropyl-1,3-dichlorodisiloxane-1,3-diyl (TIPDS), followed by acylation at the 2-position with dimethoxybenzoyl group (DMBz), gave 2-dimethoxybenzoate **31**. Introduction of DMBz at the 2-position and diastereoselective formation of sulfoxide **32**, favored in Pummerer-type glycosylation reactions, were key tactics in Matsuda's synthesis. Under optimized conditions for **32**, the desired 4'-thiouridine derivative was obtained as the sole product in excellent yield (Scheme 4).²⁵



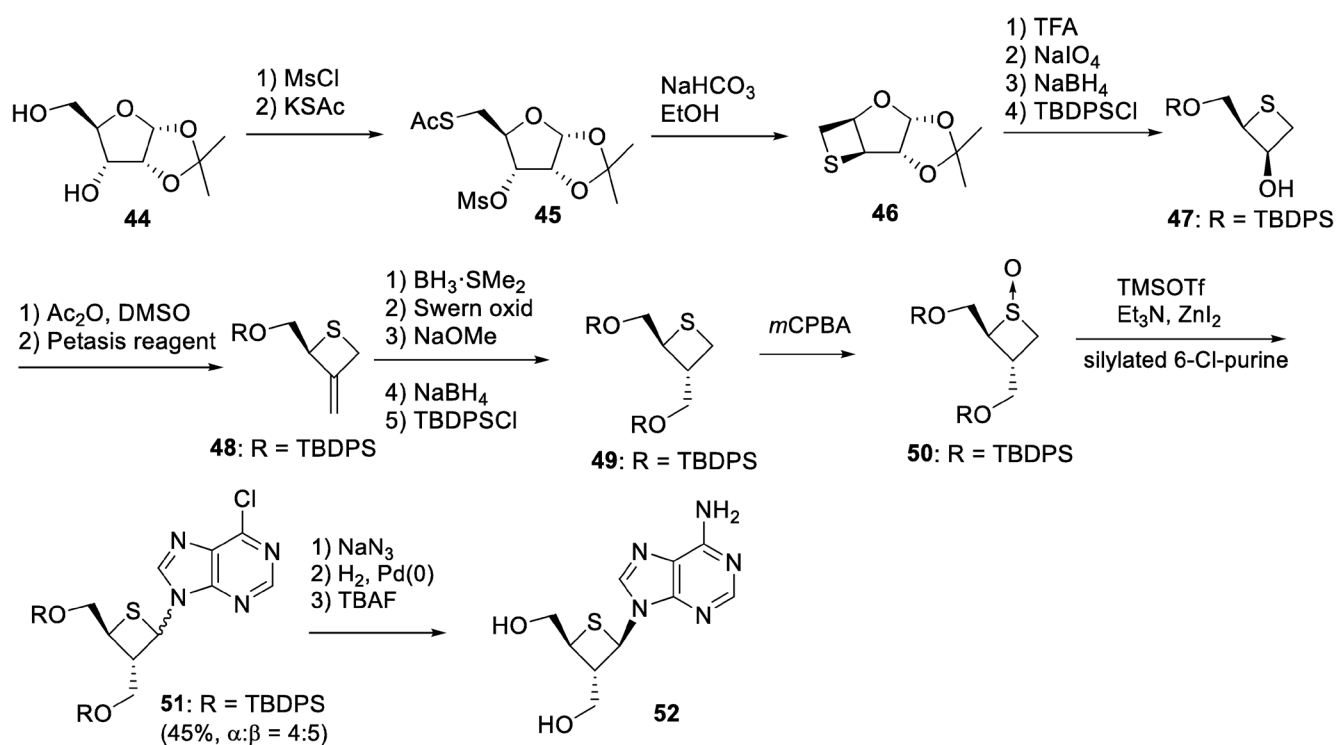
Scheme 4. Synthesis of 4'-thioribonucleoside by Matsuda's group



Scheme 5. Synthesis of 4'-thioribonucleoside by our group

We synthesized 4'-thioribonucleosides by using a different synthetic method.²⁶ The skeleton of the 4-thioribose was constructed via a ring-contraction reaction under reductive conditions. 2-Mesylate **36**, obtained from **35**, was used without any purification due to its instability. The reaction mixture containing **36** was treated with NaBH₄ in aqueous EtOH to give the ring contracted product **40** in good yield. As shown in Scheme 5, the reaction proceeded via the following three steps: 1) intramolecular nucleophilic

attack of sulfur at the 5-position and the formation of episulfonium ion **37**, 2) ring contraction and generation of 5-aldehyde **39**, and 3) hydride reduction of **39**. 5-*O*-Silylated sulfoxide **41**, prepared from **40**, was subjected to the Pummerer-type glycosylation reaction by treatment with persilylated uracil **42** and excess diisopropylethylamine (DIPEA) in the presence of TMSOTf to give 4'-thiouridine derivative **43** stereoselectively (Scheme 5).²⁶

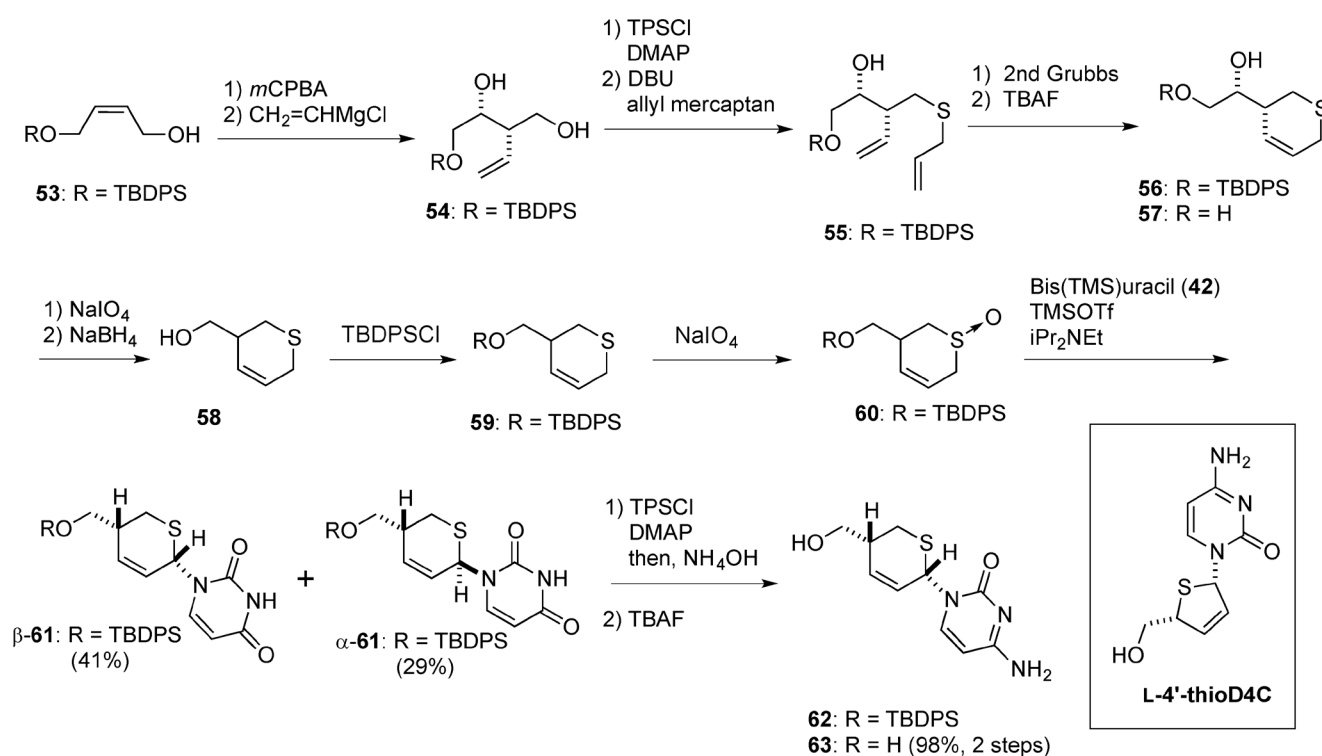


Scheme 6. Synthesis of 3'-thiooxetanocin

Chu²⁷ and Matsuda²⁸ independently studied the synthesis of 3'-thio analogues of oxetanocin A²⁹ which is a nucleoside antibiotic having oxetanose as a sugar portion, using the Pummerer-type glycosylation as a key step. Chu and his co-workers synthesized thietanose derivative **47** from ribose derivative **44** via a strategy similar to that for 4'-thioDMDC. Thietanose derivative **47** was oxidized, and the resulting ketone was treated with the Petasis reagent³⁰ to give exo-methylene **48**. Hydroboration of **48**, followed by oxidation with *m*CPBA, gave thietanose sulfoxide **50**, which was subjected to Pummerer-type glycosylation under modified conditions (silylated 6-chloropurine, TMSOTf, Et₃N, ZnI₂) to give a 4:5 mixture of α- and β-anomers of **51**. Stepwise amination at the 6-position of **51** and desilylation by treatment with TBAF yielded 3'-thiooxetanocin A (**52**) (Scheme 6).²⁷

On the basis of the reports of Chu and Matsuda, Pummerer-type glycosylation is effective for preparing thietanose, a 4-membered cyclic thiosugar. We focused on the scope and limitations of the reaction and

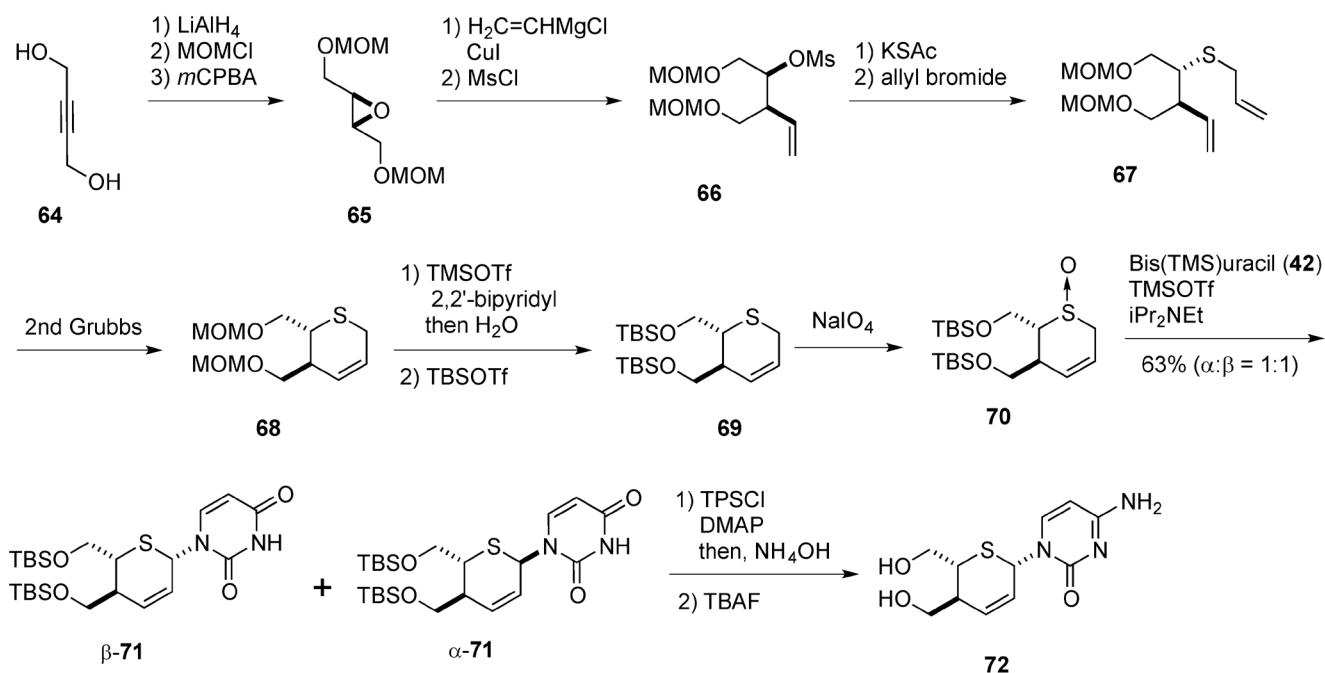
decided to apply it to a 6-membered ring system with dihydrothiopyranose as a substrate.³¹ We designed a ring-expanded analogue of L-4'-thioD4C,³² which has been reported to possess anti-HIV activity. Since the L-isomer of Lamivudine has more potent anti-HIV activity with lesser cytotoxicity,³³ it has been thought that both the D- and L-isomers of nucleosides should be active against HIV.³⁴ Therefore, we tried to synthesize the target analogue as a racemate. Monosilylated 2-butene-1,4-diol **53**³⁵ was converted to the corresponding epoxide, which was treated with vinyl Grignard reagent in the presence of copper iodide to give diol **54**. Selective introduction of a 2,4,6-triisopropylbenzenesulfonyl (TPS) group at the primary alcohol of **54** and nucleophilic substitution by allyl mercaptan gave diene **55**. The ring-closing metathesis (RCM) reaction of **55** using the second generation Grubbs catalyst³⁶ gave dihydrothiopyran derivative **56** in excellent yield. After one-carbon deletion, protection at the resulting primary hydroxyl group of **58** and oxidation gave sulfoxide **60**. Sulfoxide **60** was subjected to the Pummerer-type glycosylation reaction. Treatment of sulfoxide **60** with bis-*O*^{2,4}-(trimethylsilyl)uracil (**42**), TMSOTf, and DIPEA gave dihydrothiopyranyluracil derivatives β -**61** and α -**61** in 41% and 29% yields, respectively. Finally, conversion of the uracil moiety of β -**61** to cytosine and desilylation afforded dihydrothiopyranyl cytosine **63** (Scheme 7).³¹



Scheme 7. Synthesis of dihydrothiopyranyl cytosine derivative

However, **63** did not show anti-HIV activity. Thus, we prepared an analogue with an extra hydroxymethyl unit at the 4'-position of **63**, which resembles the structure of oxetanocin.³⁷ Epoxide **65** was prepared

from 2-butyne-1,4-diol (**64**) in 3 steps and was treated with vinyl Grignard reagent, as described above, followed by mesylation, to give mesylate **66**. Introduction of an allyl sulfide unit in **66** gave diene **67**, followed by RCM with the second generation Grubbs catalyst,³⁶ afforded dihydrothiopyran **68**. After transformation of the protecting group from MOM³⁸ to TBS and oxidation, Pummerer-type glycosylation of the resulting sulfoxide **70** gave a mixture of β -**71** and α -**71** in 63% yield (α : β = 1:1). Using the same procedure as that for **63**, bis(hydroxymethyl)dihydrothiopyranyl cytosine derivative **72** was synthesized and was shown to have anti-HIV activity (Scheme 8).³⁷



Scheme 8. Synthesis of bis(hydroxymethyl)dihydrothiopyranyl cytosine derivative

3. DEVELOPMENT OF A SULFUR-ASSISTED MITSUNOBU REACTION TOWARD THE SYNTHESIS OF ISONUCLEOSIDES

During the synthesis of 4'-thioFAC, we confirmed that the reaction of **13** by using DAST gave a fluorinated compound with retention at the reaction site.²² Marquez reported similar results, suggesting that the reaction proceeded via the neighboring group participation of the ring sulfur to form an episulfonium ion as an intermediate.³⁹ Thus, we synthesized iso-4'-thio-ddA **75**⁴⁰ as a potential anti-HIV agent since iso-ddA **74**⁴¹ was known to have anti-HIV activity comparable to that of ddA, a parental compound of the anti-HIV drug didanosine (**73**).⁴²

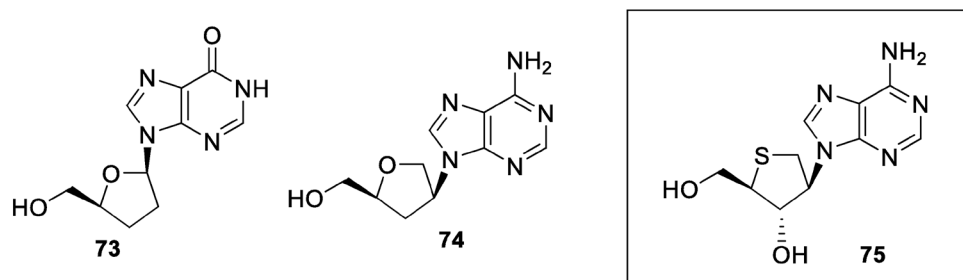
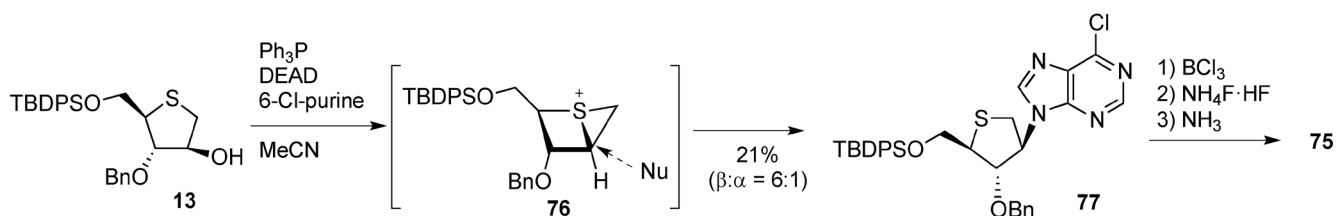


Figure 3. Structures of isonucleosides

After optimizing the reaction conditions, we found that the Mitsunobu reaction with 6-chloropurine in acetonitrile selectively gave the β -isomer of **77**, although the reaction yield was low. Deprotection and amination at the 6-position of **77** gave desired **75** (Scheme 9).⁴⁰



Scheme 9. Synthesis of iso-4'-thionucleoside

Although **75** did not show anti-HIV activity, the results prompted us to study 4'-substituted isonucleosides. With iso-ddA as an example, isonucleosides are a unique category of nucleoside derivatives and have superior tolerance against acid and enzymatic hydrolysis.⁴¹ On the other hand, since 4'-ethynyl nucleosides, such as **78**,⁴³ show potent anti-HIV-1 activity, the corresponding D4T derivative **79**, which exhibited anti-HIV activity, was synthesized.⁴⁴ From these results, 4'-substituted isonucleosides are attractive target molecules for anti-HIV agents. At that time, only the report on the synthesis of 4'-substituted isonucleosides by Nair was available.⁴⁵ The development of a new method to access 4'-substituted isonucleosides was necessary to study the SAR of these analogues. Therefore, we developed a strategy for the synthesis of 4'-hydroxymethylisonucleosides, such as **80**, which could serve as an intermediate for the synthesis of a variety of 4'-substituted isonucleosides (Figure 4).^{46,47}

We synthesized **85** from intermediate **84** by desulfurization. From the synthesis of iso-4'-thionucleosides described above, the reaction occurred via a Mitsunobu reaction using a nucleobase accompanied by sulfide migration.⁴⁰ On the other hand, by using the sulfide attachment at the 3'-position of **84**, the formation of a thietane ring around the 3'- and 4'-positions would afford bicyclo-isonucleoside **81**, an analogue structurally resembling Lamivudine (Scheme 10).

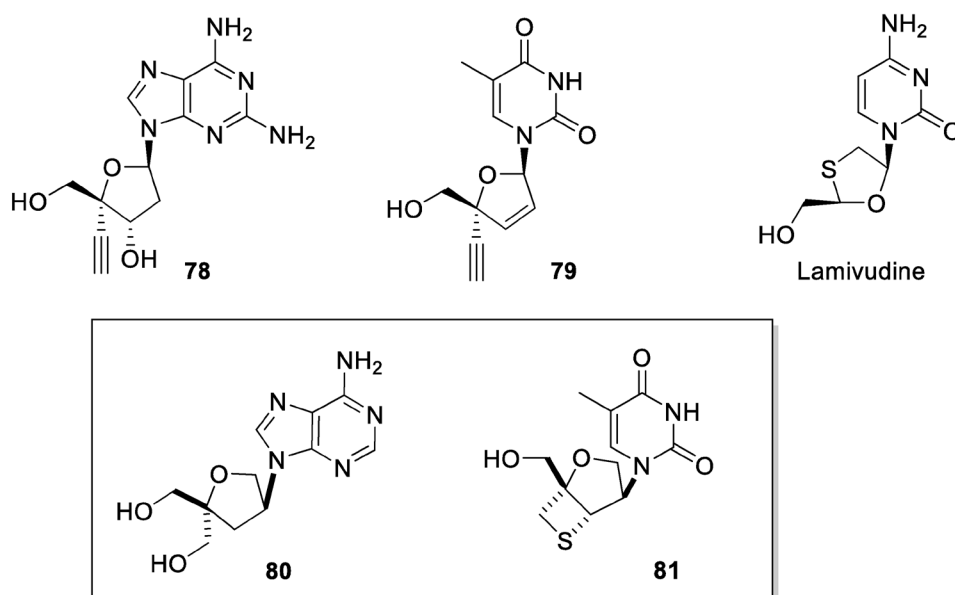
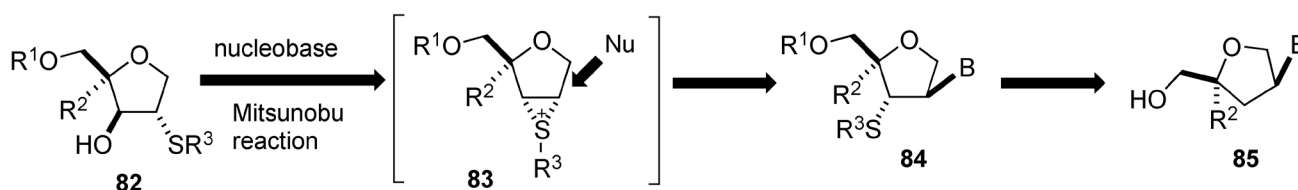
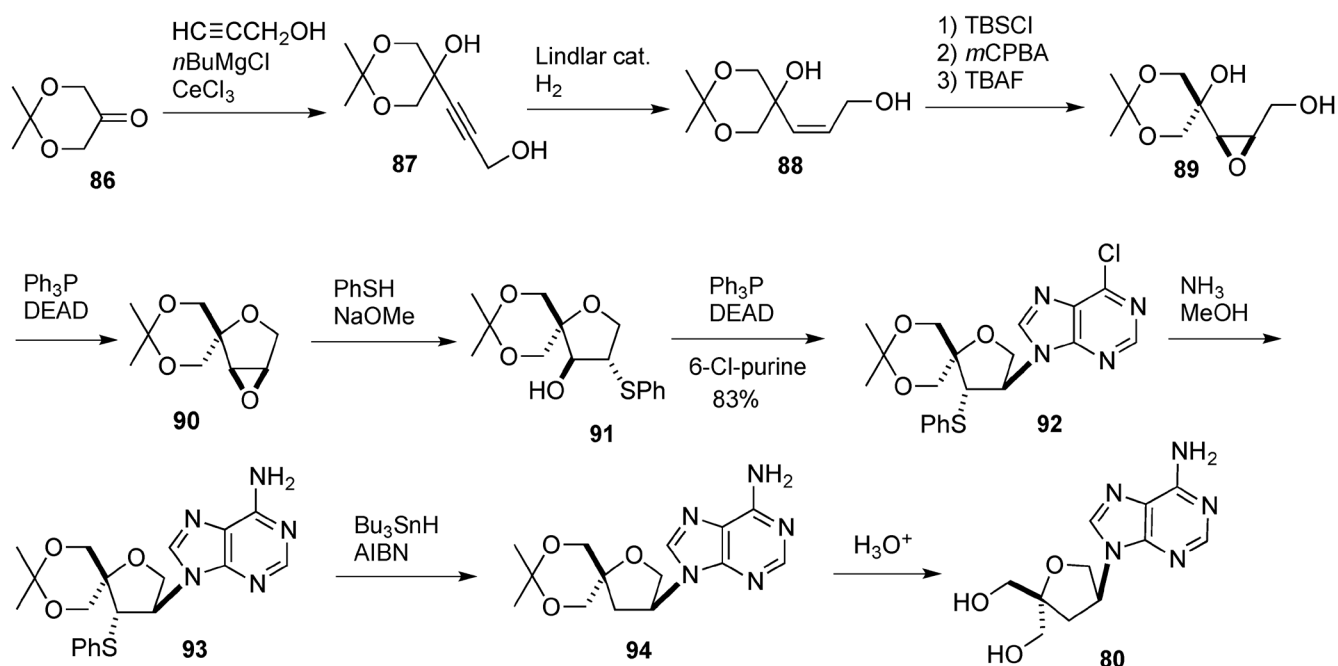


Figure 4. Structures of 4'-substituted nucleosides

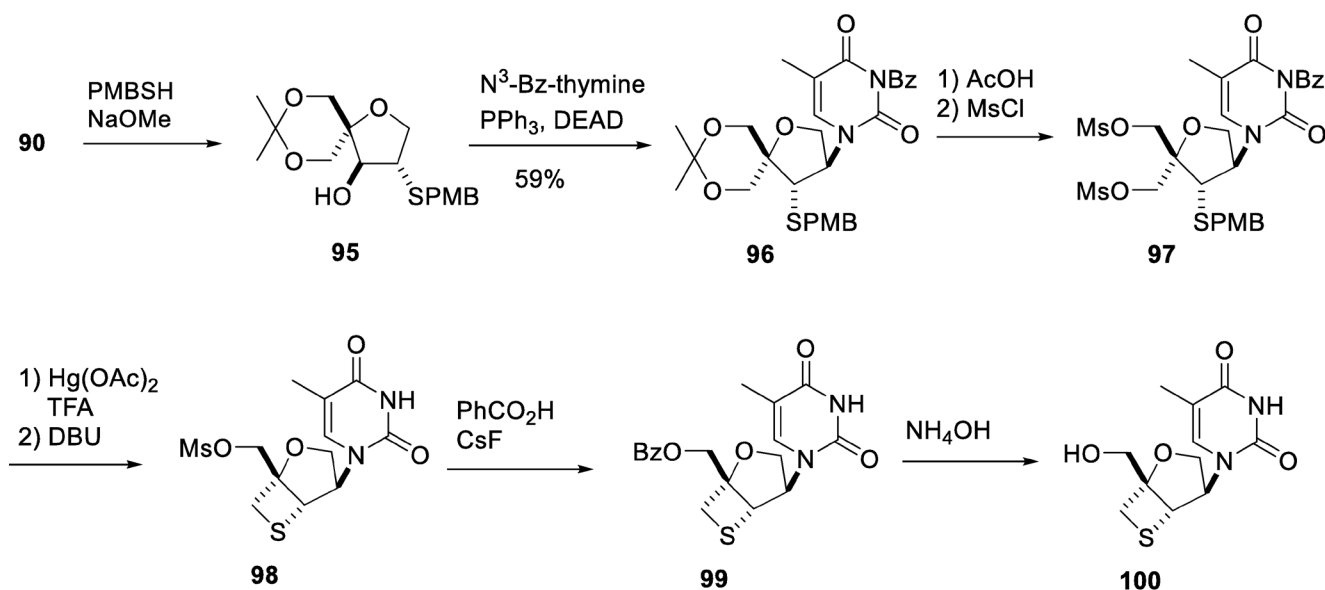


Scheme 10. Strategy for the synthesis of 4'-substituted isonucleosides

The reaction of the dianion of propargyl alcohol and **86** gave diol **87**. Semi-hydrogenation of **87** in the presence of a Lindlar catalyst gave (*Z*)-allyl alcohol derivative **88**. Silylation of the primary alcohol of **88**, followed by treatment with *m*CPBA and desilylation, gave epoxide **89**. Intramolecular etherification of **89** was carried out under Mitsunobu reaction conditions to give the desired dioxabicyclohexane derivative **90**. Cleavage of the epoxide ring of **90** was achieved by treatment with sodium thiophenoxide to give thiophenyl derivative **91** as the sole product. As we expected, the Mitsunobu reaction of **91** with 6-chloropurine in the presence of DEAD and triphenylphosphine proceeded in a regiospecific manner and stereoselectively gave purine isonucleoside derivative **92** in 83% yield. After amination at the 6-position of **92**, desulfurization by radical reduction gave **94**, which was deprotected by acid treatment to give the desired 4'-hydroxymethyl-iso-ddA **80** (Scheme 11).^{46,47}



Scheme 11. Synthesis of 4'-hydroxymethyl-iso-ddA



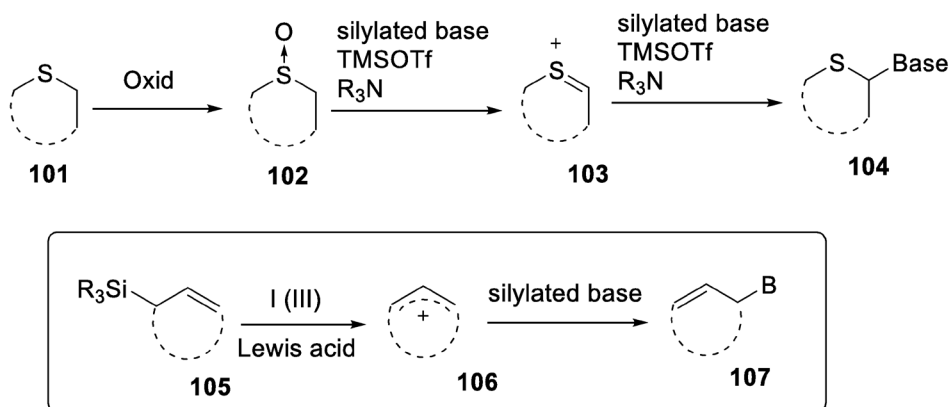
Scheme 12. Synthesis of bicyclo-isonucleoside structurally resembling Lamivudine

Using a similar procedure as that described above, the oxirane ring of **90** was cleaved by treatment with the sodium salt of PMB mercaptan to give PMB sulfide **95** as the sole product. Compound **95** was subjected to the sulfur-assisted Mitsunobu reaction in the presence of *N*³-benzoylthymine to give isothymidine derivative **96** in 59% yield. After removal of the acetal group, followed by mesylation, the PMB group of dimesylate **97** was removed, and the resulting thiol was treated with DBU to give thietane

98. The desired bicyclo-isothymidine **100** was synthesized by converting the mesylate moiety to a benzoate moiety via an S_N2 reaction of **98**, followed by treatment with aqueous NH_3 (Scheme 12).⁴⁷

4. DEVELOPEMENT OF AN OXIDATIVE COUPLING REACTION CATALYZED BY HYPAERVALENT IODINE TOWARD THE SYNTHESIS OF CARBOCYCLIC NUCLEOSIDES

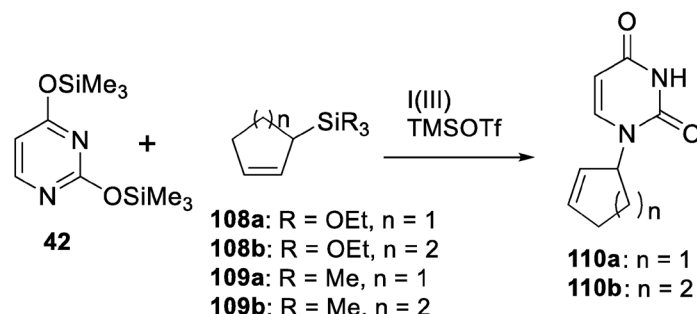
As described above, we developed a Pummerer-type glycosylation reaction, where silylated nucleobases are directly coupled with sulfoxides. Since this glycosylation reaction could be coupled with oxidation, we thought that the reaction was applicable to carbocyclic nucleoside synthesis. In other words, allylsilanes act as a pseudosugar donor for a carbocyclic nucleoside by using a hypervalent iodine reagent.⁴⁸ In the Pummerer-type glycosylation, thiosugar donor **101** was oxidized to sulfoxide **102**, the reaction of which was mediated by a Lewis acid (TMSOTf) and a base to give desired thionucleoside **104** via the formation of sulfenium ion **103**. Following the concept of the Pummerer-type glycosylation, the coupling reaction of cyclic allylsilane **105**, a pseudosugar donor for carbocyclic nucleosides **107**, with a persilylated nucleobase was achieved by using hypervalent iodine in the presence of an appropriate Lewis acid (Scheme 13).



Scheme 13. Oxidative coupling reaction for the synthesis of carbocyclic nucleosides

First, model reactions of the oxidative coupling reaction were examined using simple cycloalkenylsilanes **108a,b** and **109a,b**, prepared by hydrosilylation of cyclopentadiene and cyclohexadiene,⁴⁹ respectively. The coupling reactions of **108a,b** and **109a,b** with bis(trimethylsilyl)uracil (**42**) in the presence of a hypervalent iodine reagent and TMSOTf were examined, and the results are summarized in Scheme 14 and Table 1. The reactions of allylsilane **108a** and **108b** with **42** in the presence of (diacetoxyiodo)benzene ($PhI(OAc)_2$) gave cycloalkenyluracil **110a** and **110b** in moderate yields (entries 1 and 2, respectively). Treatment of **109a** and **109b** under the same conditions gave **110a** and **110b** in 65%

yield (entries 3 and 4, respectively). The use of [di(trifluoroacetoxy)iodo]benzene ($\text{PhI}(\text{O}_2\text{CCF}_3)_2$) (entry 5) and iodosobenzene (PhIO) (entry 6) slightly decreased the reaction yields. On the other hand, the reaction using [hydroxy(tosyloxy)iodo]benzene ($\text{PhI}(\text{OH})\text{OTs}$) gave **110b** in a poor yield (entry 7).⁵⁰



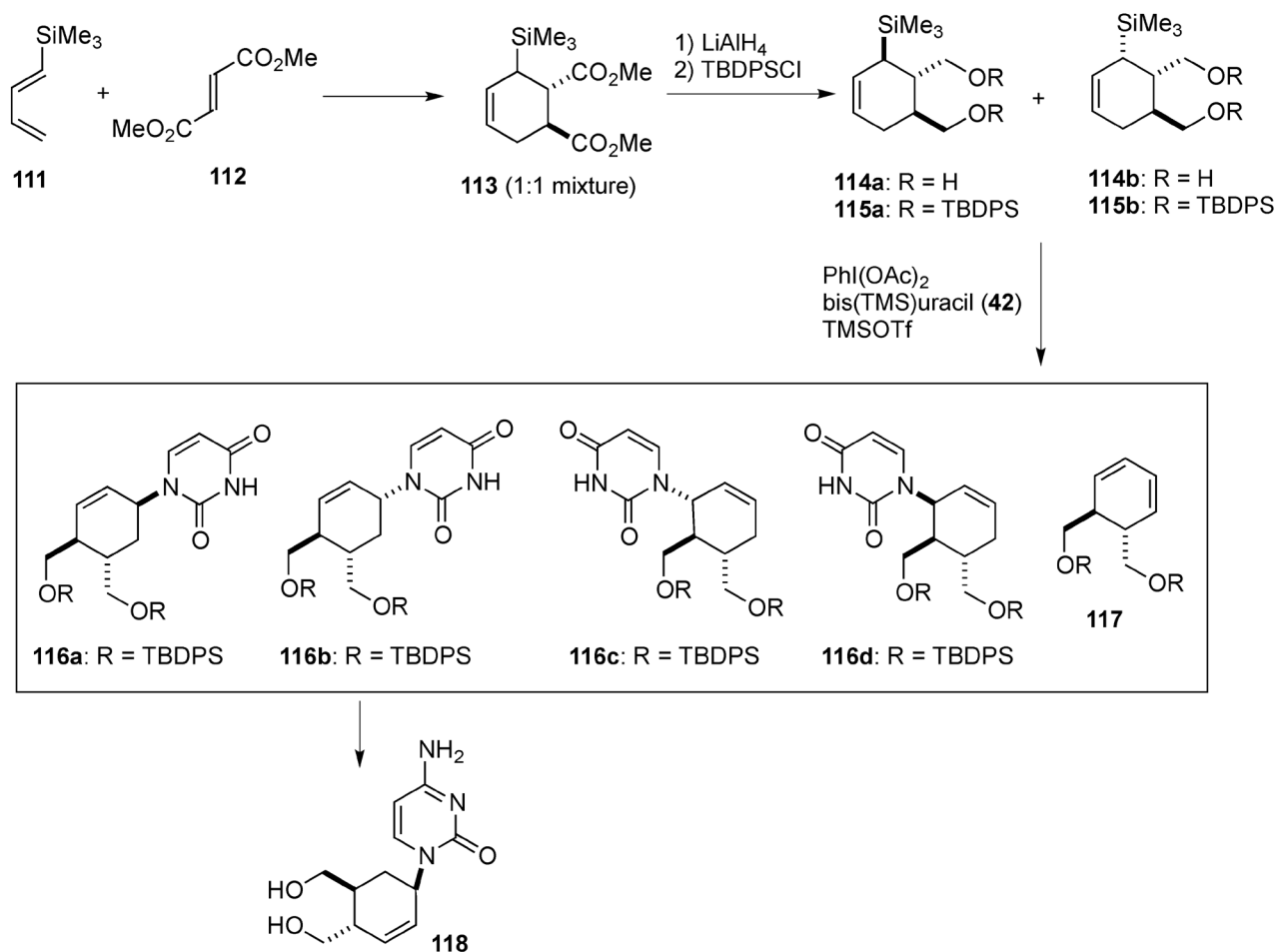
Scheme 14. Oxidative coupling reaction of cyclic allylsilanes and persilylated uracil

Table 1. Summary of the oxidative coupling reaction of cyclic allylsilanes **108** and **109** and persilylated uracil

entry	comp	I(III)	time (h)	yield (%)
1	108a	$\text{PhI}(\text{OAc})_2$	15	45
2	108b	$\text{PhI}(\text{OAc})_2$	15	49
3	109a	$\text{PhI}(\text{OAc})_2$	1	65
4	109b	$\text{PhI}(\text{OAc})_2$	1	65
5	109b	$\text{PhI}(\text{O}_2\text{CCF}_3)_2$	1	55
6	109b	PhIO	1	57
7	109b	$\text{PhI}(\text{OH})\text{OTs}$	1	29

The developed oxidative coupling reaction was applied to the synthesis of new carbocyclic nucleoside derivatives **118**, designed as potential anti-HIV agents. The Diels-Alder reaction of trimethylsilylbutadiene **111** and dimethyl fumarate (**112**) gave cyclohexene diester **113** as a 1:1 mixture.⁵¹ Hydride reduction of **113** and subsequent separation by silica gel column chromatography gave **114a,b**, which were protected by the silyl group to give di-*O*-TBDPS derivatives **115a** and **115b**. The coupling reaction of **115a** and **115b** with persilylated uracil **42** was performed by using (diacetoxyiodo)benzene as an oxidant. The results are shown in Table 2. Since the reaction proceeds via an allyl cation, the reaction of **115a** gave an inseparable mixture containing 4 stereoisomers of **116a–d** in a ratio of 6:10:2:1.5, estimated from the ^1H NMR spectrum of the reaction mixture, and the reaction of **115b** gave similar results.⁵⁰ Cyclohexadiene **117**, obtained in both cases, was consistent with the proposed reaction mechanism shown above and was formed via an E1 elimination of the allyl cation intermediate. The

different reactivities of **115a** and **115b** were explained by steric interaction of the substituents on the cyclohexene ring with the approaching nucleobase (Scheme 15 and Table 2).



Scheme 15. Synthesis of carbocyclic nucleosides using oxidative coupling reaction

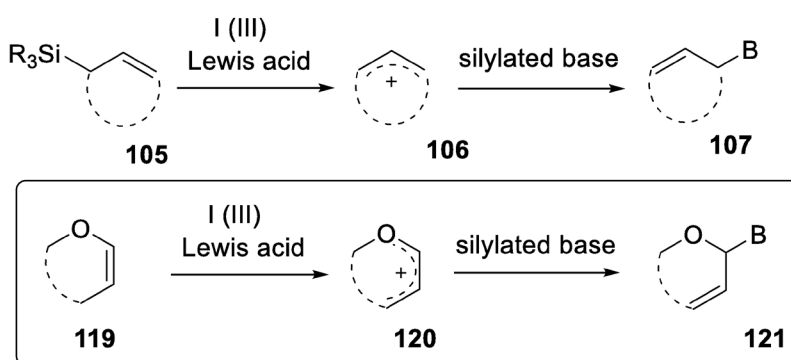
Table 2. Summary of the oxidative coupling reaction of cyclic cyclohexenylsilanes **115a,b** and uracil

comp	time (h)	yield (%)			ratio
		116a-d	117	recov.	
115a	1	60	18	0	6:10:2.0:1.5
115b	24	50	11	20	3:10:2.5:0.5

During the conversion of **116a-d** to cytosine analogues by the same procedure described above, all the stereoisomers were separated. Among them, cytosine derivative **118** only showed weak anti-HIV activity.⁵⁰

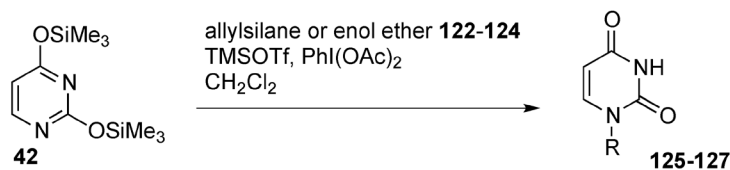
5. APPLICATION OF HYPERVALENT IODINE CHEMISTRY TO THE SYNTHESIS OF DIHYDROPYRANONUCLEOSIDES

We developed a hypervalent iodine-catalyzed reaction for condensing bases and pseudosugars to form the skeleton of carbocyclic nucleosides. The success of the oxidative coupling reaction led us to develop a glycosylation reaction applicable to another sugar donor, i.e., a glycal. The direct coupling of glycals with nucleobases is challenging since it is formally a C-N bond forming reaction with cleavage of an inactive C-H bond. Similar C-N bond forming reactions have been extensively studied in the field of hypervalent iodine chemistry.⁵² The hypervalent iodine-catalyzed coupling reaction occurs via two steps: 1) the generation of carbocation **106** by the oxidative reaction of allylsilane **105** with $\text{PhI}(\text{OAc})_2$ and TMSOTf, followed by 2) the addition of a persilylated base, as shown in Scheme 16. We thought that the reaction of electron-rich glycal **119** under the oxidation conditions described above generated oxocarbenium ion **120**, which would serve as an intermediate to give nucleoside **121** (Scheme 16).



Scheme 16. Oxidative coupling reaction of glycals using hypervalent iodine

First, we performed model reactions of the oxidative coupling of an allylsilane or enol ether using the TMSOTf/ $\text{PhI}(\text{OAc})_2$ system. The reaction of allyltrimethylsilane **122** gave 1-allyluracil **125** in 69% yield by treatment with 1 equiv of $\text{PhI}(\text{OAc})_2$, TMSOTf, and **42** in dichloromethane (entry 1 in Table 3). Although the same reaction was applied to benzyltrimethylsilane **123**, the desired product **126** did not form (entry 2). Next, we tried the reaction with 3,4-dihydro-2*H*-pyran (**124**). The conditions for the reaction involving **124** needed to be optimized. After several attempts, it was found that dihydropyranyluracil derivative **127** was obtained in 31% yield when **124** was treated under the conditions labeled method A (entry 3). $\text{Cu}(\text{OTf})_2$ could also catalyze the reaction, and the reaction of **124** with 0.2 equiv of $\text{Cu}(\text{OTf})_2$ at room temperature (method B) gave **127** in 24% yield (entry 4).⁵³

Table 3. Summary of the oxidative coupling of bis(TMS)uracil **42** with allylsilanes and enol ethers

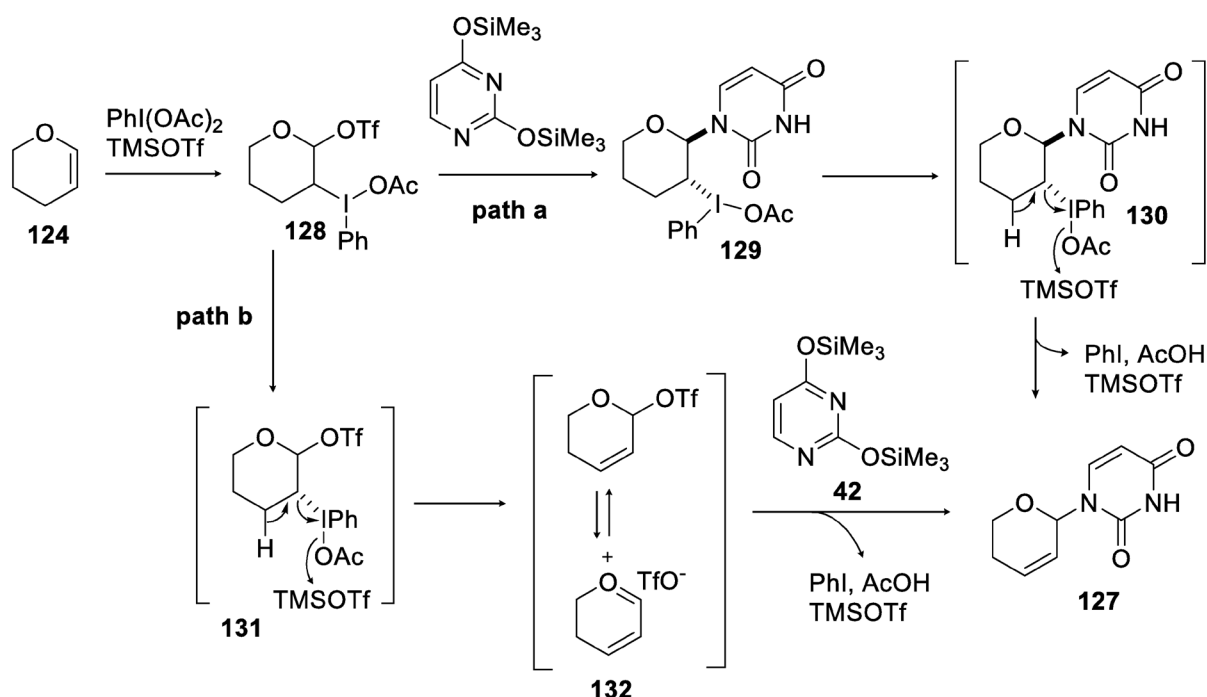
entry	comp	product	yield	entry	comp	product	yield
1			69%	3			31% (method A)
2			ND	4			24% (method B)

Method A: PhI(OAc)_2 (1.5 equiv), TMSOTf (0.4 equiv), and **2** (2.0 equiv) from $-40\text{ }^\circ\text{C}$ to rt.

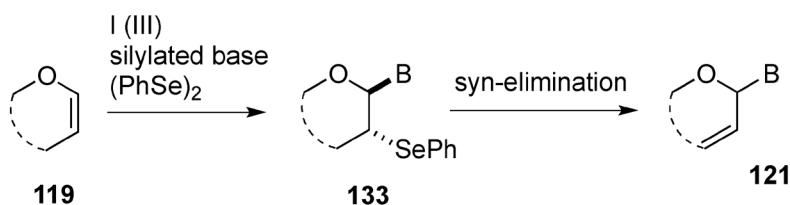
Method B: PhI(OAc)_2 (1.5 equiv), Cu(OTf)_2 (0.2 equiv), and **2** (2.0 equiv) at rt.

A possible reaction mechanism for the oxidative coupling reaction is shown in Scheme 17. When dihydropyran **124** was reacted with PhI(OAc)_2 , acetoxyiodobenzene derivative **128** formed first upon reaction with TMSOTf. There are two plausible reaction paths from intermediate **128** to the N^1 -substituted uracil **127**: nucleophilic attack of bis(TMS)uracil **42** occurs prior to elimination (path a), and an allylic carbocation **132** formed from **131** reacts with **42** (path b). In the reaction with dihydrofuran, side products generated from intermediate **130** were isolated (data not shown). The results strongly suggest that path a occurs more than path b does (Scheme 17).

It was impossible to optimize the oxidative coupling reaction further. To improve the reaction yield of the oxidative coupling reaction, we examined the use of a co-catalyst. The proposed reaction mechanism described above suggested that the instability of intermediate **128** caused the low yield. Therefore, we used $(\text{PhSe})_2$ as a co-catalyst, which should prevent the formation of unstable **128**, to obtain **121** in one step (Scheme 18).



Scheme 17. A proposed reaction mechanism for the oxidative coupling of 3,4-dihydro-2*H*-pyran **124** with TMSOTf/PhI(OAc)₂

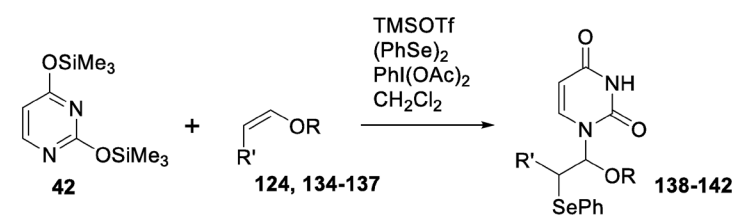
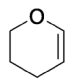
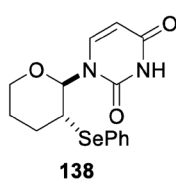
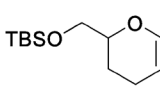
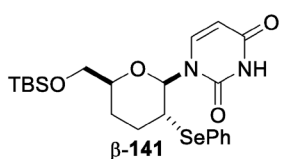
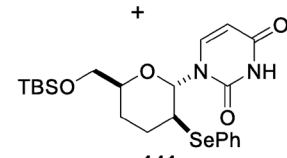
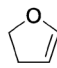
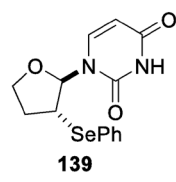
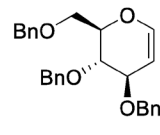
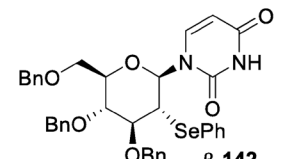
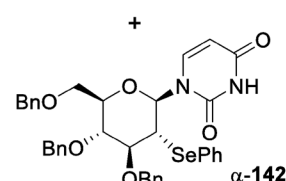
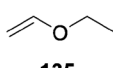
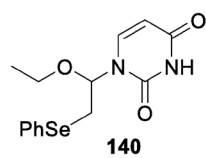


Scheme 18. Synthesis of 1-(3-phenylselanyltetrahydropyran-2-yl)uracil **121** using a co-catalyst

When **124** and **42** were treated with PhI(OAc)₂ and (PhSe)₂ in the presence of catalytic amounts of TMSOTf, the trans-isomer of 1-(3-phenylselanyltetrahydropyran-2-yl)uracil **138** was selectively obtained, as depicted in entry 1 of Table 4. Although the results were different from those expected, they suggested that the reaction could be used to obtain 2'-deoxynucleosides as well as dideoxydidehydronucleosides. Moreover, by using the conditions mentioned above, we avoided the use of an unstable reagent, like PhSeBr, to obtain 2'-phenylselanyl nucleoside derivatives.

The oxidative coupling reaction of **42** with enol ethers and glycals using the TMSOTf/PhI(OAc)₂/(PhSe)₂ system were performed, and the results are summarized in Table 4.

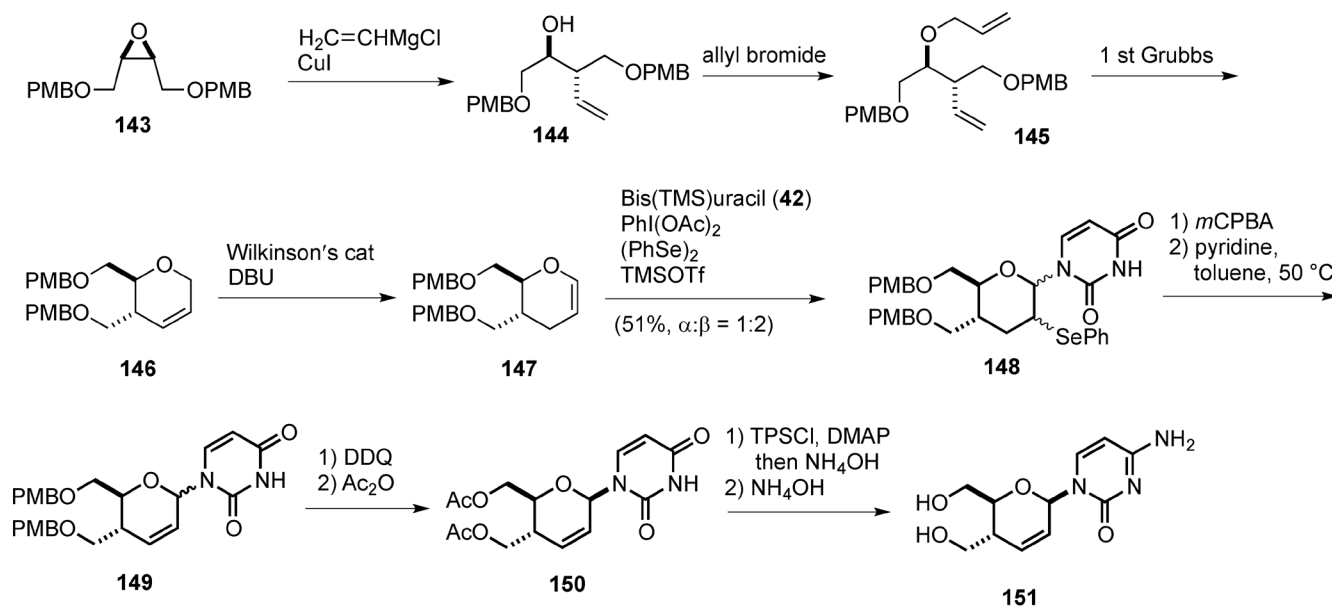
Table 4. Summary of the oxidative coupling reaction of bis(TMS)uracil **42** with enol ethers using the TMSOTf/PhI(OAc)₂/(PhSe)₂ system

							
entry	enol ether	product	yield	entry	enol ether	product	yield
1			73%	4		 β-141  α-141	80% (α:β = 1:2)
2			31%	5		 β-142  α-142	64% (α:β = 1:1)
3			69%				

The reaction with **134** afforded 1-(3-phenylselanyltetrahydrofuran-2-yl)uracil **139** in 31% yield (entry 2). The reaction of **135** with **42** at -5°C afforded **140** in 69% yield (entry 3). The reaction involving **136** gave α-**141** and β-**141** in 80% yield with the β-nucleoside as the major product (entry 4). On the other hand, the oxidative glycosylation reaction of D-glucal **137** gave a mixture of α-**142** and β-**142** in 64% yield without stereoselectivity (entry 5). The oxidative coupling reaction of glycal derivatives, like **136** and **137**, is a new glycosylation reaction, by which 2'-deoxy- and 2',3'-dideoxydidehydronucleosides can be accessed (Table 4).⁵³

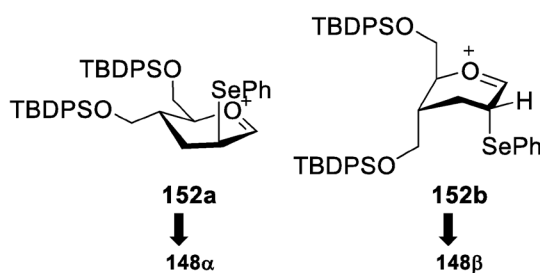
As part of our studies on SAR of nucleoside derivatives constructed on a 6-membered pseudosugar, like dihydrothiophenonucleoside **72** and carbocyclic nucleoside **118**, we designed the synthesis of a

dihydropyranonucleoside by using the oxidative coupling reaction described above.⁵⁴ PMB-protected epoxide **143** was treated with vinylmagnesium chloride to give homoallyl alcohol derivative **144**, the hydroxyl group of which was then allylated to give diene **145**. To construct the dihydropyran ring, RCM of **145** catalyzed with the first generation Grubbs catalyst⁵⁵ was performed to give dihydropyran derivative **146**. Isomerization of the double bond in **146** was achieved by treatment with a Wilkinson catalyst under basic conditions⁵⁶ to afford glycal **147** (Scheme 19).



Scheme 19. Synthesis of dihydropyranonucleoside

Oxidative glycosylation of bis(trimethylsilyl)uracil (**42**) and glycal **147** gave an inseparable mixture of α - and β -anomers of **148** (α : β = 1:2) in 51% yield. Steric repulsion and dipole interactions between two siloxymethyl substituents should favor the formation of the all axial-substituted carbocation intermediate **152b** having a structure similar to the carbocation generated from conformationally “super armed glycosyl donor”.⁵⁷ As a result, the β -anomer **148 β** should predominantly form (Scheme 20).



Scheme 20. Possible carbocation intermediates **152a** and **152b**

Compound **148** was oxidized by treatment with *m*CPBA to give the corresponding selenoxides. An elimination reaction of the resulting selenoxides without any purification gave **149**. Then the PMB group of **149** was deprotected by treatment with DDQ to give a mixture of free nucleosides. After acetylation of the products, an anomeric mixture of diacetates **150** was separated by using simple silica gel column chromatography. The major β -anomer of **150** was converted into a cytosine derivative, followed by deprotection, to give the desired dihydropyranylcytosine derivative **151**.⁵⁴ Antiviral evaluations of the final compound revealed that **151** did not show any activity against HIV though its 5'-thio counterpart **72** showed anti-HIV activity (Scheme 19).⁵⁴

6. CONCLUSION

We synthesized many structurally unique nucleoside derivatives by using new glycosylation reactions. Our early products were 4'-thioDMDC and 4'-thioisonucleoside, for which we developed the Pummerer-type glycosylation. In the case of isonucleosides, a sulfur-assisted Mitsunobu reaction was developed and applied to construct the glycosidic bond of bicyclic isonucleosides, which have structures similar to that of Lamivudine. The Pummerer-type glycosylation, on the other hand, was efficiently applied to synthesize dihydrothiopyranonucleosides. As can be seen, the Pummerer-type glycosylation included oxidation of a sulfide to the corresponding sulfoxide, followed by a TMSOTf-mediated coupling reaction. Considering the Pummerer-type glycosylation, a new glycosylation reaction for carbocyclic nucleosides using allylsilane derivatives and hypervalent iodine was developed to synthesize cyclohexenylnucleosides. In the glycosylation reaction, hypervalent iodine chemistry was applied to build a glycosyl bond between nucleobases and glycal derivatives. This new method was employed for the synthesis of dihydropyranonucleosides. From our synthetic studies on nucleoside derivatives, we found many biologically interesting nucleosides active against tumors as well as viruses. The results prove the power of glycoside bond forming reactions toward the synthesis of and search for biologically active nucleoside derivatives.

ACKNOWLEDGEMENTS

This work was supported in part by a Grant-in-Aid for Scientific Research from JSPS and by a grant from the Strategic Research Foundation Grant-aided Project for Private Universities from Ministry of Education, Culture, Sport, Science, and Technology, Japan (MEXT).

REFERENCES

1. Y. Xie, C. A. Ogah, X. Jiang, J. Li, and J. Shen, *Curr. Drug Targets*, 2016, **17**, 1560; P. J. Thornton, H. Kadri, A. Miccoli, and Y. Mehellou, *J. Med. Chem.*, 2016, **59**, 10400; P. L. Patel, N. K. Rana, M.

- R. Patel, S. D. Kozuch, and D. Sabatino, *ChemMedChem*, 2016, **11**, 252; U. Pradere, E. C. Garnier-Amblard, S. J. Coats, F. Amblard, and R. F. Schinazi, *Chem. Rev.*, 2014, **114**, 9154; E. De Clercq, *Curr. Opin. Pharmacol.*, 2010, **10**, 507; A. Matsuda and T. Sasaki, *Gann Monogr. Cancer Res.*, 2004, **52**, 215.
2. W. H. Prusoff, *Biochim. Biophys. Acta*, 1959, **32**, 295.
 3. G. B. Elion, P. A. Furman, J. A. Fyfe, P. de Miranda, L. Beauchamp, and H. J. Schaeffer, *Proc. Natl. Acad. Sci. USA*, 1977, **74**, 5716.
 4. H. Mitsuya, K. J. Weinhold, P. A. Furman, M. H. St Clair, S. N. Lehrman, R. C. Gallo, D. Bolognesi, D. W. Barry, and S. Broder, *Proc. Natl. Acad. Sci. USA*, 1985, **82**, 7096.
 5. L. W. Hertel, G. B. Boder, J. S. Kroin, S. M. Rinzel, G. A. Poore, G. C. Todd, and G. B. Grindey, *Cancer Res.*, 1990, **50**, 4417; R. P. Abratt, W. R. Bezwoda, G. Falkson, L. Goedhals, D. Hacking, and T. A. Rugg, *J. Clin. Oncol.*, 1994, **12**, 1535.
 6. M. J. Sofia, D. Bao, W. Chang, J. Du, D. Nagarathnam, S. Rachakonda, P. G. Reddy, B. S. Ross, P. Wang, H. R. Zhang, S. Bansal, C. Espiritu, M. Keilman, A. M. Lam, H. M. Steuer, C. Niu, M. J. Otto, and P. A. Furman, *J. Med. Chem.*, 2010, **53**, 7202.
 7. Selected recent reports: K. Tatani, M. Hiratochi, N. Kikuchi, Y. Kuramochi, S. Watanabe, Y. Yamauchi, F. Itoh, M. Isaji, and S. Shuto, *J. Med. Chem.*, 2016, **59**, 3719; G. Wang, J. Deval, J. Hong, N. Dyatkina, M. Prhavc, J. Taylor, A. Fung, Z. Jin, S. K. Stevens, V. Serebryany, J. Liu, Q. Zhang, Y. Tam, S. M. Chanda, D. B. Smith, J. A. Symons, L. M. Blatt, and L. Beigelman, *J. Med. Chem.*, 2015, **58**, 1862; S. K. V. Vernekar, L. Qiu, J. Zhang, J. Kankanala, H. Li, R. J. Geraghty, and Z. Wang, *J. Med. Chem.*, 2015, **58**, 4016; M. Petrová, O. Páv, M. Buděšínský, E. Zborníková, P. Novák, Š. Rosenbergová, O. Pačes, R. Liboska, I. Dvořáková, O. Šimák, and I. Rosenberg, *Org. Lett.*, 2015, **17**, 3426; S. Martínez-Montero, G. F. Deleavey, A. Dierker-Viik, P. Lindovska, T. Ilina, G. Portella, M. Orozco, M. A. Parniak, C. González, and M. J. Damha, *J. Org. Chem.*, 2015, **80**, 3083; S. Dawadi, K. Viswanathan, H. I. Boshoff, C. E. Barry, and C. C. Aldrich, *J. Org. Chem.*, 2015, **80**, 4835; J. C. Salinas, M. T. Migawa, B. L. Merner, and S. Hanessian, *J. Org. Chem.*, 2014, **79**, 11651; P. Gopinath, L. Wang, H. Abe, G. Ravi, T. Masuda, T. Watanabe, and M. Shibasaki, *Org. Lett.*, 2014, **16**, 3364.
 8. Selected recent reports: Y. Yoshimura, S. Kobayashi, H. Kaneko, T. Suzuki, and T. Imamichi, *Molecules*, 2015, **20**, 4623; B. Domínguez-Pérez, É. Ferrer, M. Figueredo, J.-D. Maréchal, J. Balzarini, R. Alibés, and F. Busqué, *J. Org. Chem.*, 2015, **80**, 9495; S. Takano, T. Tsuzuki, T. Murayama, T. Sakurai, H. Fukuda, M. Arisawa, and S. Shuto, *J. Org. Chem.*, 2015, **80**, 6619; S. Dalençon, R. A. Youcef, M. Pipelier, V. Maisonneuve, D. Dubreuil, F. Huet, and S. Legoupy, *J. Org. Chem.*, 2011, **76**, 8059; H. Saneyoshi, J. R. Deschamps, and V. E. Marquez, *J. Org. Chem.*, 2010, **75**,

- 7659; M. X.-W. Jiang, B. Jin, J. L. Gage, A. Priour, G. Savela, and M. J. Miller, *J. Org. Chem.*, 2006, **71**, 4164.
9. Selected recent reports: M. McLaughlin, J. Kong, K. M. Belyk, B. Chen, A. W. Gibson, S. P. Keen, D. R. Lieberman, E. M. Milczek, J. C. Moore, D. Murray, F. Peng, J. Qi, R. A. Reamer, Z. J. Song, L. Tan, L. Wang, and M. J. Williams, *Org. Lett.*, 2017, **19**, 926; T. Hara, T. Kodama, Y. Takegaki, K. Morihiro, K. R. Ito, and S. Obika, *J. Org. Chem.*, 2017, **82**, 25; S. P. Sau, N. E. Fahmi, J.-Y. Liao, S. Bala, and J. C. Chaput, *J. Org. Chem.*, 2016, **81**, 2302; C. Liu, S. G. Dumbre, C. Pannecouque, C. Huang, R. G. Ptak, M. G. Murray, S. De Jonghe, and P. Herdewijn, *J. Med. Chem.*, 2016, **59**, 9513; A. Istrate, M. Medvecky, and C. J. Leumann, *Org. Lett.*, 2015, **17**, 1950; K. Fukuyama, H. Ohru, and S. Kuwahara, *Org. Lett.*, 2015, **17**, 828; R. Clarkson, Z. Komsta, B. A. Mayes, A. Moussa, M. Shelbourne, A. Stewart, A. J. Tyrrell, L. L. Wallis, and A. C. Weymouth-Wilson, *J. Org. Chem.*, 2015, **80**, 2198; G. Tambutet, F. Becerril-Jiménez, S. Dostie, R. Simard, M. Prévost, P. Mochirian, and Y. Guindon, *Org. Lett.*, 2014, **16**, 5698; Z. Komsta, B. A. Mayes, A. Moussa, M. Shelbourne, A. Stewart, A. J. Tyrrell, L. L. Wallis, A. C. Weymouth-Wilson, and A. Yurek-George, *Org. Lett.*, 2014, **16**, 4878.
10. M. R. Dyson, P. L. Coe, and R. T. Walker, *J. Med. Chem.*, 1991, **34**, 2782; J. Balzarini, C. Bohman, R. T. Walker, and E. De Clercq, *Mol. Pharmacol.*, 1994, **45**, 1253.
11. J. A. Secrist III, K. N. Tiwari, J. M. Riordan, and J. A. Montgomery, *J. Med. Chem.*, 1991, **34**, 2361.
12. A. Matsuda, K. Takenuki, M. Tanaka, T. Sasaki, and T. Ueda, *J. Med. Chem.*, 1991, **34**, 812; K. Yamagami, A. Fujii, M. Arita, T. Okumoto, S. Sakata, A. Matsuda, T. Ueda, and T. Sasaki, *Cancer Res.*, 1991, **51**, 2319.
13. E. J. Reist, L. V. Fisher, and L. Goodman, *J. Org. Chem.*, 1968, **33**, 189; D. J. Hoffman and R. L. Whistler, *Biochemistry*, 1970, **9**, 2367.
14. R. L. Whistler, L. W. Doner, and U. G. Nayak, *J. Org. Chem.*, 1971, **36**, 108; N. Ototani and R. L. Whistler, *J. Med. Chem.*, 1974, **17**, 535.
15. U. Niedballa and H. Vorbrüggen, *J. Org. Chem.*, 1974, **39**, 3654.
16. M. Bobek, A. Bloch, R. Parthasarathy, and R. L. Whistler, *J. Med. Chem.*, 1975, **18**, 784.
17. Y. Kita, H. Yasuda, O. Tamura, F. Itoh, and Y. Tamura, *Tetrahedron Lett.*, 1984, **25**, 4681; Y. Kita, H. Yasuda, O. Tamura, F. Itoh, and Y. Tamura, *Chem. Pharm. Bull.*, 1985, **33**, 4235.
18. A. Nishida, T. Hamada, and O. Yonemitsu, *Chem. Pharm. Bull.*, 1990, **38**, 2977.
19. Y. Yoshimura, K. Kitano, H. Satoh, M. Watanabe, S. Miura, S. Sakata, T. Sasaki, and A. Matsuda, *J. Org. Chem.*, 1996, **61**, 822; Y. Yoshimura, K. Kitano, K. Yamada, H. Satoh, M. Watanabe, S. Miura, S. Sakata, T. Sasaki, and A. Matsuda, *J. Org. Chem.*, 1997, **62**, 3140.
20. C. Meier, T. Knispel, V. E. Marquez, M. A. Siddiqui, E. De Clercq, and J. Balzarini, *J. Med. Chem.*,

- 1999, **42**, 1615.
21. S. Miura, M. Tanaka, Y. Yoshimura, H. Satoh, S. Sakata, H. Machida, A. Matsuda, and T. Sasaki, *Biol. Pharm. Bull.*, 1996, **19**, 1311.
22. Y. Yoshimura, M. Endo, S. Miura, and S. Sakata, *J. Org. Chem.*, 1999, **64**, 7912.
23. S. Miura, Y. Yoshimura, M. Endo, H. Machida, A. Matsuda, M. Tanaka, and T. Sasaki, *Cancer Lett.*, 1998, **129**, 103; S. Miura, Y. Yoshimura, M. Endo, H. Satoh, H. Machida, and T. Sasaki, *Cancer Lett.*, 1999, **144**, 177; S. Miura, Y. Endo, Y. Yoshimura, M. Endo, Y. Yonemura, and T. Sasaki, *Oncol. Rep.*, 2002, **9**, 1319.
24. H. Machida, N. Ashida, S. Miura, M. Endo, K. Yamada, K. Kitano, Y. Yoshimura, S. Sakata, O. Ijichi, and Y. Eizuru, *Antiviral Res.*, 1998, **39**, 129; Y. Yoshimura, K. Kitano, K. Yamada, S. Sakata, S. Miura, N. Ashida, and H. Machida, *Bioorg. Med. Chem.*, 2000, **8**, 1545.
25. T. Naka, N. Minakawa, H. Abe, D. Kaga, and A. Matsuda, *J. Am. Chem. Soc.*, 2000, **122**, 7233.
26. Y. Yoshimura, T. Kuze, M. Ueno, F. Komiya, K. Haraguchi, H. Tanaka, F. Kano, K. Yamada, K. Asami, N. Kaneko, and H. Takahata, *Tetrahedron Lett.*, 2006, **47**, 591.
27. H. Choo, X. Chen, V. Yadav, J. Wang, R. F. Schinazi, and C. K. Chu, *J. Med. Chem.*, 2006, **49**, 1635.
28. N. Nishizono, N. Koike, Y. Yamagata, S. Fujii, and A. Matsuda, *Tetrahedron Lett.*, 1996, **42**, 7569.
29. N. Shimada, S. Hasegawa, T. Harada, T. Tomisawa, A. Fujii, and T. Takita, *J. Antibiot.*, 1986, **39**, 1623; H. Nakamura, S. Hasegawa, N. Shimada, A. Fujii, T. Takita, and Y. Iitaka, *J. Antibiot.*, 1986, **39**, 1626.
30. N. A. Petasis and E. I. Bzowej, *J. Am. Chem. Soc.*, 1990, **112**, 6392.
31. Y. Yoshimura, Y. Yamazaki, M. Kawahata, K. Yamaguchi, and H. Takahata, *Tetrahedron Lett.*, 2007, **48**, 4519; Y. Yoshimura, Y. Yamazaki, Y. Saito, and H. Takahata, *Tetrahedron*, 2009, **65**, 9091.
32. R. J. Young, S. Saw-Ponter, J. B. Thomson, J. A. Miller, J. G. Cumming, A. W. Pugh, and P. Rider, *Bioorg. Med. Chem. Lett.*, 1995, **5**, 2599.
33. J. A. Coates, N. Cammack, H. J. Jenkinson, I. M. Mutton, B. A. Pearson, R. Storer, J. M. Cameron, and C. R. Penn, *Antimicrob. Agents Chemother.*, 1992, **36**, 202; R. F. Schinazi, C. K. Chu, A. Peck, A. McMillan, R. Mathis, D. Cannon, L. S. Jeong, J. W. Beach, W. B. Choi, and S. Yeola, *Antimicrob. Agents Chemother.*, 1992, **36**, 672; J. A. Coates, N. Cammack, H. J. Jenkinson, A. J. Jowett, M. I. Jowett, B. A. Pearson, C. R. Penn, P. L. Rouse, K. C. Viner, and J. M. Cameron, *Antimicrob. Agents Chemother.*, 1992, **36**, 733; J. P. Sommadossi, R. F. Schinazi, C. K. Chu, and M. Y. Xie, *Biochem. Pharmacol.*, 1992, **44**, 1921.
34. K. Lee and C. K. Chu, *Antimicrob. Agents Chemother.*, 2001, **45**, 138; C. Mathe and G. Gosselin,

Antiviral Res., 2006, **71**, 276.

35. P. G. McDougal, J. G. Rico, Y.-I. Oh, and B. D. Condon, *J. Org. Chem.*, 1986, **51**, 3388; T. Ayad, Y. Génisson, and M. Baltas, *Org. Biomol. Chem.*, 2005, **3**, 2626.
36. D. A. Evans, K. R. Campos, J. S. Tedrow, F. E. Michael, and M. R. Gagné, *J. Am. Chem. Soc.*, 2000, **122**, 7905.
37. Y. Yoshimura, Y. Yamazaki, Y. Saito, Y. Natori, T. Imamichi, and H. Takahata, *Bioorg. Med. Chem. Lett.*, 2011, **21**, 3313.
38. H. Fujioka, Y. Sawama, N. Murata, T. Okitsu, O. Kubo, S. Matsuda, and Y. Kita, *J. Am. Chem. Soc.*, 2004, **126**, 11800; H. Fujioka, O. Kubo, K. Senami, Y. Minamitsuji, and T. Maegawa, *Chem. Commun.*, 2009, 4429; H. Fujioka, T. Okitsu, T. Ohnaka, R. Li, O. Kubo, K. Okamoto, Y. Sawama, and Y. Kita, *J. Org. Chem.*, 2007, **72**, 7898.
39. L. S. Jeong, M. C. Nicklaus, C. George, and V. E. Marquez, *Tetrahedron Lett.*, 1994, **35**, 7569.
40. K. Yamada, S. Sakata, and Y. Yoshimura, *J. Org. Chem.*, 1998, **63**, 6891.
41. V. Nair and Z. M. Nuesca, *J. Am. Chem. Soc.*, 1992, **114**, 7951; D. M. Huryn, B. C. Sluboski, S. Y. Tam, M. Weigle, I. Sim, B. D. Anderson, H. Mitsuya, and S. Broder, *J. Med. Chem.*, 1992, **35**, 2347; V. Nair and T. S. Jahnke, *Antimicrob. Agents Chemother.*, 1995, **39**, 1017; V. Nair, In *Recent Advances in Nucleosides*, ed. by C. K. Chu, Elsevier Science B.V., Amsterdam, 2002, pp. 149–166 and references cited therein.
42. H. Mitsuya and S. Broder, *Proc. Natl. Acad. Sci. USA*, 1986, **83**, 1911.
43. H. Ohrui, S. Kohgo, K. Kitano, S. Sakata, E. Kodama, K. Yoshimura, M. Matsuoka, S. Shigeta and H. Mitsuya, *J. Med. Chem.*, 2000, **43**, 4516; E. I. Kodama, S. Kohgo, K. Kitano, H. Machida, H. Gatanaga, S. Shigeta, M. Matsuoka, H. Ohrui, and H. Mitsuya, *Antimicrob. Agents Chemother.*, 2001, **45**, 1539.
44. G. E. Dutschman, S. P. Grill, E. A. Gullen, K. Haraguchi, S. Takeda, H. Tanaka, M. Baba, and Y.-C. Cheng, *Antimicrob. Agents Chemother.*, 2004, **48**, 1640.
45. L. B. Zintek, G. S. Jeon, and V. Nair, *Heterocycles*, 1994, **37**, 1853; V. Nair, L. B. Zintek, and G. S. Jeon, *Nucleosides Nucleotides*, 1995, **14**, 389.
46. Y. Yoshimura, K. Asami, H. Matsui, H. Tanaka, and H. Takahata, *Org. Lett.*, 2006, **8**, 6015.
47. Y. Yoshimura, K. Asami, T. Imamichi, T. Okuda, K. Shiraki, and H. Takahata, *J. Org. Chem.*, 2010, **75**, 4161.
48. M. Ochiai, E. Fujita, M. Arimoto, and H. Yamaguchi, *Chem. Pharm. Bull.*, 1985, **33**, 41.
49. M. Kira, T. Hino, and H. Sakurai, *Tetrahedron Lett.*, 1989, **30**, 1099.
50. Y. Yoshimura, M. Ohta, T. Imahori, T. Imamichi, and H. Takahata, *Org. Lett.*, 2008, **10**, 3449.
51. M. E. Jung and B. Gaede, *Tetrahedron*, 1979, **35**, 621.

52. J. A. Souto, D. Zian, and K. Muniz, *J. Am. Chem. Soc.*, 2012, **134**, 7242; M. Ochiai, *Science*, 2011, **332**, 448; S. H. Cho, J. Yoon, and S. Chang, *J. Am. Chem. Soc.*, 2011, **133**, 5996; A. P. Antonchick, R. Samanta, K. Kulikov, and J. Lategahn, *Angew. Chem. Int. Ed.*, 2011, **50**, 8605; T. Dohi, A. Maruyama, Y. Minamitsuji, N. Takenaga, and Y. Kita, *Chem. Commun.*, 2007, 1224; T. Dohi, K. Morimoto, N. Takenaga, A. Goto, A. Maruyama, Y. Kiyono, H. Tohma, and Y. Kita, *J. Org. Chem.*, 2007, **72**, 109.
53. Y. Yoshimura, H. Kan-no, Y. B. Kiran, Y. Natori, Y. Saito, and H. Takahata, *Synthesis*, 2012, **44**, 1163.
54. H. Kan-no, Y. Saito, S. Omoto, S. Minato, H. Wakamatsu, Y. Natori, T. Imamichi, H. Takahata, and Y. Yoshimura, *Synthesis*, 2014, **46**, 879.
55. P. Schwab, M. B. France, J. W. Ziller, and R. H. Grubbs, *Angew. Chem., Int. Ed. Engl.*, 1995, **34**, 2039.
56. B. Schmidt, *J. Org. Chem.*, 2004, **69**, 7672.
57. C. M. Pedersen, L. U. Nordstrøm, and M. Bols, *J. Am. Chem. Soc.*, 2007, **129**, 9222; L. K. Mydock, and A. V. Demchenko, *Org. Lett.*, 2008, **10**, 2103.
-



Prof. Yuichi Yoshimura obtained his B.S degree in 1985 and his M.S degree in 1987 from Hokkaido University. He then obtained his Ph.D. degree in 1991 from Hokkaido University and joined Yamasa Corporation after one year of work in the Faculty of Pharmaceutical Sciences, Hokkaido University as a Research Associate. In 1999, he moved to the School of Pharmacy, Showa University as a Lecturer and joined Tohoku Pharmaceutical University in 2004. In 2005, he was promoted to Associate Professor at the same university. In 2014, he became a Professor of Faculty of Pharmaceutical Sciences, Tohoku Pharmaceutical University, the name of which changed to Tohoku Medical and Pharmaceutical University in 2016. He was awarded the Sato Memorial Domestic Award by the Pharmaceutical Society of Japan in 2008. His research interests focus on synthetic and medicinal chemistry of nucleosides and nucleotides.

SYNLETT Accounts and Rapid Communications in Chemical Synthesis

This electronic reprint is provided for non-commercial and personal use only: this reprint may be forwarded to individual colleagues or may be used on the author's homepage. This reprint is not provided for distribution in repositories, including social and scientific networks and platforms.

Publishing House and Copyright:

© 2017 by
Georg Thieme Verlag KG
Rüdigerstraße 14
70469 Stuttgart
ISSN 0936-5214

Any further use
only by permission
of the Publishing House

Palladium-Catalyzed Regioselective Hydroarylation of Ynamides with Aryl Iodides: Easy Synthesis of Various Substituted Enamides Containing Stilbene Derivatives

Hideaki Wakamatsu*

Rika Yanagisawa

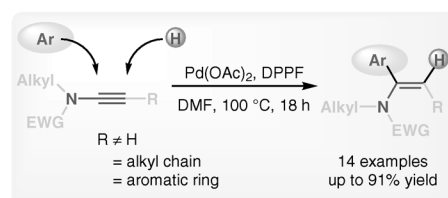
Sho Kimura

Nao Osawa

Yoshihiro Natori

Yuichi Yoshimura*

Faculty of Pharmaceutical Sciences, Tohoku Medical and Pharmaceutical University, Komatsushima 4-4-1, Aoba-ku, Sendai 981-8558, Japan
hiwaka@tohoku-mpu.ac.jp
yoshimura@tohoku-mpu.ac.jp



Received: 20.04.2017
Accepted after revision: 19.05.2017
Published online: 06.07.2017
DOI: 10.1055/s-0036-1588874; Art ID: st-2017-u0276-l

Abstract Palladium-catalyzed hydroarylation of ynamides has been developed. The desired coupling products were obtained in good yields and with high regioselectivities. Various aryl iodides can be used in this reaction, permitting the syntheses of many different kinds of enamides from ynamides.

Key words ynamides, hydroarylation, palladium catalysis, cross-coupling, enamides, arylation

Over the past 20 years, the ynamide group has begun to be recognized as a functional group that participates in a new C–C bond-forming reaction.¹ The useful C–C bond-forming reaction of ynamides has been reported by several research groups, who described the different π -orbital electron density in these compounds compared with that in other C≡C triple bonds.² We have also become interested in the reactions of ynamides with transition-metal complexes. A ring-closing metathesis (RCM) of ene-ynamides³ and a copper-free Sonogashira coupling of unsubstituted ynamides⁴ have already been reported by our research group. Our continuing interests have focused on developing additional transition-metal-catalyzed C–C bond-formation reactions of ynamides. The hydroarylation of C≡C triple bonds is known to be a useful method for the construction of carbon frameworks.^{5–7} These reactions have been successfully used for the synthesis of heterocycles.⁸ Here, we describe a palladium-catalyzed regioselective hydroarylation reaction of substituted ynamides.

When the reaction of ynamide **1a**⁹ and aryl iodide **2a** in the presence of a catalytic amount of Pd(OAc)₂ and Ph₃P in the presence of HCO₂NH₄ as a reducing agent was performed in *N,N*-dimethylformamide (DMF) at 80 °C for 20

hours, the desired coupling product **3a** was obtained in 10% yield, together with recovered **1a** in 44% yield (Table 1, entry 1). Several phosphine ligands were tested for this reaction (entries 2–5). Tricyclohexylphosphine did not work, and **1a** was recovered in 59% yield (entry 2). When 1,2-bis(diphenylphosphino)ethane (DPPE), a typical bidentate ligand, was used, a similar result was obtained to that with Ph₃P (entry 3). The use of 1,4-bis(diphenylphosphino)butane (DPPB) slightly improved the chemical yield of **3a** (entry 4), but the best result was obtained when 1,1'-bis(diphenylphosphino)ferrocene (DPPF) was used (entry 5).

The stereochemistry of the enamide **3a** was determined by an NOE experiment, as shown in Figure 1.

Table 1 Palladium-Catalyzed Hydroarylation of Ynamide **1a** and Screening of Ligands^a

Entry	Ligand	Time (h)	Yield (%) of 3a	Recovery (%) of 1a
1	Ph ₃ P ^b	20	10	44
2	PCy ₃ ^b	18	–	59
3	DPPE	18	12	63
4	DPPB	18	23	30
5	DPPF	18	24	45

^a Reaction conditions: **2a** (1.2 equiv), ligand (5 mol%), HCO₂NH₄ (1.2 equiv).

^b 10 mol% of the ligand was used.

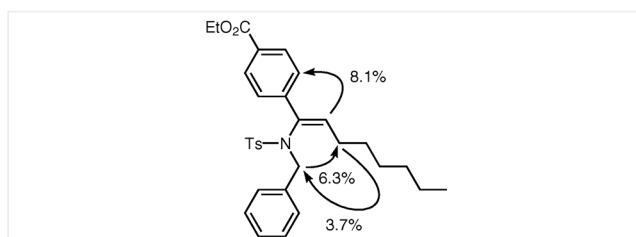
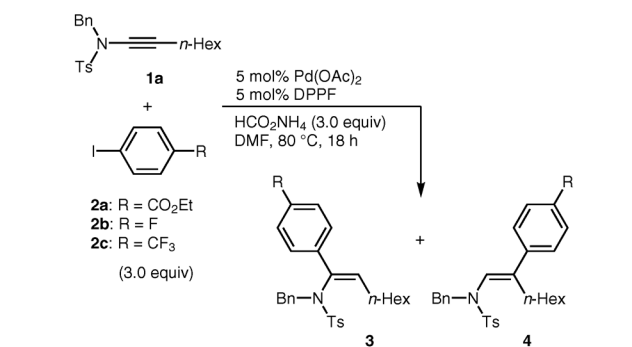


Figure 1 NOE experiment for enamide product **3a**

When the reaction of **1a** with three equivalents each of **2a** and HCO_2NH_4 was carried out at 80 °C for 18 hours, the yield of the coupling product **3a** increased to 56% (Table 2, entry 1). At this point, we recovered **2a** together with a deiodination product. Hydroarylation was restricted by the reduction of **2a**, as in the case shown in Table 1, entry 5. Encouraged by these results, we decided to examine the reactions of various aryl iodides. However, this required further optimization of the reaction conditions, because decreased coupling product yields were obtained in the cases of 1-fluoro-4-iodobenzene (**2b**) and 1-iodo-4-(trifluoromethyl)benzene (**2c**) (entries 2 and 3). The yields were slightly improved on prolonging the reaction time (entry 4). Finally, a satisfactory result in terms of regioselectivity was obtained when the reaction was carried out at 100 °C; the major isomer **3a** was obtained in 76% yield together with a 15% yield of **4a** (entry 5).¹⁰

Next, we examined the reactions of various aryl iodides with ynamide **1a** (Table 3). When the reactions of **2b** and **2c** were repeated, the yields increased to 73% and 59%, respec-

Table 2 Optimization of the Reaction Temperature and Time



Entry	2	Yield (%) of 3	Yield (%) of 4	Recovery (%) of 1a
1	2a	56	7	22
2	2b	30	–	48
3	2c	38	4	52
4 ^a	2a	59	9	18
5 ^b	2a	76	15	4

^a Reaction was carried out for 24 h.

^b At 100 °C.

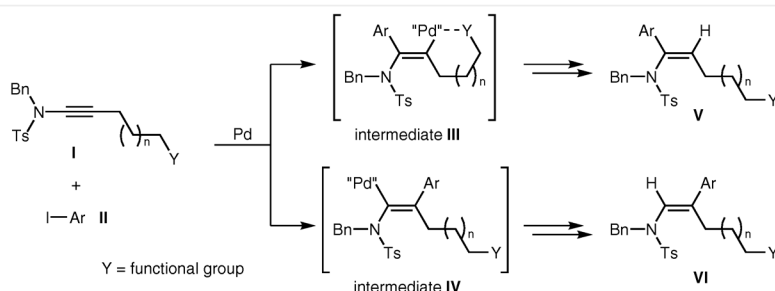
tively (Table 3, entries 1 and 2). 4-Iodobenzonitrile (**2d**), which contains an additional electron-withdrawing group, gave a satisfactory yield (entry 3). The C–C bond-forming reaction proceeded smoothly to introduce the aryl substituent at the α -position of the ynamide in the case of iodide **2e**, which has a *p*-methoxy substituent as an electron-donating group (entry 4). Aryl iodide **2f**, with a methoxycarbonyl group in the *ortho* position, did not give a satisfactory reaction (entry 5).

Table 3 Reactivity of Various Aryl Iodides to Hydroarylation of Ynamide **1a**

Entry	Substrate	Ar	Yield (%) of 3	Yield (%) of 4	Recovery (%) of 1a
1	2b	4-FC ₆ H ₄	73	12	3
2	2c	4-F ₃ CC ₆ H ₄	59	2	–
3	2d	4-NCC ₆ H ₄	57	13	2
4	2e	4-MeOC ₆ H ₄	77	5	–
5	2f	2-MeO ₂ CC ₆ H ₄	10	9	–

At this point, we designed new substrates with the aim of improving the regioselectivity. We surmised that if a functional group was introduced onto the carbon substituent of the ynamide, it might coordinate with the palladium to provide the palladacycle intermediate **III**, with suppression of the intermediate **IV**. Consequently, we predicted that the yield of product **V** might be improved (Scheme 1).

When the reaction of ynamide **1b**, having a benzoyloxymethyl group at the terminal position of the alkyne, was performed under the standard conditions, the desired product was not obtained (Table 4, entry 1), and a complex mixture was obtained on introduction of an ethoxycarbonyl group (entry 2). When ynamide **1d**, in which a siloxy group was introduced at the end of the carbon chain, was exposed to the standard reaction conditions, a good yield and high regioselectivity were obtained (entry 3). Unfortunately, the regioselectivity completely disappeared when the carboxy amide **1e** was used (entry 4). These results showed that an improvement in the regioselectivity was difficult to achieve through coordination of the functional group to the palladium metal. Because the regioselectivity disappeared on changing the 4-toluenesulfonamide group on the alkyne to a carboxy amide group, the reaction of **1** should proceed re-



Scheme 1 Our hypothesis for the improvement of the regioselectivity

Table 4 Hydroarylation of Various Ynamides

Entry	Ynamide	Time (h)	Yield (%) of 5	Yield (%) of 6
1	1b	18	–	–
2	1c	18	–	–
3	1d	24	57	13
a				
4	1e	18	30	31

^a *n*-Hex = (CH₂)₅Me.

gioselectively to provide compound **5** through steric repulsion between the *N*-benzyl-*N*-(4-toluenesulfonyl)amide group and the palladium metal.

Next, we attempted to synthesize various stilbene derivatives by introducing a phenyl group onto the terminal carbon atom of the alkyne part of the ynamide (Table 5). Under the optimized conditions, the reaction of ynamide **1f**, substituted by a methyl group on the nitrogen atom and a phenyl group on the terminal carbon of the alkyne, gave the desired enamide **7f** in 43% yield, together with a 25% recovery of substrate **1f** (entry 1). An improved chemical yield of **7g** compared with that of **7f** was observed on changing the phenyl group to an electron-donating anisyl group (entry 2). The alkyl substituent on the nitrogen did not appear to affect the product yield when the *N*-benzyl ynamide **1h** was used as a substrate (entry 3). However, we found that the benzyl group had a slightly positive effect on the product yield compared with that of the methyl group, and improved yields were obtained when an anisyl group was present on the terminal carbon atom of the alkyne (entry 4).

Table 5 Synthesis of Stilbene Derivatives **7**

Entry	Substrate	R ¹	R ²	Yield (%) of 7	Recovery (%) of 1
1	1f	Me	H	43	25
2	1g	Me	4-MeO	55	–
3	1h	Bn	H	40	48
4	1i	Bn	4-MeO	71	15

In conclusion, we have studied the palladium-catalyzed hydroarylation of ynamides to establish a new method for constructing C–C bonds. When ynamides were exposed to a catalytic amount of Pd(OAc)₂ and DPPF in the presence of 3.0 equivalents of an aryl iodide and HCO₂NH₄ in DMF at 100 °C, the reactions proceeded smoothly to provide the desired products in good yields. Regioselective C–C bond

formation on a carbon atom neighboring a nitrogen atom was achieved by using various ynamides containing a tosyl group as an electron-withdrawing group; however, the regioselectivity was not satisfactory by using ynamides containing a carboxy group as an electron-withdrawing group. Various aryl iodides can be used in this reaction, and many different kinds of enamide can now be synthesized from ynamides. Further studies on this type of reaction and on the possibility of using ynamides for transition-metal-catalyzed reactions are now in progress in our laboratory.

Supporting Information

Supporting information for this article is available online at <https://doi.org/10.1055/s-0036-1588874>.

References and Notes

- (1) For recent reviews on the chemistry of ynamines and ynamides, see: (a) Nayak, S.; Prabagar, B.; Sahoo, A. K. *Org. Biomol. Chem.* **2016**, *14*, 803. (b) Wang, X.-N.; Yeom, H.-S.; Fang, L.-C.; He, S.; Ma, Z.-X.; Kedrowski, B. L.; Hsung, R. P. *Acc. Chem. Res.* **2014**, *47*, 560. (c) Evano, G.; Jouvin, K.; Coste, A. *Synthesis* **2013**, 45, 17. (d) DeKorver, K. A.; Li, H.; Lohse, A. G.; Hayashi, R.; Lu, Z.; Zhang, Y.; Hsung, R. P. *Chem. Rev.* **2010**, *110*, 5064. (e) Evano, G.; Coste, A.; Jouvin, K. *Angew. Chem. Int. Ed.* **2010**, *49*, 2840.
- (2) For recent examples of transition-metal-catalyzed reactions of ynamide, see: (a) Chen, M.; Sun, N.; Chen, H.; Liu, Y. *Chem. Commun. (Cambridge)* **2016**, 52, 6324. (b) He, G.; Qiu, S.; Huang, H.; Zhu, G.; Zhang, D.; Zhang, R.; Zhu, H. *Org. Lett.* **2016**, *18*, 1856. (c) Liu, H.; Yang, Y.; Wu, J.; Wang, X.-N.; Chang, J. *Chem. Commun. (Cambridge)* **2016**, 52, 6801. (d) Singh, R. R.; Liu, R.-S. *Adv. Synth. Catal.* **2016**, *358*, 1421. (e) Chen, Y.-L.; Sharma, P.; Liu, R.-S. *Chem. Commun. (Cambridge)* **2016**, 52, 3187. (f) Jadhav, A. M.; Huple, D. B.; Singh, R. R.; Liu, R. S. *Adv. Synth. Catal.* **2016**, *358*, 1017. (g) Nonaka, S.; Sugimoto, K.; Ueda, H.; Tokuyama, H. *Adv. Synth. Catal.* **2016**, *358*, 380. (h) Gillie, A. D.; Reddy, R. J.; Davies, P. W. *Adv. Synth. Catal.* **2016**, *358*, 226. (i) Reddy, A. S.; Kumari, A. L. S.; Saha, S.; Swamy, K. C. K. *Adv. Synth. Catal.* **2016**, *358*, 1625. (j) Straker, R. N.; Peng, Q.; Mekareeya, A.; Paton, R. S.; Anderson, E. A. *Nat. Commun.* **2016**, *7*, 10109. (k) Lin, W.-J.; Shia, K.-S.; Song, J.-S.; Wu, M.-H.; Li, W.-T. *Org. Biomol. Chem.* **2016**, *14*, 220. (l) Zheng, N.; Chang, Y.-Y.; Zhang, L.-J.; Gong, J.-X.; Yang, Z. *Chem. Asian J.* **2016**, *11*, 371.
- (3) (a) Mori, M.; Wakamatsu, H.; Saito, N.; Sato, Y.; Narita, R.; Sato, Y.; Fujita, R. *Tetrahedron* **2006**, *62*, 3872. (b) Wakamatsu, H.; Sakagami, M.; Hanata, M.; Takeshita, M.; Mori, M. *Macromol. Symp.* **2010**, *293*, 5.
- (4) Wakamatsu, H.; Takeshita, M. *Synlett* **2010**, 2322.
- (5) (a) Mizoroki, T.; Mori, K.; Ozaki, A. *Bull. Chem. Soc. Jpn.* **1971**, *44*, 581. (b) Heck, R. F.; Nolley, J. P. *J. Org. Chem.* **1972**, *37*, 2320. For recent reviews, see: (c) Beletskaya, I. P.; Cheprakov, A. V. *Chem. Rev.* **2000**, *100*, 3009. (d) Felpin, F.-X.; Nassar-Hardy, L.; Le Calonnec, F.; Fouquet, E. *Tetrahedron* **2011**, *67*, 2815.
- (6) (a) Zhang, Y.; Negishi, E. J. *Am. Chem. Soc.* **1989**, *111*, 3454. For reviews on the reactions of transition metals with alkynes, see: (b) Alonso, F.; Beletskaya, I. P.; Yus, M. *Chem. Rev.* **2004**, *104*, 3079. (c) Chinchilla, R.; Nájera, C. *Chem. Rev.* **2007**, *107*, 874. (d) Schore, N. E. *Chem. Rev.* **1988**, *88*, 1081. (e) Fürstner, A.; Davies, P. W. *Chem. Commun. (Cambridge)* **2005**, 2307.
- (7) Bates, R. *Organic Synthesis using Transition Metals*, 2nd ed.; Wiley: Chichester, **2012**.
- (8) For a recent review on the synthesis of heterocycles by hydroarylation of C≡C triple bonds, see: Yamamoto, Y. *Chem. Soc. Rev.* **2014**, *43*, 1575.
- (9) (a) Dunetz, J. R.; Danheiser, R. L. *Org. Lett.* **2003**, *5*, 4011. (b) Hirano, S.; Tanaka, R.; Urabe, H.; Sato, F. *Org. Lett.* **2004**, *6*, 727. (c) Zhang, Y.; Hsung, R. P.; Tracey, M. R.; Kurtz, K. C. M.; Vera, E. L. *Org. Lett.* **2004**, *6*, 1151.
- (10) **Ethyl 4-[(1Z)-1-(Benzyl[(4-tolyl)sulfonyl]amino)oct-1-en-1-yl]benzoate (3a) and Ethyl 4-[(E)-2-(Benzyl[(4-tolyl)sulfonyl]amino)-1-hexylvinyl]benzoate (4a); Typical Procedure**
Ethyl 4-iodobenzoate (**2a**; 0.21 mL, 1.23 mmol, 3.0 equiv) was added a solution of ynamide **1a** (150.0 mg, 0.41 mmol), Pd(OAc)₂ (4.6 mg, 20.5 μmol, 5 mol%), DPPF (11.4 mg, 20.5 μmol, 5 mol%), and HCO₂NH₄ (77.6 mg, 1.23 mmol, 3.0 equiv) in DMF (20 mL) at 0 °C under argon. The mixture was stirred at 100 °C for 18 h and then cooled to 0 °C. H₂O (22 mL) was added, and the aqueous phase was extracted with Et₂O (3 × 50 mL). The organic phases were combined, washed with brine (1 × 50 mL), and dried (Na₂SO₄). The volatiles were removed under reduce pressure, and the residue was purified by column chromatography [silica gel, hexane–Et₂O (20:1) to hexane–EtOAc (10:1)] to afford **3a**, **4a**, and recovered **1a** (6.0 mg; 4%).
3a: off-white solid; yield: 161.1 mg (76%); mp 71 °C. IR (KBr): 3059, 2921, 1705, 1605 cm⁻¹. ¹H NMR (400 MHz, CDCl₃): δ = 0.88 (t, J = 7.2 Hz, 3 H), 1.04–1.28 (m, 8 H), 1.38 (t, J = 7.2 Hz, 3 H), 1.92 (br s, 2 H), 2.48 (s, 3 H), 4.14 (br s, 1 H), 4.36 (q, J = 7.2 Hz, 2 H), 4.71 (br s, 1 H), 6.11 (t, J = 7.4 Hz, 1 H), 7.06–7.12 (m, 4 H), 7.21–7.23 (m, 3 H), 7.35 (d, J = 7.6 Hz, 2 H), 7.81–7.85 (m, 4 H). ¹³C NMR (100 MHz, CDCl₃): δ = 14.0, 14.3, 21.5, 22.5, 28.7, 29.1, 29.9, 31.6, 52.4, 60.9, 126.4, 127.6, 128.0, 128.2, 129.3, 129.5, 129.5, 129.7, 134.6, 135.5, 137.3, 137.9, 141.7, 143.6, 166.2. EI-LRMS: m/z = 519 [M⁺], 364, 155, 91. EI-HRMS: m/z [M⁺] calcd for C₃₁H₃₇NO₄S: 519.2443; found: 519.2442.
4a: off-white solid; yield: 31.9 mg (15%); mp 73–74 °C. IR (KBr): 2929, 1716, 1607 cm⁻¹. ¹H NMR (400 MHz, CDCl₃): δ = 0.65–0.75 (m, 2 H), 0.81 (t, J = 7.2 Hz, 3 H), 0.97–1.05 (m, 4 H), 1.10–1.18 (m, 2 H), 1.38 (t, J = 7.2 Hz, 3 H), 2.42–2.49 (m, 2 H), 2.44 (s, 3 H), 4.25 (s, 2 H), 4.36 (q, J = 7.2 Hz, 2 H), 5.32 (s, 1 H), 7.17 (d, J = 8.2 Hz, 2 H), 7.26–7.35 (m, 7 H), 7.70 (d, J = 8.2 Hz, 2 H), 7.95 (d, J = 8.2 Hz, 2 H). ¹³C NMR (100 MHz, CDCl₃): δ = 14.0, 14.3, 21.5, 22.5, 27.2, 29.3, 29.8, 31.5, 55.2, 60.9, 123.7, 126.8, 127.6, 127.9, 128.4, 129.3, 129.5, 129.7, 129.7, 134.7, 135.5, 143.7, 144.0, 149.2, 166.3. EI-LRMS: m/z = 519 [M⁺], 364, 155, 91. EI-HRMS: m/z [M⁺] calcd for C₃₁H₃₇NO₄S: 519.2443; found: 519.2423.



Original Article

CYP3A4 induction mechanism of polycyclic aromatic hydrocarbons differs from that of rifampicin in PXR binding element

**Yusuke Aratsu^{1,2}, Reo Odagiri¹, Rie Shoji¹, Kouki Watanabe¹, Takeshi Kumagai¹,
Sawako Shindo¹, Takamitsu Sasaki^{1,3} and Kiyoshi Nagata¹**

¹*Department of Environmental Health Science, Faculty of Pharmaceutical Sciences, Tohoku Medical and Pharmaceutical University, 4-4-1 Komatsushima, Aoba-ku Sendai, Miyagi 981-8558, Japan*

²*Drug Metabolism and Pharmacokinetics Research Laboratories, Central Pharmaceutical Research Institute, Japan tobacco Inc., 1-1 Murasaki-cho Takatsuki, Osaka 569-1125, Japan*

³*Department of Molecular Toxicology, School of Pharmaceutical Sciences, University of Shizuoka, 52-1 Yada, Suruga-ku, Shizuoka 422-8526, Japan*

(Received September 22, 2017; Accepted September 27, 2017)

ABSTRACT — CYP3A4 is an important drug-metabolizing enzyme induced by various compounds causing drug-drug interactions. However, the molecular mechanism of CYP3A4 induction is not completely understood. CYP3A4 induction is caused by pregnane X receptor (PXR) through binding to some PXR binding elements. These elements comprise an everted repeat separated by six nucleotides in the promoter region and distal nuclear receptor binding element 1 (dNR-1) as well as the essential distal nuclear receptor binding element for CYP3A4 induction (eNR3A4) in the enhancer region of the *CYP3A4* gene. Recently, we found that polycyclic aromatic hydrocarbons including anthracene induce CYP3A4 in HepG2 cells with a different induction profile from that of rifampicin (RF), a typical PXR ligand. When a CYP3A4 reporter plasmid in which the eNR3A4 DNA fragment binds directly to the CYP3A4 promoter (-362 bases) was evaluated in a reporter assay, dibenz[a,h]anthracene (DBA) induced reporter activity, while RF did not. To be induced reporter activity by RF, more 14 nucleotides 5' upstream of the eNR3A4 (rifampicin eNR3A4: reNR3A4) DNA fragment were required. However, eNR3A4 and reNR3A4 did not respond to recombinant PXR without dNR-1. These results suggest that eNR3A4 and reNR3A4 are necessary for CYP3A4 induction by DBA and RF, respectively, and that dNR-1 is indispensable for full induction through PXR.

Key words: CYP3A4 induction, Pregnane X receptor, Rifampicin, Polycyclic aromatic hydrocarbons, Dibenz[a,h]anthracene, PXR binding element

INTRODUCTION

CYP3A4 is one of the most important drug-metabolizing enzymes involved in the metabolism of more than 50% of marketed drugs (Wienkers and Heath, 2005). Numerous studies have examined drug-drug interac-

tions (DDIs) mediated by CYP3A4. DDIs may cause serious problems from a clinical perspective. Particularly, CYP3A4 induction decreases concomitant drug exposure and efficacy in the human body. Therefore, the U.S. Food and Drug Administration (FDA, 2012), European Medicines Agency (EMA, 2012), and Pharmaceuti-

Correspondence: Kiyoshi Nagata (E-mail: nagataki@tohoku-mpu.ac.jp)

cals and Medical Devices Agency (PMDA, 2014) have released guidance for DDI where required to be included in the package insert and examined through clinical trials. Many pharmaceutical companies have attempted to estimate the risk of DDI on the clinical side and develop low-risk compounds by estimating inducibility using *in vitro* tools such as hepatocytes. However, it is very difficult to precisely evaluate the induction potency of individual compounds because of their complicate mechanisms compared to CYP inhibition.

A number of studies have demonstrated that CYP3A4 inducers activate transcription of *CYP3A4* mediated by nuclear receptors such as pregnane X receptor (PXR, NR1I2) (Bertilsson *et al.*, 1998; Blumberg *et al.*, 1998; Lehmann *et al.*, 1998), constitutive androstane receptor (NR1I3) (Goodwin *et al.*, 2002), and vitamin D receptor (NR1I1) (Drocourt *et al.*, 2002). PXR is a main regulator of drug-metabolizing enzymes and transporters (Synold *et al.*, 2001; Geick *et al.*, 2001). Human PXR is activated by binding to various drugs such as rifampicin (RF), phenytoin, and carbamazepine (Kamiguchi, 2010), transferred into the nucleus, and activates *CYP3A4* transcription by binding to the regulatory region of the gene as a heterodimer with retinoid X receptor (Wan *et al.*, 2000).

New activation pathways of *CYP3A4* transcription have also been reported. For example cyclin-dependent kinase 2 negatively regulates PXR activity through phosphorylation of Ser³⁵⁰ (Lin *et al.*, 2008). Other reports indicated that promoter transactivation on *CYP3A4* and *UDP-glucuronosyltransferase 1A1* were reduced by mutation of Ser³⁵⁰ (Elias *et al.*, 2014; Sugatani *et al.*, 2010).

Several nucleotide sequences of the PXR binding element have been identified in CYP3A4, but are not fully understood. Some PXR binding elements are composed of an everted repeat separated by six nucleotides (ER-6) in the promoter region and distal nuclear receptor binding element1 (dNR-1) (Blumberg *et al.*, 1998; Lehmann *et al.*, 1998; Goodwin *et al.*, 1999), as well as the essential distal nuclear receptor binding element for CYP3A4 induction (eNR3A4) (Toriyabe *et al.*, 2009) in the enhancer region of *CYP3A4*. These elements have a cluster of TGA(A/C)CT-like sequences recognized by the nuclear receptor family of transcription factors (Goodwin *et al.*, 1999).

We recently reported that poly aromatic hydrocarbons (PAHs) and indirubin, which were thought to be aryl hydrocarbon receptor (AhR) ligands, induced CYP3A4 in HepG2 cells. Their induction is mediated through PXR, but not through AhR (Kumagai *et al.*, 2012; Kumagai *et al.*, 2016). In addition, the molecular mech-

anism of CYP3A4 induction by PAHs and indirubin differ from those by RF and clotrimazole (CTZ), typical CYP3A4 inducers, in the responsible element of the *CYP3A4* gene. In this study, the roles of PXR binding element in eNR3A4 and dNR-1 were investigated to clarify the CYP3A4 induction mechanism.

MATERIALS AND METHODS

Materials

RF, 3-methylcholanthrene, benzo[e]pyrene, and 1,2-benzanthracene were purchased from Sigma-Aldrich (St. Louis, MO, USA). The other PAHs listed Fig. 1. were obtained from Tokyo Chemical Industry (Tokyo, Japan). Dimethyl sulfoxide (DMSO) was purchased from Nacalai Tesque (Kyoto, Japan). CTZ and 2, 3, 7, 8-tetrachlorodibenzo-*p*-dioxin (TCDD) were purchased from Wako Pure Chemical Industries (Osaka, Japan).

Cell culture

Human hepatoma cell line HepG2 cells were obtained from the RIKEN BRC (Tukuba, Japan) through Cell Resource Center for Biomedical Research (Tohoku University). The HepG2-derived cell line clone 3-1-20 stably expressing the CYP3A4-luciferase reporter gene was established as reported previously (Noracharttiyapot *et al.*, 2006). These cells were cultured in Dulbecco's modified Eagle's medium (Wako Pure Chemical Industries) supplemented with non-essential amino acids (Invitrogen, Carlsbad, CA, USA), 10% heat-inactivated fetal bovine serum (Biowest, Nuaille, France), and antibiotic-antimycotic (Invitrogen).

Reporter gene constructs and expression vectors

pCYP3A4-362, pCYP3A4-362-7.7k, pCYP3A4-362-m-7.7k, pCYP3A4-362-7.7km, and pCYP3A4-362m-7.7km and pCYP3A4-362-7.7ΔBsite were constructed as described previously (Takada *et al.*, 2004). pCYP3A4-362-7.7kΔeNR3A4 was reported previously (Toriyabe *et al.*, 2009). pCYP3A4-362+dNR-1, pCYP3A4-362+eNR3A4, pCYP3A4-362+rifampicin eNR3A4 (reNR3A4), and pCYP3A4-362+14αβ were prepared by inserting the dNR1, eNR3A4, reNR3A4, and 14αβ DNA fragments, which were isolated by PCR with primers (Table 1) and digested with *MluI* and *BglII*, into the *MluI* and *BglII* sites of pCYP3A4-362. pCYP3A4-362+eNR3A4+dNR-1 and pCYP3A4-362+reNR3A4+dNR-1 were made from pCYP3A4-362+eNR3A4 and pCYP3A4-362+reNR3A4 by inserting the dNR-1 DNA fragment digested with *Acc65I* and *MulI* into those of

Table 1. Primers used for construction of reporter gene plasmids

		Primer sequence
dNR1	FW	gcgggtaccATCTCAGCTGAATGAACTTGCTGAC
	RV	gcgacgcgtAGGAAAGCAGAGGGTCAGCAAGTTC
eNR3A4	FW	gcgacgcgtATTAAACCTTGTCCTGTGTTGACCCAGGT
	RV	gcgagatctTGAAAAGAATATGATAGCTTGT
reNR3A4	FW	gcgacgcgtCAGTGATTATTAAACCTTGTC
	RV	gcgagatctTGAAAAGAATATGATAGCTTGT
14 α β	FW	gcgacgcgtCAGTGATTATTAAACCTTGTC
	RV	gcgagatctTTCACCTGGGGTCAACACAGG

the *Acc65I* and *MulI* sites. pCYP3A4-362-7.7k Δ α , pCYP3A4-362-7.7k Δ β , pCYP3A4-362-7.7k Δ γ , pCYP3A4-362-7.7k Δ δ , and pCYP3A4-362-7.7k Δ ϵ were prepared from reporter plasmids mutated in the α , β , γ , δ , and ϵ sites as previously reported (Toriyabe *et al.*, 2009) by digestion with *XhoI*, treatment with S1 nuclease, and self-ligation. Point-mutated reporter plasmids were constructed with the QuikChange II site-directed mutagenesis kit (Stratagene, La Jolla, CA, USA) using pCYP3A4-362-7.7k as a template.

Luciferase assay for reporter plasmid

HepG2 cells were seeded into a 48-well tissue culture plate (BD Biosciences, Franklin Lakes, NJ, USA) at 3.0×10^4 cells per well the day before transfection. Each reporter plasmid and pGL4.82 (Promega, Madison, WI, USA) were cotransfected using Targefect F-1 (Targeting Systems, El Cajon, CA, USA) according to the manufacturer's protocols. Transfection efficiency was normalized by Renilla luciferase activity of pGL4.82. After transfection, HepG2 cells were cultured in the presence of various compounds dissolved in DMSO for 48 hr. Control cells were treated with vehicle (0.1% DMSO). After 48 hr incubation, the cells were washed with PBS and suspended in passive lysis buffer (Promega). Luciferase activities were evaluated using the Dual-Luciferase assay system and GloMaxTM 96 Microplate Luminometer (Promega) according to the manufacturer's protocols. Fold-induction values were calculated from the luminescence normalized as the ratio of control samples.

Luciferase assay for PAHs

3-1-20 cells were seeded into 96-well tissue cultured plate at 1.0×10^4 cells per well the day before treatment with various compounds dissolved in DMSO. After 48 hr incubation, the cells were washed with PBS and suspended in passive lysis buffer. Luciferase activities were evaluated using the Luciferase assay system (Promega) with GloMaxTM 96 Microplate Luminometer. The luminescence of each sample was normalized to the pro-

tein concentration using the Protein Assay Kit (Bio-Rad, Hercules, CA, USA).

Construction of adenovirus expression vector and infection

The human PXR-expressing adenovirus (AdhPXR) was constructed as described previously (Matsubara *et al.*, 2007). The β -galactosidase-expressing adenovirus (AdCont; AxCALacZ), used as a control adenovirus, was provided by Dr. Izumi Saito (Tokyo University, Tokyo, Japan) (Miyake, 1996). The titer of the adenoviruses, the 50% titer culture infectious dose (TCID₅₀), was determined as reported previously (Matsubara *et al.*, 2007). Multiplicity of infection was calculated as the TCID₅₀ based on the number of cells. One day before transfection, cells were seeded in 48-well plates. The adenovirus infection protocol was described previously (Kumagai *et al.*, 2012).

Statistical analysis

Data are presented as the mean \pm standard deviation (S.D.) and were evaluated by paired Student's *t*-test. A *P* value < 0.05 was considered significant.

RESULTS

Effect of PAHs on CYP3A4 reporter activity in 3-1-20 cells

First, CYP3A4 reporter activity by PAHs was investigated by using HepG2-derived cell line clone, 3-1-20 stably expressing the CYP3A4-luciferase reporter gene. Many PAHs increased CYP3A4 reporter activity. Among them, dibenz[a,h]anthracene (DBA) and dibenz[a, c]anthracene strongly increased reporter activity (20-30-fold), while benzo[e]pyrene, pyrene, naphthalene showed no activation, and dibenz[de,kl]anthracene showed minimal activation of *CYP3A4* transcription (Fig. 2).

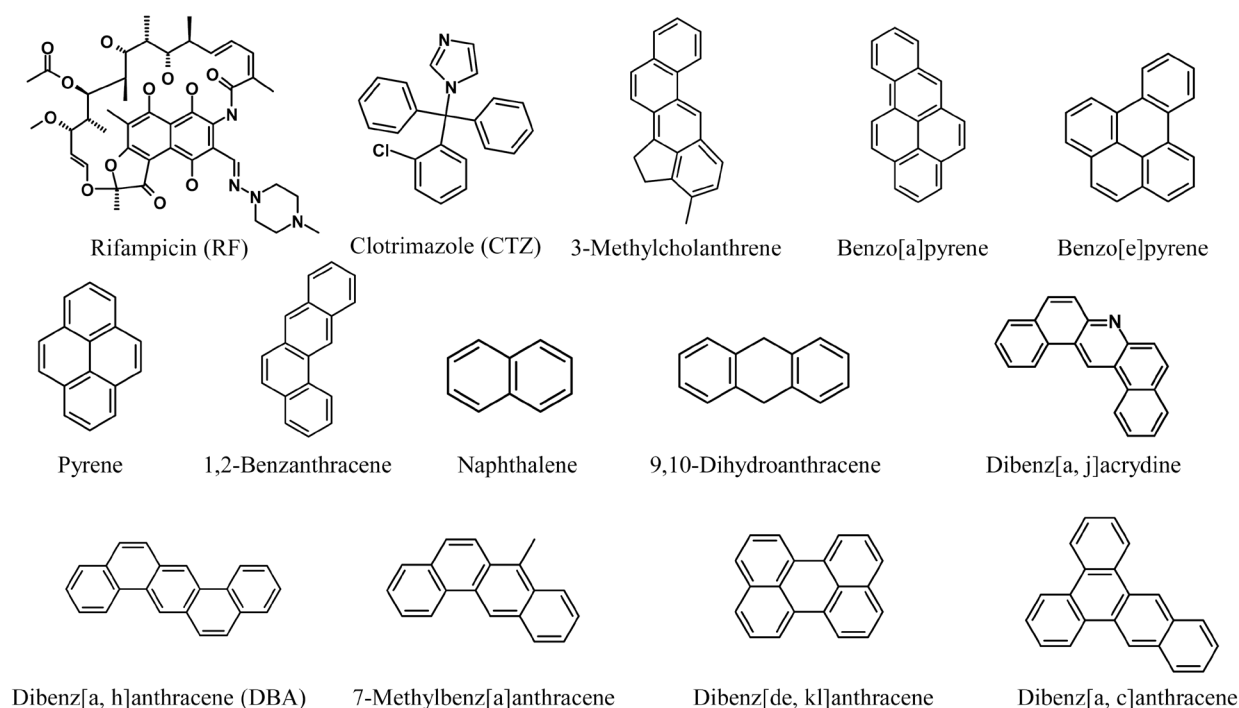


Fig. 1. Structure of RF, CTZ and PAHs.

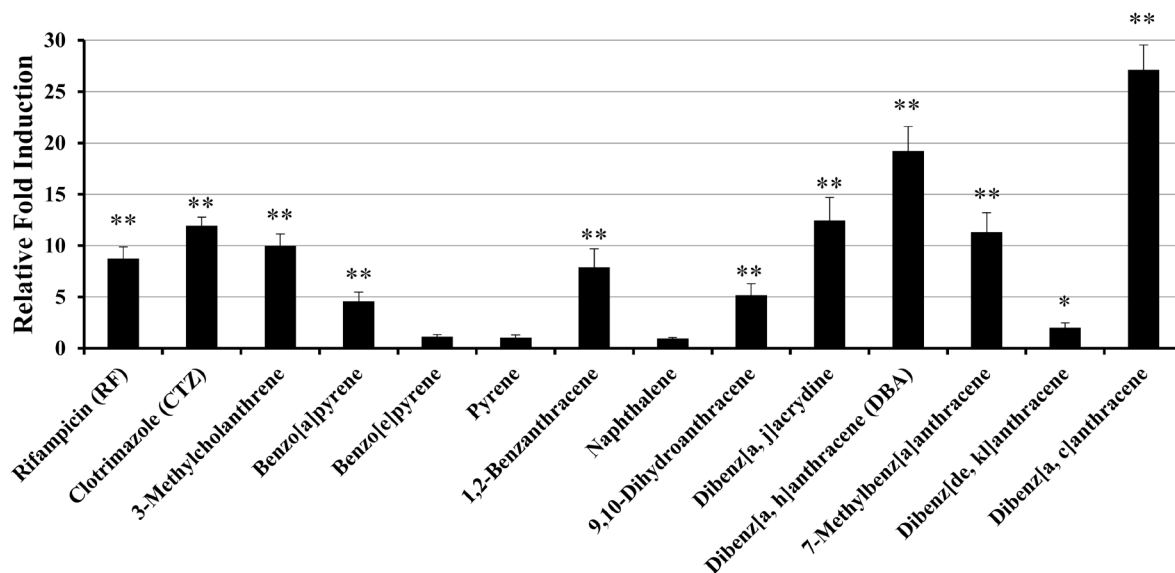


Fig. 2. Effect of PAHs on CYP3A4 reporter activity in 3-1-20 cells. Clone 3-1-20 cells were seeded at 1×10^4 cells in a 96-well tissue culture plate and pre-incubated for 24 hr before treatment with various compounds. The cells were treated with RF (10 μ M), CTZ (10 μ M) and various PAHs (1 μ M) for 48 hr and reporter activity was measured by the luciferase assay. Reporter activities are expressed as the fold to that in the vehicle-treated cells. Data are shown as the mean \pm S.D. from three different samples. * $P < 0.05$, ** $P < 0.005$, differences from vehicle-treated cells.

Effect of mutation in prER-6 and dNR-1 on reporter activity

Next, transient transfection assays were conducted by using CYP3A4 luciferase reporter plasmids containing three elements (dNR-1, eNR3A4, and prER-6), which bind to PXR (pCYP3A4-362-7.7k). The role of these elements was investigated using reporter plasmids containing mutations in dNR-1 and/or prER-6 (pCYP3A4-362-7.7km, pCYP3A4-362m-7.7k, pCYP3A4-362m-7.7km). Reporter activity was compared among the reporter plasmids using PXR ligands (RF and CTZ) and AhR ligands (DBA and TCDD) (Fig. 3). All inducers increased reporter activity (8.2-, 7.9-, 11.0-, and 9.1-fold, respectively) in cells transfected with pCYP3A4-362-7.7k. The construct mutated in prER-6, pCYP3A4-362m-7.7k, showed nearly the same activity as pCYP3A4-362-7.7k for all inducers. In contrast, the constructs mutated in dNR-1, pCYP3A4-362-7.7km, in dNR-1 and prER-6, pCYP3A4-362m-7.7km showed very low responses to RF and CTZ (pCYP3A4-362-7.7km: 2.7- and 1.8-fold and pCYP3A4-362m-7.7km: 1.5- and 2.3-fold, respectively). However, DBA and TCDD showed relatively high responses compared to those of RF and CTZ in pCYP3A4-362-7.7km (10.4- and 6.2-fold) and pCYP3A4-362m-7.7km (5.0- and 5.1-fold). Similar results were observed in cells treated with indirubin (data not shown).

Effect of deletion in enhancer region on the reporter activity

To verify the involvement of eNR3A4 for CYP3A4 induction, transient transfection assays were conducted by using several CYP3A4 luciferase reporter plasmids with deletions in various enhancer regions (Fig. 4). RF did not increase reporter activity in cells treated with deleted plasmids in this experiment, pCYP3A4-362-7.7kΔeNR3A4, pCYP3A4-362-7.7kΔBsite, pCYP3A4-362+dNR-1, pCYP3A4-362+eNR3A4, and pCYP3A4-362, although RF increased reporter activity in cells treated with pCYP3A4-362-7.7k (17.9-fold). In contrast, DBA increased reporter activity to some extent in all plasmids used in this experiment. Of all deleted plasmids, pCYP3A4-362-7.7kΔBsite and pCYP3A4-362+eNR3A4 showed a high reporter activity (5.4- and 16.3-fold, respectively) following treatment with DBA.

Effect of overexpressing PXR on the reporter activity

It is widely known that PXR is a major transcription factor involved in CYP3A4 induction. The effect of PXR on CYP3A4 induction by RF and DBA was investigated by overexpressing human PXR in HepG2 cells using adenovirus (Fig. 4). The induced reporter activity (17.9-fold) by RF was dramatically increased (51.3-

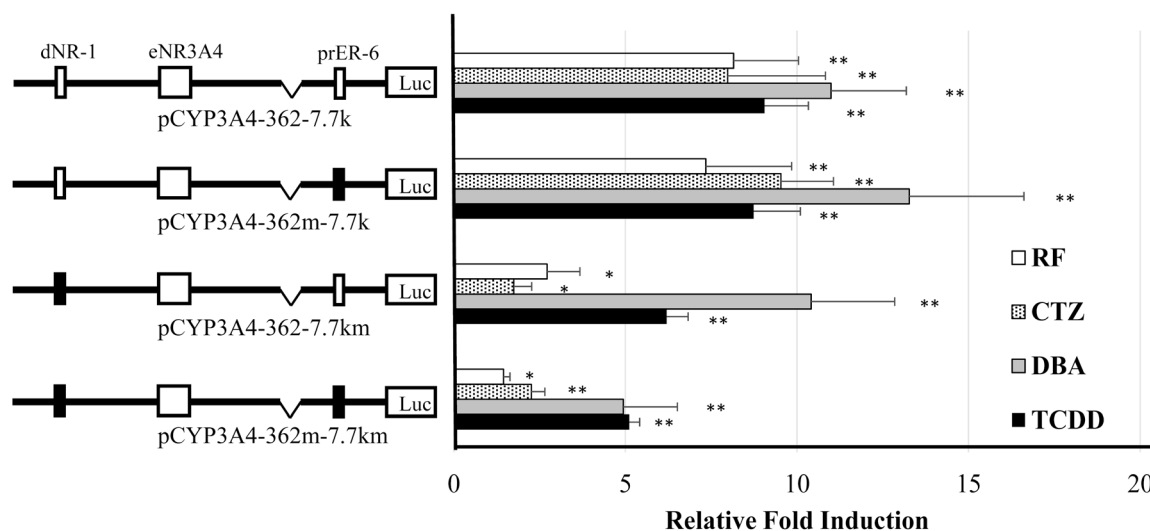


Fig. 3. Effect of mutation in CYP3A4 promoter and/or enhancer region on reporter activity induced by various compounds. HepG2 cells were seeded at 3×10^4 cells in a 48-well tissue culture plate. The cells were incubated for 24 hr before transfection. The transfection protocol is described in the "Materials and Methods". Closed boxes represent mutated PXR-binding elements. The cells were treated with RF (10 μ M), CTZ (10 μ M), DBA (10 μ M), or TCDD (10 nM) for 48 hr. Luciferase activity was normalized to Renilla luciferase activity. The values were expressed as the fold induction of the vehicle control (DMSO) group. Data are shown as the mean \pm S.D. from six different samples. * $P < 0.05$, ** $P < 0.005$, differences from vehicle-treated cells.

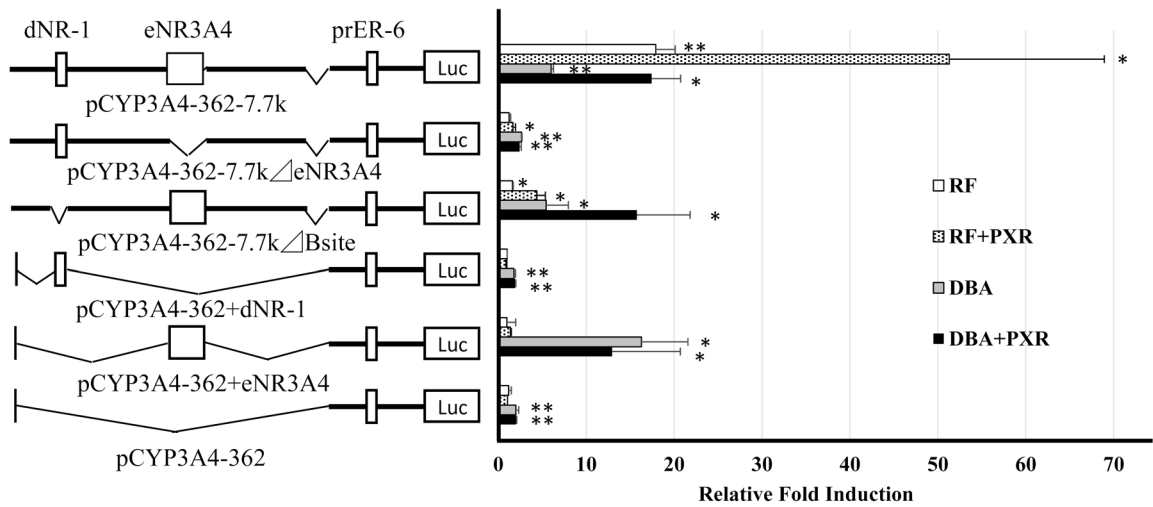


Fig. 4. Effect of overexpressing PXR on CYP3A4 reporter activity in HepG2 cells by RF and DBA. HepG2 cells were seeded at 3×10^4 cells in a 48-well tissue culture plate. The cells were incubated for 24 hr before transfection. The transfection protocol is described in the “Materials and Methods”. After 24 hr of Ad-PXR (3 MOI) infection, the cells were treated with RF (10 μ M) or DBA (10 μ M) for 48 hr. Luciferase activity was normalized to Renilla luciferase activity. The values were expressed as the fold induction of the vehicle control (DMSO) group. Data are shown as the mean \pm S.D. from three different samples. * $P < 0.05$, ** $P < 0.005$, differences from vehicle-treated cells.

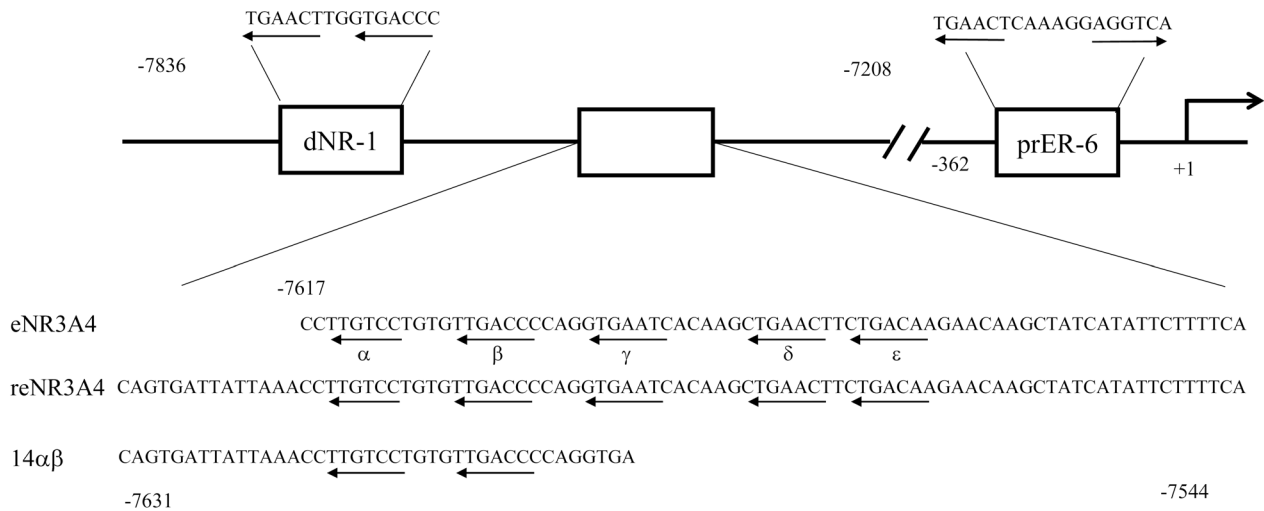


Fig. 5. Sequence of eNR3A4 and reNA3A4 of CYP3A4 and reporter constructs containing mutations and or deletions. These elements contain a cluster of TGA(A/C)CT-like sequences recognized in the nuclear receptor family of transcription factors.

fold) in cells by overexpressing PXR after transfection of pCYP3A4-362-7.7k. In cells transfected with pCYP3A4-362-7.7kΔBsite, reporter activity also increased by overexpressing PXR. Similarly, DBA highly increased the reporter activity (6.0- and 5.4-fold, respectively) in cells transfected with pCYP3A4-362-7.7k and pCYP3A4-

362-7.7kΔBsite, and these activities were dramatically increased (17.5- and 15.8-fold, respectively) by overexpressing PXR. In contrast, increased reporter activity by treatment with DBA was not activated by overexpressing PXR in cells transfected with pCYP3A4-362+eNR3A4 in which the eNR3A4 element binds directly to the promot-

er region (-362).

Effect of 14 bases 5'-upstream of eNR3A4 on reporter activity

Because increased reporter activity was not observed in pCYP3A4-362+eNR3A4 treated with RF, pCYP3A4-362+reNR3A4 containing 14 additional bases 5'-upstream of eNR3A4 was transfected into HepG2 cells. The results are shown in Fig. 6. RF and DBA increased reporter activity in cells transfected with pCYP3A4-362+reNR3A4 (5.1- and 7.2-fold, respectively), but these reporter activities were not significantly increased by overexpressing PXR (8.3- and 7.3-fold, respectively). Similar results were observed in cells transfected with pCYP3A4-362+14 $\alpha\beta$, although the reporter activity was increased to some extent without overexpressing PXR.

Role of dNR-1 for CYP3A4 induction

In the study above shown, we suggest that eNR3A4 and reNR3A4 are essential elements for *CYP3A4* gene activation by DBA and RF. However, it remained unclear how dNR-1, eNR3A4, and reNR3A4 function in CYP3A4 induction. To verify the involvement of dNR-1, eNR3A4, and reNR3A4, further transient transfection assays were conducted using CYP3A4 luciferase reporter plasmids with or without dNR-1 (Fig. 7). RF did not increase reporter activity in cells treated with pCYP3A4-362+eNR3A4 and pCYP3A4-362+dNR-1+eNR3A4. However,

RF induced reporter activity (4.5-fold) was dramatically increased (29.7-fold) in cells overexpressing PXR after transfection of pCYP3A4-362+dNR-1+reNR3A4. In contrast, DBA increased reporter activity in cells transfected with any reporter constructs and the induced activity was increased by overexpressing PXR in cells transfected with pCYP3A4-362+dNR-1+eNR3A4 and pCYP3A4-362+dNR-1+reNR3A4 (8.4- and 18.1-fold).

Effect of deletion in eNR3A4 region on reporter activity

Several TGA(A/C)CT-like sequences binding to nuclear receptor family members were observed in the eNR3A4 region. To verify the role of half-sites in eNR3A4 for CYP3A4 induction, several CYP3A4 luciferase reporter plasmids with mutated and deleted half-sites were constructed. The results are shown in Fig. 8. RF did not increase reporter activity in cells treated with pCYP3A4-362-7.7k $\Delta\alpha$ and pCYP3A4-362-7.7k $\Delta\beta$, even by overexpressing PXR. However, DBA increased reporter activity in pCYP3A4-362-7.7k $\Delta\alpha$ and pCYP3A4-362-7.7k $\Delta\beta$ and the activity was not increased by overexpressing PXR. Moreover, reporter activity increased by RF and DBA was lower in pCYP3A4-362-7.7k $\Delta\gamma$ and pCYP3A4-362-7.7k $\Delta\delta$ than in pCYP3A4-362-7.7k, although these activities were increased by overexpressing PXR.

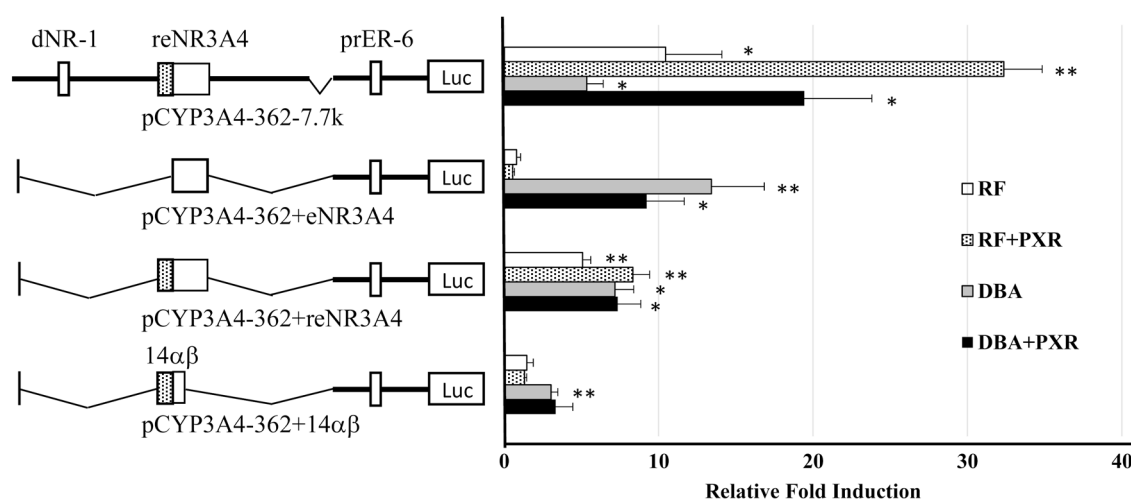


Fig. 6. Effect of DNA deletion in CYP3A4 enhancer region and overexpressing PXR on reporter activity in HepG2 cells induced by RF and DBA. HepG2 cells were seeded at 3×10^4 cells in a 48-well tissue culture plate. The cells were incubated for 24 hr before transfection. The transfection protocol is described in the "Materials and Methods". After 24 hr of Ad-PXR (3 MOI) infection, the cells were treated with RF (10 μ M) or DBA (10 μ M) for 48 hr. Luciferase activity was normalized to Renilla luciferase activity. The values were expressed as the fold induction of the vehicle control (DMSO) group. Data are shown as the mean \pm S.D. from three different samples. * $P < 0.05$, ** $P < 0.005$, differences from vehicle-treated cells.

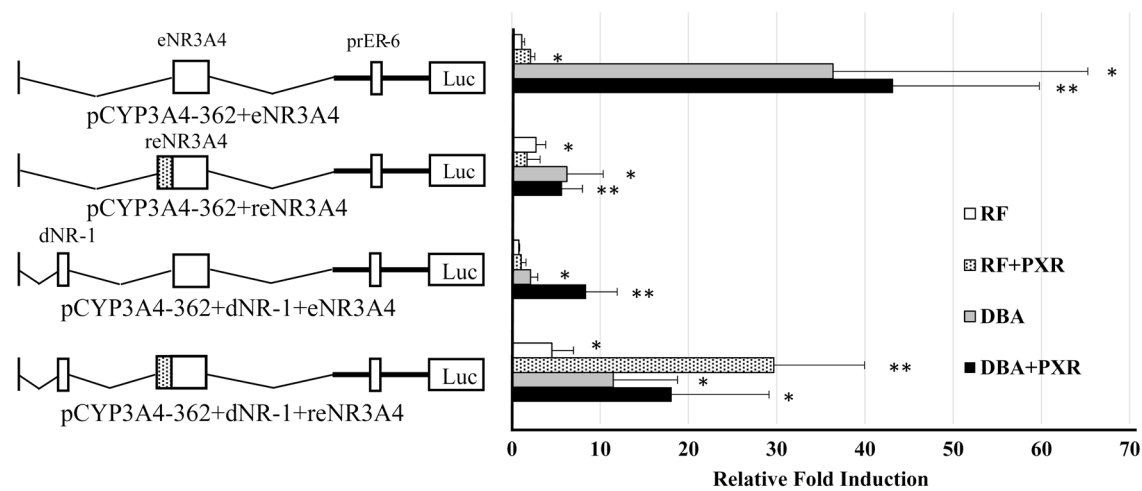


Fig. 7. Effect of DNA deletion in CYP3A4 enhancer region and overexpressing PXR on reporter activity in HepG2 cells induced by RF and DBA. HepG2 cells were seeded at 3×10^4 cells in a 48-well tissue culture plate. The cells were incubated for 24 hr before transfection. The transfection protocol is described in the “Materials and Methods”. After 24 hr of Ad-PXR (3 MOI) infection, the cells were treated with RF (10 μ M) or DBA (10 μ M) for 48 hr. Luciferase activity was normalized to Renilla luciferase activity. The values are expressed as the fold induction of the vehicle control (DMSO) group. Data are shown as the mean \pm S.D. from six different samples. *P < 0.05, **P < 0.005, differences from vehicle-treated cells.

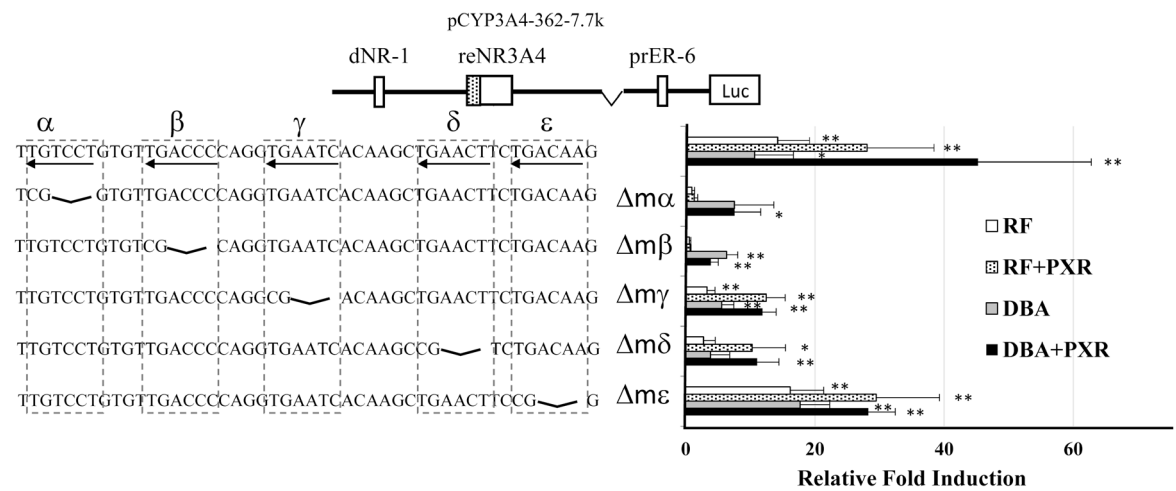


Fig. 8. Effect of DNA deletion in eNR3A4 and overexpressing PXR on reporter activity in HepG2 cells induced by RF and DBA. HepG2 cells were seeded at 3×10^4 cells in 48-well tissue culture plate. The cells were incubated for 24 hr before transfection. The transfection protocol is described in the “Materials and Methods”. After 24 hr of Ad-PXR (3 MOI) infection, the cells were treated with RF (10 μ M) or DBA (10 μ M) for 48 hr. Luciferase activity was normalized to Renilla luciferase activity. The values are expressed as the fold induction of the vehicle control (DMSO) group. Data are shown as the mean \pm S.D. from five different samples. *P < 0.05, **P < 0.005, differences from vehicle-treated cells.

Effect of point mutation in eNR3A4 region on reporter activity

To confirm the role of the half-site in eNR3A4 in detail, point mutations were introduced into pCYP3A4-

362-7.7k at several bases of the eNR3A4 DNA fragment as indicated with an arrow by changing to A. Mutation No. 3, 4, 8, and 9 showed low activity compared to that of pCYP3A4-362-7.7k by RF and DBA.

DISCUSSION

We first evaluated CYP3A4 induction by PAHs using 3-1-20 cells stably expressing the CYP3A4-luciferase reporter gene (Noracharttiyapot *et al.*, 2006). The results showed that many PAHs increased CYP3A4 reporter activity (Fig. 2). PAHs are known as AhR ligands, and activated AhR binds to a cluster of CACGC-like sequences (Watson and Hankinson, 1992), but a CACGC-like sequence was not identified in the promoter and enhancer region of *CYP3A4* used in this experiment. As shown previously, *CYP3A4* activation by PAHs such as 3-methylchoranthrene and TCDD was increased by overexpressing PXR and decreased by PXR-siRNA (Kumagai *et al.*, 2012). One of the PAHs, DBA, increased reporter activity in cells transfected with pCYP3A4-362-7.7k by overexpressing PXR (Fig. 4). PAHs including anthracene in their chemical structure likely activate the CYP3A4 reporter gene in HepG2 cells, but compounds such as benzo[e]pyrene, pyrene and dibenz[de, kl]anthracene categorized as condensed-ring annulation types only minimally activated the CYP3A4 reporter gene. However, it is unclear whether PXR binds to these compounds. In this study, because of its high induction potency, we used DBA to evaluate the CYP3A4 induction mechanism of PAHs.

It has been reported that dNR-1, eNR3A4, and prER-6 are very important for CYP3A4 induction (Blumberg *et al.*, 1998; Lehmann *et al.*, 1998; Goodwin *et al.*, 1999; Toriyabe *et al.*, 2009). In this study, we investigated the role of these PXR binding elements on CYP3A4 induction in detail by using several reporter plasmids, including CYP3A4 enhancer region into which we introduced deletion and mutations. The results indicate strong involvement not only of dNR-1, but also of eNR3A4 in the transcriptional activation of *CYP3A4* by RF and CTZ, while eNR3A4 appeared to be important for transcriptional activation of *CYP3A4* by DBA and TCDD (Fig. 3). To confirm the involvement of eNR3A4, the reporter activities of each plasmid containing deletions in the enhancer region were measured. The results showed that eNR3A4 is more important than dNR-1 in activating *CYP3A4* transcription by DBA, as demonstrated by the pCYP3A4-362-7.7kΔBsite and CYP3A4-362+eNR3A4 containing an eNR3A4 DNA fragment (Fig. 4).

We previously reported that indirubin, a ligand of AhR, induces CYP3A4 through PXR (Kumagai *et al.*, 2012; Kumagai *et al.*, 2016) and other group also reported PAHs induce CYP3A4 (Luckert *et al.*, 2013). In addition, indirubin showed a similar profile of transcriptional activation of *CYP3A4* to that of TCDD and DBA (data

not shown) in HepG2 cells. To confirm the involvement of PXR in DBA, CYP3A4 reporter activity was examined by overexpressing PXR in HepG2 cells. As a result, plasmids containing eNR3A4, pCYP3A4-362-7.7k, and pCYP3A4-362-7.7kΔBsite showed increased reporter activity by overexpressing PXR. pCYP3A4-362+eNR3A4 showed increased the reporter activity by DBA, but not by RF. The increased reporter activity was not enhanced by overexpressing PXR (Fig. 4). These results suggest that CYP3A4 induction through eNR3A4 by DBA does not depend only on PXR. There are some reports of new activation pathways of *CYP3A4* transcription. For example, cyclin-dependent kinase2 negatively regulates the activity of PXR through phosphorylation of Ser³⁵⁰ (Lin *et al.*, 2008) and cell proliferation in Huh7 cells (Sivertsson *et al.*, 2013), but the mechanism of CYP3A4 induction by DBA remains unclear. Therefore, further studies are needed to determine the CYP3A4 induction mechanism by DBA.

In addition, RF did not increase reporter activity in cells transfected with pCYP3A4-362+eNR3A4 (Fig. 4). The present results suggest that eNR3A4 is not sufficient for the *CYP3A4* transcription. We previously reported that the α and β sites in the eNR3A4 DNA fragment are key elements for induction of CYP3A4 (Toriyabe *et al.*, 2009). Therefore, we predicted that a specific DNA fragment is required for CYP3A4 induction other than the α and β sites. Reporter plasmids containing an extra 14-base pair DNA fragment 5'-upstream of eNR3A4 named as reNR3A4 were constructed. In addition, we constructed a reporter plasmid, pCYP3A4-362+14 $\alpha\beta$, with the extra 14-base pair DNA fragment and α and β sites. The results of transient transfection assays indicated that the 14-base pair DNA fragment is necessary for CYP3A4 induction by RF other than the PXR binding element (Fig. 5). However, overexpressing PXR did not increase reporter activity in either pCYP3A4-362+eNR3A4 or pCYP3A4-362+reNR3A4. Therefore, to verify the role of dNR-1, pCYP3A4-362+dNR-1+reNR3A4 and pCYP3A4-362+dNR-1+eNR3A4 were prepared. The increased reporter activity of pCYP3A4-362+dNR-1+reNR3A4 by DBA and RF was dramatically enhanced by overexpressing PXR, but the reporter activity of pCYP3A4-362+dNR-1+eNR3A4 was enhanced by overexpressing PXR following DBA treatment. These results indicate that for full CYP3A4 induction, dNR-1 is indispensable and the 14-base pair DNA fragment 5'-upstream of eNR3A4 is necessary for RF other than binding elements of dNR-1, but not for DBA.

We further verified the role of each half-site (α , β , γ , δ , ϵ) in eNR3A4 using CYP3A4 reporter constructs in

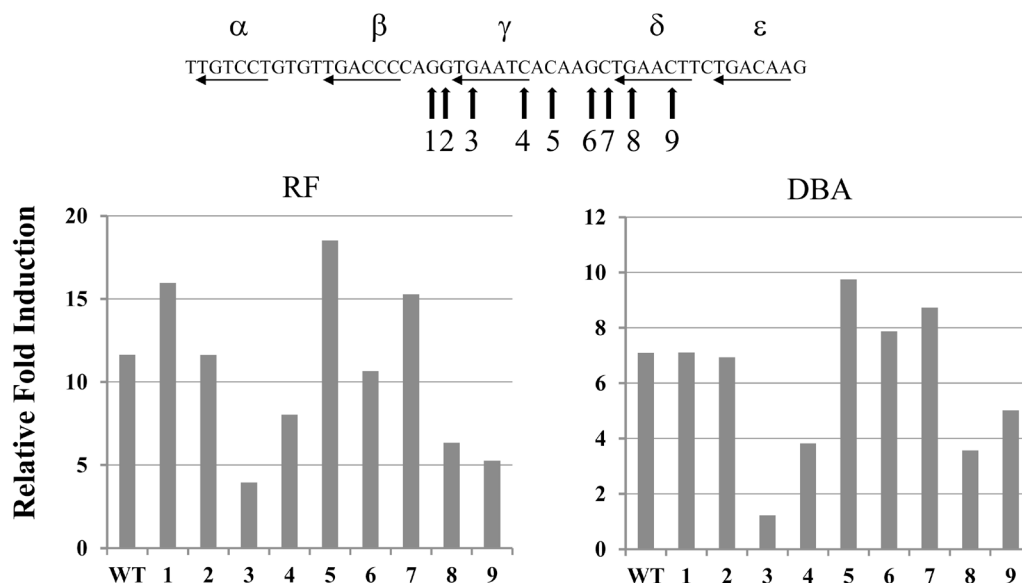


Fig. 9. Effect of DNA point mutation in γ and δ half-sites of eNR3A4 on reporter activity induced by RF and DBA. HepG2 cells were seeded at 3×10^4 cells in a 48-well tissue culture plate. The cells were incubated for 24 hr before transfection. The transfection protocol is described in the “Materials and Methods”. After 24 hr of Ad-PXR (3 MOI) infection, the cells were treated with RF (10 μ M) or DBA (10 μ M) for 48 hr. Luciferase activity was normalized to Renilla luciferase activity. The values are expressed as the fold-induction of the vehicle control (DMSO) group. Data are shown as the mean from two different samples.

which various DNA deletions and single mutations were introduced. As previously reported, α and β sites are very important for CYP3A4 induction by RF (Fig. 8) (Toriyabe *et al.*, 2009), but this study showed that α and β sites are not essential for CYP3A4 induction by DBA. Similar results were also observed by mutation of α and β sites (data not shown). Deletion of the γ and δ sites decreased reporter activity, which was increased by DBA and RF, but did not disappear. These results suggest that the γ and δ sites are also important for CYP3A4 induction. This idea was confirmed by mutation analysis of γ and δ sites as shown in Fig. 9.

In conclusion, we demonstrated that the molecular mechanism of CYP3A4 induction differs between RF and DBA in the PXR binding element. While reNR3A4 is an important DNA fragment for CYP3A4 induction by RF, eNR3A4 is an important DNA fragment for CYP3A4 induction by DBA. Furthermore, our results might suggest that CYP3A4 induction by DBA and RF use different transcription factors, although we did not confirm transcription factor binding to eNR3A4 and reNR3A4. The results of our study revealed the role of each half-sites in eNR3A4. The α and β sites are essential for CYP3A4 induction by RF, but not by DBA; in addition to the α and

β sites, the γ and δ sites are necessary for CYP3A4 induction. Moreover, to obtain full CYP3A4 induction through PXR by RF and DBA, dNR-1 was indispensable.

ACKNOWLEDGMENTS

This work was supported by a Health and Labor Sciences Research Grant for Research on Food Safety (No. 22230301) from the Ministry of Health, Labor and Welfare of Japan; Grant-in-Aid for Scientific Research (B) (No. 23790193); and Japanese Ministry of Education, Culture, Sports, Science and Technology (MEXT)-Supported Program for the Strategic Research Foundation at Private Universities.

Conflict of interest---- The authors declare that there is no conflict of interest.

REFERENCES

- Bertilsson, G., Heidrich, J., Svensson, K., Asman, M., Jendeberg, L., Sydow-Bäckman, M., Ohlsson, R., Postlind, H., Blomquist, P. and Berkenstam, A. (1998): Identification of a human nuclear receptor defines a new signaling pathway for CYP3A induction. *Proc. Natl. Acad. Sci. USA*, **95**, 12208-12213.

Different CYP3A4 induction mechanism between rifampicin and PAHs

- Blumberg, B., Sabbagh, W., Juguilon, H., Bolado, J., Van Meter, C.M., Ong, E.S. and Evans, R.M. (1998): SXR, a novel steroid and xenobiotic-sensing nuclear receptor. *Genes Dev.*, **12**, 3195-3205.
- Drocourt, L., Ourlin, J.C., Pascussi, J.M., Maurel, P. and Vilarem, M.J. (2002): Expression of CYP3A4, CYP2B6, and CYP2C9 is regulated by the vitamin D receptor pathway in primary human hepatocytes. *J. Biol. Chem.*, **277**, 25125-25132.
- Elias, A., High, A.A., Mishra, A., Sien, S., Wu, J., Peng, J. and Chen, T. (2014): Identification and characterization of phosphorylation sites within the pregnane X receptor protein. *Biochem. Pharmacol.*, **87**, 360-370.
- EMA (2012): Guideline on the investigation of drug interactions. *Guid. Doc.*, **44**, 59.
- FDA (2012): Guidance for industry. Drug interaction studies study design, data analysis, implications for dosing, and labeling recommendations. *Guid. Doc.*, 79.
- Geick, A., Eichelbaum, M. and Burk, O. (2001): Nuclear receptor response elements mediate induction of intestinal MDR1 by rifampin. *J. Biol. Chem.*, **276**, 14581-14587.
- Goodwin, B., Hodgson, E., Costa, D.J.D. and Robertson, G.R. (2002): Transcriptional regulation of the human CYP3A4 gene by the constitutive androstane receptor. *Mol. Pharmacol.*, **62**, 359-365.
- Goodwin, B., Hodgson, E. and Liddle, C. (1999): The orphan human pregnane X receptor mediates the transcriptional activation of CYP3A4 by rifampicin through a distal enhancer module. *Mol. Pharmacol.*, **56**, 1329-1339.
- Kamiguchi, N. (2010): A 96-well plate assay for CYP450A induction using cryopreserved human hepatocyte. **38**, 1912-1916.
- Kumagai, T., Aratsu, Y., Sugawara, R., Sasaki, T., Miyairi, S. and Nagata, K. (2016): Indirubin, a component of Ban-Lan-Gen, activates CYP3A4 gene transcription through the human pregnane X receptor. *Drug Metab. Pharmacokinet.*, **31**, 139-145.
- Kumagai, T., Suzuki, H., Sasaki, T., Sakaguchi, S., Miyairi, S., Yamazoe, Y. and Nagata, K. (2012): Polycyclic aromatic hydrocarbons activate CYP3A4 gene transcription through human pregnane X receptor. *Drug Metab. Pharmacokinet.*, **27**, 200-206.
- Lehmann, J.M., McKee, D.D., Watson, M.A., Willson, T.M., Moore, J.T. and Kliewer, S.A. (1998): The human orphan nuclear receptor PXR is activated by compounds that regulate CYP3A4 gene expression and cause drug interactions. *J. Clin. Invest.*, **102**, 1016-1023.
- Lin, W., Wu, J., Dong, H., Bouck, D., Zeng, F.Y. and Chen, T. (2008): Cyclin-dependent kinase 2 negatively regulates human pregnane X receptor-mediated CYP3A4 gene expression in HepG2 liver carcinoma cells. *J. Biol. Chem.*, **283**, 30650-30657.
- Luckert, C., Ehlers, A., Buhrke, T., Seidel, A., Lampen, A. and Hessel, S. (2013): Polycyclic aromatic hydrocarbons stimulate human CYP3A4 promoter activity via PXR. *Toxicol. Lett.*, **222**, 180-188.
- Matsubara, T., Noracharttiyapot, W., Toriyabe, T., Yoshinari, K., Nagata, K. and Yamazoe, Y. (2007): Assessment of human pregnane X receptor involvement in pesticide-mediated activation of CYP3A4 Gene. *Drug Metab. Dispos.*, **35**, 728-733.
- Miyake, S., Makimura, M., Kanegae, Y., Harada, S., Sato, Y., Takamori, K., Tokuda, C. and Saito, I. (1996): Efficient generation of recombinant adenoviruses using adenovirus DNA-terminal protein complex and a cosmid bearing the full-length virus genome. *Proc. Natl. Acad. Sci. USA*, **93**, 1320-1324.
- Noracharttiyapot, W., Nagai, Y., Matsubara, T., Miyata, M., Shimada, M., Nagata, K. and Yamazoe, Y. (2006): Construction of several human derived stable cell lines displaying distinct profiles of CYP3A4 induction. *Drug Metab. Pharmacokinet.*, **21**, 99-108.
- PMDA (2014): Drug interaction guideline for drug development and labeling recommendations (final draft)
- Sivertsson, L., Edebert, I., Palmertz, M.P., Ingelman-Sundberg, M. and Neve, E.P. (2013): Induced CYP3A4 expression in confluent Huh7 hepatoma cells as a result of decreased cell proliferation and subsequent pregnane X receptor activation. *Mol. Pharmacol.*, **83**, 659-670.
- Sugatani, J., Osabe, M., Kurosawa, M., Kitamura, N. and Ikari, A. (2010): Induction of UGT1A1 and CYP2B6 by an antimitogenic factor in HepG2 cells is mediated through suppression of cyclin-dependent kinase 2 activity : Cell cycle-dependent expression. *Drug Metab. Dispos.*, **38**, 177-186.
- Synold, T.W., Dussault, I. and Forman, B.M. (2001): The orphan nuclear receptor SXR coordinately regulates drug metabolism and efflux. *Nat. Med.*, **7**, 584-590.
- Takada, T., Ogino, M., Miyata, M., Shimada, M., Nagata, K. and Yamazoe, Y. (2004): Differences in transactivation between rat CYP3A1 and human CYP3A4 genes by human pregnane X receptor. *Drug Metab. Pharmacokinet.*, **19**, 103-113.
- Toriyabe, T., Nagata, K., Takada, T., Aratsu, Y., Matsubara, T., Yoshinari, K. and Yamazoe, Y. (2009): Unveiling a new essential cis element for the transactivation of the CYP3A4 gene by xenobiotics. *Mol. Pharmacol.*, **75**, 677-684.
- Wan, Y.Y., An, D., Cai, Y.A.N., Repa, J.J., Chen, T.I.M.H., Flores, M., Postic, C., Magnuson, M.A., Chen, J.U., Chien, K.R., French, S., Mangelsdorf, D.J. and Sucov, H.M. (2000): Hepatocyte-specific mutation establishes retinoid X receptor alpha as a heterodimeric integrator of multiple physiological processes in the liver. *Mol. Cell. Biol.*, **20**, 4436-4444.
- Watson, A.J. and Hankinson, O. (1992): Dioxin- and Ah receptor-dependent protein binding to xenobiotic responsive elements and G-rich DNA studied by *in vivo* footprinting. *J. Biol. Chem.*, **266**, 6874-6878.
- Wienkers, L.C. and Heath, T.G. (2005): Predicting *in vivo* drug interactions from *in vitro* drug discovery data. *Nat. Rev. Drug Discov.*, **4**, 825-833.

RESEARCH ARTICLE

Open Access



Effect of health foods on cytochrome P450-mediated drug metabolism

Takamitsu Sasaki^{1,2}, Yu Sato¹, Takeshi Kumagai¹, Kouichi Yoshinari² and Kiyoshi Nagata^{1*} 

Abstract

Background: Health foods have been widely sold and consumed in Japan. There has been an increase in reports of adverse effects in association with the expanding health food market. While health food-drug interactions are a particular concern from the viewpoint of safe and effective use of health foods, information regarding such interactions is limited owing to the lack of established methods to assess the effects of health food products on drug metabolism. We therefore developed cells that mimicked the activities of cytochrome P450 1A2 (CYP1A2), CYP2C9, CYP2C19, CYP2D6, and CYP3A4, which strongly contribute to drug metabolism in human hepatocytes, and established a system to assess the inhibitory activity of health foods toward P450-mediated metabolism.

Methods: We simultaneously infected HepG2 cells with five P450-expressing adenoviruses (Ad-CYP1A2, Ad-CYP2C9, Ad-CYP2C19, Ad-CYP2D6, and Ad-CYP3A4) to mimic the activity levels of these P450s in human hepatocytes, and named them Ad-P450 cells. The activity levels of P450s in Ad-P450 cells and human hepatocytes were calculated via simultaneous liquid chromatography/tandem mass spectrometry analysis utilizing a P450 substrate cocktail.

Results: We established Ad-P450 cells mimicking the activity levels of CYP1A2, CYP2C9, CYP2C19, CYP2D6, and CYP3A4 in human hepatocytes. We determined the K_m values of P450 substrates and IC_{50} values of P450 inhibitors in Ad-P450 cells. These values were approximately equivalent to those obtained in previous studies. We investigated the inhibitory effects of 172 health foods that were recently in circulation in Japan on P450-mediated metabolism using Ad-P450 cells. Of the 172 health foods, five products (two products having dietary effects, one turmeric-based product, one collagen-based product, and one propolis-containing product) simultaneously inhibited the five P450s by more than 50%. Another 29 products were also confirmed to inhibit one or more P450s.

Conclusions: We established a comprehensive assessment system to elucidate the effects of health foods on P450-mediated metabolism and identified the inhibitory activity of 34 of 172 health foods toward the drug-metabolizing P450s. Our results may provide useful information to predict health food-drug interactions.

Keywords: Health food, Health food-drug interaction, Cytochrome P450, Inhibition

Background

Foods with health claims and so-called 'health foods' have been widely sold and consumed in Japan. Among these foods, Foods for Specified Health Uses (FOSHU) have shown scientific evidence-based beneficial effects on physiological conditions in both healthy and diseased individuals. Although most health foods contain ingredients that promote health and improve health-related conditions, the effectiveness of these products has not

been proven. Consumers therefore select products based on advertisements, which are usually non-scientific. However, the consumption of health foods has increased rapidly, because they are inexpensive and readily available in comparison with FOSHU. Reporting of adverse effects has also increased in association with the expansion of the health food market [1]. Several studies have reported that drug-induced liver injury is caused not only by prescription drugs but also by dietary and herbal supplements [2, 3]. Consumers have recently become more aware of the benefits and risks of using health foods, through information provided by relevant regulatory agencies. However, many consumers believe that

* Correspondence: nagataki@tohoku-mpu.ac.jp

¹Department of Environmental and Health Science, School of Pharmaceutical Sciences, Tohoku Medical and Pharmaceutical University, 4-4-1 Komatsushima, Aoba-ku, Sendai, Miyagi 981-8558, Japan

Full list of author information is available at the end of the article



© The Author(s). 2017 **Open Access** This article is distributed under the terms of the Creative Commons Attribution 4.0 International License (<http://creativecommons.org/licenses/by/4.0/>), which permits unrestricted use, distribution, and reproduction in any medium, provided you give appropriate credit to the original author(s) and the source, provide a link to the Creative Commons license, and indicate if changes were made. The Creative Commons Public Domain Dedication waiver (<http://creativecommons.org/publicdomain/zero/1.0/>) applies to the data made available in this article, unless otherwise stated.

products derived from natural substances are harmless. Furthermore, some consumers use multiple health foods at the same time. Provision of information that is accompanied by scientific evidence on the safety and efficacy of health foods is essential to maintain public health and decrease medical expenses.

Health food-drug interactions are a particular concern from the viewpoint of safe and effective use of health foods. Common interactions are associated with the inhibition of drug-metabolizing enzymes, particularly cytochrome P450s (CYPs, P450s). For example, green tea extract has been reported to inhibit CYP2C9, CYP2D6, and CYP3A4 in human liver microsomes [4]. Epigallocatechin gallate, the most abundant catechin in green tea, is also a potent inhibitor of CYP3A in human liver and intestinal microsomes [5]. While ginkgolide A, B, C, J, and bilobalide, known as constituents of *Ginkgo biloba*, have shown weak or negligible inhibition of CYP1A2, CYP2C9, and CYP3A in human liver microsomes, other constituents, such as ginkgolic acid I and II, have been reported to inhibit CYP1A2, CYP2C9, and CYP2C19 [6, 7]. Although many reports have provided useful information on the safe and effective use of health foods in patients taking drugs, most of this information is limited to the effects of the health foods main ingredients on P450-mediated metabolism. However, health foods that are on the market in Japan contain a number of ingredients, and such products may contain impurities. We recently reported the effects of health foods that are available in Japan on CYP2D6-mediated metabolism [8]. We have confirmed that a product containing curcumin is a potent inhibitor of CYP2D6. *Coleus forskohlii* extract- and collagen-based products also inhibit CYP2D6. The inhibition by forskolin and collagen had not been previously reported. Thus, it is difficult to deduce the effects of health foods on P450-mediated metabolism solely from the assessment of their main ingredients. We therefore believe that the development of a P450 inhibition screening system for complete health food products, rather than their main ingredients, may lead to more appropriate use of the products.

Human hepatocytes are recommended as the most reliable tool for the assessment of drug metabolism and drug-drug interactions [9]. However, due to their high cost and lot-to-lot variations in drug metabolism, it is difficult to continuously obtain human primary hepatocytes that have the same metabolic activities, and therefore these cells are unsuitable for high-throughput testing. In this study, we have utilized hepatocellular carcinoma cells (HepG2 cells) and P450-expressing adenoviruses to establish cells (named Ad-P450 cells) that mimic the activities of CYP1A2, CYP2C9, CYP2C19, CYP2D6, and CYP3A4, which strongly contribute to human drug metabolism in human hepatocytes [10]. We

have established a system to assess the inhibitory effects of health foods on P450-mediated metabolism using Ad-P450 cells.

Methods

Reagents

Phenacetin, acetaminophen, dextromethorphan, dextrorphan, furafyllin, and sulfaphenazole were purchased from Sigma-Aldrich (St. Louis, MO, USA). Quinidine was purchased from Tokyo Chemical Industry (Tokyo, Japan). 4-hydroxydiclofenac and 1-hydroxymidazolam were purchased from Becton Dickinson (Franklin Lakes, NJ, USA). 5-Hydroxyomeprazole was purchased from Toronto Research Chemical (North York, Canada). Ketoconazole was purchased from LKT Laboratories (St. Paul, MN, USA). Health foods were purchased from Japanese retail markets. All other reagents were of the highest grade available from Wako Pure Chemical Industries (Osaka, Japan) and Sigma-Aldrich. Oligonucleotides were commercially synthesized by Fasmac (Atsugi, Japan).

Construction of recombinant adenovirus

The open reading frames of *CYP1A2*, *CYP2C9*, *CYP2C19*, and *CYP3A4* were amplified by PCR from cDNA obtained from human hepatocytes by using primers specific for CYP1A2 (forward: 5'-CACCATGGCATTGTCCCAGTCTGTTTC-3'; reverse: 5'-TCAGTTGATGGA GAAGCGCAGCCG-3'), CYP2C9 (forward: 5'-CACCA TGGATTCTCTTGTGGTCCTTG-3'; reverse: 5'-TCA GACAGGAATGAAGCACAGCTGGTAG-3'), CYP2C19 (forward: 5'-CACCATGGATCCTTTTGTGGTCCTTG TG-3'; reverse: 5'-TCAGACAGGAATGAAGCACAG CTGA-3'), and CYP3A4 (forward: 5'-CACCATGGCT CTCATCCCAGACTTGGC-3'; reverse: 5'-TCAGGCT CCACTTACGGTGCCATC-3'), respectively. Constructs of these P450-expressing adenoviruses, Ad-CYP1A2, Ad-CYP2C9, Ad-CYP2C19, and Ad-CYP3A4, were made according to the procedure described [11]. Preparation of Ad-CYP2D6 was previously described [8].

Human hepatocytes and cell culture

Human cryopreserved primary hepatocytes (lot HEP187265, 54-year-old Caucasian woman) were purchased from Biopredic International (Rennes, France). The hepatocytes were thawed and cultured using the medium kit (Biopredic International) according to the manufacturer's protocol. The cells were seeded in type I collagen-coated 48-well plate at 8.5×10^4 cells/well. After 12 h, the cell medium was changed with culture medium (Biopredic International) containing P450 substrate cocktail (100 μ M phenacetin, 25 μ M diclofenac, 10 μ M omeprazole, 10 μ M dextromethorphan, and 10 μ M midazolam) and then the cells were incubated for 24 h.

Preparation of HepG2 cells mimicking the activity levels of CYP1A2, CYP2C9, CYP2C19, CYP2D6, and CYP3A4 in human hepatocytes (Ad-P450 cells)

HepG2 cells were purchased from RIKEN cell Bank (Tsukuba, Japan) and were cultured in Dulbecco's modified Eagle's medium (Wako Pure Chemical Industries) supplemented with 10% fetal bovine serum (Biowest, Miami, FL, USA), non-essential amino acids (Thermo Fisher Scientific, Maltham, MA, USA), and antibiotic-antimycotic (Thermo Fisher Scientific) under 5% CO₂-95% air at 37 °C. The cells were seeded in a 48-well tissue culture plate (Becton Dickinson) at 5.0×10^4 cells/well. After 48 h, the cells were simultaneously infected with Ad-CYP1A2 at 5 multiplicity of infection (MOI), Ad-CYP2C9 at 1 MOI, Ad-CYP2C19 at 2 MOI, Ad-CYP2D6 at 0.05 MOI, and Ad-CYP3A4 at 10 MOI. The cells were cultured for 72 h and subsequently used as Ad-P450 cells. The cells were incubated in culture medium containing P450 substrate cocktail for 5 h.

Assessment of P450 activity and inhibition in Ad-P450 cells

Ad-P450 cells were incubated in culture medium containing phenacetin (2.5–100 µM), diclofenac (0.5–20 µM), omeprazole (0.25–10 µM), dextromethorphan (1–50 µM), or midazolam (0.25–10 µM) for 5 h. In P450 inhibition assessments, Ad-P450 cells were incubated in culture medium containing P450 substrate cocktail and each typical P450 inhibitors (furafylline for CYP1A2 [0.05–30 µM], sulfaphenazole for CYP2C9 [0.01–10 µM], ticlopidine for CYP2C19 [0.3–300 µM], quinidine for CYP2D6 [0.01–10 µM], or ketoconazole for CYP3A4 [0.01–10 µM]) for 5 h.

Preparation of health food extracts and curcumin

Recommended daily dose of health foods (tablet, capsule, and powder) was incubated in 10 mL of 70% ethanol for 2 h at 37 °C. The resulting solution was centrifuged at $3500 \times g$ for 15 min and the supernatant was used as a test solution. Liquid-type health foods were used as test solutions without extraction procedure. Curcumin was dissolved in dimethyl sulfoxide (DMSO).

Effect of health foods and curcumin on P450-mediated metabolism

Ad-P450 cells were incubated in culture medium containing P450 substrate cocktail and test solution (0.5%) or curcumin (10–300 µM) for 5 h.

Liquid chromatography/tandem mass spectrometry (LC-MS/MS) analysis

Collected medium was mixed with an equal volume of ethyl acetate containing 0.1 µM nitrazepam (internal standard). After shaking, the mixtures were centrifuged at $2500 \times g$ for 10 min and the supernatants were evaporated to dryness at 60 °C in a block incubator. The residues were dissolved in acetonitrile containing 0.1% acetic acid and the solutions were subjected to liquid chromatography/tandem mass spectrometry (LC-MS/MS) analysis.

The Prominence system (Shimadzu Corporation, Kyoto, Japan) equipped with LCMS-8040 system (Shimadzu Corporation) was used for LC-MS/MS analysis with an electrospray ionization interface. The ionization mode used was positive in the multiple reaction monitoring. The chromatographic separation was performed on Xterra MS C18 columns (2.1 mm \times 100 mm, 5 µm) (Waters, Milford, MA, USA). The column oven temperature was maintained at 40 °C. The mobile phase consisted of acetonitrile containing 0.1% acetic acid and water containing 0.1% acetic acid (85:15) with a flow rate of 200 µL/min. The LC-MS/MS conditions were shown in Table 1. Desolvation line temperature and heat block temperature was 250 and 400 °C, respectively. Nebulizer gas flow rate and drying gas flow rate were 3 and 15 L/min, respectively.

Data analysis

The K_m , V_{max} , and IC_{50} values were determined using Prism software (version 6.0; GraphPad Software Inc., San Diego, CA, USA). The other calculations were performed using Excel (Microsoft, Seattle, MA, USA).

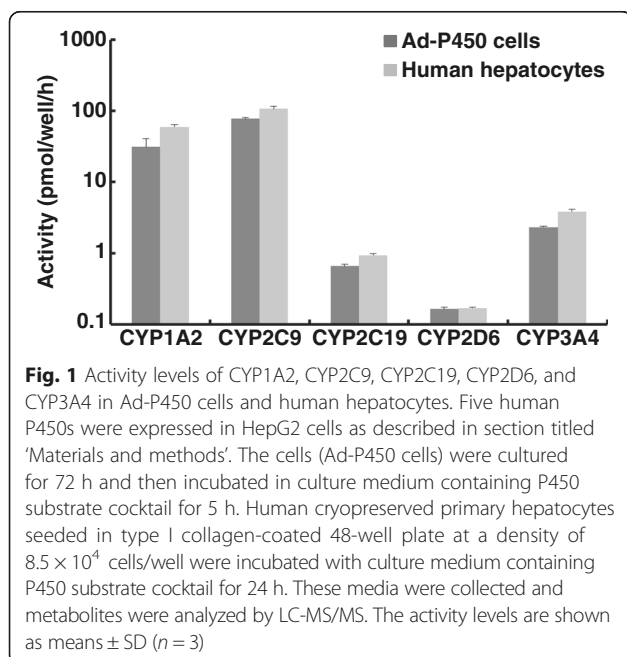
Results

Establishment of Ad-P450 cells

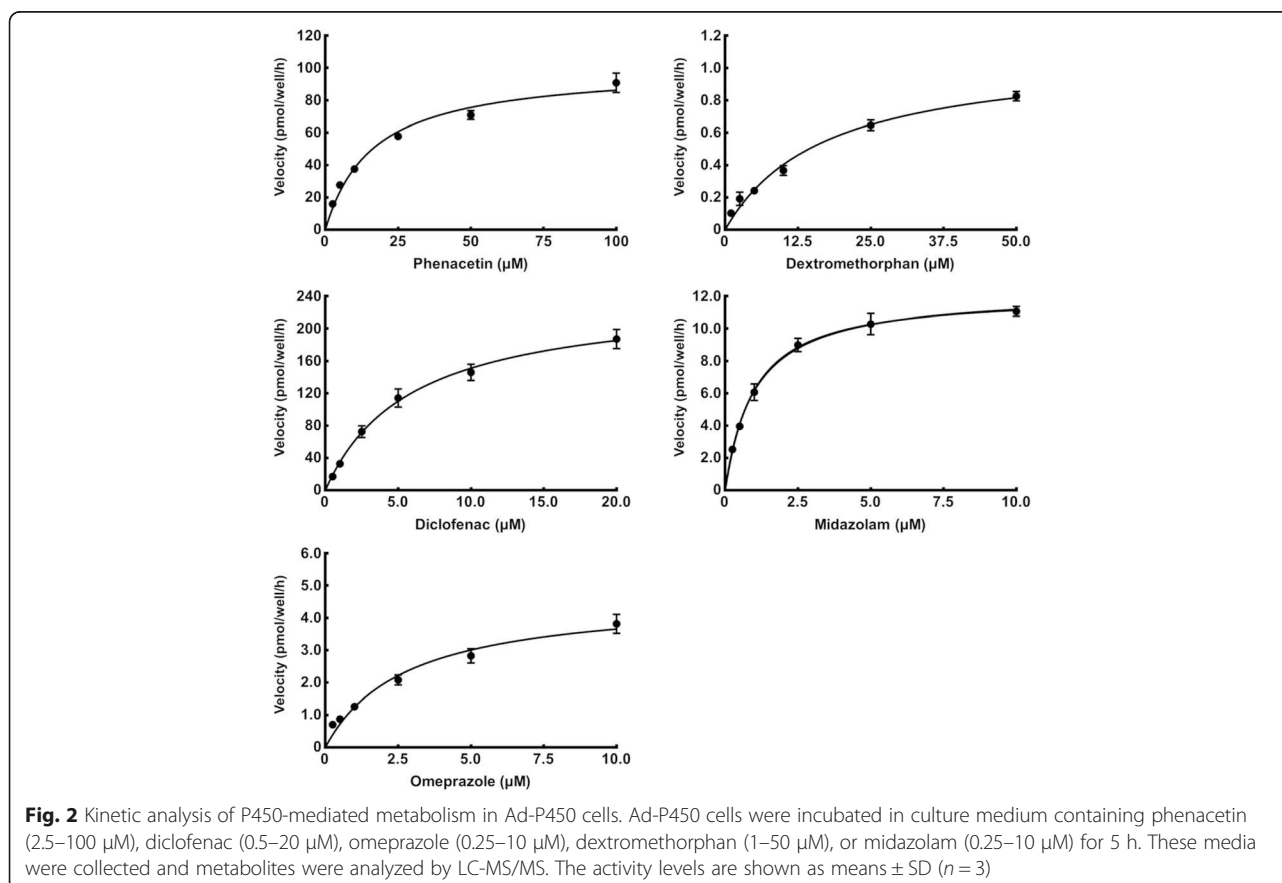
The activity levels of CYP1A2 (phenacetin *O*-deethylation activity), CYP2C9 (diclofenac 4'-hydroxylation activity), CYP2C19 (omeprazole 5-hydroxylation activity), CYP2D6 (dextromethorphan *O*-demethylation activity),

Table 1 MS/MS selected reaction monitoring transitions and collision energies for ions of metabolite and internal standard in the cocktail assays

	CYP1A2	CYP2C9	CYP2C19	CYP2D6	CYP3A4	IS
Substrate	Phenacetin	Diclofenac	Omeprazole	Dextromethorphan	Midazolam	Nitrazepam
Metabolite	Acetaminophen	4'-Hydroxy-diclofenac	5-Hydroxy-omeprazole	Dextrorphan	1'-Hydroxy-midazolam	-
Collision energy (eV)	19	33	13	42	23	25
Product ion (m/z)	110.05	229.95	213.95	157.05	324.05	236.10



and CYP3A4 (midazolam 1'-hydroxylation activity) in human hepatocytes were calculated via simultaneous LC-MS/MS analysis utilizing the P450 substrate cocktail. The activities of CYP1A2, CYP2C9, CYP2C19, CYP2D6, and CYP3A4 were 59.48, 106.71, 0.94, 0.17, and 3.86 pmol/well/h, respectively (Fig. 1). Based on these data, we simultaneously infected HepG2 cells with Ad-CYP1A2 (5 MOI), Ad-CYP2C9 (1 MOI), Ad-CYP2C19 (2 MOI), Ad-CYP2D6 (0.05 MOI), and Ad-CYP3A4 (10 MOI) to mimic the activity levels of CYP1A2, CYP2C9, CYP2C19, CYP2D6, and CYP3A4 in human hepatocytes. The activities of CYP1A2, CYP2C9, CYP2C19, CYP2D6, and CYP3A4 in the infected HepG2 cells were 31.22, 77.02, 0.66, 0.16, and 2.33 pmol/well/h, respectively (Fig. 1). Although the P450 activities in HepG2 cells infected with five P450-expressing adenoviruses were slightly lower in comparison with those in human hepatocytes, the ratios of the activities of each P450 were almost identical between these two cells (Fig. 1). We thus named the established HepG2 cells mimicking the activity levels of CYP1A2, CYP2C9, CYP2C19, CYP2D6, and CYP3A4 in human hepatocytes, Ad-P450 cells.



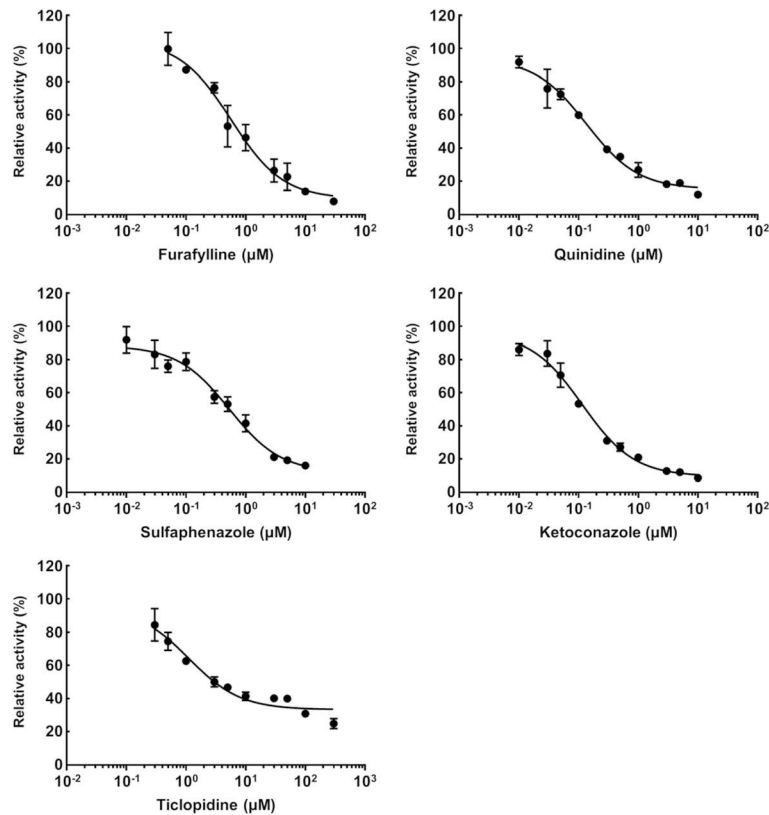


Fig. 3 Effect of representative inhibitors on P450-mediated metabolism in Ad-P450 cells. Ad-P450 cells were incubated in culture medium containing P450 substrate cocktail and each typical P450 inhibitor (furfurylline [0.05–30 μ M], sulfaphenazole [0.01–10 μ M], ticlopidine [0.3–300 μ M], quinidine [0.01–10 μ M], or ketoconazole [0.01–10 μ M]) for 5 h. These media were collected and metabolites were analyzed by LC-MS/MS. The activity levels are shown as means \pm SD ($n = 3$)

Kinetic analysis and inhibition assessment in Ad-P450 cells

To investigate the properties of Ad-P450 cells, we performed kinetic analyses using P450 substrates and calculated IC_{50} values for specific representative P450 inhibitors (CYP1A2, furfurylline; CYP2C9, sulfaphenazole; CYP2C19, ticlopidine; CYP2D6, quinidine; CYP3A4, ketoconazole) in Ad-P450 cells (Figs. 2 and 3). The Michaelis-Menten equation was used to calculate the K_m and V_{max} values from the metabolic reaction rates of the five P450s (Table 2). The specific P450 inhibitors used showed concentration-dependent inhibition, and the IC_{50} values are shown in Table 2. These values are similar to those previously reported [12, 13]. These results suggest that Ad-P450 cells

are useful for the assessment of P450-mediated drug metabolism, and drug-drug or health food-drug interactions.

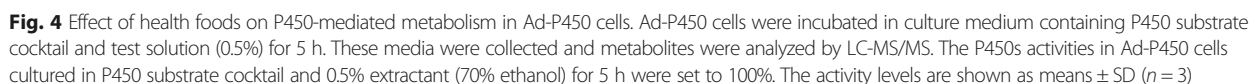
Effects of health foods on P450-mediated metabolism

We investigated the inhibitory effects of 172 health foods, whose uses in Japan were confirmed in our previous survey [8], on P450-mediated metabolism in Ad-P450 cells. The results, classified by main ingredients or expected effects, are shown in Fig. 4 and are summarized in Table 3. Products that inhibited any P450 by more than 50% were considered to have P450 inhibitory activity.

Of the 172 products, five products [two products having dietary effects (diet, no. 65 and 66), one turmeric-based product (no. 125), one collagen-based product (no. 152),

Table 2 Kinetic parameters of P450-mediated drug metabolism and IC_{50} values of P450 inhibitors in Ad-P450 cells

Enzyme	Metabolic reaction	Inhibitor	K_m (μ M)	V_{max} (pmol/well/hr)	IC_{50} (μ M)
CYP1A2	Phenacetin <i>O</i> -deethylation	Furfurylline	16.32	100.30	0.57
CYP2C9	Diclofenac 4'-hydroxylation	Sulfaphenazole	5.87	239.9	0.53
CYP2C19	Omeprazole 5-hydroxylation	Ticlopidine	2.75	4.66	1.11
CYP2D6	Dextromethorphan <i>O</i> -demethylation	Quinidine	17.14	1.10	0.14
CYP3A4	Midazolam 1'-hydroxylation	Ketoconazole	1.00	12.30	0.12



and one other product (propolis-containing product, no. 168)] simultaneously inhibited the five P450s by more than 50%. Two sesamin-based products (no. 135 and 136) simultaneously inhibited the four P450s except CYP1A2. Five products [collagen-based (no. 36), diet (no. 70), turmeric-based (no. 124), St. John's wort (SJW)-based (no. 145 and 146)] simultaneously inhibited three P450s (CYP1A2, CYP2C9/CYP2D6, and CYP3A4). A vitamin-, an isoflavone, and a vitamin/mineral-based product (no. 15, 62, and 131) simultaneously inhibited two P450s (CYP1A2 and CYP2C9). In addition, nineteen other products were found to inhibit one of the five P450s. Therefore, our results demonstrated that 34 (19.8%) of 172 health foods have P450 inhibitory activities.

Effects of curcumin on P450-mediated metabolism

Of the five products that simultaneously inhibited the five P450s, we further examined the effects of their ingredients in the turmeric-based products on P450-mediated metabolism. Curcumin is a known constituent of turmeric and a P450 inhibitor [14]. In our system using Ad-P450 cells, curcumin inhibited the five P450s in a concentration-dependent manner (Fig. 5). The residual activities in Ad-P450 cells treated with 50 μ M curcumin were 58.3% for CYP1A2, 25.9% for CYP2C9, 72.7% for CYP2C19, 71.9% for CYP2D6, and 61.9% for CYP3A4. Similar to the results of turmeric-based products, CYP2C9 was most strongly inhibited by curcumin, although this inhibition was observed only at a relatively high concentration.

Discussion

In order to comprehensively elucidate health food-drug interactions, we developed Ad-P450 cells mimicking the activity levels of CYP1A2, CYP2C9, CYP2C19, CYP2D6, and CYP3A4 in human hepatocytes and established a P450 inhibition assessment system. Of the 172 health food products tested, five products simultaneously inhibited all the five P450s, and another 29 products inhibited at least one of the P450s. Furthermore, the results of the inhibition of CYP2D6 in Ad-P450 cells were consistent with those obtained using Ad-CYP2D6-infected cells in our previous study [8].

To develop Ad-P450 cells that mimicked the drug-metabolizing activity of human hepatocytes, the five P450s that most strongly contribute to drug metabolism in human livers were expressed in HepG2 cells at levels showing the same activity as those of human hepatocytes (Fig. 1). We determined the K_m values for typical P450 reactions and IC_{50} values of representative P450 inhibitors in the Ad-P450 cells. These

values were approximately equivalent to those obtained in previous studies (Figs. 2 and 3, Table 2) [12, 13]. These results show that the Ad-P450 cells are useful tools to assess drug metabolism and health food-drug interactions.

Based on the data from our previous survey [8], we investigated the effects of health foods, for which actual use in Japan has been confirmed, on the five P450s. Our results showed that five products (two diet products, one turmeric-based product, one collagen-based product, and one propolis-containing product) inhibited the five P450s by more than 50% (Fig. 4). The two diet products (no. 65 and 66) contained *C. forskohlii* extract powder (containing 10% forskolin). However, there are few reports concerning their P450 inhibitory activities. These results suggest that unidentified ingredients might be involved in P450 inhibition, since these two diet products do not include common ingredients other than *C. forskohlii* extract.

A turmeric-based product (no. 125) also inhibited the five P450s, with CYP2C9 being the most inhibited. Curcumin is a polyphenolic component in turmeric that inhibits CYP1A2, CYP2B6, CYP2C9, CYP2D6, and CYP3A4, and its IC_{50} values are particularly low for CYP2C9 [14]. Since the product was obtained from *Curcuma longa*, which is curcumin-rich, and strong inhibitory activity of other turmeric-based products (no. 124 and 126) with little/no *C. longa* had not been observed, the inhibition of the five P450s by the turmeric-based product was thought to be due to curcumin. In this study, we confirmed that curcumin inhibited the five P450s in a concentration-dependent manner in Ad-P450 cells (Fig. 5). However, strong inhibition was found only at relatively high concentrations. These results suggest that P450 inhibition by the turmeric-based product could also be associated with ingredients other than curcumin.

Based on the product labels, the collagen-based product (no. 152) that showed inhibitory activities toward the five P450s contained silibinin in addition to collagen, but other collagen-based products (no. 29–38 and 151) did not. Silibinin has been reported to inhibit CYP2C9 and CYP3A4 through mechanism-based inhibition (MBI) [15]. It was recently reported that a metabolite of *rutaecarpine*, a principal constituent of *Evodia rutaecarpa*, strongly inhibits P450s [16], suggesting that health food-drug interactions could be caused by P450 inhibition through MBI.

We also revealed that two sesamin-based products (no. 135 and 136) inhibited CYP2C9, CYP2C19, CYP2D6, and CYP3A4. Sesamin is a known competitive inhibitor of CYP1A2, CYP2C9, and CYP3A4 and the reported K_i

Table 3 Health foods with inhibitory activity and residual activity of P450s

Product classification	Number ^a	Product name	Inhibited P450	Relative activity (%) ^b				
				CYP1A2	CYP2C9	CYP2C19	CYP2D6	CYP3A4
Vitamin	4/19	Vitamin-4	CYP2C9	73.0	8.6	—	62.8	64.0
		Vitamin-11	CYP2C9	95.1	18.1	—	—	65.4
		Vitamin-13	CYP2C9	92.4	23.3	—	88.1	65.3
		Vitamin-15	CYP1A2, CYP2C9	38.2	7.3	—	62.6	72.6
Glucosamine	2/11	Glucosamine-27	CYP1A2	45.1	83.6	92.4	65.6	56.2
		Glucosamine-28	CYP1A2	36.4	70.0	70.2	50.7	53.2
Collagen	3/12	Collagen-29	CYP2C9	96.1	31.8	—	81.4	71.4
		Collagen-36	CYP2C9, CYP2D6, CYP3A4	61.4	27.7	69.1	46.2	42.2
		Collagen-152	CYP1A2, CYP2C9, CYP2C19, CYP2D6, CYP3A4	26.3	8.0	30.4	35.6	26.6
Mineral	1/14	Mineral-39	CYP2C9	52.3	41.5	—	—	70.1
Plant	1/6	Plant-57	CYP2C9	58.1	28.4	63.6	63.5	98.3
Isoflavone	1/10	Isoflavone-62	CYP1A2, CYP2C9	35.7	8.5	—	97.4	75.0
Diet	6/9	Diet-65	CYP1A2, CYP2C9, CYP2C19, CYP2D6, CYP3A4	22.3	3.8	32.4	34.7	23.9
		Diet-66	CYP1A2, CYP2C9, CYP2C19, CYP2D6, CYP3A4	24.2	3.4	20.4	19.7	17.1
		Diet-67	CYP2C9	76.5	44.3	—	77.6	55.1
		Diet-68	CYP2C9	77.4	46.3	99.1	75.8	55.3
		Diet-69	CYP2C9	94.7	48.5	—	68.2	60.0
		Diet-70	CYP1A2, CYP2C9, CYP3A4	49.1	19.0	68.4	65.3	40.2
Garlic	1/10	Garlic-160	CYP1A2	45.2	77.3	—	53.4	56.3
Lutein/berry	0/11	—	—	—	—	—	—	—
Aojiru	0/10	—	—	—	—	—	—	—
Amino acid	0/6	—	—	—	—	—	—	—
Chlorella	0/7	—	—	—	—	—	—	—
Lactic acid bacterium	0/5	—	—	—	—	—	—	—
Other	1/3	Other-168	CYP1A2, CYP2C9, CYP2C19, CYP2D6, CYP3A4	7.6	5.3	0.0	20.9	32.5
Oyster	0/3	—	—	—	—	—	—	—
Vinegar	1/6	Vinegar-169	CYP2C9	—	46.4	70.8	83.9	59.6
CoQ10	0/4	—	—	—	—	—	—	—
Turmeric	3/4	Turmeric-124	CYP1A2, CYP2C9, CYP3A4	47.2	49.4	67.6	66.4	30.2
		Turmeric-125	CYP1A2, CYP2C9, CYP2C19, CYP2D6, CYP3A4	19.2	5.6	10.2	35.4	25.1
		Turmeric-126	CYP1A2	18.3	70.9	85.7	61.8	57.8
DHA	0/3	—	—	—	—	—	—	—
Vitamin/mineral	2/3	Vitamin/mineral-131	CYP1A2, CYP2C9	49.2	7.3	89.6	71.7	59.0
		Vitamin/mineral-133	CYP2C9	—	28.4	—	—	71.5
Enzyme	1/1	Enzyme-134	CYP2D6	—	94.6	—	36.6	62.5
Sesamin	3/3	Sesamin-135	CYP2C9, CYP2C19, CYP2D6, CYP3A4	56.8	12.5	25.6	31.5	31.4
		Sesamin-136	CYP2C9, CYP2C19, CYP2D6, CYP3A4	58.5	15.7	32.4	43.4	31.0
		Sesamin-172	CYP2C9	83.0	49.4	62.8	57.3	51.1
Vegetable	1/3	Vegetable-139	CYP1A2	36.8	86.8	97.4	—	71.5

Table 3 Health foods with inhibitory activity and residual activity of P450s (Continued)

Royal jelly	0/3	—	—	—	—	—	—	—
Animal	1/1	Animal-143	CYP2C9	88.5	24.6	—	88.6	61.5
Tea	0/1	—	—	—	—	—	—	—
SJW	2/2	SJW-145	CYP1A2, CYP2C9, CYP3A4	26.5	31.3	78.0	57.0	32.5
		SJW-146	CYP1A2, CYP2C9, CYP3A4	21.4	22.3	64.3	53.8	29.9
α-Lipoic acid	0/2	—	—	—	—	—	—	—

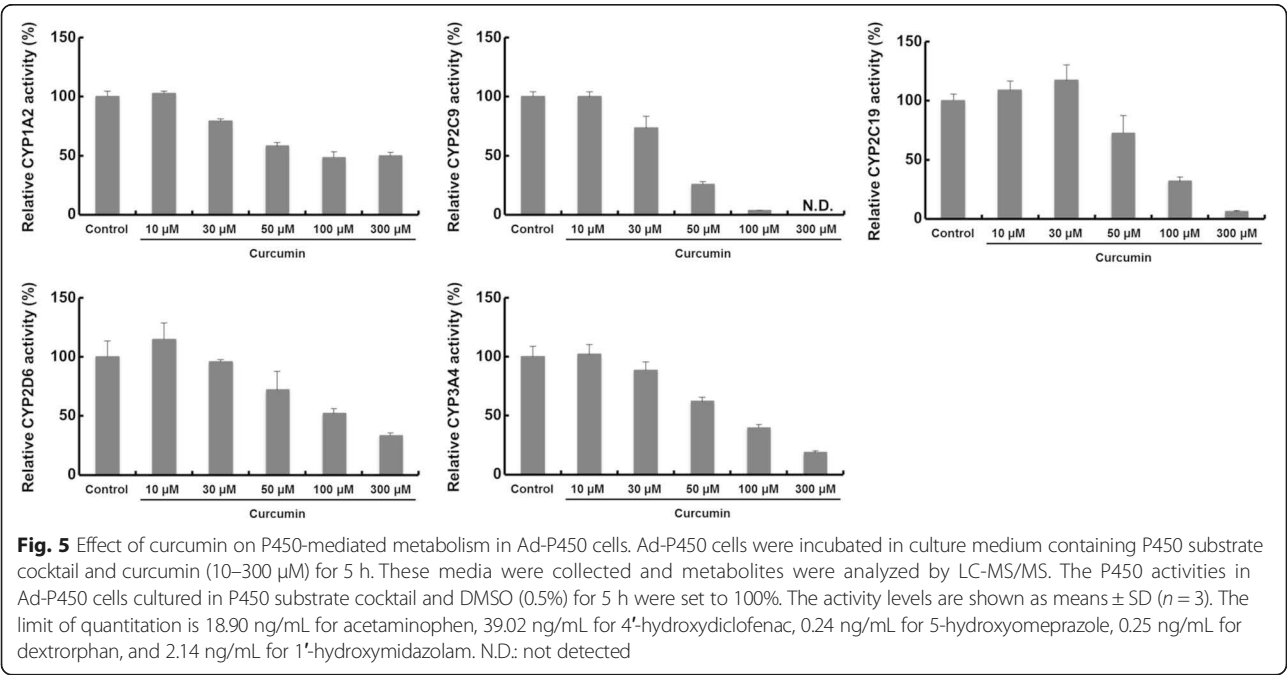
^aNumber of products with inhibitory activity/Number of products examined
^bP450s that were not inhibited by products are shown as —

values are 75, 24, and 4.2 μM, respectively [17]. Our results support the previous study, since the inhibition of CYP1A2 by two sesamin-based products was weaker than that of other P450s.

We confirmed that one isoflavone-based (no. 62) and one vitamin-based (no. 15) product inhibited CYP1A2 and CYP2C9. The isoflavone-based product contained isoflavones derived from soybean and red clover, such as genistein and biochanin A, which reportedly inhibit CYP1A2 [18, 19]. In contrast, few reports are available on P450 inhibition by vitamins in vitamin-based products, although lipid-soluble vitamins, such as vitamin A and vitamin D, have been reported to induce CYPs [20, 21]. Based on the product label, the vitamin-based product (no. 15) does not contain vitamin A and vitamin D, while the amounts of water-soluble vitamins, such as vitamins B1, B2, B6, B12, and pantothenic acid, were higher than those in other vitamin-based products. Although further study is needed to elucidate the P450

inhibition by vitamin-based product, the use of excessive amounts of water-soluble vitamins should be avoided to prevent health food-drug interactions.

In this study, we established a system to assess the inhibitory effects of health foods on P450-mediated metabolism using Ad-P450 cells. In contrast to the assessment of health food-drug interactions using human hepatocytes, assessment using Ad-P450 cells might not provide an accurate prediction of the interaction because of the limited number of P450s expressed in Ad-P450 cells. However, this established assessment system is easily applicable to health food-drug interactions testing for many health foods, because Ad-P450 cells are inexpensive with little to no lot-to-lot variations. In comparison with common assessment systems of health food-drug interactions using liver microsomes, our established system is including absorption process of chemical compounds in health foods into cells [11]. Moreover, this system has a valuable advantage, where it can mimic hepatocytes



of P450-mediated metabolism, which showed inter-individual variations by adjusting the ration of infection amount and species of P450-expressing adenovirus [22]. Furthermore, it is of great importance to assess the effects of health foods on the five P450s that most strongly contribute to drug metabolism in human livers in order to obtain beneficial and fundamental information under the current situation where there is limited scientific evidence regarding health food-drug interactions.

Conclusions

We established a comprehensive assessment system to investigate the effects of health foods on P450-mediated metabolism and found that 34 of the 172 health foods have the potential to inhibit human P450 activities. This report is the first to investigate the P450 inhibitory effects of a large number of health foods under the same conditions. Our results provide useful information to understand and predict health food-drug interactions.

Abbreviations

Ad: Adenovirus; FOSHU: Foods for Specified Health Uses; LC-MS/MS: Liquid chromatography/tandem mass spectrometry; MBI: Mechanism-based inhibition; MOI: Multiplicity of infection; PCR: Polymerase chain reaction

Acknowledgements

Not applicable

Funding

This work was supported by a Health and Labor Sciences Research Grant for Research on Food Safety (No. 22230301) from the Ministry of Health, Labor, and Welfare, Japan.

Availability of data and material

Data sharing not applicable to this article as no datasets were generated or analyzed during the current study.

Authors' contributions

TS and KN participated in the research design. TS and YS conducted experiments. TS, YS, and TK performed the data analysis. TS and KN contributed new reagents or analytic tools. TS, KY, and TK wrote or contributed to the writing of the manuscript. All authors read and approved the final manuscript.

Competing interests

The authors declare that they have no competing interests.

Consent for publication

Not applicable

Ethics approval and consent to participate

Not applicable

Publisher's Note

Springer Nature remains neutral with regard to jurisdictional claims in published maps and institutional affiliations.

Author details

¹Department of Environmental and Health Science, School of Pharmaceutical Sciences, Tohoku Medical and Pharmaceutical University, 4-4-1 Komatsushima, Aoba-ku, Sendai, Miyagi 981-8558, Japan. ²Department of Molecular Toxicology, School of Pharmaceutical Sciences, University of Shizuoka, 52-1 Yada, Suruga-ku, Shizuoka 422-8526, Japan.

Received: 23 February 2017 Accepted: 19 April 2017

Published online: 10 May 2017

References

- Koike M, Otsu F, Sakakibara J, Goto N. The current status of health food- or supplement-related adverse health effects. *Jpn J Drug Inform.* 2013;14:134–43 (in Japanese).
- Takikawa H, Murata Y, Horiike N, Fukui H, Onji M. Drug-induced liver injury in Japan: an analysis of 1676 cases between 1997 and 2006. *Hepatol Res.* 2009;39:427–31.
- Chalasani N, Bonkovsky HL, Fontana R, Lee W, Stolz A, Talwalkar J, et al. Features and outcomes of 899 patients with drug-induced liver injury: the DILIN prospective study. *Gastroenterology.* 2015;148:1340–52.
- Nishikawa M, Ariyoshi N, Kotani A, Ishii I, Nakamura H, Nakasa H, et al. Effects of continuous ingestion of green tea or grape seed extracts on the pharmacokinetics of midazolam. *Drug Metab Pharmacokinet.* 2004;19:280–9.
- Misaka S, Kawabe K, Onoue S, Werba JP, Girolini M, Tamaki S, et al. Effects of green tea catechins on cytochrome P450 2B6, 2C8, 2C19, 2D6 and 3A activities in human liver and intestinal microsomes. *Drug Metab Pharmacokinet.* 2013;28:244–9.
- Zou L, Harkey MR, Henderson GL. Effects of herbal components on cDNA-expressed cytochrome P450 enzyme catalytic activity. *Life Sci.* 2002;71:1579–89.
- von Moltke LL, Weemhoff JL, Bedir E, Khan IA, Hartzel JS, Goldman P, et al. Inhibition of human cytochromes P450 by components of Ginkgo biloba. *J Pharm Pharmacol.* 2004;56:1039–44.
- Sasaki T, Kumagai T, Sasaki H, Inami K, Sato Y, Takahashi S, et al. Assessment of inhibitory activity of CYP2D6 based on survey of use of health foods among customers of dispensing pharmacy and relevant data obtained. *Jpn J Pharm Health Care Sci.* 2014;40:488–99.
- Food and Drug Administration. Drug Development and Drug Interactions. <http://www.fda.gov/Drugs/DevelopmentApprovalProcess/DevelopmentResources/DrugInteractionsLabeling/ucm080499.htm>. Accessed 24 Dec 2015.
- Zanger UM, Turpeinen M, Klein K, Schwab M. Functional pharmacogenetics/genomics of human cytochromes P450 involved in drug biotransformation. *Anal Bioanal Chem.* 2008;392:1093–108.
- Sato Y, Sasaki T, Takahashi S, Kumagai T, Nagata K. Development of a highly reproducible system to evaluate inhibition of cytochrome P450 3A4 activity by natural medicines. *J Pharm Pharm Sci.* 2015;18:316–27.
- Li G, Huang K, Nikolic D, van Breemen RB. High-throughput cytochrome P450 cocktail inhibition assay for assessing drug-drug and drug-botanical interactions. *Drug Metab Dispos.* 2015;43:1670–8.
- Zientek M, Miller H, Smith D, Dunklee MB, Heinle L, Thurston A, et al. Development of an in vitro drug-drug interaction assay to simultaneously monitor five cytochrome P450 isoforms and performance assessment using drug library compounds. *J Pharmacol Toxicol Methods.* 2008;58:206–14.
- Appiah-Opong R, Commandeur JN, van Vugt-Lussenburg B, Vermeulen NP. Inhibition of human recombinant cytochrome P450s by curcumin and curcumin decomposition products. *Toxicology.* 2007;235:83–91.
- Sridar C, Goosen TC, Kent UM, Williams JA, Hollenberg PF. Silybin inactivates cytochromes P450 3A4 and 2C9 and inhibits major hepatic glucuronosyltransferases. *Drug Metab Dispos.* 2004;32:587–94.
- Zhang FL, He X, Zhai YR, He LN, Zhang SC, Wang LL, et al. Mechanism-based inhibition of CYPs and RMs-induced hepatotoxicity by rutaecarpine. *Xenobiotica.* 2015;45:978–89.
- Yasuda K, Ikushiro S, Kamakura M, Ohta M, Sakaki T. Metabolism of sesamin by cytochrome P450 in human liver microsomes. *Drug Metab Dispos.* 2010;38:2117–23.
- Liu Y, Santillo MF, Flynn TJ, Ferguson MS. Sex hormone modulation of both induction and inhibition of CYP1A by genistein in HepG2/C3A cells. *In Vitro Cell Dev Biol Anim.* 2015;51:426–31.
- Arora S, Taneja I, Challagundla M, Raju KS, Singh SP, Wahajuddin M. In vivo prediction of CYP-mediated metabolic interaction potential of formononetin and biochanin A using in vitro human and rat CYP450 inhibition data. *Toxicol Lett.* 2015;239:1–8.
- Wang K, Chen S, Xie W, Wan YJ. Retinoids induce cytochrome P450 3A4 through RXR/VDR-mediated pathway. *Biochem Pharmacol.* 2008;75:2204–8.

21. Drocourt L, Ourlin JC, Pascussi JM, Maurel P, Vilarem MJ. Expression of CYP3A4, CYP2B6, and CYP2C9 is regulated by the vitamin D receptor pathway in primary human hepatocytes. *J Biol Chem*. 2002;277:25125–32.
22. Aoyama K, Yoshinari K, Kim HJ, Nagata K, Yamazoe Y. Simultaneous expression of plural forms of human cytochrome P450 at desired ratios in HepG2 cells: adenovirus-mediated tool for cytochrome P450 reconstitution. *Drug Metab Pharmacokinet*. 2009;24:244–9.

Submit your next manuscript to BioMed Central and we will help you at every step:

- We accept pre-submission inquiries
- Our selector tool helps you to find the most relevant journal
- We provide round the clock customer support
- Convenient online submission
- Thorough peer review
- Inclusion in PubMed and all major indexing services
- Maximum visibility for your research

Submit your manuscript at
www.biomedcentral.com/submit





Contents lists available at ScienceDirect

European Journal of Medicinal Chemistry

journal homepage: <http://www.elsevier.com/locate/ejmech>

Research paper

Synthesis and biological evaluation of novel FK228 analogues as potential isoform selective HDAC inhibitors

Koichi Narita^a, Keisuke Matsuhara^a, Jun Itoh^a, Yui Akiyama^a, Singo Dan^b, Takao Yamori^{b, c}, Akihiro Ito^d, Minoru Yoshida^d, Tadashi Katoh^{a, *}^a Laboratory of Synthetic and Medicinal Chemistry, Faculty of Pharmaceutical Sciences, Tohoku Medical and Pharmaceutical University, 4-4-1 Komatsushima, Aoba-ku, Sendai 981-8558, Japan^b Division of Molecular Pharmacology, Cancer Chemotherapy Center, Japanese Foundation for Cancer Research, 3-10-6 Ariake, Koto-ku, Tokyo 135-8550, Japan^c Pharmaceuticals and Medical Devices Agency (PMDA), 3-3-2 Kasumigaseki, Chiyoda-ku, Tokyo 100-0013, Japan^d Chemical Genetics Laboratory, RIKEN, 2-1 Hirosawa, Wako-shi, Saitama 351-0198, Japan

ARTICLE INFO

Article history:

Received 24 February 2016

Received in revised form

14 May 2016

Accepted 16 May 2016

Available online 18 May 2016

Keywords:

FK228 analogues

Histone deacetylase inhibitors

Structure-activity relationship

Bicyclic depsipeptide

Total synthesis

ABSTRACT

Novel C4- and C7-modified FK228 analogues were efficiently synthesized in a highly convergent and unified manner. This synthesis features the amide condensation of glycine-D-cysteine-containing segments with D-valine-containing segments for the direct assembly of the corresponding *seco*-acids, which are key precursors of macrolactones. The HDAC inhibition assay and cell-growth inhibition analysis of the synthesized analogues revealed novel aspects of their structure-activity relationship. This study demonstrated that simple modification at the C4 and C7 side chains in FK228 is effective for improving both HDAC inhibitory activity and isoform selectivity; moreover, potent and highly isoform-selective class I HDAC1 inhibitors were identified.

© 2016 Elsevier Masson SAS. All rights reserved.

1. Introduction

The reversible acetylation and deacetylation of histones plays an important role for regulating gene expression by altering chromatin architecture [1]. Histone acetyltransferases (HATs) catalyse the transfer of acetyl groups from acetyl-CoA to the ϵ -amino groups on histone lysine residues, which relaxes the chromatin structure and epigenetically promotes gene transcription. Conversely, histone deacetylases (HDACs) catalyse the removal of acetyl groups from the N-acetyl lysine residues on histones, which contracts the chromatin structure and epigenetically suppresses gene transcription. The inhibition of HDAC enzymatic activity has been demonstrated to affect transcriptional events that are involved in growth arrest, differentiation, proliferation, cell cycle regulation, protein turnover and/or apoptosis in transformed tumour cell cultures. Consequently, HDAC-inhibiting compounds are considered to be potential drugs for targeted cancer therapy [2].

There are 18 human HDAC isoforms, which are grouped into four major classes: class I (HDACs 1, 2, 3 and 8), class II (class IIa: HDACs 4, 5, 7 and 9; class IIb: HDACs 6 and 10), and class IV (HDAC 11) are Zn²⁺-dependent metallohydrolases, whereas class III HDACs (SirTs 1–7) are NAD⁺-dependent sirtuins [3]. Inhibiting class I HDACs is considered to be an effective mechanism for anticancer agents, whereas inhibiting class II HDACs may cause undesirable side effects such as serious cardiac hypertrophy [4]; therefore, in cancer chemotherapy, the potent and selective inhibition of class I HDACs is highly desirable.

In 2009, the U.S. Food and Drug Administration (FDA) approved the bicyclic depsipeptide HDAC inhibitor FK228 (romidepsin, **1**, Fig. 1) for treating cutaneous T-cell lymphoma and other peripheral T-cell lymphomas [5]; however, FK228 is known to be associated with an unresolved cardiotoxicity issue [5b,6], which highlights the requirement for further identifying and developing new HDAC inhibitors with high efficacy and low toxicity. FK228 was first discovered by researchers from Fujisawa Pharmaceutical Co. Ltd. (now Astellas Pharma Inc.) in 1994, who isolated it from a culture broth of *Chromobacterium violaceum* (No. 968) [7]. Yoshida et al. proposed a molecular mechanism by which FK228 inhibits HDAC

* Corresponding author.

E-mail address: katoh@tohoku-mpu.ac.jp (T. Katoh).

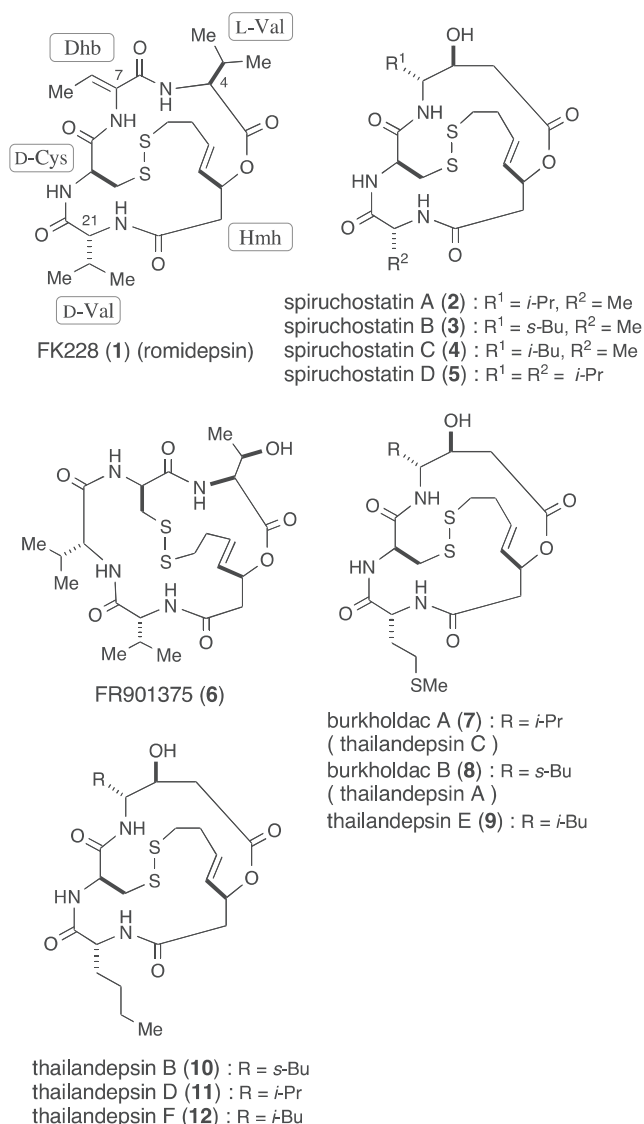


Fig. 1. Structures of FK228 (romidepsin; **1**), spiruchostatins A–D (**2–5**), FR901375 (**6**), burkholdacs A (thailandepsin C; **7**) and B (thailandepsin A; **8**), and thailandepsins E (**9**), B (**10**), D (**11**) and F (**12**). $i\text{-Pr}$ = isopropyl, $s\text{-Bu}$ = sec-butyl, $i\text{-Bu}$ = isobutyl.

[8]. In that mechanism, FK228, which itself serves as a stable pro-drug, is activated by reductive cleavage of the disulfide bond after incorporation into the cells, and the released sulfhydryl group in the butenyl side chain interacts with the zinc cation located at the binding pocket of the HDACs, resulting in a potent inhibitory effect. The structural features of FK228 are a 16-membered bicyclic depsipeptide comprising dehydrobutyrine (Dhb), L-valine, D-cysteine, D-valine, (3*S*,4*E*)-3-hydroxy-7-mercapto-4-heptenoic acid (Hmh) and a characteristic disulfide bond linkage. Since the discovery of FK228, several structurally similar bicyclic depsipeptide HDAC inhibitors have been isolated from bacterial fermentations, including spiruchostatins A–D (**2–5**) [9], FR901375 (**6**) [10], burkholdacs A (**7**) and B (**8**) [11] and thailandepsins A–F (**7–12**) [12] (thailandepsins A and C are identical to burkholdacs B and A, respectively). The potentially therapeutic biological properties and unique structural features of **1–12** have made them attractive targets for total synthesis, and several such syntheses of these natural products have been published in the literature [13–19].

During our research on the synthesis and biological evaluation of bicyclic depsipeptide HDAC inhibitors such as **1–5**, **7** and **8**

[13a,14c,15b,16,18a], we became interested in synthesizing FK228 analogues and evaluating their isoform selectivity in order to identify the potent and class I-selective HDAC inhibitors. There are several studies in the literature on synthesizing FK228 analogues [20]. Note that the synthesis and evaluation of FK228 analogues, which was reported by Ganesan et al., revealed novel aspects of their structure–activity relationship (SAR) [20c]. From this SAR study, three primary critical features that were related to the HDAC inhibitory activity of **1** were identified; i) the 16-membered macrocyclic scaffold is indispensable, ii) the unsaturated Dhb moiety can be replaced with other amino acids and iii) the C4 isopropyl group in the L-valine moiety is not always necessary. Although these results are very useful for designing novel FK228 analogues, no information on the effects of the stereochemistry in the amino acid components was reported.

Based on the results presented by Ganesan et al., we designed eight novel C4- and C7-modified FK228 analogues, which were denoted as FK-A1 to FK-A8 (**13a–h**, Fig. 2). Note that the L-valine and Dhb moieties of **1** were replaced by simple amino acids such as glycine, D-/L-alanine, D-/L-phenylalanine and D-/L-leucine. We envisaged that **13a–h** could be readily synthesized via the total synthesis we had previously developed for bicyclic depsipeptide natural products.

In this study, we describe the synthesis of FK228 analogues **13a–h** using a synthetic strategy that was developed previously in our laboratory. Then, to investigate the effect of the C7 stereochemistry and amino acid substituent groups, these synthesized analogues were subjected to an HDAC inhibition assay and anti-proliferative analysis.

2. Results and discussion

2.1. Chemistry

2.1.1. General synthetic strategy for the novel FK228 analogues FK-A1 to FK-A8 (**13a–h**)

The selection of the method that was used for constructing the

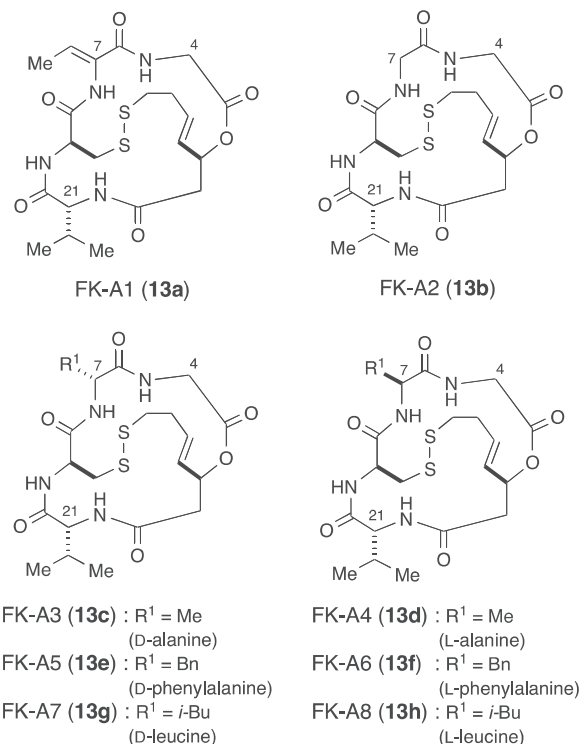


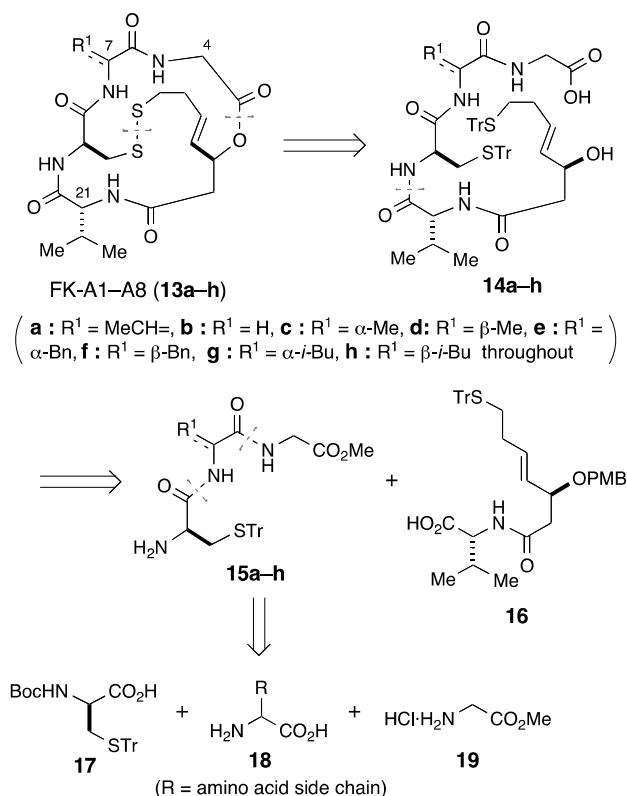
Fig. 2. Structures of the novel FK228 analogues FK-A1 to FK-A8 (**13a–h**). Bn = benzyl.

16-membered macrocyclic ring is crucial to successfully achieve the total synthesis of this class of natural products. In our previously reported total syntheses of FK228 (**1**) [13a], spiruchostatins A–D (**2–5**) [14c,15b,16] and burkholdacs A (**7**) and B (**8**) [18a], we employed two different reliable methods such as Shiina's macrocyclization [21] and Mitsunobu macrocyclization [22]. For synthesizing **2–5**, **7** and **8**, we employed Shiina's macrocyclization, whereas for synthesizing **1**, we employed Mitsunobu macrocyclization. Note that Shiina's macrocyclization was superior to the Mitsunobu macrocyclization in terms of chemical yield, reaction cleanness and ease of purification; however, in the case of **1**, all attempts to conduct Shiina's macrocyclization proved unsuccessful, most possibly because of the sterically hindered isopropyl group in the L-valine unit. Remarkably, using Shiina's macrolactonization, Ganesan et al. successfully synthesized FK228 analogues in which the L-valine moiety was replaced by glycine [20c]; therefore, we decided to perform the key macrolactonization using Shiina's method in our synthesis.

Our general synthetic plan is outlined in Scheme 1. We envisioned that the target molecules **13a–h** could be synthesized by Shiina's macrolactonization of the corresponding *seco*-acids **14a–h**, followed by internal disulfide bond formation. The key element of this scheme is the highly convergent assembly of **14a–h** by the direct condensation of the glycine-D-cysteine-containing segments **15a–h** and the D-valine-containing segment **16**. Segments **15a–h** are formed by the condensation of the D-cysteine derivative **17**, amino acid **18** and glycine methyl ester hydrochloride (**19**). The remaining segment **16** is obtained using our previously described total synthesis of **1** [13a] and **5** [16].

2.1.2. Synthesis of FK-A1 (**13a**)

First, the synthesis of segment **15a** was performed from L-



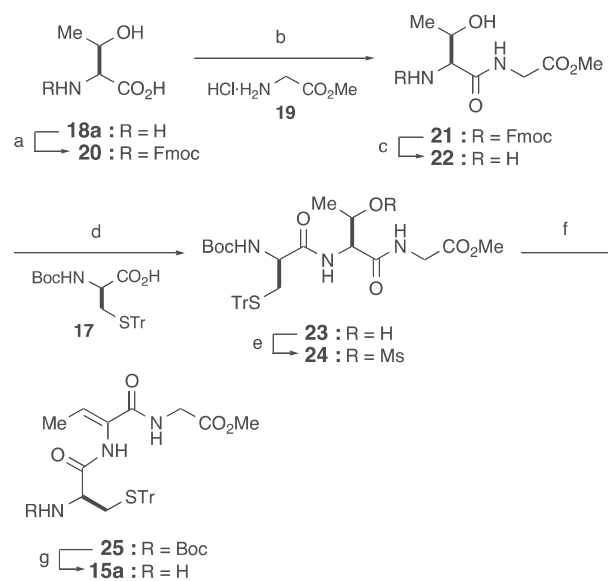
Scheme 1. Retrosynthetic analysis for **13a–h**. Tr = triphenylmethyl, PMB = 4-methoxybenzyl, Boc = *tert*-butoxycarbonyl.

threonine (**18a**), as shown in Scheme 2. Protection of the amino group in **18a** with a 9-fluorenylmethoxycarbonyl (Fmoc) group, which was followed by condensation of the resulting carbamate **20** with glycine methyl ester hydrochloride (**19**), provided the desired dipeptide **21** in 88% yield over the two steps. After deprotection of the *N*-Fmoc group in **21**, the free amine **22** was subjected to condensation with the D-cysteine derivative **17**, which resulted in the tripeptide **23** in 53% yield over the two steps. At this stage, the threonine part of **23** is converted to an unsaturated Dhb moiety via a two-step sequence that involves mesylation of the hydroxy group (94% yield) followed by elimination of the resulting mesylate **24** (89% yield), thus affording the desired product **25**. Deprotection of the *N*-Boc group in **25** is efficiently achieved using $\text{BF}_3 \cdot \text{OEt}_2$, leading to the desired segment **15a** in 88% yield.

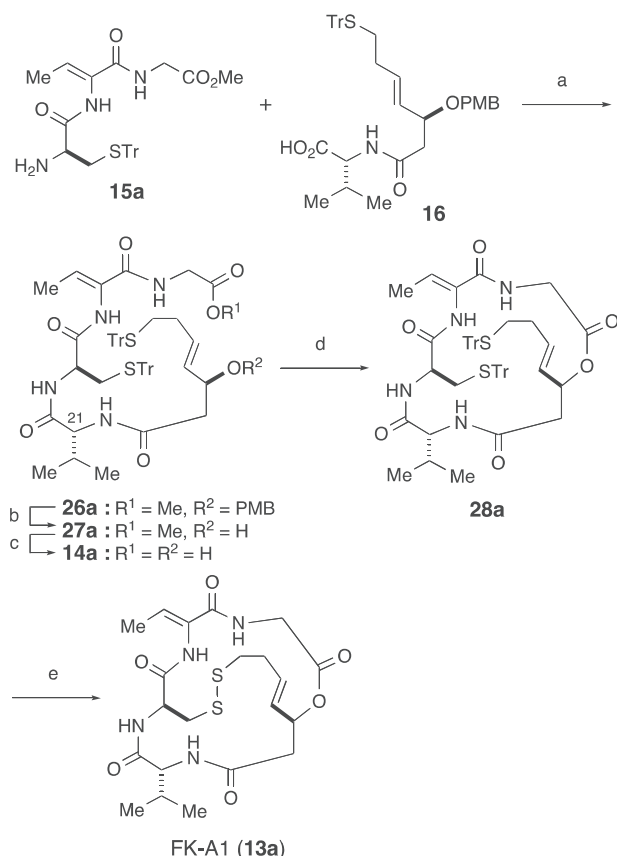
Subsequently, the synthesis of FK-A1 (**13a**) was accomplished by assembling the two segments **15a** and **16**, as shown in Scheme 3. Treating **15a** and **16** with HATU (1.3 equiv) and HOAt (1.3 equiv) in the presence of *i*-Pr₂NEt (2.6 equiv) in $\text{CH}_2\text{Cl}_2/\text{MeCN}$ at -20°C for 5 h afforded the desired condensation product **26a** in 80% yield without appreciable epimerization at the C21 stereogenic centre [13a]. Then, the condensation product **26a** was converted to the required *seco*-acid **14a** with an overall yield of 87% via the successive removal of both the PMB and methyl-protecting groups. The critical macrolactonization of **14a** is successfully performed using Shiina's method [MNBA (1.3 equiv), DMAP (3.0 equiv), CH_2Cl_2 (1.0 mM), rt, 12 h] [21], and the desired cyclization product **28a** is obtained in 64% yield. Finally, disulfide bond formation accompanied by oxidative S-Tr deprotection of **28a** is efficiently achieved by brief exposure to I_2 in a dilute $\text{CH}_2\text{Cl}_2/\text{MeOH}$ solution (0.5 mM) at room temperature, which results in the production of the desired FK-A1 (**13a**) in 97% yield.

2.1.3. Synthesis of FK-A2 to FK-A8 (**13b–h**)

As shown in Scheme 4, using glycine (**18b**: $R^1 = R^2 = \text{H}$), D-/L-alanine (**18c,d**: $R^1 = \alpha/\beta\text{-Me}$, $R^2 = \text{H}$), D-/L-phenylalanine (**18e,f**: $R^1 = \alpha/\beta\text{-Bn}$, $R^2 = \text{H}$) and D-/L-leucine (**18g,h**: $R^1 = \alpha/\beta\text{-i-Bu}$, $R^2 = \text{H}$) as starting materials, the remaining FK228 analogues, i.e.



Scheme 2. Synthesis of segment **15a**. a) FmocCl, 10% aq. Na_2CO_3 , dioxane, rt; b) **19**, PyBOP, *i*-Pr₂NEt, MeCN, rt, 88% (2 steps); c) Et_2NH , MeCN, rt; d) **17**, PyBOP, *i*-Pr₂NEt, MeCN, rt, 53% (2 steps); e) MsCl , Et_3N , CH_2Cl_2 , 0°C , 94%; f) DABCO, THF, rt, 89%; g) $\text{BF}_3 \cdot \text{Et}_2\text{O}$, CH_2Cl_2 , rt, 88%. FmocCl = 9-fluorenylmethoxycarbonyl chloride, PyBOP = (benzotriazol-1-yloxy)tripyrrolidinophosphonium hexafluorophosphate, MsCl = methanesulfonyl chloride, DABCO = 1,4-diazabicyclo-[2.2.2]octane.



FK-A2 to FK-A8 (**13b–h**), were efficiently synthesized in a manner similar to that described for synthesizing FK-A1 (**13a**).

2.2. Biological evaluation

2.2.1. HDAC inhibition assay

To determine their potency and isoform selectivity, the synthesized FK228 analogues **13a–h** were tested for their HDAC inhibitory activity against HDAC1 (class I) and HDAC6 (class IIb). In this assay, the clinically approved FK228 (**1**) was used as a positive control, and the results are summarized in Table 1. FK-A1 (**13a**), which lacks the C4 isopropyl group that is present in **1**, exhibited high HDAC1 inhibitory activity (IC₅₀ = 4.7 nM), although its potency is approximately half of that of **1** (IC₅₀ = 2.4 nM). This observation is in good agreement with a previous SAR study that was conducted by Ganesan et al. [20c]. On the other hand, FK-A2 (**13b**), which lacks both the C4 isopropyl and the C7 ethylidene groups present in **1**, exhibits much lower inhibition potency (IC₅₀ = 92.4 nM) compared to **1**. These results indicate that the C4 substituent is not responsible for HDAC inhibitory activity, whereas the C7 substituent is indispensable.

With respect to the effect of the R¹ substituent (including the C7 stereochemistry), FK-A3 (**13c**), FK-A5 (**13e**) and FK-A7 (**13g**), which were synthesized from the corresponding *D*-amino acids, exhibit excellent potency against HDAC1 in the low nanomolar range (IC₅₀ = 0.54–2.1 nM). Importantly, the potencies of **13c**, **13e** and **13g**

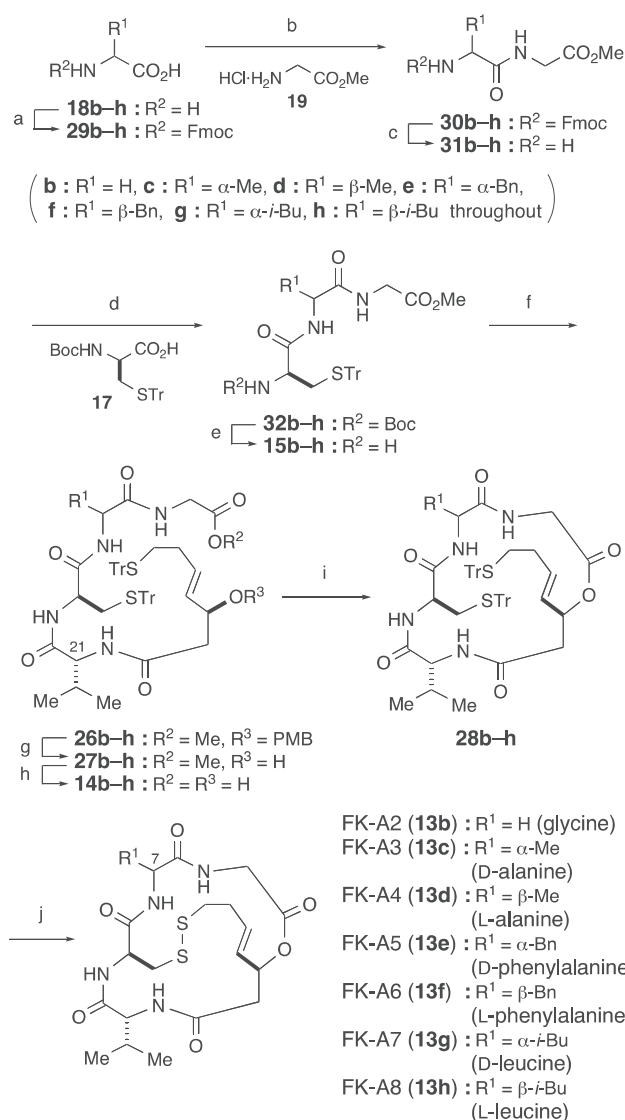


Table 1
HDAC inhibitory activity of FK228 and analogues FK-A1–FK-A8 (**13a–h**).

Compound	HDAC1 (class I) ^b	HDAC6 (class IIb) ^b	SI ^d
FK228 (1) ^c	2.4 ± 0.16	109 ± 35.8	45
FK-A1 (13a)	4.7 ± 0.88	859 ± 117	182
FK-A2 (13b)	92.4 ± 30.0	1316 ± 178	14
FK-A3 (13c)	2.1 ± 1.0	1008 ± 461	480
FK-A4 (13d)	184 ± 69.1	1022 ± 38.6	6
FK-A5 (13e)	0.54 ± 0.10	54.9 ± 14.5	102
FK-A6 (13f)	40.8 ± 4.9	355 ± 82	9
FK-A7 (13g)	0.96 ± 0.14	8452 ± 1066	8804
FK-A8 (13h)	11.4 ± 4.1	2255 ± 577	198

^a The concentration that induces 50% inhibition against HDACs.

^b The enzyme assay was performed in the presence of 0.1 mM dithiothreitol (DTT).

^c Positive control used in this study was synthesized in our laboratory [13a].

^d Selectivity index (HDAC6 IC₅₀/HDAC1 IC₅₀) as the selectivity towards class I HDAC1 over class IIb HDAC6.

were estimated to be equal to or two-fold higher than that of **1**. FK-A5 shows the highest potency ($IC_{50} = 0.54$ nM) among the analogues that were tested in this assay; however, FK-A4 (**13d**), FK-A6 (**13f**) and FK-A8 (**13h**), which were synthesized from the corresponding L-amino acids, showed considerably lower inhibitory activity ($IC_{50} = 11.4$ – 184 nM). These results suggest that the C7 stereochemistry plays an important role in conferring potency and that the D-amino acid side chains are preferable as the R^1 substituents. To the best of our knowledge, the SAR of the C7 stereochemistry in FK228 has not been previously reported. Thus, these findings provide new insight for designing novel synthetic depsipeptide HDAC inhibitors.

As we expected, **13a–h** exhibit much lower HDAC6 inhibitory activity, with IC_{50} values in the range of 55–8452 nM. For convenience, isoform selectivity (class I HDAC1/class IIb HDAC6) is expressed as a selective index (SI) value ($HDAC6\ IC_{50}/HDAC1\ IC_{50}$). The isoform selectivity of **13a** (SI = 182) is four-fold higher than that of **1** (SI = 45), suggesting that removal of the C4 substituent is effective for increasing isoform selectivity. However, FK-A2 (**13b**) exhibits lower isoform selectivity (SI = 14), suggesting that removal of the C7 substituent reduces isoform selectivity. Among the remaining analogues **13c–h**, compounds **13c**, **13e** and **13g**, which possess D-amino acid side chains at the C7 position, exhibit higher isoform selectivity (SI = 102–8804) compared to compounds **13d**, **13f** and **13h**, which possess L-amino acid side chains (SI = 6–198). Note that FK-A7 (**13g**, SI = 8804) exhibits approximately 200-fold higher isoform selectivity compared to **1** (SI = 45), which, to the best of our knowledge, represents the highest level of class I/II selectivity among the naturally occurring and synthetic bicyclic depsipeptides that have been reported to date.

These results reveal that a simple transformation of the C7 substituent (an ethylidene group) of **1** into a D-amino acid side chain is effective for improving both the HDAC inhibitory activity and the isoform selectivity. This structural alternation may confer a preferable conformational change onto the macrocyclic depsipeptide scaffold, thereby enhancing the discrimination and interactions between the macrocycle and the HDAC1 enzyme 'rim' located outside the active site binding pocket [23].

2.2.2. Cell-growth inhibition assay

The growth inhibitory activity of the synthesized analogues **13a–h** was simultaneously evaluated with FK228 (**1**) as a reference compound, using a panel of 39 human cancer cell lines at the Japanese Foundation for Cancer Research [24]. The organs from which the cell lines were derived were as follows (number of cells in parentheses): breast (5), central nervous system (6), colon (5), lung (7), melanoma (1), ovary (5), kidney (2), stomach (6) and prostate (2). Dose-response curves were measured at 5 different concentrations (from 10^{-11} to 10^{-7} M, from 10^{-10} to 10^{-6} M or from 10^{-8} to 10^{-4} M) for each compound, and the concentration that caused 50% cell growth inhibition (GI_{50}) was compared with that of the control.

The GI_{50} values of the tested analogues **13a–h** together with **1** are shown in Table 2. The potency order of these analogues was estimated using the MG-MID value (mean value of GI_{50} over all of the cell lines tested) to be **1** (6.2 nM) > **13e** (9.5 nM) > **13c** (43 nM) > **13g** (56 nM) > **13a** (115 nM) >> **13f** (1071 nM) > **13h** (1259 nM) >> **13b** (14,000 nM) > **13d** (20,000 nM).

These results correspond reasonably with the abilities of the analogues to inhibit HDAC1, as discussed above. Analogues **13c**, **13e** and **13g**, which possess D-amino acid side chains, exhibit considerably more potency ($GI_{50} = 9.5$ – 56 nM) compared to analogues **13d**, **13f** and **13h**, which possess L-amino acid side chains ($GI_{50} = 1071$ – $20,000$ nM). Interestingly, analogue **13g**, which exhibits the highest HDAC isoform selectivity (SI = 8804), exhibits the

lowest sensitivity against SF-295 (brain cancer) among the 39 cell lines. This result is significantly different from the analogues **13a–f** and **13h**, all of which exhibit their lowest sensitivity against HCT-15 (colon cancer). The change in the cell-growth inhibition pattern for **13g** might be caused by its HDAC isoform selectivity. Moreover, analogue **13e**, which exhibits the highest MG-MID value ($GI_{50} = 9.5$ nM) among the tested analogues, exhibits two-fold higher sensitivity to NCI-H522 (lung cancer, $GI_{50} = 0.72$ nM) compared to that of **1** ($GI_{50} = 1.8$ nM). One possible explanation for this observation is that analogue **13e**, which possesses an aromatic ring in the C7 side chain, has an additional molecular target (e.g. a different type of protein kinase) [25]; therefore, further investigation is necessary. Considering both HDAC inhibitory and anti-proliferative activities, **13c**, **13e** and **13g** are promising candidates for developing novel anticancer agents with high efficacy and low toxicity.

3. Conclusion

We synthesized eight new FK228 analogues, i.e. FK-A1 to FK-A8 (**13a–f**), in a highly convergent and unified manner. The present preliminary biological evaluation revealed novel aspects of the SAR for this class of depsipeptide HDAC inhibitor. In particular, replacement of the C4 isopropyl and C7 ethylidene substituents of FK228 by a hydrogen atom and a D-amino acid side chain, respectively (**13c**, **13e** and **13g**), was quite effective for improving HDAC1 inhibitory activity and isoform selectivity. Furthermore, incorporating an aromatic ring into the C7 side chain (**13e**) was demonstrated to result in an improvement of the specificity to cancer cell lines. These findings are useful for designing and developing new anticancer agents that work by the isoform-selective inhibition of HDACs. Further investigation of the activity of the synthesized analogues **13c**, **13e** and **13g** using an animal model is currently underway in our laboratories and will be reported in due course.

4. Experimental

4.1. Chemistry

All reactions involving air- and moisture-sensitive reagents were carried out using oven dried glassware and standard syringe-septum cap techniques. Routine monitorings of reaction were carried out using glass-supported Merck silica gel 60 F₂₅₄ TLC plates. Flash column chromatography was performed on Kanto Chemical Silica Gel 60N (spherical, neutral 40–50 nm) with the solvents indicated.

All solvents and reagents were used as supplied with following exceptions. Tetrahydrofuran (THF) was freshly distilled from Na metal/benzophenone under argon. CH_2Cl_2 , MeCN, Et_2NH , and i -Pr₂NEt were distilled from calcium hydride under argon.

Measurements of optical rotations were performed with a JASCO DIP-370 automatic digital polarimeter. 1H and ^{13}C NMR spectra were measured with a JEOL AL-400 (400 MHz) spectrometer. Chemical shifts were expressed in ppm using Me_4Si ($\delta = 0$) as an internal standard. The following abbreviations are used: singlet (s), doublet (d), triplet (t), quartet (q), multiplet (m) and broad (br). Infrared (IR) spectral measurements were carried out with a JASCO FT/IR-4100 spectrometer. Low- and High-resolution mass (HRMS) spectra were measured on a JEOL JMS-700 high resolution mass spectrometer.

4.1.1. Fmoc-L-Thr-Gly-OMe (**21**)

A solution of 9-fluorenylmethyl chloroformate (FmocCl) (652 mg, 2.5 mmol) in dioxane (10 mL) was added dropwise to a stirred solution of L-threonine (L-Thr) (**18a**) (300 mg, 2.5 mmol) in

Table 2Growth inhibition of FK228 analogues FK-A1 to FK-A8 (**13a–h**) against a panel of 39 human cancer cell lines.

GI ₅₀ ^a (nM)										
Origin of cancer	Cell line	1	13a	13b	13c	13d	13e	13f	13g	13h
Breast	HBC-4	6.9	170	13,000	30	17,000	37	690	70	1400
	BSY-1	8.5	200	18,000	36	27,000	36	1300	69	1500
	HBC-5	13	630	39,000	160	21,000	84	1900	270	1700
	MCF-7	4.2	190	33,000	37	17,000	62	1900	52	1600
	MDA-MB-231	5.5	53	9200	21	16,000	8.7	1200	39	1200
Central nervous system (Brain)	U-251	3.9	120	17,000	19	17,000	22	1500	10 ^b	330
	SF-268	4.9	110	12,000	31	17,000	5.0	220	11	820
	SF-295	4.0	280	40,000	71	51,000	21	1800	1100 ^c	1500
	SF-539	3.6	10 ^b	3300	10 ^b	15,000	3.3	860	57	1500
	SNB-75	7.2	10 ^b	950	10 ^b	14,000	8.7	1300	43	1000
	SNB-78	9.6	10 ^b	610 ^b	10 ^b	13,000	8.6	540	30	1800
	HCC2998	3.1	32	13,000	14	13,000	3.2	1100	27	1300
	KM-12	3.4	45	12,000	20	15,000	2.8	740	33	1100
Colon	HT-29	3.3	42	2700	13	12,000	3.0	570	33	690
	HCT-15	450 ^c	20,000 ^c	100,000 ^c	6700 ^c	100,000 ^c	100 ^c	26,000 ^c	590	17,000 ^c
	HCT-116	3.1	26	2500	10 ^b	11,000	2.6	250	22	340
	NCI-H23	4.6	130	36,000	31	27,000	4.4	1100	39	1200
	NCI-H226	8.9	410	61,000	110	21,000	4.8	1200	59	1600
	NCI-H522	1.8 ^b	10 ^b	680	10 ^b	1700 ^b	0.72 ^b	200	10 ^b	200
	NCI-H460	3.0	56	15,000	15	43,000	6.2	1100	39	1100
	A549	2.6	52	10,000	15	18,000	3.4	880	23	720
Lung	DMS273	5.8	230	47,000	89	47,000	20	1500	74	1400
	DMS114	3.6	43	5200	17	15,000	4.1	620	36	680
	LOX-IMVI	2.5	25	2900	11	4500	2.2	160 ^b	23	180 ^b
	OVCAR-3	4.6	64	13,000	22	16,000	17	1100	40	1500
	OVCAR-4	20	270	46,000	100	22,000	27	1900	87	1600
	OVCAR-5	2.8	49	3100	14	15,000	6.8	1400	31	1200
	OVCAR-8	5.5	54	18,000	31	31,000	4.6	1400	42	1500
	SK-OV-3	3.3	63	12,000	19	16,000	2.4	1200	23	1500
Melanoma	RXF-631L	6.6	230	91,000	110	100,000 ^c	7.9	1800	68	3200
	ACHN	20	460	43,000	270	100,000 ^c	24	11,000	200	9400
	St-4	22	1100	81,000	410	62,000	34	2000	230	2100
	MKN1	3.2	73	12,000	36	14,000	2.6	290	21	1100
	MKN7	4.9	380	47,000	260	43,000	35	1900	280	1800
	MKN28	17	1400	95,000	440	24,000	78	2100	270	1800
	MKN45	14	1900	100,000 ^c	500	100,000 ^c	64	1800	240	2200
	MKN74	3.0	100	16,000	35	18,000	5.9	500	44	1500
Ovary	DU-145	6.0	39	5400	21	15,000	3.6	590	37	830
	PC-3	18	170	11,000	70	13,000	5.7	1100	69	1400
Kidney	MG-MID ^d	6.2	115	14,000	43	20,000	9.5	1071	56	1259

^a Concentration that induces 50% inhibition of cell growth compared to the control.^b The most sensitive cell.^c The least sensitive cell.^d Mean value of GI₅₀ over all cell lines tested.

10% aqueous Na₂CO₃ (10 mL) at room temperature. After 2 h, the reaction mixture was diluted with H₂O (130 mL), and the resulting mixture was washed with Et₂O (2 × 40 mL). Concentrated H₂SO₄ was slowly added to the aqueous layer until pH was 2–3, and the resulting solution was extracted with EtOAc (3 × 100 mL). The combined extracts were washed with H₂O (2 × 50 mL) and brine (2 × 50 mL), then dried over Na₂SO₄. Concentration of the solvent in vacuo afforded Fmoc-L-Thr (**20**) (859 mg) as a colorless amorphous solid, which was used for the next reaction without further purification.

i-Pr₂NEt (1.71 mL, 10 mmol) was added dropwise to a stirred solution of the crude **20** (859 mg) and glycine methyl ester (Gly-OMe) hydrochloride (**19**) (348 mg, 2.8 mmol) in MeCN (25 mL) containing (benzotriazol-1-yloxy)tripyrrolidinophosphonium hexafluorophosphate (PyBOP) (1.97 g, 3.8 mmol) at room temperature under argon. After 1 h, concentration of the solvent in vacuo afforded a residue, which was purified by column chromatography (hexane/EtOAc 1:1) to give **21** (912 mg, 88%, 2 steps) as a colorless amorphous solid. [α]_D²⁷ –29.1 (c 1.0, CHCl₃); ¹H NMR (400 MHz, CDCl₃): δ 1.18 (3H, d, *J* = 6.3 Hz), 3.62 (1H, s), 3.70 (3H, s), 4.02 (2H, d, *J* = 5.4 Hz), 4.21 (2H, q, *J* = 6.8 Hz), 4.37–4.40 (3H, m), 5.99 (1H, d, *J* = 7.8 Hz), 7.15 (1H, br t, *J* = 4.9 Hz), 7.29 (2H, t, *J* = 7.3 Hz), 7.38 (2H,

t, *J* = 7.6 Hz), 7.58 (2H, d, *J* = 7.3 Hz), 7.75 (2H, d, *J* = 7.3 Hz); ¹³C NMR (100 MHz, CDCl₃): δ 18.1, 41.1, 47.1, 52.4, 58.8, 67.0, 67.2, 120.0 (2C), 125.0 (2C), 127.0 (2C), 127.71, 127.72, 141.3 (2C), 143.59, 143.64, 156.8, 170.2, 171.3; IR (neat): 3331, 3017, 2975, 2952, 1724, 1714, 1667, 1530, 1449, 1215, 1106, 758, 740 cm^{–1}; HRMS (EI): *m/z* calcd for C₂₂H₂₄N₂O₆ (M⁺) 412.1634, found 412.1628.

4.1.2. Boc-D-Cys–L-Thr–Gly-OMe (**23**)

Et₂NH (2.3 mL, 22 mmol) was added to a stirred solution of **21** (912 mg, 2.2 mmol) in MeCN (30 mL) at room temperature. After 3 h, the reaction mixture was concentrated in vacuo to afford NH₂-L-Thr–Gly-OMe (**22**) (421 mg) as a colorless oil, which was used for the next reaction without further purification.

i-Pr₂NEt (0.98 mL, 5.8 mmol) was added dropwise to a stirred solution of the crude amine **22** (421 mg, 2.2 mmol) and *N*-Boc-D-Cys(Tr)-OH (**17**) (1.23 g, 2.7 mmol) in MeCN (22 mL) containing PyBOP (1.50 g, 2.9 mmol) at room temperature under argon. After 1 h, concentration of the solvent in vacuo afforded a residue, which was purified by column chromatography (hexane/EtOAc 1:1) to give **23** (745 mg, 53%, 2 steps) as a colorless amorphous solid. [α]_D²⁸ –27.5 (c 0.10, CHCl₃). ¹H NMR (400 MHz, CDCl₃): δ 1.12 (3H, d, *J* = 6.3 Hz), 1.40 (9H, s), 2.59 (1H, dd, *J* = 12.9, 4.9 Hz), 2.78 (1H, dd,

$J = 12.4, 7.8 \text{ Hz}$), 3.30 (1H, br s), 3.60 (1H, br d, $J = 4.9 \text{ Hz}$), 3.65–3.74 (4H, m), 4.04 (1H, dd, $J = 17.6, 5.4 \text{ Hz}$), 4.23 (1H, d, $J = 7.8 \text{ Hz}$), 4.46 (1H, br s), 5.00 (1H, d, $J = 6.3 \text{ Hz}$), 6.82 (1H, d, $J = 7.8 \text{ Hz}$), 7.21–7.31 (9H, m), 7.39–7.44 (7H, m); ^{13}C NMR (100 MHz, CDCl_3): δ 18.5, 28.2 (3C), 33.5, 41.0, 52.3, 54.3, 57.8, 66.6, 67.3, 80.7, 127.0 (3C), 128.1 (6C), 129.5 (6C), 144.2 (3C), 155.5, 170.2, 171.4 (2C); IR (neat): 3387, 3303, 3275, 2979, 2921, 2852, 1685, 1676, 1654, 1642, 1541, 1533, 1508, 1219, 1163, 1101, 877, 700 cm^{-1} ; HRMS (FAB): m/z calcd for $\text{C}_{34}\text{H}_{42}\text{N}_3\text{O}_7\text{S}$ ($\text{M}^+ + \text{H}$) 636.2738, found 636.2759.

4.1.3. Boc-D-Cys(Tr)-L-Thr(OMs)-Gly-OMe (**24**)

Methanesulfonyl chloride (MsCl) (0.245 μL , 3.2 mmol) was added slowly to a stirred solution of **23** (745 mg, 1.2 mmol) in THF (23 mL) containing Et_3N (0.98 mL, 7.0 mmol) at 0°C under argon, and stirring was continued for 1 h at room temperature. The reaction was quenched with 1 M HCl (5 mL) at 0°C . The resulting mixture was extracted with CHCl_3 ($3 \times 30 \text{ mL}$), and the combined extracts were washed with brine ($2 \times 20 \text{ mL}$), then dried over MgSO_4 . Concentration of the solvent in vacuo afforded a residue, which was purified by column chromatography (hexane/ EtOAc 2:1) to give **24** (785 mg, 94%) as a colorless amorphous solid. $[\alpha]_D^{27} -21.0$ (c 1.0, CHCl_3); ^1H NMR (400 MHz, CDCl_3): δ 1.35–1.44 (12H, 2.60 (1H, dd, $J = 13.3, 5.3 \text{ Hz}$), 2.84 (1H, dd, $J = 13.5, 7.7 \text{ Hz}$), 3.02 (3H, s), 3.21–3.34 (1H, m), 3.50 (1H, dd, $J = 17.4, 5.3 \text{ Hz}$), 3.68 (3H, s), 4.06 (1H, dd, $J = 17.4, 6.3 \text{ Hz}$), 4.60 (1H, d, $J = 8.7 \text{ Hz}$), 4.87 (1H, d, $J = 4.4 \text{ Hz}$), 5.44 (1H, qd, $J = 6.5, 1.4 \text{ Hz}$), 6.38 (1H, d, $J = 8.7 \text{ Hz}$), 7.24–7.34 (9H, m), 7.40–7.42 (6H, m), 7.69 (1H, br s); ^{13}C NMR (100 MHz, CDCl_3): δ 18.5, 28.2 (3C), 31.5, 33.0, 37.7, 41.0, 52.2, 54.8, 56.5, 67.6, 81.2, 127.2 (3C), 128.2 (6C), 129.4 (6C), 144.0 (3C), 155.8, 168.9, 169.4, 171.2; IR (neat): 3330, 3057, 2979, 2935, 1752, 1675, 1517, 1491, 1364, 1211, 1175, 975, 912, 742, 700 cm^{-1} ; HRMS (FAB): m/z calcd for $\text{C}_{35}\text{H}_{42}\text{N}_3\text{O}_9\text{S}_2$ ($\text{M}^+ - \text{H}$) 712.2357, found 712.2363.

4.1.4. Boc-D-Cys(Tr)-Dhb-Gly-OMe (**25**)

1,4-Diazabicyclo[2.2.2]octane (DABCO) (478 mg, 4.3 mmol) was added to a stirred solution of **24** (761 mg, 1.1 mmol) in THF (21 mL) at room temperature under argon. After 24 h, concentration of the solvent in vacuo afforded a residue, which was purified by column chromatography (hexane/ EtOAc 2:1) to give **25** (585 mg, 89%) as a colorless amorphous solid. $[\alpha]_D^{29} -3.6$ (c 1.0, CHCl_3); ^1H NMR (400 MHz, CDCl_3): δ 1.40 (9H, s), 1.69 (3H, d, $J = 7.3 \text{ Hz}$), 2.64 (1H, dd, $J = 12.7, 5.9 \text{ Hz}$), 2.80 (1H, dd, $J = 12.7, 6.8 \text{ Hz}$), 3.64–3.73 (4H, m), 3.87 (2H, d, $J = 5.4 \text{ Hz}$), 4.90 (1H, d, $J = 5.4 \text{ Hz}$), 6.86 (1H, q, $J = 6.8 \text{ Hz}$), 7.12–7.22 (2H, m), 7.22–7.32 (9H, m), 7.41–7.43 (6H, m); ^{13}C NMR (100 MHz, CDCl_3): δ 13.5, 28.2 (3C), 33.2, 41.2, 52.1, 54.3, 67.4, 81.0, 127.1 (3C), 128.0, 128.2 (6C), 129.4 (6C), 134.0, 144.1 (3C), 155.9, 164.2, 169.4, 170.1; IR (neat): 3390, 3345, 3235, 3059, 3019, 2974, 2932, 1739, 1713, 1671, 1659, 1650, 1538, 1518, 1495, 1440, 1367, 1218, 1167, 1063, 910, 738, 700 cm^{-1} ; HRMS (FAB): m/z calcd for $\text{C}_{34}\text{H}_{40}\text{N}_3\text{O}_6\text{S}$ ($\text{M}^+ + \text{H}$) 618.2632, found 618.2628.

4.1.5. $\text{H}_2\text{N-D-Cys(Tr)-Dhb-Gly-OMe}$ (**15a**)

A solution of $\text{BF}_3 \cdot \text{Et}_2\text{O}$ (0.41 mL, 3.2 mmol) in CH_2Cl_2 (3.2 mL) was added dropwise to a stirred solution of **25** (571 mg, 0.93 mmol) in CH_2Cl_2 (46 mL) at 0°C , and stirring was continued for 5 h at room temperature. The reaction was quenched with saturated aqueous NaHCO_3 (15 mL) at 0°C . The resulting mixture was extracted with CHCl_3 ($3 \times 40 \text{ mL}$), and the combined extracts were washed with brine ($2 \times 20 \text{ mL}$), then dried over MgSO_4 . Concentration of the solvent in vacuo afforded a residue, which was purified by column chromatography ($\text{CHCl}_3/\text{MeOH}$ 20:1) to give **15a** (422 mg, 88%) as a colorless amorphous solid. $[\alpha]_D^{27} +2.0$ (c 1.0, CHCl_3); ^1H NMR (400 MHz, CDCl_3): δ 1.62 (2H, br s), 1.67 (3H, d, $J = 7.3 \text{ Hz}$), 2.65 (1H, dd, $J = 12.2, 4.4 \text{ Hz}$), 2.77 (1H, dd, $J = 12.2, 4.4 \text{ Hz}$), 3.25 (1H, dd, $J = 6.1, 4.4 \text{ Hz}$), 3.67 (3H, s), 3.79 (1H, dd, $J = 18.0, 5.4 \text{ Hz}$), 3.92 (1H,

dd, $J = 18.0, 5.9 \text{ Hz}$), 6.63 (1H, q, $J = 7.3 \text{ Hz}$), 6.97 (1H, br t, $J = 4.9 \text{ Hz}$), 7.19–7.30 (9H, m), 7.40–7.42 (6H, m), 8.53 (1H, br s); ^{13}C NMR (100 MHz, CDCl_3): δ 13.5, 37.2, 41.1, 52.1, 53.9, 66.9, 126.8 (3C), 127.9 (6C), 128.8, 129.4 (6C), 130.7, 144.3 (3C), 164.6, 170.2, 172.1; IR (neat): 3304, 3057, 3015, 2951, 1749, 1669, 1642, 1525, 1488, 1443, 1212, 1033, 847, 745, 700 cm^{-1} ; HRMS (FAB): m/z calcd for $\text{C}_{29}\text{H}_{32}\text{N}_3\text{O}_4\text{S}$ ($\text{M}^+ + \text{H}$) 518.2108, found 518.2127.

4.1.6. (5*E*,7*S*,11*R*,14*S*,17*Z*)-Methyl 17-ethylidene-11-isopropyl-7-(4-methoxybenzyloxy)-9,12,15,18-tetraoxo-1,1,1-triphenyl-14-tritylthiomethyl-2-thia-10,13,16,19-tetraazahenicos-5-en-21-oate (**26a**)

$i\text{-Pr}_2\text{NEt}$ (0.16 mL, 0.96 mmol) was added dropwise to a stirred solution of **15a** (190 mg, 0.37 mmol) and **16** (234 mg, 0.37 mmol) in $\text{CH}_2\text{Cl}_2/\text{MeCN}$ 2:1 (8.0 mL) containing O -(7-azabenzotriazol-1-yl)- N,N,N' -tetramethyluronium hexafluorophosphate (HATU) (182 mg, 0.48 mmol) and 1-hydroxy-7-azabenzotriazole (HOAt) (65 mg, 0.48 mmol) at -20°C under argon. After 5 h, the reaction mixture was diluted with CHCl_3 (80 mL). The organic layer was washed successively with 10% aqueous HCl ($2 \times 20 \text{ mL}$), saturated aqueous NaHCO_3 ($2 \times 20 \text{ mL}$) and brine ($2 \times 20 \text{ mL}$), then dried over MgSO_4 . Concentration of the solvent in vacuo afforded a residue, which was purified by column chromatography (hexane/ EtOAc 2:1) to give **26a** (334 mg, 80%) as a colorless amorphous solid. $[\alpha]_D^{29} 0$ (c 1.0, CHCl_3); ^1H NMR (400 MHz, CDCl_3): δ 0.71 (3H, d, $J = 7.0 \text{ Hz}$), 0.99 (3H, d, $J = 6.8 \text{ Hz}$), 1.69 (3H, d, $J = 6.8 \text{ Hz}$), 1.91–2.27 (5H, m), 2.37–2.45 (2H, m), 2.54 (1H, dd, $J = 12.9, 5.6 \text{ Hz}$), 2.93 (1H, dd, $J = 12.7, 6.3 \text{ Hz}$), 3.64 (3H, s), 3.79 (3H, s), 3.85–4.03 (5H, m), 4.21 (1H, d, $J = 11.2 \text{ Hz}$), 4.46 (1H, d, $J = 10.7 \text{ Hz}$), 5.27 (1H, dd, $J = 15.4, 8.0 \text{ Hz}$), 5.51 (1H, dt, $J = 15.1, 6.8 \text{ Hz}$), 6.64 (1H, d, $J = 6.8 \text{ Hz}$), 6.81–6.87 (3H, m), 7.07 (1H, t, $J = 5.6 \text{ Hz}$), 7.17–7.29 (21H, m), 7.36–7.41 (12H, m), 7.68 (1H, s); ^{13}C NMR (100 MHz, CDCl_3): δ 13.5, 17.7, 19.4, 29.4, 31.25, 31.30, 32.9, 41.3, 42.3, 52.0, 53.0, 55.3, 59.7, 66.6, 67.2, 70.0, 76.4, 113.9 (2C), 126.6 (3C), 127.0 (3C), 127.9 (6C), 128.1 (6C), 128.3, 129.4 (6C), 129.5 (7C), 129.6, 129.8 (2C), 133.6, 133.7, 144.1 (3C), 144.8 (3C), 159.4, 164.2, 168.7, 170.3, 171.9, 172.3; IR (neat): 3271, 3057, 3016, 2959, 2930, 1752, 1634, 1536, 1512, 1443, 1247, 1216, 1078, 1034, 768, 744, 700 cm^{-1} ; HRMS (FAB): m/z calcd for $\text{C}_{68}\text{H}_{73}\text{N}_4\text{O}_8\text{S}_2$ ($\text{M}^+ + \text{H}$) 1137.4864, found 1137.4889.

4.1.7. (5*E*,7*S*,11*R*,14*S*,17*Z*)-Methyl 17-ethylidene-7-hydroxy-11-isopropyl-9,12,15,18-tetraoxo-1,1,1-triphenyl-14-tritylthiomethyl-2-thia-10,13,16,19-tetraazahenicos-5-en-21-oate (**27a**)

2,3-dichloro-5,6-dicyano-1,4-benzoquinone (DDQ) (112 mg, 0.49 mmol) was added in small portions to a stirred solution of **26a** (373 mg, 0.33 mmol) in $\text{CH}_2\text{Cl}_2/\text{H}_2\text{O}$ 9:1 (16 mL) at room temperature. After 3 h, the mixture was diluted with CHCl_3 (60 mL), and the organic layer was washed with saturated aqueous NaHCO_3 ($2 \times 20 \text{ mL}$) and brine ($2 \times 20 \text{ mL}$), then dried over MgSO_4 . Concentration of the solvent in vacuo afforded a residue, which was purified by column chromatography (hexane/ EtOAc 1:5) to give **27a** (299 mg, 90%) as a colorless amorphous solid. $[\alpha]_D^{29} +0.19$ (c 1.0, CHCl_3); ^1H NMR (400 MHz, CDCl_3): δ 0.93 (3H, d, $J = 6.8 \text{ Hz}$), 0.98 (3H, d, $J = 6.3 \text{ Hz}$), 1.71 (3H, d, $J = 7.3 \text{ Hz}$), 1.97–2.31 (6H, m), 2.36 (1H, dd, $J = 13.2, 2.0 \text{ Hz}$), 2.64 (1H, dd, $J = 12.7, 4.9 \text{ Hz}$), 2.75 (1H, dd, $J = 12.7, 7.8 \text{ Hz}$), 3.61 (3H, s), 3.79 (1H, br s), 3.84 (1H, dd, $J = 18.0, 4.9 \text{ Hz}$), 4.02 (1H, dd, $J = 18.0, 5.4 \text{ Hz}$), 4.11 (1H, t, $J = 5.6 \text{ Hz}$), 4.20 (1H, td, $J = 7.8, 5.4 \text{ Hz}$), 4.29–4.37 (1H, m), 5.35 (1H, dd, $J = 15.1, 5.9 \text{ Hz}$), 5.49 (1H, dt, $J = 15.1, 6.3 \text{ Hz}$), 6.32 (1H, d, $J = 5.9 \text{ Hz}$), 6.67 (1H, q, $J = 7.1 \text{ Hz}$), 6.90 (1H, t, $J = 5.4 \text{ Hz}$), 7.13–7.29 (19H, m), 7.35–7.41 (12H, m), 7.78 (1H, br s); ^{13}C NMR (100 MHz, CDCl_3): δ 13.2, 17.8, 19.5, 29.1, 31.3 (2C), 33.1, 41.3, 43.9, 52.2, 52.5, 60.2, 66.6, 67.0, 69.6, 126.6 (3C), 126.9 (3C), 127.8 (6C), 128.0 (6C), 129.0, 129.4 (6C), 129.5 (6C), 129.9, 132.5, 132.6, 144.3 (3C), 144.8 (3C), 164.7, 169.2, 170.7, 171.4, 173.1; IR (neat): 3284, 3057, 3017, 2962, 2928,

1747, 1634, 1531, 1489, 1443, 1215, 1033, 745, 700 cm^{-1} ; HRMS (FAB): m/z calcd for $\text{C}_{60}\text{H}_{65}\text{N}_4\text{O}_7\text{S}_2$ ($\text{M}^+ + \text{H}$) 1017.4289, found 1017.4280.

4.1.8. (5*E*,7*S*,11*R*,14*S*,17*Z*)-17-Ethylidene-7-hydroxy-11-isopropyl-9,12,15,18-tetraoxo-1,1,1-triphenyl-14-tritylthiomethyl-2-thia-10,13,16,19-tetraazahenicos-5-en-21-oic acid (**14a**)

$\text{LiOH} \cdot \text{H}_2\text{O}$ (24.7 mg, 0.59 mmol) was added dropwise to a stirred solution of **27a** (299 mg, 0.94 mmol) in THF/ H_2O 4:1 (15 mL) at 0 °C. After 4 h, 10% aqueous HCl was added to the mixture at 0 °C until pH was 6. The resulting mixture was extracted with EtOAc (3 \times 30 mL), and the combined extracts were washed with saturated aqueous NaHCO_3 (2 \times 15 mL) and brine (2 \times 15 mL), then dried over Na_2SO_4 . Concentration of the solvent in vacuo afforded a residue, which was purified by column chromatography ($\text{CHCl}_3/\text{MeOH}$ 6:1) to give **14a** (289 mg, 97%) as a colorless amorphous solid. $[\alpha]_D^{29} + 5.5$ (c 1.0, CHCl_3); ^1H NMR (400 MHz, $\text{CDCl}_3/\text{CD}_3\text{OD}$ 10:1): δ 0.83 (3H, d, $J = 5.9$ Hz), 0.85 (3H, d, $J = 5.4$ Hz), 1.65 (3H, d, $J = 6.8$ Hz), 1.96–2.09 (3H, m), 2.12–2.22 (2H, m), 2.33 (2H, d, $J = 6.3$ Hz), 2.49–2.71 (2H, m), 3.57–3.82 (2H, m), 4.00–4.19 (2H, m), 4.33 (1H, q, $J = 5.9$ Hz), 5.37 (1H, dd, $J = 15.1, 5.9$ Hz), 5.50 (1H, dt, $J = 15.1, 6.3$ Hz), 6.67 (1H, q, $J = 5.9$ Hz), 7.18–7.28 (19H, m), 7.33–7.40 (15H, m); ^{13}C NMR (100 MHz, $\text{CDCl}_3/\text{CD}_3\text{OD}$ 10:1): δ 13.3, 17.7, 19.0, 30.0, 31.2, 31.3, 32.3, 43.1, 43.3, 53.1, 59.0, 66.4, 66.9, 68.9, 126.5 (3C), 126.8 (3C), 127.7 (6C), 127.9 (6C), 128.5, 129.3 (6C), 129.4 (6C), 131.9, 132.1, 132.6, 144.1 (3C), 144.7 (3C), 164.7, 169.8, 172.9, 176.0, 183.3; IR (neat): 3290, 3056, 3016, 2963, 2927, 1628, 1528, 1489, 1443, 1317, 1217, 1033, 744, 700 cm^{-1} ; HRMS (FAB): m/z calcd for $\text{C}_{59}\text{H}_{63}\text{N}_4\text{O}_7\text{S}_2$ ($\text{M}^+ + \text{H}$) 1003.4133, found 1003.4124.

4.1.9. (9*S*,12*R*,16*S*,*Z*)-6-Ethylidene-12-isopropyl-16-[(*E*)-4-tritylthiobut-1-enyl]-9-tritylthiomethyl-1-oxa-4,7,10,13-tetraazacyclohexadecane-2,5,8,11,14-pentaone (**28a**)

A solution of **14a** (154 mg, 0.15 mmol) in CH_2Cl_2 (15 mL) was added very slowly to a stirred solution of 2-methyl-6-nitrobenzoic anhydride (MNBA) (68.7 mg, 0.20 mmol) in CH_2Cl_2 (150 mL, 1.0 mM concentration) containing 4-dimethylaminopyridine (DMAP) (56.3 mg, 0.46 mmol) at room temperature over 10 h. After 2 h, the mixture was diluted with CH_2Cl_2 (150 mL), and the organic layer was washed with saturated aqueous NaHCO_3 (2 \times 50 mL), water (2 \times 20 mL) and brine (2 \times 50 mL), then dried over MgSO_4 . Concentration of the solvent in vacuo afforded a residue, which was purified by column chromatography (EtOAc) to give **28a** (97.3 mg, 64%) as a colorless amorphous solid. $[\alpha]_D^{28} - 24.0$ (c 1.0, CHCl_3); ^1H NMR (400 MHz, $\text{CDCl}_3/\text{CD}_3\text{OD}$ 10:1): δ 0.86 (3H, d, $J = 6.8$ Hz), 0.94 (3H, d, $J = 6.8$ Hz), 1.64 (3H, d, $J = 6.8$ Hz), 1.94–2.26 (5H, m), 2.44 (1H, dd, $J = 14.6, 2.0$ Hz), 2.58 (1H, dd, $J = 14.1, 10.2$ Hz), 2.80 (1H, dd, $J = 13.7, 4.9$ Hz), 2.86 (1H, dd, $J = 13.7, 8.8$ Hz), 3.27–3.38 (1H, m), 3.71 (1H, dd, $J = 16.6, 3.9$ Hz), 4.24–4.41 (2H, m), 5.37 (1H, dd, $J = 15.6, 6.3$ Hz), 5.54–5.62 (2H, m), 6.85 (1H, q, $J = 6.8$ Hz), 7.15–7.32 (20H, m), 7.38–7.42 (13H, m), 8.16 (1H, d, $J = 6.3$ Hz); ^{13}C NMR (100 MHz, $\text{CDCl}_3/\text{CD}_3\text{OD}$ 10:1): δ 13.2, 17.2, 19.3, 30.9, 31.1, 31.2, 31.8, 41.3, 41.6, 53.9, 58.2, 66.5, 67.0, 72.2, 126.5 (3C), 126.6 (3C), 127.7 (6C), 127.8 (6C), 128.0, 129.27 (6C), 129.34 (7C), 132.6, 135.3, 144.2 (3C), 144.6 (3C), 164.2, 168.9, 169.0, 170.5, 173.0; IR (neat): 3316, 3057, 3018, 2964, 2929, 1749, 1667, 1659, 1650, 1644, 1538, 1488, 1444, 1217, 1193, 1033, 768, 700 cm^{-1} ; HRMS (FAB): m/z calcd for $\text{C}_{59}\text{H}_{61}\text{N}_4\text{O}_6\text{S}_2$ ($\text{M}^+ + \text{H}$) 985.4027, found 985.4037.

4.1.10. FK-A1 (**13a**)

A solution of **28a** (87.7 mg, 89 μmol) in $\text{CH}_2\text{Cl}_2/\text{MeOH}$ 9:1 (22 mL) was added dropwise to a vigorously stirred solution of I_2 (226 mg, 0.89 mmol) in $\text{CH}_2\text{Cl}_2/\text{MeOH}$ 9:1 (178 mL, 0.5 mM concentration) over 10 min at room temperature. After 10 min, the reaction was quenched with 0.2 M ascorbic acid/citric acid buffer

(10 mL, adjusted to pH 4.0) at room temperature. The resulting mixture was diluted with CH_2Cl_2 (100 mL) and water (50 mL). The organic layer was washed with brine (2 \times 50 mL) and dried over MgSO_4 . Concentration of the solvent in vacuo afforded a residue, which was purified by column chromatography ($\text{CHCl}_3/\text{MeOH}$, 15:1) to give **13a** (42.8 mg, 97%) as a colorless amorphous solid. $[\alpha]_D^{28} + 54.9$ (c 1.0, CHCl_3); ^1H NMR (400 MHz, $\text{CDCl}_3/\text{CD}_3\text{OD}$ 10:1): δ 1.11 (3H, d, $J = 6.3$ Hz), 1.12 (3H, d, $J = 6.3$ Hz), 1.76 (3H, d, $J = 6.8$ Hz), 2.24 (1H, dq, $J = 12.7, 6.8$ Hz), 2.41–2.53 (1H, m), 2.66–2.78 (2H, m), 2.81 (1H, dd, $J = 13.2, 6.3$ Hz), 2.93 (1H, ddd, $J = 13.2, 8.8, 3.4$ Hz), 3.13–3.25 (3H, m), 3.97 (1H, dd, $J = 4.9, 3.4$ Hz), 4.10 (1H, dd, $J = 18.0, 3.9$ Hz), 4.26 (1H, dd, $J = 17.6, 4.9$ Hz), 4.82 (1H, q, $J = 5.4$ Hz), 5.72–5.91 (3H, m), 6.71 (1H, q, $J = 7.3$ Hz), 7.03 (1H, t, $J = 4.1$ Hz), 7.67 (1H, d, $J = 6.3$ Hz), 8.01 (1H, d, $J = 2.9$ Hz), 8.55 (1H, s); ^{13}C NMR (100 MHz, $\text{CDCl}_3/\text{CD}_3\text{OD}$ 10:1): δ 13.6, 18.8, 18.9, 29.2, 30.4, 35.5, 37.3, 38.0, 42.8, 56.3, 62.5, 69.7, 128.0, 129.0, 129.5, 132.6, 164.2, 166.9, 168.7, 171.6, 172.1; IR (neat): 3434, 3356, 3011, 2965, 2929, 1748, 1650, 1519, 1406, 1252, 979, 753 cm^{-1} ; HRMS (FAB): m/z calcd for $\text{C}_{21}\text{H}_{31}\text{N}_4\text{O}_6\text{S}_2$ ($\text{M}^+ + \text{H}$) 499.1680, found 499.1695.

4.1.11. Fmoc-Gly-Gly-OMe (**30b**)

Compound **30b** was synthesized from Gly (**18b**) (300 mg, 4.0 mmol) in a manner similar to that described for the synthesis of **21**. Purification by column chromatography ($\text{CHCl}_3/\text{MeOH}$ 30:1) gave **30b** (1.12 g, 78%, 2 steps) as colorless amorphous solid. ^1H NMR (400 MHz, CDCl_3): δ 3.76 (3H, s), 3.93 (2H, d, $J = 4.9$ Hz), 4.06 (2H, d, $J = 4.9$ Hz), 4.23 (1H, t, $J = 6.8$ Hz), 4.45 (2H, d, $J = 6.8$ Hz), 5.47 (1H, br s), 6.48 (1H, br s), 7.31 (2H, td, $J = 7.3, 1.0$ Hz), 7.40 (2H, t, $J = 7.3$ Hz), 7.59 (2H, d, $J = 7.3$ Hz), 7.77 (2H, d, $J = 7.3$ Hz); ^{13}C NMR (100 MHz, CDCl_3): δ 41.1, 44.3, 47.1, 52.4, 67.2, 120.0 (2C), 125.0 (2C), 127.0 (2C), 127.7 (2C), 141.3 (2C), 143.7 (2C), 156.6, 169.3, 170.1; IR (KBr): 3387, 3294, 3076, 2948, 1742, 1715, 1653, 1555, 1536, 1285, 1243, 1234, 1166, 756, 733 cm^{-1} ; HRMS (EI): m/z calcd for $\text{C}_{20}\text{H}_{20}\text{N}_2\text{O}_5$ (M^+) 368.1372, found 368.1364.

4.1.12. Boc-D-Cys(Tr)-Gly-Gly-OMe (**32b**)

Compound **32b** was synthesized from **30b** (500 mg, 1.4 mmol) in a manner similar to that described for the synthesis of **23**. Purification by column chromatography ($\text{CHCl}_3/\text{MeOH}$ 20:1) gave **32b** (588 mg, 73%, 2 steps) as a colorless amorphous solid. $[\alpha]_D^{28} - 14.4$ (c 1.0, CHCl_3); ^1H NMR (400 MHz, CDCl_3): δ 1.40 (9H, s), 2.63 (1H, dd, $J = 12.9, 5.4$ Hz), 2.76 (1H, dd, $J = 12.7, 7.3$ Hz), 3.65–3.73 (4H, m), 3.89 (2H, d, $J = 5.9$ Hz), 3.95 (2H, t, $J = 5.4$ Hz), 4.79 (1H, br d, $J = 4.4$ Hz), 6.51 (1H, br t, $J = 5.9$ Hz), 7.00 (1H, br s), 7.22–7.32 (9H, m), 7.40–7.42 (6H, m); ^{13}C NMR (100 MHz, CDCl_3): δ 28.2 (3C), 33.6, 40.8, 42.9, 52.2, 54.0, 67.3, 80.7, 127.0 (3C), 128.1 (6C), 129.5 (6C), 144.2 (3C), 155.6, 169.0, 169.9, 170.9; IR (neat): 3317, 3008, 2978, 1749, 1667, 1521, 1490, 1443, 1367, 1247, 1214, 1166, 1033, 852, 752, 700 cm^{-1} ; HRMS (FAB): m/z calcd for $\text{C}_{32}\text{H}_{38}\text{N}_3\text{O}_6\text{S}$ ($\text{M}^+ + \text{H}$) 592.2476, found 592.2475.

4.1.13. H₂N-D-Cys(Tr)-Gly-Gly-OMe (**15b**)

Compound **15b** was synthesized from **32b** (1.46 g, 2.5 mmol) in a manner similar to that described for the synthesis of **15a**. Purification by column chromatography ($\text{CHCl}_3/\text{MeOH}$ 20:1) gave **15b** (873 mg, 72%) as a colorless amorphous solid. $[\alpha]_D^{28} - 13.8$ (c 1.1, CHCl_3); ^1H NMR (400 MHz, CDCl_3): δ 1.48 (2H, br s), 2.69 (2H, d, $J = 5.9$ Hz), 3.16 (1H, t, $J = 5.9$ Hz), 3.70 (3H, s), 3.80–3.99 (4H, m), 6.82 (1H, t, $J = 5.9$ Hz), 7.20–7.31 (9H, m), 7.41–7.43 (6H, m), 7.69 (1H, t, $J = 5.9$ Hz); ^{13}C NMR (100 MHz, CDCl_3): δ 37.3, 40.8, 42.8, 52.2, 53.8, 66.9, 126.8 (3C), 128.0 (6C), 129.5 (6C), 144.4 (3C), 169.2, 169.9, 173.8; IR (neat): 3353, 3317, 3057, 2951, 1748, 1660, 1520, 1489, 1443, 1372, 1212, 1183, 1033, 984, 886, 848, 745, 700 cm^{-1} ; HRMS (FAB): m/z calcd for $\text{C}_{27}\text{H}_{30}\text{N}_3\text{O}_4\text{S}$ ($\text{M}^+ + \text{H}$) 492.1952, found 492.1942.

4.1.14. (7S,11R,14S,E)-Methyl 11-isopropyl-7-(4-methoxybenzyloxy)-9,12,15,18-tetraoxo-1,1,1-triphenyl-14-tritylthiomethyl-2-thia-10,13,16,19-tetraazahenicos-5-en-21-oate (26b)

Compound **26b** was synthesized from **15b** (77.1 mg, 0.16 mmol) in a manner similar to that described for the synthesis of **26a**. Purification by column chromatography (CHCl₃/MeOH 30:1) gave **26b** (152 mg, 87%) as a colorless amorphous solid. [α]_D²⁷ +10.4 (c 1.0, CHCl₃); ¹H NMR (400 MHz, CDCl₃): δ 0.73 (3H, d, *J* = 6.8 Hz), 0.82 (3H, d, *J* = 6.8 Hz), 1.95 (1H, dq, *J* = 13.2, 6.8 Hz), 2.06–2.16 (2H, m), 2.21–2.25 (2H, m), 2.44 (2H, d, *J* = 5.9 Hz), 2.58 (1H, dd, *J* = 13.2, 5.9 Hz), 2.78 (1H, dd, *J* = 13.2, 6.8 Hz), 3.65 (3H, s), 3.75 (3H, s), 3.81–3.89 (3H, m), 3.96 (2H, dt, *J* = 18.0, 6.3 Hz), 4.08 (1H, q, *J* = 6.3 Hz), 4.14 (1H, t, *J* = 6.8 Hz), 4.21 (1H, d, *J* = 10.7 Hz), 4.41 (1H, d, *J* = 10.7 Hz), 5.29 (1H, dd, *J* = 15.1, 8.3 Hz), 5.54 (1H, dt, *J* = 15.1, 6.8 Hz), 6.81 (2H, d, *J* = 8.3 Hz), 6.97 (1H, d, *J* = 7.3 Hz), 7.02 (1H, t, *J* = 5.6 Hz), 7.15–7.30 (22H, m), 7.35–7.42 (12H, m); ¹³C NMR (100 MHz, CDCl₃): δ 17.8, 19.3, 29.9, 31.2, 31.3, 33.3, 40.8, 42.3, 42.8, 52.1, 52.6, 55.2, 59.0, 66.5, 67.0, 70.0, 76.5, 113.7 (2C), 126.5 (3C), 126.8 (3C), 127.8 (6C), 128.0 (6C), 129.4 (6C), 129.5 (6C), 129.6, 129.8 (2C), 129.9, 133.2, 144.2 (3C), 144.7 (3C), 159.3, 169.1, 169.9, 170.2, 171.5, 171.6; IR (neat): 3287, 3082, 3058, 3016, 2960, 2931, 1744, 1691, 1634, 1513, 1490, 1443, 1247, 1216, 1181, 1079, 1034, 975, 822, 752, 700 cm⁻¹; HRMS (FAB): *m/z* calcd for C₆₆H₇₁N₄O₈S₂ (M⁺+H) 1111.4708, found 1111.4731.

4.1.15. (7S,11R,14S,E)-Methyl 7-hydroxy-11-isopropyl-9,12,15,18-tetraoxo-1,1,1-triphenyl-14-tritylthiomethyl-2-thia-10,13,16,19-tetraazahenicos-5-en-21-oate (27b)

Compound **27b** was synthesized from **26b** (108 mg, 97 μ mol) in a manner similar to that described for the synthesis of **27a**. Purification by column chromatography (CHCl₃/MeOH 30:1) gave **27b** (95.6 mg, 99%) as a colorless amorphous solid. [α]_D²⁶ –17.0 (c 1.0, CHCl₃); ¹H NMR (400 MHz, CDCl₃): δ 0.89 (3H, d, *J* = 6.8 Hz), 0.93 (3H, d, *J* = 6.8 Hz), 2.03–2.08 (2H, m), 2.12–2.22 (3H, m), 2.28 (1H, dd, *J* = 13.7, 9.8 Hz), 2.39 (1H, dd, *J* = 13.7, 2.9 Hz), 2.61–2.69 (2H, m), 3.60 (3H, s), 3.73 (1H, dd, *J* = 17.1, 5.4 Hz), 3.79 (1H, dd, *J* = 18.0, 5.4 Hz), 3.89 (1H, br s), 3.96 (1H, dd, *J* = 18.0, 5.9 Hz), 4.03 (1H, dd, *J* = 16.6, 6.3 Hz), 4.18 (1H, t, *J* = 6.3 Hz), 4.23 (1H, q, *J* = 7.1 Hz), 4.33–4.43 (1H, m), 5.38 (1H, dd, *J* = 15.1, 5.9 Hz), 5.53 (1H, dt, *J* = 15.1, 6.3 Hz), 6.54 (1H, d, *J* = 6.8 Hz), 7.14–7.28 (20H, m), 7.31–7.41 (13H, m); ¹³C NMR (100 MHz, CDCl₃): δ 17.7, 19.4, 29.4, 31.2 (2C), 33.4, 40.8, 43.0, 43.7, 52.2, 52.3, 59.5, 66.5, 66.8, 69.4, 126.5 (3C), 126.8 (3C), 127.8 (6C), 127.9 (6C), 129.4 (6C), 129.5 (6C), 129.7, 132.6, 144.2 (3C), 144.7 (3C), 169.5, 170.46, 170.50, 171.3, 172.8; IR (neat): 3289, 3082, 3058, 3016, 2962, 2929, 1744, 1635, 1531, 1489, 1443, 1216, 1183, 1082, 1033, 973, 851, 752, 700 cm⁻¹; HRMS (FAB): *m/z* calcd for C₅₈H₆₃N₄O₇S₂ (M⁺+H) 991.4133, found 991.4120.

4.1.16. (7S,11R,14S,E)-7-Hydroxy-11-isopropyl-9,12,15,18-tetraoxo-1,1,1-triphenyl-14-tritylthiomethyl-2-thia-10,13,16,19-tetraazahenicos-5-en-21-oic acid (14b)

Compound **14b** was synthesized from **27b** (106 mg, 0.11 mmol) in a manner similar to that described for the synthesis of **14a**. Purification by column chromatography (CHCl₃/MeOH 5:1) gave **14b** (79.5 mg, 76%) as a colorless amorphous solid. [α]_D²⁹ –12.5 (c 1.0, CHCl₃). ¹H NMR (400 MHz, CD₃OD/CDCl₃ 5:1): δ 0.93 (3H, d, *J* = 5.8 Hz), 0.94 (3H, d, *J* = 6.3 Hz), 1.98–2.07 (2H, m), 2.09–2.21 (3H, m), 2.35 (1H, dd, *J* = 13.5, 4.3 Hz), 2.46 (1H, dd, *J* = 13.5, 9.2 Hz), 2.62 (1H, dd, *J* = 12.6, 8.7 Hz), 2.70 (1H, dd, *J* = 12.6, 5.8 Hz), 3.74 (1H, d, *J* = 16.9 Hz), 3.76 (2H, s), 3.96 (1H, d, *J* = 16.9 Hz), 4.12–4.15 (2H, m), 4.36–4.40 (1H, m), 5.42 (1H, dd, *J* = 15.0, 6.3 Hz), 5.54 (1H, dt, *J* = 15.0, 6.8 Hz), 7.13–7.24 (18H, m), 7.24–7.39 (12H, m); ¹³C NMR (100 MHz, CD₃OD/CDCl₃ 5:1, 40 °C): δ 18.4, 19.7, 30.9, 32.2,

32.4, 34.0, 42.1, 43.4, 44.1, 54.0, 60.6, 67.6, 67.9, 70.2, 127.5 (3C), 127.7, (3C), 128.6 (6C), 128.8 (6C), 130.4 (6C), 130.46, 130.50 (6C), 134.1, 145.5 (3C), 146.0 (3C), 171.3, 172.2, 173.3, 173.5, 174.5; IR (neat): 3299, 3057, 3017, 2964, 2928, 1725, 1635, 1536, 1488, 1444, 1218, 1033, 971, 752, 700 cm⁻¹; HRMS (FAB): *m/z* calcd for C₅₇H₆₁N₄O₇S₂ (M⁺+H) 977.3976, found 977.3962.

4.1.17. (9S,12R,16S)-12-Isopropyl-16-[(E)-4-tritylthiobut-1-enyl]-9-tritylthiomethyl-1-oxa-4,7,10,13-tetraazacyclohexadecane-2,5,8,11,14-pentaone (28b)

Compound **28b** was synthesized from **14b** (72.1 mg, 74 μ mol) in a manner similar to that described for the synthesis of **28a**. Purification by column chromatography (CHCl₃/MeOH 30:1) gave **28b** (59.9 mg, 85%) as a colorless amorphous solid. [α]_D²⁹ –24.5 (c 1.0, CHCl₃); ¹H NMR (400 MHz, CDCl₃): δ 0.79 (3H, d, *J* = 6.8 Hz), 0.91 (3H, d, *J* = 6.3 Hz), 1.85–2.03 (2H, m), 2.08–2.24 (3H, m), 2.42 (1H, dd, *J* = 13.7, 9.8 Hz), 2.47–2.54 (1H, m), 2.75 (1H, dd, *J* = 13.2, 3.9 Hz), 2.86 (1H, dd, *J* = 13.2, 9.8 Hz), 3.32–3.42 (1H, m), 3.42–3.55 (2H, m), 4.30 (1H, dd, *J* = 17.1, 8.3 Hz), 4.46 (1H, dd, *J* = 16.6, 9.3 Hz), 4.72 (1H, dd, *J* = 9.3, 3.9 Hz), 5.34 (1H, dd, *J* = 15.6, 6.3 Hz), 5.49–5.64 (2H, m), 6.30 (1H, d, *J* = 8.8 Hz), 7.12–7.28 (20H, m), 7.33–7.39 (12H, m), 8.08 (1H, d, *J* = 5.9 Hz); ¹³C NMR (100 MHz, CDCl₃): δ 16.7, 19.6, 30.9, 31.4, 31.6, 32.4, 40.9, 42.7, 43.6, 54.8, 56.6, 66.7, 67.0, 72.4, 126.6 (3C), 126.7, (3C), 127.6, 127.8 (6C), 127.9 (6C), 129.4 (6C), 129.5 (6C), 132.5, 144.5 (3C), 144.7 (3C), 169.8, 169.9, 170.2, 170.4, 172.7; IR (neat): 3300, 3057, 3018, 2964, 2931, 1737, 1661, 1539, 1489, 1444, 1214, 1033, 974, 744, 700 cm⁻¹; HRMS (FAB): *m/z* calcd for C₅₇H₅₉N₄O₆S₂ (M⁺+H) 959.3871, found 959.3891.

4.1.18. FK-A2 (13b)

Compound **13b** was synthesized from **28b** (59.9 mg, 62 μ mol) in a manner similar to that described for the synthesis of **13a**. Purification by column chromatography (CHCl₃/MeOH 10:1) gave **13b** (22.0 mg, 75%) as a colorless amorphous solid. [α]_D²⁴ –39.7 (c 0.70, CHCl₃); ¹H NMR (400 MHz, CDCl₃): δ 1.09 (3H, d, *J* = 3.4 Hz), 1.10 (3H, d, *J* = 2.9 Hz), 2.30 (1H, dq, *J* = 12.1, 6.3 Hz), 2.45–2.60 (1H, m), 2.63–2.80 (2H, m), 2.88–2.99 (2H, m), 3.08 (1H, ddd, *J* = 13.0, 9.7, 2.9 Hz), 3.18 (1H, dd, *J* = 15.0, 4.3 Hz), 3.27 (1H, dd, *J* = 15.5, 10.1 Hz), 3.51 (1H, dd, *J* = 16.4, 3.4 Hz), 4.04 (1H, t, *J* = 3.9 Hz), 4.10–4.21 (2H, m), 4.44 (1H, dd, *J* = 16.4, 8.7 Hz), 4.76–4.84 (1H, m), 5.68–5.82 (2H, m), 5.82–5.95 (1H, m), 6.78 (1H, d, *J* = 2.9 Hz), 6.95 (1H, t, *J* = 4.3 Hz), 7.49 (1H, d, *J* = 6.8 Hz), 7.68 (1H, dd, *J* = 8.2, 2.9 Hz); ¹³C NMR (100 MHz, CDCl₃): δ 18.6, 19.4, 29.3, 31.1, 37.1, 37.5, 39.2, 42.3, 43.5, 55.9, 62.3, 69.7, 129.1, 129.5, 167.0, 168.9, 170.3, 171.2, 171.3; IR (neat): 3298, 3011, 2965, 2932, 1742, 1658, 1529, 1258, 1191, 1031, 979, 754 cm⁻¹; HRMS (EI): *m/z* calcd for C₁₉H₂₈N₄O₆S₂ (M⁺) 472.1450, found 472.1463.

4.1.19. Fmoc-D-Ala-Gly-OMe (30c)

Compound **30c** was synthesized from D-alanine (D-Ala) (**18c**) (500 mg, 5.6 mmol) in a manner similar to that described for the synthesis of **21**. Purification by column chromatography (hexane/EtOAc 2:3) gave **30c** (1.98 g, 92%, 2 steps) as a colorless amorphous solid. [α]_D²⁹ +13.5 (c 1.1, CHCl₃); ¹H NMR (400 MHz, CDCl₃): δ 1.40 (3H, d, *J* = 6.8 Hz), 3.70 (3H, s), 4.01 (2H, d, *J* = 4.8 Hz), 4.19 (1H, t, *J* = 6.8 Hz), 4.29–4.40 (1H, m), 4.39 (2H, d, *J* = 6.8 Hz), 5.61 (1H, d, *J* = 7.7 Hz), 6.82 (1H, br s), 7.29 (2H, t, *J* = 7.2 Hz), 7.38 (2H, t, *J* = 7.2 Hz), 7.57 (2H, dd, *J* = 7.2, 3.6 Hz), 7.74 (2H, d, *J* = 7.7 Hz); ¹³C NMR (100 MHz, CDCl₃): δ 18.5, 41.2, 47.1, 50.4, 52.4, 67.1, 120.0 (2C), 125.0 (2C), 127.1 (2C), 127.7 (2C), 141.3 (2C), 143.7 (2C), 156.0, 170.1, 172.5; IR (KBr): 3323, 3293, 3067, 2982, 2951, 2940, 2890, 1731, 1720, 1693, 1648, 1541, 1449, 1329, 1301, 1266, 1254, 1105, 1089, 1051, 1023, 758, 741, 670, 645 cm⁻¹; HRMS (EI): *m/z* calcd for C₂₁H₂₂N₂O₅ (M⁺) 382.1529, found 382.1526.

4.1.20. Boc-D-Cys(Tr)-D-Ala-Gly-OMe (**32c**)

Compound **32c** was synthesized from **30c** (200 mg, 0.52 mmol) in a manner similar to that described for the synthesis of **23**. Purification by column chromatography (hexane/EtOAc 1:2) gave **32c** (260 mg, 82%, 2 steps) as a colorless amorphous solid. $[\alpha]_D^{24} +5.3$ (c 1.0, CHCl₃); ¹H NMR (400 MHz, CDCl₃): δ 1.36 (3H, d, *J* = 6.8 Hz), 1.41 (9H, s), 2.61 (1H, dd, *J* = 12.9, 5.9 Hz), 2.70 (1H, dd, *J* = 12.7, 6.8 Hz), 3.69 (3H, s), 3.70–3.84 (2H, m), 3.96 (1H, dd, *J* = 17.6, 5.9 Hz), 4.47 (1H, dq, *J* = 7.4, 7.2 Hz), 4.81 (1H, br s), 6.35 (1H, br s), 6.96 (1H, br s), 7.21–7.32 (9H, m), 7.41–7.43 (6H, m); ¹³C NMR (100 MHz, CDCl₃): δ 17.9, 28.1 (3C), 33.7, 40.8, 48.6, 52.0, 53.4, 67.0, 80.2, 126.8 (3C), 127.9 (6C), 129.3 (6C), 144.1 (3C), 155.3, 169.8, 170.2, 172.0; IR (neat): 3285, 3058, 2978, 2928, 1756, 1680, 1645, 1523, 1491, 1445, 1367, 1209, 1167, 1049, 1020, 851, 751, 700 cm⁻¹; HRMS (FAB): *m/z* calcd for C₃₃H₄₀N₃O₆S (M⁺+H) 606.2632, found 606.2641.

4.1.21. H₂N-D-Cys(Tr)-D-Ala-Gly-OMe (**15c**)

Compound **15c** was synthesized from **32c** (70.0 mg, 0.12 mmol) in a manner similar to that described for the synthesis of **15a**. Purification by column chromatography (CHCl₃/MeOH 20:1) gave **15c** (52.0 mg, 89%) as a colorless amorphous solid. $[\alpha]_D^{25} +26.9$ (c 1.0, CHCl₃); ¹H NMR (400 MHz, CDCl₃): δ 1.35 (3H, d, *J* = 6.8 Hz), 1.42 (2H, br s), 2.58 (1H, dd, *J* = 12.6, 8.2 Hz), 2.70 (1H, dd, *J* = 12.6, 4.3 Hz), 3.00 (1H, dd, *J* = 8.2, 4.3 Hz), 3.71 (3H, s), 3.89 (1H, dd, *J* = 17.9, 5.3 Hz), 3.98 (1H, dd, *J* = 17.9, 5.3 Hz), 4.42 (1H, quint, *J* = 7.2 Hz), 6.87 (1H, t, *J* = 5.3 Hz), 7.20–7.31 (9H, m), 7.39–7.45 (7H, m); ¹³C NMR (100 MHz, CDCl₃): δ 17.4, 37.1, 41.0, 48.3, 52.2, 53.9, 67.0, 126.8 (3C), 128.0 (6C), 129.5 (6C), 144.5 (3C), 170.0, 172.2, 173.4; IR (neat): 3311, 3057, 3016, 2952, 1751, 1652, 1514, 1444, 1369, 1211, 1182, 1032, 982, 886, 848, 746, 700 cm⁻¹; HRMS (FAB): *m/z* calcd for C₂₈H₃₂N₃O₄S (M⁺+H) 506.2108, found 506.2106.

4.1.22. (7S,11R,14S,17R,E)-Methyl 11-isopropyl-7-(4-methoxybenzyloxy)-17-methyl-9,12,15,18-tetraoxo-1,1,1-triphenyl-14-tritylthiomethyl-2-thia-10,13,16,19-tetraazahenicos-5-en-21-oate (**26c**)

Compound **26c** was synthesized from **15c** (101 mg, 0.20 mmol) in a manner similar to that described for the synthesis of **26a**. Purification by column chromatography (CHCl₃/MeOH 30:1) gave **26c** (193 mg, 86%) as a colorless amorphous solid. $[\alpha]_D^{27} -0.39$ (c 1.0, CHCl₃); ¹H NMR (400 MHz, CDCl₃): δ 0.72 (3H, d, *J* = 6.8 Hz), 0.79 (3H, d, *J* = 6.8 Hz), 1.33 (3H, d, *J* = 6.8 Hz), 1.96 (1H, dq, *J* = 13.4, 6.7 Hz), 2.05–2.15 (2H, m), 2.21–2.25 (2H, m), 2.38–2.52 (3H, m), 2.70 (1H, dd, *J* = 13.2, 7.3 Hz), 3.65 (3H, s), 3.76 (3H, s), 3.89 (2H, d, *J* = 5.4 Hz), 4.00 (1H, td, *J* = 4.4, 2.9 Hz), 4.08 (1H, q, *J* = 6.3 Hz), 4.19 (1H, d, *J* = 10.7 Hz), 4.30 (1H, t, *J* = 7.1 Hz), 4.34 (1H, d, *J* = 10.7 Hz), 4.72 (1H, dq, *J* = 7.2, 7.1 Hz), 5.28 (1H, dd, *J* = 16.4, 7.8 Hz), 5.51 (1H, dt, *J* = 15.1, 6.8 Hz), 6.81 (2H, d, *J* = 8.3 Hz), 6.91 (1H, br s), 7.14–7.28 (22H, m), 7.35–7.42 (12H, m), 7.49 (1H, br s); ¹³C NMR (100 MHz, CDCl₃): δ 17.9, 18.3, 19.2, 30.6, 31.2, 31.3, 34.0, 41.0, 42.5, 48.7, 52.0, 52.1, 55.2, 58.8, 66.5, 67.0, 69.9, 76.4, 113.7 (2C), 126.6 (3C), 126.8 (3C), 127.8 (6C), 128.0 (6C), 129.4 (6C), 129.5 (6C), 129.7, 129.8 (2C), 130.0, 133.1, 144.2 (3C), 144.8 (3C), 159.2, 169.4, 170.0, 171.3 (2C), 172.3; IR (neat): 3277, 3082, 3059, 3029, 3018, 2960, 2931, 1752, 1692, 1631, 1537, 1489, 1444, 1246, 1215, 1181, 1080, 1034, 976, 822, 752, 700 cm⁻¹; HRMS (FAB): *m/z* calcd for C₆₇H₇₃N₄O₈S₂ (M⁺+H) 1125.4864, found 1125.4873.

4.1.23. (7S,11R,14S,17R,E)-Methyl 7-hydroxy-11-isopropyl-17-methyl-9,12,15,18-tetraoxo-1,1,1-triphenyl-14-tritylthiomethyl-2-thia-10,13,16,19-tetraazahenicos-5-en-21-oate (**27c**)

Compound **27c** was synthesized from **26c** (193 mg, 0.17 mmol) in a manner similar to that described for the synthesis of **27a**. Purification by column chromatography (CHCl₃/MeOH 40:1) gave **27c** (140 mg, 81%) as a colorless amorphous solid. $[\alpha]_D^{27} -1.6$ (c 1.0,

CHCl₃); ¹H NMR (400 MHz, CDCl₃): δ 0.89 (3H, d, *J* = 7.3 Hz), 0.96 (3H, d, *J* = 6.8 Hz), 1.40 (3H, d, *J* = 7.3 Hz), 2.05–2.10 (2H, m), 2.20–2.28 (4H, m), 2.36 (1H, dd, *J* = 13.7, 2.9 Hz), 2.53–2.63 (2H, m), 2.92 (1H, br s), 3.67 (3H, s), 3.81 (1H, dd, *J* = 18.0, 5.4 Hz), 3.96 (1H, dd, *J* = 18.0, 5.9 Hz), 4.10–4.20 (2H, m), 4.29–4.33 (1H, m), 4.42 (1H, quint, *J* = 7.3 Hz), 5.36 (1H, dd, *J* = 15.6, 6.3 Hz), 5.39 (1H, dt, *J* = 15.6, 6.3 Hz), 6.20 (1H, d, *J* = 6.8 Hz), 6.81 (1H, d, *J* = 7.8 Hz), 7.01 (1H, t, *J* = 4.9 Hz), 7.05 (1H, d, *J* = 7.3 Hz), 7.17–7.30 (18H, m), 7.36–7.42 (12H, m); ¹³C NMR (100 MHz, CDCl₃): δ 17.9, 18.1, 19.2, 30.4, 31.30, 31.32, 33.9, 41.0, 43.5, 49.0, 52.0, 52.2, 58.8, 66.6, 66.8, 69.6, 126.6 (3C), 126.9 (3C), 127.8 (6C), 128.0 (6C), 129.4 (6C), 129.5 (6C), 130.0, 132.5, 144.2 (3C), 144.8 (3C), 169.7, 170.3, 171.3, 172.2, 172.3; IR (neat): 3279, 3083, 3060, 3030, 3017, 2963, 2928, 1746, 1691, 1632, 1537, 1488, 1444, 1217, 1183, 1081, 1033, 971, 853, 751, 699 cm⁻¹; HRMS (FAB): *m/z* calcd for C₅₉H₆₅N₄O₇S₂ (M⁺+H) 1005.4289, found 1005.4321.

4.1.24. (7S,11R,14S,17R,E)-7-Hydroxy-11-isopropyl-17-methyl-9,12,15,18-tetraoxo-1,1,1-triphenyl-14-tritylthiomethyl-2-thia-10,13,16,19-tetraazahenicos-5-en-21-oic acid (**14c**)

Compound **14c** was synthesized from **27c** (106 mg, 0.11 mmol) in a manner similar to that described for the synthesis of **14a**. Purification by column chromatography (CHCl₃/MeOH 5:1) gave **14c** (134 mg, 97%) as a colorless amorphous solid. $[\alpha]_D^{29} -15.4$ (c 1.0, CHCl₃); ¹H NMR (400 MHz, CD₃OD/CDCl₃ 3:1): δ 0.91 (3H, d, *J* = 6.8 Hz), 0.93 (3H, d, *J* = 7.3 Hz), 1.34 (3H, d, *J* = 6.8 Hz), 2.01–2.06 (2H, m), 2.10–2.21 (3H, m), 2.36 (1H, dd, *J* = 13.7, 4.4 Hz), 2.46 (1H, dd, *J* = 13.7, 8.8 Hz), 2.57 (1H, dd, *J* = 11.7, 8.8 Hz), 2.64 (1H, dd, *J* = 12.2, 5.9 Hz), 3.69 (1H, d, *J* = 17.6 Hz), 3.79 (1H, d, *J* = 18.0 Hz), 4.16 (1H, d, *J* = 5.9 Hz), 4.18–4.26 (1H, m), 4.30–4.43 (2H, m), 5.43 (1H, dd, *J* = 15.6, 5.9 Hz), 5.53 (1H, dt, *J* = 15.1, 6.3 Hz), 7.14–7.24 (18H, m), 7.33–7.39 (12H, m); ¹³C NMR (100 MHz, CD₃OD/CDCl₃ 3:1): δ 18.0, 18.3, 19.7, 30.9, 32.2, 32.3, 34.0, 42.5, 44.1, 50.2, 53.7, 60.4, 67.5, 67.8, 70.3, 127.5 (3C), 127.7, (3C), 128.6 (6C), 128.8 (6C), 130.36 (6C), 130.44 (6C), 130.5, 133.9, 145.4 (3C), 145.9 (3C), 171.4, 173.4, 173.9, 174.1, 174.2; IR (neat): 3291, 3057, 3017, 2965, 2929, 1727, 1636, 1527, 1490, 1444, 1405, 1217, 1034, 971, 754, 700 cm⁻¹; HRMS (FAB): *m/z* calcd for C₅₈H₆₂N₄O₇S₂Na (M⁺+Na) 1013.3952, found 1013.3991.

4.1.25. (6R,9S,12R,16S)-12-Isopropyl-6-methyl-16-[(E)-4-tritylthiobut-1-enyl]-9-tritylthiomethyl-1-oxa-4,7,10,13-tetraazacyclohexadecane-2,5,8,11,14-pentaone (**28c**)

Compound **28c** was synthesized from **14c** (134 mg, 0.14 mmol) in a manner similar to that described for the synthesis of **28a**. Purification by column chromatography (CHCl₃/MeOH 40:1) gave **28c** (108 mg, 85%) as a colorless amorphous solid. $[\alpha]_D^{27} -2.2$ (c 1.0, CHCl₃); ¹H NMR (400 MHz, CDCl₃): δ 0.85 (3H, d, *J* = 6.8 Hz), 0.92 (3H, d, *J* = 6.8 Hz), 1.44 (3H, d, *J* = 7.3 Hz), 1.92–2.17 (5H, m), 2.38 (1H, dd, *J* = 14.1, 9.8 Hz), 2.43–2.52 (1H, m), 2.64 (1H, dd, *J* = 12.7, 5.4 Hz), 2.81 (1H, dd, *J* = 12.2, 8.8 Hz), 3.56 (1H, q, *J* = 6.8 Hz), 3.90–4.02 (2H, m), 4.16 (1H, quint, *J* = 7.3 Hz), 4.25 (1H, t, *J* = 7.1 Hz), 5.31 (1H, dd, *J* = 15.6, 6.3 Hz), 5.49–5.61 (2H, m), 6.33 (1H, d, *J* = 8.3 Hz), 7.16–7.30 (20H, m), 7.36–7.39 (12H, m), 7.81 (1H, br s); ¹³C NMR (100 MHz, CDCl₃, 40 °C): δ 16.7, 18.0, 19.6, 30.9, 31.1, 31.4, 31.8, 41.7, 42.4, 50.2, 56.0, 58.4, 66.7, 67.2, 72.1, 126.6 (3C), 126.9 (3C), 127.9 (6C), 128.0, 128.1 (6C), 129.4 (6C), 129.6 (6C), 132.5, 144.4 (3C), 144.9 (3C), 168.9, 169.8, 170.2, 172.2, 173.0; IR (neat): 3307, 3057, 3016, 2964, 2932, 1745, 1660, 1651, 1538, 1490, 1444, 1265, 1215, 1033, 972, 750, 700 cm⁻¹. HRMS (FAB): *m/z* calcd for C₅₈H₆₀N₄O₆S₂Na (M⁺+Na) 995.3846, found 995.3847.

4.1.26. FK-A3 (**13c**)

Compound **13c** was synthesized from **28c** (108 mg, 0.11 mmol) in a manner similar to that described for the synthesis of **13a**.

Purification by column chromatography (CHCl₃/MeOH 20:1) gave **13c** (42.4 mg, 79%) as a colorless amorphous solid. [α]_D²⁵ +19.8 (c 1.0, CHCl₃); ¹H NMR (400 MHz, CDCl₃): δ 1.09 (6H, d, J = 5.9 Hz), 1.54 (3H, d, J = 6.8 Hz), 2.23 (1H, dq, J = 12.7, 6.8 Hz), 2.49–2.59 (1H, m), 2.66–2.77 (2H, m), 2.94–3.03 (3H, m), 3.11 (1H, ddd, J = 13.2, 9.3, 3.4 Hz), 3.33 (1H, dd, J = 16.1, 11.2 Hz), 3.77 (1H, q, J = 6.8 Hz), 3.88 (1H, dd, J = 17.6, 2.0 Hz), 4.06 (1H, dd, J = 5.9, 4.4 Hz), 4.41 (1H, dd, J = 17.6, 6.3 Hz), 4.76 (1H, ddd, J = 11.2, 7.3, 3.9 Hz), 5.69–5.80 (2H, m), 5.80–5.91 (1H, m), 6.64 (1H, d, J = 3.9 Hz), 7.11 (1H, d, J = 3.9 Hz), 7.59 (1H, d, J = 7.3 Hz), 7.73 (1H, d, J = 6.3 Hz); ¹³C NMR (100 MHz, CDCl₃): δ 15.1, 19.3, 19.5, 29.2, 31.1, 34.2, 37.5, 38.1, 43.1, 51.2, 55.1, 62.0, 69.4, 129.7, 130.3, 168.0, 170.03, 170.05, 170.8, 172.4; IR (neat): 3342, 3012, 2965, 2934, 1742, 1659, 1525, 1260, 1186, 1024, 979, 754 cm⁻¹; HRMS (EI): m/z calcd for C₂₀H₃₀N₄O₆S₂ (M⁺) 486.1607, found 486.1616.

4.1.27. Fmoc-L-Ala-Gly-OMe (**30d**)

Compound **30d** was synthesized from L-alanine (L-Ala) (**18d**) (500 mg, 5.6 mmol) in a manner similar to that described for the synthesis of **21**. Purification by column chromatography (hexane/EtOAc, 2:3) gave **30d** (1.99 g, 93%, 2 steps) as a colorless amorphous solid. [α]_D²⁹ –13.2 (c 1.0, CHCl₃); ¹H NMR (400 MHz, CDCl₃): δ 1.41 (3H, d, J = 6.3 Hz), 3.72 (3H, s), 4.02 (2H, d, J = 4.9 Hz), 4.20 (1H, t, J = 6.8 Hz), 4.27–4.38 (1H, m), 4.40 (2H, d, J = 6.3 Hz), 5.51 (1H, d, J = 6.3 Hz), 6.71 (1H, br s), 7.30 (2H, t, J = 7.3 Hz), 7.39 (2H, t, J = 7.3 Hz), 7.58 (2H, dd, J = 6.8, 2.4 Hz), 7.75 (2H, d, J = 7.3 Hz); ¹³C NMR (100 MHz, CDCl₃): δ 18.5, 41.2, 47.1, 50.4, 52.4, 67.1, 120.0 (2C), 125.0 (2C), 127.1 (2C), 127.7 (2C), 141.3 (2C), 143.7 (2C), 156.0, 170.0, 172.5; IR (KBr): 3322, 3293, 3067, 2983, 2951, 2941, 2890, 1731, 1720, 1693, 1648, 1541, 1449, 1329, 1301, 1266, 1254, 1105, 1089, 1051, 1023, 758, 741, 671, 645 cm⁻¹; HRMS (EI): m/z calcd for C₂₁H₂₂N₂O₅ (M⁺) 382.1529, found 382.1520.

4.1.28. Boc-D-Cys(Tr)-L-Ala-Gly-OMe (**32d**)

Compound **32d** was synthesized from **30d** (1.65 g, 4.3 mmol) in a manner similar to that described for the synthesis of **23**. Purification by column chromatography (hexane/EtOAc 1:2) gave **32d** (2.24 g, 86%, 2 steps) as a colorless amorphous solid. [α]_D²⁵ –31.4 (c 1.0, CHCl₃); ¹H NMR (400 MHz, CDCl₃): δ 1.36 (3H, d, J = 6.8 Hz), 1.40 (9H, s), 2.55 (1H, dd, J = 12.9, 5.4 Hz), 2.75 (1H, dd, J = 12.0, 6.8 Hz), 3.66–3.73 (4H, m), 3.82 (1H, dd, J = 18.0, 5.4 Hz), 4.00 (1H, dd, J = 18.0, 5.4 Hz), 4.48 (1H, dq, J = 7.2, 7.1 Hz), 4.90 (1H, br s), 6.39 (1H, br s), 7.04 (1H, br s), 7.04–7.31 (9H, m), 7.39–7.41 (6H, m); ¹³C NMR (100 MHz, CDCl₃): δ 17.9, 28.0 (3C), 33.7, 40.8, 48.5, 51.9, 53.6, 66.8, 80.0, 126.7 (3C), 127.8 (6C), 129.3 (6C), 144.1 (3C), 155.2, 169.9, 170.2, 172.2; IR (neat): 3299, 3058, 3006, 2978, 2932, 1752, 1652, 1518, 1491, 1445, 1367, 1213, 1166, 1049, 1021, 854, 751, 700 cm⁻¹; HRMS (FAB): m/z calcd for C₃₃H₄₀N₃O₆S (M⁺+H) 606.2632, found; 606.2625.

4.1.29. H₂N-D-Cys(Tr)-L-Ala-Gly-OMe (**15d**)

Compound **15d** was synthesized from **32d** (1.83 g, 3.0 mmol) in a manner similar to that described for the synthesis of **15a**. Purification by column chromatography (CHCl₃/MeOH 15:1) gave **15d** (1.43 g, 94%) as a colorless amorphous solid. [α]_D²⁵ –64.5 (c 1.0, CHCl₃); ¹H NMR (400 MHz, CDCl₃): δ 1.34 (3H, d, J = 6.8 Hz), 1.47 (2H, br s), 2.64 (2H, d, J = 4.9 Hz), 3.05 (1H, t, J = 5.6 Hz), 3.64 (3H, s), 3.78 (1H, dd, J = 17.6, 5.4 Hz), 3.90 (1H, dd, J = 17.6, 5.9 Hz), 4.49 (1H, dq, J = 7.2, 7.1 Hz), 7.18–7.28 (10H, m), 7.39–7.41 (6H, m), 7.58 (1H, d, J = 7.8 Hz); ¹³C NMR (100 MHz, CDCl₃): δ 17.6, 37.3, 40.7, 48.2, 51.9, 53.8, 66.7, 126.7 (3C), 127.8 (6C), 129.3 (6C), 144.3 (3C), 169.8, 172.3, 173.0; IR (neat): 3308, 3057, 3016, 2951, 1750, 1654, 1509, 1444, 1369, 1211, 1183, 1032, 981, 886, 848, 745, 700 cm⁻¹; HRMS (FAB): m/z calcd for C₂₈H₃₂N₃O₄S (M⁺+H) 506.2108, found 506.2109.

4.1.30. (7S,11R,14S,17S,E)-Methyl 11-isopropyl-7-(4-methoxybenzyloxy)-17-methyl-9,12,15,18-tetraoxo-1,1,1-triphenyl-14-tritylthiomethyl-2-thia-10,13,16,19-tetraazahenicos-5-en-21-oate (**26d**)

Compound **26d** was synthesized from **15d** (119 mg, 0.24 mmol) in a manner similar to that described for the synthesis of **26a**. Purification by column chromatography (CHCl₃/MeOH 40:1) gave **26d** (240 mg, 91%) as a colorless amorphous solid. [α]_D²⁷ –4.0 (c 1.0, CHCl₃); ¹H NMR (400 MHz, CDCl₃): δ 0.69 (3H, d, J = 6.8 Hz), 0.79 (3H, d, J = 6.8 Hz), 1.34 (3H, d, J = 7.3 Hz), 2.27 (1H, dq, J = 13.2, 6.6 Hz), 2.05–2.14 (2H, m), 2.21–2.25 (2H, m), 2.47 (2H, d, J = 5.4 Hz), 2.56 (1H, dd, J = 12.7, 5.4 Hz), 2.78 (1H, dd, J = 13.4, 7.1 Hz), 3.64 (3H, s), 3.77 (3H, s), 3.82 (1H, dd, J = 18.0, 5.4 Hz), 3.89–3.99 (2H, m), 4.06 (1H, q, J = 6.7 Hz), 4.16 (1H, t, J = 6.6 Hz), 4.23 (1H, d, J = 10.7 Hz), 4.41 (1H, d, J = 10.7 Hz), 4.57 (1H, dq, J = 7.4, 7.2 Hz), 5.29 (1H, dd, J = 15.4, 8.0 Hz), 5.55 (1H, dt, J = 15.1, 6.8 Hz), 6.78 (1H, d, J = 8.3 Hz), 6.82 (2H, d, J = 8.8 Hz), 7.01 (1H, d, J = 7.3 Hz), 7.16–7.28 (22H, m), 7.33–7.42 (12H, m); ¹³C NMR (100 MHz, CDCl₃): δ 17.7, 17.8, 19.3, 30.3, 31.2, 31.3, 33.7, 40.9, 42.4, 48.9, 52.1, 52.5, 55.2, 58.9, 66.5, 67.0, 69.9, 76.4, 113.8 (2C), 126.6 (3C), 126.8 (3C), 127.8 (6C), 128.0 (6C), 129.45 (6C), 129.48 (6C), 129.7, 129.8 (2C), 129.9, 133.1, 144.3 (3C), 144.8 (3C), 159.3, 169.5, 170.1, 171.2, 171.6, 172.4; IR (neat): 3291, 3058, 3016, 2961, 2931, 1752, 1635, 1513, 1490, 1444, 1390, 1368, 1247, 1215, 1181, 1079, 1034, 975, 847, 823, 751, 700 cm⁻¹; HRMS (FAB): m/z calcd for C₆₇H₇₃N₄O₈S₂ (M⁺+H) 1125.4864, found 1125.4873.

4.1.31. (7S,11R,14S,17S,E)-Methyl 7-hydroxy-11-isopropyl-17-methyl-9,12,15,18-tetraoxo-1,1,1-triphenyl-14-tritylthiomethyl-2-thia-10,13,16,19-tetraazahenicos-5-en-21-oate (**27d**)

Compound **27d** was synthesized from **26d** (240 mg, 0.21 mmol) in a manner similar to that described for the synthesis of **27a**. Purification by column chromatography (CHCl₃/MeOH 50:1) gave **27d** (213 mg, 99%) as a colorless amorphous solid. [α]_D²⁷ –37.8 (c 1.0, CHCl₃); ¹H NMR (400 MHz, CDCl₃): δ 0.95 (3H, d, J = 6.8 Hz), 1.00 (3H, d, J = 6.8 Hz), 1.42 (3H, d, J = 7.3 Hz), 2.03–2.08 (2H, m), 2.18–2.37 (4H, m), 2.42 (1H, dd, J = 13.2, 2.0 Hz), 2.64 (2H, d, J = 6.8 Hz), 3.54 (3H, s), 3.61 (1H, dd, J = 18.0, 4.4 Hz), 4.00 (1H, br s), 4.08–4.10 (2H, m), 4.33–4.45 (3H, m), 5.38 (1H, dd, J = 15.6, 5.9 Hz), 5.59 (1H, dt, J = 15.6, 6.3 Hz), 6.01 (1H, d, J = 5.8 Hz), 6.96 (1H, t, J = 5.6 Hz), 7.02 (1H, d, J = 6.8 Hz), 7.16–7.30 (19H, m), 7.33–7.42 (12H, m); ¹³C NMR (100 MHz, CDCl₃): δ 16.1, 17.4, 19.5, 29.0, 31.1, 31.3, 33.6, 40.7, 43.7, 48.8, 51.9, 52.1, 59.9, 66.5, 66.7, 69.3, 126.5 (3C), 126.6 (3C), 127.7 (6C), 127.8 (6C), 129.38 (6C), 129.42 (6C), 129.7, 132.7, 144.3 (3C), 144.7 (3C), 170.3, 170.7, 170.8, 172.9, 173.0; IR (neat): 3291, 3082, 3058, 3017, 2964, 2930, 1745, 1633, 1531, 1490, 1444, 1391, 1370, 1216, 1183, 1081, 1033, 972, 850, 751, 700 cm⁻¹; HRMS (FAB): m/z calcd for C₅₉H₆₅N₄O₇S₂ (M⁺+H) 1005.4289, found 1005.4293.

4.1.32. (7S,11R,14S,17S,E)-7-Hydroxy-11-isopropyl-17-methyl-9,12,15,18-tetraoxo-1,1,1-triphenyl-14-tritylthiomethyl-2-thia-10,13,16,19-tetraazahenicos-5-en-21-oic acid (**14d**)

Compound **14d** was synthesized from **27d** (213 mg, 0.21 mmol) in a manner similar to that described for the synthesis of **14a**. Purification by column chromatography (CHCl₃/MeOH 5:1) gave **14d** (209 mg, 99%) as a colorless amorphous solid. [α]_D³⁰ –16.9 (c 1.0, CHCl₃); ¹H NMR (400 MHz, CD₃OD/CDCl₃ 3:1): δ 0.94 (3H, d, J = 5.4 Hz), 0.95 (3H, d, J = 6.3 Hz), 1.37 (3H, d, J = 6.8 Hz), 2.01–2.06 (2H, m), 2.09–2.21 (3H, m), 2.36 (1H, dd, J = 13.7, 4.4 Hz), 2.48 (1H, dd, J = 13.7, 9.6 Hz), 2.57 (1H, dd, J = 12.2, 8.8 Hz), 2.64 (1H, dd, J = 12.7, 5.9 Hz), 3.79 (2H, s), 4.08 (1H, d, J = 5.4 Hz), 4.13 (1H, dd, J = 8.3, 6.3 Hz), 4.29 (1H, q, J = 6.8 Hz), 4.39–4.43 (1H, m), 5.43 (1H, dd, J = 15.1, 6.3 Hz), 5.55 (1H, dt, J = 15.1, 6.3 Hz), 7.15–7.26 (18H, m), 7.35–7.39 (12H, m); ¹³C NMR (100 MHz, CD₃OD/CDCl₃ 3:1, 45 °C):

δ 17.6, 18.2, 19.6, 30.5, 32.0, 32.2, 33.8, 41.7, 43.9, 50.0, 53.7, 60.4, 67.4, 67.7, 69.8, 127.3 (3C), 127.5, (3C), 128.4 (6C), 128.6 (6C), 130.2 (6C), 130.26, 130.27 (6C), 133.7, 145.3 (3C), 145.7 (3C), 171.3, 172.5, 173.1, 174.2, 174.3; IR (neat): 3297, 3057, 3018, 2964, 2928, 1725, 1638, 1531, 1490, 1444, 1217, 1033, 970, 750, 700 cm^{-1} ; HRMS (FAB): m/z calcd for $\text{C}_{58}\text{H}_{63}\text{N}_4\text{O}_7\text{S}_2$ ($\text{M}^+ + \text{H}$) 991.4133, found 991.4153.

4.1.33. (6S,9S,12R,16S)-12-Isopropyl-6-methyl-16-[(E)-4-tritylthiobut-1-enyl]-9-tritylthiomethyl-1-oxa-4,7,10,13-tetraazacyclohexadecane-2,5,8,11,14-pentaone (**28d**)

Compound **28d** was synthesized from **14d** (104 mg, 0.11 mmol) in a manner similar to that described for the synthesis of **28a**. Purification by column chromatography ($\text{CHCl}_3/\text{MeOH}$ 40:1) gave **28d** (87.6 mg, 86%) as a colorless amorphous solid. $[\alpha]_D^{27} -16.3$ (c 1.0, CHCl_3); ^1H NMR (400 MHz, CDCl_3): δ 0.85 (3H, d, $J = 6.3$ Hz), 0.95 (3H, d, $J = 6.3$ Hz), 1.20 (3H, d, $J = 7.2$ Hz), 1.88–2.18 (5H, m), 2.42–2.57 (2H, m), 2.75 (1H, dd, $J = 12.6, 3.4$ Hz), 2.91 (1H, dd, $J = 12.6, 9.7$ Hz), 3.49 (1H, dd, $J = 16.4, 3.4$ Hz), 3.56–3.64 (1H, m), 4.29 (1H, dd, $J = 16.4, 8.2$ Hz), 4.34–4.51 (2H, m), 5.37 (1H, dd, $J = 15.5, 6.3$ Hz), 5.47–5.62 (2H, m), 6.17 (1H, br d, $J = 5.3$ Hz), 7.13–7.27 (20H, m), 7.33–7.38 (12H, m), 7.67 (1H, br s); ^{13}C NMR (100 MHz, CDCl_3 , 40 °C): δ 17.2, 17.6, 19.8, 31.1, 31.4, 32.1, 32.2, 42.1, 42.5, 48.5, 54.6, 57.7, 66.7, 66.9, 72.0, 126.6 (3C), 126.8 (3C), 127.8 (6C), 127.9 (6C), 128.0, 129.5 (6C), 129.6 (6C), 132.8, 144.6 (3C), 144.8 (3C), 169.0, 169.2, 169.8, 172.3, 172.8; IR (neat): 3289, 3058, 3016, 2965, 2933, 1734, 1654, 1540, 1489, 1444, 1216, 1195, 1033, 980, 751, 700 cm^{-1} ; HRMS (FAB): m/z calcd for $\text{C}_{58}\text{H}_{60}\text{N}_4\text{O}_6\text{S}_2\text{Na}$ ($\text{M}^+ + \text{Na}$) 995.3846, found 995.3822.

4.1.34. FK-A4 (**13d**)

Compound **13d** was synthesized from **28d** (87.0 mg, 93 μmol) in a manner similar to that described for the synthesis of **13a**. Purification by column chromatography ($\text{CHCl}_3/\text{MeOH}$ 20:1) gave **13d** (40.0 mg, 89%) as a colorless amorphous solid. $[\alpha]_D^{27} -30.4$ (c 1.0, CHCl_3); ^1H NMR (400 MHz, CDCl_3): δ 1.09 (3H, d, $J = 4.4$ Hz), 1.10 (3H, d, $J = 3.9$ Hz), 1.42 (3H, d, $J = 7.3$ Hz), 2.30 (1H, dq, $J = 12.2, 6.8$ Hz), 2.46–2.57 (1H, m), 2.62–2.76 (2H, m), 2.89–2.96 (2H, m), 3.08 (1H, ddd, $J = 13.2, 8.8, 2.9$ Hz), 3.14 (1H, dd, $J = 15.1, 3.9$ Hz), 3.27 (1H, dd, $J = 15.1, 10.2$ Hz), 4.06 (1H, t, $J = 4.4$ Hz), 4.11 (1H, dd, $J = 17.6, 5.4$ Hz), 4.20 (1H, dd, $J = 17.6, 5.4$ Hz), 4.54 (1H, q, $J = 7.3$ Hz), 4.80 (1H, ddd, $J = 10.2, 6.8, 3.9$ Hz), 5.70–5.81 (2H, m), 5.83–5.94 (1H, m), 6.48 (1H, d, $J = 2.9$ Hz), 6.90 (1H, t, $J = 4.9$ Hz), 7.43 (1H, d, $J = 6.8$ Hz), 7.48 (1H, d, $J = 8.3$ Hz); ^{13}C NMR (100 MHz, CDCl_3): δ 17.2, 18.7, 19.4, 29.3, 31.3, 37.5, 37.6, 39.5, 42.3, 49.5, 56.0, 62.2, 69.5, 128.9, 129.7, 167.3, 169.6, 171.0, 171.1, 171.9; IR (neat): 3297, 3009, 2966, 2933, 1742, 1655, 1524, 1253, 1190, 1136, 1024, 979, 754 cm^{-1} ; HRMS (EI): m/z calcd for $\text{C}_{20}\text{H}_{30}\text{N}_4\text{O}_6\text{S}_2$ (M^+) 486.1607, found 486.1601.

4.1.35. Fmoc-D-Phe-Gly-OMe (**30e**)

Compound **30e** was synthesized from D-phenylalanine (D-Phe) (**18e**) (500 mg, 3.0 mmol) in a manner similar to that described for the synthesis of **21**. Purification by column chromatography ($\text{CHCl}_3/\text{MeOH}$ 30:1) gave **30e** (971 mg, 70%, 2 steps) as a colorless amorphous solid. $[\alpha]_D^{25} +11.1$ (c 1.0, CHCl_3); ^1H NMR (400 MHz, CDCl_3): δ 3.07–3.11 (2H, m), 3.68 (3H, s), 3.89–4.02 (2H, m), 4.15 (1H, t, $J = 6.8$ Hz), 4.26–4.30 (1H, m), 4.37–4.41 (1H, m), 4.52 (1H, d, $J = 5.9$ Hz), 5.55 (1H, br d, $J = 6.8$ Hz), 6.57 (1H, br s), 7.19–7.29 (7H, m), 7.38 (2H, t, $J = 7.3$ Hz), 7.50 (2H, t, $J = 7.3$ Hz), 7.74 (2H, d, $J = 7.3$ Hz); ^{13}C NMR (100 MHz, CDCl_3): δ 38.4, 41.1, 46.3, 52.2, 55.9, 67.0, 119.9 (2C), 125.0, 126.9 (2C), 127.0 (2C), 127.6 (2C), 128.6 (2C), 129.2 (2C), 136.3, 141.2 (2C), 143.6 (2C), 156.0, 169.8, 171.3; IR (neat): 3301, 3064, 3029, 2952, 1748, 1660, 1538, 1449, 1259, 1213, 1036, 758, 740, 700 cm^{-1} ; HRMS (FAB): m/z calcd for $\text{C}_{27}\text{H}_{27}\text{N}_2\text{O}_5$ ($\text{M}^+ + \text{H}$) 459.1920, found 459.1924.

4.1.36. Boc-D-Cys(Tr)-D-Phe-Gly-OMe (**32e**)

Compound **32e** was synthesized from **30e** (775 mg, 1.7 mmol) in a manner similar to that described for the synthesis of **23**. Purification by column chromatography (hexane/EtOAc 1:1) gave **32e** (1.07 g, 92%, 2 steps) as a colorless amorphous solid. $[\alpha]_D^{25} +15.4$ (c 1.0, CHCl_3); ^1H NMR (400 MHz, CDCl_3): δ 1.34 (9H, s), 2.52–2.62 (2H, m), 3.08 (1H, dd, $J = 14.2, 6.3$ Hz), 3.15 (1H, dd, $J = 13.9, 6.8$ Hz), 3.60 (1H, dd, $J = 11.7, 5.9$ Hz), 3.65 (3H, s), 3.71 (1H, dd, $J = 17.8, 5.9$ Hz), 3.93 (1H, dd, $J = 18.1, 5.9$ Hz), 4.64 (1H, d, $J = 5.4$ Hz), 4.73 (1H, dd, $J = 14.9, 6.3$ Hz), 6.32 (1H, d, $J = 8.3$ Hz), 7.00 (1H, br s), 7.13–7.29 (14H, m), 7.37–7.40 (6H, m); ^{13}C NMR (100 MHz, CDCl_3): δ 28.1 (3C), 33.2, 37.0, 41.0, 52.1, 53.4, 54.2, 67.4, 80.6, 126.9, 127.0 (3C), 128.1 (6C), 128.6 (2C), 129.3 (2C), 129.4 (6C), 136.1, 144.1 (3C), 155.7, 169.6, 170.2, 170.8; IR (neat): 3277, 3060, 3030, 2979, 2928, 1740, 1698, 1675, 1645, 1531, 1443, 1392, 1366, 1279, 1173, 1032, 746, 700 cm^{-1} ; HRMS (FAB): m/z calcd for $\text{C}_{39}\text{H}_{44}\text{N}_3\text{O}_6\text{S}$ ($\text{M}^+ + \text{H}$) 682.2951, found 682.2957.

4.1.37. H₂N-D-Cys(Tr)-D-Phe-Gly-OMe (**15e**)

Compound **15e** was synthesized from **32e** (1.14 g, 1.7 mmol) in a manner similar to that described for the synthesis of **15a**. Purification by column chromatography ($\text{CHCl}_3/\text{MeOH}$ 40:1) gave **15e** (837 mg, 86%) as a colorless amorphous solid. $[\alpha]_D^{25} +11.5$ (c 1.0, CHCl_3); ^1H NMR (400 MHz, CDCl_3): δ 1.26 (2H, br s), 2.39 (1H, dd, $J = 12.9, 8.3$ Hz), 2.59 (1H, dd, $J = 13.2, 4.4$ Hz), 2.85 (1H, dd, $J = 8.3, 4.4$ Hz), 3.01 (1H, dd, $J = 13.9, 7.3$ Hz), 3.11 (1H, dd, $J = 13.9, 6.8$ Hz), 3.67 (3H, s), 3.80 (1H, dd, $J = 15.3, 5.4$ Hz), 3.94 (1H, dd, $J = 18.1, 5.4$ Hz), 4.64 (1H, dd, $J = 15.1, 7.8$ Hz), 6.80 (1H, t, $J = 5.4$ Hz), 7.13–7.28 (14H, m), 7.39–7.45 (7H, m); ^{13}C NMR (100 MHz, CDCl_3): δ 36.9, 37.4, 41.0, 52.2, 53.6, 53.9, 66.9, 126.8 (4C), 127.9 (6C), 128.5 (2C), 129.2 (2C), 129.5 (6C), 136.4, 144.4 (3C), 170.0, 171.0, 173.5; IR (neat): 3308, 3059, 3029, 2926, 1748, 1652, 1539, 1517, 1443, 1372, 1208, 1082, 1033, 744, 700, 667 cm^{-1} ; HRMS (FAB): m/z calcd for $\text{C}_{34}\text{H}_{36}\text{N}_3\text{O}_4\text{S}$ ($\text{M}^+ + \text{H}$) 582.2427, found 582.2421.

4.1.38. (7S,11R,14S,17R,E)-Methyl 17-benzyl-11-isopropyl-7-(4-methoxybenzyloxy)-9,12,15,18-tetraoxo-1,1,1-triphenyl-14-tritylthiomethyl-2-thia-10,13,16,19-tetraazahenicos-5-en-21-oate (**26e**)

Compound **26e** was synthesized from **15e** (200 mg, 0.34 mmol) in a manner similar to that described for the synthesis of **26a**. Purification by column chromatography ($\text{CHCl}_3/\text{MeOH}$ 40:1) gave **26e** (409 mg, 99%) as a colorless amorphous solid. $[\alpha]_D^{25} -3.4$ (c 1.0, CHCl_3); ^1H NMR (400 MHz, CDCl_3): δ 0.65 (3H, d, $J = 6.8$ Hz), 0.78 (3H, d, $J = 6.8$ Hz), 1.89–1.98 (1H, m), 2.07–2.16 (2H, m), 2.19–2.27 (2H, m), 2.32–2.48 (3H, m), 2.70 (1H, dd, $J = 12.7, 6.3$ Hz), 3.08 (1H, dd, $J = 14.1, 9.3$ Hz), 3.26 (1H, dd, $J = 14.4, 5.4$ Hz), 3.66 (3H, s), 3.74–3.80 (4H, m), 3.87 (1H, dd, $J = 5.9, 12.4$ Hz), 3.95–4.05 (3H, m), 4.17 (1H, d, $J = 10.7$ Hz), 4.43 (1H, d, $J = 10.7$ Hz), 4.80 (1H, dt, $J = 8.7, 4.9$ Hz), 5.29 (1H, dd, $J = 15.4, 7.8$ Hz), 5.51 (1H, dt, $J = 15.1, 6.4$ Hz), 6.52 (1H, br d, $J = 5.9$ Hz), 6.79–6.82 (3H, m), 7.11–7.32 (33H, m), 7.41–7.43 (6H, m); ^{13}C NMR (100 MHz, CDCl_3): δ 17.7, 19.4, 29.7, 31.2, 31.3, 33.1, 36.9, 41.0, 42.3, 52.0, 52.4, 54.0, 55.2, 59.5, 66.6, 67.1, 70.0, 76.4, 113.8 (2C), 126.5, 126.6 (3C), 126.9 (3C), 127.7 (6C), 127.8 (6C), 128.1 (2C), 128.3, 129.2 (2C), 129.4 (6C), 129.5 (6C), 129.6, 129.9 (2C), 133.6, 137.1, 144.0 (3C), 144.8 (3C), 159.4, 169.6, 169.8, 171.1, 171.6, 171.9; IR (neat): 3280, 3059, 3030, 2959, 2929, 1743, 1635, 1514, 1443, 1247, 1216, 1079, 1034, 976, 745, 699 cm^{-1} ; HRMS (FAB): m/z calcd for $\text{C}_{73}\text{H}_{77}\text{N}_4\text{O}_8\text{S}_2$ ($\text{M}^+ + \text{H}$) 1201.5183, found 1201.5183.

4.1.39. (7S,11R,14S,17R,E)-Methyl 17-benzyl-7-hydroxy-11-isopropyl-9,12,15,18-tetraoxo-1,1,1-triphenyl-14-tritylthiomethyl-2-thia-10,13,16,19-tetraazahenicos-5-en-21-oate (**27e**)

Compound **27e** was synthesized from **26e** (409 mg, 0.34 mmol) in a manner similar to that described for the synthesis of **27a**.

Purification by column chromatography (CHCl₃/MeOH 50:1) gave **27e** (331 mg, 90%) as a colorless amorphous solid. [α]_D²⁵ +3.2 (c 1.0, CHCl₃); ¹H NMR (400 MHz, CDCl₃): δ 0.85 (3H, d, J = 7.3 Hz), 0.92 (3H, d, J = 7.3 Hz), 2.04–2.35 (7H, m), 2.43 (1H, dd, J = 12.7, 5.4 Hz), 2.49 (1H, dd, J = 12.7, 7.3 Hz), 2.70 (1H, br s), 3.10 (1H, dd, J = 14.6, 9.3 Hz), 3.29 (1H, dd, J = 14.6, 4.7 Hz), 3.66 (3H, s), 3.76 (1H, dd, J = 18.1, 5.4 Hz), 3.96–4.02 (2H, m), 4.14–4.16 (2H, m), 4.77 (1H, dt, J = 8.8, 4.9 Hz), 5.31 (1H, dd, J = 15.4, 6.3 Hz), 5.42 (1H, dt, J = 15.1, 6.6 Hz), 6.29 (1H, br d, J = 6.8 Hz), 6.87 (1H, br d, J = 7.8 Hz), 6.98 (1H, br d, J = 6.8 Hz), 7.09–7.32 (30H, m), 7.39–7.44 (6H, m); ¹³C NMR (100 MHz, CDCl₃): 17.6, 19.5, 29.4, 31.27, 31.31, 33.0, 33.6, 41.1, 43.8, 52.1, 52.9, 53.9, 59.7, 66.7, 66.9, 69.6, 126.5, 126.7 (3C), 127.0 (3C), 127.9 (6C), 128.1 (6C), 128.4 (2C), 129.0 (2C), 129.3 (6C), 129.6 (6C), 130.4, 132.3, 137.2, 144.0 (3C), 144.8 (3C), 169.9, 170.0, 171.1, 171.7, 172.4; IR (neat): 3275, 3060, 3030, 2962, 2925, 1742, 1633, 1538, 1490, 1443, 1218, 1184, 1081, 1034, 972, 855, 745, 699 cm⁻¹; HRMS (FAB): m/z calcd for C₆₅H₆₉N₄O₇S₂ (M⁺+H) 1081.4608, found 1081.4601.

4.1.40. (7S,11R,14S,17R,E)-17-Benzyl-7-hydroxy-11-isopropyl-9,12,15,18-tetraoxo-1,1,1-triphenyl-14-tritylthiomethyl-2-thia-10,13,16,19-tetraazahenicos-5-en-21-oic acid (14e)

Compound **14e** was synthesized from **27e** (331 mg, 0.31 mmol) in a manner similar to that described for the synthesis of **14a**. Purification by column chromatography (CHCl₃/MeOH 20:1 to 4:1) gave **14e** (327 mg, 100%) as a colorless amorphous solid. [α]_D²⁵ –17.1 (c 1.0, CHCl₃); ¹H NMR (400 MHz, CD₃OD/CDCl₃ 10:1): δ 0.83–0.85 (6H, m), 1.97–2.03 (3H, m), 2.15–2.19 (2H, m), 2.32 (1H, dd, J = 14.0, 4.8 Hz), 2.40 (1H, dd, J = 13.8, 8.7 Hz), 2.48 (2H, d, J = 6.8 Hz), 2.91 (1H, dd, J = 14.0, 8.7 Hz), 3.15 (1H, dd, J = 13.8, 4.8 Hz), 3.66 (1H, d, J = 17.4 Hz), 3.77 (1H, d, J = 17.9 Hz), 3.98–4.01 (1H, m), 4.11 (1H, d, J = 5.8 Hz), 4.28 (1H, dd, J = 12.3, 5.8 Hz), 4.59–4.62 (1H, m), 5.36 (1H, dd, J = 15.9, 6.3 Hz), 5.46 (1H, dt, J = 15.5, 6.3 Hz), 7.07–7.32 (35H, m); ¹³C NMR (100 MHz, CD₃OD/CDCl₃ 10:1): δ 18.4, 19.8, 31.1, 32.3, 32.4, 34.2, 38.1, 42.0, 44.3, 54.0, 55.7, 60.2, 67.6, 67.9, 70.3, 127.6 (4C), 127.8 (3C), 128.7 (6C), 128.9 (6C), 129.3 (2C), 130.0, (2C), 130.45 (6C), 130.54 (6C), 130.7, 133.9, 138.0, 145.5 (3C), 146.0 (3C), 171.7, 172.8, 172.9, 173.3, 174.0; IR (neat): 3299, 3059, 3029, 2964, 2927, 1723, 1636, 1532, 1490, 1444, 1219, 1033, 972, 751, 700 cm⁻¹; HRMS (FAB): m/z calcd for C₆₄H₆₇N₄O₇S₂ (M⁺+H) 1067.4451, found 1067.4442.

4.1.41. (6R,9S,12R,16S)-6-benzyl-12-isopropyl-16-[(E)-4-(tritylthio)but-1-en-1-yl]-9-tritylthiomethyl-1-oxa-4,7,10,13-tetraazacyclohexadecane-2,5,8,11,14-pentaone (28e)

Compound **28e** was synthesized from **14e** (206 mg, 0.19 mmol) in a manner similar to that described for the synthesis of **28a**. Purification by column chromatography (hexane/EtOAc 2:1) gave **28e** (184 mg, 91%) as a colorless amorphous solid. [α]_D²⁵ –2.8 (c 1.0, CHCl₃); ¹H NMR (400 MHz, CDCl₃): δ 0.83 (3H, d, J = 6.8 Hz), 0.89 (3H, d, J = 6.8 Hz), 1.89–2.02 (3H, m), 2.13–2.16 (2H, m), 2.26–2.32 (2H, m), 2.39–2.43 (1H, m), 2.84–2.90 (1H, m), 3.00 (1H, dd, J = 13.5, 9.7 Hz), 3.22–3.29 (2H, m), 3.58 (1H, d, J = 14.0 Hz), 4.00–4.10 (2H, m), 4.38–4.44 (1H, m), 5.26 (1H, dd, J = 15.5, 6.3 Hz), 5.40–5.52 (2H, m), 6.10 (1H, br d, J = 6.8 Hz), 6.97 (5H, m), 7.10–7.26 (26H, m), 7.32–7.34 (6H, m), 7.57 (1H, br s); ¹³C NMR (100 MHz, CDCl₃): δ 18.0, 19.4, 29.7, 31.04, 31.06, 31.2, 31.3, 41.7, 42.1, 55.1, 56.4, 58.2, 66.6, 67.0, 72.2, 126.5, 126.6 (3C), 126.8 (3C), 127.8 (6C), 127.9 (6C), 128.4 (2C), 129.3 (2C), 129.4 (6C), 129.5 (7C), 132.3, 137.3, 144.3 (3C), 144.8 (3C), 168.9, 169.4, 170.6, 170.8, 173.1; IR (neat): 3309, 3058, 3029, 2963, 2929, 1745, 1651, 1540, 1490, 1444, 1274, 1216, 1033, 973, 849, 745, 700 cm⁻¹; HRMS (FAB): m/z calcd for C₆₄H₆₅N₄O₆S₂ (M⁺+H) 1049.4346, found 1049.4342.

4.1.42. FK-A5 (13e)

Compound **13e** was synthesized from **28e** (184 mg, 0.18 mmol) in a manner similar to that described for the synthesis of **13a**. Purification by column chromatography (CHCl₃/MeOH 40:1) gave **13e** (92.0 mg, 93%) as a colorless amorphous solid. [α]_D²⁵ –16.3 (c 1.1, CHCl₃); ¹H NMR (400 MHz, CDCl₃): δ 1.05 (3H, d, J = 6.4 Hz), 1.06 (3H, d, J = 6.3 Hz), 2.12–2.21 (1H, m), 2.52–2.61 (2H, m), 2.68–2.73 (1H, m), 2.94–3.11 (4H, m), 3.30–3.36 (2H, m), 3.46 (1H, dd, J = 4.4, 14.1 Hz), 3.81–3.89 (2H, m), 4.00 (1H, dd, J = 4.9, 6.1 Hz), 4.51 (1H, dd, J = 6.8, 17.6 Hz), 4.59–4.65 (1H, m), 5.71–5.75 (2H, m), 5.80–5.86 (1H, m), 6.41 (1H, d, J = 4.4 Hz), 7.10–7.11 (3H, m), 7.21 (1H, d, J = 9.8 Hz), 7.26–7.30 (2H, m), 7.37 (1H, d, J = 6.8 Hz), 7.58 (1H, d, J = 7.3 Hz); ¹³C NMR (100 MHz, CDCl₃): δ 19.36, 19.42, 29.2, 31.0, 33.9, 34.0, 37.5, 37.9, 43.1, 54.9, 57.5, 61.8, 69.5, 126.6, 128.6 (2C), 129.0 (2C), 129.6, 130.5, 138.6, 168.1, 169.78, 169.81, 170.2, 172.3; IR (neat): 3332, 3024, 2966, 2932, 1743, 1659, 1522, 1260, 1184, 979, 753, 700, 666 cm⁻¹; HRMS (FAB): m/z calcd for C₂₆H₃₅N₄O₆S₂ (M⁺+H) 563.1998, found 563.2000.

4.1.43. Fmoc-L-Phe-Gly-OMe (30f)

Compound **30f** was synthesized from L-phenylalanine (L-Phe) (**18f**) (500 mg, 3.0 mmol) in a manner similar to that described for the synthesis of **21**. Purification by column chromatography (CHCl₃/MeOH 30:1) gave **30f** (1.03 g, 73%, 2 steps) as a colorless amorphous solid. [α]_D²⁵ –10.0 (c 1.0, CHCl₃); ¹H NMR (400 MHz, CDCl₃): δ 3.10–3.11 (2H, m), 3.72 (3H, s), 3.90–4.05 (2H, m), 4.18 (1H, t, J = 6.8 Hz), 4.34–4.47 (3H, m), 5.35 (1H, br d, J = 5.3 Hz), 6.33 (1H, br s), 7.21–7.32 (7H, m), 7.40 (2H, t, J = 7.8 Hz), 7.52 (2H, t, J = 7.8 Hz), 7.76 (2H, d, J = 7.3 Hz); ¹³C NMR (100 MHz, CDCl₃): δ 38.4, 41.1, 47.0, 52.3, 55.9, 67.0, 119.9 (2C), 125.0, 126.95 (2C), 126.98 (2C), 127.6 (2C), 128.6 (2C), 129.2 (2C), 136.3, 141.2 (2C), 143.62, 143.64, 156.0, 169.8, 171.3; IR (neat): 3300, 3063, 3029, 2950, 1748, 1661, 1540, 1449, 1259, 1214, 1036, 758, 740, 701 cm⁻¹; HRMS (FAB): m/z calcd for C₂₇H₂₇N₂O₅ (M⁺+H) 459.1920, found 459.1924.

4.1.44. Boc-D-Cys(Tr)-L-Phe-Gly-OMe (32f)

Compound **32f** was synthesized from **30f** (1.01 g, 2.2 mmol) in a manner similar to that described for the synthesis of **23**. Purification by column chromatography (hexane/EtOAc 1:1) gave **32f** (1.13 g, 75%, 2 steps) as a colorless amorphous solid. [α]_D²⁵ –29.8 (c 1.0, CHCl₃); ¹H NMR (400 MHz, CDCl₃): δ 1.37 (9H, s), 2.49 (1H, dd, J = 13.0, 5.3 Hz), 2.63 (1H, dd, J = 13.0, 7.7 Hz), 3.04–3.14 (2H, m), 3.43 (1H, dd, J = 12.8, 7.3 Hz), 3.66 (3H, s), 3.76 (1H, dd, J = 17.9, 5.3 Hz), 3.97 (1H, dd, J = 17.6, 5.3 Hz), 4.74 (1H, dd, J = 14.5, 6.8 Hz), 4.93 (1H, d, J = 6.8 Hz), 6.41 (1H, d, J = 8.7 Hz), 7.10–7.18 (5H, m), 7.21–7.27 (10H, m), 7.36–7.37 (6H, m); ¹³C NMR (100 MHz, CDCl₃): δ 28.2 (3C), 33.4, 37.2, 41.1, 52.2, 53.8, 54.0, 67.3, 80.5, 126.9, 127.0 (3C), 128.1 (6C), 128.6 (2C), 129.2 (2C), 129.5 (6C), 136.2, 144.2 (3C), 155.5, 169.7, 170.6, 170.8; IR (neat): 3297, 3059, 3028, 2977, 1749, 1651, 1495, 1443, 1391, 1366, 1213, 1168, 1033, 867, 744, 700 cm⁻¹; HRMS (FAB): m/z calcd for C₃₉H₄₄N₃O₆S (M⁺+H) 682.2951, found 682.2957.

4.1.45. H₂N-D-Cys(Tr)-L-Phe-Gly-OMe (15f)

Compound **15f** was synthesized from **32f** (1.13 g, 1.7 mmol) in a manner similar to that described for the synthesis of **15a**. Purification by column chromatography (CHCl₃/MeOH 40:1) gave **15f** (846 mg, 88%) as a colorless amorphous solid. [α]_D²⁵ –51.6 (c 1.0, CHCl₃); ¹H NMR (400 MHz, CDCl₃): δ 1.26 (2H, br s), 2.55 (1H, dd, J = 12.6, 4.3 Hz), 2.61 (1H, dd, J = 12.6, 7.3 Hz), 2.85 (1H, dd, J = 7.2, 4.4 Hz), 3.00 (1H, dd, J = 14.0, 7.7 Hz), 3.14 (1H, dd, J = 14.0, 5.8 Hz), 3.64 (3H, s), 3.71 (1H, dd, J = 18.3, 5.3 Hz), 3.89 (1H, dd, J = 17.9, 5.8 Hz), 4.67 (1H, dd, J = 14.0, 7.7 Hz), 6.98 (1H, t, J = 5.6 Hz), 7.13–7.27 (14H, m), 7.37–7.40 (7H, m); ¹³C NMR (100 MHz, CDCl₃):

δ 37.1, 37.3, 40.9, 52.1, 53.8, 53.9, 67.0, 126.8, 126.9 (3C), 128.0 (6C), 128.5 (2C), 129.2 (2C), 129.5 (6C), 136.5, 144.4 (3C), 169.8, 171.0, 173.0; IR (neat): 3298, 3059, 2950, 1750, 1654, 1509, 1492, 1442, 1370, 1209, 1032, 743, 700 cm^{-1} ; HRMS (FAB): m/z calcd for $\text{C}_{34}\text{H}_{36}\text{N}_3\text{O}_4\text{S}$ ($\text{M}^+ + \text{H}$) 582.2427, found 582.2421.

4.1.46. (7S,11R,14S,17S,E)-Methyl 17-benzyl-11-isopropyl-7-(4-methoxybenzyloxy)-9,12,15,18-tetraoxo-1,1,1-triphenyl-14-tritylthiomethyl-2-thia-10,13,16,19-tetraazahenicos-5-en-21-oate (26f)

Compound **26f** was synthesized from **15f** (200 mg, 0.34 mmol) in a manner similar to that described for the synthesis of **26a**. Purification by column chromatography ($\text{CHCl}_3/\text{MeOH}$ 40:1) gave **26f** (400 mg, 97%) as a colorless amorphous solid. $[\alpha]_D^{25} -5.0$ (c 1.0, CHCl_3); ^1H NMR (400 MHz, $\text{CDCl}_3/\text{CD}_3\text{OD}$ 10:1): δ 0.68 (3H, d, $J = 6.8$ Hz), 0.77 (3H, d, $J = 6.8$ Hz), 1.87–1.95 (1H, m), 2.07–2.16 (2H, m), 2.21–2.25 (2H, m), 2.41–2.48 (3H, m), 2.65 (1H, dd, $J = 8.3$, 13.2 Hz), 2.94 (1H, dd, $J = 8.8$, 14.1 Hz), 3.20 (1H, dd, $J = 5.4$, 14.4 Hz), 3.51 (1H, dt, $J = 5.4$, 7.8 Hz), 3.65 (3H, s), 3.76–3.83 (4H, m), 3.94–4.05 (3H, m), 4.20 (1H, d, $J = 10.7$ Hz), 4.37 (1H, d, $J = 10.7$ Hz), 4.71–4.77 (1H, m), 5.28 (1H, dd, $J = 7.8$, 15.1 Hz), 5.54 (1H, dt, $J = 6.8$, 15.5 Hz), 6.44 (1H, brd, $J = 8.3$ Hz), 6.59 (1H, d, $J = 5.4$ Hz), 6.79–6.83 (2H, m), 7.07 (1H, d, $J = 6.8$ Hz), 7.06–7.12 (26H, m), 7.34–7.37 (6H, m), 7.39–7.42 (6H, m); ^{13}C NMR (100 MHz, $\text{CDCl}_3/\text{CD}_3\text{OD}$ 10:1): δ 17.5, 18.9, 30.3, 31.05, 31.14, 32.5, 36.9, 40.8, 42.2, 51.9, 52.8, 53.9, 55.0, 58.4, 66.4, 66.9, 69.7, 76.2, 113.6 (2C), 126.4 (3C), 126.5, 126.6 (3C), 127.6 (6C), 127.8 (6C), 128.2 (2C), 128.5, 128.9 (2C), 129.27 (6C), 129.31 (6C), 129.5 (2C), 129.8, 133.1, 136.4, 144.1 (3C), 144.6 (3C), 159.0, 170.0 (2C), 171.4, 171.6, 171.8; IR (neat): 3290, 3060, 3029, 2957, 1753, 1676, 1632, 1539, 1515, 1250, 1215, 1180, 1034, 825, 744, 700 cm^{-1} ; HRMS (FAB): m/z calcd for $\text{C}_{73}\text{H}_{77}\text{N}_4\text{O}_8\text{S}_2$ ($\text{M}^+ + \text{H}$) 1201.5183, found 1201.5183.

4.1.47. (7S,11R,14S,17S,E)-Methyl 17-benzyl-7-hydroxy-11-isopropyl-9,12,15,18-tetraoxo-1,1,1-triphenyl-14-tritylthiomethyl-2-thia-10,13,16,19-tetraazahenicos-5-en-21-oate (27f)

Compound **27f** was synthesized from **26f** (400 mg, 0.33 mmol) in a manner similar to that described for the synthesis of **27a**. Purification by column chromatography ($\text{CHCl}_3/\text{MeOH}$ 50:1) gave **27f** (343 mg, 95%) as a colorless amorphous solid. $[\alpha]_D^{25} -20.8$ (c 1.0, CHCl_3); ^1H NMR (400 MHz, $\text{CDCl}_3/\text{CD}_3\text{OD}$ 10:1): δ 0.92 (3H, d, $J = 7.3$ Hz), 0.97 (3H, d, $J = 6.8$ Hz), 2.03–2.10 (2H, m), 2.20–2.30 (4H, m), 2.43 (1H, dd, $J = 3.4$, 13.2 Hz), 2.52–2.63 (2H, m), 3.01 (1H, dd, $J = 8.3$, 14.1 Hz), 3.26 (1H, dd, $J = 5.9$, 13.9 Hz), 3.54 (3H, s), 3.62 (1H, dd, $J = 4.9$, 17.6 Hz), 3.95 (1H, br s), 4.05 (1H, dd, $J = 6.8$, 18.1 Hz), 4.11–4.17 (2H, m), 4.47–4.56 (2H, m), 5.40 (1H, dd, $J = 5.9$, 15.4 Hz), 5.58–5.65 (1H, m), 6.12 (1H, br d, $J = 6.8$ Hz), 6.94–7.01 (2H, m), 7.11–7.34 (30H, m), 7.39–7.42 (6H, m); ^{13}C NMR (100 MHz, $\text{CDCl}_3/\text{CD}_3\text{OD}$ 10:1): δ 17.4, 19.1, 29.3, 31.1, 31.3, 32.6, 36.7, 40.9, 43.3, 52.0, 52.3, 54.4, 59.5, 66.4, 66.8, 69.1, 126.45 (3C), 126.54, 126.6 (3C), 127.6, 127.7 (6C), 127.8 (6C), 128.3 (2C), 128.5, 128.9 (2C), 129.3 (6C), 129.4 (6C), 136.6, 144.2 (3C), 144.7 (3C), 170.2 (2C), 170.4, 171.7, 171.7; IR (neat): 3289, 3059, 3029, 2962, 2961, 2926, 1744, 1634, 1532, 1491, 1443, 1392, 1217, 1183, 1034, 972, 744, 700 cm^{-1} ; HRMS (FAB): m/z calcd for $\text{C}_{65}\text{H}_{69}\text{N}_4\text{O}_7\text{S}_2$ ($\text{M}^+ + \text{H}$) 1081.4608, found 1081.4601.

4.1.48. (7S,11R,14S,17S,E)-17-Benzyl-7-hydroxy-11-isopropyl-9,12,15,18-tetraoxo-1,1,1-triphenyl-14-tritylthiomethyl-2-thia-10,13,16,19-tetraazahenicos-5-en-21-oic acid (14f)

Compound **14f** was synthesized from **27f** (343 mg, 0.32 mmol) in a manner similar to that described for the synthesis of **14a**. Purification by column chromatography ($\text{CHCl}_3/\text{MeOH}$ 20:1 to 4:1) gave **14f** (338 mg, 100%) as a colorless amorphous solid. $[\alpha]_D^{25} -4.0$ (c 1.0, CHCl_3); ^1H NMR (400 MHz, $\text{CDCl}_3/\text{CD}_3\text{OD}$ 10:1): δ 0.84–0.88

(6H, m), 2.02–2.08 (3H, m), 2.19–2.22 (2H, m), 2.35–2.42 (3H, m), 2.47–2.53 (1H, m), 2.88–2.94 (1H, m), 3.20–3.24 (1H, m), 3.69–4.09 (4H, m), 4.39–4.43 (1H, m), 4.53–4.57 (1H, m), 5.41 (1H, dd, $J = 15.1$, 5.9 Hz), 5.54 (1H, dt, $J = 15.1$, 5.9 Hz), 7.09–7.42 (35H, m); ^{13}C NMR (100 MHz, $\text{CDCl}_3/\text{CD}_3\text{OD}$ 10:1): δ 17.5, 18.9, 29.4, 31.1, 31.2, 32.3, 36.8, 42.3, 43.1, 52.6, 54.6, 59.2, 66.4, 66.8, 68.8, 126.4 (3C), 126.5, 126.6, (3C), 127.6 (6C), 127.8 (6C), 128.2 (2C), 128.5, 128.8 (2C), 129.2 (6C), 129.3 (6C), 132.5, 136.5, 144.1 (3C), 144.5 (3C), 170.6, 171.5, 172.3, 172.9, 173.9; IR (neat): 3318, 3059, 3029, 2962, 2928, 1643, 1535, 1490, 1444, 1316, 1218, 1083, 1034, 972, 746, 700 cm^{-1} ; HRMS (FAB): m/z calcd for $\text{C}_{64}\text{H}_{67}\text{N}_4\text{O}_7\text{S}_2$ ($\text{M}^+ + \text{H}$) 1067.4451, found 1067.4442.

4.1.49. (6S,9S,12R,16S)-6-Benzyl-12-isopropyl-16-[(E)-4-tritylthiobut-1-en-1-yl]-9-tritylthiomethyl-1-oxa-4,7,10,13-tetraazacyclohexadecane-2,5,8,11,14-pentaone (28f)

Compound **28f** was synthesized from **14f** (95.7 mg, 90 μmol) in a manner similar to that described for the synthesis of **28a**. Purification by column chromatography (Hexane/EtOAc 2:1) gave **28f** (82.0 mg, 87%) as a colorless amorphous solid. $[\alpha]_D^{25} -22.2$ (c 1.0, CHCl_3); ^1H NMR (400 MHz, CDCl_3): δ 0.84 (3H, d, $J = 6.8$ Hz), 0.91 (3H, d, $J = 6.8$ Hz), 1.96–2.08 (3H, m), 2.14–2.22 (2H, m), 2.47–2.54 (2H, m), 2.72–2.86 (2H, m), 2.92–3.04 (2H, m), 3.38 (1H, dd, $J = 14.6$, 4.4 Hz), 3.52 (1H, dd, $J = 16.8$, 3.4 Hz), 4.10–4.13 (1H, m), 4.33 (1H, dd, $J = 17.1$, 8.3 Hz), 4.74 (1H, dt, $J = 9.5$, 4.4 Hz), 5.40–5.44 (2H, m), 5.54–5.62 (1H, m), 6.16 (1H, br d, $J = 6.8$ Hz), 6.98–7.00 (2H, m), 7.06–7.39 (36H, m); ^{13}C NMR (100 MHz, $\text{CDCl}_3/\text{CD}_3\text{OD}$ 10:1): δ 17.3, 19.0, 30.5, 30.8, 31.0, 31.9, 36.0, 40.7, 41.3, 53.1, 53.6, 58.7, 66.4, 66.7, 72.1, 126.3 (3C), 126.5 (3C), 127.4, 127.5 (6C), 127.6 (6C), 128.1 (2C), 128.36, 128.43 (2C), 129.1 (6C), 129.2 (6C), 132.5, 137.0, 144.1 (3C), 144.5 (3C), 168.7, 170.0, 170.5, 171.3, 172.4; IR (neat): 3304, 3058, 3029, 2963, 2928, 1735, 1647, 1540, 1490, 1444, 1217, 1033, 978, 852, 744, 700 cm^{-1} ; HRMS (FAB): m/z calcd for $\text{C}_{64}\text{H}_{65}\text{N}_4\text{O}_6\text{S}_2$ ($\text{M}^+ + \text{H}$) 1049.4346, found 1049.4342.

4.1.50. FK-A6 (13f)

Compound **13f** was synthesized from **28f** (82.0 mg, 78 μmol) in a manner similar to that described for the synthesis of **13a**. Purification by column chromatography ($\text{CHCl}_3/\text{MeOH}$ 40:1) gave **13f** (41.5 mg, 94%) as a colorless amorphous solid. $[\alpha]_D^{25} -93.0$ (c 1.0, CHCl_3); ^1H NMR (400 MHz, CDCl_3): δ 1.08 (3H, d, $J = 6.8$ Hz), 1.10 (3H, d, $J = 6.8$ Hz), 2.29–2.37 (1H, m), 2.48–2.52 (1H, m), 2.60–2.69 (2H, m), 2.86–3.03 (4H, m), 3.07 (1H, dd, $J = 4.4$, 15.4 Hz), 3.17–3.26 (2H, m), 4.04–4.09 (2H, m), 4.20 (1H, dd, $J = 17.8$, 5.4 Hz), 4.62–4.73 (2H, m), 5.67–5.75 (2H, m), 5.81–5.88 (1H, m), 6.60 (1H, d, $J = 3.9$ Hz), 7.01 (1H, t, $J = 4.6$ Hz), 7.20–7.32 (5H, m), 7.37 (1H, d, $J = 7.3$ Hz), 7.53 (1H, d, $J = 8.3$ Hz); ^{13}C NMR (100 MHz, CDCl_3): δ 18.6, 19.6, 29.2, 31.4, 37.4, 37.5, 37.6, 39.5, 42.4, 55.4, 55.6, 62.1, 69.4, 126.8, 128.5 (2C), 129.0, 129.4 (2C), 129.8, 136.5, 167.4, 169.8, 170.6, 170.7, 170.8; IR (neat): 3296, 2965, 2930, 1741, 1653, 1525, 1252, 1191, 1024, 978, 752, 700, 667 cm^{-1} ; HRMS (FAB): m/z calcd for $\text{C}_{26}\text{H}_{35}\text{N}_4\text{O}_6\text{S}_2$ ($\text{M}^+ + \text{H}$) 563.1998, found 563.2000.

4.1.51. Fmoc-D-Leu-Gly-OMe (30g)

Compound **30g** was synthesized from D-leucine (D-Leu) (**18g**) (500 mg, 3.8 mmol) in a manner similar to that described for the synthesis of **21**. Purification by column chromatography (Hexane/EtOAc 1:1) gave **30g** (1.16 g, 72%, 2 steps) as a colorless amorphous solid. $[\alpha]_D^{25} +19.4$ (c 1.0, CHCl_3); ^1H NMR (400 MHz, CDCl_3): δ 0.90–0.99 (6H, m), 1.54–1.67 (3H, m), 3.74 (3H, s), 4.03–4.07 (2H, m), 4.20–4.26 (2H, m), 4.44 (2H, d, $J = 5.4$ Hz), 5.19 (1H, d, $J = 7.3$ Hz), 6.52 (1H, br s), 7.29–7.35 (2H, m), 7.40 (2H, t, $J = 7.1$ Hz), 7.57–7.63 (2H, m), 7.76–7.79 (2H, m); ^{13}C NMR (100 MHz, CDCl_3): δ 21.9, 22.9, 24.7, 41.2, 41.3, 47.2, 52.4, 65.2, 67.0, 120.0 (2C), 124.7 (2C), 127.1 (2C), 127.7 (2C), 141.3 (2C), 143.8 (2C), 156.0, 170.1, 172.3;

IR (neat): 3298, 2953, 2358, 1700, 1663, 1540, 1449, 1211, 1043, 758, 740 cm^{-1} ; HRMS (FAB): m/z calcd for $\text{C}_{24}\text{H}_{29}\text{N}_2\text{O}_5$ ($\text{M}^+ + \text{H}$) 425.2076, found 425.2067.

4.1.52. Boc-D-Cys(S-Tr)-D-Leu-Gly-OMe (**32g**)

Compound **32g** was synthesized from **30g** (1.62 g, 3.8 mmol) in a manner similar to that described for the synthesis of **23**. Purification by column chromatography (hexane/EtOAc 1:1) gave **32g** (2.01 g, 81%, 2 steps) as a colorless amorphous solid. $[\alpha]_D^{25} + 8.0$ (c 1.0, CHCl_3); ^1H NMR (400 MHz, CDCl_3): δ 0.84–0.94 (6H, m), 1.40 (9H, s), 1.48–1.55 (1H, m), 1.60–1.67 (1H, m), 1.75–1.81 (2H, m), 2.59 (1H, dd, $J = 12.2, 5.9$ Hz), 2.74 (1H, dd, $J = 12.7, 6.8$ Hz), 3.68 (3H, s), 3.71–3.79 (1H, m), 3.98 (1H, dd, $J = 18.1, 5.9$ Hz), 4.44–4.50 (1H, m), 4.81 (1H, d, $J = 6.9$ Hz), 6.28 (1H, d, $J = 7.8$ Hz), 7.00 (1H, br s), 7.21–7.41 (15H, m); ^{13}C NMR (100 MHz, CDCl_3): δ = 21.4, 23.1, 24.6, 28.2 (3C), 33.2, 40.2, 40.9, 51.5, 52.1, 53.9, 67.2, 80.7, 127.0 (3C), 128.1 (6C), 129.4 (6C), 144.2 (3C), 155.7, 169.9, 170.6, 171.9; IR (neat): 3331, 3271, 1675, 1536, 1280, 1175, 1023, 745, 701 cm^{-1} ; HRMS (FAB): m/z calcd for $\text{C}_{36}\text{H}_{46}\text{N}_3\text{O}_6\text{S}$ ($\text{M}^+ + \text{H}$) 648.3107, found; 648.3104.

4.1.53. H₂N-D-Cys(Tr)-D-Leu-Gly-OMe (**15g**)

Compound **15g** was synthesized from **32g** (2.01 g, 3.1 mmol) in a manner similar to that described for the synthesis of **15a**. Purification by column chromatography ($\text{CHCl}_3/\text{MeOH}$ 40:1) gave **15g** (1.34 g, 78%) as a colorless amorphous solid. $[\alpha]_D^{25} + 30.1$ (c 1.0, CHCl_3); ^1H NMR (400 MHz, CDCl_3): δ 0.87 (3H, dd, $J = 6.3$ Hz), 0.91 (3H, dd, $J = 5.9$ Hz), 1.44–1.73 (5H, m), 2.55 (1H, dd, $J = 12.7, 7.8$ Hz), 2.65 (1H, dd, $J = 12.5, 4.4$ Hz), 3.11 (1H, dd, $J = 7.6, 3.9$ Hz), 3.69 (3H, s), 3.86–3.98 (2H, m), 4.38–4.44 (1H, m), 6.98 (1H, t, $J = 5.4$ Hz), 7.19–7.44 (16H, m); ^{13}C NMR (100 MHz, CDCl_3): δ 21.8, 22.9, 24.6, 37.0, 40.2, 40.9, 51.1, 52.2, 53.8, 66.8, 126.8 (3C), 127.9 (6C), 129.5 (6C), 144.5 (3C), 170.0, 172.1, 173.5; IR (neat): 3310, 2955, 1749, 1652, 1520, 1444, 1208, 1181, 744, 701 cm^{-1} ; HRMS (FAB): m/z calcd for $\text{C}_{31}\text{H}_{38}\text{N}_3\text{O}_4\text{S}$ ($\text{M}^+ + \text{H}$) 548.2583, found 548.2577.

4.1.54. (7S,11R,14S,17R,E)-Isobutyl 11-isopropyl-7-(4-methoxybenzyloxy)-17-isobutyl-9,12,15,18-tetraoxo-1,1,1-triphenyl-14-tritylthiomethyl-2-thia-10,13,16,19-tetraazahenicos-5-en-21-oate (**26g**)

Compound **26g** was synthesized from **15g** (172 mg, 0.31 mmol) in a manner similar to that described for the synthesis of **26a**. Purification by column chromatography (hexane/EtOAc 1:2) gave **26g** (316 mg, 86%) as a colorless amorphous solid. $[\alpha]_D^{25} - 4.1$ (c 1.1, CHCl_3); ^1H NMR (400 MHz, CDCl_3): δ 0.60 (3H, d, $J = 6.8$ Hz), 0.75 (3H, d, $J = 6.8$ Hz), 0.80–0.84 (6H, m), 1.59–1.70 (3H, m), 1.87–1.97 (1H, m), 1.99–2.06 (2H, m), 2.12–2.18 (2H, m), 2.22–2.32 (3H, m), 2.88 (1H, dd, $J = 12.2, 5.4$ Hz), 3.58 (3H, s), 3.72–3.76 (4H, m), 3.87–3.96 (3H, m), 4.07 (1H, dd, $J = 12.2, 5.9$ Hz), 4.10 (1H, d, $J = 10.7$ Hz), 4.37 (1H, d, $J = 10.2$ Hz), 4.40–4.46 (1H, m), 5.17–5.23 (1H, m), 5.35–5.42 (1H, m), 6.57 (1H, d, $J = 6.4$ Hz), 6.75 (2H, d, $J = 8.3$ Hz), 6.87 (1H, d, $J = 7.8$ Hz), 7.05–7.34 (34H, m); ^{13}C NMR (100 MHz, CDCl_3): δ 17.6, 19.4, 21.2, 23.2, 24.8, 29.5, 31.2, 31.3, 33.3, 38.6, 39.8, 41.0, 42.3, 52.0, 52.4, 55.3, 59.9, 66.6, 66.9, 70.1, 76.5, 113.9 (2C), 126.6 (3C), 127.0 (3C), 127.82 (6C), 128.1 (6C), 129.3 (6C), 129.40, 129.45, 129.48 (6C), 129.9 (2C), 133.7, 144.1 (3C), 144.8 (3C), 159.4, 169.6, 169.9, 171.5, 172.2, 172.3; IR (neat): 3274, 2955, 1749, 1637, 1540, 1514, 1490, 1443, 1247, 1213, 1181, 1078, 1034, 744, 700 cm^{-1} ; HRMS (FAB): m/z calcd for $\text{C}_{70}\text{H}_{79}\text{N}_4\text{O}_8\text{S}_2$ ($\text{M}^+ + \text{H}$) 1167.5339, found 1167.5356.

4.1.55. (7S,11R,14S,17R,E)-Isobutyl 7-hydroxy-11-isopropyl-17-methyl-9,12,15,18-tetraoxo-1,1,1-triphenyl-14-tritylthiomethyl-2-thia-10,13,16,19-tetraazahenicos-5-en-21-oate (**27g**)

Compound **27g** was synthesized from **26g** (258 mg, 0.22 mmol)

in a manner similar to that described for the synthesis of **27a**. Purification by column chromatography (Hexane/EtOAc 1:3) gave **27g** (209 mg, 90%) as a colorless amorphous solid. $[\alpha]_D^{25} - 9.8$ (c 1.0, CHCl_3); ^1H NMR (400 MHz, CDCl_3): δ 0.84–0.93 (12H, m), 1.62–1.67 (2H, m), 1.73–1.75 (1H, m), 2.03–2.22 (5H, m), 2.25–2.39 (2H, m), 2.46 (1H, dd, $J = 12.2, 5.4$ Hz), 2.63–2.68 (1H, m), 3.19 (1H, br s), 3.63 (3H, s), 3.75–3.90 (2H, m), 4.21–4.24 (1H, m), 4.26–4.34 (2H, m), 4.49–4.55 (1H, m), 5.35 (1H, dd, $J = 15.1, 5.9$ Hz), 5.44 (1H, dt, $J = 15.1, 6.3$ Hz), 6.68 (1H, brs), 7.14–7.42 (33H, m); ^{13}C NMR (100 MHz, CDCl_3): δ 17.8, 19.3, 21.4, 23.1, 24.8, 29.8, 31.3, 33.4, 38.6, 40.0, 40.9, 43.6, 52.0, 52.1, 52.5, 59.5, 66.6, 66.8, 69.6, 126.6 (3C), 126.9 (3C), 127.8 (6C), 128.1 (6C), 129.3 (6C), 129.5 (6C), 130.1, 132.4, 144.1 (3C), 144.8 (3C), 170.0, 170.1, 171.6, 172.3, 172.5; IR (neat): 3279, 3059, 2957, 2926, 1753, 1637, 1543, 1491, 1443, 1216, 1034, 745, 700, 676 cm^{-1} ; HRMS (FAB): m/z calcd for $\text{C}_{62}\text{H}_{71}\text{N}_4\text{O}_7\text{S}_2$ ($\text{M}^+ + \text{H}$) 1047.4764, found 1047.4758.

4.1.56. (7S,11R,14S,17R,E)-7-Hydroxy-11-isopropyl-17-isobutyl-9,12,15,18-tetraoxo-1,1,1-triphenyl-14-tritylthiomethyl-2-thia-10,13,16,19-tetraazahenicos-5-en-21-oic acid (**14g**)

Compound **14g** was synthesized from **27g** (250 mg, 0.24 mmol) in a manner similar to that described for the synthesis of **14a**. Purification by column chromatography ($\text{CHCl}_3/\text{MeOH}$ 10:1 to 8:1) gave **14g** (230 mg, 93%) as a colorless amorphous solid. $[\alpha]_D^{25} - 13.4$ (c 1.1, CHCl_3); ^1H NMR (400 MHz, $\text{CD}_3\text{OD}/\text{CDCl}_3$ 10:1): δ 0.85–0.94 (12H, m), 1.50–1.66 (3H, m), 2.05–2.62 (7H, m), 2.54–2.76 (2H, m), 3.65–3.78 (2H, m), 4.10–4.19 (2H, m), 4.32–4.38 (2H, m), 5.39–5.54 (2H, m), 7.19–7.40 (30H, m); ^{13}C NMR (100 MHz, $\text{CD}_3\text{OD}/\text{CDCl}_3$ 10:1): δ 18.1, 19.7, 21.7, 23.6, 25.4, 30.4, 30.7, 32.1, 32.3, 33.8, 41.1, 44.0, 53.0, 53.8, 60.3, 67.4, 67.8, 70.1, 127.4 (3C), 127.7 (3C), 128.5 (6C), 128.8 (6C), 130.2 (6C), 130.3 (6C), 130.6, 133.7, 145.2 (3C), 145.8 (3C), 170.0, 171.6, 171.7, 173.4, 174.1; IR (neat): 3296, 3057, 2958, 2928, 1637, 1538, 1490, 1444, 1219, 1034, 744, 700, 675, 617 cm^{-1} ; HRMS (FAB): m/z calcd for $\text{C}_{61}\text{H}_{68}\text{N}_4\text{O}_7\text{S}_2\text{Na}$ ($\text{M}^+ + \text{Na}$) 1055.4427, found 1055.4436.

4.1.57. (6R,9S,12R,16S)-12-Isopropyl-6-isobutyl-16-[(E)-4-tritylthiobut-1-enyl]-9-tritylthiomethyl-1-oxa-4,7,10,13-tetraazacyclohexadecane-2,5,8,11,14-pentaone (**28g**)

Compound **28g** was synthesized from **14g** (230 mg, 0.22 mmol) in a manner similar to that described for the synthesis of **28a**. Purification by column chromatography (hexane/EtOAc 1:3) gave **28g** (157 mg, 69%) as a colorless amorphous solid. $[\alpha]_D^{25} - 3.6$ (c 1.0, CHCl_3); ^1H NMR (400 MHz, CDCl_3): δ 0.84–0.91 (12H, m), 1.62–1.68 (1H, m), 1.79–1.85 (2H, m), 1.95–2.03 (3H, m), 2.14–2.17 (2H, m), 2.33–2.56 (3H, m), 2.87–2.92 (1H, m), 3.67–3.69 (2H, m), 4.12–4.17 (2H, m), 4.25–4.31 (1H, m), 5.31 (1H, dd, $J = 14.6, 6.8$ Hz), 5.53–5.57 (2H, m), 6.29–6.31 (1H, m), 7.14–7.40 (32H, m), 7.66–7.76 (1H, m); ^{13}C NMR (100 MHz, CDCl_3): δ 18.2, 19.5, 21.3, 23.2, 24.9, 29.7, 30.8, 31.1, 31.3, 31.8, 39.3, 41.8, 42.4, 52.5, 58.4, 66.6, 67.0, 72.3, 126.6 (3C), 126.8 (3C), 127.8 (6C), 128.0 (6C), 129.4 (6C), 129.5 (7C), 132.4, 144.3 (3C), 144.8 (3C), 169.1, 169.6, 170.9, 172.0, 173.2; IR (neat): 3305, 3056, 2958, 2927, 1743, 1655, 1542, 1490, 1444, 1278, 1215, 1035, 744, 700, 667 cm^{-1} ; HRMS (FAB): m/z calcd for $\text{C}_{61}\text{H}_{67}\text{N}_4\text{O}_6\text{S}_2$ ($\text{M}^+ + \text{H}$) 1015.4502, found; 1015.4503.

4.1.58. FK-A7 (**13g**)

Compound **13g** was synthesized from **28g** (157 mg, 0.16 mmol) in a manner similar to that described for the synthesis of **13a**. Purification by column chromatography ($\text{CHCl}_3/\text{MeOH}$ 20:1) gave **13g** (67.7 mg, 83%) as a colorless amorphous solid. $[\alpha]_D^{25} + 26.7$ (c 0.56, CHCl_3); ^1H NMR (400 MHz, CDCl_3): δ 0.89 (3H, d, $J = 6.8$ Hz), 0.93 (3H, d, $J = 5.9$ Hz), 1.09–1.11 (6H, m), 1.55–1.66 (1H, m), 1.82–1.89 (1H, m), 2.03–2.10 (1H, m), 2.18–2.26 (1H, m), 2.52–2.65 (1H, m), 2.64 (1H, d, $J = 12.7$ Hz), 2.70–2.74 (1H, m), 2.92–3.02 (3H, m),

3.06–3.12 (1H, m), 3.38 (1H, d, J = 15.9, 10.7 Hz), 3.64–3.69 (1H, m), 3.92 (1H, dd, J = 17.6, 2.4 Hz), 4.06 (1H, t, J = 5.1 Hz), 4.38 (1H, dd, J = 17.8, 6.3 Hz), 4.77–4.82 (1H, m), 5.73–7.76 (2H, m), 5.85–5.90 (1H, m), 6.60 (1H, d, J = 3.4 Hz), 7.13 (1H, d, J = 1.0 Hz), 7.54 (1H, d, J = 7.3 Hz), 7.72 (1H, d, J = 6.3 Hz); ^{13}C NMR (100 MHz, CDCl_3): δ 19.4, 19.5, 21.5, 23.1, 25.0, 29.3, 31.3, 34.6, 36.7, 37.5, 38.3, 43.0, 54.5, 54.9, 62.0, 69.4, 129.8, 130.3, 168.0, 170.0, 170.2, 171.0, 172.5; IR (neat): 3340, 2960, 2927, 2871, 1756, 1653, 1523, 1260, 1187, 981, 756, 668 cm^{-1} ; HRMS (FAB): m/z calcd for $\text{C}_{23}\text{H}_{37}\text{N}_4\text{O}_6\text{S}_2$ ($\text{M}^+ + \text{H}$) 529.2155, found 529.2155.

4.1.59. Fmoc-L-Leu-Gly-OMe (30h)

Compound **30h** was synthesized from L-leucine (L-Leu) (**18h**) (500 mg, 3.8 mmol) in a manner similar to that described for the synthesis of **21**. Purification by column chromatography (Hexane/EtOAc 1:1) gave **30h** (158 g, 97%, 2 steps) as a colorless amorphous solid. $[\alpha]_D^{25}$ –21.0 (c 1.0, CHCl_3); ^1H NMR (400 MHz, CDCl_3): δ 0.92–0.95 (6H, m), 1.54–1.67 (3H, m), 3.72 (3H, s), 4.01–4.03 (2H, m), 4.18–4.26 (2H, m), 4.37–4.43 (2H, m), 5.33 (1H, br s), 6.67 (1H, br s), 7.25–7.31 (2H, m), 7.37–7.40 (2H, m), 7.57 (2H, d, J = 7.3 Hz), 7.75 (2H, d, J = 7.3 Hz); ^{13}C NMR (100 MHz, CDCl_3): δ 21.9, 22.9, 24.6, 41.1, 41.3, 47.2, 52.3, 53.3, 67.0, 120.0 (2C), 125.0 (2C), 127.1 (2C), 127.7 (2C), 141.3 (2C), 143.8 (2C), 156.2, 170.1, 172.3; IR (neat): 3302, 2956, 2361, 1749, 1704, 1665, 1539, 1449, 1213, 1045, 758, 740 cm^{-1} ; HRMS (FAB): m/z calcd for $\text{C}_{24}\text{H}_{29}\text{N}_2\text{O}_5$ ($\text{M}^+ + \text{H}$) 425.2076, found 425.2071.

4.1.60. Boc-D-Cys(Tr)-L-Leu-Gly-OMe (32h)

Compound **32h** was synthesized from **30h** (1.62 g, 3.8 mmol) in a manner similar to that described for the synthesis of **23**. Purification by column chromatography (hexane/EtOAc 1:1) gave **32h** (1.85 g, 83%, 2 steps) as a colorless amorphous solid. $[\alpha]_D^{25}$ –25.5 (c 1.0, CHCl_3); ^1H NMR (400 MHz, CDCl_3): δ 0.87 (3H, d, J = 6.8 Hz), 0.89 (3H, d, J = 6.3 Hz), 1.48 (9H, s), 1.46–1.55 (1H, m), 1.55–1.64 (1H, m), 1.72–1.79 (1H, m), 2.56 (1H, dd, J = 12.7, 5.4 Hz), 2.76 (1H, dd, J = 12.7, 6.8 Hz), 3.69 (3H, s), 3.71–3.80 (2H, m), 4.01 (1H, dd, J = 14.9, 4.4 Hz), 4.43–4.48 (1H, m), 4.89 (1H, d, J = 6.4 Hz), 6.32 (1H, d, J = 6.3 Hz), 7.04 (1H, brs), 7.16–7.40 (15H, m); ^{13}C NMR (100 MHz, CDCl_3): δ 21.5, 23.0, 24.6, 28.1 (3C), 33.5, 40.2, 40.9, 51.5, 52.1, 54.1, 67.2, 80.5, 127.0 (3C), 128.0 (6C), 129.4 (6C), 144.2 (3C), 155.3, 167.0, 170.7, 171.9; IR (neat): 3290, 2953, 1753, 1653, 1540, 1490, 1445, 1366, 1212, 1168, 1036, 743 cm^{-1} ; HRMS (FAB): m/z calcd for $\text{C}_{36}\text{H}_{46}\text{N}_3\text{O}_6\text{S}$ ($\text{M}^+ + \text{H}$) 648.3107, found 648.3109.

4.1.61. H₂N-D-Cys(Tr)-L-Leu-Gly-OMe (15h)

Compound **15h** was synthesized from **32h** (1.85 g, 2.9 mmol) in a manner similar to that described for the synthesis of **15a**. Purification by column chromatography ($\text{CHCl}_3/\text{MeOH}$ 40:1) gave **15h** (1.31 g, 77%) as a colorless amorphous solid. $[\alpha]_D^{25}$ –55.0 (c 1.0, CHCl_3); ^1H NMR (400 MHz, CDCl_3): δ 0.88 (3H, d, J = 6.3 Hz), 0.91 (3H, d, J = 6.8 Hz), 1.48–1.64 (4H, m), 1.72–1.79 (1H, m), 2.65 (1H, dd, J = 12.2, 3.9 Hz), 2.73 (1H, dd, J = 12.7, 6.8 Hz), 3.10 (1H, dd, J = 7.8, 6.8 Hz), 3.67 (3H, s), 3.78 (1H, dd, J = 18.1, 5.4 Hz), 3.96 (1H, dd, J = 18.1, 5.9 Hz), 4.37–4.43 (1H, m), 6.86 (1H, t, J = 5.4 Hz), 7.20–7.45 (16H, m); ^{13}C NMR (100 MHz, CDCl_3): δ 21.8, 22.9, 24.8, 37.5, 40.1, 40.9, 51.3, 52.2, 53.9, 67.0, 126.9 (3C), 128.0 (6C), 129.5 (6C), 144.5 (3C), 169.9, 172.1, 173.4; IR (neat): 3286, 3060, 2954, 1752, 1650, 1555, 1490, 1444, 1208, 1035, 743, 700 cm^{-1} ; HRMS (FAB): m/z calcd for $\text{C}_{31}\text{H}_{38}\text{N}_3\text{O}_4\text{S}$ ($\text{M}^+ + \text{H}$) 548.2583, found 548.2575.

4.1.62. (7S,11R,14S,17S,E)-Isobutyl 11-isopropyl-7-(4-methoxybenzyloxy)-17-isobutyl-9,12,15,18-tetraoxo-1,1,1-triphenyl-14-tritylthiomethyl-2-thia-10,13,16,19-tetraazahenicos-5-en-21-oate (26h)

Compound **26h** was synthesized from **15h** (167 mg, 0.30 mmol)

in a manner similar to that described for the synthesis of **26a**. Purification by column chromatography (hexane/EtOAc 1:2) gave **26h** (195 mg, 50%) as a colorless amorphous solid. $[\alpha]_D^{25}$ +7.6 (c 1.1, CHCl_3); ^1H NMR (400 MHz, CDCl_3): δ 0.69 (3H, d, J = 6.8 Hz), 0.79 (3H, d, J = 6.8 Hz), 0.84 (3H, d, J = 5.8 Hz), 0.87 (3H, d, J = 6.3 Hz), 1.53–1.72 (3H, m), 1.93–1.96 (1H, m), 2.04–2.18 (2H, m), 2.21–2.25 (2H, m), 2.46 (2H, d, J = 5.4 Hz), 2.56 (1H, dd, J = 12.7, 5.4 Hz), 2.79 (1H, dd, J = 12.7, 7.3 Hz), 3.63 (3H, s), 3.78 (3H, s), 3.78–3.84 (1H, m), 3.88–3.95 (2H, m), 4.06 (1H, dd, J = 13.4, 5.9 Hz), 4.14 (1H, t, J = 6.3 Hz), 4.21 (1H, d, J = 10.7 Hz), 4.40 (1H, d, J = 10.7 Hz), 4.49–4.54 (1H, m), 5.29 (1H, dd, J = 14.6, 7.3 Hz), 5.54 (1H, dt, J = 15.1, 6.8 Hz), 6.60 (1H, d, J = 7.8 Hz), 6.82 (2H, d, J = 8.7 Hz), 6.96 (1H, br s), 7.16–7.31 (34H, m); ^{13}C NMR (100 MHz, CDCl_3): δ 17.8, 19.4, 21.5, 23.1, 24.6, 30.3, 31.28, 31.34, 33.7, 40.7, 41.0, 42.4, 51.7, 52.0, 52.6, 55.3, 59.1, 66.6, 67.1, 70.0, 76.5, 113.8 (2C), 126.6 (3C), 126.9 (3C), 127.8 (6C), 128.0 (6C), 129.47 (6C), 129.52 (6C), 129.7, 129.8 (2C), 129.9, 133.2, 144.3 (3C), 144.8 (3C), 159.3, 169.7, 170.0, 171.2, 171.7, 172.3; IR (neat): 3237, 3058, 2956, 2929, 1755, 1633, 1539, 1514, 1489, 1443, 1248, 1206, 1180, 1034, 744, 700 cm^{-1} ; HRMS (FAB): m/z calcd for $\text{C}_{70}\text{H}_{79}\text{N}_4\text{O}_8\text{S}_2$ ($\text{M}^+ + \text{H}$) 1167.5339, found 1167.5322.

4.1.63. (7S,11R,14S,17S,E)-Methyl 7-hydroxy-11-isopropyl-17-isobutyl-9,12,15,18-tetraoxo-1,1,1-triphenyl-14-tritylthiomethyl-2-thia-10,13,16,19-tetraazahenicos-5-en-21-oate (27h)

Compound **27h** was synthesized from **26h** (160 mg, 0.14 mmol) in a manner similar to that described for the synthesis of **27a**. Purification by column chromatography (hexane/EtOAc 1:3) gave **27h** (97 mg, 68%) as a colorless amorphous solid. $[\alpha]_D^{25}$ –36.7 (c 1.0, CHCl_3); ^1H NMR (400 MHz, CDCl_3): δ 0.85 (3H, d, J = 5.9 Hz), 0.92 (3H, d, J = 5.9 Hz), 0.95 (3H, d, J = 7.3 Hz), 1.00 (3H, d, J = 7.3 Hz), 1.64–1.78 (3H, m), 2.00–2.09 (2H, m), 2.16–2.23 (2H, m), 2.25–2.36 (2H, m), 2.44 (1H, dd, J = 13.2, 3.4 Hz), 2.58–2.68 (2H, m), 3.54 (3H, s), 3.64 (1H, dd, J = 18.0, 4.9 Hz), 4.03–4.14 (2H, m), 4.29–4.34 (1H, m), 4.39–4.45 (2H, m), 5.39 (1H, dd, J = 15.4, 6.3 Hz), 5.59 (1H, dt, J = 15.1, 6.8 Hz), 6.05 (1H, d, J = 6.3 Hz), 6.91–6.99 (2H, m), 7.15–7.42 (31H, m); ^{13}C NMR (100 MHz, CDCl_3): δ 17.5, 19.6, 21.6, 23.0, 24.6, 29.7, 31.2, 31.4, 33.7, 38.6, 40.8, 44.0, 51.7, 52.0, 52.3, 60.2, 66.6, 66.8, 69.5, 126.6 (3C), 126.7 (3C), 127.85 (6C), 127.90 (6C), 129.5 (6C), 129.5 (6C), 129.8, 132.8, 144.5 (3C), 144.8 (3C), 170.7 (2C), 171.0, 172.8, 173.1; IR (neat): 3288, 3058, 2957, 2926, 1747, 1633, 1539, 1489, 1444, 1215, 1183, 1034, 744, 699 cm^{-1} ; HRMS (FAB): m/z calcd for $\text{C}_{62}\text{H}_{71}\text{N}_4\text{O}_7\text{S}_2$ ($\text{M}^+ + \text{H}$) 1047.4764, found 1047.4791.

4.1.64. (7S,11R,14S,17S,E)-7-Hydroxy-11-isopropyl-17-isobutyl-9,12,15,18-tetraoxo-1,1,1-triphenyl-14-tritylthiomethyl-2-thia-10,13,16,19-tetraazahenicos-5-en-21-oic acid (14h)

Compound **14h** was synthesized from **27h** (147 mg, 0.13 mmol) in a manner similar to that described for the synthesis of **14a**. Purification by column chromatography ($\text{CHCl}_3/\text{MeOH}$ 10:1 to 8:1) gave **14h** (115 mg, 89%) as a colorless amorphous solid. $[\alpha]_D^{25}$ –19.6 (c 1.0, CHCl_3); ^1H NMR (400 MHz, $\text{CDCl}_3/\text{CD}_3\text{OD}$ 10:1): δ 0.83–0.94 (12H, m), 1.59–1.69 (3H, m), 2.01–2.23 (5H, m), 2.37–2.39 (2H, m), 2.50–2.55 (1H, m), 2.59–2.64 (1H, m), 3.64–3.92 (2H, m), 4.08–4.12 (2H, m), 4.30–4.35 (1H, m), 4.40–4.45 (1H, m), 5.42 (1H, dd, J = 15.4, 5.4 Hz), 5.55 (1H, dt, J = 15.1, 6.3 Hz), 7.17–7.45 (30H, m); ^{13}C NMR (100 MHz, $\text{CDCl}_3/\text{CD}_3\text{OD}$ 10:1): δ 17.5, 19.1, 21.1, 22.9, 24.5, 29.5, 31.2, 31.3, 32.7, 39.7, 41.4, 43.1, 51.9, 52.6, 59.4, 66.5, 66.8, 68.9, 126.5 (3C), 126.7 (3C), 127.7 (6C), 127.8 (6C), 128.5, 129.3 (6C), 129.4 (6C), 132.6, 144.2 (3C), 144.7 (3C), 170.6, 170.7, 171.98, 172.03, 172.9; IR (neat): 3287, 3057, 2959, 2928, 1726, 1636, 1538, 1490, 1468, 1444, 1218, 1034, 744, 700 cm^{-1} ; HRMS (FAB): m/z calcd for $\text{C}_{61}\text{H}_{69}\text{N}_4\text{O}_7\text{S}_2$ ($\text{M}^+ + \text{H}$) 1033.4608, found 1033.4608.

4.1.65. (6S,9S,12R,16S)-12-Isopropyl-6-isobutyl-16-[(E)-4-tritylthiobut-1-enyl]-9-tritylthiomethyl-1-oxa-4,7,10,13-tetraazacyclohexadecane-2,5,8,11,14-pentaone (**28h**)

Compound **28h** was synthesized from **14h** (49.6 mg, 0.14 mmol) in a manner similar to that described for the synthesis of **28a**. Purification by column chromatography (CHCl₃/MeOH 40:1) gave **28h** (56.0 mg, 50%) as a colorless amorphous solid. [α]_D²⁵ –24.1 (c 1.0, CHCl₃); ¹H NMR (400 MHz, CDCl₃): δ 0.80–0.85 (9H, m), 0.91 (3H, d, *J* = 6.8 Hz), 1.36–1.44 (1H, m), 1.51–1.57 (1H, m), 1.71–1.74 (1H, m), 1.93–2.07 (3H, m), 2.09–2.15 (2H, m), 2.49–2.55 (2H, m), 2.71–2.75 (1H, m), 2.82–2.87 (1H, m), 3.53–3.59 (2H, m), 4.22–4.29 (2H, m), 4.41–4.47 (1H, m), 5.38 (1H, dd, *J* = 15.6, 6.3 Hz), 5.48–5.41 (1H, m), 5.59 (1H, dt, *J* = 14.6, 6.8 Hz), 6.42 (1H, brs), 7.12–7.38 (33H, m); ¹³C NMR (100 MHz, CDCl₃): δ 17.8, 19.7, 21.0, 21.3, 23.2, 24.7, 28.2, 31.0, 31.2, 31.4, 32.3, 41.9, 51.5, 54.0, 58.9, 66.7, 66.8, 71.8, 126.6 (3C), 126.7 (3C), 127.8 (6C), 128.0 (6C), 129.4 (6C), 129.5 (7C), 133.0, 144.4 (3C), 144.7 (3C), 168.8, 169.5, 170.0, 172.2, 172.3; IR (neat): 3292, 3059, 2959, 2928, 1739, 1653, 1537, 1492, 1444, 1214, 1034, 750, 700 cm^{–1}; HRMS (FAB): *m/z* calcd for C₆₁H₆₇N₄O₆S₂ (M⁺+H) 1015.4502, found 1015.4501.

4.1.66. FK-A8 (**13h**)

Compound **13h** was synthesized from **28h** (56.0 mg, 56 μ mol) in a manner similar to that described for the synthesis of **13a**. Purification by column chromatography (CHCl₃/MeOH 20:1) gave **13h** (19.0 mg, 64%) as a colorless amorphous solid. [α]_D²⁵ –41.1 (c 1.4, CHCl₃); ¹H NMR (400 MHz, CDCl₃): δ 0.92 (3H, d, *J* = 5.9 Hz), 0.96 (3H, d, *J* = 5.9 Hz), 1.09 (3H, d, *J* = 2.4 Hz), 1.11 (3H, d, *J* = 2.4 Hz), 1.59–1.74 (3H, m), 2.28–2.34 (1H, m), 2.48–2.51 (1H, m), 2.65–2.68 (2H, m), 2.89–2.95 (2H, m), 3.08–3.13 (1H, m), 3.20 (2H, d, *J* = 7.3 Hz), 4.02–4.07 (2H, m), 4.24 (1H, dd, *J* = 17.1, 4.9 Hz), 4.52 (1H, td, *J* = 9.3, 4.4 Hz), 4.79 (1H, dd, *J* = 14.4, 6.8 Hz), 5.72–5.88 (3H, m), 6.51 (1H, br s), 7.61 (1H, br s), 8.29 (1H, d, *J* = 8.3 Hz), 7.45 (1H, d, *J* = 6.8 Hz); ¹³C NMR (100 MHz, CDCl₃): δ 18.8, 19.5, 21.6, 23.0, 24.8, 29.3, 31.0, 37.1, 37.4, 39.6, 40.8, 42.5, 52.7, 56.1, 62.3, 69.4, 129.0, 129.7, 167.3, 169.6, 171.0, 171.1, 171.8; IR (neat): 3299, 2960, 2930, 1743, 1653, 1530, 1468, 1437, 1254, 1220, 1189, 770, 665 cm^{–1}; HRMS (FAB): *m/z* calcd for C₂₃H₃₇N₄O₆S₂ (M⁺+H) 529.2155, found 529.2158.

4.2. Biological evaluation

4.2.1. HDACs preparation and enzyme inhibition assay [26]

In a 100-mm dish, 293T cells (1–2 × 10⁷) were grown for 24 h and transiently transfected with 10 μ g each of the vector pcDNA3-HDAC1 for human HDAC1 or pcDNA3-mHDA2/HDAC6 for mouse HDAC6, using the LipofectAMINE2000 reagent (Invitrogen). After successive cultivation in DMEM for 24 h, the cells were washed with PBS and lysed by sonication in lysis buffer containing 50 mM Tris–HCl (pH 7.5), 120 mM NaCl, 5 mM EDTA, and 0.5% NP40. The soluble fraction collected by microcentrifugation was precleared by incubation with protein A/G agarose beads (Roche). After the cleared supernatant had been incubated for 1 h at 4 °C with 4 μ g of an anti-FLAG M2 antibody (Sigma–Aldrich Inc.) for HDAC1 and HDAC6, the agarose beads were washed three times with lysis buffer and once with histone deacetylase buffer consisting of 20 mM Tris–HCl (pH 8.0), 150 mM NaCl, and 10% glycerol. The bound proteins were released from the immune complex by incubation for 1 h at 4 °C with 40 μ g of the FLAG peptide (Sigma–Aldrich Inc.) in histone deacetylase buffer (200 μ L). The supernatant was collected by centrifugation. For the enzyme assay, 10 μ L of the enzyme fraction was added to 1 μ L of fluorescent substrate (2 mM Ac-KGLGK(Ac)-MCA) and 9 μ L of histone deacetylase buffer, and the mixture was incubated at 37 °C for 30 min. The reaction was stopped by the addition of 30 μ L of trypsin

(20 mg/mL) and incubated at 37 °C for 15 min. The released aminomethylcoumarin (AMC) was measured using a fluorescence plate reader. The 50% inhibitory concentrations (IC₅₀) were determined as the means with SD calculated from at least three independent dose–response curves. The HDAC inhibitory activity of all test compounds was measured in the presence of 0.1 mM DTT.

4.2.2. Cell-growth inhibition assay [24]

This experiment was carried out at the Cancer Chemotherapy Center, Japanese Foundation for Cancer Research. The screening panel consisted of the following 39 human cancer cell lines (HCC panel): breast cancer HBC-4, BSY-1, HBC-5, MCF-7, and MDA-MB-231; brain cancer U-251, SF-268, SF-295, SF-539, SNB-75, and SNB-78; colon cancer HCC2998, KM-12, HT-29, HCT-15, and HCT-116; lung cancer NCI-H23, NCI-H226, NCI-H522, NCI-H460, A549, DMS273, and DMS114; melanoma LOX-IMVI; ovarian cancer OVCAR-3, OVCAR-4, OVCAR-5, OVCAR-8, and SK-OV-3; renal cancer RXF-631L and ACHN; stomach cancer St-4, MKN1, MKN7, MKN28, MKN45, and MKN74; prostate cancer DU-145 and PC-3. The GI₅₀ (50% cell growth inhibition) value for these cell lines was determined by using the sulforhodamine B colorimetric method.

Acknowledgements

We are grateful to the Screening Committee of New Anticancer Agents, which is supported by a Grant-in-Aid for Scientific Research on Innovative Area ‘Scientific Support Programs for Cancer Research (No. 221S0001, 2010–2014)’ from the Ministry of Education, Culture, Sports, Science and Technology, Japan (MEXT), for assistance with the biological evaluation of compounds **1** and **13a–h**. This study was also supported by a Grant-in-Aid for the Strategic Research Foundation Program at Private Universities (No. S1511001L, 2015–2019), a Grant-in-Aid for Scientific Research (C) (No. 15K07865, 2015–2017), and a Grant-in-Aid for Scientific Research (S) (No. 26221204, 2014–2018) from MEXT.

Appendix A. Supplementary data

Supplementary data related to this article can be found at <http://dx.doi.org/10.1016/j.ejmech.2016.05.031>.

References

- [1] (a) M. Mottamal, S. Zheng, T.L. Huang, G. Wang, *Molecules* 20 (2015) 3898–3941; (b) C. Micelli, G. Rastelli, *Drug Discov. Today* 20 (2015) 718–735; (c) S. Tan, Z.-P. Liu, *ChemMedChem* 10 (2015) 441–450; (d) B. Kim, J. Hong, *Curr. Top. Med. Chem.* 14 (2015) 2759–2782; (e) A. Abend, I. Kehat, *Pharmacol. Ther.* 147 (2015) 55–62; (f) L. Zhang, Y. Han, Q. Jiang, C. Wang, X. Chen, X. Li, F. Xu, Y. Jiang, Q. Wang, W. Xu, *Med. Res. Rev.* 35 (2015) 63–84; (g) K.J. Falkenberg, R.W. Johnstone, *Nat. Rev. Drug Discov.* 13 (2014) 673–691; (h) W. Feng, B. Zhang, D. Cai, X. Zou, *Cancer Lett.* 347 (2014) 183–190; (i) A.C. West, R.W. Johnstone, *J. Clin. Invest.* 124 (2014) 30–39; (j) J. Li, G. Li, W. Xu, *Curr. Med. Chem.* 20 (2013) 1853–1886.
- [2] (a) X. Li, J. Hou, X. Li, Y. Jiang, X. Liu, W. Mu, Y. Jin, Y. Zhang, W. Xu, *Eur. J. Med. Chem.* 89 (2015) 628–637; (b) C.-Q. Ning, C.L.L. Hu, Y.-J. Bi, L. Yao, Y.-J. He, L.-F. Liu, X.-Y. Liu, N.-F. Yu, *Eur. J. Med. Chem.* 95 (2015) 104–115; (c) X. Zhang, Y. Kong, J. Zhang, M. Su, Y. Zhou, Y. Zang, J. Li, Y. Chen, Y. Fang, X. Zhang, W. Lu, *Eur. J. Med. Chem.* 95 (2015) 127–135; (d) I. Denis, F. Bahhaj, F. Collette, R. Delatouche, F. Gueugnon, D. Pouliquen, L. Pichavant, V. Héroguez, M. Grégoire, P. Bertrand, C. Blanquar, *Eur. J. Med. Chem.* 95 (2015) 369–376.
- [3] (a) O. Witt, H.E. Deubzer, T. Milde, I. Oehme, *Cancer Lett.* 277 (2009) 8–21; (b) M. Haberland, R.L. Montgomery, E.N. Olson, *Nat. Rev. Genet.* 10 (2009) 32–42; (c) M.A. Holbert, R. Marmorstein, *Curr. Opin. Struct. Biol.* 15 (2005) 673–680; (d) S. Voelt-Mahlknecht, A.D. Ho, U. Mahlnecht, *Int. J. Mol. Med.* 16 (2005) 589–598; (e) A.J.M. De Ruijter, A.H. Van Gennip, H.N. Caron, S. Kemp, A.B.P. Van

- Kuilenburg, *Biochem. J.* 370 (2003) 737–749.
- [4] (a) T.A. McKinsey, *J. Mol. Cell. Cardiol.* 51 (2011) 491–496;
(b) A.P. Kozikowski, K.V. Butler, *Curr. Pharm. Des.* 14 (2008) 505–528;
(c) A.V. Bieliauskas, M.K.H. Pflum, *Chem. Soc. Rev.* 37 (2008) 1402–1413;
(d) S. Senese, K. Zaragoza, S. Minardi, I. Muradore, S. Ronzoni, A. Passafaro, L. Bernard, G.F. Draetta, M. Alcalay, C. Seiser, S. Chiocca, *Mol. Cell. Biol.* 27 (2007) 4784–4795;
(e) P. Kahnberg, A.J. Lucke, M.P. Glenn, G.M. Boyle, J.D.A. Tyndall, P.G. Parsons, D.P. Fairlie, *J. Med. Chem.* 49 (2006) 7611–7622;
(f) S. Chang, T.A. McKinsey, C.L. Zhang, J.A. Richardson, J.A. Hill, E.N. Olson, *Mol. Cell. Biol.* 24 (2004) 8467–8476.
- [5] (a) K.M. Van der Molen, W. McCulloch, C.J. Pearce, N.H. Oberlies, *J. Antibiot.* 64 (2011) 525–531;
(b) C. Grant, F. Rahman, R. Piekarz, C. Peer, R. Frye, R.W. Robey, E.R. Gardner, W.D. Figg, S.E. Bates, *Expert Rev. Anticancer Ther.* 10 (2010) 997–1008.
- [6] M.H. Shah, P. Binkley, K. Chan, J. Xiao, D. Arbogast, M. Collamore, Y. Farra, D. Young, M. Grever, *Clin. Cancer Res.* 12 (2006) 3997–4003.
- [7] (a) H. Ueda, H. Nakajima, Y. Hori, T. Fujita, M. Nishimura, T. Goto, M. Okuhara, *J. Antibiot.* 47 (1994) 301–310;
(b) N. Shigematsu, H. Ueda, S. Takase, H. Tanaka, *J. Antibiot.* 47 (1994) 311–314;
(c) H. Ueda, T. Manda, S. Matsumoto, S. Mukumoto, F. Nishigaki, I. Kawamura, K. Shimomura, *J. Antibiot.* 47 (1994) 315–323.
- [8] R. Furumai, A. Matsuyama, N. Kobashi, K.-H. Lee, M. Nishiyama, H. Nakajima, A. Tanaka, Y. Komatsu, N. Nishino, M. Yoshida, S. Horinouchi, *Cancer Res.* 62 (2002) 4916–4921.
- [9] (a) K. Nagai, M. Taniguchi, N. Shindo, Y. Terada, M. Mori, N. Amino, K. Suzumura, I. Takahashi, M. Amase, (Yamanouchi Pharmaceutical Co. Ltd., Japan), *PCT WO 20460 A1* (2004). (b) Y. Masuoka, A. Nagai, K. Shin-ya, K. Furihata, K. Nagai, K. Suzuki, Y. Hayakawa, H. Seto, *Tetrahedron Lett.* 42 (2001) 41–44;
(c) N. Shindo, A. Terada, M. Mori, N. Amino, K. Hayata, K. Nagai, Y. Hayakawa, K. Shin-ya, Y. Masuoka, (Yamanouchi Pharmaceutical Co. Ltd., Japan), *Japan Kokai Tokkyo Koho JP 348340A* (2001).
- [10] M. Okuhara, T. Goto, T. Fujita, Y. Hori, H. Ueda, *Japan Kokai Tokkyo Koho JP 3141296*, (1991).
- [11] J.B. Biggins, C.D. Gleber, S.F. Brady, *Org. Lett.* 13 (2011) 1536–1539.
- [12] (a) C. Wang, C.J. Flemming, Y.-Q. Cheng, *MedChemComm* 3 (2012) 976–981;
(b) C. Wang, L.M. Henkes, L.B. Dougherty, M. He, D. Wang, F.J. Meyer-Almes, Y.-Q. Cheng, *J. Nat. Prod.* 74 (2011) 2031–2038.
- [13] **Total synthesis of FK228 (1):** (a) K. Narita, T. Kikuchi, K. Watanabe, T. Takizawa, T. Yamori, M. Yoshida, T. Katoh, *Chem. A Eur. J.* 15 (2009) 11174–11186;
(b) T.J. Greshock, D.M. Johns, Y. Noguchi, R.M. Williams, *Org. Lett.* 10 (2008) 613–616;
(c) S. Wen, G. Packham, A. Ganesan, *J. Org. Chem.* 73 (2008) 9353–9361;
(d) K.W. Li, J. Wu, W. Xing, J.A. Simon, *J. Am. Chem. Soc.* 118 (1996) 7237–7238.
- [14] **Total synthesis of spiruchostatin A (2):** (a) M. Yoshida, K. Sasahara, T. Doi, *Tetrahedron* 71 (2015) 7647–7653;
(b) N.A. Calandra, Y.L. Cheng, K.A. Kocak, J.S. Miller, *Org. Lett.* 11 (2009) 1971–1974;
(c) T. Takizawa, K. Watanabe, K. Narita, K. Kudo, T. Oguchi, H. Abe, T. Katoh, *Heterocycles* 76 (2008) 275–290;
(d) T. Doi, Y. Iijima, K. Shin-ya, A. Ganesan, T. Takahashi, *Tetrahedron Lett.* 47 (2006) 1177–1180;
(e) A. Yurek-George, F. Habens, M. Brimmell, G. Packham, A. Ganesan, *J. Am. Chem. Soc.* 126 (2004) 1030–1031.
- [15] **Total synthesis of spiruchostatin B (3):** (a) S. Fuse, K. Okada, Y. Iijima, A. Munakata, K. Machida, T. Takahashi, M. Takagi, K. Shin-ya, T. Doi, *Org. Biomol. Chem.* 9 (2011) 3825–3833;
(b) T. Takizawa, K. Watanabe, K. Narita, K. Kudo, T. Oguchi, H. Abe, T. Katoh, *Chem. Commun.* (2008) 1677–1679.
- [16] **Total synthesis of spiruchostatins C (4) and D (5):** K. Narita, Y. Fukui, Y. Sano, T. Yamori, A. Ito, M. Yoshida, T. Katoh, *Eur. J. Med. Chem.* 60 (2013) 295–304.
- [17] **Total synthesis of FR901375 (6):** Y. Chen, C. Gambis, Y. Abe, P. Wentworth Jr., K.D. Janda, *J. Org. Chem.* 68 (2003) 8902–8905.
- [18] **Total synthesis of burkholdacs A (7) and/or B (8):** (a) Y. Fukui, K. Narita, S. Dan, T. Yamori, A. Ito, M. Yoshida, T. Katoh, *Eur. J. Med. Chem.* 76 (2014) 301–313;
(b) J.Y. Liu, X. Ma, Y. Liu, Z. Wang, S. Kwong, Q. Ren, S. Tang, Y. Meng, Z. Xu, T. Ye, *Synlett* 23 (2012) 783–787;
(c) H. Benelkebir, A.M. Donlevy, G. Packham, A. Ganesan, *Org. Lett.* 13 (2011) 6334–6337.
- [19] **Total synthesis of thailandepsin B (10):** Y.-Q. Cheng, S. Yang, P. Wang, (ChinAn PharmaTech Wuhan Co., Ltd., China) *PCT WO 131355A1* (2015).
- [20] (a) A.A. Bowers, T.J. Greshock, N. West, G. Estiu, S.L. Schreiber, O. Wiest, R.M. Williams, J.E. Bradner, *J. Am. Chem. Soc.* 131 (2009) 2900–2905;
(b) S.D. Maro, R.-C. Pong, J.-T. Hsieh, J.-M. Ahn, *J. Med. Chem.* 51 (2008) 6639–6641;
(c) A. Yurek-George, A.R.L. Cecil, A.H.K. Mo, S. Wen, H. Rogers, F. Habens, S. Maeda, M. Yoshida, G. Packham, A. Ganesan, *J. Med. Chem.* 50 (2007) 5720–5726.
- [21] (a) I. Shiina, T. Katoh, S. Nagai, M. Hashizume, *Chem. Rec.* 9 (2009) 305–320;
(b) I. Shiina, A. Sasaki, T. Kikuchi, H. Fukui, *Chem. – An Asian J.* 3 (2008) 462–472;
(c) I. Shiina, *Chem. Rev.* 107 (2007) 239–273;
(d) I. Shiina, M. Hashizume, *Tetrahedron* 62 (2006) 7934–7939;
(e) I. Shiina, M. Kubota, H. Oshiumi, M. Hashizume, *J. Org. Chem.* 69 (2004) 1822–1830.
- [22] O. Mitsunobu, *Synthesis* (1981) 1–28.
- [23] (a) C. Hildmann, D. Wegener, D. Riester, R. Hempel, A. Schober, J. Merana, L. Giurato, S. Guccione, T.K. Nielsen, R. Ficner, A. Schwienhorst, *J. Biotechnol.* 124 (2006) 258–270;
(b) T.K. Nielsen, C. Hildmann, A. Dickmanns, A. Schwienhorst, R. Ficner, *J. Mol. Biol.* 354 (2005) 107–120;
(c) R. Furumai, Y. Komatsu, N. Nishino, S. Khochbin, M. Yoshida, S. Horinouchi, *Proc. Natl. Acad. Sci. U. S. A.* 98 (2001) 87–92.
- [24] (a) S. Yaguchi, Y. Fukui, I. Koshimizu, H. Yoshimi, T. Matsuno, H. Gouda, S. Hirano, K. Yamazaki, T. Yamori, *J. Natl. Cancer Inst.* 98 (2006) 545–556;
(b) T. Yamori, *Cancer Chemother. Pharmacol.* 52 (Suppl. 1) (2003) 74–79;
(c) S. Dan, T. Tsunoda, O. Kitahara, R. Yanagawa, H. Zembutsu, T. Katagiri, K. Yamazaki, Y. Nakamura, T. Yamori, *Cancer Res.* 62 (2002) 1139–1147;
(d) T. Yamori, A. Matsunaga, S. Sato, K. Yamazaki, A. Komi, K. Ishizu, I. Mita, H. Edatsugi, Y. Matsuba, K. Takezawa, O. Nakanishi, H. Kohno, Y. Nakajima, H. Komatsu, T. Andoh, T. Tsuruo, *Cancer Res.* 59 (1999) 4042–4049.
- [25] **Recently, we have demonstrated that analogues 13e directly inhibits phosphatidylinositol 3-kinase (PI3K) activity and potently induces apoptosis through HDAC/PI3K dual inhibition:** (a) A. Oda, K. Saijo, C. Ishioka, K. Narita, T. Katoh, Y. Watanabe, S. Fukuyoshi, T. Ohgi, *J. Mol. Graph. Model.* 54 (2014) 46–53;
(b) K. Saijo, T. Katoh, H. Shimodaira, A. Oda, T. Ohgi, C. Ishioka, *Cancer Sci.* 103 (2012) 1994–2001.
- [26] G.M. Shivashimpi, S. Amagai, T. Kato, N. Nishino, S. Maeda, T.G. Nishino, M. Yoshida, *Bioorg. Med. Chem.* 15 (2007) 7830–7839.

Natural Product Synthesis

Enantioselective Total Synthesis of (–)-Siphonodictyal B and (+)-8-*epi*-Siphonodictyal B with Phosphatidylinositol 3-Kinase α (PI3K α) Inhibitory Activity

Takuya Kikuchi,^[a] Koichi Narita,^[a] Ken Saijo,^[b] Chikashi Ishioka,^[b] and Tadashi Katoh^{*[a]}

Abstract: The biologically interesting marine meroterpenoids (–)-siphonodictyal B and (+)-8-*epi*-siphonodictyal B were efficiently synthesized in 29–40 % overall yield in a longest linear sequence of 11 steps, starting from commercially available (+)-sclareolide. The synthesis involved the following crucial steps: (i) stereodivergent hydrogenation of a homoallylic decalin alcohol to install the requisite C8 stereogenic centre present in the decalin fragments; (ii) coupling of the decalin fragments with

an aromatic moiety to assemble the desired carbon skeletons; and (iii) deprotection from multiple *O*-protective groups on the aromatic ring to complete the project synthesis. Both (–)-siphonodictyal B and (+)-8-*epi*-siphonodictyal B showed PI3K α inhibitory activity, with potencies comparable to that of liphalgal, a naturally occurring PI3K α inhibitor. New structure–activity relationships for this class of marine meroterpenoids were also revealed.

Introduction

In recent years, numerous biologically active meroterpenoids (terpenoid–polyketide hybrid structures) having unique structural features have been isolated from marine organisms, particularly from algae and marine sponges.^[1] Several of these meroterpenoids have received considerable attention owing to their potential for use as new therapeutic agents. In most cases, however, biological studies – including those focussing on structure–activity relationships (SARs) – have been severely restricted, probably because of the scarcity of samples and/or the structural diversity of the natural products derived from marine organisms. Consequently, the development of efficient and flexible methods for the synthesis of biologically active meroterpenoids and their analogues is desirable and worthwhile from the viewpoint of medicinal/pharmaceutical chemistry.

Siphonodictyal B (**1a**; Figure 1) was originally isolated in 1981 by Faulkner et al. from the marine sponge *Aka coralliphagum* (also known as *Siphonodictyon coralliphagum*), and its structure was proposed as shown in formula **1c** by the same researchers.^[2] Subsequently, the first proposed structure (i.e., **1c**) was revised to formula **1b** (8-*epi*-siphonodictyal B) by Faulkner and Clardy et al. in 1986.^[3] Quite recently, the second proposed structure (i.e., **1b**) was revised again to formula **1a**, the true structure (C8 epimer of **1b**), by George et al. (2015) through

total synthesis of this marine natural product.^[4] Siphonodictyal B has a *trans*-fused decalin ring connected to a highly substituted aromatic ring through a methylidene linkage; the decalin unit contains three asymmetric carbon centres.^[4,5] A closely related meroterpenoid, liphalgal (**2**), which comprises a fused 6,7,5,6-tetracyclic skeleton (ABCD ring system) with the same carbon framework and substitution pattern on the aromatic ring, was also isolated from the same *Aka coralliphagum* marine sponge by Andersen et al. in 2006.^[6] George et al. proposed a hypothesis that siphonodictyal B (**1a**) is a biogenetic

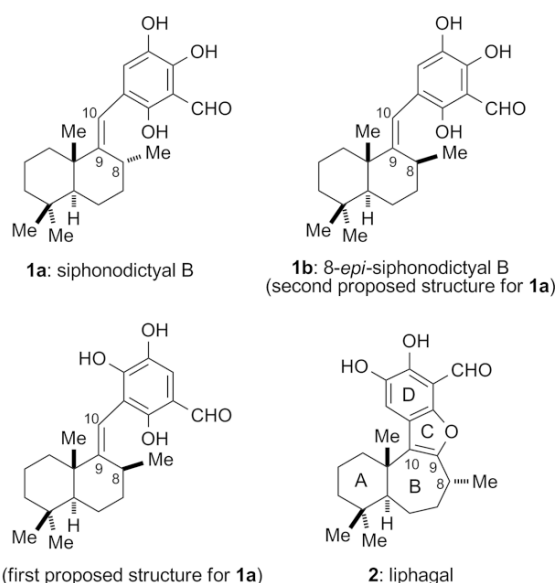


Figure 1. Structure of siphonodictyal B (**1a**), earlier proposed structures for **1a** (**1b** and **1c**), and structure of liphalgal (**2**).

[a] Laboratory of Synthetic and Medicinal Chemistry, Faculty of Pharmaceutical Sciences, Tohoku Medical and Pharmaceutical University, 4-4-1 Komatsushima, Aoba-ku, Sendai 981-8558, Japan
E-mail: katoh@tohoku-mpu.ac.jp
http://www.tohoku-mpu.ac.jp/laboratory/iyakugo/index.html

[b] Department of Clinical Oncology, Institute of Development, Aging and Cancer, Tohoku University, 4-1 Seiryomachi, Aoba-ku, Sendai 980-8575, Japan

Supporting information for this article is available on the WWW under <http://dx.doi.org/10.1002/ejoc.201600949>.

precursor of liphagal (**2**), and this hypothesis was strongly supported by their successful biomimetic conversion of **1a** into **2**.^[4] Liphagal has been reported to show potent and selective inhibitory activity against phosphatidylinositol 3-kinase α (PI3K α), which has become a new potential target for cancer chemotherapy.^[6,7] Siphonodictyal B has been reported to show biological properties such as antimicrobial and antiproliferative activities;^[2,3,5] however, its PI3K α inhibitory activity has not yet been assessed.

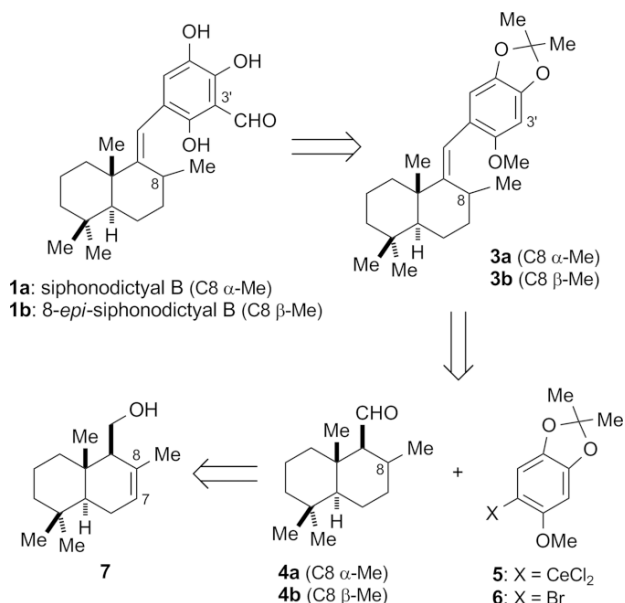
The interesting structural features, attractive biological properties, and limited availability from natural resources of (–)-siphonodictyal B (**1a**) and (+)-8-*epi*-siphonodictyal B (**1b**) prompted us to undertake a project directed towards their total synthesis in enantiomerically pure form. Recently, while our studies into the synthesis of **1a** and **1b** were in progress, George et al.^[4] reported the first and elegant total synthesis of **1a** and **1b**, which was achieved in a longest linear sequence of 10 steps, in 11 and 8 % overall yields, respectively. An approach to the total synthesis of **1b** has also been reported by Seifert et al.^[8]

In this paper, we describe our total synthesis of **1a** and **1b** by applying a synthetic strategy developed previously in our laboratory.^[9] The synthesized compounds **1a** and **1b** were subjected to a PI3K α inhibition assay to evaluate their biological potency as compared to liphagal (**2**). This evaluation represents the first report on the PI3K α inhibition efficacy of siphonodictyal B (**1a**) and its C8 epimer (**1b**).

Results and Discussion

Synthetic Plan for Siphonodictyal B (**1a**) and 8-*epi*-Siphonodictyal B (**1b**)

Our retrosynthetic analysis is outlined in Scheme 1. With reference to the synthetic approach to liphagal (**2**) previously re-

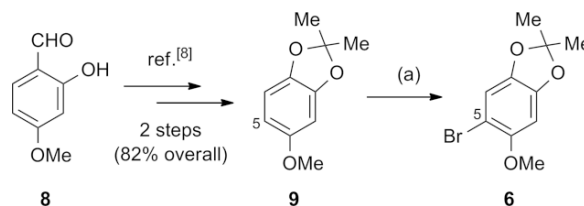


Scheme 1. Retrosynthetic analysis of siphonodictyal B (**1a**) and 8-*epi*-siphonodictyal B (**1b**).

ported by us,^[9] we envisaged that target molecules **1a** and **1b** could be synthesized by site-specific formylation of the aromatic ring at the C3' position in the corresponding intermediates (i.e., **3a** and **3b**), followed by deprotection from multiple *O*-protective groups on the aromatic ring. Intermediates **3a** and **3b** would be formed by condensation of the corresponding optically active decalin aldehydes (i.e., **4a** and **4b**) with trioxysubstituted arylcerium reagent **5**, which is accessible from trioxaryl bromide **6**. Two sets of C8 diastereomeric isomers **4a** and **4b** would be separately prepared from common homoallylic decalin alcohol **7** by stereodivergent hydrogenation of the C7–C8 double bond.

Synthesis of Aromatic Fragment **6**

We initially pursued the synthesis of aromatic fragment **6**, which is a condensation partner for decalin fragments **4a** and **4b**, starting from commercially available 2-hydroxy-4-methoxybenzaldehyde (**8**), as shown in Scheme 2. Trioxylbenzene **9** was prepared from **8** in two steps (82 % overall yield) according to a known procedure.^[8] Site-specific monobromination at the C5 position in **9** was carried out by exposure to *N*-bromosuccinimide (NBS; 1.1 equiv.) in *N,N*-dimethylformamide (DMF) at room temperature, giving the requisite aromatic fragment (i.e., **6**) in 86 % yield.

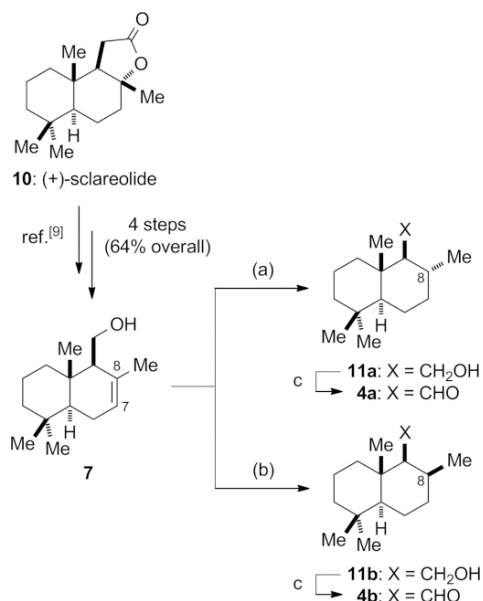


Scheme 2. Synthesis of aromatic fragment **6**. (a) NBS, DMF, room temp., 13 h, 86 %. NBS = *N*-bromosuccinimide, DMF = *N,N*-dimethylformamide.

Synthesis of Decalin Fragments **4a** and **4b**

The synthesis of **4a** and **4b** was efficiently achieved in a stereodivergent manner from a common intermediate, homoallylic decalin alcohol **7**. Intermediate **7** was prepared from commercially available (+)-sclareolide (**10**) in four steps and 64 % overall yield according to our reported method,^[9] as shown in Scheme 3. Thus, hydroxy-group-directed hydrogenation of **7** using Crabtree's catalyst {[Ir(COD)(PCy₃)(py)]⁺[PF₆][–]}^[10] (1.0 mol-%) gave C8 α -methyl compound **11a** as the major product (89 % yield), along with a small amount of C8 β -methyl compound **11b** (9 % yield; **11a**/**11b**, 10:1). Conversely, when the hydrogenation of **7** was carried out using PtO₂ as the catalyst, C8 β -methyl compound **11b** was produced as the major product (90 % yield) along with a small amount of C8 α -methyl compound **11a** (8 % yield; **11a**/**11b**, 1:11). These stereoisomers were separated by silica-gel column chromatography. The hydrogenation of **7** using PtO₂ as a catalyst must have mainly taken place at the sterically less hindered α -face of the molecule to preferentially give **11b**. To take the synthesis forward, Swern

oxidation of **11a** and **11b** gave decalin fragments **4a** and **4b**, respectively, in almost quantitative yield.

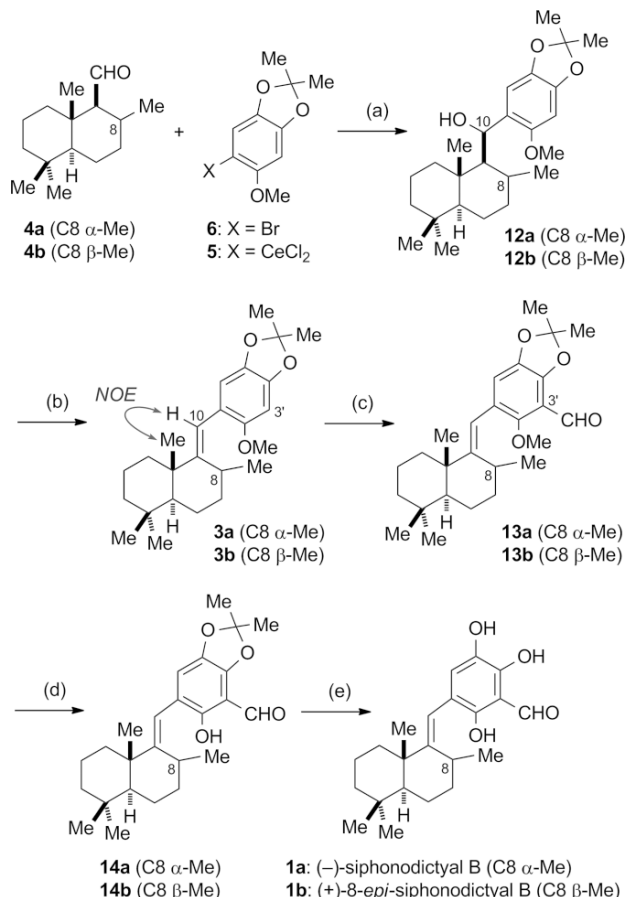


Scheme 3. Synthesis of decalin fragments **4a** and **4b**. (a) H_2 (1 atm), Crabtree's catalyst (1.0 mol-%), CH_2Cl_2 , 0 °C, 2 h, 89 % for **11a**, 9 % for **11b**; (b) H_2 (1 atm), PtO_2 (5.0 mol-%), EtOAc , 0 °C, 30 min, 90 % for **11b**, 8 % for **11a**; (c) $(\text{COCl})_2$, DMSO, $i\text{Pr}_2\text{NEt}$, CH_2Cl_2 , –78 °C, 30 min; –78 to 0 °C, 1 h, 97 % for **4a**, 99 % for **4b**. Crabtree's catalyst = $[\text{Ir}(\text{COD})(\text{PCy}_3)(\text{py})]^+[\text{PF}_6]^-$ (COD = 1,5-cyclooctadiene, Cy = cyclohexyl, py = pyridine), DMSO = dimethyl sulfoxide.

Synthesis of (–)-Siphonodictyal B (**1a**)

Having obtained the aromatic fragment **6** and the two decalin fragments **4a** and **4b**, we next carried out the synthesis of the first target molecule, (–)-siphonodictyal B (**1a**), as shown in Scheme 4. The crucial coupling reaction of sterically hindered and sensitive decalin aldehyde **4a**, which has the C8 α -methyl group in an equatorial orientation, with highly functionalized aromatic fragment **6** was efficiently achieved by using an organocerium reagent.^[11] Thus, treatment of aryl bromide **6** with $n\text{BuLi}$ in THF at –78 °C, followed by addition of the organolithium reagent generated in situ to anhydrous cerium chloride in THF at –78 °C, resulted in the production of the corresponding organocerium reagent (i.e., **5**). This was then allowed to react with **4a** at –78 °C to give the desired coupling product (i.e., **12a**) in excellent yield (98 %) as a single stereoisomer at the C10 position. The stereochemistry at C10 in **12a** was not determined, because this stereogenic centre would disappear in the following dehydration step. The dehydration of **12a** was best achieved by MgBr_2 -catalysed acetylation^[12] of the C10 hydroxy group followed by elimination of the resulting acetate in a one-pot operation. This gave olefin **3a** in 82 % yield. The (*E*) configuration of the olefinic double bond in **3a** was confirmed by a NOESY experiment (see Supporting Information). When the dehydration of alcohol **12a** was attempted under conventional conditions (e.g., MsCl , Et_3N , CH_2Cl_2 , 0 °C to reflux temp.), the requisite dehydration product (i.e., **3a**) was not ob-

tained, and unidentified decomposition products were generated. Site-specific formylation of the aromatic ring at the C3' position in **3a** ($n\text{BuLi}$, DMF, THF, –20 °C) gave the corresponding aldehyde (i.e., **13a**) in 95 % yield.



Scheme 4. Synthesis of (–)-siphonodictyal B (**1a**) and (+)-8-*epi*-siphonodictyal B (**1b**). (a) **6**, $n\text{BuLi}$, THF, –78 °C, 30 min; CeCl_3 , –78 °C, 1 h; addition of **4a** or **4b**, –78 °C, 1 h, 98 % for both **12a** (single diastereomer) and **12b** (ca. 5:3 mixture of C10 diastereomers); (b) conversion of **12a** into **3a**: MgBr_2 , Ac_2O , CH_2Cl_2 , room temp., 30 min, 82 %; conversion of **12b** into **3b**: MsCl , Et_3N , CH_2Cl_2 , 0 °C, 30 min, 94 %; (c) $n\text{BuLi}$, DMF, THF, –20 °C, 30 min, 95 % for **13a**, 97 % for **13b**; (d) $n\text{BuSLi}$, HMPA, 0 °C to room temp., 1 h, 91 % for **14a**, 88 % for **14b**; (e) BCl_3 , CH_2Cl_2 , –40 °C, 1 h, 75 % for **1a**, 91 % for **1b**. MsCl = methanesulfonyl chloride, HMPA = hexamethylphosphoramide.

In the final stage of the synthesis, the deprotection of the two types of protective groups (i.e., *O*-methyl ether and acetonide moieties) in **13a** was thoroughly investigated. Thus, treatment of **13a** with $n\text{BuSLi}$ ^[13] in hexamethylphosphoramide (HMPA) at 0 °C rising to room temperature efficiently deprotected the aromatic *O*-methyl group, leading to the free phenol derivative **14a** in 91 % yield. It is noteworthy that the sensitive formyl group on the aromatic ring remained intact during *O*-demethylation. Finally, exposure of **14a** to BCl_3 in CH_2Cl_2 at –40 °C resulted in deprotection of the acetonide moiety to give the first target, (–)-siphonodictyal B (**1a**), in 75 % yield after purification by gel-filtration chromatography on Sephadex LH-20 (using MeOH as an eluent). When the purification of **1a** was attempted using conventional silica-gel column chromatogra-

phy (with hexane/EtOAc as an eluent), a lower yield of **1a** (ca. 50 %) was obtained, probably because partial oxidative decomposition occurred during the operation, due to the presence of the highly oxygenated aromatic ring. The spectroscopic data (IR, ^1H and ^{13}C NMR, and HRMS) of our synthetic **1a** are identical with those reported for natural **1a**^[2,3] and synthetic **1a**.^[4] The optical rotation of our synthetic **1a**, $[\alpha]_{\text{D}}^{25} = -78.8$ ($c = 0.20$ in CHCl_3), is in good agreement with that reported for George's synthetic **1a**, $[\alpha]_{\text{D}}^{25} = -61.2$ ($c = 0.67$ in CHCl_3);^[4] no optical rotation data was reported for natural **1a**.^[2,3]

Synthesis of (+)-8-*epi*-Siphonodictyal B (**1b**)

Using decalin fragment **4b** (C8 β -Me in axial orientation) instead of **4a** (C8 α -Me in equatorial orientation) as the starting material, the second target, (+)-8-*epi*-siphonodictyal B (**1b**), was synthesized in a manner similar to that described for the synthesis of (–)-siphonodictyal B (**1a**) (Scheme 4). This sequence of reactions deserves comment. In the coupling reaction (**4b** + **5** → **12b**), the product (i.e., **12b**; 98 % yield) was formed as a mixture of diastereomers (ca. 5:3 ratio) at the C10 hydroxy group, and the mixture could not be separated by silica-gel column chromatography. Furthermore, in the subsequent dehydration step (**12b** → **3b**), the reaction proceeded well under conventional conditions (MsCl , Et_3N , CH_2Cl_2 , 0 °C, 30 min), and the requisite dehydration product (i.e., **3b**) was obtained in excellent yield (94 %). These differences in reactivity between the α - and β -methyl series (i.e., **4a** + **5** → **12a** vs. **4b** + **5** → **12b**; and **12a** → **3a** vs. **12b** → **3b**) may be caused by steric effects around the C8 position in the *trans*-decalin scaffold.

The spectroscopic data (IR, ^1H and ^{13}C NMR, and HRMS) of our synthetic **1b** were identical to those reported for George's synthetic **1b**.^[4] The optical rotation of our synthetic **1b**, $[\alpha]_{\text{D}}^{25} = +42.1$ ($c = 0.33$ in CHCl_3), is essentially consistent with that reported for George's synthetic **1b**, $[\alpha]_{\text{D}}^{25} = +5.3$ ($c = 0.75$ in CHCl_3).^[4]

Biological Evaluation and PI3K α Inhibition Assay

Phosphatidylinositol 3-kinases (PI3Ks) are key enzymes that control the signalling pathways used by a wide variety of cell-surface receptors on neutrophils.^[14] There are several isoforms of PI3Ks, including PI3K α , PI3K β , PI3K γ , and PI3K δ , that show different expression patterns and different pathophysiological roles.^[15] PI3K α is considered to be a potential anticancer target,^[16] and PI3K β , PI3K γ , and PI3K δ are expected to be promising targets for other pathogenic states, such as cardiovascular disorders (PI3K β)^[17] and inflammation and autoimmune diseases (PI3K γ and PI3K δ).^[18] Therefore, the potent and selective inhibition of PI3K α is highly desirable in cancer chemotherapy.

The synthesized siphonodictyal B (**1a**) and its C8 epimer (**1b**) were tested for their PI3K α inhibitory activity to elucidate their potency. In this assay, liphagal (**2**) was used as a reference compound, and the results are summarized in Table 1. In multiple side-by-side assays, **1a** and **1b** showed remarkable PI3K α inhibitory activity, with IC_{50} values of 2.6 and 3.3 μM , respectively. Their potency is equal to or better than that of liphagal ($\text{IC}_{50} =$

4.1 μM). These results indicate that the characteristic ring-fused bicyclic cyclohepta[*b*]furan ring (the BC system) present in liphagal is not responsible for the pronounced PI3K α inhibitory activity. In addition, the C8 stereochemistry in siphonodictyal B does not significantly affect its PI3K α inhibition efficacy. To the best of our knowledge, the PI3K α inhibitory activity of siphonodictyal B has not been previously reported in the literature; thus, these findings provide new knowledge that the structurally less complex siphonodictyal B is a useful seed compound for designing new synthetic PI3K α inhibitors.

Table 1. PI3K α inhibitory activity of siphonodictyal B (**1a**) and 8-*epi*-siphonodictyal B (**1b**).

Compound	IC_{50} ^[a] [μM]
Siphonodictyal B (1a)	2.6
8- <i>epi</i> -Siphonodictyal B (1b)	3.3
Liphagal (2) ^[b]	4.1

[a] Concentration that induces 50 % inhibition against PI3K α . [b] Positive control used in this study, synthesized in our laboratory.^[9]

Conclusions

We have achieved the enantioselective total synthesis of (–)-siphonodictyal B (**1a**) and (+)-8-*epi*-siphonodictyal B (**1b**) in a convergent and unified manner in 29–40 % overall yield over a linear sequence of 11 steps, starting from commercially available (+)-sclareolide (**10**). Compared to the previously reported method, the main advantage of the synthesis reported here is the higher overall yields [George's synthesis:^[4] 8–11 % overall yield over 10 steps]. A preliminary biological evaluation of **1a** and **1b** against PI3K α revealed their inhibitory potency (**1a**: $\text{IC}_{50} = 2.6 \mu\text{M}$; **1b**: $\text{IC}_{50} = 3.3 \mu\text{M}$). New aspects of the SAR of this class of marine meroterpenoids were also revealed. These results may be useful for the design and development of anticancer agents that target the inhibition of PI3K α . Further studies concerning the synthesis of unnatural siphonodictyal B analogues and the study of their SAR are currently underway in our group, and the results will be reported in due course.

Experimental Section

General Methods: All reactions involving air- and moisture-sensitive reagents were carried out using oven-dried glassware and standard syringe/septum-cap techniques. Routine monitoring of reactions was carried out using glass-supported Merck silica gel 60 F₂₅₄ TLC plates. Flash column chromatography was carried out on Kanto Chemical Silica Gel 60N (spherical, neutral, 40–50 nm) with the solvents indicated. All solvents and reagents were used as supplied, with the following exceptions: tetrahydrofuran (THF) was freshly distilled from Na metal/benzophenone under argon; dimethyl sulfoxide (DMSO), *N,N*-diisopropylethylamine, *N,N*-dimethylformamide (DMF), and CH_2Cl_2 were distilled from calcium hydride under argon. Optical rotations were measured with a JASCO DIP-370 and an Anton Paar MCP 100 automatic digital polarimeter. Melting points were measured with a Yanaco MP-3 micro melting-point apparatus. ^1H and ^{13}C NMR spectra were measured with a JEOL AL-400 (400 MHz) spectrometer. Chemical shifts are expressed in ppm, and Me_4Si ($\delta = 0$ ppm) was used as an internal standard. The following

abbreviations are used: singlet (s), doublet (d), triplet (t), quartet (q), multiplet (m), and broad (br.). Infrared (IR) spectroscopic measurements were carried out with a JASCO FTIR-4100 spectrometer. Low- and high-resolution mass (HRMS) spectra were measured with a JEOL JMS-700 MStation high-resolution mass spectrometer.

5-Bromo-6-methoxy-2,2-dimethylbenzo[d][1,3]dioxole (6): *N*-Bromosuccinimide (NBS; 1.65 g, 9.3 mmol) was added to a stirred solution of 5-methoxy-2,2-dimethylbenzo[d][1,3]dioxole (**9**)^[8] (1.52 g, 8.4 mmol) in DMF (8 mL) at room temperature. After 13 h, the reaction was quenched with water (10 mL), and the mixture was extracted with Et₂O (2 × 40 mL). The combined extracts were washed with brine (2 × 20 mL), then dried with MgSO₄. Concentration in vacuo gave a residue, which was purified by column chromatography (hexane/EtOAc, 100:1) to give **6** (1.88 g, 86 %) as a colourless viscous liquid. ¹H NMR (400 MHz, CDCl₃): δ = 1.66 (s, 6 H), 3.81 (s, 3 H), 6.49 (s, 1 H), 6.90 (s, 1 H) ppm. ¹³C NMR (100 MHz, CDCl₃): δ = 25.6 (2 C), 57.2, 96.0, 100.7, 112.3, 119.1, 141.9, 147.5, 150.7 ppm. IR (neat): ν̄ = 2991, 2938, 2864, 2833, 1625, 1604, 1495, 1396, 1384, 1351, 1272, 1191, 1164, 1084, 1040, 980, 965, 859, 819, 786, 669, 641 cm⁻¹. HRMS (EI): calcd. for C₁₀H₁₁BrO₃ [M]⁺ 257.9892; found 257.9883.

[(1S,2R,4aS,8aS)-2,5,5,8a-Tetramethyldecahydronaphthalen-1-yl]methanol (11a) and [(1S,2S,4aS,8aS)-2,5,5,8a-Tetramethyldecahydronaphthalen-1-yl]methanol (11b)

Method A: Stereocontrolled Hydrogenation of 7 Using Crabtree's Catalyst, Leading to 11a as the Major Product:

[Ir(COD)(PCy₃)(py)]⁺[PF₆]⁻ (Crabtree's catalyst; 46.9 mg, 58 μmol) was added to a solution of [(1S,4aS,8aS)-2,5,5,8a-tetramethyl-1,4,4a,5,6,7,8,8a-octahydronaphthalen-1-yl]methanol (**7**)^[9] (1.30 g, 5.8 mmol) in CH₂Cl₂ (58 mL) at room temperature. The mixture was degassed using ultrasound, then it was stirred under hydrogen (balloon) at 0 °C for 2 h. The reaction mixture was concentrated in vacuo to give a residue, which was purified by column chromatography (hexane/EtOAc, 10:1) to give **11a** (1.17 g, 89 %, less polar) and **11b** (118 mg, 9 %, more polar).

Data for 11a: White solid; m.p. 63–65 °C. [α]_D²⁷ = +1.5 (c = 1.0, CHCl₃). ¹H NMR (400 MHz, CDCl₃): δ = 0.67 (dt, J = 3.4, 11.2 Hz, 1 H), 0.82 (s, 3 H), 0.85 (s, 3 H), 0.87 (s, 3 H), 0.97 (d, J = 6.8 Hz, 3 H), 1.00–1.19 (m, 4 H), 1.24–1.49 (m, 4 H), 1.54–1.65 (m, 3 H), 1.79 (ddd, J = 3.9, 7.3, 12.9 Hz, 1 H), 1.88 (br. d, J = 12.7 Hz, 1 H), 3.63 (dd, J = 3.4, 11.2 Hz, 1 H), 3.79 (dd, J = 2.9, 11.7 Hz, 1 H) ppm. ¹³C NMR (100 MHz, CDCl₃): δ = 15.6, 18.8, 21.0, 21.8, 21.9, 30.8, 33.3, 33.6, 36.8, 37.6, 39.5, 42.1, 55.1, 60.7, 61.9 ppm. IR (KBr): ν̄ = 3356, 2923, 2869, 2844, 1457, 1387, 1366, 1231, 1205, 1118, 1088, 1066, 980, 940, 839, 815, 666 cm⁻¹. HRMS (EI): calcd. for C₁₅H₂₈O [M]⁺ 224.2140; found 224.2147.

Data for 11b: White solid; m.p. 104–105 °C. [α]_D²⁷ = +17.5 (c = 1.1, CHCl₃). ¹H NMR (400 MHz, CDCl₃): δ = 0.82 (s, 3 H), 0.85 (d, J = 2.4 Hz, 1 H), 0.86 (s, 6 H), 0.88 (d, J = 2.4 Hz, 1 H), 0.96 (d, J = 7.3 Hz, 3 H), 1.00–1.05 (m, 2 H), 1.16 (dt, J = 4.4, 13.7 Hz, 1 H), 1.34–1.70 (m, 8 H), 2.12–2.17 (m, 1 H), 3.59 (t, J = 9.8 Hz, 1 H), 3.86 (dd, J = 4.4, 10.5 Hz, 1 H) ppm. ¹³C NMR (100 MHz, CDCl₃): δ = 15.6, 17.1, 17.5, 18.4, 21.6, 28.6, 33.2, 33.6, 34.5, 37.6, 39.9, 42.0, 55.8, 56.5, 61.1 ppm. IR (KBr): ν̄ = 3298, 2991, 2920, 2864, 1683, 1521, 1455, 1368, 1215, 1084, 1040, 984, 839, 756, 668 cm⁻¹. HRMS (EI): calcd. for C₁₅H₂₈O [M]⁺ 224.2140; found 224.2139.

Method B: Stereocontrolled Hydrogenation of 7 Using Pt₂O as a Catalyst, Leading to 11b as the Major Product: PtO₂ (39.5 mg, 0.17 mmol) was added to a solution of **7** (773 mg, 3.5 mmol) in EtOAc (35 mL) at 0 °C. The mixture was stirred under hydrogen (balloon) at 0 °C for 30 min. The reaction mixture was diluted with

EtOAc (50 mL), and the catalyst was removed by filtration through a small pad of Celite®. The filtrate was concentrated in vacuo to give a residue, which was purified by column chromatography (hexane/EtOAc, 100:1 → 20:1) to give **11a** (65.8 mg, 8 %, less polar) and **11b** (706 mg, 90 %, more polar). The spectroscopic data (IR, ¹H and ¹³C NMR, and HRMS) for these samples are identical with those recorded for **11a** and **11b** as described before.

[(1S,2R,4aS,8aS)-2,5,5,8a-Tetramethyldecahydronaphthalen-1-carbaldehyde (4a): DMSO (0.41 mL, 6.2 mmol) was added dropwise to a stirred solution of oxalyl chloride (0.30 mL, 3.6 mmol) in CH₂Cl₂ (12 mL) at –78 °C under argon. After 20 min, a solution of **11a** (525 mg, 2.3 mmol) in CH₂Cl₂ (12 mL) was slowly added to the mixture at –78 °C. After 20 min, *N,N*-diisopropylethylamine (2.3 mL, 13 mmol) was added to the mixture at –78 °C. The resulting mixture was gradually warmed to 0 °C and stirred for a further 1 h. The reaction was quenched with water (20 mL) at 0 °C, and the mixture was extracted with CH₂Cl₂ (3 × 50 mL). The combined extracts were washed with brine (2 × 50 mL), then dried with MgSO₄. Concentration in vacuo gave a residue, which was purified by column chromatography (hexane/EtOAc, 30:1) to give **4a** (502 mg, 97 %) as a colourless viscous liquid. [α]_D²⁰ = +14.4 (c = 1.2, CHCl₃). ¹H NMR (400 MHz, CDCl₃): δ = 0.79 (s, 3 H), 0.84 (s, 3 H), 0.86 (s, 3 H), 0.90–1.05 (m, 3 H), 1.09 (s, 3 H), 1.18–1.64 (m, 7 H), 1.76–1.93 (m, 2 H), 2.03–2.15 (m, 1 H), 9.69 (d, J = 4.8 Hz, 1 H) ppm. ¹³C NMR (100 MHz, CDCl₃): δ = 15.9, 18.3, 20.6, 21.6, 21.8, 27.6, 33.3, 33.5, 35.5, 38.2, 40.2, 41.9, 54.2, 70.3, 207.7 ppm. IR (neat): ν̄ = 3366, 2946, 2922, 2864, 2864, 1456, 1441, 1387, 1364, 1270, 1213, 1136, 1079, 1033, 983, 963, 812, 771, 678, 643 cm⁻¹. HRMS (FAB): calcd. for C₁₅H₂₅O [M – H]⁺ 221.1900; found 221.1902.

[(1S,2S,4aS,8aS)-2,5,5,8a-Tetramethyldecahydronaphthalen-1-carbaldehyde (4b): DMSO (0.24 mL, 3.4 mmol) was added dropwise to a stirred solution of oxalyl chloride (0.15 mL, 1.7 mmol) in CH₂Cl₂ (6 mL) at –78 °C. After 20 min, a solution of **11b** (254 mg, 1.1 mmol) in CH₂Cl₂ (6 mL) was added to the mixture at –78 °C. After 20 min, *N,N*-diisopropylethylamine (2.0 mL, 11 mmol) was added to the mixture at the same temperature. The resulting mixture was gradually warmed to 0 °C and stirred for a further 1 h. The reaction was quenched with water (10 mL) at 0 °C, and the mixture was extracted with CH₂Cl₂ (3 × 30 mL). The combined extracts were washed with brine (2 × 20 mL), then dried with MgSO₄. Concentration in vacuo gave a residue, which was purified by column chromatography (hexane/EtOAc, 30:1) to give **4b** (248 mg, 99 %) as a colourless viscous liquid. [α]_D²⁰ = +22.9 (c = 1.2, CHCl₃). ¹H NMR (400 MHz, CDCl₃): δ = 0.85 (s, 3 H), 0.87 (s, 3 H), 0.81–0.89 (m, 1 H), 1.04 (d, J = 7.3 Hz, 3 H), 0.96–1.08 (m, 1 H), 1.18 (s, 3 H), 1.15–1.26 (m, 1 H), 1.37–1.73 (m, 7 H), 1.96–1.99 (m, 2 H), 2.36–2.41 (m, 1 H), 9.88 (s, 1 H) ppm. ¹³C NMR (100 MHz, CDCl₃): δ = 17.2, 17.3, 17.9, 18.0, 21.5, 29.8, 33.2, 33.4, 34.2, 37.1, 39.7, 41.9, 55.7, 65.6, 206.5 ppm. IR (neat): ν̄ = 2924, 2870, 2849, 2681, 1868, 1771, 1715, 1684, 1653, 1636, 1557, 1541, 1522, 1507, 1457, 1387, 1365, 1339, 1113, 1068, 1038, 638 cm⁻¹. HRMS (EI): calcd. for C₁₅H₂₆O [M]⁺ 222.1984; found 222.1982.

(6-Methoxy-2,2-dimethylbenzo[d][1,3]dioxol-5-yl)-[(1S,2R,4aS,8aS)-2,5,5,8a-tetramethyldecahydronaphthalen-1-yl]methanol (12a): Anhydrous CeCl₃ (1.24 g, 5.0 mmol) was prepared by heating CeCl₃·H₂O (finely ground powder; 1.87 g, 5.0 mmol) at 140 °C for 12 h under reduced pressure. The material was then cooled to room temperature, and THF (12 mL) was added. The resulting suspension was stirred at room temperature under argon for 4 h. Separately, a solution of *n*BuLi (1.6 M in *n*-hexane; 3.3 mL, 5.0 mmol) was added dropwise to a stirred solution of **6** (1.30 g, 5.0 mmol) in THF (12 mL) at –78 °C under argon. After

30 min, the resulting solution was added to the stirred solution of anhydrous CeCl_3 in THF at -78°C under argon. After 1 h, a solution of **4a** (312 mg, 1.4 mmol) in THF (1 mL) was added to the organocerium reagent, prepared in situ before, at -78°C , and stirring was continued at the same temperature for a further 1 h. The reaction was quenched with saturated aqueous NH_4Cl (15 mL) at -78°C , and the resulting mixture was extracted with EtOAc (3×50 mL). The combined extracts were washed with brine (2×30 mL), then dried with MgSO_4 . Concentration in vacuo gave a residue, which was purified by column chromatography (hexane/ EtOAc , 50:1 \rightarrow 30:1) to give **12a** (548 mg, 98 %) as a colourless amorphous solid. $[\alpha]_D^{25} = -6.8$ ($c = 1.1$, CHCl_3). ^1H NMR (400 Hz, CDCl_3): $\delta = 0.84$ (d, $J = 7.8$ Hz, 3 H), 0.85 (s, 3 H), 0.86 (s, 3 H), 0.90 (d, $J = 2.4$ Hz, 1 H), 0.98–1.08 (m, 2 H), 1.09 (s, 3 H), 1.11–1.19 (m, 1 H), 1.25–1.46 (m, 4 H), 1.55–1.61 (m, 2 H), 1.64 (s, 3 H), 1.66 (s, 3 H), 1.74–1.79 (m, 1 H), 1.91–1.99 (m, 2 H), 2.48 (d, $J = 4.4$ Hz, 1 H), 3.77 (s, 3 H), 5.26 (d, $J = 4.4$ Hz, 1 H), 6.40 (s, 1 H), 6.91 (s, 1 H) ppm. ^{13}C NMR (100 Hz, CDCl_3): $\delta = 15.0$, 19.0, 22.0 (2 C), 23.4, 25.6 (2 C), 28.7, 33.5, 33.8, 37.8, 39.1, 39.4, 42.3, 55.1, 56.0, 59.3, 67.2, 94.3, 107.7, 117.8, 126.9, 140.7, 146.0, 150.9 ppm. IR (neat): $\tilde{\nu} = 3461$, 2989, 2933, 2868, 2843, 1627, 1493, 1464, 1418, 1385, 1375, 1345, 1298, 1268, 1244, 1216, 1191, 1156, 1124, 1081, 1065, 1009, 980, 958, 934, 886, 844, 820, 802, 788, 758, 667 cm^{-1} . HRMS (EI): calcd. for $\text{C}_{25}\text{H}_{38}\text{O}_4$ $[\text{M}]^+$ 402.2770; found 402.2773.

6-Methoxy-5-((E)-[(2R,4aS,8aS)-2,5,5,8a-tetramethyloctahydronaphthalen-1(2H)-ylidene)methyl]-2,2-dimethylbenzo[d][1,3]dioxole (3a): MgBr_2 (432 mg, 2.4 mmol) and acetic anhydride (1.0 mL, 10.6 mmol) were slowly added to a stirred solution of **12a** (189 mg, 0.47 mmol) in CH_2Cl_2 (4 mL) at room temperature. After 30 min, the reaction mixture was diluted with CH_2Cl_2 (30 mL). The organic layer was washed successively with water (2×10 mL), saturated aqueous NaHCO_3 (2×10 mL), and brine (2×10 mL), and then dried with MgSO_4 . Concentration in vacuo gave a residue, which was purified by column chromatography (hexane/ EtOAc , 100:1) to give **3a** (148 mg, 82 %) as a colourless viscous liquid. $[\alpha]_D^{25} = -75.3$ ($c = 0.88$, CHCl_3). ^1H NMR (400 Hz, CDCl_3): $\delta = 0.87$ (s, 3 H), 0.90 (s, 3 H), 0.91 (d, $J = 6.8$ Hz, 3 H), 1.16 (s, 3 H), 1.18–1.26 (m, 2 H), 1.32–1.57 (m, 6 H), 1.66 (s, 3 H), 1.65 (s, 3 H), 1.68–1.79 (m, 2 H), 1.85 (d, $J = 11.2$ Hz, 1 H), 2.66–2.70 (m, 1 H), 3.71 (s, 3 H), 6.14 (s, 1 H), 6.39 (s, 1 H), 6.52 (s, 1 H) ppm. ^{13}C NMR (100 Hz, CDCl_3): $\delta = 19.6$, 19.9, 21.7, 22.1, 23.1, 25.7 (2 C), 31.7, 32.2, 33.2, 34.0, 39.7, 40.8, 42.4, 49.5, 56.9, 95.2, 110.0, 115.4, 117.6, 121.3, 140.6, 146.0, 151.6, 156.9 ppm. IR (neat): $\tilde{\nu} = 2989$, 2932, 2869, 2844, 1615, 1492, 1463, 1416, 1385, 1374, 1349, 1268, 1247, 1216, 1190, 1158, 1067, 1013, 980, 888, 842, 828, 818, 789, 759 cm^{-1} . HRMS (EI): calcd. for $\text{C}_{25}\text{H}_{36}\text{O}_3$ $[\text{M}]^+$ 384.2665; found 384.2663.

5-Methoxy-6-((E)-[(2R,4aS,8aS)-2,5,5,8a-tetramethyloctahydronaphthalen-1(2H)-ylidene)methyl]-2,2-dimethylbenzo[d][1,3]dioxole-4-carbaldehyde (13a): $n\text{BuLi}$ (2.6 M in n -hexane; 0.43 mL, 1.2 mmol) was added dropwise to a stirred solution of **3a** (148 mg, 0.49 mmol) in THF (4 mL) at -20°C under argon. After 30 min, DMF (0.29 mL, 3.9 mmol) was added dropwise to the reaction mixture at -20°C , and the mixture was stirred at the same temperature for a further 30 min. The reaction was quenched with saturated aqueous NH_4Cl (5 mL) at -20°C , and the resulting mixture was extracted with Et_2O (3×10 mL). The combined extracts were washed with brine (2×5 mL), then dried with MgSO_4 . Concentration in vacuo gave a residue, which was purified by column chromatography (hexane/ EtOAc , 20:1) to give **13a** (151 mg, 95 %) as a yellow amorphous solid. $[\alpha]_D^{25} = -71.4$ ($c = 1.0$, CHCl_3). ^1H NMR (400 Hz, CDCl_3): $\delta = 0.88$ (s, 3 H), 0.92 (s, 3 H), 0.93 (d, $J = 6.8$ Hz, 3 H), 1.18 (s, 3 H), 1.15–1.23 (m, 1 H), 1.31 (dd, $J = 4.9$, 12.2 Hz, 1 H), 1.36–1.59 (m, 6 H), 1.73 (s, 3 H), 1.74 (s, 3 H), 1.65–1.81 (m, 2 H), 1.85 (d, $J = 12.2$ Hz,

1 H), 2.66–2.72 (m, 1 H), 3.75 (s, 3 H), 6.17 (s, 1 H), 6.72 (s, 1 H), 10.27 (s, 1 H) ppm. ^{13}C NMR (100 Hz, CDCl_3): $\delta = 19.5$, 20.1, 21.7, 22.1, 22.8, 25.9 (2 C), 32.1, 32.5, 33.2, 34.0, 39.7, 41.0, 42.4, 49.9, 62.2, 113.9, 114.0, 115.4, 120.6, 125.8, 143.8, 146.3, 152.9, 158.5, 188.8 ppm. IR (neat): $\tilde{\nu} = 2931$, 2868, 1689, 1616, 1599, 1469, 1386, 1282, 1225, 1202, 1088, 1048, 1004, 978, 883, 836, 790, 756, 712 cm^{-1} . HRMS (EI): calcd. for $\text{C}_{26}\text{H}_{36}\text{O}_4$ $[\text{M}]^+$ 412.2613; found 412.2604.

5-Hydroxy-6-((E)-[(2R,4aS,8aS)-2,5,5,8a-tetramethyloctahydronaphthalen-1(2H)-ylidene)methyl]-2,2-dimethylbenzo[d][1,3]dioxole-4-carbaldehyde (14a): $n\text{BuLi}$ (2.6 M in n -hexane; 0.69 mL, 1.8 mmol) was added to a stirred solution of $n\text{BuSH}$ (0.20 mL, 1.8 mmol) in hexamethylphosphoramide (HMPA; 5 mL) at room temperature under argon. After 15 min, a solution of **13a** (151 mg, 0.37 mmol) in HMPA (2 mL) was added to the mixture at 0°C . The resulting mixture was warmed to room temperature, and stirring was continued for 1 h. The reaction was quenched with saturated aqueous NH_4Cl (5 mL) at 0°C , and the resulting mixture was extracted with Et_2O (3×20 mL). The combined extracts were washed with brine (2×20 mL), then dried with MgSO_4 . Concentration in vacuo gave a residue, which was purified by column chromatography (hexane/ EtOAc , 200:1 \rightarrow 100:1) to give **14a** (133 mg, 91 %) as an orange-yellow solid; m.p. 99 – 101°C . $[\alpha]_D^{25} = -112.5$ ($c = 1.2$, CHCl_3). ^1H NMR (400 Hz, CDCl_3): $\delta = 0.87$ (s, 3 H), 0.90 (s, 3 H), 0.91 (d, $J = 7.3$ Hz, 3 H), 1.17 (s, 3 H), 1.19–1.23 (m, 1 H), 1.30–1.57 (m, 7 H), 1.71 (s, 3 H), 1.71 (s, 3 H), 1.63–1.79 (m, 2 H), 1.85 (d, $J = 12.7$ Hz, 1 H), 2.64–2.70 (m, 1 H), 6.09 (s, 1 H), 6.76 (s, 1 H), 10.08 (s, 1 H), 10.59 (s, 1 H) ppm. ^{13}C NMR (100 Hz, CDCl_3): $\delta = 19.5$, 20.0, 21.7, 22.1, 23.1, 25.7 (2 C), 32.0, 32.5, 33.2, 34.0, 39.6, 41.0, 42.4, 49.8, 106.5, 113.4, 118.1, 119.1, 120.4, 139.4, 148.4, 151.5, 158.9, 191.5 ppm. IR (KBr): $\tilde{\nu} = 3435$, 2930, 2869, 1655, 1639, 1610, 1475, 1467, 1459, 1397, 1377, 1300, 1253, 1221, 1200, 1163, 1162, 1020, 1002, 701 cm^{-1} . HRMS (EI): calcd. for $\text{C}_{25}\text{H}_{34}\text{O}_4$ $[\text{M}]^+$ 398.2457; found 398.2464.

(-)-Siphonodictyal B (1a): BCl_3 (1.0 M in CH_2Cl_2 ; 0.62 mL, 0.62 mmol) was added to a stirred solution of **14a** (49.7 mg, 0.13 mmol) in CH_2Cl_2 (2 mL) at -40°C under argon. After 30 min, the reaction was quenched with saturated aqueous NaHCO_3 (2 mL) at -40°C , and the resulting mixture was extracted with CH_2Cl_2 (3×15 mL). The combined extracts were washed with brine (2×10 mL), then dried with MgSO_4 . Concentration in vacuo gave a residue, which was purified by gel-filtration chromatography on Sephadex LH-20 using MeOH as an eluent to give **1a** (33.4 mg, 75 %) as a yellow solid; m.p. 118 – 120°C . $[\alpha]_D^{25} = -78.8$ ($c = 0.20$, CHCl_3) [ref.^[4]]. $[\alpha]_D^{25} = -61.2$ ($c = 0.67$, CHCl_3). ^1H and ^{13}C NMR spectra of **1a** were recorded in three different solvents (i.e., CDCl_3 , $[\text{D}_6]\text{DMSO}$, and CD_3OD) to compare with the data reported in the literature.^[4] The ^1H and ^{13}C NMR, IR, and MS data (see below) are identical to those reported^[4] (see also the Supporting Information). ^1H NMR (400 Hz, CDCl_3): $\delta = 0.75$ (d, $J = 6.8$ Hz, 3 H), 0.86 (s, 3 H), 0.89 (s, 3 H), 1.16 (s, 3 H), 1.11–1.30 (m, 3 H), 1.41–1.82 (m, 8 H), 2.52–2.61 (m, 1 H), 5.12 (br. s, 1 H), 5.41 (br. s, 1 H), 5.90 (s, 1 H), 6.83 (s, 1 H), 10.29 (s, 1 H), 11.45 (br. s, 1 H) ppm. ^{13}C NMR (100 Hz, CDCl_3): $\delta = 19.4$, 21.1, 21.2, 21.7, 22.6, 33.2, 33.9, 34.1, 34.7, 39.3, 41.9, 42.3, 52.3, 109.1, 109.5, 116.9, 123.7, 136.9, 147.6, 148.5, 165.8, 194.5 ppm. ^1H NMR (400 Hz, $[\text{D}_6]\text{DMSO}$): $\delta = 0.84$ (s, 3 H), 0.86 (d, $J = 4.8$ Hz, 3 H), 0.87 (s, 3 H), 1.11 (s, 3 H), 1.12–1.18 (m, 1 H), 1.25–1.41 (m, 4 H), 1.44–1.52 (m, 2 H), 1.58–1.78 (m, 4 H), 2.56–2.65 (m, 1 H), 6.02 (s, 1 H), 6.83 (s, 1 H), 9.00 (s, 1 H), 10.02 (s, 1 H), 10.24 (s, 1 H), 10.89 (s, 1 H) ppm. ^{13}C NMR (100 Hz, $[\text{D}_6]\text{DMSO}$): $\delta = 19.0$, 19.3, 21.4, 21.8, 22.9, 31.3, 31.7, 32.9, 33.6, 39.1, 40.3, 41.9, 49.0, 110.2, 113.4, 116.6, 126.2, 136.1, 147.8, 151.2, 157.0, 194.7 ppm. ^1H NMR (400 Hz, CD_3OD): $\delta = 0.86$ (d, $J = 6.8$ Hz, 3 H), 0.88 (s, 3 H), 0.93 (s, 3 H), 1.19 (s, 3 H), 1.20–1.26 (m, 1 H), 1.29–1.48 (m, 3 H), 1.50–1.62 (m, 3 H), 1.68–1.82

(m, 4 H), 2.61–2.69 (m, 1 H), 6.05 (s, 1 H), 6.80 (s, 1 H), 10.34 (s, 1 H) ppm. ^{13}C NMR (100 Hz, CD_3OD): δ = 20.6, 21.7, 22.1, 22.4, 23.2, 33.7, 34.1, 34.2, 34.9, 40.5, 42.2, 43.6, 51.9, 111.5, 114.4, 119.1, 127.6, 137.3, 149.5, 152.9, 159.8, 196.0 ppm. IR (KBr): $\tilde{\nu}$ = 3383, 2929, 2870, 1644, 1458, 1389, 1375, 1306, 1270, 938, 757 cm^{-1} . HRMS (EI): calcd. for $\text{C}_{22}\text{H}_{30}\text{O}_4$ $[\text{M}]^+$ 358.2144; found 358.2159.

(6-Methoxy-2,2-dimethylbenzo[d][1,3]dioxol-5-yl)-[(1S,2S,4aS,8aS)-2,5,5,8a-tetramethyldecahydronaphthalen-1-yl]methanol (12b): Anhydrous CeCl_3 (1.20 g, 4.9 mmol) was prepared by heating $\text{CeCl}_3 \cdot \text{H}_2\text{O}$ (finely ground powder; 1.82 g, 4.9 mmol) at 140 °C under reduced pressure for 4 h. The material was then cooled to room temperature, and THF (12 mL) was added. The resulting suspension was stirred at room temperature under argon for 4 h. Separately, a solution of *n*BuLi (1.6 M in *n*-hexane; 3.2 mL, 4.9 mmol) was added dropwise to a stirred solution of **6** (1.26 g, 4.9 mmol) in THF (12 mL) at –78 °C under argon. After 30 min, the resulting solution was added to the above stirred solution of anhydrous CeCl_3 in THF at –78 °C under argon. After 1 h, a solution of **4b** (272 mg, 1.2 mmol) in THF (1 mL) was added to the organocerium reagent, prepared in situ above, at –78 °C, and the mixture was stirred at the same temperature for a further 1 h. The reaction was quenched with saturated aqueous NH_4Cl (20 mL) at –78 °C, and the resulting mixture was extracted with EtOAc (2 × 100 mL). The combined extracts were washed with brine (2 × 50 mL), then dried with MgSO_4 . Concentration in vacuo gave a residue, which was purified by column chromatography (hexane/EtOAc, 50:1 → 10:1) to give **12b** (483 mg, 98 %) as a yellow amorphous solid. This product comprised a mixture of diastereomers (ca. 5:3 ratio) at the hydroxy group, and the mixture could not be separated by silica gel column chromatography. ^1H NMR (400 Hz, CDCl_3): δ = 0.67–2.23 (m, 32 H), 3.76 (s, 15/8 H), 3.78 (s, 9/8 H), 4.91–4.95 (m, 3/8 H), 5.36–5.38 (m, 5/8 H), 6.39 (s, 5/8 H), 6.41 (s, 3/8 H), 6.66 (s, 3/8 H), 6.85 ppm (s, 5/8 H). ^{13}C NMR (100 Hz, CDCl_3): δ = 16.4 (5/8 C), 17.2 (3/8 C), 17.5 (3/8 C), 17.8 (5/8 C), 17.9 (5/8 C), 18.3 (5/8 C), 18.5 (3/8 C), 18.6 (3/8 C), 21.6 (5/8 C), 21.7 (5/8 C), 22.6 (3/8 C), 22.8 (3/8 C), 25.66 (3/8 C), 25.69 (10/8 C), 28.7, 30.7 (3/8 C), 31.0 (5/8 C), 33.7 (5/8 C), 33.8 (3/8 C), 35.3 (3/8 C), 36.0 (5/8 C), 39.3 (3/8 C), 39.6 (5/8 C), 42.0 (5/8 C), 42.2 (3/8 C), 56.1 (3/8 C), 56.3 (5/8 C), 56.9 (3/8 C), 57.0 (5/8 C), 57.2 (5/8 C), 58.8 (3/8 C), 69.2 (5/8 C), 72.4 (3/8 C), 94.4 (5/8 C), 94.5 (3/8 C), 107.5 (5/8 C), 108.6 (3/8 C), 117.8 (5/8 C), 118.0 (3/8 C), 124.5 (3/8 C), 126.6 (5/8 C), 140.9 (3/8 C), 141.0 (5/8 C), 146.4 (3/8 C), 146.7 (5/8 C), 150.2 (5/8 C), 151.3 ppm (3/8 C). IR (neat): $\tilde{\nu}$ = 3550, 2991, 2993, 2869, 2848, 1626, 1494, 1464, 1421, 1385, 1376, 1342, 1224, 1216, 1191, 1156, 1112, 1065, 1038, 1010, 980, 909, 886, 843, 822, 804, 787, 759, 737, 667 cm^{-1} . HRMS (EI): calcd. for $\text{C}_{25}\text{H}_{38}\text{O}_4$ $[\text{M}]^+$ 402.2770; found 402.2773.

6-Methoxy-5-[(E)-[(2S,4aS,8aS)-2,5,5,8a-tetramethyloctahydronaphthalen-1(2H)-ylidene)methyl]-2,2-dimethylbenzo[d][1,3]dioxole (3b): Methanesulfonyl chloride (0.18 mL, 2.3 mmol) was added dropwise to a stirred solution of **12b** (308 mg, 0.77 mmol) in CH_2Cl_2 (7 mL) containing triethylamine (0.53 mL, 3.8 mmol) at 0 °C. After 30 min, the reaction was quenched with saturated aqueous NH_4Cl (3 mL) at 0 °C, and the resulting mixture was extracted with Et₂O (2 × 50 mL). The combined extracts were washed with brine (2 × 30 mL), then dried with MgSO_4 . Concentration in vacuo gave a residue, which was purified by column chromatography (hexane/EtOAc, 200:1) to give **12b** (277 mg, 94 %) as a white solid; m.p. 96–98 °C. $[\alpha]_D^{25}$ = +106.2 (*c* = 0.98, CHCl_3). ^1H NMR (400 Hz, CDCl_3): δ = 0.87 (s, 3 H), 0.89 (s, 3 H), 1.03 (dd, *J* = 2.4, 11.7 Hz, 1 H), 1.18 (s, 3 H), 1.20–1.25 (m, 5 H), 1.40 (d, *J* = 12.7 Hz, 1 H), 1.48–1.61 (m, 6 H), 1.65 (s, 3 H), 1.68 (s, 3 H), 1.78 (d, *J* = 12.2 Hz, 1 H), 3.01–3.09 (m, 1 H), 3.73 (s, 3 H), 6.13 (s, 1 H), 6.43 (s, 1 H), 6.59 (s, 1

H) ppm. ^{13}C NMR (100 Hz, CDCl_3): δ = 17.8, 18.9, 21.8, 22.6, 22.8, 25.7, 25.8, 30.7, 33.3, 34.0, 34.1, 38.6, 40.9, 42.1, 54.6, 57.0, 95.3, 109.4, 115.1, 117.7, 120.4, 140.7, 146.0, 152.2, 155.5 ppm. IR (KBr): $\tilde{\nu}$ = 2934, 2869, 2854, 1615, 1493, 1463, 1420, 1385, 1375, 1348, 1273, 1248, 1217, 1190, 1157, 1068, 1011, 980, 890, 841, 818, 759, 736 cm^{-1} . HRMS (EI): calcd. for $\text{C}_{25}\text{H}_{36}\text{O}_3$ $[\text{M}]^+$ 384.2665; found 384.2663.

5-Methoxy-6-[(E)-[(2S,4aS,8aS)-2,5,5,8a-tetramethyloctahydronaphthalen-1(2H)-ylidene)methyl]-2,2-dimethylbenzo[d][1,3]dioxole-4-carbaldehyde (13b): *n*BuLi (2.6 M in *n*-hexane; 0.49 mL, 1.3 mmol) was added dropwise to a stirred solution of **3b** (165 mg, 0.43 mmol) in THF (5 mL) at –20 °C under argon. After 30 min, DMF (0.32 mL, 4.3 mmol) was added dropwise to the reaction mixture at –20 °C, and stirring was continued at the same temperature for 30 min. The reaction was quenched with saturated aqueous NH_4Cl (2 mL) at –20 °C, and the resulting mixture was extracted with Et₂O (2 × 25 mL). The combined extracts were washed with brine (2 × 10 mL), then dried with MgSO_4 . Concentration in vacuo gave a residue, which was purified by column chromatography (hexane/EtOAc, 20:1) to give **13b** (172 mg, 97 %) as a yellow amorphous solid. $[\alpha]_D^{25}$ = +59.4 (*c* = 1.12, CHCl_3). ^1H NMR (400 Hz, CDCl_3): δ = 0.89 (s, 3 H), 0.91 (s, 3 H), 0.98 (dd, *J* = 2.9, 11.7 Hz, 1 H), 1.21 (s, 3 H), 1.24 (d, *J* = 7.3 Hz, 3 H), 1.16–1.28 (m, 2 H), 1.42–1.69 (m, 7 H), 1.73 (s, 3 H), 1.75 (s, 3 H), 1.82 (d, *J* = 12.2 Hz, 1 H), 2.95–3.02 (m, 1 H), 3.75 (s, 3 H), 6.15 (s, 1 H), 6.74 (s, 1 H), 10.28 (s, 1 H) ppm. ^{13}C NMR (100 Hz, CDCl_3): δ = 17.8, 18.9, 21.8, 22.4, 22.5, 26.0 (2 C), 31.0, 33.4, 34.0, 34.1, 38.8, 41.0, 42.1, 55.0, 62.6, 114.2, 114.3, 114.7, 120.7, 124.8, 144.0, 146.2, 153.6, 157.6, 188.7 ppm. IR (neat): $\tilde{\nu}$ = 2981, 2933, 2869, 2854, 1691, 1614, 1600, 1470, 1386, 1284, 1253, 1221, 1203, 1089, 1049, 999, 979, 757 cm^{-1} . HRMS (EI): calcd. for $\text{C}_{26}\text{H}_{36}\text{O}_4$ $[\text{M}]^+$ 412.2613; found 412.2604.

5-Hydroxy-6-[(E)-[(2S,4aS,8aS)-2,5,5,8a-tetramethyloctahydronaphthalen-1(2H)-ylidene)methyl]-2,2-dimethylbenzo[d][1,3]dioxole-4-carbaldehyde (14b): *n*BuLi (2.6 M in *n*-hexane; 0.82 mL, 2.2 mmol) was added to a stirred solution of *n*BuSH (0.23 mL, 2.2 mmol) in hexamethylphosphoramide (HMPA; 5 mL) at room temperature under argon. After 15 min, a solution of **13b** (172 mg, 0.43 mmol) in HMPA (2 mL) was added to the above mixture at 0 °C. The resulting mixture was warmed to room temperature, and stirring was continued for 1 h. The reaction was quenched with saturated aqueous NH_4Cl (3 mL) at 0 °C, and the resulting mixture was extracted with Et₂O (2 × 25 mL). The combined extracts were washed with brine (2 × 10 mL), then dried with MgSO_4 . Concentration in vacuo gave a residue, which was purified by column chromatography (hexane/EtOAc, 200:1 → 100:1) to give **14b** (151 mg, 88 %) as an orange-yellow solid; m.p. 167–169 °C. $[\alpha]_D^{25}$ = +175.7 (*c* = 0.96, CHCl_3). ^1H NMR (400 Hz, CDCl_3): δ = 0.87 (s, 3 H), 0.89 (s, 3 H), 1.05 (dd, *J* = 2.9, 11.7 Hz, 1 H), 1.19 (s, 3 H), 1.25 (d, *J* = 7.3 Hz, 3 H), 1.21–1.26 (m, 2 H), 1.40 (d, *J* = 13.2 Hz, 1 H), 1.49–1.69 (m, 6 H), 1.71 (s, 3 H), 1.74 (s, 3 H), 1.80 (d, *J* = 11.7 Hz, 1 H), 2.95–2.98 (m, 1 H), 6.11 (s, 1 H), 6.83 (s, 1 H), 10.09 (s, 1 H), 10.71 (s, 1 H) ppm. ^{13}C NMR (100 Hz, CDCl_3): δ = 17.8, 18.9, 21.8, 22.5, 22.9, 25.8 (2 C), 31.0, 33.3, 34.0, 34.1, 38.5, 41.0, 42.0, 54.5, 106.5, 113.3, 117.4, 118.0, 120.5, 139.5, 148.4, 152.2, 157.4, 191.5 ppm. IR (KBr): $\tilde{\nu}$ = 3435, 2984, 2962, 2929, 2869, 1658, 1641, 1478, 1459, 1389, 1376, 1317, 1301, 1255, 1237, 1159, 1065, 1029, 1003, 691, 676 cm^{-1} . HRMS (EI): calcd. for $\text{C}_{25}\text{H}_{34}\text{O}_4$ $[\text{M}]^+$ 398.2457; found 398.2464.

(+)-8-*epi*-Siphonodictyal B (1b): BCl_3 (1.0 M in CH_2Cl_2 ; 0.76 mL, 0.76 mmol) was added to a stirred solution of **14b** (60.7 mg, 0.15 mmol) in CH_2Cl_2 (3 mL) at –40 °C under argon. After 30 min, the reaction was quenched with saturated aqueous NaHCO_3 (3 mL) at –40 °C, and the resulting mixture was extracted with CH_2Cl_2 (2 ×

25 mL). The combined extracts were washed with brine (2 × 10 mL), then dried with MgSO₄. Concentration in vacuo gave a residue, which was purified by gel-filtration chromatography on Sephadex LH-20 using MeOH as an eluent to give **1b** (49.4 mg, 91 %) as a yellow solid; m.p. 86–88 °C. $[\alpha]_D^{25} = +42.1$ ($c = 0.33$, CHCl₃) {ref.^[4] $[\alpha]_D^{25} = +5.3$ ($c = 0.75$, CHCl₃)}. The ¹H and ¹³C NMR, IR, and MS data (see below) are identical to those reported^[4] (see also the Supporting Information). ¹H NMR (400 Hz, CDCl₃): $\delta = 0.88$ (s, 6 H), 1.93–1.96 (m, 1 H), 1.09 (d, $J = 7.3$ Hz, 3 H), 1.20 (s, 3 H), 1.14–1.22 (m, 1 H), 1.40–1.76 (m, 8 H), 1.83 (d, $J = 12.6$ Hz, 1 H), 2.66–2.73 (m, 1 H), 5.08 (br. s, 1 H), 5.51 (br. s, 1 H), 5.83 (s, 1 H), 6.81 (s, 1 H), 10.31 (s, 1 H), 11.35 (br. s, 1 H) ppm. ¹³C NMR (100 Hz, CDCl₃): $\delta = 17.7$, 18.8, 21.8, 22.5, 22.7, 31.6, 33.4, 34.0, 34.1, 38.0, 41.3, 42.0, 55.0, 109.4, 110.7, 115.7, 123.7, 137.0, 147.6, 148.9, 165.6, 194.6 ppm. IR (KBr): $\tilde{\nu} = 3398$, 2921, 2869, 1655, 1638, 1609, 1459, 1439, 1399, 1388, 1254, 1204, 1018, 947 cm⁻¹. HRMS (EI): calcd. for C₂₂H₃₀O₄ [M]⁺ 358.2144; found 358.2146.

PI3K α Inhibition Assay: The PI3K α (p110 α /p85 α) activity was evaluated using the mobility shift assay (Carna Biosciences, Kobe, Japan). Compound solutions containing the kinase and substrate were prepared with assay buffer (Carna Biosciences). The mixed solutions were incubated in a 384-well microplate at room temperature for 5 h. The reaction mixtures were then applied to the LabChip (Caliper Life Sciences, MA, USA), and the product and substrate peaks were separated and quantified. The PI3K reaction was evaluated from the product ratio, calculated from the peak heights of the product and substrate. Data are the mean of two independent experiments carried out in duplicate. IC₅₀ values were determined from concentration vs. %-inhibition curves by fitting to a four-parameter logistic curve.

Acknowledgments

This study was supported by the Ministry of Education, Culture, Sports, Science and Technology, Japan (MEXT) through a Grant-in-Aid for the Strategic Research Foundation Program at Private Universities (no. S1511001L, 2015–2019) and a Grant-in-Aid for Scientific Research (C) (no. 15K07865, 2015–2017).

Keywords: Natural products · Total synthesis · Terpenoids · Polyketides · Biological activity

[1] For reviews, see: a) J. W. Blunt, B. R. Copp, R. A. Keyzers, M. H. G. Munro, M. R. Prinsep, *Nat. Prod. Rep.* **2016**, 33, 382–431; b) X.-M. Hou, R.-F. Xu,

- Y.-C. Gu, C.-Y. Wang, C.-L. Shao, *Curr. Med. Chem.* **2015**, 22, 3707–3762; c) J. W. Blunt, B. R. Copp, R. A. Keyzers, M. H. G. Munro, M. R. Prinsep, *Nat. Prod. Rep.* **2015**, 32, 116–211.
- [2] B. Sullivan, P. Djura, D. E. McIntyre, D. J. Faulkner, *Tetrahedron* **1981**, 37, 979–982.
- [3] B. W. Sullivan, D. J. Faulkner, G. K. Matsumoto, H. Cun-heng, J. Clardy, *J. Org. Chem.* **1986**, 51, 4568–4573.
- [4] A. W. Markwell-Heys, K. K. W. Kuan, J. H. George, *Org. Lett.* **2015**, 17, 4228–4231.
- [5] A. Grube, M. Assmann, E. Lichte, F. Sasse, J. R. Pawlik, M. Köch, *J. Nat. Prod.* **2007**, 70, 504–509.
- [6] F. Marion, D. E. Williams, B. O. Patrick, I. Hollander, R. Mallon, S. C. Kim, D. M. Roll, L. Feldberg, R. V. Soest, R. J. Andersen, *Org. Lett.* **2006**, 8, 321–324.
- [7] A. R. Pereira, W. K. Strangman, F. Marion, L. Feldberg, D. Roll, R. Mallon, I. Hollander, R. J. Andersen, *J. Med. Chem.* **2010**, 53, 8523–8533.
- [8] A. Bernet, K. Seifert, *Helv. Chim. Acta* **2006**, 89, 784–796.
- [9] T. Kamishima, T. Kikuchi, K. Narita, T. Katoh, *Eur. J. Org. Chem.* **2014**, 3443–3450.
- [10] a) R. H. Crabtree, M. H. Davis, *J. Org. Chem.* **1986**, 51, 2655–2661; b) P. G. Nell, *Synlett* **2001**, 160 and references cited therein.
- [11] For a review on organocerium reagents in organic synthesis, see: H.-J. Liu, K.-S. Shia, X. Shang, B.-Y. Zhu, *Tetrahedron* **1999**, 55, 3803–3830.
- [12] S. V. Pansare, M. G. Malusare, A. N. Rai, *Synth. Commun.* **2000**, 30, 2587–2592.
- [13] a) J. Sakurai, T. Oguchi, K. Watanabe, H. Abe, S. Kanno, M. Ishikawa, T. Katoh, *Chem. Eur. J.* **2008**, 14, 829–837; b) M. Nakatani, M. Nakamura, A. Suzuki, M. Inoue, T. Katoh, *Org. Lett.* **2002**, 4, 4483–4486; c) T. Taishi, S. Takechi, S. Mori, *Tetrahedron Lett.* **1998**, 39, 4347–4350; d) P. A. Aristoff, A. W. Harrison, A. M. Huber, *Tetrahedron Lett.* **1984**, 25, 3955–3958; e) S. C. Welch, A. S. C. P. Pao, *Tetrahedron Lett.* **1977**, 18, 505–508; f) G. I. Feutrill, R. N. Mirrington, *Aust. J. Chem.* **1972**, 25, 1719–1729; g) P. A. Bartlett, W. S. Johnson, *Tetrahedron Lett.* **1970**, 11, 4459–4412.
- [14] For reviews, see: a) B. Vanhaesebroeck, L. Stephens, P. Hawkins, *Nat. Rev. Mol. Cell Biol.* **2012**, 13, 195–203; b) M. P. Wymann, C. Schultz, *ChemBioChem* **2012**, 13, 2022–2035.
- [15] For reviews, see: a) K. Blajec, A. Borgström, A. Arcaro, *Curr. Drug Targets* **2011**, 12, 1056–1081; b) S. G. Ward, P. Finan, *Curr. Opin. Pharmacol.* **2003**, 3, 426–434; c) S. Ward, Y. Sotsios, J. Dowden, I. Bruce, P. Finan, *Chem. Biol.* **2003**, 10, 207–213.
- [16] For reviews, see: a) I. Brana, L. L. Siu, *BMC Med.* **2012**, 10, 161; b) Q.-W. Fan, W. A. Weiss, *Cell Cycle* **2006**, 5, 2301–2305.
- [17] For reviews, see: a) B. A. McLean, P. Zhabyeyev, E. Pituskin, I. Paterson, M. J. Haykowsky, G. Y. Oudit, *J. Card. Failure* **2013**, 19, 268–282; b) A. Eisenreich, U. Rauch, *Cardiovasc. Ther.* **2011**, 29, 29–36.
- [18] For reviews, see: a) L. So, D. A. Fruman, *Biochem. J.* **2012**, 442, 465–481; b) M. D. Blunt, S. G. Ward, *Curr. Opin. Pharmacol.* **2012**, 12, 444–451; c) P. Norman, *Expert Opin. Ther. Pat.* **2011**, 21, 1773–1790; d) C. Rommel, M. Camps, H. Ji, *Nat. Rev. Immunol.* **2007**, 7, 191–201.

Received: August 1, 2016

Published Online: November 2, 2016

Enantioselective Total Synthesis of Mandelalide A and Isomandelalide A: Discovery of a Cytotoxic Ring-Expanded Isomer

Nagarathanam Veerasamy,[†] Ankan Ghosh,[†] Jinming Li,[†] Kazuhiro Watanabe,^{†,‡} Jeffrey D. Serrill,[§] Jane E. Ishmael,[§] Kerry L. McPhail,[§] and Rich G. Carter^{*,†}

[†]Department of Chemistry and [§]Department of Pharmaceutical Sciences, Oregon State University, Corvallis, Oregon 97331, United States

[‡]Laboratory of Synthetic and Medicinal Chemistry, Tohoku Pharmaceutical University, Sendai 981-8558, Japan

Supporting Information

ABSTRACT: The total synthesis of mandelalide A and its ring-expanded macrolide isomer isomandelalide A has been achieved. Unexpected high levels of cytotoxicity were observed with the ring-expanded isomandelalide A with a rank order of potency: mandelalide A > isomandelalide A > mandelalide B. Key aspects of the synthesis include Ag-catalyzed cyclizations (AgCC's) to construct both the THF and THP rings present in the macrocycle, diastereoselective Sharpless dihydroxylation of a *cis*-enyne, and lithium acetylide coupling with a chiral epoxide.

In 2012, McPhail et al. reported the isolation of a series of novel macrolides in small quantities from a new species of *Lissoclinum* ascidian found in Algoa Bay, South Africa.¹ These compounds were named mandelalides A–D, and their structures were proposed by extensive spectroscopic analysis. Given the small quantities of material obtained from isolation, only preliminary evaluation of their biological properties could be performed. Mandelalides A and B showed low nanomolar cytotoxicity to lung (NCI-H460) and neuroblastoma (Neuro-2A) cancer cell lines. Not surprisingly, these structurally complex, cytotoxic compounds have attracted considerable synthetic attention from multiple laboratories. In 2014, Willwacher and Fürstner reported the total synthesis of the proposed structure **1**, which did not match the spectroscopic data of the natural product.² Shortly thereafter, Ghosh et al. reported the synthesis of the aglycone of the proposed structure of mandelalide A.³ Ye et al. synthesized a series of structural variants of mandelalide A, which allowed them to unequivocally establish the absolute structure of mandelalide A as compound **2**.^{4,5} Given the scarcity of **2** and our laboratory's long-standing interest in the synthesis of cytotoxic macrolides,⁶ we sought to develop a robust synthesis of compound **2** to enable additional biological evaluation. Herein, we report the enantioselective total synthesis of mandelalide A (**2**).

As shown in Scheme 1, our synthesis strategy builds on the observation that both the THF and the THP rings present in macrolide **2** could be accessed by a silver-catalyzed cyclization (AgCC) from the requisite propargylic benzoates. Our laboratory had previously demonstrated the utility of this general concept in our synthesis of amphidinolides C and F;^{6b,d} however, we are unaware of any examples for accessing six-membered oxygenated heterocycles using AgCC.⁷ Another

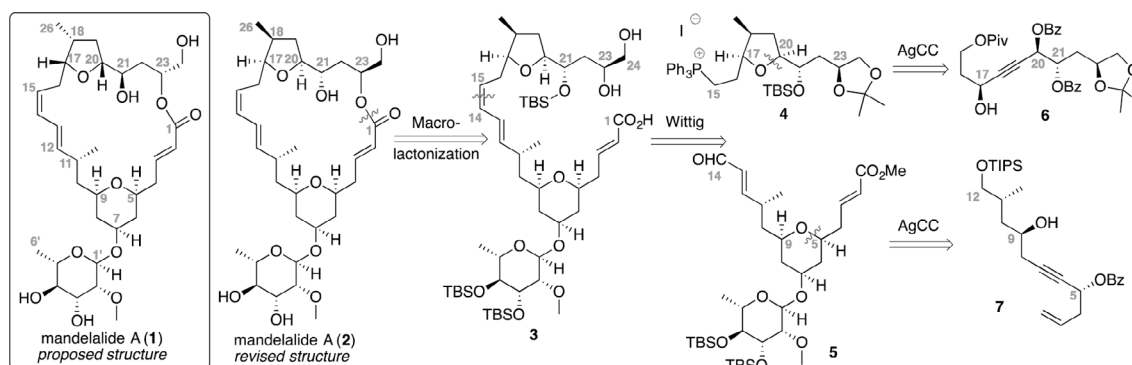
intriguing strategic premise was the possibility that the macrocyclization event could be conducted with both the C₂₃ and C₂₄ alcohols exposed and governed by strong, preferential translocation to the desired C₂₃ macrolactone. Support for this premise can be seen in the observations that translocation was operable with the originally proposed structure **1**⁴ as well as with other macrolides such as amphidinolides G/H;⁸ however, the revised structure **2** exists exclusively as the C₂₃ macrolactone. If this hypothesis proved problematic, the C₂₄ position could be masked prior to macrolactonization.

Synthesis of the northern C₁₅–C₂₄ fragment **4** commenced from the alkyne **9**^{6b,d} and iodide **10**⁹ (Scheme 2). These building blocks were readily available from (*S*)-malic acid (**8**). Sonogashira coupling provided the *cis*-enyne in excellent yield using diisopropylamine as the solvent. Sharpless asymmetric dihydroxylation of *cis*-alkenes¹⁰ has seen limited use in total synthesis¹¹ despite the widespread utility and prevalence of *anti*-diols. We were pleased to observe that Sharpless dihydroxylation using commercially available (DHQD)₂PHAL provided the desired diastereomer **12** in good yield and reasonable diastereoselectivity (76%, 3.5:1 dr). Use of the pseudo-enantiomeric ligand (DHQ)₂PHAL gave the opposite diastereomer in similar selectivity (1:3.6 dr). Interestingly, the Sharpless ligand specifically designed for *cis*-alkenes (DHQD-IND)¹⁰ proved less effective (2.2:1 dr). Bisesterification using benzoyl chloride followed by desilylation generated the AgCC precursor. While our laboratory has explored the utility of diols as viable nucleophiles in the AgCC process,^{6b,d} the alternate combination of using dibenzoates (e.g., **6**) has not been reported. We were pleased to discover that this substrate rapidly and smoothly undergoes cyclization to provide the unstable enol benzoate **13**. Subsequent *in situ* treatment with MeLi·LiBr revealed ketone **14** which also proved unstable until protection as its silyl ether **15** in good overall yield with excellent stereoselectivity (68%, > 10:1 dr). Ketone **15** was next olefinated with the Petasis reagent followed by diastereoselective reduction using Rh/Al₂O₃ to provide the 18*S* stereochemistry. Finally, removal of the Piv ester followed by conversion to Wittig salt **4** proceeded smoothly.

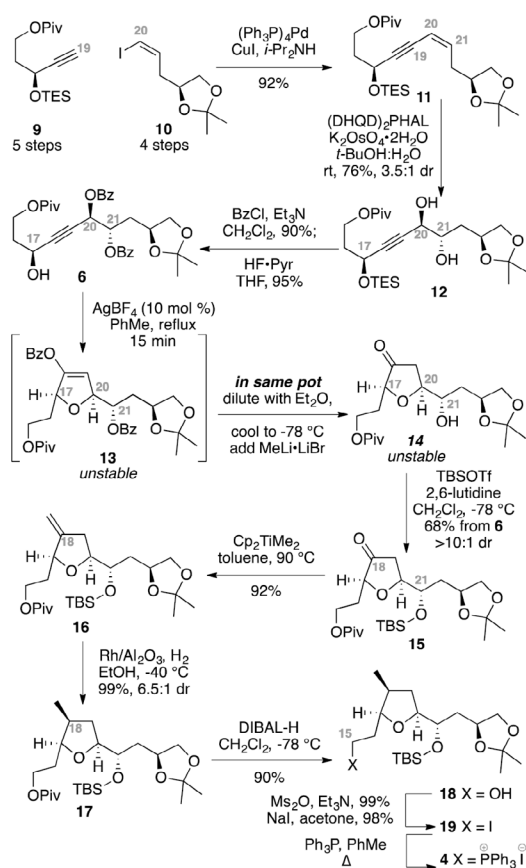
Received: November 24, 2015

Published: January 13, 2016

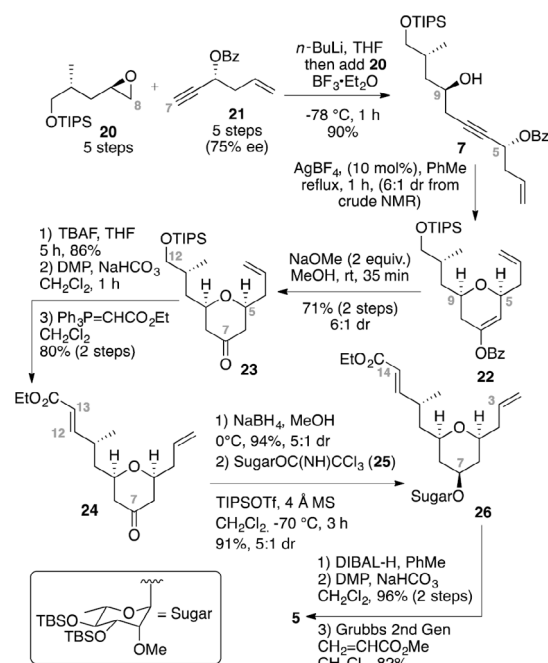
Scheme 1. Retrosynthetic Analysis of Mandelalide A (2)



Scheme 2. Synthesis of Northern Fragment 4



Scheme 3. Synthesis of Southern Fragment 5

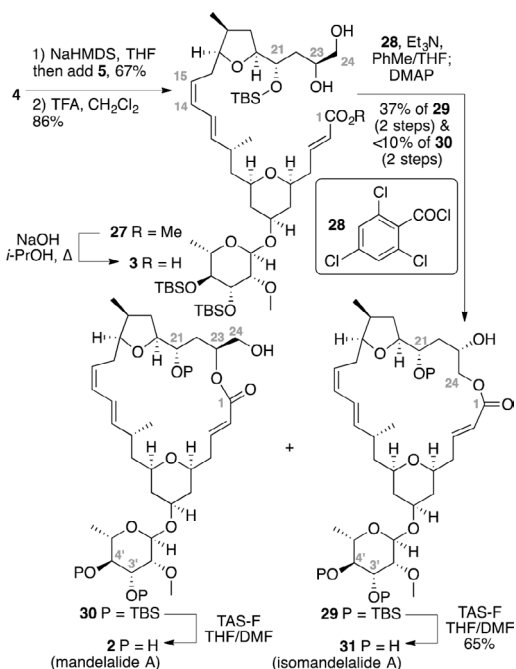


With the northern phosphonium salt in hand, we shifted our focus to the southern C₁–C₁₄ subunit (Scheme 3). Starting from the readily available epoxide **20** and alkyne **21** (each accessible in 5 steps from commercially available sources), BF₃·Et₂O-mediated coupling under optimized conditions provided the homopropargylic alcohol **7**. While examples exist of alkyne/epoxide couplings in the presence of an ester,¹² propargylic benzoates have not been used before in the process. With the cyclization precursor **7** in hand, we explored the key AgCC to access the pyran **22**. While we are unaware of prior examples of related silver-catalyzed cyclizations for extending the AgCC process to larger ring systems,⁷ we were gratified to discover

that the transformation proceeded smoothly to yield **22** in a 6:1 dr at C₅ based on crude ¹H NMR. This level of diastereoselectivity may be explained by the modest level of enantiopurity (7:1 er) in the alkyne precursor **21**. The crude benzoate was immediately submitted to hydrolysis conditions (NaOMe, MeOH, rt) to generate the desired C₇ ketone **23** in good yield with no loss in stereochemical integrity. It is important to note that alternate protocols to convert the enol benzoate **22** into the ketone **23** (including MeLi·LiBr)^{6b,d} led to inferior yields and/or reduced dr. Removal of the C₁₂ silyl ether followed by oxidation and Wittig olefination generated the ester **24**. Borohydride reduction followed by Schmidt glycosylation⁵ produced the target glycoside **26** in good yield and reasonable dr at C₁. Finally, conversion of the C₁₄ ester into its corresponding aldehyde and cross metathesis¹³ generated the southern fragment **5**.

Our first generation approach to coupling and macrocyclization is shown in Scheme 4. Treatment of phosphonium salt **4** with NaHMDS followed by addition of the aldehyde **5**

Scheme 4. Total Synthesis of Isomandelalide A (31)



cleanly provided the C₁₂–C₁₅ *E,Z*-diene. Next, selective deprotection of the C₂₃–C₂₄ acetonide in the presence of the C₇ glycoside and the acid-sensitive *E,Z*-diene motif was accomplished using TFA to generate the C_{23,24} diol in excellent yield. Yamaguchi conditions smoothly induced macrolactonization; however, the ring-expanded, 25-membered isomer **29** was the primary isolable product from this reaction. Removal of the three silyl moieties in **29** using TAS-F provided the previously unknown, 25-membered macrocycle called isomandelalide A (**31**). A second product **30** was also observed in the macrolactonization. Subsequent TAS-F treatment of the crude mixture from the macrolactonization revealed the desired mandelalide A (**2**); however, only minor amounts of **2** could be accessed through this route. The preference for **29** over **30** is surprising based on the observation by Ye et al. that **2** appeared to prefer the smaller, 24-membered macrocycle.^{4,14}

In order to selectively access the desired natural product, the C₂₄ position was masked as its TBS ether on diol **27** (Scheme 5). Subsequent conversion of the methyl ester into the acid **32** was accomplished by a redox process. Attempted direct saponification of the C₁ methyl ester on the C₂₄ silylated product led to extensive silyl migration. We were pleased to see that Yamaguchi macrolactonization of the seco acid **32** proved effective on the C₂₄ silyl ether series to give the known Ye intermediate.⁴ Finally, global desilylation generated the natural product, the data for which matched with the literature values (¹H, ¹³C, [α]_D).¹ A modest amount of a second macrocycle was observed under the cyclization process, which we hypothesize to be the C₂₁ macrolactone (likely due to C₂₁/C₂₃ silyl migration); however, this minor product decomposed under the TAS-F conditions.

Isomandelalide A (**31**) showed potent cytotoxicity in comparative testing with synthetic mandelalide A (**2**) and relative to the natural mandelalide B (**33**) (Table 1). Using assay conditions comparable to those used in the original

Scheme 5. Total Synthesis of Mandelalide A (2)

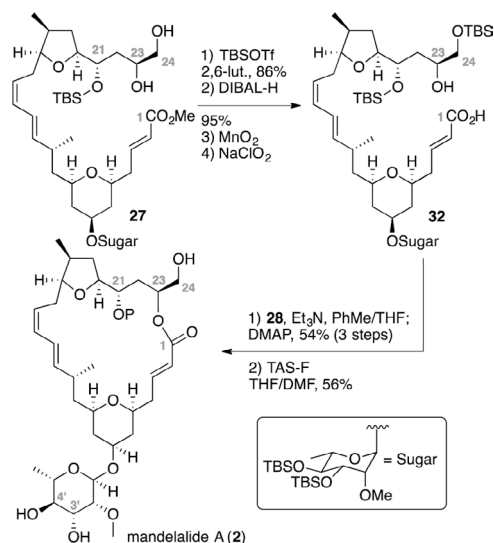


Table 1. Cytotoxic Effects of Compounds **2**, **31**, and **33** Against Human Cancer Cell Lines

compd. no.	HeLa cervix		H460 lung	
	EC ₅₀ (nM)	95% C.I. (nM)	EC ₅₀ (nM)	95% C.I. (nM)
2	10.5	8.6–12.2	13.2	8.6–18.0
31	17.1	13.1–21.7	30.3	15.0–42.5
33	35.5	16.1–52.4	35.5	26.3–61.2

bioassay-guided drug discovery screen,¹ synthetic **2** showed biological activity that was entirely consistent with the cytotoxicity observed in earlier testing of the natural product. Synthetic **2** was approximately 3-fold more potent than **33** against human HeLa cervical and H460 lung cancer cells. Although slightly less potent than **2**, isomandelalide A (**31**) was also a fully efficacious cytotoxin against both human cancer cell types with EC₅₀ values of 17.1 and 30.3 nM for HeLa and NCI-H460 cells, respectively.

In conclusion, efficient total syntheses of mandelalide A (**2**) and its ring-expanded isomer isomandelalide A (**31**) have been completed. The unexpected potency of isomandelalide A raises intriguing questions about the biology of these natural products, given that variation in ring size of a macrocycle often leads to conformational changes that can have a notable impact on biological activity (e.g., amphotolide G/H¹⁵ and isoapoptolide/apoptolide¹⁶). The disclosed synthetic campaign demonstrated the utility of the AgCC for the construction of oxygenated heterocycles, including the first reported example for accessing a pyran ring system. The *E,Z*-diene motif was incorporated smoothly through a Wittig reaction. The macrocyclization preferences for the C_{23,24} diol were explored. Further application of this methodology to access other members of the mandelalide family will be disclosed in due course.

■ ASSOCIATED CONTENT

§ Supporting Information

The Supporting Information is available free of charge on the ACS Publications website at DOI: 10.1021/jacs.5b12318.

Complete experimental details and biological protocols (PDF)

¹H and ¹³C NMR spectra (PDF)

AUTHOR INFORMATION

Corresponding Author

*rich.carter@oregonstate.edu

Funding

No competing financial interests have been declared.

Notes

The authors declare no competing financial interest.

ACKNOWLEDGMENTS

Financial support provided by Oregon State University. Tohoku Pharmaceutical University is acknowledged for their fellowship for K.W. Prof. Claudia Maier and Jeff Morré (OSU) are acknowledged for mass spectra. Dr. Mohamed F. El-Mansy (OSU) is acknowledged for his assistance with organizing the spectral data. Finally, the authors are grateful to Prof. Paul Ha-Yeon Cheong (OSU) and Dr. Roger Hanselmann (Akebia Therapeutics) for their helpful discussions.

REFERENCES

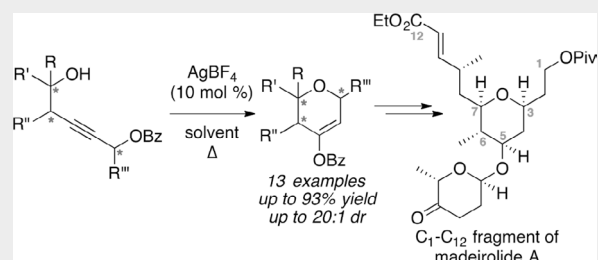
- (1) (a) Sikorska, J.; Hau, A. M.; Anklin, C.; Parker-Nance, S.; Davies-Coleman, M. T.; Ishmael, J. E.; McPhail, K. L. *J. Org. Chem.* **2012**, *77*, 6066–6075. (b) Sikorska, J.; Hau, A. M.; Anklin, C.; Parker-Nance, S.; Davies-Coleman, M. T.; Ishmael, J. E.; McPhail, K. L. *J. Org. Chem.* **2013**, *78*, 2812. (c) Davies-Coleman, M. T.; Veale, C. G. L. *Mar. Drugs* **2015**, *13*, 6366–6383.
- (2) (a) Willwacher, J.; Fürstner, A. *Angew. Chem., Int. Ed.* **2014**, *53*, 4217–4221. See also: (b) Fürstner, A. *Angew. Chem., Int. Ed.* **2014**, *53*, 8587–8598.
- (3) Reddy, K. M.; Yamini, V.; Singarapu, K. K.; Ghosh, S. *Org. Lett.* **2014**, *16*, 2658–2660.
- (4) Lei, H.; Yan, J.; Yu, J.; Liu, Y.; Wang, Z.; Xu, Z.; Ye, T. *Angew. Chem., Int. Ed.* **2014**, *53*, 6533–6537.
- (5) (a) Willwacher, J.; Heggen, D.-I. B.; Wirtz, C.; Thiel, W.; Fürstner, A. *Chem. - Eur. J.* **2015**, *21*, 10416–10430. (c) Brütisch, T. M.; Bucher, P.; Altmann, K.-H. *Eur. J. Chem.* DOI: 10.1002/chem.201504918.
- (6) (a) Lu, L.; Zhang, W.; Carter, R. G. *J. Am. Chem. Soc.* **2008**, *130*, 7253–7255. (b) Mahapatra, S.; Carter, R. G. *Angew. Chem., Int. Ed.* **2012**, *51*, 7948–7951. (c) Lu, L.; Zhang, W.; Nam, S.; Horne, D. A.; Jove, R.; Carter, R. G. *J. Org. Chem.* **2013**, *78*, 2213–2247. (d) Mahapatra, S.; Carter, R. G. *J. Am. Chem. Soc.* **2013**, *135*, 10792–10803.
- (7) (a) Gockel, B.; Krause, N. *Org. Lett.* **2006**, *8*, 4485–4488. (b) Wang, Y.-M.; Kuzniewski, C. N.; Rauniyar, V.; Hoong, C.; Toste, F. D. *J. Am. Chem. Soc.* **2011**, *133*, 12972–12975. (c) Kotikalapudi, R.; Kumara Swamy, K. C. *Tetrahedron* **2013**, *69*, 8002–8012.
- (8) Kobayashi, J.; Shimbo, K.; Sato, M.; Tsuda, M. *J. Org. Chem.* **2002**, *67*, 6585–6592.
- (9) Taguchi, T.; Kitagawa, O.; Morikawa, T.; Nishiwaki, T.; Uehara, H.; Endo, H.; Kobayashi, Y. *Tetrahedron Lett.* **1986**, *27*, 6103–6106.
- (10) Wang, L.; Sharpless, K. B. *J. Am. Chem. Soc.* **1992**, *114*, 7568–7570.
- (11) (a) Dong, S.; Paquette, L. A. *J. Org. Chem.* **2005**, *70*, 1580–1596. (b) Halim, R.; Brimble, M. A.; Merten, J. *Org. Lett.* **2005**, *7*, 2659–2662. (c) Hicks, J. D.; Flamme, E. M.; Roush, W. R. *Org. Lett.* **2005**, *7*, 5509–5512. (d) Ermolenko, L.; Sasaki, N. A. *J. Org. Chem.* **2006**, *71*, 693–703. (e) Yuen, T.-Y.; Brimble, M. A. *Org. Lett.* **2012**, *14*, 5154–5157.
- (12) (a) Ramana, C. V.; Raghupathi, N.; Gujar, M. K.; Chorghade, M. S. *Tetrahedron Lett.* **2005**, *23*, 4073–4075. (b) Tinsley, J. M.; Roush, W. R. *J. Am. Chem. Soc.* **2005**, *127*, 10818–10819.
- (13) Carlson, E. C.; Rathbone, L. K.; Yang, H.; Collett, N. D.; Carter, R. G. *J. Org. Chem.* **2008**, *73*, 5155–5158.
- (14) Blakemore, P. R.; Browder, C. C.; Hong, J.; Lincoln, C. M.; Nagorney, P. A.; Robarge, L. A.; Wardrop, D. J.; White, J. D. *J. Org. Chem.* **2005**, *70*, 5449–5460.
- (15) Kobayashi, J.; Shigemori, H.; Ishibashi, M.; Yamasu, T.; Hirota, H.; Sasaki, T. *J. Org. Chem.* **1991**, *56*, 5221–5224.
- (16) Wender, P. A.; Gullledge, A. V.; Jankowski, O. D.; Seto, H. *Org. Lett.* **2002**, *4*, 3819–3822.

Stereoselective, Ag-Catalyzed Cyclizations To Access Polysubstituted Pyran Ring Systems: Synthesis of C₁–C₁₂ Subunit of Madeirolide AKazuhiro Watanabe,^{†,‡} Jinming Li,[‡] Nagarathanam Veerasamy, Ankan Ghosh, and Rich G. Carter*

Department of Chemistry, Oregon State University, 153 Gilbert Hall, Corvallis, Oregon 97331, United States

Supporting Information

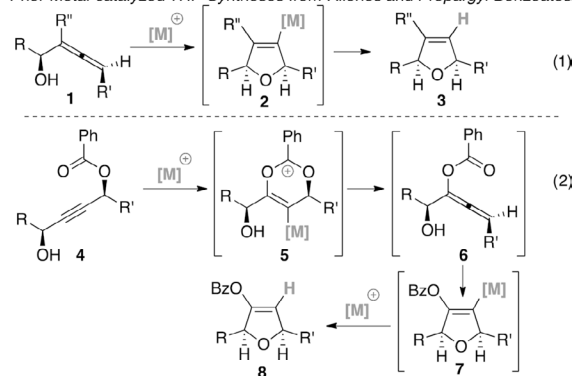
ABSTRACT: The exploration into the scope of a silver-catalyzed cyclization (AgCC) of propargyl benzoates for accessing pyran ring systems has been reported. The impact of the degree of substitution, nature of the substitution on the carbon backbone/benzoate moiety, and stereochemistry has been evaluated. The application of this methodology to the synthesis of the C₁–C₁₂ southern fragment of madeirolide A is disclosed.



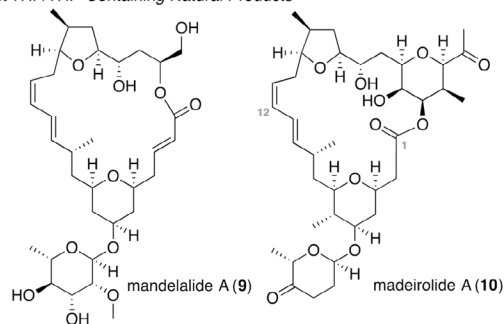
Nature produces a diverse array of polyketide natural products that have shown interesting biological activity. Many of these polyketides contain stereodefined, polysubstituted tetrahydrofurans and tetrahydropyrans (Scheme 1). Consequently, a broad array of synthetic tools have been developed to access these structural classes,¹ including various transition-metal-mediated processes. The use of allenyl alcohols as suitable precursors has proven effective in metal-catalyzed (primarily Au and Ag) methods for accessing dihydrofurans (eq 1)² and dihydropyrans.³ Our laboratory has had a long-standing interest in macrolides including those containing furan and pyran ring systems.⁴ More recently, we have been focused on the potential of silver-catalyzed cyclizations (AgCCs) with propargyl benzoates for accessing furanyl ring systems (eq 2).⁵ This work was inspired by Shigemasa and other pioneering authors in the area.^{6,7} In these transformations, the propargyl benzoate **4** must first undergo metal-catalyzed rearrangement to an allenyl enol ether **6** which then undergoes a second metal-catalyzed process, this time a 5-*endo* cyclization to access a presumed vinyl metallo intermediate **7** which subsequently protodemetalates to give the final, dihydrofuranyl enol ether product **8**. We became intrigued by the potential of extending this concept to access tetrahydropyrans using the corresponding homopropargylic alcohols. Toste and co-workers demonstrated the potential of phenolic-containing propargylic benzoates for accessing enantioenriched benzopyrans.⁸ Kotikalapudi and Swamy utilized highly unsaturated propargyl benzoate systems for access to diethyl pyran systems.⁹ In our recent total synthesis of mandelalide A (**9**), we demonstrated the first example of using a AgCC to access a *cis*-disubstituted pyran moiety.^{5c} Concurrent with our mandelalide A synthesis, Fürstner and co-workers reported a *exo*-cyclic version of this transformation in their synthesis of enigazole A.¹⁰ Herein, we disclose the exploration of a general method for accessing enol benzoate-containing dihydropyrans and its application to the

Scheme 1. Background of Metal-Catalyzed THF Synthesis and Select Natural Product Examples

Prior Metal-catalyzed THF Syntheses from Allenes and Propargyl Benzoates



Select THF/THP Containing Natural Products



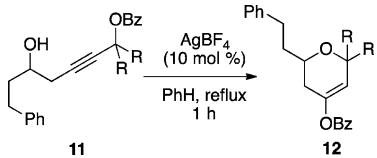
Received: February 11, 2016

Published: March 31, 2016

synthesis of the C₁–C₁₂ fragment of the antifungal macroide madeirolide A (**10**).¹¹

We first sought to explore the impact of substitution on the propargylic benzoate carbon¹² in the AgCC process (Table 1).

Table 1. Exploration of Scope of AgCC



entry	R	yield (%)
a	Me	73
b	Et	76
c	Ph	decomp
d	–(CH ₂) ₄ –	89
e	–(CH ₂) ₅ –	83
f	–(CH ₂) ₂ –O–(CH ₂) ₂ –	73
g ^a	H	decomp

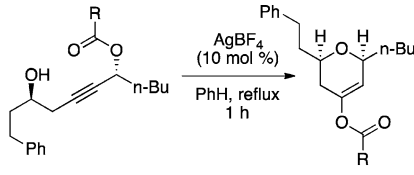
^aThis result was observed in refluxing toluene (3 h) and xylenes (1 h). No reaction was observed under refluxing benzene (4 h).

The optimum conditions for these cyclizations were in refluxing benzene. The reaction proceeded faster at higher temperatures (e.g., refluxing toluene or xylenes); however, slightly lower yields were typically observed (ca. 5–10% lower). We were pleased to see clean conversion with both the dimethyl benzoate **11a** and the diethyl variant **11b** to their desired products in 73% and 76% yield, respectively. Interestingly, the diphenyl benzoate **11c** proved problematic, as decomposition was observed under the reaction conditions. We attribute this outcome to the strong propensity of the benzoate moiety to ionize to the corresponding 3° carbocation which would be highly stabilized by the two phenyl substituents as well as the alkyne. Cyclic systems (e.g., **11d**–**11f**) worked smoothly to provide the spirocyclic products in good to excellent yields (73–89%). The absence of any substitution at the propargylic benzoate carbon was problematic as the primary benzoate **11g** led to no reaction under refluxing benzene conditions and decomposition at higher temperatures.

We next set out to study the impact of substituents on the benzoate moiety in the cyclization (Table 2). We focused on the disubstituted AgCC, as we recently demonstrated the utility of this transformation in our mandelalide A synthesis.^{5c} These cyclization precursors were accessed from known chiral building blocks.¹³ We observed a modest temperature dependent stereoselectivity in the cyclization process. Interestingly, higher reaction temperatures appeared to have a slight, positive impact on the stereochemical outcome of the process. The use of more electron-rich benzoates (e.g., **13d**) led to an increase in the reaction rate, likely due to the increased nucleophilicity of the benzoate to attack the silver-activated alkyne (entries 10–12); however, a decrease in the overall selectivity was observed. In contrast, the use of a more electron-deficient benzoate (**13e**) led to dramatically lower yields and slightly reduced diastereoselectivity (entries 13–15).

Varying substitution of the carbon backbone led to interesting results (Scheme 2).¹² The use of a primary alcohol as the terminal nucleophile (compound **15**) in the AgCC worked smoothly and in high yield. This result is in contrast to the primary propargylic benzoate **11g** which led to decom-

Table 2. Exploration of Diastereoselective AgCC

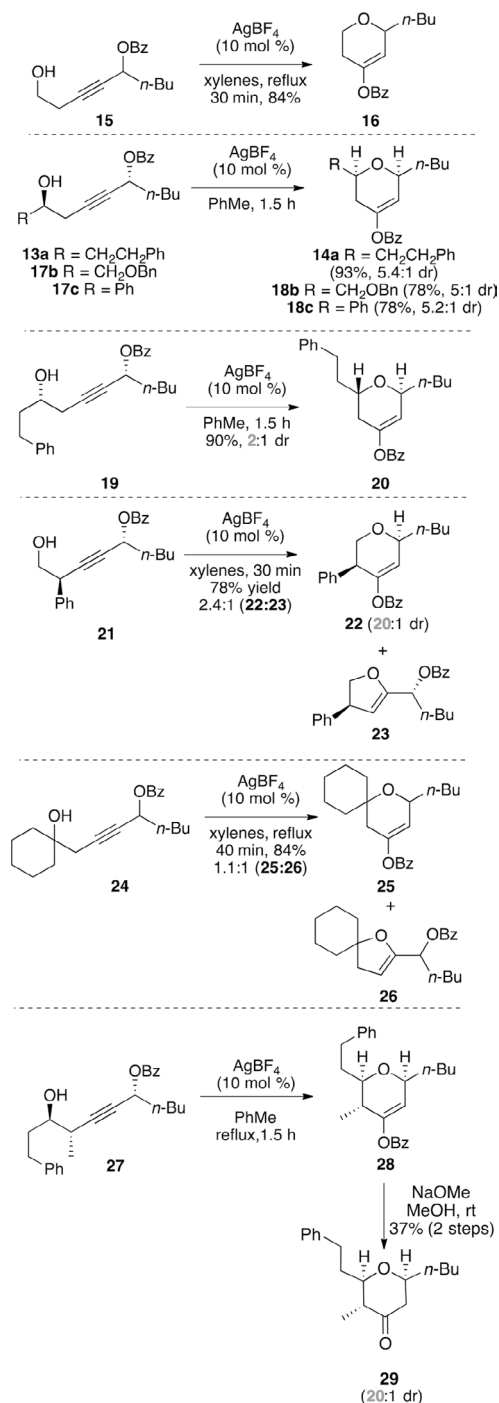


entry	substrate	conditions	% yield (dr)
1	13a	PhH, reflux, 3.5 h	92 (4.6:1)
2	13a	PhMe, reflux, 1.5 h	93 (5.4:1)
3	13a	xylenes, reflux, 50 min	93 (5.5:1)
4	13b	PhH, reflux, 4 h	79 (4.2:1)
5	13b	PhMe, reflux, 5 h	87 (4.8:1)
6	13b	xylenes, reflux, 50 min	86 (4.6:1)
7	13c	PhH, reflux, 3.5 h	93 (3.8:1)
8	13c	PhMe, reflux, 1.5 h	94 (4.0:1)
9	13c	xylenes, reflux, 50 min	90 (4.3:1)
10	13d	PhH, reflux, 2.5 h	77 (2.6:1)
11	13d	PhMe, reflux, 1.5 h	93 (3.8:1)
12	13d	xylenes, reflux, 30 min	91 (3.8:1)
13	13e	PhH, reflux, 7 h	13 (3.0:1)
14	13e	PhMe, reflux, 5 h	45 (3.2:1)
15	13e	xylenes, reflux, 1 h	62 (3.5:1)

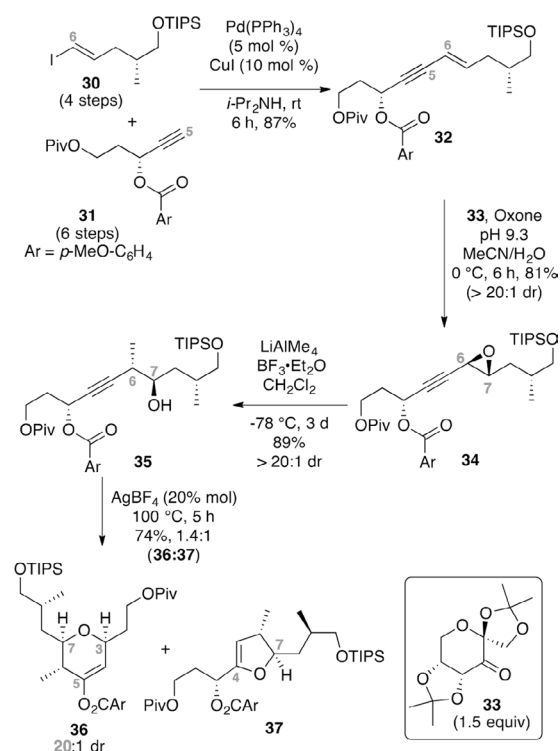
position. A series of cyclization precursors containing multiple stereochemistries were studied. The stereoselectivities on alcohols **17b**–**c** were modest (5–6:1 dr), but the reactions proceeded in generally good yields. Interestingly, the epimeric alcohol stereochemistry **19** did produce the expected trans-pyran ring **20**, but in low diastereoselectivity (2:1 dr). This example clearly demonstrates that significant stereochemical scrambling is occurring on a similar time frame to cyclization. The presence of a second propargylic stereocenter proved beneficial, leading to excellent stereoconversion (20:1 dr) for alcohol **21** to enol benzoate **22**; however, the formation of a dihydrofuran (DHF) byproduct **23** was also observed.¹⁴ The use of tertiary alcohols produced nearly equal amounts of five- and six-membered products. Finally, the use of the stereochemically dense alcohol **27** did provide the target dihydropyran **28**.¹⁴ Crude NMR indicated a similar DHF byproduct was also formed in nearly equal amounts (approximately 1:1); however, this presumed DHF compound proved too unstable to verify. Subsequent hydrolysis of the enol benzoate **28** provided the pyranone **29** in 20:1 dr.

With a firm knowledge of the reaction scope, we applied the AgCC protocol to the synthesis of the C₁–C₁₂ fragment of madeirolide A (Scheme 3). Starting from readily available vinyl iodide **30**¹⁵ and alkyne **31**,^{5b} Sonogashira cross-coupling generated the enyne **32** in good yield. Shi epoxidation of enyne **32** proceeded in excellent diastereoselectivity and good overall yield. Subsequent ring opening at the propargylic position was best accomplished using LiAlMe₄/BF₃·Et₂O to provide clean stereoconversion to alcohol **35**. We were pleased to see that the key AgCC proceeded in excellent diastereoselectivity to provide the enol *p*-methoxybenzoate **36** in >20:1 dr along with a minor amount of the undesired DHF **37** in an approximately 1.4:1 ratio (**36**:**37**). The *p*-methoxy

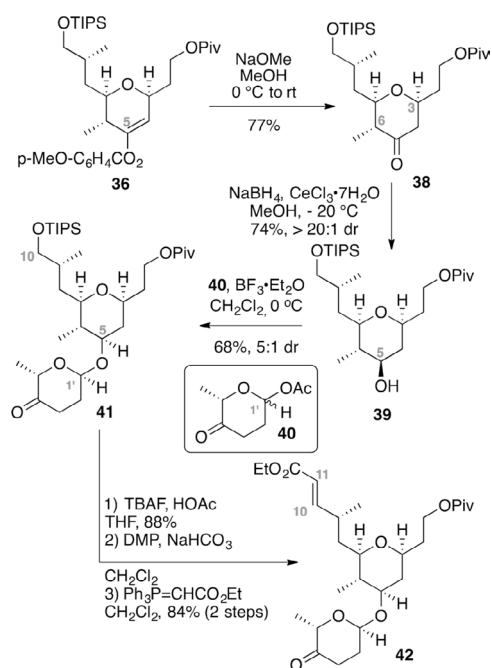
Scheme 2. Exploration of Stereochemistry in AgCC



group on the aromatic ring of the benzoate was essential for obtaining reasonable yields. Interestingly, the DHF product¹⁴ was formed in greater quantities at lower temperatures, indicating a higher activation barrier for isomerization of the propargylic benzoate to the allene as compared to direct cyclization by the alcohol to the activated alkyne. The DHF 37 proved unstable and decomposed partially under SiO₂ purification conditions and upon storage in CDCl₃.

Scheme 3. AgCC for Accessing the C₃–C₇ THP Ring in Madeirolide A

The completion of the southern, C₁–C₁₂ fragment of madeirolide A is shown in Scheme 4. NaOMe cleavage^{5c} of the enol benzoate revealed the desired ketone with no

Scheme 4. Synthesis of the C₁–C₁₂ Subunit of Madeirolide A

stereoreduction at C₃ or C₆. Stereoselective reduction of the C₅ ketone followed by attachment of the glycoside **40**^{11b} provided product **41**. Finally, buffered TBAF deprotection of the C₁₀ OTIPS ether followed by DMP oxidation and Wittig olefination introduced the key *trans* C_{10,11} alkene **42**.

In summary, the scope of AgCC to access pyran ring systems has been explored. The impact of the degree of substitution, nature of substituents, and stereochemistry has been studied. Extension of this work to the synthesis of the southern, C₁–C₁₂ subunit of madeirolide A has been demonstrated. Further work exploring the AgCC reaction and its application in synthesis will be reported in due course.

■ ASSOCIATED CONTENT

Supporting Information

The Supporting Information is available free of charge on the ACS Publications website at DOI: 10.1021/acs.orglett.6b00414.

Complete experimental procedures (PDF)

Copies of ¹H and ¹³C spectra for all new compounds (PDF)

■ AUTHOR INFORMATION

Corresponding Author

*E-mail: rich.carter@oregonstate.edu.

Present Address

[†]Tohoku Pharmaceutical University, 4-1-1 Komatsushima, Aoba-ku, Sendai, 981-8558, Japan.

Author Contributions

[‡]K.W. and J.L. contributed equally.

Notes

The authors declare no competing financial interest.

■ ACKNOWLEDGMENTS

Financial support was provided by Oregon State University. K.W. acknowledges Tohoku Pharmaceutical University for fellowship support. We thank Professor Claudia Maier and Dr. Jeff Morré (OSU) for mass spectrometric data.

■ REFERENCES

- (1) (a) Nasir, N. M.; Ermanis, K.; Clarke, P. A. *Biomol. Chem.* **2014**, *12*, 3323–3335. (b) Perry, M. A.; Rychnovsky, S. D.; Sizemore, N. Synthesis of Saturated Oxygenated Heterocycles I. In *Topics in Heterocyclic Chemistry*, Vol. 35; Cossy, J., Ed.; Springer VCH: 2014; pp 43–95. DOI: 10.1007/978-3-642-41473-2_2.
- (2) (a) Aurecochea, J. M.; Solay, M. *Tetrahedron* **1998**, *54*, 3851–3856. (b) Marshall, J. A.; Yu, R. H.; Perkins, J. F. *J. Org. Chem.* **1995**, *60*, 5550–5555. (c) VanBrunt, M. P.; Standaert, R. F. *Org. Lett.* **2000**, *2*, 705–708. (d) Hoffmann-Röder, A.; Krause, N. *Org. Lett.* **2001**, *3*, 2537–2538. (e) Yoshida, M.; Ueda, H.; Ihara, M. *Tetrahedron Lett.* **2005**, *46*, 6705–6708. (f) Fürstner, A.; Kattnig, E.; Lepage, O. *J. Am. Chem. Soc.* **2006**, *128*, 9194–9204. (g) Kolakowski, R. V.; Williams, L. J. *Tetrahedron Lett.* **2007**, *48*, 4761–4764. (h) Xu, B.; Hammond, G. B. *Angew. Chem., Int. Ed.* **2008**, *47*, 689–692. (i) Chen, B.; Lu, Z.; Chai, G.; Fu, C.; Ma, S. *J. Org. Chem.* **2008**, *73*, 9486–9489. (j) Gao, Z.; Li, Y.; Cooksey, J. P.; Snaddon, T. N.; Schunk, S.; Viseux, E. M. E.; McAteer, S. M.; Kocienski, P. J. *Angew. Chem., Int. Ed.* **2009**, *48*, 5022–5025. (k) Larivée, A.; Unger, J. B.; Thomas, M.; Wirtz, C.; Dubost, C.; Handa, S.; Fürstner, A. *Angew. Chem., Int. Ed.* **2011**, *50*, 304–309. (l) Minkler, S. R. K.; Lipshutz, B. H.; Krause, N. *Angew. Chem., Int. Ed.* **2011**, *50*, 7820–7823. (m) Belger, K.; Krause, N. *Eur. J. Org. Chem.* **2015**, *2015*, 220–225. (n) Roy, A.; Bhat, B. A.; Lepore, S. D. *Org. Lett.* **2015**, *17*, 900–903.
- (3) (a) Gockel, B.; Krause, N. *Org. Lett.* **2006**, *8*, 4485–4488. (b) Zriba, R.; Gandon, V.; Aubert, C.; Fensterbank, L.; Malacria, M. *Chem. - Eur. J.* **2008**, *14*, 1482–1491. (c) Axet, M. R. A.; Barbazanges, M.; Augé, M.; Desmarests, C.; Moussa, J.; Ollivier, C.; Aubert, C.; Fensterbank, L.; Gandon, V.; Malacria, M.; Chamoreau, L. M.; Amouri, H. *Organometallics* **2010**, *29*, 6636–6638. (d) Kilpin, K. J.; Paul, U. S. D.; Lee, A.-L.; Crowley, J. D. *Chem. Commun.* **2011**, *47*, 328–330. (e) Dupré, N.; Brazel, C.; Fensterbank, L.; Malacria, M.; Thorimbert, S.; Hasenknopf, B.; Lacôte, E. *Chem. - Eur. J.* **2012**, *18*, 12962–12965. (f) Gockel, B.; Krause, N. *Eur. J. Org. Chem.* **2010**, *2010*, 311–316. (g) Mundal, D. A.; Lutz, K. E.; Thomson, R. J. *J. Am. Chem. Soc.* **2012**, *134*, 5782–5785. (h) Cox, N.; Uehling, M. R.; Haelsig, K. T.; Lalic, G. *Angew. Chem., Int. Ed.* **2013**, *52*, 4878–4882. (i) Kawade, R. K.; Liu, R.-S. *Org. Lett.* **2013**, *15*, 4094–4097. (j) Liu, Z.; Gu, P.; Shi, M. *Chem. - Eur. J.* **2011**, *17*, 5796–5799.
- (4) (a) Carter, R. G.; Bourland, T. C.; Zhou, X.-T.; Gronemeyer, M. A. *Tetrahedron* **2003**, *59*, 8963–74. (b) Zhou, X.-T.; Carter, R. G. *Angew. Chem., Int. Ed.* **2006**, *45*, 1787–1790. (c) Zhou, X.-T.; Lu, L.; Furkert, D. P.; Wells, C. E.; Carter, R. G. *Angew. Chem., Int. Ed.* **2006**, *45*, 7622–7626.
- (5) (a) Mahapatra, S.; Carter, R. G. *Angew. Chem., Int. Ed.* **2012**, *51*, 7948–7951. (b) Mahapatra, S.; Carter, R. G. *J. Am. Chem. Soc.* **2013**, *135*, 10792–10803. (c) Veerasamy, N.; Ghosh, A.; Li, J.; Watanabe, K.; Serrill, J. D.; Ishmael, J. E.; McPhail, K. L.; Carter, R. G. *J. Am. Chem. Soc.* **2016**, *138*, 770–773.
- (6) Shigemasa, Y.; Yasui, M.; Ohrai, S.-I.; Sasaki, M.; Sashiwa, H.; Saimoto, H. *J. Org. Chem.* **1991**, *56*, 910–912.
- (7) (a) Buzas, A.; Istrate, F.; Gagosz, F. *Org. Lett.* **2006**, *8*, 1957–1959. (b) Yeom, H.-S.; Yoon, S.-J.; Shin, S. *Tetrahedron Lett.* **2007**, *48*, 4817–4820.
- (8) Wang, Y.-M.; Kuzniewski, C. N.; Rauniyar, V.; Hoong, C.; Toste, F. D. *J. Am. Chem. Soc.* **2011**, *133*, 12972–12975.
- (9) Kotikalapudi, R.; Swamy, K. C. K. *Tetrahedron* **2013**, *69*, 8002–8012.
- (10) Ahlers, A.; de Haro, T.; Gabor, B.; Fürstner, A. *Angew. Chem., Int. Ed.* **2016**, *55*, 1406–1411.
- (11) (a) Winder, P. L. Ph.D. Thesis, Florida Atlantic University, 2009. (b) Paterson, I.; Haslett, G. W. *Org. Lett.* **2013**, *15*, 1338–1341.
- (12) The synthetic routes for each one of the cyclization precursors provided in the Supporting Information.
- (13) (a) Yue, Y.; Turlington, M.; Yu, X.-Q.; Pu, L. *J. Org. Chem.* **2009**, *74*, 8681–8689. (b) Bae, H. J.; Jeong, W.; Lee, J. H.; Rhee, Y. H. *Chem. - Eur. J.* **2011**, *17*, 1433–1436.
- (14) A mechanistic explanation for the formation of unwanted DHP byproduct is provided in the Supporting Information.
- (15) (a) Ni, Y.; Kassab, R.; Cheviakov, M.; Montgomery, J. J. *Am. Chem. Soc.* **2009**, *131*, 17714–17718. (b) Huang, Z.; Negishi, E. *Org. Lett.* **2006**, *8*, 3675–3678.

Activation of p38 Mitogen-Activated Protein Kinase by Clotrimazole Induces Multidrug Resistance–Associated Protein 3 Activation through a Novel Transcriptional Element

Takamitsu Sasaki, Keita Inami, Yoshihiro Numata, Kodai Funakoshi, Midori Yoshida, Takeshi Kumagai, Shuichi Kanno, Satomi Matsui, Takayoshi Toriyabe, Yasushi Yamazoe, Kouichi Yoshinari, and Kiyoshi Nagata

Department of Environmental and Health Science (T.S., K.I., Y.N., K.F., M.Y., T.K., K.N.) and Clinical Pharmacotherapeutics (S.K.), Faculty of Pharmaceutical Sciences, Tohoku Medical and Pharmaceutical University, Aoba-ku, Sendai, Miyagi, Japan; Department of Molecular Toxicology, School of Pharmaceutical Sciences, University of Shizuoka, Suruga-ku, Shizuoka, Japan (T.S., K.Y.); and Division of Drug Metabolism and Molecular Toxicology, Graduate School of Pharmaceutical Sciences, Tohoku University, Aoba-ku, Sendai, Miyagi, Japan (S.M., T.T., Y.Y.)

Received February 23, 2016; accepted August 2, 2016

ABSTRACT

Multidrug resistance–associated protein 3 (MRP3) is a basolaterally localized transporter in the liver and contributes to the transport of various metabolites such as conjugates of endogenous compounds and drugs from hepatocytes. MRP3 expression in the human liver is low under normal physiologic conditions but is induced by drug treatment. Although several studies have identified a region necessary for the basal transcription of *MRP3*, no region that responds to drugs has been reported. To identify the xenobiotic-responsive elements of *MRP3*, we constructed a luciferase reporter plasmid containing the *MRP3* 5′-flanking region up to −10 kb upstream from the transcription start site. Among typical nuclear receptor ligands, clotrimazole dramatically enhanced MRP3 reporter activity in HepG2 cells, whereas rifampicin had no effect. We then conducted *MRP3* reporter assays with deletion or mutation constructs to identify a clotrimazole-responsive element. The

element was located approximately −6.8 kb upstream from the *MRP3* transcription start site. Overexpression of the pregnane X receptor did not enhance clotrimazole-mediated transcription. We found that clotrimazole was toxic to HepG2 cells and we therefore investigated whether mitogen-activated protein kinase (MAPK) activation is involved in the transactivation of *MRP3* by clotrimazole. p38 MAPK inhibitor SB203580 [4-(4-fluorophenyl)-2-(4-methylsulfinylphenyl)-5-(4-pyridyl)1*H*-imidazole] suppressed *MRP3* mRNA expression induced by clotrimazole, whereas c-Jun N-terminal kinase inhibitor SP600125 (1,9-pyrazoloanthrone) and extracellular signal-regulated kinase inhibitor PD98059 [2-(2-amino-3-methoxyphenyl)-4*H*-1-benzopyran-4-one] did not. Phosphorylated p38 MAPK was detected in HepG2 cells treated with clotrimazole. These results suggest that activation of the p38 MAPK pathway induces the transcriptional activation of *MRP3*.

Introduction

Multidrug resistance–associated proteins (MRPs) belong to the ATP-binding cassette family of membrane transporters and transport endogenous and exogenous compounds across biologic membranes (Borst and Elferink, 2002). Eight MRP isoforms have been identified as organic anion transporters. Among them, MRP2 and MRP3 are primary transporters in the liver, which transport various metabolites (e.g., conjugates of endogenous compounds and drugs) from hepatocytes. Both

isoforms show similar substrate specificity, including several sulfate, glutathione, and glucuronate conjugates, but have different physiologic roles (Bodo et al., 2003; Borst et al., 2007; Nies and Keppler, 2007; Bachour-El Azzi et al., 2015). MRP2 is located at the apical membrane of hepatocytes and transports conjugated metabolites into the bile canaliculus, whereas MRP3 is expressed on the basolateral membrane of hepatocytes and eliminates its substrates toward blood circulation (König et al., 1999; Borst et al., 2006).

MRP3 expression is induced by treatment with pregnane X receptor (PXR) activators, including rifampicin and clotrimazole, in human hepatoma cell lines (Teng et al., 2003). Aryl hydrocarbon receptor activators omeprazole and β -naphthoflavone also appear to induce MRP3 expression (Hitzl et al., 2003). Recent studies in PXR or nuclear factor E2–related factor-2

This research was supported by the Japanese Ministry of Education, Culture, Sports, Science and Technology–supported Program for the Strategic Research Foundation at Private Universities (No. S1511001L) and Grant-in-Aid for Scientific Research (C) (No. 25460195).
 dx.doi.org/10.1124/jpet.115.231589.

ABBREVIATIONS: CAR, constitutive androstane receptor; CDCA, chenodeoxycholic acid; DMSO, dimethylsulfoxide; DR, direct repeat; GAPDH, glyceraldehyde-3-phosphate dehydrogenase; hPXR, human pregnane X receptor; hRXR α , human retinoid X receptor α ; JNK, c-Jun N-terminal kinase; LDH, lactate dehydrogenase; MAPK, mitogen-activated protein kinase; MRP, multidrug resistance–associated protein; PCR, polymerase chain reaction; PD98059, 2-(2-amino-3-methoxyphenyl)-4*H*-1-benzopyran-4-one; PXR, pregnane X receptor; SB203580, 4-(4-fluorophenyl)-2-(4-methylsulfinylphenyl)-5-(4-pyridyl)1*H*-imidazole; SP600125, 1,9-pyrazoloanthrone; TNF α , tumor necrosis factor α ; VD₃, 1 α , 25-dihydroxyvitamin D₃.

(Nrf2) knockout mouse models have examined the roles of the transcription factors in the regulation of *Mrp3* and suggest that these factors are involved in the induction of *Mrp3* expression (Teng et al., 2003; Maher et al., 2007). Constitutive androstane receptor (CAR) activators 1,4-bis[2-(3,5-dichloropyridyloxy)]benzene and phenobarbital have also been reported to induce *Mrp3* expression in mice (Cherrington et al., 2003; Maher et al., 2005). Taken together, MRP3/*Mrp3* expression is thought to be induced via nuclear receptor-mediated pathways in human and mouse livers.

MRP3 expression in the human liver is low under normal physiologic conditions, but the expression is markedly upregulated in patients with cholestasis and Dubin–Johnson syndrome as a result of deficient MRP2 expression (König et al., 1999; Chai et al., 2012). In cholestasis, the enhancement of MRP3 expression is mediated via the activation of c-Jun N-terminal kinase (JNK), a member of mitogen-activated protein kinase (MAPK) family. *Mrp3* expression was also found to be upregulated in a rat model of cholestasis and Dubin–Johnson syndrome (Soroka et al., 2001; Kuroda et al., 2004). These results suggest that MRP3/*Mrp3* expression is induced by signal pathways, including MAPK, independently of nuclear receptor-mediated pathways and that MRP3/*Mrp3* may work as a compensatory transporter for MRP2.

Few studies have examined the molecular mechanism of transcriptional regulation of human *MRP3*. In reporter assays with a *MRP3* 5'-flanking region up to -4235 bp from the transcriptional start site, a GC-rich region located between -127 and -23 bp was reported to be important for its basal expression (Takada et al., 2000). *MRP3* gene expression is under the control of a TATA-less promoter, and some putative binding sites for transcription factors such as Sp1 are found in this GC-rich region. Another study demonstrated that a *MRP3* 5'-flanking region up to -1287 bp from the transcriptional start site includes regions involved in basal expression (Stöckel et al., 2000). However, xenobiotic-responsive elements of the *MRP3* 5'-flanking region have not been identified, indicating that the elements may be further upstream.

In this study, we constructed a luciferase reporter plasmid containing the *MRP3* 5'-flanking region up to -10 kb to investigate nuclear receptor ligand-induced *MRP3* expression using reporter assays and we identified a novel xenobiotic-responsive element involved in clotrimazole-induced *MRP3* expression. We demonstrate that *MRP3* induction by clotrimazole occurs through the p38 MAPK pathway. Our results suggest an association between drug-induced hepatotoxicity and transcriptional activation of human *MRP3*.

Materials and Methods

Materials. Restriction and DNA modification enzymes were obtained from Takara Bio Inc. (Shiga, Japan). Rifampicin, clotrimazole, chenodeoxycholic acid (CDCA), and 1 α ,25-dihydroxyvitamin D₃ (VD₃) were purchased from Sigma-Aldrich (St. Louis, MO). Anisomycin, SB203580 [4-(4-fluorophenyl)-2-(4-methylsulfinylphenyl)-5-(4-pyridyl)1H-imidazole], PD98059 [2-(2-amino-3-methoxyphenyl)-4H-1-benzopyran-4-one], and SP600125 (1,9-pyrazoloanthrone) were purchased from Wako Pure Chemicals (Osaka, Japan). Dimethylsulfoxide (DMSO) was obtained from Nacalai Tesque (Kyoto, Japan).

Reporter Gene Constructs and Expression Vector. The luciferase reporter plasmid pGL3-Basic was purchased from Promega (Madison, WI). An approximately 10-kb fragment (nucleotides from +16 to -10,136) of the *MRP3* 5'-flanking region was isolated by polymerase

chain reaction (PCR) amplification from human genomic DNA using the forward primer 5'-GCGACGCGTGCCAGGGTCATGCCTATCTGG-3' and the reverse primer 5'-GCGGTCTGACGCGGCTGCAAGGAAGGC-GAGC-3'. The underlined sequences represent the MluI and SalI restriction sites, respectively. The fragment was subcloned into a pCR-XL-TOPO vector (Invitrogen, Carlsbad, CA). The plasmid was then digested with the MluI and SalI restriction enzymes and then ligated into the MluI and XhoI sites of the pGL3-Basic vector (pGL3-MRP3-10k). The resultant construct was used as a template to generate various reporter plasmids lacking portions of the 5'-flanking region of *MRP3*. To generate an internal deletion construct (pGL3-MRP3-Acc65), a region (nucleotides from -5913 to -837) was removed from the pGL3-MRP3-10k vector by EcoRI digestion. In addition, the construct was digested with Acc65 and the nucleotides from -10,136 to -8021 were deleted. Successive deletions of the reporter plasmid to -7.9, -7.6, -7.4, -7.2, -7.1, -6.8, and -6.4 kb were created from pGL3-MRP3-Acc65 as a template. The -6.8- and -6.4-kb deleted fragments were isolated by PCR amplification using the forward primers for the -6.8-kb fragment (5'-GCGACGCGTGCTGACTGGCATTACAGG-CACTGTCC-3') and the -6.4-kb fragment (5'-GCGACGCGT-CACCTGTCTGGTGTCTACTGCAGAC-3') and the reverse primer (5'-GCGGTCTGACGCGGCTGCAAGGAAGGCGAGC-3'). The underlined sequences represent the MluI restriction sites in the forward primer and the SalI restriction site in the reverse primer. The fragments were subcloned into the pGEM-T vector (Promega). The plasmids were digested with MluI and SalI and then ligated into the MluI and XhoI sites of the pGL3-Basic vector (pGL3-MRP3-6.8k and pGL3-MRP3-6.4k). The -7.9-kb, -7.6-kb, -7.4-kb, -7.2-kb, and -7.1-kb deleted fragments were isolated by PCR amplification using the forward primers for the -7.9-kb fragment (5'-GCGACGCGTGTTTCCGACACCAGAAGCTGTTGG-3'), the -7.6-kb fragment (5'-GCGACGCGTATTTTGGAACTGTA-ATGTAAC-3'), the -7.4-kb fragment (5'-GCGACGCGTTGAT-GAGAGAGAGATCCTGGAGATGG-3'), the -7.2-kb fragment (5'-GCGACGCGTTCTGAGAGTGAGAGAACCTGAAC-3'), and the -7.1-kb fragment (5'-GCGACGCGTCTCTAGCTAGGCAGCTCAGT-GAATGG-3') and the reverse primer (5'-AACATGTGTGAATTCTA-CAAAAATATAAAG-3'). The underlined sequences represent the MluI restriction sites in the forward primers and EcoRI restriction site in the reverse primer. These fragments were subcloned into the pGEM-T vector. The plasmids were then digested with MluI and EcoRI and then ligated into the MluI and EcoRI sites of the pGL3-MRP3-10k vector (resulting in pGL3-MRP3-7.9k, pGL3-MRP3-7.6k, pGL3-MRP3-7.4k, pGL3-MRP3-7.2k, and pGL3-MRP3-7.1k). Mutated reporter plasmids were constructed by the QuikChange II site-directed mutagenesis kit (Stratagene, La Jolla, CA) using pGL3-MRP3-Acc65 as a template. Preparation of the human pregnane X receptor (hPXR) expression plasmid was previously described (Takada et al., 2004). All plasmids were sequenced to confirm their integrity.

Cell Culture and Reporter Assays. The human hepatoma cell line HepG2 was obtained from American Type Culture Collection (Manassas, VA) and cultured in Dulbecco's modified Eagle's medium (Nissui Pharmaceutical, Tokyo, Japan) supplemented with 10% fetal calf serum (Boehringer, Mannheim, Germany) and minimum Eagle's medium nonessential amino acids (Invitrogen). Cells were seeded in 12-well tissue culture plates (BD Biosciences, Franklin Lakes, NJ) at 1.2×10^5 cells per well 1 day before transfection. Each reporter plasmid and a pSV- β -galactosidase control vector (Promega) were cotransfected using the CellPhect Transfection Kit (GE Healthcare, Little Chalfont, UK) according to the manufacturer's instructions. In overexpression analyses of hPXR, either the hPXR expression vector or the pCMV4 control plasmid was simultaneously transfected into HepG2 cells with a reporter plasmid. After transfection, the cells were incubated in culture medium containing various compounds (rifampicin, clotrimazole, CDCA, or VD₃) dissolved in DMSO (final concentration 0.1%) for 48 hours. Control cells were treated with 0.1% DMSO. Subsequently, cells were washed with phosphate-buffered saline and suspended in 0.1 ml passive lysis buffer (Promega). Luciferase

activities were determined using a luciferase assay system (Promega). To normalize transfection efficiency, β -galactosidase assays were performed as previously described (Herbomel et al., 1984).

Electrophoretic Mobility Shift Assays. hPXR and human retinoid X receptor- α (hRXR α) were synthesized in vitro with the pT_NT-hPXR and pT_NT-hRXR α plasmids, respectively, using the T_NT Quick Coupled Transcription/Translation System (Promega) following the manufacturer's protocol. Preparation of the pT_NT-hPXR and pT_NT-hRXR α plasmids was previously described (Toriyabe et al., 2009). Double-strand oligonucleotides (Fig. 4) were labeled with [γ -³²P]ATP using T4 polynucleotide kinase (New England BioLabs, Ipswich, MA) and purified using NAP5 columns (GE Healthcare). The binding reactions were carried out as previously described (Toriyabe et al., 2009).

Cytotoxicity Assays. HepG2 cells were seeded in 96-well tissue culture plates (BD Biosciences) at 1.5×10^4 cells per well. The culture medium was replaced with fresh medium containing clotrimazole or rifampicin 24 hours after cell seeding. After 72 hours of exposure, the release of lactate dehydrogenase (LDH) was determined using the Cytotoxicity Detection Kit (Roche Applied Science, Mannheim, Germany) according to the manufacturer's instructions.

HepaRG Cells and Cell Culture. Differentiated HepaRG cells were obtained from Life Technologies (Carlsbad, CA). The cells were thawed and cultured in William's medium E containing GlutaMAXI and HepaRG Thaw, Plate, and General Purpose Medium Supplement (all from Life Technologies) according to the manufacturer's protocol. The cells were seeded in type I collagen-coated 48-well tissue culture plates (Corning, Corning, NY) at 2.0×10^5 cells per well and cultured for 72 hours before drug treatment. The cells were then cultured in William's medium E containing GlutaMAXI, HepaRG Induction Medium Supplement, and clotrimazole or rifampicin for 48 hours.

Small Interfering RNA Transfection. Trypsinized HepG2 cells were reverse transfected with 40 nM ON-TARGETplus SMART Pool MAPK14 or 40 nM ON-TARGETplus Non-Targeting Pool (GE Healthcare) using Lipofectamine RNAiMAX (Invitrogen). After 24 hours, the medium was changed to fresh medium containing clotrimazole and the cells were cultured for an additional 24 hours. Next, the cells were forward transfected with the small interfering RNAs for 6 hours and subsequently treated with clotrimazole for an additional 48 hours.

Quantitative Analysis of mRNA Levels. HepG2 cells were seeded in 24-well tissue culture plates (BD Biosciences) at 1.0×10^5 cells per well. The culture medium was replaced with fresh medium containing clotrimazole or rifampicin 24 hours after cell seeding. In MAPK inhibitor experiments, the cells were pretreated with SB203580, PD98059, or SP600125 1 hour before exposure to the various compounds. After 72 hours of exposure, total RNA was extracted using TRI Reagent (Molecular Research Center, Cincinnati, OH). First-strand cDNA was synthesized from 2 μ g total RNA in a 25- μ l reaction mixture using Moloney murine virus reverse transcriptase (Promega), oligo (dT)₂₀ primers, and ribonuclease inhibitor (Takara Bio Inc.). cDNA was used to carry out real-time PCR using SYBR premix ExTaq (Takara Bio Inc.) to measure the mRNA levels of *MRP3*, *activating transcription factor 3* (*ATF3*), and glyceraldehyde-3-phosphate dehydrogenase (*GAPDH*). The amplification reaction was performed using specific primers for *MRP3* (forward: 5'-GTCCGCA-GAATGGACTTGAT-3'; reverse: 5'-TCACCACTTGGGGATCATTT-3'), *ATF3* (forward: 5'-AGCCTGGAGCAAAATGATGCTT-3'; reverse: 5'-AGGTTAGCAAAATCCTCAACAC-3'), and *GAPDH* (forward: 5'-GAAGGTGAAGTCTCGAGTCAAC-3'; reverse: 5'-CAGAGTTAAAG-GCAGCCCTGGT-3'). The relative mRNA levels in each sample were normalized according to those of *GAPDH*.

Immunoblot Analysis. Immunoblot analysis was performed to evaluate the expression of phospho-p38 MAPK proteins. Whole cell lysates were size fractionated by gel electrophoresis on a 10% polyacrylamide/0.1% sodium dodecyl sulfate gel after denaturation by heating in loading buffer containing 2-mercaptoethanol. The proteins were electrotransferred onto Immobilon-P membranes

(Millipore, Billerica, MA), which were then incubated for 16 hours with a phospho-p38 MAPK (Thr180/Tyr182) antibody (Cell Signaling Technology, Beverly, MA) diluted in Tris-buffered saline (1:1000). The membrane was also incubated with p38 MAPK antibody (dilution, 1:500; Cell Signaling Technology) or β -actin antibody (dilution, 1:1000; Cell Signaling Technology) for 1 hour. The membranes were subsequently incubated for 1 hour with horseradish peroxidase-conjugated secondary antibody diluted in Tris-buffered saline (1:5000; Santa Cruz Biotechnology, Santa Cruz, CA). After development with the SuperSignal West Pico chemiluminescent substrate (Thermo Fisher Scientific, Waltham, MA), the membrane was scanned using a Lumino Imaging Analyzer FAS-1000 (Toyobo, Osaka, Japan).

Statistical Analysis. Data are presented as means \pm S.E.M. Data were analyzed with the Welch *t* test or one-way analysis of variance followed by the Dunnett or Bonferroni post hoc test. All statistical analyses were performed using Prism software (version 6.0; GraphPad Software Inc., San Diego, CA). A *P* value less than 0.05 was considered statistically significant.

Results

Effect of Typical Nuclear Receptor Ligands on MRP3 Reporter Activity in HepG2 Cells. Previous studies demonstrated that the *MRP3* 5'-flanking region up to -1287 bp or -4235 bp including the GC-rich region regulates *MRP3* basal expression (Stöckel et al., 2000; Takada et al., 2000). However, to our knowledge, a role of the far upstream region in the drug-induced expression of *MRP3* has not been investigated. To identify xenobiotic-responsive elements of *MRP3*, we constructed a luciferase reporter plasmid containing the *MRP3* 5'-flanking region up to -10 kb (pGL-MRP3-10k) and transfected the plasmid into HepG2 cells. We investigated whether treatment with typical ligands of PXR (rifampicin and clotrimazole), the vitamin D receptor (VD₃), and the farnesoid X receptor (CDCA) increased *MRP3* reporter activity. Clotrimazole treatment resulted in a 132-fold increase in *MRP3* reporter activity (Fig. 1). In contrast, treatment with rifampicin and other compounds did not increase the luciferase activities in HepG2 cells.

We also used the *CYP3A4* reporter plasmid (pCYP3A4-362-7.7k), including everted repeat separated by six nucleotides

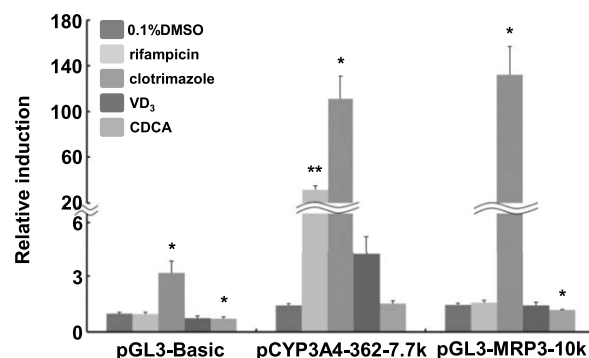


Fig. 1. Effects of typical nuclear receptor ligands on *MRP3* reporter activity in HepG2 cells. HepG2 cells seeded in 12-well tissue culture plates at 1.2×10^5 cells/well 1 day before transfection were transfected with each reporter plasmid and pSV- β -galactosidase as an internal control. The cells were treated with vehicle (0.1% DMSO), rifampicin (10 μ M), clotrimazole (5 μ M), VD₃ (10 nM), or CDCA (100 μ M) for 48 hours. Relative luciferase activities are shown as means \pm S.E.M. (*n* = 4). **P* < 0.05; ***P* < 0.01, significantly different from the activities in corresponding vehicle-treated cells based on the Welch *t* test.

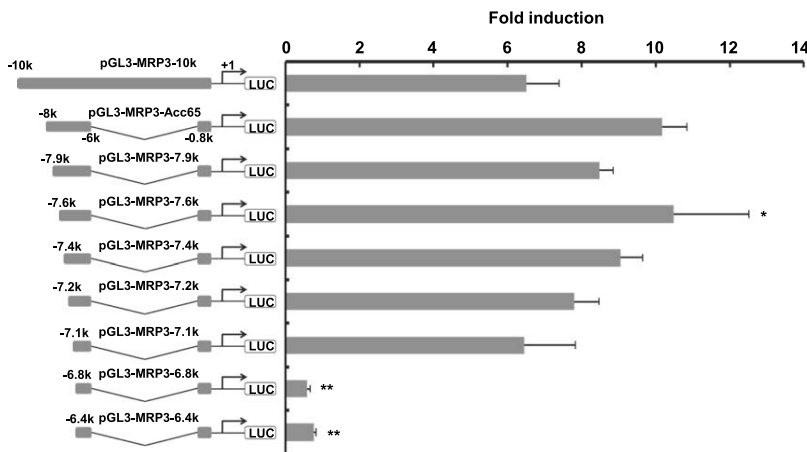


Fig. 2. Effects of deletions of the *MRP3* 5'-flanking region on reporter activity. HepG2 cells seeded in 12-well tissue culture plates at 1.2×10^5 cells/well 1 day before transfection were transfected with various reporter plasmids lacking portions of the *MRP3* 5'-flanking region of pGL3-MRP3-10k and with pSV- β -galactosidase as an internal control. The cells were treated with vehicle (0.1% DMSO) or clotrimazole (5 μ M) for 48 hours. The reporter activity of cells treated with vehicle was set to 1.0. The data represent means \pm S.E.M. ($n = 4$). * $P < 0.05$; ** $P < 0.01$, significantly different from the reporter activity of the cells transfected with pGL3-MRP3-10k based on one-way analysis of variance with the Dunnett post hoc test.

located in the *CYP3A4* proximal promoter (prER6; +11 to -362 bp) and essential distal nuclear receptor-binding element for *CYP3A4* induction and distal nuclear receptor-binding element 1 (-7.2 to -7.8 kb) as the positive control. *CYP3A4* reporter activities were significantly increased by clotrimazole and rifampicin treatment. The reporter activity was also enhanced by VD₃.

Effect of Deletions of the *MRP3* 5'-Flanking Region on Reporter Activity. To identify a clotrimazole-responsive region in *MRP3*, reporter assays were carried out with various plasmids lacking portions of the *MRP3* 5'-flanking region. The reporter plasmid, in which the regions from -10 to -8.0 kb and -6.0 to -0.8 kb were removed (pGL3-MRP3-Acc65), was more responsive to clotrimazole treatment compared with pGL-MRP3-10k, although the difference was not significant (Fig. 2).

Deletion constructs of pGL3-MRP3-Acc65 were transiently transfected into HepG2 cells. Reporter activities of pGL3-MRP3-Acc65 with successive deletions from the 5' end to -7.9, -7.6, -7.4, -7.2, and -7.1 kb were not affected by clotrimazole. However, further deletion from -7.1 to -6.8 kb dramatically reduced the clotrimazole-induced *MRP3* reporter activity. These results suggest that an unidentified region responding to clotrimazole is present between -7.1 and -6.8 kb on *MRP3*.

Mutation Analysis of the Clotrimazole-Responsive Element in the *MRP3* 5'-Flanking Region. We next performed mutation analysis to identify a clotrimazole-responsive element located between -7.1 and -6.8 kb. Several nuclear receptor binding half-sites, AG(G/T)TCA-like sequence, are present between -6831 and -6810 bp. To assess the roles of the half-sites in the transcriptional activation of *MRP3* in response to clotrimazole, a series of reporter plasmids constructed by site-directed mutagenesis were used. The introduction of mutations into and surrounding the half-sites significantly reduced the reporter activities (Fig. 3). These results suggest that the clotrimazole-responsive element including half-sites is present in this region between -6831 and -6810 bp.

Role of PXR in the Transcriptional Activation of *MRP3*. We investigated whether PXR was involved in the clotrimazole-mediated activation of *MRP3*. *CYP3A4* reporter activity was significantly increased in hPXR-overexpressing HepG2 cells (173-fold) and clotrimazole treatment further increased the reporter activity (328-fold). However, overexpression of PXR did not increase *MRP3* reporter activity (Fig. 4A). On the contrary, PXR suppressed the reporter activity induced by clotrimazole. The hPXR/hRXR α heterodimer binding site located within prER6 of *CYP3A4* was recognized by the hPXR/hRXR α heterodimer (Fig. 4B). The DNA-protein complex was competed out by an 100-fold excess of unlabeled prER6.

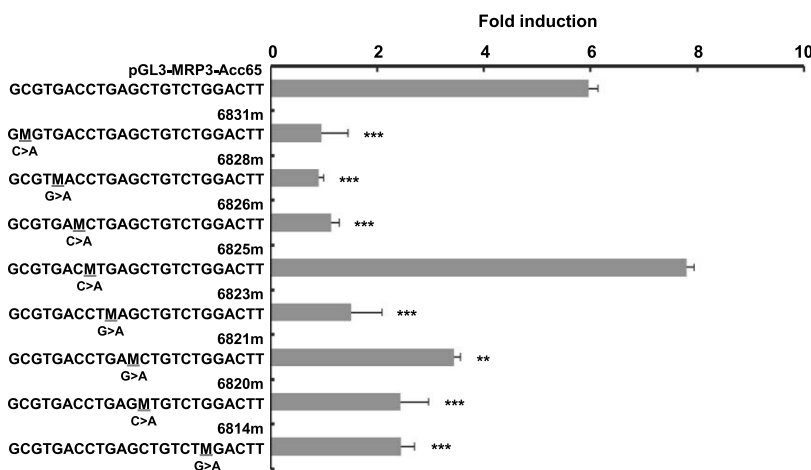


Fig. 3. Mutation analysis of the clotrimazole-responsive element in the *MRP3* 5'-flanking region. HepG2 cells seeded in 12-well tissue culture plates at 1.2×10^5 cells/well 1 day before transfection were transfected with various mutation constructs of pGL3-MRP3-Acc65 and with pSV- β -galactosidase as an internal control. The cells were treated with vehicle (0.1% DMSO) or clotrimazole (3 μ M) for 48 hours. The reporter activity of cells treated with vehicle was set to 1.0. The data represent means \pm S.E.M. ($n = 4$). The mutations are indicated as M and all mutations changed the original nucleotide (G or C) to A. ** $P < 0.01$; *** $P < 0.001$, significantly different from the reporter activity of the cells transfected with pGL3-MRP3-Acc65 based on one-way analysis of variance with the Dunnett post hoc test.

However, binding of the hPXR/hRXR α heterodimer to the clotrimazole-responsive element of *MRP3* was not observed. These results suggest that PXR is not likely to be involved in *MRP3* transactivation via the clotrimazole-responsive element.

Effect of Clotrimazole on Cytotoxicity and *MRP3* mRNA Levels in HepG2 Cells. Our results suggest that the activation of PXR by clotrimazole is less effective on the transcriptional activation of *MRP3* in HepG2 cells. We therefore focused on the hepatotoxicity of azole antifungal agents (García Rodríguez et al., 1999; Kuroda et al., 2004; Girois et al., 2005), because it has been reported that *Mrp3*

expression is significantly increased in cholestasis-induced liver injury (Wagner et al., 2003). To confirm the cytotoxicity of clotrimazole, LDH activity was measured in HepG2 cells treated with clotrimazole or rifampicin. Clotrimazole resulted in a significantly high LDH activity level compared with that in control cells (Fig. 5A). In contrast, the LDH release from HepG2 cells treated with rifampicin was similar to that from control cells. To investigate the effect of clotrimazole and rifampicin on intrinsic *MRP3* mRNA expression, HepG2 cells were treated with these drugs. *MRP3* mRNA levels were markedly induced by clotrimazole (8.7-fold) (Fig. 5B). In contrast, *MRP3* mRNA levels were not affected by rifampicin treatment. We also tested whether *MRP3* mRNA expression was induced by treatment with troglitazone, which is known to be a hepatotoxicity-inducing drug. *MRP3* mRNA levels were significantly increased by the treatment (5.9-fold) (Fig. 5C). Furthermore, we confirmed that the *MRP3* mRNA levels were increased in HepaRG cells, which retain many characteristics of primary human hepatocytes, treated with clotrimazole but not with rifampicin (Fig. 5D).

Effect of MAPK Inhibitors on Clotrimazole-Induced *MRP3* mRNA Expression in HepG2 Cells. We next investigated whether *MRP3* transcriptional activation by clotrimazole was associated with the activation of MAPKs, which are essential for the cellular response to injuries caused by drug treatment and inflammatory diseases, including cholestasis (Hanawa et al., 2008; Boaglio et al., 2012). To assess the effects of MAPK inhibitors on *MRP3* mRNA expression induced by clotrimazole, HepG2 cells were preincubated with a p38 MAPK inhibitor (SB203580), JNK inhibitor (SP600125), or extracellular signal-regulated kinase inhibitor (PD98059) for 1 hour, followed by with clotrimazole. SB203580 pretreatment suppressed *MRP3* mRNA expression induced by clotrimazole, whereas SP600125 and PD98059 did not (Fig. 6A). We also investigated whether *ATF3*, which is known to be induced by the stress-activated p38 signaling pathway (Lu et al., 2007), was enhanced by clotrimazole treatment. Clotrimazole induced *ATF3* mRNA expression as well as *MRP3* mRNA expression, and the increased expression was inhibited only by pretreatment with SB203580. Furthermore, treatment with anisomycin, a p38 MAPK activator (Saito et al., 2013), resulted in a 12.8-fold increase in *MRP3* mRNA levels, and the induced expression was also suppressed by pretreatment with SB203580 (Fig. 6B). To confirm the activation of p38 MAPK by clotrimazole, Western blotting was carried out to detect phosphorylated p38 MAPK. Increased phosphorylated p38 MAPK protein levels were detected in HepG2 cells treated with clotrimazole (Fig. 6C). In contrast, phosphorylated p38 MAPK was not detected in HepG2 cells treated with rifampicin, which did not induce *MRP3* mRNA expression. We also demonstrated that clotrimazole-induced *MRP3* mRNA expression was significantly suppressed in HepG2 cells transfected with p38 MAPK small interfering RNA (Fig. 6D).

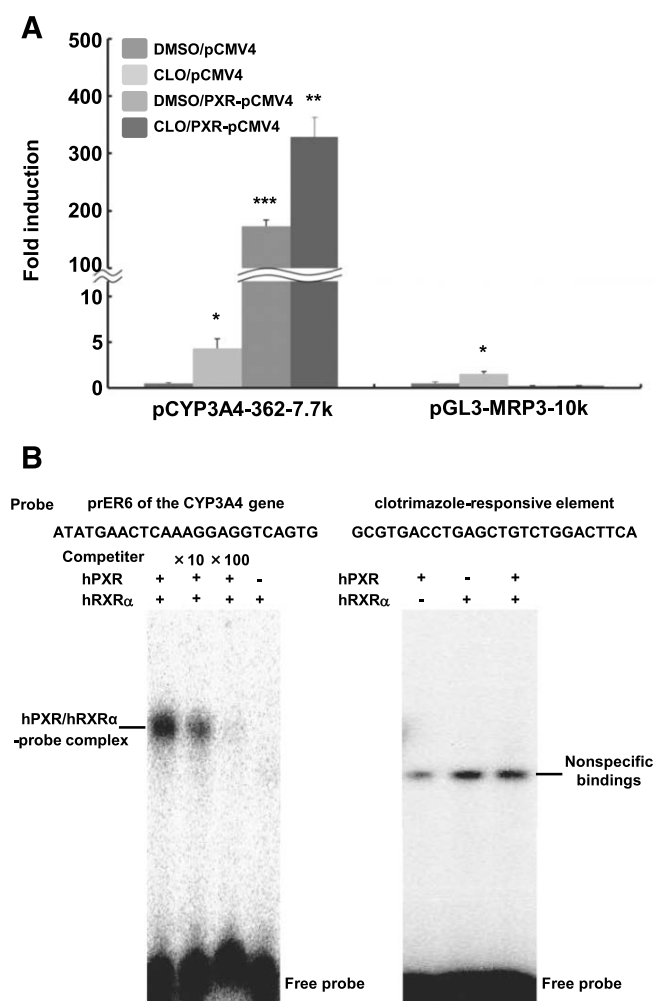


Fig. 4. Role of PXR in the transcriptional activation of *MRP3*. (A) HepG2 cells seeded in 12-well tissue culture plates at 1.2×10^5 cells/well 1 day before transfection were transfected with each reporter plasmid and with pSV- β -galactosidase as an internal control. The hPXR expression plasmid or pCMV4 was simultaneously transfected into the HepG2 cells. The cells were treated with vehicle (0.1% DMSO) or clotrimazole (3 μ M) for 48 hours. The reporter activity of HepG2 cells treated with vehicle was set to 1.0. The data represent means \pm S.E.M. ($n = 4$). * $P < 0.05$; ** $P < 0.01$; *** $P < 0.001$, significantly different from the activities of the vehicle-treated/pCMV4-transfected cells based on the Welch t test. (B) Sequences of the oligonucleotides used for the gel electrophoresis mobility shift assays are shown. The assays were carried out with radiolabeled prER6 and the clotrimazole-responsive element. Incubations were carried out with hPXR and/or hRXR α synthesized in vitro as indicated. Competition assays were performed with radiolabeled prER6 as probes. Ten- or 100-fold molar excesses of unlabeled competitors were added to the reaction solution. CLO, clotrimazole.

Discussion

In this study, we investigated whether ligands of PXR and other nuclear receptors induced *MRP3* expression (Fig. 1). Among the PXR ligands tested, clotrimazole dramatically enhanced *MRP3* reporter activity in HepG2 cells, whereas rifampicin had no effect. However, these compounds significantly increased CYP3A4 reporter activity. Our results

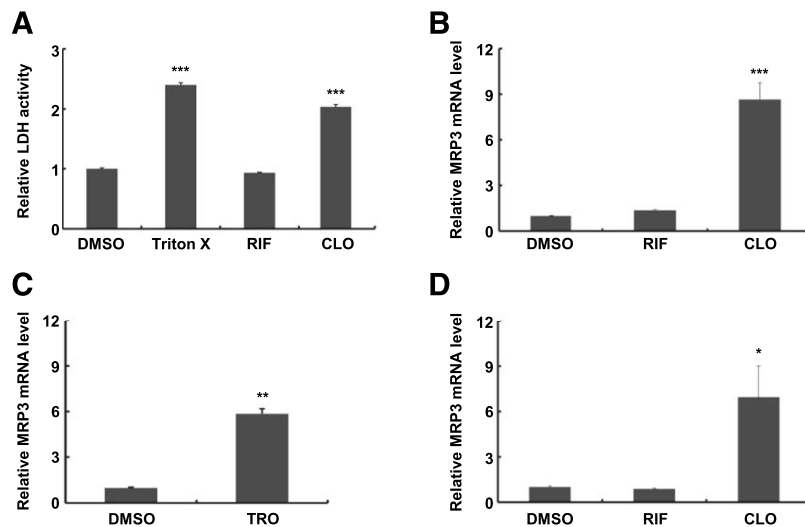


Fig. 5. Effects of clotrimazole on cytotoxicity and *MRP3* mRNA expression in HepG2 cells and HepaRG cells. HepG2 cells were seeded in 24-well tissue culture plates at 1.0×10^5 cells/well 1 day before drug treatment. The cells were treated with vehicle (0.1% DMSO), rifampicin (20 μ M), clotrimazole (20 μ M), or troglitazone (50 μ M) for 72 hours. (A) The medium in each well was collected and LDH activities were measured. The media from Triton X-100-treated cells were used as a positive control for cytotoxicity. (B and C) Total RNA was extracted and the *MRP3* mRNA levels were determined. (D) HepaRG cells were seeded in type I collagen-coated 48-well tissue culture plates at 2.0×10^5 cells/well 3 days before drug treatment. The cells were treated with vehicle (0.1% DMSO), rifampicin (20 μ M), or clotrimazole (20 μ M). Total RNA was extracted and the *MRP3* mRNA levels were determined. The mRNA levels were normalized to those of GAPDH. The relative LDH activity and mRNA levels in HepG2 cells treated with vehicle were set to 1.0. The data represent means \pm S.E.M. ($n = 3$). * $P < 0.05$; ** $P < 0.01$; *** $P < 0.001$, significantly different from the activity and mRNA levels of the vehicle-treated cells based on the Welch t test or one-way analysis of variance with the Dunnett post hoc test. CLO, clotrimazole; RIF, rifampicin; TRO, troglitazone.

suggest that transcriptional activation of *MRP3* and *CYP3A4* by clotrimazole might be regulated via different pathways.

To identify the clotrimazole-responsive element, we conducted reporter assays with various plasmids lacking portions of the *MRP3* 5'-flanking region. The responsive element was located between the -7.1 and -6.8 kb region, far upstream from the transcription start site of *MRP3* (Fig. 2). Furthermore, we confirmed that the clotrimazole-responsive element including half-site-like sequences were present between -6831 and -6810 bp (Fig. 3). However, our results showed that the activation of PXR by clotrimazole was less effective on the transcriptional activation of *MRP3* (Fig. 4). Several studies have demonstrated that *Mrp3* mRNA expression was increased in wild-type and PXR knockout mice upon cholestasis induced by α -naphthyl isothiocyanate or cholic acid (Teng and Piquette-Miller, 2007; Cui et al., 2009), suggesting that PXR-independent pathways are involved in the induction of *Mrp3* expression.

Azole antifungal agents have been reported to induce hepatotoxicity in patients (Somchit et al., 2009; Kao et al., 2014). We confirmed that clotrimazole caused significant cytotoxicity in HepG2 cells (Fig. 5A). Furthermore, we demonstrated that intrinsic *MRP3* mRNA levels increased in HepG2 cells treated with clotrimazole or troglitazone, two drugs that are known to induce hepatotoxicity (8.7- and 5.9-fold, respectively) (Fig. 5, B and C). These results suggest that the enhancement of *MRP3* mRNA expression by clotrimazole in HepG2 cells is associated with drug-induced hepatotoxicity. MAPKs are activated under hepatotoxicity caused by drug treatment and inflammatory diseases, including cholestasis (Hanawa et al., 2008; Boaglio et al., 2012). We therefore investigated whether MAPK activation was involved in the transactivation of *MRP3* by clotrimazole. In our study, the p38 MAPK inhibitor and p38 MAPK knockdown suppressed the *MRP3* mRNA expression induced by clotrimazole, whereas

the JNK or extracellular signal-regulated kinase inhibitor showed no effect on *MRP3* mRNA expression levels (Fig. 6, A and D). We also found that anisomycin, a p38 MAPK activator, significantly increased *MRP3* mRNA levels (Fig. 6B). Furthermore, phosphorylated p38 MAPK was detected in HepG2 cells treated with clotrimazole but not with rifampicin (Fig. 6C). These results suggest that the p38 MAPK pathway is involved in clotrimazole-induced *MRP3* expression.

MRP3 expression is reported to be markedly upregulated in a rat model of bile duct ligation and in human cholestatic liver disease (Soroka et al., 2001; Schaap et al., 2009). LDH release from the liver is observed in cholestatic conditions. Furthermore, the expression levels of tumor necrosis factor α (TNF α) and fibroblast growth factor 19 are significantly elevated (Bohan et al., 2003; Schaap et al., 2009). TNF α induces the activation of stress-activated protein kinase, JNK, and p38 MAPK (Wajant et al., 2003). Chai et al. (2012) reported that *MRP3* mRNA levels in liver are significantly correlated with plasma TNF α levels in patients with obstructive cholestasis and that the induction involves activated JNK. These results suggest that MAPKs are involved in inducing *MRP3* expression in liver injury.

A novel link between nuclear receptors, such as PXR and CAR, and the p38 MAPK pathway was recently demonstrated (Kodama and Negishi, 2011; Saito et al., 2013). In addition, another study reported that PXR has anti-inflammation functions via suppression of signal transduction pathways (Sun et al., 2015). Although we did not observe the binding of PXR to the clotrimazole-responsive element, the increase in clotrimazole-induced *MRP3* reporter activity was suppressed by PXR overexpression (Fig. 4). These findings suggest that PXR might suppress clotrimazole-induced cytotoxicity, resulting in the suppression of *MRP3* reporter activity induced by clotrimazole. In addition, it has been reported that activated

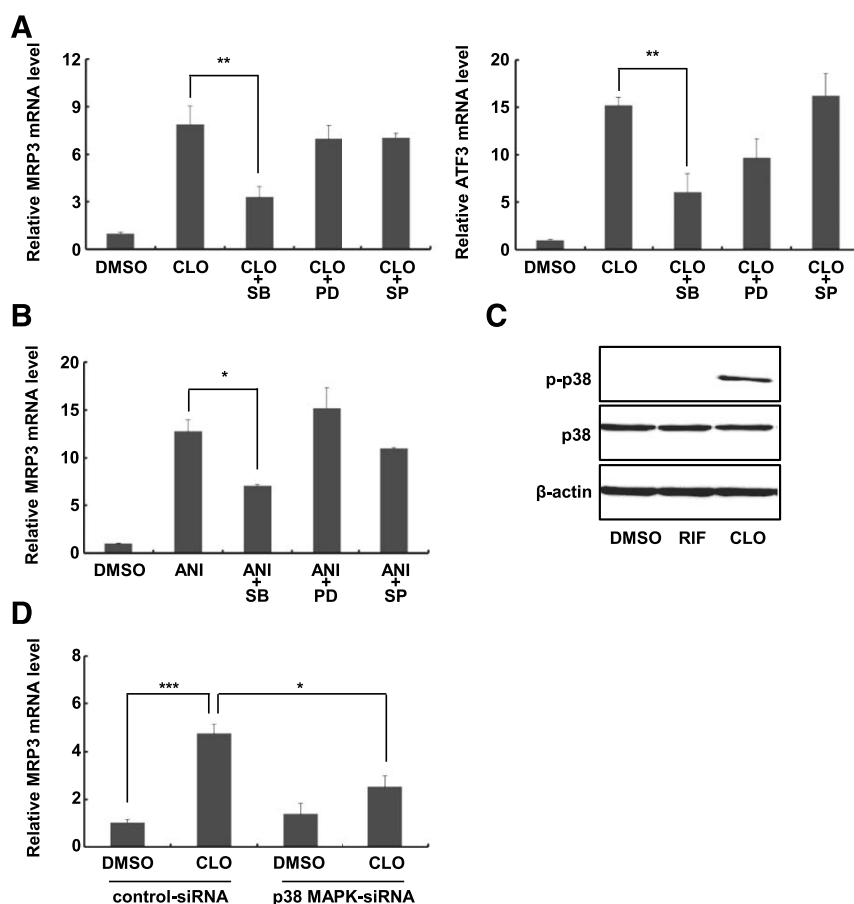


Fig. 6. Effects of MAPK inhibitors on clotrimazole-induced *MRP3* mRNA expression in HepG2 cells. HepG2 cells were seeded in 24-well tissue culture plates at 1.0×10^5 cells/well 1 day before drug treatment. The cells were pretreated with or without MAPK inhibitors ($5 \mu\text{M}$) for 1 hour. (A) The cells were treated with vehicle (0.1% DMSO) or clotrimazole ($20 \mu\text{M}$) for 72 hours and the *MRP3* and *ATF3* mRNA levels were determined. (B) The cells were treated with anisomycin ($1 \mu\text{M}$) for 12 hours and the *MRP3* mRNA levels were determined. (C) Whole cell lysates were subjected to immunoblot analyses with an antibody for phospho-p38 MAPK, p38 MAPK, or β -actin. (D) HepG2 cells were transfected with control or p38 MAPK small interfering RNA. The cells were treated with vehicle (0.1% DMSO) or clotrimazole ($20 \mu\text{M}$) for 72 hours and the *MRP3* mRNA levels were determined. The mRNA levels were normalized to those of GAPDH. The relative mRNA levels in HepG2 cells treated with vehicle were set to 1.0. The data represent means \pm S.E.M. ($n = 3$). * $P < 0.05$; ** $P < 0.01$; *** $P < 0.001$, significantly different from the expression levels of the corresponding clotrimazole-treated cells based on one-way analysis of variance with the Dunnett or Bonferroni post hoc test. ANI, anisomycin; CLO, clotrimazole; PD, PD98059; RIF, rifampicin; SB, SB203580; siRNA, small interfering RNA; SP, SP600125.

Nrf2, known as a cellular sensor for oxidative stress, binds to the regulatory region of *Mrp3* and activates gene expression (Maher et al., 2007). Further studies are required to reveal whether Nrf2 is activated by clotrimazole treatment.

In conclusion, we identified a novel clotrimazole-response element, located at -6.8 kb upstream from the transcription start site of *MRP3*, and we found that there are differences in the transactivation mechanism by clotrimazole between *MRP3* and *CYP3A4*. Furthermore, our results suggest that the transcriptional activation of *MRP3* via the clotrimazole-responsive element involves the p38 MAPK pathway.

Authorship Contributions

Participated in research design: Sasaki, Toriyabe, Yamazoe, Yoshinari, Nagata.

Conducted experiments: Sasaki, Inami, Numata, Funakoshi, Yoshida, Kanno, Matsui, Toriyabe.

Contributed new reagents or analytic tools: Sasaki, Toriyabe, Nagata.

Performed data analysis: Sasaki, Kumagai, Toriyabe.

Wrote or contributed to the writing of the manuscript: Sasaki, Inami, Yoshinari, Nagata.

References

- Bachour-El Azzi P, Sharanek A, Burban A, Li R, Guével RL, Abdel-Razzak Z, Stieger B, Guguen-Guillouzo C, and Guillouzo A (2015) Comparative localization and functional activity of the main hepatobiliary transporters in HepaRG cells and primary human hepatocytes. *Toxicol Sci* **145**:157–168.
- Boaglio AC, Zucchetti AE, Toledo FD, Barosso IR, Sánchez Pozzi EJ, Crocenzi FA, and Roma MG (2012) ERK1/2 and p38 MAPKs are complementarily involved in estradiol 17 β -D-glucuronide-induced cholestasis: crosstalk with cPKC and PI3K. *PLoS One* **7**:e49255.

- Bodo A, Bakos E, Szeri F, Varadi A, and Sarkadi B (2003) Differential modulation of the human liver conjugate transporters MRP2 and MRP3 by bile acids and organic anions. *J Biol Chem* **278**:23529–23537.
- Bohan A, Chen WS, Denson LA, Held MA, and Boyer JL (2003) Tumor necrosis factor alpha-dependent up-regulation of Lrh-1 and Mrp3(Abcc3) reduces liver injury in obstructive cholestasis. *J Biol Chem* **278**:36688–36698.
- Borst P, de Wolf C, and van de Wetering K (2007) Multidrug resistance-associated proteins 3, 4, and 5. *Pflugers Arch* **453**:661–673.
- Borst P and Elferink RO (2002) Mammalian ABC transporters in health and disease. *Annu Rev Biochem* **71**:537–592.
- Borst P, Zelcer N, and van de Wetering K (2006) MRP2 and 3 in health and disease. *Cancer Lett* **234**:51–61.
- Chai J, He Y, Cai SY, Jiang Z, Wang H, Li Q, Chen L, Peng Z, He X, Wu X, et al. (2012) Elevated hepatic multidrug resistance-associated protein 3/ATP-binding cassette subfamily C 3 expression in human obstructive cholestasis is mediated through tumor necrosis factor alpha and c-Jun NH2-terminal kinase/stress-activated protein kinase-signaling pathway. *Hepatology* **55**:1485–1494.
- Cherrington NJ, Slitt AL, Maher JM, Zhang XX, Zhang J, Huang W, Wan YJ, Moore DD, and Klaassen CD (2003) Induction of multidrug resistance protein 3 (MRP3) in vivo is independent of constitutive androstane receptor. *Drug Metab Dispos* **31**:1315–1319.
- Cui YJ, Aleksunes LM, Tanaka Y, Goedken MJ, and Klaassen CD (2009) Compensatory induction of liver efflux transporters in response to ANIT-induced liver injury is impaired in FXR-null mice. *Toxicol Sci* **110**:47–60.
- García Rodríguez LA, Duque A, Castellsague J, Pérez-Gutthann S, and Stricker BH (1999) A cohort study on the risk of acute liver injury among users of ketoconazole and other antifungal drugs. *Br J Clin Pharmacol* **48**:847–852.
- Girois SB, Chapuis F, Decullier E, and Revol BG (2005) Adverse effects of antifungal therapies in invasive fungal infections: review and meta-analysis. *Eur J Clin Microbiol Infect Dis* **24**:119–130.
- Hanawa N, Shinohara M, Saberi B, Gaarde WA, Han D, and Kaplowitz N (2008) Role of JNK translocation to mitochondria leading to inhibition of mitochondria bioenergetics in acetaminophen-induced liver injury. *J Biol Chem* **283**:13565–13577.
- Herbomel P, Bourachot B, and Yaniv M (1984) Two distinct enhancers with different cell specificities coexist in the regulatory region of polyoma. *Cell* **39**:653–662.
- Hitzl M, Klein K, Zanger UM, Fritz P, Nüssler AK, Neuhaus P, and Fromm MF (2003) Influence of omeprazole on multidrug resistance protein 3 expression in human liver. *J Pharmacol Exp Ther* **304**:524–530.
- Kao WY, Su CW, Huang YS, Chou YC, Chen YC, Chung WH, Hou MC, Lin HC, Lee FY, and Wu JC (2014) Risk of oral antifungal agent-induced liver injury in Taiwanese. *Br J Clin Pharmacol* **77**:180–189.

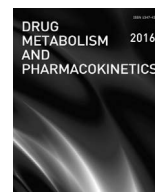
- Kodama S and Negishi M (2011) Pregnane X receptor PXR activates the GADD45beta gene, eliciting the p38 MAPK signal and cell migration. *J Biol Chem* **286**:3570–3578.
- König J, Rost D, Cui Y, and Keppler D (1999) Characterization of the human multidrug resistance protein isoform MRP3 localized to the basolateral hepatocyte membrane. *Hepatology* **29**:1156–1163.
- Kuroda M, Kobayashi Y, Tanaka Y, Itani T, Mifuji R, Araki J, Kaito M, and Adachi Y (2004) Increased hepatic and renal expressions of multidrug resistance-associated protein 3 in Eisai hyperbilirubinuria rats. *J Gastroenterol Hepatol* **19**:146–153.
- Lu D, Chen J, and Hai T (2007) The regulation of ATF3 gene expression by mitogen-activated protein kinases. *Biochem J* **401**:559–567.
- Maher JM, Cheng X, Slitt AL, Dieter MZ, and Klaassen CD (2005) Induction of the multidrug resistance-associated protein family of transporters by chemical activators of receptor-mediated pathways in mouse liver. *Drug Metab Dispos* **33**:956–962.
- Maher JM, Dieter MZ, Aleksunes LM, Slitt AL, Guo G, Tanaka Y, Scheffer GL, Chan JY, Manautou JE, Chen Y, et al. (2007) Oxidative and electrophilic stress induces multidrug resistance-associated protein transporters via the nuclear factor-E2-related factor-2 transcriptional pathway. *Hepatology* **46**:1597–1610.
- Nies AT and Keppler D (2007) The apical conjugate efflux pump ABCC2 (MRP2). *Pflügers Arch* **453**:643–659.
- Saito K, Moore R, and Negishi M (2013) p38 Mitogen-activated protein kinase regulates nuclear receptor CAR that activates the CYP2B6 gene. *Drug Metab Dispos* **41**:1170–1173.
- Schaap FG, van der Gaag NA, Gouma DJ, and Jansen PL (2009) High expression of the bile salt-homeostatic hormone fibroblast growth factor 19 in the liver of patients with extrahepatic cholestasis. *Hepatology* **49**:1228–1235.
- Somchit N, Ngee CS, Yaakob A, Ahmad Z, and Zakaria ZA (2009) Effects of cytochrome p450 inhibitors on itraconazole and fluconazole induced cytotoxicity in hepatocytes. *J Toxicol* **2009**:912320.
- Soroka CJ, Lee JM, Azzaroli F, and Boyer JL (2001) Cellular localization and up-regulation of multidrug resistance-associated protein 3 in hepatocytes and cholangiocytes during obstructive cholestasis in rat liver. *Hepatology* **33**:783–791.
- Stöckel B, König J, Nies AT, Cui Y, Brom M, and Keppler D (2000) Characterization of the 5'-flanking region of the human multidrug resistance protein 2 (MRP2) gene and its regulation in comparison with the multidrug resistance protein 3 (MRP3) gene. *Eur J Biochem* **267**:1347–1358.
- Sun M, Cui W, Woody SK, and Staudinger JL (2015) Pregnane X receptor modulates the inflammatory response in primary cultures of hepatocytes. *Drug Metab Dispos* **43**:335–343.
- Takada T, Ogino M, Miyata M, Shimada M, Nagata K, and Yamazoe Y (2004) Differences in transactivation between rat CYP3A1 and human CYP3A4 genes by human pregnane X receptor. *Drug Metab Pharmacokinet* **19**:103–113.
- Takada T, Suzuki H, and Sugiyama Y (2000) Characterization of 5'-flanking region of human MRP3. *Biochem Biophys Res Commun* **270**:728–732.
- Teng S, Jekerle V, and Piquette-Miller M (2003) Induction of ABCC3 (MRP3) by pregnane X receptor activators. *Drug Metab Dispos* **31**:1296–1299.
- Teng S and Piquette-Miller M (2007) Hepatoprotective role of PXR activation and MRP3 in cholic acid-induced cholestasis. *Br J Pharmacol* **151**:367–376.
- Toriyabe T, Nagata K, Takada T, Aratsu Y, Matsubara T, Yoshinari K, and Yamazoe Y (2009) Unveiling a new essential cis element for the transactivation of the CYP3A4 gene by xenobiotics. *Mol Pharmacol* **75**:677–684.
- Wagner M, Fickert P, Zollner G, Fuchsbichler A, Silbert D, Tsybrovskyy O, Zatloukal K, Guo GL, Schuetz JD, Gonzalez FJ, et al. (2003) Role of farnesoid X receptor in determining hepatic ABC transporter expression and liver injury in bile duct-ligated mice. *Gastroenterology* **125**:825–838.
- Wajant H, Pfizenmaier K, and Scheurich P (2003) Tumor necrosis factor signaling. *Cell Death Differ* **10**:45–65.

Address correspondence to: Kiyoshi Nagata, Department of Environmental and Health Science, Faculty of Pharmaceutical Sciences, Tohoku Medical and Pharmaceutical University, 4-4-1, Komatsushima, Aoba-ku, Sendai 981-8558, Japan. E-mail: nagataki@tohoku-mpu.ac.jp



Contents lists available at ScienceDirect

Drug Metabolism and Pharmacokinetics

journal homepage: <http://www.journals.elsevier.com/drug-metabolism-and-pharmacokinetics>

Regular article

Indirubin, a component of Ban-Lan-Gen, activates CYP3A4 gene transcription through the human pregnane X receptor

Takeshi Kumagai^{a,*}, Yusuke Aratsu^{a,b}, Ryosuke Sugawara^a, Takamitsu Sasaki^{a,c}, Shinichi Miyairi^d, Kiyoshi Nagata^a^a Department of Environmental Health Science, Tohoku Pharmaceutical University, 4-4-1 Komatsushima, Aoba-ku, Sendai, Miyagi 981-8558, Japan^b Drug Metabolism and Pharmacokinetics Research Laboratories, Central Pharmaceutical Research Institute, Japan Tobacco Inc., 1-1 Murasaki-cho, Takatsuki, Osaka 569-1125, Japan^c Department of Molecular Toxicology, School of Pharmaceutical Sciences, University of Shizuoka, 52-1 Yada, Suruga-ku, Shizuoka 422-8526, Japan^d Laboratory of Organic Chemistry, School of Pharmacy, Nihon University, 7-7-1 Narashino, Funabashi, Chiba 274-8555, Japan

ARTICLE INFO

Article history:

Received 22 October 2015

Received in revised form

14 January 2016

Accepted 14 January 2016

Available online 22 January 2016

Keywords:

AhR activator

Indirubin

CYP3A4 induction

PXR

Herb–drug interactions

ABSTRACT

Ban-Lan-Gen is the common name for the dried roots of indigo plants, including *Polygonum tinctorium*, *Isatis indigotica*, *Isatis tinctoria*, and *Strobilanthes cusia*. Ban-Lan-Gen is frequently used as an anti-inflammatory and an anti-viral for the treatment of hepatitis, influenza, and various types of inflammation. One of the cytochrome P450 (CYP) enzymes, CYP3A4, is responsible for the metabolism of a wide variety of xenobiotics, including an estimated 60% of all clinically used drugs. In this study, we investigated the effect of Ban-Lan-Gen on the transcriptional activation of the CYP3A4 gene. Ban-Lan-Gen extract increased CYP3A4 gene reporter activity in a dose-dependent manner. Indirubin, one of the biologically active ingredients in the Ban-Lan-Gen, also dose-dependently increased CYP3A4 gene reporter activity. Expression of short hairpin RNA for the human pregnane X receptor (hPXR-shRNA) inhibited CYP3A4 gene reporter activity, and overexpression of human PXR increased indirubin- and rifampicin-induced CYP3A4 gene reporter activity. Furthermore, indirubin induced CYP3A4 mRNA expression in HepG2 cells. Taken together, these results indicate that indirubin, a component of Ban-Lan-Gen, activated CYP3A4 gene transcription through the activation of the human PXR.

Copyright © 2016, Published by Elsevier Ltd on behalf of The Japanese Society for the Study of Xenobiotics.

1. Introduction

Chinese herbal medicines are an integral part of health care in Asia, and many herbal medicines are extensively used as alternative and/or complementary therapies. However, the clinical efficacy, mechanisms of action, and safety profiles of most herbal medicines are not well characterized. Moreover, herbal medicines are often

co-administered with therapeutic drugs, creating the potential for herb–drug interactions [1,2]. While the underlying mechanism of most herb–drug interactions is not known, induction and inhibition of drug-metabolizing enzymes or drug transporters have been implicated as potential mechanisms.

Ban-Lan-Gen is the common name for the dried roots of indigo plants, including *Polygonum tinctorium*, *Isatis indigotica*, *Isatis tinctoria*, and *Strobilanthes cusia*. Indigo plants have been an important source of dyes in Asia since ancient times, and today, they are commonly used as therapeutics in traditional Chinese medicine. Ban-Lan-Gen is frequently used as an anti-inflammatory and anti-viral for the treatment of hepatitis, influenza, and various kinds of inflammation [3,4]. Several biologically active ingredients have been identified in Ban-Lan-Gen, including indigoid alkaloids (e.g., indigo and indirubin) and quinazolinone alkaloids (e.g., tryptanthrin) [5]. In fact, indigo, indirubin, and tryptanthrin are three marker compounds found in Ban-Lan-Gen [6]. Among these marker compounds, it has been reported that indirubin causes trans-activation of cytochrome P450 1A1 (CYP1A1) and CYP1A2 genes via

Abbreviations: AdCont, β -galactosidase-expressing adenovirus; AdPXR, human PXR-expressing adenovirus; AdhPXR-shRNA, AdhPXR-short hairpin RNA; AhR, aryl hydrocarbon receptor; Ct, threshold PCR cycle; CAR, constitutive androstane receptor; CYP, cytochrome P450; DMEM, Dulbecco's modified Eagle's medium; dNR1, distal nuclear receptor-binding protein 1; DMSO, dimethyl sulfoxide; D-PBS, Dulbecco's phosphate buffered saline; DR3, direct repeats spaced by 3 bases; eNR3A4, essential distal nuclear receptor-binding element; ER6, everted repeats separated by 6 bases; GAPDH, glyceraldehyde-3-phosphate dehydrogenase; GBE, *Ginkgo biloba* extract; GR α , glucocorticoid receptor- α ; MOI, multiplicity of infection; PAHs, polycyclic aromatic hydrocarbons; prER6, ER6 in the CYP3A4 proximal promoter; PXR, pregnane X receptor; RXR α , retinoid X receptor α ; SJW, St. John's wort; TCID₅₀, 50% titer culture infectious dose; VDR, vitamin D receptor.

* Corresponding author.

E-mail address: ta-kuma@tohoku-pharm.ac.jp (T. Kumagai).

<http://dx.doi.org/10.1016/j.dmpk.2016.01.002>

1347-4367/Copyright © 2016, Published by Elsevier Ltd on behalf of The Japanese Society for the Study of Xenobiotics.

the aryl hydrocarbon receptor (AhR) [7]. In addition, a content of indirubin have been reported in the roots of *I. indigotica* as main raw materials of Ban-Lan-Gen (0.224–34.4 µg/g) [5,6].

Members of the CYP supergene family of monooxygenases play an important role in detoxification by converting pollutants, plant toxins, carcinogens, and drugs to products that are then excreted in to urine or bile [8,9]. Human CYP3A4 is of particular significance in this respect, because it is involved in the metabolism of approximately two-thirds of clinically relevant drugs [10]. A number of compounds, including pesticides, herbal supplements, vitamins, and drugs, activate CYP3A4 gene transcription both in the liver and in the small intestine [11,12]. This induction process is the molecular basis for a number of important drug interactions that occur in patients taking multiple medications.

The pregnane X receptor (PXR; NR1I2) is the principal regulator of CYP3A4 gene expression and binds as a heterodimer with retinoid X receptor α (RXR α) to regulatory DNA sequences. These sequences include: (1) AG(G/T)TCA-like direct repeats spaced by 3 bases (DR3) located –8 kb upstream from the transcription start point and identified as distal nuclear receptor-binding element 1 (dNR1), and (2) everted repeats separated by 6 bases (ER6) located in the CYP3A4 proximal promoter (prER6) [13]. Recently, Toriyabe et al. identified a distinct PXR response element as an essential distal nuclear receptor-binding element (eNR3A4) for CYP3A4 gene induction [14]. PXR is activated by a number of structurally and chemically diverse ligands, such as drugs [rifampicin (RIF), clotrimazole] [15], pesticides (pyributicarb, endosulfan) [16,17], natural and synthetic steroids (dexamethasone) [15], bile acids (lithocholic acid) [18], and herbal medicines (St. John's wort [SJW], *Ginkgo biloba*, and *Sophora flavescens*) [19–21]. CYP3A4 induction by these PXR activators leads to accelerated metabolism of the activators themselves and concomitantly-administered drugs that are metabolized by CYP3A4.

Induction and inhibition of CYP3A4 by Ban-Lan-Gen are not fully understood. In this study, we investigated the effect of Ban-Lan-Gen on transcriptional activation of the CYP3A4 gene.

2. Materials and methods

2.1. Materials

Ban-Lan-Gen (lot. 9115476) was purchased from Beijing Tong Ren Group Co., Ltd. (Beijing, China). SJW was purchased from ChromaDex (Irvine, CA). Indirubin and tryptanthrin were purchased from Enzo Life Sciences, Inc. (Farmingdale, NY). Indican, isatin, and indigo were purchased from Tokyo Chemical Industry Co., Ltd. (Tokyo, Japan). *Ginkgo biloba* extract (GBE) was purchased from Tama Biochemicals Co., Ltd (Tokyo, Japan). RIF was purchased from Sigma–Aldrich (St. Louis, MO). The chemicals used for this study were dissolved in dimethyl sulfoxide (DMSO). Ban-Lan-Gen, SJW, and GBE were extracted with culture medium used for the cell culture in this study, for 2 h at 37 °C. These extract solutions were centrifuged at 2,000 × g for 15 min at 4 °C and the supernatants were used for this study. All other reagents used were of the highest quality available. Dulbecco's modified Eagle's medium (DMEM) and fetal bovine serum were obtained from Wako Pure Chemical Industries, Ltd. (Osaka, Japan) and Hyclone Laboratories (Logan, UT), respectively. MEM non-essential amino acids and antibiotic-antimycotic were purchased from Invitrogen (Paisley, UK).

2.2. Cell culture

HepG2 cells were obtained from RIKEN cell bank (Tsukuba, Japan). The HepG2-derived cell line stably expressing the CYP3A4-

luciferase reporter gene, clone 3-1-20, was maintained as reported previously [22]. Cells were cultured in DMEM supplemented with 10% fetal bovine serum, MEM non-essential amino acids, and antibiotic-antimycotic. The cells were seeded at 3×10^4 cells per well onto 48-well tissue culture plate (BD Biosciences, Heidelberg, Germany) for luciferase gene reporter assay, and 5×10^4 cells per well onto 24-well tissue culture plate (BD Biosciences) for real-time polymerase chain reaction (PCR). After 24 h, the cell medium was changed with the extract solutions or various subjects dissolved in DMSO (final concentration, 0.1%) and cultured for 48 h.

2.3. Luciferase gene reporter assay

3-1-20 cells were washed with Dulbecco's phosphate buffered saline (D-PBS) and suspended in passive lysis buffer (Promega, Madison, WI) in a microcentrifuge tube. The cell suspension was centrifuged at 12,000 × g for 5 min at 4 °C, and the cell extract was used for the luciferase assay. The luciferase assay was performed using the Luciferase Assay System and a GloMax™ 96 Microplate Luminometer (Promega) according to the manufacturer's instructions. The resulting data are presented as the ratio of luminescence of treated cell samples to that of control. The luminescence of each sample was normalized by its protein concentration as determined with the Protein Assay Kit (Bio-Rad Laboratories, Hercules, CA).

2.4. Reporter gene constructs and transient transfection

The luciferase reporter plasmids, pGL3-Basic and pGL4.70, were purchased from Promega. Preparation of the CYP3A4 luciferase reporter gene constructs, including pCYP3A4-362-7.7k, pCYP3A4-362-7.7km, pCYP3A4-362m-7.7k, pCYP3A4-362m-7.7km, and pCYP3A4-362-7.7km $\Delta\alpha$, was described previously [14]. One day before transfection, cells were seeded in 48-well plates. Each reporter plasmid and pGL4.70 was transfected using Targefect F-1 (Targeting System, El Cajon, CA) according to the manufacturer's protocol. pGL4.70 was used for the normalization of transfection efficiency. After transfection, cells were cultured in medium in the presence of various chemicals for 48 h. Control cells were cultured with vehicle (0.1% DMSO) alone. Subsequently, the cells were harvested and suspended in passive lysis buffer (Promega). Luciferase activities were determined with Dual-Luciferase® Reporter Assay System (Promega).

2.5. Construction of recombinant adenovirus and infection

Construction of the human PXR-expressing adenovirus (AdhPXR) and AdhPXR-short hairpin RNA (AdhPXR-shRNA) was described previously [17]. Control adenovirus, a β -galactosidase-expressing adenovirus (AdCont; AxCALacZ), was provided by Dr. Izumi Saito (Tokyo University, Japan) [23]. The titer of the adenoviruses, 50% titer culture infectious dose (TCID₅₀), was determined as reported previously [17]. Multiplicity of infection (MOI) was calculated by dividing the TCID₅₀ by the number of cells. One day before transfection, cells were seeded in 24-well plates. Adenovirus infection was carried out as described previously [24].

2.6. Isolation of RNA and analysis of quantitative real-time polymerase chain reaction

Total RNA was isolated from HepG2 cells using TRI Reagent (Molecular Research Center, Inc., Montgomery, AL) according to the manufacturer's protocol. cDNA was prepared from 2.0 µg of total RNA with Moloney murine leukemia virus (MMLV) reverse transcriptase (Promega) using oligo(dT)₂₀ primer (Greiner Japan, Japan)

and porcine RNase inhibitor (TaKaRa Bio, Japan). Quantitative real-time PCR was performed using Permixon Ex Taq (Perfect Real Time, TaKaRa Bio) in a Thermal Cycler Dice Real Time System (TaKaRa Bio). All samples were quantified using a comparative threshold PCR cycle (Ct) method for relative quantification of gene expression, normalized to that of glyceraldehyde-3-phosphate dehydrogenase (GAPDH). The sequences of the primers used are shown in Table 1.

2.7. Statistical analysis

Data are presented as mean \pm standard deviation (S.D.) and were evaluated by paired Student's *t*-test. A *P* value < 0.05 was considered to be significant.

3. Results

3.1. Ban-Lan-Gen increases CYP3A4 gene reporter activity

The effects of Ban-Lan-Gen, SJW, and GBE on CYP3A4 gene reporter activity were confirmed in HepG2-derived cells stably expressing the CYP3A4 gene reporter (3-1-20 cells) as reported previously [22]. SJW and GBE served as positive controls for CYP3A4 induction. Similar to SJW and GBE, Ban-Lan-Gen extract increased CYP3A4 gene reporter activity, increasing luminescence 11-fold over control levels (Fig. 1). Furthermore, Ban-Lan-Gen extract increased CYP3A4 gene reporter activity in a dose-dependent manner (Fig. 2).

3.2. Indirubin, a component of Ban-Lan-Gen, activates CYP3A4 gene transcription

We next examined the effect of components of Ban-Lan-Gen on CYP3A4 gene reporter activity. RIF was used as a positive control. 3-1-20 cells were treated with RIF (5 μ M) or various Ban-Lan-Gen components (5 μ M), such as indirubin, indigo, isatin, indicant, and tryptanthrin, for 48 h. The CYP3A4 gene reporter activity was significantly elevated in response to indirubin, and the induction level reached the same level as that of RIF (Fig. 3). Indirubin increased reporter activity in a dose-dependent manner (Fig. 4). We further investigated the effect of indirubin on intrinsic CYP3A4 mRNA expression in HepG2 cells. In these cells, indirubin increased CYP3A4 mRNA expression to a similar magnitude as that observed with RIF (Fig. 5). Previous studies reported that indirubin is a prototypical AhR ligand [25]. In this study, indirubin also resulted in an increase in CYP1A1 mRNA expression. Furthermore, we investigated the effect of indirubin on CYP3A4 mRNA expression in human hepatocyte. When human cryopreserved hepatocyte was incubated with 5 μ M of RIF and indirubin, CYP3A4 mRNA expression was increased 6.3-fold by RIF compared with untreated cells, but not by indirubin (data not shown).

Table 1
Sequences of the oligonucleotide primers used for PCR amplification.

	Primer sequence
Human CYP3A4	
Sense	5'-CTGTGTGTTCCAAGAGAAGTTAC-3'
Antisense	5'-TGCATCAATTTCTCTGCAG-3'
Human CYP1A1	
Sense	5'-CATCCCCACAGCACAACA-3'
Antisense	5'-CAGGGGTGAGAAACCGTTCA-3'
Human GAPDH	
Sense	5'-CATGGGTGTGAACCATGAGAA-3'
Antisense	5'-GGTCATGAGTCTTCCACGAT-3'

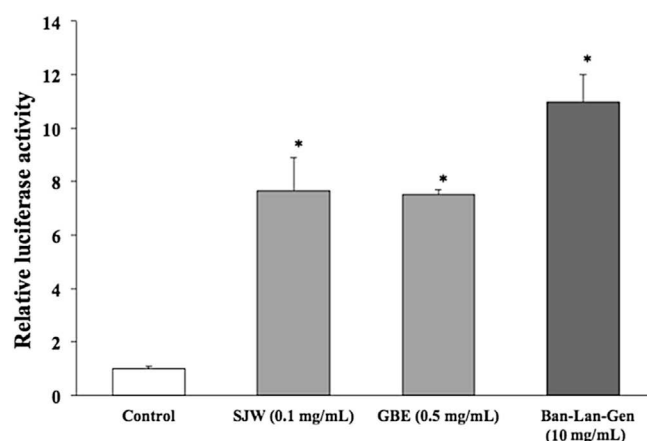


Fig. 1. Effects of SJW, GBE, and Ban-Lan-Gen on CYP3A4 gene reporter activity in 3-1-20 cells. Clone 3-1-20 was seeded at 3×10^4 cells in 24-well tissue culture plates with 0.3 mL of DMEM, 24 h before SJW, GBE, and Ban-Lan-Gen extract treatment. The cells were treated with SJW (0.1 mg/mL), GBE (0.5 mg/mL), and Ban-Lan-Gen extract (10 mg/mL) for 48 h, and the reporter activity was measured by luciferase assay. Reporter activities are expressed as fold increase compared with that in the vehicle-treated cells. Results represent the mean \pm S.D. of three separate experiments. **P* < 0.005, difference from the vehicle-treated cells.

3.3. Transcriptional activation of CYP3A4 reporter genes by indirubin

To elucidate the molecular mechanism of CYP3A4 gene transcriptional activation by indirubin, we performed transient transfection assays with reporter gene constructs containing mutations in the hPXR binding elements. As shown in Fig. 6, treatment of HepG2 cells with 5 μ M indirubin or RIF resulted in an increase in luciferase activity (18.1-fold and 32.9-fold, respectively) after transfection of pCYP3A4-362-7.7k, which included the CYP3A4 5'-flanking regions dNR1, eNR3A4, and prER6, all known to be highly involved in the transcriptional regulation of the CYP3A4 gene [14]. Mutation of either dNR1 (pCYP3A4-362-7.7km) or prER6 (pCYP3A4-362m-7.7k) of pCYP3A4-362-7.7k did not abolish the indirubin response completely (6.8- and 13.9-fold, respectively).

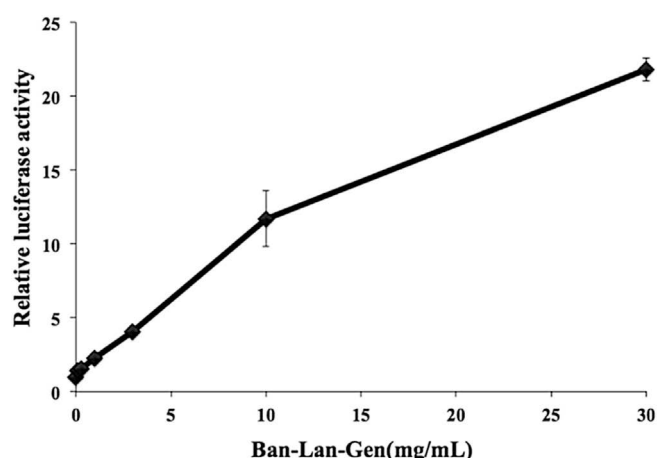


Fig. 2. Effect of various concentrations of Ban-Lan-Gen on the CYP3A4 gene reporter activity in 3-1-20 cells. Clone 3-1-20 was seeded at 3×10^4 cells in 24-well tissue culture plates with 0.3 mL of DMEM 24 h before Ban-Lan-Gen treatment. The cells were treated with 1–30 mg/mL Ban-Lan-Gen for 48 h, and the reporter activity was measured by luciferase assay. Reporter activities are expressed as fold increase compared with that in the vehicle-treated cells. Results represent the mean \pm S.D. of three separate experiments.

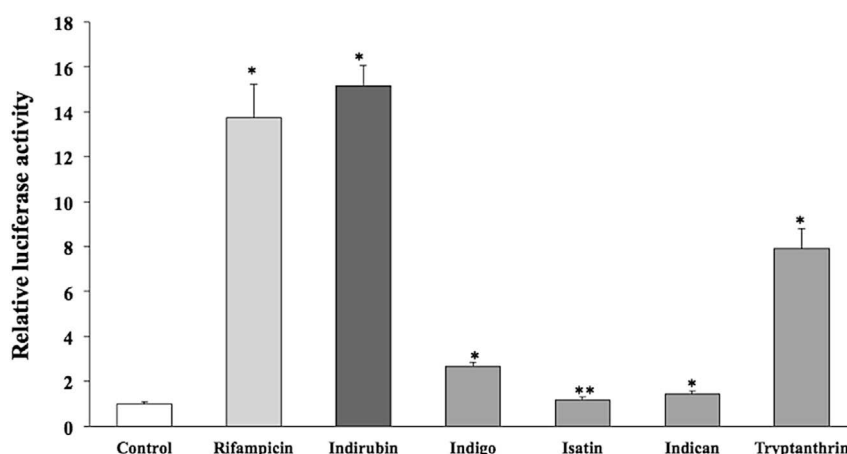


Fig. 3. Effect of various components of Ban-Lan-Gen on CYP3A4 gene reporter activity in 3-1-20 cells. Clone 3-1-20 was seeded at 3×10^4 cells in 48-well tissue culture plates with 0.3 mL DMEM, 24 h before Ban-Lan-Gen treatment. The cells were treated with each 5 μ M of indirubin, indigo, isatin, indicant, tryptanthrin, and RIF for 48 h, and the reporter activity was measured by luciferase assay. Reporter activities are expressed as fold increase compared with that in the vehicle-treated cells. Results represent the mean \pm S.D. of three separate experiments. * $P < 0.005$, ** $P < 0.05$, difference from the vehicle-treated cells.

However, the response was significantly decreased by the introduction of a mutation into the α half-site of eNR3A4 (pCYP3A4-362-7.7km $\Delta\alpha$) of pCYP3A4-362-7.7k (2.5-fold). RIF, in contrast, significantly decreased the response in cells transfected with the mutated pCYP3A4-362-7.7ks in dNR1, prER6, or eNR3A4 motifs (3.4-, 9.4- and 0.8-fold, respectively).

3.4. Indirubin increases CYP3A4 gene reporter activity through the PXR pathway

PXR is widely known as a major transcription factor mediating CYP3A4 induction. To clarify whether indirubin activates the CYP3A4 reporter gene via this pathway, we utilized knockdown of PXR using AdhPXR-shRNA and overexpression of PXR using AdhPXR (hPXR-expressing adenovirus). Indirubin-induced CYP3A4 gene reporter activities were significantly increased by the introduction of AdhPXR (Fig. 7). In addition, CYP3A4 gene reporter activation after treatment with indirubin, as well as RIF, was significantly decreased by the introduction of AdhPXR-shRNA in 3-1-20 cells (Fig. 8).

4. Discussion

Herbal medicines and supplements are used worldwide [26]. Because the safety and efficacy of herb–drug combinations are largely unknown, research on herb–drug interactions is urgently needed to guide the therapeutic use of herbs [27]. Metabolism-mediated herb–drug interactions are very common and can decrease the efficacy or increase the toxicity of the drug. Although various studies have described the actions of Ban-Lan-Gen [3,4], there are few reports on Ban-Lan-Gen–drug interactions.

In this study, we investigated the effect of Ban-Lan-Gen on transactivation of the CYP3A4 gene using 3-1-20 cells, which have a CYP3A4 reporter gene incorporated into their chromosomes. In general, there is a plurality of the extraction method of herbal medicine such as Ban-Lan-Gen. Thus, it is considered that the difference of the extraction method of Ban-Lan-Gen might be reflected on the CYP3A4 induction activity. However, to mimic extraction of components from herbal medicine and their absorption in human intestine, we used the extraction from the Ban-Lan-Gen product extracted with culture medium for CYP3A4 induction study. As a result, Ban-Lan-Gen extract dose-dependently activated

the CYP3A4 reporter gene (Figs. 1 and 2). These results indicate that Ban-Lan-Gen extract induces CYP3A4 gene expression. In addition, indirubin, a biological ingredient found in Ban-Lan-Gen, increased CYP3A4 gene reporter activity in a dose-dependent manner (Fig. 4) and increased CYP3A4 mRNA expression (Fig. 5). Although indirubin activated CYP3A4 gene transcription in HepG2 cells, it did not increase CYP3A4 mRNA expression in human hepatocytes. A major difference between these two cells types is cell proliferation. HepG2 cells grow without limitation, but human hepatocytes dose not. It is known that indirubin is a potent inhibitor of cyclin-dependent kinase 2 (CDK2), a modulator of cell cycle [28]. In addition, Sivertsson et al. reported that the CYP3A4 induction in confluent Huh 7 cells was regulated by the endogenous activation of PXR as a result of decreased CDK2 activity, which was linked to reduced cell proliferation in the confluent cell culture [29]. Therefore, the difference in CYP3A4 induction by indirubin between HepG2 cells and the human hepatocytes may be due to CDK2 activity. Further studies are needed to resolve this issue.

CYP3A4 induction by xenobiotics and hormones is mediated by the PXR [30–32], the constitutive androstane receptor (CAR, NR1I3) [33], the vitamin D receptor (VDR, NR1I1) [34], and the

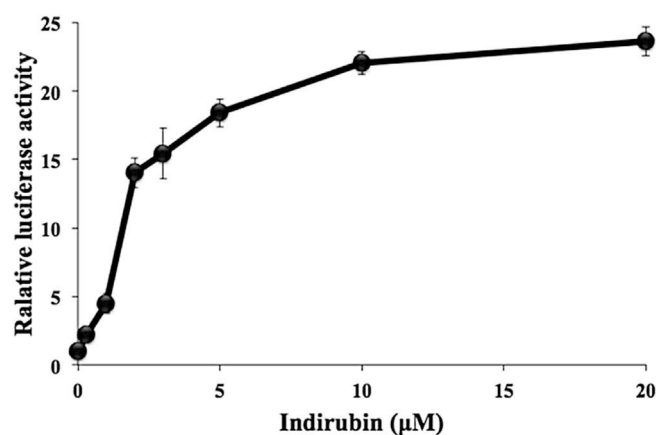


Fig. 4. Dose effect of indirubin on the CYP3A4 gene reporter activity in 3-1-20 cells. Clone 3-1-20 was seeded at 3×10^4 cells in 24-well tissue culture plates with 0.3 mL of DMEM 1 day before indirubin treatment. The cells were treated with 1–20 μ M indirubin for 48 h, and the reporter activity was measured by luciferase assay. Reporter activities are expressed as fold increase compared with that in the vehicle-treated cells. Results represent the mean \pm S.D. of three separate experiments.

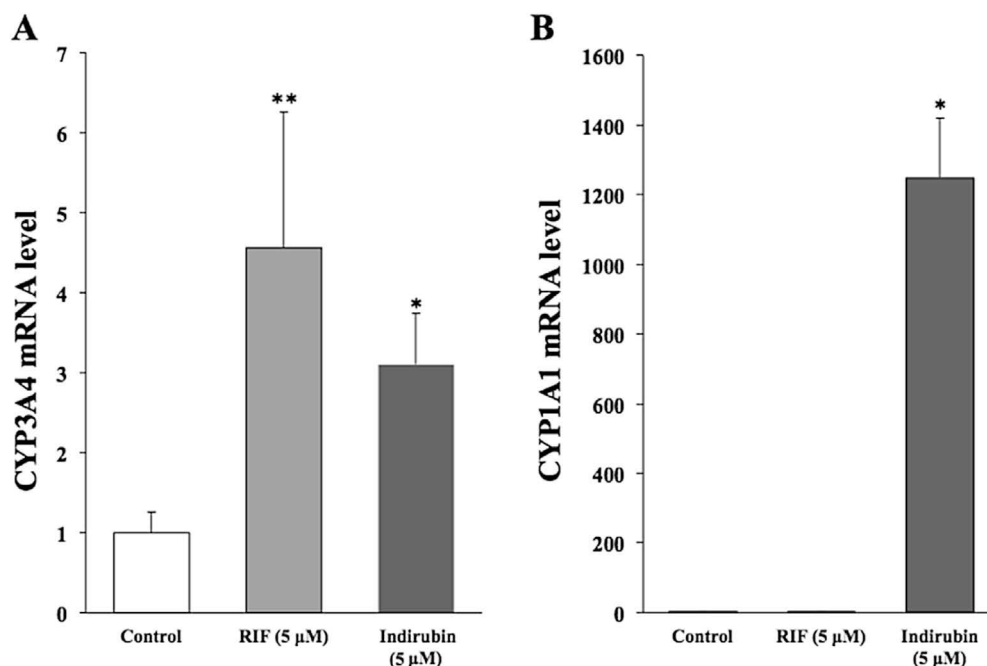


Fig. 5. Effect of indirubin on CYP mRNA expression in HepG2 cells. HepG2 cells were seeded at 5×10^4 cells in 24-well tissue culture plates with 0.5 mL DMEM, 24 h before RIF and indirubin treatment. The cells were treated with 5 μM RIF and 5 μM indirubin for 48 h and then assayed using quantitative polymerase chain reaction (qPCR). CYP3A4 mRNA or CYP1A1 mRNA expression was normalized by expression of GAPDH housekeeping gene and presented as fold increase compared with that of vehicle-treated cells. Results represent the mean \pm S.D. of three separate experiments. (A) CYP3A4 mRNA level, (B) CYP1A1 mRNA level. * $P < 0.005$, ** $P < 0.01$, difference from the vehicle-treated cells.

glucocorticoid receptor- α (GR α , NR3C1) [35] in the liver. Chemically-induced activation of the *CYP3A4* gene is mainly mediated by PXR binding to the *CYP3A4* 5'-flanking region [30,32,36]. Therefore, we knocked down hPXR expression using AdhPXR-shRNA. When AdhPXR-shRNA was introduced into the 3-1-20 cells, the activation of the *CYP3A4* reporter gene by indirubin, as well as by RIF, was significantly decreased (Fig. 8). Furthermore, the overexpression of PXR using AdhPXR increased CYP3A4 reporter activity by indirubin in an infection dose-dependent manner (Fig. 7). These results strongly suggest that indirubin enhanced the transactivation of the *CYP3A4* gene through PXR activation.

Since indirubin is a natural AhR ligand isolated from human urine [7], it is possible that indirubin activation of the *CYP3A4* gene is through the AhR pathway. We previously demonstrated that polycyclic aromatic hydrocarbons (PAHs) enhance the trans-activation of the *CYP3A4* gene through PXR activation but not AhR activation [24]. Recently, Luckert et al. also reported that PAHs and their metabolites induce *CYP3A4* gene expression via PXR [37]. Thus, indirubin and other PAHs activate *CYP3A4* gene transcription through the PXR pathway but not the AhR pathway.

A number of independent studies have examined the relative contribution of the individual functional PXR-binding motifs (dNR1,

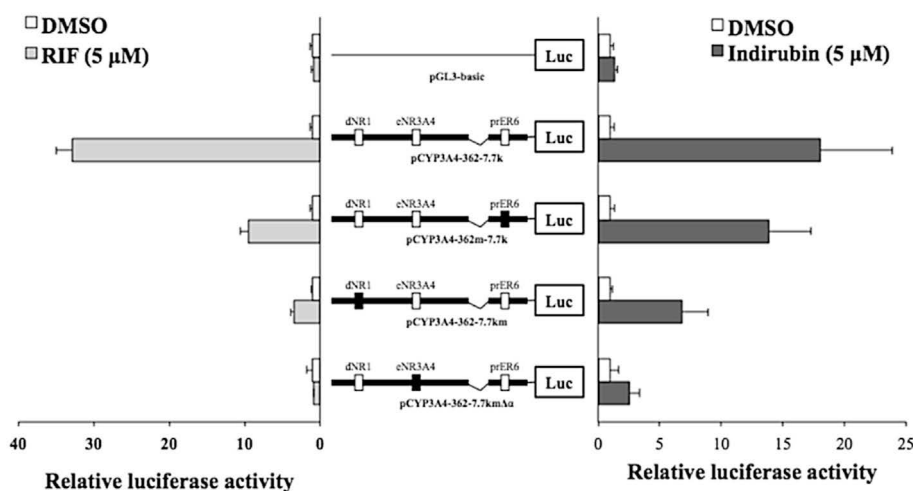


Fig. 6. Mutational analysis of putative human PXR responsive elements in the *CYP3A4* gene. Schematic structures of reporter plasmids used are shown in the middle. Closed boxes represent mutated PXR binding elements. HepG2 cells seeded at 3×10^4 cells in 48-well tissue culture plates pre-incubated for 24 h before transfection. Transfection into HepG2 cells was performed as described in the Materials and methods section. The cells were treated with 5 μM RIF and 5 μM indirubin for 48 h, and the reporter activity was measured by luciferase assay. Reporter activities are expressed as fold increase compared with that in the vehicle-treated cells. Results represent the mean \pm S.D. of three separate experiments. * $P < 0.005$, ** $P < 0.05$, difference from the indirubin- or RIF-treated cells transfected with the pCYP3A4-362-7.7k.

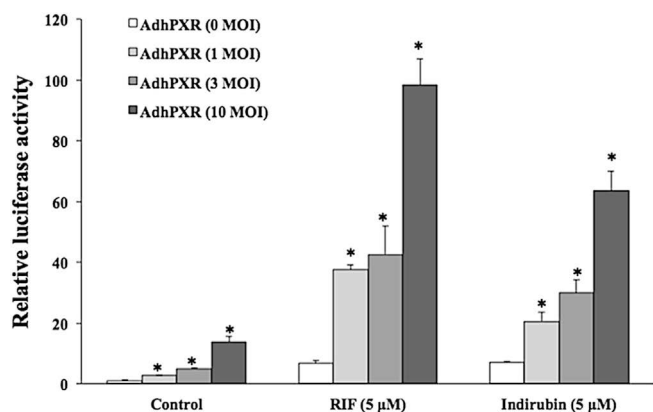


Fig. 7. Effect of PXR on *CYP3A4* gene reporter activity in 3-1-20 cells. Clone 3-1-20 was seeded at 2×10^4 cells in 24-well tissue culture plates pre-incubated for 24 h and then treated with AdhPXR (MOI of 0, 1, 3, and 10). Forty-eight hours after infection, these cells were treated with 5 μ M RIF and 5 μ M indirubin for 48 h, and the reporter activity was measured by luciferase assay. Reporter activities are expressed as fold increase compared with that in the vehicle-treated cells uninfected with AdhPXR. Results represent the mean \pm S.D. of three separate experiments. * $P < 0.005$, difference from the corresponding AdLacZ-infected cells.

prER6, and eNR3A4) on PXR-mediated transactivation of the *CYP3A4* gene. In particular, a novel functional *cis*-acting PXR-binding element designated eNR3A4 has been discovered to be essential for RIF-inducible *CYP3A4* transactivation in human liver [14]. This element is located approximately 7.6 kb upstream from the transcription initiation site of the *CYP3A4* gene to which PXR binds as a heterodimer with RXR α . Furthermore, Pavék et al. reported that eNR3A4 has negligible or no effect on *CYP3A4* transactivation through VDR [38]. These findings strongly suggest that eNR3A4 is a key regulatory element for the xenobiotic induction of *CYP3A4* through PXR in the liver. Thus, we investigated the involvement of eNR3A4 in the transactivation of the *CYP3A4* through PXR activation by indirubin with the *CYP3A4* reporter gene constructs that have a mutation in three PXR response elements

(dNR1, prER6, and eNR3A4). Notably, the introduction of a mutation into eNR3A4 significantly decreased the indirubin-induced transcriptional activation, whereas mutations of dNR1 and prER6 did not (Fig. 6). These results indicate that eNR3A4 might be involved in the activation of *CYP3A4* gene through PXR by indirubin.

In conclusion, we have demonstrated that Ban-Lan-Gen activated *CYP3A4* gene transcription and that indirubin, a component of Ban-Lan-Gen, played an important role in *CYP3A4* gene transcription. In addition, we have shown that indirubin activated *CYP3A4* gene through the activation of PXR in HepG2 cells. More detailed studies on the molecular mechanism of *CYP3A4* induction by indirubin may provide important information on the herb–drug and drug–drug interactions.

Conflict of interest

None.

Acknowledgments

This work was supported by a Health and Labour Sciences Research Grant for Research on Food Safety (No. 22230301) from the Ministry of Health, Labour and Welfare, Japan. We would like to thank Ms. Machi Miura for the excellent technical assistance provided.

References

- [1] Fugh-Berman A. Herb–drug interactions. *Lancet* 2000;355:134–8.
- [2] Hu Z, Yang X, Ho PC, Chan SY, Heng PW, Chan E, et al. Herb–drug interaction: a literature review. *Drugs* 2005;65:1239–82.
- [3] Hamburger M. *Isatis tinctoria* – from the rediscovery of an ancient medical plant towards a novel anti-inflammatory phytopharmaceutical. *Phytochem Rev* 2002;1:333–44.
- [4] Ho YL, Chang YS. Studies on the antinociceptive, anti-inflammatory and anti pyretic effects of *Isatis indigotica* root. *Phytomedicine* 2002;9:419–24.
- [5] Honda G, Tosirisuk V, Tabata M. Isolation of an antidermatophytic, tryptanthrin, from indigo plants, *Polygonum tinctorium* and *Isatis tinctoria*. *Planta Med* 1980;38:275–6.
- [6] Liao BC, Jong TT, Lee MR, Chen SS. LC–APCI–MS method for detection and analysis of tryptanthrin, indigo, and indirubin in daqingye and banlangen. *J Pharm Biomed Anal* 2007;43:346–51.
- [7] Adachi J, Mori Y, Matsui S, Takigami H, Fujino J, Kitagawa H, et al. Indirubin and indigo are potent aryl hydrocarbon receptor ligands present in human urine. *J Biol Chem* 2001;276:31475–8.
- [8] Gonzalez FJ. Human cytochromes P450: problem and prospects. *Trends Pharmacol Sci* 1992;13:346–52.
- [9] Nebert DW, Russell DW. Clinical importance of cytochromes P450. *Lancet* 2002;360:1155–62.
- [10] Thummel KE, Wilkinson GR. In vitro and in vivo drug interactions involving human CYP3A. *Annu Rev Pharmacol Toxicol* 1998;38:389–430.
- [11] Quattrochi LC, Guzelian PS. CYP3A regulation: from pharmacology to nuclear receptors. *Drug Metab Dispos* 2001;29:615–22.
- [12] Thelen K, Dressman JB. Cytochrome P450-mediated metabolism in the human gut wall. *J Pharm Pharmacol* 2009;61:541–58.
- [13] Tolson AH, Wang H. Regulation of drug-metabolizing enzymes by xenobiotic receptors: PXR and CAR. *Adv Drug Deliv Rev* 2010;62:1238–49.
- [14] Toriyabe T, Nagata K, Takada T, Aratsu Y, Matsubara T, Yoshinari K, et al. Unveiling a new essential *cis* element for the transactivation of the *CYP3A4* gene by xenobiotics. *Mol Pharmacol* 2009;75:677–84.
- [15] Luo G, Cunningham M, Kim S, Burn T, Lin J, Sinz M, et al. CYP3A4 induction by drugs: correlation between a pregnane X receptor reporter gene assay and CYP3A4 expression in human hepatocytes. *Drug Metab Dispos* 2002;30:795–804.
- [16] Casbar RC, Das PC, DeKrey GK, Gardiner CS, Cao Y, Rose R, et al. Endosulfan induce CYP2B6 and CYP3A4 by activating the pregnane X receptor. *Toxicol Appl Pharmacol* 2010;245:335–43.
- [17] Matsubara T, Noracharttiyapont W, Toriyabe T, Yoshinari K, Nagata K, Yamazoe Y. Assessment of human pregnane X receptor involvement in pesticide mediated activation of CYP3A4 gene. *Drug Metab Dispos* 2007;35:728–33.
- [18] Matsubara T, Yoshinari K, Aoyama K, Sugawara M, Sekiya Y, Nagata K, et al. Role of vitamin D receptor in the lithocholic acid-mediated CYP3A induction in vitro and in vivo. *Drug Metab Dispos* 2008;36:2058–63.

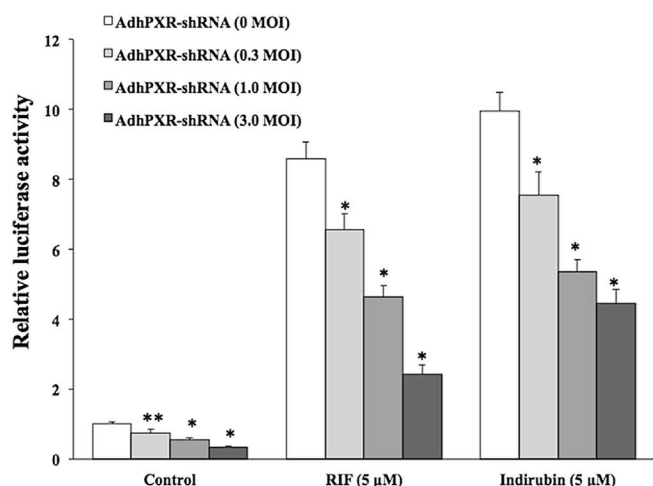


Fig. 8. Effects of PXR-shRNA on *CYP3A4* gene reporter activity in 3-1-20 cells. Clone 3-1-20 was seeded at 2×10^4 cells in 24-well tissue culture plates pre-incubated for 24 h and then treated with AdhPXR-shRNA (MOI of 0, 0.3, 1, and 3). Forty-eight hours after infection, these cells were treated with 5 μ M RIF and 5 μ M indirubin for 48 h, and the reporter activity was measured by luciferase assay. Reporter activities are expressed as fold increase compared with that in the vehicle-treated cells uninfected with AdhPXR-shRNA. Results represent the mean \pm S.D. of three separate experiments. * $P < 0.005$, ** $P < 0.01$, difference from the corresponding AdLacZ-infected cells.

- [19] Moore LB, Goodwin B, Jones SA, Wisely GB, Serabjit-Singh CJ, Willson TM, et al. St. John's wort induces hepatic drug metabolism through activation of the pregnane X receptor. *Proc Natl Acad Sci U S A* 2000;97:7500–2.
- [20] Yeung EY, Sueyoshi T, Negishi M, Chang TK. Identification of *Ginkgo biloba* as a novel activator of pregnane X receptor. *Drug Metab Dispos* 2008;36:2270–6.
- [21] Wang L, Li F, Lu J, Li G, Li D, Zhong X, et al. The Chinese herbal medicine *Sophora flavescens* activates pregnane X receptor. *Drug Metab Dispos* 2010;38:2226–31.
- [22] Noracharttiyapont W, Nagai Y, Matsubara T, Miyata M, Shimada M, Nagata K, et al. Construction of several human-derived stable cell lines displaying distinct profiles of CYP3A4 induction. *Drug Metab Pharmacokinet* 2006;21:99–108.
- [23] Miyake S, Makimura M, Kanegae Y, Harada S, Sato Y, Takamori K, et al. Efficient generation of recombinant adenoviruses using adenovirus DNA-terminal protein complex and a cosmid bearing the full-length virus genome. *Proc Natl Acad Sci U S A* 1996;93:1320–4.
- [24] Kumagai T, Suzuki H, Sasaki T, Sakaguchi S, Miyairi S, Yamazoe Y, et al. Polycyclic aromatic hydrocarbons activate CYP3A4 gene transcription through human pregnane X receptor. *Drug Metab Pharmacokinet* 2012;27:200–6.
- [25] Sato W, Suzuki H, Sasaki T, Kumagai T, Sakaguchi S, Mizugaki M, et al. Construction of a system that simultaneously evaluates CYP1A1 and CYP1A2 induction in a stable human-derived cell line using a dual reporter plasmid. *Drug Metab Pharmacokinet* 2010;25:180–9.
- [26] Kraft K. Complementary/alternative medicine in the context of prevention of disease and maintenance of health. *Prev Med* 2009;49:88–92.
- [27] Chan E, Tan M, Xin J, Sudarsanam S, Johnson DE. Interactions between traditional Chinese medicines and Western therapeutics. *Curr Opin Drug Discov Devel* 2010;13:50–65.
- [28] Eisenbrand G, Hippe F, Jakobs S, Muehlbeyer S. Molecular mechanisms of indirubin and its derivatives: novel anticancer molecules with their origin in traditional Chinese phytomedicine. *J Cancer Res Clin Oncol* 2004;130:627–35.
- [29] Sivertsson L, Edebert I, Palmertz MP, Ingelman-Sundberg M, Neve EP. Induction CYP3A4 expression in confluent Huh7 hepatoma cells as a result of decreased cell proliferation and subsequent pregnane X receptor activation. *Mol Pharmacol* 2013;83:659–70.
- [30] Bertilsson G, Heidrich J, Svensson K, Asman M, Jendeberg L, Sydow-Backman M, et al. Identification of a human nuclear receptor defines a new signaling pathway for CYP3A induction. *Proc Natl Acad Sci U S A* 1998;95:12208–13.
- [31] Goodwin B, Hodgson E, Liddle C. The orphan human pregnane X receptor mediates the transcriptional activation of CYP3A4 by rifampicin through a distal enhancer module. *Mol Pharmacol* 1999;56:1329–39.
- [32] Lehman JM, McKee DD, Watson MA, Willson TM, Moore JT, Kliewer SA. The human orphan nuclear receptor PXR is activated by compounds that regulate CYP3A4 gene expression and cause drug interactions. *J Clin Invest* 1998;102:1016–23.
- [33] Goodwin B, Hodgson E, D'Costa DJ, Roberson GR, Liddle C. Transcriptional regulation of the human CYP3A4 gene by the constitutive androstane receptor. *Mol Pharmacol* 2002;62:359–65.
- [34] Drocourt L, Ourlin JC, Pascucci JM, Maurel P, Vilarem MJ. Expression of CYP3A4, CYP2B6, and CYP2C9 is regulated by the vitamin D receptor pathway in primary human hepatocytes. *J Biol Chem* 2002;277:25125–32.
- [35] Pascucci JM, Drocourt L, Gerbal-Chaloin S, Fabre JM, Maurel P, Vilarem MJ. Dual effect of dexamethasone on CYP3A4 gene expression in human hepatocytes. Sequential role of glucocorticoid receptor and pregnane X receptor. *Eur J Biochem* 2001;268:6346–58.
- [36] Blumberg B, Sabbagh Jr W, Juguilon H, Bolado Jr J, Van Meter CM, et al. SXR, a novel steroid and xenobiotic-sensing nuclear receptor. *Genes Dev* 1998;12:3195–205.
- [37] Luckert C, Ehlers A, Buhrke T, Seidel A, Lampen A, Hessel S. Polycyclic aromatic hydrocarbons stimulate human CYP3A4 promoter activity via PXR. *Toxicol Lett* 2013;222:180–8.
- [38] Pavek P, Pospechova K, Svecova L, Syrova Z, Stejkalova L, Blazkova J, et al. Intestinal cell-specific vitamin D receptor (VDR)-mediated transcriptional regulation of CYP3A4 gene. *Biochem Pharmacol* 2010;79:277–87.



Contents lists available at ScienceDirect

Tetrahedron Letters

journal homepage: www.elsevier.com/locate/tetlet

Directed synthesis of 2-spiroindolines from indole derivatives by formic acid-induced *N*-acyliminium ion-conjugated diene spirocyclization



Hideki Abe^{a,*}, Naohiro Miyagawa^a, Sho Hasegawa^a, Toyoharu Kobayashi^a, Sakae Aoyagi^b, Chihiro Kibayashi^b, Tadashi Katoh^c, Hisanaka Ito^{a,*}

^a School of Life Sciences, Tokyo University of Pharmacy and Life Sciences, 1432-1 Horinouchi, Hachioji, Tokyo 192-0392, Japan

^b School of Pharmacy, Tokyo University of Pharmacy and Life Sciences, 1432-1 Horinouchi, Hachioji, Tokyo 192-0392, Japan

^c Department of Chemical Pharmaceutical Science, Tohoku Pharmaceutical University, 4-4-1 Komatsushima, Aoba-ku, Sendai 981-8558, Japan

ARTICLE INFO

Article history:

Received 15 November 2014

Revised 17 December 2014

Accepted 26 December 2014

Available online 7 January 2015

Keywords:

2-Spiroindoline

Spirocyclization

2-Substituted indole

Formic acid

N-Acyliminium ion

ABSTRACT

Synthesis of 2-spiroindolines from 2-substituted indole derivatives via acid-induced *N*-acyliminium ion-conjugated diene spirocyclization was demonstrated. This methodology can be used to direct transformations of 2-substituted indole moieties into 3-nonsubstituted-2-spiroindoline skeletons.

© 2015 Elsevier Ltd. All rights reserved.

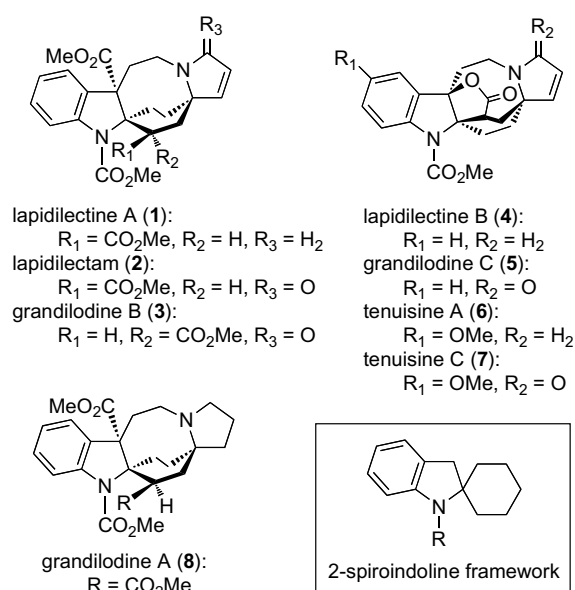
Introduction

Indole and indoline frameworks are common substructures in a number of biologically active compounds and natural products. 2-Spiroindoline alkaloids, such as lapidilectines, lapidilectam, tenuisines, and grandilodines (Fig. 1 and 1–8), have been isolated from plants, including *Kopsia lapidilecta*, *Kopsia tenuis*, and *Kopsia grandifolia*.^{1–4} Lapidilectine B (**4**), grandilodine C (**5**), and tenuisine A (**6**) have been found to reverse multidrug resistance in vincristine-resistant KB cells without showing any cytotoxicity against either drug-sensitive or drug-resistant cells in the absence of added vincristine.⁴ The only synthetic studies on these biologically active and complex alkaloids reported to date are the total synthesis of lapidilectine B (**4**)⁵ by Pearson and the total synthesis of lundurine B,⁶ from *Kopsia tenuis*, by Nishida. There have been several synthetic studies on the construction of the alkaloids' indole core fused to an azacyclooctane ring,^{7–10} but to our knowledge there have as yet been no attempts to synthesize complex 2-spiroindoline alkaloids. Although some synthetic methods for 2-spiroindolines, for example, intramolecular CH insertion^{11,12} and spiro ring

formation from 2,2-disubstituted indoline,¹³ have been reported, there are few known methodologies for direct transformation of 2-substituted indoles to 2-spiroindolines. Additionally, there have been few reports of directed alkylations at the C2 position to give 2-substituted indoles due to the high reactivity of the C3 position toward electrophilic reagents. In fact, many reactions of indole at the C3 position, such as Friedel–Crafts-type reactions, have been developed.¹⁴ Harrowven and co-workers¹⁵ reported the only example of direct synthesis of 2-spiroindoline from indole by 5-*exo* or 6-*exo* radical cyclization of indoles tethered to aromatic rings. We previously reported formic-acid-induced spirocyclization of *N*-acyliminium ions with conjugated dienes and the total synthesis of tricyclic marine alkaloids¹⁶ using a prepared spiro-compound as the key intermediate. This key reaction was used for stereoselective construction of a 1-azaspiro[4.5]decane skeleton tethered to an allyl alcohol moiety from an amide ketone in a single operation. Therefore, the possibility of synthesizing 2-spiroindoline by acid-induced spirocyclization attracted our interest. We recently reported the spirocyclization of a 3,3-ethylenedioxy-2-hydroxy indoline derivative to afford an octahydroacridine derivative¹⁷ via spirocyclization followed by rearrangement. Herein, we report the directed transformation of a 2-substituted indole to 2-spiroindoline by spirocyclization.

* Corresponding authors. Tel.: +81 42 676 7293; fax: +81 42 676 7282.

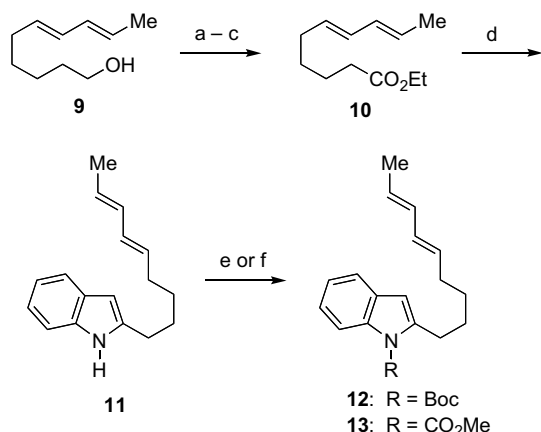
E-mail addresses: abehidek@toyaku.ac.jp (H. Abe), itohisa@toyaku.ac.jp (H. Ito).

Figure 1. Structures of *Kopsia* alkaloids and 2-spiroindoline framework.

Results and discussion

Our investigation of the construction of 2-spiroindoline began with the synthesis of 2-substituted indole derivatives **12** and **13**. Initially, 2-substituted indole **11** was derived from *E,E*-dienol **9**¹⁸ in 4 steps, including Smith's synthesis method for indole,¹⁹ as shown in Scheme 1. Thus, two-step oxidation (Parikh–Doering oxidation²⁰/Pinnick oxidation²¹) of alcohol **9**, followed by esterification of the resulting carboxylic acid, gave the ethyl ester **10**. Condensation of **10** with *N*-TMS-*o*-toluidine,²² obtained easily from *o*-toluidine, was achieved by Smith's method to provide **11** in moderate yield. Finally, protection of the nitrogen atom of **11** with a *tert*-butoxycarbonyl group or a methoxycarbonyl group gave the requisite *N*-Boc indole **12** and *N*-methoxycarbonyl indole **13**, respectively.

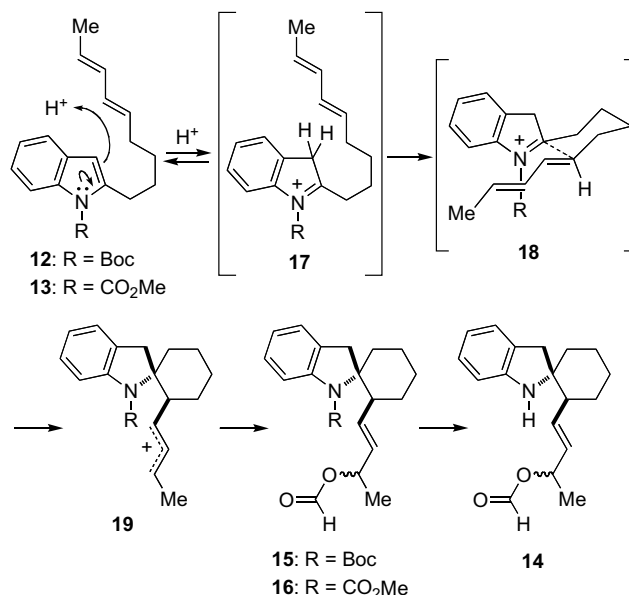
Having obtained the *N*-Boc derivative **12** and the *N*-methoxycarbonyl derivative **13** in an efficient manner, we then investigated the transformation to 2-spiroindolines via formic acid-induced spirocyclization of *N*-acyliminium ions with conjugated dienes



Scheme 1. Reagents and conditions: (a) SO_3 -pyridine, Et_3N , DMSO, rt, 10 min; (b) NaClO_2 , 2-methyl-2-butene, NaH_2PO_4 , *tert*-BuOH– H_2O , rt, 10 min; (c) *p*-TsOH, EtOH, reflux, 2 h, 63%, 3 steps; (d) *N*-TMS-*o*-toluidine, *n*-BuLi, hexane, reflux, 10 h, then **10**, THF, $-78^\circ\text{C} \rightarrow \text{rt}$, 1 h, 58%; (e) di-*tert*-butyl-dicarbonate, Et_3N , DMAP, CH_2Cl_2 , rt, 1 h, 98% for **12**; (f) methyl chloroformate, *n*-BuLi, -78°C , 1 h, then 0°C , 1 h, 96% for **13**.

Table 1
Spirocyclization of 2-substituted indole derivatives **12** and **13**

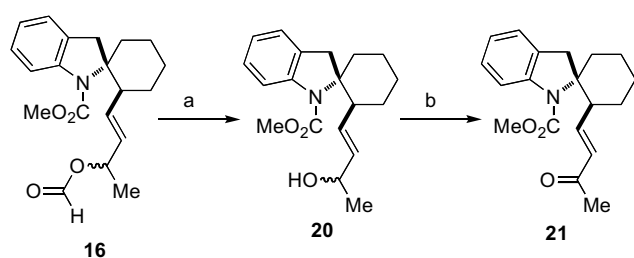
Entry	Substrate	Temp	Time (h)	Products (yield %)
1	12	Rt	14	14 (36)
2	12	0°C	48	15 (14) and 14 (18)
3	13	Rt	4	16 (53)
4	13	0°C	48	16 (22)



Scheme 2. Proposed mechanism for spirocyclization.

(Table 1).²³ The first attempt at formic-acid induced spirocyclization of **12**, under the same conditions as in our previous report ($\text{HCO}_2\text{H}-\text{CH}_2\text{Cl}_2$, rt),¹⁷ gave the deBoc 2-spiroindoline **14** in 36% yield as a 1:1 mixture of diastereoisomers at the C3' position (entry 1). When the reaction was performed at 0°C for 48 h (entry 2), the desired 2-spiroindoline derivative **15** and the spiro compound **14** were detected, but in poor yields (14% and 18%, respectively), along with recovered **12**. However, the spirocyclization of *N*-methoxycarbonyl derivative **13** with formic acid proceeded smoothly at room temperature to afford the desired 2-spiroindoline **16** in 53% yield as a 1:1 mixture of diastereoisomers at C3' (entry 3). When the reaction time was lengthened and the temperature decreased to 0°C , the spiro compound **16** was obtained in only 22% yield, along with a complex mixture of unidentified products. When using indole **11** as a starting material in this reaction, complex mixtures were obtained.

The proposed mechanism for the transformation of *N*-acyl-2-substituted indoles to 2-spiroindolines is shown in Scheme 2. The 2-substituted indoles **12** and **13** are in equilibrium with



Scheme 3. Reagents and conditions: (a) satd K_2CO_3 aqueous solution, MeOH, rt, 30 min; (b) MnO_2 , CH_2Cl_2 , rt, 3 h, 95% for 2 steps.

iminium ions **17**, generated by protonation at the C3 position of the indole ring in the presence of formic acid.²⁴ Spirocyclization of the iminium ion **17** with the conjugated diene occurs via the chair-like transition state **18**¹⁶ to afford spiro compound **19**, which contains an allyl cation moiety. Addition of formic acid to the C3' position of the side chain gives the desired 2-spiroindolines **15** and **16**, respectively. In the case of the reaction of *N*-Boc derivative **12**, cleavage of the Boc group of **12** and the desired product **15** competed with spirocyclization under acidic conditions, decreasing the yields of the desired spiro compounds. Fortunately, the *N*-methoxycarbonyl group was more suitable for use under acidic conditions than the Boc group. Thus, spirocyclization of *N*-methoxycarbonyl indole **13** proceeded without cleavage of the methoxycarbonyl group in the presence of formic acid to give the desired *N*-methoxycarbonyl-2-spiroindoline **16** in moderate yield.

To confirm that the resulting 2-spiroindoline mixture was a mixture of diastereoisomers at the C3' position, transformation of formate to a conjugated enone was carried out as shown in Scheme 3. Hydrolysis of spiro formate **16** under basic conditions gave the allyl alcohol **20** as a 1:1 mixture of diastereoisomers. Oxidation of allyl alcohol **20** with activated MnO_2 afforded the conjugated enone **21** as a single diastereomer in 95% yield over 2 steps. This result proved that the spiro compounds obtained consisted of a mixture of diastereoisomers at the C3' position.

The substrate scope of the spirocyclization of 2-substituted indoles²⁵ to 2,2-spiro indoline derivatives was investigated (Table 2). Spirocyclization of 5-methyl substituted indole derivative **22** using formic acid gave the desired spiroindoline **26** in

67% yield as a 1:1 mixture of diastereoisomers (entry 1). In the case of the reaction of 5-methoxy indole derivative **23** (entries 2 and 3), the spiroindoline **27**, which is a component of tenuisine-type alkaloids, was obtained in 42% (66% brsm) yield. When this reaction time was prolonged, the yield of **27** decreased to 30% due to decomposition of the product. Spirocyclization of the 5-fluoro-substituted compound **24**, containing an electron-withdrawing group (entry 4), gave **28** in low yield (30%). The reaction of a 6-methyl indole derivative afforded the corresponding spiroindoline **29** in moderate yield (entry 5). Although the construction of indole-2-spiro-2'-cyclohexane derivatives from 2-nona-5,7-dienyl indole derivatives **12**, **13**, and **22–25** was achieved as stated above, attempts to transform the 2-octa-4,6-dienyl indole to the corresponding indole-2-spiro-2'-cyclopentane derivative under the same conditions failed.²⁶

In conclusion, directed synthesis of 2-spiroindoline derivatives by spirocyclization of indoles tethered to conjugated dienes at the C2 position was demonstrated. The transformation of indoles to spiroindolines proceeded via protonation at the C3 position in the presence of formic acid, followed by spirocyclization of the resulting iminium ion with the conjugated diene. This synthetic methodology is expected to be useful for total synthesis of *Kopsia* alkaloids with *N*-methoxycarbonyl-2-spiroindoline components, a project that is now in progress in our laboratory.

Acknowledgments

This work was supported by the Platform for Drug Discovery, Informatics, and Structural Life Science project of the Ministry of Education, Culture, Sports, Science, and Technology, Japan. H.A. thanks the Takeda Science Foundation and the Uehara Memorial Foundation for financial support.

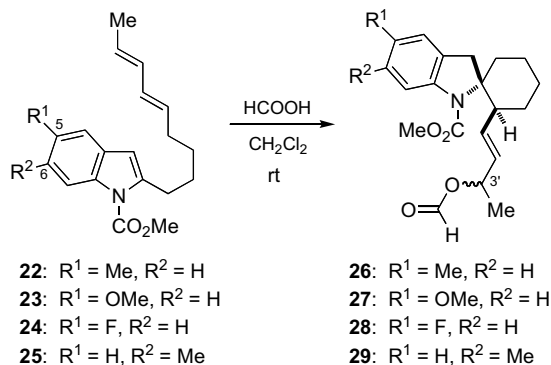
Supplementary data

Supplementary data associated with this article can be found, in the online version, at <http://dx.doi.org/10.1016/j.tetlet.2014.12.130>.

References and notes

- Awang, K.; Sévenet, T.; Hadi, A. H. A.; David, B.; Païs, M. *Tetrahedron Lett.* **1992**, 33, 2493.
- Awang, K.; Sévenet, T.; Païs, M.; Hadi, A. H. A. *J. Nat. Prod.* **1993**, 56, 1134.
- Kam, T.-S.; Lim, K.-H.; Yoganathan, K.; Hayashi, M.; Komiyama, K. *Tetrahedron* **2004**, 60, 10739.
- Yap, W.-S.; Gan, C.-Y.; Low, Y.-Y.; Choo, Y.-M.; Etoh, T.; Hayashi, M.; Komiyama, K.; Kam, T.-S. *J. Nat. Prod.* **2011**, 74, 1309.
- (a) Pearson, W. H.; Lee, I. Y.; Mi, Y.; Stoy, P. J. *Org. Chem.* **2004**, 69, 9109; (b) Pearson, W. H.; Mi, Y.; Lee, I. Y.; Stoy, P. J. *Am. Chem. Soc.* **2001**, 123, 6724.
- Hoshi, M.; Kaneko, O.; Nakajima, M.; Arai, S.; Nishida, A. *Org. Lett.* **2014**, 16, 768.
- Schultz, E. E.; Pujanauski, B. G.; Sarpong, R. *Org. Lett.* **2012**, 14, 648.
- Donets, P. A.; Van Hecke, K.; Van Meervelt, L.; Van der Eycken, E. V. *Org. Lett.* **2009**, 11, 3618.
- (a) Ferrer, C.; Escribano-Cuesta, A.; Echavarren, A. M. *Tetrahedron* **2009**, 65, 9015; (b) Ferrer, C.; Amijs, C. H. M.; Echavarren, A. M. *Chem. Eur. J.* **2007**, 13, 1358.
- (a) Maruyama, J.; Yamashita, H.; Watanabe, T.; Arai, S.; Nishida, A. *Tetrahedron* **2009**, 65, 1327; (b) Watanabe, T.; Arai, S.; Nishida, A. *Synlett* **2004**, 907.
- Whipp, C. J.; de Turiso, F. G.-L. *Tetrahedron Lett.* **2008**, 49, 5508.
- Bremner, J. B.; Sengpracha, W. *Tetrahedron* **2005**, 61, 5489.
- Malapel-Andrieu, M.; Mérour, J.-Y. *J. Heterocycl. Chem.* **1998**, 35, 421.
- For a review: Bandini, M.; Eichholzer, A. *Angew. Chem., Int. Ed.* **2009**, 48, 9608.
- Flanagan, S. R.; Harrowven, D. C.; Bradley, M. *Tetrahedron Lett.* **2003**, 44, 1795.
- Abe, H.; Aoyagi, S.; Kibayashi, C. *J. Am. Chem. Soc.* **2005**, 127, 1473.
- Abe, H.; Sato, Y.; Watanabe, K.; Aoyagi, S.; Kibayashi, C.; Katoh, T. *Heterocycles* **2009**, 77, 533.
- Baldwin, J. E.; Gerald Lopez, R. C. *Tetrahedron* **1983**, 39, 1487.
- Smith, A. B., III; Visnick, M. *Tetrahedron Lett.* **1985**, 26, 3757.
- Parikh, J. R.; Doering, W. E. *J. Am. Chem. Soc.* **1967**, 89, 5505.
- Bal, B. S.; Childers, W. E., Jr.; Pinnick, H. W. *Tetrahedron* **1981**, 37, 2091.
- Smith, A. B., III; Visnick, M.; Haseltine, J. N.; Sprengeler, P. A. *Tetrahedron* **1986**, 42, 2957.

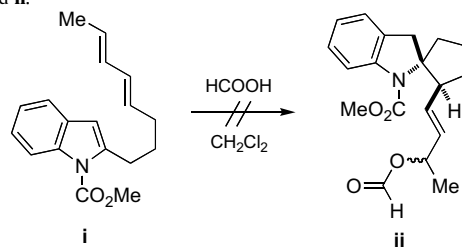
Table 2
Spirocyclization of 2-substituted indole derivatives **22–25**



Entry	Substrate	Time (h)	Products (yield %)
1	22	6	26 (67)
2	23	2	27 (42, 66% brsm)
3	23	6	27 (30, 46% brsm)
4	24	8	28 (30, 39% brsm)
5	25	8	29 (48)

23. *General procedure:* To a solution of 2-substituted indole (0.1 mmol) in CH_2Cl_2 (1 mL) at 0 °C was added formic acid dropwise (1 mL). After stirring for the indicated times and temperatures, the reaction mixture was made basic by addition of 28% NH_3 aqueous solution, and then extracted with CHCl_3 three times. The combined organic layers were washed with water and dried over MgSO_4 , and the solvent was removed in vacuo. Purification of the resulting residue by flash column chromatography gave the 2-spiroindolines.
24. The spirocyclization reaction of **13** with acetic acid (room temperature for 5 days) did not proceed, and 94% of **13** was recovered.
25. The 5- or 6-substituted indole derivatives used as starting materials were synthesized by the same procedure used for the synthesis of **13**, as shown in Scheme 1, condensation of ethyl ester **10** and the corresponding *N*-TMS-*o*-toluidine derivatives.

26. The reaction of methyl 2-((4*E*,6*E*)-octa-4,6-dien-1-yl)-1*H*-indole-1-carboxylate **i** with formic acid gave only a complex mixture and did not afford the spiro compound **ii**.



Article

Construction of an Isonucleoside on a 2,6-Dioxobicyclo[3.2.0]-heptane Skeleton

Yuichi Yoshimura ^{1,*}, Satoshi Kobayashi ¹, Hitomi Kaneko ¹, Takeshi Suzuki ¹ and Tomozumi Imamichi ²

¹ Faculty of Pharmaceutical Sciences, Tohoku Pharmaceutical University, 4-4-1 Komatsushima, Aoba-ku, Sendai 981-8558, Japan; E-Mails: s-kobayashi@fujichemical.co.jp (S.K.); hitomi.f528@gmail.com (H.K.); suzutake19851109@coral.plala.or.jp (T.S.)

² Laboratory of Human Retrovirology, Leidos Biochemical Research Inc., Frederick National Laboratory for Cancer Research, Frederick, MD 21702, USA; E-Mail: timamichi@mail.nih.gov

* Author to whom correspondence should be addressed; E-Mail: yoshimura@tohoku-pharm.ac.jp; Tel./Fax: +81-22-727-0144.

Academic Editors: Mahesh K. Lakshman and Fumi Nagatsugi

Received: 2 February 2015 / Accepted: 4 March 2015 / Published: 12 March 2015

Abstract: We have built a new isonucleoside derivative on a 2,6-dioxobicyclo[3.2.0]heptane skeleton as a potential anti-HIV agent. To synthesize the target compound, an acetal-protected dihydroxyacetone was first converted to a 2,3-epoxy-tetrahydrofuran derivative. Introduction of an azide group, followed by the formation of an oxetane ring, gave a pseudosugar derivative with a 2,6-dioxobicyclo[3.2.0]heptane skeleton. The desired isonucleoside was obtained by constructing a purine base moiety on the scaffold, followed by amination.

Keywords: nucleoside; bicyclo; oxetane ring; conformation

1. Introduction

Since the discovery of 3'-azidothymidine (AZT), much attention has been paid to the development of effective chemotherapeutic agents against the human immunodeficiency virus (HIV), a causative agent for AIDS [1,2]. More than 20 anti-HIV drugs have now been approved and are clinically used for the treatment of AIDS. Among them, nucleoside reverse transcriptase inhibitors (NRTIs) play a

critical role in the treatment of AIDS patients. In the most successful regimen for AIDS referred to as ART (Anti-Retroviral Therapy), a cocktail of anti-HIV drugs, including NRTIs, non-nucleoside reverse transcriptase inhibitors (NNRTIs), and protease inhibitors (PIs) [3], is used. Although ART greatly contributes to increasing the lifespan of patients, drug-resistant strains of the virus are still a serious problem [4,5]. Therefore, new drugs that are effective against the resistant virus strains are constantly needed.

Most NRTIs belong to a category of dideoxynucleosides, e.g., zalcitabine (ddC) [6] and didanosine (ddI) [6]. AZT [7] and lamivudine [8] are 3'-substituted dideoxynucleoside derivatives, and abacavir is a carbocyclic analogue of dideoxynucleoside. Only tenofovir [9], which is a nucleoside phosphonate (Figures 1 and 2), is different. From the viewpoint of designing new anti-HIV agents, nucleosides constructed on a novel scaffold are expected to have antiviral activity against the resistant virus strains and may avoid cross-resistance to the known NRTIs.

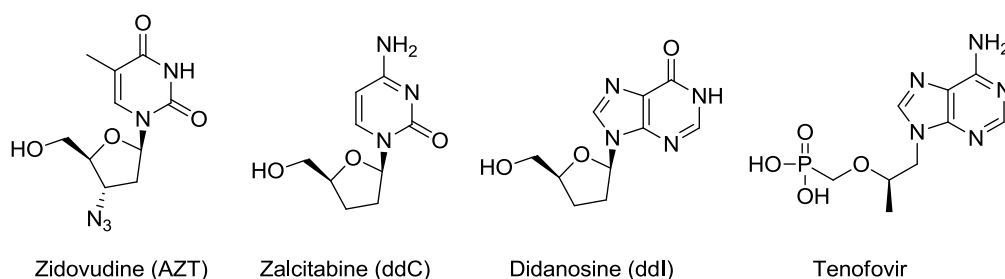


Figure 1. Approved NRTIs.

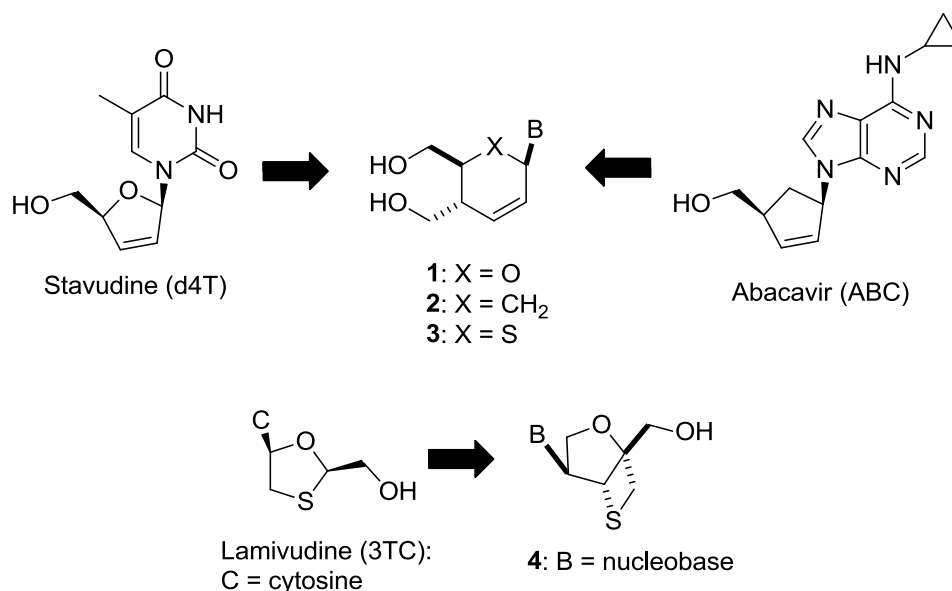


Figure 2. Our previous works searching for anti-HIV nucleosides built on a new scaffold.

Thus, we have been focusing on the design and synthesis of nucleoside derivatives attached to a pseudosugar scaffold [10–17]. Among them, nucleosides with cyclohexenyl [13], dihydrothiophenyl [15], and dihydropyranyl [17] groups in place of a furanose ring have been synthesized as “ring-expanded” analogues of stavudine and abacavir. Dihydropyranyl derivative **1** did

not show any activity, whereas cyclohexenyl derivative **2** showed weak anti-HIV activity [13,17]. On the other hand, dihydrothiophenyl derivative **3** showed significant anti-HIV activity [15]. In addition, we have applied the “ring-expanding” concept to lamivudine and synthesized isonucleosides **4** constructed on 2-oxa-6-thiabicyclo[3.2.0]heptane [14]. The isonucleoside **4** was also considered as conformationally-restricted analogue of lamivudine by introducing a fused thietane ring (*vide infra*). However, **4** showed no anti-HIV activity (Figure 2). In this study, we planned to build isonucleoside **6** on a 2,6-dioxobicyclo[3.2.0]heptane skeleton, an analogue of dioxolane nucleoside **5** which exhibited potent anti-HIV activity [18–20]. The similar conformationally-restricted analogue of d4T was known: cyclopropane-fused carbocyclic d4T (*N*-MCd4T), fixed in north conformation, was originally reported by Marquez and his colleagues and had significant anti-HIV activity with lesser cytotoxicity [21]. In addition, D-enantiomer of **5** was known to have potent cytotoxicity [18–20]. Thus, isonucleoside **6** should be promising although the thietane-fused derivative **4** was inactive (Figure 3).

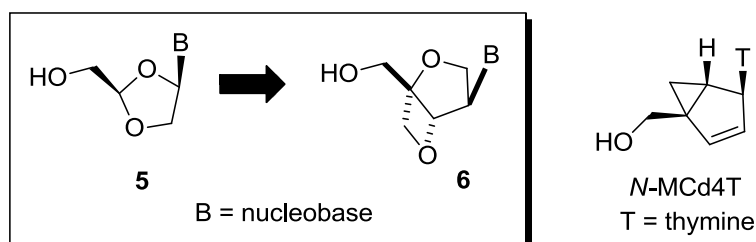
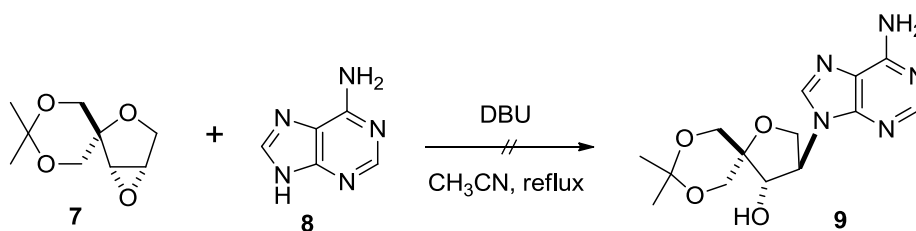


Figure 3. Design of nucleoside derivative built on a 2,6-bicyclo[3.2.0]heptane skeleton.

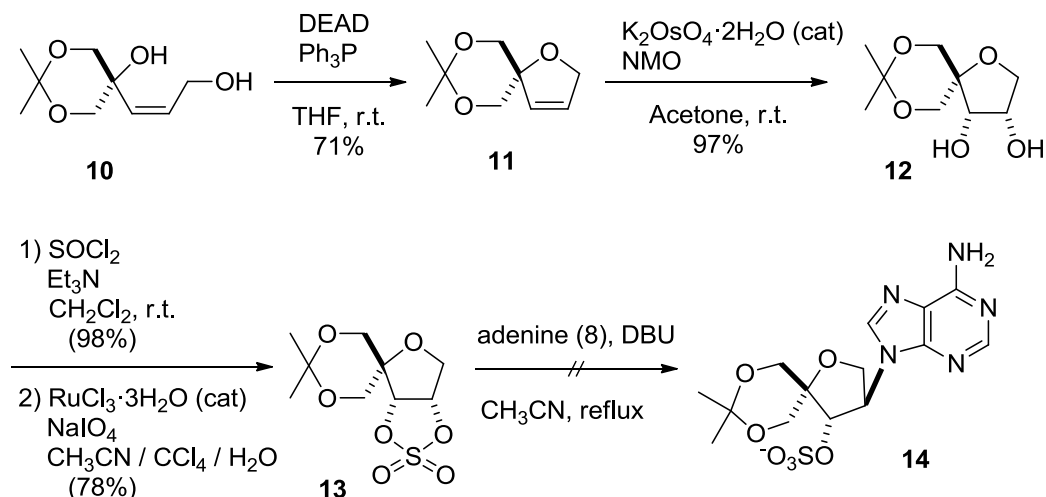
2. Results and Discussion

Following our previous reports [11,14], epoxide **7** was synthesized. We first attempted to introduce an adenine onto **7** by treating it with DBU [22]. However, the reaction did not give the desired product **9** (Scheme 1).



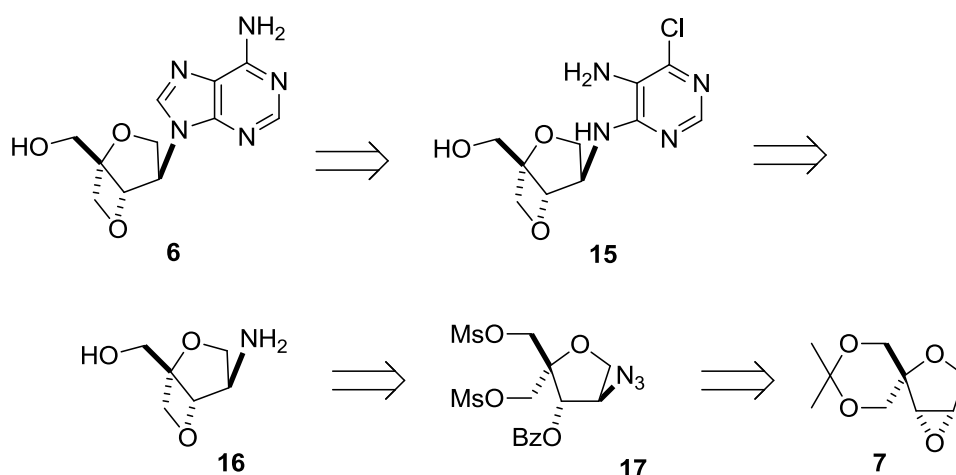
Scheme 1. Attempt to introduce adenine moiety.

In addition, Lewis acid-catalyzed reactions did not afford **9** either (data not shown). Since the low reactivity of **7** might be due to its rigid structure, we next tried nucleophilic substitution using a more reactive cyclic sulfate derivative [23]. *Cis*-allyl alcohol **10**, a precursor of epoxide **7** [11,14], was cyclized under Mitsunobu conditions, as in the case of epoxide **7** [11,14], to give dihydrofuran **11** in 71% yield. Treatment of dihydrofuran **11** with potassium osmate in the presence of *N*-methylmorpholine *N*-oxide afforded *cis*-diol **12**. The desired cyclic sulfate **13** was obtained by treatment of **12** with thionyl chloride, followed by oxidation. However, the nucleophilic substitution of **13** with adenine did not afford the desired isonucleoside **14** (Scheme 2).



Scheme 2. Second attempt to introduce adenine using a cyclic sulfate.

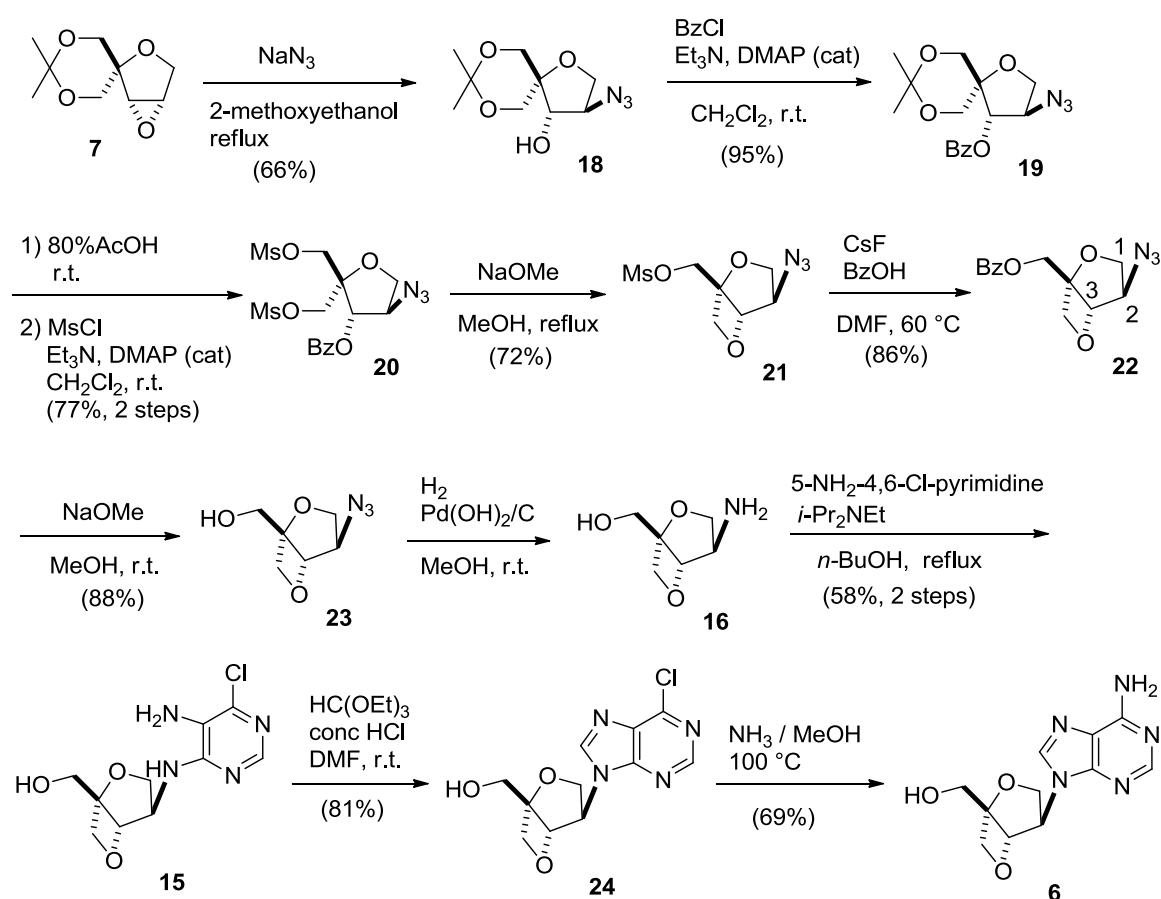
Therefore, we revised our plan to synthesize an isoadenosine constructed on a 2,6-dioxobicyclo[3.2.0]heptane scaffold, and the revised scheme is shown in Scheme 3 in a retrosynthetic manner. Instead of the direct introduction of adenine, we decided to build the adenine ring on the 2,6-dioxobicyclo[3.2.0]heptane pseudosugar skeleton in a stepwise manner. According to this plan, compound **16** was thought to be a suitable intermediate for preparing **15** since it can be transformed to **6** by the formation of an imidazole ring, followed by amination. Fused oxetane derivative **16** can be obtained from dimesylate **17**. Finally, epoxide **7**, described above, was selected as the starting compound because it can be converted to **17** by the selective cleavage of the oxirane ring with an azide anion (Scheme 2).



Scheme 3. Revised retrosynthesis of isoadenosine **6** built on a 2,6-dioxobicyclo[3.2.0]heptane skeleton.

First, regioselective cleavage of the oxirane ring of **7** with sodium azide in 2-methoxyethanol under reflux conditions gave the desired azide-alcohol **18** as a single regioisomer in 66% yield. It is obvious that the nucleophilic azide anion attacked from the less hindered side since similar regioselective epoxide opening was observed in our previous report [11,14]. After benzylation of the hydroxyl group, the acetal group of **19** was removed by using acidic hydrolysis, and the resulting diol was

mesylated to give dimesylate **20** in good yield. Deprotection of the benzoyl group and the subsequent formation of an oxetane ring were achieved by treating **20** with sodium methoxide under reflux conditions to give mesylate **21** in 72% yield. The structure of **21** was unambiguously determined by comparison of 1D NMR spectrum with that of 2-oxa-6-thiabicyclo[3.2.0]heptane skeleton [14] after converting it to benzoate **22** by treatment with benzoic acid in the presence of cesium fluoride. In ^1H -NMR spectra of **22**, the peaks corresponding to the methyl groups of the dimesylate were absent, and only the peaks corresponding to the benzoyl group in the range of 8.1–7.4 ppm were present. In addition, one of the methylene protons at the 2-position was observed as a doublet at 4.42 ppm, meaning that the coupling with H-3 disappeared. This indicates that the conformation around the tetrahydrofuran ring changes and becomes fixed, which causes a loss of coupling between one pair of H-2 and H-3 protons. A similar correlation between conformation and couplings in ^1H -NMR spectra has been reported for the 2-oxa-6-thiabicyclo[3.2.0]heptane skeleton [14]. Moreover, in the mass spectrum of the compound, a molecular ion peak was observed at $m/z = 276$, further supporting the assignment of the structure. Finally, **22** was deprotected to afford azido-alcohol **23** in 88% yield (Scheme 4).



Scheme 4. Synthesis of isoadenosine **6**.

Azido-alcohol **23** was reduced by catalytic hydrogenation to give key intermediate **16**, which was treated with 5-amino-4,6-dichloropyrimidine and diisopropylethylamine in refluxing n -butanol [23] to give diaminopyrimidine derivative **15** in 58% yield from **23**. Formation of the imidazole ring of **15** was

accomplished by treatment with orthoethyl formate under acidic conditions [24] to give 6-chloropurine nucleoside **24**. Finally, the isoadenosine was built on the 2,6-dioxobicyclo[3.2.0]heptane scaffold **6** by heating **24** with methanolic ammonia in a sealed tube in 69% yield (Scheme 4). Isoadenosine **6** did not show any significant activity against HIV even at a concentration of 100 μ M.

3. Experimental Section

General Information

Melting points are uncorrected. NMR spectra were recorded at 400 MHz (^1H), 100 MHz (^{13}C) using CDCl_3 as a solvent. As an internal standard, tetramethylsilane was used for CDCl_3 . Mass spectra were obtained by EI or FAB mode. Silica gel for chromatography was Silica Gel 60N (spherical, neutral, 100–210 μm , Kanto Chemical Co. Inc., Tokyo, Japan). When the reagents sensitive to moisture were used, the reaction was performed under argon atmosphere.

8,8-Dimethyl-1,7,9-trioxaspiro[4.5]dec-3-ene (11). To a solution of PPh_3 (2.49 g, 9.48 mmol) in THF (10 mL) was added DEAD (4.31 mL, 9.48 mmol) and the mixture was stirred at room temperature for 5 min. To this mixture, a solution of **10** [11,14] (1.04 g, 5.58 mmol) in THF (10 mL) was added. The mixture was stirred at room temperature for 1 h. After the solvent was removed under reduced pressure, the residue was purified by silica gel column chromatography (hexane–ethyl acetate = 19:1) to give **11** (677 mg, 71%) as a white crystal. mp 47–49 $^\circ\text{C}$; ^1H -NMR (CDCl_3) δ 1.45 (3H, s), 1.48 (3H, s), 3.76 (2H, d, J = 11.6 Hz), 3.81 (2H, d, J = 11.6 Hz), 4.71 (2H, t, J = 1.9 Hz), 5.84–5.87 (1H, m), 6.02 (1H, d, J = 6.3 Hz); ^{13}C -NMR (CDCl_3) δ 22.6, 24.6, 66.7, 74.9, 98.0, 128.1, 129.1; IR (neat) 2924.2, 2853.1, 1724.1, 1215.9, 758.3 cm^{-1} ; FAB-MS (m/z) 155 [$\text{M}-15$] $^+$; Anal. Calcd for $\text{C}_9\text{H}_{14}\text{O}_3$; C, 62.84; H, 8.32. Found; C, 62.78; H, 8.44.

(3*S,4*S**)-8,8-Dimethyl-1,7,9-trioxaspiro[4.5]decane-3,4-diol (12)**. To a solution of **11** (73 mg, 0.43 mmol) and NMO (0.22 mL) in acetone (4 mL), was added a solution of $\text{K}_2\text{OsO}_4 \cdot 2\text{H}_2\text{O}$ (1 mg, 0.004 mmol) in H_2O (0.4 mL) at 0 $^\circ\text{C}$. After stirred at room temperature for 60 h, $\text{Na}_2\text{S}_2\text{O}_3 \cdot 5\text{H}_2\text{O}$ (125 mg) was added and the mixture was stirred at room temperature for 30 min. After the whole mixture was dried over Na_2SO_4 , the solid materials were removed by suction and washed with ethyl acetate. The combined filtrate was concentrated under reduced pressure. The residue was purified by silica gel column chromatography (CHCl_3 –MeOH = 19:1) to give **12** (84 mg, 97%). ^1H -NMR (CDCl_3) δ 1.43 (3H, s), 1.49 (3H, s), 3.59 (1H, dd, J = 11.6, 1.9 Hz), 3.80 (1H, d, J = 9.7 Hz), 3.82–3.87 (2H, m), 3.94 (1H, dd, J = 9.7, 4.9 Hz), 4.14 (1H, dd, J = 11.6, 1.9 Hz), 4.22 (1H, d, J = 5.3 Hz) 4.34 (1H, q, J = 5.0 Hz); ^{13}C -NMR (CDCl_3) δ 21.0, 25.8, 63.3, 66.5, 71.0, 71.4, 74.9, 76.7, 98.4; IR (KBr) 3306.4, 2953.6, 2741.6, 1452.2, 524.19 cm^{-1} ; EI-MS (m/z): 204 [$\text{M}+1$] $^+$; HRMS Calcd for $\text{C}_9\text{H}_{15}\text{N}_3\text{O}_4$: 204.0998, Found: 204.0992.

(3*S,4*S**)-8,8-Dimethyl-1,7,9-trioxaspiro[4.5]decane-3,4-cyclicsulfate (13)**. To a solution of **12** (410 mg, 2.01 mmol) and Et_3N (672 μL , 4.82 mmol) in CH_2Cl_2 (10 mL), was added dropwise a solution of SOCl_2 (113 μL , 1.55 mmol) in CH_2Cl_2 (10 mL) at 0 $^\circ\text{C}$. After stirred at room temperature for 15 min, the mixture was washed with water. The water layer was extracted with CHCl_3 twice and the combined

organic layer was washed with brine, then dried over Na₂SO₄. After filtration, the residue was passed through a short silica gel column (eluate: hexane–ethyl acetate = 1:1). After the solvents were removed under reduced pressure, the residue was dissolved in CCl₄–CH₃CN–H₂O (2:2:3, 3 mL). To this solution, were added RuCl₃·3H₂O (2.7 mg) and NaIO₄ (73 mg, 0.34 mmol) at 0 °C. The mixture was stirred at the same temperature for 1.5 h. After diluted with ether, the mixture was washed with water, sat. NaHCO₃ and brine, then dried over Na₂SO₄. After filtration, the solvents were removed under reduce pressure, the residue was purified by silica gel column chromatography (hexane–ethyl acetate = 6:1) to give **13** (82 mg, 77%). ¹H-NMR (CDCl₃) δ 1.43 (3H, s), 1.50 (3H, s), 3.56 (1H, dd, *J* = 12.1, 2.4 Hz), 3.82 (1H, d, *J* = 12.1 Hz), 3.91 (1H, d, *J* = 12.1 Hz), 3.97 (1H, dd, *J* = 12.6, 4.4 Hz), 4.06 (1H, dd, *J* = 12.1, 2.4 Hz), 4.28 (1H, d, *J* = 12.6 Hz), 5.42 (1H, d, *J* = 6.3 Hz), 5.48 (1H, t, *J* = 5.1 Hz); ¹³C-NMR (CDCl₃) δ 19.6, 27.1, 61.0, 62.4, 69.7, 79.0, 83.3, 84.5, 99.2; IR (KBr) 3000.8, 2892.3, 1699.7, 1380.9, 1089.9 cm^{−1}; EI-MS (*m/z*): 267 [M+1]⁺; HRMS Calcd for C₉H₁₅N₃O₄: 266.0460, Found: 266.0467.

(3*R**,4*S**)-3-Azido-8,8-dimethyl-1,7,9,-trioxaspiro[4.5]decan-4-ol (**18**). A mixture of **7** [11,14] (433 mg, 2.33 mmol) and NaN₃ (752 mg 11.6 mmol) in 2-methoxyethanol (26 mL) was kept at 100 °C for 5 h. After the solvent was removed under reduced pressure, the residue was dissolved in ethyl acetate. After washed with water and brine, the organic layer was dried over Na₂SO₄. After filtration, the solvents were removed under reduce pressure, the residue was purified by silica gel column chromatography (hexane–ethyl acetate = 5:1) to give **18** (351 mg, 66%). ¹H-NMR (CDCl₃) δ 1.40 (3H, s), 1.49 (3H, s), 3.69–3.80 (3H, m), 3.84 (1H, d, *J* = 11.6 Hz), 4.01–4.08 (3H, m), 4.38 (1H, t, *J* = 1.9, 2.4 Hz); ¹³C-NMR (CDCl₃) δ 19.5, 27.4, 62.3, 66.0, 67.6, 69.4, 78.2, 79.1, 98.5; IR (neat) 3419.0, 2104.8, 1086.6, 831.7 cm^{−1}; EI-MS (*m/z*): 229 [M+1]⁺; HRMS Calcd for C₉H₁₅N₃O₄: 229.1063, Found: 229.1062.

(3*R**,4*S**)-3-Azido-8,8-dimethyl-1,7,9,-trioxaspiro[4.5]decan-4-yl benzoate (**19**). To a solution of **18** (432 mg, 1.88 mmol), Et₃N (0.59 mL, 4.24 mmol), and DMAP (23 mg, 0.19 mmol) in CH₂Cl₂ (15 mL) was added benzoyl chloride (0.40 mL, 3.39 mmol) and the mixture was stirred at room temperature for 6.5 h. The reaction was quenched by addition of MeOH, and the whole was stirred at room temperature for 10 min. The mixture was diluted with CH₂Cl₂ and washed with water and brine, then dried over Na₂SO₄. After filtration, the solvents were removed under reduce pressure, the residue was purified by silica gel column chromatography (hexane–ethyl acetate = 4:1) to give **19** (598 mg, 95%). ¹H-NMR (CDCl₃) δ 1.37 (3H, s), 1.47 (3H, s), 3.84–3.91 (3H, m), 3.99 (1H, dd, *J* = 1.4, 10.6 Hz), 4.07 (1H, dd, *J* = 1.4, 10.6 Hz), 4.18–4.25 (2H, m), 5.47 (1H, d, *J* = 1.0 Hz), 7.48 (2H, t, *J* = 7.2 Hz), 7.62 (1H, *J* = 7.2 Hz), 8.03 (2H, *J* = 7.2 Hz); ¹³C-NMR (CDCl₃) δ 22.4, 24.2, 62.1, 65.0, 66.2, 69.9, 78.9, 79.2, 98.4, 128.6, 129.0, 129.6, 133.6, 165.3; IR (neat) 2993.1, 2107.2, 1725.4, 1267.4, 1091.3, 711.5 cm^{−1}; EI-MS (*m/z*): 333 [M]⁺; HRMS Calcd for C₁₆H₁₉N₃O₅: 333.1325, Found: 333.1336.

(3*S**,4*R**)-4-Azido-2,2-bis((methylsulfonyloxy)methyl)tetrahydrohuran-3-yl benzoate (**20**). A mixture of **19** (1.01 g, 3.04 mmol) in 80% AcOH (80 mL) was stirred at room temperature for 5 h. After the solvent was removed under reduced pressure, the residue was co-evaporated with EtOH five times to remove residual AcOH. The resulting crude product was dissolved in CH₂Cl₂ (40 mL). To this mixture, were added, MsCl (1.19 mL, 15.18 mmol), Et₃N (2.14 mL, 15.18 mmol), and DMAP (38 mg,

0.30 mmol). After stirred at room temperature for 1 h, the mixture was diluted with CH₂Cl₂ washed with 5% HCl, sat. NaHCO₃ and brine. The separated organic layer was dried over Na₂SO₄. After filtration, the solvents were removed under reduced pressure, the residue was purified by silica gel column chromatography (hexane–ethyl acetate = 2:1) to give **20** (1.05 g, 77%). ¹H-NMR (CDCl₃) δ 3.00 (3H, s), 3.12 (3H, s), 3.94 (1H, dd, *J* = 5.80, 4.37 Hz), 4.33–4.48 (6H, m), 5.48 (1H, d, *J* = 3.4 Hz), 7.50 (2H, t, *J* = 7.7 Hz), 7.64 (1H, t, *J* = 8.0 Hz), 8.04 (2H, d, *J* = 7.3 Hz); ¹³C-NMR (CDCl₃) δ 37.7, 65.5, 65.8, 67.4, 70.3, 77.2, 78.9, 82.8, 128.1, 128.8, 129.9, 134.2, 165.2; IR (neat) 2110.7, 1728.8, 1360.0, 1267.0 cm^{−1}; FAB-MS (*m/z*): 450 [M+1]⁺; HRMS Calcd for C₁₅H₂₀N₃O₉S₂: 450.0641, Found: 450.0631.

((1*R**,4*R**,5*S**)-4-Azido-2,6-dioxabicyclo[3.2.0]heptan-1-yl)methyl methanesulfonate (**21**). A mixture of **20** (36 mg, 0.08 mmol) and NaOCH₃ (4.6 mg, 0.08 mmol) in MeOH (2 mL) was kept at 75 °C overnight. After the solvent was removed under reduced pressure, the residue was dissolved in CHCl₃ and washed with water and brine, then dried over Na₂SO₄. After filtration, the solvents were removed under reduced pressure, the residue was purified by silica gel column chromatography (hexane–ethyl acetate = 2:1) to give **21** (14 mg, 72%). ¹H-NMR (CDCl₃) δ 3.09 (3H, s), 4.05 (1H, d, *J* = 3.4 Hz), 3.40 (1H, d, *J* = 11.1 Hz), 4.29–4.77 (4H, m), 4.76 (1H, d, *J* = 8.2 Hz), 5.06 (1H, s); ¹³C-NMR (CDCl₃) δ 37.8, 63.6, 67.4, 71.9, 77.1, 84.4, 89.9; IR (neat) 2098.2, 1360.4, 1175.0, 960.2, 815.5 cm^{−1}; FAB-MS (*m/z*): 250 [M+1]⁺; HRMS Calcd for C₇H₁₂N₃O₅S: 250.0498, Found: 250.0490.

((1*R**,4*R**,5*S**)-4-Azido-2,6-dioxabicyclo[3.2.0]heptan-1-yl)methyl benzoate (**22**). A mixture of CsF (332 mg, 2.19 mmol) and PhCOOH (267 mg, 2.19 mmol) in DMF (40 mL) was stirred at room temperature for 20 min. To this mixture was added a solution of **21** (182 mg, 0.73 mmol) in DMF (20 mL). After stirred at 60 °C overnight, the mixture was partitioned between EtOAc and H₂O. The separated water layer was extracted with EtOAc, and the organic layer was washed with sat. NaHCO₃, brine, then dried over Na₂SO₄. After filtration, the filtrate was concentrated under reduced pressure. The residue was purified by silica gel column chromatography (hexane–ethyl acetate = 5:1) to give **22** (170 mg, 86%). ¹H-NMR (CDCl₃) δ 4.08 (1H, d, *J* = 3.4 Hz), 4.42 (1H, d, *J* = 10.6 Hz), 4.52 (2H, dd, *J* = 10.6, 3.4 Hz), 4.60 (2H, s), 4.83 (1H, d, *J* = 7.7 Hz), 5.15 (1H, s), 7.61 (2H, t, *J* = 15.5 Hz), 7.59 (1H, t, *J* = 17.4 Hz), 8.10 (2H, d, *J* = 9.7 Hz); ¹³C-NMR (CDCl₃) δ 63.1, 63.8, 71.5, 77.8, 85.1, 90.4, 128.4, 129.4, 129.7, 133.3, 166.1; IR (neat) 2099.7, 1723.1, 1284.3, 713.4 cm^{−1}; FAB-MS (*m/z*): 276 [M+1]⁺; HRMS Calcd for C₁₃H₁₄N₃O₄: 276.0984, Found: 276.0977.

((1*S**,4*R**,5*S**)-4-Azido-2,6-dioxabicyclo[3.2.0]heptan-1-yl)methanol (**23**). A mixture of **22** (184 mg, 0.67 mmol) and NaOCH₃ (19 mg, 0.33 mmol) in MeOH (15 mL) was stirred at room temperature. After the mixture was neutralized with AcOH (19 μL), the solvents were removed under reduced pressure and the residue was purified by silica gel column chromatography (hexane–ethyl acetate = 4:1) to give **23** (90 mg, 79%). ¹H-NMR (CDCl₃) δ 3.91 (2H, d, *J* = 6.3 Hz), 4.04 (1H, d, *J* = 3.9 Hz), 4.36 (1H, d, *J* = 10.6 Hz), 4.48 (2H, dd, *J* = 10.6, 3.4 Hz), 4.48 (1H, d, *J* = 8.2 Hz), 4.68 (1H, d, *J* = 8.2 Hz), 5.05 (1H, s); ¹³C-NMR (CDCl₃) δ 62.3, 64.0, 71.5, 77.6, 86.9, 90.2; IR (neat) 3431.5, 2101.6, 1248.2, 870.88 cm^{−1}; EI-MS (*m/z*): 171 [M]⁺; HRMS Calcd for C₆H₉N₃O₃: 171.0644, Found: 171.0643.

((1*S**,4*R**,5*S**)-4-(5-Amino-6-chloropyrimidin-4-ylamino)-2,6-dioxo-bicyclo[3.2.0]heptan-1-yl)methanol (**15**). A mixture of **23** (69 mg, 0.40 mmol) and Pd(OH)₂ (6.2 mg, 0.04 mmol) in MeOH (5 mL) was stirred at room temperature overnight under H₂ atmosphere. After insoluble materials were removed by filtration, the solvents were removed under reduced pressure. The resulting crude product was dissolved in *n*-BuOH (3 mL). To this mixture, were added 5-amino-4,6-dichloropyrimidine (140.1 mg, 0.86 mmol) and *i*-Pr₂NEt (298 µL, 1.71 mmol). The mixture was kept under reflux overnight. After the solvents were removed under reduced pressure, the residue was purified by silica gel column chromatography (chloroform–methanol = 19:1) to give **15** (64 mg, 58%). ¹H-NMR (CD₃OD) δ 3.67 (2H, q, *J* = 12.6 Hz), 4.24 (1H, d, *J* = 10.1 Hz), 4.38 (1H, d, *J* = 7.7 Hz), 4.45 (1H, d, *J* = 4.4 Hz), 4.50 (1H, d, *J* = 10.1, 4.4 Hz), 4.63 (1H, d, *J* = 7.2 Hz), 4.90 (1H, s), 7.72 (1H, s); ¹³C NMR (CD₃OD) δ 58.1, 58.3, 62.7, 73.1, 88.3, 92.1, 125.5, 138.9, 147.3, 153.3; IR (KBr) 3381.3, 2926.7, 1578.6, 1056.3 cm⁻¹; EI-MS (*m/z*): 272 [M]⁺; HRMS Calcd for C₁₀H₁₃ClN₄O₃: 272.0676, Found: 272.0673.

((1*S**,4*R**,5*S**)-4-(6-Chloro-9H-purin-9-yl)-2,6-dioxo-bicyclo[3.2.0]heptan-1-yl)methanol (**24**). To a solution of **15** (18 mg, 0.07 mmol) in DMF (0.5 mL), were added orthoethyl formate (0.7 mL, 4.21 mmol) and *conc* HCl (2 µL, 0.024 mmol) at 0 °C. After the mixture was stirred at room temperature, the solvents were removed under reduced pressure. The residue was dissolved in 0.5 M aqHCl (1 mL) and the mixture was stirred at room temperature for 1 h. The mixture was neutralized with 1M aqNaOH (0.5 mL) and concentrated under reduced pressure. The residue was extracted with a solution of chloroform–methanol = 1:1. After the insoluble materials were removed by filtration, the solvents were removed under reduced pressure. The residue was purified by *p*TLC (developed by chloroform-methanol = 5:1) to give **24** (14.9 mg, 81%). ¹H-NMR (CDCl₃) δ 4.12 (2H, q, *J* = 12.6 Hz), 4.59 (1H, d, *J* = 11.6 Hz), 4.66 (1H, d, *J* = 9.7 Hz), 4.68 (1H, d, *J* = 9.7 Hz), 4.66 (1H, d, *J* = 9.7 Hz), 4.90 (1H, dd, *J* = 11.1, 4.8 Hz), 5.24 (1H, s), 5.38 (1H, d, *J* = 4.4 Hz), 8.68 (1H, s), 8.76 (1H, s); ¹³C-NMR (CDCl₃-CD₃OD = 19 : 1) δ 58.6, 61.2, 71.9, 77.2, 87.8, 90.9, 130.7, 144.6, 150.7, 151.2, 151.8; IR (KBr) 3401.4, 2931.1, 1597.4, 1567.4, 1056.6 cm⁻¹; EI-MS (*m/z*): 282 [M]⁺; HRMS Calcd for C₁₁H₁₁ClN₄O₃: 282.0520, Found: 282.0506.

((1*S**,4*R**,5*S**)-4-(6-Amino-9H-purin-9-yl)-2,6-dioxo-bicyclo[3.2.0]heptan-1-yl)methanol (**6**). Compound **24** (29.4 mg, 0.10 mmol) was dissolved in *sat.* methanolic ammonia (7 mL) and the mixture was kept at 100 °C for 21 h in a glass sealed tube. After the solvents were removed under reduced pressure, the residue was purified by *p*TLC (developed by chloroform–methanol = 5:1) to give **6** (18.8 mg, 69%). ¹H-NMR (CDCl₃-CD₃OD = 17:3) δ 3.91 (1H, d, *J* = 12.6 Hz), 4.00 (1H, d, *J* = 12.1 Hz), 4.57 (1H, d, *J* = 10.6 Hz), 4.64 (1H, d, *J* = 7.7 Hz), 4.70 (1H, d, *J* = 7.7 Hz), 4.87 (1H, dd, *J* = 11.1, 4.8 Hz), 5.19 (1H, s), 5.25 (1H, d, *J* = 4.8 Hz), 8.25 (1H, s), 8.28 (1H, s); ¹³C-NMR (CDCl₃-CD₃OD = 17:3) δ 29.5, 58.3, 61.3, 72.1, 87.6, 91.0, 118.2, 139.1, 148.9, 152.6, 155.3; IR (KBr) 3192.2, 2409.9, 1660.5, 1615.0, 1054.9 cm⁻¹; EI-MS (*m/z*): 263 [M]⁺; HRMS Calcd for C₁₁H₁₃N₅O₃: 263.1018, Found: 263.1021.

4. Conclusions

We constructed an isoadenosine derivative on a 2,6-dioxobicyclo[3.2.0]heptane scaffold. Since our initial attempt to synthesize **6** by directly introducing the adenine moiety was not successful, we

synthesized it by the de novo synthesis of an adenine ring on a pseudosugar moiety. However, this unique adenosine analogue showed no activity against HIV. Previously, we have reported that neither thymine nor adenine analogues **4** built on a 2-oxa-6-thiabicyclo[3.2.0]heptane skeleton inhibit HIV [14]. The structural rigidities of these analogues and isoadenosine **6** due to the introduction of fused thietane and oxetane rings, respectively, appear to inhibit anti-HIV activity. In particular, phosphorylation at the 5'-hydroxyl group would be inhibited since deoxynucleoside kinase recognizes the puckering of sugars [25]. Thus, we are currently preparing new substituted nucleoside derivatives based on **4** and **6**, and the results will be reported elsewhere.

Acknowledgments

This work was supported in part by a Grant-in-Aid for Scientific Research (No. 24590143, Y.Y.) from JSPS and by a grant of Strategic Research Foundation Grant-aided Project for Private Universities from Ministry of Education, Culture, Sport, Science, and Technology, Japan (MEXT), 2010–2014.

Author Contributions

YY and TI designed research; SK, HK and TS performed the synthesis of compounds and TI assayed anti-HIV activity. YY wrote the paper. All authors read and approved the final manuscript.

Conflicts of Interest

The authors declare no conflict of interest.

References

1. Cihlar, T.; Ray, A.S. Nucleoside and nucleotide HIV reverse transcriptase inhibitors: 25 years after zidovudine. *Antivir. Res.* **2010**, *85*, 39–58.
2. Mehellou, Y.; de Clercq, E. Twenty-six years of anti-HIV drug discovery: Where do we stand and where do we go? *J. Med. Chem.* **2010**, *53*, 521–538.
3. WHO. Consolidated Guidelines on the Use of Antiretroviral Drugs for Treating and Preventing HIV Infection. Available online: <http://www.who.int/hiv/pub/guidelines/arv2013/download/en/> (accessed on 30 June 2013).
4. Meadows, D.C.; Gervy-Hague, J. Current developments in HIV chemotherapy. *ChemMedChem* **2006**, *1*, 16–29.
5. Imamichi, T. Action of anti-HIV drugs and resistance: Reverse transcriptase inhibitors and protease inhibitors. *Curr. Pharm. Des.* **2004**, *10*, 4039–4053.
6. Mitsuya, H.; Broder, S. Inhibition of the *in vitro* infectivity and cytopathic effect of human T-lymphotrophic virus type III/lymphadenopathy-associated virus (HTLV-III/LAV) by 2',3'-dideoxynucleosides. *Proc. Natl. Acad. Sci. USA* **1986**, *83*, 1911–1915.
7. Mitsuya, H.; Weinhold, K.J.; Furman, P.A.; St Clair, M.H.; Lehrman, S.N.; Gallo, R.C.; Bolognesi, D.; Barry, D.W.; Broder, S. 3'-Azido-3'-deoxythymidine (BW A509U): An antiviral agent that inhibits the infectivity and cytopathic effect of human T-lymphotropic virus type III/lymphadenopathy-associated virus *in vitro*. *Proc. Natl. Acad. Sci. USA* **1985**, *82*, 7096–7100.

8. Schinazi, R.F.; Chu, C.K.; Peck, A.; McMillan, A.; Mathis, R.; Cannon, D.; Jeong, L.S.; Beach, J.W.; Choi, W.B.; Yeola, S.; *et al.* Activities of the four optical isomers of 2',3'-dideoxy-3'-thiacytidine (BCH-189) against human immunodeficiency virus type 1 in human lymphocytes. *Antimicrob. Agents Chemother.* **1992**, *36*, 672–676.
9. Balzarini, J.; Holy, A.; Jindrich, J.; Naesens, L.; Snoeck, R.; Schols, D.; de Clercq, E. Differential antiherpesvirus and antiretrovirus effects of the (*S*) and (*R*) enantiomers of acyclic nucleoside phosphonates: Potent and selective *in vitro* and *in vivo* antiretrovirus activities of (*R*)-9-(2-phosphonomethoxypropyl)-2,6-diaminopurine. *Antimicrob. Agents Chemother.* **1993**, *37*, 332–338.
10. Yoshimura, Y.; Yamazaki, Y.; Kawahata, M.; Yamaguchi, K.; Takahata, H. Design and synthesis of a novel ring-expanded 4'-Thio-*apio*-nucleoside derivatives. *Tetrahedron Lett.* **2007**, *48*, 4519–4522.
11. Yoshimura, Y.; Asami, K.; Matsui, H.; Tanaka, H.; Takahata, H. New synthesis of (\pm)-isonucleosides. *Org. Lett.* **2006**, *8*, 6015–6018.
12. Yoshimura, Y.; Yamazaki, Y.; Saito, Y.; Takahata, H. Synthesis of 1-(5,6-dihydro-2H-thiopyran-2-yl)uracil by a Pummerer-type thioglycosylation reaction: The regioselectivity of allylic substitution. *Tetrahedron* **2009**, *65*, 9091–9102.
13. Yoshimura, Y.; Ohta, M.; Imahori, T.; Imamichi, T.; Takahata, H. A new entry to carbocyclic nucleosides: Oxidative coupling reaction of cycloalkenylsilanes with a nucleobase mediated by hypervalent iodine reagent. *Org. Lett.* **2008**, *10*, 3449–3452.
14. Yoshimura, Y.; Asami, K.; Imamichi, T.; Okuda, T.; Shiraki, K.; Takahata, H. Design and synthesis of isonucleosides constructed on a 2-oxa-6-thiabicyclo[3.2.0]heptane scaffold. *J. Org. Chem.* **2010**, *75*, 4161–4171.
15. Yoshimura, Y.; Yamazaki, Y.; Saito, Y.; Natori, Y.; Imamichi, T.; Takahata, H. Synthesis of 5-thiodidehydropyranylcytosine derivatives as potential anti-HIV agents. *Bioorg. Med. Chem. Lett.* **2011**, *21*, 3313–3316.
16. Kiran, Y.B.; Wakamatsu, H.; Natori, Y.; Takahata, H.; Yoshimura, Y. Design and synthesis of a nucleoside and a phosphonate analogue constructed on a branched-*threo*-tetrofurranose skeleton. *Tetrahedron Lett.* **2013**, *54*, 3949–3952.
17. Kan-no, H.; Saito, Y.; Omoto, S.; Minato, S.; Wakamatsu, H.; Natori, Y.; Imamichi, T.; Takahata, H.; Yoshimura, Y. Synthesis of a dihydropyranonucleoside using an oxidative glycosylation reaction mediated by hypervalent iodine. *Synthesis* **2014**, *46*, 879–886.
18. Chu, C.K.; Ahn, S.K.; Kim, H.O.; Beach, J.W.; Alves, A.J.; Jeong, L.S.; Islam, Q.; van Roey, P.; Schinazi, R.F. Asymmetric synthesis of enantiomerically pure (–)-(1'*R*,4'*R*)-dioxolane-thymine and its anti-HIV activity. *Tetrahedron Lett.* **1991**, *32*, 3791–3794.
19. Kim, H.O.; Schinazi, R.F.; Nampalli, S.; Shanmuganathan, K.; Cannon, D.L.; Alves, A.J.; Jeong, L.S.; Beach, J.W.; Chu, C.K. 1,3-dioxolanylpurine nucleosides (2*R*,4*R*) and (2*R*,4*S*) with selective anti-HIV-1 activity in human lymphocytes. *J. Med. Chem.* **1993**, *36*, 30–37.
20. Kim, H.O.; Schinazi, R.F.; Shanmuganathan, K.; Jeong, L.S.; Beach, J.W.; Nampalli, S.; Cannon, D.L.; Chu, C.K. L-beta-(2*S*,4*S*)- and L-alpha-(2*S*,4*R*)-dioxolanyl nucleosides as potential anti-HIV agents: Asymmetric synthesis and structure-activity relationships. *J. Med. Chem.* **1993**, *36*, 519–528.

21. Choi, Y.; George, C.; Comin, M.J.; Brachi, J.J.; Kim, H.S.; Jacobsen, K.A.; Balzarini, J.; Mitsuya, H.; Boyer, P.L.; Hughes, S.H.; *et al.* A conformationally locked analogue of the anti-HIV agent stavudine. An important correlation between pseudorotation and maximum amplitude. *J. Med. Chem.* **2003**, *46*, 3292–3299.
22. D'Alonzo, D.; van Aerschot, A.; Guaragna, A.; Palumbo, G.; Schepers, G.; Capone, S.; Rozenski, J.; Herdewijn, P. Synthesis and base pairing properties of 1',5'-anhydro-L-hexitol nucleic acids (L-HNA). *Chem. Eur. J.* **2009**, *15*, 10121–10131.
23. Bera, S.; Nair, V. A new general synthesis of isomeric nucleosides. *Tetrahedron Lett.* **2001**, *42*, 5813–5815.
24. Quadrelli, P.; Piccanello, A.; Mella, M.; Corsaro, A.; Pistarà, V. From cyclopentadiene to isoxazoline-carbocyclic nucleosides: A rapid access to biological molecules through aza-Diels-Alder reactions. *Tetrahedron* **2008**, *64*, 3541–3547.
25. Comin, M.J.; Vu, B.C.; Boyer, P.L.; Liao, C.; Hughes, S.H.; Marquez, V.E. D-(+)-iso-methanocarbothymidine: A high-affinity substrate for herpes simplex virus 1 thymidine kinase. *ChemMedChem* **2008**, *3*, 1129–1134.

Sample Availability: Sample of the final compound is available from the authors. About the other compounds, please contact the authors.

© 2015 by the authors; licensee MDPI, Basel, Switzerland. This article is an open access article distributed under the terms and conditions of the Creative Commons Attribution license (<http://creativecommons.org/licenses/by/4.0/>).

Simultaneous evaluation of human CYP3A4 and ABCB1 induction by reporter assay in LS174T cells, stably expressing their reporter genes

Keita Inami, Takamitsu Sasaki, Takeshi Kumagai, and Kiyoshi Nagata*

Department of Environmental and Health Science, Tohoku Pharmaceutical University, Sendai, Japan

ABSTRACT: The bioavailability of orally administered therapies are often significantly limited in the human intestine by the metabolic activities of cytochrome P450 3A4 (CYP3A4) and P-glycoprotein (P-gp). Predicting whether candidate compounds induce CYP3A4 and P-gp is a crucial stage in the drug development process, as drug–drug interactions may result in the induction of intestinal CYP3A4 and P-gp. However, the assay systems needed to evaluate both CYP3A4 and P-gp induction in the intestine are yet to be established. To address this urgent requirement, LS174T cells were used to create two stable cell lines expressing the *CYP3A4* or *ATP-binding cassette subfamily B member 1* (*ABCB1*, encoding P-gp) reporter genes. First, these stable cells were tested by treatment with 1 α ,25-dihydroxyvitamin D₃ (1,25(OH)₂D₃), all-*trans*-retinoic acid (ATRA) and 9-*cis*-retinoic acid (9-*cis* RA) that induce CYP3A4 and P-gp in the intestines. All these compounds significantly increased both *CYP3A4* and *ABCB1* reporter activities in the stable cell lines. To simultaneously assess the induction of *CYP3A4* and *ABCB1*, both stable cells were co-cultivated to measure their reporter activities. The mixed cells showed a significant increase in the *CYP3A4* and *ABCB1* reporter activities following treatment with 1,25(OH)₂D₃, ATRA, and 9-*cis* RA. These activity levels were maintained after passaging more than 20 times and following multiple freeze–thaw cycles. These results demonstrate that our established cell lines can be used to evaluate simultaneously *CYP3A4* and *ABCB1* induction in the intestines, providing a valuable *in vitro* model for the evaluation of future drug candidates. Copyright © 2014 John Wiley & Sons, Ltd.

Key words: CYP3A4; P-gp; stable cell line; LS174T; reporter assay

Introduction

Cytochrome P450 (CYP) plays important roles in the metabolism of various xenobiotics and endogenous compounds [1]. Of the CYPs isoforms, CYP3A4 is the most abundant, found in the adult human liver and small intestines. It is estimated that hepatic and intestinal CYP3A4 activity metabolizes approximately half of the prescribed drugs

used today [2–4]. In addition to CYP, the ATP dependent efflux transporter, P-glycoprotein (P-gp) has a crucial role in limiting intracellular drug concentrations, therefore reducing the bioavailability of many prescribed drugs [5]. P-gp, also known as the multi-drug resistance protein 1, is encoded by the *ATP-binding cassette subfamily B member 1* gene (*ABCB1*) and is expressed in various tissues including the liver, small intestine, the blood–brain barrier, kidney and the adrenal glands [6].

Both CYP3A4 and P-gp contribute significantly in limiting the bioavailability of orally administered drugs. This is due to similar substrate specificities, as well as to high levels of expression in

*Correspondence to: Department of Environmental and Health Science, Tohoku Pharmaceutical University, 4-4-1, Komatsushima, Aoba-ku, Sendai 981-8558, Japan.
E-mail: nagataki@tohoku-pharm.ac.jp

the liver and small intestine [7]. Furthermore, the expression of CYP3A4 and P-gp is often induced simultaneously by many drug therapies [8]. To date, many researchers have reported clinically relevant drug–drug interactions, mediated through CYP3A4 and/or P-gp [9,10]. It is therefore important in the drug development process, to consider whether candidate compounds induce CYP3A4 and ABCB1 expression.

Recently, studies have shown that expression of the CYP3A4 and ABCB1 genes are regulated by nuclear receptors, such as the pregnane X receptor (PXR), constitutive androstane receptor, and the vitamin D receptor (VDR) [11–13]. Nuclear receptors are ligand-activated transcription factors, which mediate the body's defense mechanism against toxic compounds and xenobiotics. The PXR is activated by a broad spectrum of xenobiotics and plays a key role in mediating the body's defense mechanism against toxic substances, including prescription drugs. Upon ligand-binding, the PXR receptor is translocated to the nucleus where it forms a heterodimer with the retinoid X receptor α [14]. The heterodimer then binds to the regulatory *cis*-elements, which specifically activates a number of genes involved in xenobiotic elimination that include CYP3A4. Hepatic and intestinal induction of CYP3A4 and P-gp occurs via different ligand-specific, receptor-defined pathways. For example, rifampicin activation of PXR, mediates transactivation of the CYP3A4 predominantly in the liver. However, 1 α ,25-dihydroxyvitamin D₃ (1,25(OH)₂D₃), mediates activation of the VDR, resulting in intestinal transactivation of CYP3A4 [15]. As with CYP3A4, the induction of P-gp in the liver and intestine also occurs via different pathways. This is because the expression of PXR is higher than VDR in the liver; however, VDR expression is higher than PXR in the intestines [16]. Consequently, the expression profiles for nuclear receptors would need to be considered, when selecting a suitable cell line for evaluating intestinal CYP3A4 and P-gp induction. Several *in vitro* systems exist for the assessment of CYP3A4 and P-gp induction in the liver [17–19]. However, an *in vitro* system for evaluating the effect of drug absorption on intestinal CYP3A4 and P-gp induction has yet to be established.

A reporter gene under the control of the CYP3A4 and ABCB1 regulatory regions provides

a rapid and sensitive expression system. However, a plasmid based reporter system is both time-consuming and cost-intensive, because transient transfection of the reporter plasmid is required before each experiment. In addition, the data from these experiments often vary, due to variations in the transfection efficiency. To solve this problem several research groups, including our own, have developed a stable reporter CYP gene expression system, constructed by inserting the reporter gene into the chromosomes of HepG2 cells [20–22]. The reporter cell lines have the advantage of being easily maintained and readily available, as well as increasing experimental reproducibility in comparison with the transient expression systems.

In this study, two stable cell lines were established, expressing chromosomally integrated reporter genes driven by CYP3A4 and ABCB1 regulatory regions. The stable cell lines are termed 1-2-10 and 3-13, respectively, and were generated using LS174T. The utility of these stable gene reporter systems was demonstrated, using the CYP3A4 and ABCB1 inducers, 1,25(OH)₂D₃, 9-*cis*-retinoic acid (9-*cis* RA), and all-*trans*-retinoic acid (ATRA) [18,23]. Our results clearly demonstrate a highly sensitive and reproducible expression system for measuring the induction response for both CYP3A4 and ABCB1. It is concluded that these two cell lines provide a rapid and reproducible assay for identifying compounds that simultaneously induce CYP3A4 and ABCB1.

Materials and Methods

Materials

The 1,25(OH)₂D₃ was purchased from Sigma-Aldrich (St Louis, MO). The 9-*cis* RA and ATRA were purchased from Wako Pure Chemicals (Osaka, Japan). Dimethyl sulfoxide (DMSO) was obtained from Nacalai Tesque (Kyoto, Japan). Oligonucleotides were commercially synthesized by Fasmac (Atsugi, Japan).

Construction of the reporter plasmids

The reporter plasmid pGL3-CYP3A4-362-7.7 k for the human CYP3A4 gene was described previously [21]. The pGL3-CYP3A4-362-7.7 k includes the promoter region (–362 bp to +11 bp) and distal

nuclear receptor binding elements (−7836 bp to −7208 bp) of the human *CYP3A4* gene derived from human liver. The reporter plasmid of the human *ABCB1* gene was constructed using the p-8935 construct that was reported by Tachibana *et al.* [24]. Briefly, the p-8935 construct, which included the 5'-untranslated region of the *ABCB1* gene from −8935 bp to +126 bp, was digested with *SpeI* and *AatII* (Takara Bio, Otsu, Japan), and the region between the enhancer region (from −8935 bp to −7472 bp) and the promoter region (from −601 bp to +126 bp) was removed and then both regions were directly ligated. The obtained construct pSEAP2-ABCB1-601-(9-7.5 k) and pGL4.70[hRluc] vector (Promega, Madison, MI) were digested with *Acc65I* (New England Biolabs, Ipswich, MA) and *HindIII* (Nippon Gene, Tokyo, Japan). These digested constructs were ligated together to obtain the construct pGL4.70-ABCB1-601-(9-7.5 k).

Generation of stable cell lines

In order to generate a ligation for transfection, the reporter plasmids pGL3-CYP3A4-362-7.7 k, pGL4.70-ABCB1-601-(9-7.5 k) were linearized with *BamHI* and *BglII* (Nippon Gene, Tokyo, Japan). The pQBI plasmid (Wako Pure Chemicals) was also linearized with *BamHI* and *BglII* resulting in a 4500 bp fragment, which included the neomycin resistance gene. The reporter plasmid fragments were ligated into the linearized pQBI plasmid, using the DNA ligation kit ver. 2.1 (Takara Bio). The human colon adenocarcinoma cell line, LS174T was obtained from the Institute of Development, Aging and Cancer, Tohoku University (Sendai, Japan). The cells were cultured under 5% CO₂ at 37°C in Eagle's minimum essential medium (EMEM, Wako Pure Chemicals), supplemented with 10% fetal bovine serum (FBS, Biowest, Miami, FL) and Antibiotic-Antimycotic (Invitrogen, Carlsbad, CA). The cells were seeded in 6-well tissue culture plates (BD Biosciences, Heidelberg, Germany) at 3×10^5 cells per well, one day before transfection. The ligation fragments were transfected using Targefect F-1 (Targeting Systems, El Cajon, CA), according to the manufacturer's instructions. After a 2-week incubation, the cells were selected with 500 µg/mL geneticin (G418, Invitrogen). The positive colonies were further subcloned into 24-well tissue culture plates (BD Biosciences) to obtain monoclonal cells.

G418-resistant clones were chosen for induction testing by treating the cells with 10 nM 1,25(OH)₂D₃. The induction response was measured by the luciferase assay. Clones exhibiting the strongest induction response of *CYP3A4* and *ABCB1* were termed 1-2-10 cells and 3-13 cells, respectively.

Cell culture and cell extract

The stable cells were cultured in EMEM (Wako Pure Chemicals) containing 10% FBS (Biowest) and the Antibiotic-Antimycotic (Invitrogen). The cells were seeded in 48-well tissue culture plates (BD Biosciences) at 8×10^4 cells per well in 0.2 mL EMEM. After 24 h, the cell medium was changed with the medium containing various drugs dissolved in DMSO (final concentration, 0.1%). The control cells were treated with 0.1% DMSO. After 6–48 h exposure to various drugs, the cells were washed twice with Dulbecco's phosphate buffered saline and suspended in 50 µL of passive lysis buffer (Promega). The cell suspension was centrifuged at 2000 rpm for 10 min at 4°C. The supernatant was processed for luciferase assay and determination of protein concentration. The protein concentration was measured using the Bio-Rad protein assay (Bio-Rad Laboratories, Hercules, CA).

Luciferase assay

The luciferase assay system (Promega) and the *Renilla* luciferase assay system (Promega) were used for 1-2-10 and 3-13 cells according to the manufacturer's instructions. The luciferase activity was normalized to the total protein content and expressed as a ratio of the luminescence of 0.1% DMSO-treated cells. The luminescence obtained from reaction of the luciferase assay was then monitored by a GlomaxTM 96 microplate luminometer (Promega). Simultaneous measurement of firefly and *Renilla* luciferase activity was performed using the dual-luciferase reporter assay system (Promega) according to the manufacturer's instructions.

RNA purification and real-time PCR

Total RNA was extracted using TRI reagent (Molecular Research Center, Cincinnati, OH). First-strand cDNA was synthesized from 1 µg total RNA in a 25 µL reaction mixture using Moloney murine leukemia virus reverse transcriptase

(Promega), oligo(dT)₂₀ primer and recombinant RNase inhibitor (Takara Bio). The cDNA was used as a template for real-time PCR using SYBR Premix Ex Taq (Takara Bio) to measure the expression levels of *CYP3A4* and *ABCB1*. The control used for all real-time PCR analysis was the *GAPDH* gene, which encodes glyceraldehyde-3-phosphate dehydrogenase. The amplification reactions were performed with the following specific primers: *CYP3A4* (forward: 5'-CTGTGTGTTTCCAAGAGAAGTTAC-3' and reverse: 5'-TGCATCAATTCCTCCTGCAG-3'), *ABCB1* (forward: 5'-GCCAAAGCCAAAATATCAGC-3' and reverse: 5'-TTCCAATGTGTTTCGGCATTA-3'), and *GAPDH* (forward: 5'-CATGGGTGTGAACCATGAGAA-3' and reverse: 5'-GGTCATGAGTCCTTCACGAT-3'). Quantitative values were obtained above the threshold PCR cycle number (Ct) at which an increase in signal associated with an exponential growth in PCR products was detected using Thermal Cycler Dice™ TP800 (Takara Bio). Relative mRNA expression levels for each sample were obtained using the 2- $\Delta\Delta C_t$ method, normalized to *GAPDH* expression levels.

Statistical analysis

Data were evaluated using the paired Student's *t*-test. Values of *p* < 0.05 were considered statistically significant.

Results

Dose-dependent induction of the *CYP3A4* and *ABCB1* reporter genes by 1,25(OH)₂D₃

The two stable cell lines, 1-2-10 and 3-13, were constructed by inserting the *CYP3A4* and *ABCB1* reporter plasmids, into the chromosomes of LS174T cells. To characterize the isolated stable cell lines, a dose-dependent induction of reporter activity was measured. The reporter activity for *CYP3A4* and *ABCB1* was determined at four time intervals, 6, 12, 24, and 48 h, following the addition of 1,25(OH)₂D₃ to the culture medium at concentrations in the range 1–100 nM and 3–500 nM. The results show a dose-dependent increase in the luciferase activity for both the *CYP3A4* and *ABCB1* reporter plasmids, in response to increasing concentrations of 1,25(OH)₂D₃ (Figure 1). The response peaked at 24 h, and thereafter the level decreased. The maximum induction of *CYP3A4* reporter activity occurred when the 1-2-10 cells were exposed to 100 nM of 1,25(OH)₂D₃ for 24 h. This resulted in an 80-fold increase in the reporter gene activity when compared with the control (Figure 1A). The *CYP3A4* reporter activity was readily detectable in the 1-2-10 cells, even when a low concentration of 1,25(OH)₂D₃ (1 nM) for 24 h was used (Figure 1A). A maximum increase in *ABCB1* reporter activity was seen when the 3-13 cells were treated with

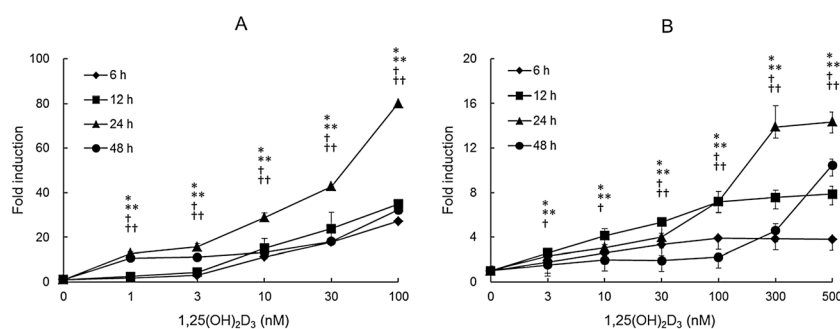


Figure 1. Dose-dependent induction of the *CYP3A4* and *ABCB1* reporter genes by 1,25(OH)₂D₃. The 1-2-10 or 3-13 cells were seeded at 8×10^4 cells per well in 48-well tissue culture plates one day before drug treatment. The following day, the cell medium was exchanged to a medium containing the various concentrations of 1,25(OH)₂D₃. The cell lysate was harvested at 6 h (closed diamonds), 12 h (closed squares), 24 h (closed triangles), and 48 h (closed circles) after drug treatment. The lysate was used to assay for luciferase activity and to determine protein concentration. The luciferase activity was normalized with protein concentration, and the reporter activity in 0.1% DMSO-treated cells was set equal to 1.0. Each point represents mean \pm SD (*n* = 3). *, **, +, and ++, *p* < 0.05 in the cells treated with 1,25(OH)₂D₃ for 6 h, 12 h, 24 h, and 48 h versus 0.1% DMSO-treated cells. (A) *CYP3A4* reporter activity, (B) *ABCB1* reporter activity

500 nM for 24 h. This gave a 14-fold increase in reporter activity in comparison with the control (Figure 1B). Generally, *Renilla* luciferase shows a higher background than firefly luciferase because of the autoluminescence. Consistent with this, the 3-13 cells showed higher background luminescence than that of the 1-2-10 cells.

The effect of cell density on 1,25(OH)₂D₃ induced reporter activity in the stable cell lines

The effect of various cell densities on luciferase activity was also examined. The stable cells were seeded at densities of 3×10^4 , 4×10^4 , 6×10^4 , 8×10^4 , 10×10^4 , and 12×10^4 cells per well in 48-well tissue culture plates. CYP3A4 and ABCB1 reporter activities were induced with 10 nM or 300 nM 1,25(OH)₂D₃ and measured after 24 h. Increases in the CYP3A4 reporter activity occurred in a cell density-dependent manner with the highest cell density (12×10^4 cells per well) exhibiting the greatest induction (Figure 2A). However, the ABCB1 reporter activity decreased in a cell density-dependent manner (Figure 2B).

Transcriptional activation of the CYP3A4 and ABCB1 genes by retinoids

Wang *et al.* (2008) have reported that retinoids such as 9-*cis* RA and ATRA, induce CYP3A4 activity through activation of the VDR in the human

colorectal adenocarcinoma cell line Caco-2 [25]. The study tested whether these compounds could induce the reporter activity in the stable cells. The results show that 9-*cis* RA at a concentration of 100 μ M caused a 2.3-fold increase in luciferase activity in 1-2-10 cells (Figure 3A). Similarly, ATRA at a concentration of 20 μ M increased the luciferase activity by 1.8-fold in 1-2-10 cells. With respect to the 3-13 cells, treatment with 100 μ M 9-*cis* RA and 20 μ M ATRA resulted in an increase of luciferase activity by 3.1-fold and 2.2-fold, respectively (Figure 3B).

The effect of 1,25(OH)₂D₃ and retinoids on CYP3A4 and ABCB1 expression levels

Real-time PCR was performed to examine the effect of 1,25(OH)₂D₃ and retinoids on the expression of intrinsic CYP3A4 and ABCB1 in the stable cell lines. When the 1-2-10 cells were treated with 10 nM 1,25(OH)₂D₃, CYP3A4 expression increased by 76-fold in comparison with the control (Figure 4A). Treatment of the 1-2-10 cells with 100 μ M 9-*cis* RA and 20 μ M ATRA resulted in a greater than 3-fold increase in CYP3A4 expression compared with the control (Figure 4A). The effect of these compounds on ABCB1 expression in 3-13 cells was also examined. Induction with 300 nM 1,25(OH)₂D₃, 100 μ M 9-*cis* RA and 20 μ M ATRA resulted in an increase of ABCB1 expression by 5.9-, 2.3-, and 3.6-fold, respectively (Figure 4B).

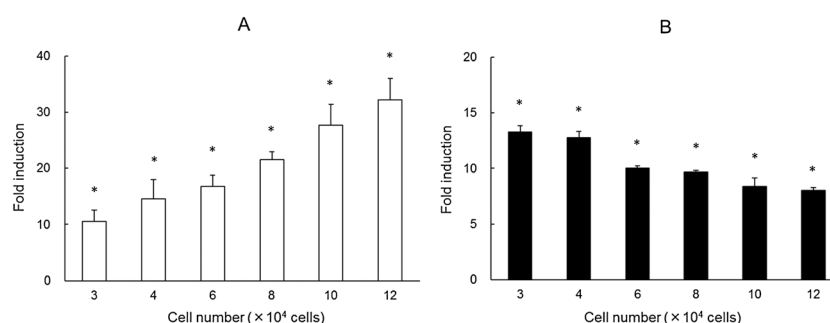


Figure 2. The effect of cell density on 1,25(OH)₂D₃ induced reporter activity in the stable cell lines. The 1-2-10 or 3-13 cells were seeded in 48-well tissue culture plates at various cell densities; 3×10^4 , 4×10^4 , 6×10^4 , 8×10^4 , 10×10^4 and 12×10^4 cells per well 24 h before drug treatment. The cells were treated with 1,25(OH)₂D₃ (10 or 300 nM) for 24 h, and then the lysate was harvested. The lysate was used to assay for luciferase activity and to determine protein concentration. The luciferase activity was normalized using protein concentration, and the reporter activity in 0.1% DMSO-treated cells was set equal to 1.0. The values represent mean \pm SD ($n = 4$). *, $p < 0.05$ versus 0.1% DMSO-treated cells. (A) CYP3A4 reporter activity, (B) ABCB1 reporter activity

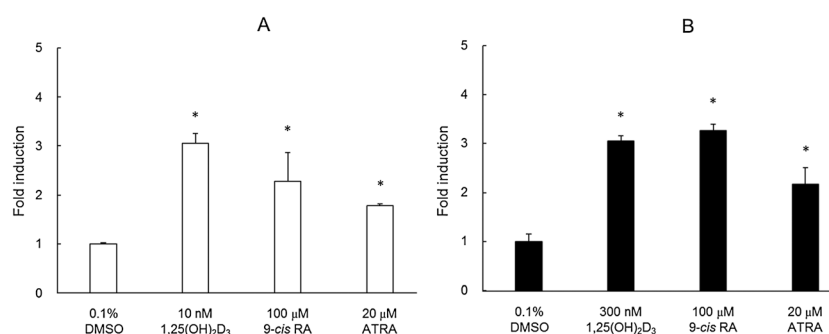


Figure 3. Transcriptional activation of the *CYP3A4* and *ABCB1* genes by retinoids. The 1-2-10 or 3-13 cells were seeded at 8×10^4 cells per well in 48-well tissue culture plates and treated with 1,25(OH)₂D₃ (10 or 300 nM), 9-*cis* RA (100 μM) or ATRA (20 μM) for 48 h. The cells were harvested and the lysate was used to assay for luciferase activity and to determine protein concentration. The luciferase activity was normalized with protein concentration, and the reporter activity in 0.1% DMSO-treated cells was set equal to 1.0. The values represent mean \pm SD ($n = 3$). *, $p < 0.05$ versus 0.1% DMSO-treated cells. (A) *CYP3A4* reporter activity, (B) *ABCB1* reporter activity

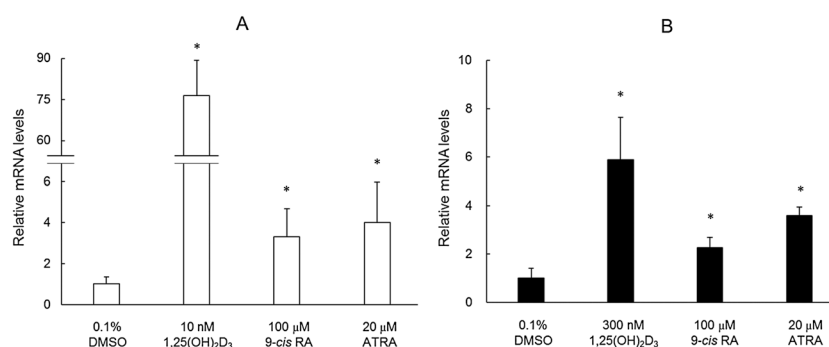


Figure 4. Effect of 1,25(OH)₂D₃ and retinoids on the expression levels of *CYP3A4* and *ABCB1* mRNA. The 1-2-10 or 3-13 cells were seeded at 1.5×10^5 cells per well in 24-well tissue culture plates 24 h before drug treatment. The cells were treated with 1,25(OH)₂D₃ (10 or 300 nM), 9-*cis* RA (100 μM) or ATRA (20 μM). After 48 h, the total RNA was extracted and real-time PCR was carried out as described in Materials and Methods. *CYP3A4* and *ABCB1* mRNA levels were normalized to those of *GAPDH*. The mRNA expression level in 0.1% DMSO-treated cells was set equal to 1.0. The values represent mean \pm SD ($n = 4$). *, $p < 0.05$ versus 0.1% DMSO-treated cells. (A) *CYP3A4* mRNA level, (B) *ABCB1* mRNA level

Simultaneous measurement of *CYP3A4* and *ABCB1* reporter activity

The 1-2-10 and 3-13 stable cells were seeded at various ratios 3:5, 1:1, 5:3, and 3:1 respectively, to a total cell number of 8×10^4 cells per well. The cells were exposed to 300 nM 1,25(OH)₂D₃ for 24 h, after which a dual-luciferase reporter assay was performed. As expected the 1-2-10 cells demonstrated an increase in *CYP3A4* reporter activity that increased in a density-dependent manner. Whereas the 3-13 cells showed a reduction in the *ABCB1*

reporter activity which decreased in a cell density-dependent manner (data not shown). These results are consistent with the results described above, shown in Figure 2. The reporter activities for both *CYP3A4* and *ABCB1* showed the greatest induction when the 1-2-10 and 3-13 cells were mixed at a ratio of 3:1. Consequently, 1-2-10 and 3-13 cells were mixed at a ratio of 3:1, and subcultured continually for more than 20 passages. The mixed cells showed a significant increase in *CYP3A4* and *ABCB1* reporter activity following treatment with 1,25(OH)₂D₃ and

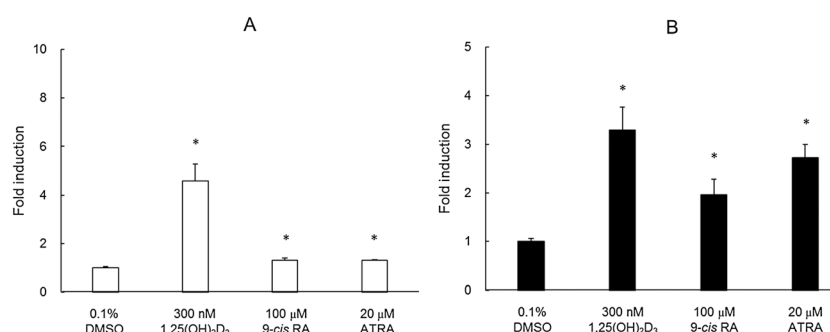


Figure 5. Simultaneous measurement of *CYP3A4* and *ABCB1* reporter activity. 1-2-10 and 3-13 cells were mixed at a ratio of 3:1, and the mixed cells were seeded at 8×10^4 cells per well in 48-well tissue culture plates 24 h before drug treatment. The cells were treated with 1,25(OH)₂D₃ (300 nM), 9-*cis*-RA (100 μM) and ATRA (20 μM) for 48 h. The cells were harvested and the lysate was used for dual-luciferase reporter assay. The reporter activity in 0.1% DMSO-treated cells was set equal to 1.0. The values represent mean \pm SD ($n = 3$). *, $p < 0.05$ versus 0.1% DMSO-treated cells. (A) *CYP3A4* reporter activity, (B) *ABCB1* reporter activity

retinoids. Induction with 300 nM 1,25(OH)₂D₃, 100 μM 9-*cis* RA and 20 μM ATRA resulted in a 4.6-, 1.3-, and 1.3-fold increase of *CYP3A4* reporter activity, respectively, in comparison with the DMSO control (Figure 5A). These activators also increased the *ABCB1* reporter activity by 3.3-, 2.0-, and 2.7-fold above the DMSO control (Figure 5B).

Discussion

In the drug development process, the efficient screening systems are required for shortening the development period and to reduce cost. Cell-based reporter assay systems have been used extensively to screen CYP inducers as reliable and high-throughput methods [26]. Predicting whether drug candidates induce intestinal CYP3A4 and P-gp is crucial as well as in the liver. In fact, Greiner *et al.* (1999) have reported clinically relevant drug interaction between digoxin and rifampicin caused by intestinal P-gp [27]. However, the *in vitro* intestinal models for predicting CYP3A4 and P-gp are yet to be established. In this study, LS174T cells were chosen for constructing the stable cell lines expressing *CYP3A4* or *ABCB1* reporter genes, because LS174T cells were used widely as an *in vitro* human intestinal model [24].

The stable cells were first characterized by measuring the transactivation of *CYP3A4* and *ABCB1* by 1,25(OH)₂D₃, which is a strong inducer of these

genes in the intestine [28]. As shown in Figure 1, 1,25(OH)₂D₃ induced the reporter activity in a dose-dependent manner in both the 1-2-10 and 3-13 cells, with the response reaching a peak at 24 h. The effect of cell density on the reporter activity was also examined. The results showed that the reporter activity increased in a cell density-dependent manner in the 1-2-10 cells, whereas reporter activity gradually diminished in the 3-13 cells (Figure 2). One reason for this may be due to a cell density-dependent increase in reporter activity in non-treated 3-13 cells resulting in a high background compared with the 1-2-10 cells. However, the 3-13 cells did display a significant reporter activity above the background level needed to assess *ABCB1* induction.

To gauge the usefulness of these stable cells, the response of the reporter activity for known inducers of *CYP3A4* and *ABCB1* in the intestine was investigated. In both the 1-2-10 and 3-13 cells, the compounds tested, which included 9-*cis* RA (100 μM) and ATRA (20 μM), caused significant increases in reporter activity (Figure 3), as well as increasing the expression of *CYP3A4*/*ABCB1* (Figure 4). Other researchers have demonstrated the transactivation of *CYP3A4* and *ABCB1* genes caused by 1,25(OH)₂D₃ using transient expression systems. Pavék *et al.* (2010) and Saeki *et al.* (2008) have reported that approximately 30- and 9-fold induction of *CYP3A4* and *ABCB1* reporter activity, respectively, has been achieved by transducing human VDR into LS174T or

Caco-2 cells [18,29]. Our data from this study is comparable to these results, without the overexpression of VDR. In addition, the stable cells created in this study, have the advantage of being more convenient than transient transfection and transduction methods.

CYP3A4 and P-gp are often co-induced and act synergistically to limit oral drug bioavailability. As one example, co-induction of CYP3A4 and P-gp by corticosteroids reduced the tacrolimus blood concentration [30]. Therefore, simultaneous assessment of CYP3A4 and P-gp induction has implications for preventing drug–drug interactions. For this reason, our group attempted to insert both the *CYP3A4* and *ABCB1* reporter plasmids into LS174T cells, to create a double-stable cell line. Unfortunately, the resulting cells showed little reporter activity in response to inducers. Therefore, the 1-2-10 and the 3-13 cells were co-cultivated at a ratio of 3:1. The mixed cells were used for a dual-luciferase reporter assay where they showed a significant increase in both *CYP3A4* and *ABCB1* reporter activity, following treatment with 1,25(OH)₂D₃ and retinoids (Figure 5). In addition, the responsiveness of the mixed cells was sustained for more than 20 subculturing passages, and after freeze-thawing. These results indicate that the mixed cells may be applicable for the simultaneous assessment of CYP3A4 and P-gp, and may be suitable for high-throughput screening of candidate compounds.

Conclusion

In this study, two stable cell lines were established to assess intestinal CYP3A4 and *ABCB1* induction. These cells showed highly sensitive and reproducible induction in response to 1,25(OH)₂D₃, 9-*cis* RA, and ATRA, and the responsiveness of the stable cell lines was comparable to those of the assay systems previously reported. Furthermore, the stable cells have the advantage of being more readily available, as well as being applicable for simultaneous measurement of *CYP3A4* and *ABCB1* reporter activity by co-cultivation. In conclusion, these cells have the potential to predict which candidate drugs cause intestinal CYP3A4 and P-gp induction, providing a useful tool in the drug development process.

Acknowledgements

This work was supported by a Health and Labor Sciences Research Grant for Research on Food Safety (No. 22230301) from the Ministry of Health, Labor and Welfare of Japan; and by the Japanese Ministry of Education, Culture, Sports, Science and Technology (MEXT)-Supported Program for the Strategic Research Foundation at Private Universities.

Conflict of Interest

The authors have no conflicts of interest to declare.

References

1. Nebert DW, Russell DW. Clinical importance of cytochromes P450. *Lancet* 2002; **360**: 1155–1162. doi:10.1016/S0140-6736(02)11203-7.
2. Shimada T, Yamazaki H, Mimura M, Inui Y, Guengerich FP. Interindividual variations in human liver cytochrome P-450 enzymes involved in the oxidation of drugs, carcinogens and toxic chemicals: studies with liver microsomes of 30 Japanese and 30 Caucasians. *J Pharmacol Exp Ther* 1994; **270**: 414–423.
3. McKinnon RA, Burgess WM, Hall PM, Roberts-Thomson SJ, Gonzalez FJ, McManus ME. Characterisation of *CYP3A* gene subfamily expression in human gastrointestinal tissues. *Gut* 1995; **36**: 259–267. doi:10.1136/gut.36.2.259.
4. Li AP, Kaminski DL, Rasmussen A. Substrates of human hepatic cytochrome P450 3A4. *Toxicology* 1995; **104**: 1–8. doi:10.1016/0300-483X(95)03155-9.
5. König J, Müller F, Fromm MF. Transporters and drug–drug interactions: important determinants of drug disposition and effects. *Pharmacol Rev* 2013; **65**: 944–966. doi:10.1124/pr.113.007518.
6. Watkins PB. The barrier function of CYP3A4 and P-glycoprotein in the small bowel. *Adv Drug Deliv Rev* 1997; **27**: 161–170. doi:10.1016/S0169-409X(97)00041-0.
7. Kivistö KT, Niemi M, Fromm MF. Functional interaction of intestinal CYP3A4 and P-glycoprotein. *Fundam Clin Pharmacol* 2004; **18**: 621–626. doi:10.1111/j.1472-8206.2004.00291.x.
8. Gupta A, Mugundu GM, Desai PB, Thummel KE, Unadkat JD. Intestinal human colon adenocarcinoma cell line LS180 is an excellent model to study pregnane X receptor, but not constitutive androstane receptor, mediated CYP3A4 and multi

- drug resistance transporter 1 induction: studies with anti-human immunodeficiency virus protease inhibitors. *Drug Metab Dispos* 2008; **36**: 1172–1180. doi:10.1124/dmd.107.018689.
9. Galetin A, Gertz M, Houston JB. Contribution of intestinal cytochrome P450-mediated metabolism to drug–drug inhibition and induction interactions. *Drug Metab Pharmacokinet* 2010; **25**: 28–47.
 10. Zhang L, Huang SM, Lesko LJ. Transporter-mediated drug–drug interactions. *Clin Pharmacol Ther* 2011; **89**: 481–484. doi:10.1038/clpt.2010.359.
 11. Lehmann JM, McKee DD, Watson MA, Willson TM, Moore JT, Kliewer SA. The human orphan nuclear receptor PXR is activated by compounds that regulate CYP3A4 gene expression and cause drug interactions. *J Clin Invest* 1998; **102**: 1016–1023. doi:10.1172/JCI3703.
 12. Goodwin B, Hodgson E, da Costa DJ, Robertson GR, Liddle C. Transcriptional regulation of the human CYP3A4 gene by the constitutive androstane receptor. *Mol Pharmacol* 2002; **62**: 359–365. doi:10.1124/mol.62.2.359.
 13. Drocourt L, Ourlin JC, Pascussi JM, Maurel P, Vilarem MJ. Expression of CYP3A4, CYP2B6, and CYP2C9 is regulated by the vitamin D receptor pathway in primary human hepatocytes. *J Biol Chem* 2002; **277**: 25125–25132. doi:10.1074/jbc.M201323200.
 14. Kliewer SA. The nuclear pregnane X receptor regulates xenobiotic detoxification. *J Nutr* 2003; **133**: 2444S–2447S.
 15. Thompson PD, Jurutka PW, Whitfield GK, et al. Liganded VDR induces CYP3A4 in small intestinal and colon cancer cells via DR3 and ER6 vitamin D responsive elements. *Biochem Biophys Res Commun* 2002; **299**: 730–738. doi:10.1016/S0006-291X(02)02742-0.
 16. Khan AA, Chow EC, van Loenen-Weemaes AM, Porte RJ, Pang KS, Groothuis GM. Comparison of effects of VDR versus PXR, FXR and GR ligands on the regulation of CYP3A isozymes in rat and human intestine and liver. *Eur J Pharm Sci* 2009; **37**: 115–125. doi:10.1016/j.ejps.2009.01.006.
 17. Toriyabe T, Nagata K, Takada T, et al. Unveiling a new essential *cis* element for the transactivation of the CYP3A4 gene by xenobiotics. *Mol Pharmacol* 2009; **75**: 677–684. doi:10.1124/mol.108.050575.
 18. Saeki M, Kurose K, Tohkin M, Hasegawa R. Identification of the functional vitamin D response elements in the human *MDR1* gene. *Biochem Pharmacol* 2008; **76**: 531–542. doi:10.1016/j.bcp.2008.05.030.
 19. Geick A, Eichelbaum M, Burk O. Nuclear receptor response elements mediate induction of intestinal *MDR1* by rifampin. *J Biol Chem* 2001; **276**: 14581–14587. doi:10.1074/jbc.M010173200.
 20. Sekimoto M, Sano S, Hosaka T, Nemoto K, Degawa M. Establishment of a stable human cell line, HPL-A3, for use in reporter gene assays of cytochrome P450 3A inducers. *Biol Pharm Bull* 2012; **35**: 677–685.
 21. Norcharttiyapot W, Nagai Y, Matsubara T, et al. Construction of several human-derived stable cell lines displaying distinct profiles of CYP3A4 induction. *Drug Metab Pharmacokinet* 2006; **21**: 99–108.
 22. Sato W, Suzuki H, Sasaki T, et al. Construction of a system that simultaneously evaluates CYP1A1 and CYP1A2 induction in a stable human-derived cell line using a dual reporter plasmid. *Drug Metab Pharmacokinet* 2010; **25**: 180–189.
 23. Chen S, Wang K, Wan YJ. Retinoids activate RXR/CAR-mediated pathway and induce CYP3A. *Biochem Pharmacol* 2010; **79**: 270–276. doi:10.1016/j.bcp.2009.08.012.
 24. Tachibana S, Yoshinari K, Chikada T, Toriyabe T, Nagata K, Yamazoe Y. Involvement of Vitamin D receptor in the intestinal induction of human ABCB1. *Drug Metab Dispos* 2009; **37**: 1604–1610. doi:10.1124/dmd.109.027219.
 25. Wang K, Chen S, Xie W, Wan YJ. Retinoids induce cytochrome P450 3A4 through RXR/VDR-mediated pathway. *Biochem Pharmacol* 2008; **75**: 2204–2213. doi:10.1016/j.bcp.2008.02.030.
 26. Luo G, Cunningham M, Kim S, et al. CYP3A4 induction by drugs: correlation between a pregnane X receptor reporter gene assay and CYP3A4 expression in human hepatocytes. *Drug Metab Dispos* 2002; **30**: 795–804. doi:10.1124/dmd.30.7.795.
 27. Greiner B, Eichelbaum M, Fritz P, et al. The role of intestinal P-glycoprotein in the interaction of digoxin and rifampin. *J Clin Invest* 1999; **104**: 147–153. doi:10.1172/JCI6663.
 28. Pfrunder A, Gutmann H, Beglinger C, Drewe J. Gene expression of CYP3A4, ABC-transporters (MDR1 and MRP1-MRP5) and hPXR in three different human colon carcinoma cell lines. *J Pharm Pharmacol* 2003; **55**: 59–66. doi:10.1111/j.2042-7158.2003.tb02434.x.
 29. Pavsek P, Pospechova K, Svecova L, et al. Intestinal cell-specific vitamin D receptor (VDR)-mediated transcriptional regulation of CYP3A4 gene. *Biochem Pharmacol* 2010; **79**: 277–287. doi:10.1016/j.bcp.2009.08.017.
 30. Anglicheau D, Flamant M, Schlageter MH, et al. Pharmacokinetic interaction between corticosteroids and tacrolimus after renal transplantation. *Nephrol Dial Transplant* 2003; **18**: 2409–2414. doi:10.1093/ndt/fgf381.

Development of a Highly Reproducible System to Evaluate Inhibition of Cytochrome P450 3A4 Activity by Natural Medicines

Yu Sato, Takamitsu Sasaki, Shogo Takahashi, Takeshi Kumagai, Kiyoshi Nagata

Department of Environmental and Health Science, Tohoku Pharmaceutical University, Miyagi, Japan.

Received, June 2, 2015; Revised, July 17, 2015; Accepted, July 28, 2015; Published, August 4, 2015.

ABSTRACT – PURPOSE: In recent years, a number of natural medicines have been reported to have inductive or inhibitive effects on the activity of drug metabolizing enzymes, upon co-administration with prescribed medicines. However, information regarding natural medicine-drug interactions that influence drug metabolism is limited owing to the lack of efficient screening method for such interactions. Therefore, to understand whether P450 activity is affected by natural medicine, we have established frozen recombinant P450-expressing cells infected with human CYP3A4 expressing adenovirus (Ad-CYP3A4) to evaluate the effect of natural medicines on CYP3A4 activity. **METHODS:** Ad-CYP3A4 cells were created by infecting HepG2 cells with Ad-CYP3A4 at 10 multiplicity of infection (MOI) and these cells were stored using cryopreservation medium (fAd-CYP3A4 cells) to obtain long-term consistent data and stable supplies of cells expressing a constant level of CYP3A4 activity. **RESULTS:** The CYP3A4 activity in fAd-CYP3A4 cells remained unaffected at the end of each frozen period (0, 1, 2, and 6 months). Inhibitory effect on CYP3A4 activity by typical inhibitors (ketoconazole, hyperforin) and natural medicines (Cat's Claw, Devil's Claw, Feverfew, Peppermint Oil, Red Clover, and Siberian Eleuthero) were evaluated. The inhibitors had nearly equal IC₅₀ values in fAd-CYP3A4 cells, Ad-CYP3A4 cells and recombinant CYP3A4 microsomes. Cat's Claw, Peppermint Oil and Siberian Eleuthero inhibited CYP3A4 activity more potently than 0.1 µM ketoconazole in fAd-CYP3A4 cells. **CONCLUSIONS:** In the present study, we have successfully developed a highly reproducible system to evaluate CYP3A4 inhibition by natural medicines.

This article is open to **POST-PUBLICATION REVIEW**. Registered readers (see "For Readers") may **comment** by clicking on ABSTRACT on the issue's contents page.

INTRODUCTION

Cytochromes P450 (P450) belong to a supergene family of monooxygenases and play an important role in the oxidative metabolism of endogenous compounds such as steroids, fatty acids, and prostaglandins and exogenous compounds such as drugs, environmental pollutants, and food components (1, 2). Of all the CYPs, CYP3A4, CYP2D6, CYP2C19, CYP2C9, and CYP1A2 are mainly expressed in human livers and are involved in ~90% of the oxidative metabolism of drugs (1). In particular, CYP3A4 is the most abundant CYP form found in livers and small intestines, comprising approximately 30% and 70% of the total P450 content, respectively (3). CYP3A4 metabolizes more than 50% of the currently used therapeutic drugs, for example, alprazolam, and nifedipine (3, 4). Thus, compounds that inhibit the CYP3A4 activity could potentially affect the pharmacokinetics/pharmacodynamics of these therapeutic drugs. For example, grapefruit juice (GFJ) has been found to increase the bioavailability

of felodipine (5-7). GFJ reduces the first-pass effect of felodipine by inhibition of its metabolism by CYP3A4. Therefore, it is important to evaluate not only drug-drug interaction but also drug-dietary substance or drug-natural product interaction.

Natural medicines have been used for various health conditions worldwide. These have been used for self-medication without medical supervision and are believed to be safe. In recent years, a number of natural medicines have been reported to have inductive or inhibitive effects on the activity of drug metabolizing enzymes, upon co-administration with prescribed medicines. A typical example is St. John's wort (SJW), which increases the activity of CYP3A4 and reduces plasma concentrations of a number of drugs (7-9). However, the information regarding natural medicine-drug interactions that influence drug

Corresponding Author: Kiyoshi Nagata; Department of Environmental and Health Science, Tohoku Pharmaceutical University; 4-4-1 Komatsushima, Aoba-ku, Sendai, Miyagi, Japan; E-mail: nagataki@tohoku-pharm.ac.jp

metabolism is limited. Therefore, one can assume that natural medicine-drug interactions pose an important problem for clinical therapeutics and it is essential to understand whether P450 activity is affected by natural medicine.

At present, human liver microsomes and primary human hepatocytes are the most desirable enzyme sources for drug metabolism experiments since they retain majority of the biological functions of human livers as well abundantly express drug-metabolizing enzymes (10-12). However, these show large donor-to-donor variability in drug metabolizing activity, which make date interpretation from different sources difficult (10-12). Human hepatoma-derived cell lines such as HepG2 cells have been used for *in vitro* drug metabolism studies owing to have an unlimited lifespan, but have drawback the limit of liver-specific functions including expression of drug-metabolizing enzymes (13-15). In order to compensate for the shortcomings of HepG2 cells, various transient P450 expression systems are generally used for drug metabolism studies.

On the other hand, viral and non-viral methods have been used as tools for intracellular gene transfer (16). In particular, adenoviral vectors are capable of introducing target genes into a variety of cells efficiently (17). The expression level of a recombinant protein can be easily controlled by transfection, depending on the amount of adenovirus. However, this process requires infection of adenovirus with biosafety regulation before each experiment and, a well-to-well difference in enzyme activity is observed within the same experiment, thus, making this system unsuitable for high-throughput screening. In order to overcome these problems, we have established frozen recombinant P450-expressing cells infected with human CYP3A4 expressing adenovirus (Ad-CYP3A4) to evaluate the effect of natural medicines on CYP3A4 activity. By create large amounts of the cells simultaneously, it is possible to obtain long-term consistent data and stable supplies of cells expressing a constant level of P450 activity.

In the present study, we examined the difference in enzymatic activity between the frozen Ad-CYP3A4-infected cells (fAd-CYP3A4 cells) and non-frozen Ad-CYP3A4-infected cells (Ad-CYP3A4 cells), and by using our new method based on fAd-CYP3A4 cells, we evaluated the extent of CYP3A4 inhibition by natural medicines.

METHODS

Materials

Ketoconazole was obtained from LKT Laboratories (St. Paul, MN). Hyperforin was obtained from Sigma-Aldrich (St. Louis, MO). Dimethyl sulfoxide (DMSO) was obtained from Nacalai Tesque (Kyoto, Japan). Oligonucleotides were commercially synthesized by Fasmac (Atsugi, Japan). Microsomes expressing human CYP3A4 prepared from baculovirus-infected insect cells (recombinant CYP3A4 microsomes) were purchased from BD Gentest (Woburn, MA). Cat's Claw, Devil's Claw, Feverfew, Peppermint Oil, Red Clover, and Siberian Eleuthero were obtained from Nature's way (Springville, UT).

Cell Culture

HepG2 and HEK293 cells were obtained from Riken cell bank (Tsukuba, Japan). Cells were cultured in Dulbecco's modified Eagle's medium (DMEM; WAKO Pure Chemicals, Osaka, Japan) supplemented with 10% fetal bovine serum (FBS; Biowest, Miami, FL), minimum essential medium nonessential amino acids (MEM NEAA; Invitrogen, Carlsbad, CA), and Antibiotic-Antimycotic (Invitrogen), under 5% CO₂ at 37°C. Before 24 h adenovirus infection, HepG2 cells were seeded at 1.5×10^5 cells per well onto 24-well tissue culture plates (BD Biosciences, Heidelberg, Germany) for real-time PCR, 1.0×10^5 cells per well onto 48-well tissue culture plates (BD Biosciences) for immunoblotting, and 0.5×10^5 cells per well onto 96-well tissue culture plates (BD Biosciences) for P450-Glo™ assay. The cells were subjected to corresponding experiments after 48 h.

Sample Preparation

Ketoconazole and hyperforin were dissolved in DMSO and the final assay concentration ranges were 0.01-10 µM (ketoconazole) and 0.1-100 µM (hyperforin). For the assessment of inhibitory activities, the daily dose of the natural medicines was extracted in 10 mL ethanol 70% (v/v) for 2 h in water-bath at 37°C. The resulting solution was centrifuged at 3,500 rpm for 15 min at 4°C and the supernatants were used as natural medicine extracts. These were added to the culture medium (0.1%, 0.25%, and 1% extracts) for CYP3A4 activity assay.

Construction of Recombinant Adenovirus

The open reading frame of CYP3A4 DNA was isolated by amplification of cDNA obtained from

human hepatocyte mRNA by PCR using the forward primer, 5'-CACCATGGCTCTCATCCAGACTTGGC-3', and the reverse primer, 5'-TCAGGCTCCACTTACGGTGCCATC-3'. The synthesis was carried out according to the manufacturer's protocol for the ViraPower™ Adenoviral Expression System, pENTR™ Directional TOPO Cloning and pAd/CMV/V5-DEST™ Gateway® Vector kits (Invitrogen). The plasmid was purified by CsCl density gradient centrifugation, linearized with *PacI* (New England Biolabs Inc, Ipswich, MA) and then transfected into HEK293 cells using Targefect F-1 (Nacalai Tesque). The control adenovirus, a β -galactosidase-expressing adenovirus (Ad-LacZ) was produced using the pAd/CMV/V5-GW/*lacZ* control plasmid (Invitrogen). The titer of adenovirus, 50% titer culture infectious dose (TCID₅₀), was determined in HEK293 cells. TCID₅₀ has been reported almost equivalent to that of the plaque-forming unit (18). Multiplicity of infection (MOI) was calculated by dividing TCID₅₀ by the number of cells at the time of seeding.

Preparation of Frozen Ad-CYP3A4 Infected HepG2 Cells

HepG2 cells were seeded at 3×10^6 cells in 100-mm² culture dish (BD Biosciences) 24 h before Ad-CYP3A4 infection at 10 MOI. After 24 h, the cells were harvested, media was replaced with cryopreservation medium (BamBanker; Nippon Genetics, Tokyo), and cells were stored in liquid nitrogen. fAd-CYP3A4 cells were thawed in a 37°C water-bath and then washed with cultured medium. The cells were seeded into 60-mm² culture dish (BD Biosciences) and incubated in fresh medium for 24 h. The cells were seeded at 1.5×10^5 cells per well onto 24-well tissue culture plates for real-time PCR, 1.0×10^5 cells per well onto 48-well tissue culture plates for immunoblotting, and 0.5×10^5 cells per well onto 96-well tissue culture plates for P450-Glo™ assay, respectively, for 24 h prior to experiments.

Quantitative Analysis of CYP3A4 mRNA Contents

Total RNA was extracted by using TRI REAGENT® (Molecular Research Center, Cincinnati, OH). First-strand cDNA was synthesized from 2 μ g total RNA in a 20 μ L reaction mixture using Moloney Murein Virus Reverse Transcriptase (Promega, Madison, MI), oligo(dT)₂₀ primer, and Ribonuclease Inhibitor

(TaKaRa Bio, Shiga, Japan). The cDNA was used to carry out real-time polymerase chain reaction (PCR) using SYBR® Premix ExTaq (TaKaRa Bio) in order to measure mRNA levels of *CYP3A4* and *glyceraldehyde-3-phosphate dehydrogenase* (*GAPDH*). The amplification reactions were performed with specific primers for CYP3A4 (forward: 5'-CTGTGTTTCCAAGAGAAGTTAC-3' and reverse: TGCATCAATTCCTCCTGCAG-3'), and GAPDH (forward: 5'-CATGGGTGTGAACCATGAGAA-3' and reverse: 5'-GGTCATGAGTCCTTCCACGAT-3') (19). Quantitative values were obtained above the threshold PCR cycle number (Ct) at which the increase in signal associated with an exponential growth in PCR products was detected using Thermal Cycler Dice™ TP800 (TaKaRa Bio). The relative mRNA expression levels in each sample were normalized to those of GAPDH.

Determination of CYP3A4 Enzymatic Activities using P450-Glo™ Assay

CYP3A4 activity was measured using a P450-Glo™ CYP3A4 assay kit (Promega) according to the manufacturer's protocol. Ad-CYP3A4 and fAd-CYP3A4 cells were rinsed twice with phosphate buffer saline. Fresh medium containing 3 μ M luciferin-IPA and/or test compound was added to the cells and incubated at 37°C for 1 h. Subsequently, 40 μ L of the medium from each well was transferred to a 96-well white luminometer plate (BD Biosciences), and the luminescence was detected by using a Glomax™ 96 microplate luminometer (Promega). The luminescence signals were calculated by subtracting background luminescence values (no-cell control) from the values of the test compound and the blank (without the test compound).

The reaction mixture consisted of recombinant CYP3A4 microsomes, potassium phosphate buffer, luciferin-IPA (final concentration is 2 nM, 100 mM and 3 μ M, respectively) and/or test compounds in a final volume of 25 μ L. The mixture was incubated at 37°C for 20 min. At the end of the reaction period, reaction mixture was transferred to a 96-well white luminometer plate, and the CYP3A4 activity was measured as described above.

Immunoblot Analysis

Immunoblot analysis was performed to detect the expression of CYP3A4 proteins in HepG2, Ad-CYP3A4, and fAd-CYP3A4 cells. Whole cell

lysates from these cells were size-fractionated by gel electrophoresis on a 10% polyacrylamide/0.1% sodium dodecyl sulfate gel after being denatured by heating in a 2-mercaptoethanol-containing loading buffer. The proteins were electrotransferred to Immobilon®-P membranes (Millipore, Billerica, MA), which were then incubated for 1 h with polyclonal goat anti-human CYP3A4 antibody (Santa Cruz Biotechnology, Inc., Santa Cruz, CA) that had been diluted in Tris-buffered saline (1:1,000). The membranes were subsequently incubated for 1 h with a horseradish peroxidase-conjugated secondary antibody diluted in Tris-buffered saline (1:10,000; Santa Cruz Biotechnology, Inc.). After development with SuperSignal West Pico chemiluminescent substrate (Thermo Fisher Scientific Inc., Waltham, MA), the membrane was scanned using LAS-4000 (GE Healthcare, Milwaukee, WI).

STATISTICAL ANALYSIS

Data are expressed as the mean \pm standard (S.D.) error from three determinations. Statistical comparison of two groups was performed using a two-tailed Student's *t*-test. *P*-values less than 0.05 were considered to be statistically significant.

RESULTS

Determination of optimal conditions for CYP3A4 expression in Ad-CYP3A4-infected HepG2 cells

To optimize the conditions of CYP3A4 expression in Ad-CYP3A4 cells, HepG2 cells were infected with various amounts (0, 3, 5, 10, and 20 MOI) of Ad-CYP3A4 and measured mRNA expression, enzyme activity, and protein expression. The levels of CYP3A4 mRNA expression, activity, and protein increased corresponding to the infection amount of Ad-CYP3A4, but not in Ad-LacZ infected cells at 20 MOI (Figure 1). The highest activity was measured in cells infected with Ad-CYP3A4 at 20 MOI, however this infection level was found to be cytotoxic. Therefore, we used Ad-CYP3A4 at 10 MOI in order to prepare the Ad-CYP3A4 cells.

Effects of cryopreservation on CYP3A4 expression

fAd-CYP3A4 cells were prepared by infecting HepG2 cells with Ad-CYP3A4 at 10 MOI and these cells were stored using cryopreservation medium. To confirm the effects of cryopreservation on

CYP3A4 expression in fAd-CYP3A4 cells, we compared CYP3A4 mRNA, activity and protein expression between fAd-CYP3A4 cells and non-frozen Ad-CYP3A4 cells at 10 MOI. The mRNA, activity, and protein expression levels of CYP3A4 were upregulated in fAd-CYP3A4 cells, as compared to the HepG2 cells (Figure 2). In fAd-CYP3A4 cells, these levels showed higher values as compared to the Ad-CYP3A4 cells. Moreover, to confirm the effects of cryopreservation period on CYP3A4 activity in fAd-CYP3A4 cells, we measured the activity after cryopreservation at the end of 0, 1, 2, and 6 months. As the results, CYP3A4 activity remained unaffected at the end of each frozen period (Figure 3). In those periods, the activities were not significantly different.

Effects of specific inhibitors on CYP3A4 activity

In order to demonstrate the utility of fAd-CYP3A4 cells for the evaluation of inhibition of CYP3A4 enzyme activity, we used ketoconazole and hyperforin as typical inhibitors (20). When fAd-CYP3A4 cells, Ad-CYP3A4 cells, and recombinant CYP3A4 microsomes were treated with ketoconazole or hyperforin, enzyme activity of CYP3A4 was decreased in a concentration-dependent manner (Figure 4). IC₅₀ values of 0.077, 0.105, and 0.096 μ M for ketoconazole were determined in fAd-CYP3A4 cells, Ad-CYP3A4 cells, and recombinant CYP3A4 microsomes, respectively. Hyperforin, a compound of SJW, were inhibited CYP3A4 activity at IC₅₀ values of 9.212, 6.738, and 4.411 μ M, respectively (Table 1). The IC₅₀ values of ketoconazole and hyperforin showed nearly equal values in each evaluation systems.

Effects of natural medicines on CYP3A4 activity

In order to substantiate the ability of fAd-CYP3A4 cells to assess CYP3A4 activity inhibition by natural medicines, the cells were treated with natural medicine extracts. As shown in Figure 5, each natural medicine extract inhibited the activity in a concentration-dependent manner. 1% extracts of Cat's Claw, Peppermint Oil, and Siberian Eleuthero strongly inhibited CYP3A4 activity in fAd-CYP3A4 cells (Figure 5A). The inhibitory levels of Devil's Claw, Feverfew, and Red Clover were found to be comparable to 0.1 μ M ketoconazole (positive control) in fAd-CYP3A4 cells.

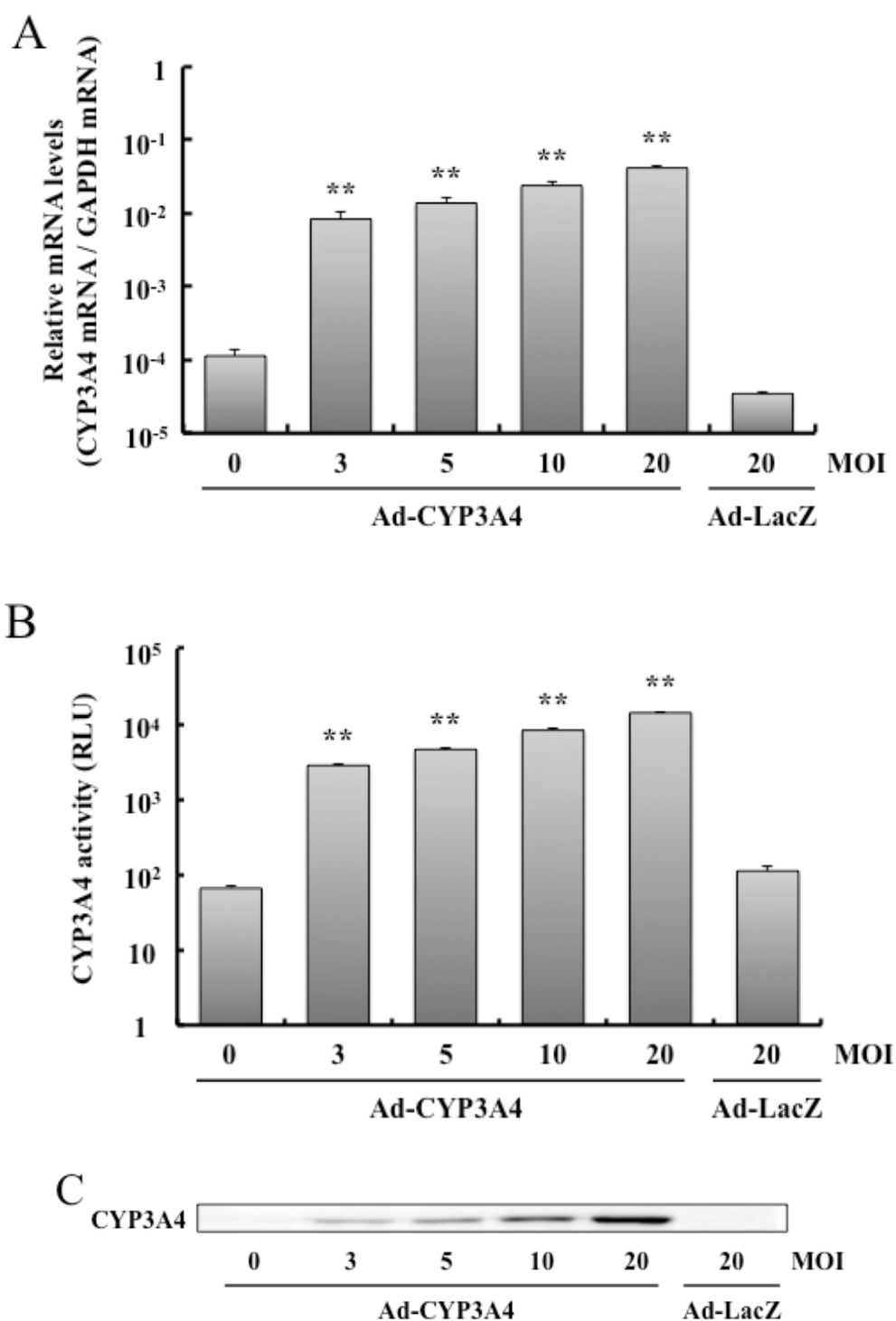


Figure 1. MOI-dependent increase of CYP3A4 levels in HepG2 cells infected with Ad-CYP3A4.

HepG2 cells were seeded in 24-well tissue culture plates at 1.5×10^5 cells per well for real-time PCR, 96-well tissue culture plates at 0.5×10^5 cells per well for P450-Glo™ assay, and 48-well tissue culture plates at 1.0×10^5 cells per well for immunoblotting. The next day, the cells were infected with Ad-CYP3A4 (MOI of 3, 5, 10, and 20) or Ad-LacZ (MOI of 20). After 48 h, mRNA expression (A), enzyme activity (B), and protein levels (C) were measured using real-time PCR, P450-Glo™ assay, and immunoblotting. Results represent the mean \pm S.D. (n = 3). Student's *t*-test: ***p* < 0.01, compared with non-infection cells (0 MOI).

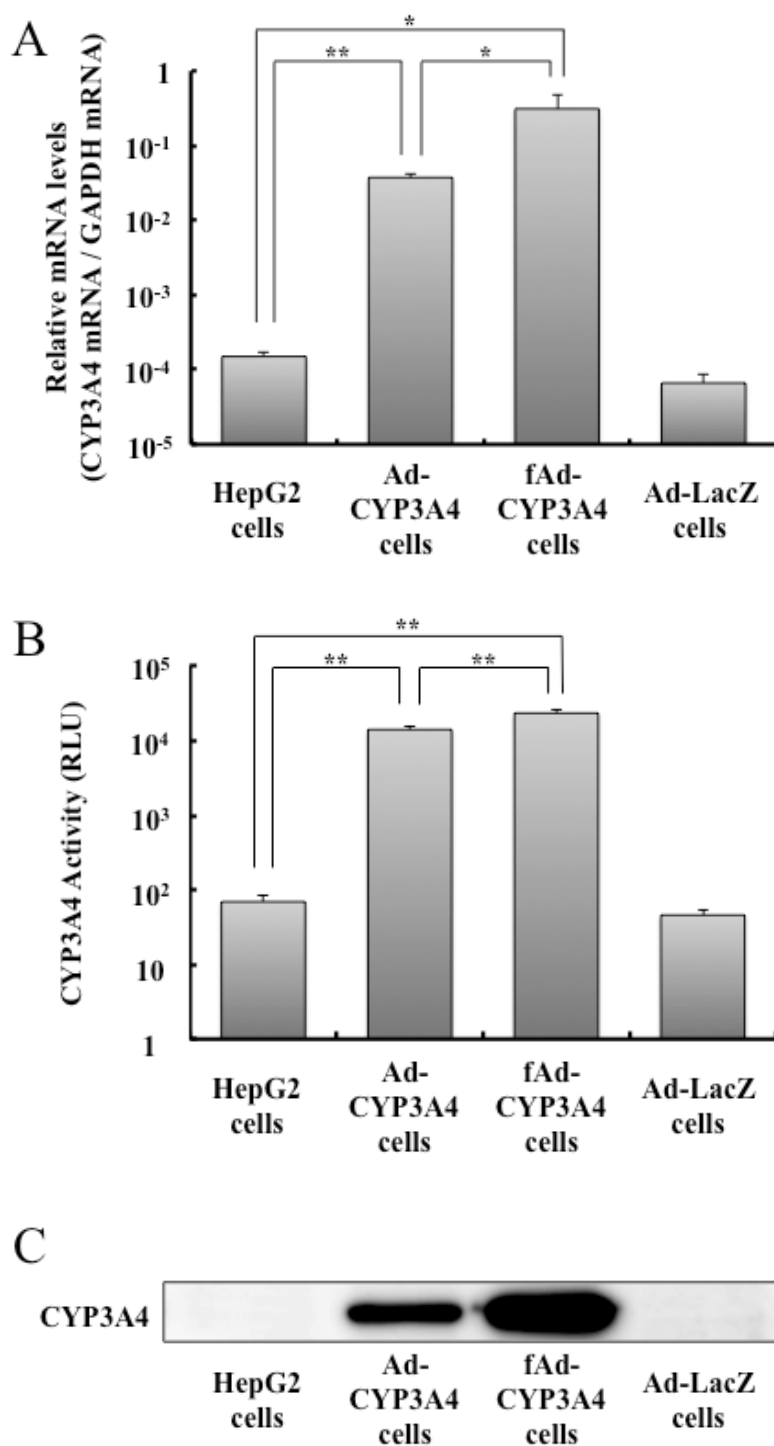


Figure 2. Comparison of CYP3A4 levels in fAd-CYP3A4 cells and Ad-CYP3A4 cells.

HepG2 cells were seeded in 24-well tissue culture plates at 1.5×10^5 cells per well for real-time PCR, 96-well tissue culture plates at 0.5×10^5 cells per well for P450-Glo™ assay, and 48-well tissue culture plates at 1.0×10^5 cells per well for immunoblotting. The next day, the cells were infected with Ad-CYP3A4 (MOI of 10) or Ad-LacZ (MOI of 10). After 48 h, mRNA expression (A), enzyme activity (B), and protein levels (C) were measured using real-time PCR, P450-Glo™ assay, and immunoblotting. fAd-CYP3A4 cells were seeded in the same way as HepG2 cells before 24 h of real-time PCR, P450-Glo™ assay, and immunoblotting. Results represent the mean \pm S.D. (n = 3). Student's *t*-test: ** $p < 0.01$, * $p < 0.05$.

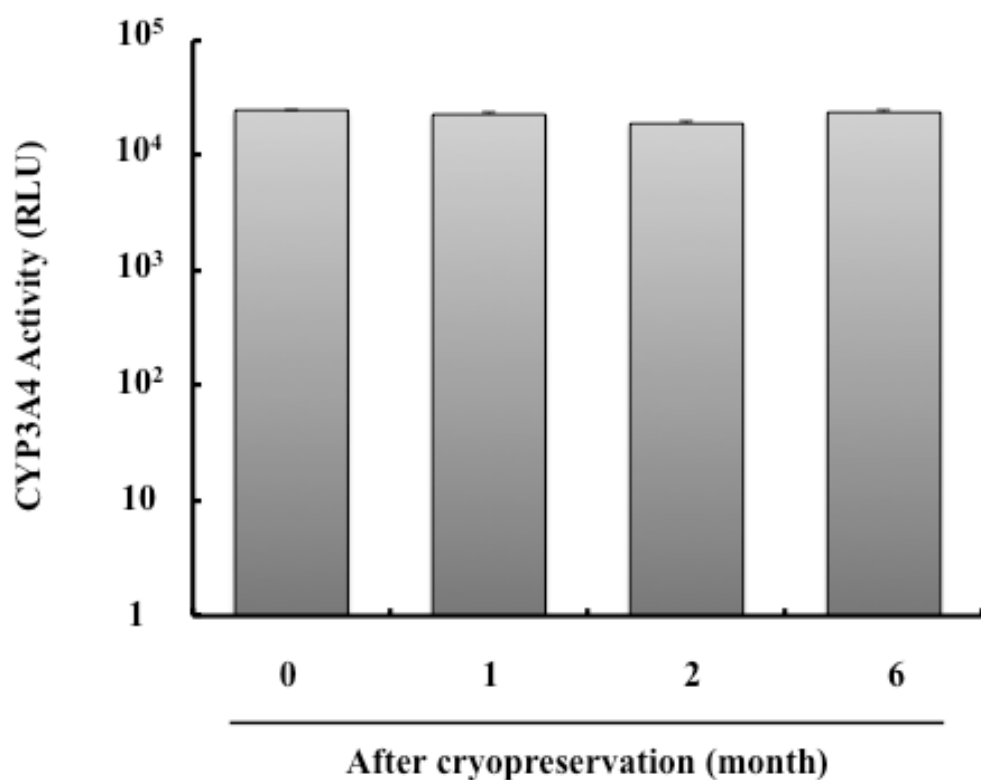


Figure 3. Effect of the frozen period on CYP3A4 activity.

After cryopreservation for 0, 1, 2 and 6 months, fAd-CYP3A4 cells were seeded in 96-well tissue culture plates at 0.5×10^5 cells per well. After 24 h, enzyme activity was measured using P450-Glo™ assay. Results represent the mean \pm S.D. (n = 3).

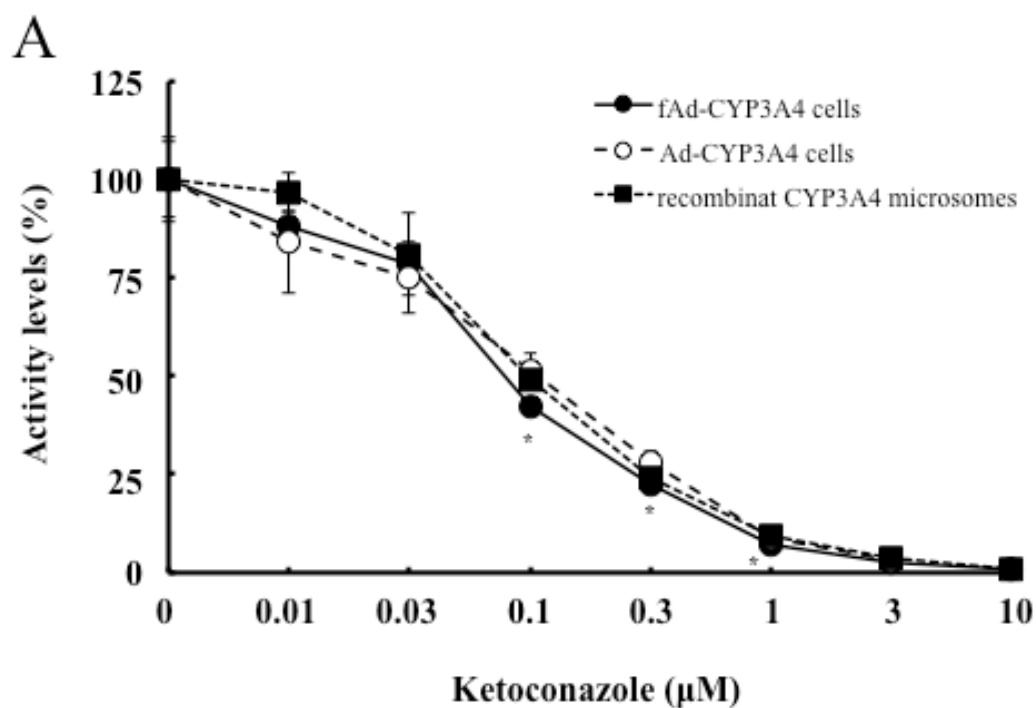


Figure 4.

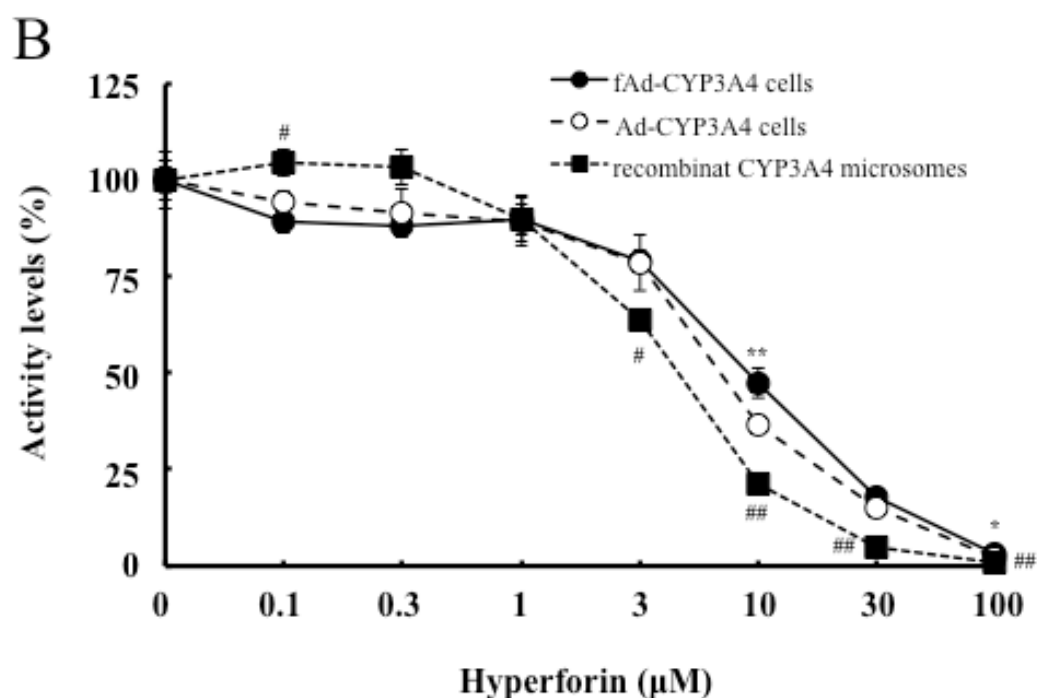


Figure 4. Inhibition of CYP3A4 activity by ketoconazole (A) and hyperforin (B).

HepG2 cells were seeded in 96-well tissue culture plates at 0.5×10^5 cells per well prior to 24 h Ad-CYP3A4 (MOI of 20) infection. After 48 h, enzyme activity was measured using P450-Glo™ assay. fAd-CYP3A4 cells were seeded in 96-well tissue culture plates at 0.5×10^5 cells per well density before 24 h measurement of enzyme activity. Recombinant CYP3A4 microsomes were incubated with ketoconazole or hyperforin before measurement of enzyme activity. Results represent the mean \pm S.D. (n = 3). Student's *t*-test: ***p* < 0.01, **p* < 0.05, compared between Ad-CYP3A4 cells and fAd-CYP3A4 cells. ##*p* < 0.01, #*p* < 0.05, compared between Ad-CYP3A4 cells and recombinant CYP3A4 microsomes.

Table 1. IC₅₀ values of CYP3A4 activity using each evaluation systems

Evaluation systems	IC ₅₀ (μM)	
	Ketoconazole	Hyperforin
fAd-CYP3A4 cells	0.077 (0.075-0.079)	9.212 (8.19-10.234)
Ad-CYP3A4 cells	0.105 (0.084-0.126)	6.738 (6.214-7.262)
Recombinat CYP3A4 microsomes	0.096 (0.091-0.101)	4.411 (4.158-4.664)

IC₅₀ values were determined with data shown in Figure 4.

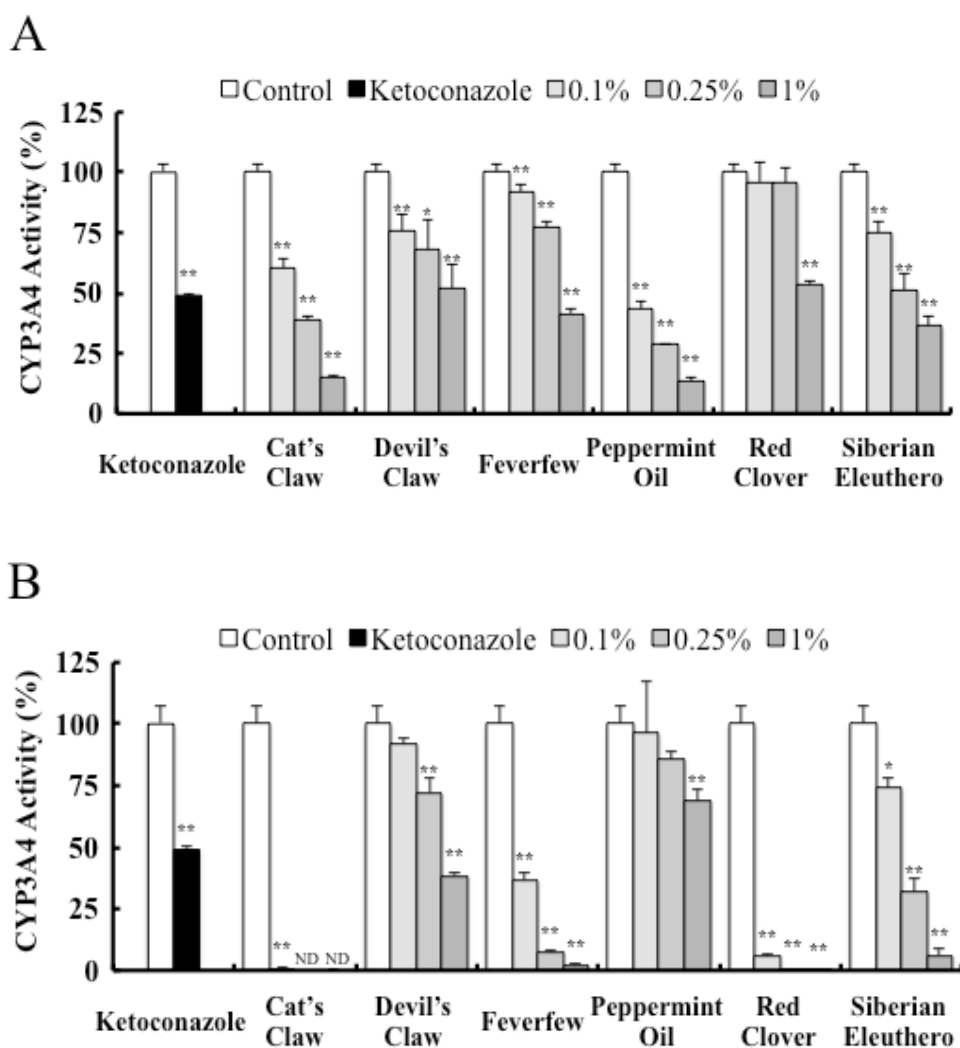


Figure 5. Inhibitory effect of natural medicines on CYP3A4 activity in fAd-CYP3A4 cells (A) and CYP3A4 microsomes (B).

fAd-CYP3A4 cells were seeded in 96-well tissue culture plates at 0.5×10^5 cells per well. After 24 h, enzyme activity of CYP3A4 was measured. Reaction mixture of recombinant CYP3A4 microsomes was incubated with ketoconazole (0.1 μ M) and test natural medicine compounds. The enzyme activity was measured using P450-Glo™ assay. The values of enzyme activity in untreated groups were set equal to 100%. Results represent the mean \pm S.D. (n = 3) ND, not detected. Student's *t*-test: ***p* < 0.01, **p* < 0.05, compared with control.

On the other hand, in recombinant CYP3A4 microsomes, CYP3A4 activity was strongly inhibited by 1% extracts of Cat's Claw, Feverfew, Red Clover, and Siberian Eleuthero, which was stronger than that of the finding in fAd-CYP3A4 cells (Figure 5B). However, this was not observed in case of Peppermint Oil.

DISCUSSION

Adenoviral vectors are highly efficient tools for gene transfer into various cell types. Furthermore,

expression levels of the target protein can be controlled by the infection amount of the adenovirus. As shown in Figure 1, Ad-CYP3A4 infection leads to increased CYP3A4 mRNA, protein levels, and enzyme activity in HepG2 cells and this increase corresponds to the infection amount of Ad-CYP3A4. However, it may cause a well-to-well difference in the enzyme activity by the virus infection in every experiment. Ugai *et al.* (21) previously reported that the function of adenoviral vectors usually does not change unless they are exposed to excessive freeze/thaw cycles.

We therefore assume that recombinant P450 activity in adenovirus-infected cells is not altered by limited cycles of freeze / thawing.

The fAd-CYP3A4 cells had higher CYP3A4 activity than Ad-CYP3A4 cells (Figure 2). The difference in activity levels among these cells corresponded to the mRNA and protein levels. This may be owing to the difference in total culture period after seeding the cells (fAd-CYP3A4 cells: 96 h, non-frozen Ad-CYP3A4 cells: 72 h). For the inhibition assays with ketoconazole, a potent inhibitor of CYP3A4-mediated metabolism, the IC₅₀ values in fAd-CYP3A4 cells, Ad-CYP3A4 cells, and recombinant CYP3A4 microsomes were in good agreement with what has been reported (20, 22) (Figure 4 and Table 1). Moreover, hyperforin (one of SJW components) inhibited CYP3A4 activity and IC₅₀ values were comparable on each experiment. Obach *et al* (23) previously reported that hyperforin potently inhibited CYP3A4 activity in studies using recombinant CYP3A4 microsomes and hepatocytes (24). Moreover, Qi *et al.* (25) reported that oral clearance of midazolam in rats decreased with SJW treatment of short period. Therefore, our results suggest that fAd-CYP3A4 cells are a useful system to evaluate P450 inhibition and are comparable to human hepatocytes and microsomes.

Further, we have compared that inhibition effect to CYP3A4 enzymes activity by natural medicines on fAd-CYP3A4 cells and recombinant CYP3A4 microsomes. A previously published clinical study has shown that Cat's Claw interacts with HIV protease inhibitors, which are known CYP3A4 inhibitors (26, 27). Unger *et al* (28) reported that Devil's Claw, Feverfew, Peppermint Oil, and Red clover were inhibitors of CYP enzymes including CYP3A4. Although extent of inhibition of CYP3A4 activity by these natural medicines differed, all the natural medicine extracts exhibited this inhibitory effect (Figure 5). The inhibitory levels in recombinant CYP3A4 microsomes were stronger than those in case of fAd-CYP3A4 cells. In contrast, the CYP3A4 activity was strongly inhibited in fAd-CYP3A4 cells treated with Peppermint Oil extracts compared to that in the recombinant CYP3A4 microsomes. This difference might be involved in the permeability of the CYP3A4 inhibitors including these natural medicines into the cells. It was not possible to evaluate the cell membrane permeability of the compounds in microsomes unlike cell-based *in vitro* test systems for P450 inhibitors. In fact, Englund *et al* (29) have reported that IC₅₀ values of

elacrider for midazolam (CYP3A substrate) metabolism in hepatocytes were found to be higher than those found in liver microsomes. They have described that this difference may be due to the difference in membrane permeability of the inhibitor into the cells. Therefore, our results suggest that our evaluation system has reflected membrane permeability of compounds into the cells of livers. Our cell based-inhibitory assay system have mimicking human drug metabolism intracellular considered for membrane permeability.

Primary human hepatocytes are the most desirable enzyme source, but there are lot to lot (donor to donor) variation and limitation to use the large amount of the each lot. Our results indicated that Ad-CYP3A4-infected cells could be cryopreserved and their activity did not decrease upon long-term storage. Thus, easy and reproducibly assessment is possible by storing a large volumes of fAd-CYP3A4 cells. Aoyama *et al.* (30) also have reported that HepG2 cells infected with two different varieties of P450-expressing adenovirus had no effect on each expression levels. Therefore, our model can be developed to evaluate a system that considers metabolic pathways in addition to other P450- and transporter-expressing adenoviruses.

In the present study, we have successfully developed a highly reproducible system, which provides large amounts of frozen CYP3A4-expressing cells after Ad-CYP3A4 infection. Our results suggested that this evaluation system become more similar to hepatocytes by expressing of multiple P450s and is more useful for screening inhibitory effect of natural medicine on P450 activity.

ACKNOWLEDGMENTS

This work was supported by a Health and Labour Sciences Research Grant for Research on Food Safety (No. 22230301) from the Ministry of Health, Labour and Welfare of Japan; and by the Japanese Ministry of Education, Culture, Sports, Science and Technology (MEXT)-Supported Program for the Strategic Research Foundation at Private Universities.

REFERENCES

1. Guengerich FP. Cytochrome P450s and other enzymes in drug metabolism and toxicity. *AAPS J.* 2006; 8(1):E101-11.
2. Guengerich FP. Cytochrome p450 and chemical

- toxicology. *Chem Res Toxicol*. 2008; 21(1):70-83.
3. Zanger UM, Schwab M. Cytochrome P450 enzymes in drug metabolism: regulation of gene expression, enzyme activities, and impact of genetic variation. *Pharmacol Ther*. 2013; 138(1):103-41.
4. Williams JA, Ring BJ, Cantrell VE, Jones DR, Eckstein J, Ruterbories K, et al. Comparative metabolic capabilities of CYP3A4, CYP3A5, and CYP3A7. *Drug Metab Dispos*. 2002; 30(8):883-91.
5. Paine MF, Widmer WW, Hart HL, Pusek SN, Beavers KL, Criss AB, et al. A furanocoumarin-free grapefruit juice establishes furanocoumarins as the mediators of the grapefruit juice-felodipine interaction. *Am J Clin Nutr*. 2006; 83(5):1097-105.
6. Bailey DG, Malcolm J, Arnold O, Spence JD. Grapefruit juice-drug interactions. *Br J Clin Pharmacol*. 1998; 46(2):101-10.
7. Nowack R. Review article: cytochrome P450 enzyme, and transport protein mediated herb-drug interactions in renal transplant patients: grapefruit juice, St John's Wort - and beyond! *Nephrology (Carlton)*. 2008; 13(4):337-47.
8. Piscitelli SC, Burstein AH, Chait D, Alfaro RM, Falloon J. Indinavir concentrations and St John's wort. *Lancet*. 2000; 355(9203):547-8.
9. Bauer S, Stormer E, John A, Kruger H, Budde K, Neumayer HH, et al. Alterations in cyclosporin A pharmacokinetics and metabolism during treatment with St John's wort in renal transplant patients. *Br J Clin Pharmacol*. 2003; 55(2):203-11.
10. Brandon EF, Raap CD, Meijerman I, Beijnen JH, Schellens JH. An update on in vitro test methods in human hepatic drug biotransformation research: pros and cons. *Toxicol Appl Pharmacol*. 2003; 189(3):233-46.
11. Gomez-Lechon MJ, Donato MT, Castell JV, Jover R. Human hepatocytes as a tool for studying toxicity and drug metabolism. *Curr Drug Metab*. 2003; 4(4):292-312.
12. Vermeir M, Annaert P, Mamidi RN, Roymans D, Meuldermans W, Mannens G. Cell-based models to study hepatic drug metabolism and enzyme induction in humans. *Expert Opin Drug Metab Toxicol*. 2005; 1(1):75-90.
13. Donato MT, Lahoz A, Castell JV, Gomez-Lechon MJ. Cell lines: a tool for in vitro drug metabolism studies. *Curr Drug Metab*. 2008; 9(1):1-11.
14. Hewitt NJ, Hewitt P. Phase I and II enzyme characterization of two sources of HepG2 cell lines. *Xenobiotica*. 2004; 34(3):243-56.
15. Rodriguez-Antona C, Donato MT, Boobis A, Edwards RJ, Watts PS, Castell JV, et al. Cytochrome P450 expression in human hepatocytes and hepatoma cell lines: molecular mechanisms that determine lower expression in cultured cells. *Xenobiotica*. 2002; 32(6):505-20.
16. Gao X, Kim KS, Liu D. Nonviral gene delivery: what we know and what is next. *AAPS J*. 2007; 9(1):E92-104.
17. Ghosh SS, Gopinath P, Ramesh A. Adenoviral vectors: a promising tool for gene therapy. *Appl Biochem Biotechnol*. 2006; 133(1):9-29.
18. Sasaki T, Takahashi S, Numata Y, Narita M, Tanaka Y, Kumagai T, et al. Hepatocyte nuclear factor 6 activates the transcription of CYP3A4 in hepatocyte-like cells differentiated from human induced pluripotent stem cells. *Drug Metab Pharmacokinet*. 2013; 28(3):250-9.
19. Takezawa T, Matsunaga T, Aikawa K, Nakamura K, Ohmori S. Lower expression of HNF4alpha and PGC1alpha might impair rifampicin-mediated CYP3A4 induction under conditions where PXR is overexpressed in human fetal liver cells. *Drug Metab Pharmacokinet*. 2012; 27(4):430-8.
20. Greenblatt DJ, Zhao Y, Venkatakrishnan K, Duan SX, Harmatz JS, Parent SJ, et al. Mechanism of cytochrome P450-3A inhibition by ketoconazole. *J Pharm Pharmacol*. 2011; 63(2):214-21.
21. Ugai H, Watanabe S, Suzuki E, Tsutsui-Nakata H, Yokoyama KK, Murata T. Stability of a recombinant adenoviral vector: optimization of conditions for storage, transport and delivery. *Jpn J Cancer Res*. 2002; 93(5):598-603.
22. Qin CZ, Ren X, Tan ZR, Chen Y, Yin JY, Yu J, et al. A high-throughput inhibition screening of major human cytochrome P450 enzymes using an in vitro cocktail and liquid chromatography-tandem mass spectrometry. *Biomed Chromatogr*. 2014; 28(2):197-203.
23. Obach RS. Inhibition of human cytochrome P450 enzymes by constituents of St. John's Wort, an herbal preparation used in the treatment of depression. *J Pharmacol Exp Ther*. 2000; 294(1):88-95.
24. Komoroski BJ, Zhang S, Cai H, Hutzler JM, Frye R, Tracy TS, et al. Induction and inhibition of cytochromes P450 by the St. John's wort constituent hyperforin in human hepatocyte cultures. *Drug Metab Dispos*. 2004; 32(5):512-8.
25. Qi JW, Nakamura K, Hosokawa S, Okada Y, Horiuchi R, Yamamoto K. Time-dependent induction of midazolam-1-hydroxylation enzymes in rats treated with St. John's wort. *Biol Pharm Bull*. 2005; 28(8):1467-71.
26. Lopez Galera RM, Ribera Pascuet E, Esteban Mur JJ, Montoro Ronsano JB, Juarez Gimenez JC. Interaction between cat's claw and protease inhibitors atazanavir, ritonavir and saquinavir. *Eur J Clin Pharmacol*. 2008; 64(12):1235-6.
27. Kumar S, Kumar A. Differential effects of ethanol on spectral binding and inhibition of cytochrome P450 3A4 with eight protease inhibitors antiretroviral drugs. *Alcohol Clin Exp Res*. 2011; 35(12):2121-7.
28. Unger M, Frank A. Simultaneous determination of the inhibitory potency of herbal extracts on the

- activity of six major cytochrome P450 enzymes using liquid chromatography/mass spectrometry and automated online extraction. *Rapid Commun Mass Spectrom*. 2004; 18(19):2273-81.
29. Englund G, Lundquist P, Skogastierna C, Johansson J, Hoogstraate J, Afzelius L, et al. Cytochrome p450 inhibitory properties of common efflux transporter inhibitors. *Drug Metab Dispos*. 2014; 42(3):441-7.
30. Aoyama K, Yoshinari K, Kim HJ, Nagata K, Yamazoe Y. Simultaneous expression of plural forms of human cytochrome P450 at desired ratios in HepG2 cells: adenovirus-mediated tool for cytochrome P450 reconstitution. *Drug Metab Pharmacokinet*. 2009; 24(3):209-17.

研究テーマ 2

老年性神経系疾患（老人性認知症、高齢者うつ病）

改善薬の開発



Research report

Role of prefrontal cortical 5-HT_{2A} receptors and serotonin transporter in the behavioral deficits in post-pubertal rats following neonatal lesion of the ventral hippocampus



Satoru Mitazaki^{a,b,1}, Osamu Nakagawasai^{a,*}, Hiroshi Onogi^{a,c}, Kenya Watanabe^{a,g}, Kohei Takahashi^{a,d}, Koichi Tan-No^a, Rémi Quirion^e, Lalit K Srivastava^e, Takeshi Tadano^{a,f}

^a Department of Pharmacology, Faculty of Pharmaceutical Sciences, Tohoku Medical and Pharmaceutical University, 4-4-1 Komatsushima, Aoba-ku, Sendai, 981-8558, Japan

^b Laboratory of Molecular Neuroscience, Faculty of Pharmacy, Takasaki University of Health and Welfare, 60 Nakaorui-machi, Takasaki, 370-0033, Japan

^c Faculty of Health Science, Tohoku Fukushi University, 1-8-1 Kunimi, Aoba-ku, Sendai, 981-8522, Japan

^d Department of Pharmacology, School of Pharmacy, International University of Health and Welfare, 2600-1 Kitakanemaru, Ohtawara, 324-8501, Japan

^e Douglas Mental Health University Institute, Department of Psychiatry, McGill University, Montreal, Québec, H4H 1R3, Canada

^f Complementary and Alternative Medicine Clinical Research and Development, Graduate School of Medicine Sciences, Kakumamachi, Kanazawa University, Kanazawa, 920-8640, Japan

^g Department of Pharmacy, Fukushima Medical University Hospital, Hikarigaoka 1, Fukushima, 960-1295, Japan

ARTICLE INFO

Keywords:

5-HT_{2A} receptor
Serotonin transporter
Prepulse inhibition
Schizophrenia
Receptor autoradiography
Prefrontal cortex

ABSTRACT

Neonatal ventral hippocampal-lesioned (NVHL) rats have been shown to display neurochemical and behavioral abnormalities at adulthood, analogous to some of those seen in schizophrenia. Serotonergic neurotransmission is implicated in the pathophysiology and treatment of schizophrenia. In this study, we evaluated possible role of serotonergic transmission in the behaviors of NVHL-lesioned rats. Bilateral lesions to the ventral hippocampus (VH) in rat pups were made using the excitotoxin ibotenic acid. We investigated 5-HT_{2A}-receptor and SERT binding sites in cortical and subcortical areas in post-pubertal NVHL and sham-lesioned rats, using quantitative receptor autoradiography. We compared a 5-HT-dependent behavior in NVHL and sham animals, the wet-dog shake response (WDSr) to a 5-HT_{2A} receptor agonist DOI. In addition, we studied prepulse inhibition (PPI) of startle responses in NVHL and Sham-lesioned animals treated with antipsychotic drugs haloperidol, risperidone and clozapine and 5-HT_{2A} antagonists ketanserin or MDL100907. The WDSr elicited by DOI was enhanced in post-pubertal NVHL rats compared to sham-lesioned controls. Moreover, post-pubertal NVHL rats exhibited PPI deficits which was reversed by atypical antipsychotics, ketanserin and MDL100907. A significant increase in 5-HT_{2A}-like receptor binding was observed in the medial prefrontal cortex (mPFC) in post-pubertal NVHL rats without any significant change in the striatum and ventral pallidum. A significant increase in SERT-like binding was also observed in the mPFC and striatum of NVHL rats at pre-pubertal period; however, at post-pubertal age, the binding remained elevated in mPFC only. These data suggest that increased prefrontal cortical 5-HT transmission may play a role in the behavioral deficits observed in this neurodevelopmental model of schizophrenia.

Abbreviations: 5-HT, serotonin; ANOVA, analysis of variance; ASR, acoustic startle response; Cg1, cingulate cortex area 1; CPu, caudate putamen; DA, dopamine; DOI, (±)-2,5-dimethoxy-4-iodoamphetamine hydrochloride; HTR, head twitch response; i.p., intraperitoneally; IL, infralimbic cortex; MIA, maternal immune activation; NAcC, nucleus accumbens core; NAcSh, nucleus accumbens shell; NVHL, Neonatal ventral hippocampal-lesioned; mPFC, medial prefrontal cortex; PD, postnatal day; PLSD, Protected Least Significant Difference; PrL, prelimbic cortex; PPI, prepulse inhibition; SEM, standard error of the mean; SERT, serotonin transporter; VP, ventral pallidum; WDSr, Wet-dog shakes response

* Corresponding author at: Department of Pharmacology, Faculty of Pharmaceutical Sciences, Tohoku Medical and Pharmaceutical University, 4-4-1 Komatsushima, Aoba-ku, Sendai, Miyagi 981-8558, Japan.

E-mail address: osamun@tohoku-mpu.ac.jp (O. Nakagawasai).

¹ These authors contributed equally to this work.

<https://doi.org/10.1016/j.bbr.2019.112226>

Received 3 June 2019; Received in revised form 23 August 2019; Accepted 10 September 2019

Available online 12 September 2019

0166-4328/ © 2019 Elsevier B.V. All rights reserved.

1. Introduction

Neonatal ventral hippocampal-lesion (NVHL) in rats have been shown to induce post-pubertal emergence of behavioral abnormalities thought to simulate some aspects of positive, negative and cognitive symptoms classically observed in schizophrenic patients. These include hyper-reactivity to stress and amphetamine, deficits in prepulse inhibition (PPI) of startle and latent inhibition, and impaired social behavior and working memory [1].

It is suggested that the serotonergic system may be related to the pathophysiology of schizophrenia due to its role in many physiologic processes related to mood, cognition, and perception [2]. Alterations in the expression of serotonin (5-HT) receptors and transporter have been reported in the brains of patients with schizophrenia [3,4] and may play a role in the differential action of atypical as compared to typical antipsychotic drugs [5]. In addition, polymorphisms in serotonergic receptor genes are related to the prediction of response to atypical antipsychotics [6]. Furthermore, the effectiveness of clozapine, an atypical antipsychotic drug with significant 5-HT receptor binding affinity, and the observation that 5-HT modulates the activity of dopaminergic neurons constitute important evidence implying a role of 5-HT in schizophrenia [7]. While genetic association studies of 5-HT_{2A} receptor and the serotonin transporter (SERT) in schizophrenia have not been conclusive, given the above-evidence, it is imperative to better explore the roles of serotonergic systems in schizophrenia [8–11].

Schizophrenia has been associated with abnormalities in information processing, attentional mechanisms and sensorimotor gating [12]. One well-established method for evaluating sensory gating is the paradigm of PPI of startle which refers to the inhibition of a startle reflex by the presentation of a weak prepulse immediately before a startling stimulus. Interestingly, PPI is a translatable phenomenon which can be measured using virtually identical techniques and parameters across species and it shows similar sensitivity to stimulus parameters in rats and human beings [13]. Disruption of PPI in schizophrenia patients has been well described in several studies [14,15]. PPI is regulated at by various brain regions and by many neurotransmitters. Previous studies have suggested that atypical antipsychotics, in contrast to typical antipsychotics, were able to attenuate NVHL lesion-induced PPI deficits [16]. Given the significant affinity of atypical antipsychotics to serotonin receptors, it is possible that the PPI deficits in NVHL rats may also involve 5-HT system, in addition to other neurotransmitters as suggested previously [16–18].

In order to assess possible alterations in serotonergic system, the present investigation was designed to evaluate the levels of 5-HT_{2A} receptor and SERT binding sites at pre- and post-pubertal ages in cortical and subcortical areas of NVHL rats, using quantitative receptor autoradiography. In addition, we assessed the role of serotonergic transmission in the behaviors of NVHL rats using the Wet-dog shakes response (WDSr), a 5-HT_{2A} receptor-associated behavior, and the effects of 5-HT_{2A} antagonists in PPI deficits observed in NVHL rats. Our data show that increased prefrontal cortical serotonergic system may contribute to some of the behavioral deficits observed in this neurodevelopmental model of schizophrenia.

2. Materials and methods

All experiments were performed following the approval of the Ethics Committee of Animal Experiment in Tohoku Medical and Pharmaceutical University and according to the National Institutes of Health Guide for the Care and Use of Laboratory Animals. Efforts were made to minimize suffering and to reduce the number of animals used. Measurements of the behaviors and post-mortem analyses were conducted by an observer blind to treatment conditions. Behavioral testing occurred between 10:00 and 18:00.

2.1. Neonatal ventral hippocampal lesion

Lesions of the ventral hippocampus were performed as previously described [19]. Pregnant Sprague-Dawley rats at 14–16 days of gestation were obtained from Japan SLC (Hamamatsu, Shizuoka, Japan), housed under conditions of constant temperature ($23 \pm 1^\circ\text{C}$) and humidity ($55 \pm 5\%$), on a 12:12 h light-dark cycle (light: 7–19 h). The rats were housed individually in plastic cages (20 cm \times 25 cm \times 40 cm). On postnatal day (PD) 7, male pups (14–18 g) within each litter (4–10 males/litter) were randomly divided to sham or lesion status. Pups were anesthetized by hypothermia by placing them on ice for 20 min and were immobilized on a platform fixed on a stereotaxic frame. An incision in the skin overlaying the skull was made and two 1 mm holes were drilled. A needle connected to an infusion pump through a Hamilton syringe was lowered into the each ventral hippocampus at the coordinates: AP -3.0 mm ML \pm 3.5 mm relative to bregma and -5.0 mm relative to the surface of the skull. Ibotenic acid (0.3 μl , 10 $\mu\text{g}/\mu\text{l}$; Sigma, St. Louis, MO, USA) in 0.15 M phosphate buffer (PB) pH 7.4 was infused bilaterally at a flow rate of 0.15 $\mu\text{l}/\text{min}$. Sham operated animals received the same volume of PB. The needle was withdrawn 2 min after completion of the infusion. Pups were placed on a warming pad (MUROMACHI KIKAI CO., LTD., Tokyo, Japan) and then returned to their mothers. On PD 21 to 25, rats were weaned and grouped 2 to 3 per cage (20 cm \times 25 cm \times 40 cm). Experiments were performed in pre- (PD 35) and post-pubertal (PD 60) animals.

2.2. Drugs

Ketanserin (Sigma Chemical Co., St. Louis, MO, USA) and (\pm) - 2, 5 - dimethoxy - 4 - iodoamphetamine hydrochloride (DOI) (Sigma) were dissolved in saline, and MDL 100907 (ABX, Radeberg, Germany) was dissolved in tween 80 (0.5%) in saline. Drugs were administered in a volume of 1 ml/kg intraperitoneally (i.p.; ketanserin) or subcutaneously (s.c.; MDL100907, DOI).

2.3. Histology

Histology was conducted in a cohort of animals used for the behavioral study. To assess the size and location of the lesion, adult rats were sacrificed by decapitation and brains were removed and frozen in isopentane at -40°C and stored at -80°C until sectioning using a cryostat. Coronal sections (20 μm) were mounted onto gelatin-coated slides and stained with cresyl violet. Lesion size was confirmed by digital camera. As shown in Fig. 1, bilateral damage including neuronal loss, atrophy and cavitation of the ventral hippocampus was observed in ibotenic acid-treated rats.

2.4. Wet-dog shakes response (WDSr)

Each rat was allowed to adapt for 1 h in an observation cage (20 cm \times 25 cm \times 40 cm) before injection of the DOI (1.0 mg/kg, s.c.) or vehicle. The number of wet-dog shakes (rapid right and left movements of the head with little or no involvement of the trunk) was counted for 30 min after injection of DOI or vehicle. All groups had 9–13 animals per condition.

2.5. PPI of the acoustic startle response

Tests were conducted using SR-LAB system (SR-LAB, San Diego Instruments, San Diego, CA, USA) that comprised five sound-attenuating chambers each equipped with a cylindrical plexiglas animal enclosure (length, 16 cm; inner diameter, 8.2 cm). Ventilation was provided by a small electric fan that also generated a 70 dB background noise. Tone pulses were presented by a speaker positioned 24 cm directly above the animal enclosure. A piezoelectric accelerometer affixed

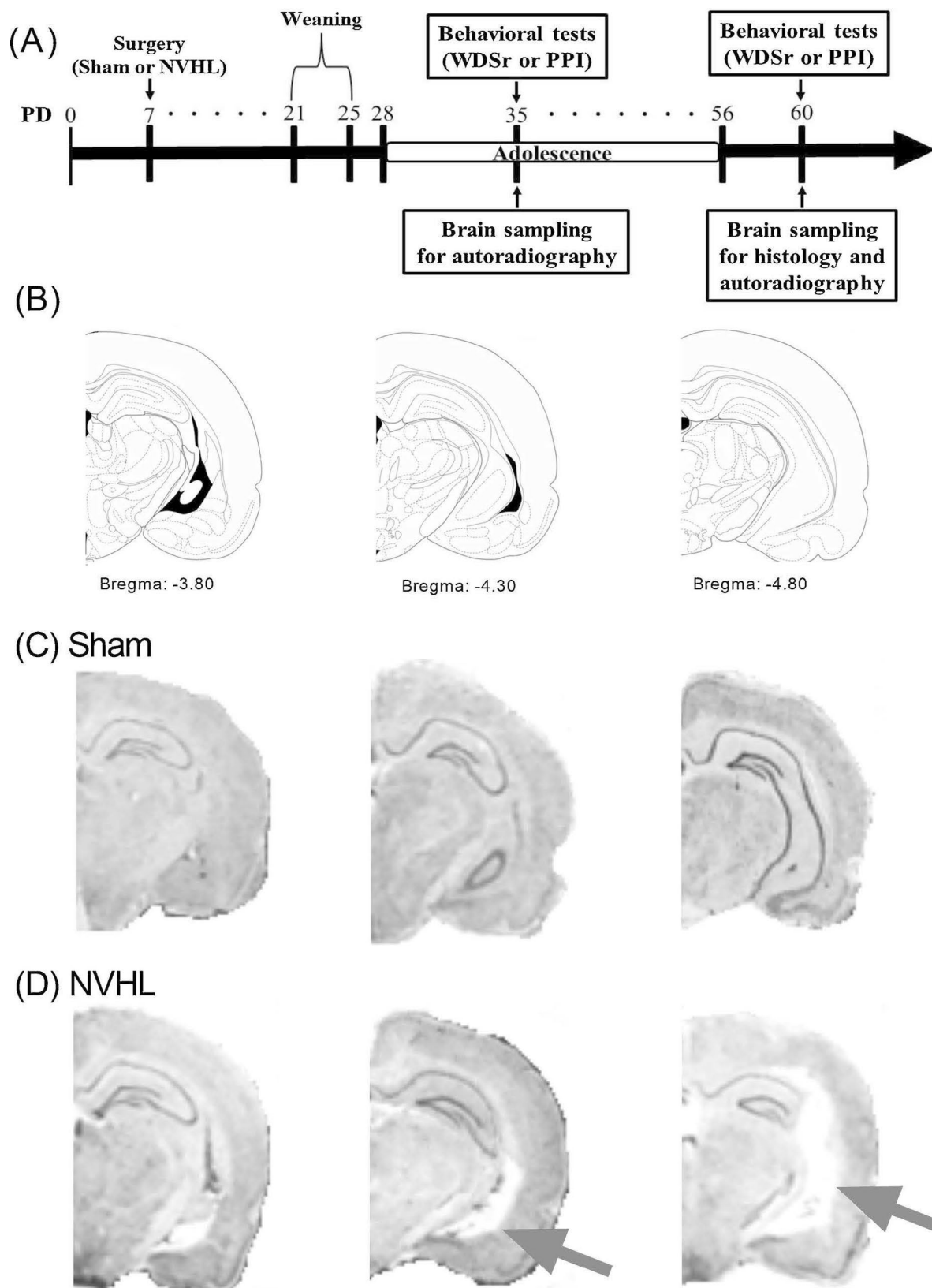


Fig. 1. Experimental time course for protocol (A). Diagram showing the dorsal to ventral hippocampus (B). (C): Sham rat. (D): NVHL rat. A typical cresyl violet stained coronal sections at the level of ventral hippocampus of a PD 60 rat indicating ibotenic acid induced neuron loss (arrow) in the ventral hippocampus (D).

to the animal enclosure frame was used to detect and transduce motion resulting from the animal's response. Tone pulse parameters were controlled by a computer using a commercial software package (SR-LAB) and interface assembly that also digitized (0–4095), rectified, and recorded stabilimeter readings.

Measures of both acoustic startle response (ASR) and PPI were obtained in a single session as described by Brake et al [20] with minor modifications. We investigated the effects of 5-HT_{2A/2C} antagonist ketanserin (0.2, 1.0 and 2.0 mg/kg, i.p.) and selective 5-HT_{2A} antagonist MDL100907 (0.1 and 0.5 mg/kg, s.c.). Thirty minutes after drug injections, rats were placed in the Plexiglas enclosure and allowed to acclimatize to the environment for 5 min before being tested during 42 discrete trials. On the first two trials, the magnitude of the ASR to a 50 ms duration of 120 dB tone was measured. These first two startle tones were presented in order to habituate the animals to the testing procedure. Therefore, the ASR magnitude of these two trials was omitted from the statistical analysis of the mean ASR amplitude. On the subsequent 40 trials, the startle tone was either presented alone or 100 ms after presentation of a 30 ms duration prepulse. Prepulse intensity ranged from 3 to 15 dB above background noise and was varied randomly between trials in 3 dB steps. Measures were taken at each of the five prepulse intensities on 5 trials; animals were randomly presented with the startle tone alone during the other 10 trials; null trials (background tone alone) during the other 5 trials. The same stimulus condition was never presented on more than two consecutive trials. The interval between each trial was programmed to a variable time schedule with an average duration of 15 s (range 5–30 s). A measure of startle response amplitude was derived from the mean of 100 digitized data points collected from stimulus onset at a rate of 1 kHz. Prepulse effectiveness in suppressing the startle response was expressed as a percentage based on the mean amplitude of responses to the startle tone alone (10 startle tones) relative to those recorded under the five prepulse conditions (5 startle tones/condition): $PPI = 100 - [(mean\ startle\ amplitude\ for\ prepulse + pulse\ trials / mean\ startle\ amplitude\ for\ pulse-alone\ trials) \times 100]\%$. The responses to five different prepulse intensities were averaged and used for statistical analysis.

2.6. Quantitative receptor autoradiography

Two cohorts of sham and NVHL rats (drug-free) were sacrificed by decapitation: one at PD 35 (pre-pubertal) and the other at PD 60 (post-pubertal). Brains were removed and frozen in isopentane at -40°C and stored at -80°C . Using a cryostat (Leica 1720, Germany), 20 μm thick coronal sections from the PFC (corresponding to plates 8–9 of the atlas of Paxinos and Watson [21]), caudate putamen (CPu) and nucleus accumbens (NAc) and ventral pallidum (VP) (plates 10–12 of the atlas of Paxinos and Watson [21]) were obtained on gelatin-coated slides and stored at -80°C until use.

5-HT_{2A} receptors and SERT binding sites were visualized using [³H] ketanserin (72.2 Ci/mmol) and [³H] citalopram (79.0 Ci/mmol) respectively (PerkinElmer Life and Analytical Sciences, Boston, MA, USA). The protocol was carried out as previously described with minor modifications [22,23]. Briefly, sections were preincubated for 15 min in 50 mM Tris-HCl buffer (NaCl 120 mM, CaCl₂ 4 mM, pH 7.4) at room temperature before a 60 min incubation into the same buffer containing either 2 nM [³H] ketanserin with 1 μM prazosin hydrochloride, and 1 μM tetrabenazine or 2 nM [³H] citalopram. Non-specific binding was determined by inclusion of 10 μM mianserin (Sigma) or 10 μM fluoxetine (TOCRIS, Ellisville, MO, USA) in the assay buffer already containing 2 nM [³H] ketanserin with 1 μM prazosin hydrochloride and 1 μM tetrabenazine or 2 nM [³H] citalopram, respectively. At the end of the incubation, sections were rinsed four times, 2 min each in ice-cold same buffer, then dipped in deionized water to remove salts and rapidly dried. All slides were exposed to tritium sensitive imaging plate (Fuji Film, Tokyo, Japan) together with [³H] microscale standards (GE Healthcare UK Ltd., Buckinghamshire, UK) for 8 days for [³H]

ketanserin binding and 10 days for [³H] citalopram binding. Specific labelling was quantified (nCi/mg wet weight) using a computer-assisted Image Reader BAS 5000 ver. 1.12 (Fuji Film).

2.7. Statistical analysis

Results are expressed as mean \pm standard error of the mean (SEM). Normality and homoscedasticity assumptions were verified prior to the use of any parametric tests (Shapiro-Wilk normality test and equality of variances F-test). An unpaired *t*-test was used to analyze the effect of the lesion on the average PPI, startle amplitude, and on the WDSr. A two-way ANOVA (group \times treatment or brain region) was used to assess the effect of drug on the average PPI and startle amplitude at PD 60 and the quantitative receptor autoradiography. Bonferroni test was used to analyze autoradiography data at both PD 35 and 60, while Tukey-kramer test was used for evaluating the effect of drugs on the average PPI and startle amplitude. In some cases, when a main effect was significant without interaction effect, we did an exploratory and limited pairwise post-hoc comparison consistent with our a priori hypothesis. All significance levels were set at a *P* value of < 0.05 .

3. Results

3.1. Histological examination of the ventral hippocampal lesion

In PD 60 (post-pubertal period) NVHL, bilateral cell loss and cavitation of the ventral hippocampus was observed while the dorsal hippocampus was spared. Fig. 1 shows a typical bilateral lesion at PD 60. Animals exhibiting damage in the dorsal hippocampus, thalamus or cortex were excluded from the study. Sham-lesioned control animals did not show any obvious damage in ventral hippocampal areas.

3.2. Changes of DOI-induced WDSr in post-pubertal NVHL rats

The administration of DOI induced WDSr in all animals; however, it was significantly greater in NVHL rats compared to sham animals at post-puberty [*t* (22) = 3.092, *p* = 0.0053, Fig. 2(B)], but not at pre-pubertal age [*t* (16) = 0.6765, *p* = 0.5084, Fig. 2(A)].

3.3. Effects of antipsychotics drugs on PPI in post-pubertal NVHL rats

Post-pubertal, but not pre-pubertal, NVHL rats exhibited significant reduction in the PPI [Pre-pubertal period: average PPI: *t* (18) = 1.742, *p* = 0.0986, startle amplitude: *t* (18) = 0.4093, *p* = 0.6871, Fig. 3(A). Post-pubertal period: average PPI: *t* (18) = 3.664, *p* = 0.0018, startle amplitude: *t* (18) = 1.088, *p* = 0.2909, Fig. 3 (B)] consistent with previous studies [20,24]. We evaluated whether administration of haloperidol (a typical antipsychotic drug) or risperidone and clozapine (atypical antipsychotics) reversed the PPI deficits in NVHL rats. The results show that NVHL-induced PPI deficits were reversed by all tested compounds except for haloperidol. The drugs produced no effect in sham animals, and had no significant effect on the startle amplitude [Fig. 3(C–E) Two-way ANOVA: haloperidol (C): average PPI: group: *F* (1, 40) = 46.62, *p* < 0.0001, treatment: *F* (1, 40) = 0.02024, *p* = 0.8876, group \times treatment: *F* (1, 40) = 0.4077, *p* = 0.5268; startle amplitude: group: *F* (1, 40) = 0.4876, *p* = 0.4890, treatment: *F* (1, 40) = 2.913, *p* = 0.0956, group \times treatment: *F* (1, 40) = 0.08907, *p* = 0.7669. Two-way ANOVA: risperidone (D): average PPI: group: *F* (1, 23) = 7.668, *p* = 0.0109, treatment: *F* (1, 23) = 17.19, *p* = 0.0004, group \times treatment: *F* (1, 23) = 4.631, *p* = 0.0421; startle amplitude: group: *F* (1, 23) = 0.2102, *p* = 0.6509, treatment: *F* (1, 23) = 0.7925, *p* = 0.3826, group \times treatment: *F* (1, 23) = 1.094, *p* = 0.3064. Post-hoc test (average PPI): *p* < 0.0001. Two-way ANOVA: clozapine (E): average PPI: group: *F* (1, 26) = 8.07, *p* = 0.0086, treatment: *F* (1, 26) = 9.01, *p* = 0.0059, group \times treatment: *F* (1, 26) = 4.075, *p* = 0.0439; startle amplitude: group: *F* (1, 26) = 0.06324, *p* = 0.8034,

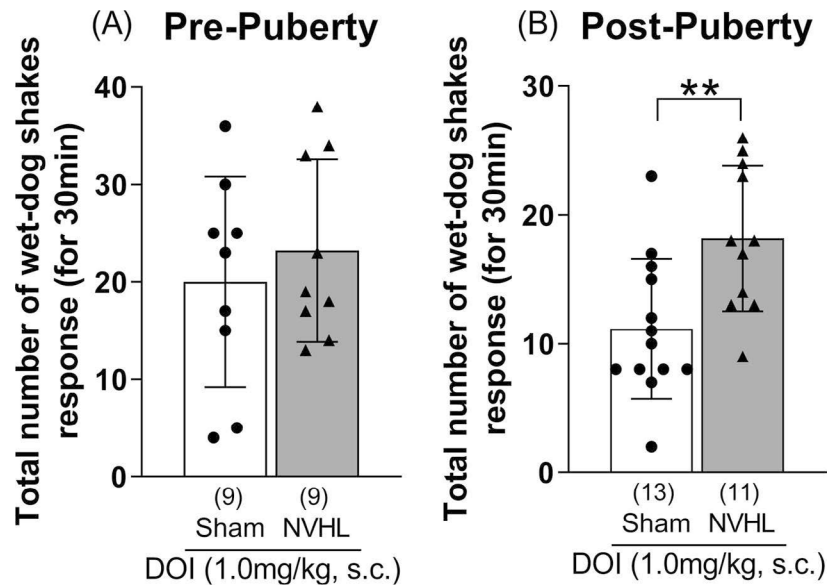


Fig. 2. Changes of DOI-induced WDSr in NVHL rats at both pre- and post-pubertal periods. Each column shows the total number of WDSr for 30 min. Vertical bars represent standard errors of means (SEM). ** $p < 0.01$ compared with sham group.

treatment: $F(1, 26) = 0.3448$, $p = 0.5622$, group \times treatment: $F(1, 26) = 0.6531$, $p = 0.4263$. Post-hoc test (average PPI): $p = 0.0010$].

3.4. Effects of 5-HT_{2A} antagonists on PPI in post-pubertal NVHL rats

In order to know whether 5-HT_{2A} receptors are involved in the impaired PPI observed in post-pubertal NVHL rats, the effects of ketanserin and MDL100907, two 5-HT_{2A} receptor antagonists, were evaluated in this behavioral test. The data show that ketanserin and MDL100907 attenuated PPI deficits in post-pubertal NVHL rats but produced no effect in sham animals. The drugs had no significant effect on the startle amplitude [Fig. 4(A) and (B) Two-way ANOVA: ketanserin (A): average PPI: group: $F(1, 45) = 29.51$, $p < 0.0001$, treatment: $F(1, 45) = 7.438$, $p = 0.0091$, group \times treatment: $F(1, 45) = 6.306$, $p = 0.0157$; startle amplitude: $F(1, 45) = 4.699$,

$p = 0.0355$, treatment: $F(1, 45) = 1.711$, $p = 0.1975$, group \times treatment: $F(1, 45) = 0.2233$, $p = 0.6388$. Post-hoc test (average PPI): $p = 0.0050$. Two-way ANOVA: MDL100907 (B): average PPI: group: $F(1, 37) = 68.83$, $p < 0.0001$, treatment: $F(1, 37) = 8.438$, $p = 0.0062$, group \times treatment: $F(1, 37) = 13.81$, $p = 0.0007$; startle amplitude: group: $F(1, 37) = 0.5083$, $p = 0.4804$, treatment: $F(1, 37) = 1.67$, $p = 0.2043$, group \times treatment: $F(1, 37) = 0.3584$, $p = 0.5530$. Post-hoc test (average PPI): $p = 0.0002$].

3.5. Quantitative receptor autoradiography of 5-HT_{2A} receptor and serotonin transporter binding sites

We investigated the levels of 5-HT_{2A} receptor binding sites in NVHL rats at both pre- and post-pubertal periods. Our observed pattern of 5HT_{2A} binding in different brain regions is consistent with previous

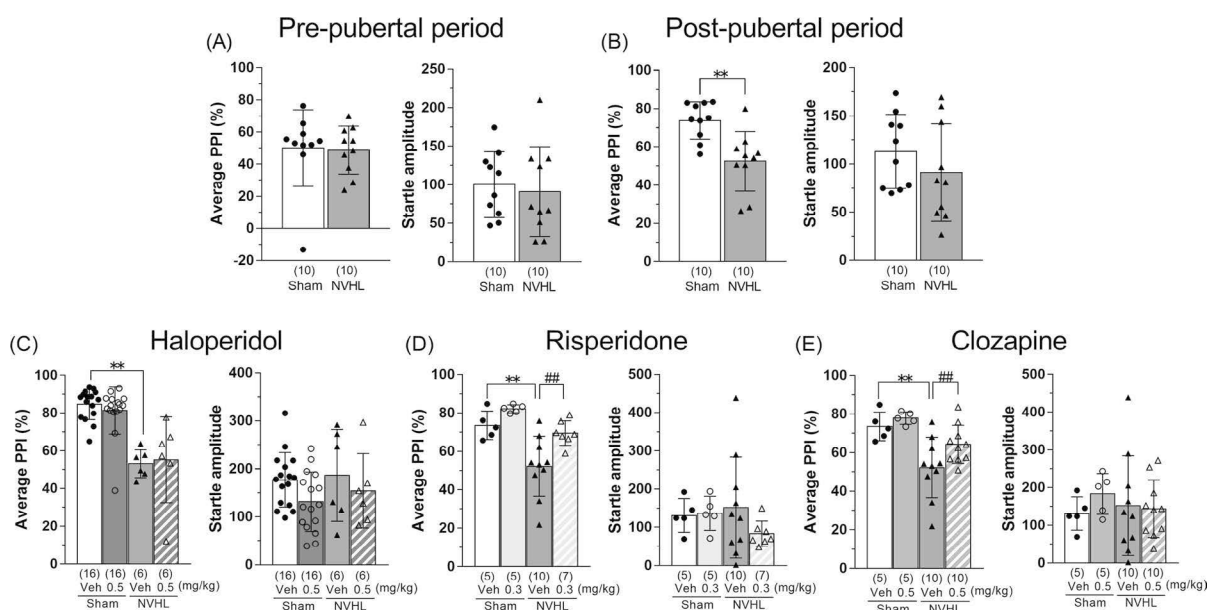


Fig. 3. Influence of NVHL rats on PPI deficits in startle reflex tested at both pre- and post-pubertal periods. Vertical bars represent SEM. ** $p < 0.01$ compared with sham/vehicle group. ## $p < 0.01$ compared with NVHL/vehicle group.

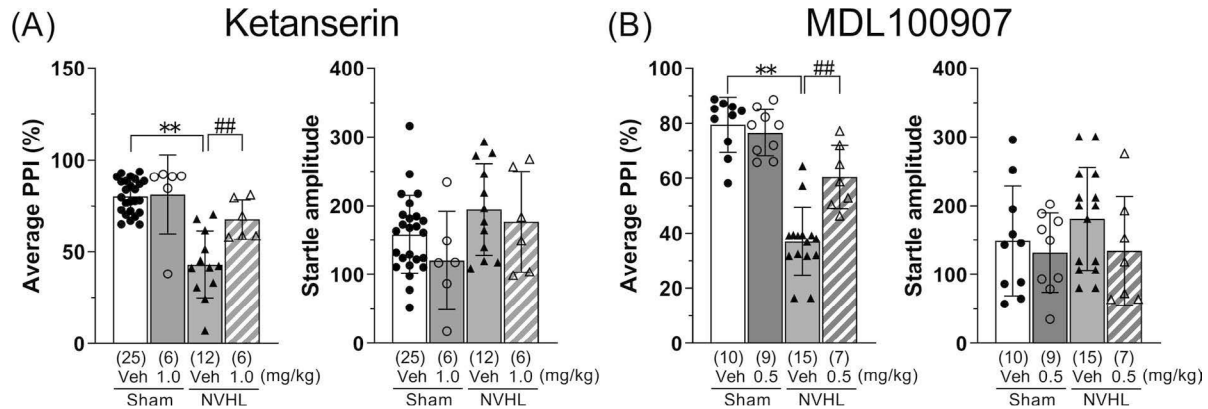


Fig. 4. Effect of ketanserin or MDL100907 in NVHL rats induced deficits in PPI of startle reflex. Vertical bars represent SEM. ** $p < 0.01$ compared with sham/vehicle group. ## $p < 0.01$ compared with NVHL/vehicle group.

literatures [3,22]. The 5-HT_{2A} receptor binding level was not significantly altered in NVHL rats at pre-pubertal period. However, significant increases in 5-HT_{2A} receptor binding sites were found in the medial prefrontal cortex (mPFC), regions viz., infralimbic cortex (IL), prelimbic cortex (PrL) and cingulate cortex area 1 (Cg1) of the post-pubertal NVHL rats compared to sham animals [Fig. 5 Two-way ANOVA: group: $F(1, 63) = 0.190$, $p = 0.6640$, brain region: $F(6, 63) = 53.422$, $p < 0.0001$ and group \times brain region: $F(6, 63) = 0.817$, $p = 0.5608$, A); group: $F(1, 133) = 15.384$, $p < 0.0001$, brain region: $F(6, 133) = 277.873$, $p < 0.0001$ and group \times brain region: $F(6, 133) = 12.376$, $p < 0.0001$, post-hoc test: IL: $p = 0.0065$, PrL: $p = 0.0012$, Cg1: $p = 0.0002$, CPu: $p > 0.9999$, NAcC: $p > 0.9999$, NAcSh: $p > 0.9999$, VP: $p = 0.4161$, B)].

The changes of SERT binding sites in different brain regions of pre- and post-pubertal NVHL rats are shown in Fig. 5(C) and (D). We observed a significant main effect of groups (sham/lesion) by ANOVA, while interaction (group \times brain region) was not significantly different at post-pubertal period [Two-way ANOVA: group: $F(1, 98) = 123.380$, $p < 0.0001$, brain region: $F(6, 98) = 25.537$, $p < 0.0001$ and group \times brain region: $F(6, 98) = 2.903$, $p = 0.0479$, post-hoc test: IL: $p = 0.0002$, PrL: $p = 0.0013$, Cg1: $p = 0.0263$, CPu: $p = 0.0082$, NAcC: $p = 0.1842$, NAcSh: $p < 0.0001$, VP: $p < 0.0001$, C); group: $F(1, 98) = 27.608$, $p < 0.0001$, brain region: $F(6, 98) = 29.601$, $p < 0.0001$, and group \times brain region: $F(6, 98) = 0.909$, $p = 0.4919$, post-hoc test: IL: $p = 0.1121$, PrL: $p = 0.0050$, Cg1: $p = 0.0595$, CPu: $p = 0.7401$, NAcC: $p = 0.0599$, NAcSh: $p = 0.0619$, VP: $p > 0.9999$, D)]. Thus, we focused on the effect of lesion, but not brain region at post-pubertal period. We found a significant increase in SERT binding all areas except NAcC at pre-pubertal period compared to sham control animals. In contrast to pre-pubertal period, increases in SERT binding of the post-pubertal NVHL rats were found PrL and Cg1 only compared to sham control animals.

4. Discussion

In the present study, we have demonstrated that post-pubertal NVHL rats exhibit increases in the levels of both 5-HT_{2A} receptors and SERT binding sites in mPFC. These increases are likely to be functionally relevant as the administration of 5-HT_{2A} agonist DOI significantly enhanced WDSr in post-pubertal NVHL rats. Moreover, we have observed that 5-HT_{2A} antagonists were able to attenuate the PPI deficits in post-pubertal NVHL rats.

The administration of DOI elicits a characteristic behavioral response that is manifested as an induction of WDSr in rats and mice [25]. The WDSr is mediated by selective activation of 5-HT_{2A} receptors, and is a useful and non-invasive marker of alterations in endogenous 5-HT_{2A} receptor activity [26]. For example, chronic administration of

antidepressants has been shown to lead to a reduction in DOI-induced WDSr, which correlates with a downregulation of central 5-HT_{2A} receptors [27]. Furthermore, it is well known that mPFC is an important region in the generation of WDSr. For example, Willins and Meltzer have found that a WDSr occurs via stimulation of 5-HT_{2A} receptor in mPFC [28]. Accordingly, the present data indicate functional hypersensitivity of 5-HT_{2A} receptors in mPFC in post-pubertal NVHL rats. The actual hyperactivation of the receptor and associated signaling pathways will be presented in a subsequent paper.

In agreement with previous reports [24,29], we have shown that NVHL rats showed significant PPI deficits at PD 60 but not PD 35. The PPI deficits in the NVHL rats are attenuated by atypical antipsychotics such as clozapine, risperidone but not by a typical antipsychotic haloperidol consistent with previous study [16]. The atypical antipsychotics, such as clozapine and risperidone, have been shown to have a high affinity for 5-HT_{2A} receptors [30]. Similar results are found in schizophrenia patients, where atypical antipsychotic drugs, but not typical antipsychotic drugs, attenuate PPI deficits in the patients [31]. Since the levels of 5-HT_{2A} binding sites were altered in several prefrontal cortical areas of post-pubertal NVHL rats, the capacity of ketanserin to attenuate the PPI deficits of NVHL rats was investigated. We observed that NVHL-induced PPI deficits were attenuated by the administration of ketanserin. However, ketanserin has affinity not only for 5-HT_{2A/2C} receptors but also α_1 and dopamine (DA) $1/2$ receptors [32,33]. It has been reported that alterations in prefrontal α_1 adrenergic receptors may contribute to altered PPI responses observed in NVHL rats [17]. However, we observed that the NVHL-induced PPI deficits were also attenuated by the administration of a more selective 5-HT_{2A} receptor antagonist MDL100907. Previous study reported that both increases and decreases in cortical 5-HT activity disrupt PPI [34]. These findings suggest that cortical serotonergic system play an important role in PPI deficit of NVHL rats.

It is possible that 5-HT system in the PFC interacts with the dopaminergic system to modulate the PPI deficit in the NVHL rats. It has been suggested that abnormalities in dopaminergic transmission in the PFC might be a critical component of abnormal behaviors in post-pubertal NVHL rats [35]. A role of prefrontal cortical DA in PPI has been reported previously. For example, reduction of dopaminergic activity in the PFC by local injection of the neurotoxin 6-hydroxydopamine was shown to induce PPI deficits [36]. Further, intra-PFC injection of a dopamine D₁ receptor antagonist enhanced DA agonist apomorphine-induced PPI deficits [37]. Systemic administration of MDL100907 has been shown to increase medial prefrontal DA efflux and 5-HT_{2A} receptor suppresses dopaminergic transmission in the PFC [38,39]. Taken together, we suggest that PPI deficits in NVHL animals may be related to increased sensitivity or activity of 5-HT_{2A} receptors which may disrupt the balance between multiple neurotransmitter

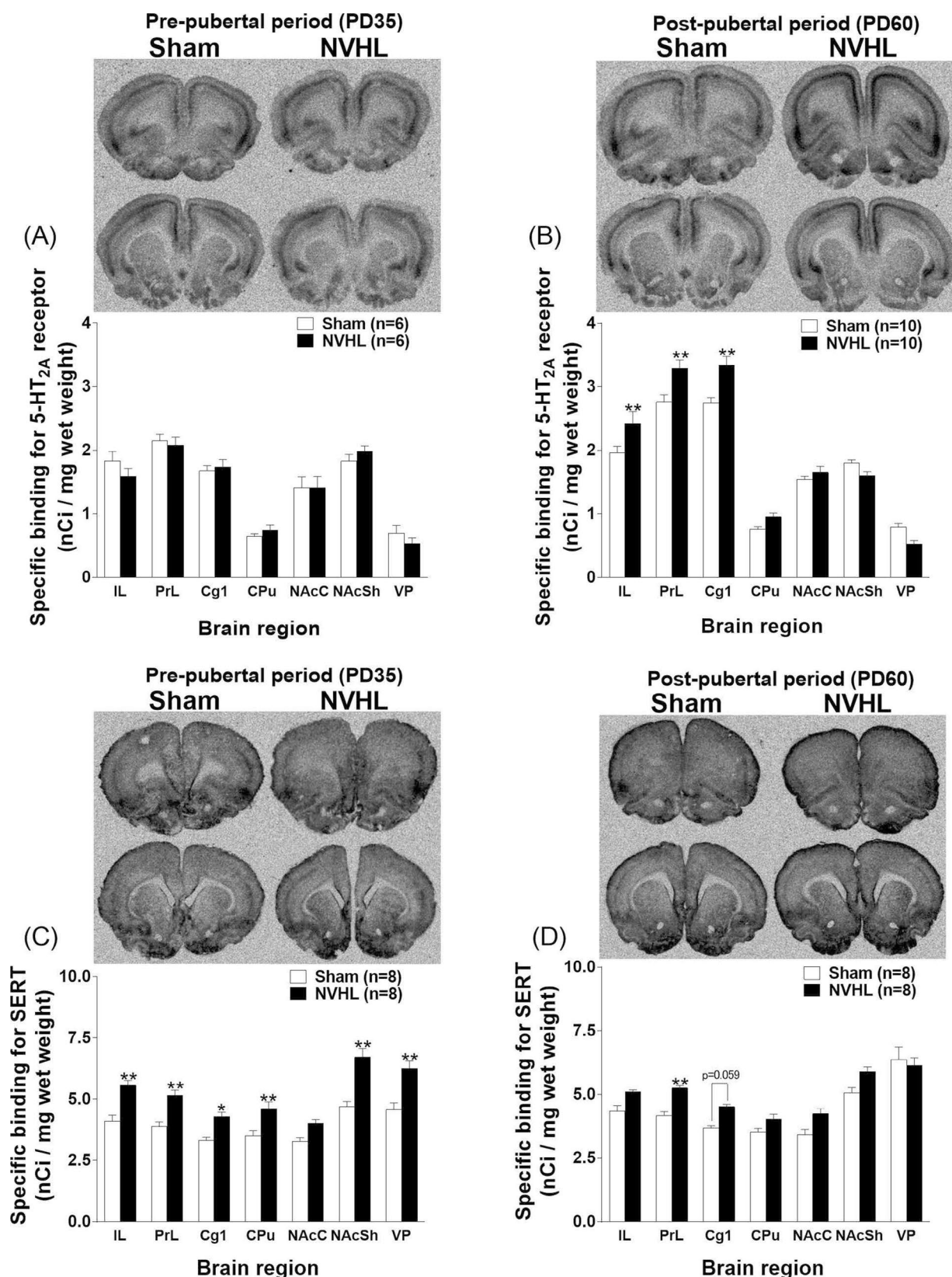


Fig. 5. Quantitative autoradiography of $[^3\text{H}]$ ketanserin or $[^3\text{H}]$ citalopram binding sites in various regions of sham and NVHL rats at PD 35 (A and C) and 60 (B and D). Non-specific binding was defined in the presence of $10\ \mu\text{M}$ mianserin for quantitative autoradiography of $[^3\text{H}]$ ketanserin and $10\ \mu\text{M}$ fluoxetine for quantitative autoradiography of $[^3\text{H}]$ citalopram. Specific binding is expressed as nCi/mg wet weight. Vertical bars represent SEM. * $p < 0.05$, ** $p < 0.01$ compared with sham group.

systems that are involved in modulating sensorimotor gating.

We found that NVHL rats have increased levels of prefrontal cortical SERT binding sites at both pre- and post-pubertal period. SERT exists at presynaptic serotonergic nerve terminal [40]. Increased SERT binding sites may indicate increased 5-HT reuptake and/or the number of 5-HT nerve terminals [41]. The present study found that SERT level in the raphe nuclei at post-pubertal period shows a tendency toward of increase ($p = 0.07$). The raphe nuclei which has 5-HT-producing neurons projects to the PFC and ventral hippocampus, respectively [42]. Thus, NVHL may induce an increase of 5-HT neurons in the PFC through the raphe nuclei. We hypothesized that increased 5-HT reuptake in the PFC results in the reduction of 5-HT levels in the subsynaptic interval, while this phenomenon induces an increase of 5-HT_{2A} receptors in the post synapse as compensatory mechanism. Interestingly, increase of SERT has been reported in PFC in schizophrenia patients [4] and genetic animal model of schizophrenia [43]. Further, an enhanced DOI-induced head twitch response (HTR) has also been shown in SERT over-expressing transgenic mice [44]. In contrast, the SERT knockout mice showed reducing HTR to DOI [45]. Thus, we consider that altered SERT binding sites in NVHL may be associated with alternation of cortical 5-HT_{2A} receptors bindings, and may indirectly induce PPI deficits.

The exact mechanism by which NVHL leads to serotonergic changes is unknown at present. However, observations in NVHL animals of altered morphology and electrophysiological properties of prefrontal pyramidal neurons [46] suggest that the lesion may initiate a re-organization within PFC with 5-HT_{2A} and SERT changes being part of this remodeling. Regardless of the mechanisms of serotonergic changes, our data in NVHL animals suggest that the alterations in serotonergic transmission may contribute to some of the behavioral changes observed in this neurodevelopmental animal model of schizophrenia. Taken together, our data also suggest that at least some of the sensorimotor gating deficits in schizophrenia patients may be due to over-stimulation of 5-HT_{2A} receptors.

Declaration of Competing Interest

Authors report no conflicts of interest.

Acknowledgments

This study was supported in part by Grants-in-Aid for Scientific Research (Grant number 18K06687) and Matching Fund Subsidy for Private University (Grant number S1511001L) from the Ministry of Education, Culture, Sports, Science and Technology of Japan.

References

- [1] B.K. Lipska, Using animal models to test a neurodevelopmental hypothesis of schizophrenia, *J. Psychiatry Neurosci.* 29 (2004) 282–286.
- [2] H.M. Abdolmaleky, S. Thiagalingam, M. Wilcox, Genetics and epigenetics in major psychiatric disorders: dilemmas, achievements, applications, and future scope, *Am. J. Pharmacogenomics* 5 (2005) 149–160.
- [3] P.W. Burnet, S.L. Eastwood, P.J. Harrison, 5-HT_{1A} and 5-HT_{2A} receptor mRNAs and binding site densities are differentially altered in schizophrenia, *Neuropsychopharmacology* 15 (1996) 442–455.
- [4] I. Hernandez, B.P. Sokolov, Abnormal expression of serotonin transporter mRNA in the frontal and temporal cortex of schizophrenics, *Mol. Psychiatry* 21 (1997) 57–64.
- [5] H.Y. Meltzer, The role of serotonin in antipsychotic drug action, *Neuropsychopharmacology* 21 (2Suppl) (1999) 106S–115S.
- [6] M.J. Arranz, R.W. Kerwin, Advances in the pharmacogenetic prediction of antipsychotic response, *Toxicology* 192 (2003) 33–35.
- [7] M.J. Arranz, J. Munro, P. Sham, G. Kirov, R.M. Murray, D.A. Collier, R.W. Kerwin, Meta-analysis of studies on genetic variation in 5-HT_{2A} receptors and clozapine response, *Schizophr. Res.* 32 (1998) 93–99.
- [8] H.M. Abdolmaleky, S.V. Faraone, S.J. Glatt, M.T. Tsuang, Meta-analysis of association between the T102C polymorphism of the 5-HT_{2A} receptor gene and schizophrenia, *Schizophr. Res.* 67 (2004) 53–62.
- [9] J.B. Fan, P. Sklar, Meta-analysis reveals association between serotonin transporter gene Stn2 VNTR polymorphism and schizophrenia, *Mol. Psychiatry* 10 (2005) 928–938.
- [10] D. Li, Y. Duan, L. He, Association study of serotonin 2A receptor (5-HT_{2A}) gene with schizophrenia and suicidal behavior using systematic meta-analysis, *Biochem. Biophys. Res. Commun.* 340 (2006) 1006–1015.
- [11] J. Williams, P. McGuffin, M. Nothen, M.J. Owen, Meta-analysis of association between the 5-HT_{2A} receptor T102C polymorphism and schizophrenia, EMAS Collaborative Group. European Multicentre Association Study of Schizophrenia, *Lancet* 349 (1997) 1221.
- [12] N.R. Swerdlow, M.A. Geyer, Using an animal model of deficient sensorimotor gating to study the pathophysiology and new treatments of schizophrenia, *Schizophr. Bull.* 24 (1998) 285–301.
- [13] N.R. Swerdlow, D.L. Braff, N. Taaid, M.A. Geyer, Assessing the validity of an animal model of deficient sensorimotor gating in schizophrenic patients, *Arch. Gen. Psychiatry* 51 (1994) 139–154.
- [14] D.L. Braff, C. Grillon, M.A. Geyer, Gating and habituation of the startle reflex in schizophrenic patients, *Arch. Gen. Psychiatry* 49 (1992) 206–215.
- [15] F. Bolino, V. Di Michele, L. Di Cicco, V. Manna, E. Daneluzzo, M. Casacchia, Sensorimotor gating and habituation evoked by electro-cutaneous stimulation in schizophrenia, *Biol. Psychiatry* 36 (1994) 670–679.
- [16] G. Le Pen, J.L. Moreau, Disruption of prepulse inhibition of startle reflex in a neurodevelopmental model of schizophrenia: reversal by clozapine, olanzapine and risperidone but not by haloperidol, *Neuropsychopharmacology* 27 (2002) 1–11.
- [17] A. Kamath, I. Al-Khairi, S. Bhardwaj, L.K. Srivastava, Enhanced alpha1 adrenergic sensitivity in sensorimotor gating deficits in neonatal ventral hippocampus-lesioned rats, *Int. J. Neuropsychopharmacol.* 11 (2008) 1085–1096.
- [18] F. Laplante, O. Nakagawasa, L.K. Srivastava, R. Quirion, Alterations in behavioral responses to a cholinergic agonist in post-pubertal rats with neonatal ventral hippocampal lesions: relationship to changes in muscarinic receptor levels, *Neuropsychopharmacology* 30 (2005) 1076–1087.
- [19] G. Flores, G. Alquier, A.B. Silva-Gomez, G. Zaldivar, J. Stewart, R. Quirion, L.K. Srivastava, Alterations in dendritic morphology of prefrontal cortical and nucleus accumbens neurons in post-pubertal rats after neonatal excitotoxic lesions of the ventral hippocampus, *Neuroscience* 133 (2005) 463–470.
- [20] W.G. Brake, G. Flores, D. Francis, M.J. Meaney, L.K. Srivastava, A. Gratton, Enhanced nucleus accumbens dopamine and plasma corticosterone stress responses in adult rats with neonatal excitotoxic lesions to the medial prefrontal cortex, *Neuroscience* 96 (2000) 687–695.
- [21] G. Paxinos, C. Watson, *The Rat Brain in Stereotaxic Coordinates*, second ed., Academic, New York, 1986.
- [22] L. Schiller, M. Jähkel, M. Kretschmar, P. Brust, J. Oehler, Autoradiographic analyses of 5-HT_{1A} and 5-HT_{2A} receptors after social isolation in mice, *Brain Res.* 980 (2003) 169–178.
- [23] S. Kusljic, M. Van den Buuse, Differential involvement of 5-HT projections within the amygdala in prepulse inhibition but not in psychotomimetic drug-induced hyperlocomotion, *Behav. Brain Res.* 168 (2006) 74–82.
- [24] G. Le Pen, J. Kew, D. Alberati, E. Borroni, M.P. Heitz, J.L. Moreau, Prepulse inhibition deficits of the startle reflex in neonatal ventral hippocampal-lesioned rats: reversal by glycine and a glycine transporter inhibitor, *Biol. Psychiatry* 54 (2003) 1162–1170.
- [25] B.B. Gorzalka, M.N. Hill, J.C. Sun, Functional role of the endocannabinoid system and AMPA/kainate receptors in 5-HT_{2A} receptor-mediated wet dog shakes, *Eur. J. Pharmacol.* 516 (2005) 28–33.
- [26] C.Y. Yap, D.A. Taylor, Involvement of 5-HT₂ receptors in the wet-dog shake behaviour induced by 5-hydroxytryptophan in the rat, *Neuropharmacology* 22 (1983) 801–804.
- [27] G.M. Goodwin, A.R. Green, P. Johnson, 5-HT₂ receptor characteristics in frontal cortex and 5-HT₂ receptor-mediated head-twitch behaviour following antidepressant treatment to mice, *Br. J. Pharmacol.* 83 (1984) 235–242.
- [28] D.L. Willins, H.Y. Meltzer, Direct injection of 5-HT_{2A} receptor agonists into the medial prefrontal cortex produces a head-twitch response in rats, *J. Pharmacol. Exp. Ther.* 282 (1997) 699–706.
- [29] G. Le Pen, L. Gaudet, P. Mortas, R. Mory, J.L. Moreau, Deficits in reward sensitivity in a neurodevelopmental rat model of schizophrenia, *Psychopharmacology (Berl.)* 161 (2002) 434–441.
- [30] B.L. Roth, D.J. Sheffler, W.K. Kroeze, Magic shotguns versus magic bullets: selectively non-selective drugs for mood disorders and schizophrenia, *Nat. Rev. Drug Discov.* 3 (2004) 353–359.
- [31] V. Kumari, E. Antonova, M.A. Geyer, D. Ffytche, S.C. Williams, T. Sharma, A fMRI investigation of startle gating deficits in schizophrenia patients treated with typical or atypical antipsychotics, *Int. J. Neuropsychopharmacol.* 10 (2007) 463–477.
- [32] K.P. Bogoso, J. Arnt, V. Boeck, A.V. Christensen, J. Hyttel, K.G. Jensen, Antihypertensive activity in a series of 1-piperazino-3-phenylindans with potent 5-HT_{2A}-antagonistic activity, *J. Med. Chem.* 31 (1988) 2247–2256.
- [33] P.H. Andersen, F.C. Gronvald, J.A. Jansen, A comparison between dopamine-stimulated adenylate cyclase and 3H-SCH23390 binding in rat striatum, *Life Sci.* 37 (1985) 1971–1983.
- [34] P.J. Fletcher, Z.F. Selhi, A. Azampanah, T.L. Sills, Reduced brain serotonin activity disrupts prepulse inhibition of the acoustic startle reflex. Effects of 5,7-dihydroxytryptamine and p-chlorophenylalanine, *Neuropsychopharmacology* 24 (2001) 399–409.
- [35] K.Y. Tseng, B.L. Lewis, B.K. Lipska, P. O'Donnell, Post-pubertal disruption of medial prefrontal cortical dopamine-glutamate interactions in a developmental animal model of schizophrenia, *Biol. Psychiatry* 62 (2007) 730–738.
- [36] M. Buser, M. Koch, Prepulse inhibition of the acoustic startle response of rats is reduced by 6-hydroxydopamine lesions of the medial prefrontal cortex, *Psychopharmacology (Berl.)* 113 (1994) 487–492.
- [37] I.E. De Jong, M. Van den Busse, SCH 23390 in the prefrontal cortex enhances the effect of apomorphine on prepulse inhibition of rats, *Neuropharmacology* 51 (2006)

- 438–446.
- [38] C.J. Schmidt, G.M. Fadayel, The selective 5-HT_{2A} receptor antagonist, MDL 100,907, increases dopamine efflux in the prefrontal cortex of the rat, *Eur. J. Pharmacol.* 273 (1995) 273–279.
 - [39] S. Kapur, G. Remington, Serotonin-dopamine interaction and its relevance to schizophrenia, *Am. J. Psychiatry* 153 (1996) 466–476.
 - [40] R. Hurlmann, A. Matusch, K.U. Kuhn, J. Berning, D. Elmenhorst, O. Winz, H. Kolsch, K. Zilles, M. Wagner, W. Maier, A. Bauer, 5-HT_{2A} receptor density is decreased in the at-risk mental state, *Psychopharmacology* 195 (2008) 579–590.
 - [41] P. Govitrapong, S. Mukda, W. Turakitwanakan, H. Dumrongphol, C. Chindaduangratn, Y. Sanvarinda, Platelet serotonin transporter in schizophrenic patients with and without neuroleptic treatment, *Neurochem. Int.* 41 (2002) 209–216.
 - [42] A. Der-Avakian, A. Markou, The neurobiology of anhedonia and other reward-related deficits, *Trends Neurosci.* 35 (2012) 68–77.
 - [43] B. Dean, T. Karl, G. Pavey, S. Boer, L. Duffy, E. Scarr, Increased levels of serotonin 2A receptors and serotonin transporter in the CNS of neuregulin 1 hypomorphic/mutant mice, *Schizophr. Res.* 99 (2008) 341–349.
 - [44] K.A. Jennings, W.J. Sheward, A.J. Harmar, T. Sharp, Evidence that genetic variation in 5-HT transporter expression is linked to changes in 5-HT_{2A} receptor function, *Neuropharmacology* 54 (2008) 776–783.
 - [45] Y. Qu, N. Villacreses, D.L. Murphy, S.I. Rapoport, 5-HT_{2A/2C} receptor signaling via phospholipase A2 and arachidonic acid is attenuated in mice lacking the serotonin reuptake transporter, *Psychopharmacology* 180 (2005) 12–20.
 - [46] P. O'Donnell, B.L. Lewis, D.R. Weinberger, B.K. Lipska, Neonatal hippocampal damage alters electrophysiological properties of prefrontal cortical neurons in adult rats, *Cereb. Cortex* 12 (2002) 975–982.



Contents lists available at ScienceDirect

Bioorganic & Medicinal Chemistry Letters

journal homepage: www.elsevier.com/locate/bmclER subtype selectivity of *m*-carborane-containing phenols: *C*-alkyl groups on the *m*-carborane cage enhance ER α selectivityKiminori Ohta^{a,*}, Takumi Ogawa^b, Koichi Kato^{c,d}, Akifumi Oda^c, Yasuyuki Endo^b^a School of Pharmacy, Showa University, 1-5-8, Hatanodai, Shinagawa-ku, Tokyo 142-8555, Japan^b Faculty of Pharmaceutical Sciences, Tohoku Medical and Pharmaceutical University, 4-4-1 Komatsushima, Aoba-ku, Sendai 981-8558, Japan^c Faculty of Pharmacy, Meijo University, 150 Yagotoyama, Tenpaku-ku, Nagoya 468-8503, Japan^d Department of Pharmacy, Kinjo Gakuin University, 2-1723 Omori, Moriyama-ku, Nagoya, Aichi 463-8521, Japan

ARTICLE INFO

Keywords:

Carborane

Estrogen receptor

ER α

Subtype selectivity

ABSTRACT

Estrogen receptor (ER) exhibits two subtypes, ER α and ER β , whose biological functions are quite different despite expression in the same tissues. We developed diiodo-*m*-carborane derivative **3a**, which showed 14-fold selectivity for ER β with high binding affinity toward ER β . Interestingly, introduction of an alkyl group into the carbon atom of the *m*-carborane cage of **3a** markedly enhanced the binding affinity toward ER α and decreased affinity toward ER β . *C*-*n*-propyl derivative **3d** showed 28-fold selectivity for ER α in an ER binding assay and promoted proliferation of MCF-7 breast cancer cells. Docking simulation studies suggest that the directions of the *n*-propyl group and the diiodo substituent introduced on the *m*-carborane cage play important roles for the control of ER subtype selectivity. As **3a** and **3d** showed ER β and ER α selectivity with high binding affinity, respectively, these ligands may be useful as biological tools to aid in understanding the different roles of ER subtypes.

Since the discovery of estrogen receptor α (ER α) in 1986,¹ ardent studies on ER have continued in a variety of research fields, such as biology,² pharmacology,² physiology,² physical chemistry,³ as well as medicinal chemistry.⁴ ER α is a well known member of the nuclear receptor superfamily and mainly present in female reproductive organs and bone.^{1,2} Additionally, transmembrane ER has also been discovered and belongs to the G-protein coupled receptor (GPCR) family.⁵ ER α is activated by endogenous estrogen, 17 β -estradiol (E2, **1**, Fig. 1), and regulates various important physiological processes, including development and function of the female reproductive system, maintenance of bone mineral density, tumor repressive effects, cardiovascular health, and protection of the central nervous system.² Decrease of E2 production after menopause induces ER α deactivation and may lead to osteoporosis and menopause. ER α agonists are often used for estrogen replacement therapy but increased risk of breast cancer. Recently, several tissue selective estrogen receptor modulators (SERMs), which show tissue selective agonist or antagonist activities by selective recruitment of co-repressors or co-activators toward ER α , have been discovered as potential therapeutic agents for osteoporosis, and menopause, in addition to breast cancer.⁶

ER-subtype β (ER β) was cloned from a rat ventral prostate cDNA library as a second form of ER α .⁷ ER β is also activated by E2, but

exhibits quite different biological functions from ER α despite expression in the same tissues.⁸ Recent studies suggest that ER subtype selective modulators offer potential as therapeutic agents for ER-related diseases, such as depression,⁹ Alzheimer's disease,¹⁰ multiple sclerosis,¹¹ metabolic disorders,¹² cardiovascular diseases,¹³ and various type of cancers.¹⁴ The subtype selective ligands can be used to elicit beneficial estrogen activities and reduce side effects.¹⁵ Thus, the discovery of subtype selective ER modulators is of particular interest to medicinal chemists, for the ultimate benefit of patients with ER-dependent diseases. However, development of ER subtype selective ligands is a major challenge, because the structural differences within the hydrophobic ligand binding domains (LBDs) of ERs occur at only two amino acid residues: Leu384 and Met421 in ER α , which are replaced by Met336 and Ile373, respectively, in ER β .¹⁶

We have developed several ER β -selective ligands using a carborane cage as a hydrophobic pharmacophore.¹⁷ Recently, we reported that *B*-iodo-*m*-carboranyl phenols **2a** and **3a** showed high ER β -selectivity with potent binding affinity toward ER β (Fig. 1).¹⁸ Table 1 summarizes the relative binding affinity (RBA) and the selectivity index (SI) values of *m*-carborane-containing ER β -selective ligands toward ER α and ER β . The SAR studies revealed that the iodine atom on the boron atom of the *m*-carborane cage enhanced the binding affinity toward ER β , while the

* Corresponding author.

E-mail address: ohta@pharm.showa-u.ac.jp (K. Ohta).<https://doi.org/10.1016/j.bmcl.2019.06.025>

Received 25 April 2019; Received in revised form 17 June 2019; Accepted 18 June 2019

Available online 19 June 2019

0960-894X/ © 2019 Elsevier Ltd. All rights reserved.

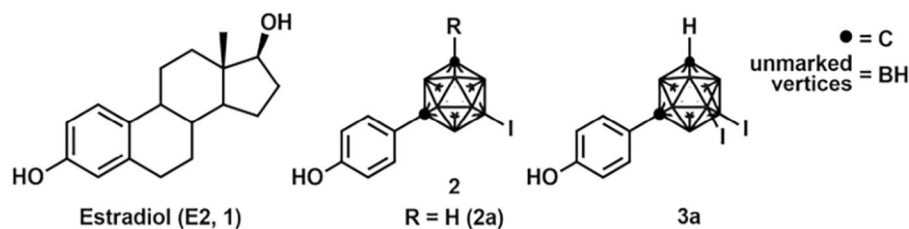


Fig. 1. Structures of 17 β -estradiol (E2, 1) and *m*-carborane-containing ER β -selective ligands 2a and 3a.

Table 1
Relative binding affinity (RBA) and selectivity index (SI) values of *m*-carborane derivatives 2a–2e and 3a.

Compound	R	RBA		
		ER α	ER β	SI for ER β
2a	H	13	129	9.9
2b	I	8.4	81	9.6
2c	Allyl	17	62	3.6
2d	<i>n</i> -Butyl	29	157	5.4
2e	Benzyl	28	19	0.68
3a	–	8.0	111	14

C-substituents of the *m*-carborane cage reduced and enhanced the binding affinities toward ER β and ER α , respectively. In particular, compound 2e, with a benzyl group, showed little selectivity. As substituents on the *m*-carborane cage greatly affected the ER subtype selectivity, the *m*-carborane cage seems both suitable and attractive as a hydrophobic pharmacophore for the discovery of ER subtype-selective ligands.

Thus, novel *m*-carborane-containing ER subtype-selective ligands, which exhibit high ER α or ER β selectivity with high binding affinity toward either ER subtype, were designed using 3a as a lead compound. Development of novel ER α selective agonist is quite important for the discovery of new functions of ER α . We were interested in the substitution on the carbon atom of the *m*-carborane cage, the transformation of the B–I bonds into B-alkyl groups, and the introduction of a methylene linker between the phenol ring and the *m*-carborane cage (Fig. 2). Herein, we describe the syntheses of several *m*-carborane-containing phenols, 3–5, evaluation of their ER binding affinities and selectivity, biological functions of 3d against the estrogen-dependent breast cancer cell line MCF-7, and results of a docking simulation study of both the parent 3a and 3d toward ER α and ER β .

The synthesis of the *m*-carborane-containing phenol derivatives 3–5 is summarized in Scheme 1. 7,9-Diiodo-*m*-carborane, 6, which was prepared by iodination of *m*-carborane with I₂ in the presence of AlCl₃,¹⁹ was treated with *n*-BuLi to obtain the C–Li salt, which was transformed into the C–Cu salt in the presence of CuCl (I) and reacted with 4-iodoanisole in the presence of pyridine as a base and a ligand for

Cu to obtain the key intermediate 7 at a 65% yield.²⁰ The C–Li salt obtained from the reaction of 7 with *n*-BuLi was reacted with an alkyl halide and I₂, followed by demethylation with BBr₃, to afford 3b–3f at 12–56% yields over two steps. The iodine atoms of 7 were transformed into methyl and ethyl groups using the corresponding alkyl Grignard reagents under conditions of Pd-catalyzed coupling.²¹ When methylmagnesium bromide was used in this coupling reaction, the *B*,*B*-dimethyl derivative was obtained, which was dimethylated to produce 4a at a 61% yield over two steps. Unexpectedly, use of ethylmagnesium bromide instead of methylmagnesium bromide afforded the *B*-monoethylated derivative owing to steric hindrance of the ethyl group, which was transformed into the corresponding phenol 4b at a 14% yield over two steps. The C–Li salt obtained from the reaction of 6 with *n*-BuLi was reacted with 4-methoxybenzyl chloride, followed by demethylation with BBr₃, to afford 5 at a 2% yield over two steps. The benzylation of *m*-carborane cage gave mono- and di-substituted intermediates which are hard to separate, and thus the yield of 5 is quite low.

The binding affinity of the synthesized compounds toward ER α and ER β was evaluated by means of a competitive binding assay using [2,4,6,7-³H]17 β -estradiol.¹⁷ Table 2 summarizes the RBA and SI values toward both ERs. Surprisingly, introduction of a methyl group onto the carbon atom of the *m*-carborane cage of 3a markedly enhanced the binding affinity toward ER α , but reduced affinity toward ER β . Thus, the C-methylated derivative 3b exhibited 4.4-fold higher selectivity toward ER α vs ER β ; nevertheless, the lead compound 3a acted as an ER β -selective ligand. The C-ethyl derivative 3c exhibited similar binding affinity toward both ER α and E2. The binding affinity of the C-propyl derivative 3d toward ER β was markedly decreased, yet 3d exhibited high ER α binding affinity, and thus showed the highest SI values among the tested compounds, and a 28-fold selectivity for ER α vs ER β . Although an alkyl group on the carbon atom of the *m*-carborane cage of 3a is important for enhancing the ER α binding affinity, likely via hydrophobic interaction with the amino acid residues of the ER α LBD, an *n*-butyl group is likely too large for similar interactions with ER α LBD. Thus, 3e exhibited lower selectivity toward ER α than 3d. 3f showed similar RBA and SI values to those of 3b, owing to the similar van der Waals radii of the iodine atom and methyl group. The RBA values of 7,9-dimethyl-*m*-carboranylphenol (4a) were similar to those of the parent compound (3a) but the ER subtype selectivity was reduced. The RBA values of 4b toward both ERs were not high, and the *B*-ethyl group of 4b may be too large for interaction with both ER LBDs. Thus, 4b showed little ER subtype selectivity. A methylene group between the *m*-carborane cage and the phenol group of 5 enhanced flexibility of the hydrophobic pharmacophore, and the binding affinities toward both ER α and ER β were markedly decreased. Additionally, the SI values of 5 were similar to those of 1 and the ER subtype selectivity was diminished.

The biological profiles, namely agonistic and antagonistic activities, of compound 3d were evaluated by means of a cell proliferation assay using the MCF-7 cell line, which shows estrogen-dependent cell growth (Fig. 3).¹⁷ Compound 3d promoted MCF-7 cell proliferation in a concentration-dependent manner, and acted as an ER agonist, similar to endogenous estrogen (E2).

To understand the effect of alkyl substituents on the carbon atom of the *m*-carborane ring in 3 on ER subtype selectivity, we performed

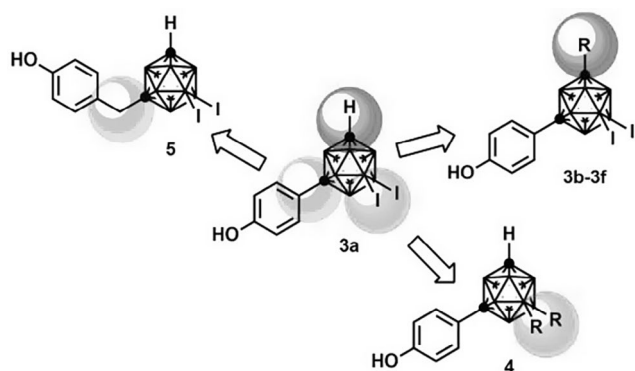
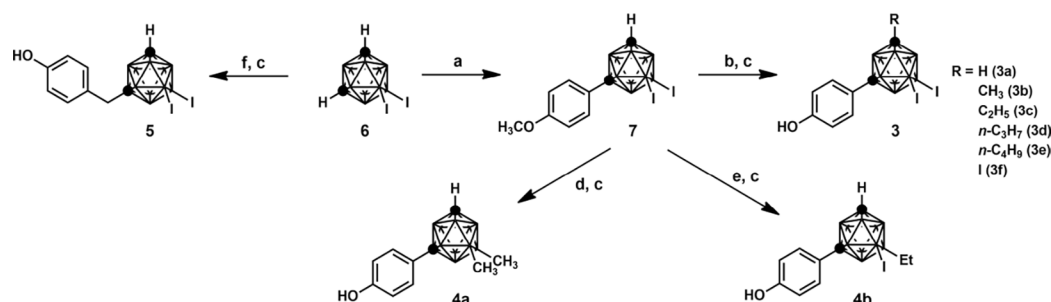


Fig. 2. Design of the ER subtype-selective ligand candidates 3–5.



Scheme 1. Synthesis of novel *m*-carborane derivatives 3–5. *Reagent and conditions:* (a) (i) *n*-BuLi, DME, 0 °C; (ii) CuCl, rt; (iii) 4-iodoanisole, pyridine, 100 °C; (b) (i) *n*-BuLi, THF, 0 °C; (ii) alkyl halides or I₂, rt; (c) BBr₃, CH₂Cl₂, 0 °C; (d) CH₃MgBr, PdCl₂(PPh₃)₂, CuI, THF, reflux; (e) C₂H₅MgBr, PdCl₂(PPh₃)₂, CuI, THF, reflux; (f) (i) *n*-BuLi, THF, 0 °C; (ii) 4-methoxybenzyl chloride, rt.

Table 2

Binding affinity and subtype selectivity of the synthesized compounds 3–5 toward ERα and ERβ.^a

Compound	R	RBA ^b		SI ^c
		ERα	ERβ	ERα/ERβ
3a	H	8	111	0.07
3b	CH ₃	61	14	4.4
3c	C ₂ H ₅	99	14	7.1
3d	<i>n</i> -C ₃ H ₇	65	2.3	28
3e	<i>n</i> -C ₄ H ₉	36	2.9	12
3f	I	59	26	2.3
4a	–	12	75	0.16
4b	–	18	30	0.6
5	–	0.005	0.004	1.3

^a All binding assays were treated with the test compounds (0.4 nM–4 μM) in the presence of [2,4,6,7-³H]17β-estradiol (4 nM) and performed in triplicate (*n* = 3).

^b RBA values were calculated from the IC₅₀ values of E2 and test compounds, taking that of E2 as 100%.

^c Subtype selectivity was estimated from the RBA values toward ERα and ERβ.

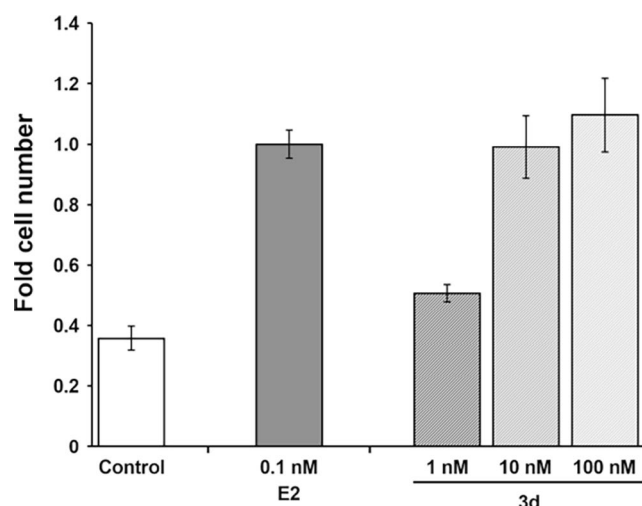


Fig. 3. Concentration-dependent MCF-7 cell proliferation induced by 3d. MCF-7 cells were incubated with 3d (100 nM–1 nM) for 5 days, and the results are shown as fold cell number, with the value for 0.1 nM E2 taken as 1. Assays were performed in triplicate (*n* = 3).

docking simulation studies of 3a and 3d for ERα²² and ERβ²² using a docking program (GOLD 5.2).²³ Results are summarized in Fig. 4. Each phenol group of 3a and 3d formed hydrogen bonds with both the

guanidino group of Arg394 and the carbonyl group of Leu384 in the backbone of the α-helix in ERα (Fig. 4A and B). Upon binding to ERβ, each phenol group of 3a and 3d formed hydrogen bonds with the amino acid residues of Arg346 and Glu304 (Fig. 4C and D). The diiodo substituent of 3a was located at the hydrophobic pocket of ERα, which contains sufficient space and is comprised of Leu387, Met421, Ile424, and Leu525 (Fig. 4A). Upon binding to ERβ, the diiodo substituent of 3a was located near the hydrophobic amino acid residues Ile373 and Ile376 (Fig. 4C). It is suggested that the diiodo-*m*-carborane cage is of a suitable size for interaction with the hydrophobic pocket of ERβ. The *n*-propyl group of 3d is much larger than the diiodo substituent and is close to both the Met421 and Ile424 residues of ERα. Thus, the diiodo substituent of 3d was turned within the hydrophobic pocket to allow the substituted-*m*-carborane structure of 3d to fit well within the hydrophobic pocket of ERα (Fig. 4B). As the alkyl substituents of 3 were made longer, the RBA values toward ERα increased, and the ethyl derivative 3c showed the highest RBA value. Methyl group of 3b would be slightly small for the hydrophobic space formed by both the Met421 and Ile424 residues of ERα. On the other hand, the *n*-propyl group of 3d exhibited steric repulsion with Ile373 of ERβ and was swung backwards against the binding mode of 3d with ERα (Fig. 4D). Compounds 3b and 3c with a methyl and ethyl groups, respectively, would be slightly large for ERβ LBD. The substituted-*m*-carborane structure of 3d is too large for interaction with the hydrophobic pocket of ERβ, and thus the binding affinity of 3d for ERβ was low. Results of the calculation explain the effects of the alkyl group of 3 on the binding affinity for ERα and ERβ.

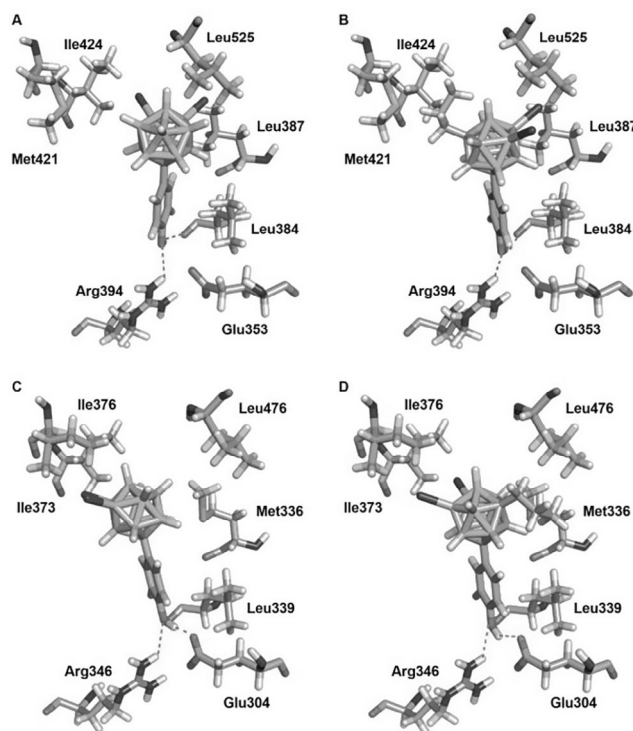


Fig. 4. Comparisons of docking models of **3a** and **3d** with ER α and ER β (atom colors: H (white), B (pink), C (gray), N (purple), O (red), S (yellow) and I (purple)). (A) Binding mode of **3a** with the ER α LBD (baggy). (B) Binding mode of **3d** with the ER α LBD (well fitted). (C) Binding mode of **3a** with the ER β LBD (well fitted). (D) Binding mode of **3d** with the ER β LBD (too tight).

In conclusion, we designed and synthesized various *m*-carborane-containing phenol derivatives as ER subtype-selective ligand candidates using **3a** as the lead compound. Although introduction of a hydrophobic substituent on the carbon atom of the *m*-carborane cage greatly affected the binding affinity toward ERs, the other chemical transformations of **3a** showed no improvements in binding affinity. Thus, we found that the 7, 9-diiodo-*m*-carboranylphenol structure acts as a suitable pharmacophore for ER subtype-selective ligands. Compound **3d** showed the highest ER α selectivity and ER agonistic activity in a MCF-7 cell proliferation assay. Docking simulation studies of **3a** and **3d** for ER α and ER β suggest that the directions of the *n*-propyl group and the diiodo substituent introduced into the *m*-carborane cage play important roles for the control of ER subtype selectivity. These findings offer useful information for the potential design of ER modulators, as well as SERMs.

Acknowledgments

This research was supported by a Grant-in-Aid for the Strategic

Research Program for Private Universities (2015–2019) and a Grant-in-Aid for Scientific Research (C) (15K08029) from the Japanese Ministry of Education, Culture, Sports, Science, and Technology (MEXT, Japan).

References


- Green S, Walter P, Kumar V, et al. *Nature*. 1986;320:134.
- (a) Bhardwaj P, Au CC, Benito-Martin A, et al. *J Steroid Biochem Mol Biol*. 2019;189:161; (b) Thomas C, Gustafsson J-A. *Trends Endocrinol Metab*. 2015;26:467.
- (a) Perkins MS, Louw-du Toit R, Africander D. *J Steroid Biochem Mol Biol*. 2017;174:27; (b) Fan P, Maximov PY, Curpan RF, Abderrahman B, Jordan VC. *Mol Cell Endocrinol*. 2015;418:245.
- (a) Gajadeera N, Hanson RN. *Steroids*. 2019;144:30; (b) McDonnell DP, Wardell SE, Norris JD. *J Med Chem*. 2015;58:4883.
- (a) Rosenfeld CS, Cooke PS. *J Steroid Biochem Mol Biol*. 2019;187:106; (b) Levin ER. *Steroids*. 2018;132:1.
- Patel HK, Bihani T. *Pharmacol Ther*. 2018;186:1.
- Kuiper GGJM, Enmark E, Peltö-Huikko M, Nilsson S, Gustafsson J-A. *Proc Natl Acad Sci USA*. 1996;93:5925.
- (a) Warner M, Huang B, Gustafsson J-A. *Trends Pharmacol Sci*. 2017;38:92; (b) Williams C, DiLeo A, Niv Y, Gustafsson J-A. *Cancer Lett*. 2016;372:48.
- Walf AA, Frye CA. *Physiol Behav*. 2010;99:169.
- George S, Petit GH, Gouras GK, Brundin P, Olsson R. *ACS Chem Neurosci*. 2013;4:1537.
- Tiwari-Woodruff S, Morales LBJ, Lee R, Voskuhl RR. *Proc Natl Acad Sci USA*. 2007;104:14813.
- (a) Ahmed MA, Hassanein KMA. *Int J Physiol Pathophysiol Pharmacol*. 2012;4:156; (b) Mauvais-Jarvis F, Clegg DJ, Hevener AL. *Endocr Rev*. 2013;34:309.
- (a) Murphy E. *Circ Res*. 2011;109:687; (b) Adlanmerini M, Solinhac R, Abot A, et al. *Proc Natl Acad Sci USA*. 2013;111:E283.
- (a) Haldosen L-A, Zhao C, Dahlman-Wright K. *Mol Cell Endocrinol*. 2014;382:665; (b) Pravettoni A, Mornati O, Martini PGV, et al. *Mol Cell Endocrinol*. 2007;263:46; (c) Kim IY, Kim B-C, Seong DH, et al. *Cancer Res*. 2002;62:5365.
- Paterni I, Granchi C, Katzenellenbogen JA, Minutolo F. *Steroid*. 2014;90:13.
- (a) Paech K, Webb P, Kuiper GGJM, et al. *Science*. 1997;277:1508; (b) Brzozowski AM, Pike AC, Dauter Z, et al. *Nature*. 1997;389:753.
- (a) Ohta K, Ogawa T, Kaise A, Endo Y. *Bioorg Med Chem Lett*. 2013;23:6555; (b) Ohta K, Ogawa T, Oda A, Kaise A, Endo Y. *Chem Pharm Bull*. 2014;62:386; (c) Ohta K, Ogawa T, Oda A, Kaise A, Endo Y. *Bioorg Med Chem Lett*. 2015;25:4174.
- Ohta K, Ogawa T, Endo Y. *Bioorg Med Chem Lett*. 2017;27:4030.
- Ohta K, Ogawa T, Kaise A, Endo Y. *Bioorg Med Chem*. 2014;22:3508.
- (a) Ohta K, Goto T, Endo Y. *Inorg Chem*. 2005;44:8569; (b) Coult R, Fox MA, Gill WR, Herbertson PL, MacBride JAH, Wade K. *J Organomet Chem*. 1993;462:19.
- Kovredov AI, Shaugumbekova Zh.S, Petrovskii PV, Zakharkin LIZh. *Obshch Khim*. 1989;59:607.
- The docking simulation study were performed using 3D structures of human ER α and ER β which were retrieved from the Protein Data Bank (PDB ID: 1ERE and 2IOG, respectively).
- Jones G, Willett P, Glen RC. *J Mol Biol*. 1995;245:43.

RESEARCH

Open Access



Effect of *Enterococcus faecalis* 2001 on colitis and depressive-like behavior in dextran sulfate sodium-treated mice: involvement of the brain–gut axis

Kohei Takahashi^{1,2}, Osamu Nakagawasai^{1*} , Wataru Nemoto¹, Takayo Odaira¹, Wakana Sakuma¹, Hiroshi Onogi³, Hiroaki Nishijima⁴, Ryuji Furihata⁵, Yukio Nemoto⁶, Hiroyuki Iwasa⁷, Koichi Tan-No¹ and Takeshi Tadano^{1,8}

Abstract

Background: Patients with inflammatory bowel disease (IBD), including those with ulcerative colitis and Crohn's disease, have higher rates of psychiatric disorders, such as depression and anxiety; however, the mechanism of psychiatric disorder development remains unclear. Mice with IBD induced by dextran sulfate sodium (DSS) in drinking water exhibit depressive-like behavior. The presence of *Lactobacillus* in the gut microbiota is associated with major depressive disorder. Therefore, we examined whether *Enterococcus faecalis* 2001 (EF-2001), a biogenic lactic acid bacterium, prevents DSS-induced depressive-like behavior and changes in peripheral symptoms.

Methods: We evaluated colon inflammation and used the tail suspension test to examine whether EF-2001 prevents IBD-like symptoms and depressive-like behavior in DSS-treated mice. The protein expression of tumor necrosis factor- α (TNF- α), interleukin-6 (IL-6), X-linked inhibitor of apoptosis protein (XIAP), and cleaved caspase-3 in the rectum and hippocampus was assessed by western blotting. Hippocampal neurogenesis, altered nuclear factor-kappa B (NFkB) p65 morphometry, and the localization of activated NFkB p65 and XIAP were examined by immunohistochemistry.

Results: Treatment with 1.5% DSS for 7 days induced IBD-like pathology and depressive-like behavior, increased TNF- α and IL-6 expression in the rectum and hippocampus, activated caspase-3 in the hippocampus, and decreased hippocampal neurogenesis. Interestingly, these changes were reversed by 20-day administration of EF-2001. Further, EF-2001 administration enhanced NFkB p65 expression in the microglial cells and XIAP expression in the hippocampus of DSS-treated mice.

Conclusion: EF-2001 prevented IBD-like pathology and depressive-like behavior via decreased rectal and hippocampal inflammatory cytokines and facilitated the NFkB p65/XIAP pathway in the hippocampus. Our findings suggest a close relationship between IBD and depression.

Keywords: Antidepressant, Apoptosis, EF-2001, Inflammatory bowel disease, Neurogenesis, Neuroinflammation

* Correspondence: osamun@tohoku-mpu.ac.jp

¹Department of Pharmacology, Faculty of Pharmaceutical Sciences, Tohoku Medical and Pharmaceutical University, 4-4-1 Komatsushima, Aoba-ku, Sendai 981-8558, Japan

Full list of author information is available at the end of the article



© The Author(s). 2019 **Open Access** This article is distributed under the terms of the Creative Commons Attribution 4.0 International License (<http://creativecommons.org/licenses/by/4.0/>), which permits unrestricted use, distribution, and reproduction in any medium, provided you give appropriate credit to the original author(s) and the source, provide a link to the Creative Commons license, and indicate if changes were made. The Creative Commons Public Domain Dedication waiver (<http://creativecommons.org/publicdomain/zero/1.0/>) applies to the data made available in this article, unless otherwise stated.

Background

Inflammatory bowel disease (IBD), which comprises ulcerative colitis and Crohn's disease, affects approximately 2.2 million people in Europe and 1.4 million people in the USA. Recent studies have demonstrated a connection between intestinal inflammation and changes in brain function [1]. Inflammation in the bowel is associated with alterations in the central nervous system, as revealed by the activation of tumor necrosis factor- α (TNF- α) signaling and microglia in the brain [2]. Other researchers have demonstrated that chronic experimental colitis increases anxiety behavior in mice [3]. Further, peripheral inflammation may account for at least some of the neurological and behavioral changes associated with chronic inflammatory diseases. Indeed, patients with IBD have higher rates of obsessive-compulsive disorder, panic disorder, depression, and anxiety [4–7].

A well-characterized mouse model of IBD is produced by repeated administration of dextran sulfate sodium (DSS) in drinking water [8]. DSS does not cross the blood–brain barrier because of its higher molecular weight. Epithelial cell toxicity, increased intestinal permeability, and macrophage activation are implicated in the deleterious effects of DSS. The DSS model is characterized by colonic epithelial cell lesions and acute (7–14 days after the beginning of the treatment) intestinal inflammation [9]. Repeated DSS cycling in combination with treatment with azoxymethane, a genotoxic agent, induced colitis-dependent neoplasia, generating a commonly used model for colorectal neoplasia and cancer in humans [10]. Recent studies have reported that DSS-treated rodents exhibit anxiety- and depressive-like behavior [11] and reduction of hippocampal neurogenesis [12].

Decreased adult hippocampal neurogenesis is associated with depression in rodents and humans [13–15]. Moreover, depression is associated with altered inflammation [16], which manifests due to increased inflammatory cytokine expression [17]. Pro-inflammatory cytokines also inhibit adult neurogenesis in the hippocampus [18–20]. Therefore, cytokine-induced disruption of neurogenesis might be a key link between inflammation and depression. Antidepressants enhance hippocampal neurogenesis [21] and regulate several apoptotic factors, which are involved in cell survival pathways [22]. Treatment of mood disorders, including depression and anxiety, is critically dependent on intact adult neurogenesis in the hippocampal dentate gyrus (DG) [23, 24]. Thus, the stimulation of neurogenesis and reduction of apoptosis may constitute important drug targets in the modulation of depressive symptoms [25].

Enterococcus faecalis 2001 (EF-2001) is a biogenic lactic acid bacterium that is used as a biological response modifier (BRM). Live *E. faecalis* 2001 can be heat-treated to produce a BRM containing high levels of β -

glucan, named EF-2001. β -Glucan, one constituent of EF-2001, is a ligand for toll-like receptor 2 (TLR2) and activates nuclear factor-kappa B (NF κ B) p65, which controls spontaneous apoptosis and anti-apoptotic effects. NF κ B p65 activation inhibits apoptosis by increasing X-linked inhibitor of apoptosis protein (XIAP), an anti-apoptotic factor that exerts its action by regulating caspase-3 activity [26, 27]. EF-2001 can decrease serum inflammatory cytokines in a contact dermatitis model mouse [28], has anti-tumor effects [29], and protects chemical-induced colitis [30]. Therefore, we hypothesized that EF-2001 may attenuate inflammation and apoptosis in DSS-treated mice. Additionally, reports indicate that *E. faecalis* modulates inflammation in colitis models [31, 32]. However, the effect of EF-2001 on colitis-induced depression is unclear.

Taken together, we examined whether EF-2001 prevents DSS-induced depressive-like behaviors and changes in peripheral symptoms and investigated the neuroprotective molecular mechanisms underlying these effects.

Materials and methods

All experiments were performed following approval of the Ethics Committee of Animal Experiments in Tohoku Medical and Pharmaceutical University (approval numbers: 16023 cn, 17015 cn, and 18031 cn) and according to the National Institutes of Health Guide for the Care and Use of Laboratory Animals. All efforts were made to minimize suffering and reduce the number of animals used.

Animals

We used male ddY mice (weight, 28–32 g; Japan SLC, Shizuoka, Japan) for all experiments (total: $n = 239$; behavioral tests: $n = 127$; immunohistochemistry: $n = 55$; western blot analysis: $n = 24$; mRNA quantification: $n = 33$). Mice were housed in cages with free access to food and water under conditions of constant temperature ($22 \pm 2^\circ\text{C}$) and humidity ($55 \pm 5\%$), on a 12-h light to dark cycle (lights on: 07:00–19:00).

Compounds

Commercially available heat-treated EF-2001 was originally isolated from healthy human feces. It was supplied as a heat-killed, dried powder by Nihon BRM Co. (Tokyo, Japan). DSS (0.75%, 1.5%, or 3%; Wako Pure Chemical Industries Ltd., Osaka, Japan) and EF-2001 (250 mg/kg) were dissolved in drinking water. Mice were given drinking water containing DSS ad libitum for 7 days to induce colitis. Dexamethasone (Dex; 0.1 mg/kg; Aspen Japan, Tokyo, Japan) and imipramine (Imi; 20 mg/kg; Sigma–Aldrich, St-Louis, USA) were dissolved in saline. EF-2001 was administered orally (per os [p.o.]) from 14 days before the beginning of DSS administration until the day prior to the

last DSS treatment. Dex and Imi were administered intraperitoneally (i.p.) starting on the same day as the first DSS administration until the last day of DSS treatment. The dose for each drug used was calculated from previous reports [29, 33, 34].

Evaluation of colon inflammation

This evaluation was conducted according to the experimental protocol shown in Fig. 1a, b. Disease activity index (DAI) scores are well correlated with pathological findings in a DSS-induced model of IBD [35]. DAI scores were calculated as described previously [36]. DAI

is the combined score of stool consistency and bleeding, as detailed in Table 1. When mice were sacrificed, the colon length, starting above the anus to the top of the cecum, was measured. All parameters were scored on days 3, 5, and 7 during DSS treatment.

Tail suspension test

This test was conducted according to the experimental protocol shown in Fig. 1a, b. The tail suspension test was conducted to assess depressive-like behaviors and antidepressant effects. The procedure was performed as described previously [37]. Mice were considered

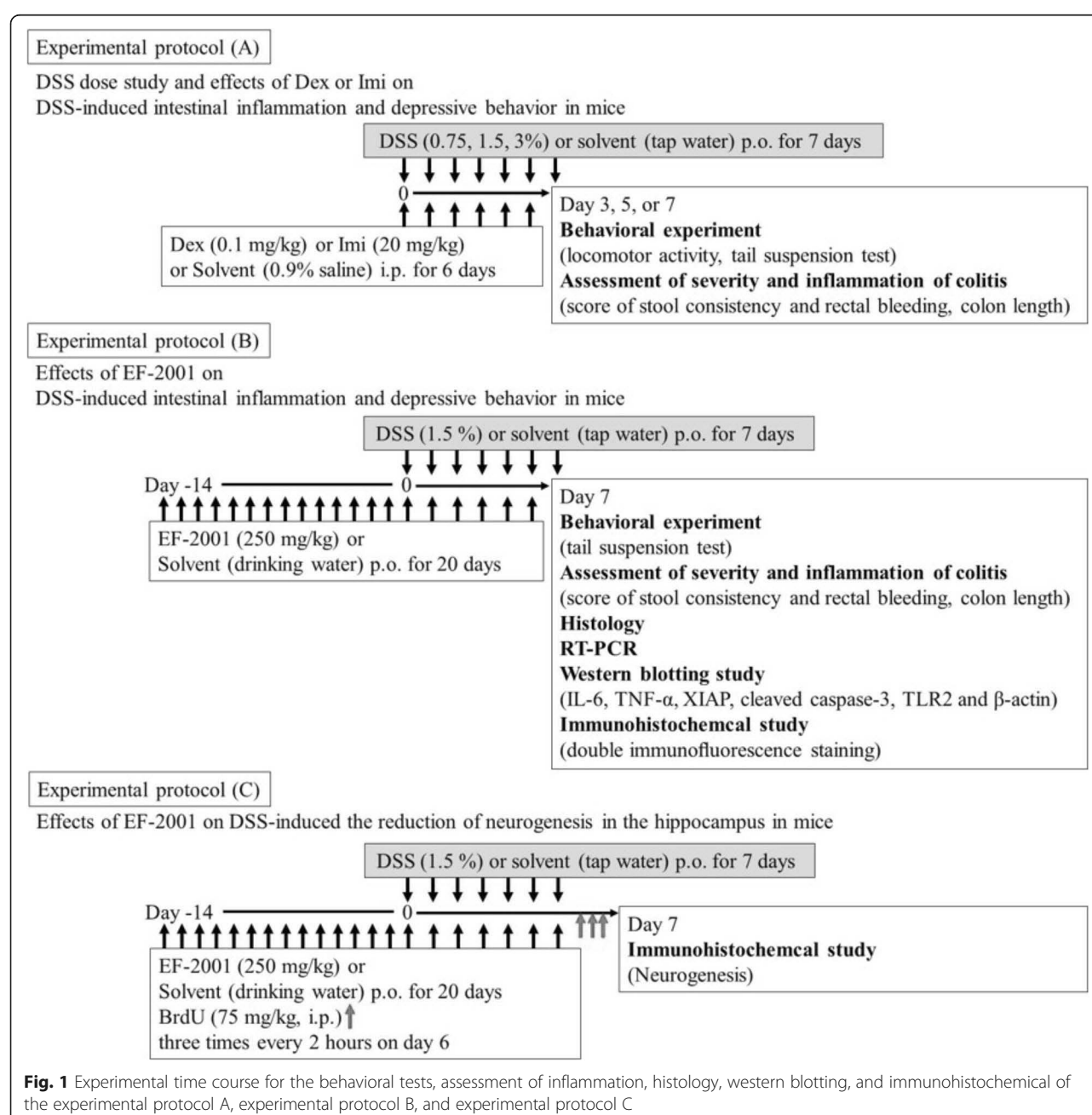


Fig. 1 Experimental time course for the behavioral tests, assessment of inflammation, histology, western blotting, and immunohistochemical of the experimental protocol A, experimental protocol B, and experimental protocol C

Table 1 Score of stool consistency and rectal bleeding

Score	Stool consistency	Rectal bleeding
1	Normal	Absent
2	Loose stool (tangible stool with high moisture content)	Visible blood stool
3	Diarrhea stool (collapsed stool with high moisture content)	Blood is attached to the anus
4	Watery diarrhea (almost intangible liquid stool)	Always bleeding from the anus

immobile only when they hung completely and passively motionless. Mice were suspended 30 cm above the floor by means of adhesive tape placed approximately 1 cm from the tip of the tail. The duration of time spent immobile was quantified during a test period of 10 min.

Locomotor activity

This test was conducted according to the experimental protocol shown in Fig. 1a. The locomotor activity of mice was evaluated using the multichannel activity-counting system SUPERMEX (Muromachi Kikai Co., Tokyo, Japan). The procedure and instrument have been reported previously [38]. This instrument can monitor even minute movements in all three planes of motion (sagittal, vertical, and horizontal) as one movement, owing to its infrared sensor with multiple Fresnel lenses that can be moved close enough to the cage to capture multidirectional locomotor alterations in a single mouse. This system interprets each movement as a count. Thus, the vertical movements, such as jumping, and horizontal movements, such as walking and running, can be counted. Activity measurements were conducted between 11:00 and 15:00 during the light phase. Mice were divided into three groups (water, DSS 1.5%, and DSS 3%) and were placed in activity boxes during 15 min for adaptation. Locomotor activity was recorded for 60 min.

Histology

The histological analysis was conducted according to the experimental protocol shown in Fig. 1b. Histology was assessed in mice following DAI and behavioral evaluations. The entire colon was collected and fixed in 4% buffered formalin for 24 h at room temperature, imbedded in paraffin, and sliced. Samples were sectioned into 5- μ m slices and subjected to staining with hematoxylin and eosin (HE). Finally, sections were examined under a light microscope to evaluate the histopathologic changes in colon tissue.

Western blotting

Western blotting was performed according to the experimental protocol shown in Fig. 1b. Mice were divided into four groups (water/water, water/EF-2001, DSS/water, and DSS/EF-2001). Mice were sacrificed by decapitation after

20 days of water or EF-2001 administration. Protein isolation and western blots were performed as described previously [37, 39]. Sectioning was performed as described previously [40, 41]. After sacrifice, the rectum of each mouse was washed in ice-cold phosphate-buffered saline (PBS). The rectal tissue, 8 mm from the edge of the cecum (side of the anus), was carefully cut into 5-mm slices on ice. The brain was removed and sectioned on ice using a mouse brain slicer (Muromachi Kikai) to produce 1-mm-thick coronal sections. To ensure precise regions, the cerebral peduncle was regarded as a landmark, and the five edge blades were anteriorly placed from this landmark. We visually confirmed the dorsal hippocampal location using Paxinos and Franklin mouse brain atlas [42]. After electrophoresis, proteins were transferred to a PVDF membrane, which was then incubated with blocking solution [10 mM Tris-HCl (pH 7.4), 100 mM NaCl, 0.01% Tween 20, and 5% skim milk] for 1 h. Next, membranes were probed with antibodies against TLR2 (1:100; Cell Signaling Technology, Danvers, USA), TNF- α (1:1000; Cell Signaling Technology), interleukin-6 (IL-6; 1:1000; Cell Signaling Technology), XIAP (1:200; Abcam Ltd., Cambridge, UK), brain-derived neurotrophic factor (BDNF; 1:100; Abcam Ltd.), and β -actin (1:1000; Cell Signaling Technology) overnight at 4 °C. Membranes were washed with blocking solution without milk and incubated with horseradish peroxidase-conjugated secondary antibody (Cell Signaling Technology) for 2 h, followed by visualization of the immunoreactive species with ECL Western Blotting Detection Reagent (Amersham Life Science, Piscataway, USA). Band densities were analyzed with ImageJ 1.43 (National Institutes of Health).

Immunohistochemical analysis

Immunohistochemical analysis was conducted according to the experimental protocol shown in Fig. 1c. To assess neurogenesis, on day 20 after EF-2001 administration, 5-bromo-2'-deoxyuridine (BrdU; Sigma-Aldrich; 75 mg/kg, i.p.) was injected three times every 2 h after the last administration of water or EF-2001. Animals were subsequently sacrificed 24 h after the last injection. Brain samples were collected as described previously [37, 38]. The brains were cut into 40- μ m sections from bregma - 2.20 to - 2.80 mm using a cryostat (MICROM HM560, Mikron Instrument, Inc., California, USA).

Frozen sections were mounted on glass slides (Matsunami Glass, Osaka, Japan). Sections were treated with HCl (2 N) at 37 °C for 30 min, followed by neutralization with sodium borate buffer (0.15 M) at room temperature twice every 10 min. After three washes every 5 min, the sections were incubated with PBS containing 1% normal goat serum (Life Technologies Corporation, Carlsbad, USA) and 0.3% Triton X-100 (PBSGT) at room temperature for 2 h. The sections were incubated

overnight at 4 °C with rat anti-BrdU monoclonal antibody (1:100; Harlan SeraLab, Loughborough, UK) and mouse anti-doublecortin (DCX) monoclonal antibody (1:50; Santa Cruz Biotech, Santa Cruz, CA). Sections were washed and incubated for 2 h at room temperature with goat anti-rat IgG Alexa Fluor 568 (1:200; Molecular Probes, Eugene, USA) and goat anti-mouse IgG Alexa Fluor 488 (1:200; Molecular Probes) with PBSGT. DAPI was used to identify the nuclei. Finally, sections were washed and coverslipped with Dako fluorescence mounting medium (Dako, Carpinteria, USA). Labeled sections were analyzed using a confocal laser-scanning microscope (A1Rsi; Nikon, Tokyo, Japan). Eight sections per mouse were used, and two images (left and right hemisphere, 640 × 640 μm) of the DG region of the hippocampus were obtained from each section. To assess neurogenesis, we counted the number of BrdU⁺/DCX⁺ cells in the DG. A mean number of eight images were analyzed for each mouse, and each group contained 6–9 mice.

Double immunofluorescence staining

Immunofluorescence analysis was conducted according to the experimental protocol shown in Fig. 1b. The brain samples were collected as described previously [43, 44]. The sections were incubated overnight at 4 °C with rabbit anti-TLR2 (1:100; Cell Signaling Technology), rabbit anti-NFκB p65 (1:500; Cell Signaling Technology), rabbit anti-XIAP (1:200; Abcam Ltd.), mouse anti-DCX monoclonal antibody (1:50; Santa Cruz Biotech), mouse anti-neuronal nuclear antigen (NeuN; 1:500; Millipore Corporation), rabbit anti-ionized calcium-binding adaptor molecule 1 (Iba1; 1:200; Wako Pure Chemical Industries Ltd., Osaka, Japan), and mouse anti-glial fibrillary acidic protein (GFAP; 1:200; Millipore Corporation) antibodies. When double labeling was performed using two primary antibodies from different host species (rabbit and mouse), sections were washed and incubated for 2 h at room temperature with goat anti-rabbit IgG Alexa Fluor 568 (1:200; Molecular Probes) and goat anti-mouse IgG Alexa Fluor 488 (1:200; Molecular Probes) in PBSGT. When double labeling was performed using two primary antibodies from the same host species (rabbit anti-TLR2, rabbit anti-NFκB p65, rabbit anti-XIAP, and rabbit anti-Iba1 antibodies), the detection of each antigen was performed sequentially and labeled goat anti-rabbit IgG Alexa Fluor 488 AffiniPure Fab fragments (Jackson ImmunoResearch Laboratories, USA), instead of whole antibodies, were used in the first detection (Iba1). The immunohistochemical staining with two primary antibodies from the same host species was carried out as described previously in detail [45]. Immunofluorescent images were analyzed with a confocal laser-scanning microscope (A1Rsi; Nikon).

Neuromorphometrical study

Morphometric assessment of the brain was conducted according to the experimental protocol shown in Fig. 1b. The brain samples were collected as described previously [37, 38]. The sections were incubated overnight at 4 °C with rabbit anti-NFκB p65 antibody (1:500; Cell Signaling Technology). Sections were washed and incubated for 2 h at room temperature with goat anti-rabbit IgG Alexa Fluor 568 (1:200; Molecular Probes) in PBSGT. We observed alterations in activation of NFκB p65-positive cells in the hippocampal DG area with a confocal laser-scanning microscope. We then evaluated the activation of NFκB p65-positive cells by observing translocation to cell nuclei.

Reverse transcription polymerase chain reaction (RT-PCR)

RT-PCR was performed according to the experimental protocol shown in Fig. 1b. Total RNA was isolated from the rectum and hippocampus of mice using TRI Reagent according to the manufacturer's protocol. Total RNA was reverse transcribed using ReverTra Ace and oligo (dT) primers. PCR was conducted using the following primer sequences: IL-6 sense primer 5'-AGGAGTGGCTAAGGACCAAGA-3' and antisense primer 5'-CATAACGCAC TAGGTTTGCCG-3', TNF-α sense primer 5'-GGCAGG TCTACTTTGGAGTCATTGC-3' and antisense primer 5'-ACATTCGAGGCTCCAGTGAATTCGG-3', and TATA-binding protein (TBP) sense primer 5'-ACCGTG AATCTTGGCTGTAAAC-3' and antisense primer 5'-GCAGCAAATCGCTTGGGATTA-3'. For quantification of mRNA expression, real-time PCR was carried out in a 20-μl solution containing Go Taq quantitative PCR Master mix (10 μl), RT template (2 μl), water (7 μl), and primers (1 μl) using the StepOnePlus Real-Time PCR System (Applied Biosystems, California, USA). The amount of each PCR product was normalized to TBP.

Statistical analysis

Normality and homoscedasticity assumptions were verified before the use of any parametric tests (Shapiro–Wilk normality test and equality of variances *F* test). Results are expressed as mean ± standard error of the mean (SEM). The significance of differences was determined by the Student's *t* test for two-group comparisons or by one or two-way analysis of variance (ANOVA), followed by Tukey–Kramer tests for multigroup comparisons using GraphPad Prism 7 (GraphPad Software, California, USA) and StatView 5.0 (HULINKS, Tokyo, Japan). For the DAI scores, statistical significance of differences was assessed with a non-parametric Mann–Whitney test for two-group comparisons or Kruskal–Wallis test followed by Steel's test for multigroup comparisons. In some cases, when a main effect was significant without interaction effect, we did an exploratory

and limited pairwise post hoc comparison consistent with our a priori hypothesis. Results were considered statistically significant if $p < 0.05$.

Results

Concentration-dependent effect of DSS on DAI scores, colon length, immobility time, and locomotor activity in mice

DAI scores of both stool consistency and rectal bleeding in DSS-treated mice (1.5% and 3%) were significantly increased compared with those in the control group [Fig. 2a, b, Kruskal–Wallis test, stool consistency: $p < 0.0001$, rectal bleeding: $p < 0.0001$]. The colon length in DSS-treated mice (0.75%: $p = 0.0007$, 1.5%: $p < 0.0001$, and 3%: $p < 0.0001$) was significantly shorter than in control mice [Fig. 2c, one-way ANOVA, $F(3, 41) = 16.2$, $p < 0.0001$]. There was a significantly prolonged duration of immobility in DSS-treated mice (0.75%: $p = 0.0337$, 1.5%: $p = 0.0165$, and 3%: $p < 0.0001$) compared with controls in the tail suspension test [Fig. 2d, one-way ANOVA, $F(3, 44) = 9.626$, $p < 0.0001$]. Furthermore, DSS (1.5% and 3%) did not affect locomotor activity in mice [Fig. 2e, one-way ANOVA, $F(2, 27) = 0.142$, $p = 0.8683$].

We observed that DSS 3% caused the death of a few mice (data not shown). Based on these results, DSS 1.5% was the appropriate dose to investigate in the IBD model with depression.

Time-dependent effects of DSS on DAI scores, colon length, and immobility time in mice

As shown in Fig. 3, diarrhea and shortened colon length were observed on day 7 of DSS treatment, but not on days 3 and 5 [Fig. 3a, Mann–Whitney test, day 3: $p > 0.9999$, day 5: $p = 0.3173$, day 7: $p = 0.0009$; Fig. 3c, two-way ANOVA, group: $F(1, 65) = 14.51$, $p = 0.0003$, time: $F(2, 65) = 0.8248$, $p = 0.4429$, group \times time: $F(2, 65) = 16.31$, $p < 0.0001$]. In contrast, bloody stool and prolonged duration of immobility were observed on days 5 and 7 of DSS treatment, but not on day 3 [Fig. 3b, Mann–Whitney test, day 3: $p > 0.9999$, day 5: $p = 0.0139$, day 7: $p = 0.0008$; Fig. 3d, two-way ANOVA, group: $F(1, 66) = 23.4$, $p < 0.0001$, time: $F(2, 66) = 3.874$, $p = 0.0257$, group \times time: $F(2, 66) = 6.591$, $p = 0.0025$]. Based on these results, day 7 after the beginning of DSS treatment was the best time point to investigate changes in the IBD model with depression.

Effects of Imi, Dex, or EF-2001 on DAI scores, colon length, and immobility time in DSS-treated mice

We investigated the effects of Imi, Dex, or EF-2001 on DSS-induced changes in mice. Imi reversed the DSS-induced prolonged duration of immobility time, while other changes were not affected. In contrast, Dex and EF-2001 prevented DSS-induced diarrhea, bloody stool (Dex showed a tendency toward prevention of bloody

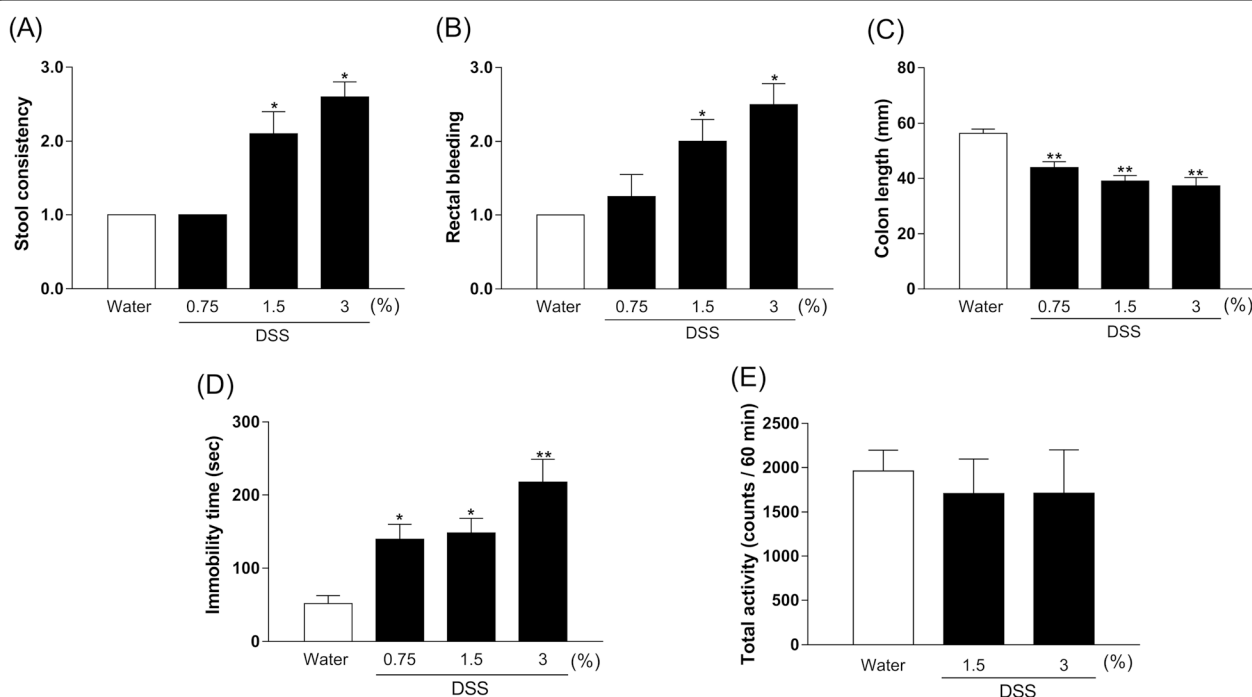


Fig. 2 Changes in stool consistency (a), rectal bleeding (b), colon length (c), immobility time (d), and locomotor activity (e) in dextran sulfate sodium (DSS)-treated mice at day 7. Bars represent means \pm standard error of mean (SEM). * $p < 0.05$ and ** $p < 0.01$ vs. water group ($n = 6$ –12 per group)

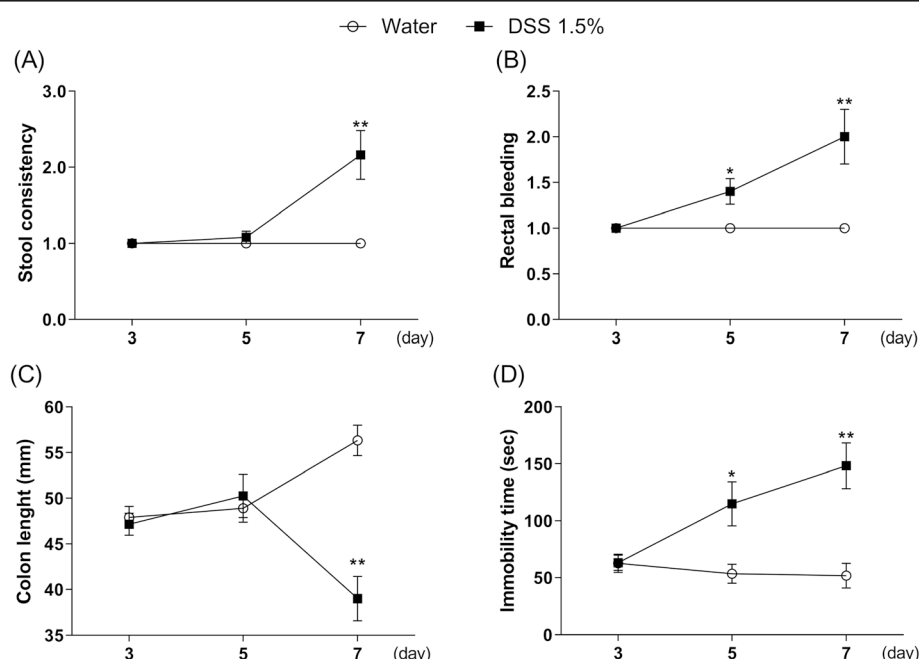


Fig. 3 Time-course of stool consistency (a), rectal bleeding (b), colon length (c), and immobility time (d) in dextran sulfate sodium (DSS; 1.5%)-treated mice at days 3, 5, and 7. Bars represent means \pm standard error of mean (SEM). * $p < 0.05$ and ** $p < 0.01$ vs. water group ($n = 11$ –12 per group)

stool), and colon atrophy. Further, it reversed the prolonged duration of immobility time [Kruskal–Wallis test, Fig. 4a, stool consistency: $p = 0.0012$; Fig. 4b, rectal bleeding: $p = 0.0181$; Fig. 4c, one-way ANOVA: $F(2, 31) = 5.089$, $p = 0.0123$; Fig. 4d, $F(2, 31) = 12.17$, $p = 0.0001$; Mann–Whitney test, Fig. 4e, stool consistency: $p = 0.0231$; Fig. 4f, rectal bleeding: $p = 0.0535$; Student's t test, Fig. 4g, colon length: $t(22) = 3.632$, $p = 0.0015$; Fig. 4h, immobility time: $t(22) = 2.939$, $p = 0.0076$]. In the histological study, EF-2001 prevented DSS-induced colon erosion similar to treatment with Dex (Fig. 4i–l).

Effect of EF-2001 on TNF- α and IL-6 levels in the rectum and hippocampus of DSS-treated mice

As shown in Fig. 5, the immunocontent of TNF- α and IL-6 in the rectum and hippocampus of DSS-treated mice was significantly increased compared with controls. Interestingly, these changes were reversed by treatment with EF-2001 [two-way ANOVA, Fig. 5b, group: $F(1, 17) = 10.01$, $p = 0.0057$, treatment: $F(1, 17) = 10.26$, $p = 0.0052$, group \times treatment: $F(1, 17) = 10.27$, $p = 0.0052$; Fig. 5c, group: $F(1, 14) = 6.676$, $p = 0.0216$, treatment: $F(1, 14) = 5.352$, $p = 0.0364$, group \times treatment: $F(1, 14) = 5.813$, $p = 0.0302$; Fig. 5e, group: $F(1, 22) = 3.273$, $p = 0.0841$, treatment: $F(1, 22) = 19.13$, $p = 0.0002$, group \times treatment: $F(1, 22) = 8.049$, $p = 0.0096$; Fig. 5f, group: $F(1, 22) = 8.157$, $p =$

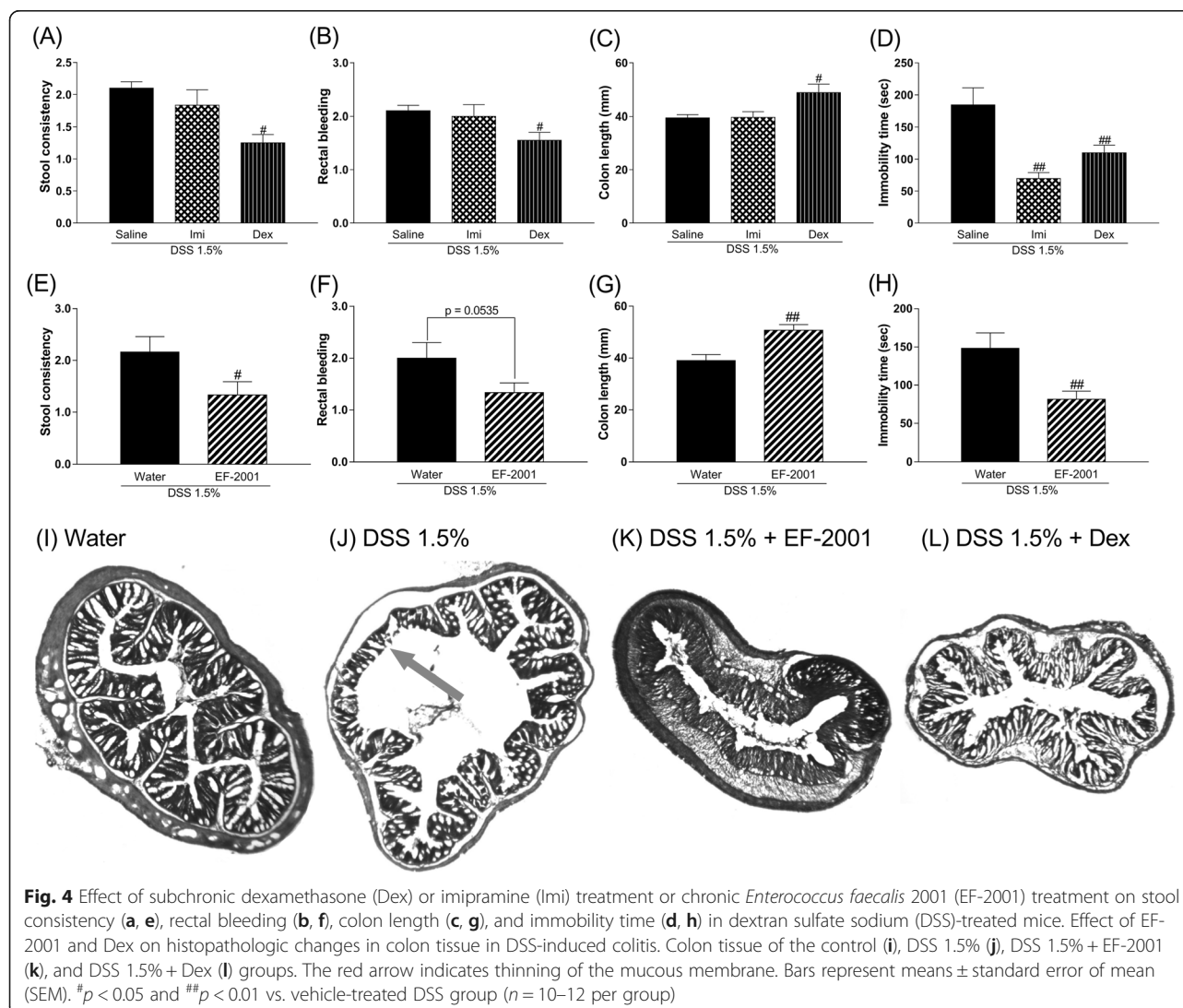
0.0092, treatment: $F(1, 22) = 16.3$, $p = 0.0006$, group \times treatment: $F(1, 22) = 4.728$, $p = 0.0407$].

Effect of EF-2001 on TNF- α and IL-6 mRNA levels in the hippocampus of DSS-treated mice

We investigated the changes in the expression of TNF- α and IL-6 mRNA levels in the hippocampus. The hippocampal TNF- α and IL-6 mRNA levels in DSS-treated mice did not change as compared to those in control mice [Fig. 6a, two-way ANOVA, group: $F(1, 17) = 0.1801$, $p = 0.6766$, treatment: $F(1, 17) = 0.2614$, $p = 0.6157$, group \times treatment: $F(1, 17) = 0.3334$, $p = 0.5713$; Fig. 6b, group: $F(1, 29) = 3.335$, $p = 0.0781$, treatment: $F(1, 29) = 0.2765$, $p = 0.6030$, group \times treatment: $F(1, 29) = 0.1689$, $p = 0.6841$].

Effect of EF-2001 on reduced neurogenesis in the hippocampal DG of DSS-treated mice

To determine any change in hippocampal neurogenesis in DSS-treated mice, animals were injected with BrdU. The incorporation of BrdU indicates that cells were replicating at the time of the BrdU injection. Further, anti-DCX staining was used to identify immature neurons in the DG. DSS-treated mice had a significantly lower number of BrdU $^+$ /DCX $^+$ cells compared with the control group, which was reversed by administration of EF-2001 [Fig. 7b, two-way ANOVA, group: $F(1, 27) = 5.927$, $p =$



0.0218, treatment: $F(1, 27) = 1.663$, $p = 0.2082$, group \times treatment: $F(1, 27) = 7.613$, $p = 0.0103$].

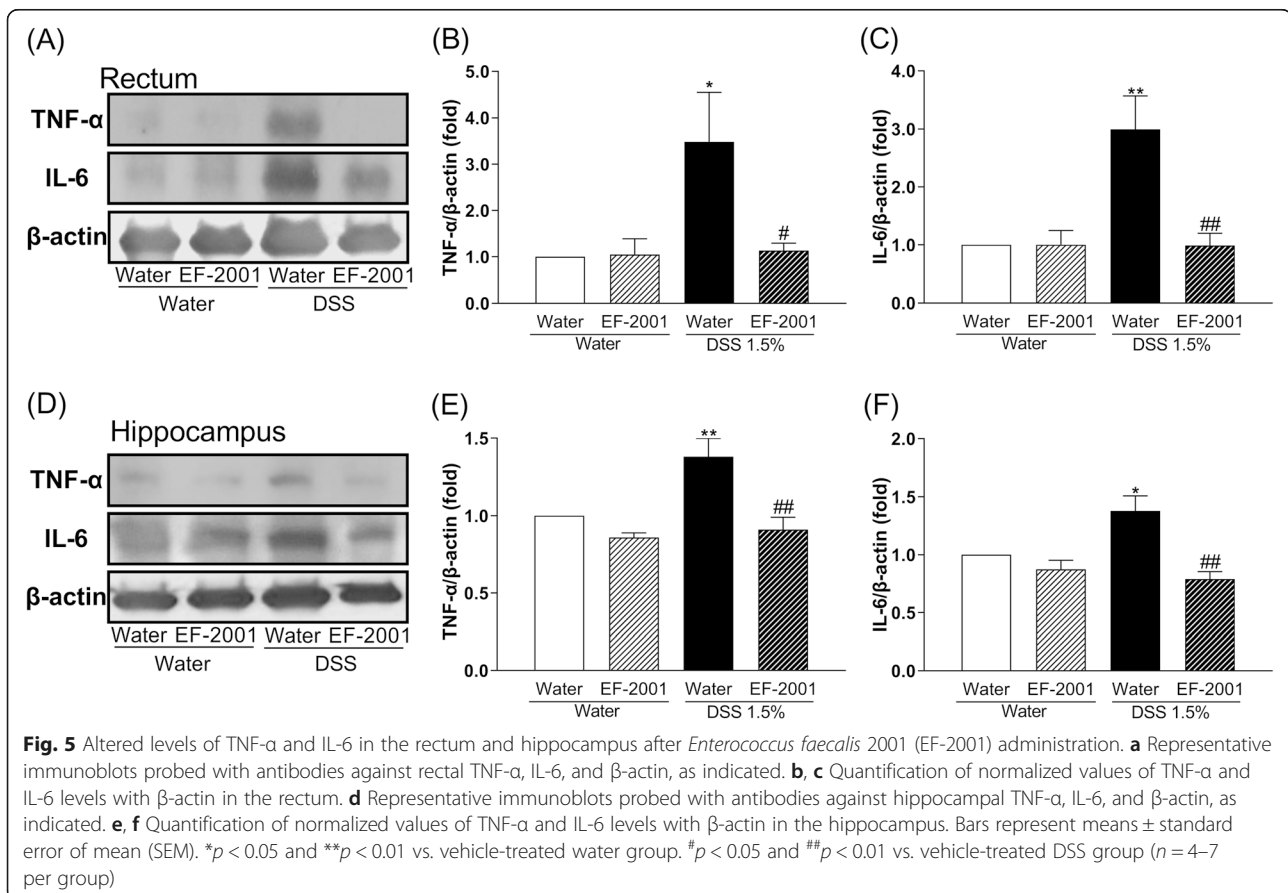
NF κ B p65-positive astrocytes and microglia in the hippocampal DG after treatment with EF-2001

NF κ B p65 may control spontaneous apoptosis, anti-apoptotic gene expression, and translocation to cell nuclei during activation. Two-way ANOVA showed significant main effects for the treatment factor but not an interaction [Fig. 8f, two-way ANOVA, group: $F(1, 15) = 3.237$, $p = 0.0922$, treatment: $F(1, 15) = 34.35$, $p < 0.0001$, group \times treatment: $F(1, 15) = 0.4169$, $p = 0.5282$]. Therefore, we focused our analysis on the effects of treatment. EF-2001 treatment significantly increased activation of NF κ B p65-positive cells in the DG compared with the water-treated group. To determine which cell types were involved, dual immunofluorescence staining for NF κ B p65 was performed in conjunction with cell-specific markers, such as

DCX, NeuN (a marker for mature neurons), GFAP (an astrocyte marker), and Iba1 (a microglia marker). Activated NF κ B p65-positive cells were identified as astrocytes and microglia (Fig. 8g).

Effect of EF-2001 on TLR2 levels in the hippocampus of DSS-treated mice

Two-way ANOVA showed statistical significance for the main effects of treatment [$F(1, 14) = 16.49$, $p = 0.0012$] but no significance for the TLR2 interaction [group \times treatment: $F(1, 14) = 0.13$, $p = 0.7239$] (Fig. 9a). Thus, we focused our analysis on the major effects of EF-2001 administration. EF-2001 significantly increased TLR2 expression in the hippocampus of DSS-treated mice. Moreover, to identify the cell types involved in the production of TLR2, dual immunofluorescence staining was performed for the localization of TLR2 and cell-specific

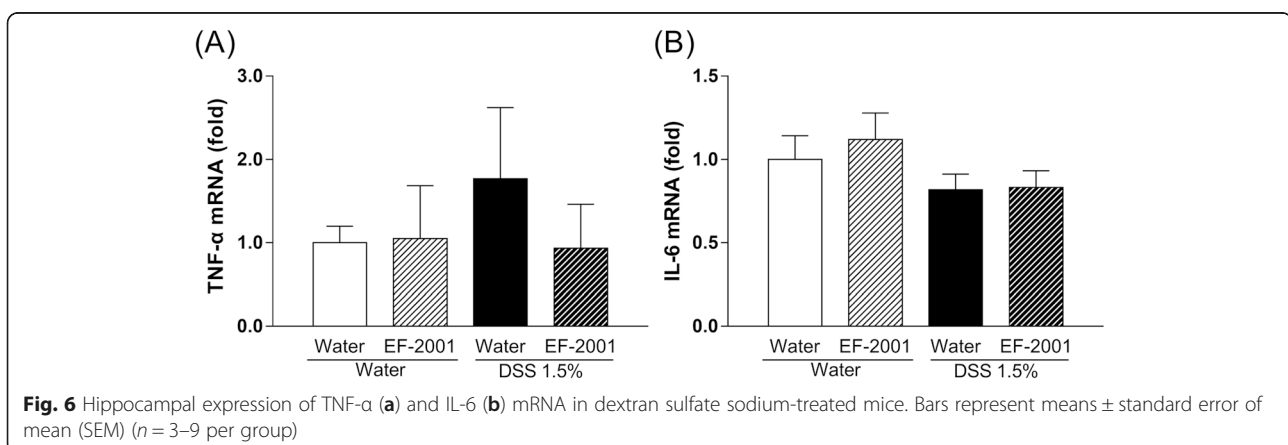


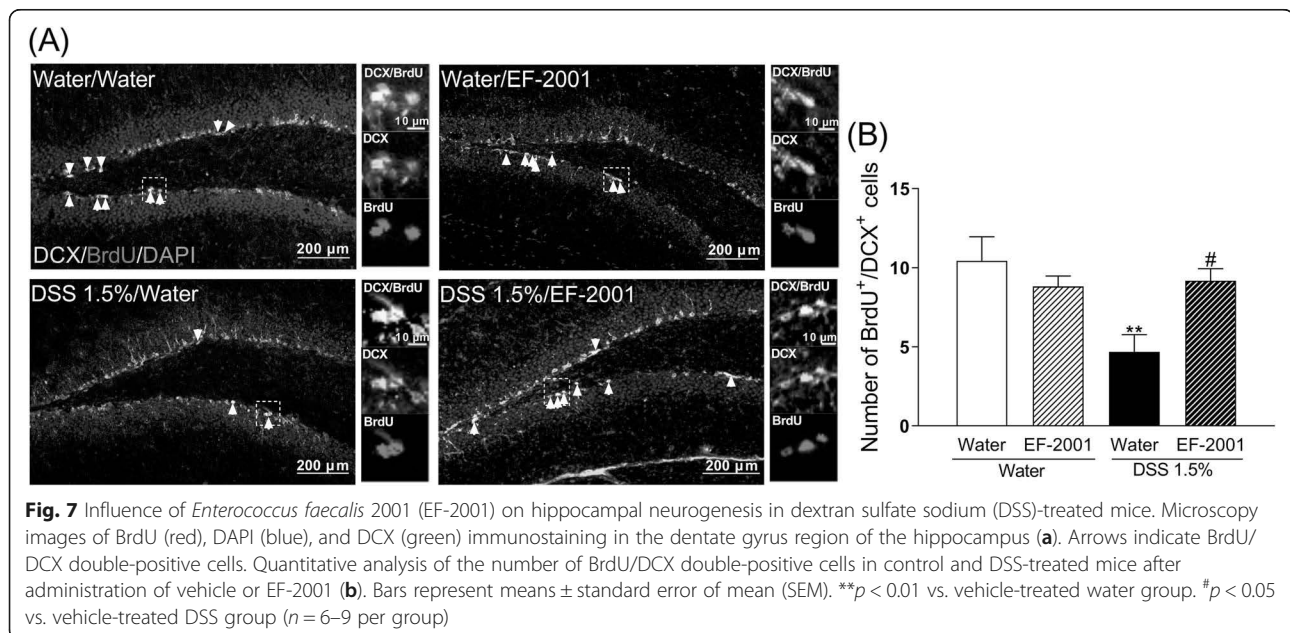
markers, such as DCX, NeuN, GFAP, and Iba1. TLR2 was localized in all assessed cell types (Fig. 9b).

Effect of EF-2001 on the enhancement of neuroinflammation and apoptosis in the hippocampus of DSS-treated mice

As shown in Fig. 10, two-way ANOVA showed significant main effects for treatment [$F(1, 20) = 11.92$, $p = 0.0025$] but no interaction for XIAP [group \times treatment: $F(1, 20) = 1.23$, $p = 0.2805$] (Fig. 10b). Thus, we focused

our analysis on the effects of treatment. EF-2001 significantly increased XIAP in the hippocampus of DSS-treated mice. Cleaved caspase-3 in the hippocampus of DSS-treated mice was significantly increased compared with controls, while EF-2001 treatment significantly decreased cleaved caspase-3 levels in DSS-treated mice [Fig. 10c, two-way ANOVA, group: $F(1, 15) = 7.46$, $p = 0.0155$, treatment: $F(1, 15) = 15.51$, $p = 0.0013$, group \times treatment: $F(1, 15) = 13.91$, $p = 0.0020$]. Moreover, to determine the cell types that are involved in the





production of XIAP, dual immunofluorescence staining for XIAP was performed in conjunction with cell-specific markers, such as GFAP and Iba-1. XIAP was localized in the microglia (Fig. 10d).

Discussion

Patients with IBD have higher rates of psychiatric disorders, such as depression and anxiety; however, the mechanisms underlying a link between intestinal inflammation and depressive-like symptoms are largely unknown. In this study, we investigated the effect of EF-2001 in IBD-like physiological changes and depressive-like behavior in DSS-treated mice. Chronic administration of EF-2001 prevented such changes. In addition, EF-2001 attenuated the increase of inflammatory cytokines in the rectum and hippocampus, attenuated the reduction of neurogenesis in the hippocampus, and facilitated the NFκB p65/XIAP pathway in the hippocampus of DSS-treated mice. This is the first report that the antidepressant effect of EF-2001 may involve hippocampal neuroprotection via decreased inflammatory cytokine expression in the rectum and hippocampus as well as apoptotic cell death regulation via inhibition of caspase-3 activity through facilitation of the NFκB p65/XIAP pathway in the hippocampus.

IBD, including Crohn's disease and ulcerative colitis, is a chronic relapsing condition characterized by intestinal damage (barrier disruption, altered microbiota) and high levels of inflammation such as elevated inflammatory cytokines [43, 46, 47]. Cytokines induce extensive inflammation in the colon, which has a negative impact on epithelial cells, resident and recruited immune cells, and stromal cells [44]. Specifically, inflammation can cause damage to epithelial cells, and activate and recruit

immune and stromal cells, ultimately leading to non-resolving chronic inflammation and the development of IBD [44]. Moreover, during acute or chronic inflammation, inflammatory cytokines can induce the development of depression [48, 49]. Clinical studies have reported that patients with IBD often exhibit obsessive-compulsive disorder, panic disorder, depression, and anxiety [4-7]. DSS treatment induces colonic epithelial cell lesions and intestinal inflammation, including elevated inflammatory cytokines, via epithelial cell toxicity, increased intestinal permeability, and macrophage activation [9]. It has been suggested that *E. faecalis* improves colitis by increasing interleukin-10 (IL-10), a factor that inhibits cytokine synthesis, in colonic epithelial cells [50, 51]. The present study showed that EF-2001 reduced inflammatory cytokines in the rectum (Fig. 5). This effect was similar to that of steroids, which are commonly prescribed for treating IBD [52]. Recently, other researchers have reported that EF-2001 protects dinitrobenzene sulfonic acid-induced colitis, a chemically induced colitis model, via a decrease in inflammatory cytokines [30]. Thus, the anti-inflammatory effect of EF-2001 may also be related to reduced inflammatory cytokines. Peripheral inflammation is a risk factor for developing mood or psychotic disorders, such as depression [53-56], and may affect hippocampal neurogenesis, including the proliferation, differentiation, and survival of newborn neurons [54, 55]. Adult neurogenesis occurs in two main regions of the brain, one of which is the subgranular zone of the DG [57, 58]. In the present study, we observed that DSS treatment significantly increased TNF-α and IL-6 levels in the rectum and hippocampus. A previous study has reported that DSS

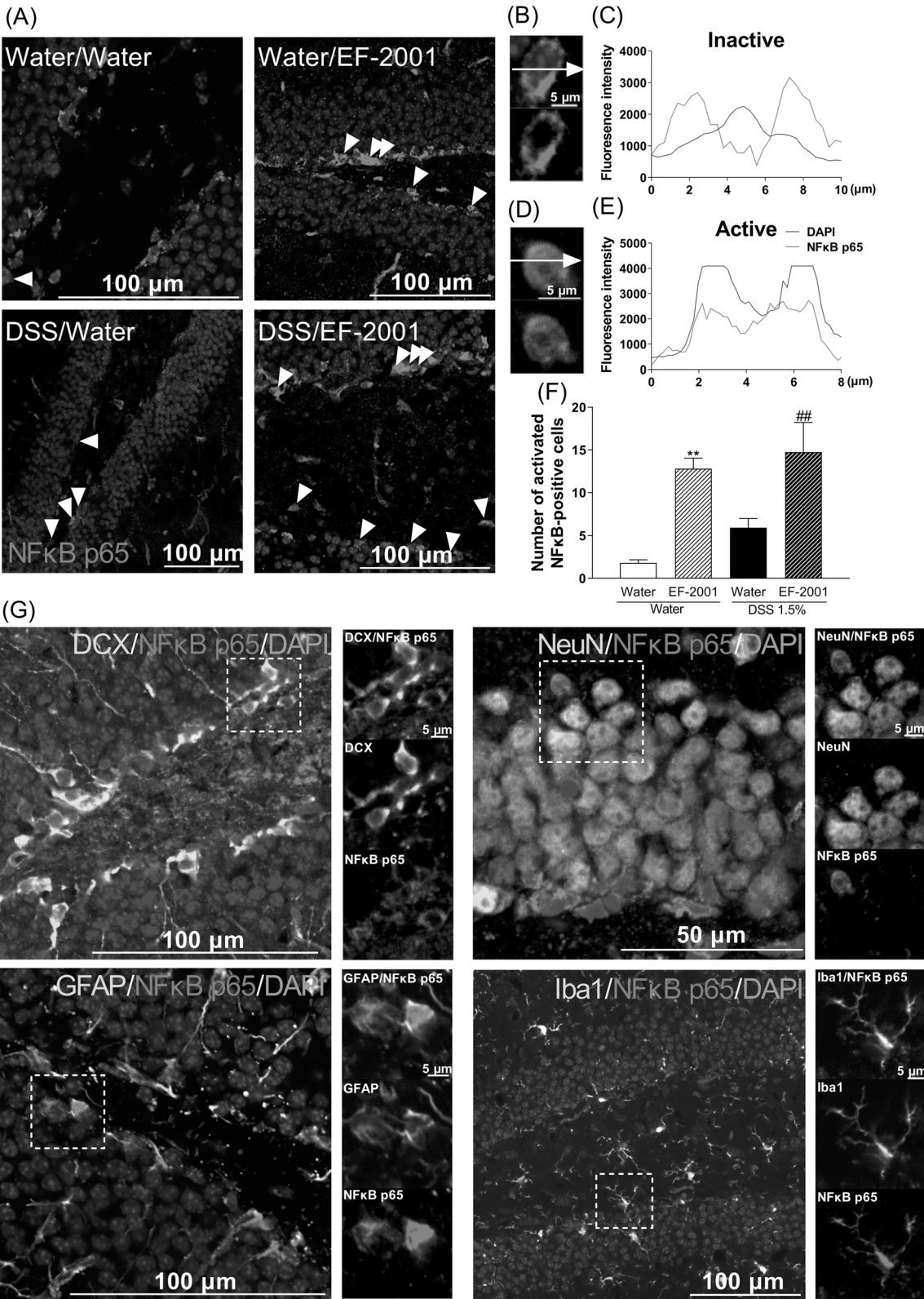


Fig. 8 (See legend on next page.)

(See figure on previous page.)

Fig. 8 Influence of *Enterococcus faecalis* 2001 (EF-2001) on hippocampal activation of NFκB p65-positive cells in dextran sulfate sodium (DSS)-treated mice. Microscopy images of NFκB p65 (red) and DAPI (blue) immunostaining in the dentate gyrus region of the hippocampus (a). The fluorescence intensity profile of DAPI (blue line) and NFκB p65 (red line) in the immunostaining indicated by the white dashed lines in the inactive NFκB p65 (b, c) and active NFκB p65 (d, e). Quantitative analysis of the number of activated NFκB p65-positive cells in control and DSS-treated mice after administration of vehicle or EF-2001 (f). Activated NFκB p65 is expressed in astrocytes and microglia in the hippocampus of DSS-treated mice treated with EF-2001. Microscopy images of NFκB p65 (red), DAPI (blue), and DCX, NeuN, GFAP, or Iba1 (green) immunostaining in the dentate gyrus region of the hippocampus (g). The boxed area is shown in higher magnification. Bars represent means ± standard error of mean (SEM). ** $p < 0.01$ vs. vehicle-treated water group. ## $p < 0.01$ vs. vehicle-treated DSS group ($n = 4-5$ per group)

treatment significantly increases rectal TNF- α and IL-6 levels [59]. Interestingly, hippocampal TNF- α and IL-6 mRNA in DSS-treated mice were unchanged compared with controls (Fig. 6). Depression is closely associated with altered inflammation [16], manifested by increased expression of inflammatory cytokines such as TNF- α and IL-6 [17]. Neuroinflammatory factors, such as TNF- α and IL-6, can negatively affect many stages of neurogenesis in the adult mammalian brain, including the proliferation, differentiation, and survival of newborn neurons [18–20, 54, 55]. Therefore, cytokine-induced reduction of neurogenesis might establish a key link between inflammation and depression. In this study, DSS-treated mice showed a significant decrease in neurogenesis in the DG, consistent with a previous study [12]. Likewise, DeCarolis and Eisch reported a reduction in neurogenesis in the hippocampus of patients with depression [60]. These findings suggest that DSS-induced depressive-like behavior may be associated with the reduction of neurogenesis in the DG via the release of

inflammatory cytokines derived from peripheral inflammation. Moreover, several studies have suggested that antidepressant effects are critically dependent on intact adult neurogenesis and may be mediated by the enhancement of neurogenesis in the hippocampal DG [21, 23, 24]. We observed that administration of EF-2001 significantly attenuated the enhancements of rectal and hippocampal inflammation and reduction of newborn neurons in the hippocampus of DSS-treated mice. Therefore, we suggest that the antidepressant effect and enhanced neurogenesis observed upon EF-2001 administration are partly independent effects, resulting from the EF-2001-mediated reduction of peripheral inflammation. Although the mechanism by which pro-inflammatory cytokines reduce neurogenesis is not fully understood, we believe that inflammatory cytokines in peripheral tissue might be key mediators of this process.

In human neutrophils, the activation of NFκB p65 seems to control spontaneous apoptosis and anti-apoptotic effects. Unexpectedly, we found that the activation of

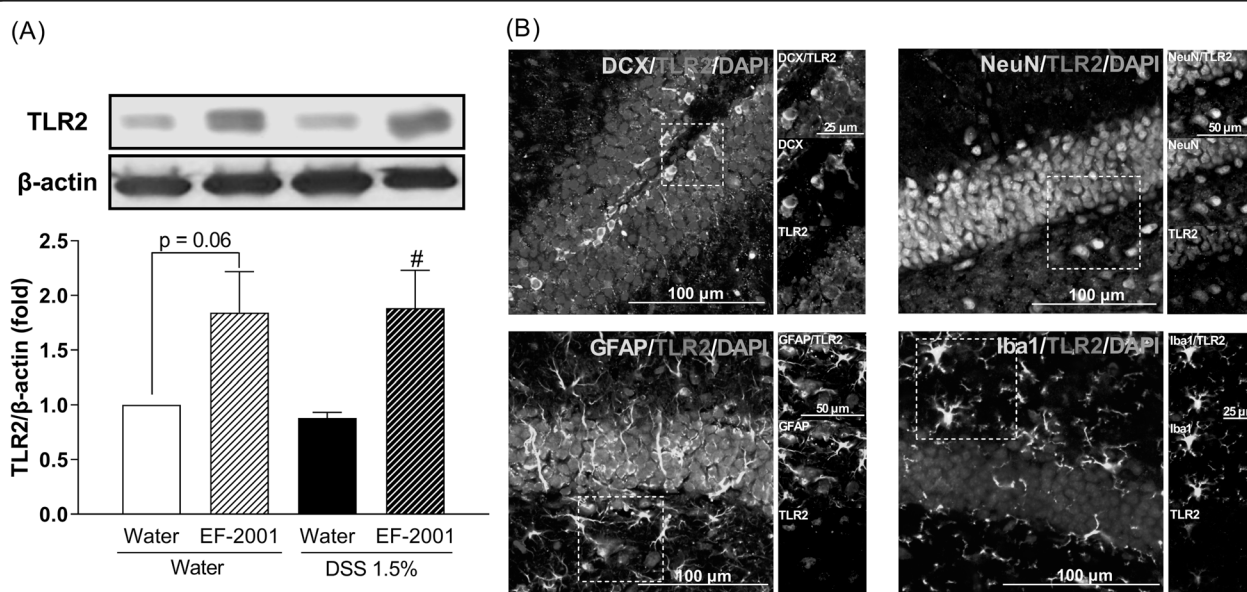


Fig. 9 Altered TLR2 protein level in the hippocampus after *Enterococcus faecalis* 2001 (EF-2001) administration. **a** TLR2 is expressed in all cell types in the hippocampus of dextran sulfate sodium (DSS)-treated mice administered with EF-2001. Fluorescence microscopy images of TLR2 (red); DAPI (blue); and DCX, NeuN, GFAP, or Iba1 (green) immunostaining in the dentate gyrus region of the hippocampus. **b** The insets (boxed area) are images of higher magnification. Bars represent means ± standard error of mean (SEM). * $p < 0.05$ vs. vehicle-treated DSS group ($n = 4-6$ per group)

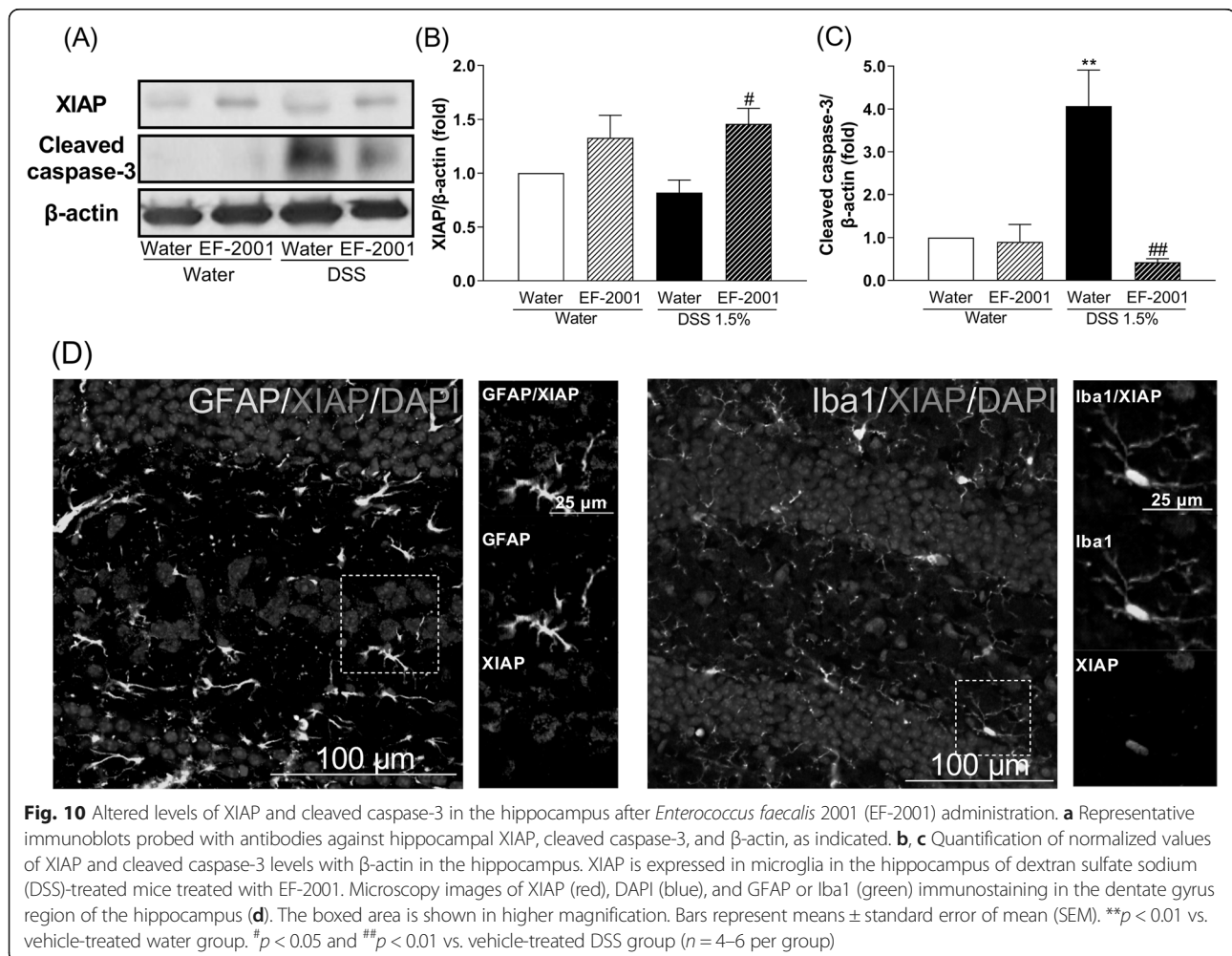
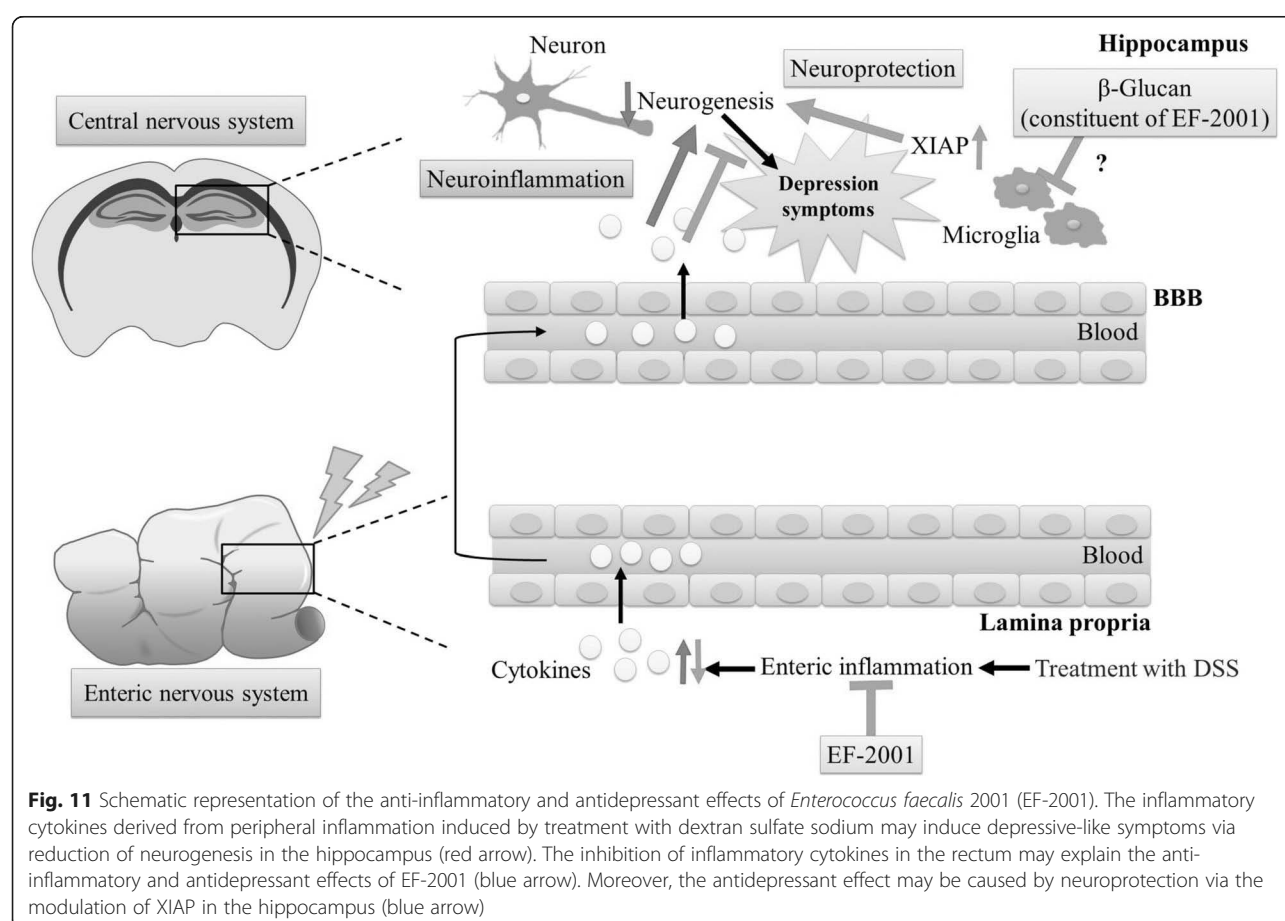


Fig. 10 Altered levels of XIAP and cleaved caspase-3 in the hippocampus after *Enterococcus faecalis* 2001 (EF-2001) administration. **a** Representative immunoblots probed with antibodies against hippocampal XIAP, cleaved caspase-3, and β -actin, as indicated. **b, c** Quantification of normalized values of XIAP and cleaved caspase-3 levels with β -actin in the hippocampus. XIAP is expressed in microglia in the hippocampus of dextran sulfate sodium (DSS)-treated mice treated with EF-2001. Microscopy images of XIAP (red), DAPI (blue), and GFAP or Iba1 (green) immunostaining in the dentate gyrus region of the hippocampus (**d**). The boxed area is shown in higher magnification. Bars represent means \pm standard error of mean (SEM). ^{**} $p < 0.01$ vs. vehicle-treated water group. [#] $p < 0.05$ and ^{##} $p < 0.01$ vs. vehicle-treated DSS group ($n = 4$ –6 per group)

NF κ B p65-positive cells were increased by EF-2001 administration in water- and DSS-treated groups compared with control groups. Moreover, we found that activation of NF κ B p65 was localized to hippocampal astrocytes and microglia; however, the mechanisms underlying this activation remain unclear. We hypothesized that β -glucan may be associated with activation of NF κ B p65 via TLR2. β -Glucan activates TLR2 and increases TLR2 expression via NF κ B p65 activation [61–63]. Interestingly, we found that hippocampal TLR2 was activated by EF-2001, which was localized in all cell types, including immature and mature neurons, astrocytes, and microglia (Fig. 9). We did not assess the migration of EF-2001 or β -glucan into the brain; we will examine them in a future study. Modulation of this pathway most likely regulates the balance between pro- and anti-apoptotic factors [64], thus affecting neutrophil survival. In this study, EF-2001 attenuated DSS-induced neuroinflammation and we hypothesized that NF κ B p65 may play a role in anti-apoptosis. The activation of NF κ B p65 inhibits apoptosis via a mechanism involving upregulation of various anti-apoptotic genes, such

as cellular FLICE-inhibitory protein, Bcl-xL, and XIAP [26, 27]. XIAP, a key member of the inhibitors of apoptosis protein family, can inhibit apoptosis by directly binding to the initiator caspases: caspase-3, -7, and -9 [65]. Moreover, hippocampal XIAP regulates synaptic plasticity, which is associated with the development of depression [66, 67]. In this study, XIAP was significantly increased by EF-2001. Further, XIAP was localized in hippocampal microglia. Moreover, cleaved caspase-3, which is crucial in the process of apoptosis and contributes to the irreversible stage of apoptosis [68], was significantly increased in the hippocampus of DSS-treated mice. In contrast, EF-2001 suppressed the increased levels of cleaved caspase-3 in the hippocampus of DSS-treated mice. These results suggested that EF-2001 might partly modulate apoptosis via regulation of the microglial NF κ B p65/XIAP pathway and caspase-3 in the hippocampus of DSS-treated mice.

As summarized in Fig. 11, EF-2001 had anti-inflammatory and antidepressant effects in DSS-treated mice, and hippocampal neuroprotection is a key factor mediating the antidepressant effect of EF-2001. Other



researchers have reported that administration of *Lactobacillus* strains had antidepressant effects and enhanced neurogenesis in the hippocampus via the vagus nerve [69, 70]. Hence, further extensive experiments examining the relationship between the vagus nerve and effects of EF-2001 will be presented in a subsequent paper.

Conclusions

The present study showed that DSS-treated mice exhibited IBD-like physiological changes and depressive-like behaviors (Figs. 2 and 3). This result was consistent with previous studies [11, 12]. In this study, we evaluated the predictive validity of the IBD animal model by using a classic antidepressant drug, Imi, or a steroid, Dex. Administration of Imi significantly improved depressive-like behavior, whereas Dex significantly improved both IBD-like peripheral symptoms and depressive-like behavior. These results demonstrated that DSS-treated mice provided a model of IBD with depression.

Our results indicate that EF-2001 attenuated IBD-like symptoms and depressive-like behavior in DSS-treated mice. EF-2001 prevented DSS-induced colitis and the mechanism may also involve the suppression of inflammatory cytokines in the rectum. The antidepressant

effect of EF-2001 may involve neuroprotection in the hippocampus via decreased TNF- α and IL-6 expression in the rectum and hippocampus and facilitation of the NF κ B p65 pathway in the hippocampus. This process is likely mediated by modulation of XIAP, which is involved in the regulation of apoptotic cell death via caspase-3 activity. Moreover, our findings suggest a close relationship between IBD and depression.

Abbreviations

ANOVA: Analysis of variance; BDNF: Brain-derived neurotrophic factor; bp: Base pair; BrdU: 5-bromo-2'-deoxyuridine; BRM: Biological response modifier; DAI: Disease activity index; DCX: Doublecortin; Dex: Dexamethasone; DG: Dentate gyrus; DSS: Dextran sulfate sodium; EF-2001: *Enterococcus faecalis* 2001; GFAP: Glial fibrillary acidic protein; HE: Hematoxylin and eosin; i.p.: Intraperitoneally; Iba1: Ionized calcium-binding adaptor molecule 1; IBD: Inflammatory bowel disease; IL-6: Interleukin-6; Imi: Imipramine; NF κ B: Nuclear factor-kappa B; p.o.: Per os; PBS: Phosphate-buffered saline; PBSGT: PBS containing 1% normal goat serum and 0.3% Triton X-100; SEM: Standard error of the mean; TBP: TATA-binding protein; TLR2: Toll-like receptor 2; TNF- α : Tumor necrosis factor- α ; XIAP: X-linked inhibitor of apoptosis protein

Acknowledgements

The authors would like to thank Mr. Takehiko Tanaka and Ms. Momona Nagasaki of the Tohoku Medical and Pharmaceutical University for their technical assistance.

Authors' contributions

TK performed the experiments (evaluation of colon inflammation, behavioral testing, western blotting, and immunohistochemical study), analyzed the data, and wrote the manuscript; NO designed the project; NW and OH performed the experiments (histology and RT-PCR) and analyzed the data; OT and SW performed the experiments (evaluation of colon inflammation and behavioral testing); and NH, FR, NY, IH, T-NK, and TT supervised the experiments. All authors critically reviewed the manuscript and approved the final version for publication.

Funding

This study was supported in part by the Grants-in-Aid for Scientific Research (Grant number 18 K06687) and Matching Fund Subsidy for Private University from the Ministry of Education, Culture, Sports, Science and Technology of Japan (grant number S1511001 L).

Availability of data and materials

The datasets used and/or analyzed in the current study are available from the corresponding author on reasonable request.

Ethics approval and consent to participate

All experiments were performed following the approval of the Ethics Committee for Animal Experiments at Tohoku Medical and Pharmaceutical University (approval numbers: 16023 cn, 17015 cn, and 18031 cn) and according to the tenets of the National Institutes of Health Guide for the Care and Use of Laboratory Animals. All efforts were made to minimize the suffering of the animals and reduce the number of animals used.

Consent for publication

Not applicable.

Competing interests

Hiroyuki Iwasa is an employee of Nihon Berm Co., Ltd. All other authors declare that they have no competing interests.

Author details

¹Department of Pharmacology, Faculty of Pharmaceutical Sciences, Tohoku Medical and Pharmaceutical University, 4-4-1 Komatsushima, Aoba-ku, Sendai 981-8558, Japan. ²Department of Pharmacology, School of Pharmacy, International University of Health and Welfare, 2600-1 Kitakanemaru, Ohtawara, Tochigi 324-8501, Japan. ³Faculty of Health Science, Tohoku Fukushi University, 1-8-1 Kunimi, Aoba-ku, Sendai, Miyagi 981-8522, Japan. ⁴Department of Healthcare and Regulatory Sciences, School of Pharmacy, Showa University, 1-5-8 Hatanodai, Shinagawa-ku, Tokyo 142-8555, Japan. ⁵Department of Psychiatry, Nihon University School of Medicine, 30-1 Oyaguchi-kamicho, Itabashi-ku, Tokyo 173-8610, Japan. ⁶Kampo and Herbal Medicine Research Center, Yokohama University of Pharmacy, 601 Matanocho, Totsuka-ku, Yokohama City, Kanagawa 245-0066, Japan. ⁷Nihon Berm Co, Ltd, 2-14-3 Nagatachou, Chiyoda-ku, Tokyo 100-0014, Japan. ⁸Complementary and Alternative Medicine Clinical Research and Development, Graduate School of Medicine Sciences, Kanazawa University, Kanazawa 920-8640, Japan.

Received: 7 June 2019 Accepted: 10 September 2019

Published online: 31 October 2019

References

- Perez-Pardo P, Hartog M, Garssen J, Kraneveld AD. Microbes tickling your tummy: the importance of the gut-brain axis in Parkinson's disease. *Curr Behav Neurosci Rep*. 2017;4:361–8.
- Riazi K, Galic MA, Kuzmiski JB, Ho W, Sharkey KA, Pittman QJ. Microglial activation and TNF α production mediate altered CNS excitability following peripheral inflammation. *Proc Natl Acad Sci U S A*. 2008;105:17151–6.
- Bercik P, Park AJ, Sinclair D, Khoshdel A, Lu J, Huang X, Deng Y, Blennerhassett PA, Fahnstock M, Moine D, Berger B, Huizinga JD, Kunze W, McLean PG, Bergonzelli GE, Collins SM, Verdu EF. The anxiolytic effect of *Bifidobacterium longum* NCC3001 involves vagal pathways for gut-brain communication. *Neurogastroenterol Motil*. 2011;23:1132–9.
- Mikocka-Walus AA, Turnbull DA, Moulding NT, Wilson IG, Andrews JM, Holtmann GJ. Antidepressants and inflammatory bowel disease: a systematic review. *Clin Pract Epidemiol Ment Health*. 2006;2:24.
- Graff LA, Walker JR, Bernstein CN. Depression and anxiety in inflammatory bowel disease: a review of comorbidity and management. *Inflamm Bowel Dis*. 2009;5:1105–18.
- Lydiard RB. Irritable bowel syndrome, anxiety, and depression: what are the links? *J Clin Psychiatry*. 2001;62(Suppl 8):38–45.
- Kurina LM, Goldacre MJ, Yeates D, Gill LE. Depression and anxiety in people with inflammatory bowel disease. *J Epidemiol Community Health*. 2001;55:716–20.
- Takedatsu H, Michelsen KS, Wei B, Landers CJ, Thomas LS, Dhall D, Braun J, Targan SR. TL1A (TNFSF15) regulates the development of chronic colitis by modulating both T-helper 1 and T-helper 17 activation. *Gastroenterology*. 2008;135:552–67.
- Strober W, Fuss IJ, Blumberg RS. The immunology of mucosal models of inflammation. *Annu Rev Immunol*. 2002;20:495–549.
- Neurath MF, Fuss I, Kelsall BL, Stuber E, Strober W. Antibodies to interleukin 12 abrogate established experimental colitis in mice. *J Exp Med*. 1995;182:1281–90.
- Chen J, Winston JH, Fu Y, Guptarak J, Jensen KL, Shi XZ, Green TA, Sarna SK. Genesis of anxiety, depression, and ongoing abdominal discomfort in ulcerative colitis-like colon inflammation. *Am J Physiol Regul Integr Comp Physiol*. 2015;308:R18–27.
- Zonis S, Pechnick RN, Ljubimov VA, Mahgerefteh M, Wawrowsky K, Michelsen KS, Chesnokova V. Chronic intestinal inflammation alters hippocampal neurogenesis. *J Neuroinflammation*. 2015;12:65.
- Scorza FA, Guerra A d B, Cavalheiro EA, Calil HM. Neurogenesis and depression: etiology or new illusion? *Rev Bras Psiquiatr*. 2005;27:249–53.
- Duman RS, Monteggia LM. A neurotrophic model for stress-related mood disorders. *Biol Psychiatry*. 2006;59:1116–27.
- Castrén E, Vöörä V, Rantamäki T. Role of neurotrophic factors in depression. *Curr Opin Pharmacol*. 2007;7:18–21.
- Yirmiya R, Rimmerman N, Reshef R. Depression as a microglial disease. *Trends Neurosci*. 2015;38:637–58.
- Milior G, Lecours C, Samson L, Bisht K, Poggini S, Pagani F, DeFlorio C, Lauro C, Alboni S, Limatola C, Branchi I, Tremblay ME, Maggi L. Fractalkine receptor deficiency impairs microglial and neuronal responsiveness to chronic stress. *Brain Behav Immun*. 2016;55:114–25.
- Ben-Hur T, Ben-Menachem O, Furer V, Einstein O, Mizrahi-Kol R, Grigoriadis N. Effects of proinflammatory cytokines on the growth, fate, and motility of multipotential neural precursor cells. *Mol Cell Neurosci*. 2003;24:623–31.
- Koo JW, Duman RS. Interleukin-1 receptor null mutant mice show decreased anxiety-like behavior and enhanced fear memory. *Neurosci Lett*. 2009;456:39–43.
- Iosif RE, Ekdahl CT, Ahlenius H, Pronk CJ, Bonde S, Kokaia Z, Jacobsen SE, Lindvall O. Tumor necrosis factor receptor 1 is a negative regulator of progenitor proliferation in adult hippocampal neurogenesis. *J Neurosci*. 2006;26:9703–12.
- Santarelli L, Saxe M, Gross C, Surget A, Battaglia F, Dulawa S, Weisstaub N, Lee J, Duman R, Arancio O, Belzung C, Hen R. Requirement of hippocampal neurogenesis for the behavioral effects of antidepressants. *Science*. 2003;301:805–9.
- Engel D, Zomkowski AD, Lieberknecht V, Rodrigues AL, Gabilan NH. Chronic administration of duloxetine and mirtazapine downregulates proapoptotic proteins and upregulates neurotrophin gene expression in the hippocampus and cerebral cortex of mice. *J Psychiatr Res*. 2013;47:802–8.
- Lehmann ML, Brachman RA, Martinowich K, Schloesser RJ, Herkenham M. Glucocorticoids orchestrate divergent effects on mood through adult neurogenesis. *J Neurosci*. 2013;33:2961–72.
- Schloesser RJ, Lehmann M, Martinowich K, Manji HK, Herkenham M. Environmental enrichment requires adult neurogenesis to facilitate the recovery from psychosocial stress. *Mol Psychiatry*. 2010;15:1152–63.
- Lucassen PJ, Heine VM, Muller MB, van der Beek EM, Wiegant VM, De Kloet ER, Joels M, Fuchs E, Swaab DF, Czeh B. Stress, depression and hippocampal apoptosis. *CNS Neurol Disord Drug Targets*. 2006;5:531–46.
- Barkett M, Gilmore TD. Control of apoptosis by Rel/NF- κ B transcription factors. *Oncogene*. 1999;18:6910–24.
- Karin M, Lin A. NF- κ B at the crossroads of life and death. *Nat Immunol*. 2002;3:221–7.
- Choi EJ, Iwasa M, Han KI, Kim WJ, Tang Y, Hwang YJ, Chae JR, Han WC, Shin YS, Kim EK. Heat-killed *Enterococcus faecalis* EF-2001 ameliorates atopic dermatitis in a murine model. *Nutrients*. 2016;8:146.

29. Gu YH, Choi H, Yamashita T, Kang KM, Iwasa M, Lee MJ, Lee KH, Kim CH. Pharmaceutical production of anti-tumor and immune-potentiating *Enterococcus faecalis*-2001 β -glucans: enhanced activity of macrophage and lymphocytes in tumor-implemented mice. *Curr Pharm Biotechnol*. 2017;18:653–61.
30. Choi EJ, Lee HJ, Kim WJ, Han KI, Iwasa M, Kobayashi K, Debnath T, Tang Y, Kwak YS, Yoon JH, Kim EK. *Enterococcus faecalis* EF-2001 protects DNBS-induced inflammatory bowel disease in mice model. *PLoS One*. 2019;14:e0210854.
31. Celiberto LS, Bedani R, Dejani NN, Ivo de Medeiros A, Sampaio Zuanon JA, Spolidorio LC, Tallarico Adorno MA, Amâncio Varesche MB, Carrilho Galvão F, Valentini SR, Font de Valdez G, Rossi EA, DCU C. Effect of a probiotic beverage consumption (*Enterococcus faecium* CRL 183 and *Bifidobacterium longum* ATCC 15707) in rats with chemically induced colitis. *PLoS One*. 2017;12:e0175935.
32. Wang S, Hibberd ML, Pettersson S, Lee YK. *Enterococcus faecalis* from healthy infants modulates inflammation through MAPK signaling pathways. *PLoS One*. 2014;9:e97523.
33. Nakamura H, Mizushima Y, Seto Y, Motoyoshi S, Kadokawa T. Dexamethasone fails to produce antipyretic and analgesic actions in experimental animals. *Agents Actions*. 1985;16:542–7.
34. Takahashi K, Nakagawasai O, Nemoto W, Nakajima T, Arai Y, Hisamitsu T, Tan-No K. Alterations in behavioral responses to dopamine agonists in olfactory bulbectomized mice: relationship to changes in the striatal dopaminergic system. *Psychopharmacology (Berl)*. 2016;233:1311–22.
35. Cooper HS, Murthy SN, Shah RS, Sedergran DJ. Clinicopathologic study of dextran sulfate sodium experimental murine colitis. *Lab Invest*. 1993;69:238–49.
36. Vasina V, Broccoli M, Ursino MG, Canistro D, Valgimigli L, Soleti A, Paolini M, De Ponti F. Non-peptidyl low molecular weight radical scavenger IAC attenuates DSS-induced colitis in rats. *World J Gastroenterol*. 2010;16:3642–50.
37. Takahashi K, Nakagawasai O, Nemoto W, Kadota S, Isono J, Odaira T, Sakuma W, Arai Y, Tadano T, Tan-No K. Memantine ameliorates depressive-like behaviors by regulating hippocampal cell proliferation and neuroprotection in olfactory bulbectomized mice. *Neuropharmacology*. 2018a;137:141–55.
38. Takahashi K, Nakagawasai O, Nemoto W, Odaira T, Arai Y, Hisamitsu T, Tan-No K. Time-dependent role of prefrontal cortex and hippocampus on cognitive improvement by aripiprazole in olfactory bulbectomized mice. *Eur Neuropsychopharmacol*. 2017;27:1000–10.
39. Takahashi K, Nakagawasai O, Nemoto W, Odaira T, Sakuma W, Tan-No K. Antidepressant-like effect of aripiprazole via 5-HT_{1A}, D₁, and D₂ receptors in the prefrontal cortex of olfactory bulbectomized mice. *J Pharmacol Sci*. 2018;137:241–7.
40. Liu D, Smith DJ. Voxellation and gene expression tomography for the acquisition of 3-D gene expression maps in the brain. *Methods*. 2003;31:317–25.
41. Li P, Tang XD, Cai ZX, Qiu JJ, Lin XL, Zhu T, Owusu L, Guo HS. CNP signal pathway up-regulated in rectum of depressed rats and the interventional effect of Xiaoyaosan. *World J Gastroenterol*. 2015;21:1518–30.
42. Paxinos G, Franklin KBJ. The mouse brain in stereotaxic coordinates. 2nd ed. San Diego: Academic Press; 2001.
43. Neurath MF. Cytokines in inflammatory bowel disease. *Nat Rev Immunol*. 2014;14:329–42.
44. Francescone R, Hou V, Grivennikov SI. Cytokines, IBD, and colitis-associated cancer. *Inflamm Bowel Dis*. 2015;21:409–18.
45. Nemoto W, Yamagata R, Ogata Y, Nakagawasai O, Tadano T, Tan-No K. Inhibitory effect of angiotensin (1–7) on angiotensin III-induced nociceptive behaviour in mice. *Neuropeptides*. 2017;65:71–6.
46. Baumgart DC, Sandborn WJ. Crohn's disease. *Lancet*. 2012;380:1590–605.
47. Danese S, Fiocchi C. Ulcerative colitis. *N Engl J Med*. 2011;365:1713–25.
48. Smith RS. The macrophage theory of depression. *Med Hypotheses*. 1991;35:298–306.
49. Maes M, Smith R, Scharpe S. The monocyte-T-lymphocyte hypothesis of major depression. *Psychoneuroendocrinology*. 1995;20:111–6.
50. Are A, Aronsson L, Wang S, Greicius G, Lee YK, Gustafsson JA, Pettersson S, Arulampalam V. *Enterococcus faecalis* from newborn babies regulate endogenous PPAR γ activity and IL-10 levels in colonic epithelial cells. *Proc Natl Acad Sci U S A*. 2008;105:1943–8.
51. Takada Y, Hisamatsu T, Kamada N, Kitazume MT, Honda H, Oshima Y, Saito R, Takayama T, Kobayashi T, Chinen H, Mikami Y, Kanai T, Okamoto S, Hibi T. Monocyte chemoattractant protein-1 contributes to gut homeostasis and intestinal inflammation by composition of IL-10-producing regulatory macrophage subset. *J Immunol*. 2010;184:2671–6.
52. Creed TJ, Lee RW, Newcomb PV, di Mambro AJ, Raju M, Dayan CM. The effects of cytokines on suppression of lymphocyte proliferation by dexamethasone. *J Immunol*. 2009;183:164–71.
53. Hashimoto K. Emerging role of glutamate in the pathophysiology of major depressive disorder. *Brain Res Rev*. 2009;61:105–23.
54. Hashimoto K. Inflammatory biomarkers as differential predictors of antidepressant response. *Int J Mol Sci*. 2015;16:7796–801.
55. Miller AH, Maletic V, Raison CL. Inflammation and its discontents: the role of cytokines in the pathophysiology of major depression. *Biol Psychiatry*. 2009;65:732–41.
56. Schoenfeld TJ, Cameron HA. Adult neurogenesis and mental illness. *Neuropsychopharmacology*. 2015;40:113–28.
57. Alvarez-Buylla A, Garcia-Verdugo JM. Neurogenesis in adult subventricular zone. *J Neurosci*. 2002;22:629–34.
58. Cayre M, Malaterre J, Scotto-Lomassese S, Strambi C, Strambi A. The common properties of neurogenesis in the adult brain: from invertebrates to vertebrates. *Comp Biochem Physiol B Biochem Mol Biol*. 2002;132:1–15.
59. Yu XT, Xu YF, Huang YF, Qu C, Xu LQ, Su ZR, Zeng HF, Zheng L, Yi TG, Li HL, Chen JP, Zhang XJ. Berberubine attenuates mucosal lesions and inflammation in dextran sodium sulfate-induced colitis in mice. *PLoS One*. 2018;13:e0194069.
60. DeCarolis NA, Eisch AJ. Hippocampal neurogenesis as a target for the treatment of mental illness: a critical evaluation. *Neuropharmacology*. 2010;58:884–93.
61. Aizawa M, Watanabe K, Tominari T, Matsumoto C, Hirata M, Grundler FMW, Inada M, Miyaura C. Low molecular-weight curdlan, (1 \rightarrow 3)- β -glucan suppresses TLR2-induced RANKL-dependent bone resorption. *Biol Pharm Bull*. 2018;41:1282–5.
62. Beaulieu LM, Lin E, Morin KM, Tanriverdi K, Freedman JE. Regulatory effects of TLR2 on megakaryocytic cell function. *Blood*. 2011;117:5963–74.
63. Bérubé J, Bourdon C, Yao Y, Rousseau S. Distinct intracellular signaling pathways control the synthesis of IL-8 and RANTES in TLR1/TLR2, TLR3 or NOD1 activated human airway epithelial cells. *Cell Signal*. 2009;21:448–56.
64. Agkul C, Moulding DA, Edwards SW. Molecular control of neutrophil apoptosis. *FEBS Lett*. 2001;487:318–22.
65. Holcik M, Korneluk RG. XIAP, the guardian angel. *Nat Rev Mol Cell Biol*. 2001;2:550–6.
66. Gibon J, Unsain N, Gamache K, Thomas RA, De Leon A, Johnstone A, Nader K, Séguéla P, Barker PA. The X-linked inhibitor of apoptosis regulates long-term depression and learning rate. *FASEB J*. 2016;30:3083–90.
67. Martínez-Mármol R, Barneda-Zahonero B, Soto D, Andrés RM, Coccia E, Gasull X, Planells-Ferrer L, Moubarak RS, Soriano E, Comella JX. FAIM-L regulation of XIAP degradation modulates synaptic long-term depression and axon degeneration. *Sci Rep*. 2016;6:35775.
68. Fiandalo MV, Kyprianou N. Caspase control: protagonists of cancer cell apoptosis. *Exp Oncol*. 2012;34:165–75.
69. Bravo JA, Forsythe P, Chew MV, Escaravage E, Savignac HM, Dinan TG, Bienenstock J, Cryan JF. Ingestion of *Lactobacillus* strain regulates emotional behavior and central GABA receptor expression in a mouse via the vagus nerve. *Proc Natl Acad Sci U S A*. 2011;108:16050–5.
70. O'Leary OF, O'Gonnaya ES, Felice D, Levone BR, Conroy LC, Fitzgerald P, Bravo JA, Forsythe P, Bienenstock J, Dinan TG, Cryan JF. The vagus nerve modulates BDNF expression and neurogenesis in the hippocampus. *Eur Neuropsychopharmacol*. 2018;28:307–16.

Publisher's Note

Springer Nature remains neutral with regard to jurisdictional claims in published maps and institutional affiliations.



Contents lists available at ScienceDirect

Neuropharmacology

journal homepage: www.elsevier.com/locate/neuropharm

Mechanisms underpinning AMP-activated protein kinase-related effects on behavior and hippocampal neurogenesis in an animal model of depression

Takayo Odaira, Osamu Nakagawasai^{*}, Kohei Takahashi, Wataru Nemoto, Wakana Sakuma, Jia-Rong Lin, Koichi Tan-No

Department of Pharmacology, Faculty of Pharmaceutical Sciences, Tohoku Medical and Pharmaceutical University, 4-4-1 Komatsushima, Aoba-ku, Sendai 981-8558, Japan

HIGHLIGHTS

- AMPK activator AICAR ameliorates depressive behavior in OBX mice.
- AICAR activates PKC ζ /NF- κ B/BDNF/TrkB/CREB pathway in the hippocampus of OBX mice.
- AICAR promotes neurogenesis, and this effect is attenuated by PKC ζ inhibitor.
- Phospho-AMPK is detected in neurons and microglia; NF- κ B is detected in neurons.
- AMPK activators may serve as new therapeutic targets in depression.

ABSTRACT

Adenosine monophosphate-activated protein kinase (AMPK) is critical for whole-body energy metabolism regulation. Recent studies have suggested that physical exercise ameliorates depressive-like behaviors via AMPK activation; however, the underlying mechanism is unclear. Here, we examined the effects and underlying mechanisms of AMPK activation on depressive-like behavior in olfactory bulbectomized (OBX) mice. We treated OBX mice with the AMPK activator, 5-aminoimidazole-4-carboxamide-1- β -D-ribose (AICAR) on the 7th or 14th day after bilateral bulbectomy and evaluated depressive-like behavior using the tail-suspension test (TST) and forced swimming test (FST) on the 21st day. The expression of phosphorylated AMPK, protein kinase C ζ (PKC ζ), nuclear factor-kappa B (NF- κ B), brain-derived neurotrophic factor (BDNF), and cAMP response element-binding protein (CREB) in the hippocampus was assessed by western blotting. Hippocampal neurogenesis and localization of AMPK and phosphorylated NF- κ B were examined by immunohistochemistry. Chronic AICAR treatment suppressed the prolonged immobility of OBX mice in the TST and FST, and increased the levels of phosphorylated AMPK, PKC ζ , NF- κ B, CREB, and BDNF. Hippocampal neurogenesis in OBX mice was promoted by chronic AICAR treatment. Co-administration of AICAR with the PKC ζ inhibitor or the neurotrophic tyrosine kinase receptor type 2 (TrkB) antagonist, ANA-12, inhibited these effects. Phosphorylated AMPK was detected in mature and immature hippocampal neurons and microglia, while phosphorylated NF- κ B was detected only in neurons in AICAR-treated OBX mice. These data indicate that AMPK activation produces anti-depressant effects, which are mediated by elevated hippocampal neurogenesis potentially via PKC ζ /NF- κ B/BDNF/TrkB/CREB signaling in neurons.

1. Introduction

Adenosine monophosphate (AMP)-activated protein kinase (AMPK) is a serine-threonine kinase and a heterotrimer composed of a catalytic subunit, α , and two regulatory subunits, β and γ (Shaw et al., 2004). AMPK is activated by physical exercise (Winder and Hardie, 1996) and an increasing AMP/ATP ratio (Hardie and Ashford, 2014), while the activity of AMPK contributes to the expression of glucose transporters and improvement in insulin sensitivity (Kong et al., 2013). Recently, we reported that an AMPK activator promotes recovery from physical fatigue in mice (Nakagawasai et al., 2015). AMPK activators, such as

metformin and resveratrol, elicit anti-depressant effects in patients with depression (Guo et al., 2014) and animal models of depression (Ali et al., 2015). However, the detailed mechanism underlying these effects in the central nervous system, via AMPK, remains unclear.

AMPK binds to and directly phosphorylates protein kinase C ζ (PKC ζ) in an isoform-specific manner in alveolar epithelial cells (Gusarova et al., 2009). Both metformin and 5-aminoimidazole-4-carboxamide-1- β -D-ribose (AICAR), an analog of AMP that directly activates AMPK, activate PKC ζ in an AMPK-dependent manner in muscle cells (Sajan et al., 2010). The PKC family is classified into three groups comprising conventional (α , β , and γ), novel (δ , ϵ , θ , μ , and η),

^{*} Corresponding author. Department of Pharmacology, Faculty of Pharmaceutical Sciences, Tohoku Medical and Pharmaceutical University, 4-4-1 Komatsushima, Aoba-ku, Sendai, Miyagi 981-8558, Japan

E-mail address: osamun@tohoku-mpu.ac.jp (O. Nakagawasai).

<https://doi.org/10.1016/j.neuropharm.2019.03.026>

Received 16 October 2018; Received in revised form 1 March 2019; Accepted 19 March 2019

Available online 23 March 2019

0028-3908/ © 2019 Elsevier Ltd. All rights reserved.

and atypical (λ and ζ) PKCs. In particular, PKC ζ plays an important role in neuronal function; it was demonstrated to be involved in long-term potentiation (Sacktor et al., 1993) and the release of neurotrophic factors, such as nerve growth factor (NGF), via the transcription factor, nuclear factor-kappa B (NF- κ B) (Obara et al., 2001). Moreover, blockade of atypical PKCs resulted in decreased NF- κ B activation (Dominguez et al., 1993). The latter promotes the expression of neurotrophic factors, such as NGF and brain-derived neurotrophic factor (BDNF) (Obara et al., 2001). BDNF is known to have high affinity for neurotrophic tyrosine kinase receptor type 2 (TrkB). The intracellular TrkB signaling cascade results in the phosphorylation of cyclic AMP response element-binding protein (CREB) and the subsequent activation of CREB-mediated gene transcription, which plays a critical role in the improvement in depressive-like behavior and promotion of neurogenesis (Berry et al., 2012). Previous studies have reported that both BDNF and CREB expression is lower in patients and animal models of depression than in healthy subjects (Chen et al., 2001a; Karege et al., 2002; Patki et al., 2013; Zhang et al., 2017). Moreover, chronic administration of anti-depressants, such as tricyclic anti-depressants (TCAs) and selective serotonin reuptake inhibitors (SSRIs), increased BDNF expression in human sera and rodent brains (Lee and Kim, 2008; Larsen et al., 2010), as well as CREB expression and activity in rodents (Nibuya et al., 1996; Thome et al., 2000). Recently, some groups have reported that physical exercise ameliorates depressive-like behavior via increased BDNF expression and promotion of neurogenesis in the dentate gyrus (DG) of the hippocampus (Widenfalk et al., 1999; Bjørnebekk et al., 2005; Yau et al., 2011). Newly generated neurons are incorporated into the hippocampal circuitry and contribute to hippocampal functions, including mood and memory (Petrik et al., 2012). Indeed, chronic anti-depressant administration promotes neurogenesis in the rodent hippocampus (Mostany et al., 2008). However, the detailed mechanism underlying the anti-depressant effects and promotion of neurogenesis via AMPK activation remains unclear.

In the present study, we used olfactory bulbectomized (OBX) mice as an animal model of depression which is caused by non-inflammatory mechanism and inflammatory. A previous study reported that patients with depression exhibit reduced olfactory bulb (OB) volumes and olfaction (Negoiias et al., 2010). These reductions negatively correlate with the depression scale, and impaired olfaction recovers after medical treatment, such as with TCAs and SSRIs (Pause et al., 2001). OBX mice exhibit depressive-like behavior, which is evidenced by their prolonged immobility in the tail-suspension test (TST) and the forced swimming test (FST) (Han et al., 2009), as well as their decreased sucrose preference (Sato et al., 2010; Nakagawasai et al., 2016). Moreover, some groups have reported that OBX rodents exhibit alternation of the serotonergic (Nakagawasai et al., 2003), noradrenergic (Cairncross et al., 1975), and dopaminergic (Takahashi et al., 2016) systems in the brain. The behavioral alternations in OBX rodents are improved by chronic, but not acute, administration of anti-depressants, such as TCAs, SSRIs, and serotonin-noradrenaline reuptake inhibitors (SNRIs). Such effects have also been observed in clinical patients. OBX has been used as an animal model of depression because it fulfills many of the necessary criteria for a depression model, which are comparable to the features observed in patients with major depression (Cryan and Mombereau, 2004). Therefore, OBX mice are an appropriate animal model for the screening of novel anti-depressants and for clarification of the mechanism of depression.

The hippocampus is divided into the ventral and dorsal hippocampus. Several groups, including our group, have reported that the bilateral infusion of BDNF into the dorsal hippocampus produces anti-depressant-like effects in behavioral depression models (Shirayama et al., 2002; Scharfman et al., 2005) and that conventional anti-depressant effects occurred via neurogenesis in the dorsal hippocampus (Mostany et al., 2008; Takahashi et al., 2018). Moreover, irradiation of the dorsal hippocampus caused a reduction in neurogenesis and a loss of fluoxetine's antidepressant effects (Santarelli et al., 2003). Therefore,

this study aimed to identify molecular and cellular changes in the dorsal hippocampus.

In this study, we examined the effects of AICAR on depressive-like behavior in OBX mice to clarify the role of AMPK in the anti-depressant effects. To identify possible mechanisms involved in the promotion of neurogenesis in the dorsal hippocampus, we measured the effect of AICAR on the PKC ζ /NF- κ B/BDNF/CREB signaling pathway.

2. Materials and methods

All experiments were performed following approval of the Ethics Committee of Animal Experiments in Tohoku Medical and Pharmaceutical University (Approval number: 16023 cn, 17015 cn) and according to the National Institutes of Health Guide for the Care and Use of Laboratory Animals. Efforts were made to minimize suffering and reduce the number of animals used.

2.1. Animals

We used male ddY mice (age: 6–7 weeks, weight: 26–28 g; Japan SLC, Japan) for all experiments (total: $n = 251$; behavioral test: $n = 187$; western blotting analysis: $n = 29$; immunohistochemical study: $n = 35$). We chose this strain of mice partly based on previous work showing that ddY mice are more vulnerable to the development of stress-induced behavioral disturbances (Mouri et al., 2012). This strain is also more responsive to treatment with anti-depressants than other mice (Sugimoto et al., 2011). We selected this age range because the peak period of first onset in most mental disorders is adolescence and young adulthood (Ströhle et al., 2007; Patel et al., 2007). The mice were housed in cages of 5–6 mice, under steady conditions ($23 \pm 1^\circ\text{C}$, $55 \pm 5\%$, 12/12 h light-dark cycle with lights on at 7:00 a.m.) with free access to food or water. All behavioral tests were performed between 9:00 and 17:00. All mice were numbered by earmarks and randomly divided into groups using a table of random numbers.

2.2. Surgical procedure

OBX surgery was performed as described previously (Hozumi et al., 2003). The mice were anesthetized with sodium pentobarbital (50 mg/kg; Kyoritsu Seiyaku, Tokyo, Japan) and subsequently placed on a stereotaxic instrument. The head was incised and drilled on the sagittal midline, and the OBs were aspirated using a micropipette tip connected to a water vacuum pump. The mice were occluded in their anterior holes using a hemostatic sponge. All mice were euthanized at the end of the experiment and it was visually confirmed that two-thirds of the OB had been lesioned. Mice were excluded from the data if the lesion did not extend to more than two-thirds of the OB or if it extended to the cortex. Sham operations followed the same surgical procedure without the removal of the OB. The OBs of sham and OBX showed in Fig. 1A.

2.3. Compounds

AICAR (50 and 100 mg/kg; Toronto Research Chemicals, Inc.; Cat# A611700) was dissolved in saline and injected intraperitoneally at a volume of 0.1 mL/10 g body weight. Previously Liu et al. reported that administration of 100 mg/kg of AICAR ameliorates depressive-like behavior in a high-fat diet and corticosterone co-treated mice (Liu et al., 2014). The protocol for AICAR administration is provided in Figs. 1, 2, 4 and 5. Myristoylated PKC pseudosubstrate (zeta-inhibitory peptide [ZIP]; PKC ζ inhibitor; AnaSpec, Inc.; Cat# AS-63361) was dissolved in Ringer's solution (Fuso Pharmaceutical Industries, Ltd, Osaka, Japan), and N-[2-[[[Hexahydro-2-oxo-1H-azepin-3-yl]amino]carbonyl]phenyl]-benzo[b]thiophene-2-carboxamide (ANA-12; Trk B receptor antagonist; Sigma-Aldrich; Cat# SML0209) was dissolved in saline containing 0.15% Tween 80. ZIP was injected into OBX mice using cannulas (Brain infusion kit 3; Muromachi Kikai, Tokyo, Japan) and an osmotic pump (Alzet 2002; Muromachi Kikai)

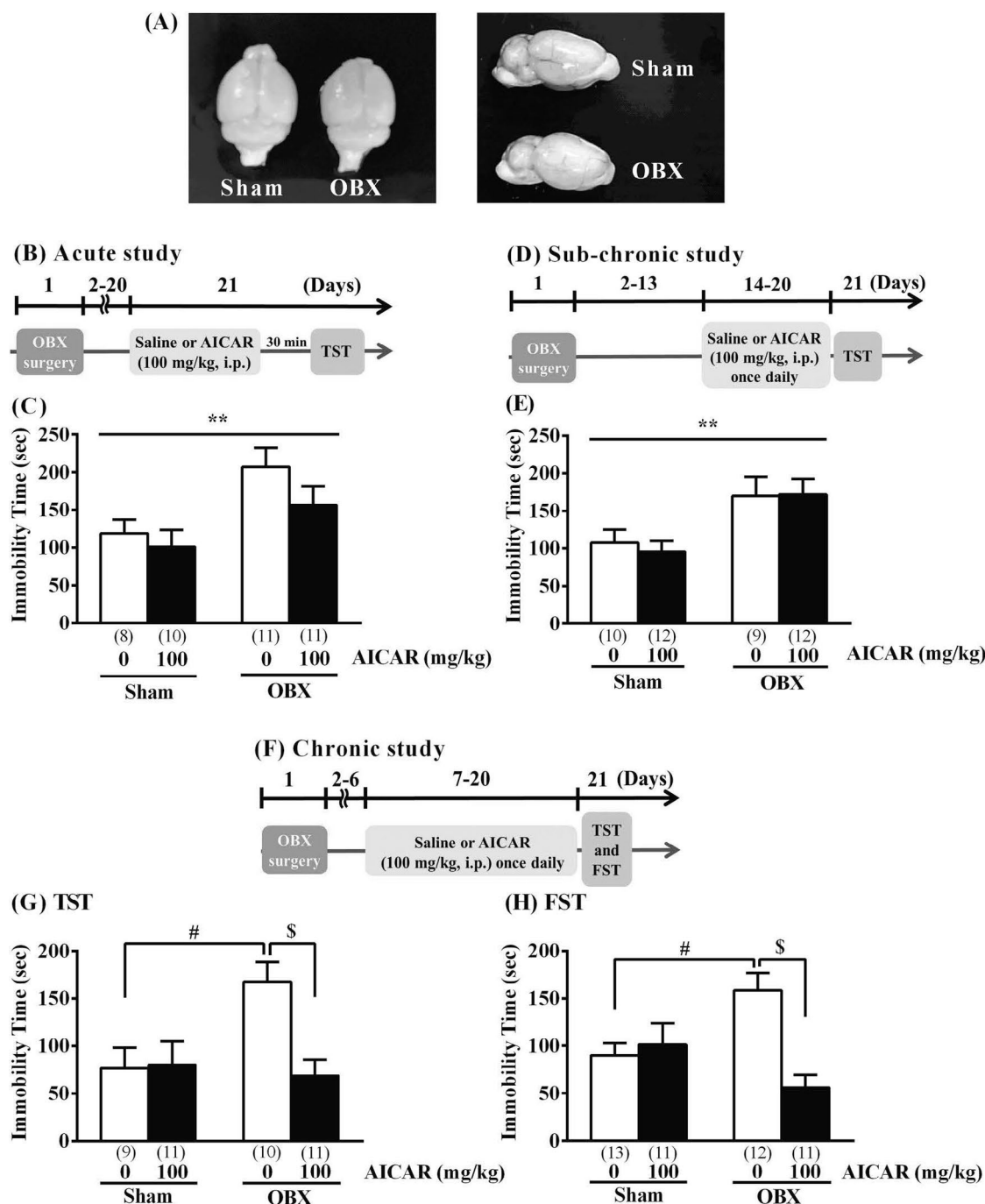


Fig. 1. Effect of AICAR on the tail-suspension test (TST) in olfactory bulbectomized (OBX) mice. (A) Representative image of whole brain in sham mice and OBX mice. (B, D, F) Time course of the experimental protocol. (C) The immobility time was evaluated by the TST 30 min after vehicle or AICAR intraperitoneal (i.p.) administration on the 21st day after surgery. (E, G) The immobility time was measured in the TST 24 h after vehicle or AICAR administration for 7 days (E) or for 14 days (G). (H) The immobility time was measured by the FST 24h after vehicle or AICAR administration for 14 days. Vertical lines above bars represent mean \pm standard error of the mean. **, $p < 0.01$ as compared between sham group and OBX group; #, $p < 0.05$ compared to sham + Vehicle group; \$, $p < 0.05$ compared to OBX + Vehicle group. $n = 9$ – 12 animals in each group.

for 14 days (5 μ g/12 μ L/day) (Migues et al., 2010; Bogard and Tavalin, 2015). The protocol for ZIP microinfusion is provided in Fig. 4. ANA-12 was injected intraperitoneally at a dose of 0.5 mg/kg (Ma et al., 2016). The protocol for ANA-12 administration is provided in Fig. 5.

2.4. Osmotic pump implantation for intracerebral ZIP microinfusion

Implantation of the osmotic pump and brain infusion were

performed as described by DeVos (DeVos and Miller, 2013). On the 7th day after surgery, OBX mice were anesthetized with sodium pentobarbital (50 mg/kg) and placed on a stereotaxic instrument. A hole was drilled in the skull, and a cannula was implanted and placed at 1.0 mm lateral, 0.22 mm posterior, and 3 mm deep in relation to the bregma. The cannula was fixed with dental cement on the skull and connected to an osmotic pump that was inserted into the lateral back of OBX mice.

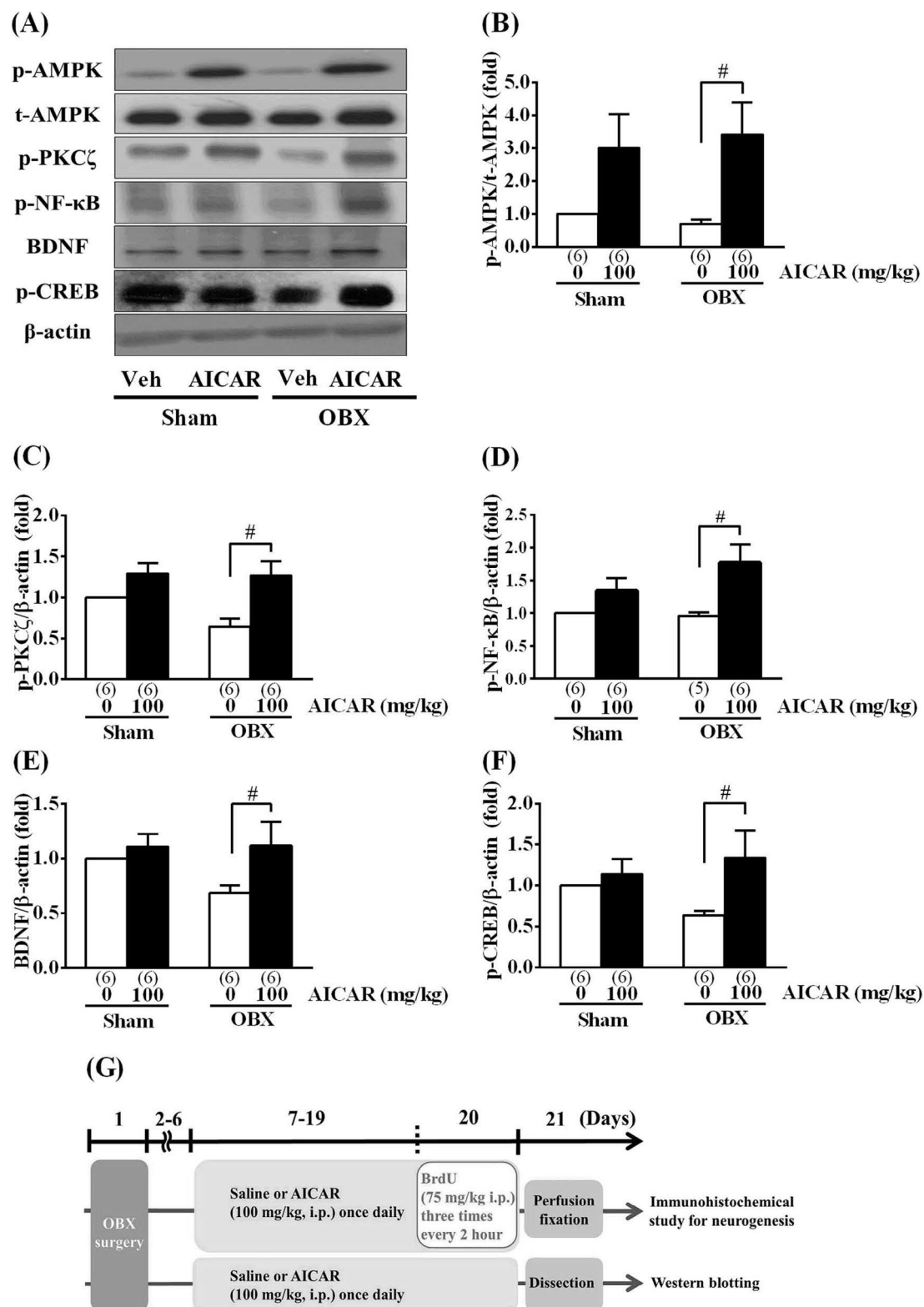


Fig. 2. AICAR administration increases phosphorylation and expression levels of proteins in the hippocampus of olfactory bulbectomized (OBX) mice. (A) Representative immunoblots probed with antibodies against p-AMPK, AMPK, p-PKC ζ , p-NF- κ B, BDNF, p-CREB, and β -actin, as indicated. (B–F) Quantification of the normalized to total AMPK values of p-AMPK (B), and of the normalized to β -actin values of p-PKC ζ (C), p-NF- κ B (D), BDNF (E) and p-CREB (F). (G) Time course of the experimental protocol. Vertical lines above bars represent mean \pm standard error of the mean. n = 6–9 per group. #, p < 0.05 compared to OBX + Vehicle group. n = 6–9 animals in each group.

2.5. Tail-suspension test

The TST was used to observe the effect of AICAR on depressive-like behavior in OBX mice. The procedure was performed as described previously (Takahashi et al., 2018). The mice were taped from the tip of their tail and suspended at a height of 30 cm from the floor for 10 min. The immobility time was measured for 10 min by an observer who was blinded to the treatment.

2.6. Forced swimming test

The FST was also conducted to evaluate the anti-depressant effect of AICAR. The procedure was performed as described previously (Han et al., 2009; Takahashi et al., 2018). After the TST, OBX and sham mice were individually placed on plastic cylinders (height: 25 cm; diameter: 20 cm) containing water maintained at $25 \pm 0.5^\circ\text{C}$ up to 14 cm for 5 min. The immobility time was measured for 5 min by an observer who was blinded to the treatment.

2.7. Western immunoblotting

Western immunoblotting analysis was performed using hippocampal samples from mice that had not undergone any behavioral testing. Mice were euthanized by decapitation 24 h after the final AICAR administration. Sectioning was performed as described by Liu and Smith (2003). Briefly, the brain was removed and sectioned on ice, using a mouse brain slicer (Muromachi Kikai), to produce 1 mm thick coronal sections. We visually confirmed the dorsal hippocampal location using mouse brain stereotaxic coordinates (Paxinos and Franklin, 2001). The two (left and right) dorsal hippocampi were isolated, frozen in liquid nitrogen, and then stored at -80°C until use. The brain samples were homogenized in 150 μL of CellLytic™ MT Cell Lysis Reagent (Sigma-Aldrich; Cat# C3228-50 ML) and centrifuged at $15,000 \times g$ for 15 min at 4°C . The supernatants were diluted in $4 \times$ Laemmli sample buffer (300 mM Tris-HCl [pH 6.8], 8% sodium dodecyl sulfate [SDS], 40% glycerol, 12% 2-mercaptoethanol, and 0.012% bromophenol blue) and then incubated at 95°C for 10 min. These extracted samples were loaded onto 10% SDS-polyacrylamide gel. After electrophoresis, proteins were transferred to polyvinylidene difluoride membranes and incubated with blocking solution (10 mM Tris-HCl [pH 7.4], 100 mM NaCl, 0.01% Tween 20, and 5% skim milk). The membranes were probed with antibodies against AMPK (1:1000; Cell Signaling Technology; Cat# 2532), phosphorylated (p)-AMPK (1:1000; Cell Signaling Technology; Cat# 2531), p-PKC ζ (1:1000; Santa Cruz Biotechnology; Cat# sc-12894-R), p-NF- κB (Ser311, 1:200; Santa Cruz Biotechnology; Cat# sc-135769), p-CREB (1:1000; Cell Signaling Technology; Cat# 9198), BDNF (1:100; Santa Cruz Biotechnology; Cat# sc-546), and β -actin (1:1000; Cell Signaling Technology; Cat# 4967) overnight at 4°C . The membranes were then washed with blocking solution without milk, incubated with horseradish peroxidase-conjugated secondary antibody (1:5000; Cell Signaling Technology; Cat# 7074) for 2 h, and visualized using an enhanced chemiluminescence western blotting detection reagent (Amersham Life Science; Cat# RPN2109). The band density was measured by densitometry (Image-J 1.43 μ , National Institute of Health).

2.8. Immunohistochemistry for neurogenesis

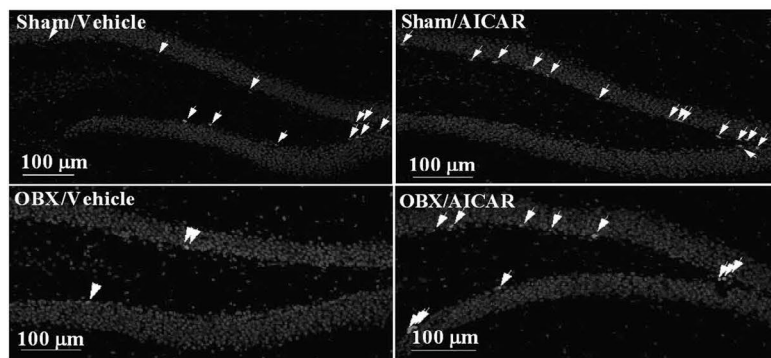
To investigate whether AICAR promotes cell proliferation in hippocampus, sham or OBX mice were injected with 5-bromo-2'-deoxyuridine (BrdU; 75 mg/kg intraperitoneal injection; Nacalai Tesque; Cat# 05650-24) three times every 2 h after the final administration of saline or AICAR on day 20 after surgery. The procedures from perfusion to immunohistochemical staining were performed as described previously (Nakagawasai et al., 2016). The mice were subsequently

euthanized under deep anesthesia 24 h after the final injection of saline or AICAR and intracardially perfused with 15 mL of 4°C phosphate-buffered saline (PBS), followed by 45 mL of 4% paraformaldehyde (PFA; Sigma-Aldrich) in 0.1 M PBS. Brains were post-fixed in 4% PFA-0.1 M PBS for 1 h at 4°C , followed by immersion in 20% sucrose-0.1 M PBS for 48 h. The brains were sliced into 40 μm sections from -1.40 mm to -2.00 mm relative to the bregma using a cryostat (MICROM HM560, Microm International GmbH, Walldorf, Germany). Three sections were confirmed visually dorsal hippocampus following mouse brain stereotaxic coordinates (Paxinos and Franklin, 2001) to evaluate neurogenesis in the same location of each mouse. Frozen sections were mounted on glass slides (Matsunami Glass, Osaka, Japan). Sections were treated with HCl (2 N) at 37°C for 30 min, followed by neutralization with sodium borate buffer (0.15 M) at room temperature, twice for 10 min each. After three 5 min washes, the sections were incubated with PBS containing 1% normal goat serum and 0.3% Tri-ton X-100 (PBST) at room temperature for 2 h and then incubated overnight at 4°C with primary monoclonal antibodies against rat anti-BrdU (1:100; Bio Rad; Cat# OBT0030) and mouse anti-doublecortin (DCX) (1:50; Santa Cruz Biotechnology; Cat# sc-271390). After incubation for 2 days, the sections were washed twice with 0.1% PBS and incubated for 2 h with goat anti-rat IgG Alexa fluor 568 (1:200; Molecular Probes; Cat# A11077) and goat anti-mouse IgG Alexa fluor 488 (1:200; Molecular Probes Cat# A11001) as secondary antibodies, and DAPI (1:100; Wako Pure Chemical Industries, Ltd; Cat# 34207431) to identify nuclei. The sections were then washed twice with 0.1% PBS and coverslipped with Dako fluorescent mounting medium (Dako, Carpinteria, USA). The labeled sections were analyzed using a confocal laser-scanning microscope (A1RSi; Nikon, Tokyo, Japan). Three sections per mouse were used, and two images (left and right hemisphere, $640 \times 640 \mu\text{m}$) of the DG region of the hippocampus were obtained from each section. We calculated the BrdU/DCX positive cells following methods outlined by Liu et al. and Ouchi et al. (Liu et al., 2017; Ouchi et al., 2013). Positive cells were counted in the region observed under a fluorescence microscope. The positive cells in 2 images \times 3 sections per mouse were added, and this total value was considered to be the total number of BrdU/DCX positive cells in the whole dorsal hippocampus. A total of six images were analyzed per mouse, and each group contained 5–6 mice.

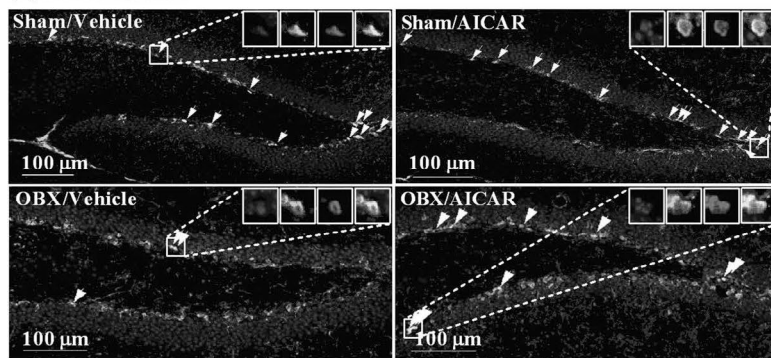
2.9. Immunohistochemistry for localization of p-AMPK and p-NF- κB

Brain samples were collected on day 21 after surgery. The sections were incubated overnight at 4°C with the following primary antibodies: rabbit anti-p-AMPK monoclonal (1:50; Cell Signaling Technology; Cat# 2535), p-NF- κB (Ser311, 1:200; Santa Cruz Biotechnology; Cat# sc-135769), mouse anti-neuronal nuclei (NeuN; 1:500; Millipore Corporation; Cat# MAB377), rabbit anti-NeuN (1:100; Cell Signaling Technology; Cat# 24307), rabbit anti-DCX (1:500; Abcam Ltd.; Cat# ab18723), rabbit anti-ionized calcium binding adaptor molecule 1 (Iba-1; 1:100; Wako; Cat# 019-19741), and mouse anti-glial fibrillary acidic protein (GFAP; 1:200; Millipore Corporation; Cat# MAB360). The sections were washed twice with 0.1% PBS and incubated for 2 h at $22 \pm 2^\circ\text{C}$ with the following secondary antibodies: goat anti-rabbit IgG Alexa fluor 568 (1:200; Molecular Probes; Cat# A11011) for anti-p-AMPK, goat anti-rabbit IgG Alexa fluor 488 (1:200; Molecular Probes; Cat# A11008) for rabbit anti-NeuN and anti-DCX, goat anti-mouse IgG Alexa fluor 568 (1:200; Molecular Probes; Cat# A11004) for anti-p-NF- κB , goat anti-mouse IgG Alexa fluor 488 (1:200; Molecular Probes; Cat# A11001) for mouse anti-NeuN and anti-GFAP, goat anti-rabbit IgG Alexa fluor 488 (1:200; Molecular Probes; Cat# A11008) for rabbit anti-Iba-1, and DAPI (1:100; Wako). Lastly, the sections were washed twice with 0.1% PBS and coverslipped with Dako medium. The fluorescence intensity was visualized on a confocal laser-scanning microscope (Nikon).

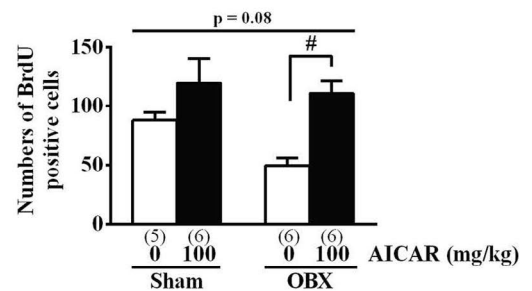
(A) DAPI/BrdU



(B) DAPI/DCX/BrdU



(C)



(D)

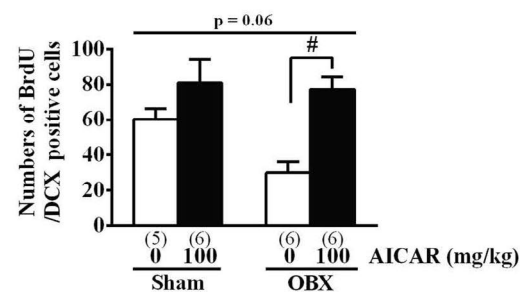


Fig. 3. Effect of AICAR on neurogenesis in the hippocampal dentate gyrus of olfactory bulbectomized (OBX) mice. (A, B) Confocal images of brain slices stained with DAPI (blue) and BrdU (red) (A) or DAPI, BrdU and DCX (green) (B). Arrowheads point to double or triple positive cells in the subgranular zone (SGZ). (C, D) Quantitative analysis of the number of BrdU⁺ and BrdU⁺/DCX⁺ cells in SGZ sham- and OBX-operated mice treated with saline or AICAR. #, $p < 0.05$ compared to OBX + Vehicle group. $n = 5$ –6 animals in each group.

2.10. Statistical analyses

Results are expressed as the mean \pm standard error of the mean. Normality and homoscedasticity assumptions were verified prior to the use of any parametric test (Shapiro–Wilk normality test and equality of variances F-test). The significance of the differences was determined by a one- or two-way analysis of variance (ANOVA) to compare groups, followed by the Tukey–Kramer test to correct for multigroup comparisons using GraphPad Prism 6 (GraphPad Software, California, USA) and StatView 5.0 (HULINKS, Tokyo, Japan), and a significant difference was defined as $p < 0.05$. When a main effect of group or treatment was significant without a group \times treatment interaction, we conducted an exploratory and limited pairwise post-hoc comparison, consistent with our a priori hypothesis. All statistical analyses, including the behavioral test, western blotting analysis, and immunohistochemistry for neurogenesis was performed by investigators other than the experimenters to avoid bias and to ensure blinding.

3. Results

3.1. AICAR exerts an anti-depressant effect in OBX mice

In TST, two-way ANOVA for the acute study of AICAR showed a significant main effect of group [$F(1, 36) = 9.014$, $p = 0.0048$] but not treatment [$F(1, 36) = 2.047$, $p = 0.1611$] or group \times treatment interaction [$F(1, 36) = 0.4639$, $p = 0.5002$] (Fig. 1C). Similarly, two-way ANOVA analysis of sub-chronic study of AICAR revealed a significant main effect of group [$F(1, 39) = 12.33$, $p = 0.0011$] but not treatment [$F(1, 39) = 0.06799$, $p = 0.7957$] or group \times treatment interaction [$F(1, 39) = 0.1238$, $p = 0.7269$] (Fig. 1E). The immobility time in OBX mice 21 days after the operation was significantly longer

than in sham-operated mice. Two-way ANOVA of administration of AICAR at 100 mg/kg for 14 days in TST indicated a marginally significant main effect of group [$F(1, 37) = 3.595$, $p = 0.0658$], AICAR treatment [$F(1, 37) = 5.044$, $p = 0.0308$], and group \times treatment interaction [$F(1, 37) = 5.955$, $p = 0.0196$]. Post-hoc analysis revealed prolonged immobility time in saline-treated OBX mice compared to saline-treated sham mice ($p < 0.05$) (Fig. 1G). Immobility time of OBX mice chronically treated with AICAR at 100 mg/kg for 14 days was significantly lower than the vehicle-treated OBX mice ($p < 0.05$) (Fig. 1G). Two-way ANOVA of the immobility time of FST showed a main effect of AICAR treatment [$F(1, 43) = 7.034$, $p = 0.0112$] and a group \times treatment interaction [$F(1, 43) = 10.97$, $p = 0.0019$], but no main effect of group [$F(1, 43) = 0.4614$, $p = 0.5006$]. Post-hoc tests confirmed the immobility time of OBX mice chronically treated with 100 mg/kg of AICAR was lower than that of vehicle-treated OBX mice ($p < 0.05$) (Fig. 1H). In addition, OBX mice that were chronically treated with AICAR at 50 mg/kg for 14 days did not significantly differ from OBX mice in the TST and FST [TST: one-way ANOVA, $F(2, 30) = 7.820$, $p = 0.0018$, post-hoc test, $p > 0.05$ at 50 mg/kg, $p < 0.05$ at 100 mg/kg; FST: one-way ANOVA, $F(2, 32) = 8.842$, $p = 0.0009$, post-hoc test, $p > 0.05$ at 50 mg/kg, $p < 0.05$ at 100 mg/kg] (Supplement Fig. 1). Thus, we investigated the mechanism underlying the AICAR-induced (at 100 mg/kg for 14 days) anti-depressant effect.

3.2. AICAR enhances p-AMPK, p-PKC ζ , p-NF- κ B, p-CREB, and BDNF levels in the hippocampi of OBX mice

To investigate whether chronic administration of AICAR changed the phosphorylation levels of AMPK, PKC ζ , NF- κ B, and CREB, and the expression level of BDNF in the hippocampus, we performed western

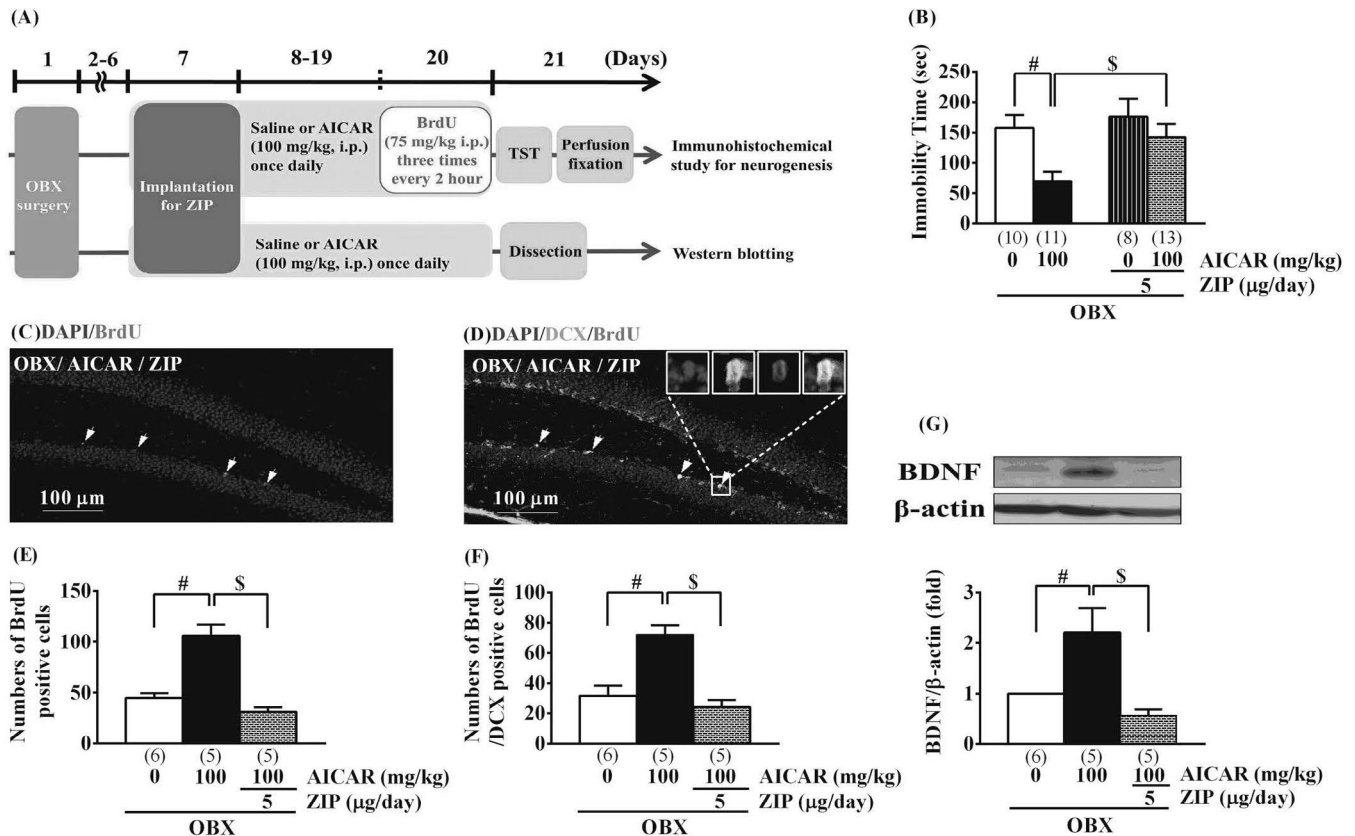


Fig. 4. Effect of ZIP on the anti-depressant effect of AICAR in olfactory bulbectomized (OBX) mice. (A) Timeline of the experimental protocol. (B) Immobility time measured with the tail-suspension test on the 21st day after OBX surgery. (C, D) Confocal images of brain slices stained DAPI (blue), BrdU (red) and DCX (green). Arrowheads point to BrdU⁺ or BrdU⁺/DCX⁺ cells in the SGZ. (E, F) Quantitative analysis of the number of BrdU⁺ and BrdU⁺/DCX⁺ cells in SGZ of OBX mice treated with AICAR [administered intraperitoneally (i.p.)] and ZIP (administered via an osmotic pump). (G) Representative immunoblots probed with antibodies against BDNF and β-actin. Quantification of normalized values of BDNF relative to β-actin levels. Vertical lines above bars represent mean ± standard error of the mean. #, $p < 0.05$ compared to OBX + Vehicle group; \$, $p < 0.05$ compared to OBX + AICAR group. $n = 6-9$ animals in each group.

blot analysis. Analysis of p -AMPK levels showed a significant main effect of treatment [$F(1, 20) = 10.92$, $p = 0.0035$] but not group [$F(1, 20) = 0.005776$, $p = 0.9402$] or group × treatment interaction [$F(1, 20) = 0.2606$, $p = 0.6153$]. Similarly, ANOVA analysis of p -PKCζ levels showed a significant main effect of treatment [$F(1, 20) = 15.15$, $p = 0.0009$] but not group [$F(1, 20) = 2.586$, $p = 0.1235$] or group × treatment interaction [$F(1, 20) = 1.966$, $p = 0.1762$]. Analysis of p -NF-κB levels also showed a significant main effect of treatment only [$F(1, 19) = 11.86$, $p = 0.0027$], without a significant effect of group [$F(1, 19) = 1.257$, $p = 0.2763$], or group × treatment interaction [$F(1, 19) = 1.931$, $p = 0.1807$]. BDNF expression showed a significant main effect of treatment [$F(1, 20) = 4.615$, $p = 0.0441$] but not group [$F(1, 20) = 1.459$, $p = 0.2411$] or group × treatment interaction [$F(1, 20) = 1.658$, $p = 0.2126$]. ANOVA of p -CREB levels demonstrated a significant main effect of treatment [$F(1, 20) = 4.777$, $p = 0.0409$] but not group [$F(1, 20) = 0.1917$, $p = 0.6662$] or two-way interaction [$F(1, 20) = 2.140$, $p = 0.1590$]. Post-hoc analysis revealed that protein levels in the hippocampus of AICAR-treated OBX mice are higher than in those vehicle-treated mice ($p < 0.05$), whereas no significant changes were observed in sham mice. These data are presented in Fig. 2 B–F.

3.3. AICAR promotes neurogenesis in the hippocampal DG

We examined whether AICAR altered neurogenesis in the DG of the hippocampus. ANOVA of BrdU⁺ and BrdU⁺/DCX⁺ cells showed a marginally significant main effect of group [BrdU⁺: $F(1, 19) = 3.404$,

$p = 0.0807$; BrdU⁺/DCX⁺: $F(1, 19) = 3.791$, $p = 0.0665$] and a significant effect of treatment [BrdU⁺: $F(1, 19) = 13.41$, $p = 0.0017$; BrdU⁺/DCX⁺: $F(1, 19) = 14.64$, $p = 0.0011$], but no group × treatment interaction [BrdU⁺: $F(1, 19) = 1.393$, $p = 0.2525$; BrdU⁺/DCX⁺: $F(1, 19) = 2.233$, $p = 0.1515$]. Post-hoc analysis revealed that BrdU⁺ and BrdU⁺/DCX⁺ cells in the chronic AICAR-treated OBX mice were significantly greater than in the vehicle-treated OBX mice ($p < 0.05$), whereas no change was observed in sham mice (Fig. 3C and D). These results indicate that AICAR promotes neurogenesis in the DGs of OBX mice.

3.4. AICAR-induced anti-depressant effect and neurogenesis are attenuated by ZIP

To investigate whether PKCζ is involved in the anti-depressant effect of AICAR, we co-administrated AICAR and ZIP, a PKCζ inhibitor, to OBX mice for 14 days. Post-hoc analysis revealed that the reduction observed in the immobility time of OBX mice treated with AICAR was significantly attenuated by co-administration of AICAR and ZIP [one-way ANOVA; $F(3, 38) = 4.306$, $p = 0.0104$; Fig. 4B]. Next, we investigated whether the PKCζ inhibitor altered neurogenesis in OBX mice. In this experiment, as a control, we used OBX mice implanted with a cannula, and treated with ringer's solution. Post-hoc analysis revealed that the increase in the number of BrdU⁺ and BrdU⁺/DCX⁺ cells in OBX mice treated with AICAR was significantly attenuated by co-administration of AICAR and ZIP [BrdU⁺ cells: one-way ANOVA, $F(2, 13) = 31.89$, $p < 0.0001$; BrdU⁺/DCX⁺ cells: one-way ANOVA, F

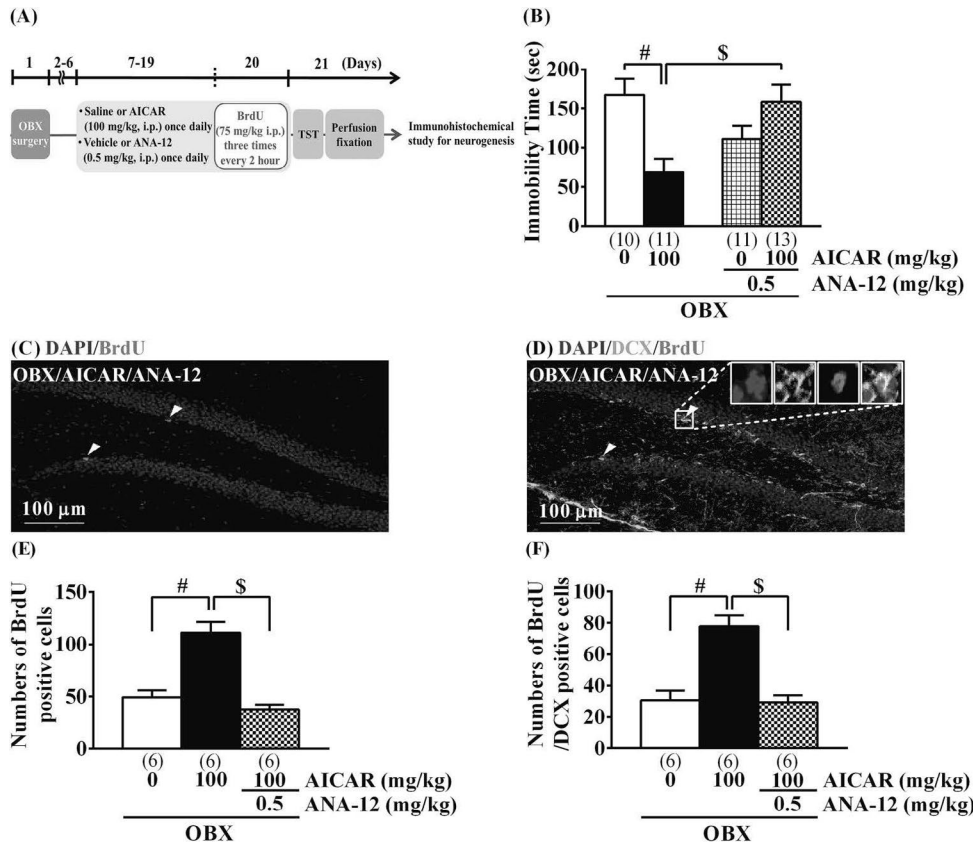


Fig. 5. Effect of ANA-12 on the anti-depressant effect of AICAR in olfactory bulbectomized (OBX) mice. (A) Timeline of the experimental protocol. (B) OBX mice immobility time was measured by the tail-suspension test on the 21st day after OBX surgery. (C, D) Confocal images of brain slices stained DAPI (blue), BrdU (red) and DCX (green). Arrowheads point to BrdU⁺ or BrdU⁺/DCX⁺ cells in the SGZ. (E, F) Quantitative analysis of the number of BrdU⁺ and BrdU⁺/DCX⁺ cells in SGZ of OBX mice treated with AICAR (administered intraperitoneally (i.p.)) and ANA-12 (i.p.). Vertical lines above bars represent mean \pm standard error of the mean. #, $p < 0.05$ compared to OBX + Vehicle group; \$, $p < 0.05$ compared to OBX + AICAR group. $n = 6-9$ animals in each group. i.p., intraperitoneally.

(2, 13) = 17.88, $p = 0.0002$; Fig. 4C–F]. These results indicate that PKC ζ is indeed involved in the anti-depressant effect and promotion of neurogenesis induced by AICAR.

3.5. ZIP attenuates the AICAR-induced increase in BDNF levels in the hippocampi of OBX mice

We next examined whether administration of ZIP changed the expression levels of BDNF in the hippocampi of OBX mice. Post-hoc analysis revealed that co-administration of AICAR and ZIP to OBX mice significantly attenuated the increase in BDNF levels in the hippocampi of OBX mice treated only with AICAR ($p < 0.05$) [one-way ANOVA; $F(2, 13) = 9.897$, $p = 0.0024$; Fig. 4G]. This data indicates that PKC ζ mediates the production of BDNF.

3.6. ANA-12 attenuates the anti-depressant effect of AICAR

To investigate whether the TrkB receptor is involved in the anti-depressant effect of AICAR, we co-administrated AICAR and the TrkB antagonist, ANA-12, to OBX mice for 14 days. Post-hoc analysis revealed that co-administration of the two drugs significantly attenuated the observed reduction in immobility time of OBX mice treated only with AICAR [one-way ANOVA; $F(3, 41) = 5.432$, $p = 0.0031$; Fig. 5B]. To investigate whether the TrkB receptor mediates neurogenesis, we examined neurogenesis in OBX mice treated with AICAR and ANA-12. Post-hoc analysis revealed that the increase in the number of BrdU⁺ and BrdU⁺/DCX⁺ cells in OBX mice treated with AICAR was blocked by co-administration of AICAR and ANA-12 [BrdU⁺ cells (Fig. 5E): one-way ANOVA, $F(2, 15) = 28.02$, $p < 0.0001$; BrdU⁺/DCX⁺ cells (Fig. 5F): one-way ANOVA, $F(2, 15) = 20.71$, $p < 0.0001$]. These data indicate the involvement of TrkB in the anti-depressant effect of AICAR.

3.7. AMPK is activated in mature hippocampal nerve cells and microglia

We performed dual immunofluorescence staining for *p*-AMPK and different markers, such as NeuN and DCX for neurons, GFAP for astrocytes, and Iba-1 for microglia, to determine which types of cells are activated by AICAR. We found that *p*-AMPK was localized in NeuN⁺, DCX⁺, and Iba-1⁺ cells, but was absent from GFAP⁺ cells (Fig. 6), indicating that AICAR activates mature neurons, immature neurons and microglia but not astrocytes in the hippocampi of OBX mice.

3.8. NF- κ B is activated in the mature nerve cells of the hippocampus

Next, we performed immunofluorescence staining to determine the cell type in which NF- κ B is activated. As illustrated in Fig. 7, *p*-NF- κ B was localized in NeuN⁺ and DCX⁺ cells but not Iba-1⁺ cells, indicating that AICAR activates AMPK/PKC ζ /NF- κ B signaling in mature and immature hippocampal neurons in OBX mice.

4. Discussion

In this study, we investigated the role of AMPK in depressive-like behavior in OBX mice. Chronic administration of AICAR caused a reduction in the immobility time in the TST and FST. In addition, *p*-AMPK induced PKC ζ /NF- κ B/BDNF/CREB signaling and increased neurogenesis in the hippocampi of OBX mice. Inhibition of PKC ζ or the TrkB receptor attenuated these effects of AICAR in OBX mice. Therefore, we report for the first time that activation of AMPK contributes to the improvement in depressive-like behavior via the PKC ζ /NF- κ B/BDNF/CREB signaling pathway and enhancement of neurogenesis in OBX mice.

In our study, OBX mice exhibited depressive-like behavior, as assessed by the TST and FST, 21 days after surgery. Chronic AICAR treatment for 14 days, but not acute or subchronic treatment for 7 days,

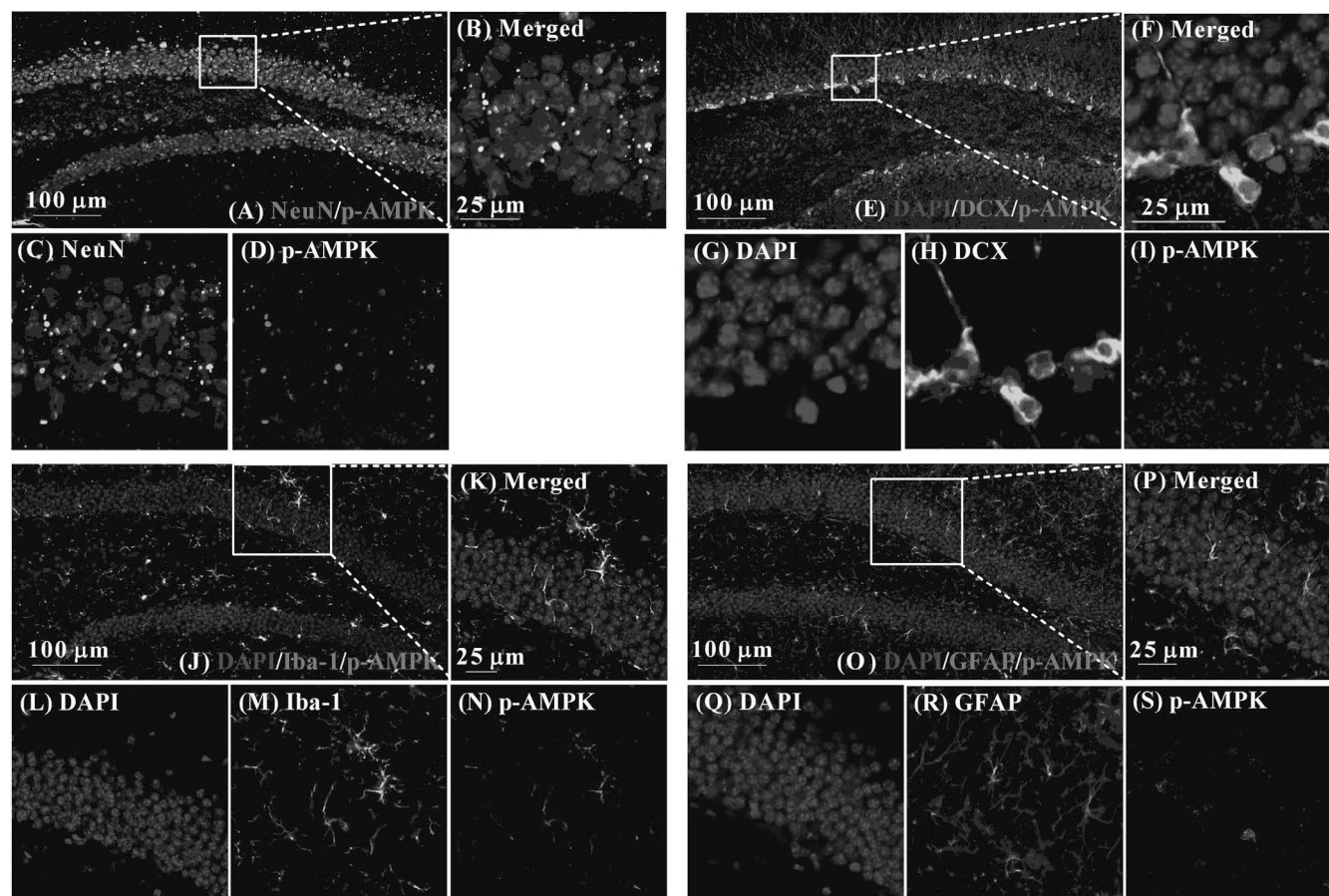


Fig. 6. Phosphorylated AMPK is expressed in mature and immature neurons and microglia in the hippocampus of olfactory bulbectomized (OBX) mice treated with AICAR. Double immunofluorescence staining for p-AMPK and either NeuN (A–D), DCX (E–I), Iba-1 (J–N), or GFAP (O–S). (A) Low magnification image of the hippocampus stained with p-AMPK and NeuN antibodies. The boxed area is shown in higher magnification in B. (C, D) Independent photomicrographs of NeuN (green; C) and p-AMPK positive cells (red; D). (E) Low magnification image of the hippocampus stained with p-AMPK and DCX antibodies. The boxed area is shown in higher magnification in F. (G–I) Independent photomicrographs of DAPI (blue; G), DCX (green; H) and p-AMPK positive cells (red; I). (J) Low magnification image of the hippocampus stained with p-AMPK and Iba-1 antibodies and counterstained with DAPI. The boxed area is shown in higher magnification in K. (L–N) Independent photomicrographs of fluorescent DAPI (blue; L), Iba-1 (green; M), and p-AMPK positive cells (red; N). (O) Low magnification image of the hippocampus stained with p-AMPK and GFAP antibodies and counterstained with DAPI. The boxed area is shown in higher magnification in P. (Q–S) Independent photomicrographs of fluorescent DAPI (blue; Q), GFAP (green; R) and p-AMPK positive cells (red; S).

resulted in an anti-depressant effect in OBX mice, which manifested as a reversal of the reduced immobility in the TST. A recent study reported that the depressive-like behaviors induced by a combination of high-fat diet and corticosterone treatment were reversed with AICAR 100 mg/kg administration for 4 weeks (Liu et al., 2014). These results indicate that AICAR requires several days to exert its anti-depressant effect. Chronic administration of conventional anti-depressants, such as SSRIs and noradrenergic and specific serotonergic antidepressants (NaSSA), takes several weeks to exhibit any clinical effect (Stahl et al., 2001). Moreover, chronic anti-depressant treatment promotes neurogenesis in the hippocampus (Zhao et al., 2008). Recently, we also reported that chronic treatment with memantine, an NMDA receptor antagonist, enhances neurogenesis in the hippocampus and ameliorates depressive-like behavior in OBX mice (Takahashi et al., 2018). It is believed that the effects of anti-depressants may be mediated by the enhancement of hippocampal neurogenesis (Santarelli et al., 2003; Kino, 2015). Moreover, AICAR at 100 mg/kg is more effective than 50 mg/kg in both TST and FST. Liu et al. also reported that the same dosage of AICAR induced anti-depressant effects (Liu et al., 2014). Therefore, we focused on the molecular mechanism that might lead to the increased neurogenesis that mediates the anti-depressant effects of AICAR (100 mg/kg).

It was previously demonstrated that the activation of AMPK by exercise or AICAR promotes glucose transport via PKC ζ activity (Chen

et al., 2002). Previous studies have reported a negative correlation between depressive-like behavior and AMPK activation (Liu et al., 2014; Yau et al., 2014). In addition, other groups have reported that the AMPK activator, metformin, promotes neurogenesis in the hippocampus via PKC ζ signaling (Wang et al., 2012), while Obara et al. found that PKC ζ activation enhances the secretion of neurotrophic factors, such as NGF and BDNF, via NF- κ B (Obara et al., 2001). The transcription factor, NF- κ B, is a heterodimer composed of p50 and p65 and plays important roles in neuronal growth and survival. Indeed, it was reported that the activated PKC ζ /NF- κ B pathway contributes to neuronal survival in PC12 cells (Macdonald et al., 1999). BDNF is known to play a critical role in neuronal survival and is believed to modulate neuroplasticity, including neurogenesis (Noble et al., 2011). Previous studies have led to the formulation of the neurotrophic hypothesis of depression (Duman and Monteggia, 2006; Groves, 2007), based on evidence that low levels of BDNF lead to a depressive condition (Chen et al., 2001b; Karege et al., 2002). Medical treatments, such as SSRIs and SNRIs, increase BDNF levels in the brains of depressive patients (Lee and Kim, 2008; Larsen et al., 2010). In the present study, BDNF levels of OBX mice increased after chronic treatment with AICAR. The activation of BDNF/TrkB signaling leads to the phosphorylation of CREB (Yan et al., 2016; Ye et al., 2017). In addition, overexpression of CREB in the hippocampus results in anti-depressant effects (Chen et al., 2001a). The

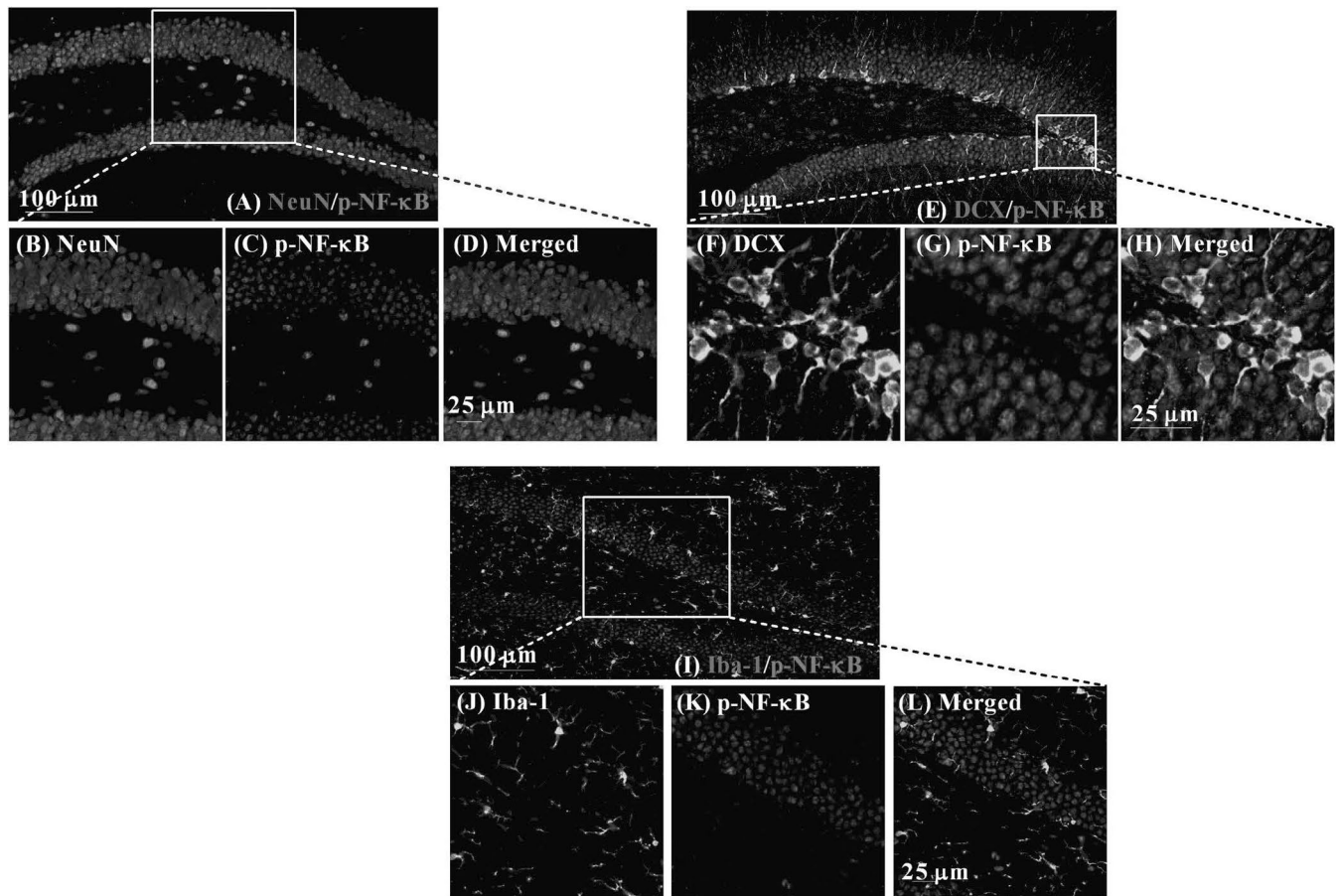


Fig. 7. Phosphorylated NF- κ B is expressed in mature and immature neurons in the hippocampus of olfactory bulbectomized (OBX) mice treated with AICAR. Double immunofluorescence staining for p-NF- κ B and either NeuN (A–D) DCX (E–H) or Iba-1 (I–L). (A) Low magnification image of the hippocampus stained with NeuN and p-NF- κ B antibodies. The boxed area is shown in higher magnification in D. (B, C) Independent photomicrographs of fluorescent NeuN (green; B) and p-NF- κ B positive cells (red; C). (E) Low magnification image of the hippocampus stained with DCX and p-NF- κ B antibodies. The boxed area is shown in higher magnification in H. (F, G) Independent photomicrographs of fluorescent DCX (green; F) and p-NF- κ B positive cells (red; G). (I) Low magnification image of the hippocampus stained with p-NF- κ B and Iba-1 antibodies. The boxed area is shown in higher magnification in L. (J, K) Independent photomicrographs of Iba-1 (green; J) and p-NF- κ B positive cells (red; K).

present study revealed that AICAR significantly increased p-CREB levels in the hippocampi of OBX mice. Thus, we consider that activation of the AMPK/PKC ζ /NF- κ B pathway by AICAR may promote the secretion of BDNF, which in turn activates the TrkB/CREB signaling pathway.

The stimulation of BDNF/TrkB/CREB signaling is critical for the regulation of hippocampal neurogenesis (Ji et al., 2010), which improves depressive-like behavior. Indeed, the volume of the hippocampus is decreased in patients with depression (MacQueen et al., 2003) and rodent models of depression (Luo et al., 2014). Chronic SSRI and SNRI treatment induces neurogenesis and subsequently ameliorates depressive-like behavior in rodents (Luo et al., 2014). In addition, neurogenesis ablation by x-ray irradiation attenuates the effect of anti-depressants in animal models of depression (Santarelli et al., 2003). Recent studies have demonstrated that activation of AMPK enhances neurogenesis (Wang et al., 2012; Arya et al., 2016) and ameliorates depressive-like behavior (Liu et al., 2014; Yau et al., 2014). We also observed enhancement of neurogenesis and improvements in depressive-like behavior in AICAR-treated OBX mice. Considering the previous findings and our current results, we suggest that AMPK activation promotes neurogenesis in a similar manner to anti-depressants, such as SSRIs and SNRIs.

Our hypothesis that activated AMPK promotes neurogenesis via PKC ζ /NF- κ B/BDNF/TrkB/CREB signaling was further confirmed using ZIP and ANA-12. In our study, inhibition of PKC ζ blocked the AICAR-

induced anti-depressant effect and promotion of neurogenesis in OBX mice, suggesting that PKC ζ activation mediates such effects of AICAR. In agreement with this notion, Wang et al. reported that fluoxetine-induced activation of atypical PKC and promotion of neurogenesis are blocked by ZIP (Wang et al., 2014). Furthermore, we found that co-treatment with AICAR and ANA-12 blocks the AICAR-induced anti-depressant effect and neurogenesis in OBX mice. Consistently, ANA-12 also blocks the anti-depressant effect of fluoxetine (Ma et al., 2016). Jiang et al. reported that the anti-depressant effect and enhancement of cell proliferation induced by ginsenoside Rg1 in the hippocampus are blocked by co-treatment with the TrkB antagonist, K252a (Jiang et al., 2012). Altogether, these results indicate that TrkB may be involved in the improvement in depressive-like behavior and enhancement of neurogenesis by inducing PKC ζ phosphorylation via the activation of AMPK.

We previously reported that OBX resulted in memory dysfunction induced by alternation of the dopaminergic system. This dysfunction was ameliorated by aripiprazole via stimulation of D₁ receptors in the prefrontal cortex and increases in NGF and neurogenesis in the hippocampus (Takahashi et al., 2017). It has been suggested that the prefrontal cortex and hippocampus are associated with not only memory, but also depression (Pan et al., 2014; Petrik et al., 2012); however, we focused on only the hippocampus due to the observed neurogenesis dysfunction in the DGs of OBX mice in this study. Therefore, further

study will be required to examine the influence of AMPK activation in other brain regions involved in the pathogenesis of depression.

In the present study, we found that *p*-AMPK exhibits a nuclear punctate distribution in NeuN⁺ and DCX⁺ cells, thus reflecting the translocation of AMPK to the nucleus (McGee et al., 2003) or the localization of the α -subunit of AMPK in the nucleus (Salt et al., 1998). A previous study demonstrated that the nuclear localization of the AMPK α 2 subunit regulates gene expression (Salt et al., 1998). Therefore, it is possible that AMPK, like NF- κ B, regulates gene expression in the hippocampi of OBX mice. Moreover, we found that *p*-AMPK was expressed in microglia but not in astrocytes. Previously, Xu et al. reported that AMPK reduces cytokines and neuroinflammation, thus promoting microglia conversion towards the M2 phenotype (Xu et al., 2015). Therefore, *p*-AMPK expressed in microglia may contribute to anti-neuroinflammation. Further work is required to examine the anti-neuroinflammation effects of AMPK in OBX mice and the detailed underlying mechanisms. Moreover, we found that AICAR-induced *p*-NF- κ B was localized in NeuN⁺ cells. Consistently, another group also reported phosphorylation of NF- κ B at Ser311 in the DG of the hippocampus (Kim et al., 2013). PKC ζ directly phosphorylates NF- κ B, and this phosphorylation contributes to neuronal survival and promotes transcription (Obara et al., 2001; Duran et al., 2003). PKC ζ , which is upstream of NF- κ B, is widely distributed in the brain and can be detected in nerve cells, microglia, and astrocytes (Slepko et al., 1999; Wang et al., 2012). However, PKC ζ expression levels and basal activity of NF- κ B in microglia are very low (Slepko et al., 1999; Kaltschmidt and Kaltschmidt, 2009). These results suggest that activation of AMPK/PKC ζ /NF- κ B occurs in nerve cells and then secretes BDNF. Samuels et al. found that the effects of the anti-depressant fluoxetine are, at least in part, mediated by 5-HT_{1A} receptor activation in mature granule cells of the ventral hippocampus but not in adult-born neurons (Samuels et al., 2015). In contrast, we observed *p*-NF- κ B expression, not only in mature neurons, but also in immature neurons. Consistently, other groups reported that inhibition of NF- κ B in neonatal nodose neurons and cortical neurons caused an impairment in the growth of these cells (Gutierrez et al., 2005). The PKC/CREB binding protein (CBP; co-activator of NF- κ B) pathway was also detected in hippocampal precursor cells, and this pathway also regulates the maturation of neurons (Gouveia et al., 2016). Moreover, autocrine function of BDNF was required for the regulation of synaptogenesis, survival, and maturation in dorsal root ganglion neurons and adult-born neurons (Acheson et al., 1995; Davies and Wright, 1995; Wang et al., 2015). From these reports, the AMPK/PKC ζ /NF- κ B/BDNF/TrkB pathway in hippocampal immature neurons of OBX mice may play an important role in neurogenesis. Therefore, it is possible that the effects of AMPK on neurogenesis are direct effects that act on adult-born neurons, or indirect effects that possibly act on mature neurons and microglia, which may lead to BDNF release from cells that could stimulate neurogenesis. Future investigation is necessary to further delineate these possibilities.

In conclusion, our data indicate that persistent AMPK activation may induce anti-depressant effects and enhancement of neurogenesis via the PKC ζ /NF- κ B/BDNF/TrkB/CREB signaling pathway. We thus provide evidence on the molecular mechanism of AMPK activation in an animal model of depression. Our findings suggest that AMPK activators may be used as novel therapeutic agents in the treatment of neuropsychiatric disorders, such as depression.

Acknowledgements and conflict of interest disclosure

This study was supported in part by the Nagai Memorial Research Scholarship from the Pharmaceutical Society of Japan, Grants-in-Aid for Scientific Research (Grant number 18K06687), and a Matching Fund Subsidy for Private University from the Ministry of Education, Culture, Sports, Science, and Technology of Japan (Grant number S1511001L). The authors have no conflicts of interest to declare.

Appendix A. Supplementary data

Supplementary data to this article can be found online at <https://doi.org/10.1016/j.neuropharm.2019.03.026>.

References

- Acheson, A., Conover, J.C., Fandl, J.P., DeChiara, T.M., Russell, M., Thadani, A., Squinto, S.P., Yancopoulos, G.D., Lindsay, R.M., 1995. A BDNF autocrine loop in adult sensory neurons prevents cell death. *Nature* 374, 450–453.
- Ali, S.H., Madhana, R.M., K. V. A., Kasala, E.R., Bodduluru, L.N., Pitta, S., Mahareddy, J.R., Lahkar, M., 2015. Resveratrol ameliorates depressive-like behavior in repeated corticosterone-induced depression in mice. *Steroids* 101, 37–42.
- Arya, A., Gangwar, A., Singh, S.K., Roy, M., Das, M., Sethy, N.K., Bhargava, K., 2016. Cerium oxide nanoparticles promote neurogenesis and abrogate hypoxia-induced memory impairment through AMPK-PKC-CBP signaling cascade. *Int. J. Nanomed.* 11, 1159–1173.
- Berry, A., Bellisario, V., Capoccia, S., Tirassa, P., Calza, A., Alleve, E., Cirulli, F., 2012. Social deprivation stress is a triggering factor for the emergence of anxiety-and depression-like behaviours and leads to reduced brain BDNF levels in C57BL/6J mice. *Psychoneuroendocrinology* 37, 762–772.
- Bjørnebekk, A., Mathé, A.A., Brené, S., 2005. The antidepressant effect of running is associated with increased hippocampal cell proliferation. *Int. J. Neuropsychopharmacol.* 8, 357–368.
- Bogard, A.S., Tavalin, S.J., 2015. Protein kinase C (PKC) ζ pseudosubstrate inhibitor peptide Promiscuously binds PKC family isoforms and Disrupts conventional PKC targeting and translocation. *Mol. Pharmacol.* 88, 728–735.
- Cairncross, K.D., Schofield, P.M., Bassett, J.R., 1975. Endogenous brain norepinephrine levels following bilateral olfactory bulb ablation. *Pharmacol. Biochem. Behav.* 3, 425–427.
- Chen, A.C., Shirayama, Y., Shin, K.H., Neve, R.L., Duman, R.S., 2001a. Expression of the cAMP response element binding protein (CREB) in hippocampus produces an antidepressant effect. *Biol. Psychiatr.* 49, 753–762.
- Chen, B., Dowlatshahi, D., MacQueen, G.M., Wang, J.F., Young, L.T., 2001b. Increased hippocampal BDNF immunoreactivity in subjects treated with antidepressant medication. *Biol. Psychiatr.* 50, 260–265.
- Chen, H.C., Bandyopadhyay, G., Sajan, M.P., Kanoh, Y., Standaert, M., Farese Jr., R.V., Farese, R.V., 2002. Activation of the ERK pathway and atypical protein kinase C isoforms in exercise- and aminoimidazole-4-carboxamide-1-beta-D-ribose (AICAR)-stimulated glucose transport. *J. Biol. Chem.* 277, 23554–23562.
- Cryan, J.F., Mombereau, C., 2004. In search of a depressed mouse: utility of models for studying depression-related behavior in genetically modified mice. *Mol. Psychiatr.* 9, 326–357.
- Davies, A.M., Wright, E.M., 1995. Neurotrophic factors. Neurotrophin autocrine loops. *Curr. Biol.* 5, 723–726.
- DeVos, S.L., Miller, T.M., 2013. Direct intraventricular delivery of drugs to the rodent central nervous system. *J. Vis. Exp.* 12, e50326.
- Dominguez, I., Sanz, L., Arenzana-Seisdedos, F., Diaz-Meco, M.T., Virelizier, J.L., Moscat, J., 1993. Inhibition of protein kinase C zeta subspecies blocks the activation of an NF-kappa B-like activity in *Xenopus laevis* oocytes. *Mol. Cell Biol.* 13, 1290–1295.
- Duman, R.S., Monteggia, L.M., 2006. A neurotrophic model for stress-related mood disorders. *Biol. Psychiatr.* 59, 1116–1127.
- Duran, A., Diaz-Meco, M.T., Moscat, J., 2003. Essential role of RelA Ser311 phosphorylation by zetaPKC in NF-kappaB transcriptional activation. *EMBO J.* 22, 3910–3918.
- Gouveia, A., Hsu, K., Niibori, Y., Seegobin, M., Cancino, G.I., He, L., Wondisford, F.E., Bennett, S., Lagace, D., Frankland, P.W., Wang, J., 2016. The aPKC-CBP pathway regulates AdultHippocampal neurogenesis in an age-dependent manner. *Stem Cell Reports* 7, 719–734.
- Groves, J.O., 2007. Is it time to reassess the BDNF hypothesis of depression? *Mol. Psychiatr.* 12, 1079–1088.
- Guo, M., Mi, J., Jiang, Q.M., Xu, J.M., Tang, Y.Y., Tian, G., Wang, B., 2014. Metformin may produce antidepressant effects through improvement of cognitive function among depressed patients with diabetes mellitus. *Clin. Exp. Pharmacol. Physiol.* 41, 650–656.
- Gusarova, G.A., Dada, L.A., Kelly, A.M., Brodie, C., Witters, L.A., Chandel, N.S., Sznajder, J.I., 2009. Alpha1-AMP-activated protein kinase regulates hypoxia-induced Na,K-ATPase endocytosis via direct phosphorylation of protein kinase C zeta. *Mol. Cell Biol.* 29, 3455–3464.
- Gutierrez, H., Hale, V.A., Dolcet, X., Davies, A., 2005. NF-kappaB signalling regulates the growth of neural processes in the developing PNS and CNS. *Development* 132, 1713–1726.
- Han, F., Nakano, T., Yamamoto, Y., Shioda, N., Lu, Y.M., Fukunaga, K., 2009. Improvement of depressive behaviors by nefiracetam is associated with activation of CaM kinases in olfactory bulbectomized mice. *Brain Res.* 1265, 205–214.
- Hardie, D.G., Ashford, M.L., 2014. AMPK: regulating energy balance at the cellular and whole body levels. *Physiology* 29, 99–107.
- Hozumi, S., Nakagawasai, O., Tan-No, K., Nijima, F., Yamadera, F., Murata, A., Arai, Y., Yasuhara, H., Tadano, T., 2003. Characteristics of changes in cholinergic function and impairment of learning and memory-related behavior induced by olfactory bulbectomy. *Behav. Brain Res.* 138, 9–15.
- Ji, Y., Lu, Y., Yang, F., Shen, W., Tang, T.T., Feng, L., Duan, S., Lu, B., 2010. Acute and gradual increases in BDNF concentration elicit distinct signaling and functions in neurons. *Nat. Neurosci.* 13, 302–309.
- Jiang, B., Xiong, Z., Yang, J., Wang, W., Wang, Y., Hu, Z.L., Wang, F., Chen, J.G., 2012.

- Antidepressant-like effects of ginsenoside Rg1 are due to activation of the BDNF signalling pathway and neurogenesis in the hippocampus. *Br. J. Pharmacol.* 166, 1872–1887.
- Kaltschmidt, B., Kaltschmidt, C., 2009. NF-kappaB in the nervous system. *Cold Spring Harb Perspect Biol* 1, a001271.
- Karege, F., Perret, G., Bondolfi, G., Schwald, M., Bertschy, G., Aubry, J.M., 2002. Decreased serum brain-derived neurotrophic factor levels in major depressed patients. *Psychiatr. Res.* 109, 143–148.
- Kim, J.E., Kim, D.S., Jin, Ryu H., Il Kim, W., Kim, M.J., Won Kim, D., Young Choi, S., Kang, T.C., 2013. The effect of P2X7 receptor activation on nuclear factor- κ B phosphorylation induced by status epilepticus in the rat hippocampus. *Hippocampus* 23, 500–514.
- Kino, T., 2015. Stress, glucocorticoid hormones, and hippocampal neural progenitor cells: implications to mood disorders. *Front. Physiol.* 6, 230.
- Kong, D., Song, G., Wang, C., Ma, H., Ren, L., Nie, Q., Zhang, X., Gan, K., 2013. Overexpression of mitofusin 2 improves translocation of glucose transporter 4 in skeletal muscle of high fat diet fed rats through AMP activated protein kinase signaling. *Mol. Med. Rep.* 8, 205–210.
- Larsen, M.H., Mikkelsen, J.D., Hay-Schmidt, A., Sandi, C., 2010. Regulation of brain-derived neurotrophic factor (BDNF) in the chronic unpredictable stress rat model and the effects of chronic antidepressant treatment. *J. Psychiatr. Res.* 44, 808–816.
- Lee, H.Y., Kim, Y.K., 2008. Plasma brain-derived neurotrophic factor as a peripheral marker for the action mechanism of antidepressants. *Neuropsychobiology* 57, 194–199.
- Liu, D., Smith, D.J., 2003. Voxellation and gene expression tomography for the acquisition of 3-D gene expression maps in the brain. *Methods* 31, 317–325.
- Liu, T.T., Peng, L., Liu, H.F., Shu, Y., Xiao, B., 2017. Altered axon initial segment in hippocampal newborn neurons, associated with recurrence of temporal lobe epilepsy in rats. *Mol. Med. Rep.* 16, 3169–3178.
- Liu, W., Zhai, X., Li, H., Ji, L., 2014. Depression-like behaviors in mice subjected to co-treatment of high-fat diet and corticosterone are ameliorated by AICAR and exercise. *J. Affect. Disord.* 156, 171–177.
- Luo, Y., Cao, Z., Wang, D., Wu, L., Li, Y., Sun, W., Zhu, Y., 2014. Dynamic study of the hippocampal volume by structural MRI in a rat model of depression. *Neurol. Sci.* 35, 1777–17783.
- Ma, M., Ren, Q., Yang, C., Zhang, J.C., Yao, W., Dong, C., Ohgi, Y., Futamura, T., Hashimoto, K., 2016. Adjunctive treatment of brexpiprazole with fluoxetine shows a rapid antidepressant effect in social defeat stress model: role of BDNF-TrkB signaling. *Sci. Rep.* 6, 39209.
- Macdonald, N.J., Perez-Polo, J.R., Bennett, A.D., Tagliatela, G., 1999. NGF-resistant PC12 cell death induced by arachidonic acid is accompanied by a decrease of active PKC zeta and nuclear factor kappa B. *J. Neurosci. Res.* 57, 219–226.
- MacQueen, G.M., Campbell, S., McEwen, B.S., Macdonald, K., Amano, S., Joffe, R.T., Nahmias, C., Young, L.T., 2003. Course of illness, hippocampal function, and hippocampal volume in major depression. *Proc. Natl. Acad. Sci. U. S. A.* 100, 1387–1392.
- McGee, S.L., Howlett, K.F., Starkie, R.L., Cameron-Smith, D., Kemp, B.E., Hargreaves, M., 2003. Exercise increases nuclear AMPK alpha2 in human skeletal muscle. *Diabetes* 52, 926–928.
- Migues, P.V., Hardt, O., Wu, D.C., Gamache, K., Sacktor, T.C., Wang, Y.T., Nader, K., 2010. PKMzeta maintains memories by regulating GluR2-dependent AMPA receptor trafficking. *Nat. Neurosci.* 13, 630–634.
- Mostany, R., Valdzán, E.M., Pazos, A., 2008. A role for nuclear beta-catenin in SNRI antidepressant-induced hippocampal cell proliferation. *Neuropharmacology* 55, 18–26.
- Mouri, A., Koseki, T., Narusawa, S., Niwa, M., Mamiya, T., Kano, S., Sawa, A., Nabeshima, T., 2012. Mouse strain differences in phenylcyclidine-induced behavioural changes. *Int. J. Neuropsychopharmacol.* 15, 767–779.
- Nakagawasai, O., Tadano, T., Arai, Y., Hozumi, S., Oba, A., Tan-No, K., Yasuhara, H., Kisara, K., Orelund, L., 2003. Enhancement of 5-hydroxytryptamine-induced head-twitch response after olfactory bulbectomy. *Neuroscience* 117, 1017–1023.
- Nakagawasai, O., Yamada, K., Nemoto, W., Sato, S., Ogata, Y., Miya, K., Sakurai, H., Tan-No, K., 2015. Liver hydrolysate attenuates the sickness behavior induced by concanavalin A in mice. *J. Pharmacol. Sci.* 127, 489–492.
- Nakagawasai, O., Nemoto, W., Onogi, H., Moriya, T., Lin, J.R., Odaira, T., Yaoita, F., Ogawa, T., Ohta, K., Endo, Y., Tan-No, K., 2016. BE360, a new selective estrogen receptor modulator, produces antidepressant and antidepressant effects through the enhancement of hippocampal cell proliferation in olfactory bulbectomized mice. *Behav. Brain Res.* 297, 315–322.
- Negoias, S., Croy, I., Gerber, J., Puschmann, S., Petrowski, K., Joraschky, P., Hummel, T., 2010. Reduced olfactory bulb volume and olfactory sensitivity in patients with acute major depression. *Neurosci.* 169, 415–421.
- Nibuya, M., Nestler, E.J., Duman, R.S., 1996. Chronic antidepressant administration increases the expression of cAMP response element binding protein (CREB) in rat hippocampus. *J. Neurosci.* 16, 2365–2372.
- Noble, E.E., Billington, C.J., Kotz, C.M., Wang, C., 2011. The lighter side of BDNF. *Am. J. Physiol. Regul. Integr. Comp. Physiol.* 300, R1053–R1069.
- Obara, Y., Kobayashi, H., Ohta, T., Ohizumi, Y., Nakahata, N., 2001. Scabronine G-methyl ester enhances secretion of neurotrophic factors mediated by an activation of protein kinase C-zeta. *Mol. Pharmacol.* 59, 1287–1297.
- Ouchi, Y., Banno, Y., Shimizu, Y., Ando, S., Hasegawa, H., Adachi, K., Iwamoto, T., 2013. Reduced adult hippocampal neurogenesis and working memory deficits in the Dgcr8-deficient mouse model of 22q11.2 deletion-associated schizophrenia can be rescued by IGF2. *J. Neurosci.* 33, 9408–9419.
- Pan, Y., Chen, X.Y., Zhang, Q.Y., Kong, L.D., 2014. Microglial NLRP3 inflammasome activation mediates IL-1 β -related inflammation in prefrontal cortex of depressive rats. *Brain Behav. Immun.* 41, 90–100.
- Patel, V., Flisher, A.J., Hetrick, S., McGorry, P., 2007. Mental health of young people: a global public-health challenge. *Lancet* 369, 1302–1313.
- Patki, G., Solanki, N., Atrooz, F., Allam, F., Salim, S., 2013. Depression, anxiety-like behavior and memory impairment are associated with increased oxidative stress and inflammation in a rat model of social stress. *Brain Res.* 1539, 73–86.
- Pause, B.M., Miranda, A., Göder, R., Aldenhoff, J.B., Ferstl, R., 2001. Reduced olfactory performance in patients with major depression. *J. Psychiatr. Res.* 35, 271–277.
- Paxinos, G., Franklin, K.B.J., 2001. *The Mouse Brain in Stereotaxic Coordinates*, second ed. Academic Press, San Diego.
- Petrik, D., Lagace, D.C., Eisch, A.J., 2012. The neurogenesis hypothesis of affective and anxiety disorders: are we mistaking the scaffolding for the building? *Neuropharmacology* 62, 21–34.
- Sacktor, T.C., Osten, P., Valsamis, H., Jiang, X., Naik, M.U., Sublette, E., 1993. Persistent activation of the zeta isoform of protein kinase C in the maintenance of long-term potentiation. *Proc. Natl. Acad. Sci. U. S. A.* 90, 8342–8346.
- Sajan, M.P., Bandyopadhyay, G., Miura, A., Standaert, M.L., Nimal, S., Longnus, S.L., Van Obberghen, E., Hainault, I., Foulfelle, F., Kahn, R., Braun, U., Leitges, M., Farese, R.V., 2010. AICAR and metformin, but not exercise, increase muscle glucose transport through AMPK-, ERK-, and PDK1-dependent activation of atypical PKC. *Am. J. Physiol. Endocrinol. Metab.* 298, E179–E192.
- Salt, I., Celler, J.W., Hawley, S.A., Prescott, A., Woods, A., Carling, D., Hardie, D.G., 1998. AMP-activated protein kinase: greater AMP dependence, and preferential nuclear localization, of complexes containing the alpha2 isoform. *Biochem. J.* 334, 177–187.
- Samuels, B.A., Anacker, C., Hu, A., Levinstein, M.R., Pickenhagen, A., Tssetsenis, T., Madroñal, N., Donaldson, Z.R., Drew, L.J., Dranovsky, A., Gross, C.T., Tanaka, K.F., Hen, R., 2015. 5-HT1A receptors on mature dentate gyrus granule cells are critical for the antidepressant response. *Nat. Neurosci.* 18, 1606–1616.
- Santarelli, L., Saxe, M., Gross, C., Surget, A., Battaglia, F., Dulawa, S., Weisstaub, N., Lee, J., Duman, R., Arancio, O., Belzung, C., Hen, R., 2003. Requirement of hippocampal neurogenesis for the behavioral effects of antidepressants. *Science* 301, 805–809.
- Sato, A., Nakagawasai, O., Tan-No, K., Onogi, H., Nijima, F., Tadano, T., 2010. Effect of non-selective dopaminergic receptor agonist on disrupted maternal behavior in olfactory bulbectomized mice. *Behav. Brain Res.* 210, 251–256.
- Scharfman, H., Goodman, J., Macleod, A., Phani, S., Antonelli, C., Croll, S., 2005. Increased neurogenesis and the ectopic granule cells after intrahippocampal BDNF infusion in adult rats. *Exp. Neurol.* 192, 348–356.
- Shaw, R.J., Kosmatka, M., Bardeesy, N., Hurley, R.L., Witters, L.A., DePino, R.A., Cantley, L.C., 2004. The tumor suppressor LKB1 kinase directly activates AMP-activated kinase and regulates apoptosis in response to energy stress. *Proc. Natl. Acad. Sci. U. S. A.* 101, 3329–3335.
- Shirayama, Y., Chen, A.C., Nakagawa, S., Russell, D.S., Duman, R.S., 2002. Brain-derived neurotrophic factor produces antidepressant effects in behavioral models of depression. *J. Neurosci.* 22, 3251–3261.
- Slepko, N., Patrizio, M., Levi, G., 1999. Expression and translocation of protein kinase C isoforms in rat microglial and astroglial cultures. *J. Neurosci. Res.* 57, 33–38.
- Stahl, S.M., Nierenberg, A.A., Gorman, J.M., 2001. Evidence of early onset of antidepressant effect in randomized controlled trials. *J. Clin. Psychiatry* 62 (Suppl. 4), 17–23 discussion 37–40.
- Ströhle, A., Höfler, M., Pfister, H., Müller, A.G., Hoyer, J., Wittchen, H.U., Lieb, R., 2007. Physical activity and prevalence and incidence of mental disorders in adolescents and young adults. *Psychol. Med.* 37, 1657–1666.
- Sugimoto, Y., Yamamoto, M., Tagawa, N., Kobayashi, Y., Mitsui-Saitoh, K., Hotta, Y., Yamada, J., 2011. Differences between mice strains in response to paroxetine in the forced swimming test: involvement of serotonergic or noradrenergic systems. *Eur. J. Pharmacol.* 672, 121–125.
- Takahashi, K., Nakagawasai, O., Nemoto, W., Nakajima, T., Arai, Y., Hisamitsu, T., Tan-No, K., 2016. Alterations in behavioral responses to dopamine agonists in olfactory bulbectomized mice: relationship to changes in the striatal dopaminergic system. *Psychopharmacology (Berl)* 233, 1311–1322.
- Takahashi, K., Nakagawasai, O., Nemoto, W., Odaira, T., Arai, Y., Hisamitsu, T., Tan-No, K., 2017. Time-dependent role of prefrontal cortex and hippocampus on cognitive improvement by aripiprazole in olfactory bulbectomized mice. *Eur. Neuropsychopharmacol.* 27, 1000–1010.
- Takahashi, K., Nakagawasai, O., Nemoto, W., Kadota, S., Isono, J., Odaira, T., Sakuma, W., Arai, Y., Tadano, T., Tan-No, K., 2018. Memantine ameliorates depressive-like behaviors by regulating hippocampal cell proliferation and neuroprotection in olfactory bulbectomized mice. *Neuropharmacology* 137, 141–155.
- Thome, J., Sakai, N., Shin, K., Steffen, C., Zhang, Y.J., Impey, S., Storm, D., Duman, R.S., 2000. cAMP response element-mediated gene transcription is upregulated by chronic antidepressant treatment. *J. Neurosci.* 20, 4030–4036.
- Wang, J., Gallagher, D., DeVito, L.M., Cancino, G.I., Tsui, D., He, L., Keller, G.M., Frankland, P.W., Kaplan, D.R., Miller, F.D., 2012. Metformin activates an atypical PKC-CBP pathway to promote neurogenesis and enhance spatial memory formation. *Cell Stem Cell* 11, 23–35.
- Wang, L., Chang, X., She, L., Xu, D., Huang, W., Poo, M.M., 2015. Autocrine action of BDNF on dendrite development of adult-born hippocampal neurons. *J. Neurosci.* 35, 8384–8393.
- Wang, Y.X., Zhang, X.R., Zhang, Z.J., Li, L., Xi, G.J., Wu, D., Wang, Y.J., 2014. Protein kinase M ζ is involved in the modulatory effect of fluoxetine on hippocampal neurogenesis in vitro. *Int. J. Neuropsychopharmacol.* 17, 1429–1441.
- Widenfalk, J., Olson, L., Thorén, P., 1999. Deprived of habitual running, rats down-regulate BDNF and TrkB messages in the brain. *Neurosci. Res.* 34, 125–132.
- Winder, W.W., Hardie, D.G., 1996. Inactivation of acetyl-CoA carboxylase and activation of AMP-activated protein kinase in muscle during exercise. *Am. J. Physiol.* 270, E299–E304.

- Xu, Y., Xu, Y., Wang, Y., Wang, Y., He, L., Jiang, Z., Huang, Z., Liao, H., Li, J., Saavedra, J.M., Zhang, L., Pang, T., 2015. Telmisartan prevention of LPS-induced microglia activation involves M2 microglia polarization via CaMKK β -dependent AMPK activation. *Brain Behav. Immun.* 50, 298–313.
- Yan, T., Xu, M., Wan, S., Wang, M., Wu, B., Xiao, F., Bi, K., Jia, Y., 2016. Schisandra chinensis produces the antidepressant-like effects in repeated corticosterone-induced mice via the BDNF/TrkB/CREB signaling pathway. *Psychiatr. Res.* 243, 135–142.
- Yau, S.Y., Lau, B.W., Tong, J.B., Wong, R., Ching, Y.P., Qiu, G., Tang, S.W., Lee, T.M., So, K.F., 2011. Hippocampal neurogenesis and dendritic plasticity support running-improved spatial learning and depression-like behaviour in stressed rats. *PLoS One* 6, e24263.
- Yau, S.Y., Li, A., Hoo, R.L., Ching, Y.P., Christie, B.R., Lee, T.M., Xu, A., So, K.F., 2014. Physical exercise-induced hippocampal neurogenesis and antidepressant effects are mediated by the adipocyte hormone adiponectin. *Proc. Natl. Acad. Sci. U. S. A.* 111, 15810–15815.
- Ye, Y.L., Zhong, K., Liu, D.D., Xu, J., Pan, B.B., Li, X., Yu, Y.P., Zhang, Q., 2017. Huanglian-jie-du-tang Extract ameliorates depression-like behaviors through BDNF-TrkB-CREB pathway in rats with chronic unpredictable stress. *Evid. Based Complement Alternat. Med.* 2017, 7903918.
- Zhang, Q., Wang, X., Bai, X., Xie, Y., Zhang, T., Bo, S., Chen, X., 2017. Resveratrol reversed chronic restraint stress-induced impaired cognitive function in rats. *Mol. Med. Rep.* 16, 2095–2100.
- Zhao, C., Deng, W., Gage, F.H., 2008. Mechanisms and functional implications of adult neurogenesis. *Cell* 132, 645–660.



Contents lists available at ScienceDirect

Neuropharmacology

journal homepage: www.elsevier.com/locate/neuropharm

Prenatal treatment with methylazoxymethanol acetate as a neurodevelopmental disruption model of schizophrenia in mice

Kohei Takahashi^{a,1}, Osamu Nakagawasai^{a,*}, Wakana Sakuma^{a,1}, Wataru Nemoto^a, Takayo Odaira^a, Jia-Rong Lin^a, Hiroshi Onogi^b, Lalit K. Srivastava^c, Koichi Tan-No^a

^a Department of Pharmacology, Faculty of Pharmaceutical Sciences, Tohoku Medical and Pharmaceutical University, 4-4-1 Komatsushima, Aoba-ku, Sendai, Miyagi 981-8558, Japan

^b Faculty of Health Science, Tohoku Fukushi University, 1-8-1 Kunimi, Aoba-ku, Sendai, Miyagi 981-8522, Japan

^c Department of Psychiatry, Douglas Mental Health University Institute, McGill University, Montreal, QC, Canada

HIGHLIGHTS

- MAM mice showed schizophrenia-like behaviors.
- MAM mice exhibited neuroanatomical changes in the hippocampus.
- DA concentrations and DOPAC/DA increased in the mPFC of MAM treated mice.
- MAM-induced PPI deficits and social withdrawal improved with atypical antipsychotics.
- Atypical and typical antipsychotics improved hyperactivity by MK-801 in MAM mice.

ARTICLE INFO

Keywords:

Antipsychotic drugs
Methylazoxymethanol acetate
Monoamine transmission
Neurogenesis
Prepulse inhibition
Schizophrenia

ABSTRACT

Methylazoxymethanol (MAM)-treated pregnant rat at gestation day (GD) 17 has been shown to be a valuable developmental animal model for schizophrenia. Yet, this model remains to be established in mice. In the present study, we examined behavioral, cytoarchitectural, and neurochemical changes in the offspring of MAM-treated mice and validated the model's face, construct and predictive validities. We found that in contrast to a single injection of MAM to dams at GD 15, 16 or 17, its daily administration from GD 15 to 17 led to deficits in prepulse inhibition (PPI) of startle in the post-pubertal offspring. In addition, we observed behavioral deficits in working memory and social interactions, as well as an increase in locomotor activity induced by the NMDA antagonist MK-801 in GD15–17 MAM offspring. These animals also showed a reduction in the volume of the prefrontal cortex (PFC) and hippocampus, neuroanatomical changes such as discontinuities and heterotopias in the hippocampus, and an increase of DA level and DOPAC/DA ratio in the medial PFC. Atypical antipsychotic drugs clozapine, risperidone, and aripiprazole, but not the typical drug haloperidol, reversed the deficit in PPI and social withdrawal in the offspring of MAM-treated dams. In contrast, MK-801-induced hyperactivity in MAM mice was reversed by both and typical or atypical antipsychotic drugs. Taken together, the treatment of pregnant mice with MAM during GD 15–17 offers a new approach to study neurobiological mechanisms involved in the pathogenesis of schizophrenia.

1. Introduction

Schizophrenia is a frequent psychiatric disorder that appears during the late adolescent stage or early adulthood and is regarded as a neurodevelopmental disorder in which alterations start early in

development. Epidemiological research (Waddington et al., 1999) suggest that during the second trimester of pregnancy, the fetus could be exposed to environmental factors that increase the risk of developing schizophrenia (Waddington et al., 1999). During this period, extensive neuronal cell migration to the cortex occurs in the human brain

Abbreviations: ANOVA, analysis of variance; BrdU, 5-bromo-2'-deoxyuridine; CA, Cornu Ammonis; DA, dopamine; DG, dentate gyrus; GD, gestation day; MAM, methylazoxymethanol; mPFC, medial prefrontal cortex; NVH, neonatal ventral hippocampal lesions; SEM, standard error of the mean

* Corresponding author.

E-mail address: osamun@tohoku-mpu.ac.jp (O. Nakagawasai).

¹ These authors contributed equally to this work.

<https://doi.org/10.1016/j.neuropharm.2019.02.034>

Received 16 April 2018; Received in revised form 12 February 2019; Accepted 25 February 2019

Available online 01 March 2019

0028-3908/ © 2019 Elsevier Ltd. All rights reserved.

(Sidman and Rakic, 1973). The current view is that during adolescence brain maturation could be inhibited by the primal developmental alterations and thus contribute to the pathophysiology of schizophrenia (Rapoport et al., 2005). A number of animal models have been described to explore this hypothesis.

Current schizophrenia models are not intended to serve as the complete animal equivalent of the human disorder. Rather, they are often designed to test specific causative or mechanistic hypotheses.

In accordance with the neurodevelopmental hypothesis of schizophrenia, animal models have been proposed using pre- or early post-natal brain damages to induce schizophrenia-like behavioral changes (Lipska and Weinberger, 2000; Boksa, 2004; Laplante et al., 2005). Prenatal toxin treatment can induce alterations in the structures of the brain, with a relative specificity given by the neurogenic timetable (Cattabeni and Di Luca, 1997). To induce neurodevelopmental damages in the hippocampus and cortex, methylazoxymethanol (MAM) can be used to briefly interfere with brain cellular proliferation during late gestation, a time when the neurons that will migrate to these areas are undergoing major cell division (Bayer and Altman, 2004). MAM administration to pregnant rats at gestation day (GD) 17 was recently used as an experimental model for schizophrenia (Moore et al., 2006). This treatment leads to aberrant methylation of DNA and interference with neurogenesis (Hoareau et al., 2006) and induces many characteristics consistent with schizophrenia, including neurochemical changes, behavioral changes [in prepulse inhibition (PPI) of startle reflex, working memory and social interaction] and increased locomotor activity to psychotropic drugs (Gomes et al., 2016). Furthermore, MAM-treated rats display an increase in the firing of dopamine (DA) neurons that is driven by hyperactivity in the ventral hippocampus (Chen et al., 2014; Gomes et al., 2016). Thus, this model is appropriate for studying the link between altered embryonic neurogenesis and transition to schizophrenia-like deficits in the adult.

Given the general advantage of mice models (for example, the availability of transgenic strains) the MAM-treated mice could enable researchers to analyze genetic influences in the pathophysiology of schizophrenia. Guo et al. (2013) have reported the effect of MAM given to adolescent mice. More recent studies have reported establishment of models based on pregnant mice treated with MAM at GD16 or 17 (Chalkiadaki et al., 2018; Huo et al., 2018). However, these models fail to exhibit many schizophrenia-like phenotypes, such as behavioral and brain changes, in the offspring.

Our validation experiments using GD 16 or 17 MAM-treated mice did not reveal significant schizophrenia-related behaviors in the offspring, e.g., deficits in prepulse inhibition of startle. Therefore, we developed a protocol in which mice are treated with MAM on GD15–17. According to species comparison of Carnegie stages of embryonic development (https://embryology.med.unsw.edu.au/embryology/index.php/Mouse_Development), GD15.5 of mice may be in accordance with GD17 of rats, regarding the morphological development of the embryo. In addition, the latest predictive model (Workman et al., 2013) proposes that equivalent maturation stages of brain development between mouse and rat differ by 1–2 days, with the latter maturing later. We anticipated that a prenatal treatment with MAM during this period would induce neuronal loss (Gaspard et al., 2008; Alsö et al., 2013) and behavioral, pathological and neurochemical changes relevant to schizophrenia. Our data shows that a number of these changes induced by prenatal MAM treatment are detectable in the offspring at post-pubertal period and can be reversed by typical and atypical antipsychotic drugs. We believe that the mice MAM model may serve as a new heuristic paradigm to further investigate the neurodevelopmental bases of schizophrenia.

2. Materials and methods

All experiments were performed following the approval of the Ethics Committee of Animal Experiment in Tohoku Medical and

Pharmaceutical University, and according to the National Institutes of Health Guide for the Care and Use of Laboratory Animals. Efforts were made to minimize suffering and to reduce the number of animals used. Measurement of the behaviors and post-mortem analyses were done in blinded manner.

2.1. Animals

Pregnant female ddY mice were obtained from Japan SLC (Shizuoka, Japan) on GD 11–13 and were housed individually in plastic cages (height: 12 cm, width: 17 cm, length: 27 cm). Our choice of this strain of mice was partly based on previous work showing that ddY mice are more vulnerable to the development of behavioral disturbance by stress or phencyclidine treatments (Mouri et al., 2012). This strain is also more responsive to treatment with antipsychotics than other strains (Sugimoto et al., 2008). The dams were injected once daily with saline or MAM (10 mg/kg, i.p.) for 3 days, between GD 15 and 17 (dams treated with higher dose of MAM, 20 mg/kg, died almost immediately after delivery and the pups didn't survive). Within 10 days after birth, all female offspring were culled. The remaining pups were weaned 21 days after birth and were housed in groups of 4–6 mice. Only the male pups were included in the studies, and each animal was tested only for one behavior at pre-pubertal age (5 weeks) and then one behavior at post-pubertal age (8 weeks). The onset of pubertal age has been described previously (Palanza et al., 2001; Naert et al., 2013). The experiments were performed on several groups of saline or MAM-treated animals. They consisted of: (1) behavioral testing ($n = 492$), (2) measurement of body and brain weights ($n = 10$), (3) determination of neurotransmitter concentrations ($n = 14$), and (4) immunohistochemistry ($n = 28$). The animals were housed in plastic cages with free access to food and water under conditions of constant temperature ($22 \pm 2^\circ\text{C}$) and humidity ($55 \pm 5\%$), on a 12 h light-dark cycle (lights on at 07:00).

2.2. Drugs

MAM (Wako Pure Chemical Industries Ltd, Osaka, Japan) and MK-801 (Sigma-Aldrich, St-Louis, USA) were dissolved in saline. Haloperidol (Sigma-Aldrich), Clozapine (Sigma-Aldrich), Risperidone (Sigma-Aldrich) and Aripiprazole (Wako Pure Chemical Industries Ltd) were dissolved in 0.5% Tween80 (Wako Pure Chemical Industries Ltd). These drugs were administered intraperitoneally (i.p.) at a volume of 0.1 ml/10 g of mouse body weight. The antipsychotic drugs were administered 30 min before the behavioral tests.

2.3. PPI of the acoustic startle response

Sensorimotor gating processes which are frequently impaired in schizophrenia patients were evaluated using the PPI of the startle response which is one of the paradigms to detect this deficit in patients (Braff et al., 2001). Tests were conducted using the commercial software package SR-LAB system (SR-LAB, San Diego Instruments, San Diego, USA) that comprised two sound-attenuating chambers each equipped with a cylindrical Plexiglas animal enclosure (length: 6.7 cm; inner diameter: 3.8 cm). Ventilation was provided by a small electric fan that also generated a 70 dB background noise. Tone pulses were presented by a speaker positioned 24 cm directly above the animal enclosure. A piezoelectric accelerometer affixed to the animal enclosure frame was used to detect and transduce motion resulting from the animal's response. Tone pulse parameters were controlled by a computer using a SR-LAB and interface assembly that also digitized, rectified and recorded stabilimeter readings.

Measures of both acoustic startle response (ASR) and PPI were obtained in a single session. Mice were placed in the Plexiglas enclosure and allowed to acclimatize to the environment for 5 min before being tested during 42 discrete trials. When antipsychotic drugs or vehicle

were administered, mice were placed in the Plexiglas enclosure 30 min after the administration. On the first two trials, the magnitude of the ASR to a 120 dB tone lasting 50 ms was measured. These first two startle tones were presented in order to habituate the animals to the testing procedure. Therefore, the ASR magnitude of these two trials was omitted from the statistical analysis of the mean ASR amplitude. On the subsequent 40 trials, the startle tone was either presented alone or 100 ms after the presentation of a 30 ms duration prepulse. Prepulse intensity ranged from 3 to 15 dB above background noise and was varied randomly between trials in 3 dB steps. Measures were taken at each of the five prepulse intensities during five trials; animals were randomly presented with the startle tone alone during another ten trials; null trials (background tone alone) were conducted during the other five trials. The same stimulus condition was never presented on more than two consecutive trials. The interval between each trial was programmed to a variable time schedule with an average duration of 15 s (range 5–30 s). A measure of startle response amplitude was derived from the mean of 100 digitized data points collected from stimulus onset at a rate of 1 kHz. Prepulse effectiveness in suppressing the startle response was expressed as a percentage based on the mean amplitude of response to the startle tone alone (10 startle tones) relative to those recorded under the five prepulse conditions (5 startle tones/condition): $PPI = 100 - [(mean\ startle\ amplitude\ for\ prepulse + pulse\ trials / mean\ startle\ amplitude\ for\ pulse-alone\ trials) \times 100]\%$. The five different prepulse intensities were averaged and used for statistical analysis.

2.4. Locomotor activity

Positive symptoms of schizophrenia develop around adulthood (Tandon et al., 2009) and are exacerbated by NMDA glutamatergic transmission in brain (Lahti et al., 1995). An increase in locomotor activity has been proposed as an animal behavioral equivalent to the positive symptoms seen in schizophrenia patients (Tandon et al., 2009). The locomotor activity of mice was evaluated using the multichannel activity-counting system SUPERMEX (Muromachi Kikai Co., Tokyo, Japan). This instrument can monitor even minute movements in all three planes of motion (vertical and horizontal) as one movement, owing to its infrared sensor with multiple Fresnel lenses that can be moved close enough to the cage to capture multidirectional locomotor alterations in a single mouse. Thus, vertical movement such as jumping as well as horizontal movements such as walking and running could be counted. The Supermex instrument was connected to a behavioral analyzing system (CompACT AMS) (Muromachi Kikai Co.) which interpreted the movements as one count. Measurements of activity were conducted between 11:00 and 15:00 during the light phase. Mice were divided into two groups (saline and MAM), placed in activity boxes for 60 min. Mice were then injected with saline or MK-801 (0.1 mg/kg, i.p.) and locomotor activity was recorded for another 60 min.

2.5. Social interaction test

Social withdrawal is frequently observed as a negative symptom of schizophrenia (Mueser and McGurk, 2004) that can be modeled in rodents. The general design of the model was adapted from Tanda et al. (2009). The test was performed in a Plexiglas cage (height: 18 cm, width: 26 cm, length: 30 cm). The measurement of social interaction was done by video recording without any observer in the room. Experiments were performed at a light intensity of 35 lux. The arena was placed in a dimly lit room and was cleaned after each test. Two unfamiliar mice that had approximately the same weight and had received an identical prenatal treatment were placed simultaneously in the opposite corners of the arena and the behavior of each mouse was recorded for a 10 min period. Behaviors such as sniffing, grooming and chasing at a distance closer than 2 cm of one another were counted as social interaction. Frequency as well as the time spent in these

behaviors were analyzed.

2.6. Y-maze test

In addition to positive and negative symptoms, schizophrenia patients consistently present cognitive deficits in working memory (Heinrichs and Zakzanis, 1998). We assessed cognitive deficits in MAM-treated using spontaneous alternation in a Y-maze. The Y-maze apparatus consisted of three compartments (height: 25 cm, width: 3 cm, length: 40 cm) radiating out from the center. The mice were placed in one of the compartments and allowed to move freely for 8 min. Experiments were performed at a light intensity of 35 lux. An arm entry was defined as three legs entering one of the arms, and the sequence of entries was manually recorded. An alternation was defined as entry into all three arms on consecutive trials. Thus, the maximum number of alternations was the total number of entries minus 2, and the percent alternation was calculated as (actual alternations/maximum alternations) \times 100. The percent spontaneous alternation behavior of the mouse was taken as a measure of spatial short-term memory.

2.7. Measurement of body and brain weights

We examined regional brain weights in MAM mice as schizophrenia patients consistently show a decrease in cortical and hippocampal volumes (Brugger and Howes, 2017). On postnatal day 56, mice were weighed and then killed by decapitation. The brain (including the cerebellum) was removed and weighed. On a separate group of saline and MAM treated mice, the prefrontal cortex (PFC), hippocampus and striatum were dissected out and weighed. The PFC corresponded to an area that included the rostral pole of the brain, and was delimited medially by the interhemispheric fissure, laterally by the corpus callosum and caudally extended to Bregma +2.68. The striatum and hippocampus were dissected from the remaining bloc of tissue.

2.8. Immunohistochemical study (cell proliferation and neurogenesis)

Some studies performed on postmortem brains revealed that the proliferation of hippocampal neural stem cell was significantly reduced in schizophrenic patients (Allen et al., 2016; Iannitelli et al., 2017). On postnatal day 42, 5-bromo-2'-deoxyuridine (BrdU) (Nacalai Tesque, Inc, Kyoto, Japan; 75 mg/kg i.p.) was injected three times every 24 h for analysis of neurogenesis. These mice were sacrificed 2 weeks after the first BrdU injection. On postnatal day 56, BrdU was injected three times every 2 h for analysis of cell proliferation. These mice were sacrificed 24 h after the first BrdU injection. Brains were fixed with 4% paraformaldehyde. The brains were cut into 40 μ m sections from bregma -1.60 mm to -2.0 mm using a cryostat (MICROM HM560, Mikron Instrument, Inc., Simi Valley, USA). For BrdU immunodetection, tissue sections were first incubated at 37 °C for 30 min in HCl (2 N) followed by primary antibody addition. The primary antibodies used were rat anti-BrdU monoclonal antibody (1:100; Harlan SeraLab, Loughborough, UK), mouse anti-doublecortin (DCX) monoclonal antibody (1:50; Santa Cruz Biotech, Santa Cruz, CA) and mouse anti-neuronal nuclear antigen (NeuN) monoclonal antibody (1:500; Millipore, Temecula, USA). The following fluorescence conjugated secondary antibodies were used: goat anti-rat IgG Alexa Fluor 568 (1:200; Molecular Probes, Eugene, USA) and goat anti-mouse IgG Alexa Fluor 488 (1:200; Molecular Probes). DAPI was used to identify nuclei. Finally, sections were washed and coverslipped with Dako fluorescence mounting medium (Dako, Carpinteria, USA). Labeled sections were analyzed using a confocal laser-scanning microscope (A1Rsi; Nikon, Tokyo, Japan). Eight sections per mouse were used, and two images (640 \times 640 μ m) of the DG region of the hippocampus were obtained from each section. We counted the number of BrdU + /DCX + cells and BrdU + /NeuN + cells in the DG for analysis of cell proliferation and neurogenesis using NIS-Elements AR analysis system, respectively. A mean number of eight

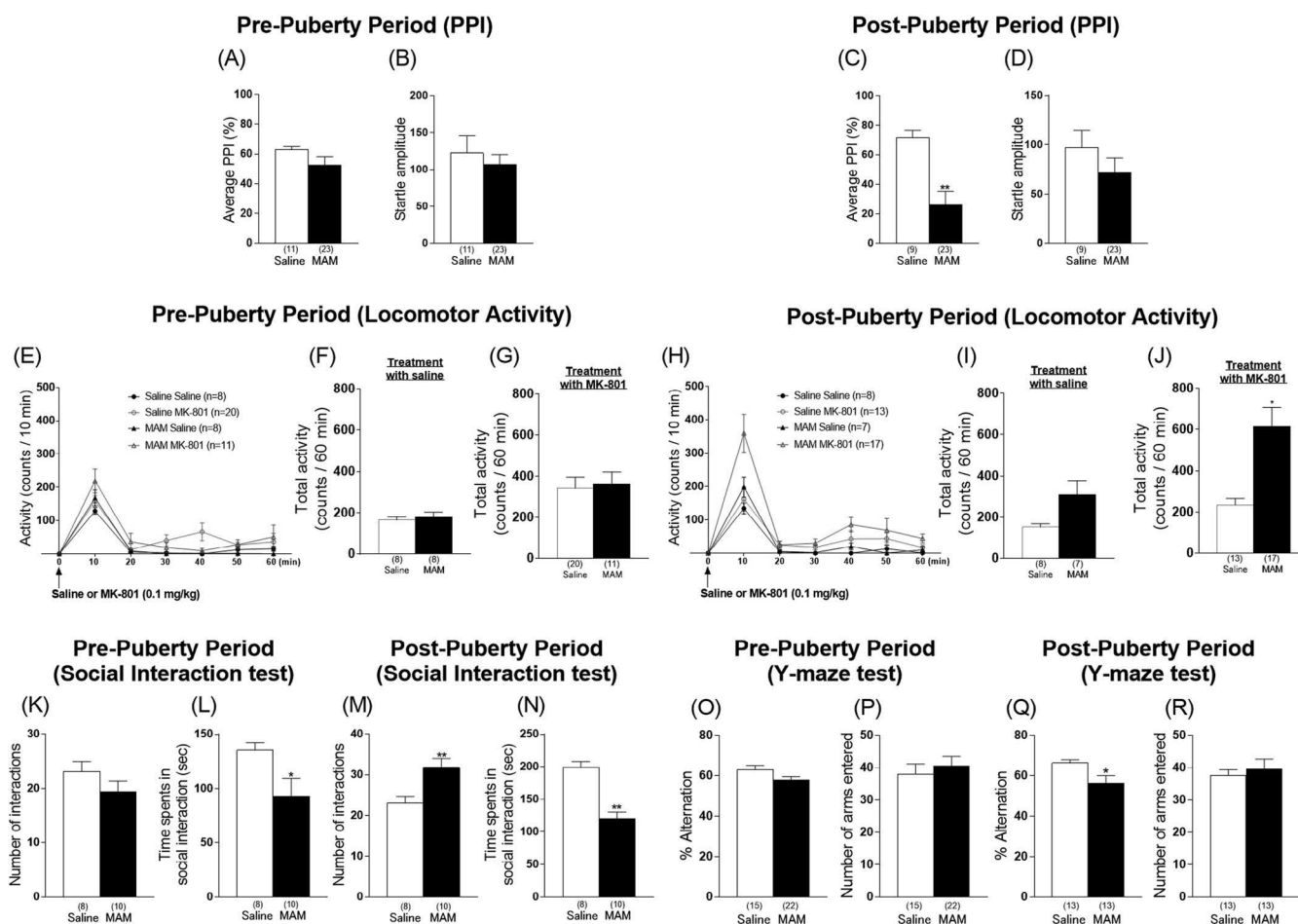


Fig. 1. Behavioral changes in mice exposed to MAM at GD 15–17. Average PPI and acoustic startle response in pre-pubertal (A and B) and post-pubertal (C and D) mice treated prenatally with saline or MAM. PPI deficits in MAM mice developed at post-pubertal, but not pre-pubertal age. Locomotor activity in pre-pubertal (E–G) and post-pubertal (H–J) mice treated prenatally with saline or MAM. (E) and (H) show the temporal profiles of MK-801-induced locomotion. (F, G, I and J) Analysis of total activity scores following MK-801 treatment reveals that MAM mice become more active than control animals only at post-pubertal period. Social interaction in pre-pubertal and post-pubertal mice treated prenatally with saline or MAM (K–N). Social withdrawal in MAM mice began development in pre-pubertal age. Working memory in the Y-maze in pre-pubertal and post-pubertal mice treated prenatally with saline or MAM (O–R). Memory deficits in MAM mice developed in post-pubertal, but not pre-pubertal age. Bars represent means \pm S.E.M. *: $p < 0.05$ and **: $p < 0.01$ vs. prenatal treatment with saline group.

images were analyzed for each mouse, and each group contained 4–5 mice.

2.9. Immunohistochemical study (cytoarchitectural and neuromorphometric alteration)

One of the structural abnormality observed in the brains of schizophrenic patients is the hippocampal cellular disarray such as selective decrease in the number of pyramidal cells in the cornu ammonis (CA)2 area and neuron of discontinuities and heterotopias (Benes et al., 1998; Heckers, 2004; Nelson et al., 1998). Brain sections were prepared as described in the preceding section (cell proliferation and neurogenesis). Antigen retrieval was performed for RGS-14 staining. Briefly, free-floating sections were incubated at 80 °C for 30 min in 50 mM sodium citrate (pH = 9.0). We used the following primary antibodies: rabbit anti-Prox1 monoclonal antibody (1:500; Abcam Ltd., Cambridge, UK), mouse anti-RGS14 monoclonal antibody (1:100; NeuroMab, Davis, USA), and rat anti-Ctip2 monoclonal antibody (1:500; Abcam Ltd). The fluorescence conjugated secondary antibodies were: goat anti-mouse IgG Alexa Fluor 488 (1:200; Molecular Probes), goat anti-rabbit IgG Alexa Fluor 568 (1:200; Molecular Probes) and goat anti-rat IgG Alexa Fluor 647 (1:200; Molecular Probes). For analyses, eight sections per mouse were used and two images (640 \times 640 μ m) of the dorsal and

ventral hippocampus were obtained from each section. We counted the number of DAPI positive cells in each sector of the hippocampus i.e. CA1, CA2, CA3 and DG. An average of eight images from each of the three mice per group was used for the analysis. Heterotopias, defined as a group of misplaced neurons, were counted in the hippocampus from MAM and control animals. Discontinuities were defined as a disruption in the CA layer characterized by the presence of interruption in the neuronal layer continuity and dispersed neurons on any side of the cellular layer. Heterotopias, defined as a group of misplaced neurons, were counted in the dorsal hippocampus from MAM and control animals.

2.10. DA and metabolite measurements with high-performance liquid chromatography (HPLC)

It has been suggested that a disturbance in the dopaminergic system, such as an increased presynaptic DA function in the various brain regions, underlies schizophrenia (Kesby et al., 2018). Mice were divided into two groups (saline and MAM) and sacrificed by decapitation on postnatal day 56. Each brain was rapidly removed and the medial PFC (mPFC), striatum and hippocampus were dissected on an ice-cold plate. These brain tissues were homogenized by sonication in ice-cold 0.1 M perchloric acid with an internal standard (Isoproterenol)

added at a concentration of 100 ng/ml. The homogenates were centrifuged at $10000 \times g$ then each supernatant was filtered through a $0.45 \mu\text{m}$ pore size membrane filter. The filtrate was used for the quantification of DA (Sigma-Aldrich) by HPLC coupled with electrochemical detection. The HPLC system was comprised of a CCPM pump, an auto-sampler equipped with a cooling plate maintained at 4°C , and CO-8010 column oven (Tosoh, Tokyo, Japan). Separation was achieved on a TSK gel ODS-100s (Tosoh, $250 \times 4.6 \text{ mm i.d.}$). The mobile phase was 95% 50 mM sodium acetate, 10 mM citric acid, 0.15 mM EDTA, 0.45 mM SOS and 5% acetonitrile adjusted to pH 3.5 with glacial acetic acid then filtered through a $0.45 \mu\text{m}$ membrane. The flow rate was 1.0 ml/min. The electrochemical detection was accomplished using an electrochemical detector (model EC8020, Tosoh) with a glass working electrode at a potential of 1700 mV. The ratio of DOPAC/DA and HVA/DA were used as indices of DA turnover.

2.11. Statistical analysis

Normality and homoscedasticity assumptions were verified prior to the use of any parametric tests (Shapiro-Wilk normality test and equality of variances F-test). Results are expressed as mean \pm standard error of the mean (SEM). The statistical significance of differences was determined by the Student's t-test for two-group comparisons. One-way, two-way or three-way analysis of variance (ANOVA) followed by Tukey-kramer test were employed for multigroup comparisons. In some cases, when a main effect was significant without interaction effect, we did an exploratory and limited pairwise post-hoc comparison consistent with our *a priori* hypothesis. Brain weights were analyzed by ANCOVA with body weight as a covariate. $p < 0.05$ represented a significant difference.

3. Results

3.1. Acoustic startle and PPI

There was no significant differences in the startle amplitude measured at either pre- or post-pubertal periods between mice treated prenatally (GD 15–17) with saline or MAM. MAM-treated mice displayed significant average PPI deficits at the post-pubertal period, but not pre-pubertal period [Fig. 1 (A–D) Pre-pubertal: Student's t-test of average PPI: $t(32) = 1.19$, $p = 0.24$, (A); startle amplitude: $t(32) = 0.61$, $p = 0.55$, (B). Post-pubertal: Student's t-test of average PPI: $t(30) = 3.01$, $p = 0.0053$, (C); startle amplitude: $t(30) = 0.94$, $p = 0.35$, (D)]. These results indicated that the prenatal administration of MAM at GD 15–17 induced schizophrenia-like behavioral deficits in PPI at adulthood, similar to that reported for MAM-treated rats at GD 17 (Gomes et al., 2016). In preliminary experiments, we found that mice prenatally treated with single injection of MAM (10 mg/kg) on either GD 15, GD 16 or GD 17 did not display PPI deficits during the post-pubertal period [Fig. S1 GD 15 (A): Student's t-test: average: $t(27) = 0.88$, $p = 0.39$. GD 16 (B): Student's t-test of average PPI: $t(49) = 0.029$, $p = 0.98$. GD 17 (C): Student's t-test of average PPI: $t(35) = 1.28$, $p = 0.21$]. Based on these results, we chose GD 15–17 as the time period to treat pregnant mice with MAM for further behavioral, pathological and neurochemical studies.

3.2. Locomotor activity

Changes in locomotor activity induced by the NMDA antagonist MK-801 was analyzed at both pre- and post-pubertal periods. For either periods, the activities of MAM and saline treated mice were not significant different following the saline treatment of the test. ANOVA showed significant main effects of treatment and prenatal treatment factors but not an interaction. Thus, we focused our analysis on the effects of MAM and drug treatments. A significant increase in total locomotor activity by treatment with MK-801 was only observed at post-

pubertal age in MAM treated mice compared to saline treated mice. [Fig. 1 (E–J) Three-way ANOVA: prenatal treatment: $F(1, 43) = 0.93$, $p = 0.76$, treatment: $F(1, 43) = 8.80$, $p = 0.005$, time: $F(3, 143) = 35.32$, $p < 0.0001$, prenatal treatment \times treatment: $F(1, 43) = 0.004$, $p = 0.95$, time \times prenatal treatment: $F(3, 143) = 1.67$, $p = 0.17$, time \times treatment: $F(3, 143) = 0.21$, $p = 0.91$, time \times prenatal treatment \times treatment: $F(3, 143) = 0.68$, $p = 0.58$, (E); Student's t-test: $t(14) = 0.50$, $p = 0.62$, (F); $t(29) = 0.26$, $p = 0.80$, (G); Three-way ANOVA: prenatal treatment: $F(1, 41) = 4.88$, $p = 0.033$, treatment: $F(1, 41) = 9.28$, $p = 0.004$, time: $F(2, 86) = 35.99$, $p < 0.0001$, prenatal treatment \times treatment: $F(1, 41) = 1.61$, $p = 0.21$, time \times prenatal treatment: $F(2, 86) = 3.55$, $p = 0.031$, time \times treatment: $F(2, 86) = 1.18$, $p = 0.31$, time \times prenatal treatment \times treatment: $F(2, 86) = 0.88$, $p = 0.43$, (H); Student's t-test: $t(19) = 1.75$, $p = 0.096$, (I); $t(22) = 2.56$, $p = 0.018$, (J)]. These results indicated that prenatal MAM treatments induced MK-801-induced hyperactivity in mice during the post-pubertal period.

3.3. Social interaction test

The effect of prenatal MAM on social behavior was evaluated at pre- and post-pubertal periods between pairs of unfamiliar mice that received the same prenatal treatments [Fig. 1 (K–N)]. Compared to saline-treated mice, MAM-treated mice showed significantly reduced time spent in social interactions at both developmental periods [Student's t-test: $t(14) = 2.38$, $p = 0.032$, (L); $t(18) = 5.91$, $p < 0.0001$, (N)]. Moreover, at the post-pubertal period, the number of interactions significantly increased in MAM treated mice compared to saline treated mice [Student's t-test: $t(14) = 1.38$, $p = 0.19$, (K); $t(18) = 3.12$, $p = 0.0059$, (M)]. These results indicate that prenatal MAM treatments induced social deficits in mice at both pre- and post-pubertal periods.

3.4. Y-maze test

Memory functions were evaluated in saline and MAM-treated mice at pre- and post-pubertal periods in the Y-maze test [Fig. 1 (O–R)]. Total arm entries were not significantly different between saline and MAM treated mice at both periods [Student's t-test: $t(35) = 0.57$, $p = 0.57$, (P); $t(24) = 0.58$, $p = 0.57$, (R)]. However, spontaneous alternation was significantly decreased in MAM-treated mice compared to saline-treated mice at the post-pubertal, but not the pre-pubertal period [Student's t-test: $t(35) = 1.82$, $p = 0.077$, (O); $t(24) = 2.48$, $p = 0.021$, (Q)]. The data indicates that prenatal MAM treatments induced post-pubertal cognitive deficits in mice.

3.5. Measurement of body and brain weights

Our data show that the weight of the PFC and hippocampus, but not the striatum, were significantly reduced in MAM-treated mice compared to saline controls on postnatal day 56 [Fig. 2 (A–E) Student's t-test: PFC: $t(8) = 3.26$, $p = 0.012$, Fig. 2 (A); striatum: $t(8) = 1.53$, $p = 0.17$, Fig. 2 (B); hippocampus: $t(8) = 4.51$, $p = 0.002$, Fig. 2 (C); whole brain: $t(8) = 4.92$, $p = 0.0012$, Fig. 2 (D); whole body: $t(8) = 3.05$, $p = 0.016$, Fig. 2 (E)]. Total brain weight was also significantly reduced by approximately 9.5% in MAM treated mice while the average body weight was smaller by 16.2%. However, an analysis by ANCOVA revealed that the body weight contribution to brain weight was not significant [ANCOVA: whole brain: $F(1, 6) = 11.23$, $p = 0.015$, whole body: $F(1, 6) = 0.013$, $p = 0.91$].

3.6. Cytoarchitectural alterations in the hippocampus of MAM treated mice

We have performed multiple immuno-labeling in order to evaluate the pyramidal/granule cell density and morphology in the dorsal and ventral hippocampus [Fig. 3 (A and B)]. Anti-Ctip2, anti-RGS14 and anti-Prox1 antibodies were used to identify the CA1, CA2 and DG areas,

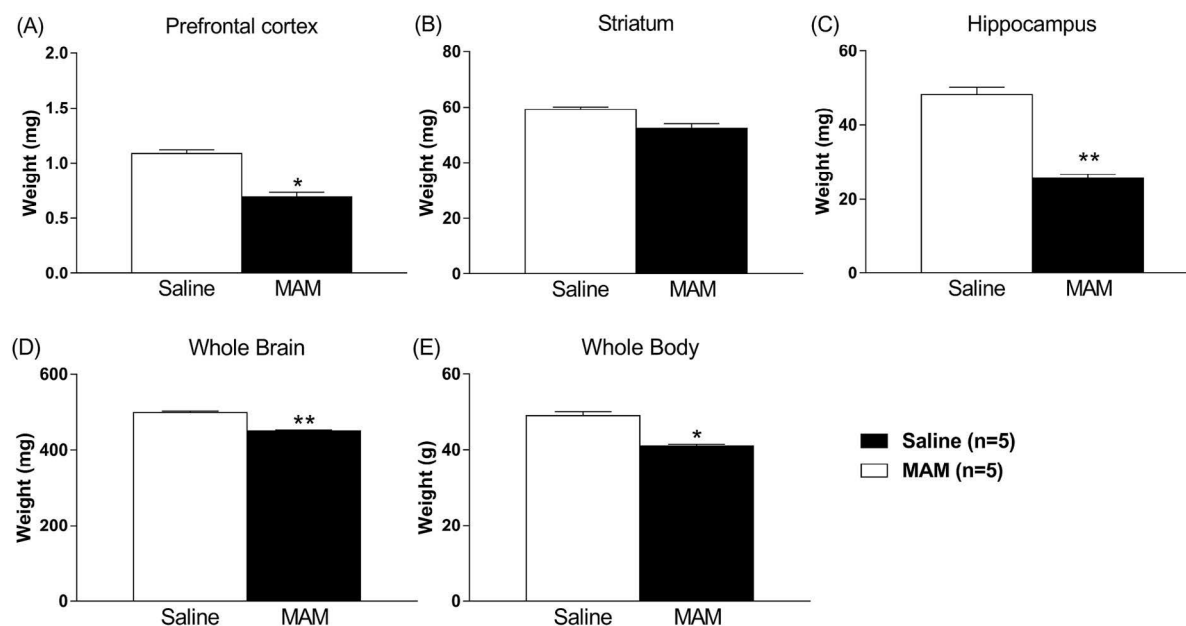


Fig. 2. Prefrontal cortex (PFC) (A), striatum (B), hippocampus (C), whole brain (D) and whole body (E) weight comparisons at postnatal day 56 between mice treated prenatally with saline or MAM. The weight of the PFC, hippocampus and whole brain, but not the striatum, were significantly reduced in MAM-treated mice compared to saline controls on postnatal day 56, while body weight contribution to brain weight was not significant. Bars represent means \pm S.E.M. *: $p < 0.05$ and **: $p < 0.01$ vs. prenatal treatment with saline group.

respectively. The pyramidal cell density in CA2 was significantly decreased in MAM-treated mice compared to saline treated mice, whereas the subfields CA1, CA3 or DG in both the dorsal and ventral hippocampus showed no significant differences [Fig. 3 (C and D) Two-way ANOVA: prenatal treatment: $F(1, 32) = 20.43$, $p < 0.0001$, brain region: $F(3, 32) = 282.1$, $p < 0.0001$, prenatal treatment \times brain region: $F(3, 32) = 11.66$, $p < 0.0001$, Post-hoc test: CA1: $p > 0.9999$, CA2: $p < 0.0001$, CA3: $p > 0.9999$, DG: $p = 0.75$, (C); prenatal treatment: $F(1, 32) = 9.27$, $p = 0.0046$, brain region: $F(3, 32) = 67.87$, $p < 0.0001$, prenatal treatment \times brain region: $F(3, 32) = 3.32$, $p = 0.032$, Post-hoc test: CA1: $p > 0.9999$, CA2: $p = 0.0007$, CA3: $p > 0.9999$, DG: $p = 0.77$, (D)]. Quantitative analyses of discontinuities and heterotopias in the dorsal hippocampus [Fig. 3 (E, F and H)] showed that, compared to control saline-treated mice. Main effect of prenatal treatment was significant by ANOVA, while interaction was not significantly different. Thus, we focused on the effect of MAM, but not brain regions. The mice treated with MAM exhibited more discontinuities in CA1, CA2 and CA3 compared to control mice [Fig. 3 (G) Two-way ANOVA: prenatal treatment: $F(1, 24) = 26.59$, $p < 0.0001$, brain region: $F(2, 24) = 0.39$, $p = 0.68$, prenatal treatment \times brain region: $F(2, 24) = 0.86$, $p = 0.44$, Post-hoc test: CA1: $p = 0.015$, CA2: $p = 0.013$, CA3: $p = 0.025$, (G)]. In addition, the number of heterotopias was also significantly increased in the MAM mice [Fig. 3 (I) Student's t-test: $t(8) = 2.43$, $p = 0.042$, (I)]. These results indicate that the prenatal treatment with MAM induced a decrease in pyramidal cell density in the CA2 area which was accompanied with an increase in discontinuities and heterotopias.

3.7. Cell proliferation and neurogenesis in the DG of the hippocampal formation

To determine the rate of hippocampal cell proliferation and neurogenesis in our model, animals were injected with BrdU. Anti-DCX antibody was used to identify immature neurons while anti-NeuN antibody was used to identify mature neurons in the DG area. The incorporation of BrdU into a cell indicates that it was dividing at the time of the BrdU injection. MAM-treated mice had a significantly lower number of both BrdU+/DCX+ cells and BrdU+/NeuN+ cells

compared to the saline-treated group [Fig. 4 (B) and (D) Student's t-test: $t(8) = 8.52$, $p < 0.0001$, (B); $t(6) = 5.70$, $p = 0.0013$, (D)]. These results indicate that the prenatal treatment with MAM in mice induced a reduction in cell proliferation and neurogenesis in the DG of the hippocampus.

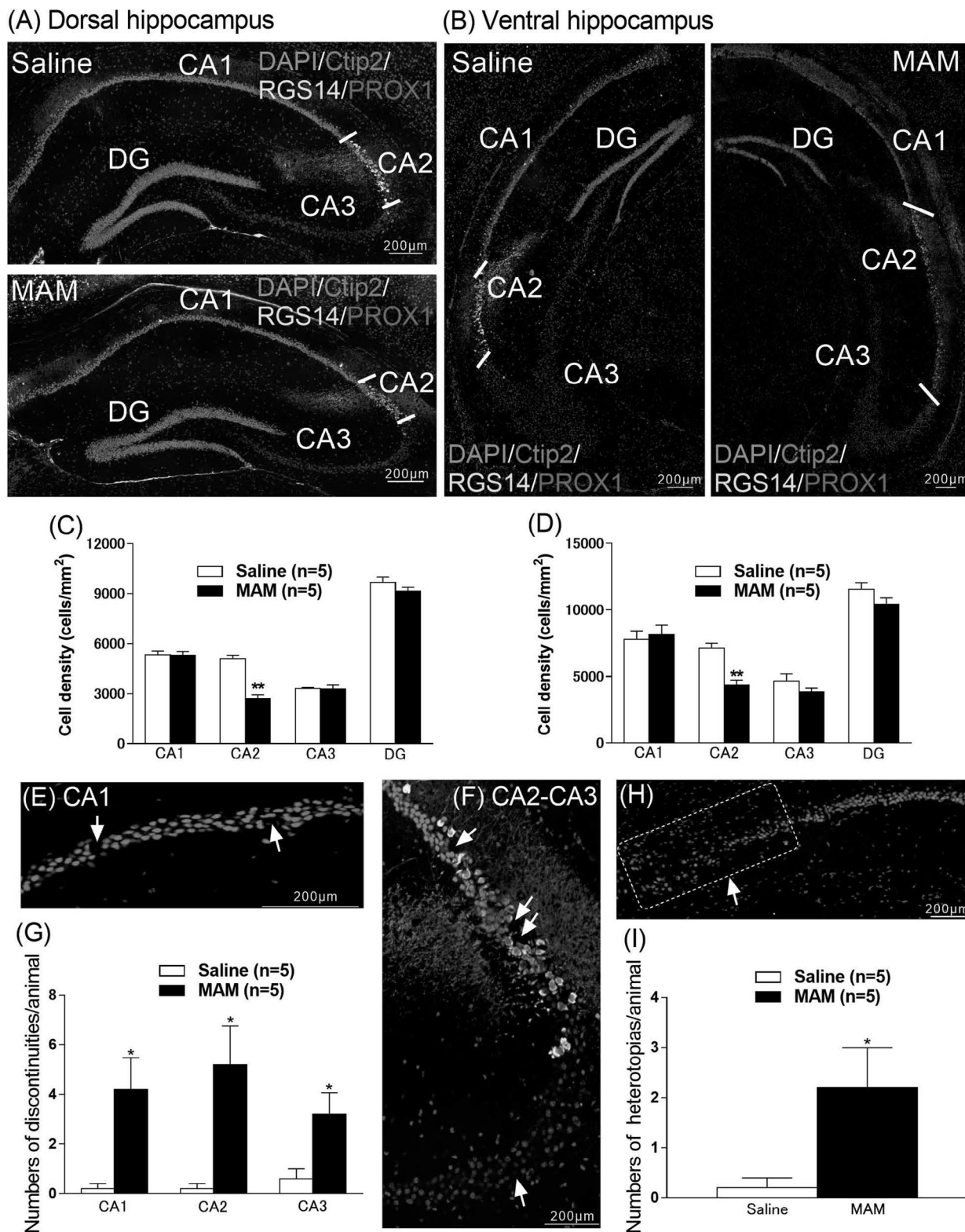
3.8. Alterations of dopaminergic system in the brain of MAM-treated mice

Tissue levels of DA, its metabolites and their turnover in the mPFC, striatum and hippocampus of mice treated prenatally with saline or MAM are shown in Fig. 5. ANOVA showed a significant main effect of prenatal treatment but not of interaction in the content and turnover in the mPFC area. Thus, we focused on the effect of MAM only. In the mPFC, the DA concentration and DOPAC/DA ratio in MAM treated mice was significantly increased compared to the saline treated group [Two-way ANOVA: prenatal treatment: $F(1, 36) = 12.56$, $p = 0.0011$, concentration: $F(2, 36) = 19.52$, $p < 0.0001$, prenatal treatment \times concentration: $F(2, 36) = 0.60$, $p = 0.55$, Post-hoc test: DA: $p = 0.038$, DOPAC: $p = 0.059$, HVA: $p = 0.12$, (A); Two-way ANOVA: prenatal treatment: $F(1, 24) = 6.53$, $p = 0.017$, turnover: $F(1, 24) = 7.08$, $p = 0.014$, prenatal treatment \times turnover: $F(1, 24) = 2.33$, $p = 0.14$, Post-hoc test: DOPAC/DA: $p = 0.032$, HVA/DA: $p = 0.36$, (B); Two-way ANOVA: prenatal treatment: $F(1, 36) = 1.54$, $p = 0.22$, concentration: $F(2, 36) = 120.7$, $p < 0.0001$, prenatal treatment \times concentration: $F(2, 36) = 1.28$, $p = 0.29$, (C); prenatal treatment: $F(1, 24) = 0.11$, $p = 0.75$, turnover: $F(1, 24) = 77.22$, $p < 0.0001$, prenatal treatment \times turnover: $F(1, 24) = 0.19$, $p = 0.66$, (D); prenatal treatment: $F(1, 36) = 3.19$, $p = 0.083$, concentration: $F(2, 36) = 10.29$, $p = 0.0003$, prenatal treatment \times concentration: $F(2, 36) = 0.46$, $p = 0.64$, (E); prenatal treatment: $F(1, 24) = 1.63$, $p = 0.21$, turnover: $F(1, 24) = 3.64$, $p = 0.068$, prenatal treatment \times turnover: $F(1, 24) = 0.25$, $p = 0.62$, (F)]. These results indicate that the treatment with MAM induced an increase in the tissue levels of DA and a disturbance in the homeostasis of the dopaminergic system.

3.9. Effect of antipsychotic drugs on MAM-induced PPI disruption

We evaluated whether haloperidol (a typical antipsychotic), risperidone and clozapine (atypical antipsychotics) or aripiprazole (dopamine-serotonin stabilizer) reversed the PPI deficits (average PPI) in MAM-treated mice. MAM-induced PPI deficits were reversed by all

tested compounds except for haloperidol [Fig. 6 (A) Two-way ANOVA: average PPI: prenatal treatment: $F(1, 78) = 18.17$, $p < 0.0001$, antipsychotic: $F(3, 78) = 1.36$, $p = 0.26$, prenatal treatment \times antipsychotic: $F(3, 78) = 0.66$, $p = 0.58$, startle amplitude: prenatal treatment: $F(1, 78) = 3.30$, $p = 0.073$, antipsychotic: $F(3, 78) = 0.82$, $p = 0.49$, prenatal treatment \times antipsychotic: $F(3, 78) = 0.91$,



(caption on next page)

Fig. 3. Alteration of pyramidal/granule cell density and cytoarchitecture in different areas of the hippocampus in mice exposed to MAM at GD 15–17. Representative tissue sections used for cell counting in the dorsal (A) and ventral (B) hippocampus. Color of the neuronal layer in the different areas after merging of labeled images: CA1 and DG (magenta), CA2 (white), CA3 (blue). An example of labeling with individual antibodies is shown on Fig. S2. Cells were counted in the pyramidal/granule cell layer (C and D). Bar designated total was the average of all hippocampal subregions and DG. Coronal slices at Bregma -2.2 mm to -3.0 mm of the dorsal and ventral hippocampus: CA1, CA2 and CA3 from MAM treated mice stained with anti-Ctip2 antibody, anti-RGS14 antibody, anti-Prox1 antibody and DAPI. The pyramidal cell density in CA2 was significantly decreased in MAM-treated mice compared to saline treated mice, whereas the subfields CA1, CA3 or DG in both the dorsal and ventral hippocampus showed no significant differences. Arrows point to discontinuities in the dorsal hippocampus (E and F). Discontinuity differences between MAM and saline treated mice in hippocampal subfields CA1, CA2 and CA3 (G). The prenatal treatment with MAM exhibited more discontinuities in CA1 and CA2. The arrow points to heterotopia in the dorsal hippocampal CA1 area (H). Comparison between the number of heterotopias in the hippocampus of MAM treated mice and controls (I). The prenatal treatment with MAM induced an increase in heterotopias in the dorsal hippocampus. Bars represent means \pm S.E.M. *: $p < 0.05$ and **: $p < 0.01$ vs. prenatal treatment with saline group.

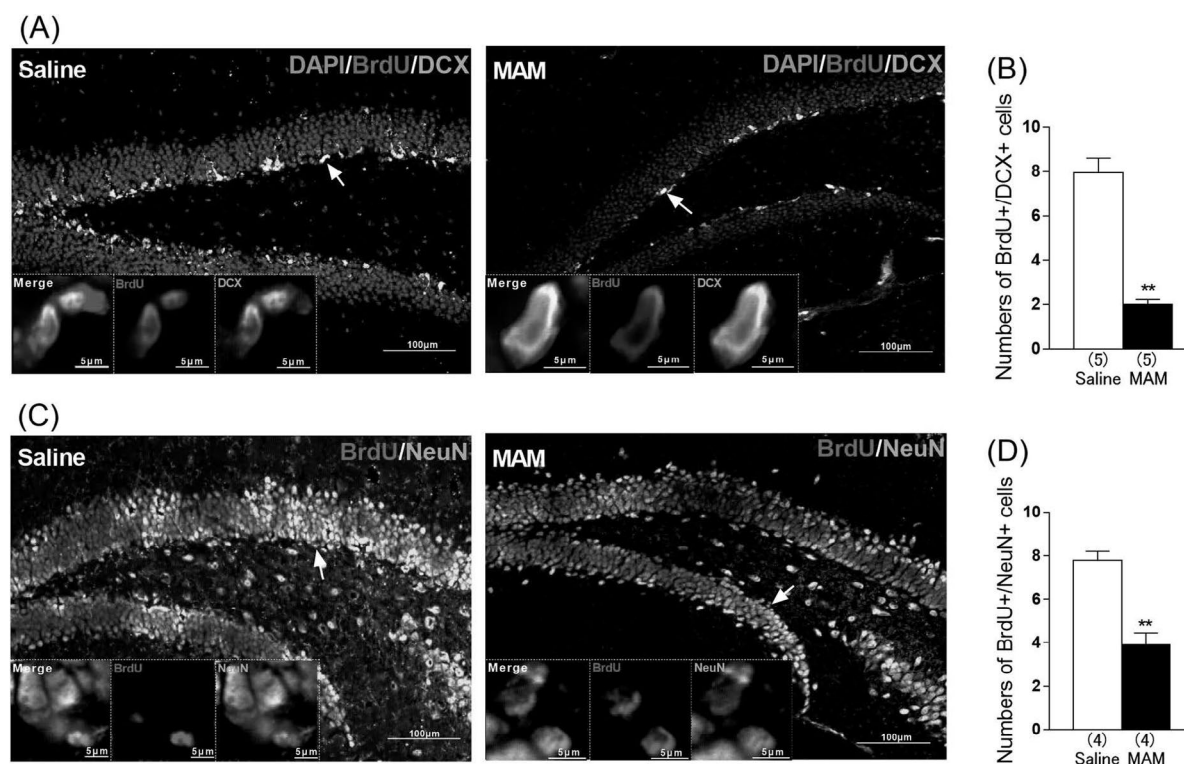


Fig. 4. Microscopy images of BrdU (red), DAPI (blue), and DCX or NeuN (green) immunostaining in the DG region of the hippocampus. The prenatal treatment with MAM in mice induced a reduction in cell proliferation and neurogenesis in the DG of the hippocampus. Bars represent means \pm S.E.M. **: $p < 0.01$ vs. prenatal treatment with saline group.

$p = 0.44$, (A)]. Risperidone (0.03 mg/kg), clozapine (0.5, 1 and 3 mg/kg) and aripiprazole (1 and 5 mg/kg) attenuated the MAM-induced PPI deficit for the average PPI, respectively [Fig. 6 (B–D) Two-way ANOVA: average PPI: prenatal treatment: $F(1, 75) = 10.28$, $p = 0.0020$, antipsychotic: $F(2, 75) = 4.21$, $p = 0.019$, prenatal treatment \times antipsychotic: $F(2, 75) = 4.076$, $p = 0.021$, startle amplitude: prenatal treatment: $F(1, 75) = 0.00047$, $p = 0.98$, antipsychotic: $F(2, 75) = 1.73$, $p = 0.19$, prenatal treatment \times antipsychotic: $F(2, 75) = 0.18$, $p = 0.84$. Post-hoc test (average PPI): 0.01 mg/kg: $p = 0.99$; 0.03 mg/kg: $p = 0.0027$, (B); Two-way ANOVA: average PPI: prenatal treatment: $F(1, 102) = 6.76$, $p = 0.011$, antipsychotic: $F(3, 102) = 7.97$, $p < 0.0001$, prenatal treatment \times antipsychotic: $F(3, 102) = 3.79$, $p = 0.013$, startle amplitude: prenatal treatment: $F(1, 102) = 0.30$, $p = 0.59$, antipsychotic: $F(3, 102) = 0.59$, $p = 0.62$, prenatal treatment \times antipsychotic: $F(3, 102) = 0.45$, $p = 0.72$. Post-hoc test (average PPI): 0.5 mg/kg: $p = 0.034$; 1 mg/kg: $p = 0.0041$; 3 mg/kg: $p < 0.0001$, (C); Two-way ANOVA: average PPI: prenatal treatment: $F(1, 70) = 1.91$, $p = 0.17$, antipsychotic: $F(3, 70) = 2.12$, $p = 0.11$, prenatal treatment \times antipsychotic: $F(3, 70) = 3.077$, $p = 0.033$, startle amplitude: prenatal treatment: $F(1, 70) = 2.86$, $p = 0.095$, antipsychotic: $F(3, 70) = 0.26$, $p = 0.85$, prenatal treatment \times antipsychotic: $F(3, 70) = 0.21$, $p = 0.89$. Post-hoc test

(average PPI): 0.2 mg/kg: $p = 0.68$; 1 mg/kg: $p = 0.027$; 5 mg/kg: $p = 0.013$, (D)]. These results indicate that prenatal MAM-induced PPI deficits in mice were improved with atypical antipsychotics but not with the typical antipsychotic drug haloperidol.

3.10. Effect of antipsychotic drugs on MK-801-induced hyperactivity in MAM-treated mice

We evaluated whether haloperidol, risperidone, clozapine or aripiprazole reversed the hyperactivity by MK-801 in MAM-treated mice. MAM-induced hyperactivity by MK-801 were reversed by all tested compounds without influence on control group [Fig. 7 (A–D) Haloperidol: Two-way ANOVA: prenatal treatment: $F(1, 47) = 6.076$, $p = 0.017$, antipsychotic: $F(3, 47) = 19.69$, $p < 0.0001$, prenatal treatment \times antipsychotic: $F(3, 47) = 3.86$, $p = 0.015$, Post-hoc test: 0.05 mg/kg: $p = 0.0002$, 0.1 mg/kg: $p < 0.0001$, 0.5 mg/kg: $p < 0.0001$, (A); Risperidone: Two-way ANOVA: prenatal treatment: $F(1, 32) = 1.89$, $p = 0.18$, antipsychotic: $F(2, 32) = 4.12$, $p = 0.026$, prenatal treatment \times antipsychotic: $F(2, 32) = 3.99$, $p = 0.028$, Post-hoc test: 0.01 mg/kg: $p = 0.0097$, 0.03 mg/kg: $p = 0.034$, (B); Clozapine: Two-way ANOVA: prenatal treatment: $F(1, 40) = 4.75$, $p = 0.035$, antipsychotic: $F(3, 40) = 3.30$, $p = 0.030$, prenatal

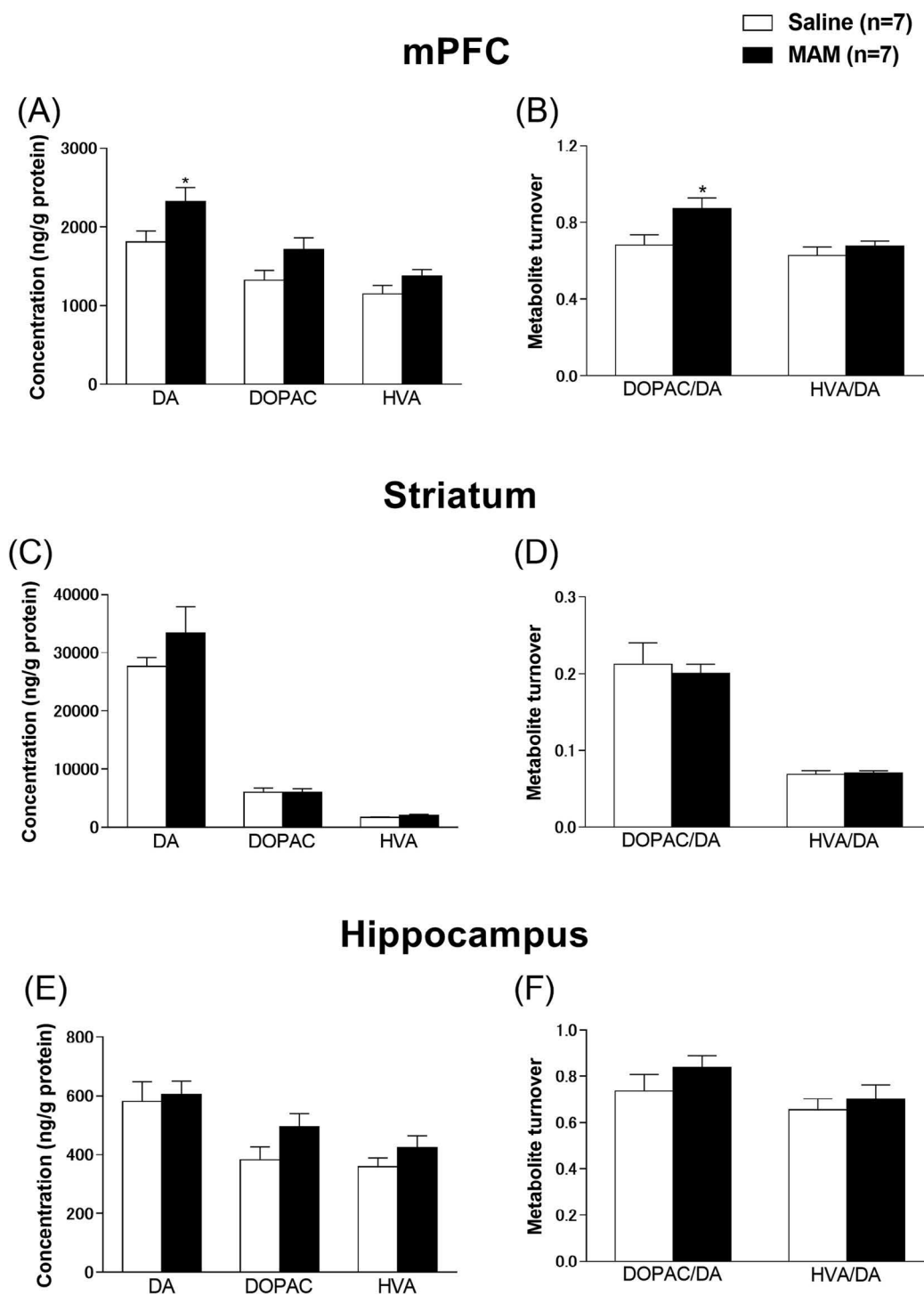


Fig. 5. Alteration of DA, DOPAC and HVA concentrations and DOPAC/DA and HVA/DA in the mPFC, striatum and hippocampus in MAM mice. Concentrations are indicated as ng per g fresh weight of brain tissue. The treatment with MAM induced an increase in the tissue levels of DA and a disturbance in the homeostasis of the dopaminergic system in the mPFC. Bars represent means \pm S.E.M. *: $p < 0.05$ vs. prenatal treatment with saline group.

treatment \times antipsychotic: $F(3, 40) = 2.47$, $p = 0.049$, Post-hoc test: 0.5 mg/kg: $p = 0.14$, 1 mg/kg: $p = 0.0091$, 3 mg/kg: $p = 0.18$, (C); Aripiprazole: Two-way ANOVA: prenatal treatment: $F(1, 45) = 2.71$, $p = 0.11$, antipsychotic: $F(3, 45) = 11.47$, $p < 0.0001$, prenatal treatment \times antipsychotic: $F(3, 45) = 2.95$, $p = 0.043$, Post-hoc test: 0.2 mg/kg: $p = 0.0006$, 1 mg/kg: $p = 0.0001$, 5 mg/kg: $p < 0.0001$, (D)]. These results indicate that prenatal MAM-induced hyperactivity by MK-801 were improved with typical and atypical antipsychotics.

3.11. Effect of antipsychotic drugs on MAM-induced deficits in social behavior

We evaluated whether haloperidol, risperidone, clozapine or aripiprazole reversed the social deficits in MAM treated mice. Haloperidol (0.05–0.5 mg/kg) did not significantly improve MAM-induced social deficits [One-way ANOVA: $F(3, 25) = 5.88$, $p = 0.0035$, Post-hoc test: 0.05 mg/kg: $p = 0.47$, 0.1 mg/kg: $p = 0.66$, 0.5 mg/kg: $p = 0.0020$,

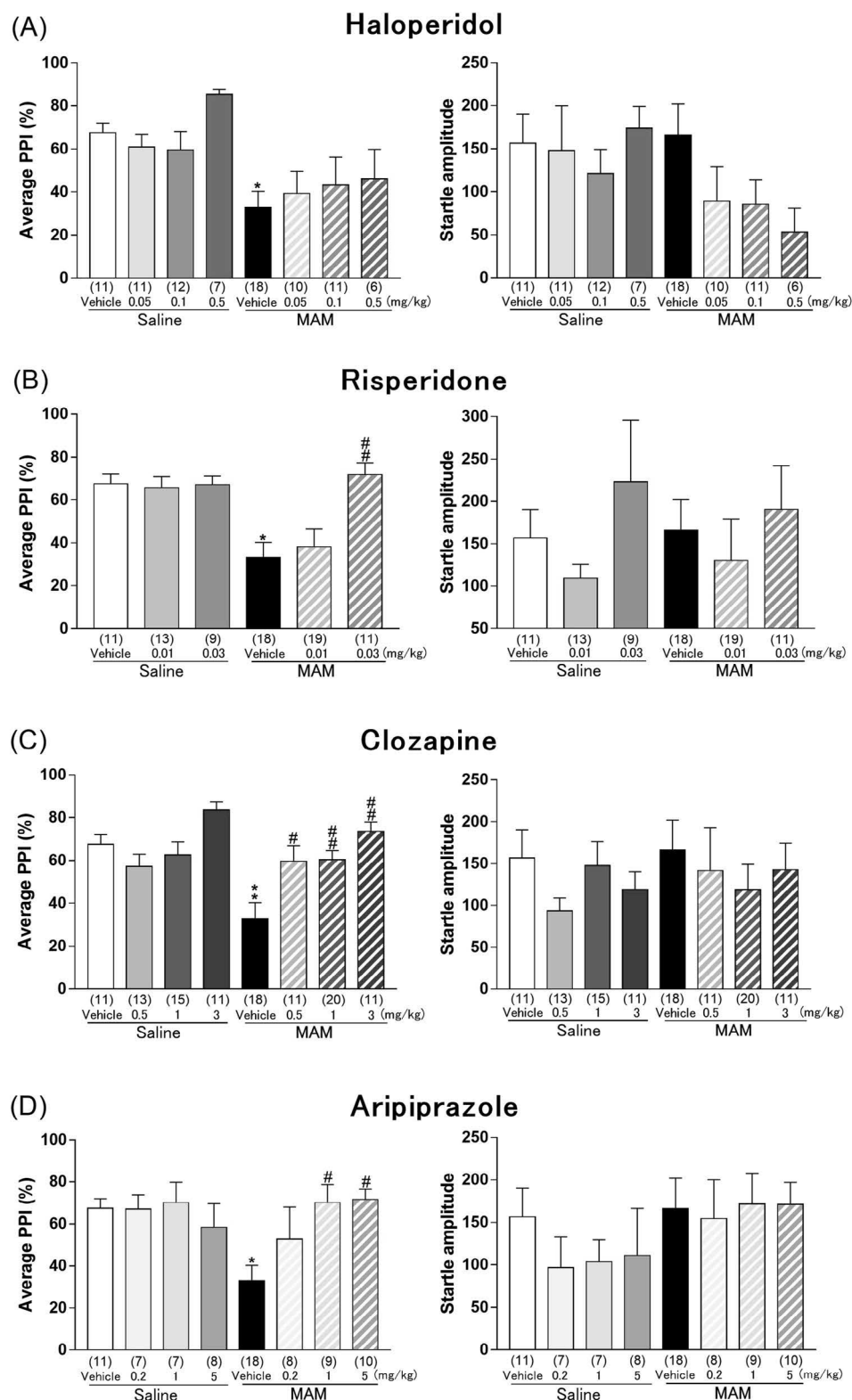


Fig. 6. Effect of haloperidol (A), risperidone (B), clozapine (C) and aripiprazole (D) on average PPI and startle amplitude in saline and MAM-treated mice. Prenatal MAM-induced PPI deficits in mice were improved with atypical antipsychotics but not with the typical antipsychotic drug haloperidol. Bars represent means \pm S.E.M. *: $p < 0.05$ and **: $p < 0.01$ vs. vehicle-treated saline group. #: $p < 0.05$ and ##: $p < 0.01$ vs. vehicle-treated MAM group.

Fig. 8 (A)]. Risperidone at 0.01 mg/kg improved the social deficits in MAM mice [One-way ANOVA: $F(2, 19) = 19.27$, $p < 0.0001$, Post-hoc test: 0.01 mg/kg: $p < 0.0001$, 0.03 mg/kg: $p = 0.075$, Fig. 8 (B)]. Clozapine at 0.5 mg/kg also improved the MAM-induced social deficit

[One-way ANOVA: $F(3, 23) = 7.52$, $p = 0.0011$, Post-hoc test: 0.5 mg/kg: $p = 0.0046$, 1 mg/kg: $p = 0.090$, 3 mg/kg: $p = 0.99$, Fig. 8 (C)]. Similarly, aripiprazole at 0.2 mg/kg improved the MAM-induced social deficits [One-way ANOVA: $F(3, 24) = 4.72$, $p = 0.010$, Post-hoc test:

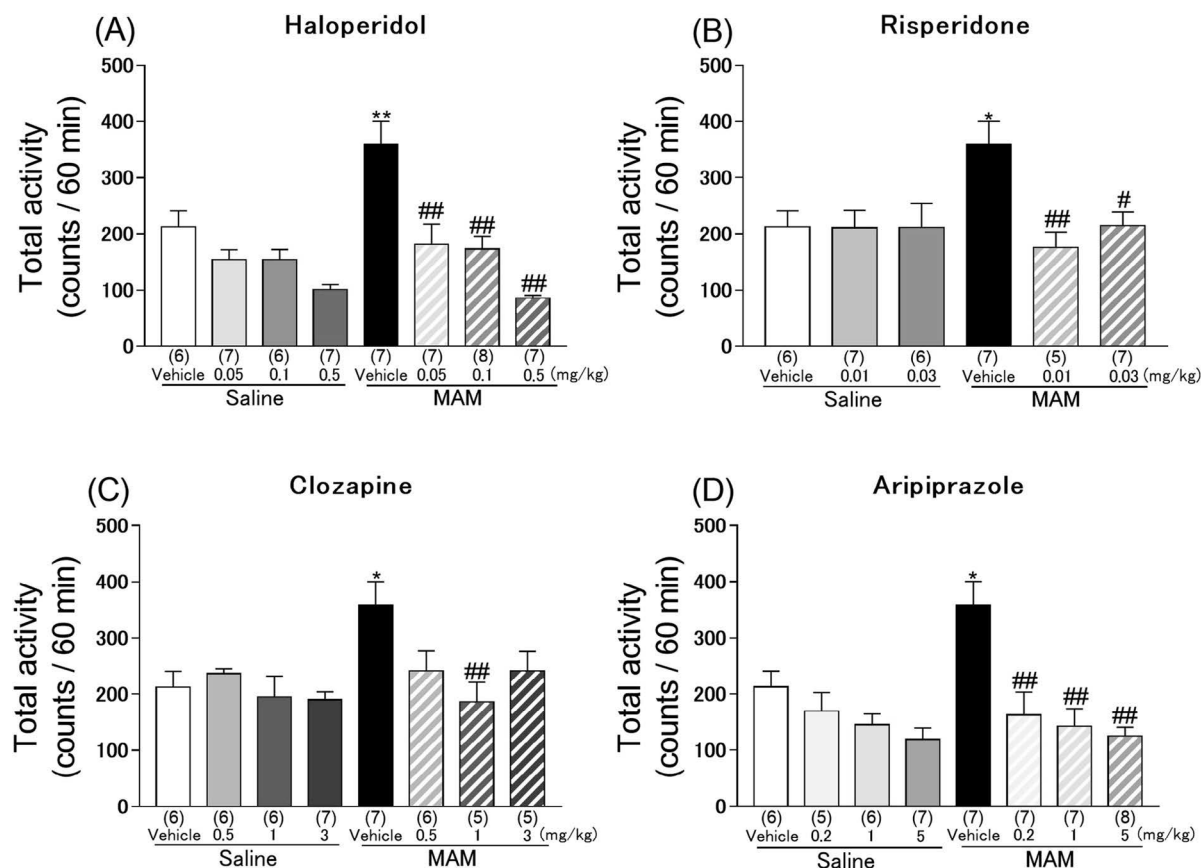


Fig. 7. Effect of haloperidol (A), risperidone (B), clozapine (C) and aripiprazole (D) on hyperactivity in saline and MAM-treated mice. Prenatal MAM-induced hyperactivity by MK-801 in mice were improved with typical and atypical antipsychotics. Bars represent means \pm S.E.M. *: $p < 0.05$ and **: $p < 0.01$ vs. vehicle-treated saline group. #: $p < 0.05$ and ##: $p < 0.01$ vs. vehicle-treated MAM group.

0.2 mg/kg: $p = 0.045$, 1 mg/kg: $p = 0.87$, 5 mg/kg: $p = 0.99$, Fig. 8 (D)]. These results indicate that prenatal MAM-induced social withdrawal were improved with atypical antipsychotics but not with the typical antipsychotic drug haloperidol.

4. Discussion

In the present study, we have examined the face, constructive and predictive validities of GD 15–17 MAM-treated mice to determine whether this model exhibits schizophrenia-like features. We initially evaluated the face validity with respect to behavioral changes such as PPI, locomotor activity, social interaction and working memory.

First, we found that mice exposed to MAM at GD 15–17 present PPI deficits during post-pubertal period, which is one of the endophenotypes of schizophrenia patients (Braff et al., 2001) and also a valid marker for sensorimotor gating in rodent models (Geyer et al., 2001). Interestingly, PPI deficits in prenatal MAM-treated rats were also observed only at post-pubertal period (Gomes et al., 2016), a finding that parallels the onset of the disorder in schizophrenia patients (Neumann et al., 1995). Secondly, we found that MK-801-induced locomotor activity was enhanced in MAM-treated mice at post-pubertal period in a similar fashion to what was observed with the neonatal ventral hippocampal (NVH) lesion rat model (Al-Amin et al., 2000). Clinical studies suggest that the antagonism of NMDA glutamatergic transmission in brain exacerbates positive symptoms of schizophrenia (Lahti et al., 1995). Thirdly, we found that GD 15–17 MAM treated mice spent less time in social interactions at both pre- and post-pubertal ages [Fig. 1 (I–L)]. Such changes have previously been observed at both pre- and post-pubertal periods in MAM-treated rats (Hazane et al., 2009) as well as in NVH lesioned rats (Sams-Dodd et al., 1997). Social

withdrawal is considered as one of the negative symptoms of schizophrenia (Mueser and McGurk, 2004) which is frequently observed before the onset of positive symptoms and is persistent (Olin and Mednick, 1996). Fourthly, we found that mice prenatally treated with MAM presented working memory deficits in the Y-maze test at post-pubertal period [Fig. 1 (M–P)]. Working memory deficits in the Y-maze test has also been reported at post-pubertal period for rats treated with MAM (Moore et al., 2006) and for NVH lesioned mice (Naert et al., 2013). In agreement, schizophrenia patients consistently present cognitive deficits involving working memory (Heinrichs and Zakzanis, 1998). From our results we can infer that treating mice with MAM on GD 15–17 can lead to behavioral deficits of relevance to positive and negative symptoms as well as cognitive dysfunctions.

Meta-analysis studies reveal that schizophrenia patients present a decrease in the volume of prefrontal cortex and hippocampus (Brugger and Howes, 2017). In the present study, the treatment with MAM resulted in a marked decrease in brain tissue weight for both the PFC and hippocampus which appears to be consistent with a previous study in rat MAM model (Flagstad et al., 2004). Studies on postmortem hippocampi of schizophrenic patients suggest that there may be a selective decrease in the number of pyramidal cells in the CA2 area which are essential for social memory (Benes et al., 1998; Hitti and Siegelbaum, 2014). In accordance, social memory deficits have been observed in patients with schizophrenia (Okuszek et al., 2017). Our MAM-treated mice also displayed a decrease in pyramidal cell density in the CA2 area compared to the control group (Fig. 3). Changes in hippocampal structure in schizophrenia patients are consistently reported in post-mortem and neuro-imaging studies (Heckers, 2004; Nelson et al., 1998). Neuronal discontinuities and heterotopias in the dorsal hippocampus observed in schizophrenia patients have also been observed in

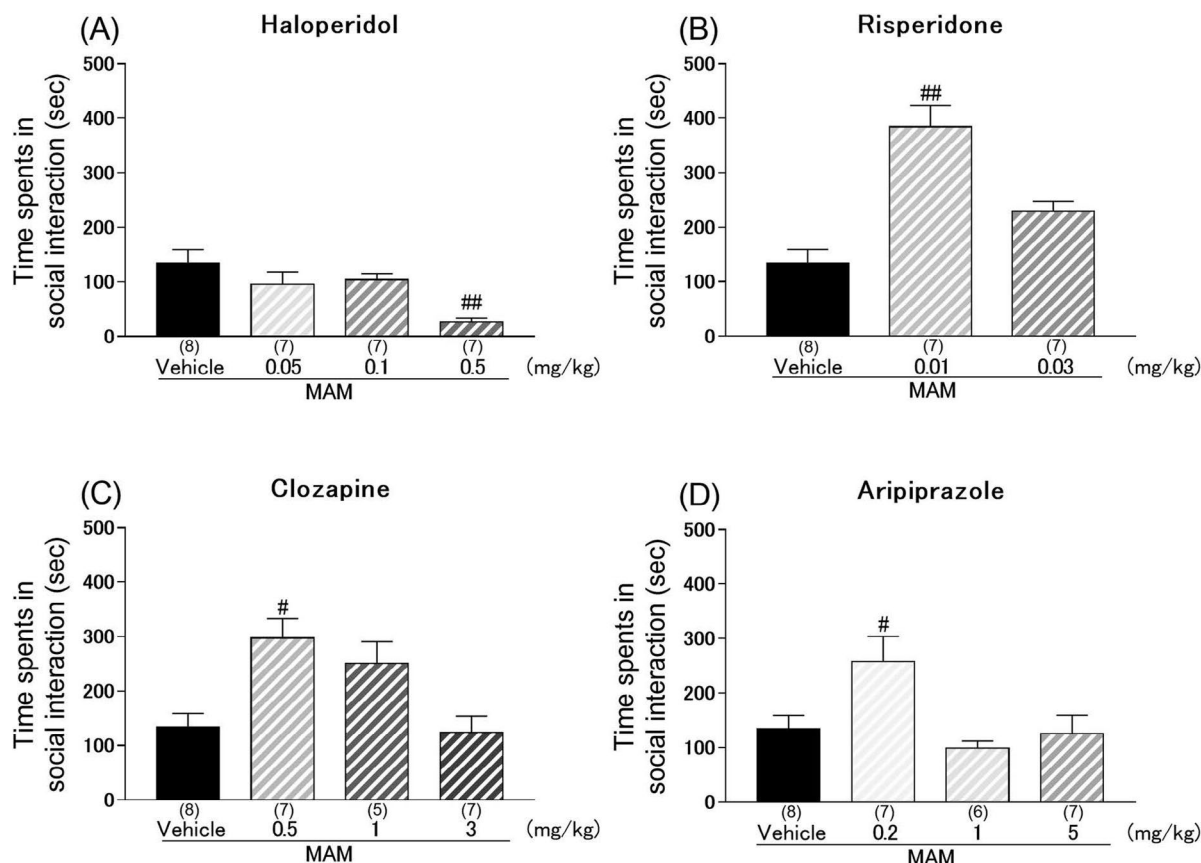


Fig. 8. Effect of haloperidol (A), risperidone (B), clozapine (C) and aripiprazole (D) on social withdrawal in saline and MAM-treated mice. Prenatal MAM-induced social withdrawal in mice were improved with atypical antipsychotics but not with the typical antipsychotic drug haloperidol. Bars represent means \pm S.E.M. #: $p < 0.05$ and ##: $p < 0.01$ vs. vehicle-treated MAM group.

the offspring of MAM-treated rat dams (Singh, 1977; Chevassus-Au-Louis et al., 1998). Consistent with these observations, we found neuronal discontinuities and heterotopias in the dorsal hippocampus in the offspring of MAM-treated pregnant mice.

Our studies show that prenatal MAM-treated mice display a decrease in cell proliferation and neurogenesis in the DG compared to the control group (Fig. 5). Some studies have suggested that a reduction in hippocampal neural stem cell proliferation may be involved in the pathogenesis of schizophrenia and an association between decreased neurogenesis and schizophrenia has been demonstrated (Allen et al., 2016; Eriksson, 2006; Iannitelli et al., 2017). Interestingly, it has been demonstrated in rodents that a reduction in hippocampal neurogenesis may lead to PPI deficits (Osumi et al., 2015), memory deficits and social withdrawal (Iwata et al., 2008). Together, these results may indicate that the schizophrenia-like behaviors induced by prenatal MAM may be related to the reductions in cell proliferation and neurogenesis we observed.

It has been demonstrated that a dysfunction in central DA efflux may be related to the positive and negative symptoms as well as the cognitive deficits of schizophrenia (Grace, 2016). DA levels and DOPAC/DA ratio in the PFC were found to be increased in the mice offspring of MAM-treated dams, which is in agreement with the enhanced cortical DA levels seen in the offspring of pregnant rats treated with MAM (Hallman and Jonsson, 1984) or after prenatal treatment with mitotic inhibitor Ara-C in rats which is proposed as a neurodevelopmental model of schizophrenia (Brown et al., 2012). Belujon et al. (2014) reported that MAM rats led to a hyperdopaminergic state and abnormally increased activity in the mPFC induced suppression of the nucleus accumbens and long-term potentiation via D_2 receptor in the mPFC. Long-term potentiation in the ventral subiculum–mPFC–

nucleus accumbens pathway plays a significant role in the performance of goal-directed behavior (Kelley, 2004; Goto and Grace, 2005a, 2005b). It is thus possible that the abnormal increased activity by hyperdopaminergic state in the mPFC may be associated with some abnormal behaviors related to schizophrenia. Interestingly, similar to our finding in the MAM mice, a clinical study has reported that schizophrenia patients show increased DA synthesis rate in the mPFC (Lindström et al., 1999). However, Abi-Dargham and colleagues suggest that schizophrenia patients exhibit reduced dopaminergic transmission in the dorsolateral PFC as revealed by neuroimaging studies (Abi-Dargham et al., 2012; Slifstein et al., 2015; Roffman et al., 2016). These paradoxical results may possibly be associated with the different of PFC regions studied in the rodents versus humans. Taken together, we suggest that hyperdopaminergic state in the mPFC of MAM mice may be associated with altered behaviors relevant to schizophrenia.

Other researchers have reported the effects of antipsychotic drugs on prenatal MAM rat model in multiple paradigms (Brown et al., 2013; Du and Grace, 2013, 2016; Goda et al., 2015; Grace and Gomes, 2018; Le Pen et al., 2011; Sonnenschein et al., 2018). This study was undertaken to evaluate the predictive validity of our mice model whether typical or atypical antipsychotic drugs could reverse the deficits in the PPI of startle reflex, hyperactivity by MK-801 and social withdrawal observed in MAM-treated mice. Using the PPI of startle paradigm or social interaction test, we showed that atypical antipsychotics such as clozapine, risperidone and the dopamine-serotonin stabilizer aripiprazole all reversed the MAM-induced sensorimotor gating deficits and social withdrawal. In contrast the typical antipsychotic haloperidol could not reverse the PPI deficits and social withdrawal in these mice. On the other hand, we found that hyperactivity by MK-801 in MAM mice was reversed by both typical and atypical antipsychotics, results

that are consistent with previous studies in MAM rat model (Le Pen et al., 2011). These results suggest that PPI deficits and social withdrawal may be particularly sensitive to some critical characteristics related to the “atypicality” of those antipsychotic drugs while alterations of DA neurotransmission may be responsible for hyperactivity by MK-801. Clinical studies reported that atypical antipsychotics such as clozapine or ziprasidone, but not typical antipsychotic haloperidol-treated schizophrenic patients occasionally showed normalization of PPI (Kumari et al., 1999; Braff et al., 1992) and negative symptoms (Stahl et al., 2010). Moreover, clinical efficacy of antipsychotic drugs for positive symptoms is correlated with their ability to block subcortical D₂ receptors (Creese et al., 1976; Seeman and Lee, 1975), suggesting DA signal is important. Thus, atypical antipsychotics such as clozapine, risperidone and aripiprazole probably interact with brain systems affected by the MAM treatment through their action on receptors other than DA receptors to normalize PPI deficits and social withdrawal, while all typical and atypical antipsychotics may improve hyperactivity by MK-801 via inhibition of D₂ receptors. In contrast to haloperidol, atypical antipsychotics also interact with 5HT_{2A}, α₂ adrenergic, muscarinic and histaminergic receptors, among others (Bymaster et al., 2003; Citrome, 2014; Kusumi et al., 2015). Any or all of these receptors could play an important role for the unique action of atypical antipsychotics in our mice model. Taken together, the data suggest that the MAM mice model may be useful for the screening of novel antipsychotic drugs for negative symptoms of schizophrenia.

In conclusion, we have established a MAM model in mice that displays behavioral changes similar to what has been found in MAM treated rats including neurodevelopment-dependent onset of behavioral alterations such as PPI deficits, hypersensitivity to MK-801, social interaction deficits and cognitive deficits. Moreover, the prenatal treatment with MAM led to a decrease in brain weight (notably in the PFC and hippocampus), cytoarchitectural alterations such as discontinues and heterotopias, reductions in cell proliferation and neurogenesis, as well as an increase of DA content and turnover in the PFC. The behavioral, anatomical and neurophysiological changes are more consistent with those observed in schizophrenia patients than prenatal MAM rat models. Moreover, we found for the first time that atypical antipsychotic drugs reversed MAM-induced PPI deficits and social withdrawal. We believe that prenatal GD 15–17 administration of MAM in mice may offer a new means to study neurobiological mechanisms involved in the pathophysiology of schizophrenia.

Acknowledgments

This study was supported in part by Grants-in-Aid for Scientific Research (Grant number 18K06687) and Matching Fund Subsidy for Private University from the Ministry of Education, Culture, Sports, Science and Technology of Japan (Grant number S1511001L). The authors would like to thank Ms. Anna Mori, Ms. Kaoru Takano, Mr. Daiki Hasegawa and Mr. Daisuke Tezuka of Tohoku Medical and Pharmaceutical University for their technical assistance and Prof. Remi Quirion of McGill University for experimental advice.

Appendix A. Supplementary data

Supplementary data to this article can be found online at <https://doi.org/10.1016/j.neuropharm.2019.02.034>.

References

- Abi-Dargham, A., Xu, X., Thompson, J.L., Gil, R., Kegeles, L.S., Urban, N., Narendran, R., Hwang, D.R., Laruelle, M., Slifstein, M., 2012. Increased prefrontal cortical D1 receptors in drug naive patients with schizophrenia: a PET study with [¹¹C]NNC112. *J. Psychopharmacol.* 26, 794–805.
- Al-Amin, H.A., Weinberger, D.R., Lipska, B.K., 2000. Exaggerated MK-801-induced motor hyperactivity in rats with the neonatal lesion of the ventral hippocampus. *Behav. Pharmacol.* 11, 269–278.
- Allen, K.M., Fung, S.J., Weickert, C.S., 2016. Cell proliferation is reduced in the hippocampus in schizophrenia. *Aust. N. Z. J. Psychiatr.* 50, 473–480.
- Alsio, J.M., Tarchini, B., Cayouette, M., Livesey, F.J., 2013. Ikaros promotes early-born neuronal fates in the cerebral cortex. *Proc. Natl. Acad. Sci. U. S. A.* 110, E716–E725.
- Bayer, S.A., Altman, J., 2004. Development of the telencephalon: neural stem cells, neurogenesis, and neuronal migration. In: Paxinos, G. (Ed.), *The Rat Nervous System*, third ed. Academic Press, London, pp. 27–73.
- Benes, F.M., Kwok, E.W., Vincent, S.L., Todtenkopf, M.S., 1998. A reduction of non-pyramidal cells in sector CA2 of schizophrenics and manic depressives. *Biol. Psychiatry* 44, 88–97.
- Belujon, P., Patton, M.H., Grace, A.A., 2014. Role of the prefrontal cortex in altered hippocampal-accumbens synaptic plasticity in a developmental animal model of schizophrenia. *Cerebr. Cortex* 24, 968–977.
- Boks, P., 2004. Animal models of obstetric complications in relation to schizophrenia. *Brain Res. Rev.* 45, 1–17.
- Braff, D.L., Geyer, M.A., Swerdlow, N.R., 2001. Human studies of prepulse inhibition of startle: normal subjects, patient groups, and pharmacological studies. *Psychopharmacology (Berlin)* 156, 234–258.
- Braff, D.L., Grillon, C., Geyer, M.A., 1992. Gating and habituation of the startle reflex in schizophrenic patients. *Arch. Gen. Psychiatr.* 49, 206–215.
- Brown, J.W., Whitehead, C.A., Basso, A.M., Rueter, L.E., Zhang, M., 2013. Preclinical evaluation of non-imidazole histamine H3 receptor antagonists in comparison to atypical antipsychotics for the treatment of cognitive deficits associated with schizophrenia. *Int. J. Neuropsychopharmacol.* 16, 9–904.
- Brown, P.L., Shepard, P.D., Elmer, G.I., Stockman, S., McFarland, R., Mayo, C.L., Cadet, J.L., Krasnova, I.N., Greenwald, M., Schoonover, C., Vogel, M.W., 2012. Altered spatial learning, cortical plasticity and hippocampal anatomy in a neurodevelopmental model of schizophrenia-related endophenotypes. *Eur. J. Neurosci.* 36, 2773–2781.
- Brugger, S.P., Howes, O.D., 2017. Heterogeneity and homogeneity of regional brain structure in schizophrenia: a meta-analysis. *JAMA Psychiatry* 74, 1104–1111.
- Bymaster, F.P., Felder, C.C., Tzavara, E., Nomikos, G.G., Calligaro, D.O., McKinzie, D.L., 2003. Muscarinic mechanisms of antipsychotic atypicality. *Prog. Neuro-Psychopharmacol. Biol. Psychiatry* 27, 1125–1143.
- Cattabeni, F., Di Luca, M., 1997. Developmental models of brain dysfunctions induced by targeted cellular ablations with methylazoxymethanol. *Physiol. Rev.* 77, 199–215.
- Creese, I., Burt, D.R., Snyder, S.H., 1976. Dopamine receptor binding predicts clinical and pharmacological potencies of antischizophrenic drugs. *Science* 192, 481–483.
- Chalkiadaki, K., Velli, A., Kyriazidis, E., Stavroulaki, V., Vouvoutsis, V., Chatzaki, E., Aivaliotis, M., Sidiropoulou, K., 2018. Development of the MAM model of schizophrenia in mice: sex similarities and differences of hippocampal and prefrontal cortical function. *Neuropharmacology* 144, 193–207.
- Chen, L., Perez, S.M., Lodge, D.J., 2014. An augmented dopamine system function is present prior to puberty in the methylazoxymethanol acetate rodent model of schizophrenia. *Dev. Neurobiol.* 74, 907–917.
- Chevassus-Au-Louis, N., Rafiki, A., Jorquera, I., Ben-Ari, Y., Represa, A., 1998. Neocortex in the hippocampus: an anatomical and functional study of CA1 heterotopias after prenatal treatment with methylazoxymethanol in rats. *J. Comp. Neurol.* 394, 520–536.
- Citrome, L., 2014. Asenapine review, part I: chemistry, receptor affinity profile, pharmacokinetics and metabolism. *Expert Opin. Drug Metabol. Toxicol.* 10, 893–903.
- Du, Y., Grace, A.A., 2013. Peripubertal diazepam administration prevents the emergence of dopamine system hyperresponsivity in the MAM developmental disruption model of schizophrenia. *Neuropsychopharmacology* 38, 1881–1888.
- Du, Y., Grace, A.A., 2016. Amygdala hyperactivity in MAM model of schizophrenia is normalized by peripubertal diazepam administration. *Neuropsychopharmacology* 41, 2455–2462.
- Eriksson, P.S., 2006. Schizophrenia—a stem cell disorder. *Exp. Neurol.* 199, 26–27.
- Flagstad, P., Mørk, A., Glenthøj, B.Y., van, Beek, J., Michael-Titus, A.T., Didriksen, M., 2004. Disruption of neurogenesis on gestational day 17 in the rat causes behavioral changes relevant to positive and negative schizophrenia symptoms and alters amphetamine-induced dopamine release in nucleus accumbens. *Neuropsychopharmacology* 29, 2052–2064.
- Gaspard, N., Bouschet, T., Hourez, R., Dimidschstein, J., Naeije, G., van, den, Ameerle, J., Espuny-Camacho, I., Herpoel, A., Passante, L., Schiffmann, S.N., Gaillard, A., Vanderhaeghen, P., 2008. An intrinsic mechanism of corticogenesis from embryonic stem cells. *Nature* 455, 351–357.
- Geyer, M.A., Krebs-Thomson, K., Braff, D.L., Swerdlow, N.R., 2001. Pharmacological studies of prepulse inhibition models of sensorimotor gating deficits in schizophrenia: a decade in review. *Psychopharmacology (Berlin)* 156, 117–154.
- Goda, S.A., Olszewski, M., Piasecka, J., Rejniak, K., Whittington, M.A., Kasicki, S., Hunt, M.J., 2015. Aberrant high frequency oscillations recorded in the rat nucleus accumbens in the methylazoxymethanol acetate neurodevelopmental model of schizophrenia. *Prog. Neuro-Psychopharmacol. Biol. Psychiatry* 61, 44–51.
- Gomes, F.V., Rincón-Cortés, M., Grace, A.A., 2016. Adolescence as a period of vulnerability and intervention in schizophrenia: insights from the MAM model. *Neurosci. Biobehav. Rev.* 70, 260–270.
- Goto, Y., Grace, A.A., 2005a. Dopamine-dependent interactions between limbic and prefrontal cortical plasticity in the nucleus accumbens: disruption by cocaine sensitization. *Neuron* 47, 255–266.
- Goto, Y., Grace, A.A., 2005b. Dopaminergic modulation of limbic and cortical drive of nucleus accumbens in goal-directed behavior. *Nat. Neurosci.* 8, 805–812.
- Grace, A.A., 2016. Dysregulation of the dopamine system in the pathophysiology of schizophrenia and depression. *Nat. Rev. Neurosci.* 17, 524–532.
- Grace, A.A., Gomes, F.V., 2018. The circuitry of dopamine system regulation and its disruption in schizophrenia: insights into treatment and prevention. *Schizophr. Bull.*

- (in press).
- Guo, N., Yoshizaki, K., Kimura, R., Suto, F., Yanagawa, Y., Osumi, N., 2013. A sensitive period for GABAergic interneurons in the dentate gyrus in modulating sensorimotor gating. *J. Neurosci.* 33, 6691–6704.
- Hallman, H., Jonsson, G., 1984. Monoamine neurotransmitter metabolism in micro-encephalic rat brain after prenatal methylazoxymethanol treatment. *Brain Res. Bull.* 13, 383–389.
- Hazane, F., Krebs, M.O., Jay, T.M., Le Pen, G., 2009. Behavioral perturbations after prenatal neurogenesis disturbance in female rat. *Neurotox. Res.* 15, 311–320.
- Heckers, S., 2004. The hippocampus in schizophrenia. *Am. J. Psychiatry* 161, 2138–2139.
- Heinrichs, R.W., Zakzanis, K.K., 1998. Neurocognitive deficit in schizophrenia: a quantitative review of the evidence. *Neuropsychology* 12, 426–445.
- Hitti, F.L., Siegelbaum, S.A., 2014. The hippocampal CA2 region is essential for social memory. *Nature* 508, 88–92.
- Hoareau, C., Hazane, F., Le Pen, G., Krebs, M.O., 2006. Postnatal effect of embryonic neurogenesis disturbance on reelin level in organotypic cultures of rathippocampus. *Brain Res.* 1097, 43–51.
- Huo, C., Liu, X., Zhao, J., Zhao, T., Huang, H., Ye, H., 2018. Abnormalities in behaviour, histology and prefrontal cortical gene expression profiles relevant to schizophrenia in embryonic day 17 MAM-Exposed C57BL/6 mice. *Neuropharmacology* 140, 287–301.
- Iannitelli, A., Quartini, A., Tirassa, P., Bersani, G., 2017. Schizophrenia and neurogenesis: a stem cell approach. *Neurosci. Biobehav. Rev.* 80, 414–442.
- Iwata, Y., Suzuki, K., Wakuda, T., Seki, N., Thanseem, I., Matsuzaki, H., Mamiya, T., Ueki, T., Mikawa, S., Sasaki, T., Suda, S., Yamamoto, S., Tsuchiya, K.J., Sugihara, G., Nakamura, K., Sato, K., Takei, N., Hashimoto, K., Mori, N., 2008. Irradiation in adulthood as a new model of schizophrenia. *PLoS One* 3, e2283.
- Kelley, A.E., 2004. Ventral striatal control of appetitive motivation: role in ingestive behavior and reward-related learning. *Neurosci. Biobehav. Rev.* 27, 765–776.
- Kesby, J.P., Eyles, D.W., McGrath, J.J., Scott, J.G., 2018. Dopamine, psychosis and schizophrenia: the widening gap between basic and clinical neuroscience. *Transl. Psychiatry* 8, 30.
- Kumari, V., Soni, W., Sharma, T., 1999. Normalization of information processing deficits in schizophrenia with clozapine. *Am. J. Psychiatry* 156, 1046–1051.
- Kusumi, I., Boku, S., Takahashi, Y., 2015. Psychopharmacology of atypical antipsychotic drugs: from the receptor binding profile to neuroprotection and neurogenesis. *Psychiatr. Clin. Neurosci.* 69, 243–258.
- Lahti, A.C., Koffel, B., LaPorte, D., Tamminga, C.A., 1995. Subanesthetic doses of ketamine stimulate psychosis in schizophrenia. *Neuropsychopharmacology* 13, 9–19.
- Laplanche, F., Nakagawasai, O., Srivastava, L.K., Quirion, R., 2005. Alterations in behavioral responses to a cholinergic agonist in post-pubertal rats with neonatal ventral hippocampal lesions: relationship to changes in muscarinic receptor levels. *Neuropsychopharmacology* 30, 1076–1087.
- Le Pen, G., Jay, T.M., Krebs, M.O., 2011. Effect of antipsychotics on spontaneous hyperactivity and hypersensitivity to MK-801-induced hyperactivity in rats prenatally exposed to methylazoxymethanol. *J. Psychopharmacol.* 25, 822–835.
- Lindström, L.H., Gefvert, O., Hagberg, G., Lundberg, T., Bergström, M., Hartvig, P., Långström, B., 1999. Increased dopamine synthesis rate in medial prefrontal cortex and striatum in schizophrenia indicated by L-(beta-11C) DOPA and PET. *Biol. Psychiatry* 46, 681–688.
- Lipska, B.K., Weinberger, D.R., 2000. To model a psychiatric disorder in animals: schizophrenia as a reality test. *Neuropsychopharmacology* 23, 223–239.
- Moore, H., Jentsch, J.D., Ghajarnia, M., Geyer, M.A., Grace, A.A., 2006. A neurobehavioral systems analysis of adult rats exposed to methylazoxymethanol acetate on E17: implications for the neuropathology of schizophrenia. *Biol. Psychiatry* 60, 253–264.
- Mouri, A., Koseki, T., Narusawa, S., Niwa, M., Mamiya, T., Kano, S., Sawa, A., Nabeshima, T., 2012. Mouse strain differences in phencyclidine-induced behavioural changes. *Int. J. Neuropsychopharmacol.* 15, 767–779.
- Mueser, K.T., McGurk, S.R., 2004. Schizophrenia. *Lancet* 363, 2063–2072.
- Naert, A., Gantois, I., Laeremans, A., Vreysen, S., Van, den, Bergh, G., Arckens, L., Callaerts-Vegh, Z., D'Hooge, R., 2013. Behavioural alterations relevant to developmental brain disorders in mice with neonatally induced ventral hippocampal lesions. *Brain Res. Bull.* 94, 71–81.
- Nelson, M.D., Saykin, A.J., Flashman, L.A., Riordan, H.J., 1998. Hippocampal volume reduction in schizophrenia as assessed by magnetic resonance imaging: a meta-analytic study. *Arch. Gen. Psychiatr.* 55, 433–440.
- Neumann, C.S., Grimes, K., Walker, E.F., Baum, K., 1995. Developmental pathways to schizophrenia: behavioral subtypes. *J. Abnorm. Psychol.* 104, 558–566.
- Okruszek, Ł., Bala, A., Wordecha, M., Jarkiewicz, M., Wysokiński, A., Szczepocka, E., Piejka, A., Zaborowska, O., Szantoch, M., Rysz, A., Marchel, A., 2017. Social cognition in neuropsychiatric populations: a comparison of theory of mind in schizophrenia and mesial temporal lobe epilepsy. *Sci. Rep.* 7, 484.
- Olin, S.C.S., Mednick, S.A., 1996. Risk factors of psychosis: identifying vulnerable populations premorbidly. *Schizophr. Bull.* 22, 223–240.
- Osumi, N., Guo, N., Matsumata, M., Yoshizaki, K., 2015. Neurogenesis and sensorimotor gating: bridging a microphenotype and an endophenotype. *Curr. Mol. Med.* 15, 129–137.
- Palanza, P., Morley-Fletcher, S., Laviola, G., 2001. Novelty seeking in periadolescent mice: sex differences and influence of intrauterine position. *Physiol. Behav.* 72, 255–262.
- Rapoport, J.L., Addington, A.M., Frangou, S., Psych, M.R., 2005. The neurodevelopmental model of schizophrenia: update 2005. *Mol. Psychiatr.* 10, 434–449.
- Roffman, J.L., Tanner, A.S., Eryilmaz, H., Rodriguez-Thompson, A., Silverstein, N.J., Ho, N.F., Nitenson, A.Z., Chonde, D.B., Greve, D.N., Abi-Dargham, A., Buckner, R.L., Manoach, D.S., Rosen, B.R., Hooker, J.M., Catana, C., 2016. Dopamine D1 signaling organizes network dynamics underlying working memory. *Sci. Adv.* 2, e1501672.
- Sams-Dodd, F., Lipska, B.K., Weinberger, D.R., 1997. Neonatal lesions of the rat ventral hippocampus result in hyperlocomotion and deficits in social behaviour in adulthood. *Psychopharmacology (Berlin)* 132, 303–310.
- Seeman, P., Lee, T., 1975. Antipsychotic drugs: direct correlation between clinical potency and presynaptic action on dopamine neurons. *Science* 188, 1217–1219.
- Sidman, R.L., Rakic, P., 1973. Neuronal migration, with special reference to developing human brain: a review. *Brain Res.* 62, 1–35.
- Singh, S.C., 1977. Ectopic neurones in the hippocampus of the postnatal rat exposed to methylazoxymethanol during foetal development. *Acta Neuropathol.* 40, 111–116.
- Slifstein, M., van, de, Giessen, E., Van, Snellenberg, J., Thompson, J.L., Narendran, R., Gil, R., Hackett, E., Girgis, R., Ojeil, N., Moore, H., D'Souza, D., Malison, R.T., Huang, Y., Lim, K., Nabulsi, N., Carson, R.E., Lieberman, J.A., Abi-Dargham, A., 2015. Deficits in prefrontal cortical and extrastriatal dopamine release in schizophrenia: a positron emission tomographic functional magnetic resonance imaging study. *JAMA Psychiatry* 72, 316–324.
- Sonnenschein, S.F., Gill, K.M., Grace, A.A., 2018. State-dependent effects of the D2 partial agonist aripiprazole on dopamine neuron activity in the MAM neurodevelopmental model of schizophrenia. *Neuropsychopharmacology* (in press).
- Stahl, S.M., Malla, A., Newcomer, J.W., Potkin, S.G., Weiden, P.J., Harvey, P.D., Loebel, A., Watsky, E., Siu, C.O., Romano, S., 2010. A post hoc analysis of negative symptoms and psychosocial function in patients with schizophrenia: a 40-week randomized, double-blind study of ziprasidone versus haloperidol followed by a 3-year double-blind extension trial. *J. Clin. Psychopharmacol.* 30, 425–430.
- Sugimoto, Y., Kajiwara, Y., Hirano, K., Yamada, S., Tagawa, N., Kobayashi, Y., Hotta, Y., Yamada, J., 2008. Mouse strain differences in immobility and sensitivity to fluvoxamine and desipramine in the forced swimming test: analysis of serotonin and noradrenaline transporter binding. *Eur. J. Pharmacol.* 592, 116–122.
- Tanda, K., Nishi, A., Matsuo, N., Nakanishi, K., Yamasaki, N., Sugimoto, T., Toyama, K., Takao, K., Miyakawa, T., 2009. Abnormal social behavior, hyperactivity, impaired remote spatial memory, and increased D1-mediated dopaminergic signaling in neuronal nitric oxide synthase knockout mice. *Mol. Brain* 2, 19.
- Tandon, R., Nasrallah, H.A., Keshavan, M.S., 2009. Schizophrenia, "just the facts" 4. Clinical features and conceptualization. *Schizophr. Res.* 110, 1–23.
- Waddington, J.L., Lane, A., Larkin, C., O'Callaghan, E., 1999. The neurodevelopmental basis of schizophrenia: clinical clues from cerebrocraniofacial dysmorphogenesis, and the roots of a lifetime trajectory of disease. *Biol. Psychiatry* 46, 31–39.
- Workman, A.D., Charvet, C.J., Clancy, B., Darlington, R.B., Finlay, B.L., 2013. Modeling transformations of neurodevelopmental sequences across mammalian species. *J. Neurosci.* 33, 7368–7383.



Involvement of catecholaminergic and GABAergic mediations in the anxiety-related behavior in long-term powdered diet-fed mice

Fukie Yaoita^{a,*}, Masahiro Tsuchiya^b, Yuichiro Arai^c, Takeshi Tadano^d, Koichi Tan-No^a

^a Department of Pharmacology, Faculty of Pharmaceutical Sciences, Tohoku Medical and Pharmaceutical University, 4-4-1 Komatsushima, Aoba-ku, Sendai, 981-8558, Japan

^b Department of Nursing, Tohoku Fukushi University, 1-8-1 Kunimi, Aoba-ku, Sendai, 981-8522, Japan

^c Tokyo Ariake University of Medical and Health Science, 2-9-1 Ariake, Koto-Ku, Tokyo, 135-0063, Japan

^d Complementary and Alternative Medicine Clinical Research and Development, Graduate School of Medicine Sciences, Kanazawa University, Kakumamachi, Kanazawa, 920-1192, Japan

ARTICLE INFO

Keywords:

Atomoxetine
Methylphenidate
PD168077
Anxiety-related behavior
Low anxiety
Bicuculline
Attention deficit/hyperactivity disorder

ABSTRACT

Dietary habits are important factors which affect metabolic homeostasis and the development of emotion. We have previously shown that long-term powdered diet feeding in mice increases spontaneous locomotor activity and social interaction (SI) time. Moreover, that diet causes changes in the dopaminergic system, especially increased dopamine turnover and decreased dopamine D4 receptor signals in the frontal cortex. Although the increased SI time indicates low anxiety, the elevated plus maze (EPM) test shows anxiety-related behavior and impulsive behavior. In this study, we investigated whether the powdered diet feeding causes changes in anxiety-related behavior. Mice fed a powdered diet for 17 weeks from weaning were compared with mice fed a standard diet (control). The percentage (%) of open arm time and total number of arm entries were increased in powdered diet-fed mice in the EPM test. We also examined the effects of diazepam, benzodiazepine anti-anxiety drug, bicuculline, GABA-A receptor antagonist, methylphenidate, dopamine transporter (DAT) and noradrenaline transporter (NAT) inhibitor, atomoxetine, selective NAT inhibitor, GBR12909, selective DAT inhibitor, and PD168077, selective dopamine D4 receptor agonist, on the changes of the EPM in powdered diet-fed mice. Methylphenidate and atomoxetine are clinically used to treat attention deficit/hyperactivity disorder (ADHD) symptoms. The % of open arm time in powdered diet-fed mice was decreased by treatments of atomoxetine, methylphenidate and PD168077. Diazepam increased the % of open arm time in control diet-fed mice, but not in powdered diet-fed mice. The powdered diet feeding induced a decrease in GABA transaminase, GABA metabolic enzymes, in the frontal cortex. Moreover, the powdered diet feeding induced an increase in NAT expression, but not DAT expression, in the frontal cortex. These results suggest that the long-term powdered diet feeding may cause low anxiety or impulsivity, possibly via noradrenergic and/or dopaminergic, and GABAergic mediations and increase the risk for onset of ADHD-like behaviors.

1. Introduction

Various changes brought on by modern lifestyle have caused an increased risk of disease. Dietary habits are particularly important factors which affect development of the central nervous system as well as emotion (Aoki et al., 2005; Kushida et al., 2008; Mitome et al., 2005; Nijijima-Yaoita et al., 2013; Yamamoto and Hirayama, 2001). It has been suggested that evolutionary changes in dietary habit to softer

foods in part explain lesser developed masticatory function (Yamanaka et al., 2009). We recently reported that long-term powdered diet feeding in mice increases spontaneous locomotor activity and social interaction (SI) time of SI test. Moreover, this diet causes changes in the dopaminergic system, in particular, increased dopamine turnover and decreased dopamine D4 receptor signals in the frontal cortex (Nijijima-Yaoita et al., 2013). However, some reports suggest that the impairment of dopaminergic activity in the hippocampus may be related to the

Abbreviations: ADHD, attention deficit/hyperactivity disorder; ANOVA, analysis of variance; BZD, benzodiazepines; DAT, dopamine transporter; EPM, elevated plus maze; GABA-A, γ -amino butyric acid receptor type A; GAPDH, glyceraldehyde-3-phosphate dehydrogenase; i.p., intraperitoneally; NA, noradrenaline; NAT, noradrenaline transporter; % of open arm time, percentage of time spent in the open arm; SI, social interaction; T-PBS, Tween-20 in phosphate-buffered saline

* Corresponding author.

E-mail address: nijijima@tohoku-mpu.ac.jp (F. Yaoita).

<https://doi.org/10.1016/j.neuint.2018.12.002>

Received 25 September 2018; Received in revised form 30 November 2018; Accepted 4 December 2018

Available online 07 December 2018

0197-0186/ © 2018 Elsevier Ltd. All rights reserved.

masticatory dysfunction induced by powdered diet feeding (Kushida et al., 2008; Yoshino et al., 2012).

In addition to the SI test, the elevated plus maze (EPM) test is useful for evaluating anxiety-related behavior (File, 1992). It is known that γ -amino butyric acid type A (GABA-A) receptor plays a critical role in anxiolytic activity. GABA-A receptor is a chloride channel composed of a pentameric hetero-oligomeric protein with binding sites for GABA, benzodiazepines (BZD), barbiturates, and steroids, etc. The activation of the GABA-A receptor induced by BZD including diazepam increases the percentage (%) of open arm time in the EPM test, indicating low anxiety (i.e. anxiolytic effect) (for review see Jacob et al., 2008; Möhler et al., 2002). On the other hand, Hwang et al. (2004) reported that the increase in expression of GABA transaminase and GABA metabolic enzymes, provide important information about the brain with GABA dysfunction. Moreover, the GABA transaminase has been primarily investigated in relation to epilepsy, but it has also been found that a decrease in GABA neurotransmission appears to be involved in the aetiology of several neurological disorders such as anxiety (for review see Kowalczyk and Kulig, 2014).

Attention deficit/hyperactivity disorder (ADHD) is a neurodevelopmental disorder characterized by inattention, hyperactivity, and impulsivity. Using the ADHD animal model, impulsive behavior can be evaluated by the EPM test (Kishikawa et al., 2014; Niimi et al., 2011; Ueno et al., 2002). This test is designed to detect anxiety-related behavior but it also reflects impulsivity for novelty seeking.

The frontal cortex is an important brain region which is related to ADHD symptoms, including impulsive behavior (for reviews see Arnsten and Pliszka, 2011; Brevet-Aeby et al., 2016; Herman et al., 2018). The etiology and pathophysiology of ADHD have not been completely clarified, however the prefrontal cortex is known to be particularly sensitive to the neurochemical environment; relatively slight changes in the levels of noradrenaline (NA) and dopamine can produce significant changes in its function (for review see Arnsten and Pliszka, 2011). Although newer drugs have been developed, methylphenidate and atomoxetine remain the predominantly prescribed drugs for the treatment of ADHD. Methylphenidate increases extracellular dopamine and NA indirectly by blocking the transporters, dopamine transporter (DAT) and NA transporter (NAT), while atomoxetine preferentially inhibits NAT (for review see Arnsten and Pliszka, 2011).

The aims of the present mice study on were to investigate the following: (a) whether long-term powdered diet feeding induces changes in anxiety-related behavior in the EPM test, (b) the effect of diazepam, benzodiazepine anti-anxiety drug, bicuculline, a GABA-A receptor antagonist, GBR12909, a selective DAT inhibitor, methylphenidate, DAT and NAT inhibitor, atomoxetine, a selective NAT inhibitor and PD168077, a selective dopamine D4 receptor agonist, on the changes in the EPM test, and (c) GABA transaminase expressions in the frontal cortex, DAT and NAT expressions in the frontal cortex and hippocampus.

2. Materials and methods

2.1. Animal treatment

Male Balb/c mice (3 weeks old) were obtained from Japan CREA (Tokyo, Japan). The animals were housed under conditions of constant temperature ($23 \pm 1^\circ\text{C}$) and humidity ($55 \pm 5\%$), on a 12/12 h light–dark cycle (light from 7 to 19 h; dark from 19 to 7 h). The mice were housed in groups of 5–6 in standard plastic cages (30 cm \times 20 cm \times 14 cm high) with wire mesh lids and a bedding of wood shavings. Mice were fed either a control diet (pellet type Labo MR stock, Nihon Nosan, Kanagawa, Japan) or powdered diet (powder type Labo MR stock, Nihon Nosan) containing the same ingredients with free access to water for 17 weeks. All experiments complied with the Guidelines for Care and Use of Laboratory Animals issued by Tohoku Medical and Pharmaceutical University.

2.2. Drugs and treatment

The following drugs were used: diazepam (Sigma–Aldrich, St. Louis, MO, USA), bicuculline (GABA-A receptor antagonist, Tocris Bioscience, Bristol, UK), methylphenidate (Novartis Pharma, Tokyo, Japan), atomoxetine (selective NET inhibitor, Sigma–Aldrich) and GBR12909 (selective DAT inhibitor, Tocris Bioscience). Diazepam, bicuculline and PD168077 (selective dopamine D4 receptor agonist, Sigma–Aldrich) were suspended in saline containing 0.5% Tween 80. Methylphenidate, atomoxetine and GBR12909 were dissolved in saline. All drugs were administered intraperitoneally (i.p.) (volume: 0.1 ml/10 g body weight) at 30 min before the behavioral test. The drug doses used in the present study were within the ranges widely used in experiments on mice and rats (Gould et al., 2005; Hiraide et al., 2013; Kanegawa et al., 2010; Leggio et al., 2011; Nijima et al., 2006; Nijima-Yaoita et al., 2013; Robinson et al., 2012; Ueno et al., 2002).

2.3. EPM test

At 20 weeks of age, the anxiety-related behavior was evaluated using the EPM test. The apparatus consisted of two open arms (6 cm \times 30 cm) opposite each other, crossed by two closed arms (6 cm \times 30 cm) (walls 10 cm) with an open roof and central platform (9 cm \times 9 cm). The maze floor and walls were constructed from acrylic plate and elevated 40 cm from the ground floor. Initially, the animals were placed on the central platform of the maze in front of a closed arm. The animal had 5 min to explore the apparatus. Activity of mice was monitored via video camera positioned above the apparatus. The time spent in each arm and the number of entries into each arm were automatically analyzed offline using the ANY-maze video tracking software (Stoelting Company, Wood Dale, IL, USA). The test area was cleaned with 20% ethanol between each session.

2.4. Western blot analysis of GABA transaminase in the frontal cortex and both NAT and DAT expressions in the frontal cortex and hippocampus

After 17 weeks of treatment, animals were sacrificed by decapitation without anesthesia. The brains were rapidly resected and two brain regions (frontal cortex and hippocampus) were dissected, and placed on an ice-cold plate. Each brain sample was quickly frozen and stored at -80°C , until use. The dissected tissues were homogenized in CelLyticTM MT Cell Lysis Reagent (Sigma–Aldrich) containing 1% protease inhibitor cocktail (Sigma–Aldrich) and centrifuged at $15,000 \times g$ for 15 min at 4°C . Supernatants were isolated and protein concentrations were measured using the Pierce BCA protein assay kit (Pierce, Rockford, IL). Equivalent amounts of protein lysates (15 μg) were separated by electrophoresis on a sodium dodecylsulphate polyacrylamide gel (10% e-PAGE, ATTO Corp., Tokyo, Japan) and transferred onto polyvinylidene fluoride membranes (Immobilon-P, Millipore, Bedford, MA). Blots were blocked for 1 h with Blocking One (Nacalai Tesque, Kyoto, Japan) at room temperature. The membranes were sequentially incubated overnight with antibodies to NAT (Norepinephrine Transporter Monoclonal Antibody, dilution 1: 2000, P21934, Thermo Scientific, Rockford, IL), DAT (Anti-Dopamine Transporter N-terminal Antibody, dilution 1:1000, D6944, Sigma–Aldrich), GABA transaminase (ABAT Antibody, dilution 1:10000, NBP1-95517, Novus Biologicals, CO) or glyceraldehyde-3-phosphate dehydrogenase (GAPDH, dilution 1:1000, 5714, Cell Signaling Technology, Danvers, MA). After repeated washing with 0.05% Tween-20 in phosphate-buffered saline (T-PBS), a peroxide-conjugated goat anti-mouse antibody (dilution 1:5000, NA931, Amersham, GE Healthcare, Buckinghamshire, UK) for the membrane of NAT, a peroxide-conjugated goat anti-rabbit antibody (dilution 1:5000, 7074, Cell Signaling Technology) for DAT, GABA transaminase or GAPDH, was added for 1 h at room temperature. After repeated washing with T-PBS, the immunoreactive bands were visualized using

ECL Western Blotting Detection Reagents (GE Healthcare) and detected by Image Quant LAS4010 (GE Healthcare). Immunoblots were quantified by Image Quant TL software (GE Healthcare).

2.5. Statistical analyses

Statistical analyses were performed with the computer program, GraphPad Prism (GraphPad Software, Inc., San Diego, CA, USA). Results are expressed as means \pm standard errors of the mean (SEM). To analyze the drug's effect on powdered diet group, the results were analyzed by a one-way analysis of variance (ANOVA) using GraphPad Prism, followed by Dunnett's test. To evaluate the effects of diazepam on the EPM test in both control diet and powdered diet groups, two-way ANOVA was used. Significant main effects or interactions were followed by Tukey's test. Statistical evaluations between two groups were performed using Student's *t*-test. Statistical significance was set at $p < 0.05$.

3. Results

3.1. Anxiety-related behavior of powdered diet-fed mice assessed by the EPM test

At 20 weeks of age, the anxiety-related behavior of powdered diet-fed group was measured for 5 min in the EPM apparatus. Fig. 1 shows the influence of powdered diet feeding on the % of open arm time and total number of arm entries. The powdered diet group had a significantly increased % of open arm time (unpaired *t*-test: $p = 0.0017$) (Fig. 1A) and the total number of arm entries (unpaired *t*-test: $p = 0.0111$) (Fig. 1B).

3.2. Effect of diazepam on the anxiety-related behavior of powdered diet-fed mice in the EPM test

To study the implication of influence of anxiolytic agent on the anxiety-related behaviors elicited by powdered diet, mice at 20 weeks of age were used; the % of open arm time and the total number of arm entries were measured in powdered diet- and control diet groups. Fig. 2 shows the % of open arm time and the total number of arm entries after treatment with diazepam, an anxiolytic agent, on powdered diet- and control diet-fed mice. Two-way ANOVA revealed the main effect for diet on the % of open arm time [$F(1, 42) = 16.21, p = 0.0002$], the main effect for drug [$F(1, 42) = 18.33, p = 0.0001$] and diet \times drug interaction [$F(1, 42) = 4.004, p = 0.0519$] (Fig. 2A). The post hoc Tukey's test revealed that diazepam (1 mg/kg) significantly increased the % of open arm time in control diet-fed group, compared with that of vehicle-treated control diet-fed mice ($p < 0.01$, Fig. 2A). The % of open time in vehicle-treated powdered diet-fed mice significantly increased, compared with vehicle-treated control diet-fed mice

($p < 0.01$, Fig. 2A). In contrast to the % of open arm time, two-way ANOVA revealed the main effect for diet on the total number of arm entries [$F(1, 42) = 8.119, p = 0.0068$], the main effect for drug [$F(1, 42) = 7.985, p = 0.0072$] and diet \times drug interaction [$F(1, 42) = 0.1310, p = 0.7192$] (Fig. 2B). The post hoc Tukey's test revealed that the total number of arm entries in the vehicle-treated powdered diet-fed mice significantly increased, compared with vehicle-treated control diet-fed mice ($p < 0.05$, Fig. 2B).

3.3. Effect of bicuculline, a GABA-A receptor antagonist, on the anxiety-related behavior of powdered diet-fed mice in the EPM test

In the experiments described above, treatment with diazepam increased the % of open arm time in control diet-fed group, but not in the powdered diet-fed group, suggesting that the alteration of GABA-A receptor function. Fig. 3 shows the % of open arm time and the total number of arm entries after treatment with bicuculline, a GABA-A receptor antagonist, on powdered diet-fed mice. The increase in the % of open arm time elicited by powdered diet feeding was attenuated by treatment with bicuculline at a dose of 5 mg/kg, compared with that of vehicle-treated powdered diet-fed group (unpaired *t*-test: $p = 0.0181$, Fig. 3A). However, the total number of arm entries in powdered diet-fed group [unpaired *t*-test: $p = 0.312$, Fig. 3B], after treatment with bicuculline (5 mg/kg) did not show any behavioral changes as compared with the vehicle-treated powdered diet-fed group. There were no significant differences between vehicle-treated control diet-fed mice and bicuculline (5 mg/kg)-treated control diet-fed mice, in the EPM test (data not shown).

3.4. Effect of GBR12909, a selective DAT transporter inhibitor, on the anxiety-related behavior of powdered diet-fed mice in the EPM test

We recently reported that mice subjected to long-term feeding on powdered diet induces the alteration of dopaminergic regulation, and in particular, it decreases the expression of dopamine D4 receptor mRNA and increases dopamine turnover in the frontal cortex (Nijima-Yaoita et al., 2013). To study the influence of selective DAT inhibitor on the anxiety-related behaviors elicited by powdered diet, the % of open arm time and the total number of arm entries after treatment with selective DAT transporter inhibitor were measured in powdered diet group. Fig. 4 shows the % of open arm time and the total number of arm entries after treatment with GBR12909, a selective DAT inhibitor, in powdered diet-fed mice. One-way ANOVA of the influence of GBR12909 on the % of open arm time [$F(2, 35) = 1.551; p = 0.2263$] (Fig. 4A) and total number of arm entries [$F(2, 35) = 1.395; p = 0.2612$] (Fig. 4B) in powdered diet-fed group revealed no significant differences. There were no significant differences between vehicle-treated control diet-fed mice and GBR 12909 (3 mg/kg)-treated control diet-fed mice, in the EPM test (data not shown).

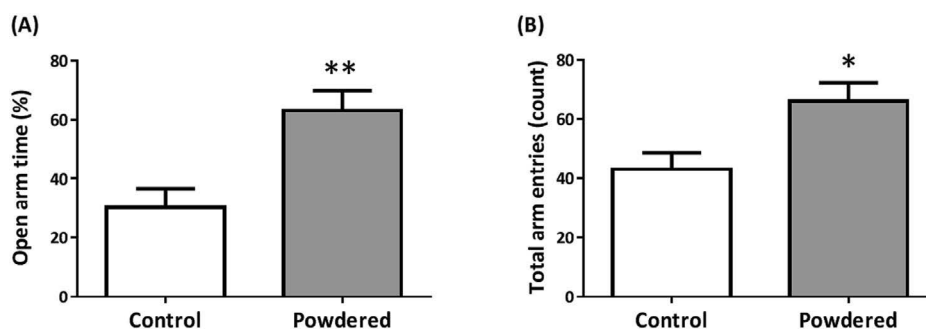


Fig. 1. Influence of powdered diet feeding for 17 weeks on the elevated plus maze test in mice. The left and right panels show time spent in the open arm (A) and total arm entries (B), respectively. The data are expressed as the mean \pm S.E.M. for 14–18 mice/group. * $p < 0.05$, ** $p < 0.01$; vs. control diet-fed mice (unpaired *t*-test).

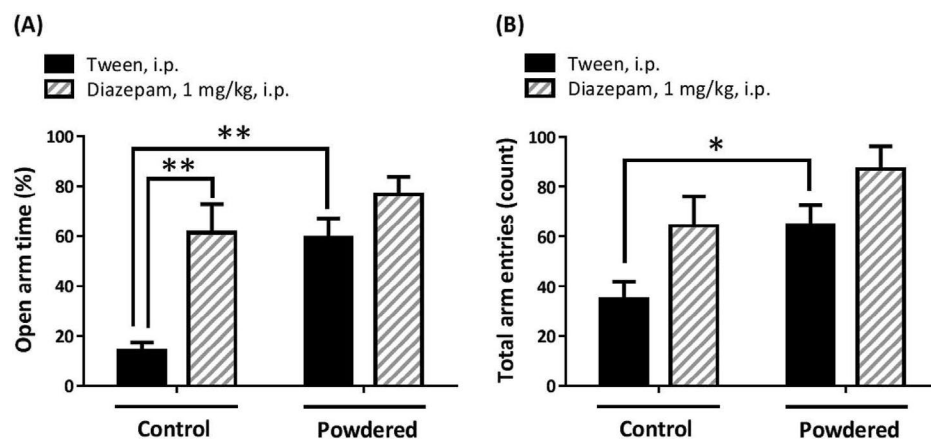


Fig. 2. Effect of diazepam on the elevated plus maze test in control diet- and powdered diet-fed mice. The left and right panels show time spent in the open arm (A) and total arm entries (B), respectively. The data are expressed as the mean \pm S.E.M. for 8–15 mice/group. * $p < 0.05$, ** $p < 0.01$; vs. vehicle-treated control diet-fed mice (Tukey's test).

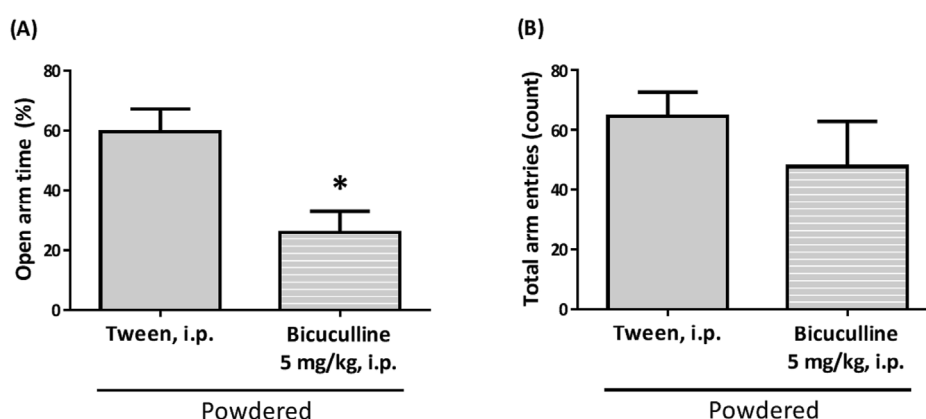


Fig. 3. Effect of bicuculline on the elevated plus maze test in powdered diet-fed mice. The left and right panels show time spent in the open arm (A) and total arm entries (B), respectively. The data are expressed as the mean \pm S.E.M. for 6–15 mice/group. * $p < 0.05$; vs. vehicle-treated mice (unpaired t -test).

3.5. Effect of atomoxetine, a selective NAT inhibitor, on the anxiety-related behavior of powdered diet-fed mice in the EPM test

To study the influence of selective NAT inhibitor on the anxiety-related behaviors elicited by powdered diet, the % of open arm time and the total number of arm entries after treatment with selective NAT transporter inhibitor were measured in powdered diet group. Fig. 5 shows the % of open arm time and the total number of arm entries after treatment with atomoxetine, a selective NAT inhibitor, in powdered diet-fed mice. One-way ANOVA of the influence of atomoxetine on the % of open arm time in powdered diet-fed group revealed significant

differences [$F(4, 58) = 3.851$; $p = 0.0077$] (Fig. 5A). The post hoc Dunnett's test revealed that atomoxetine at a dose of 0.18 mg/kg, significantly attenuated the % of open arm time in powdered diet-fed group, compared with that of saline-treated powdered diet-fed group ($p < 0.01$, Fig. 5A). On the other hand, one-way ANOVA revealed that the total number of arm entries in powdered diet-fed group [$F(4, 58) = 0.2623$; $p = 0.9009$, Fig. 5B] was not influenced by treatment with atomoxetine. There were no significant differences between saline-treated control diet-fed mice and atomoxetine (0.18 and 0.5 mg/kg)-treated control diet-fed mice, in the EPM test (data not shown).

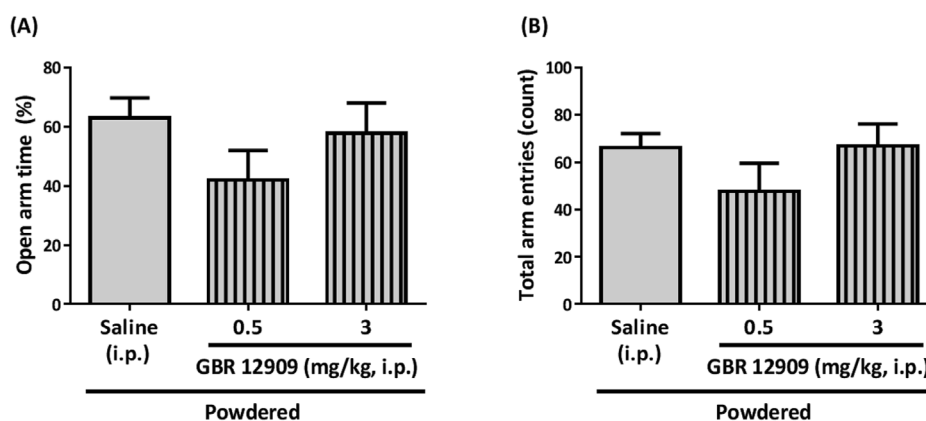


Fig. 4. Effect of GBR12909 on the elevated plus maze test in powdered diet-fed mice. The left and right panels show time spent in the open arm (A) and total arm entries (B), respectively. The data are expressed as the mean \pm S.E.M. for 10–18 mice/group.

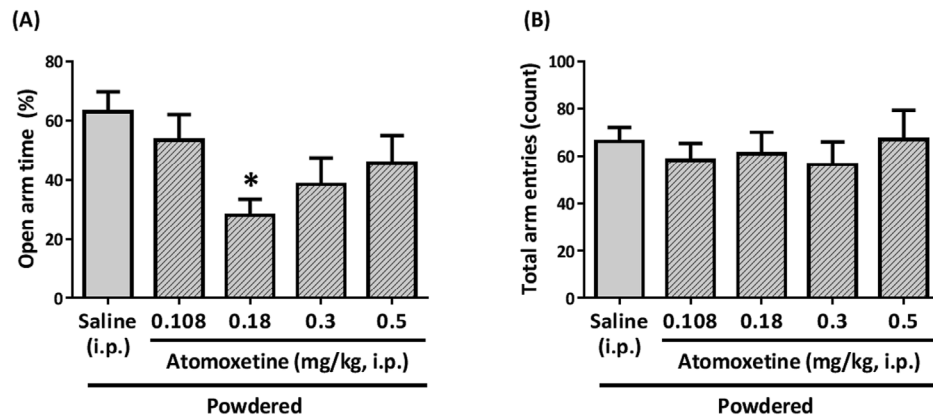


Fig. 5. Effect of atomoxetine on the elevated plus maze test in powdered diet-fed mice. The left and right panels show time spent in the open arm (A) and total arm entries (B), respectively. The data are expressed as the mean \pm S.E.M. for 10–18 mice/group. ** $p < 0.01$; vs. saline-treated mice (Dunnett's test).

3.6. Effect of methylphenidate, a DAT and NAT inhibitor, on the anxiety-related behavior of powdered diet-fed mice in the EPM test

To study the influence of methylphenidate, a DAT and NAT inhibitor, on the anxiety-related behaviors elicited by powdered diet, the % of open arm time and the total number of arm entries after treatment with methylphenidate (0.133, 0.2 and 0.3 mg/kg) were measured in powdered diet group. Fig. 6 shows the % of open arm time and the total number of arm entries after treatment with methylphenidate in powdered diet-fed mice. One-way ANOVA of the influence of methylphenidate on the % of open arm time in powdered diet-fed group revealed significant differences [$F(3, 46) = 2.839$; $p = 0.0482$] (Fig. 6A). The post hoc Dunnett's test revealed that methylphenidate (0.2 mg/kg), significantly attenuated the % of open arm time in powdered diet-fed group, compared with that of saline-treated powdered diet-fed group (saline vs. 0.2 mg/kg; $p < 0.05$, Fig. 6A). In contrast, one-way ANOVA revealed that the total number of arm entries in the powdered diet-fed group [$F(3, 46) = 1.408$; $p = 0.2525$, Fig. 6B] was not influenced by treatment with methylphenidate. There were no significant differences between saline-treated control diet-fed mice and methylphenidate (0.2 and 0.3 mg/kg)-treated control diet-fed mice, in the EPM test (data not shown).

3.7. Effect of PD168077, a selective dopamine D4 receptor agonist, on the anxiety-related behavior of powdered diet-fed mice in the EPM test

We recently reported that PD168077, a selective D4 receptor agonist, attenuates the increased SI time in powdered diet-fed mice

(Nijima-Yaoita et al., 2013). To study the influence of PD168077 on the anxiety-related behaviors elicited by powdered diet, the % of open arm time and the total number of arm entries after treatment with PD168077 (0.1 and 0.3 mg/kg) were measured in powdered diet group. Fig. 7 shows the % of open arm time and the total number of arm entries after treatment with PD168077 on powdered diet-fed mice. One-way ANOVA of the influence of PD168077 on the % of open arm time revealed significant differences in powdered diet-fed mice [$F(2, 23) = 5.651$; $p = 0.0101$, Fig. 7A]. The post hoc Dunnett's test revealed that PD168077 (0.3 mg/kg) significantly attenuated the % of open arm time in powdered diet-fed group, compared with that of vehicle-treated powdered diet-fed mice (vehicle vs. 0.3 mg/kg; $p < 0.05$, Fig. 7A). In contrast to the % of open arm time in powdered diet-fed group, the total number of arm entries in powdered diet-fed group [$F(2, 23) = 0.8001$; $p = 0.4614$, Fig. 7B] was not influenced by treatment with PD168077. There were no significant differences between vehicle-treated control diet-fed mice and PD168077 (0.3 mg/kg)-treated control diet-fed mice, in the EPM test (data not shown).

3.8. Influence of long-term powdered diet feeding on the expression of GABA transaminase in the frontal cortex

In the experiments described above, the increase in the % of open arm time elicited by long-term powdered diet feeding was attenuated by treatment with bicuculline, GABA-A receptor antagonist. Hwang et al. (2004) suggested that the increase in expression of GABA transaminase, GABA metabolic enzymes (for review see Kowalczyk and Kulig, 2014), provides important information about the brain with

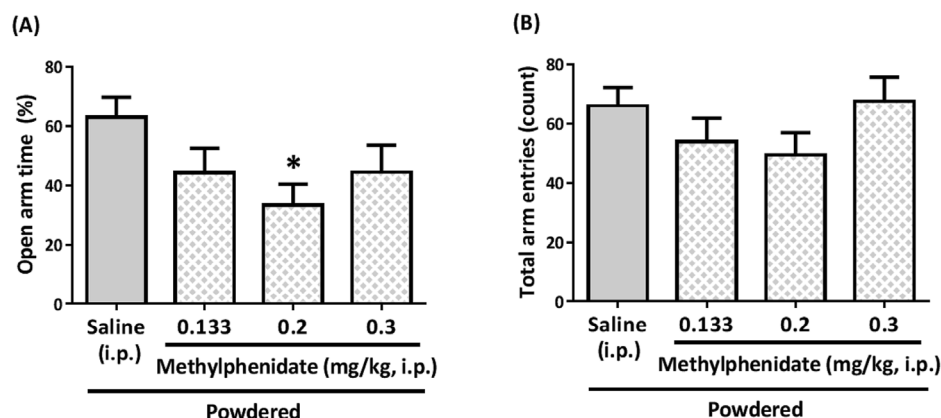


Fig. 6. Effect of methylphenidate on the elevated plus maze test in powdered diet-fed mice. The left and right panels show time spent in the open arm (A) and total arm entries (B), respectively. The data are expressed as the mean \pm S.E.M. for 10–18 mice/group. * $p < 0.05$; vs. saline-treated mice (Dunnett's test).

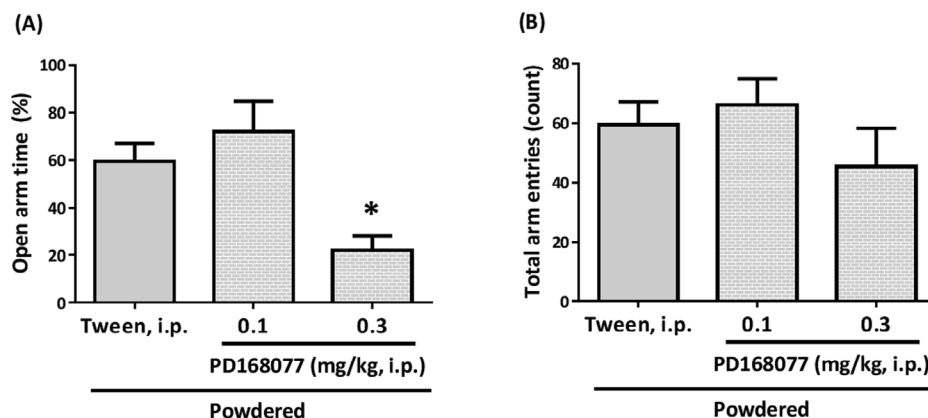


Fig. 7. Effect of PD168077 on the elevated plus maze test in powdered diet-fed mice. The left and right panels show time spent in the open arm (A) and total arm entries (B), respectively. The data are expressed as the mean \pm S.E.M. for 5–15 mice/group. * $p < 0.05$; vs. vehicle-treated mice (Dunnett's test).

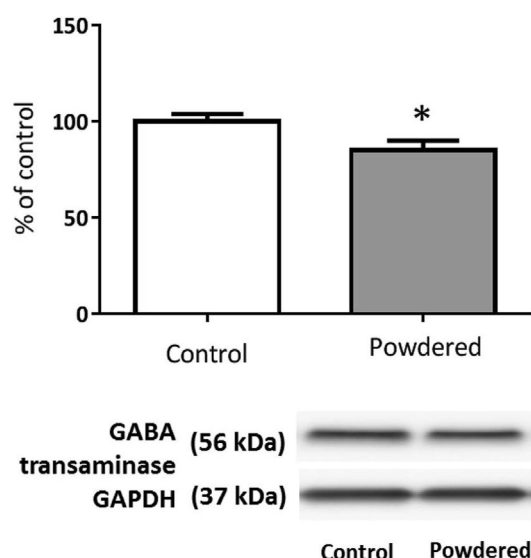


Fig. 8. Influence of powdered diet feeding for 17 weeks on the expression of GABA transaminase in the frontal cortex (FC) of mice. The data are given as the mean \pm SEM for a group of 5 mice/group. * $p < 0.05$; vs. control diet-fed mice (unpaired t -test).

GABA dysfunction. Therefore, we compared the differences in the expression levels of GABA transaminase in the frontal cortex between the powdered diet group and control diet group (Fig. 8). The levels of GABA transaminase expression in the frontal cortex of powdered diet-fed mice were lower than that of control diet-fed mice (unpaired t -test: $p = 0.026$, Fig. 8).

3.9. Influence of long-term powdered diet feeding on the expression of DAT and NAT in the frontal cortex and hippocampus

In the experiments described above, increase in the % of open arm time elicited by long-term powdered diet feeding was attenuated by treatment with atomoxetine, selective NAT inhibitor, and methylphenidate, DAT and NAT inhibitor, but not treatment with GBR12909, a selective DAT inhibitor (Figs. 4–6). Moreover, we recently reported the alteration of dopaminergic regulation, especially the increase in dopamine turnover in the frontal cortex, but not but in the hippocampus of powdered diet-fed mice (Nijima-Yaoita et al., 2013). Therefore, we compared the differences in the expression levels of both DAT and NAT in the frontal cortex and hippocampus between the powdered diet group and control diet group (Figs. 9 and 10). The levels of NAT

expression in the frontal cortex and hippocampus of powdered diet-fed mice were higher and lower in control diet-fed mice, respectively (unpaired t -test: $p = 0.0452$, Fig. 9B and $p = 0.003$, Fig. 10B). There were no significant differences in the expressions of DAT in the frontal cortex and hippocampus (unpaired t -test: $p = 0.4672$, Fig. 9A and $p = 0.4293$, Fig. 10A).

4. Discussion

The findings of the present study may be summarized as follows: (i) Long-term powdered diet increased the % of open arm time and the total number of arm entries, indicating that the mice have low anxiety, hyperactivity and impulsivity behaviors (EPM test) (Fig. 1), (ii) The % of open arm time in control diet-fed mice was increased by treatment with anxiolytic agent, while the anxiolytic agent did not influence the % of open arm time in powdered diet-fed mice (Fig. 2), (iii) GABA-A receptor antagonist attenuated the increase in the % of open arm time by powdered diet feeding (Fig. 3), (iv) selective DAT inhibitor did not influence the % of open arm time and the total number of arm entries in powdered diet-fed mice. In contrast, the increased the % of open arm time by powdered diet feeding was attenuated by treatment with selective NAT inhibitor, DAT and NAT inhibitor and dopamine D4 receptor agonist (Figs. 4–7), (v) GABA transaminase expressions in the frontal cortex of powdered diet-fed mice were decreased (Fig. 8), (vi) powdered diet feeding induced an increase and a decrease in NAT expression, but not DAT expression, in the frontal cortex and hippocampus, respectively (Figs. 9 and 10). These findings are discussed below.

We have previously reported that mice subjected to long-term feeding on powdered diet exhibits increased SI behavior (Nijima-Yaoita et al., 2013), elevation of blood catecholamine and corticosterone, hyperglycemia, hypertension and no changes in growth curves between diet types; further, we found that among daily dietary habits, mastication of food of adequate hardness is very important for the maintenance of systemic (physical and mental) health (Tsuchiya et al., 2014). Although the SI test has been widely documented as an anxiety test, mainly because of a novel partner/place, the EPM test was also developed to detect anxiety-related behavior. In this study, we chose the EPM test as an approach to study anxiety-related behavior; the long-term powdered diet-fed mice showed an increase in the % of open arm time and total number of arm entries, indicating that the mice subjected to long-term feeding on powdered diet have low anxiety behavior.

It is known that GABA-A receptor plays a critical role in anxiolytic activity and the activation of the GABA-A receptor induced by BZD including diazepam reduces anxiety (for review see Jacob et al., 2008; Möhler et al., 2002). Thus, in this study, to investigate the implication of GABA-A receptor on these behaviors, the effects of diazepam and

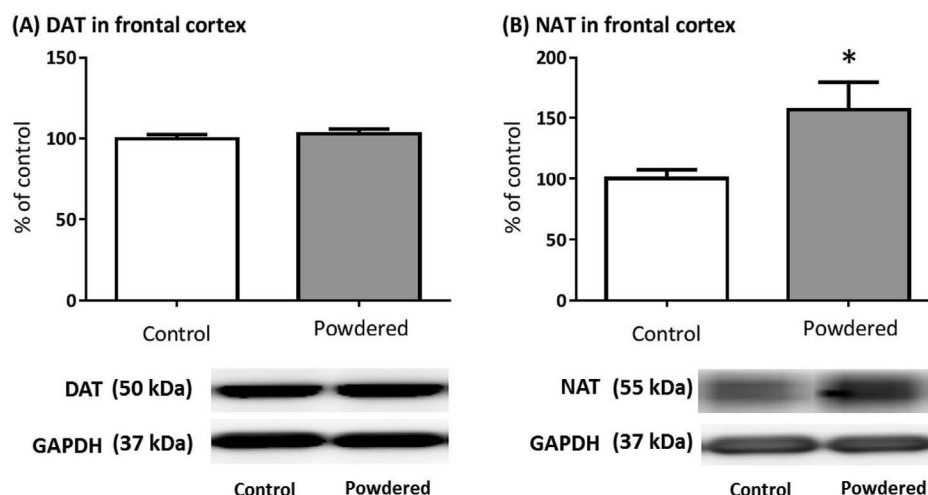


Fig. 9. Influence of powdered diet feeding for 17 weeks on the expression of dopamine transporter (DAT) (A) and noradrenaline transporter (NAT) (B) in the frontal cortex of mice. The data are given as the mean \pm SEM for a group of 5 mice/group. * $p < 0.05$; vs. control diet-fed mice (unpaired t -test).

bicuculline on the behaviors in powdered diet- and control diet-fed mice, were evaluated. We showed that the increase in the % of open arm time in powdered diet-fed mice was attenuated by treatment with GABA-A receptor antagonist bicuculline, not by treatment with anxiolytic diazepam. However, the % of open arm time in control diet-fed mice was increased by treatment with diazepam. Moreover, both diazepam and bicuculline did not affect the total number of arm entries in powdered diet- and control diet-fed groups. These data indicated that the low anxiety elicited by long-term powdered-diet feeding was mediated via the GABAergic transmission.

Recent evidence suggests that GABAergic neurotransmission within the medial prefrontal cortex may be central to the regulation of amygdala activity related to emotion and anxiety-related behavior processing (Delli Pizzi et al., 2017). Solati et al. (2013) reported that using rats, bilateral medial prefrontal cortex injection of the GABA-A receptor agonist muscimol produces a low anxiety in the EPM test. Majewska et al. (1986) reported that one of the corticosterone metabolites is allotetrahydrodeoxycorticosterone, a neuroactive 3α 5α -reduced steroid, which are potent positive allosteric modulator of GABA-A receptors. In our previous study, we demonstrated that the plasma corticosterone level of powdered diet-fed mice is higher than that of control diet-fed mice (Tsuchiya et al., 2014), suggesting that the increased corticosterone metabolites may stimulate GABA-A receptor in

the powdered diet-fed mice and the low anxiety behavior may be elicited.

Kazi and Oommen (2014) reported that using rats, chronic noise stress induced an increase in GABA levels and a decrease in activity of GABA transaminase in cortex. Moreover, to investigate the relationship between low anxiety behavior elicited by long-term powdered diet feeding and the leading cause of activated GABA-A receptors, we measured the expression of GABA transaminase, GABA metabolic enzymes, in frontal cortex of powdered diet- and control diet-fed mice. In this study, the expression levels of GABA transaminase of the frontal cortex in powdered diet-fed mice were lower than that in control diet-fed mice, indicating that the GABA-A receptor in the frontal cortex of powdered diet-fed mice may be stimulated by an increase in the concentration of GABA via attenuated GABA transaminase.

In our previous study, we proposed that the increase in SI behaviors (i.e. it prolonged SI time) in powdered diet-fed mice might be mediated via alteration of dopaminergic system, especially a decrease in dopamine D4 receptor signals in the frontal cortex (Nijima-Yaoita et al., 2013). Interestingly, dysregulation of dopamine D4 receptor signaling is linked to several pathological conditions, such as ADHD (for review see Rondou et al., 2010). Moreover, the exploratory behavior in open arms may reflect impulsivity for novelty-seeking (for review see Steimer and Driscoll (2003)). Indeed, the increase in the % of open arm time

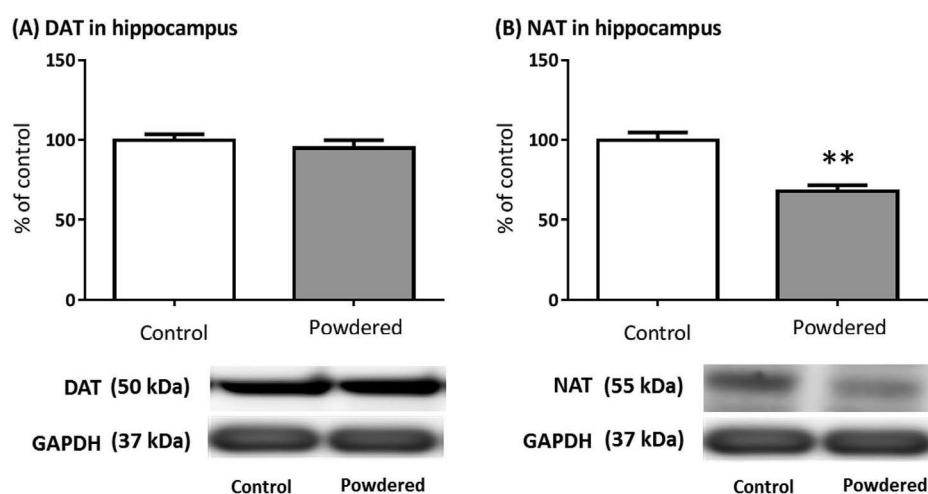


Fig. 10. Influence of powdered diet feeding for 17 weeks on the expression of dopamine transporter (DAT) (A) and noradrenaline transporter (NAT) (B) in the hippocampus of mice. The data are given as the mean \pm SEM for a group of 6 mice/group. * $p < 0.05$; vs. control diet-fed mice (unpaired t -test).

(low anxiety behavior) and total number of arm entries elicited by powdered diet feeding may relate to the impulsivity and hyperactivity-like symptoms in ADHD, indicating that the long-term powdered diet feeding may increase the risk for the onset of ADHD-like behavior or symptoms.

To investigate the implication of these behaviors in the EPM test on these symptoms in ADHD, we measured whether the ADHD therapeutic agent, methylphenidate and atomoxetine, attenuate the low anxiety or impulsivity-like behavior and hyperactivity-like behavior elicited by powdered diet feeding. In this study, treatments of methylphenidate and atomoxetine improved the impulsivity-like behavior, but not the hyperactivity-like behavior in powdered diet-fed group. Moreover, the % of open arm time and the total number of arm entries in control diet-fed group were not affected by a similar dose of methylphenidate and atomoxetine. Methylphenidate and atomoxetine appear to enhance prefrontal cortex function through inhibition of both DAT and NAT and inhibition of NAT, respectively (for review see Arnsten and Pliszka, 2011). Andrews and Lavin (2006) reported that methylphenidate acts to increase catecholaminergic tone in the prefrontal cortex, and activation of alpha-2 adrenoceptors located in GABA interneurons. Indeed, the inhibition of GABA function may influence the amygdala activity related to emotion and anxiety-related behavior processing and attenuate the low anxiety or impulsivity-like behavior. In this study, we showed an increase in the expression of NAT in the frontal cortex of powdered diet-fed mice. In contrast, DAT expression was not changed in the frontal cortex of powdered diet-fed mice. These findings may suggest the relationship between improvement of methylphenidate and atomoxetine on the low anxiety behavior or impulsive-like behavior elicited by long-term powdered diet feeding and the activation of alpha-2 adrenoceptors by an increase in the concentration of NA mainly via inhibition of NAT in the synaptic cleft. In addition, the involvement of long-term powdered diet feeding on an increased risk ADHD-like behavior onset or symptoms was suggested.

However, in this study, improvement by methylphenidate and atomoxetine on the low anxiety behavior or impulsive-like behavior elicited by long-term powdered diet feeding was not dose dependent. Berridge and Spencer (2016) reported that NA is targeted by pharmacological treatments used to treat prefrontal cortex dysfunction associated with a range of psychopathologies, including ADHD, and modulating the distinct processes via alpha-1 and alpha-2 adrenoceptors, respectively. Moreover, they described that the differential activation of adrenoceptor subtypes within the prefrontal cortex is reflected in the inverted-U shaped function. In addition to the receptor specific actions, the differences of concentration, such as low doses that are within a clinically-relevant range or doses without clinically-relevant range, are reflected in the inverted-U shaped function. These findings may support our data showing that improvements of methylphenidate and atomoxetine were not dose dependent.

Although the low anxiety behavior or impulsive-like behavior in powdered diet-fed mice may be related to changes in noradrenergic functions, i.e., decrease in the concentration of NA in the synaptic cleft via elevated NAT expressions in the frontal cortex, in the previous study we suggested that the powdered diet feeding may cause the increased SI time and the changes in the dopaminergic system, especially the decrease in dopamine D4 receptor signals in the frontal cortex (Nijima-Yaoita et al., 2013). Moreover, in this study, we showed that PD168077, a dopamine D4 receptor agonist, attenuated the low anxiety behavior or impulsive-like behavior in powdered diet-fed mice. In contrast, GBR12909, a DAT inhibitor, which increases the concentration of dopamine in the synaptic cleft, did not influence the low anxiety behavior or impulsive-like behavior in powdered diet-fed mice. Interestingly, agonism of endogenous neurotransmitters at the dopamine D4 receptor has been described not only for dopamine (Asghari et al., 1995), but also for NA and adrenaline (Lanau et al., 1997; Newman-Tancredi et al., 1997). Moreover, it is reported that in the prefrontal cortex, where the DAT density of dopaminergic neurons is low (Sesack

et al., 1998), NAT discharges dopamine reuptake (Carboni et al., 1990; Morón et al., 2002). In addition, it is well known that emotional stress induces an elevation of serum glucocorticoids. Ayada et al. (2002) observed that improved mastication behavior might reduce the stress-induced enhancement of serum cortisol. In our previous study, we showed the elevation of serum corticosterone in powdered diet-fed mice (Tsuchiya et al., 2014) and the decrease in the expression of dopamine D4 receptor mRNA, but not in D1, D2, D3 and D5 receptor mRNA in powdered diet-fed mice (Nijima-Yaoita et al., 2013). Barros et al. (2003) reported that corticosterone down-regulates dopamine D4 receptor in a mouse cerebral cortex neuronal cell line. These findings suggest that the masticatory dysfunction induced by long-term powdered diet feeding may cause the low anxiety behavior or impulsive like behavior, the decrease in not only NA but also dopamine in the synaptic cleft of the frontal cortex, and the decreased dopamine D4 receptor signaling via the elevated NAT expression and corticosterone. Indeed, the decreased expression of dopamine D4 receptor may be stimulated by the selective dopamine D4 receptor agonist PD168007, but not by an increase in the concentration of dopamine via inhibition of DAT by GBR12909.

In addition, Shah et al. (2004) reported that using rats, intra-medial prefrontal cortex infusions of the highly selective dopamine D4 receptor antagonist, increased the % of open arm time in the EPM test, indicating low anxiety. Moreover, rodent dopamine D4 receptor activation in prefrontal cortex pyramidal neurons inhibits GABAergic functions (Wang et al., 2002). Indeed, the decreased dopamine D4 signals in the frontal cortex of powdered diet-fed mice may attenuate the inhibitory effects of dopamine D4 receptors on GABAergic function in regulating amygdala activity related to emotion and anxiety-related behavior processing.

Zhang et al. (2017) reported that chronic social stress up-regulated expression of NAT in the brain is mediated by glucocorticoid receptor (GR) and the GR expressional alterations in response to chronic stress are complex and brain region-specific. However, the measurement of GR protein levels after chronic stress was inconsistent (Kohda et al., 2007; Liberzon et al., 1999; Makino et al., 2002; Trujillo et al., 2016). In this study, we showed the increase and decrease in NAT expressions in the frontal cortex and hippocampus of powdered diet-fed mice, respectively. We previously observed that long-term powdered diet feeding markedly increased the serum level of corticosterone (Tsuchiya et al., 2014). These findings may support the differences in NAT expressions between the frontal cortex and hippocampus in our study.

In conclusion, the present study demonstrated that the dietary habits, e.g. a long-term powdered diet feeding, increased the % of open arm, the total number of arm entries, the expression of NAT, and decrease in expression of GABA transaminase in the frontal cortex. In addition, the increased the % of open arm time in powdered diet-fed mice was attenuated by GABA-A receptor antagonist, ADHD therapeutic agents and selective dopamine D4 receptor agonist, but not by anxiolytic agent or DAT inhibitor. These results suggest that the long-term powdered diet feeding may cause low anxiety or impulsivity, possibly via an increase in NAT expression, decrease in dopamine D4 receptor signals and increase in GABA-A receptor functions in the frontal cortex of mice. Moreover, the long-term powdered diet feeding may increase the risk for onset of ADHD-like behavior or symptoms and the effect of ADHD therapeutic agents on the impulsive behavior might be inhibited mainly by NAT and by the increased NA and/or dopamine levels in the synaptic cleft.

Acknowledgements

We would like to express our deepest gratitude to Mr. Shunsuke Nishidate, Mr. Kota Namura, Mr. Hiroki Imaizumi and Mr. Keigo Kawanami of the Department of Pharmacology, Faculty of Pharmaceutical Sciences, Tohoku Medical and Pharmaceutical University for their excellent technical assistance.

This study was supported by JSPS KAKENHI Grant Numbers 24700433, 26500014 and 17K00768 and the MEXT (Ministry of Education, Culture, Sports, Science and Technology)-Supported Program for the Strategic Research Foundation at Private Universities (No. S1511001L, 2015–2019).

Appendix A. Supplementary data

Supplementary data to this article can be found online at <https://doi.org/10.1016/j.neuint.2018.12.002>.

References

- Andrews, G.D., Lavin, A., 2006. Methylphenidate increases cortical excitability via activation of alpha-2 noradrenergic receptors. *Neuropsychopharmacology* 31, 594–601. <https://doi.org/10.1038/sj.npp.1300818>.
- Aoki, H., Kimoto, K., Hori, N., Toyoda, M., 2005. Cell proliferation in the dentate gyrus of rat hippocampus is inhibited by soft diet feeding. *Gerontology* 51, 369–374. <https://doi.org/10.1159/000088700>.
- Arnsten, A.F., Pliszka, S.R., 2011. Catecholamine influences on prefrontal cortical function: relevance to treatment of attention deficit/hyperactivity disorder and related disorders. *Pharmacol. Biochem. Behav.* 99, 211–216. <https://doi.org/10.1016/j.pbb.2011.01.020>.
- Asghari, V., Sanyal, S., Buchwaldt, S., Paterson, A., Jovanovic, V., Van Tol, H.H., 1995. Modulation of intracellular cyclic AMP levels by different human dopamine D4 receptor variants. *J. Neurochem.* 65, 1157–1165.
- Ayada, K., Tadano, T., Endo, Y., 2002. Gnawing behavior of a mouse in a narrow cylinder: a simple system for the study of muscle activity, fatigue, and stress. *Physiol. Behav.* 77, 161–166.
- Barros, V.G., Boado, L.A., Adamo, A.M., Caviedes, R., Caviedes, P., Antonelli, M.C., 2003. Corticosterone down-regulates dopamine D4 receptor in a mouse cerebral cortex neuronal cell line. *Neurotox. Res.* 5, 369–373.
- Berridge, C.W., Spencer, R.C., 2016. Differential cognitive actions of norepinephrine $\alpha 2$ and $\alpha 1$ receptor signaling in the prefrontal cortex. *Brain Res.* 1641, 189–196. <https://doi.org/10.1016/j.brainres.2015.11.024>.
- Brevet-Aebly, C., Brunelin, J., Ictea, S., Padovan, C., Poulet, E., 2016. Prefrontal cortex and impulsivity: interest of noninvasive brain stimulation. *Neurosci. Biobehav. Rev.* 71, 112–134. <https://doi.org/10.1016/j.neubiorev.2016.08.028>.
- Carboni, E., Tanda, G.L., Frau, R., Di Chiara, G., 1990. Blockade of the noradrenergic carrier increases extracellular dopamine concentrations in the prefrontal cortex: evidence that dopamine is taken up in vivo by noradrenergic terminals. *J. Neurochem.* 55, 1067–1070.
- Delli Pizzi, S., Chiacchiaretta, P., Mantini, D., Bubbico, G., Edden, R.A., Onofri, M., Ferretti, A., Bonanni, L., 2017. GABA content within medial prefrontal cortex predicts the variability of fronto-limbic effective connectivity. *Brain Struct. Funct.* 222, 3217–3229. <https://doi.org/10.1007/s00429-017-1399-x>.
- File, S.E., 1992. Behavioral detection of anxiolytic action. In: Elliott, J.M., Heal, D.J., Marsden, C.A. (Eds.), *Experimental Approaches to Anxiety and Depression*. John Wiley and Sons, Chichester, UK, pp. 25–44.
- Gould, T.J., Rukstalis, M., Lewis, M.C., 2005. Atomoxetine and nicotine enhance prepulse inhibition of acoustic startle in C57BL/6 mice. *Neurosci. Lett.* 377, 85–90. <https://doi.org/10.1016/j.neulet.2004.11.073>.
- Herman, A.M., Critchley, H.D., Duka, T., 2018. The role of emotions and physiological arousal in modulating impulsive behaviour. *Biol. Psychol.* 133, 30–43. <https://doi.org/10.1016/j.biopsycho.2018.01>.
- Hiraide, S., Ueno, K., Yamaguchi, T., Matsumoto, M., Yanagawa, Y., Yoshioka, M., Togashi, H., 2013. Behavioural effects of monoamine reuptake inhibitors on symptomatic domains in an animal model of attention-deficit/hyperactivity disorder. *Pharmacol. Biochem. Behav.* 105, 89–97. <https://doi.org/10.1016/j.pbb.2013.01.009>.
- Hwang, I.K., Kim, D.W., Yoo, K.Y., Kim, D.S., Kim, K.S., Kang, J.H., Choi, S.Y., Kim, Y.S., Kang, T.C., Won, M.H., 2004. Age-related changes of gamma-aminobutyric acid transaminase immunoreactivity in the hippocampus and dentate gyrus of the Mongolian gerbil. *Brain Res.* 1017, 77–84. <https://doi.org/10.1016/j.brainres.2004.05.022>.
- Jacob, T.C., Moss, S.J., Jurd, R., 2008. GABA (A) receptor trafficking and its role in the dynamic modulation of neuronal inhibition. *Nat. Rev. Neurosci.* 9, 331–343. <https://doi.org/10.1038/nrn2370>.
- Kanegawa, N., Suzuki, C., Ohinata, K., 2010. Dipeptide Tyr-Leu (YL) exhibits anxiolytic-like activity after oral administration via activating serotonin 5-HT_{1A}, dopamine D1 and GABA_A receptors in mice. *FEBS Lett.* 584, 599–604. <https://doi.org/10.1016/j.febslet.2009.12.008>.
- Kazi, A.I., Oommen, A., 2014. Chronic noise stress-induced alterations of glutamate and gamma-aminobutyric acid and their metabolism in the rat brain. *Noise Health* 16, 343–349. <https://doi.org/10.4103/1463-1741.144394>.
- Kishikawa, Y., Kawahara, Y., Yamada, M., Kaneko, F., Kawahara, H., Nishi, A., 2014. The spontaneously hypertensive rat/Izm (SHR/Izm) shows attention deficit/hyperactivity disorder-like behaviors but without impulsive behavior: therapeutic implications of low-dose methylphenidate. *Behav. Brain Res.* 274, 235–242. <https://doi.org/10.1016/j.bbr.2014.08.026>.
- Kohda, K., Harada, K., Kato, K., Hoshino, A., Motohashi, J., Yamaji, T., Morinobu, S., Matsuo, N., Kato, N., 2007. Glucocorticoid receptor activation is involved in producing abnormal phenotypes of single-prolonged stress rats: a putative post-traumatic stress disorder model. *Neuroscience* 148, 22–33. <https://doi.org/10.1016/j.neuroscience.2007.05.041>.
- Kowalczyk, P., Kulig, K., 2014. GABA system as a target for new drugs. *Curr. Med. Chem.* 21, 3294–3309.
- Kushida, S., Kimoto, K., Hori, N., Toyoda, M., Karasawa, N., Yamamoto, T., Kojo, A., Onozuka, M., 2008. Soft-diet feeding decreases dopamine release and impairs aversive learning in Alzheimer model rats. *Neurosci. Lett.* 439, 208–211. <https://doi.org/10.1016/j.neulet.2008.05.017>.
- Lanau, F., Zenner, M.T., Civelli, O., Hartman, D.S., 1997. Epinephrine and norepinephrine act as potent agonists at the recombinant human dopamine D4 receptor. *J. Neurochem.* 68, 804–812.
- Leggio, G.M., Micale, V., Le Foll, B., Mazzola, C., Nobrega, J.N., Drago, F., 2011. Dopamine D3 receptor knock-out mice exhibit increased behavioral sensitivity to the anxiolytic drug diazepam. *Eur. Neuropsychopharmacol.* 21, 325–332. <https://doi.org/10.1016/j.euroneuro.2010.05.006>.
- Liberzon, I., López, J.F., Fligel, S.B., Vázquez, D.M., Young, E.A., 1999. Differential regulation of hippocampal glucocorticoid receptors mRNA and fast feedback: relevance to post-traumatic stress disorder. *J. Neuroendocrinol.* 11, 11–17.
- Majewska, M.D., Harrison, N.L., Schwartz, R.D., Barker, J.L., Paul, S.M., 1986. Steroid hormone metabolites are barbiturate-like modulators of the GABA receptor. *Science* 232, 1004–1007.
- Makino, S., Smith, M.A., Gold, P.W., 2002. Regulatory role of glucocorticoids and glucocorticoid receptor mRNA levels on tyrosine hydroxylase gene expression in the locus coeruleus during repeated immobilization stress. *Brain Res.* 943, 216–223.
- Mitome, M., Hasegawa, T., Shirakawa, T., 2005. Mastication influences the survival of newly generated cells in mouse dentate gyrus. *Neuroreport* 16, 249–252.
- Möhler, H., Fritschy, J.M., Rudolph, U., 2002. A new benzodiazepine pharmacology. *J. Pharmacol. Exp. Therapeut.* 300, 2–8.
- Morón, J.A., Brockington, A., Wise, R.A., Rocha, B.A., Hope, B.T., 2002. Dopamine uptake through the norepinephrine transporter in brain regions with low levels of the dopamine transporter: evidence from knock-out mouse lines. *J. Neurosci.* 22, 389–395.
- Newman-Tancredi, A., Audinot-Bouchet, V., Gobert, A., Millan, M.J., 1997. Noradrenaline and adrenaline are high affinity agonists at dopamine D4 receptors. *Eur. J. Pharmacol.* 319, 379–383.
- Nijijima, F., Nakagawasa, O., Tan-No, K., Tadano, T., 2006. Inhibitory effects of methylphenidate and atomoxetine on jumping behavior induced by intermittent rapid eye movement (REM) sleep deprivation stress in mice. *Biog. Amines* 20, 99–111.
- Nijijima-Yaoita, F., Tsuchiya, M., Saito, H., Nagasawa, Y., Murai, S., Arai, Y., Nakagawasa, O., Nemoto, W., Tadano, T., Tan-No, K., 2013. Influence of a long-term powdered diet on the social interaction test and dopaminergic systems in mice. *Neurochem. Int.* 63, 309–315. <https://doi.org/10.1016/j.neuint.2013.07.004>.
- Niimi, K., Nishioka, C., Miyamoto, T., Takahashi, E., Miyoshi, I., Itakura, C., Yamashita, T., 2011. Impairment of neuropsychological behaviors in ganglioside GM3-knockout mice. *Biochem. Biophys. Res. Commun.* 406, 524–528. <https://doi.org/10.1016/j.bbr.2011.02.071>.
- Robinson, A.M., Eggleston, R.L., Bucci, D.J., 2012. Physical exercise and catecholamine reuptake inhibitors affect orienting behavior and social interaction in a rat model of attention-deficit/hyperactivity disorder. *Behav. Neurosci.* 126, 762–771. <https://doi.org/10.1037/a0030488>.
- Rondou, P., Haegeman, G., Van Craenenbroeck, K., 2010. The dopamine D4 receptor: biochemical and signalling properties. *Cell. Mol. Life Sci.* 67, 1971–1986. <https://doi.org/10.1007/s00018-010-0293-y>.
- Sesack, S.R., Hawrylyk, V.A., Guido, M.A., Levey, A.I., 1998. Cellular and subcellular localization of the dopamine transporter in rat cortex. *Adv. Pharmacol.* 42, 171–174.
- Shah, A.A., Sjøvold, T., Treit, D., 2004. Selective antagonism of medial prefrontal cortex D4 receptors decreases fear-related behaviour in rats. *Eur. J. Neurosci.* 19, 3393–3397. <https://doi.org/10.1111/j.0953-816X.2004.03447.x>.
- Solati, J., Hajikhani, R., Golub, Y., 2013. Activation of GABA_A receptors in the medial prefrontal cortex produces an anxiolytic-like response. *Acta Neuropsychiatr.* 25, 221–226. <https://doi.org/10.1111/acn.12016>.
- Steimer, T., Driscoll, P., 2003. Divergent stress responses and coping styles in psychogenetically selected Roman high-(RHA) and low-(RLA) avoidance rats: behavioural, neuroendocrine and developmental aspects. *Stress* 6, 87–100. <https://doi.org/10.1080/1025389031000111320>.
- Trujillo, V., Durando, P.E., Suárez, M.M., 2016. Maternal separation in early life modifies anxious behavior and Fos and glucocorticoid receptor expression in limbic neurons after chronic stress in rats: effects of tianeptine. *Stress* 19, 91–103. <https://doi.org/10.3109/10253890.2015.1105958>.
- Tsuchiya, M., Nijijima-Yaoita, F., Yoneda, H., Chiba, K., Tsuchiya, S., Hagiwara, Y., Sasaki, K., Sugawara, S., Endo, Y., Tan-No, K., Watanabe, M., 2014. Long-term feeding on powdered food causes hyperglycemia and signs of systemic illness in mice. *Life Sci.* 103, 8–14. <https://doi.org/10.1016/j.lfs.2014.03.022>.
- Ueno, K.I., Togashi, H., Mori, K., Matsumoto, M., Ohashi, S., Hoshino, A., Fujita, T., Saito, H., Minami, M., Yoshioka, M., 2002. Behavioural and pharmacological relevance of stroke-prone spontaneously hypertensive rats as an animal model of a developmental disorder. *Behav. Pharmacol.* 13, 1–13.
- Wang, X., Zhong, P., Yan, Z., 2002. Dopamine D4 receptors modulate GABAergic signaling in pyramidal neurons of prefrontal cortex. *J. Neurosci.* 22, 9185–9193.
- Yamamoto, T., Hirayama, A., 2001. Effects of soft-diet feeding on synaptic density in the hippocampus and parietal cortex of senescence-accelerated mice. *Brain Res.* 902, 255–263.
- Yamanaka, R., Akther, R., Furuta, M., Koyama, R., Tomofuji, T., Ekuni, D., Tamaki, N., Azuma, T., Yamamoto, T., Kishimoto, E., 2009. Relation of dietary preference to bite force and occlusal contact area in Japanese children. *J. Oral Rehabil.* 36, 584–591. <https://doi.org/10.1111/j.1365-2842.2009.01971.x>.
- Yoshino, F., Yoshida, A., Hori, N., Ono, Y., Kimoto, K., Onozuka, M., Lee, M.C., 2012. Soft-food diet induces oxidative stress in the rat brain. *Neurosci. Lett.* 508, 42–46. <https://doi.org/10.1016/j.neulet.2011.12.015>.
- Zhang, J., Fan, Y., Raza, M.U., Zhan, Y., Du, X.D., Patel, P.D., Zhu, M.Y., 2017. The regulation of corticosteroid receptors in response to chronic social defeat. *Neurochem. Int.* 108, 397–409. <https://doi.org/10.1016/j.neuint.2017.05.021>.



Novel androgen receptor full antagonists: Design, synthesis, and a docking study of glycerol and aminoglycerol derivatives that contain *p*-carborane cages

Asako Kaise^a, Kiminori Ohta^{b,*}, Shinya Fujii^c, Akifumi Oda^d, Tokuhito Goto^a, Yasuyuki Endo^a

^a Faculty of Pharmaceutical Sciences, Tohoku Medical and Pharmaceutical University, 4-4-1 Komatsushima, Aoba-ku, Sendai 981-8558, Japan

^b School of Pharmacy, Showa University, 1-5-8 Hatanodai, Shinagawa-ku, Tokyo 142-8555, Japan

^c Institute of Molecular and Cellular Bioscience, The University of Tokyo, 1-1-1 Yayoi, Bunkyo-ku, Tokyo 113-0032, Japan

^d Faculty of Pharmacy, Meijo University, 150 Yagotoyama, Tenpaku-ku, Nagoya 468-8503, Japan

ARTICLE INFO

Keywords:

Androgen receptor
Hydrophobic pharmacophore
Carborane
Anti-androgen withdrawal syndrome

ABSTRACT

Based on the co-crystal structure of bicalutamide with a T877A-mutated androgen receptor (AR), glycerol and aminoglycerol derivatives were designed and synthesized as a novel type of carborane-containing AR modulators. The (*R*)-isomer of **6c**, whose chirality is derived from the glycerol group, showed 20 times more potent cell inhibitory activity against LNCaP cell lines expressing T877A-mutated AR than the corresponding (*S*)-isomer. Docking studies of both isomers with AR suggested that (*R*)-**6c** is in closer spatial proximity to helix-12 of the AR than (*S*)-**6c**, which is the most important common motif in the secondary structure of AR for the expression of antagonistic activity.

1. Introduction

Worldwide, prostate cancer (PC) is one of the major causes of cancer-related death in men.¹ The molecular basis of this disease involves an irregular behavior of the functions mediated by the androgen receptor (AR), which belongs to the nuclear receptor (NR) superfamily of transcription factors that regulate gene transcription upon ligand binding.² Synthetic AR modulators can be structurally classified as either steroidal or non-steroidal, and may exhibit various types of functional (androgenic, anti-androgenic, or anabolic) activity.³ The non-steroidal ligand flutamide (**1**),⁴ which is metabolized into the more potent AR antagonist hydroxyflutamide (OH-Flu, **2**),⁴ is a well-known AR antagonist used for the treatment of PC (Fig. 1), while bicalutamide (Bic, **3**) is used for the treatment of D2-stage metastatic PC (Fig. 1).⁵ In contrast to steroidal ligands, these two typical non-steroidal AR antagonists exhibit a high selectivity for AR.

Anti-androgens are particularly useful for the early-stage treatment of PC. However, PC often advances to a hormone-refractory state, in which the disease progresses despite continued androgen ablation or anti-androgen therapy due to the appearance of androgen-independent PC cells or the ability of adrenal androgens to support tumor growth.⁶ Instances of anti-androgen-withdrawal syndrome (AWS), i.e., a clinical improvement upon withdrawal of the anti-androgen therapy, have also been reported after prolonged treatment with anti-androgens.⁷ Thus,

the development of pure AR full antagonists which are effective for AWS represents an attractive drug discovery goal in the context of AR.⁸ Although the molecular mechanism of operation for AR is not fully understood yet, one proposed mechanism is based on the hypothesis that AR may be subject to a mutation, which has been discovered in patients treated with flutamide.⁹ AR mutations that result in receptor promiscuity and the ability of anti-androgens to exhibit agonist activity might at least partially account for this phenomenon. In particular, a point mutation at T877 has been discovered in the AR-ligand-binding domain (AR LBD) in AWS patients, and this mutation has since been considered as a hotspot for the critical pathology.⁹ Bic, which is the most widely used pure anti-androgen agent, acts as an anti-androgen for the T877A-mutated AR. However, Bic also exhibits significant androgenic activity towards W741L- or W741C-mutated AR, which is known as Bic-withdrawal syndrome (BWS).⁹

Carborane-containing ligands are of interest in medicinal chemistry, as they exhibit a different spectrum of ligand responsiveness relative to other therapeutic agents due to their unique chemical and structural features.¹⁰ We have reported several *in vivo* drug candidates, such as estrogen-receptor modulators¹¹ and retinoid-X-receptor antagonists¹² that contain a carborane cage as a hydrophobic pharmacophore. Moreover, we have obtained several useful carborane-containing AR ligands as PC-treatment-drug candidates and AR-related biochemical tools, e.g. BA341 (**4**) and BA632 (**5**).^{13,14} Compound **4** showed more

* Corresponding author.

E-mail address: k-ohta@pharm.showa-u.ac.jp (K. Ohta).

<https://doi.org/10.1016/j.bmc.2018.06.007>

Received 16 April 2018; Received in revised form 6 June 2018; Accepted 6 June 2018
Available online 07 June 2018

0968-0896/ © 2018 Elsevier Ltd. All rights reserved.

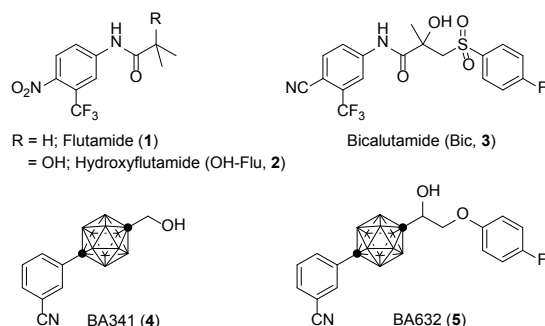


Fig. 1. Structures of non-steroidal and carborane-containing AR ligands.

potent AR-binding and AR-antagonistic activity levels than **2**, but acted as an agonist toward LNCaP cells, which express the T877A-mutated AR ($EC_{50} = 6.3 \times 10^{-7}$ M). Compound **5**, which contains a Bic-like side chain, acted as an AR full antagonist for LNCaP cells, i.e., the carborane cage acted as an effective hydrophobic pharmacophore for the AR LBD for both agonist and antagonist.

It seems that the steric repulsion between the carborane cage and several amino acid residues around helix-12 is able to directly control helix-12, which is crucial for expressing AR-antagonistic activity.² Our strategy for the development of AR full antagonists is based on a permanent AR antagonistic activity that is unaffected by the point mutation of AR LBD, using the direct repulsion between helix-12 and the carborane cage. Bohl et al. have reported that the cyano group of Bic interacts with the amino-acid residues Arg752, Glu711, and Met745 of AR LBD via a water molecule in co-crystal structure (Fig. 2a).¹⁵

Glycerol and aminoglycerol groups contain three hydrogen-bond acceptors and two or three hydrogen-bond donors, respectively. We anticipated that compounds with these groups could effectively bind to the target protein through the formation of multivalent hydrogen bonds. Although Hosoda et al. have reported that diphenylmethane

derivatives with glycerol and aminoglycerol groups bind to the vitamin D receptor (VDR) and AR LBD, the specific roles of glycerol and aminoglycerol remain unclear.¹⁶ Thus, we designed novel *p*-carborane derivatives with glycerol (**6**) and aminoglycerol groups (**7**) at the *para* position to mimic the binding mode of Bic with AR LBD containing a water molecule, and to bring the *p*-carborane cage closer to helix-12 in the AR (Fig. 2). In this paper, we describe the synthesis of novel *p*-carborane derivatives with glycerol (**6**) and aminoglycerol groups (**7**) at the *para* position and their biological activity, i.e., AR binding, their effect on AR-dependent proliferation of SC-3 and LNCaP cells, and an AR-ligand docking simulation study.

2. Results and discussion

2.1. Chemistry

Scheme 1 summarizes the synthesis of the target molecules **6** and **7**. *p*-Carborane derivative **8**,¹¹ which is protected with a *tert*-butyldimethylsilyl (TBS) group was consecutively treated with *n*-BuLi and CuCl to afford the corresponding Cu reagent, which was reacted with 4-iodoanisole or 4-iodonitrobenzene under Ullmann coupling conditions to furnish the corresponding aryl-*p*-carborane derivatives **9** and **11** in 54% and 80% yield, respectively.¹⁷ The methoxy and TBS groups of **9** were deprotected with BBr₃ to afford phenol derivative **10**, in which a phenol group between two hydroxy groups is selectively transformed with 3-chloro-1,2-propanediol to generate the corresponding glycerol derivative **6a** in 91% yield over two steps. The reduction of the nitro group of **11** was accomplished by a catalytic hydrogenation using Pd/C under an atmosphere of hydrogen. The thus quantitatively obtained aniline (**12**) was reacted with glycidol, and the TBS group was subsequently deprotected with tetra-*n*-butylammonium fluoride (TBAF) to furnish the corresponding aminoglycerol derivative (**7**) in 29% yield over two steps.

Scheme 2 summarizes the synthesis of **6b**, **6c**, and **14**, whereby the

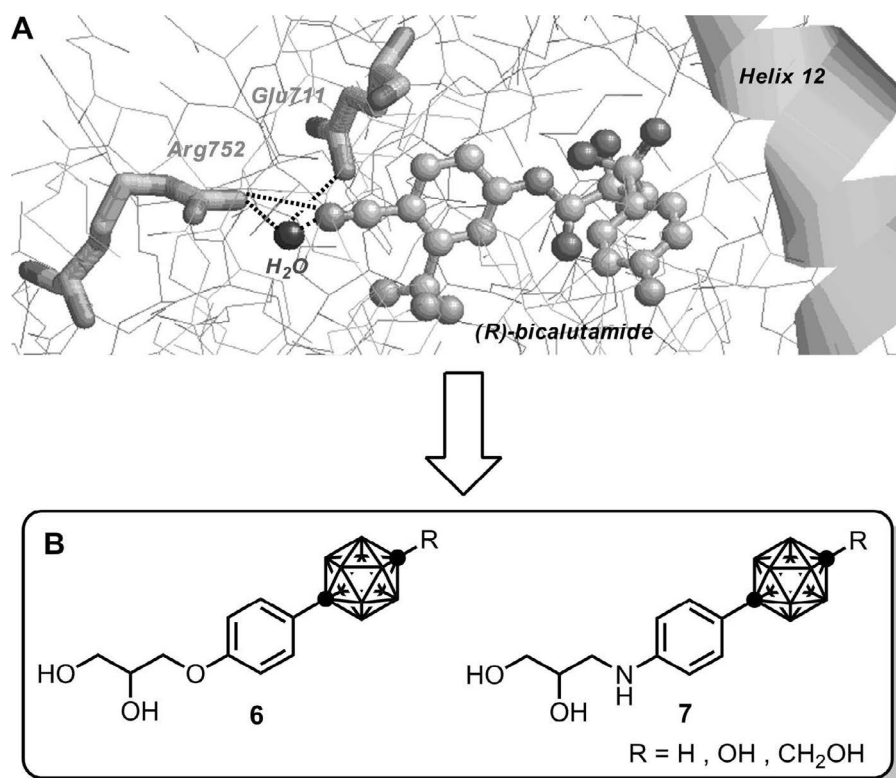
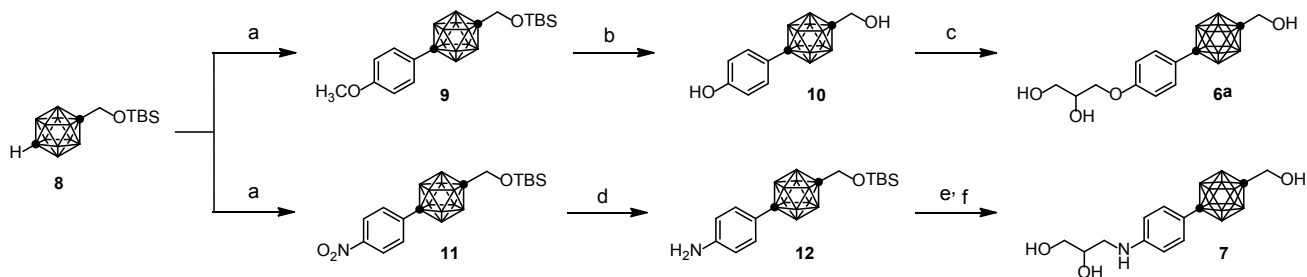


Fig. 2. (A) X-ray crystal structure of bicalutamide with AR-LBD (PDBID: 1Z95); (B) Design of novel carborane-containing AR full antagonist drug candidates **6** and **7**.



Scheme 1. Synthesis of hydroxymethyl derivatives **6a** and **7**. *Reagents and conditions:* (a) *n*-BuLi, DME, CuCl, pyridine; then 4-iodoanisole or 4-iodonitrobenzene, 100 °C; (b) BBr₃, CH₂Cl₂; (c) 3-chloro-1,2-propanediol, K₂CO₃, DMF; (d) Pd/C, H₂, MeOH; (e) glycidol, EtOH; (f) TBAF, THF.

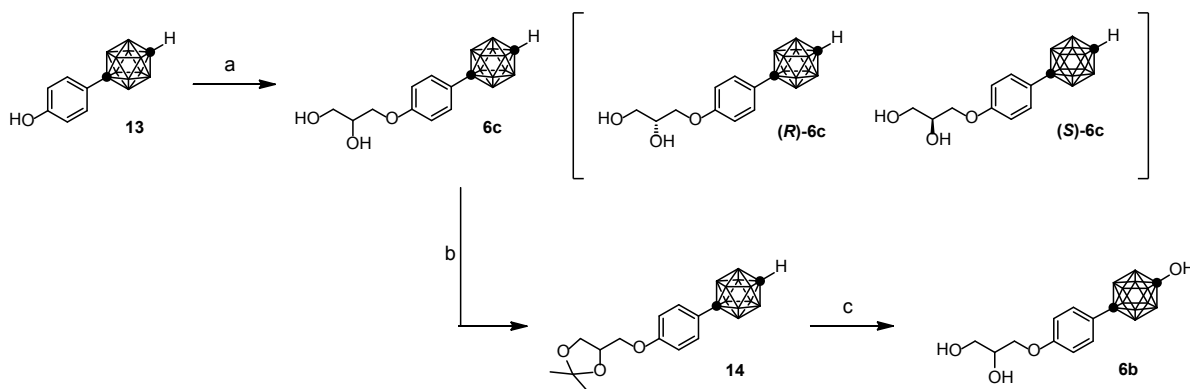
latter is the acetone-protected derivative of **6c**. *p*-Carboranyl phenol **13**¹¹ was treated with 3-chloro-1,2-propanediol in the presence of potassium carbonate to afford the corresponding glycerol derivative (**6c**) in 82% yield. In this reaction, using of (*R*)- or (*S*)-3-chloro-1,2-propanediol instead of the corresponding racemic reagent afforded chiral glycerol derivatives (*R*)-**6c** and (*S*)-**6c** in 76% and 97% yield, respectively. Both compounds showed an optical purity of > 99% (HPLC). The diol moiety of **6c** was initially protected with acetone to afford the corresponding acetonide (**14**) in 88% yield, which was transformed into the boronic ester that was subjected to an oxidative rearrangement with H₂O₂ in the presence of acetic acid, followed by deprotection of the acetonide to afford *p*-carboranol **6b** in 69% yield.¹⁸

2.2. Biological activities of the synthesized compounds

Binding affinities of **6**, **7**, and **14** for human AR (hAR) were evaluated by means of a competitive binding assay using [1,2-³H]-dihydrotestosterone ([³H]-DHT) and hAR.^{13,14} The results showed that **6a–6c** and **7** bind in a dose-dependent fashion to the AR LBD and that their affinity values are comparable to or slightly weaker than that of OH-Flu. The binding affinity of (*R*)-**6c** for hAR is slightly higher than that of (*S*)-**6c**, which suggests that the orientation of the secondary hydroxyl group in both enantiomers has little effect on the formation of hydrogen bonds with the amino acid residues Arg752 and Glu711 in the AR LBD. Our hypothesis was supported by the fact that **14**, in which the central functional group is masked by an acetonide, showed no binding affinity to the AR LBD. The glycerol or aminoglycerol groups of **6** and **7** play an important role for the binding to the AR LBD. Thus, these results strongly support the validity of our drug-design concept based on glycerol and aminoglycerol groups.

The anti-androgenic activity of **6**, **7**, and **14** was evaluated by cell-proliferation assays using SC-3 and LNCaP cell lines, which show AR-dependent proliferation. In these assay systems, endogenous steroid hormones, growth factors, and cytokines in fetal bovine serum (FBS)

were removed by the charcoal stripping treatment and these cells were only proliferated in the presence of 1 nM of testosterone. That is, we can directly understand AR-dependent cell proliferation inhibitory activity of the tested compounds in these assay systems. To further determine whether the cell proliferation activity of **6**, **7**, and **14** depends on AR, we also evaluated cell proliferation inhibitory activity against AR-independent prostate cancer cell line PC-3. OH-Flu, as an active metabolite of flutamide, showed the most potent antagonistic activity in the SC-3-proliferation assay, but acted as an agonist for LNCaP cells. On the other hand, (*R*)-Bic, an active enantiomer, showed antagonistic activity towards LNCaP cell lines (IC₅₀ = 0.43 μM). Glycerol derivatives **6a–6c** showed weaker AR antagonistic activity than OH-Flu in the SC-3-proliferation assay, but acted as AR antagonists toward LNCaP cells. Compound **6a**, which contains a hydroxymethyl group on another carbon atom of the *p*-carborane cage, showed the most potent AR-antagonistic activity toward LNCaP cell lines. Its IC₅₀ value (0.39 μM) was slightly lower than that of (*R*)-Bic. The IC₅₀ values of **6a–6c** toward LNCaP cells were affected by the size of the substituent at the carbon atom of the *p*-carborane (H > OH > CH₂OH). It seems that OH and CH₂OH groups form no strong hydrogen bond interactions with the amino acid residues of AR LBD. This result is probably due to the repulsion between the substituents and helix-12. We also examined the effects of the chirality of the secondary hydroxyl group in the glycerol group on the biological activity related to AR by using the chiral derivatives (*R*)-**6c** and (*S*)-**6c**. Interestingly, the (*R*)-isomer showed an AR-antagonistic activity in the LNCaP-proliferation assay that was 20 times more potent than that of the corresponding (*S*)-isomer, even though both enantiomers showed a similar binding affinity to hAR. As expected for **6a–6c**, the *p*-carborane cage of the (*R*)-isomer should be located closer to helix-12 in the AR LBD than that of the (*S*)-isomer. Aminoglycerol derivative **7** exhibited a similar bioactivity profile to that of the corresponding glycerol derivative **6a** in the AR-binding assay and the SC-3- and LNCaP-proliferation assays. None of the synthesized compounds showed cell proliferation inhibitory activity against AR



Scheme 2. Synthesis of glycerol derivatives **6b** and **6c** and acetonide **14**. *Reagents and conditions:* (a) *rac*-3-chloro-1,2-propanediol, K₂CO₃, DMF for **6c**; (*R*)- or (*S*)-3-chloro-1,2-propanediol, K₂CO₃, DMF for (*R*)- or (*S*)-**6c**, respectively; (b) acetone, *p*-TsOH; (c) *n*-BuLi, Et₂O, B(OMe)₃, H₂O₂, AcOH.

Table 1
Biological profiles of 6, 7, and 14.

Compound	IC ₅₀ (μM) for hAR-binding ^a	IC ₅₀ (μM) for cell proliferation ^b		
		SC-3 cell (AR+)	LNCaP cell (AR+)	PC-3 cell (AR-)
OH-Flu	10.6	0.02	Agonist	Inactive
(R)-Bic	nt	nt	0.43	Inactive
6a	15.9	0.27	0.39	Inactive
6b	16.1	0.70	1.6	Inactive
6c	12.5	0.58	5.7	Inactive
(R)-6c	10.3	1.0	0.66	Inactive
(S)-6c	12.2	0.50	11	Inactive
7	16.1	0.21	0.42	Inactive
14	Inactive	Inactive	Inactive	Inactive

^a All competitive binding assays were carried out in duplicate ($n = 2$) and IC₅₀ values were calculated based on the dose-response curves obtained from the binding assays.

^b SC-3 and LNCaP cells were incubated for 3 and 5 days, respectively, with the test compounds (0.1 nM–10 μM) in the presence of testosterone (1 nM). All assays were performed in triplicate ($n = 3$).

non-expression PC-3 cells. Therefore, cell proliferation inhibitory activity of **6** and **7** against SC-3 and LNCaP cells should be caused by the inhibition of AR activation by 1 nM of testosterone. As expected from the results of the AR-binding assay, acetamide **14** did not show any cell-proliferation activity toward the SC-3 or LNCaP cell lines. As the acetamide protecting group is stable under these assay conditions, such derivatives may be considered prodrugs of the glycerol and aminoglycerol derivatives (Table 1).¹⁹

2.3. Docking simulation study of (R)-6c and (S)-6c with AR

Docking simulation studies of (R)-6c and (S)-6c with T877A-mutated AR, using the co-crystal structure of T877A-mutated AR with cyproteron acetate (PDBID: 2OZ7), were performed with a docking program (GOLD 5.2).²⁰ The overall structure of the docking results is shown in Fig. 3A. The *p*-carborane cages of (R)-6c and (S)-6c are accommodated in a deep position of the hydrophobic pocket of the AR LBD close to helix-12, which is the most important common motif in the secondary structures of AR for the expression of antagonistic activity.

Surprisingly, we observed a difference regarding the location of both carborane cages. The *p*-carborane cage of (R)-6c is closer to the amino acid residue Met895 on helix-12 than that of the other enantiomer (Fig. 3B). We propose that the potent anti-androgenic activity of (R)-6c toward LNCaP cells is caused by the steric repulsion between the *p*-carborane cage as a hydrophobic pharmacophore and helix-12 of the AR LBD. As expected, the glycerol groups of (R)-6c and (S)-6c bind to the amino acid residues Arg752 and Gln711 of AR (Fig. 3C and D). Interestingly, the supposed interaction modes of the glycerol group of (R)-6c with the amino acid residues of Arg752 and Gln711 in the AR LBD are different from those obtained for (S)-6c. In the interaction mode of (R)-6c, an oxygen atom of the ether moiety and the secondary hydroxy group interacts with Gln711, whereas the secondary and primary hydroxy groups of (S)-6c interacts with Gln711. For Arg752 in AR, (R)-6c and (S)-6c interact with the secondary and primary hydroxy groups, respectively. Based on the results from the docking study and the biological activity, we suggest that the difference of the arrangement of the *p*-carborane cage between (R)-6c and (S)-6c should be caused by the different interaction modes of each glycerol group with the amino acid residues of Arg752 and Gln711 of AR, which was induced by the chirality of the secondary hydroxy group. It seems that the glycerol group can partially mimic the binding mode observed in the co-crystal structure of Bic with the AR LBD. These groups should thus be useful as novel functional groups for the development of AR ligands.

3. Conclusion

In summary, we have designed and synthesized *p*-carborane-containing glycerol and aminoglycerol derivatives based on the co-crystal structure of Bic with AR LBD. Glycerol and aminoglycerol groups can partially mimic the AR-Bic binding mode via a water molecule. Thus, the synthesized compounds bind to the AR LBD and exhibit anti-androgenic activity towards LNCaP cells by expressing the T877A-mutated receptor AR. The chiral secondary hydroxy group also plays an important role for the anti-androgenic activity toward LNCaP cells. Recently, it has been reported that Bic exhibits significant androgenic activity toward W741L- and W741C-mutated AR, which is called the Bic-withdrawal syndrome (BWS).⁹ We hope that **6** and **7** act as anti-androgens towards AWS and BWS owing to their significant structural differences relative to Bic. Biological assays of **6** and **7** would be performed using BWS

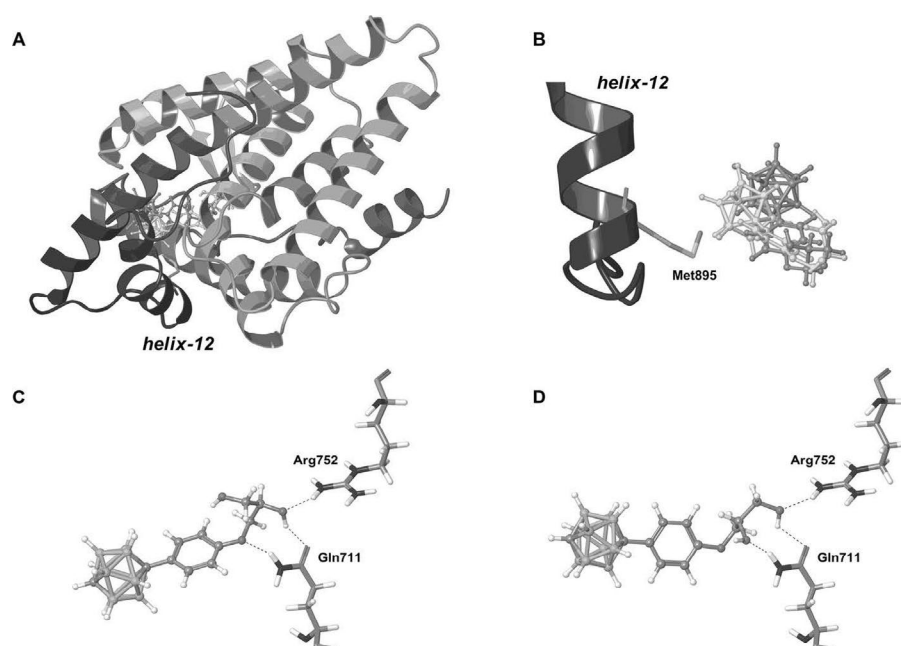


Fig. 3. Comparisons of the docking models for (R)-6c and (S)-6c with AR. (A) Overall view of the binding mode of (R)-6c (aqua) and (S)-6c (brown) with AR. (B) The arrangement of (R)-6c (aqua) and (S)-6c (brown) relative to the amino acid residue of Met895 on helix-12 in the AR LBD. (C) Proposed interaction of the glycerol group of (R)-6c with the amino acid residues of Arg752 and Gln711 in the AR LBD. (D) Proposed interaction of the glycerol group of (S)-6c with the amino acid residues of Arg752 and Gln711 in the AR LBD.

model cell lines. Further investigations, especially into the synthesis of analogues, the biological evaluation for other mutated ARs, and the tissue selectivity, are currently in progress.

4. Experimental section

4.1. General considerations

Melting points were determined on a Yanaco micro melting point apparatus and are uncorrected. ^1H NMR and $^{13}\text{C}\{^1\text{H}\}$ NMR spectra were recorded on JEOL JNM-EX-270 and JNM-LA-400 spectrometers. Chemical shifts (δ) are expressed in ppm relative to tetramethylsilane (0.0 ppm; ^1H NMR) as an internal standard, or against the signals of the deuterated solvents (^{13}C NMR). The splitting patterns are designated as follows: s (singlet), d (doublet), t (triplet), m (multiplet), and br (broad). Mass spectra were recorded on a JEOL JMS-DX-303 spectrometer. Column chromatography was carried out using Fuji Silysia BW80s, while TLC was performed on Merck silica gel F₂₅₄. *p*-Carborane was purchased from Katchem s.r.o. Other chemicals were purchased from Aldrich or Tokyo Kasei Ltd. and used without further purification. All solvents were commercial products of reagent grade, which were used without further purification.

4.2. Synthesis

4.2.1. 1-*tert*-Butyldimethylsiloxyethyl-12-(4-methoxyphenyl)-1,12-dicarba-closo-dodecaborane (9)

A 2.64 M solution of *n*-BuLi in hexane (3.96 mL, 10.5 mmol) was added dropwise to a solution of **8** (2.0 g, 6.94 mmol) in DME (5 mL) at 0 °C under argon (Ar) atmosphere.¹¹ The mixture was stirred at room temperature for 30 min, before CuCl (920 mg, 9.02 mmol) was added in one portion. Stirring was continued at room temperature for 1 h, before pyridine (4.13 mL, 51.3 mmol) and 4-iodoanisole (1.85 g, 7.92 mmol) were added in one portion. Subsequently, the mixture was heated to 100 °C for 45 h. After cooling, the reaction was quenched with 10% aq. HCl, before the insoluble materials were removed by filtration through Celite. The filtrate was extracted with AcOEt, and the organic fractions were washed with 10% aq. Na₂S₂O₃ and brine, dried over Na₂SO₄, and concentrated. Purification by column chromatography on silica gel (eluent: *n*-hexane to *n*-hexane/AcOEt = 10/1, v/v) gave **10** (1.47 g, 3.72 mmol) as a colorless solid in 54% yield; ^1H NMR (400 MHz, CDCl₃) –0.02 (s, 6H), 0.86 (s, 9H), 1.00–3.50 (brm, 10H), 3.49 (s, 2H), 3.74 (s, 3H), 6.67 (d, J = 8.8 Hz, 2H), 7.14 (d, J = 8.8 Hz, 2H); $^{13}\text{C}\{^1\text{H}\}$ NMR (100 MHz, CD₃OD) –5.7, 18.2, 25.7, 55.2, 66.5, 81.1, 81.9, 113.2, 128.3, 128.5, 159.5; MS (EI) m/z 394 (M^+), 337 (100%).

4.2.2. 1-Hydroxymethyl-12-(4-hydroxyphenyl)-1,12-dicarba-closo-dodecaborane (10)

A 1 M solution of BBr₃ in CH₂Cl₂ (0.36 mL, 0.36 mmol) was added dropwise to a solution of **9** (20 mg, 0.05 mmol) in CH₂Cl₂ (1 mL) at 0 °C under Ar atmosphere, before the reaction mixture was stirred at room temperature for 16 h. The reaction was quenched with water and the reaction mixture was extracted with CH₂Cl₂. The organic layer was washed with brine, dried over Na₂SO₄, and concentrated. Purification by column chromatography on silica gel (eluent: *n*-hexane to *n*-hexane/AcOEt = 10/1, v/v) gave **10** (16.6 mg, 0.07 mmol) as a colorless solid in quantitative yield; ^1H NMR (400 MHz, CD₃OD) 1.00–3.50 (brm, 10H), 3.55 (s, 2H), 4.96 (brs, 1H), 6.61 (d, J = 8.8 Hz, 2H), 7.06 (d, J = 8.8 Hz, 2H); $^{13}\text{C}\{^1\text{H}\}$ NMR (100 MHz, CD₃OD) 66.1, 82.7, 83.6, 115.6, 128.6, 129.6, 129.3, 158.6; MS (EI) m/z 266 (M^+), 250 (100%).

4.2.3. 1-Hydroxymethyl-12-{4-(2,3-dihydroxypropyloxy)phenyl}-1,12-dicarba-closo-dodecaborane (6a)

To a solution of **10** (200 mg, 0.76 mmol) in DMF (5 mL) was added 3-chloro-1,2-propanediol (76 μL , 0.91 mmol) and K₂CO₃ (130 mg, 0.91 mmol) at room temperature under Ar atmosphere. The mixture

was heated at 80 °C for 8 h, before 3-chloro-1,2-propanediol (456 μL , 5.47 mmol) and K₂CO₃ (455 mg, 3.19 mmol) were further added. The reaction was continued for 40 h until **10** was disappeared on TLC. After cooling, the reaction was quenched with water and the reaction mixture was extracted with AcOEt. The organic layer was washed with brine, dried over Na₂SO₄, and concentrated. Purification by column chromatography on silica gel (eluent: *n*-hexane/AcOEt = 10/1 to 5/1, v/v) gave **6a** (236 mg, 0.69 mmol) as a colorless solid in 91% yield; Colorless prisms (MeOH); mp 144.0–146.0 °C; ^1H NMR (400 MHz, CD₃OD) 1.00–3.50 (brm, 10H), 3.46 (s, 2H), 3.58–3.66 (m, 2H), 3.88–3.94 (m, 2H), 3.97–4.02 (m, 1H), 6.77 (d, J = 9.3 Hz, 2H), 7.12 (d, J = 9.3 Hz, 2H); $^{13}\text{C}\{^1\text{H}\}$ NMR (100 MHz, CD₃OD) 64.1, 66.2, 70.4, 71.7, 83.3, 115.0, 115.9, 129.4, 130.0, 160.6. MS (EI) m/z 340 (M^+), 266 (100%); HRMS Calcd for C₁₂H₂₄B₁₀O₄: 340.2678, Found: 340.2677; Anal. Calcd for C₁₂H₂₄B₁₀O₄: C, 42.35; H, 7.06; Found: C, 42.34; H, 7.11.

4.2.4. 1-*tert*-Butyldimethylsiloxyethyl-12-(4-nitrophenyl)-1,12-dicarba-closo-dodecaborane (11)

Compound **11** was prepared by the same method as described for the synthesis of **9** using 4-iodonitrobenzene (0.33 g, 1.31 mmol) instead of 4-iodoanisole; 330 mg (0.80 mmol, 80% yield); ^1H NMR (400 MHz, CDCl₃) –0.01 (s, 6H), 0.86 (s, 9H), 1.00–3.50 (brm, 10H), 3.50 (s, 2H), 7.38 (d, J = 8.8 Hz, 2H), 8.03 (d, J = 8.8 Hz, 2H); $^{13}\text{C}\{^1\text{H}\}$ NMR (100 MHz, CDCl₃) –5.7, 18.2, 25.6, 66.0, 79.9, 83.0, 123.2, 128.4, 142.9, 147.6; MS (EI) m/z 411 (M^+), 73 (100%).

4.2.5. 4-(1-*tert*-Butyldimethylsiloxyethyl-1,12-dicarba-closo-dodecaborane-1-yl)aniline (12)

A catalytic amount of Pd/C (80 mg) was added to a solution of **11** (400 mg, 0.97 mmol) in methanol (10 mL), before the mixture was stirred at room temperature for 3 h under H₂ atmosphere. Pd/C was removed by filtration through Celite, before the filtrate was evaporated. Purification by column chromatography on silica gel (eluent: *n*-hexane/AcOEt = 100/1 to 20/1, v/v) gave **12** (401 mg, 1.06 mmol) as a colorless solid in quantitative yield; ^1H NMR (400 MHz, CDCl₃) 1.00–3.50 (brm, 10H), 3.49 (s, 2H), 3.63 (brs, 2H), 6.44 (d, J = 8.8 Hz, 2H), 6.97 (d, J = 8.8 Hz, 2H); $^{13}\text{C}\{^1\text{H}\}$ NMR (100 MHz, CDCl₃) –5.7, 18.1, 25.7, 66.0, 80.6, 82.4, 114.1, 126.5, 128.1, 146.5; MS (EI) m/z 379 (M^+), 322 (100%).

4.2.6. *N*-2,3-Propanediol-4-(12-hydroxymethyl-1,12-dicarba-closo-dodecaborane-1-yl)aniline (7)

To a solution of **12** (50 mg, 0.13 mmol) in ethanol (3 mL) was added glycidol (11.7 mg, 0.16 mmol) at room temperature. The mixture was stirred at 80 °C for 48 h, before the solvent was removed under reduced pressure. Purification by column chromatography on silica gel (eluent: *n*-hexane/AcOEt = 5/1 to 2/1, v/v) gave *N*-2,3-propanediol-4-(12-*tert*-butyldimethylsiloxy-methyl-1,12-dicarba-closo-dodecaborane-1-yl)aniline (23 mg, 0.05 mmol) as a colorless solid in 39% yield; ^1H NMR (400 MHz, CDCl₃) –0.02 (s, 6H), 0.85 (s, 9H), 1.00–3.50 (brm, 10H), 3.12 (dd, J = 7.3 Hz, 13.2 Hz, 1H), 3.22 (dd, J = 4.4 Hz, 13.2 Hz, 1H), 3.49 (s, 2H), 3.60 (dd, J = 5.6 Hz, 11.2 Hz, 1H), 3.74 (dd, J = 3.5 Hz, 11.2 Hz, 1H), 3.88–3.95 (m, 1H), 6.41 (d, J = 8.8 Hz, 2H), 7.00 (d, J = 8.8 Hz, 2H); $^{13}\text{C}\{^1\text{H}\}$ NMR (100 MHz, CDCl₃) –5.6, 18.2, 25.7, 46.4, 64.7, 66.1, 70.2, 80.7, 82.4, 112.4, 126.3, 128.1, 147.7; MS (EI) m/z 453 (M^+), 393 (100%). A 1 M solution of TBAF in THF (0.07 mL, 0.07 mmol) was added to a solution of *N*-2,3-propanediol-4-(12-*tert*-butyldimethylsiloxy-methyl-1,12-dicarba-closo-dodecaborane-1-yl)aniline (20 mg, 0.04 mmol) in 1 mL of dry THF, before the reaction mixture was stirred at room temperature for 24 h. The reaction was quenched with water and the reaction mixture was extracted with AcOEt. The organic layer was washed with brine, dried over MgSO₄, and concentrated. Purification by column chromatography on silica gel (eluent: *n*-hexane/AcOEt = 1/1 to 1/2, v/v) gave **7** (10 mg, 0.03 mmol) as a colorless solid in 75% yield; Colorless cubes (CHCl₃); mp 137.5–139.0 °C; ^1H NMR (400 MHz, CDCl₃) 1.00–3.50 (brm, 10H), 3.13

(dd, $J = 7.8$ Hz, 13.2 Hz, 1H), 3.24 (dd, $J = 4.4$ Hz, 13.2 Hz, 1H), 3.54 (brs, 2H), 3.61 (dd, $J = 5.9$ Hz, 11.2 Hz, 1H), 3.75 (dd, $J = 3.3$ Hz, 11.2 Hz, 1H), 3.89–3.95 (m, 1H), 6.42 (d, $J = 8.8$ Hz, 2H), 7.00 (d, $J = 8.8$ Hz, 2H); $^{13}\text{C}\{^1\text{H}\}$ NMR (100 MHz, CD_3OD) 47.3, 65.4, 66.2, 71.6, 82.5, 84.5, 112.9, 125.7, 128.9, 150.3; MS (EI) m/z 339 (M^+), 278 (100%); HRMS Calcd for $\text{C}_{12}\text{H}_{25}\text{B}_{10}\text{NO}_3$: 339.2839; Found: 339.2836; Anal. Calcd for $\text{C}_{12}\text{H}_{25}\text{B}_{10}\text{NO}_3$: C, 42.46; H, 7.42; N, 4.13; Found: C, 42.17; H, 7.27; N, 4.32.

4.2.7. 1-{4-(2,3-Dihydroxypropyloxy)phenyl}-1,12-dicarba-closo-dodecaborane (**6c**)

Compound **6c** was prepared by the same method as described for the synthesis of **6a** using **13**¹¹ (0.33 g, 1.31 mmol) instead of **10**; 330 mg (0.80 mmol, 80% yield); Colorless needles (*n*-hexane/ CH_2Cl_2); mp 81.0–83.0 °C; ^1H NMR (400 MHz, CDCl_3) 1.00–3.50 (brm, 10H), 1.89 (t, $J = 5.9$ Hz, 1H), 2.45 (d, $J = 4.9$ Hz, 1H), 2.76 (brs, 1H), 3.71 (dd, $J = 5.9$ Hz, 11.2 Hz, 1H), 3.78–3.84 (m, 1H), 3.97–3.98 (m, 2H), 4.05–4.08 (m, 1H), 6.69 (d, $J = 8.8$ Hz, 2H), 7.12 (d, $J = 8.8$ Hz, 2H); $^{13}\text{C}\{^1\text{H}\}$ NMR (100 MHz, CDCl_3) 59.3, 63.5, 69.1, 70.2, 86.1, 113.8, 128.3, 130.0, 158.3; MS (EI) m/z 310 (M^+), 236 (100%); HRMS Calcd for $\text{C}_{11}\text{H}_{22}\text{B}_{10}\text{O}_3$: 310.2573; Found: 340.2566; Anal. Calcd for $\text{C}_{11}\text{H}_{22}\text{B}_{10}\text{NO}_3$: C, 42.56; H, 7.14; Found: C, 42.66; H, 7.17.

4.2.8. 1-{4-(1,3-Dioxolane-2,2-dimethyl-4-methyloxy)phenyl}-1,12-dicarba-closo-dodecaborane (**14**)

A solution of **6c** (1.0 g, 3.23 mmol) and TsOH (80 mg, 0.46 mmol) in acetone (10 mL) was stirred at room temperature for 4 h, before the reaction was quenched with saturated aq. NaHCO_3 and the mixture was extracted with AcOEt. The organic layer was washed with brine, dried over Na_2SO_4 , and concentrated. Purification by column chromatography on silica gel (eluent: *n*-hexane/AcOEt = 10/1 to 1/1, v/v) gave **14** (994 mg, 2.84 mmol) as a colorless solid in 88% yield. Colorless thin needles (*n*-hexane); mp 85.0–86.0 °C; ^1H NMR (400 MHz, CDCl_3) 1.38 (s, 3H), 1.43 (s, 3H), 1.00–3.50 (brm, 10H), 2.75 (brs, 1H), 3.83–3.88 (m, 2H), 3.96–4.00 (m, 2H), 4.39–4.45 (m, 1H), 6.69 (d, $J = 8.8$ Hz, 2H), 7.11 (d, $J = 9.2$ Hz, 2H); $^{13}\text{C}\{^1\text{H}\}$ NMR (100 MHz, CDCl_3) 25.2, 26.6, 59.1, 66.6, 68.6, 73.6, 86.1, 109.5, 113.7, 128.0, 129.6, 158.4; MS (EI) m/z 350 (M^+), 101 (100%); HRMS Calcd for $\text{C}_{14}\text{H}_{26}\text{B}_{10}\text{O}_3$: 350.2886; Found: 350.2894; Anal. Calcd for $\text{C}_{14}\text{H}_{26}\text{B}_{10}\text{O}_3$: C, 47.98, H, 7.48; Found: C, 48.05; H, 7.53.

4.2.9. 1-Hydroxy-12-{4-(2,3-Dihydroxypropyloxy)phenyl}-1,12-dicarba-closo-dodecaborane (**6b**)

A 2.64 M solution of *n*-BuLi in hexane (1.2 mL, 3.33 mmol) was added dropwise to a solution of **14** (1.0 g, 2.86 mmol) in dry ether (20 mL) at 0 °C under Ar atmosphere. The mixture was cooled to –30 °C, before trimethyl borate (3.6 mL, 3.33 mmol) was added in one portion. The reaction mixture was warmed to 0 °C over 1 h. A mixture of 10 mL of 30% H_2O_2 and 7 mL AcOH was added to the reaction mixture, before the reaction was continued at room temperature for 11 h. Subsequently, saturated aq. NaHSO_3 (28 mL) and 10% aq. NaOH (48 mL) were added to the reaction mixture, before the solution was stirred at room temperature for 1 h. The reaction mixture was extracted with ether and the organic layer was washed with water and brine, dried over MgSO_4 , and concentrated. Purification by column chromatography on silica gel (eluent: *n*-hexane/AcOEt = 10/1 to 1/1, v/v) gave **6b** (0.65 mg, 1.98 mmol) as a colorless solid in 69% yield; Colorless sheets (ether/*n*-hexane); mp 200.0–201.5 °C; ^1H NMR (400 MHz, CDCl_3) 1.0–3.5 (brm, 10H), 3.58–3.63 (m, 2H), 3.87–3.92 (m, 2H), 3.96–4.00 (m, 1H), 6.75 (d, $J = 8.8$ Hz, 2H), 7.11 (d, $J = 8.8$ Hz, 2H); $^{13}\text{C}\{^1\text{H}\}$ NMR (100 MHz, CDCl_3) 59.3, 63.5, 69.1, 70.2, 86.1, 113.8, 128.3, 130.0, 158.4; MS (EI) m/z 326 (M^+), 252 (100%); HRMS Calcd for $\text{C}_{11}\text{H}_{22}\text{B}_{10}\text{O}_4$: 326.2522; Found: 326.2525; Anal. Calcd for $\text{C}_{11}\text{H}_{22}\text{B}_{10}\text{O}_4$: C, 40.48; H, 6.79; Found: C, 40.53; H, 6.75.

4.3. A competitive binding assay against AR

Binding affinities of test compounds for hAR (human androgen receptor) were measured in competition experiments using [^3H]-DHT and cytosolic fraction of hAR-LBD (hAR ligand-binding domain)-transformed *Escherichia coli* as described previously. A hAR-LBD expression plasmid vector that encodes GST-hARLBD (627–919 aa, EF domain) fusion protein under the *lac* promoter (provided by Prof. S. Kato, University of Tokyo) was transfected into *E. coli* strain HB-101. An overnight culture (10 mL) of the bacteria was added to 1 L of LB medium and incubated at 27 °C until its optical density reached 0.6–0.7 at 600 nm. Following the addition of IPTG to a concentration of 1 mM, incubation was continued for an additional 4.5 h. Cells were harvested by centrifugation at 4000 g at 4 °C for 15 min and stored at –80 °C until use. All subsequent operations were performed at 4 °C. The bacterial pellet obtained from 40 mL of culture was resuspended in 1 mL of ice-cold TEGDM buffer (10 mM Tris-HCl pH 7.4, 1 mM EDTA, 10% glycerol, 10 mM DTT, 10 mM sodium molybdate). This suspension was subjected to sonication (10 × 10 s bursts) on ice, and crude GST-hARLBD fraction was prepared by centrifugation of the suspension at 12,000 g for 30 min at 4 °C. This crude receptor fraction was diluted with buffer (20 mM Tris-HCl pH 8.0, 0.3 M KCl, 1 mM EDTA) to a protein concentration of 0.3–0.5 mg/mL and used in binding assays as hAR-LBD fraction. Aliquots of the hAR-LBD fraction were incubated in the dark at 4 °C with [^3H]-DHT (NEN, 4 nM final concentration), triamcinolone acetonide (1 μM final concentration), and reference or test compounds (dissolved in DMSO). Nonspecific binding was assessed by addition of a 200-fold excess of nonradioactive DHT. After 15 h, a Dextran T-70/c-globulin-coated-charcoal suspension was added to the ligand/protein mixture (1% Norit A, 0.05% c-globulin, 0.05% Dextran T-70 final concentration each) and the whole was incubated at 4 °C for 10 min. The charcoal was removed by centrifugation for 5 min at 1300 g, and the radioactivity of the supernatant was measured in Atomlight (NEN) by using a liquid scintillation counter.

4.4. Cell growth inhibitory assay

4.4.1. SC-3 cell proliferation Assay¹⁴

SC-3 cells were cultivated in MEM α (Wako Co.) supplemented with 2% FBS, 100 IU/mL penicillin, 100 mg/mL streptomycin, and 1 nM testosterone at 37 °C in a 5% CO_2 humidified incubator. Cells were trypsinized from the maintenance dish with trypsin-EDTA and seeded in a 96-well plate at a density of 2000 cells per well (final volume: 100 μL) with MEM α supplemented with 2% charcoal-stripped FBS. After 1 day, 10 μL of the medium was removed from each well and 10 μL of solution containing serial dilutions of the test compounds or DMSO (dilute control) in the presence or absence of 1 nM testosterone were added to microcultures in triplicate. Cells were incubated at 37 °C under 5% CO_2 for 3 days and the proliferation was evaluated by using 10 μL WST-8 (DOJINDO), which was added to each well of microcultures before the cells were incubated for 4 h. Subsequently, the absorbance at 450 nm was measured with a model 680 microplate reader (BIO-RAD). This parameter is related to the number of living cells in the culture. The concentration required for 50% cell growth inhibition (GI_{50}) was calculated using the Prism 4 software.

4.4.2. LNCaP cell proliferation Assay¹⁴

LNCaP cells were cultivated in RPMI-1640 (Wako Co.) supplemented with 10% FBS at 37 °C under 5% CO_2 humidified incubator. Cells were trypsinized from the maintenance dish with trypsin-EDTA and seeded in a 96-well plate at a density of 3000 cells per well (final volume: 100 μL) with RPMI-1640 supplemented with 10% charcoal-stripped FBS. After 1 day, 10 μL of the medium was removed from each well and 10 μL of solution containing serial dilutions of the test compounds or DMSO (dilute control) in the presence or absence of 1 nM testosterone were added to microcultures in triplicate. Cells were

incubated at 37 °C under 5% CO₂ for 6 days. During this period, 50 µL of the medium was replaced from each well to the corresponding medium once after 3 days. The proliferation was evaluated by using 10 µL WST-8 (DOJINDO), which was added to each well of microcultures before the cells were incubated for 4 h. Subsequently, the absorbance at 450 nm was measured with a model 680 microplate reader (BIO-RAD). This parameter is related to the number of living cells in the culture. The concentration required for 50% cell growth inhibition (GI₅₀) was calculated using the Prism 4 software.

4.4.3. PC-3 cell proliferation Assay²¹

PC-3 cells were cultivated in RPMI-1640 (Wako Co.) supplemented with 10% FBS at 37 °C under 5% CO₂ humidified incubator. Cells were trypsinized from the maintenance dish with trypsin-EDTA and seeded in a 96-well plate at a density of 3000 cells per well (final volume: 100 µL); for the cell culture, the same media were used. After 1 day, the medium was removed from each well and 100 µL of solution containing serial dilutions of the test compounds or DMSO (dilute control) were added to microcultures in triplicate. Cells were incubated at 37 °C under 5% CO₂ for 3 days and the proliferation was evaluated by using 10 µL WST-8 (DOJINDO), which was added to each well of microcultures before the cells were incubated for 4 h. Subsequently, the absorbance at 450 nm was measured with a model 680 microplate reader (BIO-RAD). This parameter is related to the number of living cells in the culture. The concentration required for 50% cell growth inhibition (GI₅₀) was calculated using the Prism 4 software.

4.5. Computational study

Three-dimensional (3D) structures of protein-ligand complexes were predicted by GOLD 5.2 software with default settings.²⁰ The 3D structure of human AR used in this study was retrieved from the Protein DataBank (PDB) (PDB ID: 2OZ7). The active site of hAR LBD was defined as the collection of amino acids for which at least one atom was closer than 6.5 Å to any atom of the bound cyproteron acetate. The structural optimizations of ligands were carried out by B3LYP/6-31G(d,p) using Gaussian 09 (Gaussian, Inc., Wallingford, CT). Default values were used for other parameters, and the treatment of the ligand molecule was the same as in a previous study.²²

Acknowledgments

This research was supported by a grant-in-aid from the Strategic Research Program for Private Universities (2015–2019) and a grant-in-aid for Scientific Research (C) (26460151 and 15K08029) from the Japanese Ministry of Education, Culture, Sports, Science, and Technology (MEXT).

A. Supplementary data

Supplementary data associated with this article can be found, in the online version, at <http://dx.doi.org/10.1016/j.bmc.2018.06.007>.

References

- (a) Ferlay J, Soerjomataram I, Dikshit R, et al. *Int J Cancer*. 2015;136:E359
(b) Jemal A, Bray F, Center MM, Ferlay J, Ward E, Forman D. *CA Cancer J Clin*. 2011;61:69.
- (a) Evans RM. *Science*. 1988;240:889
(b) MacLean HE, Warne GL, Zajac JD. *J Steroid Biochem Mol Biol*. 1997;62:233
(c) McEwan IJ. *Biochem Soc Trans*. 2000;28:369
(d) Taplin M-E. *Expert Rev Anticancer Ther*. 2008;8:1495
(e) Castoria G, Auricchio F, Migliaccio A. *FASEB J*. 2017;31:1289.
- (a) Haendler B, Cleve A. *Mol Cell Endocrinol*. 2012;352:79
(b) Mohler ML, Bohl CE, Jones A, et al. *J Med Chem*. 2009;52:3597.
- (a) Neri RO, Peets EA. *J Steroid Biochem*. 1975;6:815
(b) Koch H. *Drugs Today*. 1984;20:561
(c) Neri R. *Urology*. 1989;34:19
(d) Wakeling AE, Furr BJ, Glen AT, Hughes LR. *J Steroid Biochem*. 1981;15:355
(e) Yeh S, Miyamoto H, Chang C. *Lancet*. 1997;349:852
(f) Bohl CE, Miller DD, Chen J, Bell CE, Dalton JT. *J Biol Chem*. 2005;280:37747.
- (a) Kolvenbag GJ, Blackledge GR, Gotting-Smith K. *Prostate*. 1998;34:61
(b) Fradet Y. *Expert Rev Anticancer Ther*. 2004;4:37.
- Scher HI, Steineck G, Kelly WK. *Urology*. 1995;46:142.
- (a) Taplin ME, Rajeshkumar B, Halabi S, et al. *J Clin Oncol*. 2003;21:2673
(b) Miyamoto H, Rahman MM, Chang C. *J Cell Biochem*. 2003;91:3
(c) Terada N, Shimizu Y, Yoshida T, et al. *Prostate*. 2010;70:252.
- (a) Guo C, Kephart S, Ornelas M, et al. *Bioorg Med Chem Lett*. 2012;22:1230
(b) Yamamoto Y, Lorient Y, Beraldi E, et al. *Clin Cancer Res*. 2015;21:1675.
- (a) Taplin ME, Bubley GJ, Ko YJ, et al. *Cancer Res*. 1999;59:2511
(b) Zhao XY, Malloy PJ, Krishnan AV, et al. *Nat Med*. 2000;6:703
(c) Hara T, Miyazaki Araki JH, Yamaoka M, Kanzaki N, Kusaka M, Miyamoto M. *Cancer Res*. 2003;63:149
(d) Yoshida T, Kinoshita H, Segawa T, et al. *Cancer Res*. 2005;65:9611
(e) Zhou J, Liu B, Geng G, Wu JH. *Proteins*. 2010;78:623.
- (a) Issa F, Kassiou M, Rendina LM. *Chem Rev*. 2011;111:5701.
(b) Endo Y, Iijima T, Yamakoshi Y, et al. *Chem Biol*. 2001;8:341
(c) Endo Y, Yoshimi T, Miyaura C. *Pure Appl Chem*. 2003;75:1197
(d) Nakagawasa O, Nemoto W, Onogi H, et al. *Behav Brain Res*. 2016;297:315.
- (a) Ohta K, Iijima T, Kawachi E, Kagechika H, Endo Y. *Bioorg Med Chem Lett*. 2004;14:5913
(b) Wietrzyk-Schindler M, Szyszka-Niagolov M, Ohta K, et al. *Biol Psychiatry*. 2011;69:788
(c) Calléja C, Messaddeq N, Chapellier B, et al. *Gene Dev*. 2006;20:1525.
- Fujii S, Goto T, Ohta K, et al. *J Med Chem*. 2005;48:4654.
- Goto T, Ohta K, Fujii S, Ohta S, Endo Y. *J Med Chem*. 2010;53:4917.
- Bohl CE, Gao W, Miller DD, Bell CE, Dalton JT. *Proc Natl Acad Sci USA*. 2005;102:6201.
- (a) Hosoda S, Tanatani A, Wakabayashi K, et al. *Bioorg Med Chem*. 2006;14:5489
(b) Hosoda S, Tanatani A, Wakabayashi K, et al. *Bioorg Med Chem Lett*. 2005;15:4327.
- (a) Coult R, Fox MA, Gill WR, Herbertson PL, MacBride JAH, Wade K. *J Organomet Chem*. 1993;462:19
(b) Ohta K, Goto T, Endo Y. *Inorg Chem*. 2005;44:8569.
- Ohta K, Goto T, Yamazaki H, Pichierri F, Endo Y. *Inorg Chem*. 2007;46:3970.
- Gupta VD. *J Pharm Sci*. 1983;72:1453.
- Jones G, Willett P, Glen RC. *J Mol Biol*. 1995;245:43.
- Kaise A, Ohta K, Endo Y. *Eur J Med Chem*. 2016;122:257.
- Ohta K, Goto T, Fujii S, et al. *Bioorg Med Chem*. 2011;19:3540.



Contents lists available at ScienceDirect

Neuropharmacology

journal homepage: www.elsevier.com/locate/neuropharm

Memantine ameliorates depressive-like behaviors by regulating hippocampal cell proliferation and neuroprotection in olfactory bulbectomized mice

Kohei Takahashi^a, Osamu Nakagawasai^{a,*}, Wataru Nemoto^a, Shogo Kadota^a,
Jinichi Isono^a, Takayo Odaira^a, Wakana Sakuma^a, Yuichiro Arai^b, Takeshi Tadano^c,
Koichi Tan-No^a

^a Department of Pharmacology, Faculty of Pharmaceutical Sciences, Tohoku Medical and Pharmaceutical University, 4-4-1 Komatsushima, Aoba-ku, Sendai 981-8558, Japan

^b Course of Judo-therapy, Faculty of Health Science, Tokyo Ariake University of Medical and Health Science, 2-9-1 Ariake, Koto-Ku, Tokyo 135-0063, Japan

^c Complementary and Alternative Medicine Clinical Research and Development, Graduate School of Medical Sciences, Kanazawa University, Kanazawa 920-8640, Japan

ARTICLE INFO

Article history:

Received 31 October 2017

Received in revised form

5 April 2018

Accepted 10 April 2018

Available online 4 May 2018

Keywords:

Apoptosis

Cell proliferation

Depression

Emotional behavior

Olfactory bulbectomy

Neuroinflammation

ABSTRACT

Our previous study suggested that the non-competitive N-methyl-D-aspartate receptor antagonist memantine (MEM) inhibits dopamine (DA) reuptake and turnover by inhibiting brain monoamine oxidase. Clinical studies have reported that MEM may improve depressive symptoms; however, specific mechanisms underlying this effect are unclear. We performed emotional behavior, tail suspension, and forced swimming tests to examine whether MEM has antidepressant effects in olfactory bulbectomized (OBX) mice, an animal model of depression. Subsequently, we investigated the effects of MEM on the distribution of tyrosine hydroxylase (TH), altered microglia morphometry, and astrocyte and cell proliferation in the hippocampus with immunohistochemistry. We also investigated MEM effects on the levels of norepinephrine (NE), DA, and their metabolites with high performance liquid chromatography, and of neurotrophic, proinflammatory, and apoptotic molecules in the hippocampus with western blotting. Forty-two days after surgery, OBX mice showed depressive-like behaviors, as well as decreased levels of monoamines, reduced cell proliferation, and lower levels of TH, phospho(p)-TH (ser31 and ser40), p-protein kinase A (PKA), p-DARPP-32, p-ERK1/2, p-CREB, brain-derived neurotrophic factor (BDNF), doublecortin, NeuN, and Bcl-2 levels. In contrast, the number of activated microglia and astrocytes and the levels of Iba1, GFAP, p-IkB- α , p-NF- κ B p65, TNF- α , IL-6, Bax, and cleaved caspase-3 were increased in the hippocampus. These changes (except for those in NE and Bax) were reversed with chronic administration of MEM. These results suggest that MEM-induced antidepressant effects are associated with enhanced hippocampal cell proliferation and neuroprotection via the PKA-ERK-CREB-BDNF/Bcl-2-caspase-3 pathway and increased DA levels.

© 2018 Elsevier Ltd. All rights reserved.

Abbreviations: ANOVA, analysis of variance; Bax, Bcl-2-associated protein X; Bcl-2, B cell lymphoma/leukemia gene 2; BDNF, brain-derived neurotrophic factor; BrdU, 5-bromo-2'-deoxyuridine; CREB, cAMP-responsive element binding protein; DA, dopamine; DARPP-32, dopamine- and cAMP-regulated phosphoprotein-32; DOPAC, dihydroxyphenylacetic acid; DG, dentate gyrus; ERK, extracellular signal-regulated protein kinase; GFAP, glial fibrillary acidic protein; HVA, homovanillic acid; Iba1, ionized calcium binding adaptor molecule 1; IL-6, interleukin-6; i.p., intraperitoneally; IkB- α , NF- κ B inhibitor- α ; MAO, monoamine oxidase; MEM, memantine; MHA, 3-methoxy-4-hydroxymandelic acid; NMDA, N-methyl-D-aspartate; NE, norepinephrine; NeuN, neuronal nuclear antigen; NF- κ B, nuclear factor-kappa B; OBX, olfactory bulbectomized; p.o., per os; PBS, phosphate-buffered saline; PFC, prefrontal cortex; PKA, protein kinase A; PLSD, Protected Least Significant Difference; ROI, region of interest; SEM, standard error of the mean; TH, tyrosine hydroxylase; TNF- α , tumor necrosis factor- α .

* Corresponding author. Department of Pharmacology, Faculty of Pharmaceutical Sciences, Tohoku Medical and Pharmaceutical University, 4-4-1 Komatsushima, Aoba-ku, Sendai, Miyagi 981-8558, Japan.

E-mail address: osamun@tohoku-mpu.ac.jp (O. Nakagawasai).

<https://doi.org/10.1016/j.neuropharm.2018.04.013>

0028-3908/© 2018 Elsevier Ltd. All rights reserved.

1. Introduction

Olfactory bulbectomized (OBX) mice are a useful experimental animal model for depression, as reported by us and several other researchers. OBX mice express abnormal behaviors, including cognitive deficits and depressive-like and hyperemotional behaviors (Kelly et al., 1997; Hozumi et al., 2003; Takahashi et al., 2011). These abnormal behaviors improve with chronic, but not acute, administration of antidepressant drugs (Breuer et al., 2009a; 2009b). Furthermore, physiological and neurochemical changes in OBX models, such as the reduction of hippocampal monoamines, cell proliferation, and brain-derived neurotrophic factor (BDNF) levels, were similar to those of clinical depression (Nakagawasai et al., 2003a, 2003b; 2016; Takahashi et al., 2016, 2017; Thakare et al., 2017). BDNF is known to play an important role in neuronal survival and is believed to regulate neuroplasticity, including neurogenesis (Waterhouse et al., 2012). Decreased adult hippocampal neurogenesis is associated with depression in both rodents and humans (Scorza et al., 2005; Duman and Monteggia, 2006; Castrén et al., 2007). Moreover, it has been reported that the effects of chronic antidepressant drug administration may be exerted through the enhancement of hippocampal neurogenesis (Santarelli et al., 2003). Thus, in some cases, enhanced neurogenesis in the hippocampus via BDNF signaling pathway activation may mediate the effects of antidepressants.

In contrast, OBX induces neuroinflammation in the hippocampus via activation of microglia, and this inflammation may be associated with depressive-like behavior (Rinwa and Kumar, 2013). The available evidence indicates that depression is closely associated with altered inflammation and microglia activation (Yirmiya et al., 2015), which manifest due to increased inflammatory cytokine levels (Miliot et al., 2016). Microglia function is affected by signaling systems associated with depression, namely BDNF (Gomes et al., 2013), glucocorticoids (Ros-Bernal et al., 2011), norepinephrine (NE), or dopamine (DA) (Färber et al., 2005). These reports suggest that microglia-induced inflammation is an important factor in depression. Furthermore, it has been reported that OBX-induced depressive-like behavior is associated with increased inflammatory cytokine and apoptotic factor levels (Rinwa et al., 2013). Antidepressants regulate several apoptotic factors, such as B cell lymphoma/leukemia gene 2 (Bcl-2) expression, which are involved in cell survival pathways (Engel et al., 2013). Thus, neurogenesis and apoptosis may constitute important drug targets for the modulation of depressive symptoms (Lucassen et al., 2006).

Recent clinical and preclinical studies have demonstrated that a subanesthetic single-dose of the N-methyl-D-aspartate (NMDA) receptor antagonist ketamine produces a rapid and sustained antidepressant effect in 70% of treatment-resistant patients with bipolar and major depressive disorder (Berman et al., 2012; Zarate et al., 2006; Diazgranados et al., 2010). Furthermore, our previous study suggested that a non-competitive NMDA receptor antagonist memantine (MEM) inhibits the reuptake and turnover of DA by inhibiting brain monoamine oxidase (MAO) (Onogi et al., 2009). In addition to the already described affinities for the NMDA and D₂ receptors, MEM binds with relatively high affinity to the $\alpha 7$ nicotinic and 5-HT₃ receptors (Berman et al., 2012; Kishi and Iwata, 2013; Parsons et al., 2007; Rammes et al., 2001) and possibly interacts with D₁ and 5-HT_{2A} receptors (Ishida et al., 2010; Nakaya et al., 2011). Clinical studies have reported that MEM may improve depressive symptoms, including emotional behavior (Matsunaga et al., 2015; Omranifard et al., 2017); however, the specific detailed mechanisms underlying this effect are unclear.

Therefore, we examined whether MEM improves OBX-induced depressive-like behaviors and investigated the molecular

mechanisms underlying this from the perspective of cell proliferation and neuroprotection.

2. Materials and methods

All experiments were performed following the approval of the Ethics Committee of Animal Experiments at Tohoku Medical and Pharmaceutical University, and according to the National Institutes of Health Guide for the Care and Use of Laboratory Animals. Efforts were made to minimize suffering and to reduce the number of animals used. The scores on the behavioral tests were determined manually and measurements were conducted by a blinded observer.

2.1. Animals

We used male ddY strain mice (weighing 28–32 g; Japan SLC, Shizuoka, Japan) for all experiments (total: $n = 330$; behavioral tests: $n = 250$; HPLC: $n = 16$; immunohistochemistry: $n = 34$; western blot analysis: $n = 30$). Mice were housed in groups in each cage with free access to food and water under conditions of constant temperature ($22 \pm 2^\circ\text{C}$) and humidity ($55 \pm 5\%$), on a 12-h light-dark cycle (lights on: 07:00–19:00).

2.2. Olfactory bulbectomized mice

OBX surgery was performed as previously described (Nakagawasai et al., 2003a). All mice were sacrificed at the end of the experiment and visually examined to confirm that two thirds of the olfactory bulb (OB) had been lesioned. We excluded data from mice in which the lesion was either not extensive enough or extended to the cortex. Sham operations were performed with the same procedure but without the removal of the OB.

2.3. Drugs

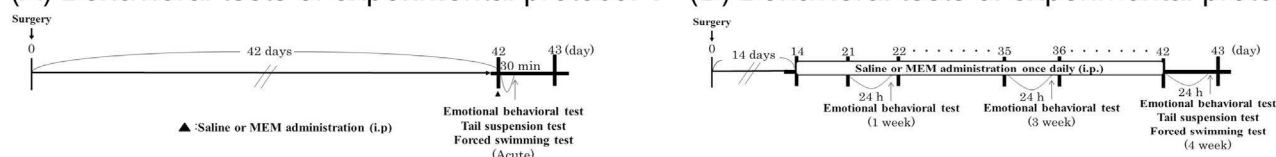
MEM (10 and 20 mg/kg; Sigma-Aldrich, St-Louis, USA) was dissolved in physiological saline and chronically intraperitoneally (i.p.) administered once daily between days 14–42 after surgery. Acute treatment of MEM was performed on the 42nd day after surgery.

2.4. Emotional assessments

The evaluation of hyperemotional behaviors in OBX rodents provide a suitable model for evaluating antidepressant efficiency (Saitoh et al., 2003, 2007). At 14–42 days after surgery, emotional behavior was measured with a modified procedure, which has been previously described (Takahashi et al., 2011). All animals underwent emotional behavior observation 30 min after a single drug injection on day 42, or 24 h after the last drug injection after 1, 3, and 4 weeks of administration. Each animal was tested within 10 min.

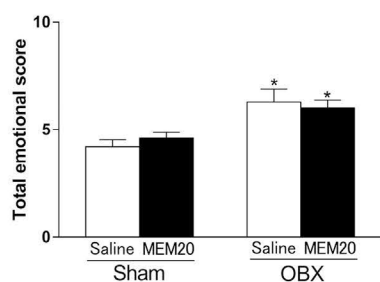
The study was conducted according to the experimental protocols shown in Fig. 1 (A and B). The emotional behavior of mice was measured by scoring their responses to the following stimuli: attack response, scored by presenting a rod of 4–5 cm in front of the snout; startle response, scored by blowing air on the dorsum using a 5-mL syringe; struggle response, scored by handling with a gloved hand; and fight response, scored by pinching the tail with forceps. The attack response was graded as follows: 0, no reaction; 1, slight; 2, moderate; 3, marked; or 4, extreme reaction. Other responses and vocalization during the test were scored and graded as follows: 0, no reaction or vocalization; 2, moderate; 4, extreme. Fewer gradations were used because it was difficult to discriminate

(A) Behavioral tests of experimental protocol 1 (B) Behavioral tests of experimental protocol 2

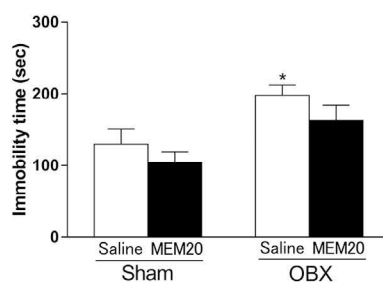


Acute administration

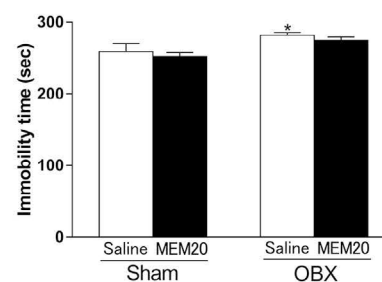
(C) Emotional behavioral test



(D) Tail suspension test

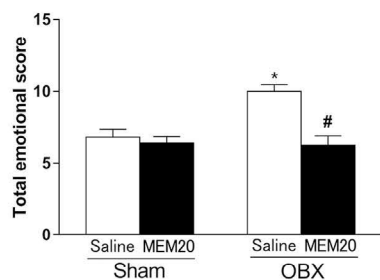


(E) Forced swimming test

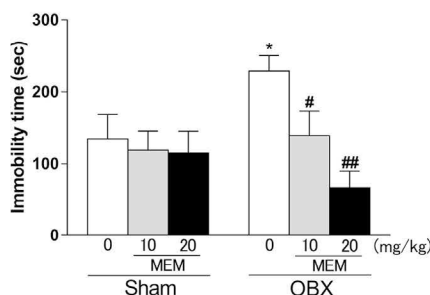


4 weeks administration

(F) Emotional behavioral test



(G) Tail suspension test



(H) Forced swimming test

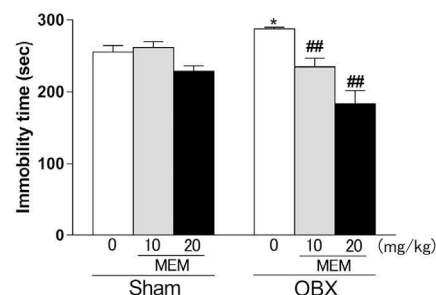


Fig. 1. Effects of memantine (MEM) on depressive-like behaviors of olfactory bulbectomized (OBX) mice. A, B: Experimental time course for behavioral tests of experimental protocol 1 (A) and of experimental protocol 2 (B). MEM effects were evaluated with an emotional behavior (C and F), tail-suspension (D and G), and forced swim (E and H) tests. The emotional behavior test was conducted after an acute, 1-week, 3-week, and 4-week administration of MEM, while the tail suspension and forced swim tests were conducted only after the acute or 4-week treatment. C–H: Quantification of the total emotional score (C and F) in the emotional test and immobility time in the tail suspension (D and G) and forced swim (E and H) tests. Bars represent means \pm SEM. Kruskal–Wallis test: (C), acute administration, $p < 0.01$; (F), chronic administration, $p < 0.01$. Two-way ANOVA [(D), group: $F(1, 38) = 11.88$, $p < 0.01$; treatment: $F(1, 38) = 2.70$, $p > 0.05$; group \times treatment: $F(1, 38) = 0.071$, $p > 0.05$; (E), group: $F(1, 37) = 13.29$, $p < 0.01$; treatment: $F(1, 37) = 1.33$, $p > 0.05$; group \times treatment: $F(1, 37) = 0.0048$, $p > 0.05$; (G), group: $F(1, 50) = 0.90$, $p > 0.05$; treatment: $F(2, 50) = 4.93$, $p < 0.05$; group \times treatment: $F(2, 50) = 3.06$, $p > 0.05$; and (H), group: $F(1, 52) = 2.08$, $p > 0.05$; treatment: $F(2, 52) = 17.79$, $p < 0.01$; group \times treatment: $F(2, 52) = 6.66$, $p < 0.01$]. * $p < 0.05$ vs. saline-treated sham group, # $p < 0.05$ and ## $p < 0.01$ vs. saline-treated OBX group ($n = 7–21$ per group).

differences in vocalization. Finally, we evaluated the total emotional score.

2.5. Tail suspension test

The tail suspension test was conducted to assess depressive-like behavior and the effects of antidepressants. Mice were suspended 30 cm above the floor by means of adhesive tape placed approximately 1 cm from the tip of the tail, 30 min after the acute or 24 h after the chronic administration. Mice were considered immobile only when they were hanging completely and were passively motionless. The duration of time spent immobile was quantified during a test period of 10 min.

2.6. Forced swimming test

The forced swimming test was conducted according to a

modified method of Porsolt et al. (1978). As a pre-test, mice were individually placed in vertical glass cylinders (height, 16 cm; diameter, 10 cm) that contained 8 cm of water, maintained at 25 °C, for 15 min. After 24 h, the time during which mice remained immobile was measured during a test period of 5 min. Mice were considered immobile when they passively floated in the water and only made movements necessary to keep their heads above the water line. The forced swimming test was performed 30 min after the acute or 24 h after the chronic drug administration on the 42nd day after surgery.

2.7. Western blotting

Mice were divided into four groups (sham/vehicle, sham/MEM 20 mg/kg, OBX/vehicle, OBX/MEM 20 mg/kg). The mice were sacrificed by decapitation after 4 weeks of saline or MEM administration. Protein isolation and western blots were performed as

described previously (Nakagawasai et al., 2016). After electrophoresis, proteins were transferred to a PVDF membrane, which was then incubated with blocking solution [10 mM Tris–HCl (pH 7.4), 100 mM NaCl, 0.01% Tween 20, and 5% skim milk] for 1 h and probed with antibodies against tyrosine hydroxylase (TH; 1:100; Millipore Corporation, Billerica, USA), phosphorylated-TH (p-TH, Ser31; 1:1000; Cell Signaling Technology, Danvers, USA), p-TH (Ser40; 1:500; Millipore Corporation), p-protein kinase A (PKA; 1:1000; Cell Signaling Technology), p-DA- and cAMP-regulated phosphoprotein-32 (DARPP-32; 1:1000; Cell Signaling Technology), extracellular signal-regulated protein kinase (ERK; 1:1000; Cell Signaling Technology), p-ERK (1:1000; Cell Signaling Technology), cAMP-responsive element binding protein (CREB; 1:1000; Cell Signaling Technology), p-CREB (1:1000; Cell Signaling Technology), BDNF (1:100; Abcam Ltd., Cambridge, UK), doublecortin (DCX; 1:100; Santa Cruz Biotech, Santa Cruz, CA), neuronal nuclear antigen (NeuN; 1:1000; Millipore Corporation), ionized calcium binding adaptor molecule 1 (Iba1; 1:500; Abcam Ltd.), glial fibrillary acidic protein (GFAP; 1:200; Millipore Corporation), tumor necrosis factor- α (TNF- α ; 1:1000; Cell Signaling Technology), interleukin-6 (IL-6; 1:1000; Cell Signaling Technology), p-nuclear factor-kappa B (NF- κ B) p65 (1:500; Cell Signaling Technology), p-NF- κ B inhibitor- α (I κ B- α ; 1:1000; Cell Signaling Technology), Bcl-2 (1:200; Santa Cruz Biotechnology), Bcl-2-associated protein X (Bax; 1:1000; Abcam Ltd.), cleaved caspase-3 (1:1000; Cell Signaling Technology), and β -actin (1:1000; Cell Signaling Technology) overnight at 4 °C. The membrane was then washed with blocking solution without milk, incubated with horseradish peroxidase-conjugated secondary antibody (Cell Signaling Technology/Abcam Ltd.) for 2 h, and the immunoreactive species were visualized with ECL Western blotting detection reagent (Amersham Life Science, Piscataway, USA). The densities of the bands were analyzed with densitometry (Image-J 1.43 μ , National Institute of Health).

2.8. High-performance liquid chromatography (HPLC)

Mice were divided into four groups (sham/saline, sham/MEM 20 mg/kg, OBX/saline, OBX/MEM 20 mg/kg). Sample isolation and measurement of monoamines were performed as described previously (Fukuda et al., 2011). The sample was homogenized in 0.1 M perchloric acid containing 100 ng/mL of isoproterenol as an internal standard. The homogenates were centrifuged at $10,000 \times g$ for 10 min. Supernatants were filtered through a 0.45- μ m pore size membrane filter. The filtrate was used for quantification of NE (Sigma-Aldrich), 3-methoxy-4-hydroxymandelic acid (MHA; Sigma-Aldrich), DA (Sigma-Aldrich), dihydroxyphenylacetic acid (DOPAC; Sigma-Aldrich), and homovanillic acid (HVA; Sigma-Aldrich) with HPLC coupled with electrochemical detection. In the mobile phase, we used 95% of 50 mM sodium acetate, 10 mM citric acid, 0.15 mM EDTA, 0.45 mM SOS, and 5% acetonitrile, adjusted to pH 3.6 with glacial acetic acid and filtered to 0.45 μ m. The flow rate was 0.4 mL/min. Electrochemical detection was accomplished with an electrochemical detector (model EC8020, Tosoh, Tokyo, Japan) with a glassy working electrode at a potential of 1700 mV. The ratios of MHA/NE, DOPAC/DA, and HVA/DA were used as an index of NE and DA turnover.

2.9. Immunohistochemistry

On day 42 after surgery, 5-bromo-2'-deoxyuridine (BrdU; Sigma-Aldrich; 75 mg/kg) was injected i.p. three times every 2 h after the last administration of saline or MEM. Animals were subsequently sacrificed 24 h after the last injection. Brain samples were collected as described previously (Nakagawasai et al., 2016). The brains were cut into 40 μ m sections from bregma –2.20

to –2.80 mm using a cryostat (MICROM HM560, Mikron Instrument, Inc., California, USA).

Frozen sections were mounted on glass slides (Matsunami Glass, Osaka, Japan). Sections were treated with HCl (2 N) at 37 °C for 30 min, followed by neutralization with sodium borate buffer (0.15 M) at room temperature twice every 10 min. After three washes every 5 min, the sections were incubated with phosphate-buffered saline (PBS) containing 1% normal goat serum (Life Technologies Corporation, Carlsbad, USA) and 0.3% Triton X-100 (PBSGT) at room temperature for 2 h. The sections were incubated overnight at 4 °C with rat anti-BrdU (1:100; Harlan SeraLab, Loughborough, UK) and mouse anti-NeuN (1:500; Millipore Corporation) monoclonal antibodies. Sections were washed and incubated for 2 h at room temperature with goat anti-rat IgG Alexa Fluor 568 (1:200; Molecular Probes, Eugene, USA) and goat anti-mouse IgG Alexa Fluor 488 (1:200; Molecular Probes) in PBSGT. Finally, sections were washed and coverslipped with Dako fluorescent mounting medium (Dako, Carpinteria, USA).

Immunofluorescent images were analyzed with a confocal laser-scanning microscope (A1Rsi; Nikon, Tokyo, Japan). Eight sections per mouse were analyzed. We counted the number of BrdU positive cells in both the right and left sides of the dentate gyrus (DG) images (640 \times 640 μ m) from each section. The total number of BrdU positive cells was extrapolated for the entire volume of the DG.

2.10. Neuromorphometrical study

The brain samples were collected as described previously (Nakagawasai et al., 2016) and in paragraph 2.9. The sections were incubated overnight at 4 °C with rabbit anti-TH (1:100; Millipore Corporation), rabbit anti-Iba1 (1:200; Wako Pure Chemical Industries Ltd, Osaka, Japan), and mouse GFAP (1:200; Millipore Corporation) antibodies. Sections were washed and incubated for 2 h at room temperature with goat anti-rabbit IgG Alexa Fluor 568 (1:200; Molecular Probes) and goat anti-mouse IgG Alexa Fluor 488 (1:200; Molecular Probes) in PBSGT. We observed alterations in TH-positive cells in OBX mice with a confocal laser-scanning microscope. We then evaluated the activation of microglia and astrocytes by observing and counting cells that typically exhibited hypertrophy with thicker processes, and larger and densely stained cell bodies.

2.11. Statistical analysis

Results are expressed as mean \pm standard error of the mean (SEM). The significance of differences was determined by a two-way analysis of variance (ANOVA), followed by Fisher's Protected Least Significant Difference (PLSD) test for multigroup comparisons. Regarding the emotional behavioral test, the statistical significance of differences was assessed with a non-parametric Kruskal–Wallis test followed by Steel's test (non-parametric statistical analysis). We considered $p < 0.05$ for representing significant differences.

3. Results

3.1. Effects of MEM on OBX-induced depressive-like behaviors

We measured emotional behavior to clarify whether emotional responses in OBX mice were affected by an acute, 1-week, 3-week, or 4-week treatment with MEM (20 mg/kg). There was a significant increase in the total emotional score in the OBX + saline group on day 42 after surgery compared with the sham + saline group [Fig. 1 (C–F)]. This was reversed after the 4-week chronic administration of MEM (20 mg/kg) [Fig. 1 (F)], but not after the acute administration

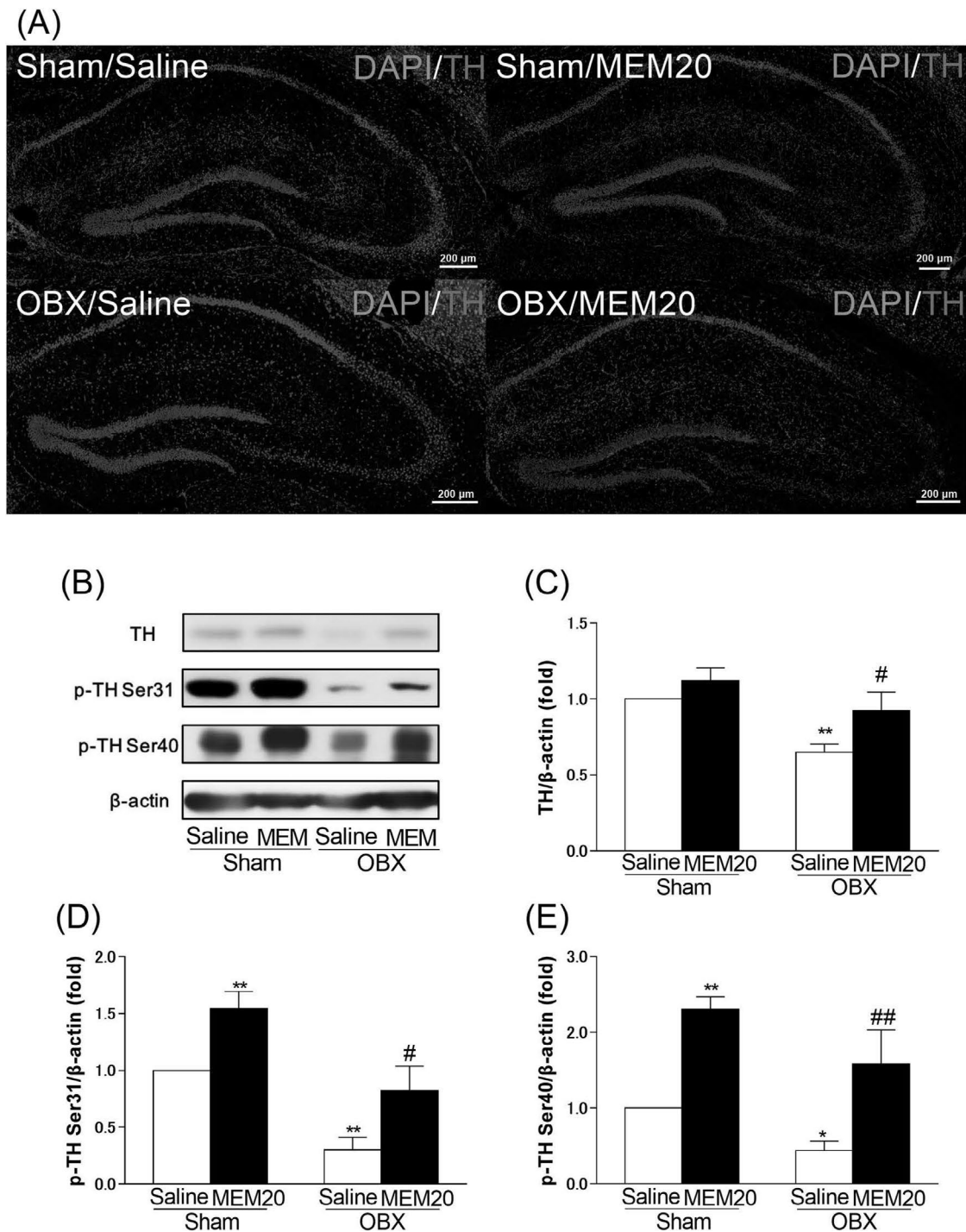


Fig. 2. Effects of memantine (MEM) on the levels of total and activated tyrosine hydroxylase (TH). A: Microscopy images of TH (red) and DAPI (blue) immunostaining in the hippocampus. Images show alterations in TH, p-TH^{Ser31}, and p-TH^{Ser40} levels in the hippocampus after MEM administration. B: Representative immunoblots probed with antibodies against TH, p-TH^{Ser31}, p-TH^{Ser40}, and β-actin. C–E: Quantification of the normalized to β-actin levels of TH, p-TH^{Ser31}, and p-TH^{Ser40} after saline or MEM treatment in sham-operated or olfactory bulbectomized (OBX) mice. Bars represent means ± SEM. Two-way ANOVA [(C), group: $F(1, 12) = 11.72$, $p < 0.01$; treatment: $F(1, 12) = 6.05$, $p < 0.05$; group × treatment: $F(1, 12) = 0.9$, $p > 0.05$; (D), group: $F(1, 12) = 34.14$, $p < 0.01$; treatment: $F(1, 12) = 19.28$, $p < 0.01$; group × treatment: $F(1, 12) = 0.011$, $p > 0.05$; and (E), group: $F(1, 12) = 6.83$, $p < 0.05$; treatment: $F(1, 12) = 25.23$, $p < 0.01$; group × treatment: $F(1, 12) = 0.11$, $p > 0.01$]. * $p < 0.05$ and ** $p < 0.01$ vs. saline-treated sham group, # $p < 0.05$ and ## $p < 0.01$ vs. saline-treated OBX group ($n = 3–5$ per group).

[Fig. 1 (C)]. On days 21 (1 week of drug treatment) and 35 (3 weeks of drug treatment) after surgery, we observed no differences between the OBX + saline and OBX + MEM groups (data not shown). Furthermore, on day 42 after surgery, OBX control mice remained

immobile for a significantly longer period than sham controls in both the tail suspension and forced swimming tests. In contrast, OBX mice, chronically treated with MEM (10 and 20 mg/kg), remained immobile for significantly shorter periods than the OBX

controls in both tests [Fig. 1 (G and H)], whereas acute administration of MEM (20 mg/kg) did not have this effect [Fig. 1 (D and E)]. In contrast, there was no change in the duration of immobility in either test between sham mice treated with MEM (10 and 20 mg/kg) and sham controls. These results suggest that chronic MEM-treatment improves OBX-induced depressive-like behaviors.

3.2. Changes in TH and monoamine levels in the hippocampus of OBX mice

Our previous study demonstrated that OBX induces a decrease in striatal TH levels, a biosynthetic rate-controlling enzyme of

catecholamines, such as NE and DA (Takahashi et al., 2016). Thakare et al. (2017) demonstrated a decrease in monoamines in the hippocampus of OBX mice. As the pathophysiology of depression is associated with low levels of monoamines in the central nervous system, like NE and DA, (Carlsson et al., 1969; Schildkraut and Kety, 1967), we examined whether OBX can decrease TH levels and activity in the hippocampus.

As shown in Fig. 2, the TH, p-TH^{ser31}, and p-TH^{ser40} immunocontent was significantly lower in OBX mice than in sham controls. Compared with saline, MEM treatment significantly increased TH levels in the hippocampus of OBX mice, and significantly increased p-TH^{ser31} and p-TH^{ser40} levels in the hippocampus of both groups.

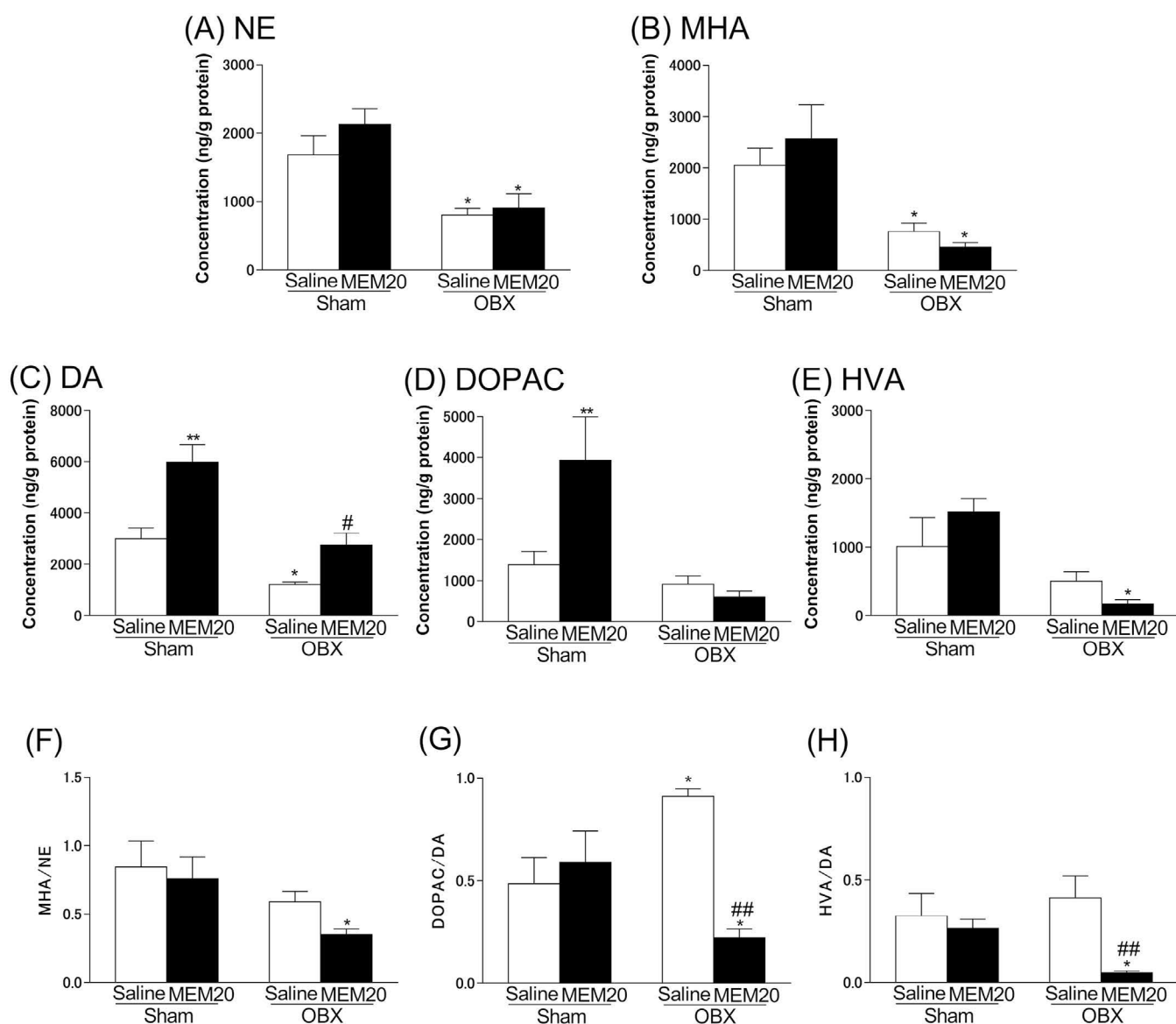


Fig. 3. Altered norepinephrine (NE), MHA (3-methoxy-4-hydroxymandelic acid), dopamine (DA), DOPAC (dihydroxyphenylacetic acid), and HVA (homovanillic acid) concentrations and turnover in the hippocampus of olfactory bulbectomized (OBX) mice. A–E: Graphs showing the quantification of the concentrations of NE (A), MHA (B), DA (C), DOPAC (D), and HVA (E) in the hippocampus of sham or OBX mice treated with saline or MEM. Concentrations are expressed as ng per g weight of fresh brain tissue. Bars represent means \pm SEM. Two-way ANOVA [(A), group: $F(1, 12) = 23.37$, $p < 0.01$; treatment: $F(1, 12) = 1.56$, $p > 0.05$; group \times treatment: $F(1, 12) = 0.62$, $p > 0.05$; (B), group: $F(1, 12) = 19.9$, $p < 0.01$; treatment: $F(1, 12) = 0.076$, $p > 0.05$; group \times treatment: $F(1, 12) = 1.16$, $p > 0.05$; (C), group: $F(1, 12) = 28.47$, $p < 0.01$; treatment: $F(1, 12) = 23.1$, $p < 0.01$; group \times treatment: $F(1, 12) = 2.41$, $p > 0.05$; (D), group: $F(1, 12) = 11.04$, $p < 0.01$; treatment: $F(1, 12) = 3.8$, $p > 0.05$; group \times treatment: $F(1, 12) = 6.29$, $p < 0.05$; and (E), group: $F(1, 12) = 14.04$, $p < 0.01$; treatment: $F(1, 12) = 0.12$, $p > 0.05$; group \times treatment: $F(1, 12) = 2.87$, $p > 0.05$]. F–H: Graphs showing the MHA/NE (F), DOPAC/DA (G), and HVA/DA (H) ratios. Bars represent means \pm SEM. Two-way ANOVA [(F), group: $F(1, 12) = 6.28$, $p < 0.05$; treatment: $F(1, 12) = 1.50$, $p > 0.05$; group \times treatment: $F(1, 12) = 0.34$, $p > 0.05$; (G), group: $F(1, 12) = 0.08$, $p > 0.05$; treatment: $F(1, 12) = 7.92$, $p < 0.05$; group \times treatment: $F(1, 12) = 14.42$, $p < 0.01$; and (H), group: $F(1, 12) = 0.43$, $p > 0.05$; treatment: $F(1, 12) = 7.19$, $p < 0.05$; group \times treatment: $F(1, 12) = 3.70$, $p > 0.05$]. * $p < 0.05$ and ** $p < 0.01$ vs. saline-treated sham group, # $p < 0.05$ and ## $p < 0.01$ vs. saline-treated OBX group ($n = 4$ per group).

From these results, we hypothesized that monoamines were decreased in the hippocampus of OBX mice, and that this could be reversed by MEM.

Next, we measured the levels of NE, DA, and their metabolites in the hippocampus of OBX mice [Fig. 3 (A–E)]. Sham mice treated with MEM had significantly higher levels of DA and DOPAC than the sham control group. We observed significantly lower NE, MHA, and DA concentrations in the OBX than the sham control group, while OBX mice treated with MEM had significantly higher DA levels. Moreover, we observed that the DOPAC/DA ratio was significantly higher in OBX mice than in sham controls, while the ratios of DOPAC/DA and HVA/DA were reduced after the administration of MEM in OBX mice [Fig. 3 (G and H)]. These results suggest that the antidepressant effects of MEM may underlie, at least in part, the increase in DA concentration in the hippocampus, via the inhibition of DA turnover.

3.3. Changes in p-PKA, p-DARPP-32, p-ERK, p-CREB, and BDNF levels in the hippocampus of OBX mice

In the present study, MEM led to increased DA levels in the hippocampus of OBX mice. We examined whether the magnitude of this increase is functionally meaningful. The stimulation of DA receptors activates PKA, DARPP-32, and the ERK-CREB-BDNF pathway (Bozzi et al., 2011). As shown in Fig. 4, the levels of p-PKA, p-DARPP-32, p-ERK, p-CREB, and BDNF were significantly lower in OBX mice than in sham controls. Compared with saline, MEM treatment significantly increased p-PKA and p-DARPP-32

levels in the hippocampal DG of both the sham and OBX groups. Similarly, MEM treatment increased p-ERK, p-CREB, and BDNF levels in the hippocampus of OBX mice. These results suggest that increased DA, induced by MEM, is functionally meaningful and that MEM-induced antidepressant effects might underlie the increased BDNF levels in the hippocampus, via the PKA-ERK-CREB pathway, by increasing DA.

3.4. Effect of MEM on reduced cell proliferation in the hippocampal DG of OBX mice

In the present study, MEM enhanced BDNF levels, which regulate forms of plasticity including neurogenesis in the hippocampus (Waterhouse et al., 2012). Therefore, animals were injected with BrdU on the 42nd day after surgery to determine the rate of hippocampal cell proliferation. Anti-NeuN antibody was used to identify mature neurons in the DG area. The incorporation of BrdU into a cell indicates that it was cycling at the time of the BrdU injection. We found a significantly lower number of BrdU positive cells in OBX than in sham mice [Fig. 5 (A and B)]. However, the chronic administration of MEM (20 mg/kg) significantly increased the number of BrdU positive cells in OBX mice.

In order to examine whether the excess of newborn cells differentiates into immature and mature neurons in the hippocampus, we investigated changes in DCX and NeuN, markers of immature and mature neurons, respectively, after MEM treatment. As shown in Fig. 5 (C–E), the immunocenters of DCX and NeuN in OBX mice were significantly lower than in sham controls. Compared with

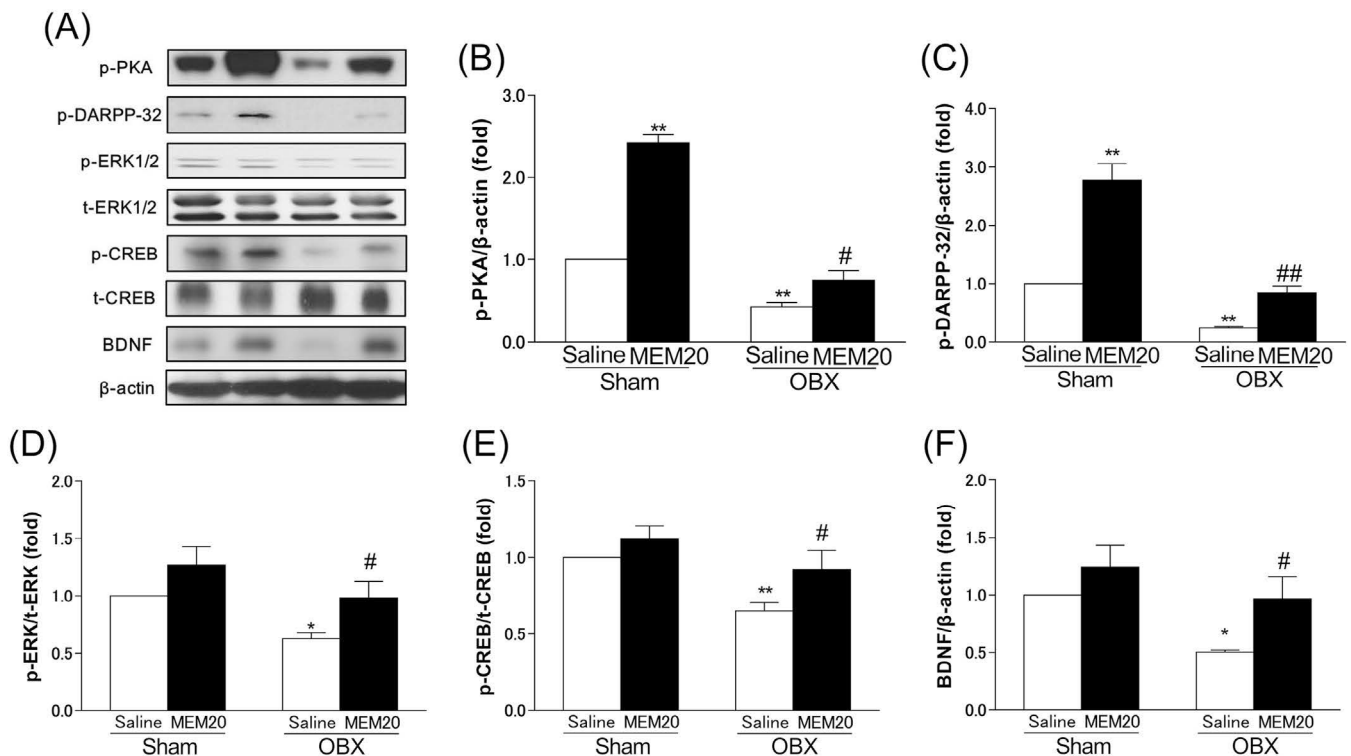


Fig. 4. Altered levels of the phosphorylated (p) forms of PKA, DARPP-32, ERK, and CREB, and of BDNF in the hippocampus after memantine (MEM) administration. A: Representative immunoblots probed with antibodies against p-PKA, p-DARPP-32, p-ERK, t-ERK, p-CREB, t-CREB, BDNF, and β-actin, as indicated. B–F: Quantification of the normalized values of p-PKA (B), p-DARPP-32 (C), and BDNF (F) levels with β-actin and of p-ERK (D) and p-CREB (E) with total (t)-ERK and t-CREB, respectively. Bars represent means ± SEM. Two-way ANOVA [(B), group: $F(1, 9) = 227.5$, $p < 0.01$; treatment: $F(1, 9) = 137.3$, $p < 0.01$; group × treatment: $F(1, 9) = 54.15$, $p < 0.01$; (C), group: $F(1, 12) = 125.8$, $p < 0.01$; treatment: $F(1, 12) = 96.87$, $p < 0.01$; group × treatment: $F(1, 12) = 23.98$, $p < 0.01$; (D), group: $F(1, 14) = 11.54$, $p < 0.01$; treatment: $F(1, 14) = 10.51$, $p < 0.01$; group × treatment: $F(1, 14) = 0.20$, $p > 0.05$; (E), group: $F(1, 12) = 11.72$, $p < 0.01$; treatment: $F(1, 12) = 6.05$, $p < 0.05$; group × treatment: $F(1, 12) = 0.90$, $p > 0.05$; and (F), group: $F(1, 15) = 9.19$, $p < 0.01$; treatment: $F(1, 15) = 7.67$, $p < 0.05$; group × treatment: $F(1, 15) = 0.73$, $p > 0.05$]. * $p < 0.05$ and ** $p < 0.01$ vs. saline-treated sham group, # $p < 0.05$ and ## $p < 0.01$ vs. saline-treated OBX group ($n = 3–5$ per group).

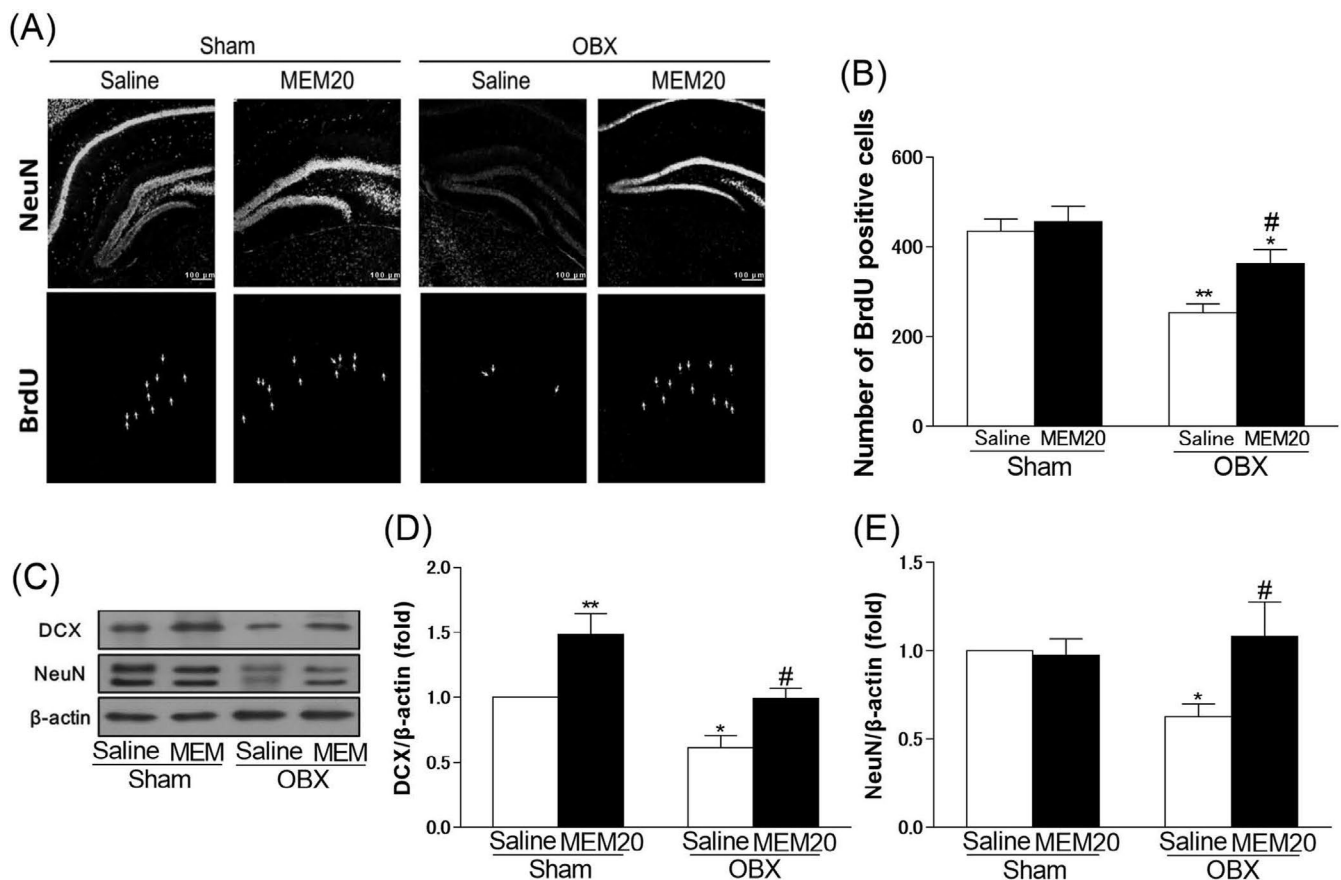


Fig. 5. Influence of memantine (MEM) on hippocampal neurogenesis in olfactory bulbectomized (OBX) mice. **A:** Microscopy images showing BrdU (red) and NeuN (green) immunostaining in the dentate gyrus region of the hippocampus. Arrows indicate BrdU-labeled cells. **B:** Quantitative analysis of the number of BrdU positive cells in sham and OBX mice treated with saline or MEM. Bars represent means ± SEM. Two-way ANOVA [(B), group: $F(1, 16) = 47.59, p < 0.01$; treatment: $F(1, 16) = 13.15, p < 0.01$; group × treatment: $F(1, 16) = 0.16, p > 0.05$]. **C:** Representative immunoblots probed with antibodies against DCX, NeuN, and β-actin, as indicated. Altered DCX and NeuN levels in the hippocampus were observed after MEM administration. **D, E:** Quantification of normalized values of DCX and NeuN levels with β-actin. Bars represent means ± SEM. Two-way ANOVA [(D), group: $F(1, 18) = 16.85, p < 0.01$; treatment: $F(1, 18) = 17.5, p < 0.01$; group × treatment: $F(1, 18) = 0.27, p > 0.05$; and (E), group: $F(1, 17) = 3.84, p > 0.05$; treatment: $F(1, 17) = 1.53, p > 0.05$; group × treatment: $F(1, 17) = 4.83, p < 0.05$]. * $p < 0.05$ and ** $p < 0.01$ vs. saline-treated sham group, # $p < 0.05$ vs. saline-treated OBX group ($n = 5–6$ per group).

saline, MEM treatment significantly decreased DCX and NeuN levels in the hippocampus of OBX mice. In contrast, DCX but not NeuN levels in the hippocampus were significantly higher in sham mice treated with MEM. We suggest that MEM-induced antidepressant effects in OBX mice may be associated with enhanced cell proliferation in the DG and the enhancement of BDNF levels.

3.5. Effect of MEM on the enhancement of inflammation in the hippocampus of OBX mice

Acute and chronic neuroinflammation can negatively affect many stages of neurogenesis in the adult mammalian brain, including proliferation, differentiation, and survival of newborn neurons (Hashimoto, 2015; Miller et al., 2009). To examine whether OBX induces the activation of microglia and astrocytes in the hippocampus, we performed immunostaining and western blotting by using antibodies for Iba1 and GFAP [Fig. 6 (A–D)]. Compared with sham controls, the microglia marker Iba1 and the astrocyte marker GFAP were significantly increased in the hippocampus of OBX mice. We observed that activated microglia and astrocytes typically exhibited hypertrophy, with thicker processes, larger and more densely stained cell bodies, while the number of activated glial cells was increased in the hippocampus of OBX mice. These phenomena were also observed in the DG area of OBX mice. In contrast,

activation of microglia and astrocytes in the hippocampus of MEM-treated OBX mice was attenuated. As shown in Fig. 6 (C and D), Iba1 and GFAP immunoreactivity was significantly higher in OBX mice than in sham controls. Compared with saline, MEM treatment significantly decreased Iba1 and GFAP levels in the hippocampus of OBX mice. Moreover, MEM reversed the effects of OBX on glial cell activation, including on cell body size, processes, cell count, and cell density [Fig. 6 (I–P)]. These results suggest that OBX induces neuroinflammation in the hippocampus via activation of microglia and astrocytes, while MEM appears to have an anti-neuroinflammatory effect.

3.6. Changes in p-IkB-α, p-NF-κB p65, TNF-α, and IL-6 levels in the hippocampus of OBX mice

Microglia are important resident immunoreactive cells in the central nervous system. The available evidence indicates that depression is intimately associated with altered inflammation and microglia (Yirmiya et al., 2015), manifesting with an increased proinflammatory profile, involving increased TNF-α and IL-6 levels (Milić et al., 2016). Thus, we examined whether OBX-induced neuromorphometrical alterations of microglia and astrocytes are functionally meaningful.

As shown in Fig. 7, the immunoreactivity of p-IkB-α, p-NF-κB p65,

TNF- α , and IL-6 was significantly higher in OBX mice than in sham controls. Compared with saline, MEM treatment significantly decreased p-I κ B- α , p-NF- κ B p65, TNF- α , and IL-6 levels in the hippocampus of OBX mice. Moreover, OBX-induced neuro-inflammation, leading to increased TNF- α and IL-6 levels via the activation of p-I κ B- α and p-NF- κ B p65, was reversed by MEM. These results suggest that OBX-induced neuromorphometrical alterations of microglia and astrocytes are functionally meaningful.

3.7. Changes in Bcl-2, Bax, and cleaved caspase-3 levels in the hippocampus of OBX mice

Modulation of apoptosis may play an important role in the modulation of depressive symptoms (Lucassen et al., 2006). Since the balance between Bcl-2 and Bax is involved in the regulation of apoptotic cell death (Cory and Adams, 2002) and cleaved caspase-3 is a crucial mediator of apoptosis (Fiandalo and Kyprianou, 2012), we next investigated whether OBX influences Bcl-2, Bax, and cleaved caspase-3 expression.

As shown in Fig. 8 (A), the Bcl-2 immunocontent was significantly lower in OBX than in sham mice. Compared with saline, MEM treatment significantly increased Bcl-2 levels in the hippocampus of OBX mice. In contrast, the Bax immunocontent was significantly higher in OBX mice treated with either saline or MEM than in sham controls [Fig. 8 (B)]. Similarly, cleaved caspase-3 levels were significantly higher in OBX than in sham mice, and this change was reversed by MEM. In contrast, cleaved caspase-3 immunocontent significantly increased in sham mice treated with MEM compared to sham controls [Fig. 8 (C)]. These results demonstrate that neuronal apoptosis is induced by OBX and that treatment with MEM significantly reverses this effect.

4. Discussion

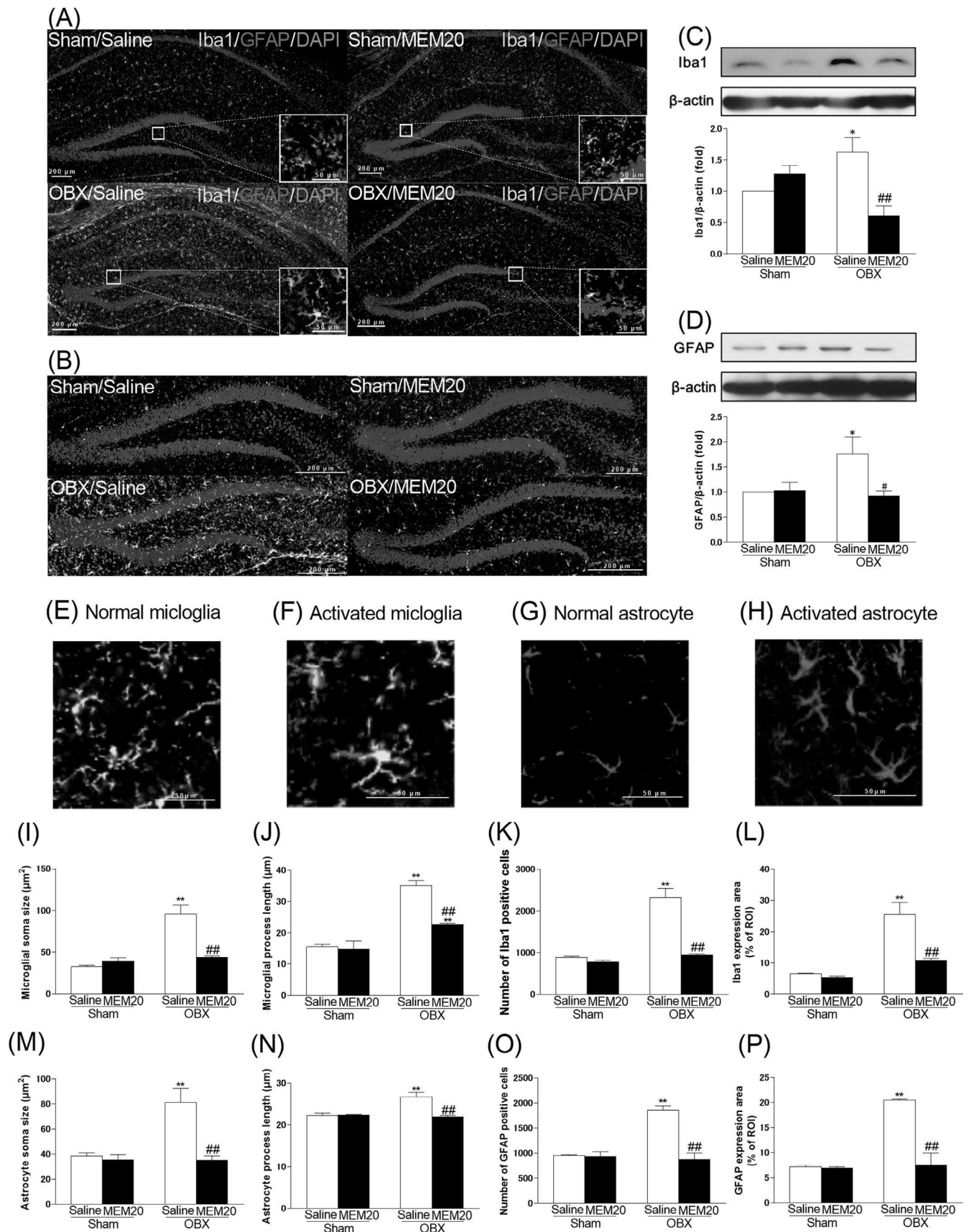
The present study showed that OBX mice exhibit depressive-like behaviors in the tail suspension, forced swimming, and emotional behavior tests, 42 days after surgery. Furthermore, chronic, but not acute, administration of MEM improved OBX-induced depressive-like behavior. We observed that MEM (10 or 20 mg/kg, i.p.) has antidepressant effects when administered chronically for 4 weeks after OBX surgery in mice. In contrast, Borre et al. reported that MEM [20 mg/kg, per os (p.o.)] has antidepressant effects when administered before the OBX surgery in rats (Borre et al., 2012). We propose that the administration method, species differences, or evaluation of specific behavioral aspects may be responsible for these discrepancies. For example, drugs reach the brain more efficiently with i.p. than p.o. administration, suggesting that the concentration of MEM in the brain examined in our study may be higher than that examined in the study by Borre et al. Moreover, it has been reported that OBX in different species occasionally exhibits different outcomes (Hendriksen et al., 2015). In the striatum, an area of the dopaminergic system associated with motivation and anhedonia in depression patients, OBX mice exhibit decreased TH levels (Takahashi et al., 2016). On the other hand, OBX rats exhibit increased DA levels in this area (Masini et al., 2004). Moreover, OBX mice but not OBX rats exhibit depressive-like behavior, including longer immobility time during the forced swimming test (Han et al., 2009; Kelly and Leonard, 1999). Regarding the behavioral aspects, Borre et al. evaluated the effects of MEM on OBX-induced hyperactivity, which may reflect psychomotor retardation or agitation. In contrast, our study evaluated MEM effects on OBX-induced hyperemotional response and immobility duration, which may reflect mood, motivation, or remissness (Abelaira et al., 2013). These factors may be responsible for the different results.

Clinical and preclinical studies have reported that MEM

ameliorates depressive-like symptoms, including emotional behavior (Matsunaga et al., 2015; Omranifard et al., 2017; Kos and Popik, 2005). Other studies have reported that the antidepressant effects of MEM are associated with the 5-HT₃ receptor and antagonism of NMDA receptors in the central nervous system (Rammes et al., 2001; Réus et al., 2010). However, we previously reported that MEM inhibits DA reuptake and turnover by inhibiting brain MAO activity (Onogi et al., 2009). Thus, in this study, we focused on the role of the dopaminergic system in the antidepressant effects of MEM.

Consistent with our results, previous studies have suggested that NE and DA levels are decreased in the hippocampus of OBX mice (Thakare et al., 2017). These changes might be, at least in part, attributed to the decreased TH levels and activity in the hippocampus of these mice. The pathophysiology of depression involves decreased 5-HT, NE, and DA levels in the central nervous system (Carlsson et al., 1969; Schildkraut and Kety, 1967). Clinical studies have reported that monoamine replacement is an important factor towards the effective treatment of patients with depression (Carroll, 1971). In the present study, MEM treatment significantly enhanced TH activity and increased DA concentration in the hippocampus of mice in both the sham and OBX groups. These effects have also been demonstrated in studies using primary midbrain neuron-glia cultures, in which MEM was shown to increase TH-positive cells and DA levels (Wu et al., 2009). Preclinical and clinical studies have reported that increased DA levels in the brain show antidepressant effects (Hosenbocus and Chahal, 2013; Chen et al., 2016). We also observed a significant increase in the DOPAC/DA ratio of OBX mice compared with the one in sham controls. Previously, we demonstrated that OBX increases MAO_B activity, which leads to DA metabolism in the forebrain (Nakagawasai et al., 2003b). Thus, we suggest that the increased DOPAC/DA ratio in OBX mice might be induced by activation of MAO_B. Moreover, DA turnover (DOPAC/DA and HVA/DA) was inhibited in OBX mice treated with MEM. This might be explained by our previous study in which we showed that MEM inhibits the reuptake of DA and MAO_B in the forebrain (Onogi et al., 2009). Taken together, these results suggest that DA is involved in the modulation of MEM-induced antidepressant effects.

Takamura et al. (2014) suggested that DA might play a role in adult hippocampal neurogenesis via DA receptors, and that activation of these receptors holds a therapeutic potential for depression. We observed that the low levels of p-PKA, p-DARPP-32, p-ERK1/2, p-CREB, and BDNF in the hippocampus of OBX mice were reversed after chronic treatment with MEM. Phosphorylation of DARPP-32 plays an important role in mediating dopaminergic transmission (Walaas et al., 1983). Furthermore, the state of phosphorylation of this protein in dopaminergic neurons is regulated by both DA and cAMP. Thus, we suggest that increased DA levels, induced by MEM, stimulate DA receptors. Moreover, enhanced DA activates the PKA and ERK1/2 pathways (Bozzi et al., 2011). In turn, these pathways lead to the activation of CREB, important for neural plasticity, as well as to the transcription of BDNF (Finkbeiner et al., 1997) and TH genes (Gueorguiev et al., 2006). Results from several studies have led to the formulation of the neurotrophic hypothesis of depression, based on which low levels of BDNF lead to a depressive condition (Castrén et al., 2007; Duman and Monteggia, 2006). Neurotrophins are trophic proteins essential for neuronal survival and differentiation, while high hippocampal BDNF levels attenuate depression symptoms (Chen et al., 2001). Moreover, ERK1/2 pathway promotes the activation of TH by increasing its phosphorylation on ser31 (Haycock et al., 1992), while PKA induces TH phosphorylation on ser40 (Funakoshi et al., 1991). The present study revealed that MEM significantly increases p-PKA, p-ERK1/2, p-TH^{ser31}, and p-TH^{ser40} levels in both the sham and OBX groups (p-



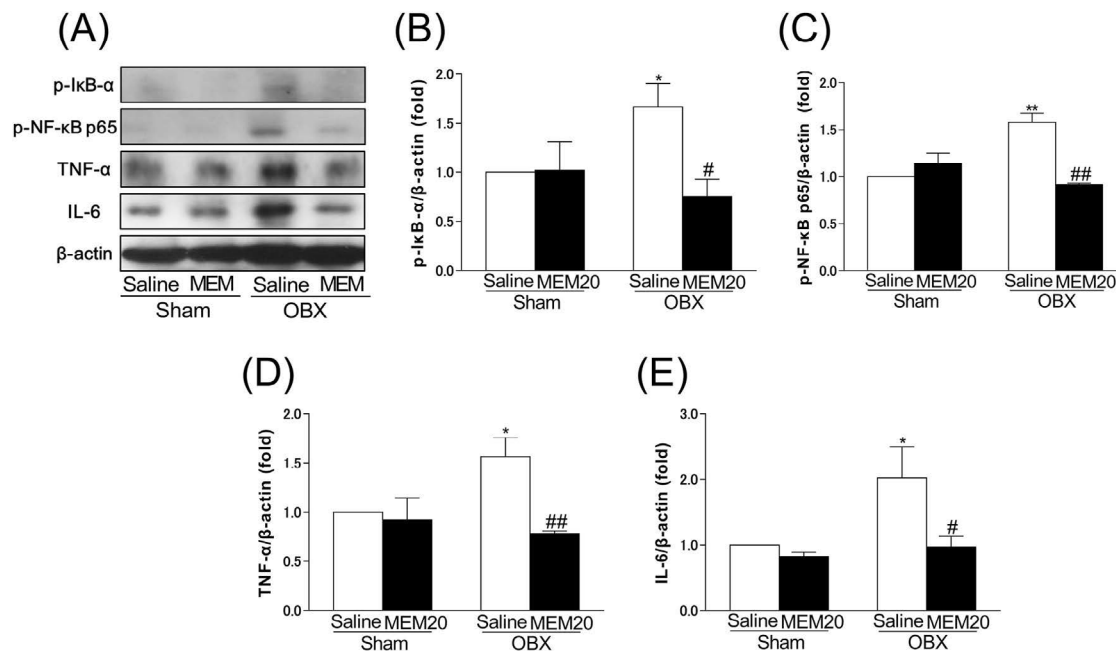


Fig. 7. Altered levels of phosphorylated (p)-IκBα, p-NF-κB p65, TNF-α, and IL-6 in the hippocampus after memantine (MEM) administration. A: Representative immunoblots probed with antibodies against p-IκBα, p-NF-κB p65, TNF-α, IL-6, and β-actin, as indicated. B–E: Quantification of normalized values of p-IκBα, p-NF-κB p65, TNF-α, and IL-6 levels with β-actin. Bars represent means ± SEM. Two-way ANOVA [(B), group: $F(1, 15) = 0.86$, $p > 0.05$; treatment: $F(1, 15) = 4.36$, $p > 0.05$; group × treatment: $F(1, 15) = 4.73$, $p < 0.05$; (C), group: $F(1, 14) = 6.11$, $p < 0.05$; treatment: $F(1, 14) = 12.96$, $p < 0.01$; group × treatment: $F(1, 14) = 30.75$, $p < 0.01$; (D), and group: $F(1, 14) = 2.01$, $p > 0.05$; treatment: $F(1, 14) = 8.55$, $p < 0.05$; group × treatment: $F(1, 14) = 5.85$, $p < 0.05$; and (E), group: $F(1, 15) = 4.83$, $p < 0.05$; treatment: $F(1, 15) = 5.35$, $p < 0.05$; group × treatment: $F(1, 15) = 2.73$, $p > 0.05$]. * $p < 0.05$ and ** $p < 0.01$ vs. saline-treated sham group, # $p < 0.05$ and ## $p < 0.01$ vs. saline-treated OBX group ($n = 3–5$ per group).

ERK1/2 levels in the sham group were slightly increased ($p = 0.08$) by MEM compared to saline). Thus, our results suggest that MEM-induced antidepressant effects might underlie the increased BDNF levels in the hippocampus and that MEM-induced enhancement of TH levels and activity in the hippocampus might be associated with PKA-ERK-CREB pathway via increasing DA.

It is well known that adult neurogenesis occurs mainly in two regions of the brain, one of which is the subgranular zone of the DG in the hippocampal formation (Alvarez-Buylla and Garcia-Verdugo, 2002; Cayre et al., 2002). In the present study, OBX mice showed a significant decrease in cell proliferation in the DG, consistently with our previous study (Nakagawasai et al., 2016; Takahashi et al., 2017). Moreover, DCX and NeuN levels in the hippocampus were significantly lower in OBX than in sham mice. Likewise, DeCarolis and Eisch (2010) reported a reduction in neurogenesis in the hippocampus of patients with depression. Moreover, Santarelli et al. (2003) suggested that antidepressant effects may be mediated by the enhancement of neurogenesis in the hippocampus. These findings suggest that enhancement of neurogenesis in the hippocampus may ameliorate depressive-like behaviors in the OBX

model. We observed that chronic administration of MEM to OBX mice significantly increases the number of newborn cells in the hippocampus. Thus, we suggest that MEM-induced antidepressant effects might be mediated by the induction of neurogenesis in the hippocampal DG of OBX mice.

Neuroinflammation can negatively affect many stages of neurogenesis in the adult mammalian brain, including proliferation, differentiation, and survival of newborn neurons (Hashimoto, 2015; Miller et al., 2009). Current evidence points to a role of inflammatory processes in the pathophysiology of depression (Hashimoto, 2009, 2015; Miller et al., 2009). Patients with depression show increased blood concentrations of pro-inflammatory cytokines, such as IL-1β, IL-6, and TNF-α (Howren et al., 2009; Kim et al., 2007). Moreover, antidepressant treatment attenuates the expression of inflammatory biomarkers in depression (Maes et al., 2009), while depression is intimately associated with altered inflammation and microglia (Yirmiya et al., 2015). Indeed, results from many studies converge to suggest that microglia are morphologically altered in frontal limbic regions of patients with depression and suicide completers (Steiner et al., 2008; Schnieder et al., 2014;

Fig. 6. Effects of memantine (MEM) on microglia and astrocyte activation in the hippocampus of olfactory bulbectomized (OBX) mice. A, B: Microscopy images of Iba1 (green), GFAP (red), and DAPI (blue) immunostaining in the hippocampus (A) and dentate gyrus (B). Altered Iba1 and GFAP levels in the hippocampus were observed after MEM administration. C, D: Representative immunoblots probed with antibodies against Iba1 (C), GFAP (D), and β-actin are shown. Graphs in panels C and D indicate the quantification of the normalized values of Iba1 and GFAP levels with β-actin. Bars represent means ± SEM. Two-way ANOVA [(C), group: $F(1, 14) = 0.016$, $p > 0.05$; treatment: $F(1, 14) = 5.04$, $p < 0.05$; group × treatment: $F(1, 14) = 15.3$, $p < 0.01$; (D), group: $F(1, 13) = 2.80$, $p > 0.05$; treatment: $F(1, 13) = 4.24$, $p > 0.05$; group × treatment: $F(1, 13) = 4.98$, $p < 0.05$]. E–H: Microscopy images showing normal and activated microglia (E and F) and astrocytes (G and H), as indicated. I–P: Quantification of soma size (I and M), process length (J and N), Iba1 positive cells (K), GFAP positive cells (O), and cell density in the region of interest (ROI), using representative tissue sections stained with Iba1 and GFAP antibodies. Bars represent means ± SEM. Two-way ANOVA [(I), group: $F(1, 9) = 38.93$, $p < 0.01$; $F(1, 9) = 17.47$, $p < 0.01$; group × treatment: $F(1, 9) = 28.98$, $p < 0.01$; (J), group: $F(1, 9) = 92.22$, $p < 0.01$; treatment: $F(1, 9) = 21.12$, $p < 0.01$; group × treatment: $F(1, 9) = 16.97$, $p < 0.01$; (K), group: $F(1, 9) = 55.9$, $p < 0.01$; treatment: $F(1, 9) = 44.7$, $p < 0.01$; group × treatment: $F(1, 9) = 34.75$, $p < 0.01$; (L), group: $F(1, 9) = 45.58$, $p < 0.01$; treatment: $F(1, 9) = 19.57$, $p < 0.01$; group × treatment: $F(1, 9) = 14.4$, $p < 0.01$; (M), group: $F(1, 9) = 10.01$, $p < 0.01$; treatment: $F(1, 9) = 13.67$, $p < 0.01$; group × treatment: $F(1, 9) = 14.66$, $p < 0.01$; (N), group: $F(1, 9) = 11.93$, $p < 0.01$; treatment: $F(1, 9) = 15.95$, $p < 0.01$; group × treatment: $F(1, 9) = 12.66$, $p < 0.01$; (O), group: $F(1, 9) = 17.19$, $p < 0.01$; treatment: $F(1, 9) = 23.79$, $p < 0.01$; group × treatment: $F(1, 9) = 21.93$, $p < 0.01$; and (P), group: $F(1, 9) = 20.4$, $p < 0.01$; treatment: $F(1, 9) = 18.34$, $p < 0.01$; group × treatment: $F(1, 9) = 16.77$, $p < 0.01$]. * $p < 0.05$ and ** $p < 0.01$ vs. saline-treated sham group, # $p < 0.05$ and ## $p < 0.01$ vs. saline-treated OBX group ($n = 3–5$ per group).

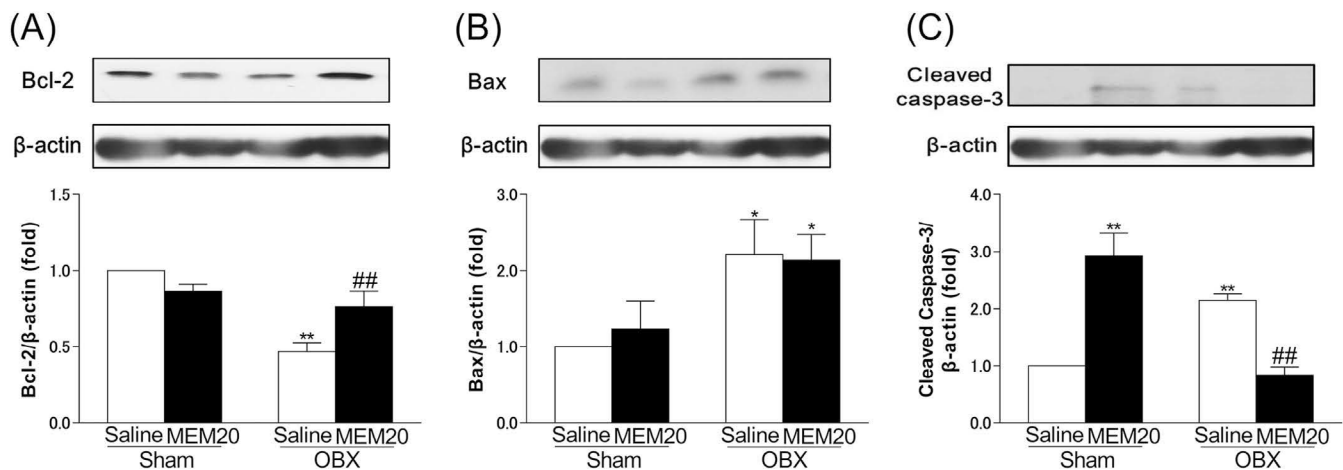


Fig. 8. Altered Bcl-2, Bax, and cleaved caspase-3 levels in the hippocampus after memantine (MEM) administration. A–C: Representative immunoblots probed with antibodies against Bcl-2, Bax, cleaved caspase-3, and β -actin, as indicated. Graphs indicate the quantification of the normalized values of Bcl-2, Bax, and cleaved caspase-3 levels with β -actin. Bars represent means \pm SEM. Two-way ANOVA [(A), group: $F(1, 15) = 29.13$, $p < 0.01$; treatment: $F(1, 15) = 1.89$, $p > 0.05$; group \times treatment: $F(1, 15) = 13.83$, $p < 0.01$; (B), group: $F(1, 15) = 9.61$, $p < 0.01$; treatment: $F(1, 15) = 0.048$, $p > 0.05$; group \times treatment: $F(1, 15) = 0.21$, $p > 0.05$; and (C), group: $F(1, 18) = 3.08$, $p > 0.05$; treatment: $F(1, 18) = 7.06$, $p < 0.05$; group \times treatment: $F(1, 18) = 84.44$, $p < 0.01$]. * $p < 0.05$ and ** $p < 0.01$ vs. saline-treated sham group, ### $p < 0.01$ vs. saline-treated OBX group ($n = 4–6$ per group).

Torres-Platas et al., 2014; Setiawan et al., 2015). Thus, the available evidence indicates that dysfunction of microglia is a core event in depression. In the present study, we observed for the first time that OBX mice show significantly increased TNF- α and IL-6 levels, possibly via the activation of p-IkB- α and p-NF- κ B p65 and reflected by the increased immunoreactivity for Iba1 (a marker of microglia) and GFAP (a marker of astrocytes) in the hippocampus. Dominguez-Mejide et al. (2017) demonstrated that DA inhibits activated microglia in vitro. Moreover, the neuroprotective effects of MEM observed in primary midbrain neuron-glia culture studies are partly mediated via alternative mechanisms, which reduce microglia-associated inflammation (Wu et al., 2009). We found that microglia-induced inflammation, observed in the hippocampus of OBX mice, was attenuated by MEM, suggesting that MEM exhibits anti-inflammatory effects by inhibiting microglial activity in these mice.

In human neutrophils, activation of NF- κ B seems to control spontaneous apoptosis and antiapoptotic effects. The modulation of this pathway most likely regulates the balance between pro- and anti-apoptotic factors, especially members of the Bcl-2 family, (Akgul et al., 2001), thus affecting neutrophil survival. The balance between Bcl-2 (an anti-apoptotic protein) and Bax (a pro-apoptotic protein) regulates apoptotic cell death. Moreover, cleaved caspase-3 is crucial in the process of apoptosis, and its activation contributes to the irreversible stage of apoptosis (Fiandalo and Kyprianou, 2012). Our results showed that MEM reverses the decreased levels of Bcl-2 in the hippocampus of OBX mice, but not the increased levels of Bax. In contrast, MEM reverses the increased levels of cleaved caspase-3 in the hippocampus of OBX mice. Interestingly, sham mice treated with MEM also showed enhanced cleaved caspase-3 levels in the hippocampus. These paradoxical results may be associated with the increased DCX and unchanged NeuN expression levels in the hippocampus of sham mice. Indeed, a previous study reported that the disequilibrium between neuronal proliferation and apoptosis may be involved in the pathogenesis of neuropsychiatric disorders (Genius et al., 2012). We hypothesize that the MEM-induced excess of immature neurons in the hippocampus of sham mice did not differentiate to mature neurons, but instead underwent apoptosis. These results suggest that MEM might partly modulate apoptosis by regulating caspase-3 and the balance between Bcl-2 and Bax in the hippocampus of OBX mice.

Besides the hippocampus, the pathogenesis of depression affects various brain regions, including the prefrontal cortex, striatum, and amygdala (Treadway and Zald, 2011). In this study, we only examined the antidepressant effects of MEM on the hippocampus. Moreover, the regulation of emotional behavior is thought to rely more on ventral hippocampal neurogenesis (Tanti et al., 2012). Hence, further experiments examining the relationship between other brain areas involved in depressive-like behavior, including the ventral hippocampus, and the effects of MEM will be presented in a subsequent paper.

When we investigated the time-dependency of MEM effects in OBX mice by emotional behavioral testing, we observed that the OBX-induced emotional behavior increase was reduced after 4 weeks of MEM administration. A previous study suggested that antidepressants may exert their action by stimulating neurogenesis in the hippocampus (Santarelli et al., 2003). Moreover, enhancement of neurogenesis was observed after chronic but not acute administration, consistently with the time course for the therapeutic action of antidepressants (Malberg et al., 2000). Chiu et al. (2015) reported that the enhancement of neurogenesis and antidepressant effects of L-DOPA (L-3,4-dihydroxyphenylalanine), the precursor of the neurotransmitter DA, or of pramipexole, a D₂/D₃ receptor agonist, were also observed after chronic, but not acute administration. These findings suggest that the dopaminergic activity-related enhancement of neurogenesis, as well as the antidepressant effects, develop later (Chiu et al., 2015). Thus, we suggest that the delayed antidepressant effect of MEM might contribute to the enhancement of neurogenesis via the enhancement of dopaminergic activity. Moreover, recent short-term clinical and meta-analysis studies have reported that MEM as adjunct to sertraline, but not MEM alone, efficiently improves depressive symptoms in patients with major depressive disorder (Amidfar et al., 2017; Kishi et al., 2017). In contrast, a 12-week course of an open-label, flexible-dose study of MEM revealed its efficacy in such patients (Ferguson and Shingleton, 2007). In the present study, MEM exhibited an antidepressant effect 4 weeks after the first treatment in OBX mice. Previous studies have reported that OBX-induced hyperemotional behaviors improve by administration of classic antidepressants, such as desipramine, milnacipran, and fluvoxamine, for 7 days (Saitoh et al., 2003, 2007). Antidepressants are the mainstay of pharmacological treatment for patients with

depressive disorders; however, evidence supporting their use in dementia is unclear (Ford and Almeida, 2017). Thus, we consider that MEM may be effective for depression and emotional disturbances in dementia but its effects might develop later than in the case of classic antidepressants. Therefore, long-term studies on MEM effects on depression are required. However, we suggest that MEM can reduce polypharmacy, a frequent problem in the elderly, which can lead to worsened cognition, increased risk of adverse drug reactions, and falls (Beer et al., 2011).

In conclusion, our results indicate that MEM has antidepressant effects in OBX mice. The mechanism of action may involve the enhancement of cell proliferation in the hippocampus, stimulated by increased BDNF levels and mediated by the activation of the DA receptor signaling pathway (PKA-ERK-CREB). This leads to increased DA via the enhancement of TH activity and inhibition of DA turnover following MEM treatment. In addition, we showed that MEM exerts neuroprotective effects in the hippocampus, by decreasing TNF- α and IL-6 levels and activating the I κ B- α and NF- κ B p65 signaling pathways. This process is likely mediated by the suppression of microglial activity, and the modulation of the balance between Bcl-2 and Bax, involved in the regulation of apoptotic cell death via caspase-3 activity. Our results provide the basis for the development of MEM strategies not only towards treating dementia, but also depression.

Conflicts of interest

We do not have any conflicts of interest in connection with this manuscript.

Acknowledgments

This study was supported in part by JSPS KAKENHI (Grant Number: JP26460102) and Matching Fund Subsidy for Private Universities from the Ministry of Education, Culture, Sports, Science and Technology of Japan (Grant Number: S1511001L). The authors would like to thank Ms. Yurika Yamamoto, Mr. Kazuya Sano, and Mr. Kotaro Yabuki of Tohoku Medical and Pharmaceutical University for their technical assistance.

Appendix A. Supplementary data

Supplementary data related to this article can be found at <https://doi.org/10.1016/j.neuropharm.2018.04.013>.

References

- Abelaira, H.M., Réus, G.Z., Quevedo, J., 2013. Animal models as tools to study the pathophysiology of depression. *Rev. Bras. Psiquiatr.* 35 (Suppl. 2), S112–S120.
- Akgul, C., Moulding, D.A., Edwards, S.W., 2001. Molecular control of neutrophil apoptosis. *FEBS Lett.* 487, 318–322.
- Amidfar, M., Khiabany, M., Kohi, A., Salardini, E., Arbabi, M., Roohi Azizi, M., Zarrindast, M.R., Mohammadnejad, P., Zeinoddini, A., Akhondzadeh, S., 2017. Effect of memantine combination therapy on symptoms in patients with moderate-to-severe depressive disorder: randomized, double-blind, placebo-controlled study. *J. Clin. Pharm. Therapeut.* 42, 44–50.
- Alvarez-Buylla, A., Garcia-Verdugo, J.M., 2002. Neurogenesis in adult subventricular zone. *J. Neurosci.* 22, 629–634.
- Beer, C., Loh, P.K., Peng, Y.G., Potter, K., Millar, A., 2011. A pilot randomized controlled trial of deprescribing. *Ther. Adv. Drug Saf.* 2, 37–43.
- Berman, K., Brodsky, H., Withall, A., Seeher, K., 2012. Pharmacologic treatment of apathy in dementia. *Am. J. Geriatr. Psychiatr.* 20, 104–122.
- Borre, Y., Bosman, E., Lemstra, S., Westphal, K.G., Olivier, B., Oosting, R.S., 2012. Memantine partly rescues behavioral and cognitive deficits in an animal model of neurodegeneration. *Neuropharmacology* 62, 2010–2017.
- Bozzi, Y., Dunleavy, M., Henshall, D.C., 2011. Cell signaling underlying epileptic behavior. *Front. Behav. Neurosci.* 5, 45.
- Breuer, M.E., Groenink, L., Oosting, R.S., Buerger, E., Korte, M., Ferger, B., Olivier, B., 2009a. Antidepressant effects of pramipexole, a dopamine D3/D2 receptor agonist, and 7-OH-DPAT, a dopamine D3 receptor agonist, in olfactory bulbectomized rats. *Eur. J. Pharmacol.* 616, 134–140.
- Breuer, M.E., van Gaalen, M.M., Wernet, W., Claessens, S.E., Oosting, R.S., Behl, B., Korte, S.M., Schoemaker, H., Gross, G., Olivier, B., Groenink, L., 2009b. SSR149415, a non-peptide vasopressin V1b receptor antagonist, has long-lasting antidepressant effects in the olfactory bulbectomy-induced hyperactivity depression model. *Naunyn-Schmiedeberg's Arch. Pharmacol.* 379, 101–106.
- Carlsson, A., Corrodi, H., Fuxe, K., Hökfelt, T., 1969. Effects of some antidepressant drugs on the depletion of intraneuronal brain catecholamine stores caused by 4, alpha-dimethyl-meta-tyramine. *Eur. J. Pharmacol.* 5, 367–373.
- Carroll, B.J., 1971. Monoamine precursors in the treatment of depression. *Clin. Pharmacol. Ther.* 12, 743–761.
- Castrén, E., Voikar, V., Rantamäki, T., 2007. Role of neurotrophic factors in depression. *Curr. Opin. Pharmacol.* 7, 18–21.
- Cayre, M., Malaterre, J., Scotto-Lomassese, S., Strambi, C., Strambi, A., 2002. The common properties of neurogenesis in the adult brain: from invertebrates to vertebrates. *Comp. Biochem. Physiol. B Biochem. Mol. Biol.* 132, 1–15.
- Chen, B., Dowlatabadi, D., MacQueen, G.M., Wang, J.F., Young, L.T., 2001. Increased hippocampal BDNF immunoreactivity in subjects treated with antidepressant medication. *Biol. Psychiatr.* 50, 260–265.
- Chen, C., Nakagawa, S., Kitaichi, Y., An, Y., Omiya, Y., Song, N., Koga, M., Kato, A., Inoue, T., Kusumi, I., 2016. The role of medial prefrontal corticosterone and dopamine in the antidepressant-like effect of exercise. *Psychoneuroendocrinology* 69, 1–9.
- Chiu, W.H., Depboylu, C., Hermanns, G., Maurer, L., Windolph, A., Oertel, W.H., Ries, V., Höglinger, G.U., 2015. Long-term treatment with L-DOPA or pramipexole affects adult neurogenesis and corresponding non-motor behavior in a mouse model of Parkinson's disease. *Neuropharmacology* 95, 367–376.
- Cory, S., Adams, J.M., 2002. The Bcl2 family: regulators of the cellular life-or-death switch. *Nat. Rev. Canc.* 2, 647–656.
- DeCarolis, N.A., Eisch, A.J., 2010. Hippocampal neurogenesis as a target for the treatment of mental illness: a critical evaluation. *Neuropharmacology* 58, 884–893.
- Diazgranados, N., Ibrahim, L., Brutsche, N.E., Newberg, A., Kronstein, P., Khalife, S., Kammerer, W.A., Quezado, Z., Luckenbaugh, D.A., Salvatore, G., Machado-Vieira, R., Manji, H.K., Zarate Jr., C.A., 2010. A randomized add-on trial of an N-methyl-D-aspartate antagonist in treatment-resistant bipolar depression. *Arch. Gen. Psychiatr.* 67, 793–802.
- Dominguez-Mejide, A., Rodriguez-Perez, A.I., Diaz-Ruiz, C., Guerra, M.J., Labandeira-Garcia, J.L., 2017. Dopamine modulates astroglial and microglial activity via glial renin-angiotensin system in cultures. *Brain Behav. Immun.* 62, 277–290.
- Duman, R.S., Monteggia, L.M., 2006. A neurotrophic model for stress-related mood disorders. *Biol. Psychiatr.* 59, 1116–1127.
- Engel, D., Zomkowski, A.D., Lieberknecht, V., Rodrigues, A.L., Gabilan, N.H., 2013. Chronic administration of duloxetine and mirtazapine downregulates proapoptotic proteins and upregulates neurotrophin gene expression in the hippocampus and cerebral cortex of mice. *J. Psychiatr. Res.* 47, 802–808.
- Ferguson, J.M., Shingleton, R.N., 2007. An open-label, flexible-dose study of memantine in major depressive disorder. *Clin. Neuropharmacol.* 30, 136–144.
- Fiandalo, M.V., Kyprianou, N., 2012. Caspase control: protagonists of cancer cell apoptosis. *Exp. Oncol.* 34, 165–175.
- Finkbeiner, S., Tavazoie, S.F., Maloratsky, A., Jacobs, K.M., Harris, K.M., Greenberg, M.E., 1997. CREB: a major mediator of neuronal neurotrophin responses. *Neuron* 19, 1031–1047.
- Ford, A.H., Almeida, O.P., 2017. Management of depression in patients with dementia: is pharmacological treatment justified? *Drugs Aging* 34, 89–95.
- Färber, K., Pannasch, U., Kettenmann, H., 2005. Dopamine and noradrenaline control distinct functions in rodent microglial cells. *Mol. Cell. Neurosci.* 29, 128–138.
- Fukuda, T., Hashimoto, H., Okayasu, N., Kameyama, A., Onogi, H., Nakagawasa, O., Nakazawa, T., Kurosawa, T., Hao, Y., Isaji, T., Tadano, T., Narimatsu, H., Taniguchi, N., Gu, J., 2011. Alpha1,6-fucosyltransferase-deficient mice exhibit multiple behavioral abnormalities associated with a schizophrenia-like phenotype: importance of the balance between the dopamine and serotonin systems. *J. Biol. Chem.* 286, 18434–18443.
- Funakoshi, H., Okuno, S., Fujisawa, H., 1991. Different effects on activity caused by phosphorylation of tyrosine hydroxylase at serine 40 by three multifunctional protein kinases. *J. Biol. Chem.* 266, 15614–15620.
- Genius, J., Benninghoff, J., Reuter, N., Braun, I., Giegling, I., Hartmann, A., Möller, H.J., Rujescu, D., 2012. Dysequilibrium of neuronal proliferation and apoptosis in a pharmacological animal model of psychosis. *Methods* 56, 519–527.
- Gomes, C., Ferreira, R., George, J., Sanches, R., Rodrigues, D.I., Gonçalves, N., Cunha, R.A., 2013. Activation of microglial cells triggers a release of brain-derived neurotrophic factor (BDNF) inducing their proliferation in an adenosine A2A receptor-dependent manner: a2A receptor blockade prevents BDNF release and proliferation of microglia. *J. Neuroinflammation* 10, 16.
- Gueorguiev, V.D., Cheng, S.Y., Sabban, E.L., 2006. Prolonged activation of cAMP-response element-binding protein and ATF-2 needed for nicotine-triggered elevation of tyrosine hydroxylase gene transcription in PC12 cells. *J. Biol. Chem.* 281, 10188–10195.
- Han, F., Nakano, T., Yamamoto, Y., Shioda, N., Lu, Y.M., Fukunaga, K., 2009. Improvement of depressive behaviors by nefaracetam is associated with activation of CaM kinases in olfactory bulbectomized mice. *Brain Res.* 1265, 205–214.
- Hashimoto, K., 2009. Emerging role of glutamate in the pathophysiology of major

- depressive disorder. *Brain Res. Rev.* 61, 105–123.
- Hashimoto, K., 2015. Inflammatory biomarkers as differential predictors of antidepressant response. *Int. J. Mol. Sci.* 16, 7796–7801.
- Haycock, J.W., Ahn, N.G., Cobb, M.H., Krebs, E.G., 1992. ERK1 and ERK2, two microtubule-associated protein 2 kinases, mediate the phosphorylation of tyrosine hydroxylase at serine-31 in situ. *Proc. Natl. Acad. Sci. U. S. A.* 89, 2365–2369.
- Hendriksen, H., Korte, S.M., Olivier, B., Oosting, R.S., 2015. The olfactory bulbectomy model in mice and rat: one story or two tails? *Eur. J. Pharmacol.* 753, 105–113.
- Hosenbocus, S., Chahal, R., 2013. Amantadine: a review of use in child and adolescent psychiatry. *J. Can. Acad. Child. Adolesc. Psychiatry* 22, 55–60.
- Howren, M.B., Lamkin, D.M., Suls, J., 2009. Associations of depression with C-reactive protein, IL-1, and IL-6: a meta-analysis. *Psychosom. Med.* 71, 171–186.
- Hozumi, S., Nakagawasai, O., Tan-No, K., Nijima, F., Yamadera, F., Murata, A., Arai, Y., Yasuhara, H., Tadano, T., 2003. Characteristics of changes in cholinergic function and impairment of learning and memory-related behavior induced by olfactory bulbectomy. *Behav. Brain Res.* 138, 9–15.
- Ishida, T., Obara, Y., Kamei, C., 2010. Studies on wakefulness-promoting effect of memantine in rats. *Behav. Brain Res.* 206, 274–278.
- Kelly, J.P., Leonard, B.E., 1999. An investigation of the antidepressant properties of lofepramine and its desmethylated metabolites in the forced swim and olfactory bulbectomized rat models of depression. *Eur. Neuropsychopharmacol.* 9, 101–105.
- Kelly, J.P., Wrynny, A.S., Leonard, B.E., 1997. The olfactory bulbectomized rat as a model of depression: an update. *Pharmacol. Ther.* 74, 299–316.
- Kim, Y.K., Na, K.S., Shin, K.H., Jung, H.Y., Choi, S.H., Kim, J.B., 2007. Cytokine imbalance in the pathophysiology of major depressive disorder. *Prog. Neuro-Psychopharmacol. Biol. Psychiatry* 31, 1044–1053.
- Kishi, T., Matsunaga, S., Iwata, N., 2017. A meta-analysis of memantine for depression. *J. Alzheimers Dis.* 57, 113–121.
- Kishi, T., Iwata, N., 2013. NMDA receptor antagonists interventions in schizophrenia: meta-analysis of randomized, placebo-controlled trials. *J. Psychiatr. Res.* 47, 1143–1149.
- Kos, T., Popik, P., 2005. A comparison of the predictive therapeutic and undesired side-effects of the NMDA receptor antagonist, memantine, in mice. *Behav. Pharmacol.* 16, 155–161.
- Lucassen, P.J., Heine, V.M., Muller, M.B., van der Beek, E.M., Wiegant, V.M., De Kloet, E.R., Joels, M., Fuchs, E., Swaab, D.F., Czeh, B., 2006. Stress, depression and hippocampal apoptosis. *CNS Neurol. Disord. - Drug Targets* 5, 531–546.
- Maes, M., Yirmiya, R., Noraberg, J., Brene, S., Hibbeln, J., Perini, G., Kubera, M., Bob, P., Lerer, B., Maj, M., 2009. The inflammatory & neurodegenerative (I&ND) hypothesis of depression: leads for future research and new drug developments in depression. *Metab. Brain Dis.* 24, 27–53.
- Malberg, J.E., Eisch, A.J., Nestler, E.J., Duman, R.S., 2000. Chronic antidepressant treatment increases neurogenesis in adult rat hippocampus. *J. Neurosci.* 20, 9104–9110.
- Masini, C.V., Holmes, P.V., Freeman, K.G., Maki, A.C., Edwards, G.L., 2004. Dopamine overflow is increased in olfactory bulbectomized rats: an in vivo microdialysis study. *Physiol. Behav.* 81, 111–119.
- Matsunaga, S., Kishi, T., Iwata, N., 2015. Memantine monotherapy for Alzheimer's disease: a systematic review and meta-analysis. *PLoS One* 10, e0123289.
- Milior, G., Lecours, C., Samson, L., Bisht, K., Poggini, S., Pagani, F., Deflorio, C., Lauro, C., Alboni, S., Limatola, C., Branchi, I., Tremblay, M.E., Maggi, L., 2016. Fractalkine receptor deficiency impairs microglial and neuronal responsiveness to chronic stress. *Brain Behav. Immun.* 55, 114–125.
- Miller, A.H., Maletic, V., Raison, C.L., 2009. Inflammation and its discontents: the role of cytokines in the pathophysiology of major depression. *Biol. Psychiatry* 65, 732–741.
- Nakagawasai, O., Hozumi, S., Tan-No, K., Nijima, F., Arai, Y., Yasuhara, H., Tadano, T., 2003a. Immunohistochemical fluorescence intensity reduction of brain somatostatin in the impairment of learning and memory-related behaviour induced by olfactory bulbectomy. *Behav. Brain Res.* 142, 63–67.
- Nakagawasai, O., Nemoto, W., Onogi, H., Moriya, T., Lin, J.R., Odaira, T., Yaoita, F., Ogawa, T., Ohta, K., Endo, Y., Tan-No, K., 2016. BE360, a new selective estrogen receptor modulator, produces antidepressant and antidepressant effects through the enhancement of hippocampal cell proliferation in olfactory bulbectomized mice. *Behav. Brain Res.* 297, 315–322.
- Nakagawasai, O., Tadano, T., Arai, Y., Hozumi, S., Oba, A., Tan-No, K., Yasuhara, H., Kisara, K., Orelund, L., 2003b. Enhancement of 5-hydroxytryptamine-induced head-twitch response after olfactory bulbectomy. *Neuroscience* 117, 1017–1023.
- Nakaya, K., Nakagawasai, O., Arai, Y., Onogi, H., Sato, A., Nijima, F., Tan-No, K., Tadano, T., 2011. Pharmacological characterizations of memantine-induced disruption of prepulse inhibition of the acoustic startle response in mice: involvement of dopamine D2 and 5-HT2A receptors. *Behav. Brain Res.* 218, 165–173.
- Omrani, F., Rajabi, F., Mohammadian-Sichani, M., Maracy, M.R., 2017. The effect of add-on memantine on positive, negative and depressive symptoms of schizophrenia: a double-blind, randomized, controlled trial. *Actas Esp. Psiquiatr.* 45, 108–115.
- Onogi, H., Ishigaki, S., Nakagawasai, O., Arai-Kato, Y., Arai, Y., Watanabe, H., Miyamoto, A., Tan-no, K., Tadano, T., 2009. Influence of memantine on brain monoaminergic neurotransmission parameters in mice: neurochemical and behavioral study. *Biol. Pharm. Bull.* 32, 850–855.
- Parsons, C.G., Stoffler, A., Danysz, W., 2007. Memantine: a NMDA receptor antagonist that improves memory by restoration of homeostasis in the glutamatergic system—too little activation is bad, too much is even worse. *Neuropharmacology* 53, 699–723.
- Porsolt, R.D., Anton, G., Blavet, N., Jalfre, M., 1978. Behavioural despair in rats: a new model sensitive to antidepressant treatments. *Eur. J. Pharmacol.* 47, 379–391.
- Rammes, G., Rupprecht, R., Ferrari, U., Zieglansberger, W., Parsons, C.G., 2001. The N-methyl-D aspartate receptor channel blockers memantine, MRZ 2/579 and other amino-alkyl-cyclohexanes antagonize 5-HT(3) receptor currents in cultured HEK-293 and N1E-115 cell systems in a non competitive manner. *Neurosci. Lett.* 306, 81–84.
- Réus, G.Z., Stringari, R.B., Kirsch, T.R., Fries, G.R., Kapczinski, F., Roesler, R., Quevedo, J., 2010. Neurochemical and behavioural effects of acute and chronic memantine administration in rats: further support for NMDA as a new pharmacological target for the treatment of depression? *Brain Res. Bull.* 81, 585–589.
- Rinwa, P., Kumar, A., 2013. Quercetin suppress microglial neuroinflammatory response and induce antidepressant-like effect in olfactory bulbectomized rats. *Neuroscience* 255, 86–98.
- Rinwa, P., Kumar, A., Garg, S., 2013. Suppression of neuroinflammatory and apoptotic signaling cascade by curcumin alone and in combination with piperine in rat model of olfactory bulbectomy induced depression. *PLoS One* 8, e61052.
- Ros-Bernal, F., Hunot, S., Herrero, M.T., Parnadeau, S., Corvol, J.C., Lu, L., Alvarez-Fischer, D., Carrillo-de Sauvage, M.A., Saurini, F., Coussieu, C., Kinugawa, K., Prigent, A., Höglinger, G., Hamon, M., Tronche, F., Hirsch, E.C., Vyas, S., 2011. Microglial glucocorticoid receptors play a pivotal role in regulating dopaminergic neurodegeneration in parkinsonism. *Proc. Natl. Acad. Sci. U. S. A.* 108, 6632–6637.
- Saitoh, A., Yamaguchi, K., Murasawa, H., Kamei, J., 2003. The approaches in the discovery of antidepressants using affective disorder models. *Nihon Shinkei Seishin Yakurigaku Zasshi* 23, 75–82.
- Saitoh, A., Yamaguchi, K., Tatsumi, Y., Murasawa, H., Nakatani, A., Hirose, N., Yamada, M., Yamada, M., Kamei, J., 2007. Effects of milnacipran and fluvoxamine on hyperemotional behaviors and the loss of tryptophan hydroxylase-positive cells in olfactory bulbectomized rats. *Psychopharmacology (Berlin)* 191, 857–865.
- Santarelli, L., Saxe, M., Gross, C., Surget, A., Battaglia, F., Dulawa, S., Weisstaub, N., Lee, J., Duman, R., Arancio, O., Belzung, C., Hen, R., 2003. Requirement of hippocampal neurogenesis for the behavioral effects of antidepressants. *Science* 301, 805–809.
- Schildkraut, J.J., Kety, S.S., 1967. Biogenic amines and emotion. *Science* 156, 21–37.
- Schneider, T.P., Trencsevska, I., Rosoklija, G., Stankov, A., Mann, J.J., Smiley, J., Dwork, A.J., 2014. Microglia of prefrontal white matter in suicide. *J. Neuropathol. Exp. Neurol.* 73, 880–890.
- Scorza, F.A., Guerra, A. de B., Cavalheiro, E.A., Calil, H.M., 2005. Neurogenesis and depression: etiology or new illusion? *Rev. Bras. Psiquiatr.* 27, 249–253.
- Setiawan, E., Wilson, A.A., Mizrahi, R., Rusjan, P.M., Miler, L., Rajkowska, G., Suridjan, I., Kennedy, J.L., Rekkas, P.V., Houle, S., Meyer, J.H., 2015. Role of translocator protein density, a marker of neuroinflammation, in the brain during major depressive episodes. *JAMA Psychiatry* 72, 268–275.
- Steiner, J., Bielau, H., Brisch, R., Danos, P., Ullrich, O., Mavrin, C., Bernstein, H.G., Bogerts, B., 2008. Immunological aspects in the neurobiology of suicide: elevated microglial density in schizophrenia and depression is associated with suicide. *J. Psychiatry. Res.* 42, 151–157.
- Takahashi, K., Nakagawasai, O., Nemoto, W., Odaira, T., Arai, Y., Hisamitsu, T., Tan-No, K., 2017. Time-dependent role of prefrontal cortex and hippocampus on cognitive improvement by aripiprazole in olfactory bulbectomized mice. *Eur. Neuropsychopharmacol.* 27, 1000–1010.
- Takahashi, K., Murasawa, H., Yamaguchi, K., Yamada, M., Nakatani, A., Yoshida, M., Iwai, T., Inagaki, M., Yamada, M., Saitoh, A., 2011. Riluzole rapidly attenuates hyperemotional responses in olfactory bulbectomized rats, an animal model of depression. *Behav. Brain Res.* 216, 46–52.
- Takahashi, K., Nakagawasai, O., Nemoto, W., Nakajima, T., Arai, Y., Hisamitsu, T., Tan-No, K., 2016. Alterations in behavioral responses to dopamine agonists in olfactory bulbectomized mice: relationship to changes in the striatal dopaminergic system. *Psychopharmacology (Berlin)* 233, 1311–1322.
- Takamura, N., Nakagawa, S., Masuda, T., Boku, S., Kato, A., Song, N., An, Y., Kitaichi, Y., Inoue, T., Koyama, T., Kusumi, I., 2014. The effect of dopamine on adult hippocampal neurogenesis. *Prog. Neuro-Psychopharmacol. Biol. Psychiatry* 50, 116–124.
- Tanti, A., Rainer, Q., Minier, F., Surget, A., Belzung, C., 2012. Differential environmental regulation of neurogenesis along the septo-temporal axis of the hippocampus. *Neuropharmacology* 63, 374–384.
- Thakare, V.N., Aswar, M.K., Kulkarni, Y.P., Patil, R.R., Patel, B.M., 2017. Silymarin ameliorates experimentally induced depressive like behavior in rats: involvement of hippocampal BDNF signaling, inflammatory cytokines and oxidative stress response. *Physiol. Behav.* 179, 401–410.
- Torres-Platas, S.G., Cruceanu, C., Chen, G.G., Turecki, G., Mechawar, N., 2014. Evidence for increased microglial priming and macrophage recruitment in the dorsal anterior cingulate white matter of depressed suicides. *Brain Behav. Immun.* 42, 50–59.
- Treadway, M.T., Zald, D.H., 2011. Reconsidering anhedonia in depression: lessons from translational neuroscience. *Neurosci. Biobehav. Rev.* 35, 537–555.
- Waterhouse, E.G., An, J.J., Orefice, L.L., Baydyuk, M., Liao, G.Y., Zheng, K., Lu, B., Xu, B., 2012. BDNF promotes differentiation and maturation of adult-born neurons through GABAergic transmission. *J. Neurosci.* 32, 14318–14330.

- Walaas, S.I., Aswad, D.W., Greengard, P., 1983. A dopamine- and cyclic AMP-regulated phosphoprotein enriched in dopamine-innervated brain regions. *Nature* 301, 69–71.
- Wu, H.M., Tzeng, N.S., Qian, L., Wei, S.J., Hu, X., Chen, S.H., Rawls, S.M., Flood, P., Hong, J.S., Lu, R.B., 2009. Novel neuroprotective mechanisms of memantine: increase in neurotrophic factor release from astroglia and anti-inflammation by preventing microglial activation. *Neuropsychopharmacology* 34, 2344–2357.
- Yirmiya, R., Rimmerman, N., Reshef, R., 2015. Depression as a microglial disease. *Trends Neurosci.* 38, 637–658.
- Zarate Jr., C.A., Singh, J.B., Carlson, P.J., Brutsche, N.E., Ameli, R., Luckenbaugh, D.A., Charney, D.S., Manji, H.K., 2006. A randomized trial of an N-methyl-D-aspartate antagonist in treatment-resistant major depression. *Arch. Gen. Psychiatr.* 63, 856–864.



Contents lists available at ScienceDirect

Bioorganic & Medicinal Chemistry Letters

journal homepage: www.elsevier.com/locate/bmclDesign and synthesis of iodocarborane-containing ligands with high affinity and selectivity toward ER β 

Kiminori Ohta*, Takumi Ogawa, Yasuyuki Endo

Faculty of Pharmaceutical Sciences, Tohoku Medical and Pharmaceutical University, 4-4-1 Komatsushima, Aoba-ku, Sendai 981-8558, Japan

ARTICLE INFO

Article history:

Received 21 June 2017

Revised 19 July 2017

Accepted 20 July 2017

Available online 25 July 2017

Keywords:

Carborane

Estrogen receptor

ER β

Subtype selectivity

ABSTRACT

The selectivity and the binding affinity of previously reported carborane-containing ligands **2** and **3** toward ER β remains to be optimized. To improve their biological profiles, a series of iodinated carboranyl phenol derivatives (**4–6**) were designed and synthesized as prospective ER β -selective ligands with high affinity. Several iodinated carboranyl phenols showed high relative binding affinity (RBA) values for both ERs, and especially for ER β , due to suitable hydrophobic interactions of the iodine atoms with the hydrophobic amino acid residues of the ER β ligand-binding domains. Among these derivatives, 9,10-diiodo-*m*-carborane **5f** exhibited a more than 100% increase of the RBA values toward ER β , a 14-fold increased selectivity for ER β over ER α , and ER-agonistic activity in MCF-7 cell proliferation assays.

© 2017 Elsevier Ltd. All rights reserved.

Estrogen receptor β (ER β)¹ was initially cloned from a rat ventral prostate cDNA library as a second form of ER α ,² and has since shown quite different biological functions compared to ER α .³ Endogenous estrogen 17 β -estradiol (E2, **1**) modulates various physiological processes, including the development and function of the female reproductive system, as well as the maintenance of bone mineral density.⁴ However, the therapeutic use of **1** is limited by an increased risk of breast cancer, which has been linked to the activation of ER α (Fig. 1).⁵ Nevertheless, the activation of ER β induces an anti-proliferative effect on breast cancer.⁶ ER β -selective agonists down-regulate the expression of the androgen receptor (AR),⁷ inhibit the proliferation and migration of prostate cancer cell lines,⁸ and delay the progression of Alzheimer's disease by including the degradation of A β aggregates.⁹ Thus, ER β -selective ligands are of interest as potential therapeutic agents for Alzheimer's disease and several other types of cancer, and as probes for ER β -related molecular biology.¹⁰

The development of ER-subtype-selective ligands remains a major challenge, as there are only two different amino acid residues in the hydrophobic pocket of the ER-ligand-binding domains (LBDs),¹¹ i.e., Leu384 and Met421 in ER α are substituted in ER β by Met336 and Ile373, respectively.¹¹ Most ER β -selective ligands obtain their subtype selectivity through electronic, hydrophobic, or steric interactions with these key amino acid residues.¹²

Based on the above theory, we have recently developed carborane-containing ER β -selective ligands **2**¹³ and **3**,¹⁴ which showed

high RBA values and high selectivity toward ER β , respectively (Fig. 1). Although **3** showed much better ER β selectivity than **2**, it is still not sufficient for the development of drug candidates or biological tools on account of the low binding affinity toward ER β . An SAR study on the ER β selectivity of **2** revealed that the iodine atom on the carbon atom of the *m*-carborane cage in **2** increases the binding affinity toward ER β . Thus, we designed novel iodinated carborane-containing ER β -selective ligands with high affinity toward ER β , using **2** as a lead compound. In this paper, we describe the syntheses of several iodinated carboranyl phenols (**4–6**) and the evaluation of their ER-binding affinity and selectivity.

The synthesis of iodinated-*o*-carborane **4** is summarized in Scheme 1. 3-Iodo-*o*-carborane **7**, which was prepared from the *o*-carborane-reconstructing reaction of *nido*-7,8-C₂B₉H₁₂[−] with BI₃,¹⁵ was treated with 4-methoxyphenylmagnesium bromide in the presence of CuI under Pd-catalyzed coupling conditions to afford 3-(4-methoxyphenyl)-*o*-carborane **8** in 98% yield.¹⁶ Two iodine atoms were introduced on two carbon atoms of the *o*-carborane cage of **8** by consecutive exposure to *n*-BuLi and I₂, which afforded **9** in 91% yield. Subsequently, **9** was treated with BBr₃ to furnish 1,2-diiodo-*o*-carboranylphenol **4** in 96% yield.

Iodinated *m*-carboranes **5a–5e** were synthesized from **11** (Scheme 2), which was obtained in 28% yield from the iodination of *m*-carborane **10** with ICl in the presence of AlCl₃,¹⁷ followed by a transformation into a copper salt and an Ullman coupling.¹⁸ In this coupling reaction, 7,9-diiodo derivative **12** was also obtained unexpectedly in 23% yield, which suggests that the copper salt of **11** reacts with the iodine liberated during the reaction. The iodinated *m*-carboranes **11** and **12** were treated with BBr₃ to

* Corresponding author.

E-mail address: k-ohta@tohoku-mpu.ac.jp (K. Ohta).

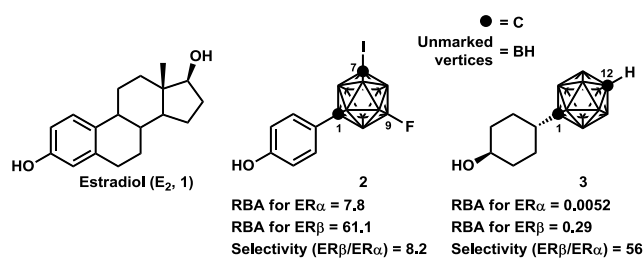
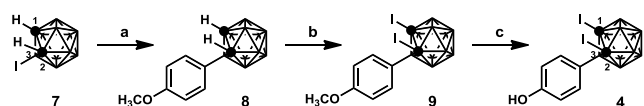
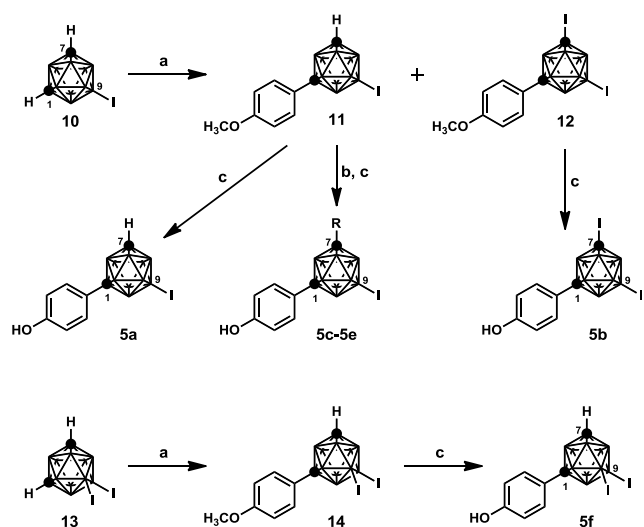


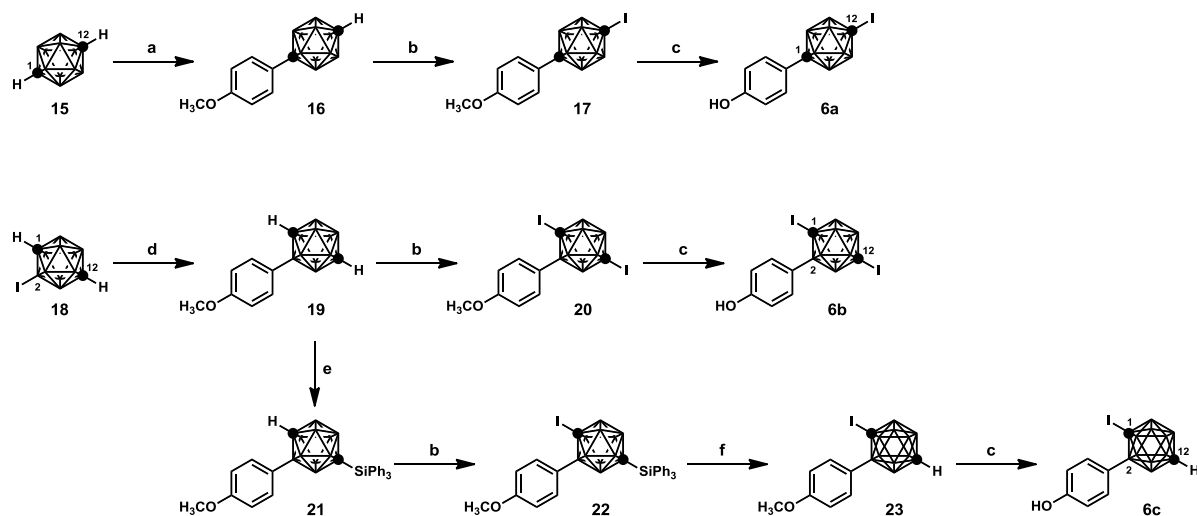
Fig. 1. Structures of 17 β -estradiol and carborane-containing $ER\beta$ -selective ligands.



Scheme 1. Synthesis of iodinated *o*-carborane 4. Reagents and conditions: (a) 4-methoxyphenylmagnesium bromide, $PdCl_2(PPh_3)_2$, CuI, THF, reflux; (b) (i) *n*-BuLi, Et_2O , 0 °C; (ii) I_2 , rt; (c) BBr_3 , CH_2Cl_2 , 0 °C.



Scheme 2. Synthesis of iodinated *m*-carborane derivatives 5a–f. Reagents and conditions: (a) (i) *n*-BuLi, DME, 0 °C; (ii) CuCl, rt; (iii) 4-iodoanisole, pyridine, 100 °C; (b) (i) *n*-BuLi, Et_2O , 0 °C; (ii) R-X, rt; (c) BBr_3 , CH_2Cl_2 , 0 °C.

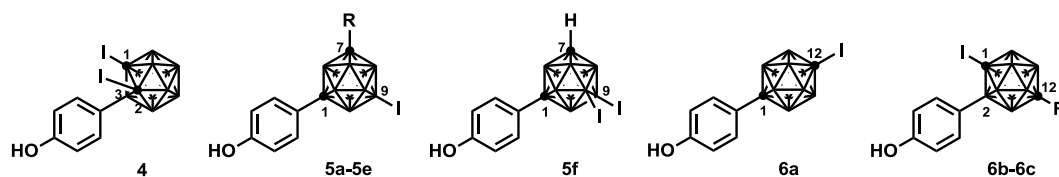


Scheme 3. Synthesis of iodinated *p*-carboranes 6a–c. Reagents and conditions: (a) (i) *n*-BuLi, DME, 0 °C; (ii) CuCl, rt; (iii) 4-iodoanisole, pyridine, 100 °C; (b) (i) *n*-BuLi, Et_2O , 0 °C; (ii) I_2 , rt; (c) BBr_3 , CH_2Cl_2 , 0 °C; (d) 4-methoxyphenylmagnesium bromide, $PdCl_2(PPh_3)_2$, CuI, THF, reflux; (e) (i) *n*-BuLi, Et_2O , 0 °C; (ii) Ph_3SiCl , rt; (f) TBAF, THF, rt.

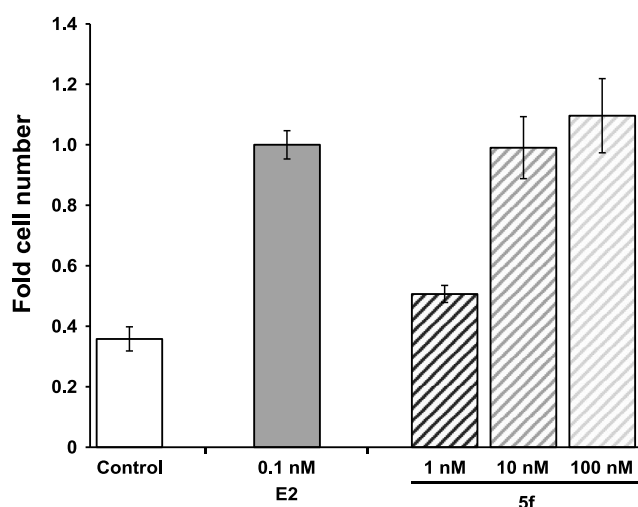
afford 9-iodo-*m*-carboranylphenol 5a and 7,9-diiodo-*m*-carboranylphenol 5b in 90% and quantitative yield, respectively. Allyl, *n*-butyl, and benzyl groups were introduced into the C–H moiety of the *m*-carborane cage of 11 using the corresponding halide reagents in 68–83% yield, which were treated with BBr_3 to afford the corresponding 9-iodophenol derivatives 5c, 5d, and 5e in 68%, 75%, and 93% yield, respectively. Scheme 2 also includes the synthesis of 9,10-diiodo-*m*-carboranylphenol 5f. 9,10-Diiodo-*m*-carborane 13,¹⁹ prepared from the iodination of the corresponding *m*-carborane, was transformed into 14 (65%) under Cu-mediated coupling conditions, followed by a deprotection of the methyl group with BBr_3 to afford 5f in 61% yield.

Scheme 3 summarizes the synthesis of iodinated *p*-carboranyl phenols 6a–6c. Compound 16, which was prepared by the Cu-mediated coupling reaction of *p*-carborane 15 with 4-iodoanisole, was consecutively treated with *n*-BuLi and I_2 , before a demethylation with BBr_3 afforded 12-iodo-*p*-carboranylphenol 6a in 33% overall yield. A Pd-catalyzed *B*-arylation of 2-iodo-*p*-carborane 18, which was obtained from the iodination of *p*-carborane with 4-methoxymagnesium bromide, afforded 19 in 90% yield.¹⁶ Compound 19 was subsequently treated with 2 equivalents of *n*-BuLi, quenched with I_2 , and demethylated to afford 6b in 73% overall yield. One of the less hindered carbon atoms of the *p*-carborane cage of 19 was protected with a triphenylsilyl group,²⁰ while another carbon atom was iodinated to afford 22 in 20% overall yield. The two protecting groups, i.e., the triphenylsilyl and methyl groups, were separately removed with TBAF and BBr_3 , respectively, to afford 6c in 90% overall yield.

The relative binding affinity (RBA) values toward $ER\alpha$, $ER\beta$, and the ER -subtype selectivity of the compounds synthesized in this study are summarized in Table 1.²¹ Interestingly, several derivatives showed RBA values of more than 100% toward $ER\beta$. Although *o*-carborane 4 showed a high $ER\beta$ -binding affinity, the $ER\beta$ selectivity was moderate due to the potent binding affinity toward $ER\alpha$. We found that iodinated *m*-carborane 5a is an $ER\beta$ -selective ligand with high binding affinity toward $ER\beta$. The introduction of an iodine atom onto the carbon atom of the *m*-carborane cage reduced the RBA values toward $ER\alpha$ and $ER\beta$, but the $ER\beta$ selectivity of 5b was almost similar to that of 5a. On the other hand, the introduction of an alkyl substituent, such as an allyl (5c), *n*-butyl (5d), or benzyl (5e) group, enhanced the $ER\alpha$ -binding affinity under concomitant decrease of the $ER\beta$ selectivity. Benzyl derivative 5e exhibited a remarkable decrease of the binding affinity

Table 1RBA values toward ER α and ER β , and ER-subtype selectivity of the iodinated carboranyl phenols **7–9**.^a

Compound	Carborane	R	RBA ^b		Selectivity ^c	
			ER α	ER β	ER α /ER β	ER β /ER α
4	<i>o</i> -Carborane	–	42	242	0.17	5.8
5a	<i>m</i> -Carborane	H	13	129	0.10	9.9
5b		I	8.4	81	0.10	9.6
5c		Allyl	17	62	0.27	3.6
5d		<i>n</i> -Butyl	29	157	0.18	5.4
5e		Benzyl	28	19	1.50	0.68
5f	<i>p</i> -Carborane	–	8.0	111	0.07	14
6a		–	574	888	0.65	1.5
6b		I	18	107	0.17	5.9
6c		H	10	38	0.26	3.8

^a In all binding assays, which were performed in triplicate ($n = 3$), the test compounds (0.4 nM–4 μ M) were examined in the presence of [2,4,6,7-³H]17 β -estradiol (4 nM).^b RBA values were calculated from the IC₅₀ values of E2 and the test compounds, whereby that of E2 was set to 100%.^c The ER-subtype selectivity was estimated from the RBA values toward ER α and ER β .**Fig. 2.** Concentration-dependent MCF-7 cell proliferation induced by **5f**. MCF-7 cells were incubated with **5f** (100 nM–1 nM) for 5 days; the results are shown as the fold cell number, whereby the value for 0.1 nM E2 was set to 100%; assays were performed in triplicate ($n = 3$).

toward ER β , and the RBA value of **5e** toward ER α surpassed that of ER β . 9,10-Diiodo-*m*-carborane **5f** showed a 14-fold higher selectivity toward ER β than toward ER α with an RBA value of more than 100% for ER β . Surprisingly, the RBA value of C-iodo-*p*-carboranyl phenol **6a** toward ER β was more than 800%. Unfortunately, the RBA value toward ER α was also more than 500%, resulting in an overall poor ER β selectivity. These results suggest that the rectilinear C-iodo-*p*-carboranyl phenol structure is particularly suitable for the hydrophobic pocket of both ERs. *p*-Carboranes **6b** and **6c** exhibit a bent core structure comparable to that of **4** and **5**, and showed 5.9- and 3.8-fold selectivity toward ER β , respectively.

The biological profiles, as well as the agonistic and antagonistic activity of **5f** were evaluated by means of a cell proliferation assay

using the MCF-7 cell line, which shows estrogen-dependent growth (Fig. 2).²¹ **5f** promoted the MCF-7 cell proliferation in a concentration-dependent manner and acted as an ER agonist.

In conclusion, we designed and synthesized various iodinated carboranyl phenols containing *o*-, *m*-, and *p*-carborane cages as prospective ligands with high selectivity and affinity toward ER β . A competitive binding assay revealed that the introduction of iodine atoms enhanced their ER β selectivity, which might be caused by a suitable hydrophobic interaction of the iodine atom with the amino acid residues of ER β LBD. **5f** showed the highest ER β selectivity, potent ER β binding affinity, and ER agonistic activity in an MCF-7 cell proliferation assay.

Acknowledgments

This research was supported by a grant-in-aid from the Strategic Research Program for Private Universities (2015–2019) and Grants-in-Aid for Scientific Research (C) (26460151 and 15K08029) from the Japanese Ministry of Education, Culture, Sports, Science, and Technology (MEXT).

References

- Kuiper GGJM, Enmark E, Pelto-Huikko M, Nilsson S, Gustafsson J-A. *Proc Natl Acad Sci USA*. 1996;93:5925.
- Green S, Walter P, Kumar V, et al. *Nature*. 1986;320:134.
- Heldring N, Pike A, Andersson S, et al. *Physiol Rev*. 2007;87:905.
- (a) Lanyon L, Armstrong V, Ong D, Zaman G, Price J. *J Endocrinol*. 2004;182:183; (b) Pfaff D, Waters E, Khan Q, Zhang X, Numan M. *Endocrinology*. 2011;152:1209; (c) Ribeiro JR, Freiman RN. *J Steroid Biochem Mol Biol*. 2014;143:160.
- Piu F, Cheevers C, Hyldtoft L, et al. *Eur J Pharmacol*. 2008;590:423.
- Haldosen L-A, Zhao C, Dahlman-Wright K. *Mol Cell Endocrinol*. 2014;382:665.
- Wu W-F, Maneix L, Insunza J, et al. *Proc Natl Acad Sci USA*. 2017;114:E3816.
- (a) Pravettoni A, Mornati O, Martini PGV, et al. *Mol Cell Endocrinol*. 2007;263:46; (b) Kim IY, Kim B-C, Seong DH, et al. *Cancer Res*. 2002;62:5365.
- George S, Petit GH, Gouras GK, Brundin P, Olsson R. *ACS Chem Neurosci*. 2013;4:1537.
- Warner M, Huang B, Gustafsson J-A. *Trends Pharmacol Sci*. 2017;38:92.
- (a) Paech K, Webb P, Kuiper GGJM, et al. *Science*. 1997;277:1508; (b) Brzozowski AM, Pike AC, Dauter Z, et al. *Nature*. 1997;389:753.

12. (a) Sun W, Cama LD, Birzin ET, et al. *Bioorg Med Chem Lett*. 2006;16:1468;
(b) Blizzard TE, Gude C, Morgan II JD, et al. *Bioorg Med Chem Lett*. 2006;16:834;
(c) Wilkening RR, Ratcliffe RW, Tynebor EC, et al. *Bioorg Med Chem Lett*. 2006;16:3489.
13. Ohta K, Ogawa T, Kaise A, Endo Y. *Bioorg Med Chem Lett*. 2013;23:6555.
14. Ohta K, Ogawa T, Oda A, Kaise A, Endo Y. *Bioorg Med Chem Lett*. 2015;25:4174.
15. (a) Viñas C, Barberà G, Oliva JM, Teixidor F, Welch AJ, Rosair GM. *Inorg Chem*. 2001;40:6555;
(b) Barberà G, Viñas C, Teixidor F, Rosair GM, Welch AJ. *J Chem Soc, Dalton Trans*. 2002;3647.
16. Ohta K, Yamazaki H, Endo Y. *J Organomet Chem*. 2009;694:1646.
17. Andrews JS, Zayas J, Jones Jr M. *Inorg Chem*. 1985;24:3715.
18. (a) Ohta K, Goto T, Endo Y. *Inorg Chem*. 2005;44:8569;
(b) Coult R, Fox MA, Gill WR, Herbertson PL, MacBride JAH, Wade K. *J Organomet Chem*. 1993;462:19.
19. Ohta K, Ogawa T, Kaise A, Endo Y. *Bioorg Med Chem*. 2014;22:3508.
20. Douglass AG, Pakhomov S, Reeves B, Janousek Z, Kaszynski P. *J Org Chem*. 2000;65:1434.
21. Ohta K, Chiba Y, Ogawa T, Endo Y. *Bioorg Med Chem Lett*. 2008;18:5050.



Contents lists available at ScienceDirect

Biochemical and Biophysical Research Communications

journal homepage: www.elsevier.com/locate/ybbrc



BA321, a novel carborane analog that binds to androgen and estrogen receptors, acts as a new selective androgen receptor modulator of bone in male mice



Kenta Watanabe^{a, b}, Michiko Hirata^a, Tsukasa Tominari^{a, c}, Chiho Matsumoto^a,
Yasuyuki Endo^d, Gillian Murphy^e, Hideaki Nagase^{c, f}, Masaki Inada^{a, b, c},
Chisato Miyaura^{a, b, c, *}

^a Department of Biotechnology and Life Science, Tokyo University of Agriculture and Technology, 2-24-16 Nakamachi, Koganei, Tokyo 184-8588, Japan

^b Cooperative Major in Advanced Health Science, Tokyo University of Agriculture and Technology, 2-24-16 Nakamachi, Koganei, Tokyo 184-8588, Japan

^c Institute of Global Innovation Research, Tokyo University of Agriculture and Technology, 2-24-16 Nakamachi, Koganei, Tokyo 184-8588, Japan

^d Faculty of Pharmaceutical Sciences, Tohoku Medical and Pharmaceutical University, 4-4-1, Komatsushima, Aoba-ku, Sendai, 981-8558, Japan

^e Department of Oncology, University of Cambridge, Cancer Research UK, Cambridge Institute, Li Ka Shing Centre, Cambridge, CB2 0RE, United Kingdom

^f Kennedy Institute of Rheumatology, Nuffield Department of Orthopaedics, Rheumatology and Musculoskeletal Sciences, University of Oxford, Oxford, OX3 7FY, United Kingdom

ARTICLE INFO

Article history:

Received 26 June 2016

Accepted 4 July 2016

Available online 9 July 2016

Keywords:

Osteoporosis

Bone mass

Carborane compound

Estrogen

Androgen

Orchidectomized mice

Selective androgen receptor modulator

ABSTRACT

Carboranes are a class of carbon-containing polyhedral boron cluster compounds with globular geometry and hydrophobic surface that interact with hormone receptors such as estrogen receptor (ER) and androgen receptor (AR). We have synthesized BA321, a novel carborane compound, which binds to AR. We found here that it also binds to ERs, ER α and ER β . In orchidectomized (ORX) mice, femoral bone mass was markedly reduced due to androgen deficiency and BA321 restored bone loss in the male, whilst the decreased weight of seminal vesicle in ORX mice was not recovered by administration of BA321. In female mice, BA321 acts as a pure estrogen agonist, and restored both the loss of bone mass and uterine atrophy due to estrogen deficiency in ovariectomized (OVX) mice. In bone tissues, the trabecular bone loss occurred in both ORX and OVX mice, and BA321 completely restored the trabecular bone loss in both sexes. Cortical bone loss occurred in ORX mice but not in OVX mice, and BA321 clearly restored cortical bone loss due to androgen deficiency in ORX mice. Therefore, BA321 is a novel selective androgen receptor modulator (SARM) that may offer a new therapy option for osteoporosis in the male.

© 2016 Elsevier Inc. All rights reserved.

1. Introduction

Osteoporosis is accompanied by severe bone loss due to a deficiency of sex hormones associated with advanced ageing. Postmenopausal osteoporosis in women is mainly due to increased trabecular bone resorption caused by estrogen deficiency. Ovariectomy (OVX) in rats and mice is commonly used to study estrogen deficiency in females, and it has been shown that estrogen treatment can prevent bone loss in OVX animals, as in patients with postmenopausal osteoporosis by suppressing bone resorption

[1–4]. Osteoporosis in elderly men is thought to be due to androgen deficiency and aging. Like estrogen, androgen suppresses bone resorption to maintain bone mass, but androgen also stimulates new bone formation. Similarly, orchidectomy (ORX) in mice causes marked bone loss by increased bone resorption and decreased bone formation. Administration of testosterone recovers bone loss in ORX mice, furthermore estrogen can also restore the bone loss due to androgen deficiency. Since testosterone may be partly converted to estrogen by aromatase, both androgen and estrogen may be effective for the maintenance of bone tissues in the male. Indeed, we have reported that aromatase-deficient (ArKO) mice showed marked bone loss due to increased osteoclastic bone resorption because of estrogen deficiency in both sexes [5].

Androgen and estrogen exert potent influences on skeletal shape, mass, and homeostasis in both men and women [6].

* Corresponding author. Department of Biotechnology and Life Science, Tokyo University of Agriculture and Technology, 2-24-16 Nakamachi, Koganei, Tokyo 184-8588, Japan. Tel.: +81 42 388 7390.

E-mail address: miyaura@cc.tuat.ac.jp (C. Miyaura).

Estrogen and androgen suppress bone resorption by ER- and AR-dependent mechanisms, respectively, and androgen also stimulates bone formation in an AR-dependent manner [6]. However, replacement therapy with sex steroids is not generally used for postmenopausal osteoporosis patients due to the risk of uterine cancer. Some synthetic compounds such as raloxifene preferentially act on bone and cardiovascular systems as agonists, whereas they antagonize the effects of estrogen in reproductive tissues [4,7,8]. These compounds are known as selective estrogen receptor modulators (SERM) and raloxifene is now available for the treatment of osteoporosis in women. For osteoporosis in men, selective androgen receptor modulators (SARM), which act as androgens in bone and muscle without androgenic action in male sex organ are useful for male patients. Various SARMs such as GTx-024, GTx-027, MK-4541, TSAA-291, NEP28, and S-101479 have been developed, but no SARM is available for clinical use [9–13].

Carboranes (dicarba-closo-dodecaboranes) are a class of carbon-containing polyhedral boron-cluster compounds with remarkable thermal stability and exceptional hydrophobicity, and have been applied in the field of boron neutron capture therapy in cancer [14–16]. On the other hand, we have focused on the binding affinity of carboranes to steroid hormone receptors and possible biological activity in various cells [17]. Previously, we reported that BE120, a carborane compound, bound to ER and acted as a potent estrogen agonist in both bone and reproductive tissues [18], and that BE360, another carborane, exhibited anti-estrogenic properties as a hydrophobic pharmacophore in ER-dependent luciferase reporter gene assays [19] and recovered bone loss in OVX mice without any action in reproductive tissues [20], indicating that BE360 is a possible SERM in female osteoporosis. We also developed several carborane compounds, which bind the AR and some of the compounds, BA321 and BA341, act as anti-androgens [21,22].

In this study, we examined the effect of the carborane compound, BA321 on bone mass and sex organs in ORX and OVX mice. BA321 showed a high binding affinity to both AR and ERs, and recovered bone loss in both ORX and OVX mice. BA321 did not influence the sex organs in male mice. On the other hand, it acted as a pure estrogen in female mice. Therefore BA321 is a novel SARM which acts as a selective agonist in bone tissue, and may be a new candidate in the treatment of osteoporosis in men.

2. Materials and methods

2.1. Animals and drugs

Eight-week-old female and male mice *ddy* strains were obtained from Japan SLC Inc. (Shizuoka, Japan). Male mice were either sham-operated or ORX. Some of the ORX mice were administered subcutaneously with BA321 dissolved in polyethyleneglycol-300 (Wako, Osaka, Japan) using a mini-osmotic pump (Alza Co., Palo Alto, CA) immediately after surgery. Female mice were sham-operated or OVX. Some of the OVX mice were administered subcutaneously with BA321 as described above. The mice were fed a laboratory chow containing 1.12% calcium and 1.07% phosphorus (Nippon Clea, Tokyo, Japan) for 4 weeks after the surgery. BA321 was synthesized in our laboratory as reported in our previous studies [22].

2.2. Binding analysis of BA321 to androgen receptor and estrogen receptors

The *in vitro* AR binding assay used the recombinant ligand binding domain (LBD) of human AR (hrAR-LBD) prepared by the Chemicals Evaluation Research Institute (CERI), Japan. The binding affinity of BA321 to AR was measured by the competitive binding

assay with [³H]-DHT, and the IC₅₀ value determined was compared with that of DHT. For *in vitro* binding assay for ER α and ER β , the recombinant LBDs of human ER α (hrER α -LBD) and human ER β (hrER β -LBD) prepared by the CERI, Japan were used. The binding affinity of BA321 to ERs was measured by the competitive binding assay with [³H]-17 β -estradiol, and the IC₅₀ values of BA321 for hrER α and for hrER β were determined and compared with those for 17 β -estradiol.

2.3. Radiographic analysis of the femur

The bone mineral density (BMD) of the femurs was measured by dual X-ray absorptiometry (model DCS-600R; Aloka, Tokyo, Japan), as reported previously [23]. The bone mineral content (BMC) of the mouse femur was closely correlated with the ash weight [23]. The BMD was calculated by dividing the BMC of the measured area by the area. The scanned area was dividing equally into three regions comprising the proximal, middle and distal femur to assess regional differences. The BMD in the total area of the femur was also measured.

2.4. Micro CT analysis

The CT scanning of the femurs was performed using a micro-focus X-ray CT system (inspeXio SMX-90T; Shimadzu). Three-dimensional microstructural image data were reconstructed using a cross-section of the distal femur for trabecular bone. The structural indices were calculated for trabecular bone, bone volume/tissue volume [BV/TV], bone surface of bone volume [BS/BV], trabecular number [Tb. N] and trabecular separation [Tb. S] using the TRI/3D-BON software program (Ratoc System Engineering Co., Ltd.), as reported [23].

2.5. Statistical analysis

Data were analyzed using one-way ANOVA, followed by Tukey's test for *post hoc* analysis. All data are presented as the means \pm SEM, and all statistical analyses were performed using IBM SPSS Statistics Ver.23 software.

3. Results

3.1. Design and synthesis of carborane BA321, and its affinity to AR and ERs

Carboranes are a class of carbon-containing polyhedral boron-cluster compounds, having globular geometry and a hydrophobic surface (Fig. 1A). We focused on the hydrophobic feature of carboranes which interact with steroid hormone receptors because their shape may be suitable as an AR or ER ligand. The size of the carborane cage seems to be appropriate for a hydrophobic structure in place of the C, D rings of sex steroid, DHT and 17 β -estradiol (Fig. 1B). We synthesized a novel carborane compound, BA321 (Fig. 1A), which has *p*-carborane skeletons and exhibits anti-androgen properties in AR-dependent luciferase reporter gene assays [22]. We first investigated the binding affinity of BA321 to AR and both ER α and ER β , in comparison with DHT and 17 β -estradiol using a binding competition assay. BA321 clearly bound to AR, and its binding affinity was 1/220 of that of DHT (Fig. 1C). Surprisingly, BA321 also bound to ERs, ER α and ER β , and its binding affinity to ER α and ER β was about 1/340 and 1/48 of that of 17 β -estradiol, respectively (Fig. 1C).

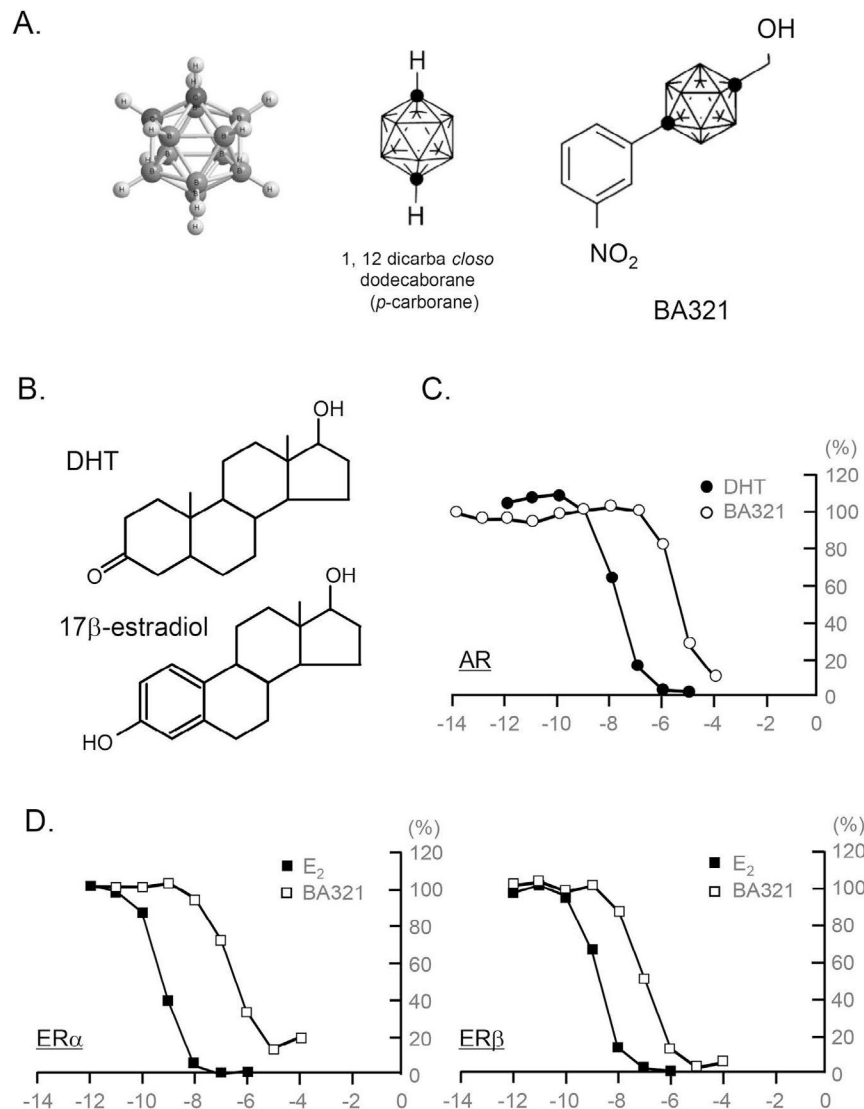


Fig. 1. Structures of the carborane cage, carborane compounds, BA321 and binding affinity to AR or ER. (A) In icosahedral cage structures, closed circles (●) represent carbon atoms and other vertices represent BH units. (B) Structures of dihydrotestosterone (DHT) and 17β-estradiol (E2). (C) Binding of BA321 (○) and DHT (●) to human AR. The binding affinities of BA321 and DHT to AR were determined by measuring their abilities to compete the binding of radiolabeled [³H]DHT to hrAR-LBD in the presence of increasing concentrations of a competitor, taking the binding of [³H]DHT to hrAR-LBD without a competitor as 100%. Log IC₅₀ values (M) of DHT and BA321 for AR were –7.82 and –5.48, respectively. (D) Binding of BA321 (□) and E2 (■) to human ERα and ERβ. The binding affinities of BA321 and E2 were determined by measuring their abilities to compete the binding of radiolabeled [³H]17β-estradiol to hrER-LBD in the presence of increasing concentrations of a competitor, taking the binding of [³H]17β-estradiol to hrER-LBD without a competitor as 100%. Log IC₅₀ values (M) of E2 and BA321 for ERα were –9.20 and –6.67, respectively. Log IC₅₀ values (M) of the two ligands for ERβ were –8.74 (E2) and –7.06 (BA321), respectively.

3.2. Effects of BA321 in sex organs in ORX and OVX mice

We first examined the effects of BA321 on the weight of sex organs in mice of both sexes. The weight of the seminal vesicles decreased markedly in ORX mice due to androgen deficiency (Fig. 2A). When ORX mice were given androgens, the weight of seminal vesicles returned to the sham level (data not shown). Administration of BA321 (10 and 30 μg/day) showed no effects on the weight of seminal vesicles in ORX mice (Fig. 2A). In OVX mice, the uterine weight decreased markedly due to estrogen deficiency, and the administration of BA321 (10 and 30 μg/day) dose-dependently restored the uterine weight to the sham level (Fig. 2B). These results indicate that BA321 exhibits estrogenic action in female sex organs, but does not act as androgen in male sex organs.

3.3. Effects of BA321 on bone mass in ORX mice

Androgen deficiency caused by ORX resulted in a marked decrease in bone mass due to the stimulation of bone resorption and a concomitant decrease in bone formation. To determine the effects of BA321 on bone mass in ORX mice, male mice were sham-operated or ORX, and some ORX mice were treated with BA321. Four weeks after the surgery, we measured the femoral BMD of the total area and of three divided areas; proximal, central and distal. Total BMD was significantly reduced by ORX, and BA321 administration (10 and 30 μg/day) caused dose-dependent recovery of bone mass to the sham level (Fig. 3A). All areas showed a decreased BMD in ORX mice, and BA321 restored the BMD to the sham level in the all area (Fig. 3A). BA321 may stimulate cortical bone formation in the central area of the femurs. Using μCT, we examined the effects

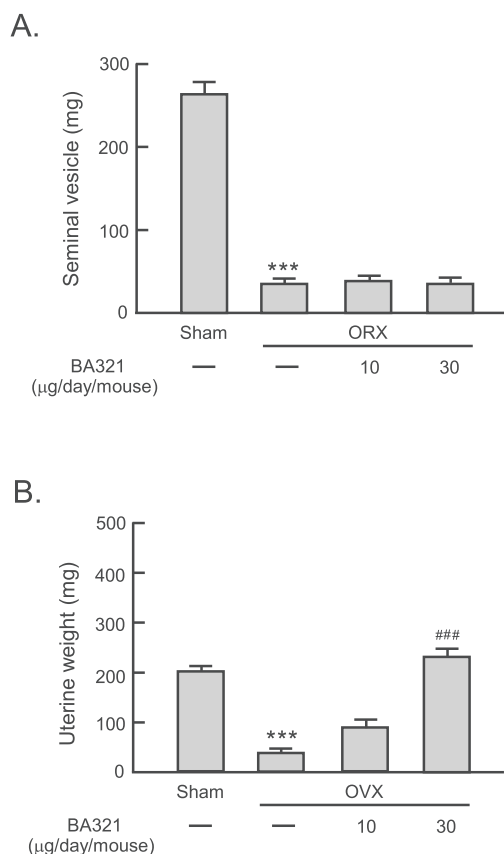


Fig. 2. Effects of BA321 on the weight of the seminal vesicles in ORX mice and the uterine weight in OVX mice. (A) Male mice were sham-operated or ORX, and some of the ORX mice were treated with 10 and 30 µg/day/mouse of BA321. At 4 weeks after the surgery, the weight of the seminal vesicles was measured. Significantly different from sham mice, *** $P < 0.001$. Data are expressed as the means \pm SEM of 6–8 mice. (B) Female mice were sham-operated or OVX, and some of the OVX mice were treated with 10 and 30 µg/day/mouse of BA321 after the surgery. The uterine weight was measured at 4 weeks after the operation. Significantly different from sham mice, *** $P < 0.001$, and from OVX mice, ### $P < 0.001$. Data are expressed as the means \pm SEM of 8–11 mice.

of BA321 on the trabecular bone architecture in ORX mice. In ORX mice, we detected a marked loss of trabecular bone in the distal femurs, which was accompanied by a decrease in BV/TV and Tb.N. and an increase in BS/BV and Tb.Sp. (Fig. 3B). Administration of BA321 (10 and 30 µg/day) dose-dependently recovered all CT markers to the sham levels, and trabecular bone architecture also recovered (Fig. 3B).

3.4. Effects of BA321 on bone mass in OVX mice

To determine the effects of BA321 on bone mass in OVX mice, OVX mice were treated for 4 weeks with BA321 and femurs were subjected to radiographic analysis. We measured the femoral BMD of total area and three divide proximal, central and distal areas. Total BMD was significantly reduced by OVX, and BA321 (10 and 30 µg/day) dose-dependently caused bone mass recovery (Fig. 4A). The distal BMD was clearly decreased by OVX, but the central BMD showed no change on OVX, and was not influenced by the administration of BA321 (Fig. 4A). In μ CT analysis, the loss of distal trabecular bone was detected in OVX mice, and BA321 dose-dependently recovered the trabecular bone architecture to the sham levels (Fig. 4B). In OVX mice, we detected a decrease in BV/TV and Tb.N. and an increase in BS/BV and Tb.Sp. (Fig. 3B). The

administration of BA321 dose-dependently recovered the all CT markers to the sham levels (Fig. 4B).

4. Discussion

In the present study, we showed that the carborane BA321 binds to the AR, and acts as an androgen in bone tissues without androgenic action in sex organs. Thus BA321 acts as a novel SARM which may be useful for the maintenance of bone mass in elderly men with accompanying androgen deficiency. In addition to AR, BA321 also binds to ER α and ER β , and exhibits a pure estrogenic action in both bone and uterus in female mice. This is unusual because SARMS generally bind to AR but not ERs and exhibit the tissues selective androgenic or anti-androgenic function. The mechanism of the tissue-specific action of SARMS is thought to depend on the AR-related recruitment of numerous cofactors, and SARMS induce recruitment of fewer cofactors than DHT [11,13]. BA321 was originally designed based on potent AR antagonists that exhibited anti-androgenic activity in reporter gene assay using NIH3T3 cells transfected with a human AR expression plasmid [22]. However, we show that BA321 also binds to ERs and exhibits estrogenic action in OVX mice. The mechanisms of action of BA321 mediated by AR and ER are unknown, and have to be examined in a future study.

Androgens and estrogens exert potent influences on the bone homeostasis in both men and women [6]. In the present study, the trabecular bone in the femur was clearly decreased with increased bone resorption in both ORX and OVX mice, and the administration of BA321 restored the trabecular bone loss to sham levels (Figs. 3B and 4B). The distal area of the femur is rich in trabecular bone, and BA321 restored the loss of distal BMD in the femur (Figs. 3A and 4A). The BMD in central area of the femur consists only of cortical bone. In ORX mice, the central BMD clearly suppressed, and the administration of BA321 restored the cortical bone loss. However, the significant loss of central BMD was not detected in OVX mice, and BA321 did not influenced the cortical bone mass in the female (Fig. 4A). These results suggest that BA321 binds to AR and acts on trabecular bone to suppress bone resorption, and on cortical bone to stimulate bone formation in the male, and that it binds to ERs and suppresses bone resorption in trabecular bone in the female. BA321 may not be useful for osteoporosis in the female, since it exhibits an estrogenic action in the uterus, which is thus a cancer risk. On the other hand, BA321 may be a potential candidate SARM for male osteoporosis without a risk of cancer in the sex organs.

Kawano et al. [24] have reported that global deletion of AR in male mice results in high bone turnover with increased trabecular bone resorption, as well as decreased cortical bone volume due to suppressed bone formation. On the other hand, data in the previous reports using global deletion of ERs are complex [6]. Cell-specific ER α knockout mice have been generated, and suggested that the ER α -dependent apoptosis occurs in osteoclasts [6,25], but the mechanisms of bone loss by the cell-specific ERs depletion are still not clear. Further studies are needed to define the mechanisms of AR-dependent and ER-dependent bone turnover in both sexes.

Loss of musculoskeletal mass and function is a natural ageing trait, and osteoporosis and sarcopenia are increasing in older people [26], but androgen therapy is not generally used due to the perceived side effects, such as prostate cancer. Therefore SARMS are potential candidate anabolic compounds that maintain bone mass and muscle function. In addition to osteoporosis and sarcopenia, SARMS are thought to be useful for the therapy of AR-dependent prostate cancer, the muscle wasting associated with cancer, and chronic illness, as well as AR-positive breast cancer [9,10,12,27]. We examined the effects of BA321 on the cell growth of AR-positive prostate cancer LNCap, and found that BA321 suppressed the DHT-dependent growth of LNCap cells (Inada, M. et al., unpublished

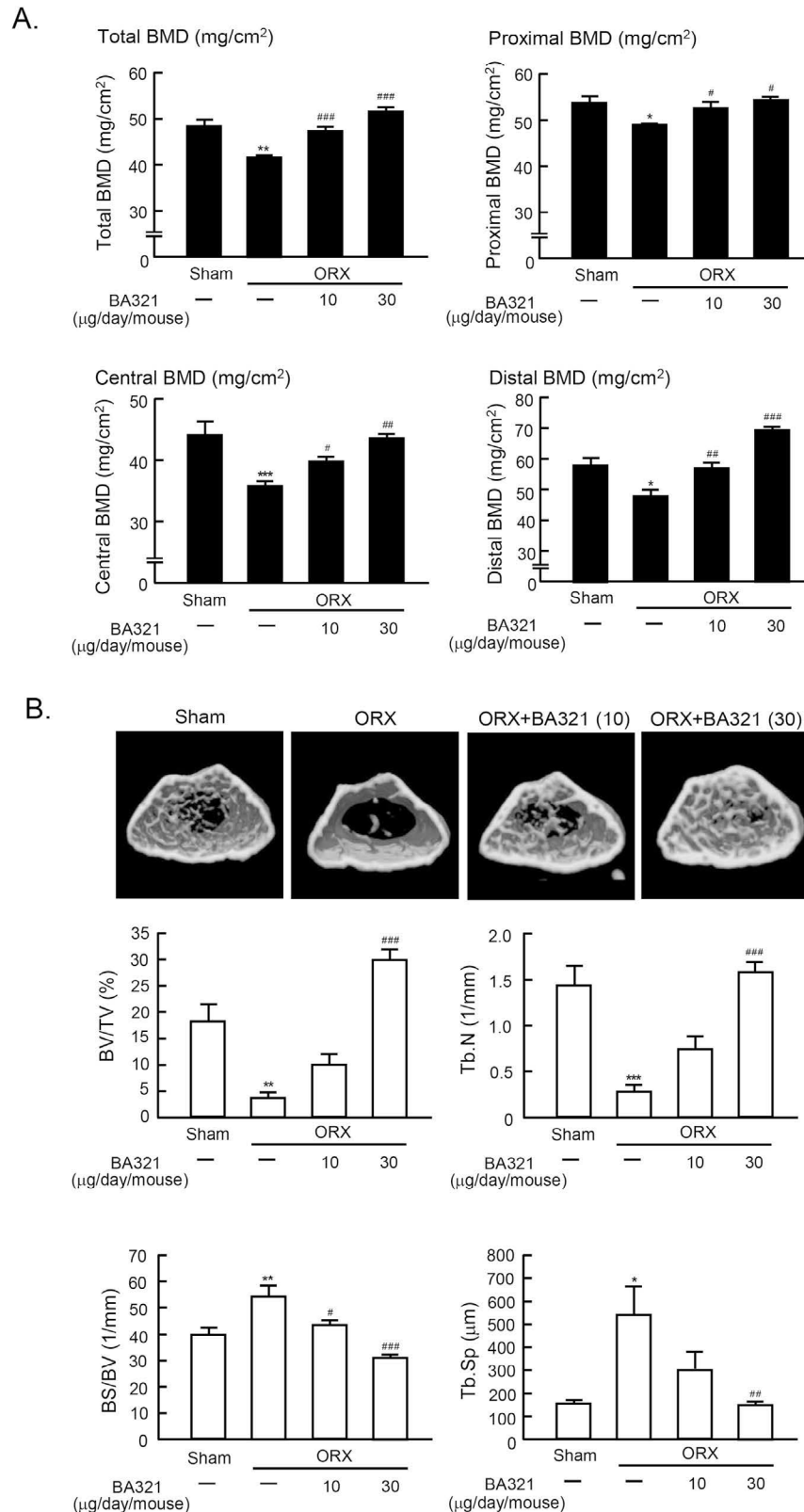


Fig. 3. Effects of BA321 on bone mass of femurs in ORX mice. (A) Mice were sham-operated or ORX, and some of the ORX mice were treated with 10 and 30 µg/day/mouse of BA321. After 4 weeks, femurs were collected and the femoral bone mineral density (BMD) in each area (total, distal, central and proximal) was measured by dual X-ray absorptiometry (DEXA). Significantly different from sham mice, * $P < 0.05$, ** $P < 0.01$, *** $P < 0.001$ and from ORX mice, # $P < 0.05$, ## $P < 0.01$, ### $P < 0.001$. Data are expressed as the means \pm SEM of 6–8 mice. (B) A three-dimensional (3D) μ CT analysis of femoral trabecular bone collected from sham, ORX, and ORX mice treated with BA321 (10 and 30 µg/day) at 4 weeks after surgery. The upper panel shows a 3D μ CT image of the femoral distal metaphysis in each group. The Bone Volume/Total tissue Volume (BV/TV), Trabecular Number (Tb.N.), Bone Surface/Bone Volume (BS/BV), and Trabecular Separation (Tb.Sp.) were calculated by a 3D μ CT analysis. The data are expressed as the mean \pm SEM of 6–8 mice. Significantly different from sham mice, * $P < 0.05$, ** $P < 0.01$, *** $P < 0.001$ and from ORX mice, # $P < 0.05$, ## $P < 0.01$, ### $P < 0.001$.

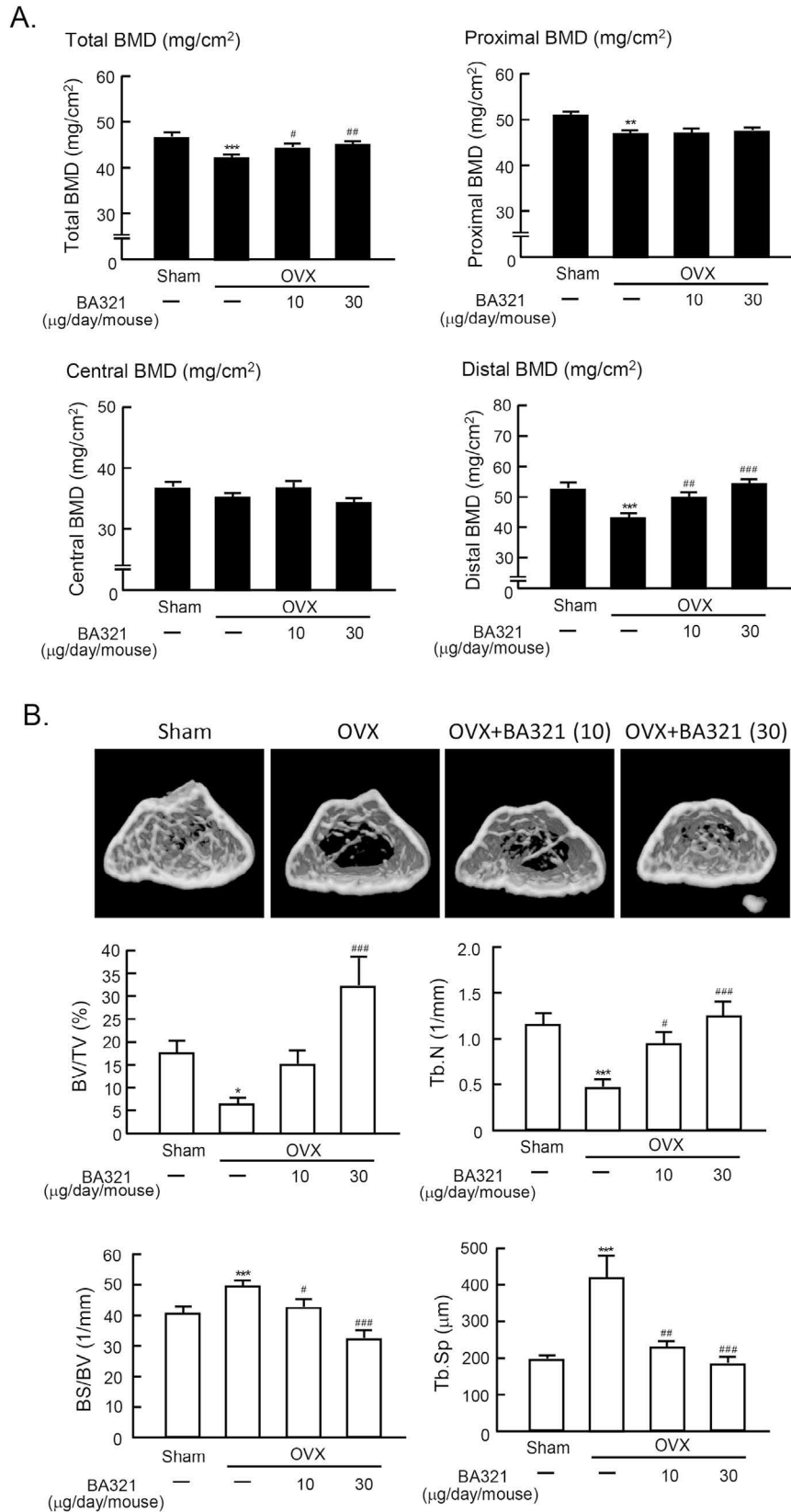


Fig. 4. Effects of BA321 on bone mass of femurs in OVX mice. (A) Mice were sham-operated or OVX, and some of the OVX mice were treated with 10 and 30 µg/day/mouse of BA321 immediately after surgery. After 4 weeks, their femurs were collected and the femoral BMD in each area (total, distal, central and proximal) was measured by DEXA. Significantly different from sham mice, ** $P < 0.01$, *** $P < 0.001$ and from OVX mice, # $P < 0.05$, ## $P < 0.01$, ### $P < 0.001$. Data are expressed as the means \pm SEM of 8–11 mice. (B) A 3D µCT analysis of femoral trabecular bone collected from sham, OVX, and OVX mice treated with BA321 (10 and 30 µg/day) at 4 weeks after surgery. The upper panel shows a 3D µCT image of the femoral distal metaphysis in each group. The BV/TV, Tb.N., BS/BV, and Tb.Sp. were calculated by a 3D µCT analysis. The data are expressed as the mean \pm SEM of 8–11 mice. Significantly different from sham mice, * $P < 0.05$, *** $P < 0.001$ and from OVX mice, # $P < 0.05$, ## $P < 0.01$, ### $P < 0.001$.

data). Therefore, it is possible that BA321 exhibits anti-androgenic action for prostate cancer as a SARM *in vivo* without the loss of musculoskeletal mass, a typical risk of anti-androgen therapy.

In conclusion, we have demonstrated that BA321, a novel carborane compound, bound to not only AR, but also ERs with a high binding affinity, and completely restored the bone loss in both ORX and OVX mice. Since BA321 did not influence the sex organ in the males, it may act as a potential SARM to prevent the loss of musculoskeletal mass due to androgen deficiency in men.

Acknowledgments

This work is partly supported by Grants-in-Aid for Scientific Research 25460062 (C.M.) and 23590069 (M.I.), National Institute of Health grant AR40994 (H.N.), Arthritis Research UK (H.N.), Cancer Research UK (G.M.) and Institute of Global Innovation Research in TUAT (M.I., H.N.). This project was supported by Open Partnership Joint Projects of JSPS Bilateral Joint Research Projects.

Transparency document

Transparency document related to this article can be found online at <http://dx.doi.org/10.1016/j.bbrc.2016.07.027>.

References

- [1] L.G. Raisz, Pathogenesis of osteoporosis: concepts, conflicts, and prospects, *J. Clin. Investig.* 115 (2005) 3318–3325.
- [2] D.J. Rickard, M. Subramaniam, T.C. Spelsberg, Molecular and cellular mechanisms of estrogen action on the skeleton, *J. Cell Biochem.* 32–33 (suppl. 32) (1999) 123–132.
- [3] M.N. Weitzmann, R. Pacifici, Estrogen deficiency and bone loss: an inflammatory tale, *J. Clin. Investig.* 116 (2006) 1186–1194.
- [4] Y. Onoe, C. Miyaura, M. Ito, H. Ohta, S. Nozawa, T. Suda, Comparative effects of estrogen and raloxifene on B lymphopoiesis and bone loss induced by sex steroid deficiency in mice, *J. Bone Min. Res.* 15 (2000) 541–549.
- [5] C. Matsumoto, M. Inada, K. Toda, C. Miyaura, Estrogen and androgen play distinct roles in bone turnover in male mice before and after reaching sexual maturity, *Bone* 28 (2006) 220–226.
- [6] S.C. Manolagas, C.A. O'Brien, M. Almeida, The role of estrogen and androgen receptors in bone health and disease, *Nat. Rev. Endocrinol.* 9 (2013) 699–712.
- [7] T.A. Grese, J.P. Sluka, H.U. Bryant, G.J. Cullinan, A.L. Glasebrook, C.D. Jones, K. Matsumoto, A.D. Palkowitz, M. Sato, J.D. Termine, M.A. Winter, N.N. Yang, J.A. Dodge, Molecular determinants of tissue selectivity in estrogen receptor modulators, *Proc. Natl. Acad. Sci. U. S. A.* 94 (1997) 14105–14110.
- [8] M. Sato, M.K. Rippey, H.U. Bryant, Raloxifene, tamoxifen, nafoxidine, or estrogen effects on reproductive and nonreproductive tissues in ovariectomized rats, *FASEB J.* 10 (1996) 905–912.
- [9] R. Narayanan, S. Ahn, M.D. Cheney, M. Yepuru, D.D. Miller, M.S. Steiner, J.T. Dalton, Selective androgen receptor modulators (SARMs) negatively regulate triple-negative breast cancer growth and epithelial:mesenchymal stem cell signaling, *PLoS One* 9 (2014) e103202.
- [10] M.J. Chisamore, M.A. Gentile, G.M. Dillon, M. Baran, C. Gambone, S. Riley, A. Schmidt, O. Flores, H. Wilkinson, S.E. Alves, A novel selective androgen receptor modulator (SARM) MK-4541 exerts anti-androgenic activity in the prostate cancer xenograft R-3327G and anabolic activity on skeletal muscle mass & function in castrated mice, *J. Steroid Biochem. Mol. Biol.* (2016), <http://dx.doi.org/10.1016/j.jsbmb.2016.04.007>. S0960-0760(16)30103-0.
- [11] Y. Hikichi, M. Yamaoka, M. Kusaka, T. Hara, Selective androgen receptor modulator activity of a steroidal antiandrogen TSAA-291 and its cofactor recruitment profile, *Eur. J. Pharmacol.* 765 (2015) 322–331.
- [12] K. Akita, K. Harada, J. Ichihara, N. Takata, Y. Takahashi, K. Saito, A novel selective androgen receptor modulator, NEP28, is efficacious in muscle and brain without serious side effects on prostate, *Eur. J. Pharmacol.* 720 (2013) 107–114.
- [13] K. Furuya, N. Yamamoto, Y. Ohyabu, T. Morikyu, H. Ishige, M. Albers, Y. Endo, Mechanism of the tissue-specific action of the selective androgen receptor modulator S-101479, *Biol. Pharm. Bull.* 36 (2013) 442–451.
- [14] V.I. Bregardze, Dicarba-closo-dodecaboranes C₂B₁₀H₁₂ and their derivatives, *Chem. Rev.* 92 (1992) 209–223.
- [15] A.H. Soloway, W. Tjarks, B.A. Barnum, F.G. Rong, R.F. Barth, I.M. Codogni, J.G. Wilson, The chemistry of neutron capture therapy, *Chem. Rev.* 98 (1998) 1515–1562.
- [16] M.F. Hawthorne, The role of chemistry in the development of boron neutron capture therapy for cancer, *Angew. Chem. Int. Ed. Engl.* 32 (1993) 950–984.
- [17] Y. Endo, T. Iijima, Y. Yamakoshi, M. Yamaguchi, H. Fukasawa, K. Shudo, Potent estrogenic agonists bearing dicarba-closo-dodecaborane as a hydrophobic pharmacophore, *J. Med. Chem.* 42 (1999) 1501–1504.
- [18] Y. Endo, T. Iijima, Y. Yamakoshi, H. Fukasawa, C. Miyaura, M. Inada, A. Kubo, A. Itai, Potent estrogen agonists based on carborane as a hydrophobic skeletal structure. A new medicinal application of boron clusters, *Chem. Biol.* 8 (2001) 341–355.
- [19] T. Ogawa, K. Ohta, T. Yoshimi, H. Yamazaki, T. Suzuki, S. Ohta, Y. Endo, *m*-Carborane bisphenol structure as a pharmacophore for selective estrogen receptor modulators, *Bioorg. Med. Chem. Lett.* 16 (2006) 3943–3946.
- [20] M. Hirata, M. Inada, C. Matsumoto, M. Takita, T. Ogawa, Y. Endo, C. Miyaura, A novel carborane analog, BE360, with a carbon-containing polyhedral boron-cluster is a new selective estrogen receptor modulator for bone, *Biochem. Biophys. Res. Commun.* 380 (2009) 218–222.
- [21] K. Ohta, T. Goto, S. Fujii, T. Suzuki, S. Ohta, Y. Endo, Design and synthesis of carborane-containing androgen receptor (AR) antagonist bearing a pyridine ring, *Bioorg. Med. Chem.* 16 (2008) 8022–8028.
- [22] S. Fujii, T. Goto, K. Ohta, Y. Hashimoto, T. Suzuki, S. Ohta, Y. Endo, Potent androgen antagonists based on carborane as a hydrophobic core structure, *J. Med. Chem.* 48 (2005) 4654–4662.
- [23] M. Inada, M. Takita, S. Yokoyama, K. Watanabe, T. Tominari, C. Matsumoto, M. Hirata, Y. Maru, T. Maruyama, Y. Sugimoto, S. Narumiya, S. Uematsu, S. Akira, G. Murphy, H. Nagase, C. Miyaura, Direct melanoma cell contact induces stromal cell autocrine prostaglandin E₂-EP4 receptor signaling that drives tumor growth, angiogenesis, and metastasis, *J. Biol. Chem.* 290 (2015) 29781–29793.
- [24] H. Kawano, T. Sato, T. Yamada, T. Matsumoto, K. Sekine, T. Watanabe, T. Nakamura, T. Fukuda, K. Yoshimura, T. Yoshizawa, K. Aihara, Y. Yamamoto, Y. Nakamichi, D. Metzger, P. Chambon, K. Nakamura, H. Kawaguchi, S. Kato, Suppressive function of androgen receptor in bone resorption, *Proc. Natl. Acad. Sci. U. S. A.* 100 (2003) 9416–9421.
- [25] T. Nakamura, Y. Imai, T. Matsumoto, S. Sato, K. Takeuchi, K. Igarashi, Y. Harada, Y. Azuma, A. Krust, Y. Yamamoto, H. Nishina, S. Takeda, H. Takayanagi, D. Metzger, J. Kanno, K. Takaoka, T.J. Martin, P. Chambon, S. Kato, Estrogen prevents bone loss via estrogen receptor α and induction of Fas ligand in osteoclasts, *Cell* 130 (2007) 811–823.
- [26] A. Nedergaard, K. Henriksen, M.A. Karsdal, C. Christiansen, Musculoskeletal ageing and primary prevention, *Best. Pract. Res. Clin. Obstet. Gynaecol.* 27 (2013) 673–688.
- [27] J. Crawford, C.M. Prado, M.A. Johnston, R.J. Gralla, R.P. Taylor, M.L. Hancock, J.T. Dalton, Study design and rationale for the phase 3 clinical development program of enobosarm, a selective androgen receptor modulator, for the prevention and treatment of muscle wasting in cancer patients (POWER Trials), *Curr. Oncol. Rep.* (2016) 18–37.



Symmetric 4,4'-(piperidin-4-ylidenemethylene)bisphenol derivatives as novel tunable estrogen receptor (ER) modulators



Manabu Sato, Kiminori Ohta*, Asako Kaise, Sayaka Aoto, Yasuyuki Endo

Faculty of Pharmaceutical Sciences, Tohoku Pharmaceutical University, 4-4-1 Komatsushima, Aoba-ku, Sendai 981-8558, Japan

ARTICLE INFO

Article history:

Received 16 December 2015

Revised 14 January 2016

Accepted 18 January 2016

Available online 18 January 2016

Keywords:

Estrogen receptor modulator

Piperidine

2,2,6,6-Tetramethylpiperidine

McMurry coupling

Hydrophobicity

ABSTRACT

We designed and synthesized 4,4'-(piperidin-4-ylidenemethylene)bisphenol derivatives as novel tunable estrogen receptor (ER) modulators. The introduction of hydrophobic substituents on the nitrogen atom of the piperidine ring enhanced ER α binding affinity. In addition, the introduction of four methyl groups adjacent to the piperidine ring nitrogen atom remarkably enhanced ER α binding affinity. *N*-Acetyl-2,2,6,6-tetramethylpiperidine derivative **3b** showed high ER α binding affinity, high MCF-7 cell proliferation inducing activity, and high metabolic stability in rat liver S9 fractions.

© 2016 Elsevier Ltd. All rights reserved.

1. Introduction

Tamoxifen (Fig. 1) has been used worldwide for more than 40 years for the treatment of breast cancer.¹ It exhibits competitive antagonism against endogenous estrogen 17 β -estradiol (E2, Fig. 1) on the estrogen receptor (ER). Tamoxifen produces a powerful effect against ER-positive but not ER-negative breast cancer.¹ In addition, since E2 is an endogenous estrogen that plays important roles in the female and male reproductive systems as well as in bone maintenance, the central nervous system, and the cardiovascular system, tamoxifen also exerts some biological actions in those tissues.² Interestingly, tamoxifen acts as either an agonist or an antagonist depending on tissue type; it exhibits anti-estrogenic action in breast cancer and hot flashes, and estrogenic action in bone and cholesterol metabolism, and is a selective estrogen receptor modulator (SERM).³

Following the success of tamoxifen, several triphenylethylene derivatives, such as toremifene⁴ and clomifene⁵, were developed as novel SERMs (Fig. 1). An alkylamino chain is attached to the terminal of benzene ring where it plays a strategic role in the expression of antagonistic activity.⁶ The three SERMs show quite varied biological activities because of the different hydrophobic side chains attached to the ethylene moiety.⁷ The hydrophobic side chain plays an important role in controlling SERM activity. The triphenylethylene structure has geometric isomers *E* and *Z*, which

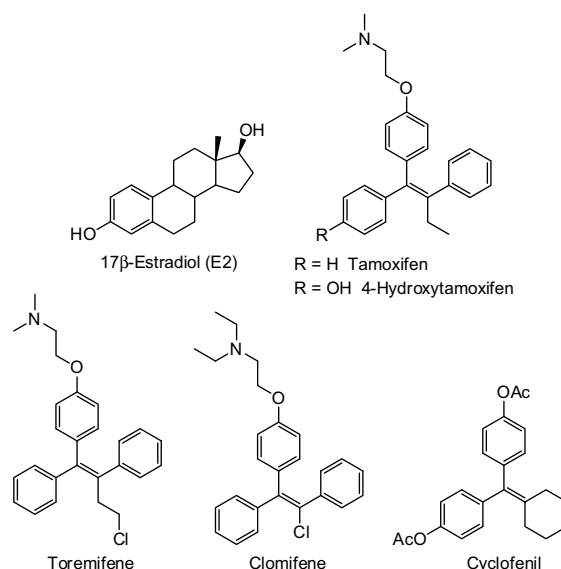


Figure 1. Chemical structures of 17 β -estradiol (E2) and clinically used SERMs.

are due to the key alkylamino chain and the asymmetric hydrophobic part. As the isomers easily isomerize between the *E* and *Z* forms, problems arise in the synthesis, purification, and preservation of the SERMs.⁸ Indeed, 4-hydroxytamoxifen, an active

* Corresponding author.

E-mail address: k-ohta@tohoku-pharm.ac.jp (K. Ohta).

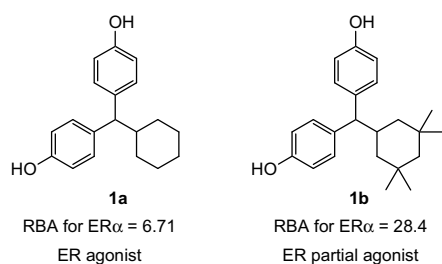


Figure 2. Chemical structures of cyclofenil derivatives **1a** and **1b**.

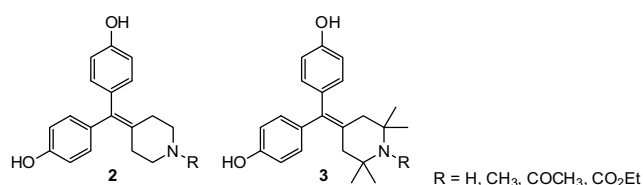


Figure 3. Novel ER modulator candidates **2** and **3** having a tunable piperidine ring.

metabolite of tamoxifen, easily isomerizes from the active *Z* form to the inactive *E* form in solution and in vitro studies (Fig. 1).⁹ In this regard, novel SERMs having other skeletons, such as benzothiophene,¹⁰ dihydronaphthalene,¹¹ benzopyrane,¹² and steroid,¹³ have been developed and used as antagonistic SERMs.

On the other hand, cyclofenil shows weak estrogenic activity because of the absence of the alkylamino chain, and thus it has been developed as an agonistic SERM (Fig. 1).¹⁴ Cyclofenil has a C-2 symmetric structure and no *E* and *Z* isomer. Recently, we have reported an SAR study of the cyclohexane ring of cyclofenil reductant **1a**, in which the diphenylmethane skeleton and the cyclohexane ring are linked by a single bond (Fig. 2).¹⁵ Transforma-

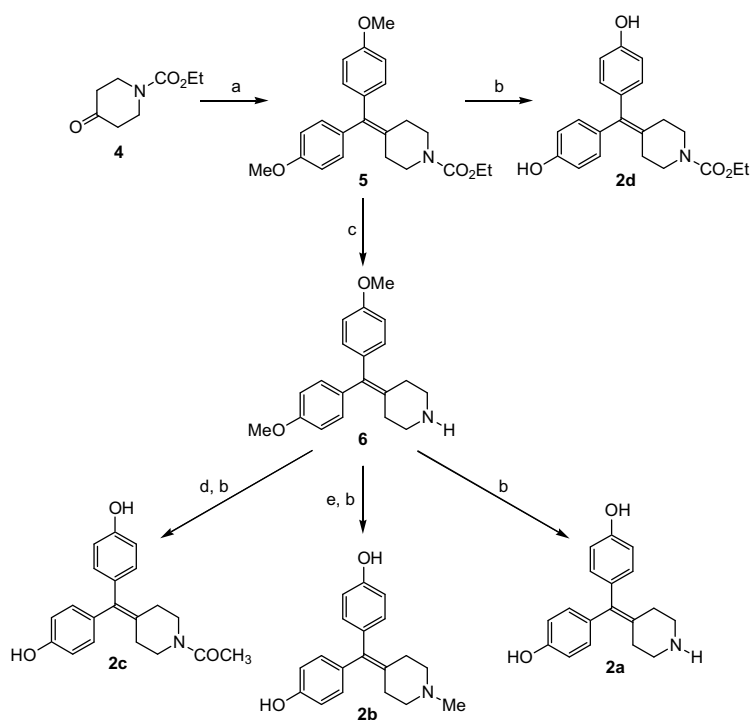
tion of the cyclohexane ring of **1a** into the 3,3,5,5-tetramethylcyclohexane ring enhanced ER α binding affinity because of the favorable hydrophobic interaction with the ER α ligand binding domain (LBD). 3,3,5,5-Tetramethylcyclohexane derivative **1b** acts as an ER partial agonist, whereas compound **1a** is an ER agonist.

The cyclohexyl moiety in **1a** and **1b** plays an important role in the hydrophobic interactions with the hydrophobic amino acid residues of ER α LBD, but is not easy tunable. A multi-tunable symmetric structure would be a very attractive tool for ER ligand studies because it would enable detailed SAR studies and not require isomer separation, and its physicochemical properties would be controllable for optimum ADME. Therefore, we focused on the discovery of readily available ER modulators with multi-tunable symmetric structures and designed novel ER ligand candidates **2a–2d**, **3a**, and **3b** containing a piperidine ring (Fig. 3). In this paper, we describe the synthesis of those compounds, their biological activities, such as ER α binding affinity and ER-dependent proliferation of MCF-7 cell line, and a metabolic study in rat liver S9 fractions.

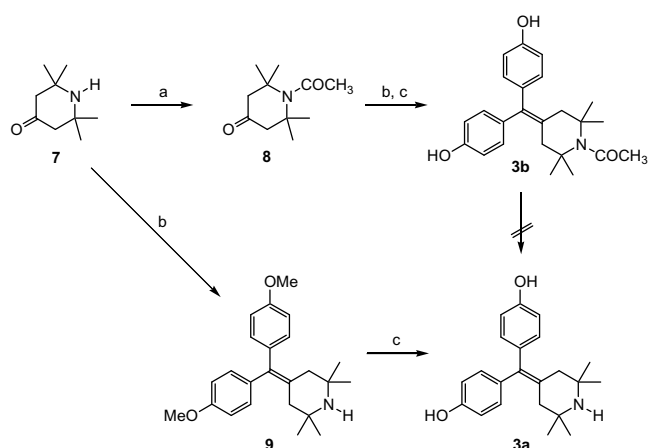
2. Results and discussion

2.1. Chemistry

A structure common to compounds **2a–2d** was synthesized from piperidinone derivatives and 4,4'-dimethoxybenzophenone by means of the McMurry coupling.¹⁶ Scheme 1 summarizes the synthesis of *N*-substituted piperidine derivatives **2a–2d**. Commercially available *N*-ethoxycarbonyl piperidin-4-one **4** was reacted with 4,4'-dimethoxybenzophenone to afford **5** in 90% yield, which was then demethylated with BBr₃ to afford **2d** in 78% yield. McMurry coupling product **5** was hydrolyzed with KOH and then subjected to spontaneous decarboxylation to afford key intermediate **6** in 90% yield. Compound **6** was transformed into **2a** with BBr₃ in 54% yield. *N*-Methylated derivative **2b** was obtained by reductive amination using paraformaldehyde and NaBH₄ in trifluoroethanol,



Scheme 1. Synthesis of the designated derivatives **2a–2d**. Reagents and conditions: (a) TiCl₄, Zn, 4,4'-dimethoxybenzophenone, THF, 90%; (b) BBr₃, CH₂Cl₂, 23–90%; (c) KOH, EtOH, 90%; (d) Ac₂O, 93%; (e) (CHO)_n, NaBH₄, CF₃CH₂OH, 87%.



Scheme 2. Synthesis of 2,2,6,6-tetramethylpiperidine derivatives **3a** and **3b**. Reagents and conditions: (a) Ac_2O , 88%; (b) TiCl_4 , Zn, 4,4'-dimethoxybenzophenone, THF, 48–75%; (c) BBr_3 , CH_2Cl_2 , 75–82%.

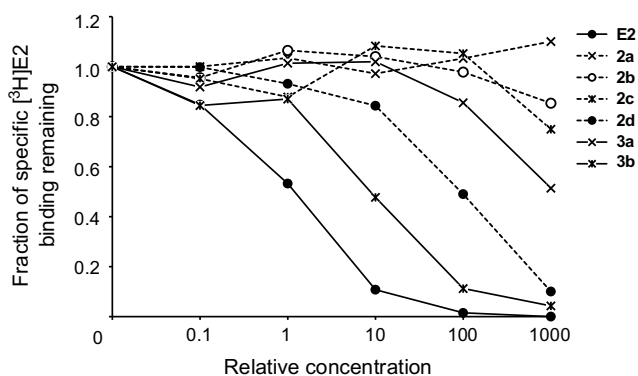


Figure 4. Binding affinities of test compounds **2a–2d**, **3a**, and **3b**. Competitive binding assay of compounds **2a–2d**, **3a**, and **3b** with $[^3\text{H}]\text{E}_2$ (4 nM) for $\text{ER}\alpha$. Binding assays of the test compounds (0.4–4 μM) were conducted in the presence of $[6,7\text{-}^3\text{H}]\text{17}\beta\text{-estradiol}$ (4 nM). The assays were performed in duplicate ($n = 2$).

followed by deprotection with BBr_3 in 20% yield over two steps. *N*-Acetylated derivative **2c** was synthesized by acetylation and subsequent demethylation in 84% yield over two steps.

The McMurry coupling of 4,4'-dimethoxybenzophenone with *N*-acetyl tetramethylpiperidinone **8**, which was obtained through the acetylation of commercially available 2,2,6,6-tetramethylpiperidin-4-one **7** followed by deprotection with BBr_3 , afforded **3b** in 38% yield over three steps (Scheme 2). To prepare **3a**, we tried to remove the *N*-acetyl group from **3b**. However, deacetylation did not proceed under both acidic and basic conditions due to the steric hindrance of the four methyl groups adjacent to the nitrogen atom of the piperidine ring. Therefore, direct McMurry coupling of 2,2,6,6-tetramethylpiperidine with 4,4'-dimethoxyphenylbenzophenone was carried out to afford corresponding coupling product **9** in 75% yield. Compound **9** was transformed into **3a** by demethylation with BBr_3 in 82% yield.

2.2. Biological evaluations

The $\text{ER}\alpha$ -binding affinity of the synthesized compounds was evaluated in a competitive binding assay using tritium-labeled E_2 and recombinant $\text{hER}\alpha$ (Fig. 4).¹⁷ Unsubstituted piperidine derivative **2a** showed no binding affinity for $\text{ER}\alpha$ LBD, whereas *N*-methyl and *N*-acetyl derivatives **2b** and **2c** bound very weakly to $\text{ER}\alpha$ LBD. Aliphatic amines **2a** and **2b** would be present in the protonated

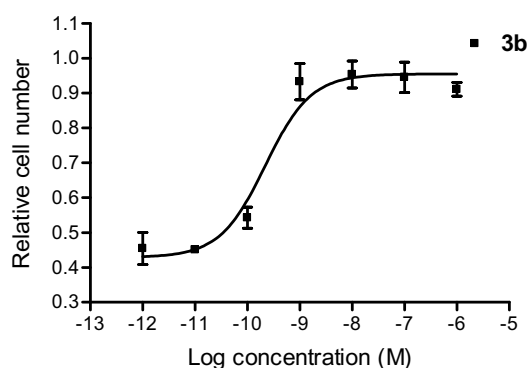


Figure 5. Dose-response curve of **3b** in the MCF-7 cell proliferation assay. MCF-7 cells were incubated with **3b** (1×10^{-6} to 1×10^{-12} M) for 5 days, and the results are shown by relative cell number with the value for E_2 taken as 1. Cell proliferation assay was performed in triplicate ($n = 3$). Values are means \pm SD of separate experiments.

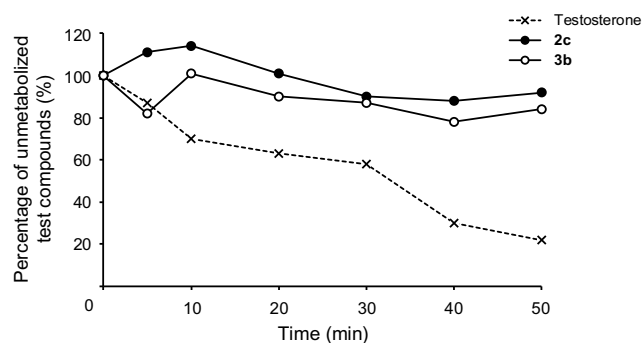


Figure 6. Percentages of **2c** and **3b** remaining in rat liver S9 fractions. The percentages were estimated from peak area ratios of corticosterone as an internal standard to the tested compounds.

form in this assay buffer. Therefore, the extremely low binding affinity of **2a** and **2b** might be caused by the polarity around the protonated nitrogen atom on the piperidine ring rather than the basicity of the nitrogen atom. *N*-Acetylated derivative **2c** also showed low binding affinity because of the high polarity (CLogP : 1.72).¹⁸ Compound **2d** having an ethyl carbamate group dose-dependently bound to $\text{ER}\alpha$ and showed higher $\text{ER}\alpha$ binding affinity than **2a–2c** owing to the increase in hydrophobicity caused by the ethyl group. Indeed, compound **2d** had the highest CLogP value at 3.90 among **2a–2d**.¹⁸ In addition, ethyl group of **2d** would be accommodated in the hydrophobic pocket of $\text{ER}\alpha$. The steric hindrance of the four methyl groups in **3a** and **3b** obscured the physicochemical properties of the nitrogen atom, such as basicity and hydrophilicity. Thus, **3a** and **3b** would show higher binding affinity than corresponding normal piperidine derivatives **2a** and **2c**, if the sterically bulky tetramethyl moiety were tolerated in the hydrophobic space of $\text{ER}\alpha$ LBD. Although the binding affinity of **3a** was low, it seemed that the four methyl groups improved incompatibility between the piperidine ring and $\text{ER}\alpha$ LBD. Interestingly, compound **3b** showed more than 100 times higher binding affinity than corresponding piperidine derivative **2c**. The four methyl groups exerted a strong positive effect on the binding of the piperidine derivatives to $\text{ER}\alpha$ LBD.

Next, cell functional assays of **3b** were performed using the MCF-7 cell line that showed $\text{ER}\alpha$ -dependent growth.¹⁷ Compound **3b** demonstrated high cell proliferation inducing activity in a dose dependent manner (Fig. 5), but no inhibition of cell proliferation activity inducing by 0.1 nM of E_2 (data not shown). The EC_{50} value

of **3b** estimated from the sigmoidal dose response curve was 0.22 nM. The maximal efficacy for MCF-7 cell proliferation inducing activity of **3b** was similar to that of E2. Interestingly, **3b** acted as ER full agonist, unlike the lead compound **1b**. We suggested that ER full agonist activity of **3b** would be caused by the nitrogen atom or the spatial configuration of 2,2,6,6-tetramethylpiperidine ring.

To examine the effect of the four methyl groups on metabolic stability, we measured the elimination rates of piperidine derivatives **2c** and **3b** in rat liver S9 fractions (Fig. 6).¹⁹ The percentage (%) of unmetabolized test compounds was estimated from the peak areas of **2c** and **3b** in HPLC analyses. Approximately 80% of testosterone used as a positive control was metabolized at 50 min under the assay conditions. Compounds **2c** and **3b** showed low metabolic rates; approximately 10% and 20% were metabolized at 50 min, respectively. Compound **3b** was more rapidly metabolized than **2c** and the tetramethyl moiety had no effect on the metabolic stability of these compounds. It seems that the piperidine rings of **2c** and **3b** are quite stable under the assay conditions.

3. Conclusion

In conclusion, we designed and synthesized novel tunable ER modulators having the 4,4'-(piperidin-4-ylidenemethylene) bisphenol structure. In contrast to the unsubstituted piperidine ring that was unfavorable for ER α LBD, the introduction of hydrophobic substituents on the nitrogen atom or the four methyl groups adjacent to the nitrogen atom improved the binding affinity of the piperidine ring for ER α LBD. Compound **3b** showed high binding affinity for ER α , high MCF-7 cell proliferation inducing activity, and good metabolic stability in rat liver S9 fractions. We are of the opinion that 2,2,6,6-tetramethylpiperidine ring is a promising core skeleton for ER modulator studies. Further investigations focusing on the chemical modification of the substituents on the nitrogen atom of the 2,2,6,6-tetramethylpiperidine ring, the introduction of alkylmino chains on the phenol group for the development of ER antagonists and SERMs, and the biological evaluation of ER subtype and tissue selectivity, are in progress.

4. Experimental section

4.1. General

Melting points were determined with a Yanaco micro melting point apparatus and were uncorrected. ¹H NMR and ¹³C NMR spectra were recorded with JEOL JNM-LA-400 spectrometers. Chemical shifts for ¹H NMR spectra were referenced to tetramethylsilane (0.0 ppm) as an internal standard. Chemical shifts for ¹³C NMR spectra were referenced to residual ¹³C present in deuterated solvents. The splitting patterns are designed as follows: s (singlet), d (doublet), t (triplet), and q (quartet). Mass spectra were recorded on a JEOL JMS-DX-303 spectrometer. Elemental analyses were performed with a Perkin Elmer 2400 CHN spectrometer. Column chromatography was carried out using Fuji Silysia silica gel BW-80S and TLC was performed on Merck silica gel F₂₅₄. Reagents were purchased from Wako Pure Chemical Industries, Ltd, Sigma-Aldrich Co., and Tokyo Chemical Industry, Ltd (TCI). All solvents were of reagent quality, purchased commercially, and were used without further purification.

4.2. Synthesis

4.2.1. Methyl 4-[(4-methoxyphenyl)(N-ethyloxy-carbonylpiperidin-4-ylidene)methyl]phenoxide (**5**)

To a stirred suspension of Zn powder (2.83 g, 43.2 mmol) in 30 mL of dry THF was added slowly titanium(IV) tetrachloride

(2.37 mL, 21.6 mmol) under an argon (Ar) atmosphere. A mixture was refluxed for 2.5 h and cooled to room temperature. To the mixture was added a solution of 4,4'-dimethoxybenzophenone (1.42 g, 5.86 mmol) and ethyl 4-oxopiperidine-1-carboxylate (1.01 g, 5.90 mmol) in 20 mL of dry THF, and it was refluxed for 12 h. The reaction mixture was poured into saturated NaHCO₃ aqueous solution. Ether was added to the aqueous solution with vigorous stirring, and insoluble materials were filtered off through Celite. The filtrate was extracted with ether, dried over MgSO₄, and concentrated. The residue was purified by column chromatography on silica gel with 40:1 *n*-hexane/AcOEt to afford the title compound **5** (2.23 g, 99%) as a yellow liquid; ¹H NMR (395 MHz, CDCl₃) δ (ppm) 7.01 (d, 2H, *J* = 7.9 Hz), 6.82 (d, 2H, *J* = 7.9 Hz), 4.14 (q, 2H, *J* = 7.9 Hz), 3.79 (s, 6H), 3.49 (t, 4H, *J* = 4.0 Hz), 2.35 (t, 4H, *J* = 4.0 Hz), 1.26 (t, 3H, *J* = 7.9 Hz); ¹³C NMR (100 MHz, CDCl₃) δ (ppm) 158.1, 155.5, 136.5, 134.8, 132.9, 130.7, 113.3, 61.2, 55.0, 44.8, 31.5, 14.6; MS (EI) *m/z* 381 (M⁺, 100%).

4.2.2. Methyl 4-[(4-methoxyphenyl)(piperidin-4-ylidene)methyl]phenoxide (**6**)

A mixture of **5** (7.54 g, 19.8 mmol) and potassium hydroxide (92.9 g, 1.66 mol) in 300 mL of ethanol was refluxed for 6 h under an Ar atmosphere. The solvent was evaporated, water (50 mL) was added to the residue, and then the aqueous mixture was extracted with AcOEt. The organic phase was dried over Na₂SO₄ and concentrated to afford the title compound **6** (5.52 g, 90%) as a yellow solid. ¹H NMR (395 MHz, CDCl₃) δ (ppm) 7.02 (d, 4H, *J* = 7.9 Hz), 6.82 (d, 4H, *J* = 7.9 Hz), 3.79 (s, 6H), 2.90 (t, 4H, *J* = 4.0 Hz), 2.33 (t, 4H, *J* = 4.0 Hz); ¹³C NMR (100 MHz, CDCl₃) δ (ppm) 157.9, 136.3, 135.2, 130.9, 129.2, 113.3, 55.1, 48.5, 33.5; MS (EI) *m/z* 309 (M⁺), 267 (100%).

4.2.3. 4-[(4-Hydroxyphenyl)(piperidin-4-ylidene)methyl]phenol (**2a**)

To a solution of **6** (2.95 g, 9.54 mmol) in 20 mL of CH₂Cl₂ was added 1 M of BBr₃ solution (17.5 mL, 17.5 mmol) at 0 °C under Ar atmosphere. The mixture was stirred for 12 h at 0 °C, the solvent was removed, water was added to the residue, and the mixture was extracted with AcOEt. The organic phase was dried over Na₂SO₄ and concentrated to afford the title compound **2a** (1.44 g, 54%) as a yellow solid; colorless cubes (MeOH); mp 205–207 °C; ¹H NMR (395 MHz, CD₃OD) δ (ppm) 6.88 (d, 4H, *J* = 7.9 Hz), 6.69 (d, 4H, *J* = 7.9 Hz), 2.83 (t, 4H, *J* = 4.0 Hz), 2.32 (t, 4H, *J* = 4.0 Hz); ¹³C NMR (100 MHz, CD₃OD) δ (ppm) 157.2, 137.6, 135.3, 134.3, 131.9, 115.8, 33.6, 32.2; MS (EI) *m/z* 281 (M⁺, 100%); Anal. Calcd for C₁₈H₁₉NO₂: C, 76.84; H, 6.81; N, 4.98. Found: C, 76.84; H, 6.81; N, 4.91.

4.2.4. 4-[(4-Hydroxyphenyl)(N-methylpiperidin-4-ylidene)methyl]phenol (**2b**)

A solution of paraformaldehyde (191 mg, 6.4 mmol) in 30 mL of trifluoroethanol was stirred at 35–40 °C. To the stirred solution was added **6** (1.18 g, 3.88 mmol), and NaBH₄ (185 mg, 4.89 mmol) was added 5 min later. After 30 min, the mixture was filtered through Celite and the filtrate was concentrated. The residue was purified by column chromatography on silica gel with AcOEt to afford *N*-methylated compound (1.09 g, 87%) as a yellow solid. ¹H NMR (395 MHz, DMSO) δ (ppm) 6.96 (d, *J* = 7.9 Hz, 4H), 6.85 (d, 4H, *J* = 7.9 Hz), 3.72 (s, 6H), 2.33 (t, 4H, *J* = 4.0 Hz), 2.25 (t, 4H, *J* = 4.0 Hz), 2.15 (s, 3H); ¹³C NMR (100 MHz, DMSO) δ (ppm) 159.8, 137.7, 136.2, 133.3, 131.8, 114.4, 58.0, 55.7, 45.9, 32.1; MS (EI) *m/z* 323 (M⁺, 100%). The *N*-methylated compound was transformed into **2b** by the same method that described the synthesis of **2a**; 23% yield; colorless needles (MeOH–CHCl₃) mp 255–257 °C; ¹H NMR (395 MHz, CD₃OD) δ (ppm) 6.99 (d, 4H, *J* = 8.0 Hz), 6.70 (d, 4H, *J* = 8.0 Hz), 2.52 (t, 4H, *J* = 8.0 Hz), 2.41

(t, 4H, $J = 4.0$ Hz), 2.32 (s, 3H); ^{13}C NMR (100 MHz, CD_3OD) δ (ppm) 157.1, 138.0, 135.3, 132.9, 131.9, 115.7, 58.1, 46.1, 32.2; MS (EI) m/z 295 (M^+ , 100%); Anal. Calcd for $\text{C}_{19}\text{H}_{21}\text{NO}_2$: C, 76.45; H, 7.17; N, 4.74; Found: C, 76.45; H, 7.15; N, 4.69.

4.2.5. 4-[(4-Hydroxyphenyl)(*N*-acetyl)piperidin-4-ylidene)methyl]phenol (2c)

A mixture of **6** (218 mg, 0.71 mmol) and 3 mL of acetic anhydride was heated at 100 °C for 6 h. After cooling to room temperature, 10% NaOH aqueous solution was added and stirred. The mixture was extracted with CH_2Cl_2 , washed with brine, dried over Na_2SO_4 , and then concentrated. The residue was purified by column chromatography on silica gel with 2:1 *n*-hexane/AcOEt to afford *N*-acetylated compound (230 mg, 93%) as a yellow solid. ^1H NMR (395 MHz, CD_3OD) δ (ppm) 7.02 (d, $J = 7.9$ Hz, 4H), 6.85 (d, 4H, $J = 7.9$ Hz), 3.77 (s, 6H), 3.60 (t, 2H, $J = 4.0$ Hz), 3.55 (t, 2H, $J = 4.0$ Hz), 2.43 (t, 2H, $J = 4.0$ Hz), 2.35 (t, 2H, $J = 4.0$ Hz), 2.11 (s, 3H); ^{13}C NMR (100 MHz, CDCl_3) δ (ppm) 168.7, 158.0, 136.7, 134.5, 132.0, 130.5, 113.2, 54.9, 47.3, 42.7, 31.8; MS (EI) m/z 351 (M^+ , 100%). The *N*-acetylated compound was transformed into **2c** by the same method that described the synthesis of **2a**; 22% yield; colorless leaflets (MeOH– CHCl_3) mp 255–257 °C; ^1H NMR (395 MHz, CD_3OD) δ (ppm) 6.99 (d, 4H, $J = 8.0$ Hz), 6.70 (d, 4H, $J = 8.0$ Hz), 2.52 (t, 4H, $J = 8.0$ Hz), 2.41 (t, 4H, $J = 4.0$ Hz), 2.32 (s, 3H); ^{13}C NMR (100 MHz, CD_3OD) δ (ppm) 157.1, 138.0, 135.3, 132.9, 131.9, 115.7, 58.1, 46.1, 32.2; MS (EI) m/z 295 (M^+ , 100%). Anal. Calcd for $\text{C}_{20}\text{H}_{21}\text{NO}_3$: C, 74.28; H, 6.55; N, 4.33; Found: C, 74.28; H, 6.58; N, 4.25.

4.2.6. 4-[(4-Hydroxyphenyl)(*N*-ethyloxycarbonyl-piperidin-4-ylidene)methyl]phenol (2d)

Compound **2d** was prepared by the same method that described the synthesis of **2a**; 90% yield; a yellow prisms (CH_2Cl_2) mp 105 °C; ^1H NMR (395 MHz, CDCl_3) δ (ppm) 6.96 (d, 4H, $J = 7.9$ Hz), 6.75 (d, 4H, $J = 7.9$ Hz), 4.14 (q, 2H, $J = 4.0$ Hz), 3.48 (t, 4H, $J = 4.0$ Hz), 2.34 (t, 4H, $J = 4.0$ Hz), 1.26 (t, 3H, $J = 7.9$ Hz); ^{13}C NMR (100 MHz, CD_3OD) δ (ppm) 157.3, 157.2, 139.0, 135.2, 133.0, 131.9, 115.8, 62.7, 46.4, 32.6, 15.0; MS (EI) m/z 353 (M^+ , 100%). Anal. Calcd for $\text{C}_{21}\text{H}_{23}\text{NO}_4$: C, 71.37; H, 6.56; N, 3.96; Found: C, 71.11; H, 6.59; N, 3.93.

4.2.7. *N*-Acetyl-2,2,6,6-tetramethyl-4-piperidone (8)

A mixture of 2,2,6,6-tetramethyl-4-piperidone (4.91 g, 31.6 mmol) and 20 mL of acetic anhydride was heated at 100 °C for 7 h. Solvent was removed, 10% NaOH aqueous solution was added, and the mixture was stirred. The mixture was extracted with CH_2Cl_2 , washed with brine, dried over Na_2SO_4 , and then concentrated. The residue was purified by column chromatography on silica gel with 3:1 *n*-hexane/AcOEt to afford the title compound **8** (5.49 g, 88%) as a colorless liquid. ^1H NMR (395 MHz, CDCl_3) δ (ppm) 2.59 (s, 4H), 2.23 (s, 3H), 1.54 (s, 12H); MS (EI) m/z 197 (M^+), 140 (100%).

4.2.8. Methyl 4-[(4-methoxyphenyl)(2,2,6,6-tetramethylpiperidin-4-ylidene)methyl]phenoxide (9)

Compound **9** was prepared by the same method that described the synthesis of **5**; 75% yield; ^1H NMR (395 MHz, CD_3OD) δ (ppm) 7.07 (d, 4H, $J = 8.0$ Hz), 6.82 (d, 4H, $J = 8.0$ Hz), 3.78 (s, 6H), 2.14 (s, 4H), 1.18 (s, 12H); ^{13}C NMR (CD_3OD) δ (ppm) 157.8, 137.3, 135.4, 132.4, 130.2, 113.4, 55.1, 52.8, 43.7, 31.2; MS (EI) m/z 365 (M^+), 98 (100%).

4.2.9. 4-[(4-Hydroxyphenyl)(2,2,6,6-tetramethylpiperidin-4-ylidene)methyl]phenol (3a)

Compound **3a** was prepared by the same method that described the synthesis of **2a**; 82% yield; colorless cubes (MeOH– CHCl_3) mp

110–112 °C; ^1H NMR (395 MHz, CD_3OD) δ (ppm) 6.96 (d, 4H, $J = 8.0$ Hz), 6.70 (d, 4H, $J = 8.0$ Hz), 2.18 (s, 4H), 1.18 (s, 12H); ^{13}C NMR (100 MHz, CD_3OD) δ (ppm) 182.2, 176.4, 157.2, 140.4, 134.7, 131.9, 115.7, 58.4, 46.1, 30.3, 28.4; MS (EI) m/z 379 (M^+), 224 (100%). Anal. Calcd for $\text{C}_{22}\text{H}_{27}\text{NO}_2$ 0.1 H_2O : C, 77.88; H, 8.08; N, 4.13. Found: C, 77.92; H, 8.19; N, 4.10.

4.2.10. 4-[(4-Hydroxyphenyl)(2,2,6,6-tetramethyl-*N*-acetyl)piperidin-4-ylidene)methyl]phenol (3b)

The product obtained from McMurry coupling reaction of compound **9** with 4,4'-dimethoxybenzophenone was transformed into **3b** by the same method that described the synthesis of **2a**; 43% yield over two steps; colorless cubes (Et_2O) mp 138–140 °C; ^1H NMR (395 MHz, CD_3OD) δ (ppm) 6.93 (d, 4H, $J = 7.9$ Hz), 6.72 (d, 4H, $J = 7.9$ Hz), 2.64 (s, 4H), 2.17 (s, 3H), 1.45 (s, 12H); ^{13}C NMR (100 MHz, CD_3OD) δ (ppm) 182.2, 176.4, 157.2, 140.4, 134.7, 131.9, 115.7, 58.4, 46.1, 30.3, 28.4; MS (EI) m/z 379 (M^+), 224 (100%). Anal. Calcd for $\text{C}_{24}\text{H}_{29}\text{NO}_3$: C, 75.96; H, 7.70; N, 3.69. Found: C, 75.91; H, 7.83; N, 3.73.

4.3. ER α binding assay

The ligand binding affinity of ER α was determined by the previously reported method.¹⁷ Briefly, ER α was diluted with an assay buffer, which contains 20 mM Tris–HCl, 0.3 M NaCl, 10 mM 2-mercaptoethanol, 0.2 mM phenylmethylsulfonyl fluoride, 1 mM EDTA, and incubated with 4 nM [6,7- ^3H]17 β -estradiol in the presence or absence of an unlabeled competitor at 4 °C for 16 h. The incubation mixture was absorbed by suction onto a nitrocellulose membrane that had been soaked in assay buffer. The membrane was washed twice with buffer, and then with 25% EtOH in distilled water. Radioactivity that remained on the membrane was measured in Atomlight using a liquid scintillation counter.

4.4. MCF-7 cell proliferation assay

The human breast adenocarcinoma cell line, MCF-7 was routinely cultivated in DMEM supplemented with 10% FBS, 100 IU/mL penicillin and 100 mg/mL streptomycin at 37 °C in a 5% CO_2 humidified incubator. Before an assay, MCF-7 cells were switched to DMEM (low glucose phenol red-free supplemented with 5% FBS, 100 IU/mL penicillin and 100 mg/mL streptomycin). Cells were trypsinized from the maintenance dish with phenol red-free trypsin–EDTA and seeded in a 96-well plate at a density of 2000 cells per final volume of 100 μL DMEM supplemented with 5% FBS, 100 IU/mL penicillin and 100 mg/mL streptomycin. After 24 h, the medium was exchanged into 90 μL of fresh DMEM and 10 μL of the drug solution, supplemented with serial dilutions of **3b** or DMSO as dilute control in the presence or absence of 1 nM E2, was added to triplicate microcultures. Cells were incubated for 5 days, and medium with **3b** or DMSO as dilute control in the presence or absence of 1 nM E2 was exchanged once after 3 days. At the end of the incubation time, proliferation was evaluated by using the WST-8. 10 nM of WST-8 was added to microcultures and cells were incubated for 4 h. The absorbance at 450 nm was measured. This parameter relates to the number of living cells in the culture.

4.5. Metabolism study of compounds **2c** and **3b** in rat liver S9 fractions

For the evaluation of metabolic stability, 40 μL of compound was incubated with 1 mg/mL pooled rat liver S9 fractions in 0.1 M potassium phosphate buffer (pH 7.4) containing 3.3 mM MgCl_2 , 1.3 mM NADP^+ , 3.3 mM glucose-6-phosphate, and 0.4 U/mL glucose-6-phosphatedehydrogenase at 37 °C for 0, 5, 10,

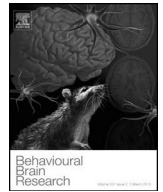
20, 30, 40, and 50 min. The incubation was stopped by the precipitation of S9 enzymes with the same volume of cold acetonitrile containing corticosterone as the internal standard. The percentage of unmetabolized test compound at the different time points was estimated from the peak area in HPLC spectrum.

Acknowledgments

This research was supported by a Grant-in-Aid of Strategic Research Program for Private Universities (2010–2014), a Grant-in-Aid for Young Scientists (B) (No. 21790116), and a Grant-in-Aid for Scientific Research (C) (No. 26460151) from the Ministry of Education, Culture, Sports, Science, and Technology, Japan.

References and notes

- (a) Powles, T.; Hickish, T.; Kanis, J. A.; Tidy, A.; Ashley, S. *J. Clin. Oncol.* **1996**, *14*, 78; (b) O'Regan, R. M.; Jordan, V. C. *Semin. Oncol.* **2001**, *28*, 260; (c) Maximov, P. Y.; Lee, T. M.; Jordan, V. C. *Curr. Clin. Pharmacol.* **2013**, *8*, 135.
- (a) Katzenellenbogen, B. S.; Choi, I.; Delage-Mourroux, R.; Ediger, T. R.; Martini, P. G. V.; Montano, M.; Sun, J.; Weis, K.; Katzenellenbogen, J. A. *J. Steroid Biochem. Mol. Biol.* **2000**, *74*, 279; (b) Lanyon, L.; Armstrong, V.; Ong, D.; Zaman, G.; Price, J. J. *Endocrinol.* **2004**, *182*, 183; (c) Pfaff, D.; Waters, E.; Khan, Q.; Zhang, X.; Numan, M. *Endocrinology* **2011**, *152*, 1209.
- (a) Fernand, L.; Claude, L.; Alain, B.; Jacques, S. In *Selective Estrogen Receptor Modulators*; Andrea, M., Michael, V., Eds.; Humana Press, 2002; (b) Komm, B. S.; Mirkin, S. *J. Steroid Biochem. Mol. Biol.* **2014**, *143*, 207.
- (a) Vogel, C. L.; Johnston, M. A.; Capers, C.; Braccia, D. *Clin. Breast Cancer* **2014**, *14*, 1; (b) Robertson, J. F. R. *Cancer Treat. Rev.* **2004**, *30*, 695.
- Bramlett, K. S.; Burris, T. P. *J. Steroid Biochem. Mol. Biol.* **2003**, *86*, 27.
- Selective Estrogen Receptor Modulator (SERMs)*; Marietta, A., Barbara, K. D., Sherry, S., Eds.; Academy of Sciences: New York, NY, 2001.
- Styles, J. A.; Davies, A.; Davies, R.; White, I. N.; Smith, L. L. *Carcinogenesis* **1997**, *18*, 303.
- (a) McCague, R.; Jarman, M.; Leung, O. T.; Foster, A. B.; Leclercq, G.; Stoessel, S. *J. Steroid Biochem.* **1988**, *31*, 545; (b) Katzenellenbogen, B. S.; Norman, M. J.; Eckert, R. L.; Peltz, S. W.; Mangel, W. F. *Cancer Res.* **1984**, *44*, 112.
- (a) Gauthier, S.; Mailhot, J.; Labrie, F. *J. Org. Chem.* **1996**, *61*, 3890; (b) Yu, D. D.; Forman, B. M. *J. Org. Chem.* **2003**, *68*, 9489.
- Mitlak, B. H.; Cohen, F. J. *Drugs* **1999**, *57*, 653.
- Swan, V. J. D.; Hamilton, C. J.; Jamal, S. A. *Adv. Ther.* **2010**, *27*, 917.
- Gara, R. K.; Sundram, V.; Chauhan, S. C.; Jaggi, M. *Curr. Med. Chem.* **2013**, *20*, 4177.
- Robertson, J. F. R.; Lindemann, J.; Garnett, S.; Anderson, E.; Nicholson, R. I.; Kuter, I.; Gee, J. M. W. *Clin. Breast Cancer* **2014**, *14*, 381.
- Garg, S.; Bindal, R. D.; Durani, S.; Kapil, R. S. *J. Steroid Biochem.* **1983**, *18*, 89.
- Kojima, T.; Ogawa, T.; Kitao, S.; Sato, M.; Oda, A.; Ohta, K.; Endo, Y. *Bioorg. Med. Chem.* **2015**, *23*, 6900.
- Cid, M. M.; Seijas, J. A.; Villaverde, M. C.; Castedo, L. *Tetrahedron* **1988**, *44*, 6197.
- Ohta, K.; Chiba, Y.; Ogawa, T.; Endo, Y. *Bioorg. Med. Chem. Lett.* **2008**, *18*, 5050.
- The ClogP values of the tested compounds were calculated with ChemDraw Ultra 12.0. CLogP: **2a** (2.67), **2b** (3.12), **2c** (1.72), **2d** (3.90), **3a** (4.75), **3b** (3.79).
- Moore, T. W.; Zhu, S.; Randolph, R.; Shoji, M.; Snyder, J. P. *ACS Med. Chem. Lett.* **2014**, *5*, 288.



Research report

BE360, a new selective estrogen receptor modulator, produces antidepressant and antidementia effects through the enhancement of hippocampal cell proliferation in olfactory bulbectomized mice



Osamu Nakagawasai^{a,*}, Wataru Nemoto^a, Hiroshi Onogi^b, Takahiro Moriya^c, Jia-Rong Lin^a, Takayo Odaira^a, Fukie Yaoita^a, Takumi Ogawa^d, Kiminori Ohta^d, Yasuyuki Endo^d, Koichi Tan-No^a

^a Department of Pharmacology, Tohoku Pharmaceutical University, 4-4-1 Komatsushima, Aoba-ku, Sendai 981-8558, Japan

^b Faculty of Health Science, Tohoku Fukushi University, 1-8-1 Kunimi, Aoba-ku, Sendai 981-8522, Japan

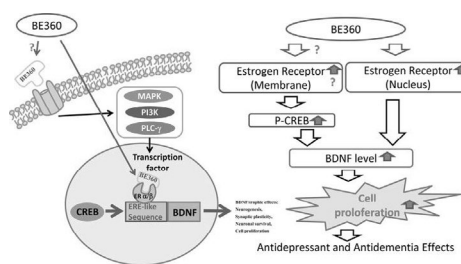
^c Department of Cellular Signaling, Graduate School of Pharmaceutical Sciences, Tohoku University, Aoba 6-3, Aramaki, Aoba-ku, Sendai 980-8578, Japan

^d Faculty of Pharmaceutical Sciences, Tohoku Pharmaceutical University, 4-4-1 Komatsushima, Aoba-ku, Sendai 981-8558, Japan

HIGHLIGHTS

- BE360 showed beneficial effects over depressive-like behavior and cognitive deficit in OBX mice.
- BE360 enhanced hippocampal cell proliferation in OBX mice.
- BE360 increased expression of pCREB and BDNF in hippocampus.
- BE360 has antidepressant and antidementia effect by hippocampal neurogenesis via CREB/BDNF signaling pathways.

GRAPHICAL ABSTRACT



ARTICLE INFO

Article history:

Received 2 May 2015

Received in revised form 2 September 2015

Accepted 15 October 2015

Available online 20 October 2015

Keywords:

Depression

Memory

Carborane compound

Olfactory bulbectomy

Cell proliferation

Selective estrogen receptor modulator

ABSTRACT

We have reported that the carborane compound BE360 is a novel selective estrogen receptor modulator and new therapy option for osteoporosis. The aim of this study was to explore the effects and underlying mechanisms of BE360 on depressive-like behavior and memory impairment in the olfactory bulbectomized (OBX) mice, an experimental animal model of depression and dementia. BE360 was administered subcutaneously to mice using a mini-osmotic pump for 2 weeks. Depressive-like behavior was measured as the reduced intake of a sweet solution in the sucrose preference test. Short-term memory was assessed using the Y-maze test. Cell proliferation was assessed by the analysis of cells expressing 5-bromo-2'-deoxyuridine (BrdU) uptake. The expression of phosphorylated cyclic-AMP response element binding protein (pCREB) and brain-derived neurotrophic factor (BDNF) were measured by immunoblot. The depressive-like behavior and memory impairment in OBX mice were improved by the chronic treatment with BE360. Immunohistochemical analysis showed that the number of BrdU-positive cells in the dentate gyrus of the hippocampus significantly decreased in OBX mice whereas they increased after the chronic treatment with BE360. Immunoblotting studies revealed that pCREB and BDNF were significantly increased in the hippocampus of OBX mice treated with BE360. The present study has shown that BE360 has antidepressant and antidementia effects characterized by hippocampal cell proliferation potentially activated via CREB/BDNF signaling pathways. These results indicate that BE360 may have valuable therapeutic potential against depression and neurodegenerative diseases.

© 2015 Elsevier B.V. All rights reserved.

* Corresponding author. Fax: +81227270123.

E-mail address: osamun@tohoku-pharm.ac.jp (O. Nakagawasai).

1. Introduction

Estrogens play important roles in numerous health issues including cardiovascular disease, osteoporosis, depression, cognition, and sexual function [1,2]. For example, several of these system dysfunctions including osteoporosis, depression and cognitive deficits frequently arise during the postmenopausal period. Recently, Hirata et al. have reported that the carborane compound 1,2-bis(4-hydroxyphenyl)-o-carborane, BE360, showed high binding affinity to the estrogen receptors (ER), ER α and ER β , and recovered bone loss in ovariectomized (OVX) and orchidectomized (ORX) mice, while not affecting the sex organs [3]. We have thus suggested that this novel selective estrogen receptor modulator (SERM) BE360 could represent a new therapy option for osteoporosis.

Accumulating data confirms the existence of olfactory dysfunctions in brain diseases, including Alzheimer's Disease (AD) and depression, much of which appear at early stages [4]. In rodents, olfactory bulbectomy (OBX) leads to numerous behavioral deficits, including cognitive deficits and anhedonia that are used to model major depression, but may also represent a valuable tool in the study of neurodegenerative disorders like AD [5–7]. Indeed, OBX has been reported to decrease hippocampal neurogenesis, a putative pathogenic mechanism in AD and depression [8,9].

Some SERMs such as tamoxifen and raloxifene are neuroprotective in a variety of experimental models of neurodegeneration, reduce anxiety and depression, promote cognition and modulate synaptic plasticity in the hippocampus of rodents [10–12]. Estradiol modulate hippocampus-related behaviors and cognition by enhancing neurogenesis in the dentate gyrus (DG) of adult animals [13]. In this region, as in the subventricular zone, neurogenesis continues into adulthood. Estrogens increase the release of brain-derived neurotrophic factor (BDNF) from the DG. BDNF is a potent modulator of neuronal functions in the hippocampus, including neurotransmission, memory formation and neurogenesis [14]. It was shown that estrogen-mediated neurogenesis following global ischemia requires the activation of the cyclic-AMP response element binding protein (CREB) pathway [15–17]. The CREB is an upstream transcription factor for BDNF expression. Thus, the effects of estrogens in hippocampal neurogenesis involve the CREB-BDNF signaling cascade.

In the present study, we examined the effects of a novel carborane compound, BE360, on depressive-like behavior and cognitive impairment in experimental animal model of dementia and depression, the OBX female mice [5]. In a final set of experiments to identify possible mechanisms involved in the increase in cell proliferation, we assessed the effect of BE360 on the expression of the neurotrophic factor BDNF and the transcription factor CREB.

2. Materials and methods

All experiments were performed according to the Guide for Care and Use of Laboratory Animals at Tohoku Pharmaceutical University.

2.1. Animals

Female ddY mice, 8 weeks of age, were obtained from Japan SLC (Hamamatsu, Japan) and acclimated for 2 weeks. The mice were maintained under conditions of constant temperature ($23 \pm 1^\circ\text{C}$) and humidity ($55 \pm 5\%$) on a 12 h/12 h light-dark cycle (light from 9 to 21 h; dark from 21 to 9 h). The mice had free access to food and water throughout the experimental period.

2.2. Estrous cycle monitoring

To determine the phase of the estrous cycle for each female, vaginal smears were taken daily for two consecutive weeks before operation and on the behavioral testing day. Samples were collected by inserting the tip of a clean glass pipette filled with $10\ \mu\text{l}$ of saline into the mouse's vagina. One drop of fluid was collected from each mouse, placed onto a glass slide, air dried, and then stained with Giemsa's solution. The cell morphology was assessed under a light microscope. The metestrus phase was defined as the presence of approximately equal proportions of nucleated epithelial cells, non-nucleated cornified epithelial cells and leukocytes. The diestrus phase was defined as a minimum amount of cells, including leukocytes and occasional epithelia. The proestrus phase was defined by the presence of more than 75% nucleated epithelial cells. The estrus phase was defined as the presence of more than 75% non-nucleated cornified epithelial cells. Only females showing four consecutive regular estrous cycles before operation were used in this study.

2.3. Olfactory bulbectomized mice

Mice, 10 weeks of age, were anesthetized with sodium pentobarbital were placed in a stereotaxic frame. The scalp was incised and two holes were drilled to expose the olfactory bulb (OB), which was then bilaterally aspirated using a suction pump. All animals were sacrificed at the end of the experiment and the lesions were verified visually. It was confirmed that at least two thirds of the OB had been removed and that some parts of the olfactory nuclei also had also been lesioned. If the lesion was either not extensive enough or extended to the cortex, data from these animals were excluded. Sham operations were performed in the same manner but without the removal of the OB. Behavioral tests (sucrose preference test and Y-maze test) were performed on the 28th day after OBX surgery.

2.4. Drugs

17 β -estradiol (E2; Sigma–Aldrich, St.-Louis, MO, USA), Tamoxifen (TAM; Sigma–Aldrich), Raloxifen hydrochloride (RAL; LKT Laboratories, Inc., St. Paul, MN, USA) and BE360 were dissolved in polyethyleneglycol-300 (Wako Pure Chemical Industries Ltd., Osaka, Japan). BE360 was synthesized in our laboratory as reported in our previous studies [18]. These compounds were administered using a mini-osmotic pump (model 2002; Alza Co., Paolo Alto, CA, USA) that was implanted subcutaneously on the back of the mouse 2 weeks after OBX surgery.

2.5. Sucrose preference test

This experiment was conducted for four days, starting 28 days post OBX surgery. The training phase lasted at least 24 h and took place before the testing phase to allow the animals to adapt to the novel solution. When starting the training phase, animals were transferred into single housing with free access to food and two bottles, one of which contained 1% sucrose solution and the second bottle contained tap water. To prevent possible effects of side preference in drinking, the position of the bottles was switched twice a day. Bottles were weighed to record the consumption of tap water and sucrose fluid every morning (9:00–11:00). A sucrose preference score was calculated using the following formula and the average of the four days was calculated. % preference = (sucrose intake/total intake) \times 100. Reduction of sucrose preference, i.e., anhedonia, is a validated index of a depression-like state in animals [19].

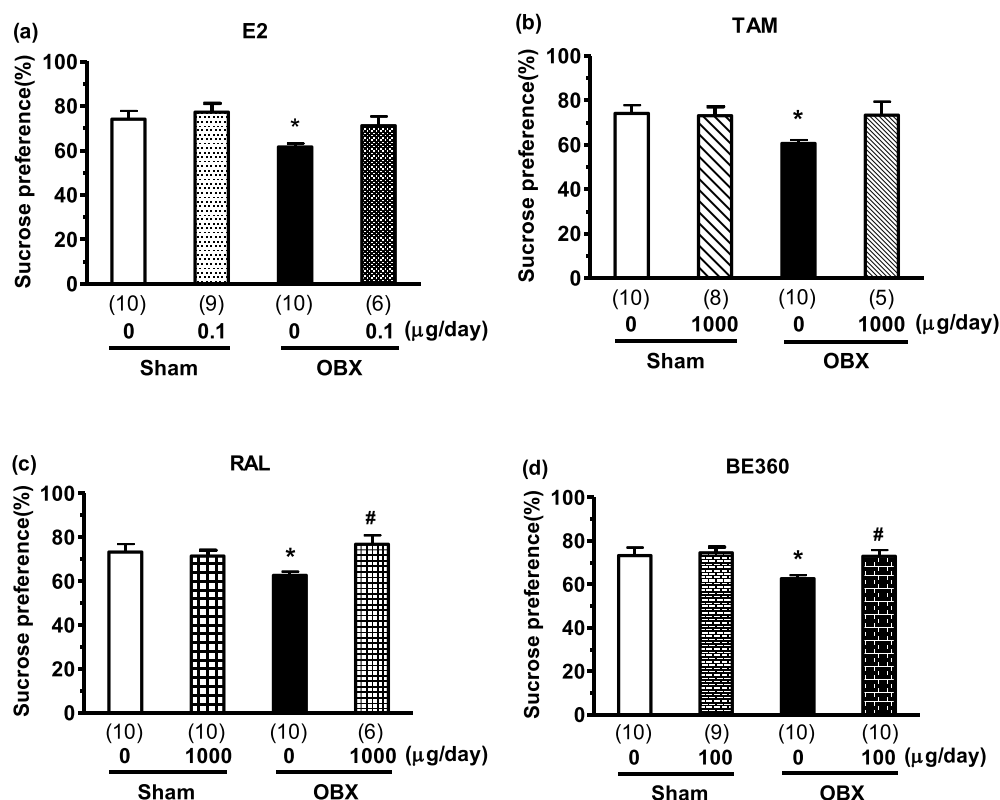


Fig. 1. Effects of estrogen receptors ligands on OBX mice in the sucrose preference test. * $p < 0.05$ vs. sham + vehicle group. # $p < 0.05$ vs. OBX + vehicle group.

2.6. Y-maze test

The Y-maze apparatus consisted of three compartments (3 cm (W) \times 40 cm (D) \times 25 cm (H)) radiating out from the center. The mice were placed in one of the compartments and allowed to move freely for 8 min. Experiments were performed at a light intensity of 35 lux. An arm entry was defined as three legs entering one of the arms, and the sequence of entries was manually recorded. An alternation was defined as entry into all three arms on consecutive choices. Thus, the maximum number of alternations was the total number of entries minus 2, and the percent alternation was calculated as (actual alternations/maximum alternations) \times 100. The percent alternation was designated as the spontaneous alternation behavior of the mouse, and was taken as a measure of short-term memory.

2.7. Immunohistochemistry

On days 27 after OBX surgery, 5-bromo-2'-deoxyuridine (BrdU) (Sigma–Aldrich; 75 mg/kg i.p.) was injected three times once every two hours for a total of three injections. Eighteen hours after the last BrdU injection, animals were deeply anesthetized with sodium pentobarbital and intracardially perfused with 15 ml of 4°C phosphate-buffered saline (PBS), followed by 45 ml of 4% paraformaldehyde (PFA; Sigma–Aldrich) in 0.1 M PBS. Brains were post-fixed in 4% PFA–0.1 M PBS for 1 h at 4°C, followed by immersion in 20% sucrose–0.1 M PBS for 48 h. The brains were cut into 40 μ m sections that included the dorsal DG from bregma -1.40 mm to -2.00 mm using a cryostat (MICROM HM560, Microm International GmbH, Walldorf, Germany). Frozen sections were mounted on glass slides (Matsunami Glass, Osaka, Japan). Sections were treated with HCl (2N) at 37°C for 30 min, followed by neutralization with sodium borate buffer (0.15 M) at room temperature, twice for 10 min each. After three 5 min washes, the sections were

incubated with PBS containing 1% normal goat serum and 0.3% Triton X-100 (PBST) at room temperature for 2 h. Then, the sections were incubated overnight at 4°C with rat anti-BrdU monoclonal antibody (1:100; Harlan SeraLab, Loughborough, UK) and mouse anti-NeuN monoclonal antibody (1:500; Millipore, Temecula, CA, USA). Sections were washed then incubated for 2 h at room temperature with goat anti-rat IgG Alexa Fluor 568 (1:200; Molecular Probes, Eugene, OR, USA) and goat anti-mouse IgM Alexa Fluor 488 (1:500; Molecular Probes) in PBST. Finally, sections were washed and coverslipped with Dako fluorescent mounting medium (Dako, Carpinteria, CA, USA). Immunofluorescent images were analyzed using a confocal laser-scanning microscope (A1Rsi; Nikon, Tokyo, Japan). Four sections per mouse were used, and two fluorescent images (640 \times 640 μ m) of DG region of the hippocampus were obtained from each section. The number of BrdU-positive cells was counted in each image. Non-specific binding of the secondary antibodies was barely detectable when tested in the absence of primary antibodies. A mean value of eight images was used for each mouse. Each group contained 8–10 mice.

2.8. Western blotting

BE360-treated mice were used for Western blotting experiments. Twelve mice were divided into four groups (Sham + vehicle, Sham + BE360, OBX + vehicle, and OBX + BE360). The mice were sacrificed by decapitation after 2 weeks of vehicle or drug administration. After sacrifice, the brains were immediately removed and washed with ice-cold PBS (pH 7.4). Then, 1 mm-thick coronal sections were cut using a mouse brain slicer (Muromachi Kikai, Tokyo, Japan) and immersed into PBS. The hippocampi were removed, frozen in liquid nitrogen, and stored at -80°C until use. The samples were homogenized in 150 μ l of CellLytic™ MT Cell Lysis Reagent (Sigma–Aldrich) and centrifuged at 15,000 $\times g$ for 15 min at 4°C. Supernatants were collected and their protein con-

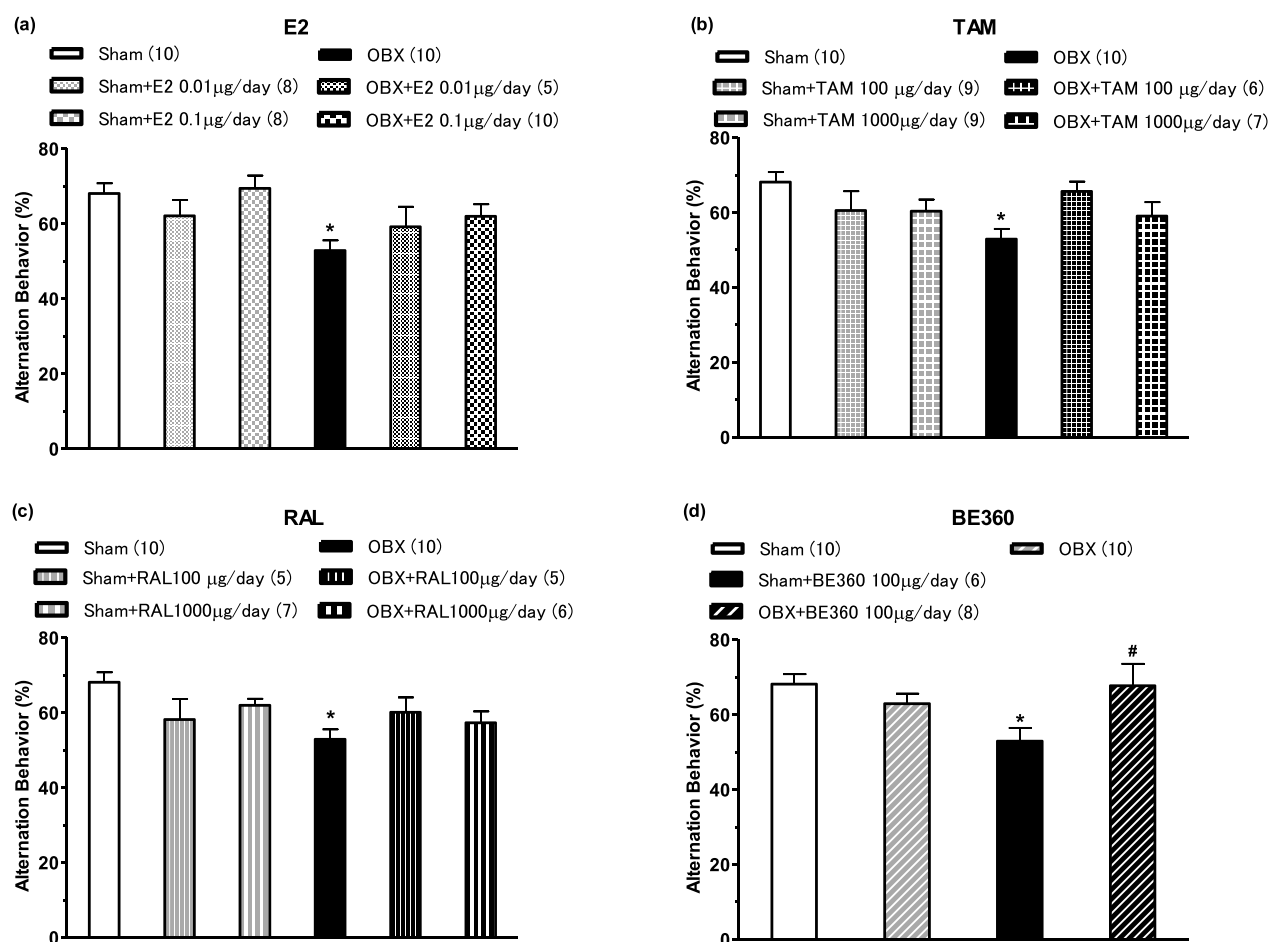


Fig. 2. Effects of estrogen receptors ligands on the impairment of spontaneous alternation behavior induced by OBX in the Y-maze test. * $p < 0.05$ vs. sham + vehicle group. # $p < 0.05$ vs. OBX + vehicle group.

centration determined using the Advanced Protein Assay Reagent (Cytoskeleton Inc., USA). Supernatants were then diluted in 4× Laemmli sample buffer (300 mM Tris-HCl (pH 6.8), 8% SDS, 40% glycerol, 12% 2-mercaptoethanol, 0.012% bromophenol blue), and incubated at 95 °C for 10 min. Aliquots of the obtained extracts (30 μg of proteins/well for each extract) were loaded onto a 10% SDS-polyacrylamide gel. After electrophoresis, proteins were transferred to a PVDF membrane, which was then incubated with blocking solution [10 mM Tris-HCl (pH 7.4), 100 mM NaCl, 0.01% Tween20 and 5% skim milk] for 1 h and probed overnight at 4 °C with antibodies against rabbit pCREB (1:1000, Cell Signaling Technology Inc., USA) or rabbit BDNF (1:1000, Abcam Ltd., UK) and rabbit β-actin (1:1000, Cell Signaling Technology Inc.). The membrane was then washed with blocking solution without milk, incubated with horseradish peroxidase-conjugated goat anti-rabbit IgG antibody (Cell Signaling Technology) for 2 h followed by visualization of the immunoreactive species with the ECL select Western blotting detection reagent (Amersham Life Sciences, USA). The densities of the bands were analyzed by densitometry (Image-J 1.43 μ, National Institute of Health).

2.9. Statistical analysis

Results are expressed as mean ± standard error of the mean (SEM). The significance of differences was determined by a one-way analysis of variance (ANOVA), followed by Fisher's PLSD test

for multigroup comparisons, respectively. $p < 0.05$ represented a significant difference.

3. Results

3.1. Effect of estrous cycle on behavior

Due to the small size of mouse samples for each of proestrus, estrus, metestrus, or diestrus phases at the time of testing ($n < 5$ per phase), we could not verify the influence that individual phases might have on behavior. To enable a preliminary evaluation of the influence of ovarian hormones, female sham and OBX mice were split into two groups: proestrus-estrus (high ovarian hormones) and metestrus-diestrus (low ovarian hormones) to increase statistical power [20–22]. In this study, we have used mice in the metestrus-diestrus phase, except for the estradiol treated group.

Effects of BE360 on sucrose preference in OBX mice Administration of RAL and BE360, but not E2 nor TAM, significantly increased the preference for sucrose in OBX mice as compared to the vehicle [E2: $F(3, 31) = 4.36$, $p = 0.01$ by one-way ANOVA, $p < 0.05$ by Fischer's PLSD, Fig. 1a; TAM: $F(3, 29) = 3.62$, $p = 0.02$ by one-way ANOVA, $p < 0.05$ by Fischer's PLSD, Fig. 1b; RAL: $F(3, 32) = 3.82$, $p = 0.02$ by one-way ANOVA, $p < 0.05$ by Fischer's PLSD, Fig. 1c; BE360: $F(3, 35) = 3.85$, $p = 0.02$ by one-way ANOVA, $p < 0.05$ by Fischer's PLSD, Fig. 1d]. Moreover, in sham mice, sucrose preference was not increased by E2, TAM, RAL or BE360 compared to vehicle.

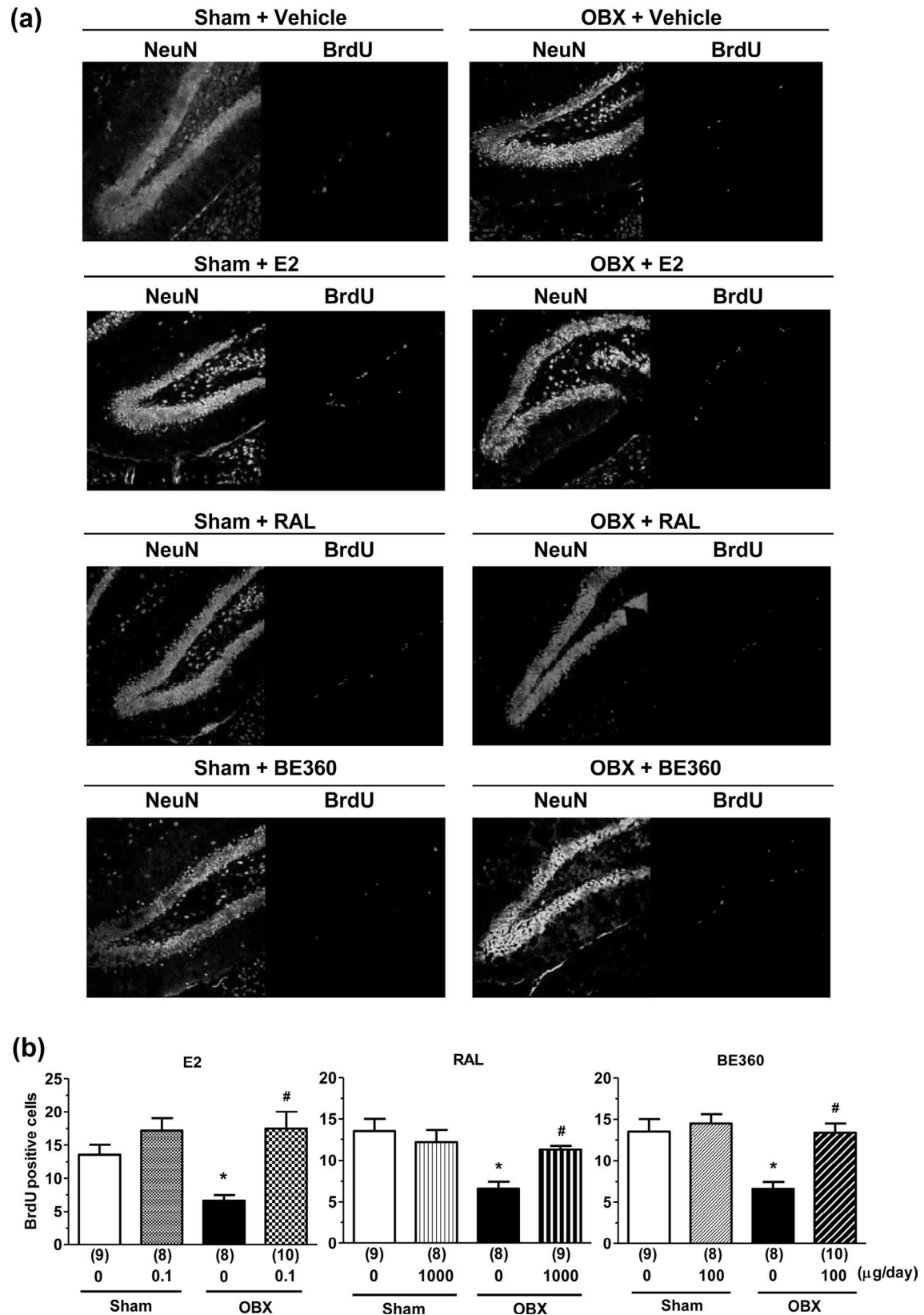


Fig. 3. Effects of estrogen receptors ligands on hippocampal cell proliferation in OBX mice. (a) Indicate NeuN⁺ (Green) and BrdU⁺ (Red) -positive cells in DG regions of the hippocampus. (b) Indicate quantitative analysis of the number of BrdU-positive cells in DG regions of the hippocampus. Numbers in parentheses indicate the number of animals in each group. * $p < 0.05$ vs. sham + vehicle group. # $p < 0.05$ vs. OBX + vehicle group. (For interpretation of the references to color in this figure legend, the reader is referred to the web version of this article.)

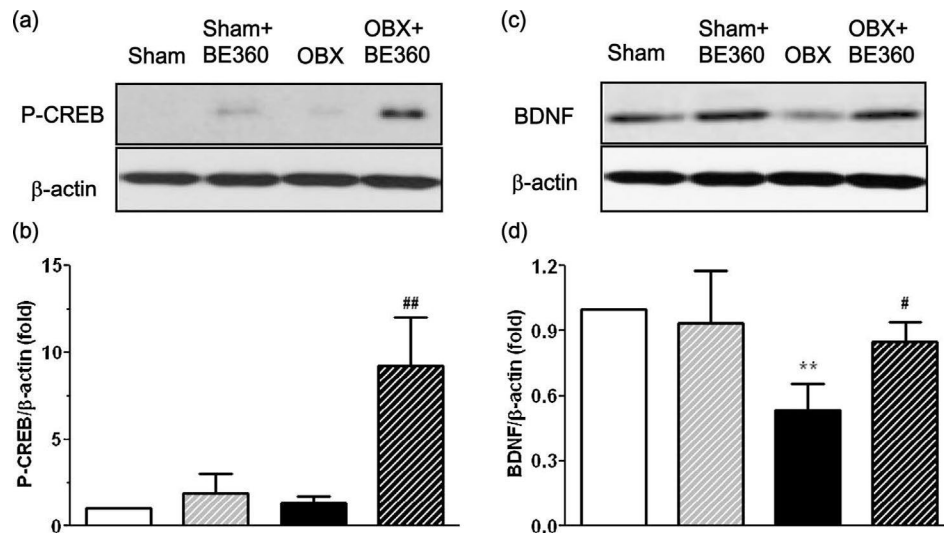


Fig. 4. Effects of chronic BE360 treatment on the hippocampal immunocontent of phosphorylated CREB (panels a and b) and BDNF (panels c and d) in OBX mice. Representative images of western blots probed with antibodies against phosphorylated CREB (P-CREB), BDNF and β -actin in the hippocampus (upper panels). Densitometric quantifications of P-CREB and BDNF are shown (lower panels). Data are expressed as fold expression relative to the sham control. $N = 4-5$ per group. ** $p < 0.01$ vs. sham + vehicle group. # $p < 0.05$ and ## $p < 0.01$ vs. OBX + vehicle group.

3.2. Effects of BE360 on spontaneous alternation behavior in OBX mice in the Y-maze test

Both the spontaneous alternation behavior and total number of arms entered were measured in this short-term memory test. The percentage of alternation behavior significantly decreased, without any change in the total number of arms entered (data not shown), in OBX compared with sham mice (Fig. 2). Administration of BE360 significantly increased the percentage of alternation behavior in OBX mice [E2: $F(5, 45) = 3.44$, $p = 0.01$ by one-way ANOVA, $p < 0.05$ by Fischer's PLSD, Fig. 2a; TAM: $F(5, 45) = 2.50$, $p = 0.04$ by one-way ANOVA, $p < 0.05$ by Fischer's PLSD, Fig. 2b; RAL: $F(5, 37) = 3.54$, $p = 0.01$ by one-way ANOVA, $p < 0.05$ by Fischer's PLSD, Fig. 2c; BE360: $F(3, 30) = 3.73$, $p = 0.02$ by one-way ANOVA, $p < 0.05$ by Fischer's PLSD, Fig. 2d].

3.3. Effects of BE360 on the decrease in cell proliferation in the dentate gyrus of OBX mice

Confocal microscopy analysis demonstrated the presence of BrdU-positive cells (red) in the granular cell layer of the DG in mice. The number of BrdU-positive cells was significantly decreased in OBX mice. However, chronic treatments of these mice with estrogen receptors ligands increased the number of BrdU-positive cells compared with vehicle [E2: $F(3, 31) = 4.53$, $p = 0.01$ by one-way ANOVA, $p < 0.05$ by Fischer's PLSD; RAL: $F(3, 30) = 6.77$, $p < 0.01$ by one-way ANOVA, $p < 0.05$ by Fischer's PLSD; BE360: $F(3, 31) = 80.32$, $p < 0.01$ by one-way ANOVA, Fig. 3b]. BrdU-positive cells were observed predominately in the deepest layers of the subgranular zone (SGZ) and hilus of hippocampal DG (Fig. 3a).

3.4. Effects of BE360 on phospho-CREB and BDNF levels in OBX mice

Chronic administration of BE360 in OBX mice significantly increased CREB phosphorylation in the hippocampus when compared with vehicle-treated OBX mice [$F(3, 8) = 19.89$, $p < 0.01$ by one-way ANOVA, $p < 0.01$ by Fischer's PLSD, Fig. 4b]. The BDNF immunocontent in vehicle-treated OBX mice was significantly decreased compared with the sham group. The OBX mice given

BE360 showed significantly higher BDNF levels than the OBX mice given vehicle [$F(3, 8) = 6.28$, $p < 0.05$ by one-way ANOVA, Fig. 4d].

4. Discussion

We have previously demonstrated that OBX female mice show a dysfunction in the brain's reward system when submitted to the sucrose preference test [7]. This validated behavioral test for depression was used in the present study to evaluate anhedonic response [23]. Here, chronic treatment with raloxifene improved the anhedonic response in OBX mice. Interestingly, we observed that chronic treatment with BE360 also improved the reduction in sucrose preference in OBX female mice. Thus, the fact that BE360 treatment was efficient in behavioral test above supports the hypothesis that this compound may be useful in modulating the depressive symptoms associated with major depression.

We have previously shown that OBX induces memory impairments in both the passive avoidance and Y-maze tasks [5,6]. In the present study, we demonstrate that a chronic treatment with BE360 improved the OBX-induced memory impairment in the Y-maze test. The Y-maze task is largely dependent on working memory, a form of short-term memory [24]. Thus, it is likely that BE360 has the potential to improve working memory deficits.

Failure in adult hippocampal neurogenesis is accompanied by cognitive deficits [25,26] and depression [27,28]. It is known that estradiol and SERMs can increase cell proliferation in the DG of the hippocampus [29–31], and that hippocampal neurogenesis can lead to changes in cognitive function and mood [32]. In this study, we also demonstrated that estradiol and RAL increases cell proliferation in the DG. Chronic treatment with antidepressants enhances hippocampal neurogenesis in OBX rodents [33,34]. Conversely, X-irradiation of the hippocampus, which reduces hippocampal neurogenesis, abolishes the behavioral and proliferative effects of many different antidepressants [35]. The OBX mice model exhibit not only characteristics of depression but also characteristics of AD, such as amyloid- β ($A\beta$) accumulation in the neocortex and hippocampus, cholinergic neuron loss in the basal forebrain, and spatial memory impairment [5,36]. Some studies have revealed a dysregulation of adult neurogenesis in AD patients and in various AD mouse models [37–39]. In the present study, BE360 enhanced hippocampal cell proliferation in OBX mice. The enhancement

of hippocampal cell proliferation by the chronic administration of BE360 could underlie the beneficial effects of BE360 on OBX-induced depressive-like behavior and cognitive deficits.

Previous reports have pointed to a role for BDNF in the control of hippocampal neurogenesis [40–42]. For example, infusion of exogenous BDNF into the DG leads to increased genesis of granule cells [43]. BDNF has been shown to promote the survival and differentiation of neurons during development, in adult brain and in cultured cells [44]. Furthermore, BDNF increases the synthesis of many proteins used in translation [45] which is required for memory formation [46] and reduce depression [47]. Moreover, pCREB is essential for memory consolidation and storage in the hippocampus [48] and increases in the rat hippocampus following a chronic administration of antidepressants [49]. Using transgenic mice overexpressing a dominant negative mutant of CREB, Nakagawa et al. reported a significant decrease in BrdU-labeled cells suggesting that CREB induces a positive effect on cell proliferation in the adult hippocampus [50]. In addition, it has been determined that increasing CREB activity may enhance cell proliferation, memory [51] and reduce depression [52]. It has been suggested that the activation of CREB-BDNF signaling may produce antidepressant and anti-dementia effects. We showed that BE360 increased the expression of BDNF and pCREB in the hippocampus. Therefore, it might be suggested that the activation of CREB and BDNF signaling pathways could mediate the effects of BE360 on cell proliferation. However, we have not examined whether BE360 shows high binding affinity to the membrane ER. Further studies are needed to determine the mechanism of action of BE360.

The present study has demonstrated that a new carborene compound BE360 has antidepressant and anti-dementia effects characterized by hippocampal cell proliferation potentially mediated through CREB/BDNF signaling pathways. These results indicate that BE360 may have a valuable therapeutic potential against depression and neurodegenerative diseases such as AD.

Conflicts of interest

None

Acknowledgments

This study was supported in part by JSPS KAKENHI (Grant Number 26460102) and Matching Fund Subsidy for Private Universities from the Ministry of Education, Culture, Sports, Science and Technology of Japan. The authors would like to thank Ms. Chie Saito, Ms. Rei Fukazawa, Ms. Anna Hoshi and Mr. Toshihiro Sasaki of Tohoku Pharmaceutical University for their technical assistance.

References

- [1] S. Green, P. Walter, V. Kumar, A. Krust, J.M. Bornert, P. Argos, P. Chambon, Human oestrogen receptor cDNA: sequence, expression and homology to v-erb-A, *Nature* 320 (1986) 134–139.
- [2] G.G. Kuiper, E. Enmark, M. Peltö-Huikko, S. Nilsson, J.A. Gustafsson, Cloning of a novel receptor expressed in rat prostate and ovary, *Proc. Natl. Acad. Sci. U. S. A.* 93 (1996) 5925–5930.
- [3] M. Hirata, M. Inada, C. Matsumoto, M. Takita, T. Ogawa, Y. Endo, C. Miyaura, A novel carborene analog, BE360, with a carbon-containing polyhedral boron-cluster is a new selective estrogen receptor modulator for bone, *Biochem. Biophys. Res. Commun.* 380 (2009) 218–222.
- [4] R.D. Strous, Y. Shoenfeld, To smell the immune system: olfaction, autoimmunity and brain involvement, *Autoimmun. Rev.* 6 (2006) 54–60.
- [5] S. Hozumi, O. Nakagawasai, K. Tan-No, F. Nijima, F. Yamadera, A. Murata, Y. Arai, H. Yasuhara, T. Tadano, Characteristics of changes in cholinergic function and impairment of learning and memory-related behavior induced by olfactory bulbectomy, *Behav. Brain Res.* 138 (2003) 9–15.
- [6] O. Nakagawasai, S. Hozumi, K. Tan-No, F. Nijima, Y. Arai, H. Yasuhara, T. Tadano, Immunohistochemical fluorescence intensity reduction of brain somatostatin in the impairment of learning and memory-related behaviour induced by olfactory bulbectomy, *Behav. Brain Res.* 142 (2003) 63–67.
- [7] A. Sato, O. Nakagawasai, K. Tan-No, H. Onogi, F. Nijima, T. Tadano, Influence of olfactory bulbectomy on maternal behavior and dopaminergic function in nucleus accumbens in mice, *Behav. Brain Res.* 210 (2010) 251–256.
- [8] J.W. Koo, S.J. Russo, D. Ferguson, E.J. Nestler, R.S. Duman, Nuclear factor-kappaB is a critical mediator of stress-impaired neurogenesis and depressive behavior, *Proc. Natl. Acad. Sci. U. S. A.* 107 (2010) 2669–2674.
- [9] N. Matsui, Y. Kido, H. Okada, M. Kubo, M. Nakai, N. Fukuishi, Y. Fukuyama, M. Akagi, Phenylbutenoid dimers isolated from *Zingiber purpureum* exert neurotrophic effects on cultured neurons and enhance hippocampal neurogenesis in olfactory bulbectomized mice, *Neurosci. Lett.* 513 (2012) 72–77.
- [10] M.A. Arevalo, I. Ruiz-Palmero, J. Simon-Areces, E. Acaz-Fonseca, I. Azcoitia, L.M. Garcia-Segura, Estradiol meets notch signaling in developing neurons, *Front. Endocrinol.* 2 (21) (2011).
- [11] N. Lagunas, I. Calmarza-Font, D. Grassi, L.M. Garcia-Segura, Estrogen receptor ligands counteract cognitive deficits caused by androgen deprivation in male rats, *Horm. Behav.* 59 (2011) 581–584.
- [12] I. Calmarza-Font, N. Lagunas, L.M. Garcia-Segura, Antidepressive and anxiolytic activity of selective estrogen receptor modulators in ovariectomized mice submitted to chronic unpredictable stress, *Behav. Brain Res.* 227 (2012) 287–290.
- [13] R.E. McClure, C.K. Barha, L.A. Galea, 17 β -Estradiol, but not estrone, increases the survival and activation of new neurons in the hippocampus in response to spatial memory in adult female rats, *Horm. Behav.* 63 (2013) 144–157.
- [14] E.G. Waterhouse, J.J. An, L.L. Orefice, M. Baydyuk, G.Y. Liao, K. Zheng, B. Lu, B. Xu, BDNF promotes differentiation and maturation of adult-born neurons through GABAergic transmission, *J. Neurosci.* 32 (2012) 14318–14330.
- [15] T. Jover, H. Tanaka, A. Calderone, K. Oguro, M.V. Bennett, A.M. Etgen, R.S. Zukin, Estrogen protects against global ischemia-induced neuronal death and prevents activation of apoptotic signaling cascades in the hippocampal CA1, *J. Neurosci.* 22 (2002) 2115–2124.
- [16] J. Kofler, P.D. Hurn, R.J. Traystman, SOD1 overexpression and female sex exhibit region-specific neuroprotection after global cerebral ischemia due to cardiac arrest, *J. Cereb. Blood Flow Metab.* 25 (2005) 1130–1137.
- [17] T. Jover-Mengual, R.S. Zukin, A.M. Etgen, MAPK signaling is critical to estradiol protection of CA1 neurons in global ischemia, *Endocrinology* 148 (2007) 1131–1143.
- [18] Y. Endo, T. Yoshimi, K. Ohta, T. Suzuki, S. Ohta, Potent estrogen receptor ligands based on bisphenols with a globular hydrophobic core, *J. Med. Chem.* 48 (2005) 3941–3944.
- [19] F.Z. Shaw, S.H. Chuang, K.R. Shieh, Y.J. Wang, Depression- and anxiety-like behaviors of a rat model with absence epileptic discharges, *Neuroscience* 160 (2009) 382–393.
- [20] C.M. Contreras, M. Molina, M. Saavedra, L. Martínez-Mota, Lateral septal neuronal firing rate increases during proestrus-estrus in the rat, *Physiol. Behav.* 68 (2000) 279–284.
- [21] L.A. Jans, C.K. Lieben, A. Blokland, Influence of sex and estrous cycle on the effects of acute tryptophan depletion induced by a gelatin-based mixture in adult Wistar rats, *Neuroscience* 147 (2007) 304–317.
- [22] P.J. Allen, K.E. D'Anci, R.B. Kanarek, P.F. Renshaw, Sex-specific antidepressant effects of dietary creatine with and without sub-acute fluoxetine in rats, *Pharmacol. Biochem. Behav.* 101 (2012) 588–601.
- [23] K.Y. Sarkisova, M.A. Kulikov, I.S. Midzyanovskaya, A.A. Folomkina, Dopamine-dependent nature of depression-like behavior in WAG/Rij rats with genetic absence epilepsy, *Neurosci. Behav. Physiol.* 38 (2008) 119–128.
- [24] M. Sarter, G. Bodewitz, D.N. Stephens, Attenuation of scopolamine-induced impairment of spontaneous alteration behaviour by antipsychotic but not inverse agonist and agonist beta-carbolines, *Psychopharmacology (Berl.)* 94 (1988) 491–495.
- [25] E. Gould, A. Beylin, P. Tanapat, A. Reeves, T.J. Shors, Learning enhances adult neurogenesis in the hippocampal formation, *Nat. Neurosci.* 2 (1999) 260–265.
- [26] T.J. Shors, G. Miesegaes, A. Beylin, M. Zhao, T. Rydel, E. Gould, Neurogenesis in the adult is involved in the formation of trace memories, *Nature* 410 (2001) 372–376.
- [27] R.S. Duman, L.M. Monteggia, A neurotrophic model for stress-related mood disorders, *Biol. Psychiatry* 59 (2006) 1116–1127.
- [28] E. Castrén, V. Vöikar, T. Rantamäki, Role of neurotrophic factors in depression, *Curr. Opin. Pharmacol.* 7 (2007) 18–21.
- [29] P. Tanapat, N.B. Hastings, A.J. Reeves, E. Gould, Estrogen stimulates a transient increase in the number of new neurons in the dentate gyrus of the adult female rat, *J. Neurosci.* 19 (1999) 5792–5801.
- [30] B.K. Ormerod, L.A. Galea, Reproductive status influences cell proliferation and cell survival in the dentate gyrus of adult female meadow voles: a possible regulatory role for estradiol, *Neuroscience* 102 (2001) 369–379.
- [31] J.A. Clark, S. Alves, C. Gundlah, B. Rocha, E.T. Birzin, S.J. Cai, et al., Selective estrogenreceptor-beta (SERM-beta) compounds modulate raphe nuclei tryptophan hydroxylase-1 (TPH-1) mRNA expression and cause antidepressant-like effects in the forced swim test, *Neuropharmacology* 63 (2012) 1051–1063.
- [32] A.A. Wolf, C.A. Frye, A review and update of mechanisms of estrogen in the hippocampus and amygdala for anxiety and depression behavior, *Neuropsychopharmacology* 31 (2006) 1097–1111.
- [33] K. Jaako-Movits, T. Zharkovsky, M. Pedersen, A. Zharkovsky, Decreased hippocampal neurogenesis following olfactory bulbectomy is reversed by repeated citalopram administration, *Cell. Mol. Neurobiol.* 26 (2006) 1559–1570.

- [34] J. Jarosik, B. Legutko, S. Werner, K. Unsicker, O. von Bohlen Und Halbach, Roles of exogenous and endogenous FGF-2 in animal models of depression, *Restor. Neurol. Neurosci.* 29 (2011) 153–165.
- [35] L. Santarelli, M. Saxe, C. Gross, A. Surget, F. Battaglia, S. Dulawa, et al., Requirement of hippocampal neurogenesis for the behavioral effects of antidepressants, *Science* 301 (2003) 805–809.
- [36] I.Y. Aleksandrova, V.V. Kuvichkin, I.A. Kashparov, N.I. Medvinskaya, I.V. Nesterova, S.M. Lunin, et al., Increased level of beta-amyloid in the brain of bulbectomized mice, *Biochemistry* 69 (2004) 176–180.
- [37] K. Jin, A.L. Peel, X.O. Mao, L. Xie, B.A. Cottrell, D.C. Henshall, D.A. Greenberg, Increased hippocampal neurogenesis in Alzheimer's disease, *Proc. Natl. Acad. Sci. U. S. A.* 101 (2004) 343–347.
- [38] T. Kimura, N. Hong, P.T. guyen, S.A. Ho, A.H. Tran, T. Ono, H. Nishijo, T-817MA, a neurotrophic agent, ameliorates the deficits in adult neurogenesis and spatial memory in rats infused i.c.v. with amyloid-beta peptide, *Br. J. Pharmacol.* 157 (2009) 451–463.
- [39] M. Demars, Y.S. Hu, A. Gadadhar, O. Lazarov, Impaired neurogenesis is an early event in the etiology of familial Alzheimer's disease in transgenic mice, *J. Neurosci. Res.* 88 (2010) 2103–2117.
- [40] E. Larsson, R.J. Mandel, R.L. Klein, N. Muzyczka, O. Lindvall, Z. Kokaia, Suppression of insult-induced neurogenesis in adult rat brain by brain-derived neurotrophic factor, *Exp. Neurol.* 177 (2002) 1–8.
- [41] J. Lee, W. Duan, M.P. Mattson, Evidence that brain-derived neurotrophic factor is required for basal neurogenesis and mediates, in part, the enhancement of neurogenesis by dietary restriction in the hippocampus of adult mice, *J. Neurochem.* 82 (2002) 1367–1375.
- [42] M. Sairanen, G. Lucas, P. Ernfors, M. Castrén, E. Castrén, Brain-derived neurotrophic factor and antidepressant drugs have different but coordinated effects on neuronal turnover, proliferation, and survival in the adult dentate gyrus, *J. Neurosci.* 25 (2005) 1089–1094.
- [43] H. Scharfman, J. Goodman, A. Macleod, S. Phani, C. Antonelli, S. Croll, Increased neurogenesis and the ectopic granule cells after intrahippocampal BDNF infusion in adult rats, *Exp. Neurol.* 192 (2005) 348–356.
- [44] J. Takahashi, T.D. Palmer, F.H. Gage, Retinoic acid and neurotrophins collaborate to regulate neurogenesis in adult-derived neural stem cell cultures, *J. Neurobiol.* 38 (1999) 65–81.
- [45] L. Liao, J. Pilotte, T. Xu, C.C. Wong, G.M. Edelman, P. Vanderklish, J.R. Yates 3rd., BDNF induces widespread changes in synaptic protein content and up-regulates components of the translation machinery: an analysis using high-throughput proteomics, *J. Proteome Res.* 6 (2007) 1059–1071.
- [46] N. Gruet, P. Richer, B. Hars, Memory consolidation and reconsolidation in the rat pup require protein synthesis, *J. Neurosci.* 24 (2004) 10488–10492.
- [47] B. Chen, D. Dowlatshahi, G.M. MacQueen, J.F. Wang, L.T. Young, Increased hippocampal BDNF immunoreactivity in subjects treated with antidepressant medication, *Biol. Psychiatry* 50 (2001) 260–265.
- [48] C. O'Connell, H.C. Gallagher, A. O'Malley, M. Bourke, C.M. Regan, CREB phosphorylation coincides with transient synapse formation in the rat hippocampal dentate gyrus following avoidance learning, *Neural Plast.* 7 (2000) 279–289.
- [49] M. Nibuya, E.J. Nestler, R.S. Duman, Chronic antidepressant administration increases the expression of cAMP response element binding protein (CREB) in rat hippocampus, *J. Neurosci.* 16 (1996) 2365–2372.
- [50] S. Nakagawa, J.E. Kim, R. Lee, J.E. Malberg, J. Chen, C. Steffen, et al., Regulation of neurogenesis in adult mouse hippocampus by cAMP and the cAMP response element-binding protein, *J. Neurosci.* 22 (2002) 3673–3682.
- [51] M. Walton, A.M. Woodgate, A. Muravlev, R. Xu, M.J. During, M. Dragunow, CREB phosphorylation promotes nerve cell survival, *J. Neurochem.* 73 (1999) 1836–1842.
- [52] J. Guo, P. Lin, X. Zhao, J. Zhang, X. Wei, Q. Wang, C. Wang, Etazolate abrogates the lipopolysaccharide (LPS)-induced downregulation of the cAMP/pCREB/BDNF signaling, neuroinflammatory response and depressive-like behavior in mice, *Neuroscience* 263 (2014) 1–14.



ELSEVIER

Contents lists available at ScienceDirect

Bioorganic & Medicinal Chemistry Letters

journal homepage: www.elsevier.com/locate/bmcl

Design and synthesis of carborane-containing estrogen receptor-beta (ER β)-selective ligands



Kiminori Ohta^{a,*}, Takumi Ogawa^a, Akifumi Oda^b, Asako Kaise^a, Yasuyuki Endo^{a,*}

^a Faculty of Pharmaceutical Sciences, Tohoku Pharmaceutical University, 4-4-1 Komatsushima, Aoba-ku, Sendai 981-8558, Japan

^b Faculty of Pharmacy, Institute of Medical, Pharmaceutical and Health Sciences, Kanazawa University, Kakuma-machi, Kanazawa, Ishikawa 920-1192, Japan

ARTICLE INFO

Article history:

Received 9 July 2015

Revised 1 August 2015

Accepted 4 August 2015

Available online 7 August 2015

Keywords:

Carborane

Estrogen receptor

Subtype selectivity

Docking study

ABSTRACT

Candidates for highly selective estrogen receptor-beta (ER β) ligands (**6a-c**, **7a-c**, **8a** and **8b**) were designed and synthesized based on carborane-containing ER ligands **1** and **2** as lead compounds. Among them, *p*-carboranylcyclohexanol derivatives **8a** and **8b** exhibited high ER β selectivity in competitive binding assay: for example, **8a** showed 56-fold selectivity for ER β over ER α . Docking studies of **8a** and **8b** with the ER α and ER β ligand-binding domains (LBDs) suggested that the *p*-carborane cage of the ligands is located close to key amino acid residues that influence ER-subtype selectivity, that is, Leu384 in the ER α LBD and Met336 in the ER β LBD. The *p*-carborane cage in **8a** and **8b** appears to play a crucial role in the increased ER β selectivity.

© 2015 Elsevier Ltd. All rights reserved.

Since estrogen receptor (ER) was cloned in 1986,¹ its biological functions have been extensively studied.² ER is activated by the binding of endogenous estrogen, 17 β -estradiol (E2, Fig. 1), and mediates the activity of estrogens in the regulation of various physiological processes, including development and function of the female reproductive system and maintenance of bone mineral density.^{1,2} Ten years later, a second form of ER, ER β , was discovered in rat prostate.³ ER β has quite different biological functions from the first form of ER, ER α . In general, the two ER subtypes show divergent roles and sometimes antagonize each other under physiological conditions.⁴ The therapeutic use of E2 is limited by estrogenic effects and an increased risk of cancer, which seem to be caused by the ER α activation.⁵ On the other hand, over-expression or activation of ER β has an anti-proliferative effect on breast cancer cells.⁶ Moreover, activation of ER β inhibits proliferation and migration of prostate cancer cell lines and stimulates differentiation of prostate.⁷ Recently, George et al. reported that an ER β -selective agonist delayed the progression of Alzheimer's disease by including degradation of A β aggregates.⁸ Thus, ER β -selective ligands are of interest as potential clinical candidates for several cancers and Alzheimer's disease, and also as probes for ER β -related molecular biology.

Carboranes, a group of carbon-containing boron clusters, have been studied as boron carriers for boron neutron capture therapy (BNCT), based on their high boron content.⁹ On the other hand, we have focused on the carborane cage as a novel hydrophobic pharmacophore for drug development, and have reported carborane derivatives with various biological activities.¹⁰ During our studies on carborane-containing ER ligands, we found that many carboranyl phenol derivatives showed more potent ER-binding affinity than E2 because the high hydrophobicity and spherical structure of carborane result in strong binding to the hydrophobic pocket of the ER ligand-binding domain (LBD).^{10,11}

1-(4-Hydroxyphenyl)-12-hydroxymethyl-*p*-carborane (**BE120**, **1**, Fig. 1) shows greater binding affinity for ER α and more potent estrogenic activity than E2.¹⁰ Recently, we also reported that introduction of a fluorine atom or an alkyl group on a boron atom of the carborane cage enhanced the ER β selectivity of the parent estrogenic carboranyl phenols.¹² For example, **BE701** (**2**, Fig. 1), which contains a *B*-fluorinated *m*-carborane cage, showed 8.5 times greater binding affinity for ER β than for ER α , although its selectivity is still not sufficient for development of drug candidates or biological tools.

The two ERs have quite similar LBDs, but in the hydrophobic pocket of the LBDs, Leu384 and Met421 of ER α are substituted by Met336 and Ile373, respectively, in ER β .¹³ E2 is accommodated equally well by the two LBDs because it has little interaction with these amino acid residues.¹³ Several ER β -selective ligands, including **2**, have been designed based on the idea of specifically decreasing the affinity for ER α by introducing ligand substituents that

* Corresponding authors. Tel./fax: +81 22 727 0143 (K.O.); tel.: +81 22 727 0142; fax: +81 22 275 2013 (Y.E.).

E-mail addresses: k-ohta@tohoku-pharm.ac.jp (K. Ohta), yendo@tohoku-pharm.ac.jp (Y. Endo).

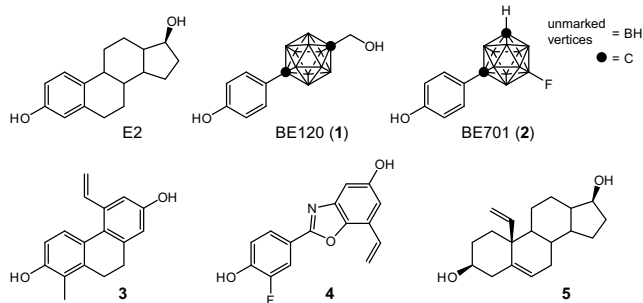


Figure 1. Structures of 17β-estradiol (E2), carborane-containing ER ligands **1** and **2**, and ERβ-selective ligands **3–5**.

interfere sterically with Met421 of ERα (Fig. 1).¹⁴ For example, compounds **3**¹⁵ and **4**¹⁶ have a methyl group and a fluorine atom at the ortho position of the phenolic hydroxyl group, respectively; these substituents moved the phenol ring closer to Met336 of ERβ and facilitate C–H...π interaction, resulting in preferential binding to ERβ. An endogenous dihydrotestosterone metabolite, 3β-androstenediol,¹⁷ and **5**,¹⁸ which contains an androstane skeleton, show high ERβ-selectivity. The androstane skeleton appears to intrinsically favor binding to ERβ rather than to ERα, and an axial substituent such as the vinyl group of **5** at the ring junction interacts sterically with Leu384 of ERα.¹⁸ In general, chemical modifications of the phenol ring of ER ligands appear to greatly influence the ER subtype selectivity.

Therefore, based on the structures of the selective ERβ ligands **3–5**, we designed carborane-containing ligands **6a–c**, **7a–c**, **8a** and **8b**. Here, we describe synthesis of **6a–c**, **7a–c**, **8a** and **8b**, evaluation of their binding affinity and selectivity for ERα and ERβ, and docking simulation studies of **8a** and **8b** with both ERs (Fig. 2).

Synthesis of *p*-carborane-containing *o*-methylated phenol derivatives **6a–c** is summarized in Scheme 1. *p*-Carborane was treated with *n*-BuLi, and then transformed into C-copper-*p*-carborane, which was reacted with 2-methyl-4-iodoanisole in the presence of pyridine as a ligand of copper to afford monoarylated *p*-carborane (**9**) and diarylated *p*-carborane (**10**) in 41% and 34% yields, respectively.¹⁹ The methoxy group of compound **9** was demethylated with BBr₃ to afford the corresponding phenol derivative **6a** in quantitative yield. Compound **9** was treated with *n*-BuLi, and then reacted with paraformaldehyde, followed by demethylation with BBr₃ to afford the *o*-methylated BE120 derivative **6b** in 97% yield over two steps. Compound **6c** was obtained by demethylation reaction of **10** with BBr₃ in 93% yield.

Scheme 2 summarizes the synthesis of *o*-halogenated-*m*-carboranyl phenol derivative **7**. *B*-Fluoro-*m*-carboranyl anisole **11**, which was obtained as a synthetic intermediate in our previous study,¹² was nitrated with potassium nitrate and concentrated sulfuric acid, followed by catalytic hydrogenation of the nitro group to afford key intermediate **12** in 77% yield over two steps. The amino group of **12** was directly transformed into a fluorine atom by treatment with nitrosonium tetrafluoroborate under Balz–Schiemann reaction conditions²⁰ and the product was demethylated with BBr₃ to afford *o*-fluorinated phenol **7a** in 23% yield over two steps.

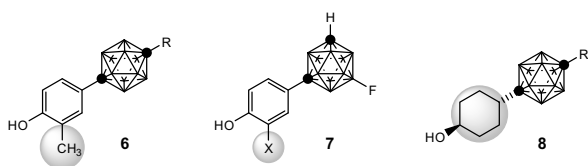
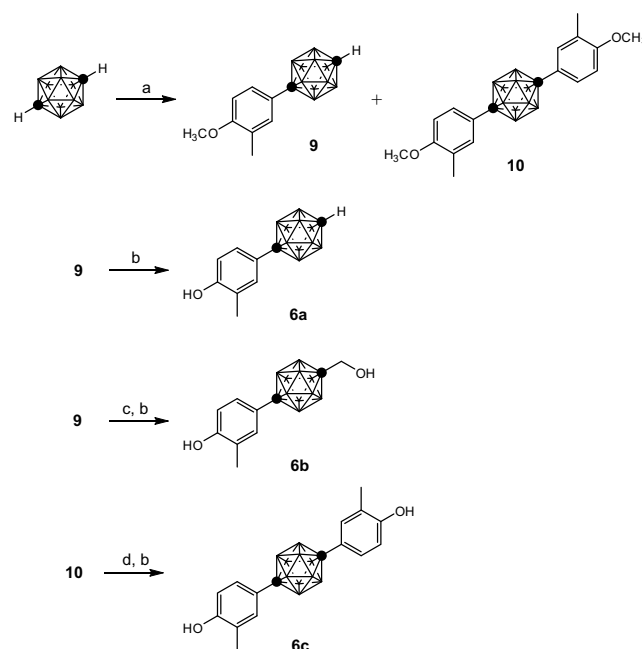


Figure 2. Structures of the target compounds **6–8**.

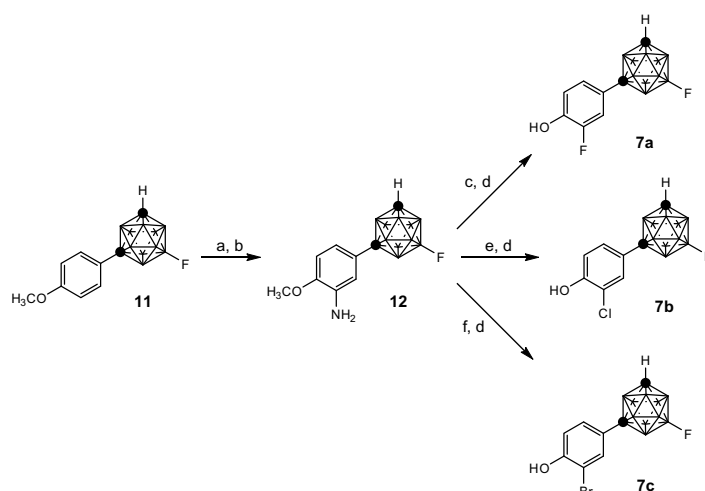


Scheme 1. Synthesis of *o*-methylated phenol derivatives **6a–c**. Reagents and conditions: (a) *n*-BuLi, DME, then CuCl, pyridine, 4-iodo-2-methylanisole, 41% for **9**, 34% for **10**; (b) BBr₃, CH₂Cl₂, 93%–quant; (c) *n*-BuLi, ether, then paraformaldehyde, 97%.

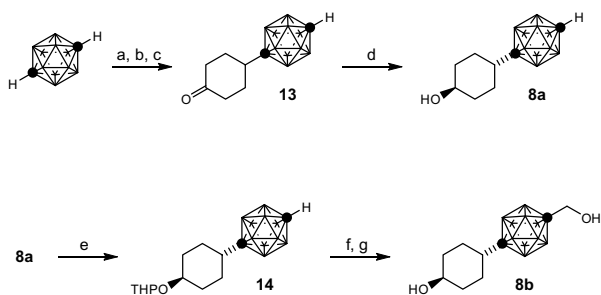
o-Chlorinated derivative **7b** and *o*-brominated derivative **7c** were synthesized via Sandmeyer reaction²¹ using *tert*-butyl nitrite and the corresponding copper halide, followed by demethylation with BBr₃, in 49% and 29% yield, respectively, over two steps.

Scheme 3 summarizes the synthesis of *p*-carborane-containing cyclohexanol derivative **8a** and **8b**. After treatment of *p*-carborane with *n*-BuLi, the resultant C-lithio-*p*-carborane was reacted with 1,4-cyclohexanedione monoethyleneketal. The tertiary alcohol was eliminated and the ketal group was deprotected under acidic conditions, and then catalytic hydrogenation of the double bond afforded 4-(*p*-carboranyl)-cyclohexanone **13** in 59% yield over three steps. Reduction of the carbonyl group of **13** with sodium borohydride afforded cyclohexanol derivative **8a** as a single *trans*-isomer.²² A hydroxyl group of **8a** was protected with a tetrahydropyran (THP) group, and then treatment with *n*-BuLi, followed by deprotection of THP, afforded completely reduced BE120 derivative **8b** in 51% yield over three steps.

Binding affinity for both ERs was evaluated by means of competitive binding assay using [2,4,6,7-³H]17β-estradiol and human recombinant ERα and ERβ, and the selectivity was estimated from the relative binding affinity (RBA) values.²³ The binding profiles of **6a–c**, **7a–c**, **8a** and **8b** are summarized in Table 1. The parent compounds **1** and **2** showed ERβ-selectivity ratios of 1.4 and 8.5, respectively. *o*-Methylphenol derivative **6a** showed a remarkable decrease of binding affinity to both ERs, but the hydroxymethyl derivatives **6b** retained high binding affinity for both ERs. This may be explained in terms of hydrogen bond formation of the hydroxymethyl group with His524. However, **6a** and **6b** showed no selectivity. Interestingly, however, symmetric bisphenol-*p*-carborane **6c** showed 10 times higher binding affinity for ERα than ERβ. Introduction of a halogen atom into the phenol ring of *m*-carboranyl phenol **2** led to decreased binding affinity for ERβ. The binding affinity of *o*-chlorinated derivative **7b** for ERβ was decreased more than 100 times compared to that of the parent compound **2**, and thus **7b** showed ERα selectivity. A bromine atom is too large to be tolerated at the *ortho*-position of phenol ring.



Scheme 2. Synthesis of *o*-halogenated phenol derivatives **7a–c**. Reagents and conditions: (a) KNO_3 , concd H_2SO_4 , CH_2Cl_2 , 79%; (b) H_2 , Pd/C, AcOEt/MeOH, 98%; (c) NOBF_4 , CH_2Cl_2 , 33%; (d) BBr_3 , CH_2Cl_2 , 70–89%; (e) $t\text{BuONO}$, CuCl_2 , CH_3CN , 56%; (f) $t\text{BuONO}$, CuBr_2 , CH_3CN , 33%.



Scheme 3. Synthesis of cyclohexanol derivatives **8a** and **8b**. Reagents and conditions: (a) $n\text{-BuLi}$, ether, then 1,4-cyclohexanedione monoethylene-ketal, 71%; (b) concd H_2SO_4 , 85%; (c) H_2 , Pd/C, MeOH, 98%; (d) NaBH_4 , MeOH, 74%; (e) 3,4-dihydro-2H-pyran, TsOH, CH_2Cl_2 , 68%; (f) $n\text{-BuLi}$, ether, then paraformaldehyde, 78%; (g) TsOH, MeOH, 96%.

Various modifications of the phenol ring of *m*- or *p*-carboranyl phenol structures failed to enhance the binding affinity for $\text{ER}\beta$ through $\text{C-H}\cdots\pi$ interaction, as observed in compounds **3** and **4**. Therefore, we concluded that ortho-substitution of carboranyl phenols is unsuitable for increasing $\text{ER}\beta$ selectivity. On the other hand, we found that *p*-carboranyl cyclohexanol derivative **8a** showed nearly 60 times higher binding affinity for $\text{ER}\beta$ than $\text{ER}\alpha$; this is the highest $\text{ER}\beta$ selectivity among known carborane-containing ER ligands. As expected, the binding affinity of compound **8b** for both ERs was greatly enhanced by hydrogen bond formation of the hydroxymethyl group on a carbon atom of the *p*-carborane cage, as seen with BE120. However, the $\text{ER}\beta$ selectivity ratio of **8b** was only 7. By analogy with **5**, we anticipate that introduction of a medium-size substituent onto carbon of the *p*-carborane cage of **8b** would enhance the $\text{ER}\beta$ selectivity. Further structural modifications and biological studies of **8b** are in progress.

Table 1
Binding affinity for $\text{ER}\alpha$ and $\text{ER}\beta$ and subtype selectivity of the phenol ring modified compounds **6–8**

Compound	R	X	Relative binding affinity ^a		Selectivity $\text{ER}\beta/\text{ER}\alpha$
			$\text{ER}\alpha$	$\text{ER}\beta$	
6a	H	—	6.3	6.3	1.0
6b	CH_2OH	—	1.2×10^2	1.4×10^2	1.2
6c		—	83	5.9	7.1×10^{-2}
7a	—	F	3.4	13	3.8
7b	—	Cl	2.2	0.30	0.14
7c	—	Br	4.5×10^{-3}	2.7×10^{-3}	0.60
8a	H	—	5.2×10^{-3}	0.29	56
8b	CH_2OH	—	1.4	9.8	7.0
1	—	—	1.6×10^2	2.2×10^2	1.4
2	—	—	4.8	41	8.5

^a All binding assays were performed in triplicate ($n = 3$). RBA values are calculated from the IC_{50} values of E2 and test compounds, taking the binding affinity of E2 as 100.

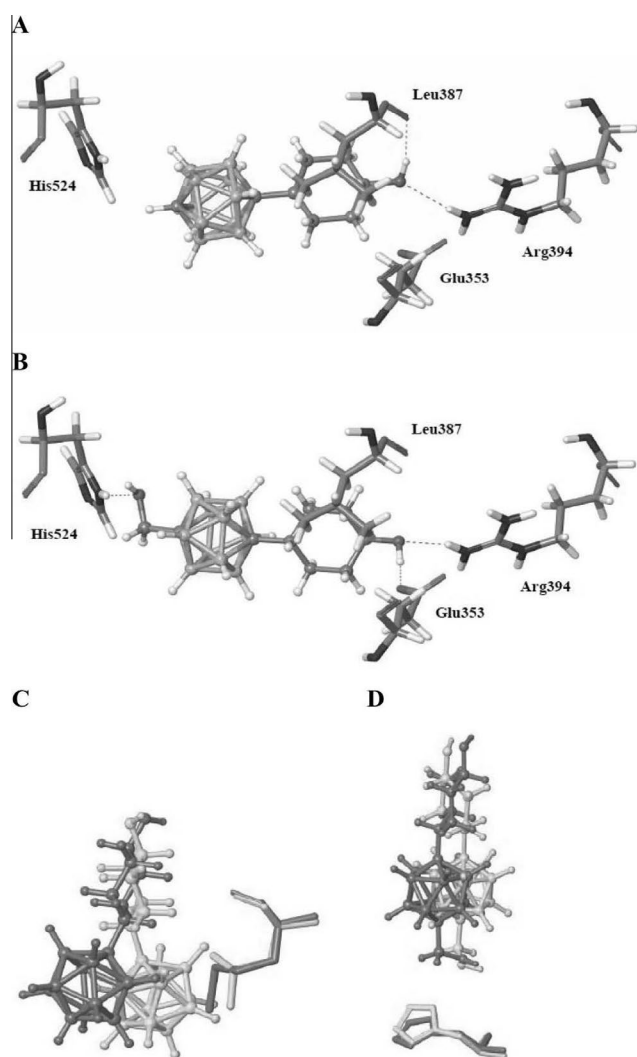


Figure 3. Comparisons of docking models of **8a** and **8b** with ER α and ER β . (A) Binding mode of **8a** with the ER α LBD. (B) Binding mode of **8b** with the ER α LBD. (C) The arrangements of **8a** and Leu384 in ER α LBD (aqua) and **8a** and Met336 in ER β LBD (brown). (D) The arrangements of **8b** and His524 in ER α LBD (aqua) and **8b** and His475 in ER β LBD (brown).

Binding modes of **8a** and **8b** with ER α ²⁴ and ER β ²⁴ were calculated using a docking program (GOLD 5.2).²⁵ The results for ER α LBD are shown in Figure 3A and B. The hydrophobic cyclohexyl-*p*-carborane skeleton of **8a** and **8b** was accommodated in the hydrophobic pocket of ER α . The hydroxyl group of **8a** forms hydrogen bonds with Arg394 and the backbone carbonyl group of Leu387 (Fig. 3A), whereas the hydroxyl group of **8b** forms a hydrogen bond with Glu353 instead of Leu387. The hydroxymethyl group of **8b** also forms a hydrogen bond with His524, which may account for the enhanced ER α -binding affinity and different hydrogen-bonding mode of the hydroxyl group. The *p*-carborane cage of **8a** is located close to Leu384 in the ER α LBD and Met336 in the ER β LBD (Fig. 3C). Since Met336 of ER β squeezes the *p*-carborane cage of **8a** into the hydrophobic pocket, the *p*-carborane cage approaches hydrophobic amino acid residues, such as Phe356, Leu298, Ile373, Ile376, and Phe377, located on the opposite side to Met336, and this may enhance the ER β -binding affinity. The hydroxymethyl group of **8b** forms hydrogen bonds with His524 in the ER α LBD and His475 in the ER β LBD, and the distances between oxygen of the hydroxyl group and nitrogen of the

imidazole ring of histidine are 2.623 Å or 3.536 Å, respectively (Fig. 3D). Although the hydrogen bond between the hydroxymethyl group of **8b** and His524 of ER α should be stronger than the corresponding hydrogen bond with His475 of ER β , the binding affinity of **8b** with ER β was higher than that with ER α owing to the interaction with the hydrophobic amino acid residues at the opposite side to Met336.

In conclusion, various carborane derivatives were designed and synthesized as candidate ER β -selective ligands, and their ER binding affinities were evaluated by means of a competitive binding assay. Introductions of a methyl group or halogen at the ortho position to the hydroxyl group on the phenol ring had little effect on ER subtype selectivity. Interestingly, cyclohexanol derivative **8a** bound to ER β with nearly 60 times greater affinity than to ER α owing to a decrease in the binding affinity for ER α . Docking studies of **8a** with both ER LBDs suggested effective hydrophobic interactions of **8a** with ER β LBD. Further structure–activity relationship studies of **8a** and ER β -related biological evaluations are in progress. These findings should be helpful for molecular design of further highly ER β -selective carborane-containing ligands.

Acknowledgments

This research was supported by a Grant-in-Aid for the Strategic Research Program for Private University (2015–2019) and a Grant-in-Aid for Scientific Research (B) (No. 26460151) from the Ministry of Education, Culture, Sports, Science and Technology, Japan.

References and notes

- Green, S.; Walter, P.; Kumar, V.; Krust, A.; Bornert, J. M.; Argos, P.; Chambon, P. *Nature* **1986**, *320*, 134.
- There are several hundred reviews on estrogen receptors and their functions. For example: (a) Lanyon, L.; Armstrong, V.; Ong, D.; Zaman, G.; Price, J. J. *J. Endocrinol.* **2004**, *182*, 183; (b) Pfaff, D.; Waters, E.; Khan, Q.; Zhang, X.; Numan, M. *Endocrinology* **2011**, *152*, 1209; (c) Ribeiro, J. R.; Freiman, R. N. *J. Steroid Biochem. Mol. Biol.* **2014**, *143*, 160.
- Kuiper, G. G. J. M.; Enmark, E.; Peltö-Huikko, M.; Nilsson, S.; Gustafsson, J.-A. *Proc. Natl. Acad. Sci. U.S.A.* **1996**, *93*, 5925.
- Matthews, J.; Gustafsson, J.-A. *Mol. Interv.* **2003**, *3*, 281.
- Piu, F.; Cheevers, C.; Hyldtoft, L.; Gardell, L. R.; Del Tredici, A. L.; Andersen, C. B.; Fairbairn, L. C.; Lund, B. W.; Gustafsson, M.; Schiffer, H. H.; Donello, J. E.; Olsson, R.; Gil, D. W.; Brann, M. R. *Eur. J. Pharmacol.* **2008**, *590*, 423.
- Haldosen, L.-A.; Zhao, C.; Dahlman-Wright, K. *Mol. Cell Endocrinol.* **2014**, *382*, 665.
- (a) Pravettoni, A.; Mornati, O.; Martini, P. G. V.; Marino, M.; Colciago, A.; Celloti, F.; Motta, M.; Negri-Cesi, P. *Mol. Cell Endocrinol.* **2007**, *263*, 46; (b) Kim, I. Y.; Kim, B.-C.; Seong, D. H.; Lee, D. K.; Seo, J.-M.; Hong, Y. J.; Kim, H.-T.; Morton, R. A.; Kim, S.-J. *Cancer Res.* **2002**, *62*, 5365.
- George, S.; Petit, G. H.; Gouras, G. K.; Brundin, P.; Olsson, R. *ACS Chem. Neurosci.* **2013**, *4*, 1537.
- (a) Soloway, A. H.; Tjarks, W.; Barnum, B. A.; Rong, F.-G.; Barth, R. F.; Codogni, I. M.; Wilson, J. G. *Chem. Rev.* **1998**, *98*, 1515; (b) Chakrabarti, A.; Hosmane, N. S. *Pure Appl. Chem.* **2012**, *84*, 2299.
- (a) Endo, Y.; Iijima, T.; Yamakoshi, Y.; Yamaguchi, M.; Fukasawa, H.; Shudo, K. *J. Med. Chem.* **1999**, *42*, 1501; (b) Endo, Y.; Iijima, T.; Yamakoshi, Y.; Fukasawa, H.; Miyaura, C.; Inada, M.; Kubo, A.; Itai, A. *Chem. Biol.* **2001**, *8*, 341.
- (a) Yamamoto, K.; Endo, Y. *Bioorg. Med. Chem. Lett.* **2001**, *11*, 2389; (b) Endo, Y.; Yamamoto, K.; Kagechika, H. *Bioorg. Med. Chem. Lett.* **2003**, *13*, 4089; (c) Ogawa, T.; Ohta, K.; Iijima, T.; Suzuki, T.; Ohta, S.; Endo, Y. *Bioorg. Med. Chem.* **2009**, *17*, 1109; (d) Endo, Y.; Yoshimi, T.; Miyaura, C. *Pure Appl. Chem.* **2003**, *75*, 1197.
- (a) Ohta, K.; Ogawa, T.; Kaise, A.; Endo, Y. *Bioorg. Med. Chem. Lett.* **2013**, *23*, 6555; (b) Ohta, K.; Ogawa, T.; Kaise, A.; Oda, A.; Endo, Y. *Chem. Pharm. Bull.* **2014**, *62*, 386.
- (a) Paech, K.; Webb, P.; Kuiper, G. G. J. M.; Nilsson, S.; Gustafsson, J.-A.; Kushner, P. J.; Scanlan, T. S. *Science* **1997**, *277*, 1508; (b) Brzozowski, A. M.; Pike, A. C.; Dauter, Z.; Hubbard, R. E.; Bonn, T.; Engstrom, O.; Ohman, L.; Greene, G. L.; Gustafsson, J.-A.; Carlquist, M. *Nature* **1997**, *389*, 753.
- (a) Wilkening, R. R.; Ratcliffe, R. W.; Tynebor, E. C.; Wildonger, K. J.; Fried, A. K.; Hammond, M. L.; Mosley, R. T.; Fitzgerald, P. M.; Sharma, N.; McKeever, B. M.; Nilsson, S.; Carlquist, M.; Thorsell, A.; Locco, L.; Katz, R.; Frisch, K.; Birzin, E. T.; Wilkinson, H. A.; Mitra, S.; Cai, S.; Hayes, E. C.; Schaeffer, J. M.; Rohrer, S. P. *Bioorg. Med. Chem. Lett.* **2006**, *16*, 3489; (b) Zhao, L.; Brinton, R. D. *Drug Dev. Res.* **2005**, *66*, 103.

15. Sun, W.; Cama, L. D.; Birzin, E. T.; Warriier, S.; Locco, L.; Mosley, R.; Hammond, M. L.; Rohrer, S. P. *Bioorg. Med. Chem. Lett.* **2006**, *16*, 1468.
16. (a) Manas, E. S.; Unwalla, R. J.; Xu, Z. B.; Malamas, M. S.; Miller, C. P.; Harris, H. A.; Hsaio, C.; Akopian, T.; Hum, W.-T.; Malakian, K.; Wolfrom, S.; Bapat, A.; Bhat, R. A.; Stahl, M. L.; Somers, W. S.; Alvarez, J. C. *J. Am. Chem. Soc.* **2004**, *126*, 15106; (b) Malamas, M. S.; Manas, E. S.; McDevitt, R. E.; Gunawan, I.; Xu, Z. B.; Collini, M. D.; Miller, C. P.; Dinh, T.; Henderson, R. A.; Keith, J. C., Jr.; Harris, H. A. *J. Med. Chem.* **2004**, *47*, 5021.
17. Weihua, Z.; Lathe, R.; Warner, M.; Gustafsson, J.-A. *Proc. Natl. Acad. Sci. U.S.A.* **2002**, *99*, 13589.
18. Blizzard, T. E.; Gude, C.; Morgan, J. D., II; Chan, W.; Birzin, E. T.; Mojena, M.; Tudela, C.; Chen, F.; Knecht, K.; Su, Q.; Kraker, B.; Mosley, R. T.; Holmes, M. A.; Sharma, N.; Fitzgerald, P. M. D.; Rohrer, S. P.; Hammond, M. L. *Bioorg. Med. Chem. Lett.* **2006**, *16*, 834.
19. (a) Coult, R.; Fox, M. A.; Gill, W. R.; Herbertson, P. L.; MacBride, J. A. H.; Wade, K. *J. Organomet. Chem.* **1993**, *462*, 19; (b) Ohta, K.; Goto, T.; Endo, Y. *Inorg. Chem.* **2005**, *44*, 8569.
20. Caldwell, J. P.; Matasi, J. J.; Zhang, H.; Fawzi, A.; Tulshian, D. B. *Bioorg. Med. Chem. Lett.* **2007**, *17*, 2281.
21. Hirano, Y.; Kojima, S.; Yamamoto, Y. *J. Org. Chem.* **2011**, *76*, 2123.
22. Compound 8a: Colorless leaflets (AcOEt/n-hexane); mp 183.5–185.0 °C; ¹H NMR (400 MHz, CDCl₃) δ (ppm): 0.90 (m, 2H), 1.09 (m, 2H), 1.40 (tt, J = 2.9 Hz, 12.1 Hz, 1H), 1.50–1.75 (m, 2H), 1.60–3.60 (brm, 10H), 1.80–1.95 (m, 2H), 2.71 (brs, 1H), 3.39 (tt, J = 4.3 Hz, 11.1 Hz, 1H); MS (EI) m/z 242 (M⁺), 57 (100%).
23. Ohta, K.; Chiba, Y.; Ogawa, T.; Endo, Y. *Bioorg. Med. Chem. Lett.* **2008**, *18*, 5050. The ligand-binding activity of ER α and ER β was determined by the nitrocellulose filter binding assay method. ER α and ER β (0.5 μ g/tube) were diluted with a binding assay buffer (20 mM Tris–HCl, pH 8.0, 0.3 M NaCl, 1 mM EDTA, pH 8.0, 10 mM 2-mercaptoethanol, 0.2 mM phenylmethylsulfonyl fluoride) and incubated with 4 nM [6,7-³H]17 β -estradiol in the presence or absence of an unlabeled competitor at 4 °C for 16 h. The incubation mixture was absorbed by suction onto a nitrocellulose membrane that had been soaked in binding assay buffer. The membrane was washed twice with buffer (20 mM Tris–HCl, pH 8.0, 0.3 M NaCl), and then with 25% ethanol in distilled water. Radioactivity that remained on the membrane was measured in Atomlight using a liquid scintillation counter.
24. The 3D structures of human ER α and ER β used in this study were retrieved from the Protein Data Bank (PDB ID: 1ERE and 2IOG, respectively).
25. Jones, G.; Willett, P.; Glen, R. C. *J. Mol. Biol.* **1995**, *245*, 43.



Contents lists available at ScienceDirect

Bioorganic & Medicinal Chemistry Letters

journal homepage: www.elsevier.com/locate/bmcl

Synthesis and biological evaluation of novel *m*-carborane-containing estrogen receptor partial agonists as SERM candidates



Kiminori Ohta, Takumi Ogawa, Asako Kaise, Yasuyuki Endo*

Faculty of Pharmaceutical Sciences, Tohoku Pharmaceutical University, 4-4-1 Komatsushima, Aoba-ku, Sendai 981-8558, Japan

ARTICLE INFO

Article history:

Received 12 May 2015

Revised 25 May 2015

Accepted 27 May 2015

Available online 3 June 2015

Keywords:

Carborane

Estrogen receptor

Partial agonist

SERM

ABSTRACT

We designed and synthesized novel *m*-carborane-containing selective estrogen receptor modulator (SERM) candidates using previously reported *m*-carborane-containing ER partial agonist **1** as the lead compound. Biological activities were evaluated by means of ER α competitive binding assay and MCF-7 cell proliferation assay. Re-positioning the *N,N*-dimethylaminoethoxy group at the *para* position of **1** to the *meta* position enhanced the ER α -binding affinity, and **4c** showed the highest relative binding affinity (RBA: 83 vs 17 β -estradiol = 100) among the tested compounds. Compound **4b** showed the most potent ER-agonist activity (EC₅₀: 1.4 nM) and the lowest maximal efficacy (*E*_{max}: 50%) in MCF-7 cell proliferation assay. Inhibition of 0.1 nM 17 β -estradiol-induced MCF-7 cell proliferation by **4b** (IC₅₀: 0.4 μ M) was at least 10 times more potent than that of the lead compound **1**.

© 2015 Elsevier Ltd. All rights reserved.

Estrogens are involved in regulation of the female and male reproductive systems, bone metabolism, and the cardiovascular system, as well as the central nervous system, and these activities are expressed through binding to and activation of nuclear estrogen receptor (ER).¹ ER has two subtypes (α and β), which show different patterns of tissue expression and mediate two different signaling pathways: transcriptional regulation and non-genomic membrane-associated transduction.¹ Many of the physiological effects of ER are subtype-specific. Non-steroidal and non-hormonal ER antagonists, such as tamoxifen² and raloxifene,³ are widely used for treatment of breast cancer (Fig. 1). Tamoxifen and its active metabolite, 4-hydroxytamoxifen, show ER agonism in endometrium and bone, whereas raloxifene acts as an antagonist in endothelium and as an agonist in bone.⁴ Therefore, raloxifene has no risk for cancer of the female reproductive system, and is used as a protective agent against osteoporosis in post-menopausal women.⁵ Compounds having tissue-specific ER agonist or antagonist activity are called selective estrogen receptor modulators (SERMs).⁶ They exhibit considerable functional diversity: for example, bazedoxifene contains an alkylamino side chain, which is critical for agonist and antagonist activities of SERMs, but its biological activities are different from those of tamoxifen and raloxifene.⁷ In addition, the binding mode of bazedoxifene to ER α is different from that of 4-hydroxytamoxifen, as evaluated by docking simulation study.⁸ The relative agonist/antagonist activities of SERMs,

including ER partial agonists, seem to be controlled by the overall shape of the ER homodimer formed after ER-ligand binding. Therefore, binding of different ligands to ER can facilitate or impede the interaction of ER homodimer with various co-regulators.⁹ The hydrophobic core structure of SERMs plays an important role in determining their elaborate biological and pharmacokinetic profiles. Therefore, development of ER modulators with novel hydrophobic core structures is expected to afford unique SERMs with distinctive biological properties.

We have developed several ER modulators having a carborane cage as a novel hydrophobic pharmacophore.¹⁰ They exhibit unique estrogen-related biological activities, different from those of the endogenous estrogen 17 β -estradiol (E2), or the above-mentioned SERMs. BE360, an *o*-carborane-containing ER modulator without an alkylamino side chain, showed partial agonist activity in MCF-7 cell proliferation assay, and it increased bone density with no effect on the uterus in ovariectomized mice (Fig. 2).¹¹ That is, BE360 is a carborane-containing SERM. We have also reported that *m*-carborane derivative **1** bearing an alkylamino group acted as a potent ER partial agonist in ER transactivation assays (Fig. 2).¹² However, the maximal efficacy of **1** is not low, and so there is a risk that **1** might induce breast cancer. SAR studies of the alkylamino chain of *m*-carborane derivative **2** revealed that compounds with an alkyl, carbamate, or thiocarbamate group instead of the alkylamino group acted as ER full agonists.¹³ Thus, the alkylamino group of **1** is essential for expression of ER partial agonist activity, as has been observed with other SERM candidates (Fig. 2).¹⁴ Recently, we have reported that the

* Corresponding author. Tel.: +81 22 727 0142; fax: +81 22 275 2013.

E-mail address: yendo@tohoku-pharm.ac.jp (Y. Endo).

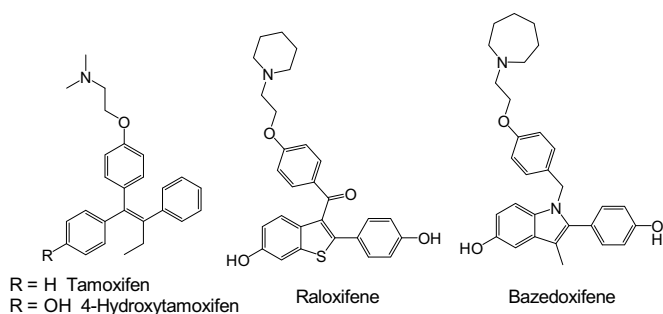


Figure 1. Structures of clinically used SERMs.

9,10-dimethyl-*m*-carborane cage is effective for obtaining ER partial agonist activity with very low maximal efficacy, as well as for increasing ER-binding affinity (compound **3**, Fig. 2).¹⁵ This may be due to a geometry change of the alkylamino group remotely induced by steric repulsion between the bulky hydrophobic structure and amino acid residues surrounding the ER ligand-binding domain (LBD). Although the 9,10-dimethyl-*m*-carborane cage of **3** seems to be more promising as a hydrophobic structure for ER partial agonist discovery than *m*-carborane, preparation of 1,7-diaryl-9,10-dimethyl-*m*-carborane derivatives is synthetically difficult in that coupling reaction of 9,10-dimethyl-*m*-carborane with aryl iodides affords the products in very low yield.

Therefore, we selected the *m*-carborane cage as a hydrophobic structure for the preparation of ER partial agonists and designed derivatives **4** in which the alkylamino side chain of **1** is transferred to a neighboring carbon (Fig. 3).

Scheme 1 summarizes the synthesis of *m*-carborane-containing ER partial agonist candidates **4**. *m*-Carborane **5** was treated with *n*-BuLi, and then transformed into C-copper-*p*-carborane, which was reacted with 4-iodoanisole in the presence of pyridine as a ligand of copper to afford 4-methoxyphenyl-*m*-carborane **6** in 71% yield.¹⁶ Next, coupling reaction of **6** with TBS-protected iodophenol under the same conditions, followed by deprotection of the TBS group, afforded key intermediate diaryl-*m*-carborane **7** in 71% yield. Dimethylaminoethyl and dimethylaminopropyl groups were introduced into **7** by using the corresponding alkyl halides in 33% and 24% yields, respectively. Demethylation of **8** with BBr₃ afforded the desired compounds **4a** and **4b** in 45% and 74% yields, respectively. Compound **7** was reacted with BBr₃ to afford bisphenol **9**

in 94% yield; its biological activity was evaluated and compared with that of bisphenol **12**, an intermediate of **1** (Scheme 1). Compound **4c** was obtained by stepwise synthesis involving two S_N2 reactions of dibromobutane. One bromine atom was changed to a phenolic hydroxyl group (**7**) in 62% yield, and the other was reacted with dimethylamine to afford **11** in 78% yield. Demethylation of **11** with BBr₃ afforded **4c** in 34% yield.

ER-binding affinity was evaluated by means of competitive binding assay using human recombinant ERα and [6,7-³H] 17β-estradiol. Relative binding affinity (RBA) values of the test compounds are summarized in Table 1.¹⁷ Compounds **1** and **12** showed low and high RBA values of 1.5 and 110, respectively, which are close to the previously reported values of 1.1 and 106, respectively.¹² Although the binding affinity of the parent bisphenol **9** is similar to that of **12**, compound **4a** with an *N,N*-dimethylaminoethoxy side chain showed 5 times more potent ERα-binding than the corresponding *p*-substituted derivative **1**. Our previous results showed that extension of the alkylamino chain of **1** has little influence on RBA values, but the same modification of the alkylamino chain of **4** led to a remarkable enhancement of RBA value, and the RBA of **4c** was 83.¹⁸ These results suggest that an alkylamino side chain at the *meta* position fits well into the cavity of the ERα LBD, and the terminal tertiary amino group of **4c** forms hydrogen bonds with amino acid residues of the ERα LBD.

Next, the functional activities of the test compounds were evaluated by means of cell proliferation assays using MCF-7 cell lines that show ER-dependent growth.¹⁷ Table 2 summarizes EC₅₀ and IC₅₀ values as parameters of the agonist and antagonist activities of the test compounds, respectively. Agonist activity is also shown as relative maximal efficacy (*E*_{max}), based on estradiol as 100%. Bisphenol **9** showed similar EC₅₀ and *E*_{max} values to **12**. Both bisphenols showed no ER-antagonist activity and acted as ER full agonists, not as side-chainless partial agonists like BE360. The lead compound **1** showed moderate agonist activity and its *E*_{max} value was 78%, which means it has lower maximal efficacy than E2. Compound **1** antagonized MCF-7 cell proliferation induced by 0.1 nM of E2 with an IC₅₀ value of 4.4 μM. Compound **4a**, which has the same side chain as the lead compound **1**, but at the *meta* position, showed potent ER agonist activity (EC₅₀ = 4.7 nM) and a low *E*_{max} value of 63%. The IC₅₀ value of **4a** was 6.5 μM, which is similar to that of **1**. Compound **4b** with a dimethylaminopropyl group showed the lowest EC₅₀ value and the lowest *E*_{max} value among the tested compounds. In addition, compound **4b** showed 10 times more potent ER antagonist activity than the lead compound **1**. Although dimethylaminobutyl derivative **4c** showed the greatest ERα-binding affinity, its biological activities parameters, EC₅₀, *E*_{max}, and IC₅₀, are similar to those of compound **4a**. These results confirm that the dimethylaminopropyl group is the most suitable ER partial agonist activity-inducing substituent in the series of *m*-carborane-containing *m*-substituted derivatives **4**. The ER-antagonist activity of **4b** was more potent than that of **3**, which contains the 9,12-dimethyl-*m*-carborane cage (IC₅₀ of **3** = 0.88 μM). The low IC₅₀ value of **4b** suggested that the side chain serves to inhibit binding of co-activators by moving helix-12 of ER to an unfavorable position. However, compound **4b** has a higher

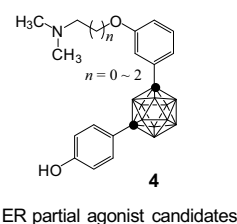


Figure 3. Structures of novel ER partial agonist candidates **4**.

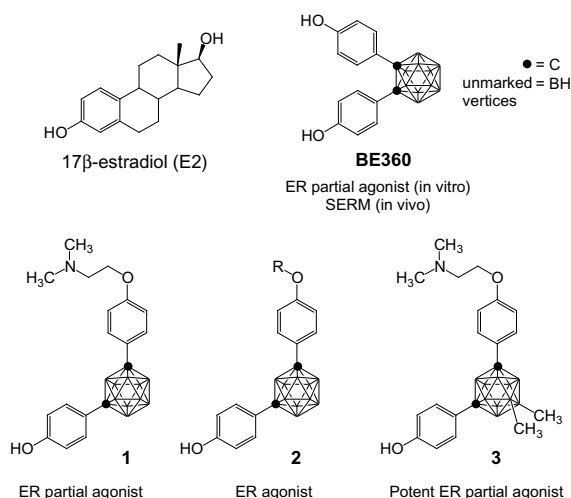
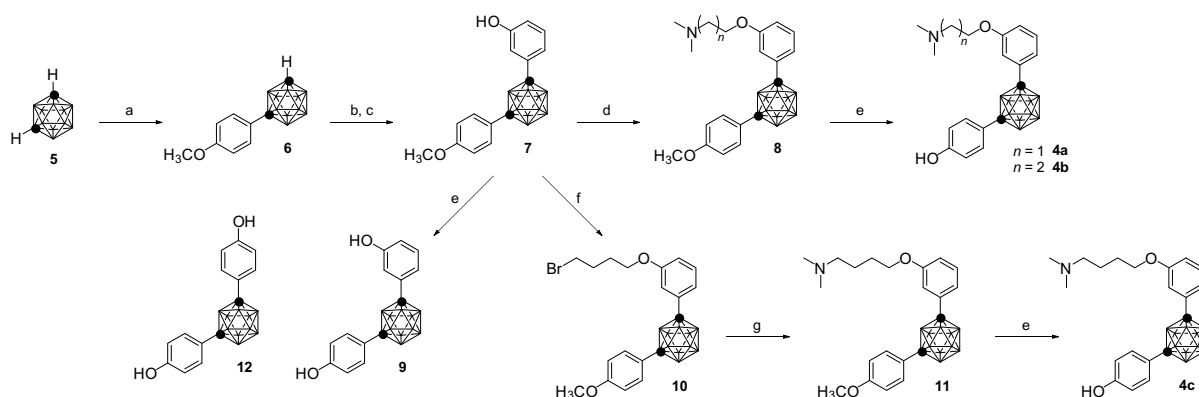


Figure 2. Structures of 17β-estradiol (E2) and *m*-carborane-containing ER modulators.



Scheme 1. Synthesis of novel ER modulators **4**. Reagents and conditions: (a) *n*-BuLi, DME, then CuCl, pyridine, 4-iodoanisole, 71%; (b) *n*-BuLi, DME, then CuCl, pyridine, 3-*tert*-butyldimethylsiloxyiodobenzene; (c) TBAF, THF, 71% over 2 steps; (d) *N,N*-dimethylaminoalkyl chloride, K₂CO₃, acetone, 24–38%; (e) BBr₃, CH₂Cl₂, 34–94%; (f) 1,4-dibromobutane, K₂CO₃, acetone, 62%; (g) dimethylamine, THF, 78%.

Table 1

Relative binding affinity (RBA) of test compounds versus specific [³H]estradiol (4 nM) binding with human recombinant ER α

Compound	Position	Substituent	RBA ^a
1	<i>p</i> -	–O–(CH ₂) ₂ –N(CH ₃) ₂	1.5
4a	<i>m</i> -	–O–(CH ₂) ₂ –N(CH ₃) ₂	7.4
4b	<i>m</i> -	–O–(CH ₂) ₃ –N(CH ₃) ₂	8.4
4c	<i>m</i> -	–O–(CH ₂) ₄ –N(CH ₃) ₂	83
9	<i>m</i> -	–OH	131
12	<i>p</i> -	–OH	110

^a All binding assay were treated with the test compounds (0.4 nM to 4 μ M) in the presence of [6,7-³H]17 β -estradiol (4 nM). The relative binding affinity is calculated from IC₅₀ values of E2 and test compounds taking that of E2 as 100%. Values represent the average of duplicate experiments.

*E*_{max} value than compound **3** (*E*_{max} of **3** = 23%), and might show moderate estrogenic activity in breast tissue. A terminal cyclic alkylamino group, such as piperidine or azepane (used in raloxifene and bazedoxifene, respectively), can often enhance ER-antagonist activity, and thus introduction of these substituents might afford better partial agonists or SERM candidates. Carborane cages are promising hydrophobic core structure for the development of ER modulators,^{10–13,15,17} and carborane-containing ER modulators may show unique biological properties.

Table 2

Biological activities of the test compounds on MCF-7 cell proliferation

Compound	Position	Substituent	EC ₅₀ ^a (nM)	<i>E</i> _{max} ^b (%)	IC ₅₀ ^c (μ M)
1	<i>p</i> -	–O–(CH ₂) ₂ –N(CH ₃) ₂	8.2	78	4.4
4a	<i>m</i> -	–O–(CH ₂) ₂ –N(CH ₃) ₂	4.7	63	6.5
4b	<i>m</i> -	–O–(CH ₂) ₃ –N(CH ₃) ₂	1.4	50	0.4
4c	<i>m</i> -	–O–(CH ₂) ₄ –N(CH ₃) ₂	2.6	62	4.3
9	<i>m</i> -	–OH	1.8	107	Inactive
12	<i>p</i> -	–OH	1.4	90	Inactive

^a MCF-7 cells were treated with the test compounds (1 \times 10^{–13} to 1 \times 10^{–5} M) alone. EC₅₀ values were estimated from the sigmoidal dose-response curves using GraphPad Prism software.

^b *E*_{max} values indicate efficacy for cell proliferation, based on the value for E2 taken as 100%.

^c MCF-7 cells were treated with the test compounds (1 \times 10^{–11} to 1 \times 10^{–5} M) in the presence of 0.1 nM E2. IC₅₀ values were estimated from the sigmoidal dose-response curves for competitive antagonism against cell proliferation activity induced by 0.1 nM E2, using GraphPad Prism software.

Novel ER modulator **3** showed better partial agonist activity than **1**, even though it contains the same alkylamino chain and has the same substitution position.¹⁵ Further syntheses of a series of diaryl-*m*-carborane derivatives, docking simulation studies, and biological investigations with other ER-expressing tissues, determination of ER expression levels, and examination of the influence of 9,12-dimethyl-*m*-carborane structure on ER partial agonist activity, as well as in vivo experiments, are in progress.

In conclusion, novel *m*-carborane-containing ER partial agonists were synthesized and their biological activities were evaluated by means of competitive ER binding assay and MCF-7 cell proliferation assay. All tested compounds **4** showed higher RBA values than the corresponding *para*-substituted derivatives, suggesting that an alkylamino side chain at the *meta* position fits well into the cavity of the ER α LBD. Compound **4b** showed the most potent ER-agonist activity and the lowest *E*_{max} value among the tested compounds. Moreover, the ER-antagonist activity of **4b** was 10 times more potent than that of the lead compound **1**. As observed in the case of bazedoxifene, the unique hydrophobic carborane cage structure provide an entry into carborane-containing ER modulators with various characteristics of ER up- or down-regulation, as well as distinctive pharmacokinetic properties. These findings should be helpful for molecular design of further carborane-containing ER modulators, including agonists, partial agonists, antagonists, and SERMs as biological tools or candidate therapeutic agents for ER-related diseases.

Acknowledgments

This research was supported by a Grant-in-Aid for the Strategic Research Program for Private University (2010–2014) and a Grant-in-Aid for Scientific Research (C) (No. 26460151) from the Ministry of Education, Culture, Sports, Science, and Technology, Japan.

References and notes

- There are several hundred reviews about estrogen receptors and their functions. For example: (a) Katzenellenbogen, B. S.; Choi, I.; Delage-Mourroux, R.; Ediger, T. R.; Martini, P. G. V.; Montano, M.; Sun, J.; Weis, K.; Katzenellenbogen, J. A. *J. Steroid Biochem. Mol. Biol.* **2000**, *74*, 279; (b) Lanyon, L.; Armstrong, V.; Ong, D.; Zaman, G.; Price, J. *J. Endocrinol.* **2004**, *182*, 183; (c) Pfaff, D.; Waters, E.; Khan, Q.; Zhang, X.; Numan, M. *Endocrinology* **2011**, *152*, 1209.
- (a) Powles, T.; Hickish, T.; Kanis, J. A.; Tidy, A.; Ashley, S. *J. Clin. Oncol.* **1996**, *14*, 78; (b) O'Regan, R. M.; Jordan, V. C. *Semin. Oncol.* **2001**, *28*, 260; (c) Maximov, P. Y.; Lee, T. M.; Jordan, V. C. *Curr. Clin. Pharmacol.* **2013**, *8*, 135.
- (a) Clemens, J. A.; Bennett, D. R.; Black, L. J.; Jones, C. D. *Life Sci.* **1983**, *32*, 2869; (b) Clemens, J. A.; Spencer, C. M. *Drugs* **2000**, *60*, 379.
- (a) Black, L. J.; Sato, M.; Rowley, E. R.; Magee, D. E.; Bekele, A.; Williams, D. C.; Cullinan, G. J.; Bendele, R.; Kauffman, R. F.; Bensch, W. R.; Frolik, C. A.; Termine,

- J. D.; Bryant, H. U. *J. Clin. Invest.* **1994**, 93, 63; (b) Turner, C. H.; Sato, M.; Bryant, H. U. *Endocrinology* **2001**, 1994, 135.
5. Silverman, S.; Christiansen, C. *Osteoporos. Int.* **2012**, 23, 797.
 6. (a) Fernand, L.; Claude, L.; Alain, B.; Jacques, S. In *Selective Estrogen Receptor Modulators*; Andrea, M., Michael, V., Eds.; Humana Press, 2002; (b) Komm, B. S.; Mirkin, S. *J. Steroid Biochem. Mol. Biol.* **2014**, 143, 207.
 7. Komm, B. S.; Kharode, Y. P.; Bodine, P. V.; Harris, H. A.; Miller, C. P.; Lyttle, C. R. *Endocrinology* **2005**, 146, 3999.
 8. Lewis-Wambi, J. S.; Kim, H.; Curpan, R.; Grigg, R.; Sarker, M. A.; Jordan, V. C. *Mol. Pharmacol.* **2011**, 80, 610.
 9. Wardell, S. E.; Nelson, E. R.; McDonnell, D. P. *Steroids* **2014**, 90, 30.
 10. (a) Endo, Y.; Iijima, T.; Yamakoshi, Y.; Yamaguchi, M.; Fukasawa, H.; Shudo, K. *J. Med. Chem.* **1999**, 42, 1501; (b) Endo, Y.; Iijima, T.; Yamakoshi, Y.; Fukasawa, H.; Miyaura, C.; Inada, M.; Kubo, A.; Itai, A. *Chem. Biol.* **2001**, 8, 341; (c) Yamamoto, K.; Endo, Y. *Bioorg. Med. Chem. Lett.* **2001**, 11, 2389; (d) Endo, Y.; Yamamoto, K.; Kagechika, H. *Bioorg. Med. Chem. Lett.* **2003**, 13, 4089; (e) Ogawa, T.; Ohta, K.; Iijima, T.; Suzuki, T.; Ohta, S.; Endo, Y. *Bioorg. Med. Chem.* **2009**, 17, 1109; (f) Ohta, K.; Ogawa, T.; Kaise, A.; Endo, Y. *Bioorg. Med. Chem. Lett.* **2013**, 23, 6555.
 11. (a) Endo, Y.; Yoshimi, T.; Miyaura, C. *Pure Appl. Chem.* **2003**, 75, 1197; (b) Hirata, M.; Inada, M.; Matsumoto, C.; Takita, M.; Ogawa, T.; Endo, Y.; Miyaura, C. *Biochem. Biophys. Res. Commun.* **2009**, 380, 218.
 12. Ogawa, T.; Ohta, K.; Yoshimi, T.; Yamazaki, H.; Suzuki, T.; Ohta, S.; Endo, Y. *Bioorg. Med. Chem. Lett.* **2006**, 16, 3943.
 13. Ohta, K.; Ogawa, T.; Suzuki, T.; Ohta, S.; Endo, Y. *Bioorg. Med. Chem.* **2009**, 17, 7958.
 14. Shiau, A. K.; Barstad, D.; Loria, P. M.; Cheng, L.; Kushner, P. J.; Agard, D. A.; Greene, G. L. *Cell* **1998**, 95, 927.
 15. Ohta, K.; Ogawa, T.; Kaise, A.; Endo, Y. *Bioorg. Med. Chem.* **2014**, 22, 3508.
 16. (a) Coult, R.; Fox, M. A.; Gill, W. R.; Herbertson, P. L.; MacBride, J. A. H.; Wade, K. *J. Organomet. Chem.* **1993**, 462, 19; (b) Ohta, K.; Goto, T.; Endo, Y. *Inorg. Chem.* **2005**, 44, 8569.
 17. Ohta, K.; Chiba, Y.; Ogawa, T.; Endo, Y. *Bioorg. Med. Chem. Lett.* **2008**, 18, 5050.
 18. RBA values of the corresponding *m*-carborane-containing *p*-substituted derivatives are as follows: *N,N*-dimethylaminoethyl = 1.1, *N,N*-dimethylaminopropyl = 1.5, and *N,N*-dimethylaminobutyl = 1.7.

研究テーマ 3

難治性疼痛に対する緩和医療法の確立

総 説

μ オピオイド受容体の多様性

溝口 広一

Variability of μ -Opioid Receptors

Hirokazu MIZOGUCHI

Department of Physiology and Anatomy, Faculty of Pharmaceutical Sciences,
Tohoku Medical and Pharmaceutical University.

(Received November 20, 2018)

The μ -opioid receptors are target receptors for narcotic analgesics. Although there is critical variability on their pharmacological effects between narcotic analgesics, only one μ -opioid receptor (MOR-1) DNA has been cloned. After the cloning of MOR-1 cDNA, many exons have been identified in the MOR-1 gene. With many exons in their gene, the MOR-1 has synthesized with a large number of splice variants. In the present review, the splice variants of MOR-1 and the possible physiological functions for specific splice variants have been discussed.

Key words — μ -opioid receptor, splice variants, analgesia, narcotic analgesics, pain

1. はじめに

疼痛は、非常に不快な感覚刺激であると共に、生体に侵害が加えられたことを知らせる重要な警告信号でもある。しかし、持続する強い痛みは苦痛以外の何物でもなく生活の質を著しく低下させることから、鎮痛薬による疼痛緩和が行われる。臨床における疼痛緩和においては、痛みの質や程度により様々な鎮痛薬が使用されており、比較的軽度な疼痛には非ステロイド性消炎鎮痛薬 (NSAID) が、中等度の疼痛には非麻薬性オピオイド鎮痛薬や弱オピオイドの麻薬性鎮痛薬が、ガン性疼痛や術後痛などの重篤な疼痛には強オピオイドの麻薬性鎮痛薬が用いられている。現在日本で用いられている麻薬性鎮痛薬には、morphine, oxycodone, fentanyl, remifentanyl, hydromorphone, methadone, tapentadol など鎮痛活性の非常に強力な強オピオイドと codeine, pethidine など鎮痛活性が比較的低い弱オピオイドが存在し、また、非麻薬性オピオイド鎮痛薬としては、tramadol, buprenorphine, pentazocine などが用いられている。オピオイドの作用するオピオイド受容体は、主に μ オピオイド受容体、 δ オピオイド受容体、 κ オピオイド受容体、ORL-1 (opioid receptor like-1) 受容体の4種のサブタイプに分類されるが、pentazocine 以外の上記オピオ

イド鎮痛薬は共に μ オピオイド受容体の作動薬であり、その鎮痛作用は μ オピオイド受容体を介して発現する。これら μ オピオイド受容体作動薬であるオピオイド鎮痛薬は、その鎮痛作用や鎮咳作用といった主作用および、嘔気・嘔吐、便秘、呼吸抑制、依存性などの副作用において、薬物間で様々な特徴的違いを示す。現在臨床では、オピオイド鎮痛薬間の薬理作用におけるこの相違を逆に利用したオピオイドローテーションが行われている。しかし、同じ μ オピオイド受容体を介して発現する薬理作用に、オピオイド鎮痛薬間で多様な差が生じる原因については、 μ オピオイド受容体の多様性による可能性が一部示唆されているものの、いまだ明確にはなっていない。

2. μ オピオイド受容体

オピオイド受容体は、morphine をはじめとするオピオイドが作用する受容体の総称である。薬物の作用点として受容体の概念が導入されて以来、morphine の作用点としてその存在は想定されていたが、その存在が初めて実験的に実際に確認されたのは1970年代初頭である。1971年から1973年にかけて複数の研究グループが、放射性標識をした各種オピオイドの結合実験を行うことにより、オピオイド受容体の存在を確認した。1971年にGoldsteinら¹⁾は、マウス脳に^[3H]levorphanolの特異的結合部位が存在することを明らかにし、そ

の後1973年に、Snyderら²⁾は $[^3\text{H}]$ naloxoneを、Simonら³⁾は $[^3\text{H}]$ etorphinを、そしてTerenius⁴⁾は $[^3\text{H}]$ dihydromorphineをそれぞれ用い、ラット脳中にその特異的結合部位の存在を明らかにした。彼らが発見した特異的結合部位が、今でいう μ オピオイド受容体であり、morphineの頭文字のMを用いて μ オピオイド受容体と名付けられている。上記放射性標識オピオイドは、 μ オピオイド受容体の他に δ オピオイド受容体や κ オピオイド受容体にも親和性を示すことから、1981年に μ オピオイド受容体に最も選択的な薬物としてDAMGO ($[\text{D-Ala}^2, \text{NMePhe}^4, \text{Gly-ol}^5]$ enkephalin) が合成された⁵⁾ 後は、 $[^3\text{H}]$ DAMGOの特異的結合部位を μ オピオイド受容体とするようになった。この $[^3\text{H}]$ DAMGOを用いた結合実験により、 μ オピオイド受容体は脳や脊髄といった中枢神経系のみならず、心臓、肺、腸管などの末梢神経系にも広範に分布していることが明らかになっている。Morphineなどの μ オピオイド受容体作動薬は、特異的部位に存在する μ オピオイド受容体を刺激することにより、鎮痛作用（脊髄、大脳皮質、視床、中脳水道周囲灰白質）、呼吸抑制作用（孤束核）、腸管運動抑制作用（腸管）、自発運動亢進作用（黒質）、鎮静作用（大脳皮質）、陶酔作用（腹側被蓋野）、心抑制作用（孤束核、心臓）など様々な薬理効果を発現すると考えられている。

μ オピオイド受容体の発見から約10年の時を経て、 μ オピオイド受容体にはサブクラスが存在することが報告された。1980年にPasternakら⁶⁾は、オピオイドペプチドとオピオイドアルカロイドの双方に等しく高い親和性を示す μ オピオイド受容体を μ_1 オピオイド受容体、オピオイドペプチドよりもオピオイドアルカロイドにより高い親和性を示す μ オピオイド受容体を μ_2 オピオイド受容体として、 μ オピオイド受容体を2つのサブクラスに分類した。また彼らは、 μ_1 オピオイド受容体選択的拮抗薬であるnaloxonazineを開発し、⁷⁾ μ_1 オピオイド受容体は上位中枢（脳）鎮痛作用、陶酔作用、acetylcholineやprolactinの放出制御作用、摂食促進作用に、一方、 μ_2 オピオイド受容体は脊髄鎮痛作用、呼吸抑制作用、腸管運動抑制作用に関与することを明らかにしている。⁸⁾ μ_1 オピオイド受容体・ μ_2 オピオイド受容体の理論は、自然発症的に μ_1 オピオイド受容体が著しく減少（ほぼ欠損）しているCXBKマウスにおいても確認されて

いる。⁹⁾ しかし、 μ_1 オピオイド受容体および μ_2 オピオイド受容体に相当する受容体の遺伝子は、いまだ発見されていない。

3. μ オピオイド受容体の遺伝子クローニングとその多様性

1992年にEvansら¹⁰⁾ およびKiefferら¹¹⁾ が δ オピオイド受容体(DOR-1) 遺伝子をクローニングして以来、オピオイド受容体に関する研究においても遺伝子工学の実験手法が多く取り入れられるようになった。DOR-1がクローニングされた翌年1993年には、Yasudaら¹²⁾ により κ オピオイド受容体(KOR-1) 遺伝子が、さらにChenら、¹³⁾ Wangら¹⁴⁾ やFukudaら¹⁵⁾ により μ オピオイド受容体(MOR-1) 遺伝子がクローニングされ、また、1994年にはORL-1受容体(ORL1) 遺伝子がクローニングされた¹⁶⁾ ことにより、現在同定されている4種のオピオイド受容体の構造（アミノ酸配列）が全て明らかとなった。MOR-1は398個のアミノ酸残基からなる受容体であり、DOR-1、KOR-1、ORL1と共にその構造中に7つの細胞膜貫通領域を持つ。細胞膜貫通領域のアミノ酸残基は他のオピオイド受容体と相同性が極めて高く、受容体全体での相同性も約60%と高い。MOR-1は他のオピオイド受容体と同様に、Gi/Go蛋白と共役した受容体であり、その受容体刺激により抑制性のシグナルを発生させることが確認されている。また、クローニングされたMOR-1遺伝子は、4つのエキソン（エキソン1～エキソン4）を含んでおり、エキソン1は細胞外N末端領域と1回目細胞膜貫通領域を、エキソン2は2回目細胞膜貫通領域～4回目細胞膜貫通領域を、エキソン3は5回目細胞膜貫通領域～7回目細胞膜貫通領域を、そしてエキソン4は細胞内C末端領域をそれぞれコードしていることが明らかとなっている。

前述したように、従来 μ オピオイド受容体は、作動薬・拮抗薬に対する感受性の違いから μ_1 オピオイド受容体と μ_2 オピオイド受容体に細分化されていた。しかし、実際に遺伝子が発見され、クローニング・単離・同定が行われた μ オピオイド受容体は、いまだMOR-1のみである。それでは、各種オピオイド鎮痛薬で認められている薬理作用の多様性は、どのようにして発現するのか。その疑問は、MOR-1遺伝子がクローニングされた翌年1994年に、Bareら¹⁷⁾ によりMOR-1のスプライス

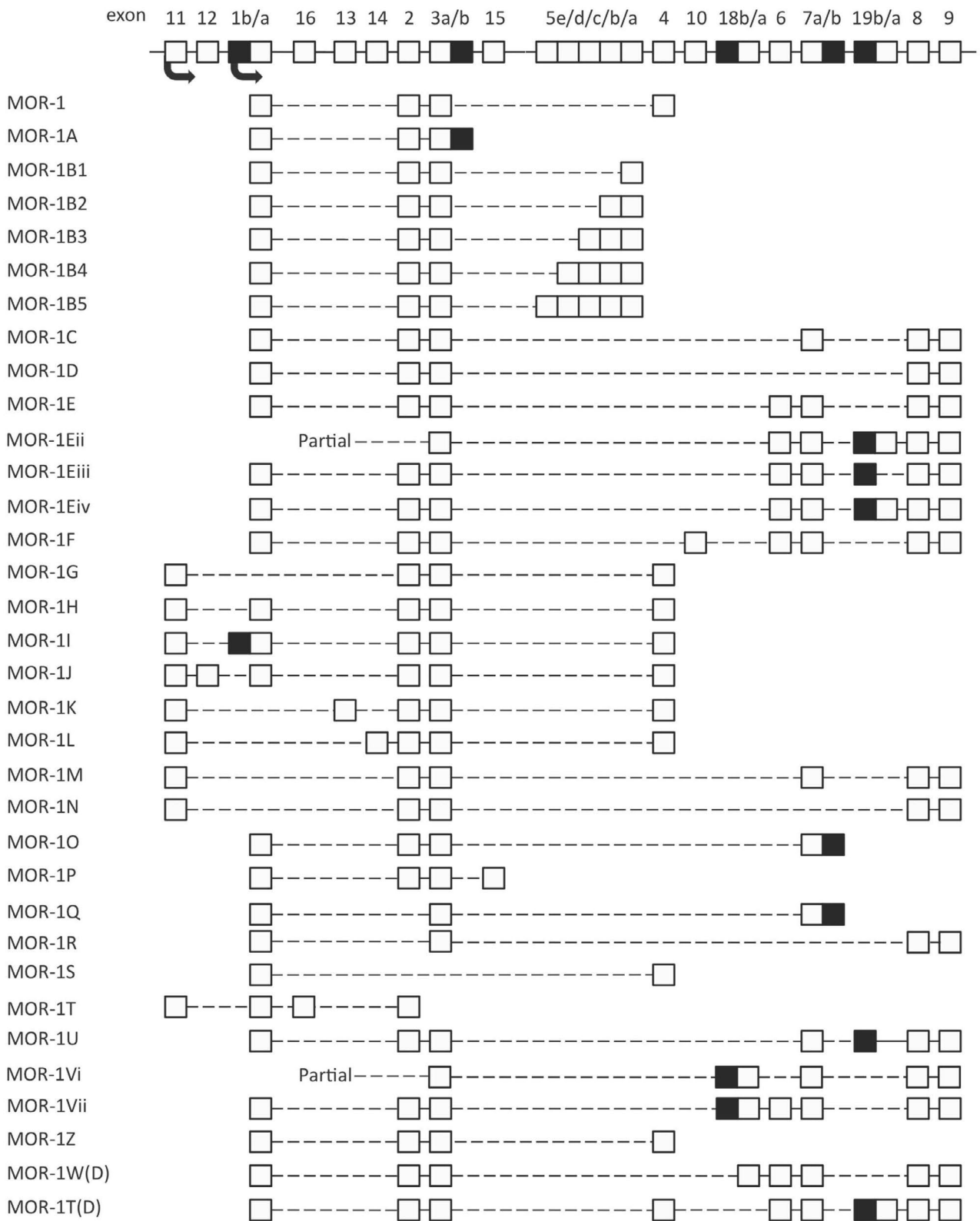


Fig. 1. Schematic of MOR-1 splicing in the mouse.

バリエントとして MOR-1A が発見されたことに端を発し、早急に解決へと向かった。スプライスバリエントとは、遺伝子に複数のエキソンが含まれている場合、遺伝子から転写された mRNA 前駆体

からイントロンが切り落とされて mRNA が産生される際に、エキソンも切り落とされることにより発現する多様性のことである。前述したように、MOR-1 は発見された当初、その遺伝子にエキソン

1~エキソン4の4つのエキソンを含む受容体とされていたが、Bareらはエキソン4相応部分が欠落したスプライスバリエントとしてMOR-1Aを発見した。一方Höhlら¹⁸⁾は、MOR-1の遺伝子中に新しいエキソンとしてエキソン5を発見し、エキソン5を含むスプライスバリエントとしてMOR-1Bを発見した。その後Panら¹⁹⁻²²⁾により、MOR-1の遺伝子中に大量のエキソンが発見され、それらエキソンに関連した大量のMOR-1スプライスバリエントが発見されている。MOR-1のスプライスバリエントは、特にマウスにおいて研究が進んでおり、現在19個のエキソンに基づく34種類のMOR-1スプライスバリエントの存在が報告されている (Fig. 1)。²³⁾ その他にも、配列の一部が発見されただけでその全配列がいまだ確定していない新規MOR-1スプライスバリエントの候補も多数存在しており、現在も新たなエキソンが発見される毎にMOR-1スプライスバリエントの種類も増加している。一方、ラットやヒトにおいてもマウスのMOR-1スプライスバリエントに相当するスプライスバリエントは存在し、現時点でラットでは17種類、ヒトでは20種類のMOR-1スプライスバリエントが報告されている。²³⁾

発見されたMOR-1スプライスバリエントの大部分は、MOR-1と同様に7回細胞膜貫通構造を持つ受容体であるが、一部のMOR-1スプライスバリエントはエキソン1が欠損した6回細胞膜貫通構造を持つ受容体である。一方、エキソン2およびエキソン3が欠損したり、エキソンの途中でストップコドンが存在することにより、結果的に1回細胞膜貫通構造となってしまうMOR-1スプライスバリエントも少数ながら存在する。これら7回細胞膜貫通構造を持たないMOR-1スプライスバリエントが、MOR-1と同様に単量体で機能するか否かに関しては、いまだ明らかになっていない。MOR-1、DOR-1やKOR-1といったオピオイド受容体は、単量体（モノマー）で機能する一方、G蛋白共役型の同種受容体や異種受容体と二量体（ホモダイマーやヘテロダイマー）を形成し、それら二量体は単量体と比較して、薬物の結合特性や受容体としての機能特性が著しく異なることが知られている。^{24,25)} このような二量体は、オピオイド受容体同士だけでなく、 β 受容体など全く異種の受容体との間でも存在する。²⁶⁾ MOR-1の複雑な多様性は、MOR-1スプライスバリエント自身の多様性に加え

て、MOR-1スプライスバリエント同士あるいは種々の受容体との様々な二量体によっても生じているのかもしれない。

4. 各種 MOR-1 スプライスバリエントの生理機能

MOR-1スプライスバリエントの存在が明らかとなってから、既に20年以上経過しているが、その生理機能に関してはいまだほとんど明らかとなっていない。個別のMOR-1スプライスバリエントに選択的な薬物が存在しないことと、各MOR-1スプライスバリエントを個別に機能低下させることが技術的に困難であることが原因である。MOR-1スプライスバリエントは、数種以外のほぼ全てがエキソン2とエキソン3を含んでおり、エキソン1による1回目細胞膜貫通領域ならびに細胞外N末端領域とエキソン4以降のC末端細胞内領域に多様性が存在する。また、大部分のMOR-1スプライスバリエントはエキソン1を含んでおり、morphineを筆頭とした全ての麻薬性鎮痛薬や μ オピオイド受容体作動薬は、このエキソン1を含んだMOR-1スプライスバリエントに選択的である。そのため、エキソン1を含んだMOR-1スプライスバリエントの発現細胞を用いても、既存の麻薬性鎮痛薬や μ オピオイド受容体作動薬の間に際立った選択性の違いは認められない。²⁷⁾ また、エキソン1を含んだMOR-1スプライスバリエントに含まれている各種エキソンは、必ず複数のMOR-1スプライスバリエントに含まれているため、エキソン選択的に個別のMOR-1スプライスバリエントを機能低下させることは不可能であり、また個々のMOR-1スプライスバリエントに対する選択的抗体も存在しない。これらの要因から、MOR-1スプライスバリエントの機能解析は不可能と判断され、その研究は一時下火となっていた。しかし著者らは、エキソン1を含まないMOR-1スプライスバリエント内には、単独のMOR-1スプライスバリエントにしか含まれていない3種類のエキソン（エキソン12、エキソン13、エキソン14）が存在することに着目して研究を行うことにより、3種のMOR-1スプライスバリエント（MOR-1J、MOR-1K、MOR-1L）の生理機能の一端を見いだすことに成功した。これら3種のMOR-1スプライスバリエントは、既存の μ オピオイド受容体作動薬に非感受性の受容体であり、これらMOR-1スプライスバリエントをエキソン選択的に発現抑制しても、既存の

μ オピオイド受容体作動薬の脊髓鎮痛作用は影響を受けない。²⁸⁾ 一方、新規ペプチド性 μ オピオイド受容体作動薬 amidino-TAPA (N ^{α} -amidino-Tyr-D-Arg-Phe- β -Ala) は、既存の μ オピオイド受容体作動薬とは異なり、脊髓で内因性オピオイドペプチド (dynorphin A, dynorphin B, α -neo-endorphin, [Leu⁵]enkephalin) を遊離する作用を持つ²⁹⁾ が、その脊髓鎮痛作用はこれら 3 種の MOR-1 スプライスバリエントをエキソン選択的に発現抑制することにより著しく抑制される。²⁸⁾ 詳細な検討により、amidino-TAPA は脊髓のこれら 3 種の MOR-1 スプライスバリエントを介して鎮痛作用を発現するが、その鎮痛作用には MOR-1J を介した dynorphin A 遊離、MOR-1K を介した dynorphin B 遊離と α -neo-endorphin 遊離、MOR-1L を介した dynorphin A 遊離と [Leu⁵]enkephalin 遊離が関与していることが明らかになっている。³⁰⁾ このように、既存の μ オピオイド受容体作動薬に非感受性の特異的 MOR-1 スプライスバリエントは、エキソン 1 を含有する麻薬性鎮痛薬感受性の MOR-1 スプライスバリエントとは異なる、特異的生理機能を持っているかもしれない。

5. 夢の鎮痛薬を創製するためのターゲット受容体

麻薬性鎮痛薬は、 μ オピオイド受容体を介して強力な鎮痛作用を発現する一方、強い精神依存性を持っており、この精神依存性による乱用が世界的に問題となっている。この麻薬性鎮痛薬の精神依存性は、 μ オピオイド受容体刺激を介して発現する陶酔感により形成される。中脳腹側被蓋野から大脳辺縁系側坐核へ投射している dopamine 神経は、快・不快に関与しており、麻薬性鎮痛薬は、腹側被蓋野の dopamine 神経細胞体を抑制的に制御している γ アミノ酪酸 (GABA) 神経上に存在する μ オピオイド受容体を刺激し、GABA 神経抑制による脱抑制により側坐核での dopamine 遊離を増加させる。³¹⁾ この側坐核での dopamine 遊離増加が陶酔感を惹起し、精神依存性が形成される。一方、側坐核の dopamine 神経終末には dynorphin 神経が投射しており、dopamine 遊離を抑制的に制御している。それ故 κ オピオイド受容体作動薬は、dopamine 遊離抑制による嫌悪作用を引き起こし、また併用することにより μ オピオイド受容体作動薬の陶酔感を打ち消すことが知られている。³¹⁾ この現象を基に、麻薬性鎮痛薬と κ オピオイド受容

体作動薬の併用による「依存性のない夢の鎮痛薬」の開発が試みられたが、当時上梓されていた κ オピオイド受容体作動薬は全て μ オピオイド受容体拮抗作用を持っていたことから、「夢の鎮痛薬」とはならなかった。一方、新規 μ オピオイド受容体作動薬 amidino-TAPA は、前出したように既存の麻薬性鎮痛薬とは異なり、内因性 κ オピオイドペプチド (dynorphin A, dynorphin B, α -neo-endorphin) を遊離する作用を持つ。 μ オピオイド受容体刺激により側坐核での dopamine 遊離を増加させる一方、遊離した内因性 κ オピオイドペプチドが側坐核の κ オピオイド受容体を刺激することによってその遊離増加を打ち消すため、amidino-TAPA は μ オピオイド受容体作動薬であるにもかかわらず、精神依存性を示さないことが明らかとなっている。³²⁾ この内因性 κ オピオイドペプチドの遊離に関わる amidino-TAPA 感受性の MOR-1 スプライスバリエントは、MOR-1J と MOR-1L であり、これら MOR-1 スプライスバリエントは、依存性のない夢の鎮痛薬を開発する上でのターゲットとなり得る受容体と考えられる。

6. おわりに

MOR-1 スプライスバリエントの機能解析は、実質的にはまだ始まったばかりである。しかし数少ない先行研究において、morphine 等の麻薬性鎮痛薬に非感受性の MOR-1 スプライスバリエントは、従来 μ オピオイド受容体で認められていた生理機能とは異なる生理機能に関与していることが示唆されている。MOR-1 スプライスバリエントの機能解析は、臨床応用可能な新たな生理機能の発見につながるかもしれない。

謝辞 本研究を遂行するにあたりご指導を賜りました、機能形態学教室の前教授である櫻田忍客員教授に衷心より御礼申し上げます。また、同教室の渡辺千寿子准教授をはじめご協力いただきました同教室の歴代諸氏に厚く御礼申し上げます。

本論文の文献 28~30 および 32 に関わる研究は、科学研究費補助金基盤研究 C (21600013, 24590731, 15K08678) の助成により行われました。

利益相反

開示すべき利益相反はない。

REFERENCES

- 1) Goldstein A., Lowney L.I., Pal B.K., *Proc. Natl. Acad. Sci. USA*, **68**, 1742–1747 (1971).
- 2) Pert C.B., Snyder S.H., *Science*, **179**, 1011–1014 (1973).
- 3) Simon E.J., Hiller J.M., Edelman I., *Proc. Natl. Acad. Sci. USA*, **70**, 1947–1949 (1973).
- 4) Terenius L., *Acta Pharmacol. Toxicol. (Copenh)*, **32**, 317–320 (1973).
- 5) Handa B.K., Land A.C., Lord J.A., Morgan B.A., Rance M.J., Smith C.F., *Eur. J. Pharmacol.*, **70**, 531–540 (1981).
- 6) Pasternak G.W., Childers S.R., Snyder S.H., *Science*, **208**, 514–516 (1980).
- 7) Pasternak G.W., Childers S.R., Snyder S.H., *J. Pharmacol. Exp. Ther.*, **214**, 455–462 (1980).
- 8) Pasternak G.W., Wood P.J., *Life Sci.*, **38**, 1889–1898 (1986).
- 9) Moskowitz A.S., Goodman R.R., *Brain Res.*, **360**, 108–116 (1985).
- 10) Evans C.J., Keith D.E. Jr., Morrison H., Magendzo K., Edwards R.H., *Science*, **258**, 1952–1955 (1992).
- 11) Kieffer B.L., Befort K., Gaveriaux-Ruff C., Hirth C.G., *Proc. Natl. Acad. Sci. USA*, **89**, 12048–12052 (1992).
- 12) Yasuda K., Raynor K., Kong H., Breder C.D., Takeda J., Reisine T., Bell G.I., *Proc. Natl. Acad. Sci. USA*, **90**, 6736–6740 (1993).
- 13) Chen Y., Mestek A., Liu J., Hurley J.A., Yu L., *Mol. Pharmacol.*, **44**, 8–12 (1993).
- 14) Wang J.B., Imai Y., Eppler C.M., Gregor P., Spivak C.E., Uhl G.R., *Proc. Natl. Acad. Sci. USA*, **90**, 10230–10234 (1993).
- 15) Fukuda K., Kato S., Mori K., Nishi M., Takeshima H., *FEBS Lett.*, **327**, 311–314 (1993).
- 16) Mollereau C., Parmentier M., Mailleux P., Butour J.L., Moisand C., Chalon P., Caput D., Vassart G., Meunier J.C., *FEBS Lett.*, **341**, 33–38 (1994).
- 17) Bare L.A., Mansson E., Yang D., *FEBS Lett.*, **354**, 213–216 (1994).
- 18) Zimprich A., Simon T., Höllt V., *FEBS Lett.*, **359**, 142–146 (1995).
- 19) Pan Y.X., Xu J., Bolan E., Abbadie C., Chang A., Zuckerman A., Rossi G., Pasternak G.W., *Mol. Pharmacol.*, **56**, 396–403 (1999).
- 20) Pan Y.X., Xu J., Bolan E., Chang A., Mahurter L., Rossi G., Pasternak G.W., *FEBS Lett.*, **466**, 337–340 (2000).
- 21) Pan Y.X., Xu J., Mahurter L., Bolan E., Xu M., Pasternak G.W., *Proc. Natl. Acad. Sci. USA*, **98**, 14084–14089 (2001).
- 22) Pan Y.X., Xu J., Bolan E., Moskowitz H.S., Xu M., Pasternak G.W., *Mol. Pharmacol.*, **68**, 866–875 (2005).
- 23) Pasternak G.W., Pan Y.X., *Pharmacol. Rev.*, **65**, 1257–1317 (2013).
- 24) Cvejic S., Devi L.A., *J. Biol. Chem.*, **272**, 26959–26964 (1997).
- 25) Gomes I., Jordan B.A., Gupta A., Trapaidze N., Nagy V., Devi L.A., *J. Neurosci.*, **20**, RC110 (2000).
- 26) Jordan B.A., Trapaidze N., Gomes I., Nivarthi R., Devi L.A., *Proc. Natl. Acad. Sci. USA*, **98**, 343–348 (2001).
- 27) Pasternak G.W., *Neuropharmacology*, **47**, 312–323 (2004).
- 28) Mizoguchi H., Watanabe C., Higashiya T., Takeda S., Moriyama K., Yonezawa A., Sato T., Komatsu T., Sakurada T., Sakurada S., *Eur. J. Pharmacol.*, **651**, 66–72 (2011).
- 29) Mizoguchi H., Watanabe C., Watanabe H., Moriyama K., Sato B., Ohwada K., Yonezawa A., Sakurada T., Sakurada S., *Eur. J. Pharmacol.*, **560**, 150–159 (2007).
- 30) Mizoguchi H., Watanabe C., Higashiya T., Takeda S., Moriyama K., Aoki Y., Kon-no T., Takagi H., Yonezawa A., Sato T., Sakurada T., Sakurada S., *Eur. J. Pharmacol.*, **711**, 80–86 (2013).
- 31) Herz A., Spanagel R., “The Pharmacology of Opioid Peptides,” ed. by Tseng L.F., Harwood Academic Publishers GmbH, Singapore, 1995, pp.445-462
- 32) Mizoguchi H., Watanabe C., Osada S., Yoshioka M., Aoki Y., Natsui S., Yonezawa A., Kanno S., Ishikawa M., Sakurada T., Sakurada S., *Psychopharmacology (Berl)*, **212**, 215–225 (2010).



Antinociceptive effect of inhalation of the essential oil of bergamot in mice

Damiana Scuteri^a, Michele Crudo^a, Laura Rombolà^a, Chizuko Watanabe^b, Hirokazu Mizoguchi^b, Shinobu Sakurada^b, Tsukasa Sakurada^c, Rosaria Greco^d, Maria Tiziana Corasaniti^e, Luigi Antonio Morrone^a, Giacinto Bagetta^{a,*}

^a Preclinical and Translational Pharmacology, Department of Pharmacy, Health Science and Nutrition, University of Calabria, 87036 Rende, CS, Italy

^b Department of Physiology and Anatomy, Faculty of Pharmaceutical Sciences, Tohoku Medical and Pharmaceutical University, 4-4-1 Komatsushima, Aoba-ku, Sendai 981-8558, Japan

^c Daiichi College of Pharmaceutical Sciences - First Department of Pharmacology Fukuoka, Japan

^d Laboratory of Neurophysiology of Integrative Autonomic Systems, Headache Science Centre, IRCCS Mondino Foundation, Pavia, Italy

^e Department of Health Sciences, University "Magna Graecia" of Catanzaro, Catanzaro, Italy

ARTICLE INFO

Keywords:

Aromatherapy
Bergamot essential oil
Pain
Inhalatory route
BPSDs

ABSTRACT

Bergamot essential oil (BEO) has proven wide evidence of pharmacological antinociceptive effectiveness both in nociceptive and in neuropathic pain models. The antinociceptive properties of BEO for inhalation have not been investigated. The purpose of this study is to evaluate the effects of the inhalation of BEO on formalin-induced nociceptive response in mice.

Male ddY-strain mice (Japan SLC, Hamamatsu, Japan) of 23–25 g of weight at the time the experiments underwent the formalin test. Twenty μ l of formalin (2% in saline) were administered into the plantar surface of the mice hindpaw and the time of licking/biting was observed and recorded at intervals of 5 min. The device for BEO inhalatory delivery consisted in a filter paper disc soaked with known volume of BEO placed on the edge of the cage.

Inhalation of BEO exerted antinociceptive activity. In particular, it reduced the formalin-induced licking/biting behaviour in a manner that was dependent on the volume of BEO used in the device for its release and on the time of exposure to the phytocomplex.

The results support the use of BEO in aromatherapy for complementary management of chronic pain relief in a stepwise therapeutic programme.

1. Introduction

According to the Farmacopea Ufficiale Italiana (1991) bergamot essential oil (BEO) is obtained by cold pressing of the epicarp and, partly, of the mesocarp of the fresh fruit of bergamot (*Citrus bergamia* Risso et Poiteau). BEO comprises a volatile fraction (93–96% of total) containing monoterpene and sesquiterpene hydrocarbons (such as limonene) and oxygenated derivatives (such as linalool) and a non-volatile fraction (4–7% of total) containing waxes, polymethoxylated flavones, coumarins and psoralens such as bergapten (5-methoxypsoralen) and bergamottine (5-geranyloxypsoralen) [1, 2]. The most abundant compounds found in the volatile fraction are the monoterpene hydrocarbons limonene, γ -terpinene, and β -pinene, the monoterpene alcohol, linalool, and the monoterpene ester, linalyl acetate, which altogether constitute > 90% of the whole oil [3–5]. The

nonvolatile residue is a natural odor fixative which influences the olfactory properties of the oil; however, it contains about 0.2% bergapten which is responsible for the phototoxicity of BEO [6, 7]. Therefore, a bergapten-free extract of the essence (BEO-BF) together with a natural essence deprived of the hydrocarbon fraction and of bergapten (BEO-HF/BF) are prepared by extractive industries for perfumery and cosmetic uses. Recently, this essential oil has been rigorously studied and some pharmacological activities of the utmost importance have been deciphered. In particular, strong evidence has been gathered for BEO to be endowed with analgesic activity, both in nociceptive and in neuropathic pain models (see [8]). In fact, intraplantar (i.pl.) BEO, or its components linalool and linalyl acetate, reduced the nociceptive response as assayed by the capsaicin test [9]. The latter antinociceptive effects were antagonized by the ipsilateral i.pl. injection of naloxone hydrochloride and by intraperitoneal (i.p.) naloxone methiodide, an

Abbreviations: BPSDs, Behavioural and psychological symptoms of dementia; BEO, Bergamot Essential Oil; BEO-BF, Bergapten-free extract of the essence; BEO-HF/BF, Essence deprived of the hydrocarbon fraction and of bergapten; i.p., Intraperitoneal; i.pl., Intraplantar; i.t., Intrathecal; PSNL, Partial Sciatic Nerve Ligation

* Corresponding author.

E-mail address: g.bagetta@unical.it (G. Bagetta).

<https://doi.org/10.1016/j.fitote.2018.06.007>

Received 14 May 2018; Received in revised form 9 June 2018; Accepted 11 June 2018

Available online 12 June 2018

0367-326X/ © 2018 Published by Elsevier B.V.

antagonist acting at the peripheral opioid receptors; morphine-induced antinociception after i.p. and intrathecal (i.t.) injections was markedly enhanced by the combined injection of i.pl. BEO or linalool, its main oxygenated monoterpene [9]. Interestingly, for i.pl. injection BEO or linalool reduced partial sciatic nerve ligation (PSNL)-induced neuropathic pain symptoms in mice and inhibition of spinal ERK phosphorylation seems to be involved in this anti-allodynic effect [10]. These same Authors [9] have shown that BEO or linalool modulate morphine-induced anti-allodynic effect under neuropathic pain, a condition known to be resistant to opioid treatment (see [11]). More recently, for i.pl. injection BEO and linalool have been reported to reduce behavioural signs of formalin-induced nociception in a dose-dependent manner. The formalin test is characterized by formalin-induced biphasic nociceptive behaviour of licking/biting, with the early nociceptive phase being followed by a late, second, phase that involves peripheral inflammation and central sensitization (see [12]). Due to the lack of relevant information about the effects of the inhalation of BEO on nociceptive behaviour, the purpose of this study was to investigate the antinociceptive action of BEO via the inhalatory route of administration. Indeed, according to the literature, BEO inhalation was found to produce anxiolytic-like behaviour [13], but there are no data available about its effect on nociception and this may be relevant to the use of BEO in aromatherapy.

2. Materials and methods

2.1. Animals

For the study, male ddY-strain mice (Japan SLC, Hamamatsu, Japan) of 23–25 g of weight at the time of these experiments were used. Mice were individually housed in a colony maintained in a controlled environment (12 h light/dark cycle, room temperature 23 °C, 50–60% relative humidity), with food and water *ad libitum*. All of the experiments were performed in agreement with the Guidelines on Ethical Standards for Investigation of Experimental Pain in Animals and approved by the Committee of Animal Care and Use of Tohoku Medical and Pharmaceutical University, for minimizing animal suffering and to use only the number of animals necessary to produce reliable results.

2.2. Experimental protocol for BEO administration via inhalatory route

The habituation of mice was carried out in a transparent cage (22.0 cm × 15.0 cm × 12.5 cm), that also served as observation chamber. Another plexiglass cage was turned upside down and placed over the first cage, in order to avoid any leaks of BEO. A filter paper dry disc (control) or soaked with different volumes of BEO according to the experiment (100, 200, 400, 800 µl) was applied on the edge of the cage 5 min before placing the mice in the observation chamber, so that it was saturated with BEO. Mice were divided into three experimental groups (post-inhalation, pre-inhalation and double-inhalation). In the post-inhalation group the inhalation of BEO was carried out immediately after the i.pl. injection of formalin and for the whole duration of the formalin test. In the pre-inhalation group the inhalation of BEO was carried out as pre-treatment for 1 h, during the mice habituation, at the end of which BEO-releasing filter paper was removed and the formalin test was performed. In the double-inhalation group the inhalation of BEO was carried out both as pre-treatment for 1 h during the habituation and immediately after formalin administration for the whole duration of the formalin test, in order to assess the total effects of these two different options of delivery of BEO.

2.3. Formalin test

After 1 h of habituation 20 µl of formalin (2% in saline) were i.pl. administered to the mice, using a microsyringe with 26-gauge needle. The time of licking/biting was recorded with a handheld stop-watch at

intervals of 5 min: during the early phase, beginning immediately after formalin administration and lasting for 10 min (0–10 min), and during the late phase, starting 10 min after formalin injection and lasting for 20 min (10–30 min).

2.4. BEO composition

BEO was obtained from “Capua Company1880 S.r.l.,” Campo Calabro, Reggio Calabria (Italy). According to chromatographic analysis provided in the certificate of analysis, this batch of BEO contains: α -limonene (39.60%), linalyl acetate (31.09%), linalool (9.55%).

2.5. Statistical analysis

The results are presented as mean \pm s.e.m. duration (seconds) of nociceptive response and evaluated statistically for differences by ANOVA followed by Bonferroni's test and considered significant when $p < 0.05$.

3. Results

3.1. Effect of BEO inhalation as post-treatment on formalin test evoked licking/biting

In the post-inhalation group (see treatment scheme in Fig. 1 a) the filter paper disc, applied on the edge of the cage, was soaked with 200, 400 or 800 µl of BEO and the mice were subjected to BEO inhalation from the time of formalin injection for the following 30 min, during which the formalin test was carried out. Under these experimental conditions, BEO did not show significant effects on the early phase (0–10 min) (Fig. 2). However, administration of 400 and 800 µl of BEO significantly reduced the time of licking/biting in the late phase (10–30 min) in a dose-dependent manner (Fig. 2).

3.2. Effect of BEO inhalation as pre-treatment on licking/biting

Mice were subjected to the inhalation of BEO (filter paper disc soaked with 200, 400 or 800 µl) for the whole habituation period of 1 h (see treatment scheme in Fig. 1 b) but not during the formalin test.

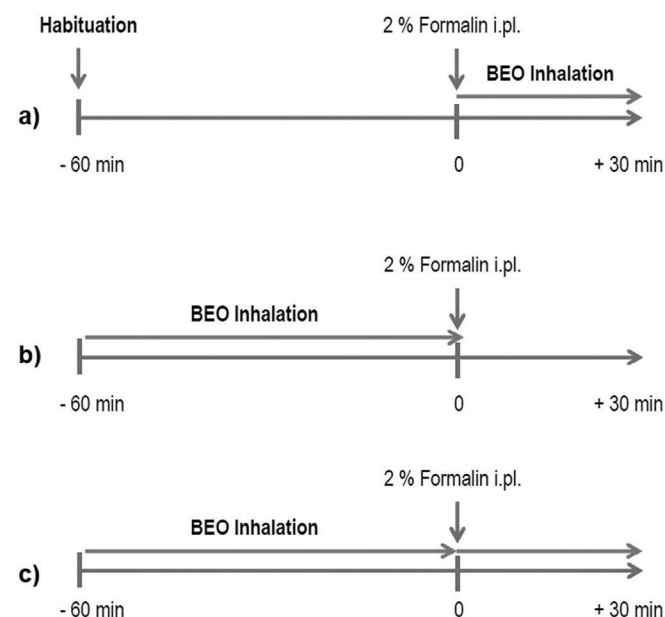


Fig. 1. BEO inhalation scheme. Schematic representation of the administration scheme of BEO as: a) post-inhalation, b) pre-inhalation and c) double-inhalation in relation to formalin intraplantar (i.pl.) administration.

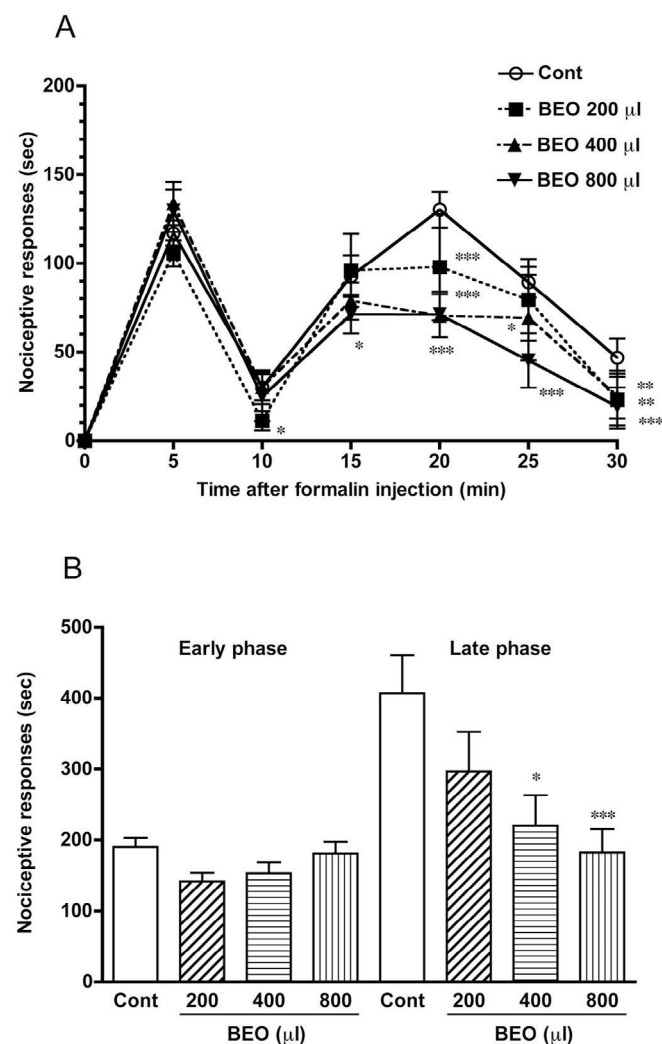


Fig. 2. Effect of BEO inhalation on the time of licking/biting in the post-inhalation group. Time of licking/biting is represented as mean \pm s.e.m. duration expressed in seconds (sec). Statistical significance was by ANOVA followed by Bonferroni's test ($n = 8$ mice per group). * $p < 0.05$, ** $p < 0.01$, *** $p < 0.001$ vs control (Cont).

Under these experimental conditions, the effects of BEO were dose-dependent and even the smaller volume, which had previously resulted ineffective in the post-inhalation group, resulted effective (Fig. 3).

3.3. Effect of the inhalation of BEO on licking/biting after formalin administration (post-inhalation group) as compared with the effect reported in the pre-inhalation and the double-inhalation groups

Comparison of the effects of the inhalation of BEO (800 µl) on the time of licking/biting, recorded at 5 min intervals, in the 3 experimental groups (post-, pre- and double-inhalation groups) unraveled that, while in the early phase BEO was efficacious in a statistically significant manner only at 5 min and if administered as pre-treatment (pre-inhalation group) or both as pre-treatment and after formalin injection (double-inhalation group) ($p < 0.001$; Fig. 4 a), in the late phase it resulted effective also when administered just immediately after formalin injection (post-inhalation group) (Fig. 4 a and b). However, BEO administered in pre-inhalation and in double-inhalation scheme resulted more effective than when administered after formalin injection (post-inhalation group).

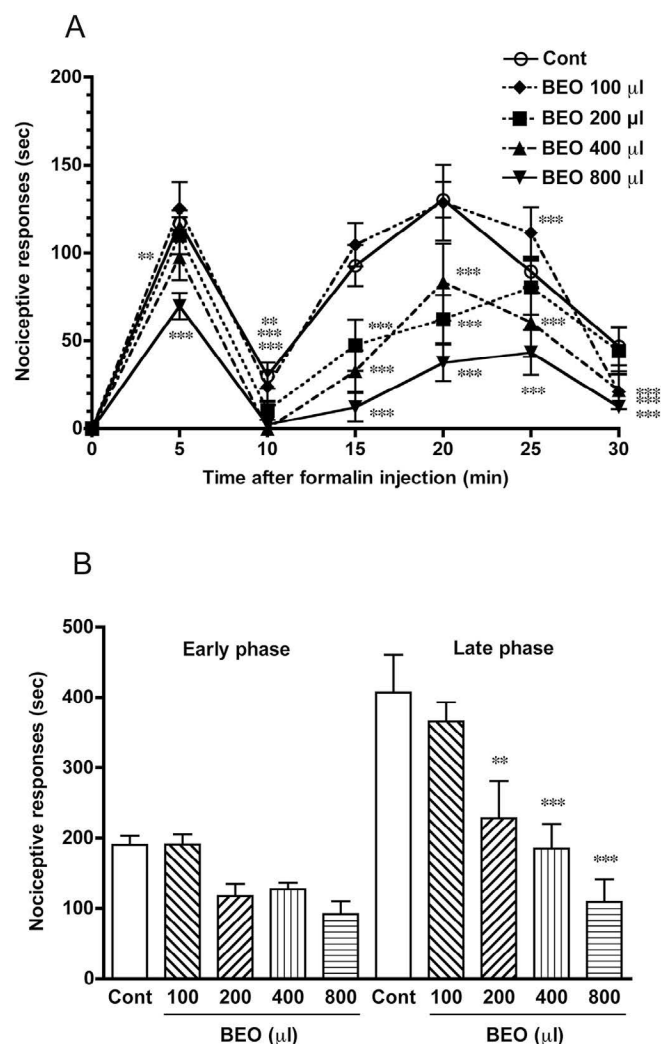


Fig. 3. Effect of BEO inhalation as pre-treatment (pre-inhalation group) on the time of licking/biting. Time of licking/biting is represented as mean \pm s.e.m. duration expressed in seconds (sec). Statistical significance was by ANOVA followed by Bonferroni's test ($n = 8$ mice per group). * $p < 0.05$, ** $p < 0.01$, *** $p < 0.001$ vs control (Cont).

4. Discussion

BEO is often used in aromatherapy (see [13]), a specialized form of phytotherapy recorded for thousand years, used nowadays in industrialized countries as complementary medicine to control symptoms of anxiety, depression, pain and sleep disorders, among others. At variance with the psychological responses, most reliant on the individual experience, pharmacological mechanisms for inhalatory aromatherapy stem from components of the phytocomplex entering the body via the bloodstream by absorption through the lungs or olfactory mucosa [14]. In line with the latter concept, our data demonstrate that BEO is endowed with antinociceptive effects when administered via the inhalatory route in mice. In fact, under our present experimental conditions, a paper filter disc soaked with different volumes of BEO and applied at the edge of a plexiglass cage allowed the effects of inhalation of BEO to be studied in the formalin-induced nociceptive response in ddY-strain mice. Exposure to BEO via inhalation occurred according to three different treatment schedules (Fig. 1): the post-inhalation group of mice was exposed to BEO immediately after formalin injection, the pre-inhalation group was exposed for the whole habituation, but not during the formalin test, and the double-inhalation group was exposed

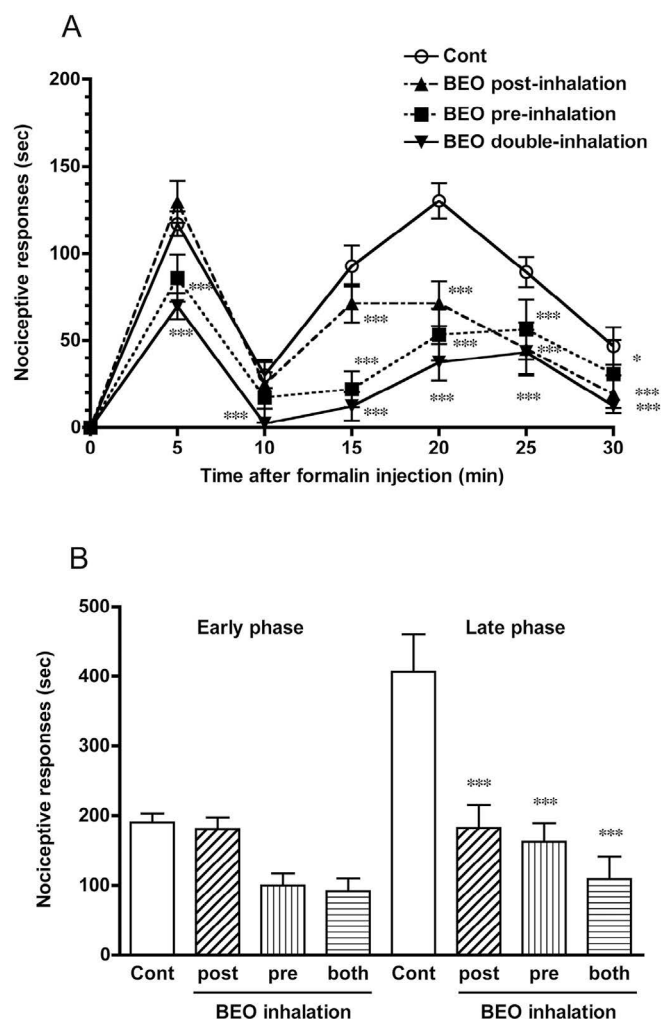


Fig. 4. Effect of the inhalation of BEO (800 μ l) after formalin administration (post-inhalation group) compared with its inhalation as pre-treatment (pre-inhalation group) and with its inhalation during habituation and for the whole duration of the formalin test (double inhalation group) on the duration of licking/biting. Time of licking/biting is represented as mean \pm s.e.m. duration expressed in seconds (sec). Statistical significance was by ANOVA followed by Bonferroni's test ($n = 8$ mice per group). * $p < 0.05$, ** $p < 0.01$, *** $p < 0.001$ vs control (Cont).

to BEO both during habituation and immediately after formalin injection, in order to evaluate the total effect of either inhalation times. The results demonstrate that, when administered immediately after formalin, BEO reduced in a dose-dependent and statistically significant manner the nociceptive behaviour in the late phase. When administered as pre-treatment, during the habituation of the mice, BEO was dose-dependently effective; interestingly, the lower volume used, inactive in the post-treatment (post-inhalation group), here resulted active. Finally, BEO resulted effective in the late phase when administered immediately after formalin and this is at variance with the effect on the early phase that has been observed only at 5 min, after pre-treatment administration or if administered both as pre-treatment and after formalin. Nevertheless, the administration of BEO carried out as pre-treatment and, both as pre-treatment and immediately after formalin for the whole duration of the formalin test, remained more effective than BEO given immediately after formalin injection. These results demonstrate that BEO is endowed with consistent and reproducible antinociceptive properties when administered *via* the inhalatory route. It has been previously reported that in the formalin test *i.p.* linalool

recapitulates the antinociception of BEO (given *i.p.*) and that opioid receptor antagonists (e.g. naloxone hydrochloride and methiodide, the latter being unable to cross the blood brain barrier) could attenuate BEO- or linalool-induced antinociception, suggesting that the peripheral opioid system takes part in the analgesic activity of the essential oil [12]. Indeed, for systemic administration BEO interferes with exocytotic and membrane transporter-mediated release of glutamate in the rat hippocampus and this effect is lost when the monoterpene hydrocarbon-free fraction of the essential oil is used [15]. Most recently, BEO has been shown to enhance basal and induced autophagy [16], a mechanism whose derangement has been implicated in pain sensitization [17]. On the other hand, linalool inhibited the licking/biting response induced by *i.t.* injection of proinflammatory cytokines, e.g. IL-1 β or TNF- α [18]. Furthermore, it has been reported that linalool could produce antinociception through interactions with opioid, muscarinic M2 or adenosine A1 receptors, or by modulating nitric oxide (NO) synthesis [19–22]. There is also evidence to suggest that linalool may modulate glutamatergic neurotransmission *via* NMDA receptors [9, 23, 24]. Accordingly, it is conceivable that antinociceptive properties of systemic administration of BEO and linalool may involve additional, central, mechanisms to the demonstrated activation of the opioid system in the periphery [8, 9], [11]. Altogether, our findings could support the development of aromatherapy clinical trials for the inhalatory administration of BEO for the treatment of chronic pain and of age-related pathological conditions often associated with chronic pain (see osteoarthritis, post-diabetic and post-herpetic neuropathic pain and behavioural and psychological symptoms of dementia, BPSDs). Indeed, the data gathered so far demonstrating a strong analgesic effectiveness of BEO do support aromatherapy with BEO for the control of chronic pain and a reduced use of drugs like opioids, bearing serious side effects. The latter are very often prescribed despite the lack of strong evidence for their efficacy in chronic non-cancer pain [25]. Some 40–60% among care homes demented patients suffer from BPSDs [26] and these are still not adequately controlled through atypical antipsychotics; in fact, BPSDs are strongly associated with pain states [27] and atypical antipsychotics are devoid of analgesic effects. At variance with the latter concept, aromatherapy with BEO, known to be endowed with analgesic activity, may be a promising management option for the control of BPSDs. Quite importantly, aromatherapy for inhalation might have its effects on pain in the absence of any psychological perception of the fragrance and this is of primary importance, since most demented people may be anosmic because of the early loss of olfactory neurons [28]. Recently, the inhalatory administration of BEO in clinical setting was found to exert an effect on mental health, assessed through the Positive and Negative Affect Scale, improving mood states [29]. Furthermore, the recent finding that the anxiolytic-like/relaxant effects of BEO are devoid of sedation, in contrast with benzodiazepines [30], strengthens the usefulness of aromatherapeutic treatment with BEO in the elderly. Therefore, additional studies are needed for a deeper knowledge of the effects of BEO given *via* inhalation, both from a basic and clinical perspective.

Conflict of interest

The authors declare that there is no conflict of interests regarding the publication of this paper.

Acknowledgements

Dr. Michele Crudo was a post-doc recipient of a research bursary in the frame of a research project (Principal Investigator: Prof. Giacinto Bagetta) on “Analgesic properties of the essential oil of bergamot” (PADOEB) funded by Calabria Region and carried out at the Tohoku Medical and Pharmaceutical University (Sendai, Japan). Financial support from the Tohoku Medical and Pharmaceutical University and from Fondazione Istituto Neurologico Nazionale (IRCCS) “Casimiro

Mondino” (Ricerca Corrente 2017, Ministry of Health, Rome), Pavia (Italy) is gratefully acknowledged.

References

- [1] L. Mondello, I. Stagno D'Alcontres, R. Del Duce, F. Crispo, On the genuineness of citrus essential oils, part XL. The composition of the coumarins and psoralens of calabrian bergamot essential oil (*Citrus bergamia* Risso), *Flav. Fragr. J.* 8 (1993) 17–24.
- [2] P. Dugo, L. Mondello, L. Dugo, R. Stancanelli, G. Dugo, LC-MS for the identification of oxygen heterocyclic compounds in citrus essential oils, *J. Pharm. Biomed. Anal.* 24 (2000) 147–150.
- [3] A. Verzera, G. Lamonica, L. Mondello, A. Trozzi, G. Dugo, The composition of bergamot oil, *Perfum. Flavor* 21 (1996) 19–34.
- [4] A. Verzera, A. Tca, F. Gazea, G. Ciccirello, A. Cotroneo, Effects of rootstock on the composition of bergamot (*Citrus bergamia* Risso et Poiteau) essential oil, *J. Agric. Food Chem.* 51 (2003) 206–210.
- [5] L. Mondello, P. Dugo, K. Bartle, G. Dugo, A. Cotroneo, Automated HPLCHRG: a powerful method for essential oils analysis. Part V. Identification of terpene hydrocarbons of bergamot, lemon, mandarin, sweet orange, bitter orange, grapefruit, clementine and mexican lime oils by coupled HPLC-HRGCMS(ITD), *Flav. Fragr. J.* 10 (1995) 33–42.
- [6] S.T. Zaynoun, B.E. Johnson, W. Frain-Bell, A study of oil of bergamot and its importance as a phototoxic agent. I. Characterization and quantification of the photoactive component, *Br. J. Dermatol.* 96 (1977) 475–482.
- [7] M.J. Ashwood-Smith, G.A. Poulton, M. Barker, M. Mildnerberger, 5-Methoxypsoralen, an ingredient in several suntan preparations, has lethal, mutagenic and clastogenic properties, *Nature* 285 (1980) 407–409.
- [8] G. Bagetta, L.A. Morrone, L. Rombola, D. Amantea, R. Russo, L. Berliocchi, S. Sakurada, T. Sakurada, D. Rotiroli, M.T. Corasaniti, Neuropharmacology of the essential oil of bergamot, *Fitoterapia* 81 (2010) 453–461.
- [9] T. Sakurada, H. Mizoguchi, H. Kuwahata, S. Katsuyama, T. Komatsu, L.A. Morrone, M.T. Corasaniti, G. Bagetta, S. Sakurada, Intraplantar injection of bergamot essential oil induces peripheral antinociception mediated by opioid mechanism, *Pharmacol. Biochem. Behav.* 97 (2011) 436–443.
- [10] H. Kuwahata, T. Komatsu, S. Katsuyama, M.T. Corasaniti, G. Bagetta, S. Sakurada, T. Sakurada, K. Takahama, Peripherally injected linalool and bergamot essential oil attenuate mechanical allodynia via inhibiting spinal ERK phosphorylation, *Pharmacol. Biochem. Behav.* 103 (2013) 735–741.
- [11] S. Arner, B.A. Meyerson, Lack of analgesic effect of opioids on neuropathic and idiopathic forms of pain, *Pain* 33 (1988) 11–23.
- [12] S. Katsuyama, A. Otowa, S. Kamio, K. Sato, T. Yagi, Y. Kishikawa, T. Komatsu, G. Bagetta, T. Sakurada, H. Nakamura, Effect of plantar subcutaneous administration of bergamot essential oil and linalool on formalin-induced nociceptive behavior in mice, *Biomed. Res.* 36 (2015) 47–54.
- [13] C.H. Ni, W.H. Hou, C.C. Kao, M.L. Chang, L.F. Yu, C.C. Wu, C. Chen, The Anxiolytic Effect of Aromatherapy on Patients Awaiting Ambulatory Surgery: a Randomized Controlled Trial. *eCAM*, (2013) 927419, <http://dx.doi.org/10.1155/2013/927419>.
- [14] A. Burns, J. Byrne, C. Ballard, C. Holmes, Sensory stimulation in dementia, *Br. Med. J.* 325 (2002) 1312–1313.
- [15] L.A. Morrone, L. Rombola, C. Pelle, M.T. Corasaniti, S. Zappettini, P. Paudice, G. Bonanno, G. Bagetta, The essential oil of bergamot enhances the levels of amino acid neurotransmitters in the hippocampus of rat: implication of monoterpene hydrocarbons, *Pharmacol. Res.* 55 (2007) 255–262.
- [16] R. Russo, M.G. Cassiano, A. Ciociaro, A. Adornetto, G.P. Varano, C. Chiappini, L. Berliocchi, C. Tassorelli, G. Bagetta, M.T. Corasaniti, Role of D-limonene in autophagy induced by bergamot essential oil in SH-SY5Y neuroblastoma cells, *PLoS ONE* 9 (2014) e113682, <http://dx.doi.org/10.1371/journal.pone.0113682>.
- [17] L. Berliocchi, R. Russo, M. Maiaru, A. Levato, G. Bagetta, M.T. Corasaniti, Autophagy impairment in a mouse model of neuropathic pain, *Mol. Pain* 7 (2011) 83, <http://dx.doi.org/10.1186/1744-8069-7-83>.
- [18] T. Sakurada, K. Katsumata, K. Tan-No, S. Sakurada, K. Kisara, The capsaicin test in mice for evaluating tachykinin antagonists in the spinal cord, *Neuropharmacology* 31 (1992) 1279–1285.
- [19] A.T. Peana, P.S. D'Aquila, M.L. Chessa, M.D. Moretti, G. Serra, P. Pippia, (-)-Linalool produces antinociception in two experimental models of pain, *Eur. J. Pharmacol.* 460 (2003) 37–41.
- [20] A.T. Peana, P. Rubattu, G.G. Piga, S. Fumagalli, G. Boatto, P. Pippia, M.G. De Montis, Involvement of adenosine A1 and A2A receptors in (-)-linalool-induced antinociception, *Life Sci.* 78 (2006) 2471–2474.
- [21] A.T. Peana, S. Marzocco, A. Popolo, A. Pinto, (-)-Linalool inhibits in vitro NO formation: probable involvement in the antinociceptive activity of this monoterpene compound, *Life Sci.* 78 (2006) 719–723.
- [22] A.T. Peana, M.G. De Montis, E. Nieddu, M.T. Spano, P.S. D'Aquila, P. Pippia, Profile of spinal and supra-spinal antinociception of (-)-linalool, *Eur. J. Pharmacol.* 485 (2004) 165–174.
- [23] E. Elisabetsky, L.F. Silva Brum, D.O. Souza, Anti-convulsant properties of linalool in glutamate-related seizure models, *Phytomedicine* 6 (1999) 107–113.
- [24] P.A. Batista, M.F. Werner, E.C. Oliveira, L. Burgos, P. Pereira, L.F. Brum, A.R. Santos, Evidence for the involvement of ionotropic glutamatergic receptors on the antinociceptive effect of (-)-linalool in mice, *Neurosci. Lett.* 440 (2008) 299–303.
- [25] L.A. Morrone, D. Scuteri, L. Rombola, H. Mizoguchi, G. Bagetta, Opioids resistance in chronic pain management, *Curr. Neuropharmacol.* 15 (2017) 444–456.
- [26] M. Margallo-Lana, A. Swann, J. O'Brien, A. Fairbairn, K. Reichelt, D. Potkins, P. Mynt, C. Ballard, Prevalence and pharmacological management of behavioural and psychological symptoms amongst dementia sufferers living in care environments, *Int. J. Geriatr. Psychiatr.* 16 (2001) 39–44.
- [27] M. Tosato, A. Lukas, H.G. van der Roest, P. Danese, M. Antocicco, H. Finne-Soveri, T. Nikolaus, F. Landi, R. Bernabei, G. Onder, Association of pain with behavioral and psychiatric symptoms among nursing home residents with cognitive impairment: results from the SHELTER study, *Pain* 153 (2012) 305–310.
- [28] D. Vance, Considering olfactory stimulation for adults with age-related dementia, *Percept. Mot. Skill* 88 (1999) 398–400.
- [29] X. Han, J. Gibson, D.L. Eggett, T.L. Parker, Bergamot (*Citrus bergamia*) essential oil inhalation improves positive feelings in the waiting room of a mental health treatment center: a pilot study, *Phytother. Res.* 31 (2017) 812–816.
- [30] L. Rombola, L. Tridico, D. Scuteri, T. Sakurada, S. Sakurada, H. Mizoguchi, P. Avato, M.T. Corasaniti, G. Bagetta, L.A. Morrone, Bergamot Essential Oil Attenuates Anxiety-like Behaviour in Rats, *Molecules*, 22 (2017), <http://dx.doi.org/10.3390/molecules22040614>.

Increased Susceptibility to Allergic Asthma with the Impairment of Respiratory Tolerance Caused by Psychological Stress

Tasuku Kawano^a Ryusuke Ouchi^a Takahiro Ishigaki^a Chiaki Masuda^a
Tomomitsu Miyasaka^a Yuichi Ohkawara^b Nobuo Ohta^c Motoaki Takayanagi^a
Tomoko Takahashi^a Isao Ohno^d

^aDivision of Pathophysiology, Department of Pharmaceutical Sciences, Faculty of Pharmaceutical Sciences, Tohoku Medical and Pharmaceutical University, Sendai, Japan; ^bDivision of Experimental Allergy and Immunology, Department of Pharmaceutical Sciences, Faculty of Pharmaceutical Sciences, Tohoku Medical Pharmaceutical University, Sendai, Japan; ^cDivision of Otorhinolaryngology, Faculty of Medicine, Tohoku Medical and Pharmaceutical University, Sendai, Japan; ^dCenter for Medical Education, Faculty of Medicine, Tohoku Medical and Pharmaceutical University, Sendai, Japan

Keywords

Asthma · Psychological stress · Immune tolerance ·
Regulatory T cell · Glucocorticoid

Abstract

Background: Bronchial asthma is characterized by type 2 T helper (Th2) cell inflammation, essentially due to a breakdown of immune tolerance to harmless environmental allergens. Etiologically, experiences of psychological stress can be associated with a heightened prevalence of asthma. However, the mechanisms underlying stress-related asthma development are unclear. In this study, we examined whether psychological stress increases susceptibility to allergic asthma by downregulating immune tolerance. **Methods:** Female BALB/c mice were sensitized with ovalbumin/alum, followed by ovalbumin inhalation. Ovalbumin inhalation induced immune tolerance before sensitization occurred. Some mice were exposed to restraint stress during tolerance induction or sensitization. Asthma development was evaluated by airway responsiveness, inflammation, cytokine expression, and IgE synthesis. Sensitization was evaluated by

measuring proliferation and cytokine production by splenocytes. The effects of stress exposure on the numbers and functions of dendritic cells and regulatory T (Treg) cells in bronchial lymph nodes and spleens were evaluated. To investigate the role of endogenous glucocorticoid in inhibiting immune tolerance after stress exposure, we examined the effects of (i) a glucocorticoid-receptor antagonist administered prior to stress exposure, and (ii) exogenous glucocorticoid (instead of stress exposure). **Results:** Asthmatic responses and Th2-biased sensitization, which were suppressed in tolerized mice, re-emerged in tolerized mice stressed during tolerance induction in association with decreased tolerogenic dendritic and Treg cell numbers. The effects of stress exposure on tolerized mice were abolished by administering a glucocorticoid-receptor antagonist and reproduced by administering exogenous glucocorticoid without stress. **Conclusions:** Our findings suggested that psychological stress can potentially increase allergic asthma susceptibility by inhibiting immune tolerance.

© 2018 S. Karger AG, Basel

Edited by: H.-U. Simon, Bern.

KARGER

© 2018 S. Karger AG, Basel

E-Mail karger@karger.com
www.karger.com/iaa

Correspondence to: Dr. Tasuku Kawano
Division of Pathophysiology, Department of Pharmaceutical Sciences
Faculty of Pharmaceutical Sciences, Tohoku Medical and Pharmaceutical University
4-4-1 Komatsushima, Aoba-ku, Sendai, Miyagi 981-8558 (Japan)
E-Mail t-kawano@tohoku-mpu.ac.jp

Introduction

Bronchial asthma is a common cause of chronic illness that is estimated to affect more than 300 million people worldwide. Asthma is caused by various environmental factors, such as allergens, infection, and stress. Asthma manifests with airway inflammation, airway hyperresponsiveness (AHR), and tissue remodeling. Asthmatic inflammatory responses are caused by eosinophil infiltration, increased mucous production, and elevated serum IgE levels, which are orchestrated by type 2 T helper (Th2) cells and Th2 cytokines, such as interleukin (IL)-4, IL-5, and IL-13. Airway inflammation leads to AHR and mucosal remodeling [1–6].

Regulatory T (Treg) cells play a critical role in balancing the immune network by suppressing or limiting effector immune responses against internal and external insults, for example, by preventing organ-specific autoimmunity and allograft rejection, and maintaining self-tolerance [7–9]. Treg cells are generated by plasmacytoid dendritic cells (pDCs) characterized by CD11c^{mid} and PDCA-1 expression, or IL-10-producing myeloid DCs (mDCs) with CD11c^{high} and IL-10 expression [9–11]. Their generation appears to be dependent on microenvironmental factors such as IL-10 and TGF- β [12, 13]. Patients with severe asthma show reduced numbers of Treg cells in the blood and sputum, with impaired suppressive activities as compared with healthy subjects [14]. Moreover, the percentage of Treg cells in bronchoalveolar lavage fluid (BALF) of children [15] and adults [16] with asthma is lower than that in healthy subjects. The failure of Treg cells to suppress Th2-mediated immune responses to innocuous inhaled antigens may lead to an imbalance between allergen activation of Treg cells and effector Th2 responses, resulting in the development and maintenance of asthmatic airway inflammation characterized by uncontrolled Th2-biased immune responses [13, 17, 18]. Recent studies have investigated the mechanisms underlying the impairment of Treg cells in maintaining immune tolerance and the association with increased susceptibility to allergic asthma. Respiratory infections with viruses such as rhinovirus and respiratory syncytial virus (RSV) in early life are risk factors for asthma development in adult life. RSV infection impairs immune tolerance by inducing phenotypic changes in Foxp3⁺ Treg cells, including GATA-3 expression, Th2 cytokine production, and loss of suppressive functions, in an IL-4-dependent pathway [19]. However, how exactly ineffective tolerogenic immune responses develop in asthmatic patients remains unclear.

Several epidemiological studies have demonstrated an association between psychological stress and asthma development [20–23]. For example, perceived stress was strongly associated with the development of adult-onset asthma and hospitalization [24]. Experiences of abuse during childhood and adolescence were positively associated with adult-onset asthma in African American women [25]. Stressful life events, such as a broken life partnership, also contributed to asthma development [26]. However, the pathogenic mechanism of asthma development by psychological stress is unknown.

Various kinds of stressors have been reported to decrease Treg cell production. The number of Treg cells in the peripheral blood of patients with PTSD (posttraumatic stress disorder) was significantly lower than that in non-PTSD subjects [27, 28]. An acute laboratory stressor decreased the number of CD4⁺FOXP3⁺ Treg cells in the peripheral blood of human subjects [29].

Psychological stress upregulates the release of glucocorticoid (GC) by activating the hypothalamic-pituitary-adrenal cortex axis. GC evokes defensive responses to stress that help to maintain homeostatic balance, including regulatory effects on immune-system activities. By affecting the immune system, GC can potentially enhance Th2 immune responses through inhibiting the development of Treg cells essential for respiratory tolerance [30, 31].

Therefore, we hypothesized that exposure to psychological stress prevents the development of respiratory tolerance by inhibiting Treg cell generation via the enhanced release of GC, resulting in Th2-biased immune responses followed by increased susceptibility to allergic asthma. To test this hypothesis, we examined the inhibitory effects of psychological stress on respiratory tolerance induction with or without a GC-receptor antagonist in a murine model of allergic asthma.

Materials and Methods

Mice

Specific pathogen-free female BALB/c mice were purchased from CLEA Japan (Tokyo, Japan). OVA-specific TCR transgenic DO11.10 (Rag2^{-/-}) mice were kindly provided by Dr. Ryo Abe (Tokyo University of Science, Noda, Japan). Animals were housed under a 12-h light/dark cycle at a constant temperature (22 \pm 2°C). Sterilized food and water were available ad libitum. All experiments described below were approved by the Committee of Animal Experiments at Tohoku Medical and Pharmaceutical University (approval numbers: 14002-cn, 15001-cn, and 16002-cn). We took the utmost care to alleviate any pain and suffering in the mice.

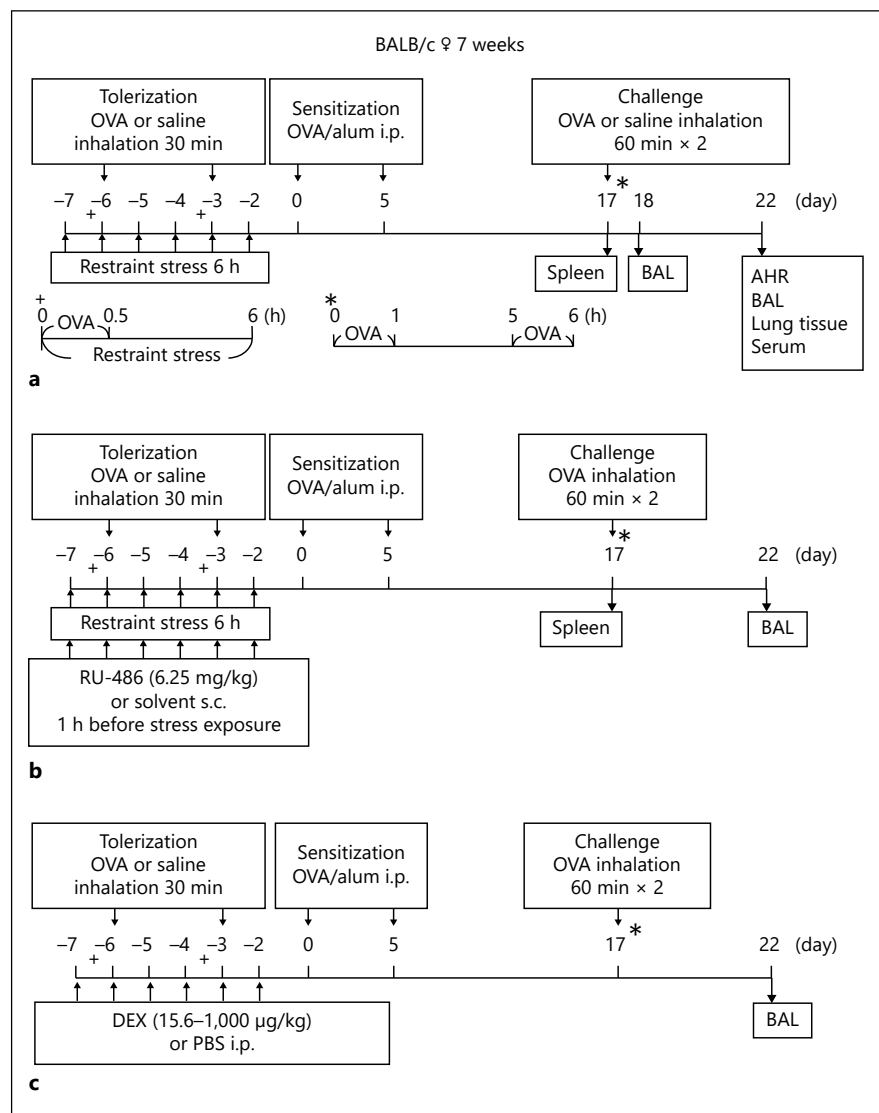


Fig. 1. Schematic representation of the protocols used for tolerization, stress exposure, sensitization, and antigen challenge.

Protocols for Tolerization, Sensitization, Antigen Challenge, and Stress Exposure

Seven-week-old mice were sensitized and made to inhale antigen, as described previously [32], with a minor modification (Fig. 1a). Briefly, mice were sensitized by intraperitoneal injections of chicken ovalbumin (OVA; grade V; Sigma-Aldrich, St. Louis, MO, USA; 8 µg/mouse) adsorbed onto aluminum hydroxide (Wako Pure Chemical Industries, Osaka, Japan; 4 mg/mouse) on days 0 and 5. Respiratory tolerance was induced by OVA inhalation without aluminum hydroxide on days -6 and -3, as described previously [33]. For the first 30 min of the period of stress exposure described below, aerosolized OVA (5 mg/mL in saline) flowed through the chambers for OVA exposure (tolerized mice). As a control for tolerance, saline alone was flowed through the chambers (asthmatic mice). For restraint stress, each mouse was placed in a 50-mL conical centrifuge tube

with multiple ventilation holes [32]. This restraint allowed mice to rotate from a supine to a prone position, but not to turn their heads toward their tails or consume food and water. Restraint stress is generally considered to induce psychological stress in animals [34]. During the tolerance phase, stressed/tolerized and stressed/asthmatic mice in 50-mL conical centrifuge tubes were left in plastic chambers for 6 h for 6 consecutive days (-7 to -2), at the same time each day. In another set of experiments, during the sensitization phase, restraint-stress exposure was performed on days 0–5 in each case. Nonstressed mice were only deprived of food and water during the period when stressed mice were exposed to stress. On day 17, all mice were challenged with aerosolized OVA (5 mg/mL) or saline. Before and after the challenge, bronchoalveolar lavage (BAL) was performed [32]. Briefly, the lungs were lavaged twice by injecting 0.25 mL of cold phosphate-buffered saline (PBS), and the recovered PBS was pooled. Ap-

proximately 0.4 mL of instilled fluid was consistently recovered from each mouse. BALFs were processed to measure cytokine contents and to count the total cell numbers and cell differentials. After centrifugation, BALF supernatants were stored at -80°C before performing cytokine measurements by an enzyme-linked immunosorbent assay (ELISA). Lung tissues were processed as described below.

Administration of a GC-Receptor Antagonist and Dexamethasone

In experiments using a GC-receptor antagonist, mifepristone (RU-486; Sigma-Aldrich) was dissolved in polyethylene glycol 400 (Nacalai Tesque, Kyoto, Japan) and subcutaneously administered (6.25 mg/kg body weight) 1 h before each stress exposure (Fig. 1b). In experiments involving GCs, dexamethasone (DEX; Sigma-Aldrich) in PBS was intraperitoneally injected at the indicated dose to substitute for restraint stress (Fig. 1c). The DEX dose administered was determined based on previous studies [35–38] to make the serum GC contents reach levels comparable to those after restraint-stress exposure. The solvents RU-486 and DEX were used as vehicle controls for these agents.

Plasma Corticosterone Measurements

Before and immediately after restraint-stress exposure on day -7 and immediately after restraint-stress exposure on days -5 and -2 , blood was collected from stressed and nonstressed mice as described [32]. Plasma samples separated from blood were stored at -80°C for corticosterone concentration measurements using an enzyme immunoassay kit (Enzo Life Sciences, Farmingdale, NY, USA) according to the manufacturer's protocol. The sensitivity of detection was 32 pg/mL.

AHR Measurements

Measurements of airway resistance (R_L) were conducted using the Buxco FinePointe Resistance and Compliance system (DSI, Minneapolis, MN, USA), as described [32] (Fig. 1a). Mice were sequentially challenged with aerosolized PBS (baseline) followed by increasing doses of methacholine (Sigma-Aldrich), ranging from 0.625 to 5 mg/mL. Maximum-resistance values were recorded during a 3-min period following each challenge. The concentration of methacholine that provoked a 200% increase in R_L (PC200) was calculated by linear interpolation of the dose-response curves.

Histological Analysis of the Lungs

Sections of lung tissues collected on day 22 were stained with periodic acid-Schiff (PAS) to evaluate mucus-containing goblet cells in the bronchial epithelium, or with hematoxylin and eosin to study eosinophil infiltration in peribronchial areas. The number of PAS-positive cells and eosinophils were determined as described previously [32].

OVA-Specific IgE Measurement

The concentrations of OVA-specific IgE in serum collected on day 22 were measured by ELISA, as described previously [32]. The sensitivity of detection was 1.9×10^{-2} EU/mL for IgE.

Preparation of Bronchial Lymph Node Cells

Bronchial lymph nodes (BLNs) obtained on day -2 from 10 nontolerized mice and from 3 tolerized mice with or without the stress exposure were pooled and weighed. BLN cells were prepared

as described previously [39], processed for flow cytometric analysis, and used for the transfer and coculture experiments described below.

Adoptive Transfer of BLN DCs

DCs as CD11c-positive cells were isolated from BLN cells from tolerized and stressed/tolerized mice on day -2 using an autoMACS Pro Separator (Miltenyi Biotec, Bergisch Gladbach, Germany) with anti-mouse CD11c (N418) MicroBeads (Miltenyi Biotec) and adoptively transferred (day -2) into naïve mice as described previously [39]. The mice were subsequently immunized (days 0–5) with OVA/alum and challenged with OVA (day 17), and BAL was performed (day 22) as described above.

Coculture of BLN DCs with Naïve DO11.10 T Cells

CD11c-positive DCs were isolated from BLN cells of tolerized and stressed/tolerized mice as mentioned above. CD4⁺ T cells were isolated from splenocytes of naïve DO11.10 (Rag2^{-/-}) female mice using an autoMACS Pro Separator (Miltenyi Biotec) with anti-mouse CD4 (L3T4) MicroBeads (Miltenyi Biotec). DCs (1×10^4 cells/well) were cocultured with CD4⁺ T cells (2×10^5 cells/well) in the presence of OVA (100 $\mu\text{g/mL}$). After culture for 3 days, cells were processed for flow-cytometric analysis.

Adoptive Transfer of CD4⁺ T Splenocytes

Splenocytes were prepared from the 4 mouse groups 1 day after the last stress exposure. CD4⁺ T cells were purified from the splenocytes, as described above. CD4⁺ T cells (2×10^7 cells/0.2 mL of saline for each mouse) were transferred into naïve BALB/c mice via the tail vein (day -1). The mice were subsequently immunized (days 0–5) with OVA/alum and challenged (day 17) with OVA, and BAL was performed (day 22) as mentioned above.

Culture of Splenocytes

Splenocytes were prepared from mice of all 4 experimental groups on day 17. The cells were cultured at 1×10^6 cells in 200 μL /well in 96-well culture plates (MICROplate; Asahi Techno Glass, Chiba, Japan) in the presence or absence of OVA (200 $\mu\text{g/mL}$) for 72 h. The samples were then centrifuged, and the supernatants were stored at -80°C for subsequent cytokine measurements. Cell proliferation was measured by performing WST-8 assays with cell-count reagent SF (Nacalai Tesque) according to the manufacturer's protocol.

Culture of Bone Marrow-Derived DCs

Bone marrow-derived DCs (BM-DCs) were prepared from BM cell cultures from female BALB/c mice (6–10 weeks old) incubated with recombinant mouse GM-CSF for 8 days in RPMI 1640 [40]. The cultured cells were more than 95% CD11c⁺. BM-DCs (2×10^4 cells in 200 μL /well in 96-well culture plates; MICROplate, Asahi Techno Glass) were stimulated with OVA (100 $\mu\text{g/mL}$) in the absence or presence of DEX at the indicated concentration for 24 h. Cell proliferation was measured by WST-8 assay as mentioned above.

Flow Cytometric Analysis

Cells were preincubated with anti-CD16/CD32 (Fc gamma III/II receptor; BD Biosciences, Franklin Lanes, NJ, USA) to reduce nonspecific binding of the subsequent antibodies. Dead cells were excluded using a LIVE/DEAD Fixable Blue Dead Cell Stain Kit

(Life Technologies/Thermo Fisher Scientific Corporation, Grand Island, NY, USA). The cells were stained for surface antigens with anti-CD11c-PE (clone N418; BioLegend, San Diego, CA, USA), anti-PDCA1-APC (clone 927; BioLegend), anti-CD3ε-FITC (clone 145-2C11; Miltenyi Biotec), anti-CD4-AF700 (clone RM4-5; BD Biosciences), anti-DO11.10-TCR-APC (clone KJ1-26; eBioscience), or isotype-control antibodies. For intracellular staining, cells were stimulated with phorbol 12-myristate 13-acetate (5 ng/mL), ionomycin (500 ng/mL), and monensin (2 mM) for 4 h before surface-antigen staining. After fixation and permeabilization, the cells were incubated with an anti-IFN-γ-PE (clone XMG1.2; eBioscience), anti-IL-4-PE-CF594 (clone 11B11; BD Biosciences), anti-IL-10-FITC (clone JES5-16E3; BioLegend), anti-Foxp3-PE or PE-Cy7 (clone FJK-16s; eBioscience), or isotype-control antibody. IL-10-producing mDCs were identified as CD11c^{high} MHC II^{high} IL-10⁺ cells, pDCs as CD11c^{mid} PDCA-1⁺ cells, DO11.10 Th1 cells as KJ1-26⁺IFN-γ⁺ cells, Th2 cells as KJ1-26⁺IL-4⁺ cells, and Treg cells as CD3⁺CD4⁺Foxp3⁺ cells. The cells were counted on a FACSAria II flow cytometer (BD Biosciences), and the analyses were performed using FACSDiva software (BD Biosciences). The flow cytometric gating strategies used to evaluate cell subsets are shown in online supplementary Figure 1 (for all online suppl. material, see www.karger.com/doi/10.1159/000488289).

Measurements of Cytokine Contents

The concentrations of IL-4, IL-5, and IL-13 in BALFs, and the concentrations of IL-4 and IFN-γ in cell culture supernatants were measured using ELISA kits (R&D Systems, Minneapolis, MN, USA) according to the manufacturer's protocol. The sensitivity of detection was 2 pg/mL for IL-4, 7 pg/mL for IL-5, 1.5 pg/mL for IL-13, and 8 pg/mL for IFN-γ.

Statistical Analysis

Data are expressed as the mean ± standard deviation (SD) from multiple independent experiments (as indicated by *n* values). Significant differences between 2 groups were determined by the non-parametric Mann-Whitney U test. For comparisons between multiple groups, analysis of variance and Bonferroni post hoc tests were performed. These analyses were performed using Prism5 (GraphPad Software, San Diego, CA, USA). *p* < 0.05 was considered statistically significant.

Results

Effects of Stress on Plasma Corticosterone Concentrations

Corticosterone concentrations (in ng/mL) in stressed mice were significantly higher than those in nonstressed mice after the 1st, 3rd, and 6th stress exposures on days -7, -5, and -2, respectively (1st: 327.2 ± 250.3 [*n* = 9] vs. 88.9 ± 29.8 [*n* = 8], *p* < 0.05; 3rd: 547.4 ± 256.0 [*n* = 7] vs. 90.0 ± 95.3 [*n* = 5], *p* < 0.05; 6th: 365.5 ± 205.7 [*n* = 11] vs. 85.1 ± 63.7 [*n* = 8], *p* < 0.01). Before stress exposure, no significant differences in corticosterone concentrations occurred between stressed and nonstressed mice. Corti-

costerone concentrations after stress exposure were significantly higher at all time points than before stress exposure, while no such increases were observed in non-stressed mice (online suppl. Fig. 2).

Effects of Stress on Asthmatic Responses in Tolerized Mice

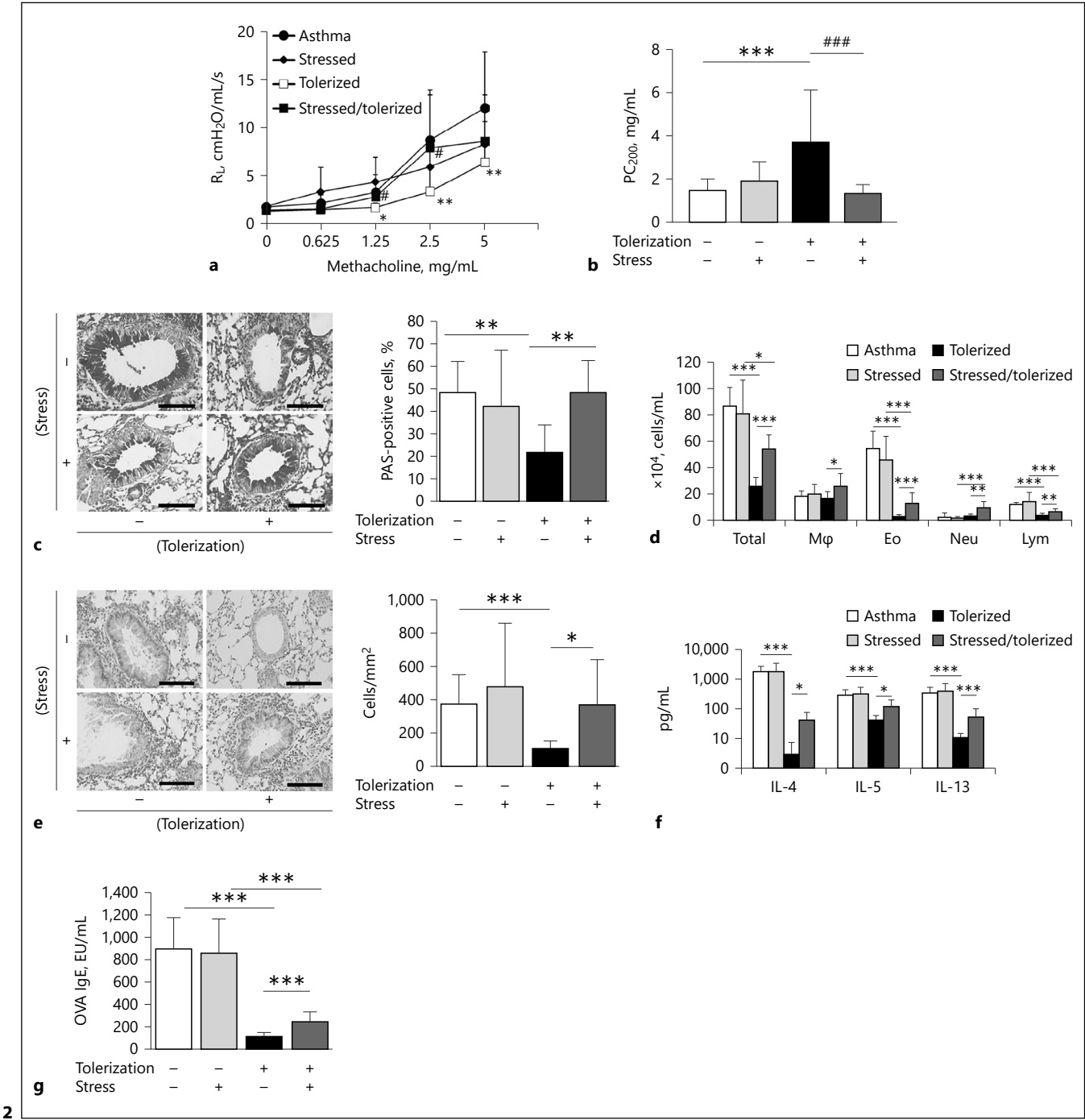
To investigate the effects of restraint stress on asthmatic responses in tolerized mice, we compared airway responsiveness, inflammation, cytokine expression, and IgE synthesis after antigen challenge in the 4 mouse groups (Fig. 2). As expected, tolerized mice showed significantly lower AHR, mucus production, numbers of total cells, eosinophils, and lymphocytes in BALFs, peribronchial eosinophil accumulation, Th2 cytokine content in BALF, and OVA-specific IgE in serum than asthmatic mice. In contrast, those airway responses and IgE levels were significantly higher in stressed/tolerized mice than in tolerized mice. However, no significant differences occurred in airway responses or IgE levels between asthmatic and stressed/asthmatic mice. The IFN-γ content in BALFs did not significantly differ between the 4 groups. Significant differences were not observed in total cell and cell differential counts in BALFs before OVA challenge (day 17) or after saline challenge (day 22) between the 4 groups (data not shown). These data indicated that stress indirectly enhanced allergic responses by inhibiting the development of respiratory tolerance. However, tolerized mice with stress exposure during sensitization (after immune tolerance establishment) showed low numbers of inflammatory cells in the BALF, similar to tolerized mice without stress exposure. No significant differences in the numbers of inflammatory cells were observed between asthmatic mice (with or without stress exposure) during sensitization (online suppl. Fig. 3).

Effects of Stress on Sensitization in Tolerized Mice

Because restraint stress caused a re-emergence of antigen-induced asthmatic responses in tolerized mice, we next investigated the effects of psychological stress on immune tolerance. As expected, pretreating mice with aerosolized OVA inhibited splenocyte proliferation upon OVA stimulation in vitro (vs. pretreatment with aerosolized saline). However, restraint stress exposure during the induction phase of tolerance significantly increased splenocyte proliferation in vitro compared with findings in tolerized mice (Fig. 3a). Moreover, we compared the OVA-induced cytokine expression (IFN-γ and IL-4) by the splenocyte in the 4 groups (Fig. 3b, c). With regard to IFN-γ (Fig. 3b), tolerance had no effects on the expression

of IFN- γ either with or without stress exposure, whereas the stress exposure decreased the cytokine expression in tolerized mice but not in nontolerized mice. On the other hand, tolerance significantly decreased IL-4 expression either with or without stress exposure, while the stress exposure did not significantly alter the cytokine expres-

sion in either nontolerized or tolerized mice (Fig. 3c). Therefore, the deviation of the Th1/Th2 balance, as seen by the IFN- γ /IL-4 ratios, toward Th2-dominant responses caused by the stress exposure in tolerized mice (Fig. 3d) could be mainly due to the decreased expression of IFN- γ .



(For legend see next page.)

Effects of Stress on the Development of Tolerogenic DCs and Tregs

Because restraint stress inhibited the induction of respiratory tolerance, we analyzed Treg cells, pDCs, and IL-10-producing mDCs as Treg-generating DCs in BLNs. The numbers and percentages of pDCs (Fig. 4a, b) and Treg cells (Fig. 4c, d) were significantly increased in toler-

ized mice compared with nontolerized mice under the nonstress condition. The stress exposure significantly decreased the numbers (Fig. 4a), but not the percentages (Fig. 4b), of pDCs and both the numbers (Fig. 4c) and percentages (Fig. 4d) of Treg cells in stressed/tolerized mice compared with tolerized mice. Few IL-10-producing mDCs were detected in BLN cells.

Fig. 3. Effects of stress on sensitization. On day 17, splenocytes were prepared from mice of each group of sensitized mice and stimulated in vitro with OVA. **a** After a 72-h culture, cell proliferation was measured in WST-8 assays. The content of IFN- γ (**b**) and IL-4 (**c**), and the content ratios of IL-4/IFN- γ (**d**) in culture supernatants were determined by ELISA. Data are expressed as the mean \pm SD of triplicate cultures from 3 independent experiments. * $p < 0.05$, ** $p < 0.01$, and *** $p < 0.001$.

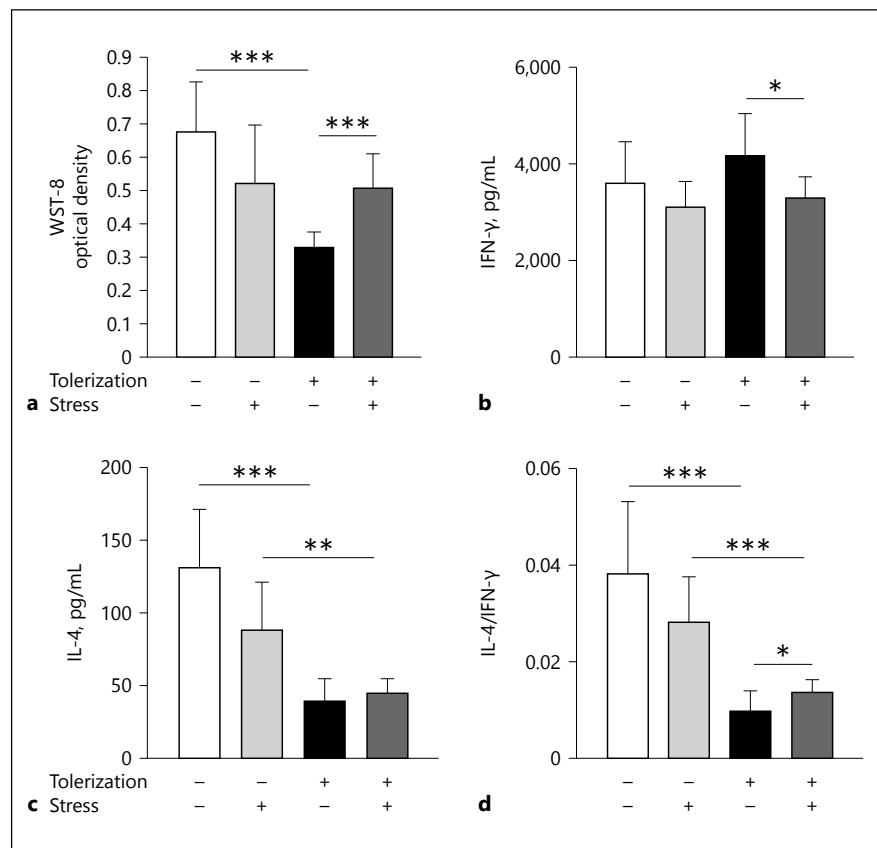
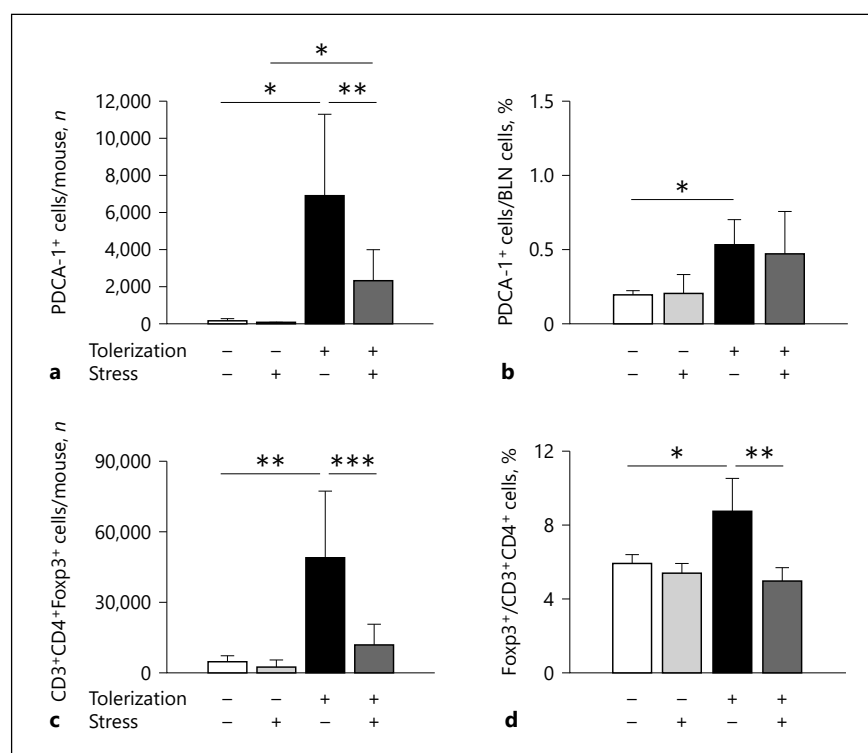


Fig. 2. Effects of stress during the tolerance induction phase on allergic airway responses. Airway reactivity (R_L ; **a**) and airway sensitivity (PC200; **b**) were measured 5 days after the last OVA challenge (day 22). Data are expressed as the mean \pm SD ($n = 9$ –13 from 4 independent experiments). * $p < 0.05$, ** $p < 0.01$, and *** $p < 0.001$, compared with asthmatic mice; # $p < 0.01$ and ### $p < 0.001$, compared with tolerized mice. **c** Lungs were isolated from mice of each group 5 days after the last OVA challenge (day 22). Lung sections were prepared and stained with PAS. Representative images of lung sections (left; scale bar, 100 μ m) and the percentage of PAS-positive cells (right) from the 4 mouse groups are shown. Data are expressed as the mean \pm SD ($n = 5$ –7 mice from 3 independent experiments). **d** BALFs were obtained from mice of each group 5 days after the last OVA challenge (day 22). Total cells (Total), macrophages (M Φ), eosinophils (Eo), neutrophils (Neu), and lymphocytes (Lym) were counted. Data are expressed as the mean \pm SD

($n = 7$ –9 from 3 independent experiments). **e** Lung sections were stained with hematoxylin and eosin. Representative images of lung sections (left; scale bar, 100 μ m) and the eosinophil counts in the peribronchial area (right) are shown. Data are expressed as the mean \pm SD ($n = 5$ –8 mice from 3 independent experiments). **f** Effects of stress on BALF cytokine contents. BALFs were obtained from mice of each group 1 day after the last OVA challenge (day 18). BALF IL-4, IL-5, and IL-13 levels were measured by ELISA. Data are expressed as the mean \pm SD ($n = 3$ –9 from 3 independent experiments). **g** Effects of stress on OVA-specific IgE in serum. Sera were obtained from mice of each treatment group 5 days after the last OVA challenge (day 22). OVA-specific IgE in serum was measured by ELISA. Data are expressed as the mean \pm SD ($n = 5$ –7 from 3 independent experiments). * $p < 0.05$, ** $p < 0.01$, and *** $p < 0.001$.

Fig. 4. Effects of stress on tolerogenic DCs and Treg cells in BLN. BLNs were collected after the final stress exposure (day -2). The numbers and percentages of PDCA-1⁺ cells (**a, b**), and CD3⁺CD4⁺Foxp3⁺ cells (**c, d**) were determined. Data from 3 independent experiments for nontolerized groups and 4 independent experiments for tolerized groups are expressed as the mean \pm SD. * $p < 0.05$, ** $p < 0.01$, and *** $p < 0.001$.



An adoptive transfer experiment was performed to examine the effects of stress exposure on DC functions that promote the development of respiratory tolerance in our stress/tolerance model. As expected, airway inflammation was suppressed in mice transferred with CD11c⁺ DCs from tolerized mice as compared with mice without transfer, although mice transferred with CD11c⁺ DCs from stressed/tolerized mice showed no significant difference compared to mice transferred with CD11c⁺ DCs from tolerized mice (online suppl. Fig. 4A). Furthermore, we investigated the effects of stress on the function of DCs in Treg development. Treg, Th2, and Th1 cell development promoted by DCs from the tolerized and stressed/tolerized mouse groups were not different (online suppl. Fig. 4B).

Transfer of the Inhibitory Effects of Stress on the Acquisition of Respiratory Tolerance by CD4⁺ T Cells

Analyses of BAL cells after sensitization followed by OVA inhalation in mice adoptively transferred with CD4⁺ T cells showed similar numbers of total cells and eosinophils between the 4 groups (Fig. 5a) compared to the variable levels observed between groups using the conventional mouse model (Fig. 2d). Adoptively trans-

ferring CD4⁺ T cells from tolerized mice resulted in significant decreases in the numbers of total cells and eosinophils in BALFs, relative to those numbers observed after transferring CD4⁺ T cells from asthmatic mice or mice injected with saline (vehicle control). The cell numbers in BALFs measured after adoptively transferring CD4⁺ T cells from stressed/tolerized mice were significantly higher than those after transferring CD4⁺ T cells from tolerized mice. However, no significant differences were found in the total numbers of cells or eosinophils between mice transferred with CD4⁺ T cells from asthmatic and stressed/asthmatic mice. The number of lymphocytes in BALFs showed a tendency similar to that of the numbers of total cells and eosinophils, although the differences between groups were not significant. In addition, the percentage of Treg cells in splenocytes from tolerized mice was significantly higher than that in asthmatic mice. In contrast, the percentage of Treg cells in splenocytes was significantly lower in stressed/tolerized mice than in tolerized mice (Fig. 5b). The percentage of CD3⁺CD4⁺ cells in splenocytes was not significantly different between the 4 groups (data not shown).

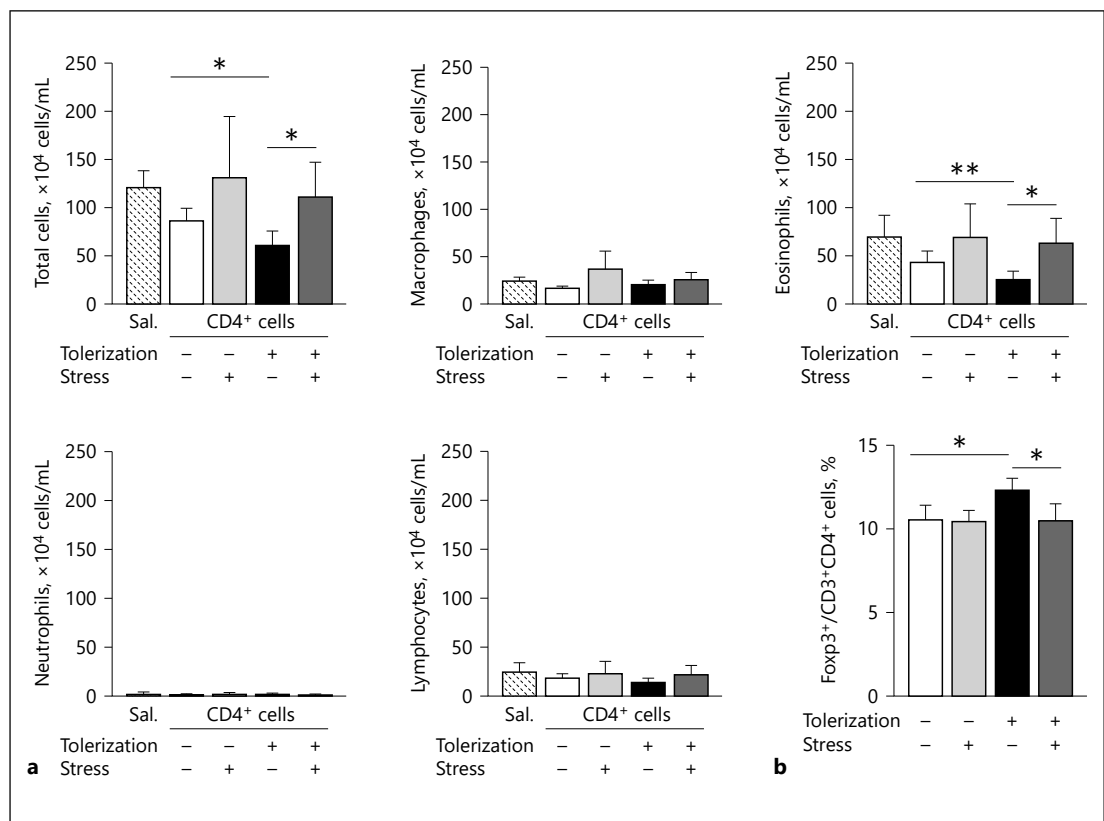


Fig. 5. Adoptive transfer of spleen CD4⁺ T cells. CD4⁺ T cells were isolated from spleens of mice of each mouse 1 day after the final stress exposure (day -1). **b** Spleen CD3⁺CD4⁺Foxp3⁺ cells were analyzed by flow cytometry. CD4⁺ T cells were intravenously injected into naïve BALB/c mice. Saline (Sal.) was injected as a control. One day postinjection, mice of all groups were sensitized with

OVA/alum and challenged with OVA. BALFs were obtained from mice of each group 5 days after the last OVA challenge. **a** Total cells, macrophages, eosinophils, neutrophils, and lymphocytes were counted. Data are expressed as the mean ± SD ($n = 3-9$ from 2 independent experiments). * $p < 0.05$ and ** $p < 0.01$.

Effects of a GC-Receptor Antagonist on Stress-Induced Inhibition of Respiratory Tolerance

The sizes and weights of BLNs and number of BLN cells in stressed/tolerized mice were lower than those in nonstressed/tolerized mice (Fig. 6a–c in solvent-treated groups). The atrophy of BLNs caused by exposure to restraint stress was abolished by treatment with RU-486 (Fig. 6a, b). Furthermore, the numbers of BLN cells, Treg cells, and tolerogenic DCs in stressed/tolerized mice recovered to the levels in nonstressed/tolerized mice after RU-486 treatment (Fig. 6c, d, f). Stress exposure appeared to affect the numbers of total cells, eosinophils, neutrophils, and lymphocytes in BALFs observed in tolerized and stressed/tolerized mice treated with solvent, but not in those treated with RU-486 (Fig. 7).

Effects of GC as a Substitute for the Stress on Respiratory Tolerance

Because the effects of stress exposure were diminished by administering the GC-receptor antagonist just before stress exposure, we examined whether exogenous GC could reproduce the effects of stress exposure. DEX administration significantly increased the numbers of total cells (250, 1,000 µg/kg), eosinophils (250, 1,000 µg/kg), and lymphocytes (250 µg/kg) in BALFs as compared to PBS administration in tolerized mice, but not in nontolerized mice (Fig. 8).

Effects of GC on BM-DC Proliferation

The proliferation of BM-DCs stimulated with OVA was reduced by DEX in a dose-dependent manner (Fig. 9).

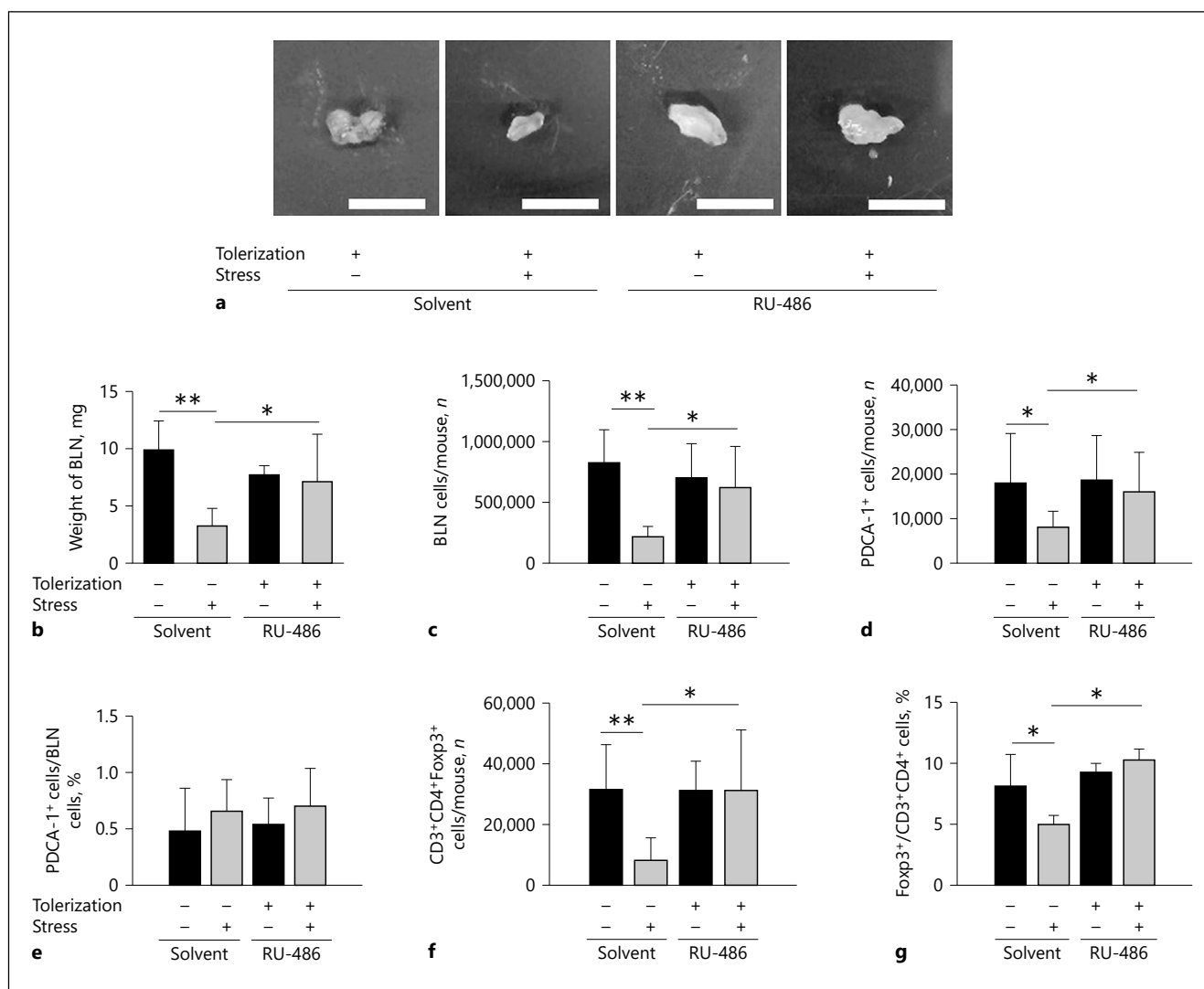


Fig. 6. Effects of a GC-receptor antagonist on BLN enlargement and cellular changes induced by stress. Tolerized mice with or without stress exposure were administered a GC-receptor antagonist, RU-486, or the solvent as a control before each stress exposure. BLNs were collected after the final stress exposure (day -2) and weighed. Representative images (**a**; scale bar, 5 mm) and weights (**b**) of BLNs in each mouse group are shown. Data are expressed as the mean \pm SD ($n = 7-8$ from 3 independent experi-

ments). Cell populations of BLN cells were analyzed by flow cytometry. The numbers of total BLN cells (**c**), PDCA-1⁺ cells (**d**), and CD3⁺CD4⁺Foxp3⁺ cells (**f**) were determined and are expressed as percentages of PDCA-1⁺ cells (**e**) and CD3⁺CD4⁺Foxp3⁺ cells (**g**) in BLN cells. Data are expressed as the mean \pm SD ($n = 6$ from 2 independent experiments). * $p < 0.05$, ** $p < 0.01$, and *** $p < 0.001$.

Discussion

In this study, we demonstrated for the first time that exposure to psychological stress during the induction phase of respiratory tolerance, but not during the sensitization phase, promoted the development of Th2-biased sensitization and, thereby, asthmatic airway responses to

inhaled allergen, while restraint-stress exposure had no effect on sensitization and allergic airway inflammation (Fig. 2; online suppl. Fig. 3). Preventing the development of immune tolerance by stress exposure was confirmed by the re-emergence of Ag-specific splenocyte proliferation and Th2-predominant cytokine secretion in stressed/tolerized mice, both of which were suppressed in tolerized

Fig. 7. Effects of a GC-receptor antagonist on the stress-induced inhibition of respiratory tolerance. A GC-receptor antagonist, RU-486, or solvent was administered before each stress exposure. BALFs were obtained from mice of each treatment group 5 days after the last OVA challenge (day 22). Total cells (Total), macrophages (MΦ), eosinophils (Eo), neutrophils (Neu), and lymphocytes (Lym) were counted. Data are expressed as the mean ± SD (*n* = 5–8 from 4 independent experiments). * *p* < 0.05, ** *p* < 0.01, and *** *p* < 0.001; # *p* < 0.05, ## *p* < 0.01, and ### *p* < 0.001, compared with solvent-treated control mice.

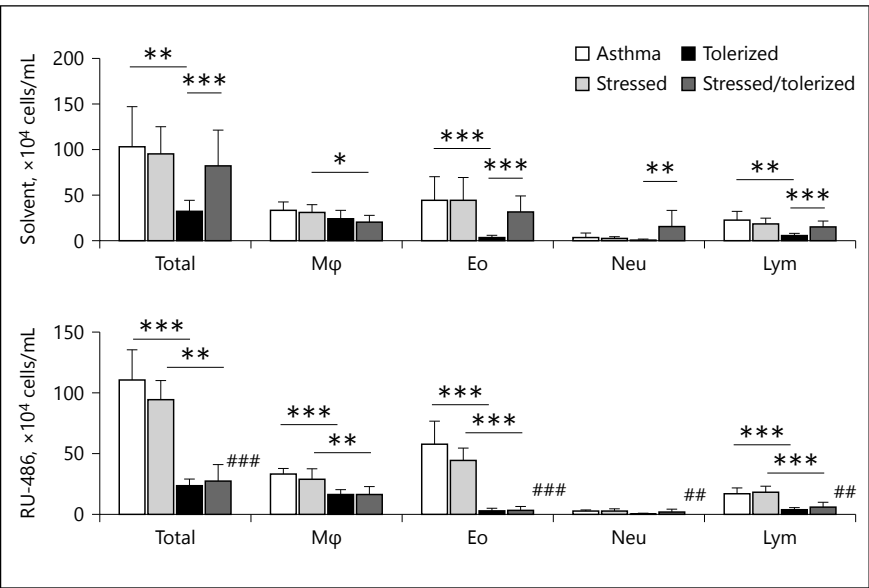
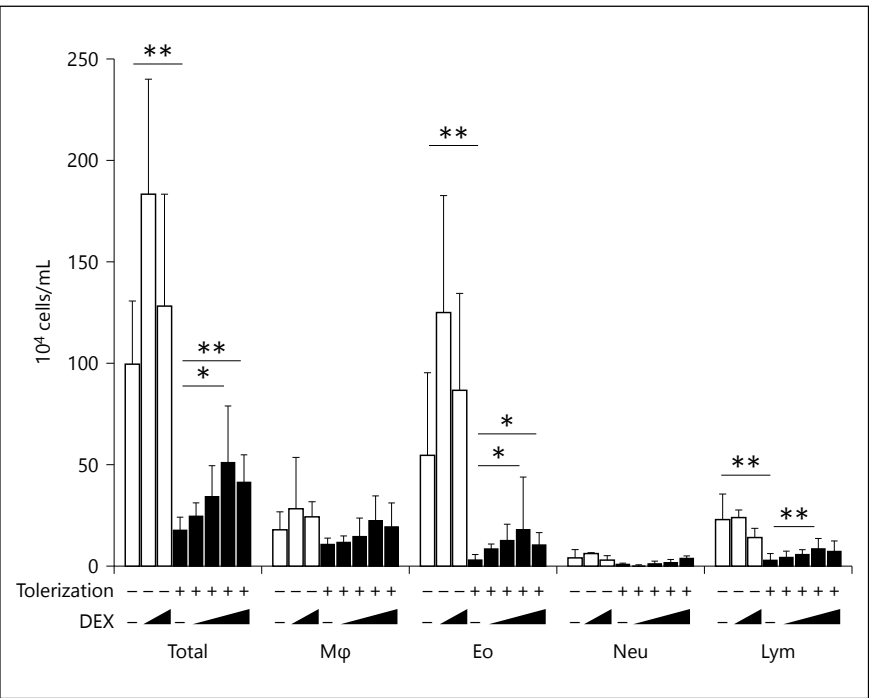


Fig. 8. Effects of DEX on the numbers of inflammatory cells. Solvent or 15.6, 62.5, 250, or 1,000 µg DEX/kg body weight was administered instead of stress exposure to nontolerized (open columns) and tolerized (closed columns) mice. BALFs were obtained from mice of each treatment group 5 days after the last OVA challenge (day 22). Total cells (Total), macrophages (MΦ), eosinophils (Eo), neutrophils (Neu), and lymphocytes (Lym) were counted. Data are expressed as the mean ± SD (*n* = 5–7 from 2 independent experiments). * *p* < 0.05 and ** *p* < 0.01.



mice as compared with asthmatic mice (Fig. 3). Stress exposure might inhibit the development of respiratory tolerance by dampening the tolerogenic DC-Treg cell axis (Fig. 4, 5), which could result from GC release upon stress exposure (Fig. 5–9).

In this study, the induction of immune tolerance by OVA inhalation correlated with BLN swelling, which was inhibited by stress exposure (Fig. 6). BLN atrophy following stress exposure has been shown in recent reports, revealing that stress leads to adverse physiological effects, such as atrophy of the thymus and lymph nodes [41, 42].

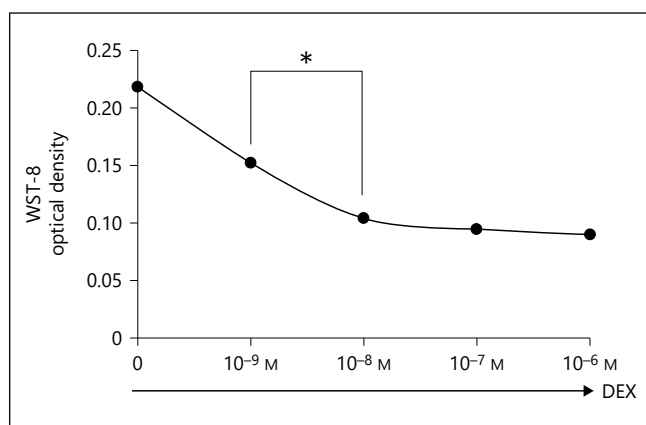


Fig. 9. Effects of DEX on BM-DC proliferation. BM-DCs were generated from female BALB/c mice. BM-DCs ($2/10^4$ cells in 200 μ L/well) in 96-well culture plates were stimulated with OVA (100 μ g/mL) in the absence or presence of DEX at the indicated concentrations for 24 h. Cell proliferation was measured in WST-8 assays.

Stress exposure caused the reduction of the absolute number of pDCs in BLNs (Fig. 4a), whereas the percentage of pDCs (Fig. 4b) and the ability of DCs to generate Treg cells (online suppl. Fig. 4B) were not altered and, furthermore, the effect of stress was not transferred by DCs (online suppl. Fig. 4A). Therefore, it is assumed that the potential roles for tolerogenic DCs in this model might not be strong. However, the transfer of CD4⁺ T cells from the spleen of stressed/tolerized mice caused the re-emergence of allergic airway inflammation, which was suppressed by the transfer of CD4⁺ T cells from tolerized mice (Fig. 5a), and the percentage of Treg cells in transferred splenocytes was significantly lower in stressed/tolerized mice than in tolerized mice (Fig. 5b). Thus, stress exposure during the tolerance-induction phase may have disturbed the induction, but not the function, of tolerogenic DCs, leading to insufficient differentiation of Treg cells, resulting in the failure to prevent Th2-biased immune sensitization. The inhibitory effects of stress exposure on Treg cell development are supported by studies showing that traumatic stress and a mental stressor reduced Treg cell numbers in peripheral blood in humans [27–29].

In airway immune responses, the stress exposure significantly increased IL-4 expression (Fig. 2f), although the stress had no effects on IFN- γ expression (data not shown), in BALF in tolerized mice. Furthermore, the number (Fig. 4c) and percentage (Fig. 4d) of Treg cells in BLNs were decreased by the stress exposure. On the other

hand, in the spleen, the deviation of the Th1/Th2 balance toward Th2-dominant responses caused by the stress exposure in tolerized mice (Fig. 3d) could be mainly due to the decreased expression of IFN- γ , while the percentage of Treg cells was decreased by the stress exposure (data not shown). Together with these findings, although the stress exposure has a potential to inhibit the development of tolerance leading to Th2-dominant immune responses, the main mechanisms underlying the deviation towards Th2-dominant immune responses might be different depending on the site of immune responses, for example systemic immunity in spleen and local immunity in airways.

To investigate the mechanisms underlying the inhibitory activity of stress on immune tolerance, we assessed the contribution of GC released upon stress exposure (online suppl. Fig. 2). The anti-tolerogenic effect of stress exposure was abolished by administering RU-486 (a GC-receptor antagonist) before each stress exposure during the tolerance-induction phase. RU-486 administration caused a re-emergence of BLN swelling (Fig. 6a) and retrieved the numbers of BLN cells, pDCs, and Treg cells in BLNs (Fig. 6) and inflammatory cells in BALFs after antigen challenge (Fig. 7) to the levels in tolerized but not stressed mice. Furthermore, the administration of DEX as a substitute for restraint stress during the tolerance-induction phase showed a similar effect as stress exposure, as demonstrated by the significant increase in the numbers of total cells, eosinophils, and lymphocytes in BALFs, compared with those in tolerized mice administered PBS (Fig. 8). These results indicated that GC signaling played a critical role in the stress exposure-induced perturbation of immune tolerance. GC can induce apoptosis of several types of immune cells [43], including mDCs [44] and pDCs [45]. Because RU-486 caused a re-emergence of BLN swelling and restored the number of pDCs, we investigated the effect of GC on DC proliferation in vitro. As expected, DEX reduced the proliferation of BM-DCs in a dose-dependent fashion (Fig. 9). Therefore, it is likely that inhibiting the acquisition of immune tolerance by stress exposure was mediated by GC, which decreased the number of pDCs and impaired Treg differentiation.

GC is recognized worldwide as a gold standard for treating and preventing asthma by its anti-allergic activities, including the reduction of airway inflammation and improvement of AHR through limiting cytokine production by T cells and epithelial cells, and impairing the recruitment, survival, and activation of eosinophils and other inflammatory cells [2, 46]. However, GC has

been shown to amplify Th2 immune responses via several mechanisms. GC treatment can potentiate Th2 differentiation, by either reducing IL-12 secretion from antigen-presenting cells [47] or directly suppressing Th1 cell polarization [48]. GC administration during sensitization enhanced Th2 responses in an allergic mouse model [31]. In addition, GC treatment during antigen inhalation (to promote the development of respiratory tolerance) eliminated IL-10-producing DCs required for the development of IL-10-producing Treg cells, leading to Th2-biased sensitization and allergic airway responses upon antigen exposure [30]. Interestingly, the development of respiratory tolerance was prevented by systemic, but not local, GC administration [49], in accordance with our finding that the GC level in the circulation had increased. Systemic administration of GC to immunocompetent humans and naïve mice significantly reduced the number, but not the suppressive function, of Foxp3⁺ Treg cells in blood [50]. More importantly, either systemic or local GC administration during the sensitization and allergen-induced inflammation phases decreased the number of Foxp3⁺ Treg cells in mouse lungs [51]. In contrast, both GC inhalation and systemic GC treatment increased the number and function of CD4⁺CD25^{high} Treg cells in blood and BALF in pediatric asthma [15], and Foxp3⁺ Treg cells in blood in adult asthma [52]. Whether the effect of GC on human Treg cells is inhibitory or stimulatory might depend on the immunocompetence status, such as healthy (immunocompetent) or asthmatic. The studies mentioned above and this study involved the use of wild-type, naïve mice so that the effect of GC treatment on Treg cells would be inhibitory, as observed with healthy subjects. The reason for the dependency was not determined and is beyond the aims of this study.

To our knowledge, it has not yet been reported that psychological stress prevents the development of respiratory tolerance. However, some studies have investigated the mechanisms underlying the impairment of immune tolerance associated with increased susceptibility to allergic asthma. Respiratory infections with viruses, such as rhinovirus and RSV, in early life are risk factors for asthma development in adult life. Simultaneous rhinovirus infection and tolerance induction in mice inhibited the acquisition of immune tolerance induced by intranasal OVA, attenuating the development of Foxp3⁺ Treg cells through OX40 ligand expression on lung DCs and thymic stromal lymphopoietin and IL-33 expression by airway epithelial cells, which increased the susceptibility to allergic airway responses [53]. Krishnamoorthy et al.

[19] demonstrated that after OVA tolerization by breast milk from maternal mice exposed to OVA, recurrent RSV infection in pups induced allergic responses, while the allergic responses were not observed in uninfected pups, in adult life (6 weeks old). RSV infection impaired immune tolerance by inducing phenotypic changes in Foxp3⁺ Treg cells, including GATA-3 expression, Th2 cytokine production, and loss of suppressive functions, in an IL-4-dependent pathway [19]. The potential of IL-33 in overcoming acquired immune tolerance was confirmed recently [54]. It was revealed that Foxp3⁺ Treg cells express the IL-33 receptor ST2, the expression of which was enhanced by the ligand, that IL-33 evoked Th2-like properties in those cells by inducing GATA-3 expression and the synthesis of Th2 cytokines associated with the loss of suppressive function, and that intranasal IL-33 administration to tolerized mice (during or after sensitization) caused allergen-induced airway inflammation.

In conclusion, psychological stress exposure inhibited the development of respiratory tolerance by GC-dependent suppression of tolerogenic DC and Treg cell induction, resulting in increased susceptibility to allergic asthma through Th2-biased immune sensitization. It is necessary to further explore the neuroendocrine pathway linking stress exposure to GC release, including neuropeptides such as opioids involved in stress-related asthma exacerbations [55, 56], as well as the endocrine-immune pathway, especially the GC-airway epithelium interaction leading to Th2-dominant immune responses.

Acknowledgements

We thank Dr. Ryo Abe (Tokyo University of Science, Noda, Japan) for providing the DO11.10 (Rag2^{-/-}) mice.

Statement of Ethics

Studies on animal subjects were approved by the Committee of Animal Experiments at Tohoku Medical and Pharmaceutical University (approval numbers: 14002-cn, 15001-cn, and 16002-cn). We took the utmost care to alleviate any pain and suffering in the mice.

Disclosure Statement

The authors have no conflicts of interest to declare.

Funding Sources

This work was supported in part by a Grant-in-Aid for Scientific Research (C; No. 25461164, 17K09624), a Grant-in-Aid for Young Scientists (B; No. 16K19608, 17K16212), and the Matching Fund Subsidy for Private Universities (No. S1001002, S1511001L) from the Ministry of Education, Culture, Sports, Science and Technology (MEXT) of Japan. The funders played no role in the study design, the collection, analysis, and interpretation of data, or the preparation of the report.

Author Contributions

T.K. and I.O. designed the study. T.K., R.O., and T.I. performed the majority of experiments. C.M. contributed to the flow cytometric analysis of lung cells and lymph node cells. T.M. contributed to the analysis of histology. Y.O. contributed to the analysis of AHR. N.O., T.T., and M.T. suggested key experiments and edited the manuscript. T.K. and I.O. wrote the manuscript.

References

- Lambrecht BN, Hammad H: The immunology of asthma. *Nat Immunol* 2015;16:45–56.
- Fahy JV: Type 2 inflammation in asthma – present in most, absent in many. *Nat Rev Immunol* 2015;15:57–65.
- Barnes PJ: Pathophysiology of allergic inflammation. *Immunol Rev* 2011;242:31–50.
- Kim RY, Rae B, Neal R, Donovan C, Pinkerton J, Balachandran L, Starkey MR, Knight DA, Horvat JC, Hansbro PM: Elucidating novel disease mechanisms in severe asthma. *Clin Trans Immunol* 2016;5:e91.
- Woodruff PG, Modrek B, Choy DF, Jia G, Abbas AR, Ellwanger A, Koth LL, Arron JR, Fahy JV: T-helper type 2-driven inflammation defines major subphenotypes of asthma. *Am J Respir Crit Care Med* 2009;180:388–395.
- Holgate ST, Wenzel S, Postma DS, Weiss ST, Renz H, Sly PD: Asthma. *Nat Rev Dis Primers* 2015;1:15025.
- Peterson RA: Regulatory T-cells: diverse phenotypes integral to immune homeostasis and suppression. *Toxicol Pathol* 2012;40:186–204.
- Sakaguchi S, Miyara M, Costantino CM, Hafler DA: FOXP3+ regulatory T cells in the human immune system. *Nat Rev Immunol* 2010;10:490–500.
- Palomares O, Yaman G, Azkur AK, Akkoc T, Akdis M, Akdis CA: Role of Treg in immune regulation of allergic diseases. *Eur J Immunol* 2010;40:1232–1240.
- Gehrie E, van der Touw W, Bromberg JS, Ochando JC: Plasmacytoid dendritic cells in tolerance. *Methods Mol Biol* 2011;677:127–147.
- Worbs T, Hammerschmidt SI, Forster R: Dendritic cell migration in health and disease. *Nat Rev Immunol* 2017;17:30–48.
- Palomares O, Martin-Fontecha M, Lauener R, Traidl-Hoffmann C, Cavkaytar O, Akdis M, Akdis CA: Regulatory T cells and immune regulation of allergic diseases: roles of IL-10 and TGF- β . *Genes Immun* 2014;15:511–520.
- Noval Rivas M, Chatila TA: Regulatory T cells in allergic diseases. *J Allergy Clin Immunol* 2016;138:639–652.
- Mamessier E, Nieves A, Lorec AM, Dupuy P, Pinot D, Pinet C, Vervloet D, Magnan A: T-cell activation during exacerbations: a longitudinal study in refractory asthma. *Allergy* 2008;63:1202–1210.
- Hartl D, Koller B, Mehlhorn AT, Reinhardt D, Nicolai T, Schendel DJ, Griesse M, Krauss-Etschmann S: Quantitative and functional impairment of pulmonary CD4⁺CD25^{hi} regulatory T cells in pediatric asthma. *J Allergy Clin Immunol* 2007;119:1258–1266.
- Barczyk A, Pierzchala W, Caramori G, Wladerkiewicz R, Kaminski M, Barnes PJ, Adcock IM: Decreased percentage of CD4⁺FOXP3⁺TGF- β ⁺ and increased percentage of CD4⁺IL-17⁺ cells in bronchoalveolar lavage of asthmatics. *J Inflamm* 2014;11:22.
- Fujita H, Meyer N, Akdis M, Akdis CA: Mechanisms of immune tolerance to allergens. *Chem Immunol Allergy* 2012;96:30–38.
- Lloyd CM, Hawrylowicz CM: Regulatory T cells in asthma. *Immunity* 2009;31:438–449.
- Krishnamoorthy N, Khare A, Oriss TB, Raundhal M, Morse C, Yarlagadda M, Wenzel SE, Moore ML, Peebles RS Jr, Ray A, Ray P: Early infection with respiratory syncytial virus impairs regulatory T cell function and increases susceptibility to allergic asthma. *Nat Med* 2012;18:1525–1530.
- Liu X, Olsen J, Agerbo E, Yuan W, Cnattingius S, Gissler M, Li J: Psychological stress and hospitalization for childhood asthma—a nationwide cohort study in two Nordic countries. *PLoS One* 2013;8:e78816.
- Yonas MA, Lange NE, Celedon JC: Psychosocial stress and asthma morbidity. *Curr Opin Allergy Clin Immunol* 2012;12:202–210.
- Lind N, Nordin M, Palmquist E, Nordt S: Psychological distress in asthma and allergy: the Vasterbotten Environmental Health Study. *Psychol Health Med* 2014;19:316–323.
- Rosenberg SL, Miller GE, Brehm JM, Celedon JC: Stress and asthma: novel insights on genetic, epigenetic, and immunologic mechanisms. *J Allergy Clin Immunol* 2014;134:1009–1015.
- Rod NH, Kristensen TS, Lange P, Prescott E, Diderichsen F: Perceived stress and risk of adult-onset asthma and other atopic disorders: a longitudinal cohort study. *Allergy* 2012;67:1408–1414.
- Coogan PF, Wise LA, O'Connor GT, Brown TA, Palmer JR, Rosenberg L: Abuse during childhood and adolescence and risk of adult-onset asthma in African American women. *J Allergy Clin Immunol* 2013;131:1058–1063.
- Loerbroeks A, Apfelbacher CJ, Thayer JF, Debling D, Sturmer T: Neuroticism, extraversion, stressful life events and asthma: a cohort study of middle-aged adults. *Allergy* 2009;64:1444–1450.
- Sommershof A, Aichinger H, Engler H, Adenauer H, Catani C, Boneberg EM, Elbert T, Groettrup M, Kolassa IT: Substantial reduction of naive and regulatory T cells following traumatic stress. *Brain Behav Immun* 2009;23:1117–1124.
- Jergovic M, Bendelja K, Vidovic A, Savic A, Vojvoda V, Aberle N, Rabatic S, Jovanovic T, Sabioncello A: Patients with posttraumatic stress disorder exhibit an altered phenotype of regulatory T cells. *Allergy Asthma Clin Immunol* 2014;10:43.
- Freier E, Weber CS, Nowotne U, Horn C, Bartels K, Meyer S, Hildebrandt Y, Luetkens T, Cao Y, Pabst C, Muzzulini J, Schnee B, Brunner-Weinzierl MC, Marangolo M, Boke-meyer C, Deter HC, Atanackovic D: Decrease of CD4⁺FOXP3⁺ T regulatory cells in the peripheral blood of human subjects undergoing a mental stressor. *Psychoneuroendocrinology* 2010;35:663–673.
- Stock P, Akbari O, DeKruyff RH, Umetsu DT: Respiratory tolerance is inhibited by the administration of corticosteroids. *J Immunol* 2005;175:7380–7387.
- Wiley RE, Cwiartka M, Alvarez D, Mackenzie DC, Johnson JR, Goncharova S, Lundblad L, Jordana M: Transient corticosteroid treatment permanently amplifies the Th2 response in a murine model of asthma. *J Immunol* 2004;172:4995–5005.
- Okuyama K, Dobashi K, Miyasaka T, Yamazaki N, Kikuchi T, Sora I, Takayanagi M, Kita H, Ohno I: The involvement of glucocorticoids in psychological stress-induced exacerbations of experimental allergic asthma. *Int Arch Allergy Immunol* 2014;163:297–306.

- 33 Behrendt AK, Hansen G: CD27 costimulation is not critical for the development of asthma and respiratory tolerance in a murine model. *Immunol Lett* 2010;133:19–27.
- 34 Wang J, Charboneau R, Barke RA, Loh HH, Roy S: μ -Opioid receptor mediates chronic restraint stress-induced lymphocyte apoptosis. *J Immunol* 2002;169:3630–3636.
- 35 Silvennoinen R, Escola-Gil JC, Julve J, Rotllan N, Llaverias G, Metso J, Valledor AF, He J, Yu L, Jauhiainen M, Blanco-Vaca F, Kovanen PT, Lee-Rueckert M: Acute psychological stress accelerates reverse cholesterol transport via corticosterone-dependent inhibition of intestinal cholesterol absorption. *Circ Res* 2012;111:1459–1469.
- 36 Carroll JC, Iba M, Bangasser DA, Valentino RJ, James MJ, Brunden KR, Lee VM, Trojanowski JQ: Chronic stress exacerbates tau pathology, neurodegeneration, and cognitive performance through a corticotropin-releasing factor receptor-dependent mechanism in a transgenic mouse model of tauopathy. *J Neurosci* 2011;31:14436–14449.
- 37 Parker CC, Ponicsan H, Spencer RL, Holmes A, Johnson TE: Restraint stress and exogenous corticosterone differentially alter sensitivity to the sedative-hypnotic effects of ethanol in inbred long-sleep and inbred short-sleep mice. *Alcohol* 2008;42:477–485.
- 38 Kainuma E, Watanabe M, Tomiyama-Miyaji C, Inoue M, Kuwano Y, Ren H, Abo T: Association of glucocorticoid with stress-induced modulation of body temperature, blood glucose and innate immunity. *Psychoneuroendocrinology* 2009;34:1459–1468.
- 39 Akbari O, DeKruyff RH, Umetsu DT: Pulmonary dendritic cells producing IL-10 mediate tolerance induced by respiratory exposure to antigen. *Nat Immunol* 2001;2:725–731.
- 40 Lutz MB, Kukutsch N, Ogilvie AL, Rossner S, Koch F, Romani N, Schuler G: An advanced culture method for generating large quantities of highly pure dendritic cells from mouse bone marrow. *J Immunol Methods* 1999;223:77–92.
- 41 Kim JJ, Diamond DM: The stressed hippocampus, synaptic plasticity and lost memories. *Nat Rev Neurosci* 2002;3:453–462.
- 42 Szabo S, Tache Y, Somogyi A: The legacy of Hans Selye and the origins of stress research: a retrospective 75 years after his landmark brief “letter” to the editor of *Nature*. *Stress* 2012;15:472–478.
- 43 Montague JW, Cidlowski JA: Glucocorticoid-induced death of immune cells: mechanisms of action. *Curr Top Microbiol Immunol* 1995;200:51–65.
- 44 Brokaw JJ, White GW, Baluk P, Anderson GP, Umemoto EY, McDonald DM: Glucocorticoid-induced apoptosis of dendritic cells in the rat tracheal mucosa. *Am J Respir Cell Mol Biol* 1998;19:598–605.
- 45 Boor PP, Metselaar HJ, Manham S, Tilanus HW, Kusters JG, Kwekkeboom J: Prednisolone suppresses the function and promotes apoptosis of plasmacytoid dendritic cells. *Am J Transplant* 2006;6:2332–2341.
- 46 John M, Lim S, Seybold J, Jose P, Robichaud A, O'Connor B, Barnes PJ, Chung KF: Inhaled corticosteroids increase interleukin-10 but reduce macrophage inflammatory protein-1 α , granulocyte-macrophage colony-stimulating factor, and interferon- γ release from alveolar macrophages in asthma. *Am J Respir Crit Care Med* 1998;157:256–262.
- 47 DeKruyff RH, Fang Y, Umetsu DT: Corticosteroids enhance the capacity of macrophages to induce Th2 cytokine synthesis in CD4+ lymphocytes by inhibiting IL-12 production. *J Immunol* 1998;160:2231–2237.
- 48 Miyaura H, Iwata M: Direct and indirect inhibition of Th1 development by progesterone and glucocorticoids. *J Immunol* 2002;168:1087–1094.
- 49 Kerzerho J, Wunsch D, Szely N, Meyer HA, Lurz L, Rose L, Wahn U, Akbari O, Stock P: Effects of systemic versus local administration of corticosteroids on mucosal tolerance. *J Immunol* 2012;188:470–476.
- 50 Sbiera S, Dexneit T, Reichardt SD, Michel KD, van den Brandt J, Schmul S, Kraus L, Beyer M, Mlynski R, Wortmann S, Allolio B, Reichardt HM, Fassnacht M: Influence of short-term glucocorticoid therapy on regulatory T cells in vivo. *PLoS One* 2011;6:e24345.
- 51 Olsen PC, Kitoko JZ, Ferreira TP, de-Azevedo CT, Arantes AC, Martins Mu A: Glucocorticoids decrease Treg cell numbers in lungs of allergic mice. *Eur J Pharmacol* 2015;747:52–58.
- 52 Karagiannidis C, Akdis M, Holopainen P, Woolley NJ, Hense G, Ruckert B, Mantel PY, Menz G, Akdis CA, Blaser K, Schmidt-Weber CB: Glucocorticoids upregulate FOXP3 expression and regulatory T cells in asthma. *J Allergy Clin Immunol* 2004;114:1425–1433.
- 53 Mehta AK, Duan W, Doerner AM, Traves SL, Broide DH, Proud D, Zuraw BL, Croft M: Rhinovirus infection interferes with induction of tolerance to aeroantigens through OX40 ligand, thymic stromal lymphopoietin, and IL-33. *J Allergy Clin Immunol* 2016;137:278–288.e6.
- 54 Chen CC, Kobayashi T, Iijima K, Hsu FC, Kita H: IL-33 dysregulates regulatory T cells and impairs established immunologic tolerance in the lungs. *J Allergy Clin Immunol* 2017;140:1351–1363.e7.
- 55 Drolet G, Dumont EC, Gosselin I, Kinkead R, Laforest S, Trotter JF: Role of endogenous opioid system in the regulation of the stress response. *Prog Neuropsychopharmacol Biol Psychiatry* 2001;25:729–741.
- 56 Miyasaka T, Dobashi-Okuyama K, Takahashi T, Takayanagi M, Ohno I: The interplay between neuroendocrine activity and psychological stress-induced exacerbation of allergic asthma. *Allergol Int* 2018;67:32–42.

The expression of 11 β -hydroxysteroid dehydrogenase in severe allergic rhinitis

Nobuo Ohta^{MD, PhD1}, Yusuke Suzuki^{MD, PhD2}, Naoya Noguchi^{MD, PhD1}, Risako Kakuta^{MD, PhD1}, Takahiro Suzuki^{MD, PhD1}, Toshiichi Awataguchi^{MD, PhD1}, Yukiko Takahashi^{MD, PhD1}, Sachiko Tomioka-Matsutani^{MD, PhD1}, Yusuke Ishida^{MD, PhD3}, Ryokichi Ikeda^{MD, PhD1}, Muneharu Yamazaki^{MD, PhD1}, Yusuke Kusano^{MD1}, Yutarou Saito^{MD1}, Fumi Shoji^{MD, PhD1}, Yuji Yaginuma^{MD, PhD1}, Tatsutoshi Suzuki^{MD, PhD4}, Hiroshi Osafune^{MD5}, Tasuku Kawano^{PhD6}, Tomomitsu Miyasaka^{PhD6}, Tomoko Takahashi^{MD, PhD6}, Isao Ohno^{MD, PhD7}, Kota Wada^{MD, PhD5}

¹Division of Otolaryngology, Tohoku Medical and Pharmaceutical University Hospital 1-12-1, Fukumuro, Miyaginoku, Sendai, Japan

²Department of Otolaryngology, Head and Neck Surgery, Yamagata University Faculty of Medicine, Yamagata, Japan

³Division of Anatomy and Cell Biology, Tohoku Medical and Pharmaceutical University, Sendai, Japan

⁴Department of Otolaryngology, Head and Neck Surgery, Kitasato University Faculty of Medicine, Kanagawa, Japan

⁵Department of Otolaryngology, Head and Neck Surgery, Toho University Faculty of Medicine, Tokyo, Japan

⁶Division of Pathophysiology, Department of Pharmaceutical Sciences, Faculty of Pharmaceutical Sciences, Tohoku Medical and Pharmaceutical University, Sendai, Japan

⁷Center for Medical Education, Faculty of Medicine, Tohoku Medical and Pharmaceutical University, Sendai, Japan

Article history: Received: 15.09.2018 Accepted: 05.10.2018 Published: 05.10.2018

ABSTRACT:

Objective: To clarify the roles of 11 β -HSD in resistance to glucocorticoid therapy for allergic rhinitis, a case series study was conducted.

Methods: The patient group consisted of 20 subjects with allergic rhinitis, aged from 21 to 46 years (mean age 26.5), who showed persistent GC resistance necessitating surgical removal of the inferior turbinate after 6 months of GC treatment. The patients with poor response to GC treatment for 6 months were defined as GC-resistant. The control group consisted of 10 subjects aged from 16 to 39 years (mean age 24.5) who underwent maxillofacial surgery, from whom nasal tissues were taken and who did not receive GC treatment. Nasal mucosal tissues from patients and control subjects were examined immunohistochemically. The sections were washed with 0.01 M phosphate-buffered saline (PBS; pH 7.2) containing 0.15 M NaCl and 0.01% Triton X-100, and incubated for 2 h with rabbit polyclonal anti-11 β -HSD1 and 11 β -HSD2 antibody (Santa Cruz Biotechnology, Inc., Santa Cruz, CA, USA), each diluted 1:200 in PBS containing 0.1% bovine serum albumin. Immunostained sections were assessed under an Olympus microscope with an eyepiece reticule at 200 \times magnification. Cell counts are expressed as means per high-power field (0.202 mm²). Control group means (arithmetic mean \pm SD) were compared with patient group means by Mann-Whitney U-test at P = 0.05.

Results: Although 11 β -HSD1 was expressed to a similar extent in patients and controls, 11 β -HSD2 was expressed more significantly in patients with severe allergic rhinitis, resulting in an increased HSD-1/HSD-2 ratio. The significantly increased expression of 11 β -HSD2 in the nasal epithelium and submucosal inflammatory cells of patients with severe nasal allergy was observed in the present study.

Conclusion: Our findings suggest that 11 β -HSD2 plays an important role in resistance to glucocorticoid therapy for allergic rhinitis, and its expression might be used as an additional parameter indicating steroid resistance in allergic rhinitis.

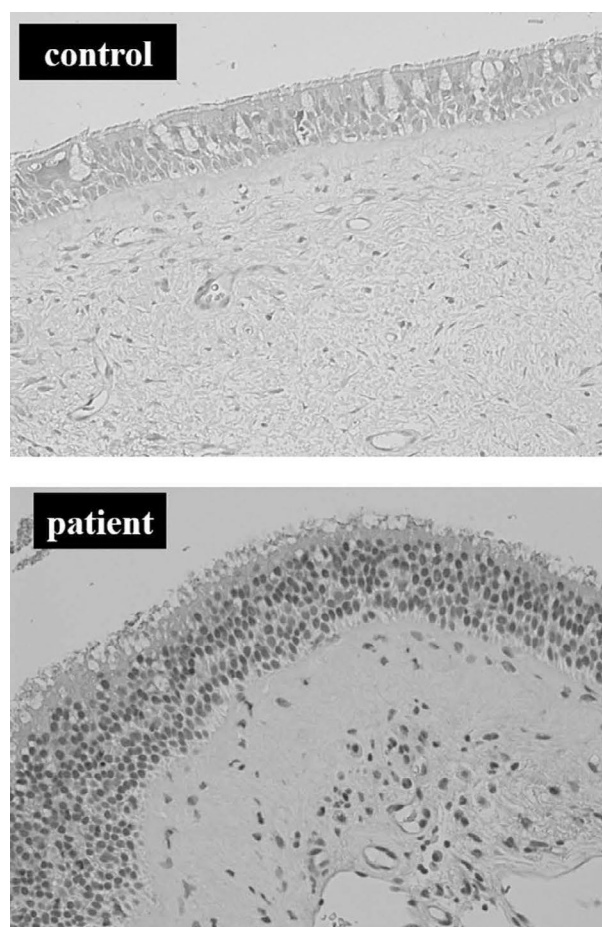
KEYWORDS:

allergic rhinitis, 11 β -hydroxysteroid dehydrogenase, glucocorticoid resistance, glucocorticoid therapy, glucocorticoid response

INTRODUCTION

Glucocorticoids (GCs) are commonly used as anti-inflammatory agents in the treatment of chronic allergic diseases, including allergic rhinitis. However, these clinical benefits are sometimes limited because some patients demonstrate persistent tissue inflammation despite repeated and high doses of GC treatment. Studies of GC receptors (GR), NF- κ B and other mediators in underlying mechanism of GC resistance have been reported (1,2). The 11 β -hydroxysteroid dehydrogenase (11 β -HSD) is a tissue-specific

regulator of glucocorticoid responses, inducing the interconversion of inactive and active glucocorticoids. The 11 β -HSD has two isoforms, 11 β -HSD1, which converts inactive 11-keto corticosteroids into active 11-hydroxy corticosteroids, thereby potentiating the effects of endogenous glucocorticoids, and 11 β -HSD2, which acts as a classic dehydrogenase by converting active 11-hydroxylated cortisol and corticosterone into inactive 11-keto forms of cortisone and 11-dehydrocorticosterone, respectively (3). Here, to clarify the roles of 11 β -HSD in resistance to glucocorticoid therapy for allergic rhinitis, a case series study was conducted.



Expression of 11β-HSD1

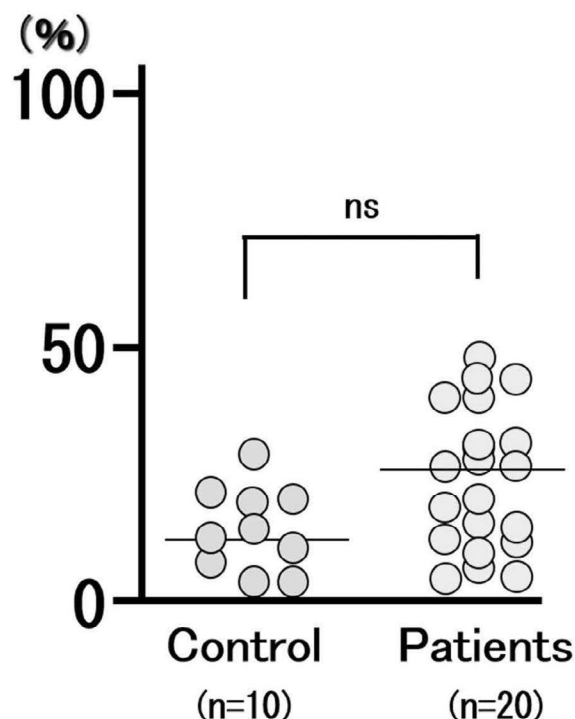


Fig. 1. Representative pathological findings of 11β-HSD1 immunoreactivities in the nasal mucosa of patients with severe nasal allergy and controls. (original magnification $\times 100$).

SUBJECTS AND METHODS

All patients were treated by experienced ENT doctors at Yamagata City Hospital Saiseikan, Yamagata University Faculty of Medicine, and Tohoku Medical and Pharmaceutical University between February 2010 and August 2017. Informed consent was obtained under protocols approved by the Institutional Review Board. The patient group consisted of 20 subjects with allergic rhinitis, aged from 21 to 46 years (mean age 26.5), who showed persistent GC resistance necessitating surgical removal of the inferior turbinate after 6 months of GC treatment. The patients with poor response to GC treatment for 6 months were defined as GC-resistant.

The control group consisted of 10 subjects aged from 16 to 39 years (mean age 24.5) who underwent maxillofacial surgery, from whom nasal tissues were taken and who did not receive GC treatment. Nasal mucosal tissues were fixed in 10% formalin for 1 to 2 days, dehydrated through an ethanol series, and embedded in paraffin wax. Sections 3 μ m thick were dewaxed in xylene and dehydrated. The sections were washed with 0.01 M phosphate-buffered saline (PBS; pH 7.2) containing 0.15 M NaCl and 0.01% Triton X-100, and incubated for 2 h with rabbit polyclonal anti-11 β -HSD1 and 11 β -HSD2 antibody (Santa Cruz Biotechnology, Inc., Santa Cruz, CA, USA), each diluted 1:200 in PBS containing 0.1% bovine serum albumin. Controls for nonspecific staining were incubated with 10 μ g/mL mouse IgG1 (DAKO, Glostrup, Denmark). Sections were

washed and incubated with biotinylated rabbit antibody to mouse IgG, IgA, and IgM (Immunotech, Tokyo, Japan) for 1 h.

The sections were incubated with Vectastain reagent (ABC Elite; Vector Laboratories, Burlingame, CA, USA), followed by 3,3'-diaminobenzidine (Dojin Chemicals, Kumamoto, Japan) as the chromogen. Finally, the slides were counterstained with hematoxylin. Immunostained sections were assessed under an Olympus microscope with an eyepiece reticule at 200 \times magnification. Cell counts are expressed as means per high-power field (0.202 mm²). At least 2 sections were immunostained, and more than 5 areas were evaluated via the graticule. Results are expressed as positive cell ratio per field. Control group means (arithmetic mean \pm SD) were compared with patient group means by Mann-Whitney U-test at $P = 0.05$.

RESULTS

Although 11 β -HSD1 was expressed to a similar extent in patients and controls, 11 β -HSD2 was expressed more significantly in patients with severe allergic rhinitis, resulting in an increased HSD-1/HSD-2 ratio. The significantly increased expression of 11 β -HSD2 in the nasal epithelium and submucosal inflammatory cells of patients with severe nasal allergy was observed in the present study (Figure 1 and Figure 2).

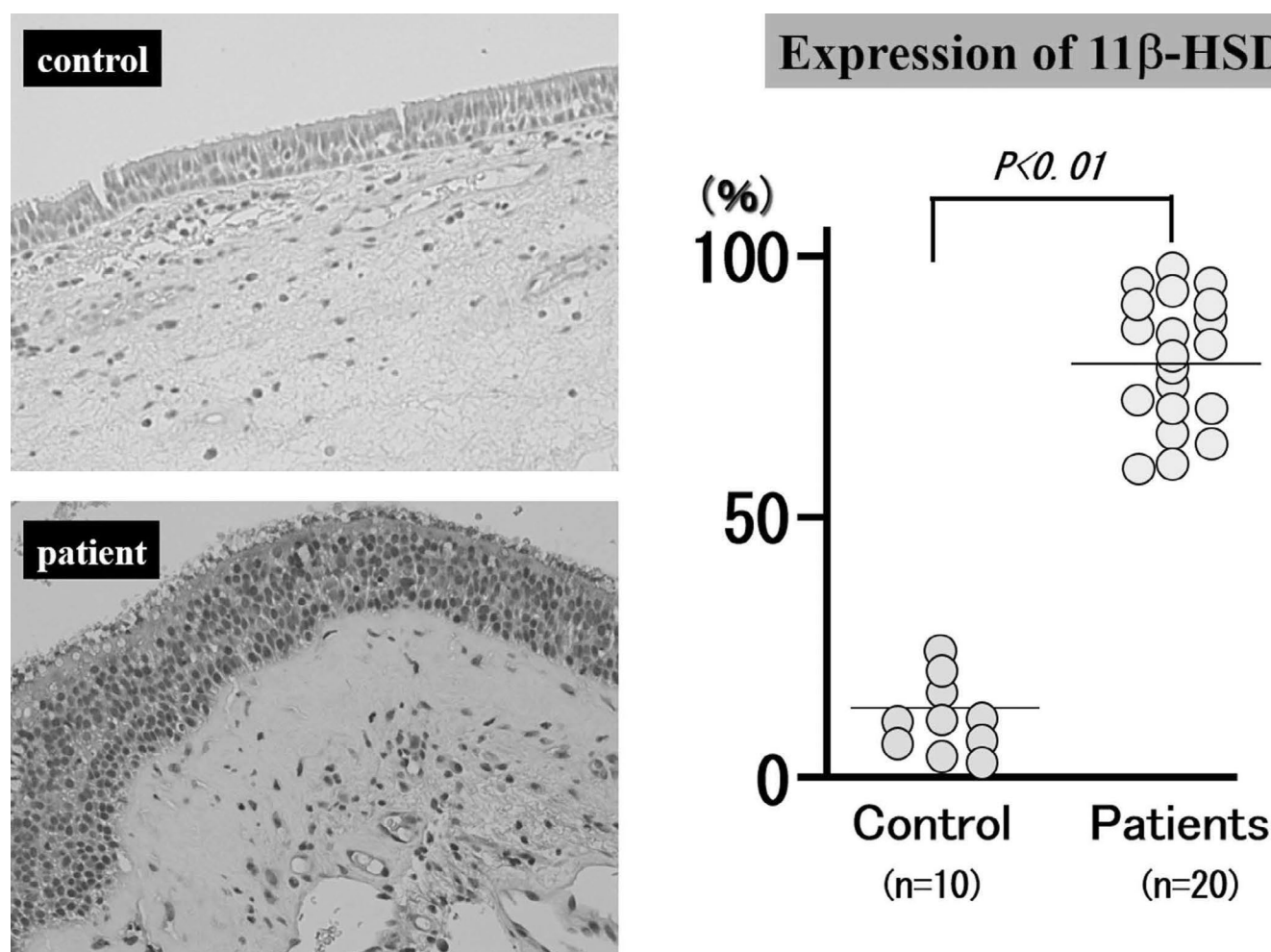


Fig. 2. Representative pathological findings of 11 β -HSD2 immunoreactivities in the nasal mucosa of patients with severe nasal allergy and controls. (original magnification $\times 100$).

DISCUSSION

The tissue levels of bioactive GCs are modulated by 11 β -HSD which interconverts corticosteroids between inactive and active states; only the active forms of corticosteroids are able to interact with GR (3). Previous studies demonstrated that the expression of 11 β -HSD1 was up-regulated and 11 β -HSD2 was decreased in allergic rhinitis and chronic rhinosinusitis (3, 4). On the other hand, a recent report suggests that 11 β -HSD1 and 11 β -HSD2 are associated with steroid sensitivity in childhood nephrotic syndrome, acute lymphoblastic leukemia and 11 β -HSD2 may contribute to steroid resistance (5). The 11 β -HSD2 is also expressed in glucocorticoid-resistant leukemic cell lines where it contributes to prednisolone resistance (6).

The expression of 11 β -HSD was regulated by Th2 type cytokines, chemical mediators and reagents (7,8). Taken together, our results strongly suggest that 11 β -HSD2 expression in nasal mucosal epithelium and inflammatory cells could influence a patient's sensitivity to GC, and explain why some patients exhibit persistent GC resistance

despite high doses and repeated treatment. The mechanisms underlying the development of steroid resistance remain unclear, and there are currently no reliable biomarkers to identify patients who will go on to develop steroid dependence and resistance.

CONCLUSION

Our findings suggest that 11 β -HSD2 plays an important role in resistance to glucocorticoid therapy for allergic rhinitis, and its expression might be used as an additional parameter indicating steroid resistance in allergic rhinitis.

ACKNOWLEDGMENTS

This work was supported by JSPS KAKENHI Grant Number JP17K11363 and the Ministry of Health, Labor, and Welfare of Japan. We express our sincere thanks to Mrs. Yuko Ohta, Uyo Gakuen college, for her editorial assistance.

REFERENCES

1. Ishida A, Ohta N, Koike S, Aoyagi M, Yamakawa M. Overexpression of glucocorticoid receptor-beta in severe allergic rhinitis. *Auris Nasus Larynx* 2010;37:584-588.
2. Ishida A, Ohta N, Suzuki Y, Kakehata S, Okubo K, Ikeda H, et al. Expression of Pendrin and Periostin in Allergic Rhinitis and Chronic Rhinosinusitis. *Allergy Int.* 2012;61:589-595.
3. Jun YJ, Park SJ, Hwang JW, Kim TH, Jung KJ, Jung JY, et al. Differential expression of 11 β -hydroxysteroid dehydrogenase type 1 and 2 in mild and moderate/severe persistent allergic nasal mucosa and regulation of their expression by Th2 cytokines: asthma and rhinitis. *Clin Exp Allergy*. 2014;44(2):197-211.
4. Jun YJ, Park SJ, Kim TH, Lee SH, Lee KJ, Hwang SM, et al. Expression of 11 β -hydroxysteroid dehydrogenase 1 and 2 in patients with chronic rhinosinusitis and their possible contribution to local glucocorticoid activation in sinus mucosa. *J Allergy Clin Immunol*. 2014;134(4):926-934.
5. Sai S, Yamamoto M, Yamaguchi R, Chapman KE, Hongo T. Reciprocal Regulation of 11 β -HSDs May Predict Steroid Sensitivity in Childhood Nephrotic Syndrome. *Pediatrics*. 2016 Sep;138(3).
6. Sai S, Nakagawa Y, Yamaguchi R, et al. Expression of 11 β -hydroxysteroid dehydrogenase 2 contributes to glucocorticoid resistance in lymphoblastic leukemia cells. *Leuk Res*. 2011;35(12):1644-1648.
7. Park SJ, Kook JH, Kim HK, Kang SH, Lim SH, Kim HJ, et al. Macrolides increase the expression of 11 β -hydroxysteroid dehydrogenase 1 in human sinonasal epithelium, contributing to glucocorticoid activation in sinonasal mucosa. *Br J Pharmacol*. 2015;172(21):5083-95.
8. Randall MJ, Kostin SF, Burgess EJ, Hoyt LR, Ather JL, Lundblad LK, et al. Anti-inflammatory effects of levalbuterol-induced 11 β -hydroxysteroid dehydrogenase type 1 activity in airway epithelial cells. *Front Endocrinol (Lausanne)*. 2015; 12;5:236.
9. Hu A, Fatma S, Cao J, Grunstein JS, Nino G, Grumbach Y, et al. Th2 cytokine-induced upregulation of 11 β -hydroxysteroid dehydrogenase-1 facilitates glucocorticoid suppression of proasthmatic airway smooth muscle function. *Am J Physiol Lung Cell Mol Physiol*. 2009;296(5):L790-803.

Word count: 1120 Tables: — Figures: 2 References: 9

Access the article online: DOI: 10.5604/01.3001.0012.6143 Table of content: <https://otolaryngologypl.com/issue/11772>

Corresponding author: Dr. Nobuo Ohta, Division of Otolaryngology, Tohoku Medical and Pharmaceutical University Hospital, 1-12-1, Fukumuro Miyaginoku, Sendai 983-8512, Japan; Email: noohta@hosp.tohoku-mpu.ac.jp

Copyright © 2019 Polish Society of Otorhinolaryngologists Head and Neck Surgeons. Published by Index Copernicus Sp. z o.o. All rights reserved.

Competing interests: The authors declare that they have no competing interests.

Cite this article as: Ohta N, Suzuki Y, Noguchi N, Kakuta R, Suzuki T, Awataguchi T, Takahashi Y, Tomioka-Matsutani S, Ishida Y, Ikeda R, Yamazaki M, Kusano Y, Saito Y, Shoji F, Yaginuma Y, Suzuki T, Osafune H, Kawano T, Miyasaka T, Takahashi T, Ohno I, Wada K.: The expression of 11 β -hydroxysteroid dehydrogenase in severe allergic rhinitis; *Otolaryngol Pol* 2019; DOI: 10.5604/01.3001.0012.6143

Maternal Separation as Early-Life Stress Causes Enhanced Allergic Airway Responses by Inhibiting Respiratory Tolerance in Mice

Ryusuke Ouchi,¹ Tasuku Kawano,¹ Hitomi Yoshida,¹ Masato Ishii,¹
Tomomitsu Miyasaka,¹ Yuichi Ohkawara,² Motoaki Takayanagi,¹
Tomoko Takahashi¹ and Isao Ohno³

¹Division of Pathophysiology, Department of Pharmaceutical Sciences, Faculty of Pharmaceutical Sciences, Tohoku Medical and Pharmaceutical University, Sendai, Miyagi, Japan

²Division of Experimental Allergy and Immunology, Department of Pharmaceutical Sciences, Faculty of Pharmaceutical Sciences, Tohoku Medical and Pharmaceutical University, Sendai, Miyagi, Japan

³Center for Medical Education, Faculty of Medicine, Tohoku Medical and Pharmaceutical University, Sendai, Miyagi, Japan

Epidemiologic studies indicate that exposure to psychosocial stress in early childhood is a risk factor of adult-onset asthma, but the mechanisms of this relationship are poorly understood. Therefore, we examined whether early-life stress increases susceptibility to adult-onset asthma by inhibiting the development of respiratory tolerance. Neonatal BALB/c female mice were aerosolized with ovalbumin (OVA) to induce immune tolerance prior to immune sensitization with an intraperitoneal injection of OVA and the adjuvant aluminum hydroxide. Maternal separation (MS) was applied as an early-life stressor during the induction phase of immune tolerance. The mice were challenged with OVA aerosol in adulthood, and allergic airway responses were evaluated, including airway hyper-responsiveness to inhaled methacholine, inflammatory cell infiltration, bronchoalveolar lavage fluid levels of interleukin (IL)-4, IL-5, and IL-13, and serum OVA-specific IgE. We then evaluated the effects of MS on the development of regulatory T (Treg) cells in bronchial lymph nodes (BLN) and on splenocyte proliferation and cytokine expression. In mice that underwent MS and OVA tolerization, the allergic airway responses and OVA-induced proliferation and IL-4 expression of splenocytes were significantly enhanced. Furthermore, exposure to MS was associated with a lower number of Treg cells in the BLN. These findings suggest that exposure to early-life stress prevents the acquisition of respiratory tolerance to inhaled antigen due to insufficient Treg cell development, resulting in Th2-biased sensitization and asthma onset. We provide the evidence for inhibitory effects of early-life stress on immune tolerance. The present findings may help to clarify the pathogenesis of adult-onset asthma.

Keywords: allergic asthma; early life stress; immune tolerance; regulatory T cell; Th2 immune polarization
Tohoku J. Exp. Med., 2018 November, **246** (3), 155-165. © 2018 Tohoku University Medical Press

Introduction

Bronchial asthma is estimated to affect more than 315 million people worldwide, making it the most common chronic inflammatory disease (To et al. 2012). Asthma is characterized by airway inflammation leading to airway hyper-responsiveness and tissue remodeling and has been shown to be related to various environmental factors, including allergens, infection, and psychosocial stress. The asthmatic inflammatory response is caused by eosinophil infiltration, increased mucous production, and elevated serum IgE levels, which are in turn orchestrated by type-2

T helper (Th2) cells and Th2 cytokines such as interleukin (IL)-4, IL-5, and IL-13. Th2 immune responses are negatively regulated by type-1 T helper (Th1) immune responses and immune tolerance in which regulatory T (Treg) cells play a central role (Fahy 2015; Holgate et al. 2015; Lambrecht and Hammad 2015; Kim et al. 2016; Rothenberg et al. 2017).

Treg cells play a critical role in maintaining immune network balance by suppressing or limiting effector immune responses against internal and external insults, including preventing organ-specific autoimmunity, preventing allograft rejection, and maintaining self-tolerance

Received August 21, 2018; revised and accepted October 18, 2018. Published online November 6, 2018; doi: 10.1620/tjem.246.155.

Correspondence: Tasuku Kawano, Division of Pathophysiology, Department of Pharmaceutical Sciences, Faculty of Pharmaceutical Sciences, Tohoku Medical and Pharmaceutical University, 4-4-1 Komatsushima, Aoba-ku, Sendai, Miyagi 981-8558, Japan.
e-mail: t-kawano@tohoku-mpu.ac.jp

(Palomares et al. 2010; Sakaguchi et al. 2010; Peterson 2012; Martin-Orozco et al. 2017). Generation of Treg cells appears to be dependent on microenvironmental factors, including IL-10 and transforming growth factor β (Palomares et al. 2014; Noval Rivas and Chatila 2016). Compared to healthy subjects, severe asthma patients show reduced numbers of Treg cells in the peripheral blood and sputum as well as impaired suppressive activities (Mamessier et al. 2008). Moreover, the percentage of Treg cells in the bronchoalveolar lavage fluid (BALF) is lower in children (Hartl et al. 2007) and adults (Barczyk et al. 2014) with asthma than in healthy subjects. The failure of Treg cells to suppress Th2-mediated immune responses to innocuous inhaled antigens may lead to an imbalance between the responses of Treg cells and effector Th2 cells to allergens, resulting in the development and maintenance of asthmatic airway inflammation characterized by an uncontrolled Th2-biased immune response (Lloyd and Hawrylowicz 2009; Fujita et al. 2012; Noval Rivas and Chatila 2016).

Recent studies have investigated the mechanisms underlying the impairment of immune tolerance associated with increased susceptibility to allergic asthma. It has been shown in a mouse model that respiratory infections with viruses such as rhinovirus and respiratory syncytial virus (RSV) in early life are risk factors for developing asthma in adult life. Simultaneous rhinovirus infection and tolerance induction in mice inhibited the acquisition of immune tolerance, attenuating the development of Treg cells characterized with the expression of a specific transcription factor, Foxp3 (Mehta et al. 2016). RSV infection impaired immune tolerance by inducing phenotypic changes in Foxp3⁺ Treg cells in an IL-4 dependent pathway, including expression of Th2-specific transcription factor, GATA-3, Th2 cytokine production, and loss of suppressive functions (Krishnamoorthy et al. 2012). IL-33 exposure evoked Th2-like properties in Foxp3⁺ Treg cells, resulting in airway inflammation in tolerized mice (Chen et al. 2017). Further, suppression of prostaglandin I₂ receptor signaling by administration of indomethacin augmented allergen-induced airway inflammation in tolerized mice without affecting Treg cells levels (Zhou et al. 2014). These results suggest that impaired respiratory tolerance leading to increased susceptibility to allergic asthma may result from multiple mechanisms and causes. However, the mechanisms by which tolerogenic immune responses are impaired in asthmatic patients remain to be explored.

Early-life stress exposure has been associated with an increased risk of adult-onset asthma (Ilmarinen et al. 2015; Rosa et al. 2018). For example, experiences of abuse during childhood and adolescence have been shown to be positively associated with adult-onset asthma in African American women (Coogan et al. 2013). Furthermore, childhood maltreatment was associated with elevated odds of lifetime diagnosis of asthma (Scott et al. 2012). However, the pathogenic mechanism underlying the relationship between adult-onset asthma development and

early-life stress is unknown.

Various kinds of stressors have been reported to decrease Treg cell production. The number of Treg cells in the peripheral blood of patients with post-traumatic stress disorder has been shown to be significantly lower than that in control subjects (Loerbroeks et al. 2009; Jergovic et al. 2014). Further, an acute laboratory stressor was able to decrease the number of CD4⁺Foxp3⁺ Treg cells in the peripheral blood of human subjects (Freier et al. 2010). Our group previously demonstrated that the use of restraint as a psychological stressor in adulthood increased susceptibility to asthma by inhibiting the development of Treg cells in a murine model of allergic asthma (Kawano et al. 2018).

Therefore, we have hypothesized that exposure to psychological stress in early life prevents the development of respiratory tolerance by inhibiting Treg cell generation, resulting in a Th2-biased immune response followed by increased susceptibility to allergic asthma. To investigate this hypothesis, we examined the effects of early-life stress on the induction of respiratory tolerance in a murine model of allergic asthma.

Materials and Methods

Mice

Specific-pathogen-free 4-postnatal day (PND)-old female BALB/c mice were purchased with their dams from CLEA Japan (Tokyo, Japan). Mice were housed under a 12-h light/dark cycle at a constant temperature. Sterilized food and water were available *ad libitum*. All experiments described below were approved by the Committee of Animal Experiments at Tohoku Medical and Pharmaceutical University (approval numbers: 14002-cn, 15001-cn, 16002-cn and 17004-cn). Further, all experiments were performed in compliance with relevant institutional guidelines. We took the utmost care to alleviate any pain and suffering in the mice.

Maternal separation

To model early-life stress, mice were subjected to maternal separation (MS) for 3 h per day for 6 consecutive days on PNDs 17-22 (MS mice). As a control for the stress exposure, MS was not performed for a subset of the mice (non-MS mice). Dams were removed from their home cages and placed in identical new cages until the end of the separation period. Each mouse was isolated in a separate container. At the end of the separation period, mice were returned to their home cages, followed by reunion with their dams. In humans, stress caused by early-life adverse events, such as parental neglect, is often associated with disorders of the hypothalamic-pituitary-adrenal (HPA) axis leading to unexpected stress responses including increased anxiety and depression (Tarullo and Gunnar 2006; Maniam et al. 2014). Also, in animal models, early-life stress, such as maternal separation, has been well known to result in reprogramming of the HPA axis associated with increased anxiety-like behavior and exaggerated stress responsiveness in adulthood (Murgatroyd and Spengler 2011; Nishi et al. 2014), and maternal separation is most commonly used as early-life stress in murine models (Tractenberg et al. 2016). Therefore, maternal separation in murine models would be feasible for the early-life stress in childhood of human beings.

Protocols for stress exposure, tolerization, sensitization, and antigen challenge

The mice were sensitized and made to inhale antigen, as described previously (Kawano et al. 2018), after stress exposure and tolerization (Fig. 1). Respiratory tolerance was induced by chicken ovalbumin (OVA) (grade V; Sigma-Aldrich, St. Louis, MO) inhalation on PNDs 18 and 21 with or without MS as described above. For 30 min before stress exposure, aerosolized OVA (5 mg/ml of saline) was flowed through the container (tolerized mice). As a control for tolerance, saline alone was flowed through the containers for a subset of the mice (non-tolerized mice). Then, all mice were ablactated on PND 23, and all 4 groups of mice (non-MS/non-tolerized group, non-MS/tolerized group, MS/non-tolerized group and MS/tolerized group) were subjected to sensitization. Briefly, OVA (8 μ g/mouse) adsorbed onto aluminum hydroxide (Wako Pure Chemical Industries, Osaka, Japan) (4 mg/mouse) was intraperitoneally injected into each mouse on PNDs 24 and 29. On PND 76, all mice were challenged with aerosolized OVA or saline. On PND 77 and PND 81, bronchoalveolar lavage fluids (BALFs) were obtained (Kawano et al. 2018) and processed to measure cytokine content, total cell counts, and cell differentials. After centrifugation, BALF supernatants were stored at -80°C before performing enzyme-linked immunosorbent assays (ELISAs) to measure cytokine levels. Lung tissues were processed for the evaluation of mucus secretion and peribronchial inflammation.

Plasma corticosterone measurements

Before and immediately after MS-stress exposure on PND 17 and immediately after MS-stress exposure on PNDs 19 and 22, blood was collected from stressed and non-stressed mice as previously described (Kawano et al. 2018). Plasma samples separated from blood were stored at -80°C for corticosterone concentration measurements using an enzyme immunoassay kit (Enzo Life Sciences, Farmingdale, NY) according to the manufacturer's protocol. The sensitivity of detection was 32 pg/ml.

Histological analysis of the lungs

Sections of lung tissues collected on PND 81 were stained with periodic acid-Schiff (PAS) to evaluate mucus-containing goblet cells in the bronchial epithelium or with hematoxylin and eosin to study eosinophil infiltration in the peribronchial areas. The number of PAS-positive cells and eosinophils were determined as described previously (Kawano et al. 2018).

OVA-specific IgE measurement

The concentrations of OVA-specific IgE in sera collected on PND 81 were measured with ELISA, as described previously (Kawano et al. 2018). The sensitivity of detection was 1.9×10^{-2} EU/ml for IgE.

Culture of splenocytes

Splenocytes were prepared from mice on PND 76 before the challenge. The cells were cultured at 1×10^6 cells in 200 μ l/well in 96-well culture plates in the presence or absence of OVA (200 μ g/ml) for 72 h. The samples were then centrifuged, and the supernatants were stored at -80°C for subsequent cytokine measurements. Cell proliferation was measured as previously described (Kawano et al. 2018).

Preparation of bronchial lymph node cells

Bronchial lymph nodes (BLNs) obtained from ten non-tolerized mice and from 3 tolerized mice with or without the stress exposure after the last MS on PND 22 were pooled and processed for the preparation of BLN cells as previously reported (Kawano et al. 2018). BLN cells were then analyzed with a flow cytometer as described below.

Flow-cytometric analysis

Cells were pre-incubated with anti-CD16/CD32 (FC gamma III/II receptor; BD Biosciences, Franklin Lakes, NJ) in order to reduce nonspecific binding of subsequent antibodies. Dead cells were excluded using a LIVE/DEAD Fixable Blue Dead Cell Stain Kit (Thermo Fisher Scientific, Waltham, MA). The cells were stained for surface antigens with anti-CD3e-FITC (clone 145-2C11; Miltenyi Biotec, Bergisch Gladbach, Germany), anti-CD4-AF700 (clone RM4-5; BD Biosciences), or isotype-control antibodies. For intracellular staining, cells were stimulated with phorbol 12-myristate 13-acetate (PMA) (5 ng/ml), ionomycin (500 ng/ml), and monensin (2 μ M) for 4 h before surface-antigen staining. After fixation and permeabilization, the cells were incubated with anti-Foxp3-PE-Cy7 (clone FJK-16s; Thermo Fisher Scientific) or an isotype-control antibody. We considered CD3⁺CD4⁺Foxp3⁺ cells to be Treg cells. Cells were counted on a FACSARIA II flow cytometer (BD Biosciences), and the analyses were performed using FACSDiva software (BD Biosciences).

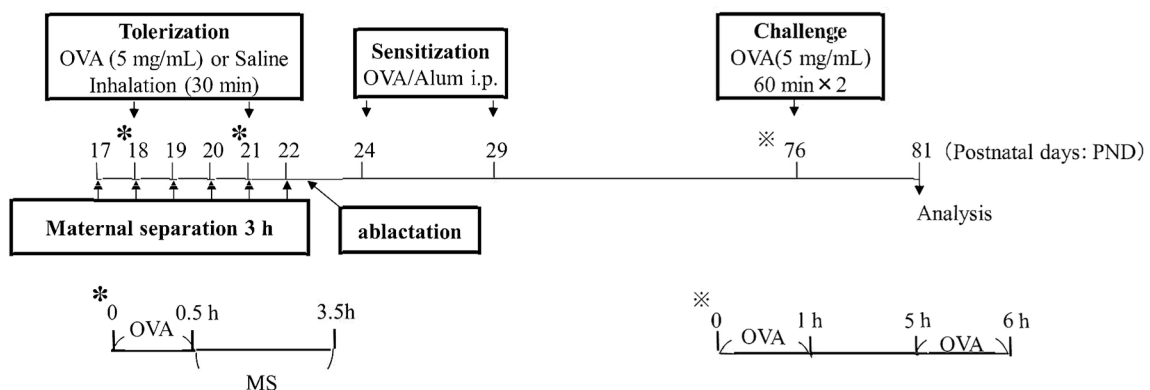


Fig. 1. Schematic representation of the protocols for tolerization, stress exposure, sensitization, and antigen challenge.

Measurements of cytokine contents

The concentrations of IL-4, IL-5, IL-13 and IFN- γ in the BALF supernatants and the splenocyte culture supernatants were measured using ELISA kits (Thermo Fisher Scientific) according to the manufacturer's protocol. The sensitivity of detection was 2 pg/ml for IL-4, 7 pg/ml for IL-5, 1.5 pg/ml for IL-13, and 8 pg/ml for IFN- γ .

Statistical analysis

Data are expressed as mean \pm standard deviation (SD) from multiple independent experiments (as indicated by *n* values). Significant differences between pairs of groups were determined by the nonparametric Mann-Whitney U-test. For comparisons between multiple groups, analysis of variance and Bonferroni's post-hoc tests were performed. These analyses were performed using Prism6 (GraphPad Software, San Diego, CA). $P < 0.05$ was considered statistically significant.

Results

Effects of maternal separation on plasma corticosterone concentrations

Blood was collected from stressed and non-stressed mice before and immediately after the 1st MS-stress exposure on PND 17 and immediately after the 3rd and 6th MS-stress exposures on PNDs 19 and 22. The mean corticosterone concentrations (ng/ml) in MS mice were significantly higher than those in non-MS mice at all 3 of the measured time points (1st: 185.2 ± 191.1 [*n* = 6] vs. 55.9 ± 38.1 [*n* = 6], $P < 0.05$; 3rd: 267.8 ± 234.9 [*n* = 6] vs. 106.4 ± 83.9 [*n* = 7], $P < 0.05$; 6th: 122.3 ± 168.7 [*n* = 7] vs. 24.1 ± 19.8 [*n* = 6], $P < 0.05$). There were no significant differences in corticosterone concentrations between MS and non-MS mice before the stress exposures (Fig. 2).

Effects of MS on airway responsiveness

To investigate the effects of early life stress on asth-

matic airway responses, we first observed airway hyper-responsiveness to inhaled methacholine. As expected, non-MS/tolerized mice (*n* = 7) showed significantly lower airway reactivity (R_L) than non-MS/non-tolerized mice (*n* = 6) at methacholine concentrations of 0.625 mg/mL (1.37 ± 0.21 vs. 2.01 ± 0.57 , $P < 0.05$), 1.25 mg/mL (1.57 ± 0.38 vs. 3.37 ± 1.24 , $P < 0.01$), 2.5 mg/mL (1.92 ± 0.46 vs. 6.79 ± 2.25 , $P < 0.01$), and 5 mg/mL (3.17 ± 1.2 vs. 6.85 ± 1.96 , $P < 0.01$) (Fig. 3A). Similarly, airway sensitivity in non-MS/tolerized mice was significantly lower, shown by higher PC₂₀₀, than in non-MS/non-tolerized mice (3.60 ± 0.87 vs. 1.18 ± 0.25 , $P < 0.01$) (Fig. 3B). Interestingly, MS completely abolished the inhibitory effects of tolerization on airway hyper-responsiveness. Both airway reactivity and airway sensitivity were significantly higher in MS/tolerized mice (*n* = 5) than in non-MS/tolerized mice (R_L , 1.25 mg/mL of methacholine: 3.15 ± 1.85 vs. 1.57 ± 0.38 , $P < 0.05$; 2.5 mg/mL: 7.80 ± 4.24 vs. 1.92 ± 0.46 , $P < 0.01$; 5 mg/mL: 6.13 ± 3.28 vs. 3.17 ± 1.20 , $P < 0.05$; Fig. 3A; PC₂₀₀: 1.44 ± 0.61 vs. 3.60 ± 0.87 , $P < 0.01$; Fig. 3B). Further, both of these measures in the MS/tolerized mice (*n* = 5) were statistically similar to those in the MS/non-tolerized mice (*n* = 3; Fig. 3). There were no significant differences in R_L and PC₂₀₀ between non-MS/non-tolerized mice and MS/non-tolerized mice, suggesting that MS affects airway hyper-responsiveness by modifying the effects of tolerization.

Effects of MS on OVA-specific IgE and airway mucus secretion

Five days after the OVA challenge (PND 81), the amount of OVA-specific IgE was significantly lower in non-MS/tolerized mice than in non-MS/non-tolerized mice (627.2 ± 519.6 EU/ml [*n* = 8] vs. $2,987.8 \pm 1,049.7$ EU/ml

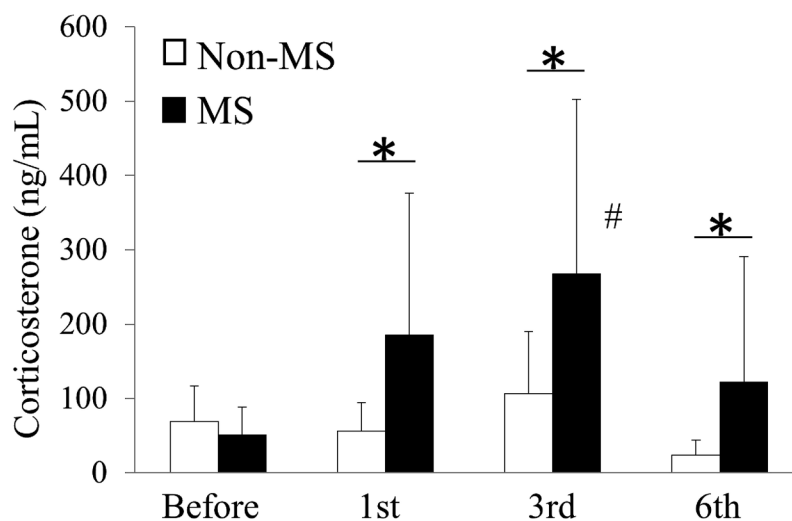


Fig. 2. Effects of MS on plasma corticosterone concentrations.

Blood was collected from MS and non-MS mice before the 1st and after the 1st, 3rd, and 6th MS exposures, and plasma corticosterone levels were measured in enzyme immunoassays. Data are expressed as the mean \pm SD (*n* = 3–11).

* $P < 0.05$ compared to values before stress exposure.

* $P < 0.05$ and ** $P < 0.01$, compared to non-stressed mice on the same day.

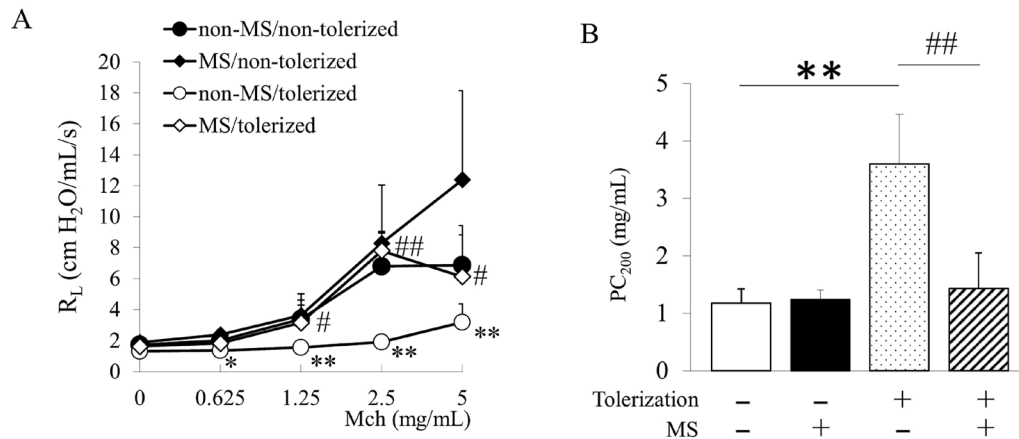


Fig. 3. Effects of MS on methacholine-induced airway hyperresponsiveness.

Airway reactivity (R_L) (A) and airway sensitivity (PC_{200}) (B) were measured 5 days after the last OVA challenge (PND 81). Data are expressed as the mean \pm SD ($n = 3-7$ from 3 independent experiments).

* $P < 0.05$ and ** $P < 0.01$ compared with non-MS/non-tolerized mice.

$P < 0.05$ and ## $P < 0.01$, compared with non-MS/tolerized mice.

[$n = 8$], $P < 0.001$). Further, the IgE levels in the MS/tolerized mice were significantly higher than the levels in the non-MS/tolerized mice ($1,501.3 \pm 1,004.0$ EU/ml [$n = 6$] vs. 627.2 ± 519.6 EU/ml [$n = 8$], $P < 0.05$). Additionally, the IgE levels in the MS/tolerized mice were statistically similar to those in the MS/non-tolerized mice. There was no significant difference in the IgE levels between the non-MS/non-tolerized mice and the MS/non-tolerized mice (Fig. 4A). The numbers of PAS-positive cells in the non-MS/tolerized mice were significantly lower than those in the non-MS/non-tolerized mice, and the numbers in the MS/tolerized mice were significantly lower than those in the non-MS/tolerized mice ($48.6 \pm 12.2\%$ [$n = 6$] vs. $27.6 \pm 10.6\%$ [$n = 8$], $P < 0.05$). The number of PAS-positive cells in the MS/tolerized mice was statistically similar to that in the MS/non-tolerized mice. No significant difference in the number of PAS cells was observed between the non-MS/non-tolerized mice and the MS/non-tolerized mice (Fig. 4B). These findings, shown in Fig. 4, suggest that MS affects OVA-specific IgE levels and mucus secretion by modifying the effects of tolerization.

Effects of MS on airway inflammation and Th2 cytokine secretion

As expected, the non-MS/tolerized mice showed significantly lower numbers of total cells, eosinophils, and lymphocytes in BALF (Fig. 5) compared with the non-MS/non-tolerized mice. OVA-specific IgE and mucus secretion were each measured to assess airway hyper-responsiveness, and the numbers of those cell types in BALF were significantly increased in the MS/tolerized mice compared with the non-MS/tolerized mice. Interestingly, MS significantly increased the number of neutrophils in tolerized, but not non-tolerized, mice. Similar effects of MS were also observed in the Th2 cytokine contents of the BALF (Fig. 6). The BALF concentrations of IFN- γ were not significantly

different between the 4 groups. No effects of MS on airway inflammation or Th2 cytokine contents were observed when comparing MS/non-tolerized mice with non-MS/non-tolerized mice. These data indicate that MS modifies the effects of respiratory tolerization.

Effects of MS on sensitization in tolerized mice

Because MS led to the development of antigen-induced asthmatic responses in tolerized mice, we also investigated the effects of MS on immune tolerance. As expected, pretreating mice with aerosolized-OVA inhibited splenocyte proliferation upon OVA stimulation in vitro. However, in vitro splenocyte proliferation was significantly higher in the mice that were exposed to MS during the induction phase of tolerance compared to the non-MS tolerized mice. Indeed, the MS/tolerized mice and the non-tolerized mice showed similar levels of in vitro splenocyte proliferation. MS had no effects on splenocyte proliferation under non-tolerized condition (Fig. 7A). Moreover, we compared OVA-induced cytokine expression (IL-4 and IFN- γ) by splenocytes in all 4 groups (Fig. 7B and C). Tolerization significantly decreased IL-4 expression in non-MS mice, while MS exposure significantly increased cytokine expression in tolerized mice. The MS/tolerized mice and the non-tolerized mice showed similar IL-4 levels (Fig. 7B). Tolerization had no effects on IFN- γ regardless of whether the mice were exposed to MS or not (Fig. 7C). MS had no effect on cytokine expression in the non-tolerized mice.

Effects of MS on regulatory T cells in BLNs

Because MS inhibited the induction of respiratory tolerance, we analyzed CD3⁺CD4⁺Foxp3⁺ cells as Treg cells in BLNs. The percentage of Treg cells was significantly increased in tolerized mice compared with non-tolerized mice under the non-MS condition. Then, the MS exposure

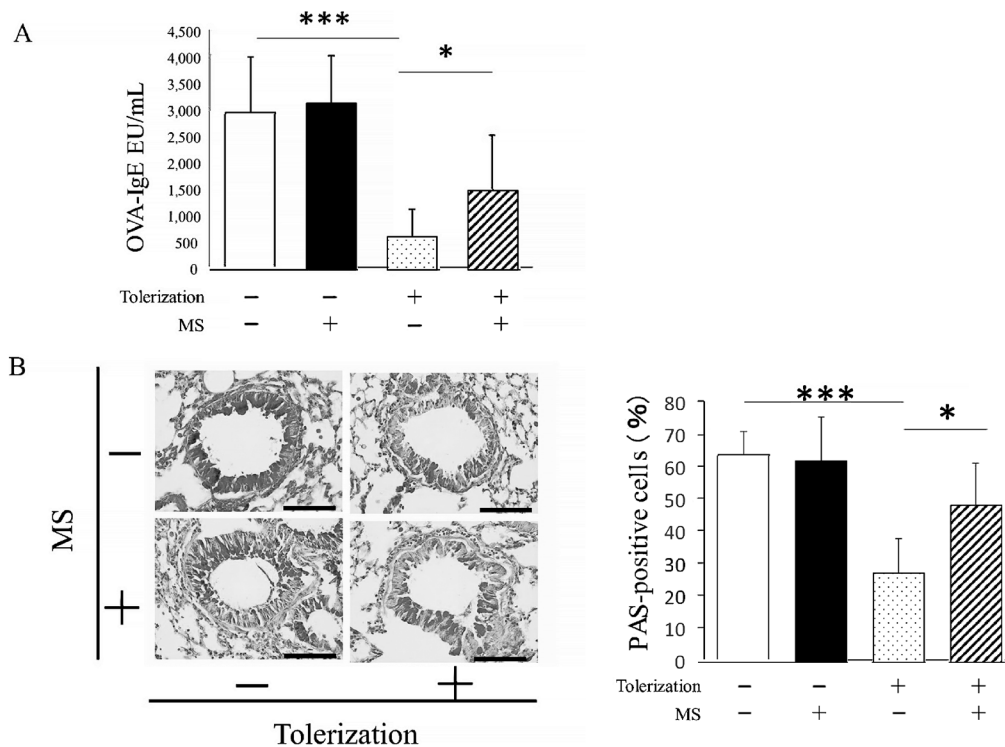


Fig. 4. Effects of MS on OVA-specific IgE and airway mucus secretion.

(A) Serum were obtained from mice of each treatment group 5 days after the last OVA challenge (PND 81). OVA-specific IgE in serum was measured by ELISA. Data are expressed as the mean \pm SD ($n = 6-8$ from 3 independent experiments).

* $P < 0.05$, and *** $P < 0.001$.

(B) Lungs were isolated from mice of each treatment group 5 days after the last OVA challenge (PND 81). Lung sections were prepared and stained with period acid–Schiff (PAS). Shown are representative images of lung sections (left, scale bar, 100 μ m) and the percentage of PAS-positive cells (right) from the 4 mice groups. Data are expressed as the mean \pm SD ($n = 6-8$ mice from 3 independent experiments).

* $P < 0.05$, and *** $P < 0.001$.

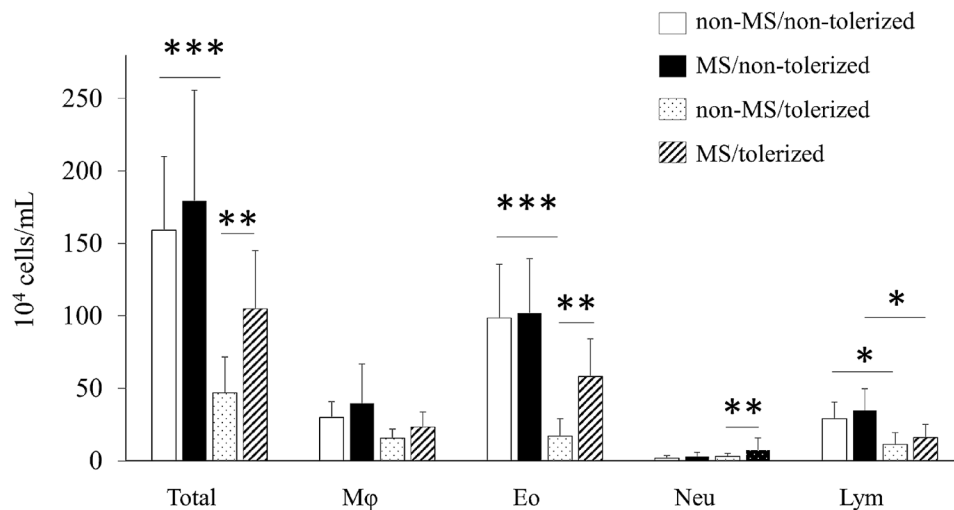


Fig. 5. Effects of MS on airway inflammation.

BALFs were obtained from mice of each group 5 days after the last OVA challenge (PND 81). Total cells (Total), macrophages (Mφ), eosinophils (Eo), neutrophils (Neu), and lymphocytes (Lym) were counted. Data are expressed as the mean \pm SD ($n = 6-8$ from 3 independent experiments).

* $P < 0.05$, ** $P < 0.01$, and *** $P < 0.001$.

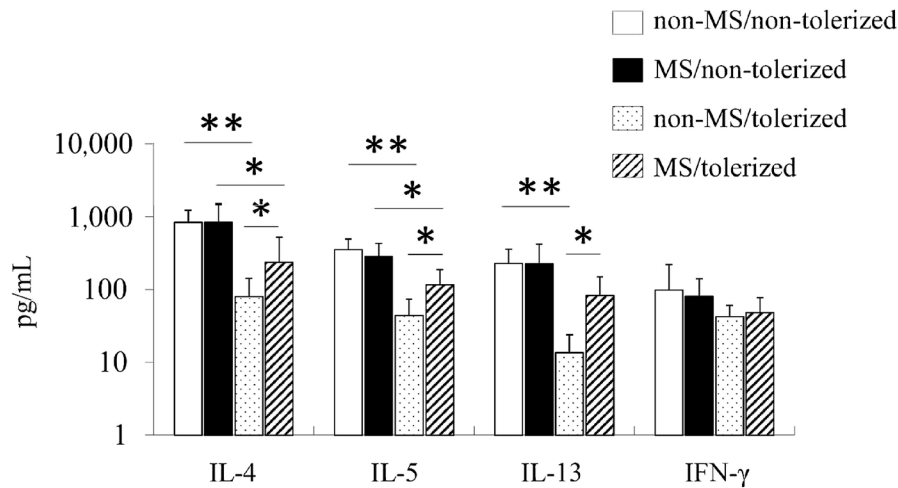


Fig. 6. Effects of MS on BALF cytokine contents.

BALFs were obtained from mice of each group 1 day after the last OVA challenge (PND 77). IL-4, IL-5, IL-13 and IFN- γ levels were measured by ELISA. Data are expressed as the mean \pm SD (n = 7-11 from 4 independent experiments).

* P < 0.05 and ** P < 0.01.

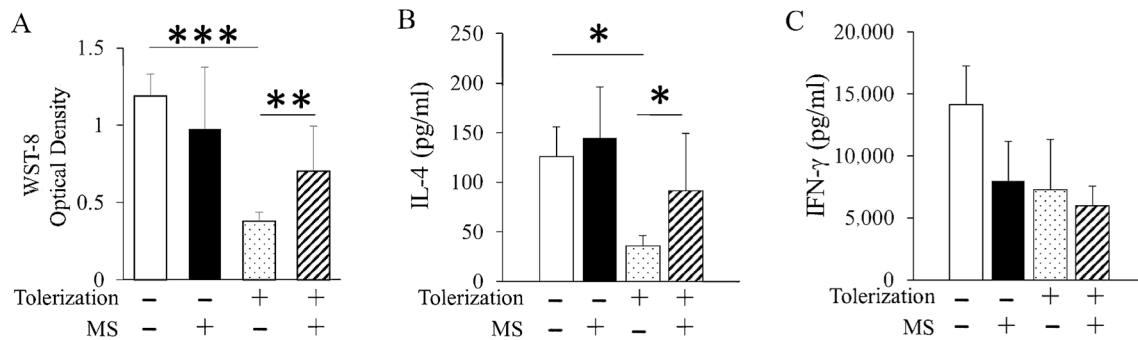


Fig. 7. Effects of MS on sensitization.

On PND 76, splenocytes were prepared from mice of each group of sensitized mice and stimulated *in vitro* with OVA. After a 72-h culture, cell proliferation was measured in WST-8 assays (A). The content of IL-4 (B) and IFN- γ (C) in culture supernatants were determined by ELISA. Data are expressed as the mean \pm SD of triplicate cultures from 3 independent experiments.

* P < 0.05, ** P < 0.01, and *** P < 0.001.

significantly decreased percentage of Treg cells in MS/tolerized mice compared with non-MS/tolerized mice. The percentage of Treg cells in MS/non-tolerized mice was statistically similar to that in non-MS/non-tolerized mice, suggesting that MS had no noticeable effects on the induction of Treg cells under non-tolerized condition. Additionally, the percentage of Treg cells was not statistically different between non-tolerized and tolerized mice under the MS condition (Fig. 8). Together with those findings, we suggest that MS could affect the induction of Treg cells by modifying the effects of tolerization.

Discussion

In this study, we demonstrated for the first time that exposure to MS as a model of early-life psychological stress during the induction phase of immune tolerance in childhood leads to Th2-biased sensitization and allergic airway inflammation in response to inhaled allergen in adult-

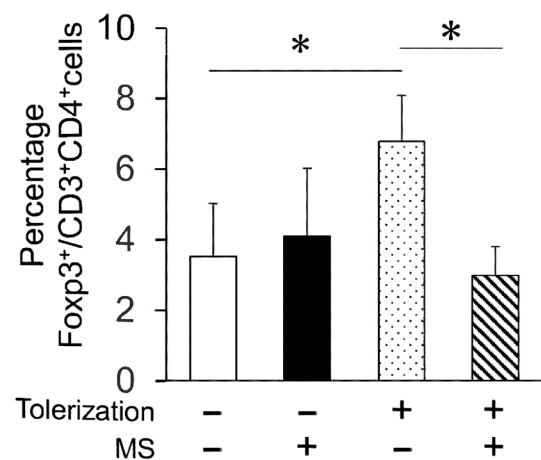


Fig. 8. Effects of MS on Treg cells in BLNs.

BLNs were collected from mice of each group after the final MS (PND 22). The percentages of CD3⁺CD4⁺Foxp3⁺ cells in CD3⁺CD4⁺ cells were determined. Data from 4 independent experiments are expressed as the mean \pm SD.

* P < 0.05.

hood (Figs. 3, 4, 5 and 6). The prevention of the induction of immune tolerance by MS exposure was confirmed by the re-emergence of antigen-specific spleen cell proliferation and IL-4 secretion in MS/tolerized mice, both of which were suppressed in tolerized mice (Fig. 7). Furthermore, MS/tolerized mice showed lower Treg cell levels in BLNs compared to non-MS/tolerized mice (Fig. 8). Thus, stress during the tolerance-induction phase may lead to insufficient differentiation of Treg cells and subsequent failure to prevent Th2-biased immune sensitization.

Antigen exposure in early life through the mucosal route can lead to a predisposition for tolerogenic responses. In mice, the inhalation of OVA by PND 7 has been demonstrated to prevent the generation of OVA-specific IgE, to decrease the accumulation of granulocytes in the BALF, and to reduce the IL-13 levels in the BALF after sensitization and challenge with OVA in adults (Wang and McCusker 2006). In humans, maturation of innate and adaptive immunity, including immune tolerance, is essentially completed by childhood (Lloyd and Marsland 2017). Infants are particularly vulnerable to the effects of psychosocial stress on immune system development, including immune tolerance, because this system is still developing and remains highly reactive and labile for the first 2 years of life (Bosquet Enlow et al. 2014; McLaughlin et al. 2015). Indeed, exposure to psychological stress in critical developmental windows, including early childhood, can result in permanently altered changes to stress-response systems, including the autonomic, neuroendocrine system, and the immune system, which are thought to play a role in the development of respiratory disorders, including asthma (Wright 2005, 2007). Based on these findings, investigating the relationship between immune tolerance and early-life stress may help to clarify the mechanisms of asthma development in adulthood.

Previous studies have shown that neutrophils activated *in vitro* mediated the migration of eosinophils (Kikuchi et al. 2006; Nishihara et al. 2015). Therefore, in the current study, it is possible that the increased neutrophils in MS/tolerized mice had influenced the migration of eosinophils into the airway. IL-17A, produced mainly by Th17, has been demonstrated to play a critical role in the induction of neutrophilic airway inflammation in severe asthma (Chesne et al. 2014; Ray and Kolls 2017). We previously observed using an adult murine model of allergic asthma that restraint stress as the psychological stress induced the airway infiltration of not only eosinophils but also neutrophils (Kawano et al. 2018), and that the neutrophil accumulation was associated with the increase of IL-17A contents and Th17 numbers in the lung of the stress/tolerized mice compared with the non-stress/tolerized mice (unpublished data). Therefore, also in the MS/tolerized mice, the development of Th17 cells and the production of IL-17A by stress exposure might be involved in the infiltration of neutrophils, which would need to be investigated.

The inhibitory effects of MS exposure on Treg cell

development are supported by human studies showing that traumatic and mental stress each reduce the number Treg cells in peripheral blood (Sommershof et al. 2009; Freier et al. 2010; Jergovic et al. 2014). Although the pathways linking stress exposure and Treg cell levels have not yet been determined, it has been shown that the stress hormone glucocorticoid (GC), released upon stress-triggered activation of the hypothalamic-pituitary-adrenal cortex axis, may play a critical role in stress-induced perturbation of immune tolerance. Indeed, GC is recognized worldwide as being effective for treating and preventing asthma due to its anti-allergic activities. GC's mechanisms of action include reducing airway inflammation and decreasing airway hyper-responsiveness by limiting cytokine production in T cells and epithelial cells and thus impairing the recruitment, survival, and activation of eosinophils and other inflammatory cells (John et al. 1998; Fahy 2015). However, GC has been shown to amplify Th2 immune responses via several mechanisms. GC treatment can potentiate Th2 differentiation by either reducing a pivotal Th1-associated cytokine, IL-12, secretion from antigen-presenting cells (DeKruyff et al. 1998) or by directly suppressing Th1 cell polarization (Miyaura and Iwata 2002). Transient GC administration during sensitization was shown to permanently enhance Th2 responses in an allergic mouse model (Wiley et al. 2004). In addition, GC treatment during antigen inhalation to promote the development of respiratory tolerance was shown to eliminate IL-10-producing dendritic cells, which are required for the development of IL-10-producing Treg cells, leading to Th2-biased sensitization and allergic airway responses upon antigen exposure (Stock et al. 2005). Interestingly, the development of respiratory tolerance was shown to be prevented by systemic, but not local, GC administration (Kerzerho et al. 2012), in accordance with our finding that respiratory tolerance was inhibited in mice that showed increased blood GC levels in response to stress exposure (Fig. 2). Systemic administration of GC to immunocompetent humans and naïve mice significantly reduced the number, but not the suppressive function, of Foxp3⁺ Treg cells in the blood (Sbiera et al. 2011). More importantly, systemic GC administration and local GC administration were each shown to decrease the number of Foxp3⁺ Treg cells in mouse lungs during sensitization and allergen-induced inflammation (Olsen et al. 2015). In addition, we previously demonstrated that restraint as a psychological stressor in adulthood inhibited the development of Treg cells through the action of glucocorticoids (Kawano et al. 2018), indicated by the result that a GC-receptor antagonist administered before each stress exposure during the tolerance-induction phase eliminated the anti-tolerogenic effects of psychological stress. Previous studies showed that the transfer of transforming growth factor β (Polte and Hansen 2008; Verhasselt et al. 2008, Verhasselt 2010) or the antigen-immunoglobulin complex (Mosconi et al. 2010; Ohsaki et al. 2018) through breast milk of tolerized-mother mice was important for the induction of immune tolerance in the

newborns by lactation. On the other hand, in the current study, the tolerance in pups was induced by OVA inhalation directly to pups but not to mother mice. Furthermore, MS showed no effect on the asthmatic responses under non-tolerized condition. Accordingly, the interruption of lactation might be considered to have little effect on the acquisition of tolerance in pups, although the influence of the interruption of lactation is not entirely excluded.

Recent studies have investigated the mechanisms underlying the absence of immune tolerance associated with increased susceptibility to allergic asthma. Viral respiratory infections in early life are risk factors for developing asthma in adult life. Simultaneous infection with rhinovirus and induction of tolerance in mice increased susceptibility to allergic airway responses by inhibiting the acquisition of immune tolerance induced by intranasal OVA and reducing the development of Foxp3⁺ Treg cells through the expression of Th2-oriented molecules such as OX40 ligand expression by lung dendritic cells and IL-33 and thymic stromal lymphopoietin expression by airway epithelial cells (Mehta et al. 2016). After OVA tolerization by breast milk from OVA-exposed maternal mice, recurrent RSV infection in pups induced allergic responses in adult life (6 weeks old), while uninfected pups showed no such responses. RSV infection was also shown to alter the phenotype of Foxp3⁺ Treg cells in an IL-4 dependent pathway, including GATA-3 expression, Th2 cytokine production, and loss of suppressive activity (Krishnamoorthy et al. 2012). The potential of IL-33 to overcome acquired immune tolerance was confirmed by a study that showed that administering intranasal IL-33 to tolerized mice (during or after sensitization) caused allergen-induced airway inflammation and that IL-33 binds Treg cells and thus evokes Th2-like properties by inducing GATA-3 expression and Th2 cytokine synthesis, which have been associated with a loss of suppressive function (Chen et al. 2017). The ability of airway epithelial cells to overwhelm acquired immune tolerance was also demonstrated using another allergic murine model. NF- κ B activation in airway epithelial cells during sensitization elicited allergic airway responses in tolerized mice in association with the activation of myeloid dendritic cells required for allergic responses in IL-4- and IL-1-dependent manners (Ather et al. 2015). There might be distinctive mechanisms which impair respiratory tolerance leading to increased susceptibility to allergic asthma. These mechanisms might depend on causative factors, such as activation of endocrine pathways by psychological stress, as in the current study, or inflammatory processes by viral infection (Krishnamoorthy et al. 2012; Mehta et al. 2016), or they may depend on developmental time points, such as insufficient Treg cell development during the induction phase of immune tolerance (Mehta et al. 2016) or Th2-like-phenotypic changes of Treg cells (Krishnamoorthy et al. 2012) or development of Th2-oriented dendritic cells (Huang et al. 2014) after the acquisition of immune tolerance.

In conclusion, we provide the evidence that MS as a psychological stressor inhibits the development of respiratory tolerance by suppressing Treg cell induction, resulting in increased susceptibility to allergic asthma through Th2-biased immune sensitization. Future studies are necessary to explore the neuroendocrine pathway linking stress exposure to GC release, including the role of neuropeptides involved in stress-related asthma exacerbations, such as opioids (Drolet et al. 2001; Miyasaka et al. 2018), as well as the endocrine-immune pathway, especially with regards to the interaction between GCs and dendritic cells leading to impaired immune tolerance.

Acknowledgments

This work was supported in part by a Grant-in-Aid for Scientific Research (C) (Nos. 25461164, 17K09624), a Grant-in-Aid for Young Scientists (B) (Nos. 16K19608, 17K16212), and the Matching Fund Subsidy for Private Universities (Nos. S1001002, S1511001L) from the Ministry of Education, Culture, Sports, Science and Technology (MEXT) of Japan. The funders played no role in the study design, the collection, analysis, and interpretation of data, or the preparation of the manuscript.

Conflict of Interest

The authors declare no conflict of interest.

References

- Ather, J.L., Foley, K.L., Suratt, B.T., Boyson, J.E. & Poynter, M.E. (2015) Airway epithelial NF- κ B activation promotes the ability to overcome inhalational antigen tolerance. *Clin. Exp. Allergy*, **45**, 1245-1258.
- Barczyk, A., Pierzchala, W., Caramori, G., Wiaderkiewicz, R., Kaminski, M., Barnes, P.J. & Adcock, I.M. (2014) Decreased percentage of CD4(+)Foxp3(+)TGF- β (+) and increased percentage of CD4(+)IL-17(+) cells in bronchoalveolar lavage of asthmatics. *J. Inflamm. (Lond)*, **11**, 22.
- Bosquet Enlow, M., King, L., Schreier, H.M., Howard, J.M., Rosenfield, D., Ritz, T. & Wright, R.J. (2014) Maternal sensitivity and infant autonomic and endocrine stress responses. *Early Hum. Dev.*, **90**, 377-385.
- Chen, C.C., Kobayashi, T., Iijima, K., Hsu, F.C. & Kita, H. (2017) IL-33 dysregulates regulatory T cells and impairs established immunologic tolerance in the lungs. *J. Allergy Clin. Immunol.*, **140**, 1351-1363.
- Chesne, J., Braza, F., Mahay, G., Brouard, S., Aronica, M. & Magnan, A. (2014) IL-17 in severe asthma. Where do we stand? *Am. J. Respir. Crit. Care Med.*, **190**, 1094-1101.
- Coogan, P.F., Wise, L.A., O'Connor, G.T., Brown, T.A., Palmer, J.R. & Rosenberg, L. (2013) Abuse during childhood and adolescence and risk of adult-onset asthma in African American women. *J. Allergy Clin. Immunol.*, **131**, 1058-1063.
- DeKruyff, R.H., Fang, Y. & Umetsu, D.T. (1998) Corticosteroids enhance the capacity of macrophages to induce Th2 cytokine synthesis in CD4⁺ lymphocytes by inhibiting IL-12 production. *J. Immunol.*, **160**, 2231-2237.
- Drolet, G., Dumont, E.C., Gosselin, I., Kinkead, R., Laforest, S. & Trotter, J.F. (2001) Role of endogenous opioid system in the regulation of the stress response. *Prog. Neuropsychopharmacol. Biol. Psychiatry*, **25**, 729-741.
- Fahy, J.V. (2015) Type 2 inflammation in asthma: present in most, absent in many. *Nat. Rev. Immunol.*, **15**, 57-65.
- Freier, E., Weber, C.S., Nowotne, U., Horn, C., Bartels, K., Meyer, S., Hildebrandt, Y., Luetkens, T., Cao, Y., Pabst, C., Muzzulini, J., Schnee, B., Brunner-Weinzierl, M.C., Marangolo, M.,

- Bokemeyer, C., et al. (2010) Decrease of CD4(+)FOXP3(+) T regulatory cells in the peripheral blood of human subjects undergoing a mental stressor. *Psychoneuroendocrinology*, **35**, 663-673.
- Fujita, H., Meyer, N., Akdis, M. & Akdis, C.A. (2012) Mechanisms of immune tolerance to allergens. *Chem. Immunol. Allergy*, **96**, 30-38.
- Hartl, D., Koller, B., Mehlhorn, A.T., Reinhardt, D., Nicolai, T., Schendel, D.J., Griese, M. & Krauss-Etschmann, S. (2007) Quantitative and functional impairment of pulmonary CD4+CD25hi regulatory T cells in pediatric asthma. *J. Allergy Clin. Immunol.*, **119**, 1258-1266.
- Holgate, S.T., Wenzel, S., Postma, D.S., Weiss, S.T., Renz, H. & Sly, P.D. (2015) Asthma. *Nat. Rev. Dis. Primers*, **1**, 15025.
- Huang, X.M., Liu, X.S., Lin, X.K., Yu, H., Sun, J.Y., Liu, X.K., Chen, C., Jin, H.L., Zhang, G.E., Shi, X.X., Zhang, Q. & Yu, J.R. (2014) Role of plasmacytoid dendritic cells and inducible costimulator-positive regulatory T cells in the immunosuppression microenvironment of gastric cancer. *Cancer Sci.*, **105**, 150-158.
- Ilmarinen, P., Tuomisto, L.E. & Kankaanranta, H. (2015) Phenotypes, risk factors, and mechanisms of adult-onset asthma. *Mediators Inflamm.*, **2015**, 514868.
- Jergovic, M., Bendelja, K., Vidovic, A., Savic, A., Vojvoda, V., Aberle, N., Rabatic, S., Jovanovic, T. & Sabioncello, A. (2014) Patients with posttraumatic stress disorder exhibit an altered phenotype of regulatory T cells. *Allergy Asthma Clin. Immunol.*, **10**, 43.
- John, M., Lim, S., Seybold, J., Jose, P., Robichaud, A., O'Connor, B., Barnes, P.J. & Chung, K.F. (1998) Inhaled corticosteroids increase interleukin-10 but reduce macrophage inflammatory protein-1alpha, granulocyte-macrophage colony-stimulating factor, and interferon-gamma release from alveolar macrophages in asthma. *Am. J. Respir. Crit. Care Med.*, **157**, 256-262.
- Kawano, T., Ouchi, R., Ishigaki, T., Masuda, C., Miyasaka, T., Ohkawara, Y., Ohta, N., Takayanagi, M., Takahashi, T. & Ohno, I. (2018) Increased susceptibility to allergic asthma with the impairment of respiratory tolerance caused by psychological stress. *Int. Arch. Allergy Immunol.*, **177**, 1-15.
- Kerzerho, J., Wunsch, D., Szely, N., Meyer, H.A., Lurz, L., Rose, L., Wahn, U., Akbari, O. & Stock, P. (2012) Effects of systemic versus local administration of corticosteroids on mucosal tolerance. *J. Immunol.*, **188**, 470-476.
- Kikuchi, I., Kikuchi, S., Kobayashi, T., Hagiwara, K., Sakamoto, Y., Kanazawa, M. & Nagata, M. (2006) Eosinophil trans-basement membrane migration induced by interleukin-8 and neutrophils. *Am. J. Respir. Cell Mol. Biol.*, **34**, 760-765.
- Kim, R.Y., Rae, B., Neal, R., Donovan, C., Pinkerton, J., Balachandran, L., Starkey, M.R., Knight, D.A., Horvat, J.C. & Hansbro, P.M. (2016) Elucidating novel disease mechanisms in severe asthma. *Clin. Transl. Immunology*, **5**, e91.
- Krishnamoorthy, N., Khare, A., Oriss, T.B., Raundhal, M., Morse, C., Yarlagaadda, M., Wenzel, S.E., Moore, M.L., Peebles, R.S. Jr., Ray, A. & Ray, P. (2012) Early infection with respiratory syncytial virus impairs regulatory T cell function and increases susceptibility to allergic asthma. *Nat. Med.*, **18**, 1525-1530.
- Lambrecht, B.N. & Hammad, H. (2015) The immunology of asthma. *Nat. Immunol.*, **16**, 45-56.
- Lloyd, C.M. & Hawrylowicz, C.M. (2009) Regulatory T cells in asthma. *Immunity*, **31**, 438-449.
- Lloyd, C.M. & Marsland, B.J. (2017) Lung homeostasis: influence of age, microbes, and the immune system. *Immunity*, **46**, 549-561.
- Loerbroeks, A., Apfelbacher, C.J., Thayer, J.F., Debling, D. & Sturmer, T. (2009) Neuroticism, extraversion, stressful life events and asthma: a cohort study of middle-aged adults. *Allergy*, **64**, 1444-1450.
- Mameessier, E., Nieves, A., Lorec, A.M., Dupuy, P., Pinot, D., Pinet, C., Vervloet, D. & Magnan, A. (2008) T-cell activation during exacerbations: a longitudinal study in refractory asthma. *Allergy*, **63**, 1202-1210.
- Maniam, J., Antoniadis, C. & Morris, M.J. (2014) Early-life stress, HPA axis adaptation, and mechanisms contributing to later health outcomes. *Front. Endocrinol. (Lausanne)*, **5**, 73.
- Martin-Orozco, E., Norte-Munoz, M. & Martinez-Garcia, J. (2017) Regulatory T cells in allergy and asthma. *Front. Pediatr.*, **5**, 117.
- McLaughlin, K.A., Sheridan, M.A., Tibu, F., Fox, N.A., Zeanah, C.H. & Nelson, C.A. 3rd (2015) Causal effects of the early caregiving environment on development of stress response systems in children. *Proc. Natl. Acad. Sci. USA*, **112**, 5637-5642.
- Mehta, A.K., Duan, W., Doerner, A.M., Traves, S.L., Broide, D.H., Proud, D., Zuraw, B.L. & Croft, M. (2016) Rhinovirus infection interferes with induction of tolerance to aeroantigens through OX40 ligand, thymic stromal lymphopoietin, and IL-33. *J. Allergy Clin. Immunol.*, **137**, 278-288.
- Miyasaka, T., Dobashi-Okuyama, K., Takahashi, T., Takayanagi, M. & Ohno, I. (2018) The interplay between neuroendocrine activity and psychological stress-induced exacerbation of allergic asthma. *Allergol. Int.*, **67**, 32-42.
- Miyaura, H. & Iwata, M. (2002) Direct and indirect inhibition of Th1 development by progesterone and glucocorticoids. *J. Immunol.*, **168**, 1087-1094.
- Mosconi, E., Rekima, A., Seitz-Polski, B., Kanda, A., Fleury, S., Tissandie, E., Monteiro, R., Dombrowicz, D.D., Julia, V., Glaichenhaus, N. & Verhasselt, V. (2010) Breast milk immune complexes are potent inducers of oral tolerance in neonates and prevent asthma development. *Mucosal Immunol.*, **3**, 461-474.
- Murgatroyd, C. & Spengler, D. (2011) Epigenetic programming of the HPA axis: early life decides. *Stress*, **14**, 581-589.
- Nishi, M., Horii-Hayashi, N. & Sasagawa, T. (2014) Effects of early life adverse experiences on the brain: implications from maternal separation models in rodents. *Front. Neurosci.*, **8**, 166.
- Nishihara, F., Nakagome, K., Kobayashi, T., Noguchi, T., Araki, R., Uchida, Y., Soma, T. & Nagata, M. (2015) Trans-basement membrane migration of eosinophils induced by LPS-stimulated neutrophils from human peripheral blood *in vitro*. *ERJ Open Res.*, **1**.
- Noval Rivas, M. & Chatila, T.A. (2016) Regulatory T cells in allergic diseases. *J. Allergy Clin. Immunol.*, **138**, 639-652.
- Ohsaki, A., Venturelli, N., Buccigrosso, T.M., Osganian, S.K., Lee, J., Blumberg, R.S. & Oyoshi, M.K. (2018) Maternal IgG immune complexes induce food allergen-specific tolerance in offspring. *J. Exp. Med.*, **215**, 91-113.
- Olsen, P.C., Kitoko, J.Z., Ferreira, T.P., de-Azevedo, C.T., Arantes, A.C. & Martins Mu, A. (2015) Glucocorticoids decrease Treg cell numbers in lungs of allergic mice. *Eur. J. Pharmacol.*, **747**, 52-58.
- Palomares, O., Martin-Fontecha, M., Lauener, R., Traidl-Hoffmann, C., Cavkaytar, O., Akdis, M. & Akdis, C.A. (2014) Regulatory T cells and immune regulation of allergic diseases: roles of IL-10 and TGF- β . *Genes Immun.*, **15**, 511-520.
- Palomares, O., Yaman, G., Azkur, A.K., Akkoc, T., Akdis, M. & Akdis, C.A. (2010) Role of Treg in immune regulation of allergic diseases. *Eur. J. Immunol.*, **40**, 1232-1240.
- Peterson, R.A. (2012) Regulatory T-cells: diverse phenotypes integral to immune homeostasis and suppression. *Toxicol. Pathol.*, **40**, 186-204.
- Polte, T. & Hansen, G. (2008) Maternal tolerance achieved during pregnancy is transferred to the offspring via breast milk and persistently protects the offspring from allergic asthma. *Clin. Exp. Allergy*, **38**, 1950-1958.
- Ray, A. & Kolls, J.K. (2017) Neutrophilic Inflammation in Asthma and Association with Disease Severity. *Trends Immunol.*, **38**,

- 942-954.
- Rosa, M.J., Lee, A.G. & Wright, R.J. (2018) Evidence establishing a link between prenatal and early-life stress and asthma development. *Curr. Opin. Allergy Clin. Immunol.*, **18**, 148-158.
- Rothenberg, M.E., Saito, H. & Peebles, R.S. Jr. (2017) Advances in mechanisms of allergic disease in 2016. *J. Allergy Clin. Immunol.*, **140**, 1622-1631.
- Sakaguchi, S., Miyara, M., Costantino, C.M. & Hafler, D.A. (2010) FOXP3⁺ regulatory T cells in the human immune system. *Nat. Rev. Immunol.*, **10**, 490-500.
- Sbiera, S., Dexneit, T., Reichardt, S.D., Michel, K.D., van den Brandt, J., Schnull, S., Kraus, L., Beyer, M., Mlynski, R., Wortmann, S., Allolio, B., Reichardt, H.M. & Fassnacht, M. (2011) Influence of short-term glucocorticoid therapy on regulatory T cells in vivo. *PLoS One*, **6**, e24345.
- Scott, K.M., Smith, D.A. & Ellis, P.M. (2012) A population study of childhood maltreatment and asthma diagnosis: differential associations between child protection database versus retrospective self-reported data. *Psychosom. Med.*, **74**, 817-823.
- Sommershof, A., Aichinger, H., Engler, H., Adenauer, H., Catani, C., Boneberg, E.M., Elbert, T., Groettrup, M. & Kolassa, I.T. (2009) Substantial reduction of naive and regulatory T cells following traumatic stress. *Brain Behav. Immun.*, **23**, 1117-1124.
- Stock, P., Akbari, O., DeKruyff, R.H. & Umetsu, D.T. (2005) Respiratory tolerance is inhibited by the administration of corticosteroids. *J. Immunol.*, **175**, 7380-7387.
- Tarullo, A.R. & Gunnar, M.R. (2006) Child maltreatment and the developing HPA axis. *Horm. Behav.*, **50**, 632-639.
- To, T., Stanojevic, S., Moores, G., Gershon, A.S., Bateman, E.D., Cruz, A.A. & Boulet, L.P. (2012) Global asthma prevalence in adults: findings from the cross-sectional world health survey. *BMC Public Health*, **12**, 204.
- Tractenberg, S.G., Levandowski, M.L., de Azeredo, L.A., Orso, R., Roithmann, L.G., Hoffmann, E.S., Brenhouse, H. & Grassi-Oliveira, R. (2016) An overview of maternal separation effects on behavioural outcomes in mice: evidence from a four-stage methodological systematic review. *Neurosci. Biobehav. Rev.*, **68**, 489-503.
- Verhasselt, V. (2010) Neonatal tolerance under breastfeeding influence: the presence of allergen and transforming growth factor-beta in breast milk protects the progeny from allergic asthma. *J. Pediatr.*, **156**, S16-20.
- Verhasselt, V., Milcent, V., Cazareth, J., Kanda, A., Fleury, S., Dombrowicz, D., Glaichenhaus, N. & Julia, V. (2008) Breast milk-mediated transfer of an antigen induces tolerance and protection from allergic asthma. *Nat. Med.*, **14**, 170-175.
- Wang, Y. & McCusker, C. (2006) Neonatal exposure with LPS and/or allergen prevents experimental allergic airways disease: development of tolerance using environmental antigens. *J. Allergy Clin. Immunol.*, **118**, 143-151.
- Wiley, R.E., Cwiartka, M., Alvarez, D., Mackenzie, D.C., Johnson, J.R., Goncharova, S., Lundblad, L. & Jordana, M. (2004) Transient corticosteroid treatment permanently amplifies the Th2 response in a murine model of asthma. *J. Immunol.*, **172**, 4995-5005.
- Wright, R.J. (2005) Stress and atopic disorders. *J. Allergy Clin. Immunol.*, **116**, 1301-1306.
- Wright, R.J. (2007) Prenatal maternal stress and early caregiving experiences: implications for childhood asthma risk. *Paediatr. Perinat. Epidemiol.*, **21** Suppl. 3, 8-14.
- Zhou, W., Goleniewska, K., Zhang, J., Dulek, D.E., Toki, S., Lotz, M.T., Newcomb, D.C., Boswell, M.G., Polosukhin, V.V., Milne, G.L., Wu, P., Moore, M.L., FitzGerald, G.A. & Peebles, R.S. Jr. (2014) Cyclooxygenase inhibition abrogates aeroallergen-induced immune tolerance by suppressing prostaglandin I₂ receptor signaling. *J. Allergy Clin. Immunol.*, **134**, 698-705.

ORIGINAL ARTICLE

Basic Mechanisms in Allergic Disease

Sex-based differences in CD103⁺ dendritic cells promote female-predominant Th2 cytokine production during allergic asthma

C. Masuda¹ | T. Miyasaka¹ | K. Kawakami¹ | J. Inokuchi² | T. Kawano¹ |
K. Dobashi-Okuyama¹ | T. Takahashi¹ | M. Takayanagi¹ | I. Ohno³

¹Division of Pathophysiology, Department of Pharmaceutical Sciences, Faculty of Pharmaceutical Sciences, Tohoku Medical and Pharmaceutical University, Sendai, Japan

²Division of Glycopathology, Institute of Molecular Biomembranes and Glycobiology, Tohoku Medical and Pharmaceutical University, Sendai, Japan

³Center for Medical Education, Faculty of Medicine, Tohoku Medical and Pharmaceutical University, Sendai, Japan

Correspondence

Tomomitsu Miyasaka, Division of Pathophysiology, Department of Pharmaceutical Sciences, Faculty of Pharmaceutical Sciences, Tohoku Medical and Pharmaceutical University, Sendai, Japan.
Email: t-miya13@tohoku-mpu.ac.jp

Present address

K. Dobashi-Okuyama, Department of Microbiology, Faculty of Medicine, Interdisciplinary Graduate School of Medicine and Engineering, University of Yamanashi, Yamanashi, Japan.

Funding information

Ministry of Education, Culture, Sports, Science and Technology of Japan, Grant/Award Number: Scientific Research (C) (No. 25461164), Research Activity Start-up (No. 25893222), Young Scientists (B) (No. 16K19608), Matching Fund Subsidy for Private Universities

Summary

Background: Gender disparities in adult patients with asthma regarding its prevalence and severity are mainly due to enhanced type 2 T-helper (Th2) cytokine production in female patients compared to that in male patients. However, the pathways mediating this effect remain unclear.

Objective: We aimed to determine the roles of two major subsets of dendritic cells (DCs) in females, specifically those displaying CD11b or CD103, during enhanced Th2 priming after allergen exposure, using an ovalbumin-induced asthma mouse model.

Methods: Sex-based differences in the number of DCs at inflamed sites, costimulatory molecule expression on DCs, and the ability of DCs to differentiate naïve CD4⁺ T cells into Th2 population were evaluated after allergen exposure in asthmatic mice. In addition, we assessed the role of 17 β -oestradiol in CD103⁺ DC function during Th2 priming in vitro.

Results: The number of CD11b^{high} DCs and CD103⁺ DCs in the lung and bronchial lymph node (BLN) was increased to a greater extent in female mice than in male mice at 16 to 20 hours after ovalbumin (OVA) inhalation. In BLNs, CD86 and I-A/I-E expression levels and antigen uptake ability in CD103⁺ DCs, but not in CD11b^{high} DCs, were greater in female mice than in male mice. Furthermore, CD4⁺ T cells cultured with CD103⁺ DCs from female mice produced higher levels of interleukin (IL)-4, IL-5, and IL-13, compared with CD4⁺ T cells cultured with CD103⁺ DCs from male mice. The 17 β -oestradiol-oriented enhancement of CD86 expression on CD103⁺ DCs after allergen exposure induced the enhanced IL-5 production from CD4⁺ T cells.

Conclusions and Clinical Relevance: These findings suggest that with regard to asthma, enhanced Th2 cytokine production in females might be attributed to 17 β -oestradiol-mediated Th2-oriented CD103⁺ DCs in the BLN.

KEYWORDS

bronchial asthma, CD103⁺ dendritic cells, oestradiol, sex-based differences, Th2

1 | INTRODUCTION

In medicine, sex has been recognized as a biological characteristic that defines cellular, molecular, and immunological differences, and is an important modulator of disease severity and response to therapeutic intervention.^{1,2} Additionally, sex is deeply associated with the prevalence and severity of asthma, effectiveness of asthma treatment and adverse reactions to asthma treatment.³ The relapse rate after discharge from the emergency department is evidently higher for female patients than for male patients.⁴ Moreover, sex was found to be significantly associated with bronchial hyperresponsiveness in systemic inflammatory conditions.⁵ Meanwhile, the prevalence and severity of asthma are greater in boys than in girls; however, this difference is reversed after puberty due to age-related changes, particularly, alterations in sex hormone levels.^{6–8} In addition, postmenopausal use of oestrogen alone was associated with an increased rate of newly diagnosed asthma in menopausal women.^{9,10} Gender-based epidemiological differences^{4–8} are frequently associated with the specific overproduction of type 2 T-helper (Th2) cytokines in females. Actually, more interleukin (IL)-13-producing T cells are observed in female patients with atopic asthma than in male patients.¹¹ Thus, increasing evidence has indicated that symptom-based features of asthma in female patients are based on the differences in pathogenic features, including enhanced Th2-type immune responses.¹²

Animal studies have verified the influence of sex on the pathogenesis of asthma. Using an ovalbumin (OVA)-induced asthma mouse model, an increased number of CD4⁺ T cells and eosinophils, higher Th2 cytokine content in broncho-alveolar lavage (BAL) fluid and higher Th2 cytokine production by the spleen and bronchial lymph node (BLN) cells were noted in female asthmatic mice compared to those in male asthmatic mice.^{13–15} Furthermore, ovariectomy before OVA inhalation significantly inhibited lung eosinophil infiltration. Moreover, oestradiol treatment in ovariectomized mice partially restored the number of eosinophils in the BAL fluids of asthmatic mice.¹⁶

Dendritic cells (DCs), the most proficient antigen-presenting cells, bridge the gap between innate and adaptive immune responses by priming Th cells, including Th1, Th2, and Th17 cells, to respiratory allergens, which is a critical step for the development and exacerbation of allergic asthma.¹⁷ In patients with asthma, circulating myeloid DCs extravasate from the circulation within 4–5 hours after allergen inhalation to the bronchial wall during the first 24 hours,^{18,19} facilitating acquired immunity to the inhaled allergen. In humans, BDCA1⁺ myeloid (m) DCs accumulate to a greater extent in the airway epithelia of patients with Th2-high asthma, compared to that in patients with Th2-low asthma or healthy controls.²⁰ Mature BDCA1⁺ DCs from patients with atopic dermatitis induce fewer interferon (IFN)- γ -producing and more IL-4-producing helper T cells, compared with DCs from healthy controls.²¹ In patients with allergic rhinitis, local allergen challenge resulted in an increase in mDC and plasmacytoid DC numbers in the nasal mucosa and skin.²² Meanwhile,

allergen challenge increases the BDCA3 on mDC levels in the sputum of subjects with asthma, and the frequency of BDCA3⁺ mDCs and extent of allergy to house dust mites are reportedly positively correlated,²³ suggesting both BDCA1⁺ and BDCA3⁺ DC subsets are involved in asthmatic immune responses. However, sex-related differences in DC subsets responsible for enhanced-Th2 cytokine production in female patients with asthma remain unclear.

Recent studies in mice have shown that the CD11b⁺ CD103[−] (CD11b⁺) and CD11b[−] CD103⁺ (CD103⁺) DCs, homologs of human CD1c (BDCA1)⁺ and CD141 (BDCA3)⁺ DCs, respectively, play crucial roles in priming the Th2 response after allergen encounter.^{24–26} Upon allergen inhalation, conditional depletion of total DCs abolished Th2 cytokine production by lymph node cells and accumulation of airway eosinophils in a murine asthma model.²⁷ Moreover, the selective depletion of either CD11b⁺ DCs or CD103⁺ DCs significantly reduced these asthmatic responses.^{28,29} Therefore, both DC subsets are required to induce a complete immune response to inhaled allergen.

In this study, we aimed to clarify the role of DCs in sex-related enhanced Th2 cytokine production upon allergen inhalation using a mouse model.

2 | MATERIALS AND METHODS

2.1 | Mice

Male and female C57BL/6 (wild-type; WT) mice, and OT-I and OT-II transgenic (Tg) mice were obtained from CLEA Japan (Osaka, Japan) and the Jackson Laboratory (Bar Harbor, ME, USA), respectively. All mice were maintained under specific pathogen-free conditions at the Institute for Animal Experimentation, Tohoku Medical and Pharmaceutical University (Sendai, Japan). All experimental procedures involving animals were approved by the Committee of Animal Experiments at Tohoku Medical and Pharmaceutical University (approval numbers: 14002-cn, 15001-cn, and 16002-cn). We took utmost care to alleviate any pain and suffering of the mice.

2.2 | Sensitization and antigen challenge

Mice, 6–8 weeks old, were sensitized through intraperitoneal injection of 8 μ g OVA (Grade V; Sigma-Aldrich, St Louis, MO, USA) adsorbed with 4 mg aluminium hydroxide (Wako Pure Chemical Industries, Osaka, Japan) in 500 μ L saline, on days 0 and 5. On day 26, mice were challenged with aerosolized OVA (0.5% in saline) for 1 hour on two occasions 4 hour apart.^{15,30}

2.3 | Preparation of the lung white blood cells

Mice were sacrificed before or at various time intervals after OVA challenge. Pulmonary leucocytes were prepared as previously described.³¹ Briefly, the lung vascular bed was flushed by injecting 5 mL chilled saline into the right ventricle. The entire lungs were

teased with a 40- μ m cell strainer (BD Falcon, Bedford, MA, USA) and incubated in RPMI 1640 medium (Nakaraï Tesque, Kyoto, Japan) with 10% foetal calf serum (FCS; Thermo Fisher Scientific, Waltham, MA, USA), 100 U/mL penicillin G, 100 μ g/mL streptomycin, 10 mmol/L HEPES and 2 mmol/L L-glutamine, containing 20 U/mL collagenase D and 1 μ g/mL DNase I (Roche Diagnostics GmbH, Mannheim, Germany). After incubation for 60 minutes at 37°C with vigorous shaking, cells were resuspended in 4 mL 40% (v/v) Percoll (Pharmacia, Uppsala, Sweden) and layered onto 4 mL 80% (v/v) Percoll. After centrifugation at 600 \times g for 20 minutes at 15°C, cells at the interface were collected. For some experiments, the cells were centrifuged and mounted onto a glass slide, stained with Diff-Quick (Sysmex Corp., Kobe, Japan), and then observed under a microscope. The number of leucocyte fractions was estimated by multiplying the total leucocyte number by the proportion of each fraction, for 200 cells.

2.4 | Preparation of the BAL fluids

BAL fluids were prepared as previously described.¹⁵ Briefly, BAL samples collected on day 3 or 5 after OVA inhalation with 2 \times 0.25 mL chilled PBS through a cannula inserted in the trachea were centrifuged at 450 \times g for 10 minutes at 4°C, and the supernatants were stored at -80°C for the cytokine assay. Cells (2 \times 10⁵) were stained with Diff-Quick solution, and cell differential percentage was determined by counting a minimum of 200 cells under light microscopy. The number of effector Th2 cells in BAL fluids was determined by flow cytometry.

2.5 | Preparation of DCs

Entire lungs and BLNs were extracted from sensitized and challenged WT mice 16 or 20 hours after OVA inhalation, respectively. Pulmonary leucocytes and BLN cells were prepared as previously described.¹⁴ The number of each DC subset per lung and BLN was calculated based on the total number of leucocytes, and percentage of each DC subset in those populations was estimated using a BD ARIALL flow cytometer (BD Biosciences, San Jose, CA, USA). In another experiment, CD11c⁺ cells were enriched using an autoMACS Separator (Miltenyi Biotec, Bergish Gladbach, Germany) and anti-mouse Pan DC MicroBeads (Miltenyi Biotec). SSC^{low} CD11c^{hi} I-A/I-E^{hi} CD11b^{hi} CD103⁻ DCs and SSC^{low} CD11c^{hi} I-A/I-E^{hi} CD103⁺ DCs were purified by cell sorting using a BD ARIALL flow cytometer. The proportion of CD11c^{hi} I-A/I-E^{hi} cells in the sorted cells was consistently 95%-98%. Furthermore, the proportion of CD11b^{hi} and CD103⁺ cells in DCs was consistently 96%-98%. Following centrifugation, morphologies were assessed using a microscope by mounting cells onto a glass slide and subsequent staining with Diff-Quick. To assess antigen uptake ability of lung DCs and migration into the BLN, Alexa Fluor 647-conjugated OVA (100 μ g; Thermo Fisher Scientific) and LPS (0.1 μ g; Sigma-Aldrich) or non-labelled endotoxin-free OVA (Hyglos GmbH, Bernried am Starnberger See, Germany) and LPS in 50 μ L saline were injected intratracheally into sensitized WT mice.

2.6 | Preparation of the lung and BLN homogenate

For RT-PCR, the entire lungs were excised from WT mice before and 3 and 16 hours after OVA challenge. BLNs were excised from WT mice before and 16 and 20 hours after OVA inhalation. These tissues were homogenized in buffer RLT (Qiagen, Valencia, CA, USA) supplemented with 1% 2-mercaptoethanol. For cytokine assay, the entire lungs were excised 1 day after OVA inhalation and homogenized in chilled 0.1% Triton-X PBS with 1% protease inhibitor (Sigma-Aldrich). After centrifugation at 15 000 \times g for 15 minutes at 4°C, the supernatants were stored at -80°C.¹⁵

2.7 | Culture of DCs with T cells

CD4⁺ T cells or CD8⁺ T cells were isolated from the spleen cell population of naïve male and female OT-II or OT-I Tg mice using an auto MACS Separator (Miltenyi Biotec) and anti-mouse CD4 or CD8 Micro Beads (Miltenyi Biotec), respectively. Furthermore, CD3⁺ CD4⁺ CD11c⁻ and CD3⁺ CD8⁺ CD11c⁻ cells were purified from CD4⁺ and CD8⁺ T cell population by cell sorting using a BD ARIALL flow cytometer. The proportion of CD4⁺ T cells or CD8⁺ T cells in the sorted cell population was >99%. For the culture experiment of DCs with T cells, T cell population was prepared as a mixture of T cells from both male and female mice at the ratio of 1:1 to exclude the influence of sex-related differences in the ability of T cells, based on our previous observation that the potential of CD4⁺ T cells to produce Th2 cytokine is different between male and female mice.³² CD4⁺ T cells from OT-II mice or CD8⁺ T cells from OT-I mice were cultured with each DC subset at a ratio of 3:1 in the presence of OVA₃₂₃₋₃₃₉ or OVA₂₅₇₋₂₆₄ peptide, respectively, for 4 days in RPMI 1640 medium supplemented with 10% FCS, 100 U/mL penicillin G, 100 μ g/mL streptomycin, 2 mmol/L L-glutamine, and 50 μ mol/L 2-mercaptoethanol. Following primary culture, T cells were further cultured in microwells coated with 1 μ g/mL purified anti-CD3 ϵ (Clone 145-2C11; BioLegend, San Diego, CA, USA) and 5 μ g/mL anti-CD28 (Clone 37.51; BioLegend). For some experiments, CD4⁺ T cells were labelled with 1 μ mol/L 5,6-carboxyfluorescein diacetate succinimidyl ester (CFSE; Dojindo Laboratories, Kumamoto, Japan) for 10 minutes before coculture with CD103⁺ DCs for 2 or 4 days.

2.8 | CD103⁺ bone marrow-derived DCs

CD103⁺ bone marrow-derived DCs (BM-DCs) were prepared as described previously by Mayer et al.³³ In brief, BM-derived cells from WT male mice were cultured at a density of 1.5 \times 10⁶ cells/mL in 10 mL RPMI 1640 medium without phenol red supplemented with 10% FCS, 100 U/mL penicillin G, 100 μ g/mL streptomycin, 2 mmol/L L-glutamine, and 50 μ mol/L 2-mercaptoethanol, and containing 3 ng/mL murine granulocyte-macrophage colony-stimulating factor (GM-CSF; Wako pure Chemical Industries, Ltd., Osaka, Japan), and 200 ng/mL murine FMS-like tyrosine kinase 3 ligand (Flt3L; PeproTech Inc., Rocky Hill, NJ, USA) in the presence of vehicle, 17 β -oestradiol (1 \times 10⁻⁷ M; Sigma-Aldrich), or 17 β -oestradiol

plus ICI182,780 (Tocris Bioscience, Ellisville, MO, USA). ICI182,780 is an oestrogen receptor antagonist. On day 9, the non-adherent cells were harvested and replated at a density of 3×10^6 cells/mL in 10 mL complete medium supplemented with GM-CSF and Flt3L in the presence of the vehicle, 17β -oestradiol, or 17β -oestradiol plus ICI182,780, as on day 0. On day 15, non-adherent cells were collected and used as CD103⁺ BM-DCs. CD103⁺ BM-DCs, at a density of 5×10^5 cells/mL, were stimulated for 24 hours with OVA and/or murine recombinant IL-33 (R&D Systems, Inc., Minneapolis, MN, USA) in the presence of vehicle, 17β -oestradiol, or 17β -oestradiol plus ICI182,780. For some experiments, 0.25 μ g/mL recombinant anti-B7-2/CD86 antibody (R&D Systems, Inc.) or isotype-matched control antibody was used to block CD86/CD28 costimulatory signals.

2.9 | Measurement of cytokine and chemokine concentration

Levels of IL-4, IL-5, IL-13, IL-17A, IL-33, and IFN- γ were assayed using enzyme-linked immunosorbent assay (ELISA) kits (eBioscience, San Diego, CA, USA). The detection limits were 4 pg/mL for IL-4, IL-5, IL-13, and IL-17A; 25 pg/mL for IL-33; and 15 pg/mL for IFN- γ . The CCL20 content in the lung homogenate was measured using ELISA kit (R&D Systems, Inc.). The limit of detection was 0.30 pg/mL. Total protein levels of the lung homogenates were assayed using a detergent-compatible protein assay kit (Bio-Rad Laboratory, Hercules, CA, USA). The cytokine and chemokine concentrations in the lung were adjusted for the protein levels of each lung.¹⁵

2.10 | Flow cytometric analysis

Cells were diluted to attain a density of 1×10^6 /100 μ L, and pre-incubated with anti-Fc γ R/II and III mAb (Clone 93; BioLegend) on ice for 15 minutes in PBS containing 1% FCS and 0.1% sodium azide. To identify DC subsets, the lung cells and BLN cells were stained with FITC-conjugated anti-I-A/I-E (Clone M5/114.15.2; BioLegend), PE-conjugated anti-CD11c (Clone N418; BioLegend), PerCP-conjugated anti-CD11b (Clone M1/70; BioLegend), and PE/Cy7-conjugated anti-CD103 (Clone 2E7; BioLegend). In addition, to evaluate surface molecule expression levels on DCs, APC-conjugated anti-CD40 (Clone 3/23; BioLegend), CD80 (Clone 16-10A1; BioLegend), CD86 (Clone GL-1; BioLegend), or Alexa Fluor 700-conjugated anti-CCR7 (Clone 4B12; eBioscience, San Diego, CA, USA) were used. In another experiment, to evaluate ST2 expression levels on DCs, they were stained with FITC-conjugated anti-ST2 (Clone DJ8; MD Biosciences, Oakdale, MN, USA), PE-conjugated anti-CD11c, PerCP-conjugated anti-CD11b, PE/Cy7-conjugated anti-CD103, and APC/Cy7-conjugated anti-I-A/I-E (Clone M5/114.15.2; BioLegend). In the *in vitro* experiments, to evaluate CD86 and I-A/I-E expression levels on CD103⁺ BM-DCs, they were stained with FITC-conjugated anti-I-A/I-E and APC-conjugated anti-CD86. Furthermore, to isolate CD4⁺ T cells used in coculture experiments, the spleen cells from OT-II Tg mice were stained with FITC-conjugated anti-CD4 (Clone GK1.5;

BioLegend), PE-conjugated anti-CD11c, and PerCP-conjugated anti-CD3 ϵ (Clone 145-2C11; BioLegend). In the isolation of CD4⁺ T cells for division-tracking experiments with CFSE, the spleen cells from OT-II Tg mice were stained with PE-conjugated anti-CD11c, APC/Cy7-conjugated anti-CD4 (Clone GK1.5; BioLegend), and PerCP-conjugated anti-CD3 ϵ or APC-conjugated anti-CD3 ϵ (Clone 145-2C11; BioLegend). In addition, to isolate CD8⁺ T cells for coculture experiments, the spleen cells from OT-I Tg mice were stained with FITC-conjugated anti-CD8 α (Clone 53-6.7; BioLegend), PE-conjugated anti-CD11c, and PerCP-conjugated anti-CD3 ϵ . Furthermore, to evaluate ST2 expression on BLN CD4⁺ T cells after the culture with CD103⁺ BM-DCs, cells were stained with FITC-conjugated anti-ST2 and APC-conjugated anti-CD3 ϵ . Cells in the BAL fluid were stained with FITC-conjugated anti-CD3 ϵ (Clone 145-2C11; BioLegend) or APC/Cy7-conjugated anti-CD3 (Clone 17A2; BioLegend), PE-conjugated anti-CD44 (Clone IM7; BioLegend), PerCP-conjugated anti-CD62L (Clone MEL-14; BioLegend), APC-conjugated anti-ST2 (Clone DIH9; BioLegend), and Alexa Fluor 700-conjugated anti-CD4 (Clone RM4-5; BD Biosciences) to identify effector Th2 cells. The positive populations or mean values of the fluorescence intensity are defined based on isotype-matched control IgG for each Ab or fluorescence minus one (FMO) controls. To distinguish false-positive signals from real positive ones, delta mean fluorescence intensity (MFI), defined as the ratio of MFI of sample histogram to MFI of control histogram, was used in evaluation of the results in some experiments. Dead cells, stained with the LIVE/DEAD fixable blue dead cell stain kit (Thermo Fisher Scientific), were excluded from analysis. Data showed that 95%–99% of the lung leucocytes were viable. Data from these studies were analysed using Diva (BD Biosciences) and FlowJo (Tree Star Inc., Ashland, OR, USA) software. The number of DCs was estimated by multiplying the leucocyte number, calculated as mentioned previously, by the proportion of each subset. However, the interpretation of flow cytometry data presents limitations owing to various factors, such as the types of antibodies included and the gating strategy.

2.11 | Real-time RT-PCR analysis

Total RNA was extracted from DCs, entire lung homogenates, and BLN homogenates using a ReliaPrep RNA cell miniprep system (Promega Corporation, WI, USA) or an RNeasy micro kit (Qiagen, Valencia, CA, USA). First-strand cDNA was synthesized using the PrimeScript RT reagent kit with gDNA Eraser (TaKaRa Bio Inc., Otsu, Japan). Real-time reverse transcription (RT)-PCR was performed using gene-specific primers and Power SYBR Green PCR Master Mix (Applied Biosystems, Foster City, CA, USA) and a Step One Plus Real-Time PCR system (Applied Biosystems).¹⁵ The primer sequences used for amplification are shown in Table S1. The expression levels of target genes and hypoxanthine-guanine phosphoribosyltransferase (Hprt) as a reference gene were calculated for each sample using the reaction efficiency, as determined by performing amplifications using standards.

2.12 | Confocal microscopic analysis

DCs were prepared from the BLN of male and female mice sensitized with non-labelled OVA and then intratracheally administered with Alexa Fluor 647-conjugated OVA. Cells were stained with Cell Mask green plasma membrane stain (Thermo Fisher Scientific) and SYTO 82 orange fluorescent nucleic acid stain (Thermo Fisher Scientific) according to manufacturer's instructions. After incubation, the cells were diluted to a density of $1 \times 10^5/200 \mu\text{L}$ in Opti-MEM (Thermo Fisher Scientific) containing 10% FCS, 0.1% sodium azide, and 10 mmol/L HEPES and then seeded in 35-mm glass bottom dishes (Matsunami Glass Ind., Ltd, Osaka, Japan). Confocal studies were performed using an oil immersion objective ($60 \times$ UPLSAPO, numerical aperture 1.35) and Fluoview FV1000 confocal laser scanning microscopy (Olympus, Tokyo, Japan). FV1000 software version 4.2 (Olympus) was used to acquire and process the confocal images. Tri-colour images were acquired using a sequential acquisition mode to avoid cross-excitation.

2.13 | Measurement of airway responsiveness

Airway responsiveness was measured as previously described.^{34,35} In brief, to measure airway responsiveness, lung resistance at the baseline and in response to aerosolized saline and acetyl- β -methylcholine (methacholine; Sigma-Aldrich) was measured for 3 minutes under each condition using Buxco whole body plethysmography (Buxco Electronics, Sharon, CT, USA).

2.14 | Statistical analysis

Statistical analysis was performed using GraphPad Prism 5 software (GraphPad Software, La Jolla, CA, USA). Differences between the two groups were tested using a two-tailed analysis and an unpaired Student's *t* test. Differences among the three groups or more were tested using ANOVA with a post hoc analysis (Turkey's multiple comparison test). A *P*-value of <0.05 was considered significant.

3 | RESULTS

3.1 | Sex-based differences in the accumulation of the lung DCs

To investigate sex-associated differences during the initial pulmonary cell responses within 24 hours of allergen inhalation in asthmatic mice, the number of lung inflammatory cells between male and female mice was compared. The number of total cells and mononuclear cells, such as monocytes, macrophages, and DCs, in the lungs 16 hours after OVA inhalation was higher in female mice than in male mice (Figure 1A,B). A similar tendency was also observed with respect to the number of eosinophils and lymphocytes, although the differences between male and female mice did not reach significance at the time points examined (Figure 1B). Meanwhile, the number of lung leucocytes 20 hours after OVA inhalation was not significantly different between male and female mice. Furthermore, the number

of total cells 24 hours after OVA inhalation in female mice was lower than that in male mice, although there was no statistical significance (Figure 1A). In this model, increased accumulation of eosinophils (Figure 1C) and effector Th2 cells (Figure 1D) in the BAL fluids on day 5, and higher IL-4, IL-5, and IL-13 production (Figure 1E) in the BAL fluids on day 3 post-OVA inhalation were observed in female mice compared with those in male mice. In addition, the lung resistance in response to inhaled methacholine increased in a dose-dependent manner in both male and female mice. Moreover, the lung resistance was significantly enhanced in female mice compared to that in male mice, 1 day after OVA inhalation (Figure 1F).

Next, to address sex-specific differences in the number of DCs in response to inhaled allergens, two major DC subsets from alveolar macrophages (CD11c^{hi} I-A/I-E^{low} SSC^{hi} cells) and monocytes (CD11c^+ I-A/I-E⁺ cells) were distinguished using internal complexity [side scatter (SSC) parameters], and the expression levels of I-A/I-E on CD11c^+ cells, followed by the expression levels of CD11b and CD103, were determined (Figure 2A). The number of total DCs and CD11b^{hi} DCs in male mice significantly increased 20 hours after allergen inhalation and was maintained up to 24 hours after inhalation, whereas the number of these cells in female mice was significantly elevated, peaked 20 hours after allergen inhalation, and decreased thereafter. The number of total DCs and CD11b^{hi} DCs was significantly higher in female mice than in male mice at 16 hours, but was not significantly different at 20 and 24 hours post-OVA inhalation. In contrast, the number of CD103^+ DCs in the lung was not significantly changed within 24 hours of OVA inhalation in both male and female mice, although the number at 16 hours post-OVA inhalation was significantly higher in female mice than in male mice (Figure 2B,C). These results suggest that initial pulmonary cell responses after allergen exposure, particularly, the increase in DCs occurring within 20 hours after allergen inhalation, are enhanced in the lungs of female mice compared to that in male mice.

To further address this possibility, we next examined the mRNA expression of CCL2, CCL7, CCL19, CCL20, and CCL21 in the lung, which attract monocytes, immature DCs, and precursors of DCs to the inflammatory sites.³⁶ As shown in Figure 3A, CCL20 mRNA levels in the lung at 3 and 16 hours post-OVA inhalation were significantly higher in female mice than in male mice, although other chemokine levels in the lung were not different between the sexes. Furthermore, mRNA expression of Flt3L and IL-33, cytokines that are associated with DC differentiation and activation in the lung during an asthma attack,^{24,37} was significantly increased in the lung of female mice compared to that in male mice at 3 or 16 hours post-OVA inhalation (Figure 3B). In addition, CCL20 and IL-33 protein levels in the lung at 16 hours post-OVA inhalation were also significantly higher in female mice than in male mice (Figure 3C).

3.2 | Sex-based differences in DC migration into BLN

To define sex-associated differences in the number of DCs in the BLN after allergen inhalation, the number of CD11b^{hi} and CD103^+

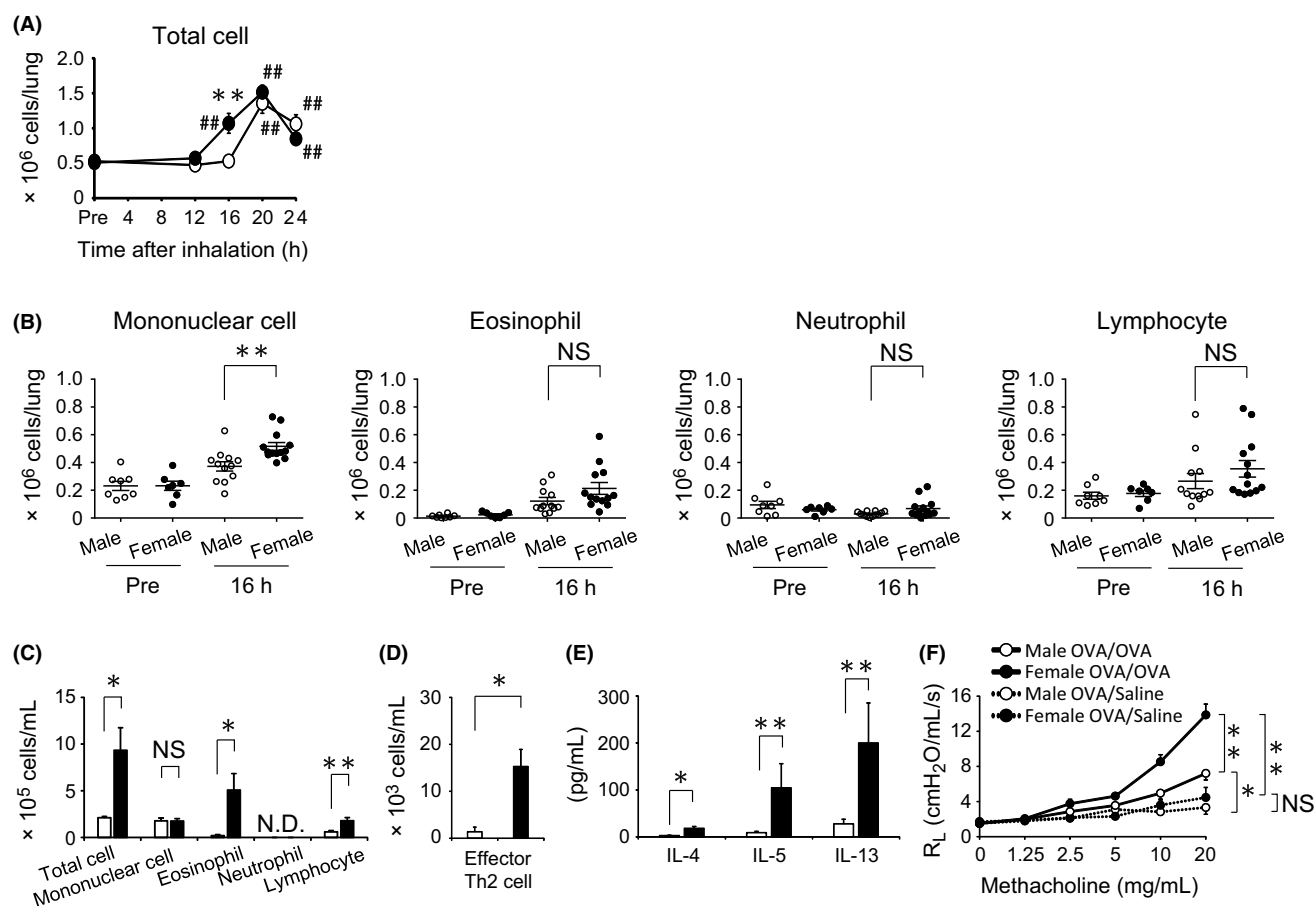


FIGURE 1 Sex-based differences in inflammatory cell infiltration in the lung. (A) The number of white blood cells in the mice lungs was counted before (Pre) and 12, 16, 20, and 24 h after (post) ovalbumin (OVA) challenge. (B) The lung white blood cells pre- and 16 h post-OVA challenge were stained with Diff-Quick and then observed using a microscope. The number of leucocyte fractions was estimated by multiplying the total leucocyte number by the proportion of each fraction. (C) The amount of cells in each leucocyte fraction and (D) the number of effector Th2 cells in the BAL fluids 5 days post-OVA challenge were measured. (E) IL-4, IL-5, and IL-13 levels in the BAL fluids 3 days post-OVA challenge were measured by ELISA. (F) Airway responsiveness in male and female sensitized mice were measured 1 day after OVA (OVA/OVA) or saline (OVA/Saline) challenge using whole body plethysmography. Data are shown as the mean \pm SEM based on at least two independent experiments ($n = 7$ –13). Open bar and circles, male mice; closed bar and circles, female mice. * $P < .05$ compared to male mice; ** $P < .01$ compared to male mice; ## $P < .01$ compared to the level before OVA inhalation; NS, not significant

DCs in the BLN was initially examined, as shown in Figure 4A. Female mice exhibited an increasingly robust accumulation of DCs from 16 to 20 hours after OVA inhalation compared to that in male mice (Figure 4B,C). The number of total DCs, CD11b^{hi} DCs, and CD103⁺ DCs in BLN had reached to peak levels 20 to 24 hours after OVA inhalation and then further decreased to basal levels at 72 hours after OVA inhalation in both male and female mice. The number of CD11b^{hi} DCs at 16 hours post-OVA inhalation was significantly higher in female mice than in male mice (Figure 4C), similar to the time-dependent change that was observed in the lung (Figure 2C). In contrast, the number of CD103⁺ DCs in the BLN 16 to 20 hours after OVA inhalation was significantly higher in female mice than in male mice (Figure 4C); nevertheless, the number of the cells in the lung was not altered in both male and female mice after allergen inhalation (Figure 2C). To address the discrepancy in the distribution of CD103⁺ DCs after allergen exposure, we next examined

sex-associated differences in the migratory properties of each DC subset. The percentage of CCR7-expressing cells in CD103⁺ DCs was significantly increased in the lungs of female mice, but not in male mice, after OVA inhalation (Figure 5A). However, such sex-associated differences were not observed in the case of CD11b^{hi} DCs (Figure 5A). Meanwhile, total number of CCR7⁺ CD11b^{hi} DCs and CCR7⁺ CD103⁺ DCs in the lung 16 hours after OVA inhalation was significantly higher in female mice than in male mice (Figure 5B). In the BLN, the mRNA expression levels of ligands for CCR7, including CCL19 and CCL21, were not statistically different between male and female mice either before or 16 and 20 hours after OVA inhalation (Figure 5C). These results suggest that increase in the number and proportion of CCR7⁺ DCs together results in the sex difference in the kinetics of each DC subsets in the BLN; DCs from the female mice responded earlier and resolved sooner than those from the male mice did in the lungs of asthmatic mice.

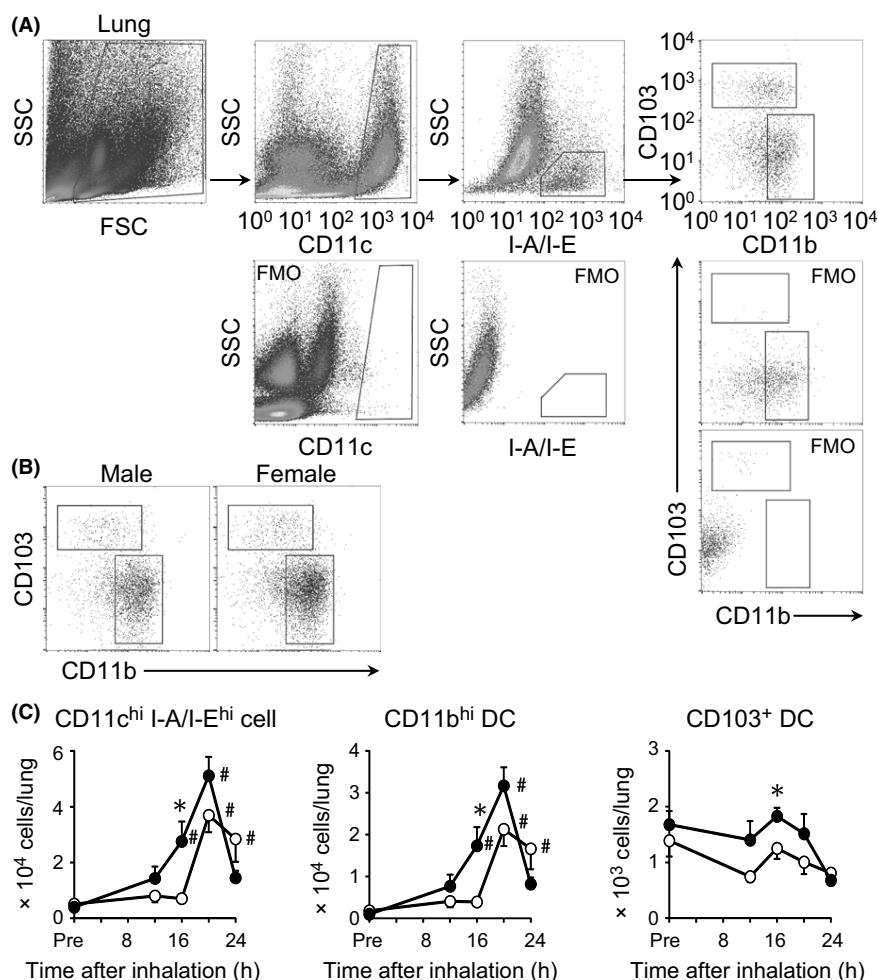


FIGURE 2 Sex-based differences in the number of dendritic cells in the lung. (A) Flow cytometric gating for SSC^{low} CD11c^{hi} I-A/I-E^{hi} dendritic cells (DCs) from the mouse lungs. Positive populations are defined based on fluorescence minus one (FMO) controls. (B) Representative profile of the expression of CD11b and CD103 on DCs in the lung of male and female mice 16 h after OVA challenge. (C) Total DCs, CD11b^{hi} DCs, and CD103⁺ DCs in the lung were counted pre- and 12, 16, 20 and 24 h post-OVA challenge. Data are shown as the mean ± SEM based on at least three independent experiments (n = 8-12). Open circle, male mice; closed circle, female mice. *P < .05 compared to male mice; #P < .05 compared to the level before OVA inhalation

3.3 | Sex-based differences in the antigen-presenting potential of BLN DCs

The pathogenesis of asthma is directed by allergen-specific Th2 cells that are generated in the secondary lymphoid organs, such as the BLN, where DC antigen presentation and signalling through costimulatory molecules are critical for the generation of Th2 cells. Therefore, to test sex-associated differences in the ability of BLN DCs to act as antigen-presenting cells, we initially examined the antigen uptake ability. As shown in Figure S1, OVA was actually taken up intracellularly by DCs of both male and female mice. Furthermore, a high frequency of OVA-positive DCs was observed in migrated DCs (male mice vs. female mice: $74.6 \pm 2.2\%$ vs. $84.2 \pm 3.2\%$; $P = .054$), but low levels were found in resident DCs in the BLNs from both male and female mice (Figure 6A). In the BLN, $81.3 \pm 2.8\%$ of DCs in male mice and $79.2 \pm 5.6\%$ of DCs in female mice were migratory (Figure 6B). Moreover, fluorescent OVA signals were more intense in migrated CD103⁺ DCs from female mice than those from male mice, although such sex-associated differences were not observed in migrated CD11b^{hi} DCs (Figure 6C). Next, the analysis of costimulatory molecule expression on BLN DCs revealed enhanced expression of CD86 and I-A/I-E, but not CD40 and CD80, in CD103⁺ DCs from

female mice, compared to those in CD103⁺ DCs from male mice, although sex-associated differences were not observed for costimulatory molecule expression on CD11b^{hi} DCs (Figure 6D). Furthermore, IL-33 receptor expression on BLN DCs was significantly enhanced in CD103⁺ DCs compared to that in CD11b^{hi} DCs in female mice, whereas such differences were not observed between CD11b^{hi} and CD103⁺ DCs in male mice (Figure 6E). These results suggest that enhanced activation and antigen uptake in BLN CD103⁺ DCs from female mice, as compared to those in corresponding DCs from male mice, are responsible for sex-based differences in Th2 cytokine production during asthma.

3.4 | Sex-based differences in BLN DC-induced T cell differentiation

To directly address the contribution of DCs to sex-related Th2 cytokine production, we initially purified CD11b^{hi} and CD103⁺ DCs from BLNs. These sorted populations were consisted of DCs, although there is the possibility of contamination with CD3⁺ cells in these populations (Figure 7A). In addition, sex-associated differences in the morphology of each DC subset were not observed between male and female mice (Figure 7A). Next, we cultured each BLN DC subset

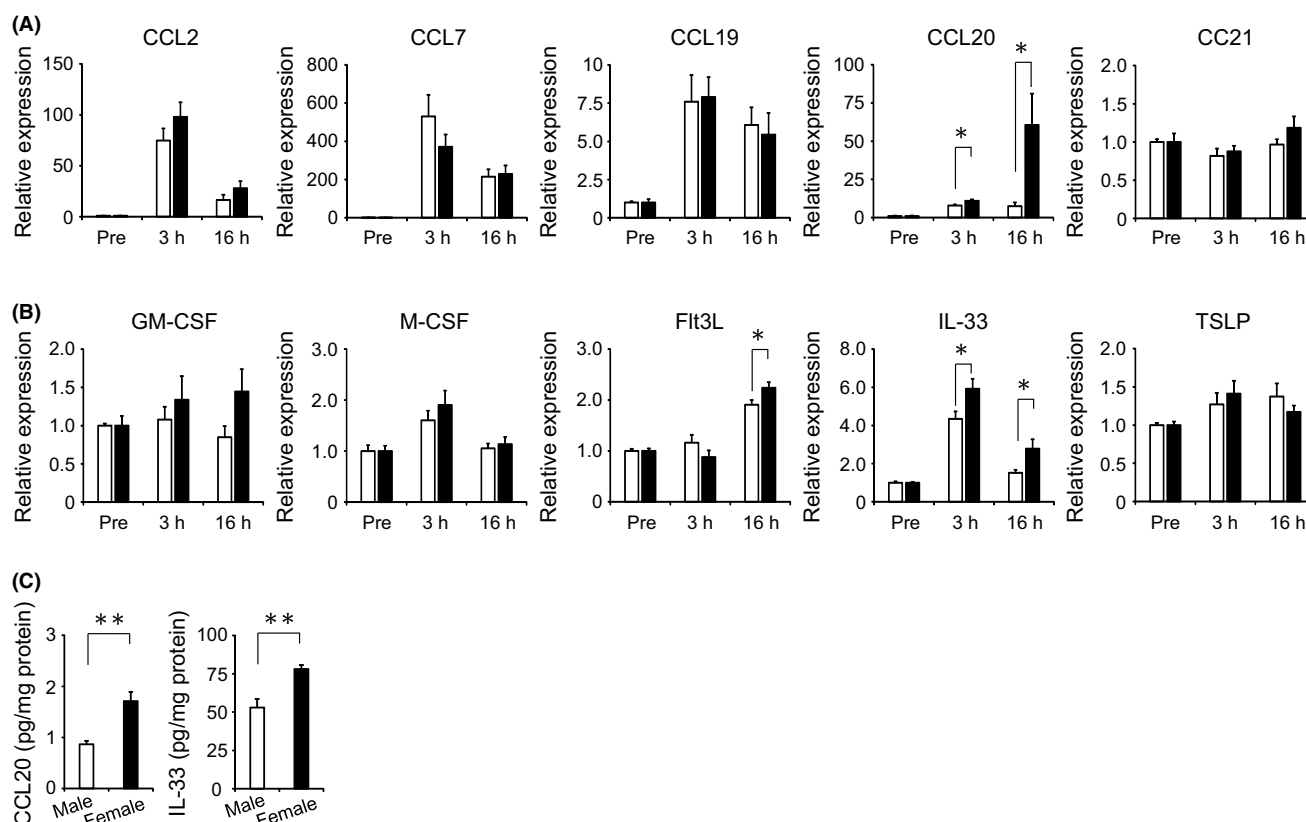


FIGURE 3 Sex-based differences in cytokine and chemokine expression in the lung. The mouse lungs were excised pre-, and 3 and 16 h post-OVA challenge. (A) Chemokine mRNA expression and (B) cytokine mRNA expression in the lungs were determined by real-time RT-PCR. (C) CCL20 and IL-33 protein levels in the lung 16 h post-OVA challenge were measured by ELISA. Data are shown as the mean \pm SEM based on two to three independent experiments ($n = 6-14$). Open bar, male mice; closed bar, female mice. * $P < .05$ compared to male mice; ** $P < .01$ compared to male mice

with OVA peptide-specific T cell receptor-expressing CD4⁺ T cells. As shown in Figure 7B, IL-4, IL-5, and IL-13 levels in the supernatants were higher after culturing with CD103⁺ DCs than with CD11b^{hi} DCs in case of both male and female mice. In addition, CD103⁺ DCs from female mice induced higher IL-4, IL-5, and IL-13 production from CD4⁺ T cells than that by CD103⁺ DCs from male mice; however, sex-associated differences in Th2 cytokine production were not observed after culturing these cells with CD11b^{hi} DCs from male and female mice. IFN- γ was also produced from CD4⁺ T cells, the levels of which were 10- to 100-fold higher than those of Th2 cytokine in both male and female mice; however, no sex-associated differences were observed with either CD11b^{hi} or CD103⁺ DCs. Furthermore, CD11b^{hi} DCs and CD103⁺ DCs from male and female mice induced similar levels of IL-17 production from CD4⁺ T cells, which were 40- to 4000-fold lower than those of other cytokines. For cytokine production in CD8⁺ T cells, CD103⁺ DCs from female mice induced higher levels of IL-5, but not IFN- γ , production than that by CD103⁺ DCs from male mice (Figure 7C). Finally, sex-associated differences in CD4⁺ T cell proliferation induced by CD103⁺ DCs were assessed. As expected, CD103⁺ DCs from female mice induced greater T cell proliferation than CD103⁺ DCs from male mice did, as determined by CFSE dilution in dividing cells

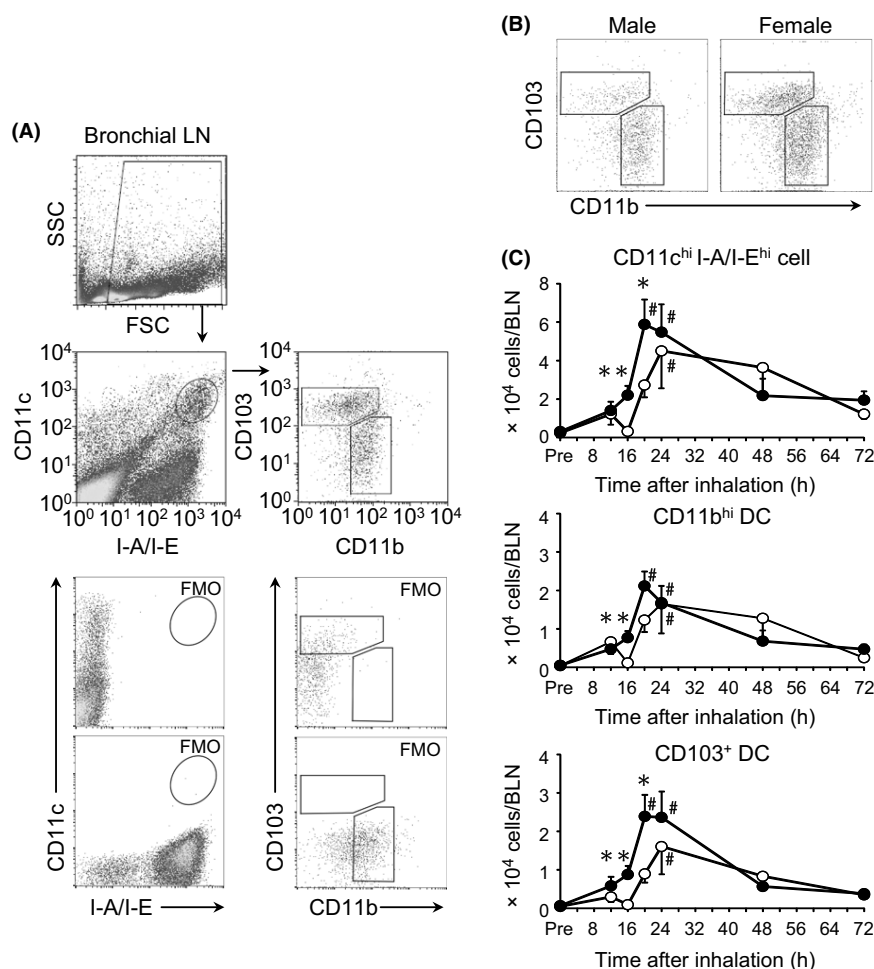
(Figure 7D,E). These results suggest that CD103⁺ DCs, but not CD11b^{hi} DCs, promote female-predominant Th2 cell differentiation, followed by female-predominant Th2 cytokine production.

3.5 | Oestradiol induces enhanced Th2-type immunity in CD103⁺ DCs

Female hormones can reportedly enhance Th2-type immune responses via their effects on DCs.^{38,39} We tested the role of 17 β -oestradiol, the most common circulating form of oestrogen, in the associated Th2-type immune response in CD103⁺ DCs. Oestradiol enhanced the expression of CD86 and I-A/I-E on CD103⁺ BM-DCs stimulated with OVA, which was further enhanced by IL-33 (Figure 8A). However, in the case of CD103⁺ DCs developed from the BM cells in the absence of 17 β -oestradiol, enhanced expression of CD86 and I-A/I-E was not observed upon stimulation with OVA plus 17 β -oestradiol (Figure S2).

CD86 and I-A/I-E expression on CD103⁺ BM-DCs was not different between oestradiol-primed CD103⁺ BM-DCs and vehicle-primed CD103⁺ BM-DCs on IL-33 stimulation (Figure 8A). Oestradiol-primed CD103⁺ BM-DCs also induced ST2 expression on CD4⁺ T cells in the presence of OVA (Figure 8B). An oestrogen receptor

FIGURE 4 Sex-based differences in the number of DCs in the bronchial lymph node. (A) Flow cytometric gating for SSC^{low} $CD11c^{hi}$ I-A/I-E hi DCs from bronchial lymph nodes (BLNs) of mice. Positive populations are defined based on FMO controls. (B) Representative profile of the expression of CD11b and CD103 on DCs in the BLN of male and female mice 20 h after OVA challenge. (C) Numbers of total DCs, $CD11b^{hi}$ DCs, and $CD103^{+}$ DCs in the BLN were counted pre- and 12, 16, 20, 24, 48, and 72 h post-OVA challenge. Data are shown as the mean \pm SEM based on two to three independent experiments ($n = 8-9$). Open circle, male mice; closed circle, female mice. * $P < .05$ compared to male mice; ** $P < .01$ compared to male mice; # $P < .05$ compared to the level before OVA inhalation



antagonist abolished the expression of these molecules on oestradiol-primed $CD103^{+}$ BM-DCs and $CD4^{+}$ T cells (Figure 8A,B). In addition, enhanced IL-5 production from $CD4^{+}$ T cells was observed after culture with oestradiol-primed $CD103^{+}$ BM-DCs, compared to that after culture with vehicle-treated $CD103^{+}$ BM-DCs, and an anti-CD86 antibody completely abolished this effect (Figure 8C).

4 | DISCUSSION

This study reports the first evidence of $CD103^{+}$ DCs being involved in the development of sex-based differences in Th2 cytokine production in asthma. We previously demonstrated that BLN cells from female mice with OVA-stimulated asthma, but not those treated with anti-CD3/CD28 antibodies, produced higher levels of IL-5 and IL-13 than those from male mice, suggesting the involvement of antigen-presenting cells in the sex-associated differences in Th2 cytokine production during asthma.³² With regard to migratory DCs in the BLN, Nembrini et al⁴⁰ showed, using an OVA-induced asthma mouse model, that $1-2 \times 10^5$ DCs were observed in the lung-draining lymph node 24 hours after OVA inhalation, of which $1.5-4 \times 10^4$ DCs were identified as migratory DCs based on their uptake of FITC-conjugated OVA. In their study, the numbers of migratory DCs in the lung-

draining lymph node reached a peak 24 hours after OVA inhalation and then decreased to almost half of their peak levels at the end of 48 hours.⁴⁰ Furthermore, Plantinga et al⁴¹ reported, using a house dust mite-induced asthma mouse model, that 60% of BLN DCs on day 3 post-house dust mite challenge were migratory ($CD11c^{hi}$ MHCII hi) DCs, and 40% of BLN DCs were resident ($CD11c^{hi}$ MHCII dim) DCs, although the sex of mice used was not described in these studies. Our data regarding the proportions of migratory DCs in the BLN 20 hours after allergen exposure (Figure 6A,B) indicate a similar tendency, in either sex, to those of migratory DCs in the BLN reported previously as mentioned above.^{40,41} Regarding the sex difference in the number of DCs, Melgert et al⁴² showed that T cell expansion in female mice appeared to be driven by a greater number of inflammatory mDCs, defined as $CD11c^{hi}$ MHC-II hi cells, migrating from the lungs to the lymph nodes, during asthma. Consistent with this observation, we showed that the total number of DCs, defined as $CD11c^{hi}$ I-A/I-E hi cells in the lung and BLN, was increased in female mice compared to those in male mice.

Chemokines, such as CCL2 and CCL20, from the airway epithelial cells activated in response to allergens, attract monocytes and DC precursors to the lung.⁴³ In contrast, TSLP, IL-25, and IL-33 in the lung confer a Th2 polarizing profile to DCs through the upregulation of B7-1, B7-2, and OX40L, which instructs naive T cells to

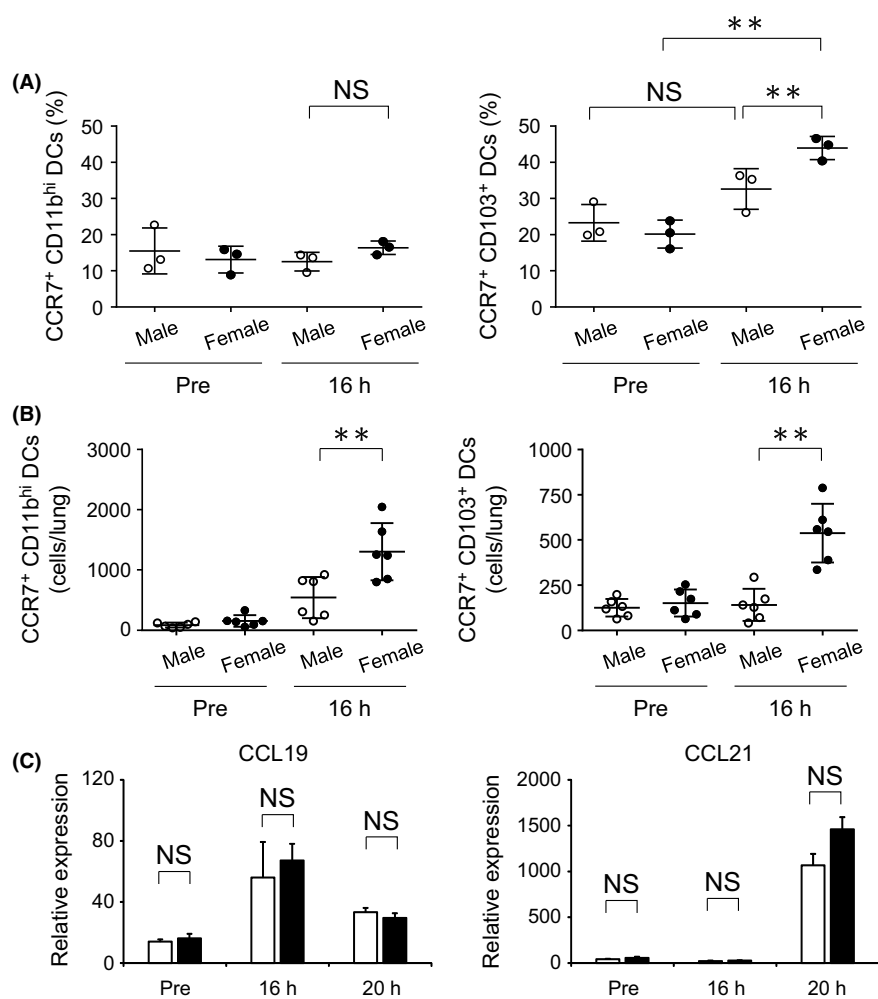


FIGURE 5 Sex-based differences in the migration capacity of pulmonary DCs to the BLN. (A) The percentages of CCR7⁺ population in the pulmonary CD11b^{hi} DCs and CD103⁺ DCs, and (B) the total numbers of CCR7⁺ CD11b^{hi} DCs and CCR7⁺ CD103⁺ DCs in the lungs pre- and 16 h post-OVA challenge. (C) CCL19 and CCL21 mRNA expression in the BLN pre- and 16 and 20 h post-OVA challenge was quantitated by RT-PCR. Data are shown as mean \pm SEM based on three to six mice. Experiments were repeated twice with similar results. Open bar and circles, male mice; closed bar and circles, female mice. ** $P < .01$; NS, not significant

differentiate into Th2 cells.^{44–47} Development of CD11b⁺ DCs from precursors in the lung depends on cytokines M-CSF and GM-CSF levels, but does not require an interaction between Flt3 and Flt3L, whereas CD103⁺ DC development from common DC precursors relies on the stepwise activity of Flt3 signalling.⁴⁸ In contrast, Plantinga et al.⁴¹ reported that Flt3L^{−/−} mice lacked both CD11b⁺ and CD103⁺ DCs, and exhibited significantly reduced numbers of eosinophil, neutrophil, and lymphocytic infiltration in the BAL fluids compared to that in the asthmatic WT mice, after exposure to house dust mites. In the present study, we showed that Flt3L and IL-33 expression in the lung tissues was enhanced in female mice compared to male mice (Figure 3), whereas TSLP expression levels were similar between the sexes, and IL-25 was not detected in either sex (data not shown). These observations suggest that close proximity of lung DCs to IL-33- or Flt3L-secreting cells might be responsible, at least in part, for the sex-associated differences in DC development and in conferring a Th2 polarizing profile to DCs in the asthmatic lung.

Developmental lineage affects the differential expression of CCR7, a chemokine receptor required for migration to lung-draining mediastinal lymph nodes; Ly-6C^{hi} CD11b⁺ DCs, and CD14^{hi} CD11b⁺ DCs, which are Flt3-independently derived from monocytes in the lungs,²⁴ express lower levels of *Ccr7*, whereas pulmonary CD103⁺

DCs express higher levels of *Ccr7* in the lung 24 hours after LPS instillation, indicating that migratory capacities of CD103⁺ DCs are superior to those of CD11b⁺ DCs.²⁵ Furthermore, Besnard et al.³⁷ demonstrated that IL-33 induces CCR7 expression on DCs and DC activation in the lung. Recently, Chen et al.⁴⁹ suggested the possibility that airway exposure to IL-33 might increase the number of cells expressing ST2, a receptor for IL-33, in the lung. Here, the enhanced population of ST2-expressing CD103⁺ DCs in female mice was accompanied by increased expression of IL-33 mRNA and protein in the lungs of these animals (Figures 3B,C and 6E). Consistent with this observation, the increased CCR7⁺ cell population in CD103⁺ DCs and the increased number of CCR7⁺ CD103⁺ DCs in the lung were observed in female mice (Figure 5A,B). These results suggest that the development of the CD103⁺ DC lineage, in association with CCR7 expression and further activation by enhanced IL-33 in females, might be involved in the sex-related differences in CCR7 expression on CD103⁺ DCs, which might lead to the corresponding differences in the number of CD103⁺ DCs in the BLN (Figure 4B,C).

CD103⁺ DCs comprise a primary DC subset in the lung and mediastinal lymph nodes that prime Th2 responses upon allergen encounter, whereas CD11b^{hi} DCs prime Th1 responses.²⁸ Furthermore, CD103⁺ DCs in the BLN are specialized for the cross-presentation of

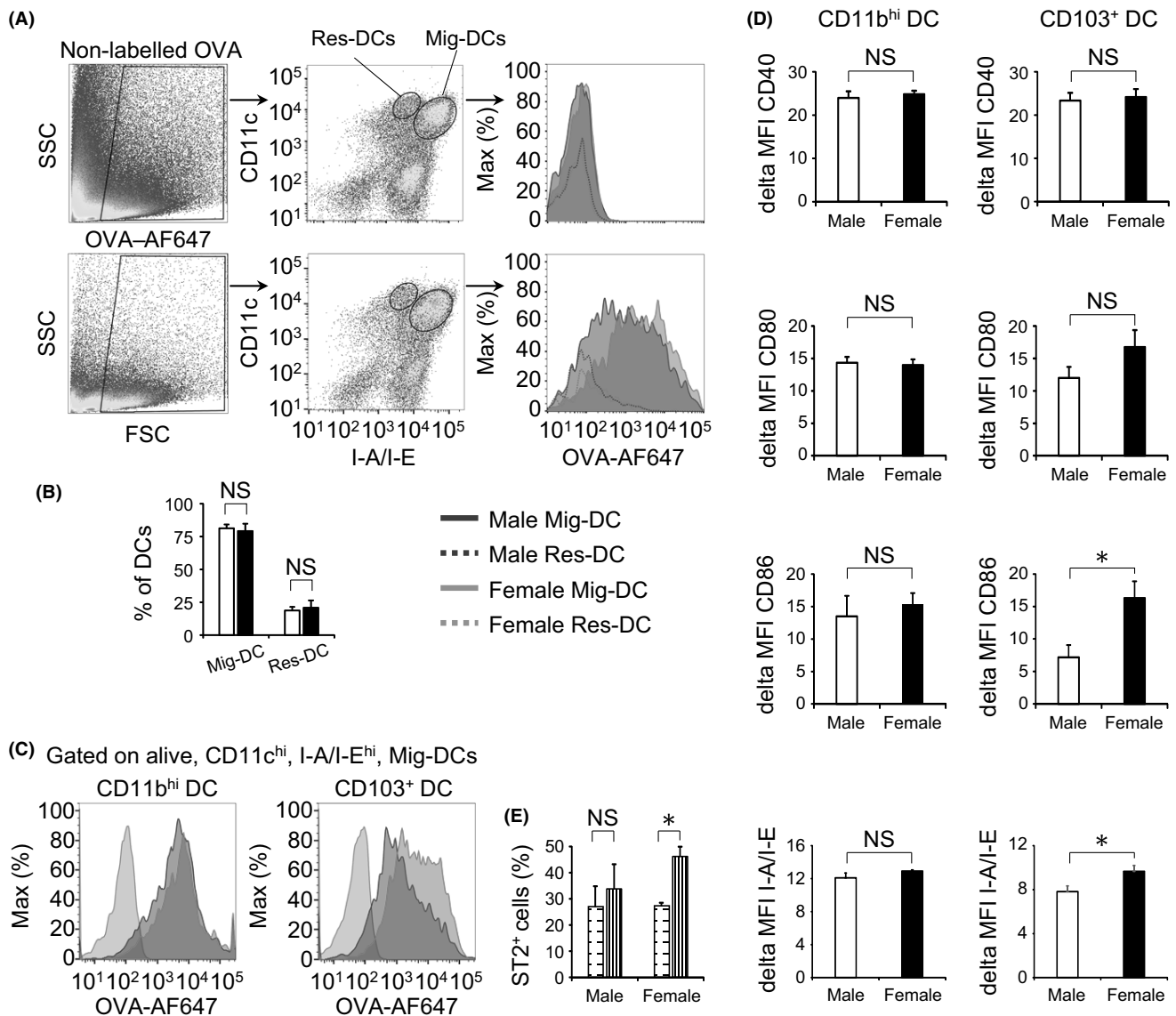


FIGURE 6 Sex-based differences in Th2 priming ability of DCs in the BLN. (A) Sex-based differences in OVA uptake by CD11c^{hi} I-A/I-E^{dim} BLN-resident DCs and CD11c^{hi} I-A/I-E^{hi} migratory DCs (from the lung to the BLN). Solid blue line, migratory DCs from male mice; solid red line, migratory DCs from female mice; dotted blue line, resident DCs from male mice; dotted red line, resident DCs from female mice. (B) The percentages of resident DCs and migratory DCs in BLN DCs of male and female mice. (C) Sex-based differences in OVA uptake by CD11b^{hi} and CD103⁺ DCs in the BLN. Representative results of three independent experiments are shown. Grey line, DCs that took up non-conjugated OVA; blue line, migratory DCs of each subset from male mice; red line, migratory DCs of each subset from female mice. (D) Sex-based differences in mean fluorescent intensity of CD40, CD80, CD86, and I-A/I-E on migratory CD11b^{hi} DCs and CD103⁺ DCs in the BLN. (E) Differences in ST2 expression on migratory BLN CD11b^{hi} DCs and CD103⁺ DCs from male and female mice. Horizontal line bars, CD11b^{hi} DCs; vertical line bars, CD103⁺ DCs. Open bar, male mice; closed bar, female mice. Data are shown as the mean \pm SEM based on four to six mice. Experiments were repeated twice with similar results. * $P < .05$; NS, not significant

inhaled antigens to CD8⁺ T cells, in contrast to CD11b⁺ DCs, which are characterized by the differential expression of MHC-I and MHC-II processing pathways.^{50,51} In accordance with the cross-presentation activity of CD103⁺ DCs, these cells mediated sex-associated differences in the Th2 cytokine production, but not IFN- γ production, from not only CD4⁺ T cells (Figure 7B), but also CD8⁺ T cells (Figure 7C). In the enhanced Th2 cytokine production, the expression of CD40, CD80, CD86, or OX40L is required for directional T cell

differentiation and activation of Th1, Th2, and Th17 cells.⁵² Moreover, OX40L, Jagged2, ICOSL, and TSLPR expression on DCs has been associated with Th2 induction by DCs during Th2 cell differentiation.⁵³⁻⁵⁵ In the current study, mRNA expression of OX40L, Jagged2, ICOSL, and TSLPR in CD103⁺ DCs is not different between male and female mice (Figure S3). Therefore, the enhanced expression of CD86 on CD103⁺ DCs may be directly responsible for the corresponding enhanced Th2 cell differentiation (Figures 6D and 8C).

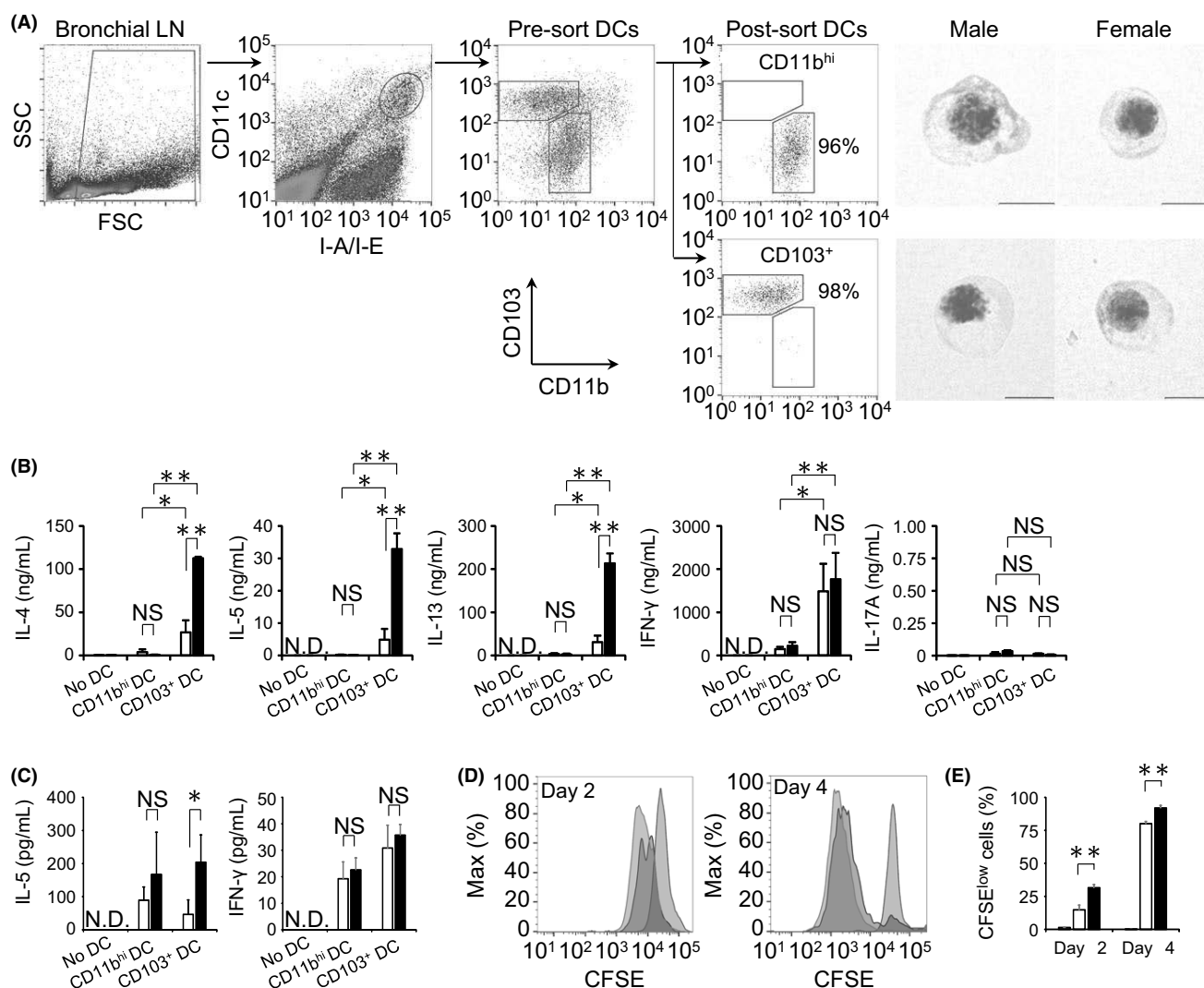


FIGURE 7 Sex-based differences in T cell differentiation promoted by BLN DCs. (A) Purity of sorted BLN CD11b^{hi} DCs and CD103⁺ DCs. Representative images of each population are shown. Scale bar = 10 μ m. (B) Cytokine levels in cultures of CD4⁺ T cells from the spleen of OT-II transgenic (Tg) mice with CD11b^{hi} DCs or CD103⁺ DCs from the BLN of male or female mice. (C) Cytokine production in CD8⁺ T cells from OT-I transgenic (Tg) mice cultured with each DC subset from the BLN of male or female mice. Cytokine levels in the culture supernatants were determined by enzyme-linked immunosorbent assay (ELISA). (D, E) 5,6-carboxyfluorescein diacetate succinimidyl ester (CFSE)-labelled CD4⁺ T cells were cultured with CD103⁺ DCs from male or female mice. (D) The dilution of the CFSE signal on day 2 or 4 post-culture was assayed by flow cytometry. Representative results of two independent experiments are shown. Grey line, CFSE-labelled CD4⁺ T cells cultured without DCs; blue line, CD4⁺ T cells cultured with CD103⁺ DCs from male mice; red line, CD4⁺ T cells cultured with CD103⁺ DCs from female mice. (E) Percentage of CFSE^{low} cells in CD4⁺ T cells cultured with CD103⁺ DCs from the BLN of male and female mice after 2 or 4 days of culture. Grey bar, CFSE-labelled CD4⁺ T cells cultured without DCs; open bar, CFSE-labelled CD4⁺ T cells cultured with CD103⁺ DCs from male mice; closed bar, CFSE-labelled CD4⁺ T cells cultured with CD103⁺ DCs from female mice. Data are shown as the mean \pm SD based on triplicate cultures. Experiments were repeated twice with similar results. * P < .05; ** P < .01; NS, not significant; N.D., not detected

Oestrogen likely induces enhanced immune responses in females through interaction with its receptors.^{38,56} Yang et al³⁹ showed that 17 β -oestradiol upregulates costimulatory molecules and MHC-II on CD11c-positive murine splenic DCs, which promotes T cell priming. In the present study, CD86 and I-A/I-E expression on CD103⁺ DCs was not enhanced through culture with 17 β -oestradiol alone, but rather through incubation with IL-33, as previously suggested by Rank et al⁵⁷ Furthermore, sustained

exposure to 17 β -oestradiol, including that during the period of CD103⁺ DC development, might enhance CD103⁺ DC activation and maturation in females upon allergen exposure, which could lead to female-enhanced Th2 cell differentiation and activation (Figure 8 and Figure S2). Meanwhile, 17 β -oestradiol enhanced the expression of CD86 and I-A/I-E on DCs after stimulation with OVA, but not with IL-33 (Figure 8A). Our results suggest that 17 β -oestradiol has a limited role in the IL-33-ST2 axis-mediated

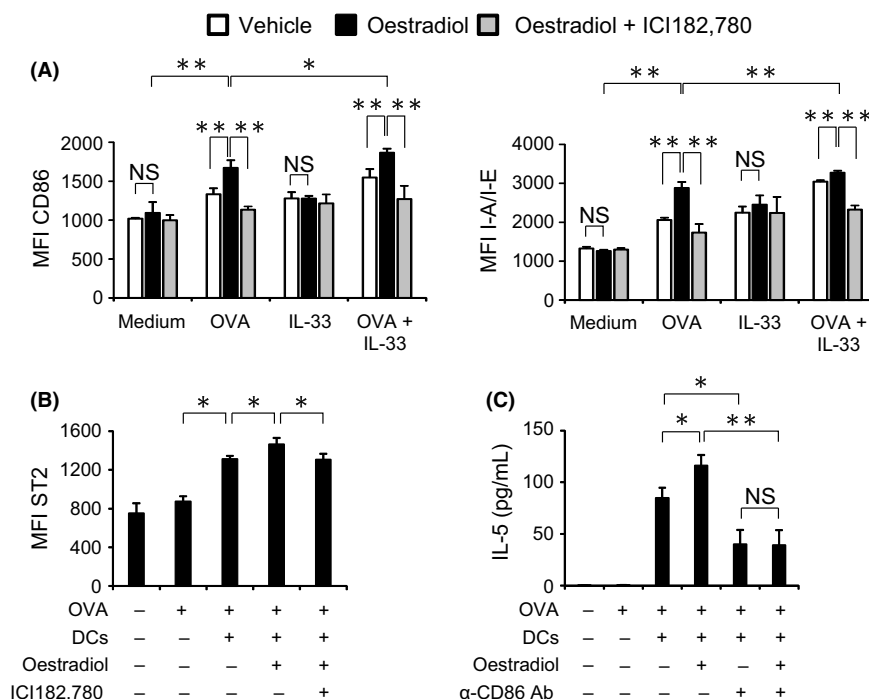


FIGURE 8 17β-oestradiol enhances Th2 cell priming by bone marrow-derived CD103⁺ DCs. CD103⁺ bone marrow (BM)-DCs were induced from BM cells of male mice in the presence of 17β-oestradiol, 17β-oestradiol plus ICI182,780, or vehicle. (A) Each set of CD103⁺ BM-DCs was cultured in the presence of OVA, IL-33, or OVA plus IL-33 for 24 h. CD86 and I-A/I-E expression levels on CD103⁺ BM-DCs were assayed by flow cytometry. (B) BLN CD4⁺ T cells were cultured with 17β-oestradiol-primed, 17β-oestradiol plus ICI182, 780-primed, or vehicle-primed CD103⁺ BM-DCs in the presence or absence of OVA. ST2 expression on CD4⁺ T cell from BLNs was determined by flow cytometry. (C) BLN CD4⁺ T cells were cultured with 17β-oestradiol-primed or vehicle-primed CD103⁺ BM-DCs in the presence or absence of OVA and recombinant anti-mouse CD86 antibody. IL-5 levels in the culture supernatants were determined by enzyme-linked immunosorbent assay (ELISA). Data are shown as the mean ± SD based on triplicate cultures. Experiments were repeated twice with similar results. **P* < .05; ***P* < .01; NS, not significant

activation of CD103⁺ DCs in female mice; however, this requires further investigation.

The present study has important implications for understanding the pathophysiological role of DCs in sex-associated asthma phenotypes. Recently, the possibility that CD103⁺ DCs might even have tolerogenic ability towards inhaled allergens through the induction of regulatory T cells in the absence of DC maturation stimulus has been reported.^{58,59} Further research is needed to completely investigate the precise role of CD103⁺ DCs in the pathogenesis of asthma. Furthermore, it still remains unclear whether BDCA3⁺ DCs, the human homolog of mice CD103⁺ DCs, play an important role in enhanced Th2 cytokine production in female patients with asthma. Therefore, the results of this study have limitations regarding their application to humans. Additional clinical studies are already ongoing in our laboratory to confirm the results, which could lead to the development of more effective strategies to treat female patients with asthma.

ACKNOWLEDGEMENTS

This work was supported in part by a grant-in-aid for Scientific Research (C) (No. 25461164), grant-in-aid for Research Activity Start-up (No. 25893222), grant-in-aid for Young Scientists (B) (No.

16K19608), and the Matching Fund Subsidy for Private Universities from the Ministry of Education, Culture, Sports, Science and Technology of Japan. The funders played no role in the study design, the collection, analysis, and interpretation of data, or the preparation of the manuscript.

CONFLICT OF INTEREST

The authors declare no conflict of interests.

AUTHOR CONTRIBUTIONS

IO and TM conceived and designed the experiments; CM, KK, TM, and KO-D performed the experiments; TM, IO, TT, CM, KK, TK, and JI analysed the data; IO, JI, and MT contributed reagents/materials/analysis tools; TM, CM, IO, TT, and MT contributed to the writing of the manuscript.

REFERENCES

- Legato MJ, Johnson PA, Manson JE. Consideration of sex differences in medicine to improve health care and patient outcomes. *JAMA*. 2016;316:1865-1866.

2. Clayton JA, Tannenbaum C. Reporting sex, gender, or both in clinical research? *JAMA*. 2016;316:1863-1864.
3. Choi IS. Gender-specific asthma treatment. *Allergy Asthma Immunol Res*. 2011;3:74-80.
4. Rowe BH, Villa-Roel C, Majumdar SR, et al. Rates and correlates of relapse following ED discharge for acute asthma: a Canadian 20-site prospective cohort study. *Chest*. 2015;147:140-149.
5. Kony S, Zureik M, Driss F, Neukirch C, Leynaert B, Neukirch F. Association of bronchial hyperresponsiveness and lung function with C-reactive protein (CRP): a population based study. *Thorax*. 2004;59:892-896.
6. Akinbami LJ, Moorman JE, Bailey C, et al. Trends in asthma prevalence, health care use, and mortality in the United States, 2001-2010. *NCHS Data Brief*. 2012;94:1-8.
7. Siroux V, Curt F, Oryszczyn MP, Maccario J, Kauffmann F. Role of gender and hormone-related events on IgE, atopy, and eosinophils in the Epidemiological Study on the Genetics and Environment of Asthma, bronchial hyperresponsiveness and atopy. *J Allergy Clin Immunol*. 2004;114:491-498.
8. Almqvist C, Worm M, Leynaert B, Working Group of GA2LEN WP 2.5 Gender. Impact of gender on asthma in childhood and adolescence: a GA2LEN review. *Allergy*. 2008;63:47-57.
9. Romieu I, Fabre A, Fournier A, et al. Postmenopausal hormone therapy and asthma onset in the E3N cohort. *Thorax*. 2010;65:292-297.
10. Troisi RJ, Speizer FE, Willett WC, Trichopoulos D, Rosner B. Menopause, postmenopausal estrogen preparations, and the risk of adult-onset asthma. A prospective cohort study. *Am J Respir Crit Care Med*. 1995;152:1183-1188.
11. Loza MJ, Foster S, Bleecker ER, Peters SP, Penn RB. Asthma and gender impact accumulation of T cell subtypes. *Respir Res*. 2010;11:103.
12. Haldar P, Pavord ID, Shaw DE, et al. Cluster analysis and clinical asthma phenotypes. *Am J Respir Crit Care Med*. 2008;178:218-224.
13. Okuyama K, Wada K, Chihara J, Takayanagi M, Ohno I. Sex-related splenocyte function in a murine model of allergic asthma. *Clin Exp Allergy*. 2008;38:1212-1219.
14. Wada K, Okuyama K, Ohkawara Y, Takayanagi M, Ohno I. Gender differences in transcriptional regulation of IL-5 expression by bronchial lymph node cells in a mouse model of asthma. *Respirology*. 2010;15:629-635.
15. Ito C, Okuyama-Dobashi K, Miyasaka T, et al. CD8 + T cells mediate female-dominant il-4 production and airway inflammation in allergic asthma. *PLoS One*. 2015;10:e0140808.
16. Rizzo-Vasquez Y, Ligeiro de Oliveira AP, Page CP, Spina D, Tavares-de-Lima W. Role of sex hormones in allergic inflammation in mice. *Clin Exp Allergy*. 2007;37:459-470.
17. Gaurav R, Agrawal DK. Clinical view on the importance of dendritic cells in asthma. *Expert Rev Clin Immunol*. 2013;9:899-919.
18. Upham JW, Denburg JA, O'Byrne PM. Rapid response of circulating myeloid dendritic cells to inhaled allergen in asthmatic subjects. *Clin Exp Allergy*. 2002;32:818-823.
19. Jahnsen FL, Moloney ED, Hogan T, Upham JW, Burke CM, Holt PG. Rapid dendritic cell recruitment to the bronchial mucosa of patients with atopic asthma in response to local allergen challenge. *Thorax*. 2001;56:823-826.
20. Greer AM, Matthay MA, Kukreja J, et al. Accumulation of BDCA1+ dendritic cells in interstitial fibrotic lung diseases and Th2-high asthma. *PLoS One*. 2014;9:e99084.
21. Lebre MC, van Capel TM, Bos JD, Knol EF, Kapsenberg ML, de Jong EC. Aberrant function of peripheral blood myeloid and plasmacytoid dendritic cells in atopic dermatitis patients. *J Allergy Clin Immunol*. 2008;122:969-976.
22. Pilette C, Jacobson MR, Ratajczak C, et al. Aberrant dendritic cell function conditions Th2-cell polarization in allergic rhinitis. *Allergy*. 2013;68:312-321.
23. Dua B, Tang W, Watson R, Gauvreau G, O'Byrne PM. Myeloid dendritic cells type 2 after allergen inhalation in asthmatic subjects. *Clin Exp Allergy*. 2014;44:921-929.
24. Belz GT, Nutt SL. Transcriptional programming of the dendritic cell network. *Nat Rev Immunol*. 2012;12:101-113.
25. Nakano H, Burgents JE, Nakano K, et al. Migratory properties of pulmonary dendritic cells are determined by their developmental lineage. *Mucosal Immunol*. 2013;6:678-691.
26. Chang CC, Wright A, Punnonen J. Monocyte-derived CD1a+ and CD1a- dendritic cell subsets differ in their cytokine production profiles, susceptibilities to transfection, and capacities to direct Th cell differentiation. *J Immunol*. 2000;165:3584-3591.
27. Hammad H, Plantinga M, Deswarte K, et al. Inflammatory dendritic cells—not basophils—are necessary and sufficient for induction of Th2 immunity to inhaled house dust mite allergen. *J Exp Med*. 2010;207:2097-2111.
28. Nakano H, Free ME, Whitehead GS, et al. Pulmonary CD103(+) dendritic cells prime Th2 responses to inhaled allergens. *Mucosal Immunol*. 2012;5:53-65.
29. Zhou Q, Ho AW, Schlitzer A, et al. GM-CSF-licensed CD11b+ lung dendritic cells orchestrate Th2 immunity to Blomiatropicalis. *J Immunol*. 2014;193:496-509.
30. Nagafuku M, Okuyama K, Onimaru Y, et al. CD4 and CD8 T cells require different membrane gangliosides for activation. *Proc Natl Acad Sci U S A*. 2012;109:E336-E342.
31. Kawakami K, Kohno S, Morikawa N, Kadota J, Saito A, Hara K. Activation of macrophages and expansion of specific T lymphocytes in the lungs of mice intratracheally inoculated with *Cryptococcus neoformans*. *Clin Exp Immunol*. 1994;96:230-237.
32. Okuyama K, Suenaga M, Furuki S, et al. Contribution of CD4 + T cells and dendritic cells to female-dominant antigen-induced T helper type 2 cytokine production by bronchial lymph node cells. *Int Arch Allergy Immunol*. 2013;161(Suppl 2):58-65.
33. Mayer CT, Ghorbani P, Nandan A, et al. Selective and efficient generation of functional Batf3-dependent CD103 + dendritic cells from mouse bone marrow. *Blood*. 2014;124:3081-3091.
34. Miyasaka T, Okuyama-Dobashi K, Masuda C, et al. The involvement of central nervous system histamine receptors in psychological stress-induced exacerbation of allergic airway inflammation in mice. *Allergol Int*. 2016;65:S38-S44.
35. Okuyama K, Dobashi K, Miyasaka T, et al. The involvement of glucocorticoids in psychological stress-induced exacerbations of experimental allergic asthma. *Int Arch Allergy Immunol*. 2014;163:297-306.
36. McColl SR. Chemokines and dendritic cells: a crucial alliance. *Immunol Cell Biol*. 2002;80:489-496.
37. Besnard AG, Togbe D, Guillo N, Erard F, Quesniaux V, Ryffel B. IL-33-activated dendritic cells are critical for allergic airway inflammation. *Eur J Immunol*. 2011;41:1675-1686.
38. Uemura Y, Liu TY, Narita Y, Suzuki M, Matsushita S. 17 Beta-estradiol (E2) plus tumor necrosis factor-alpha induces a distorted maturation of human monocyte-derived dendritic cells and promotes their capacity to initiate T-helper 2 responses. *Hum Immunol*. 2008;69:149-157.
39. Yang L, Hu Y, Hou Y. Effects of 17 beta-estradiol on the maturation, nuclear factor kappa B p65 and functions of murine spleen CD11c-positive dendritic cells. *Mol Immunol*. 2006;43:357-366.
40. Nembrini C, Sichelstiel A, Kisielow J, Kurrer M, Kopf M, Marsland BJ. Bacterial-induced protection against allergic inflammation through a multicomponent immunoregulatory mechanism. *Thorax*. 2011;66:755-763.
41. Plantinga M, Guillems M, Vanheerswynghe M, et al. Conventional and monocyte-derived CD11b(+) dendritic cells initiate and maintain T helper 2 cell-mediated immunity to house dust mite allergen. *Immunity*. 2013;38:322-335.

42. Melgert BN, Oriss TB, Qi Z, et al. Macrophages: regulators of sex differences in asthma? *Am J Respir Cell Mol Biol*. 2010;42:595-603.
43. Lambrecht BN, Hammad H. Allergens and the airway epithelium response: gateway to allergic sensitization. *J Allergy Clin Immunol*. 2014;134:499-507.
44. Ito T, Wang YH, Duramad O, et al. TSLP-activated dendritic cells induce an inflammatory T helper type 2 cell response through OX40 ligand. *J Exp Med*. 2005;202:1213-1223.
45. Su Z, Lin J, Lu F, et al. Potential autocrine regulation of interleukin-33/ST2 signaling of dendritic cells in allergic inflammation. *Mucosal Immunol*. 2013;6:921-930.
46. Chu DK, Llop-Guevara A, Walker TD, et al. IL-33, but not thymic stromal lymphopoietin or IL-25, is central to mite and peanut allergic sensitization. *J Allergy Clin Immunol*. 2013;131:187-200.
47. Hongja L, Caiqing Z, Degan L, et al. IL-25 promotes Th2 immunity responses in airway inflammation of asthmatic mice via activation of dendritic cells. *Inflammation*. 2014;37:1070-1077.
48. Holgate ST. Innate and adaptive immune responses in asthma. *Nat Med*. 2012;18:673-683.
49. Chen CC, Kobayashi T, Iijima K, Hsu FC, Kita H. IL-33 dysregulates regulatory T cells and impairs established immunologic tolerance in the lungs. *J Allergy Clin Immunol*. 2017;pii:S0091-S6749 (17)30228-2.
50. Dudziak D, Kamphorst AO, Heidkamp GF, et al. Differential antigen processing by dendritic cell subsets in vivo. *Science*. 2007;315:107-111.
51. del Rio ML, Rodriguez-Barbosa JL, Kremmer E, Förster R. CD103- and CD103 + bronchial lymph node dendritic cells are specialized in presenting and cross-presenting innocuous antigen to CD4 + and CD8 + T cells. *J Immunol*. 2007;178:6861-6866.
52. Walsh KP, Mills KH. Dendritic cells and other innate determinants of T helper cell polarisation. *Trends Immunol*. 2013;34:521-530.
53. Amsen D, Blander JM, Lee GR, Tanigaki K, Honjo T, Flavell RA. Instruction of distinct CD4 T helper cell fates by different notch ligands on antigen-presenting cells. *Cell*. 2004;117:515-526.
54. Shen C, Hupin C, Froidure A, Detry B, Pilette C. Impaired ICOSL in human myeloid dendritic cells promotes Th2 responses in patients with allergic rhinitis and asthma. *Clin Exp Allergy*. 2014;44:831-841.
55. Froidure A, Shen C, Pilette C. Dendritic cells revisited in human allergic rhinitis and asthma. *Allergy*. 2016;71:137-148.
56. Keselman A, Heller N. Estrogen signaling modulates allergic inflammation and contributes to sex differences in asthma. *Front Immunol*. 2015;6:568.
57. Rank MA, Kobayashi T, Kozaki H, Bartemes KR, Squillace DL, Kita H. IL-33-activated dendritic cells induce an atypical TH2-type response. *J Allergy Clin Immunol*. 2009;123:1047-1054.
58. Semmrich M, Plantinga M, Svensson-Frej M, et al. Directed antigen targeting in vivo identifies a role for CD103 + dendritic cells in both tolerogenic and immunogenic T-cell responses. *Mucosal Immunol*. 2012;5:150-160.
59. Khare A, Krishnamoorthy N, Oriss TB, Fei M, Ray P, Ray A. Cutting edge: inhaled antigen upregulates retinaldehyde dehydrogenase in lung CD103 + but not plasmacytoid dendritic cells to induce Foxp3 de novo in CD4 + T cells and promote airway tolerance. *J Immunol*. 2013;191:25-29.

SUPPORTING INFORMATION

Additional Supporting Information may be found online in the supporting information tab for this article.

How to cite this article: Masuda C, Miyasaka T, Kawakami K, et al. Sex-based differences in CD103⁺ dendritic cells promote female-predominant Th2 cytokine production during allergic asthma. *Clin Exp Allergy*. 2018;48:379-393. <https://doi.org/10.1111/cea.13081>



Contents lists available at ScienceDirect

European Journal of Pharmacology

journal homepage: www.elsevier.com/locate/ejphar

The involvement of spinal release of histamine on nociceptive behaviors induced by intrathecally administered spermine



Hirokazu Mizoguchi^a, Chizuko Watanabe^a, Takafumi Hayashi^b, Yoko Iwata^a,
Hiroyuki Watanabe^c, Soh Katsuyama^d, Kengo Hamamura^e, Tsukasa Sakurada^e, Hiroshi Ohtsu^f,
Kazuhiko Yanai^g, Shinobu Sakurada^{a,*}

^a Department of Physiology and Anatomy, Faculty of Pharmaceutical Sciences, Tohoku Medical and Pharmaceutical University, 4-4-1 Komatsushima, Aoba-ku, Sendai 981-8558, Japan

^b Department of Pharmaceutical Sciences, Faculty of Pharmaceutical Sciences, Tohoku Medical and Pharmaceutical University, 4-4-1 Komatsushima, Aoba-ku, Sendai 981-8558, Japan

^c Department of Pharmaceutical Biosciences, Division of Biological Research on Drug Dependence, Uppsala University, Husargatan 3, Uppsala 751 24, Sweden

^d Center for Experiential Pharmacy Practice, School of Pharmacy, Tokyo University of Pharmacy and Life Sciences, 1432-1 Horinouchi, Hachioji, Tokyo 192-0392, Japan

^e First Department of Pharmacology, Daiichi College of Pharmaceutical Sciences, 22-1 Tamagawa-cho, Minami-ku, Fukuoka 815-8511, Japan

^f Department of Quantum Science and Energy Engineering, Graduate School of Engineering, Tohoku University, 6-6-01-2 Aobayama, Aoba-ku, Sendai, 980-8579, Japan

^g Department of Pharmacology, Tohoku University Graduate School of Medicine, 2-1 Seiryō-machi, Aoba-ku, Sendai 980-8575, Japan

ARTICLE INFO

Keywords:

Spermine
Histamine
Release
NMDA receptor
Nociception
Spinal cord

ABSTRACT

The involvement of spinal release of histamine on nociceptive behaviors induced by spermine was examined in mice. Intrathecal spermine produced dose-dependent nociceptive behaviors, consisting of scratching, biting and licking. The nociceptive behaviors induced by spermine at 0.02 amol and 10 pmol were markedly suppressed by i.t. pretreatment with antiserum against histamine and were abolished in histidine decarboxylase-deficient mice. In histamine H₁ receptor-deficient mice, the nociceptive behaviors induced by spermine were completely abolished after treatment with 0.02 amol of spermine and significantly suppressed after treatment with 10 pmol of spermine. The i.t. pretreatment with tatykinin NK₁ receptor antagonists eliminated the nociceptive behaviors induced by 0.02 amol of spermine, but did not affect the nociceptive behaviors induced by 10 pmol of spermine. On the other hand, the nociceptive behaviors induced by spermine at both 0.02 amol and 10 pmol were suppressed by i.t. pretreatment with antagonists for the NMDA receptor polyamine-binding site. The present results suggest that the nociceptive behaviors induced by i.t. administration of spermine are mediated through the spinal release of histamine and are elicited via activation of NMDA receptors.

1. Introduction

The polyamines spermine, spermidine and putrescine are endogenous aliphatic amines that are widely distributed (Gilad and Gilad, 1992). Since they have a polycationic structure, they electrically bind to negatively charged cellular molecules, including nucleic acids, acidic lipids and proteins (Ahern et al., 2006; Scott et al., 1993). Therefore, polyamines are considered to be closely involved with cellular functions (Ekegren et al., 2004; Gilad and Gilad, 1992; Scott et al., 1993; Tanabe et al., 2004). Polyamines are mainly synthesized from ornithine by ornithine decarboxylase, spermidine synthase and spermine synthase (Gilad and Gilad, 1992; Laube et al., 2002; Silva et al., 2011; Wolff

et al., 2003). Putrescine is formed from ornithine by ornithine decarboxylase, and then, putrescine is converted to spermidine and spermidine is converted to spermine by spermidine synthase and spermine synthase, respectively. Polyamine synthesis has been observed in both neurons and glial cells in the central nervous system (Bernstein and Müller, 1999; Ekegren et al., 2004; Laube 2002). Immunoreactivity for spermine/spermidine was detected in both neurons and glial cells in most regions in the central nervous system (Laube, 2002). Immunoreactivity for ornithine decarboxylase was detected in neurons and glial cells in the brains under several pathophysiological conditions (Bernstein and Müller, 1999). The physiological functions of polyamines in the central nervous system

* Corresponding author.

E-mail address: s-sakura@tohoku-mpu.ac.jp (S. Sakurada).

<http://dx.doi.org/10.1016/j.ejphar.2017.01.031>

Received 27 August 2016; Received in revised form 6 January 2017; Accepted 24 January 2017

Available online 26 January 2017

0014-2999/ © 2017 Elsevier B.V. All rights reserved.

are considered to include the control of neuronal excitability involved in the variable physiological responses related to pathophysiological conditions (Gilad and Gilad, 1992).

In the neurons and glial cells of the central nervous system, the molecular target for polyamines is considered to be the N-methyl-D-aspartate (NMDA) receptor. The NMDA receptor is a hetero-tetramer consisting of 7 NMDA receptor subunits (NR1, NR2A-D and NR3A-B) that form a $\text{Ca}^{2+}/\text{Na}^{+}$ channel (Dingledine et al., 1999). The NR1 subunit is an essential subunit for NMDA receptors and is ubiquitously distributed in the central nervous system (Nagy et al., 2004). It contains a polyamine-binding site, through which endogenous polyamines positively modulate the functions of the NMDA receptors (Dingledine et al., 1999). On the other hand, the NR2A-D subunits contain binding sites for the endogenous ligand glutamate, and the activation of the glutamate-binding site opens the $\text{Ca}^{2+}/\text{Na}^{+}$ channel and results in neural excitation. This response plays an important role in pain transmission in the spinal cord (Dickenson et al., 1997). Glutamate is contained in and released from primary afferent nerves (Ueda et al., 1994) and binds to NMDA receptors on the cell body of the second order neuron for pain transmission.

It has been reported that intrathecal (i.t.) administration of spermine induced nociceptive behaviors, consisting of scratching, biting and licking (Tan-No et al., 2000). However, the mechanism of spermine-induced nociceptive behaviors is not fully understood. We reported the possible interactions among spinal neurotransmitters/neuromodulators, histamine, substance P and polyamines in spinal pain transmission (Sakurada et al., 2003, 2004; Watanabe et al., 2008). Therefore, in the present study, the mechanism of nociceptive behaviors induced by i.t. administration of spermine was investigated, with a focus on the involvement of histamine and NMDA receptors in the mouse spinal cord.

2. Materials and methods

All experiments were performed following the approval of the Ethics Committee for Animal Experiments at Tohoku Medical and Pharmaceutical University and according to the National Institutes of Health Guide for the Care and Use of Laboratory Animals. Every effort was made to minimize the number of animals and any suffering by the animals used in the following experiments.

2.1. Animals

Male ddY mice (Japan SLC, Hamamatsu, Japan), histidine decarboxylase-deficient mice (supplied by Dr. Ohtsu: Ohtsu et al., 2001), histamine H_1 receptor-deficient mice (supplied by Dr. Yanai: Inoue et al., 1996), histamine H_2 receptor-deficient mice (supplied by Dr. Kobayashi: Kobayashi et al., 2000) and respective wild-type mice weighing 22–25 g were used. The histidine decarboxylase-deficient mice have 129/Sv and CD-1 mixed genetic backgrounds. The histamine H_1 receptor-deficient mice have C57BL/6 and 129/ola mixed genetic backgrounds. The histamine H_2 receptor-deficient mice have C57BL/6 and 129/ola mixed genetic backgrounds and were backcrossed eight times to the C57BL/6 mice. The genotypes of histidine decarboxylase-deficient mice, histamine H_1 receptor-deficient mice, histamine H_2 receptor-deficient mice and wild-type mice, which have the same genetic backgrounds as the respective knockout mice, were identified by the polymerase chain reaction. The animals were housed in a room maintained at 22–23 °C and 50–60% relative humidity with an alternating 12-h light/dark cycle. Food and water were available *ad libitum*. Mice only were used once.

2.2. Intrathecal injections

I.t. injection was performed following the method described by Hylden and Wilcox (1980) using a 29-gauge stainless-steel needle

attached to a 50- μl Hamilton microsyringe. The volume of the i.t. injections was 5 μl .

2.3. Behavioral procedures

The nociceptive behaviors of mice were evaluated according to the methods described in our previous report (Mizoguchi et al., 2011). Approximately 1 h before i.t. injection, mice were adapted to individual plastic cages (22.0 \times 15.0 \times 12.5 cm), which also served as observation chambers. Immediately after i.t. injection of spermine, each mouse was placed in the transparent cage, and the nociceptive behaviors induced by spermine were observed for 30 min at 5 min intervals. The nociceptive behaviors observed included caudally directed biting and licking along with reciprocal hindlimb scratching. The total response times of these nociceptive behaviors were pooled and recorded as a single value for each animal.

2.4. Drugs

The drugs used were spermine tetrahydrochloride (Nacalai Tesque, Kyoto, Japan), arcaine sulfate (Tocris Cookson Ltd., Bristol, UK), agmatine sulfate (Tocris Cookson Ltd.), (5R,10S)-(+)-5-methyl-10,11-dihydro-5H-dibenzo[*a,d*]cycloheptene-5,10-imine (MK-801) hydrogen maleate (Sigma-Aldrich Chemical Co., St. Louis, MO), D-(-)-2-amino-5-phosphonovaleric acid (D-APV) (Sigma-Aldrich Chemical Co.), 3-((+)-2-carboxypiperazin-4-yl)-propyl-1-phosphonic acid (CPP) (Sigma-Aldrich Chemical Co.), rabbit antiserum against histamine (Progen Biotechnik GMBH, Heidelberg, German), normal rabbit serum (Vector Laboratories, Burlingame, CA). [Tyr^6 ,D-Phe 7 ,D-His 9] substance P-(6–11) (sendide) and [D-Phe 7 ,D-His 9] substance P-(6–11) were synthesized by solid-phase peptide methodology. (+)-[(2S,3S)-3-(2-methoxy-benzyl-amino)-2-phenylpiperidine] (CP-99,994) was a gift from Pfizer Pharmaceuticals (New York, NY). These drugs were dissolved or diluted in sterile artificial cerebrospinal fluid (aCSF) containing 126.6 mM NaCl, 2.5 mM KCl, 2.0 mM MgCl_2 , and 1.3 mM CaCl_2 .

2.5. Statistical analysis of data

The time spent performing nociceptive behaviors (s) was presented as the mean \pm S.E.M for 10 mice. The statistical significance of the differences between groups was assessed with Student's *t*-test and one-way analysis of variance (ANOVA) followed by Bonferroni's test or two-way ANOVA followed by Bonferroni's test.

3. Results

3.1. Involvement of histamine release in spermine-induced nociceptive behaviors

Spermine-induced nociceptive behaviors were observed in mice. Groups of mice were treated with various i.t. doses of spermine (from 0.001 amol to 10 pmol) or aCSF, and nociceptive behaviors were observed for 30 min at 5 min intervals. The i.t. administration of spermine at a dose of 0.001 amol to 1 amol dose-dependently evoked characteristic nociceptive behaviors mainly consisting of vigorous biting and/or licking with a little scratching (Fig. 1). However, at doses over 1 amol, the nociceptive behavior response elicited by spermine was saturated, and no additional increase in nociceptive behaviors was observed with 10 pmol of spermine. The nociceptive behaviors peaked at 5–10 min and disappeared at 25–30 min after the injection (data not shown).

To elucidate the involvement of the spinal release of histamine on spermine-induced nociceptive behaviors, the effect of an antiserum against histamine on spermine-induced nociceptive behaviors was determined. Groups of mice were pretreated with i.t. antiserum against

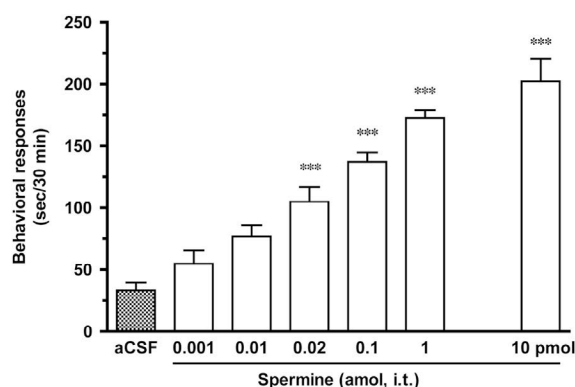


Fig. 1. Spermine-induced nociceptive behaviors in mice. Groups of mice were treated with i.t. spermine (0.001 amol–10 pmol) or aCSF, and nociceptive behaviors induced by spermine were observed for 30 min. Each column represents the mean \pm S.E.M. for 10 mice. The statistical significance of the differences between groups was assessed with one-way ANOVA followed by Bonferroni's test. The F -value of one-way ANOVA was $F[6,63] = 33.18$ ($P < 0.001$). ***, $P < 0.001$ vs. aCSF.

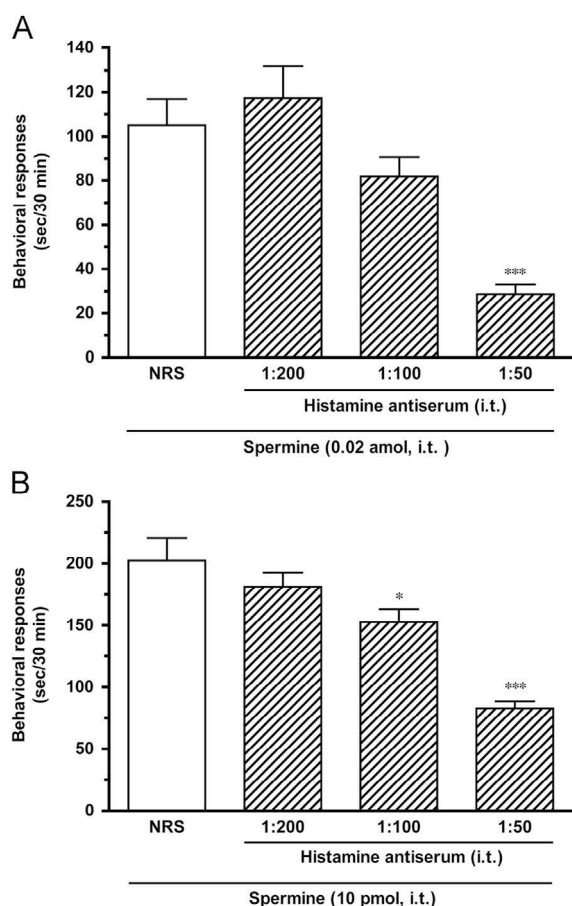


Fig. 2. Effect of histamine antiserum on spermine-induced nociceptive behaviors in mice. Groups of mice were treated with i.t. histamine antiserum (1:200–1:50 dilution) or normal rabbit serum (NRS; 1:50 dilution) 5 min prior spermine treatment, and nociceptive behaviors induced by i.t. spermine injection (A: 0.02 amol or B: 10 pmol) were observed for 30 min. Each column represents the mean \pm S.E.M. for 10 mice. The statistical significance of the differences between groups was assessed with one-way ANOVA followed by Bonferroni's test. (A) The F -value of one-way ANOVA was $F[3,36] = 13.80$ ($P < 0.001$). ***, $P < 0.001$ vs. NRS. (B) The F -value of one-way ANOVA was $F[3,36] = 17.83$ ($P < 0.001$). *, $P < 0.05$ and ***, $P < 0.001$ vs. NRS.

histamine (1:200–1:50 dilution) or normal rabbit serum (1:50 dilution) 5 min prior i.t. treatment with spermine (0.02 amol or 10 pmol), and the nociceptive behaviors induced by spermine were measured for

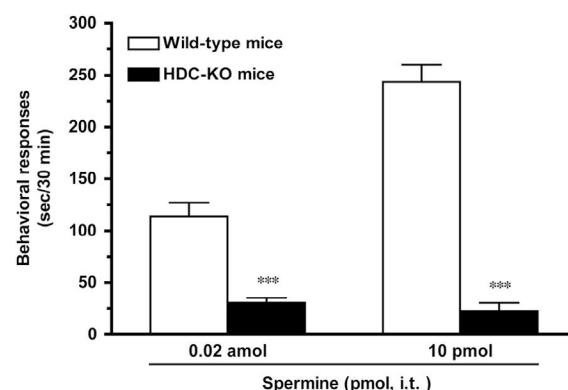


Fig. 3. Spermine-induced nociceptive behaviors in histidine decarboxylase-deficient mice (HDC-KO mice). Groups of HDC-KO mice and corresponding wild-type mice were treated with i.t. spermine (0.02 amol or 10 pmol), and nociceptive behaviors induced by spermine were observed for 30 min. Each column represents the mean \pm S.E.M. for 10 mice. The statistical significance of the differences between groups was assessed with two-way ANOVA followed by Bonferroni's test. The F -value of two-way ANOVA was $F[1,36] = 171.2$ ($P < 0.001$). ***, $P < 0.001$ vs. wild-type mice.

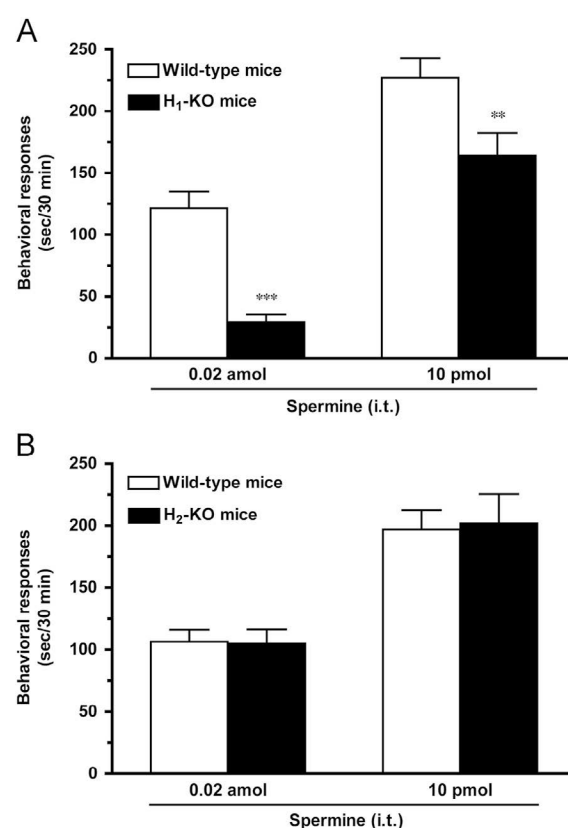


Fig. 4. Spermine-induced nociceptive behaviors in histamine H_1 receptor-deficient mice (H_1 -KO mice), histamine H_2 receptor-deficient mice (H_2 -KO mice) and respective wild-type mice. Groups of H_1 -KO mice (A), H_2 -KO mice (B) and respective wild-type mice were treated with i.t. spermine (0.02 amol or 10 pmol), and nociceptive behaviors induced by spermine were observed for 30 min. Each column represents the mean \pm S.E.M. for 10 mice. The statistical significance of the differences between groups was assessed with two-way ANOVA followed by Bonferroni's test. (A) The F -value of two-way ANOVA was $F[1,36] = 29.70$ ($P < 0.001$). **, $P < 0.01$ and ***, $P < 0.001$ vs. wild-type mice.

30 min. The nociceptive behaviors induced by spermine at both 0.02 amol and 10 pmol were suppressed by i.t. pretreatment with antiserum against histamine in a concentration-dependent manner (Fig. 2). In particular, the nociceptive behaviors induced by 0.02 amol of spermine were eliminated by the 1:50 histamine antiserum dilution (Fig. 2A).

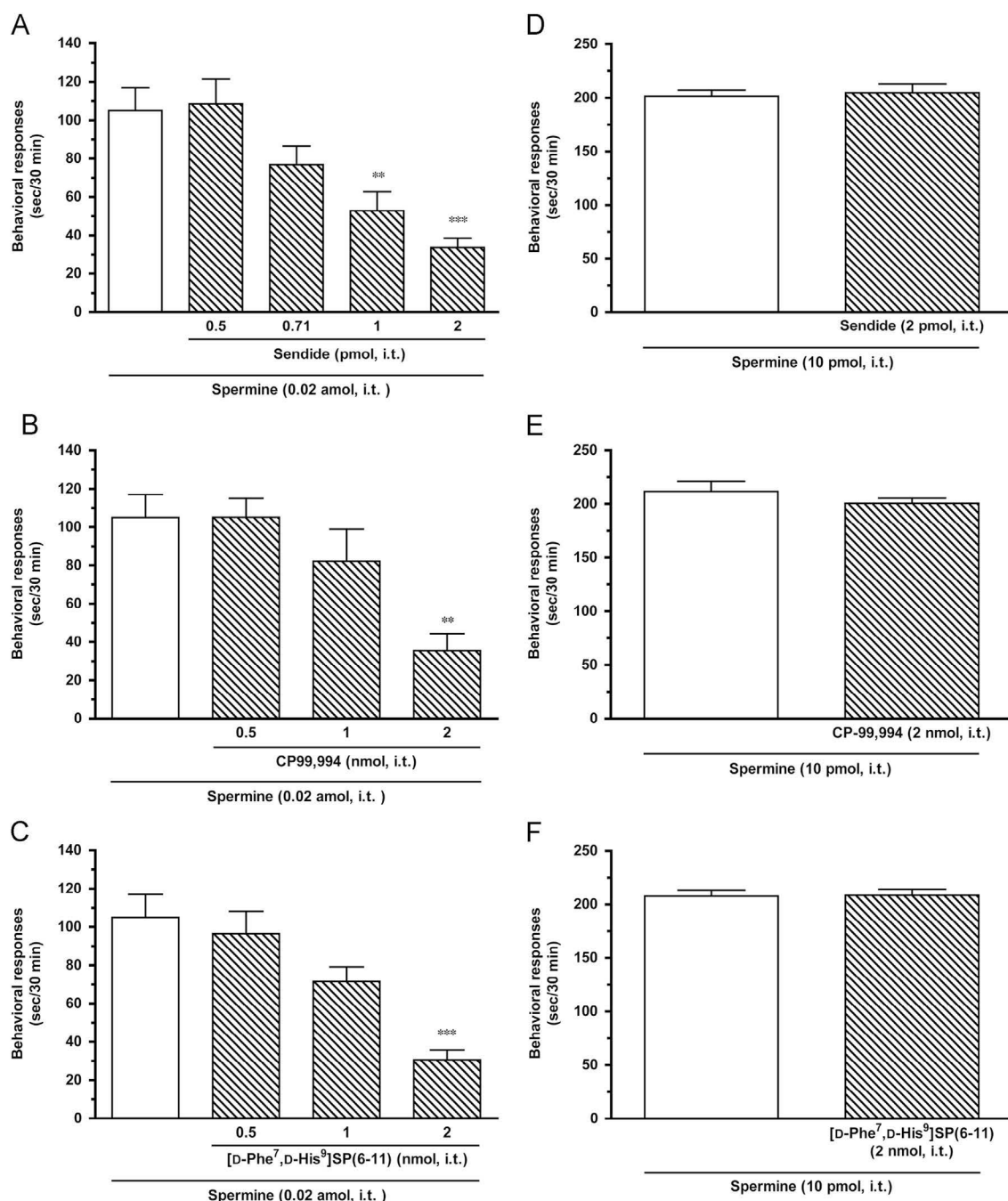


Fig. 5. Effects of the takykinin NK₁ receptor antagonists on spermine-induced nociceptive behaviors in the mouse spinal cord. Groups of mice were co-administered i.t. sendide (A and D: 0.5–2 pmol), CP99,994 (B and E: 0.5–2 nmol) or [D-Phe⁷,D-His⁹]SP(6–11) (C and F: 0.5–2 nmol) with spermine (A, B and C: 0.02 amol or D, E and F: 10 pmol), and nociceptive behaviors induced by spermine were observed for 30 min. Each column represents the mean \pm S.E.M. for 10 mice. The statistical significance of the differences between groups was assessed with one-way ANOVA followed by Bonferroni's test (A, B and C) or with Student's *t*-test (D, E and F). (A) The *F*-value of one-way ANOVA was $F_{(4,45)} = 9.937$ ($P < 0.001$). **, $P < 0.01$ and ***, $P < 0.001$ vs. spermine alone. (B) The *F*-value of one-way ANOVA was $F_{(3,36)} = 7.192$ ($P < 0.001$). **, $P < 0.01$ vs. spermine alone. (C) The *F*-value of one-way ANOVA was $F_{(3,36)} = 12.28$ ($P < 0.001$). ***, $P < 0.001$ vs. spermine alone.

The contribution of endogenous spinal histamine to the nociceptive behaviors induced by spermine was confirmed using histidine decarboxylase-deficient mice. Groups of histidine decarboxylase-deficient mice and corresponding wild-type mice were treated with spermine (0.02 amol or 10 pmol) i.t., and nociceptive behaviors were observed for 30 min. The nociceptive behaviors induced by spermine at both 0.02 amol and 10 pmol were abolished in histidine decarboxylase-deficient mice (Fig. 3).

3.2. Involvement of histamine receptors in spermine-induced nociceptive behaviors

The involvement of histamine receptor subtypes in spermine-induced nociceptive behaviors was determined using histamine H₁ receptor-deficient mice and histamine H₂ receptor-deficient mice. Groups of histamine H₁ receptor-deficient mice, histamine H₂ receptor-deficient mice and corresponding wild-type mice were treated with i.t. spermine (0.02 amol or 10 pmol), and nociceptive behaviors were observed for 30 min. The nociceptive behaviors induced by 0.02 amol of

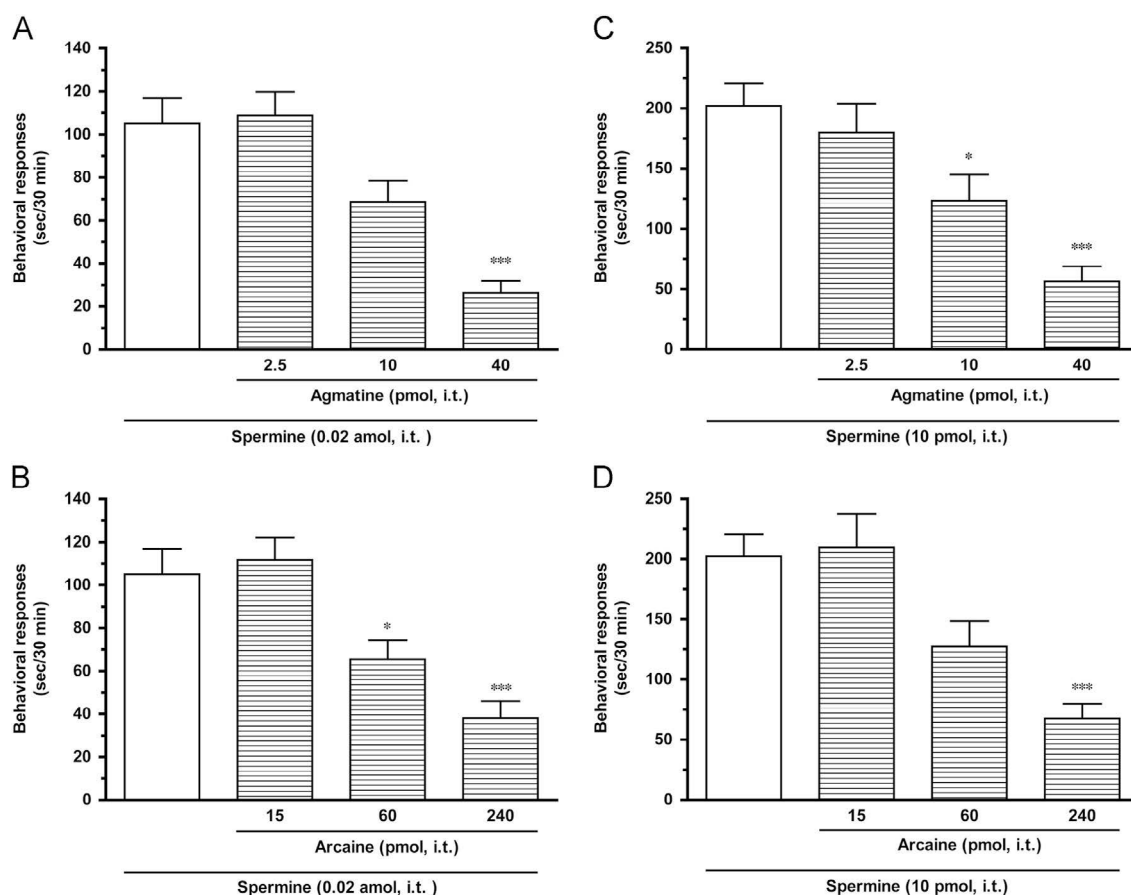


Fig. 6. Effects of the antagonists for the polyamine-binding site of the NMDA receptor on the spermine-induced nociceptive behaviors in mice. Groups of mice were co-administered i.t. agmatine (A and C: 2.5–40 pmol) or arcaine (B and D: 15–240 pmol) with spermine (A and B: 0.02 amol or C and D: 10 pmol), and nociceptive behaviors induced by spermine were observed for 30 min. Each column represents the mean \pm S.E.M. for 10 mice. The statistical significance of the differences between groups was assessed with one-way ANOVA followed by Bonferroni's test. (A) The F -value of one-way ANOVA was $F[3,36] = 15.14$ ($P < 0.001$). ***, $P < 0.001$ vs. spermine alone. (B) The F -value of one-way ANOVA was $F[3,36] = 12.09$ ($P < 0.001$). *, $P < 0.05$ and ***, $P < 0.001$ vs. spermine alone. (C) The F -value of one-way ANOVA was $F[3,36] = 11.10$ ($P < 0.001$). *, $P < 0.05$ and ***, $P < 0.001$ vs. spermine alone. (D) The F -value of one-way ANOVA was $F[3,36] = 10.71$ ($P < 0.001$). ***, $P < 0.001$ vs. spermine alone.

spermine were abolished in histamine H_1 receptor-deficient mice, whereas the nociceptive behaviors induced by 10 pmol of spermine were suppressed in histamine H_1 receptor-deficient mice (Fig. 4A). On the other hand, the nociceptive behaviors induced by spermine at both 0.02 amol and 10 pmol were not affected in histamine H_2 receptor-deficient mice (Fig. 4B).

3.3. Involvement of tachykinin NK_1 receptors in spermine-induced nociceptive behaviors

The involvement of the tachykinin NK_1 receptor in spermine-induced nociceptive behaviors was determined. Groups of mice were co-administered the i.t. tachykinin NK_1 receptor antagonists sendide (0.5–2 pmol), CP99,994 (0.5–2 nmol) or [D-Phe⁷,D-His⁹]SP(6–11) (0.5–2 nmol) with spermine (0.02 amol or 10 pmol), and nociceptive behaviors induced by spermine were observed for 30 min. The nociceptive behaviors induced by 0.02 amol of spermine were dose-dependently attenuated by the co-administration of tachykinin NK_1 receptor antagonists (Fig. 5A–C). The highest dose of tachykinin NK_1 receptor antagonists eliminated the nociceptive behaviors induced by 0.02 amol of spermine. In contrast, the nociceptive behaviors induced by 10 pmol of spermine were not affected by the co-administration of tachykinin NK_1 receptor antagonists (Fig. 5D–F).

3.4. Involvement of NMDA receptors in spermine-induced nociceptive behaviors

The NMDA receptor has multiple ligand-binding sites, including a glutamate-binding site, a glycine-binding site, an ion channel modulator-binding site and a polyamine-binding site. Therefore, the involvement of each ligand-binding site of the NMDA receptor in spermine-induced nociceptive behaviors was determined. Groups of mice were co-administered i.t. agmatine (2.5–40 pmol) or arcaine (15–240 pmol), antagonists for the polyamine-binding site of the NMDA receptor, with spermine (0.02 amol or 10 pmol), and the nociceptive behaviors induced by spermine were observed for 30 min. The nociceptive behaviors induced by both 0.02 amol and 10 pmol of spermine were dose-dependently attenuated by the co-administration of antagonists for the polyamine-binding site of the NMDA receptor (Fig. 6A–D).

Other groups of mice were co-administered i.t. D-APV (0.25–1 nmol) or CPP (1.95–31.25 pmol), antagonists for the glutamate-binding site of the NMDA receptor, or MK-801 (5–10 nmol), an antagonist for the ion channel modulator-binding site of the NMDA receptor, with spermine (0.02 amol), and the nociceptive behaviors induced by spermine were observed for 30 min. The nociceptive behaviors induced by 0.02 amol of spermine were dose-dependently reduced by the co-administration of these antagonists for the NMDA receptor (Fig. 7A–C).

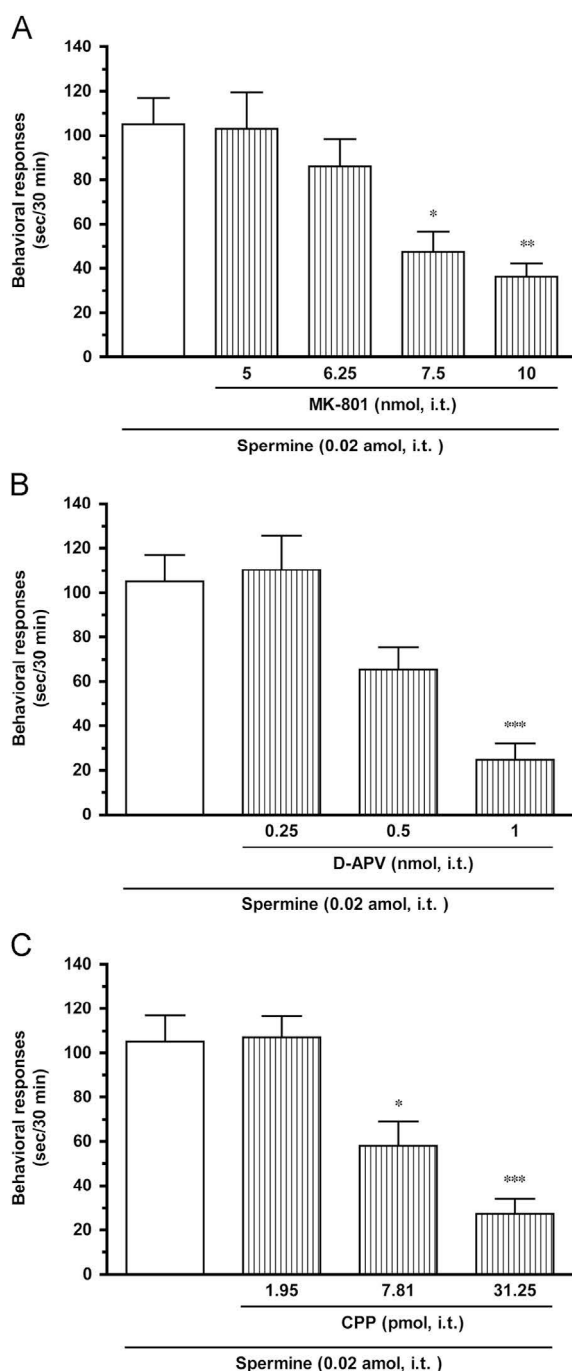


Fig. 7. Effects of the antagonists for the glutamate-binding site and ion channel modulator-binding site of the NMDA receptor on spermine-induced nociceptive behaviors in the mouse spinal cord. Groups of mice were co-administered i.t. MK-801 (5–10 nmol), D-APV (0.25–1 nmol) or CPP (1.95–31.25 pmol) with spermine (0.02 amol), and nociceptive behaviors induced by spermine were observed for 30 min. Each column represents the mean \pm S.E.M. for 10 mice. The statistical significance of the differences between groups was assessed with one-way ANOVA followed by Bonferroni's test. (A) The F -value of one-way ANOVA was $F[4,45] = 7.577$ ($P < 0.001$). *, $P < 0.05$ and **, $P < 0.01$ vs. spermine alone. (B) The F -value of one-way ANOVA was $F[3,36] = 11.67$ ($P < 0.001$). ***, $P < 0.001$ vs. spermine alone. (C) The F -value of one-way ANOVA was $F[3,36] = 14.83$ ($P < 0.001$). *, $P < 0.05$ and ***, $P < 0.001$ vs. spermine alone.

4. Discussion

Polyamines, including spermine, are aliphatic molecules that are widely distributed in the body and are involved in a variety of physiological functions and responses (Gilad and Gilad, 1992). In the

spinal transmission of pain, endogenous polyamines are thought to bind to the polyamine-binding site of the NMDA receptor and to modulate the Ca^{2+} channel function of this receptor to potentiate neural excitation (Williams et al., 1991). In fact, i.t. -administration of spermine leads to nociceptive behaviors in mice (Tan-No et al., 2000). In the present study, the mechanism of spermine-induced nociceptive behaviors was investigated in the mouse spinal cord. Intrathecal administration of spermine was previously reported to induce dose-dependent nociceptive behaviors at doses of 100 amol–10 fmol and showed saturated responses at doses of 10 fmol–10 pmol (Tan-No et al., 2000). In the present study, we found that i.t. -administered spermine showed dose-dependent nociceptive behaviors at much lower doses (0.001–1 amol) (Fig. 1). Surprisingly, 0.02 amol of spermine was adequate to stimulate significant nociceptive behaviors. It may be a lowest dose to elicit pharmacological effect in any drugs or compounds. At present, there is unfortunately no evidence to explain the mechanism of this extraordinarily high potency of spermine. The extensive research should be required to explain this phenomenon. To describe the mechanism of spermine-induced nociceptive behaviors, the present study was conducted using 0.02 amol (a very low dose) and 10 pmol (a high dose) of spermine. As a result, we found evidence that the nociceptive behaviors induced by i.t. administration of spermine at both 0.02 amol and 10 pmol were eliminated by i.t. pretreatment with histamine antiserum (Fig. 2), suggesting that the nociceptive behaviors induced by i.t. administration of spermine are mediated by the spinal release of histamine. This hypothesis was supported by the finding that the nociceptive behaviors induced by i.t. administration of spermine at both 0.02 amol and 10 pmol were abolished in histidine decarboxylase-deficient mice lacking endogenous histamine (Fig. 3). Herein, we report the remarkable physiological function of spermine to regulate the spinal release of histamine. In contrast to the results of the present study, we previously reported that i.t. administration of histamine stimulates the polyamine-binding site of the NMDA receptor to induce nociceptive behaviors (Watanabe et al., 2008). Taken together with the previously reported results, the current findings indicate that pain transmission in the spinal cord involves a complicated mutual regulation between spermine and histamine.

In the present study, the nociceptive behaviors induced by i.t. administration of spermine at both 0.02 amol and 10 pmol were suppressed in histamine H_1 receptor-deficient mice (Fig. 4A), but not in histamine H_2 receptor-deficient mice (Fig. 4B), suggesting that the histamine released by i.t. administration of spermine stimulates the histamine H_1 receptor, but not the histamine H_2 receptor, in the spinal cord. It is noteworthy that the nociceptive behaviors induced by 0.02 amol of spermine were abolished in histamine H_1 receptor-deficient mice, whereas the nociceptive behaviors induced by 10 pmol of spermine were only partially suppressed in histamine H_1 receptor-deficient mice. We previously reported that the nociceptive behaviors induced by low doses of i.t. histamine are mediated by the activation of the histamine H_1 receptor in the spinal cord (Sakurada et al., 2003), whereas the nociceptive behaviors induced by high doses of i.t. histamine are mediated by the activation of the NMDA receptor via the binding of histamine to the polyamine-binding site of the NMDA receptor in the spinal cord (Watanabe et al., 2008). Although there is no direct evidence to demonstrate that the i.t. administration of spermine dose-dependently increases the release of histamine in the spinal cord, the nociceptive behaviors induced by 0.02 amol and 10 pmol of spermine may be primarily mediated by the activation of the histamine H_1 receptor and NMDA receptor in the spinal cord, respectively, via the release of histamine.

It is well established that histamine-containing neurons project from the tuberomammillary nucleus of the posterior hypothalamus to a variety of brain regions and to the dorsal spinal cord (Haas and Panula, 2003; Panula et al., 1984, 1989a, 1989b; Watanabe et al., 1984). Histamine released at the dorsal spinal cord stimulates histamine H_1 receptors on the terminals of primary afferent nerves and subsequently

causes the release of substance P and glutamate from primary afferent nerves, which bind to tachykinin NK₁ receptors and NMDA receptors on the dorsal horn of the spinal cord, respectively (Sakurada et al., 2003, 2004). In the present study, the nociceptive behaviors induced by i.t. administration of 0.02 amol of spermine were dose-dependently reduced by the co-administration of antagonists for the polyamine-binding site of the NMDA receptor (Fig. 6A,B), antagonists for the glutamine-binding site of the NMDA receptor (Fig. 7A,B) or an antagonist for the ion channel modulator-binding site of the NMDA receptor (Fig. 7C). Moreover, the nociceptive behaviors induced by i.t. administration of 0.02 amol of spermine were suppressed by the co-administration of tachykinin NK₁ receptor antagonists (Fig. 5A–C). These results clearly suggest that the nociceptive behaviors associated with i.t. administration of 0.02 amol of spermine are due to the spinal release of histamine, which stimulates histamine H₁ receptors on the primary afferent nerves and leads to the release of substance P and glutamate from the primary afferent nerves, which bind to the tachykinin NK₁ receptor and the NMDA receptor on the dorsal spinal cord, respectively.

In the present study, the nociceptive behaviors induced by i.t. administration of 10 pmol of spermine were suppressed by co-administration of antagonists for the polyamine-binding site of the NMDA receptor (Fig. 6C–D). Moreover, it has been reported that the nociceptive behaviors induced by i.t. administration of 10 pmol of spermine were dose-dependently suppressed by the co-administration of the antagonists for the glutamine-binding site of the NMDA receptor or the antagonist for the ion channel modulator-binding site of the NMDA receptor (Tan-No et al., 2000). These results clearly suggest that the nociceptive behaviors induced by 10 pmol of spermine are mediated by the activation of the spinal NMDA receptor. However, in contrast to the 0.02 amol spermine-induced nociceptive behaviors, the mechanism for the nociceptive behaviors induced by 10 pmol of spermine may be more complicated. In the present study, administration of tachykinin NK₁ receptor antagonists failed to suppress the nociceptive behaviors induced by 10 pmol of spermine (Fig. 5D–F). Taken together with the finding that the nociceptive behaviors induced by 10 pmol of spermine were completely abolished in histidine decarboxylase-deficient mice (Fig. 3), but only partially suppressed in histamine H₁ receptor-deficient mice (Fig. 4A), the nociceptive behaviors associated with i.t. administration of 10 pmol of spermine may be due to the spinal release of histamine, which preferentially and directly stimulates the polyamine-binding site of the NMDA receptor, but not the histamine H₁ receptor, on the dorsal spinal cord.

In conclusion, the nociceptive behaviors induced by i.t. administration of spermine are mediated by the spinal release of histamine. Histamine indirectly activates the tachykinin NK₁ receptor and NMDA receptor via the spinal release of substance P and glutamate and directly stimulates the polyamine-binding site of the NMDA receptor. The receptor that is indirectly or directly stimulated by the released histamine may depend on the dose of spermine injected.

Acknowledgements

This work was supported by JSPS KAKENHI Grant numbers 15K08678 and 25460725, and a MEXT (Ministry of Education, Culture, Sports, Science and Technology)-Supported Program for the Strategic Research Foundation at Private Universities (2015–2019).

References

- Ahern, G.P., Wang, X., Miyares, R.L., 2006. Polyamines are potent ligands for the capsaicin receptor TRPV1. *J. Biol. Chem.* 281, 8991–8995.
- Bernstein, H.G., Müller, M., 1999. The cellular localization of the L-ornithine decarboxylase/polyamine system in normal and diseased central nervous systems. *Prog. Neurobiol.* 57, 485–505.
- Dickenson, A.H., Chapman, V., Green, G.M., 1997. The pharmacology of excitatory and inhibitory amino acid-mediated events in the transmission and modulation of pain in the spinal cord. *Gen. Pharmacol.* 28, 633–638.
- Dingledine, R., Borges, K., Bowie, D., Traynelis, S.F., 1999. The glutamate receptor ion channels. *Pharmacol. Rev.* 51, 7–61.
- Ekegren, T., Gomes-Trolin, C., Nygren, I., Askmark, H., 2004. Maintained regulation of polyamines in spinal cord from patients with amyotrophic lateral sclerosis. *J. Neurol. Sci.* 222, 49–53.
- Gilad, G.M., Gilad, V.H., 1992. Polyamines in neurotrauma. Ubiquitous molecules in search of a function. *Biochem. Pharmacol.* 44, 401–407.
- Haas, H., Panula, P., 2003. The role of histamine and the tuberomammillary nucleus in the nervous system. *Nat. Rev. Neurosci.* 4, 121–130.
- Hylden, J.L., Wilcox, G.L., 1980. Intrathecal morphine in mice: a new technique. *Eur. J. Pharmacol.* 67, 313–316.
- Inoue, I., Yanai, K., Kitamura, D., Taniuchi, I., Kobayashi, T., Niimura, K., Watanabe, T., Watanabe, T., 1996. Impaired locomotor activity and exploratory behavior in mice lacking histamine H₁ receptors. *Proc. Natl. Acad. Sci. USA* 93, 13316–13320.
- Kobayashi, T., Tonai, S., Ishihara, Y., Koga, R., Okabe, S., Watanabe, T., 2000. Abnormal functional and morphological regulation of the gastric mucosa in histamine H₂ receptor-deficient mice. *J. Clin. Invest.* 105, 1741–1749.
- Laube, G., Bernstein, H.G., Wolf, G., Veh, R.W., 2002. Differential distribution of spermidine/spermine-like immunoreactivity in neurons of the adult rat brain. *J. Comp. Neurol.* 444, 369–386.
- Mizoguchi, H., Komatsu, T., Iwata, Y., Watanabe, C., Watanabe, H., Orito, T., Katsuyama, S., Yonezawa, A., Onodera, K., Sakurada, T., Sakurada, S., 2011. Involvement of glial cells in the nociceptive behaviors induced by a high-dose of histamine administered intrathecally. *Eur. J. Pharmacol.* 653, 21–25.
- Nagy, G.G., Watanabe, M., Fukaya, M., Todd, A., 2004. Synaptic distribution of NR1, NR2A and NR2B subunits of the N-methyl-D-aspartate receptor in the rat lumbar spinal cord revealed with an antigen-unmasking technique. *Eur. J. Neurosci.* 20, 3301–3312.
- Ohtsu, H., Tanaka, S., Terui, T., Hori, Y., Makabe-Kobayashi, Y., Pejler, G., Tchougounova, E., Hellman, L., Gertsenstein, M., Hirasawa, N., Sakurai, E., Buzás, E., Kovács, P., Csaba, G., Kittel, A., Okada, M., Hara, M., Mar, L., Numayama-Tsuruta, K., Ishigaki-Suzuki, S., Ohuchi, K., Ichikawa, A., Falus, A., Watanabe, T., Nagy, A., 2001. Mice lacking histidine decarboxylase exhibit abnormal mast cells. *FEBS Lett.* 502, 53–56.
- Panula, P., Yang, H.Y., Costa, E., 1984. Histamine-containing neurons in the rat hypothalamus. *Proc. Natl. Acad. Sci. USA* 81, 2572–2576.
- Panula, P., Flüggé, G., Fuchs, E., Pirvola, U., Auvinen, S., Airaksinen, M.S., 1989a. Histamine-immunoreactive nerve fibers in the mammalian spinal cord. *Brain Res.* 484, 234–239.
- Panula, P., Pirvola, U., Auvinen, S., Airaksinen, M.S., 1989b. Histamine immunoreactive nerve fibers in the rat brain. *Neuroscience* 28, 585–610.
- Sakurada, S., Orito, T., Furuta, S., Watanabe, H., Mobarakeh, J.I., Yanai, K., Watanabe, T., Sato, T., Onodera, K., Sakurada, C., Sakurada, T., 2003. Intrathecal histamine induced spinally mediated behavioral responses through tachykinin NK₁ receptors. *Pharmacol. Biochem. Behav.* 74, 487–493.
- Sakurada, S., Watanabe, H., Mizoguchi, H., Yonezawa, A., Orito, T., Katsuyama, S., Kuramasu, A., Sakurada, C., Yanai, K., Sakurada, T., 2004. Involvement of the histaminergic system in the nociceptin-induced pain-related behaviors in the mouse spinal cord. *Pain* 112, 171–182.
- Scott, R.H., Sutton, K.G., Dolphin, A.C., 1993. Interactions of polyamines with neuronal ion channels. *Trends Neurosci.* 16, 153–160.
- Silva, M.A., Klafke, J.Z., Rossato, M.F., Gewehr, C., Guerra, G.P., Rubin, M.A., Ferreira, J., 2011. Role of peripheral polyamines in the development of inflammatory pain. *Biochem. Pharmacol.* 82, 269–277.
- Tanabe, T., Shin, M., Fujiwara, K., 2004. Immunoelectron microscopy study of polyamines using a newly prepared monoclonal antibody against spermidine: use of a mixture of glutaraldehyde and paraformaldehyde as a cross-linking agent in the preparation of the antigen. *J. Biochem.* 135, 501–507.
- Tan-No, K., Taira, A., Wako, K., Nijima, F., Nakagawasa, O., Tadano, T., Sakurada, C., Sakurada, T., Kisara, K., 2000. Intrathecally administered spermine produces the scratching, biting and licking behaviour in mice. *Pain* 86, 55–61.
- Ueda, M., Kuraishi, Y., Sugimoto, K., Satoh, M., 1994. Evidence that glutamate is released from capsaicin-sensitive primary afferent fibers in rats: study with on-line continuous monitoring of glutamate. *Neurosci. Res.* 20, 231–237.
- Watanabe, C., Orito, T., Watanabe, H., Mizoguchi, H., Yonezawa, A., Yanai, K., Mobarakeh, J.I., Onodera, K., Sakurada, T., Sakurada, S., 2008. Intrathecal high-dose histamine induces spinally-mediated nociceptive behavioral responses through a polyamine site of NMDA receptors. *Eur. J. Pharmacol.* 581, 54–63.
- Watanabe, T., Taguchi, Y., Shiosaka, S., Tanaka, J., Kubota, H., Terano, Y., Tohyama, M., Wada, H., 1984. Distribution of histaminergic neuron system in the central nervous system of rats; a fluorescent immunohistochemical analysis with histidine decarboxylase as a marker. *Brain Res.* 295, 13–25.
- Williams, K., Romano, C., Dichter, M.A., Molinoff, P.B., 1991. Modulation of the NMDA receptor by polyamines. *Life Sci.* 48, 469–498.
- Wolff, A.C., Armstrong, D.K., Fetting, J.H., Carducci, M.K., Riley, C.D., Bender, J.F., Casero, R.A., Jr., Davidson, N.E., 2003. A Phase II study of the polyamine analog N¹,N¹¹-diethylnorspermine (DENSpm) daily for five days every 21 days in patients with previously treated metastatic breast cancer. *Clin. Cancer Res.* 9, 5922–5928.

REVIEW ARTICLE

Opioids Resistance in Chronic Pain Management

Luigi A. Morrone^{a,b,*}, Damiana Scuteri^a, Laura Rombolà^a, Hirokazu Mizoguchi^c and Giacinto Bagetta^{a,b}

^aDepartment of Pharmacy, Health and Nutritional Sciences, University of Calabria, Rende, Italy; ^bUniversity Consortium for Adaptive Disorders and Head Pain (UCADH), Section of Neuropharmacology of Normal and Pathological Neuronal Plasticity, University of Calabria, Rende, Italy; ^cDepartment of Physiology and Anatomy, Tohoku Pharmaceutical University, 4-4-1 Komatsushima, Aoba-ku, Sendai 981-8558, Japan

ARTICLE HISTORY

Received: June 27, 2015
Revised: August 11, 2016
Accepted: October 24, 2016

DOI:
10.2174/1570159X174666161101092
822

Abstract: Chronic pain management represents a serious healthcare problem worldwide. Chronic pain affects approximately 20% of the adult European population and is more frequent in women and older people. Unfortunately, its management in the community remains generally unsatisfactory and rarely under the control of currently available analgesics. Opioids have been used as analgesics for a long history and are among the most used drugs; however, while there is no debate over their short term use for pain management, limited evidence supports their efficacy of long-term treatment for chronic non-cancer pain. Therapy with opioids is hampered by inter-individual variability and serious side effects and some opioids often result ineffective in the treatment of chronic pain and their use is controversial. Accordingly, for a better control of chronic pain a deeper knowledge of the molecular mechanisms underlying resistance to opiates is mandatory.

Keywords: Chronic pain, opiate resistance, polymorphisms.

INTRODUCTION

Chronic pain management is one of the most debated issues in pharmacology and public healthcare. Epidemiological studies show that in Europe one in five adults suffer from chronic pain [1], often of unknown etiology and rarely under the control of currently available analgesics [2]. Opioids have been used as analgesics for a long history and are among the most used drugs [3]. Interestingly, they have been used for centuries for the treatment of pain but their molecular targets were discovered only about forty years ago, in the early 70s, when the full blossom of receptor binding studies made it possible [4]. Opioid receptors belong to the family of G-protein coupled receptors and, in particular, they are coupled to pertussis toxin (PTX)-sensitive or PTX-insensitive $G_{i/o}$ proteins. The discovery of the second messenger system coupled to the receptor binding of opioid drugs led to the understanding of their mechanism of action. These receptors mediate an inhibitory signal of neural transmission involved in the analgesic action of opioids. The discovery of opioid receptors prompted the isolation of the first two endogenous opioid neurotransmitters called Met-enkephalin and Leu-enkephalin [5]. Since then, several opioid peptides were identified and the following studies led to a better understanding of their properties [6]. However, while there is

no debate over the short term use of opioids for pain management, there is limited evidence to support the efficacy of long-term treatment for chronic non-cancer pain [7, 8] and some of them are often ineffective in the treatment of chronic pain and their use is controversial. This is likely due to the inter-individual variability originating from the presence of several polymorphisms which attract genes involved in the actions of the opioid system. In addition, the use of chronic opioid therapy is limited by a set of problems. These include tolerance, addiction, pseudo-addiction, opioid induced hyperalgesia, bowel dysfunction, suppression of testosterone, cognitive impairment, substance abuse and diversion [9]. In this article we review the literature to draw a comprehensive picture of the mechanisms underlying resistance to opioids for a better control in chronic pain management.

CAUSES OF CHRONIC PAIN

Chronic pain is a multifactorial condition, caused by the complex interplay of several pathogenic mechanisms [10, 11]. This condition can be triggered by lesions or diseases affecting the somatosensory nervous system [12]. Costigan and colleagues described it as an expression of maladaptive plasticity within the nociceptive system [13]. Particularly, several changes, *e.g.*, facilitation and disinhibition of synaptic transmission and neuroimmune interactions, spreaded across the nervous system contribute to dysregulation of pain neurocircuitry and neurochemistry resulting in complex pain phenotypes. Chronic pain is associated with specific and nonspecific medical conditions and generally, it is broadly

*Address correspondence to this author at the Department of Pharmacy, Health and Nutritional Sciences, University of Calabria, Rende, Italy;
Tel: 0039 0984493054; Fax: 0039 0984493107; E-mail: luigimorrone@libero.it

categorised as cancer pain and non-cancer pain [11]. Non-cancer pain can be caused by specific chronic medical conditions such as osteoarthritis, back pain, fibromyalgia, diabetic neuropathy and migraine headaches [11, 14]. However, several pathophysiological situations might also induce it, such as alcoholism [15], HIV/AIDS [16, 17] and neurodegenerative disorders, such as multiple sclerosis [18, 19]. All these diseases have a different impact on the opioid system. For example, several animal and human studies have shown a decreased analgesic potency of μ opioid agonists in diabetic neuropathic pain [20-24]. Chen and Pan reported that the inhibitory effect of systemic morphine on spinothalamic tract neurons is substantially reduced in diabetic rats suggesting a reduction in or dysfunction of opioid receptors in the spinal cord dorsal horn in diabetes [25]. Interestingly, some studies demonstrated a reduction in spinal μ opioid receptors [26, 27] whereas others suggested that the reduced analgesic action of opioid agonists in diabetic neuropathic pain is due, at least in part, to impaired receptor-G protein coupling [28]. Following nerve injury, primary afferents reduce their expression of μ opioid receptors (MOR), and dorsal horn neurons are less sensitive to inhibition by μ opioid agonists [29]. Some authors reported a deficient functioning of MOR at the supraspinal level and κ -opioid receptors (KOR) at the spinal level in diabetic mice related to the activation of δ opioid receptors (DOR) at both the supraspinal level and spinal levels [30]. Moreover, the dysfunction of adenosine triphosphate-sensitive potassium channels may contribute to the reduction in MOR-mediated analgesia in diabetic mice [31]. Alcoholism also impacts the opioid system. In fact, prolonged exposure to ethanol can promote an upregulation of functional DOR in the spinal cord and modulate MOR-mediated analgesia [32]. In addition, Hull and colleagues suggested that ethanol may reduce opioid tolerance in mice at the cellular level acting on the γ -aminobutyric acid (GABA)ergic system either at the level of GABA release or GABA receptors [33]. Furthermore, the HIV-1 envelope glycoprotein 120 (gp120) has been shown to increase MOR mRNA expression in human vascular endothelium [34] and also in HL-60 human promyelocytic leukemia cells differentiated into macrophage-like cells by 12-O-tetradecanoylphorbol-13-acetate (TPA) [35]. In addition, more recently, Dever and colleagues reported that the expression of MOR-1 and other MOR variants may be differentially regulated by HIV-1 [36]. Interestingly, the combination of opioids and HIV-1 infection may promote the damage of neurons and glia in the pain-processing neural pathway [17]. Preclinical investigations utilizing animal models, as well as clinical observations with multiple sclerosis patients, also suggested alteration of endogenous opioid systems in the disease. Particularly, Gironi and colleagues found reduced β -endorphin concentrations in peripheral blood mononuclear cells of patients with multiple sclerosis [37]. More recently, in a Theiler's murine encephalomyelitis virus model of multiple sclerosis, Lynch and colleagues reported that mRNA levels of MOR, KOR and DOR are significantly decreased in the spinal cord [38].

LIFE STRESSFUL EVENTS AND CHRONIC PAIN

Several evidences in rodents and humans have highlighted a crucial role of early life stressful events (such

as early maternal separation, physical violence, sexual or psychological abuses) in the development and worsening of chronic pain [39-44]. The neurobiological mechanisms underlying the relationship between early-life stress and development of chronic pain are unclear, however, clinical and preclinical data suggested a key role for some neurobiological substrates, *e.g.* the hypothalamic-pituitary-adrenal axis, neurotransmissions (monoaminergic, opioidergic, endocannabinoid) and immune systems [45-47]. In this regard, Interestingly, in maternal separation, one of the most commonly used models of early-life stress, Ploj and colleagues reported altered expression of the endogenous opioids dynorphin and enkephalin in the hypothalamus, substantia nigra, amygdala, and periaqueductal gray key brain areas in the modulation of emotional and nociceptive processes [48]. Moreover, Alexander and colleagues reported that stress potentiates nerve injury-induced tactile allodynia through a mechanism involving glucocorticoids acting at glucocorticoid receptors and glutamate receptor-mediated extracellular signal-regulated kinase (ERK) activation in dorsal horn neurons suggesting that these pathways converge to cause central sensitization [42]. Epigenetic alterations may also represent one of the key mechanisms underlying the development of chronic pain in later life [43, 47, 49-51].

Recently, several data supported a relationship between early life stressful events and increased oxidative stress in the central nervous system (CNS) suggesting a crucial role in the etiopathogenesis of psychiatric disorders such as anxiety, depression, drug abuse or psychosis [52, 53] and also chronic pain [54-57]. Interestingly, some reports have shown that impaired mitochondrial energy production reduced MOR but not DOR or KOR function in neuronal SK-N-SH cells [58, 59]. Moreover, DOR agonists may exert neuroprotective effects on cells [60] and rat brain [61] attenuating intracellular oxidative stress. In particular, Wallace and colleagues demonstrated that δ agonists can act in human SK-N-SH cells in part through a receptor-mediated mechanism [60], whereas Yang and colleagues reported that DOR activation attenuates oxidative injury in the ischemic brain by enhancing the activity of antioxidant enzymes such as superoxide dismutase and glutathione peroxidase and reduces free radicals, malondialdehyde and nitric oxide (NO) [61]. More recently, Chao and colleagues, reported that DOR activation may exert neuroprotective effects against hypoxic/ischemic Na^+ influx through Na^+ channels *via* a protein kinase C (PKC)-dependent pathway in the cortex [62]. Xe and colleagues also suggested that DOR signaling could act at multiple levels to confer neuronal tolerance to harmful insult [63].

PAIN: PHARMACOLOGY AND CLINIC USE OF OPIOID DRUGS

The control of pain is the most used therapeutic action of opioids. Opioids are commonly prescribed because they are effective in relieving many types of pain. At the moment, opioids represent the most effective treatment for chronic cancer pain conditions [64]. Moreover, in these years, despite limited strong scientific evidences, use of opioids for chronic non-cancer pain has increased remarkably [8, 65]. However, the use of opioids in pain management requires careful dose escalation and empirical adjustments based on

clinical response and the presence of side effects or adverse drug reactions. The forefather of opioid analgesics, that still remains the most used drug in the management of chronic pain conditions, is morphine. Morphine is extracted from opium obtained through *Papaver somniferum* because it accounts for 10% of the alkaloids contained in this latex. The first firm reference to opium employment is traceable in Teofrasto's writings dating back to the third century b.C. [66]. The pioneer study of Snyder and his colleagues led in the 1970s to identify high affinity binding sites for opioids in intestine and brain [4]. Opioid receptors belong to the large superfamily of seven transmembrane spanning G protein-coupled receptors and are classified as μ (μ_1 , μ_2 , μ_3), δ (δ_1 , δ_2), κ (κ_1 , κ_2 , κ_3) and ORL1 [67]. These receptors have been cloned and their cDNAs described in the years from 1992 to 1994 demonstrating that their corresponding mRNAs present more than 60%-homology [68]. Opioid receptors activation inhibits adenylate cyclase (AC)-cyclic adenosine 3',5'-monophosphate (cAMP) – protein kinase-A (PKA) signal transduction pathway thus modulating a wide series of effectors up to mitogen-activated protein kinase (MAPK) family [69, 70]. For a long time it has been thought that opioid receptors could be coupled only to PTX-sensitive Gi/o proteins but, after several studies, it was demonstrated that all of these receptors can transduce their signal even through the PTX-insensitive subunits G α_z , G14 and G16 which also stimulate G protein-coupled inwardly rectifying K $^+$ channel (GIRK) and inhibit AC [71, 72]. Inhibition of the signal transduction of the pathway AC-cAMP-PKA by opioid receptors activation leads to reduced neuronal excitability and consequently nociceptive stimuli transmission. It was demonstrated that opioid receptors were particularly expressed in pain-modulating descending pathways, which include the medulla, *locus coeruleus*, medial thalamus and periaqueductal gray area. They were also expressed in limbic, midbrain, cortical structures and in the spinal cord *substantia gelatinosa* [73]. Pain stimuli are perceived by nociceptors and are inserted at level of the dorsal horn of spinal cord [74]. At this point opioid drugs come into action because the cells of the *substantia gelatinosa* are inhibitory interneurons rich of opioid receptors that are activated by the antinociceptive descending system and regulate painful stimuli transmission from primary afferents to spino-thalamic neurons. Characterization of the properties of opioid receptors sharpened the interest for identifying endogenous opioid-like neurotransmitters. In 1975 Hughes and Kosterlitz isolated two pentapeptides endowed with high affinity for opioid receptors, *i.e.* Met-enkephalin and Leu-enkephalin [5]. Additional opioid peptides were successively isolated and classified as enkephalins, endorphins, dynorphins and endomorphins according to their structure [73]. Several other non-mammalian opioid peptides, which show affinity to opioid receptors, have been discovered to date. These include opioid peptides derived from amphibian skin [75], opioid peptides derived from plant proteins [76] and opioid receptor ligands derived from food proteins [77]. Today, opioids can be classified in different groups comprehending morphine analogues, thebaine analogues, phenylpiperidines, methadone analogues and benzomorphanes [78]. In the class of morphine analogues we can recognize heroin, codeine, nalorphine, naloxone, naltrexone *etc.* The baine analogues,

like buprenorphine, are synthetic derivatives of which the chemical structure is unrelated to morphine. Among phenylpiperidines we can find fentanyl and the methadone analogues (*e.g.* dextropropoxyphene). The main representatives of the class of benzomorphanes are pentazocine and cyclazocine. For what concerns the pharmacodynamic of opioids, they are distinguished in agonists (morphine, codeine, meperidine, methadone, tramadol, tapentadol, fentanyl, oxycodone), partial agonists (buprenorphine), mixed agonist-antagonists (pentazocine) and antagonists (naloxone, naltrexone). For the clinical use the most employed drugs are tramadol, codeine and oxycodone (often in combination therapy with paracetamol), that are classified as mild opioids, and morphine and fentanyl categorized as strong opioids. Opioids are strong or mild according to the pain conditions in which they are used [79, 80]. Tramadol is a synthetic analogue of codeine very useful both in the treatment of nociceptive chronic pain and in neuropathic pain syndromes [81], in which it represents a second line therapy when gabapentin, pregabalin or tricyclic antidepressants seem not to work anymore. It is very interesting to know that this drug is sold in the shape of racemic mixture since this is more effective than the single enantiomers. It is well known that in this mixture (+) enantiomer binds μ receptor and inhibits serotonin reuptake, while (-) enantiomer inhibits noradrenaline uptake and stimulates α_2 -adrenergic receptors [82]. Tramadol has a better potency ratio relative to morphine in neuropathic pain than in nociceptive pain models suggesting that this increase in potency of tramadol is likely due to its monoaminergic mechanism [83]. Tapentadol is a novel MOR agonist whose activity is several-fold greater than tramadol, with prominent norepinephrine reuptake inhibition (NRI) and minimal serotonin effect [84]. Tapentadol showed antinociceptive and antihyperalgesic activity in various models of acute and chronic inflammatory pain, and both MOR agonism and NRI were found to contribute to these effects [85]. In addition, tapentadol has the benefit of greater gastrointestinal tolerability compared to classical strong opioids. Codeine, a mild μ opioid agonist, has gained much popularity as a single agent or in combination with a non-opioid agent, such as paracetamol, for the treatment of mild to moderate pain. Codeine has a very low affinity for opioid receptors and its analgesic effect is dependent on its conversion to morphine through the cytochrome P-450 enzyme 2D6, enzyme highly polymorphic (see below) and responsible of variability in inter-individual response to this opioid [86]. Oxycodone is a semisynthetic opioid analgesic derived from thebaine that acts at MOR and KOR. Oxycodone has a high oral bioavailability and produces more predictable plasma concentrations than morphine [87]. The clinical efficacy of oxycodone is similar to that of morphine and it, alone and in combination with paracetamol, is a useful opioid analgesic in acute postoperative pain, cancer pain, visceral pain and chronic nonmalignant pain [88]. Oxycodone combined with a μ receptor antagonist may improve pain control, reduce physical tolerance and withdrawal, minimizing opioid-related bowel dysfunction and act as an abuse deterrent [89]. Morphine and fentanyl have strong agonist activity for μ receptors and they bind more selectively these opioid receptors compared to the others. Morphine is commonly used as a reference for all other opioids. Its main

indications of use are for postoperative and chronic malignant pain, however, it is also used for other severe pain conditions (e.g. colic pain, angina pectoris) [90]. Fentanyl is a potent synthetic μ -opioid receptor agonist with a rapid onset and short duration of action [91]. This compound is 75-125 times more active than morphine [92] and is extensively used for anesthesia and analgesia in intensive care units in combination with propofol and midazolam [93]. At present, fentanyl is the only rapid-onset analgesic that is suitable for the treatment of breakthrough pain [91]. The pure agonists have no apparent ceiling effect for analgesia, however, meperidine is associated with excitatory side effects with a risk of seizures and it is not recommended for the treatment of chronic pain [81]. Partial agonists with mixed agonist-antagonist action are generally not indicated for the treatment of chronic pain [94], however, in 2011 the Food and Drug Administration has approved a transdermal formulation of buprenorphine for treatment of moderate to severe chronic pain [86]. Interestingly, buprenorphine may also act as a potent local anesthetic and blocks voltage-gated sodium channels *via* the local anesthetic binding site [95] and this property is likely to be relevant when buprenorphine is used for pain treatment and for local anesthesia. Ideally, the greatest analgesic activity would be obtained by a drug able to activate μ receptors and to inhibit k receptors. Activation of μ receptors present on GABA-ergic interneurons in the nucleus of the *raphe magnus* reduces GABA release, removing the inhibition of the primary neurons that give origin to the descending pathway inhibiting painful stimuli transmission at spinal level. On the contrary, k receptors localized on primary neurons of the nucleus of the *raphe magnus* cause hyperpolarization and consequent blockade of the inhibitory descending pathway. Opioid receptors may interact with each other to form heteromeric complexes and these interactions affect morphine signaling [96, 97]. Since chronic morphine administration leads to an enhanced level of these heteromers, these opioid receptor heteromeric complexes represent novel therapeutic targets for the treatment of pain and opioid addiction [98]. At the cellular level, opioid receptors are inhibitory and prevent the presynaptic release of a number of neurotransmitters. Of particular interest were the observations that opioids inhibited the release of glutamate, calcitonin gene related protein (CGRP), and substance P in view of their established roles in pain circuitry and nociceptive transmission [99]. Glutamate has a unique place in nociception since activation of N-methyl-aspartate (NMDA) receptors has been associated with centrally mediated chronic neuropathic pain and hyperalgesia and 'wind up', which is induced by sustained depolarization of wide dynamic range (WDR) neurons found in deeper layers of the dorsal horn [100]. Substance P is known to contribute to chronic inflammatory pain and participate in central sensitization and associated hyperalgesia [101-103]. CGRP is released from primary afferents and facilitates the activity of substance P within the dorsal horn [100]. Recently, in *in vivo* experiments, Endres-Becker and colleagues [104] found that locally applied morphine reduced capsaicin-induced thermal allodynia, suggesting that MOR activation can also inhibit the activity of the transient receptor potential vanilloid type 1 (TRPV1) *via* G(i/o) proteins and the cAMP pathway. Opioids show a wealth of side effects, among

which one of the most dangerous is respiratory depression due to a reduction of sensitivity of the brainstem respiratory centers to CO₂ tension. Moreover, these drugs depress pontine and bulbar centers involved in the modulation of the respiratory rhythm [105]. Other side effects are constipation, vomiting, myosis, cough reflex suppression and modulation of the immune system. In particular, opioids have the capability to modulate immune system both through direct effects on immune cells and *via* indirect effects mediated by central neuronal mechanisms [106]. However, it has been suggested that not all the opioids affect immune function in the same way [107] in particular, morphine and tramadol at analgesic doses induce different effects on immune system [108]. A repeated or prolonged use of opioids causes adaptive modifications that lead to tolerance, craving and addiction [109]. These adaptive modifications range from the receptors modulation and uncoupling with G protein to the hyperactivation of the cAMP-pathway, and so of the AC, with consequent increase of the proteins CREB (cAMP response element-binding protein) and fos. Hyperactivation of AC is encountered in tolerance and addiction [81]. One of the future challenges in this field is to obtain non-addictive opioids. To pursue this purpose, Mizoguchi and colleagues [110] synthesized compounds like amidino-TAPA. This drug probably exerts its pharmacologic action *via* the release of endogenous k opioid peptides and appears to be non-addictive and more effective on neuropathic pain [111].

OPIOIDS RESPONSIVENESS IN NEUROPATHIC PAIN

Neuropathic pain is a clinical manifestation characterized by the presence of allodynia and hyperalgesia, and it is difficult to treat with the most potent analgesic compounds [112]. Since the fundamental pathophysiologic mechanisms of neuropathic pain remain unclear, the exact mechanisms which may account for the weak efficacy of opioids in certain neuropathic pain states remain elusive [80, 113]. It has been suggested that this reduced opioid responsiveness may be related to inter-individual variability (see below) but also to multiple factors including desensitization of opioid receptors [114], functional changes in glutamate receptors [115] and transporters [116] and uncoupling of G-protein from opioid receptors [117]. β -arrestin has been also demonstrated as playing an important role in regulating opioid receptors [118, 119]. It has been suggested that reduced opioid responsiveness may be related to the lack of supraspinal/spinal synergy that is normally associated with morphine efficacy in conditions of acute pain determining a disturbance of normal opioid mechanisms/signaling in the spinal cord [120, 121]. In fact, the analgesic efficacy of opioids is significantly reduced from an intrathecal opioid injection compared with an intraperitoneal opioid injection for neuropathic pain states [122, 123]. Particularly, the failure of intrathecal opioids to produce antiallodynic effects may be due, in part, to the lack of available functional spinal opioid μ -receptors which may occur following nerve injury. A reorganization of MORs in the dorsal horn spinal cord follow peripheral axotomy and the reduced effectiveness of opioids may be related to a crucial functional change involving downregulation or desensitization of μ -opioid receptors. Functional downregulation and/or desensitization of these

receptors in the dorsal horn of the spinal cord and particularly in *laminae* I and II has been observed in nerve-injury neuropathy [121, 124] and diabetic neuropathy [125, 126]. The reduced analgesic effect of intrathecal morphine in diabetes is probably due to impairment of μ -opioid receptor-G protein coupling rather than reduction in μ -opioid receptor number in the spinal cord dorsal horn and may be related to increased production of PKC [127, 128]. Neuroadaptation of MOR in the brain may also contribute to the reduced efficacy of opioids in neuropathic pain [129]. A reducing μ -opioid receptor-mediated G-protein activity has been demonstrated in a model of neuropathic pain in the thalamic region of mice [130] and impairment of G transducer proteins $Gi2\alpha$, $Gi3\alpha$, and $G\alpha$ function led to weaker analgesic responses to various opioids (e.g., methadone, buprenorphine) [131]. Opioid receptor heterodimerization may be an additional contributing factor to clinical variability of opioids. In fact, opioid receptor dimerization can alter opioid receptor selectivity and trafficking [132]. Heterodimers may have different opioid binding profiles compared with monomers, as shown by the association of DORs-1 and KORs-1 [132, 133] to form a receptor consistent with the KORs-2 first proposed from binding assays [134]. Perhaps the most prominent change in ligand selectivity within the opioid field is the dimerization of MORs and the orphanin FQ receptor, ORL-1 [135]. OFQ/N binds to its own receptor with very high affinity and is insensitive to traditional opioids. Coexpression of opioid receptors has been shown to alter opioid ligand properties and affect receptor signaling in cell culture model systems [97, 132, 136-138] and these differences are hypothesized to occur as a consequence of receptor heteromerization.

Sustained agonist activation of MOR initiates rapid regulatory events, including receptor desensitization and trafficking, that are thought to contribute to the behavioral opioid tolerance that develops during prolonged opioid administration [139]. β -arrestins, including β -arrestin 1 and β -arrestin 2, are predominantly expressed in neuronal tissues and regulate G-protein-coupled receptor coupling and signaling [140]. In β -arrestin 2 knockout mice, the tolerance to the antinociceptive effects was significantly attenuated in the tail-flick test [119]. The capacity of opioids to alleviate inflammatory pain is also negatively regulated by the glutamate-binding NMDA receptor (R) [141]. μ -opioid receptors and NMDAR NR1 subunits are associated in the postsynaptic structures of PAG neurons and MOR desensitization secondary to neuropathic pain appears to involve PKA. Therefore, PKA may be responsible for the dissociation of NR1 subunits from MORs, which occurs as a result of NMDAR activation leading to MOR Ser phosphorylation and uncoupling from G-proteins [141]. NMDA receptor and PKC translocation are importantly involved in neuropathic pain and morphine tolerance [142]. In fact, the development of the hyperalgesia and allodynia in neuropathic pain states is suppressed by administration of NMDAR antagonists or PKC inhibitors [110, 143, 144]. The development of morphine analgesic tolerance by increased NMDA receptor activity seems to occur *via* neural nitric oxide synthase (nNOS) [145]. On the other hand, several studies have shown that NO mediates numerous neuropathic pain symptoms [146] and modulates the peripheral

antinociceptive effects induced by certain drugs during inflammatory pain, including opioids [147-149]. NO also regulates the transcription of μ - and κ -opioid receptor genes under basal and inflammatory conditions [150, 151]. In the brain, morphine increases the production of NO *via* the PI3K/Akt/nNOS pathway [152]. Subsequently, NO enhances NMDAR/calmodulin-dependent protein kinase II (CaMKII) cascade, promotes MOR phosphorylation and its uncoupling from regulated G-proteins [141, 145] diminishing the strength of morphine-activated μ -opioid receptor signaling. An increase in dynorphin A has also been suggested to be involved in the diminished opioid responsiveness that may be seen in neuropathic pain states [153]. Despite dynorphin A is an endogenous opioid with activity at κ -opioid receptors [154], many of its effects are blocked by MK-801 but not naloxone, implicating direct or indirect interaction with NMDAR [155]. Neuropathic pain may also inhibit endogenous analgesia in PAG through an increase in presynaptic GABA release [156].

The evidence of increased rates of opioid tolerance development in neuropathic pain states has been examined and found to involve an opioid-induced increase in central immune signaling [157-160]. Opioid exposure induces profound short- and long-term modulations of central immune signaling and recently, it has been suggested that the activation of glial cells, including astrocytes and microglia, at the level of the spinal cord plays an important role in the development of opioid tolerance [160-163]. The opposition of opioid analgesia by acute central immune signaling seems started, at least in part, by an opioid-induced toll-like receptor 4 (TLR4) response. TLR4 knockout mice exhibit a three-fold leftward shift in the systemic dose of morphine necessary for analgesia when compared with wild-type mice [164]. The hypothesis of opioid-induced TLR4 signaling is further supported by the potentiation of acute morphine analgesia after blockade of TLR4 activity [165, 166]. However, recent findings suggest that microglial activation in the development of morphine tolerance is not mediated by TLR4 [167]. The activation of microglia and astrocytes by repeated morphine administration also increased TNF α , IL-1 β and IL-6 expression in the spinal cord [168, 169]. Particularly, IL-1 β (by intrathecal administration) produces mechanical and thermal hyperalgesia [170, 171] and has been shown to oppose opioid-induced analgesia [172], decreasing morphine efficacy and contributing to the development of morphine tolerance.

Pharmacogenetic of Opioids

The individual variability of opioid pharmacology suggests that the patients' genetic disposition influences the response to opioids. Several studies suggest a genetic variability between individuals and in their ability to metabolize and respond to drugs [113]. Some drug-metabolizing enzymes and transporters (including cytochrome P450 [CYP], uridine 5'-diphosphate [UDP]-glucuronosyltransferases [UGT], and adenosine triphosphate (ATP)-binding cassette [ABC] transporters) may play a significant role in opioid metabolism and affect inter-individual differences in opioid concentrations in the human body and brain. For example, codeine is converted in morphine through a particular isoform of the

cytochrome P450, the CYP2D6 that is involved in the metabolism of several drugs. A well characterized genetic polymorphism of CYP2D6, that affects at least 10% of caucasian population, leads to the incapability to carry out this conversion and so makes codeine ineffective [173]. Chinese population is also less sensitive to codeine. Moreover, in this population even morphine is less effective, likely because of a decreased production of morphine-6-glucuronide [174]. On the other end of the spectrum, those with gene variants resulting in extra copies of CYP2D6 may metabolize codeine to morphine more rapidly and completely than others [175]. Tramadol undergoes metabolism by CYP2D6 to an active metabolite (*O*-desmethyl tramadol), which has greater affinity for the μ -opioid receptor than the parent compound [176]. The modulation of CYP2D6 also affects oxycodone pharmacodynamics [177]. In addition to CYP2D6, CYP2B6, 2C19, 3A4, and 3A5 isoforms are involved in opioids metabolism.

The CYP2B6 gene is highly polymorphic, with at least 50 allelic variants identified [178] and its polymorphism influence the plasma concentration and clearance of the methadone S-enantiomer [179]. CYP3A4 polymorphism is related to the pharmacokinetics of fentanyl and patients with CYP3A4*1G variant A allele have a lower metabolic rate of drug [180]. In Japanese patients with CYP3A5*3 polymorphism the plasma disposition of noroxycodone is altered [181]. In addition, multiple single nucleotide polymorphisms in the promoter region of uridine diphosphate glucuronosyl transferase 2B7 (UGT2B7), the predominant enzyme that catalyzes morphine glucuronidation, have been reported [182]. Presence of the UGT2B7-840G allele is associated with significantly reduced glucuronidation of morphine and thus contributes to the variability in hepatic clearance of morphine in sickle cell disease [183]. The efficacy of opioids in humans may be affected by allelic variants in the genes of transporters, structural proteins that can influence the absorption, distribution, and elimination of opioids [184]. The most characterized of the ATP binding cassette (ABC) superfamily of efflux transporters is *ABCB1* encoding P-glycoprotein. Opioid induced analgesia is increased and prolonged in mice lacking P-glycoprotein [185]. P-glycoprotein can limit the concentration of pain management drugs, such as morphine, in the brain because it actively pumps drugs out of the CNS. Also methadone, loperamide, and fentanyl have all been confirmed as P-glycoprotein substrates [186-188]. *ABCB1* gene is highly polymorphic. The most investigated *ABCB1* genetic polymorphism is the non-synonymous exon 26 SNP, C3435T, which is observed with a frequency of 50-60% in Caucasians, 40-50% in Asians, and 10-30% in Africans [189, 190]. Genetic variation in the multidrug-resistance gene MDR-1 (which encodes for P-glycoprotein), may account for the genetic variability in P-glycoprotein activity [191]. However, about opioids there are not the only genetic variations of the metabolic system to take into account. For example, A118G single nucleotide polymorphism (SNP) in exon 1 of the μ -opioid receptor gene (OPRM1) has been linked to the variability of the analgesic effect of morphine. Individuals with G118 polymorphism have a reduced or variable response to morphine and increased opioid dose requirements during

opioid therapy [192]. The SNPs interesting OPRM1 underlie the expression of μ -opioid receptors variants in humans. In particular, A118G SNP causes an asparagine to an aspartate substitution in the extracellular domain of the μ -opioid receptor. This allele has a frequency from 4% to 48% according to the population [193]. Recent studies suggest that this amino acid substitution causes a different capability of the receptor to inhibit native $\text{Ca}_v2.2$ calcium currents with a consequent difference in pain perception. It seems that patients endowed with the mutated μ -opioid receptor containing the aspartate show higher sensitivity to the analgesic action due to this receptor activation [194]. A118G SNP has been associated with elevated pain responses and decreased pain threshold in a variety of populations and it seems that A118G genotypes may influence migraine-associated head pain in females [195]. It has also been shown that this polymorphism A118G could be a clinical marker of the outcome of the progression of pain intensity and disability in patients affected by sciatic pain after lumbar disc herniation, since it seems to increase pain stimuli sensitivity in female patients and to protect male patients in the first year following to herniation [196].

In human studies, low catechol-O-methyltransferase (COMT) activity has been associated with increased sensitivity to acute clinical preoperative or postoperative pain [197]. As a result, genetic variability in the COMT gene can contribute to differences in pain sensitivity and response to analgesics. Low COMT activity also increases opioid receptors and enhances opioid analgesia and adverse effects in some cancer [198, 199]. Environmental and/or genetic influences that alter central immune signaling may also contribute to altered acute opioid analgesia. For example, single-nucleotide polymorphisms in the genes encoding IL-6 [200] or IL-1ra [201], which are associated with increased proinflammation, lead to increased opioid requirements after surgery, suggesting a possibly reduced opioid analgesic efficacy combined with or separate from increased pain.

CONCLUSION

Actually, some of the most powerful analgesics belong to the opioid drugs family which is, thus, object of intense study. Opioid receptors field is remarkable among the other fields in pharmacology because of the fact that the earliest findings, made without the aid of the modern molecular biology tools, still remain irrefutable, both about receptors and about endogenous opioid peptides, and the opioid binding sites identified in the 1973 are responsible for the main pharmacological actions of the most clinically used opioids [68]. It remains to clarify the mechanisms of addiction in order to develop non-addictive opioids and to dissect more and more the pharmacogenetic of the opioid system to obtain always the best clinical outcome with opioids therapy. In this way, through translational pharmacology, we would be able to use better the opioid drugs already available and to produce new drugs more effective in pain control and less addictive. The achievement of opioid drugs really active even in neuropathic pain syndromes is a very interesting topic. Indeed, neuropathic pain control is a so debated question that in recent years great effort has been put in understanding the mechanisms of spinal cord synaptic

plasticity which may contribute to neuropathic pain [202]. In fact, it is now clear that pain shares a lot of similarities with other neurobiological processes such as learning and memory [203] and the participation of cellular and molecular mechanisms typical of conditions in which these processes are altered, *i.e.* in neurodegenerative diseases, seems to play an important role in the development and maintenance of pain states. In this regard, autophagy, a major intracellular degradation pathway lately implicated in several pathological conditions and brain diseases [204], represents a novel pathway regulating neuroinflammation and neuropathic pain [205, 206] thus offering a new target for the development of more effective treatments and that could help us understand the different sensitivity to opioids in some pain states.

CONFLICT OF INTEREST

The authors confirm that this article content has no conflict of interest.

ACKNOWLEDGEMENTS

Declared none.

REFERENCES

- [1] Gupta, S.; Gupta, M.; Nath, S.; Hess, G.M. Survey of European pain medicine practice. *Pain Physician*, **2012**, *15*(6), E983-E994. [PMID: 23159983]
- [2] Cherubino, P.; Sarzi-Puttini, P.; Zuccaro, S.M.; Labianca, R. The management of chronic pain in important patient subgroups. *Clin. Drug Investig.*, **2012**, *32*(Suppl. 1), 35-44. [http://dx.doi.org/10.2165/11630060-000000000-00000]
- [3] Pasternak, G.W. Molecular insights into mu opioid pharmacology: From the clinic to the bench. *Clin. J. Pain*, **2010**, *26*(Suppl. 10), S3-S9. [http://dx.doi.org/10.1097/AJP.0b013e3181c49d2e] [PMID: 20026962]
- [4] Pert, C.B.; Snyder, S.H. Opiate receptor: demonstration in nervous tissue. *Science*, **1973**, *179*(4077), 1011-1014. [http://dx.doi.org/10.1126/science.179.4077.1011] [PMID: 4687585]
- [5] Hughes, J.; Smith, T.W.; Kostertitz, H.W.; Fothergill, L.A.; Morgan, B.A.; Morris, H.R. Identification of two related pentapeptides from the brain with potent opiate agonist activity. *Nature*, **1975**, *258*(5536), 577-580. [http://dx.doi.org/10.1038/258577a0] [PMID: 1207728]
- [6] Snyder, S.H. Opiate receptors and beyond: 30 years of neural signaling research. *Neuropharmacology*, **2004**, *47*(Suppl. 1), 274-285. [http://dx.doi.org/10.1016/j.neuropharm.2004.06.006] [PMID: 15464143]
- [7] Reinecke, H.; Sorgatz, H. S3 guideline LONTS. Long-term administration of opioids for non-tumor pain. *Schmerz*, **2009**, *23*(5), 440-447. [http://dx.doi.org/10.1007/s00482-009-0839-9] [PMID: 19730894]
- [8] Kissin, I. Long-term opioid treatment of chronic nonmalignant pain: unproven efficacy and neglected safety? *J. Pain Res.*, **2013**, *6*, 513-529. [http://dx.doi.org/10.2147/JPR.S47182] [PMID: 23874119]
- [9] Furlan, A.D.; Sandoval, J.A.; Mailis-Gagnon, A.; Tunks, E. Opioids for chronic noncancer pain: a meta-analysis of effectiveness and side effects. *CMAJ*, **2006**, *174*(11), 1589-1594. [http://dx.doi.org/10.1503/cmaj.051528] [PMID: 16717269]
- [10] Nicholson, B. Responsible prescribing of opioids for the management of chronic pain. *Drugs*, **2003**, *63*(1), 17-32. [http://dx.doi.org/10.2165/00003495-200363010-00002] [PMID: 12487620]
- [11] Vellucci, R. Heterogeneity of chronic pain. *Clin. Drug Investig.*, **2012**, *32*(Suppl. 1), 3-10. [http://dx.doi.org/10.2165/11630030-000000000-00000]
- [12] Treede, R.D.; Jensen, T.S.; Campbell, J.N.; Cruccu, G.; Dostrovsky, J.O.; Griffin, J.W.; Hansson, P.; Hughes, R.; Nurmikko, T.; Serra, J. Neuropathic pain: redefinition and a grading system for clinical and research purposes. *Neurology*, **2008**, *70*(18), 1630-1635. [http://dx.doi.org/10.1212/01.wnl.0000282763.29778.59] [PMID: 18003941]
- [13] Costigan, M.; Scholz, J.; Woolf, C.J. Neuropathic pain: a maladaptive response of the nervous system to damage. *Annu. Rev. Neurosci.*, **2009**, *32*, 1-32. [http://dx.doi.org/10.1146/annurev.neuro.051508.135531] [PMID: 19400724]
- [14] Trescot, A.M.; Helm, S.; Hansen, H.; Benyamin, R.; Glaser, S.E.; Adlaka, R.; Patel, S.; Manchikanti, L. Opioids in the management of chronic non-cancer pain: an update of American Society of the Interventional Pain Physicians (ASIPP) Guidelines. *Pain Physician*, **2008**, *11*(2)(Suppl.), S5-S62. [PMID: 18443640]
- [15] Egli, M.; Koob, G.F.; Edwards, S. Alcohol dependence as a chronic pain disorder. *Neurosci. Biobehav. Rev.*, **2012**, *36*(10), 2179-2192. [http://dx.doi.org/10.1016/j.neubiorev.2012.07.010] [PMID: 22975446]
- [16] Lebovits, A.H.; Lefkowitz, M.; McCarthy, D.; Simon, R.; Wilpon, H.; Jung, R.; Fried, E. The prevalence and management of pain in patients with AIDS: a review of 134 cases. *Clin. J. Pain*, **1989**, *5*(3), 245-248. [http://dx.doi.org/10.1097/00002508-198909000-00009] [PMID: 2520410]
- [17] Liu, B.; Liu, X.; Tang, S.J. Interactions of Opioids and HIV Infection in the Pathogenesis of Chronic Pain. *Front. Microbiol.*, **2016**, *7*, 103. [http://dx.doi.org/10.3389/fmicb.2016.00103] [PMID: 26903982]
- [18] Svendsen, K.B.; Jensen, T.S.; Overvad, K.; Hansen, H.J.; Koch-Henriksen, N.; Bach, F.W. Pain in patients with multiple sclerosis: a population-based study. *Arch. Neurol.*, **2003**, *60*(8), 1089-1094. [http://dx.doi.org/10.1001/archneur.60.8.1089] [PMID: 12925364]
- [19] Potter, L.E.; Paylor, J.W.; Suh, J.S.; Tenorio, G.; Caliaipernumal, J.; Colbourne, F.; Baker, G.; Winship, I.; Kerr, B.J. Altered excitatory-inhibitory balance within somatosensory cortex is associated with enhanced plasticity and pain sensitivity in a mouse model of multiple sclerosis. *J. Neuroinflammation*, **2016**, *13*(1), 142. [http://dx.doi.org/10.1186/s12974-016-0609-4] [PMID: 27282914]
- [20] Arner, S.; Meyerson, B.A. Lack of analgesic effect of opioids on neuropathic and idiopathic forms of pain. *Pain*, **1988**, *33*(1), 11-23. [http://dx.doi.org/10.1016/0304-3959(88)90198-4] [PMID: 2454440]
- [21] Courteix, C.; Bardin, M.; Chantelauze, C.; Lavarenne, J.; Eschaliere, A. Study of the sensitivity of the diabetes-induced pain model in rats to a range of analgesics. *Pain*, **1994**, *57*(2), 153-160. [http://dx.doi.org/10.1016/0304-3959(94)90218-6] [PMID: 8090511]
- [22] Field, M.J.; McCleary, S.; Hughes, J.; Singh, L. Gabapentin and pregabalin, but not morphine and amitriptyline, block both static and dynamic components of mechanical allodynia induced by streptozotocin in the rat. *Pain*, **1999**, *80*(1-2), 391-398. [http://dx.doi.org/10.1016/S0304-3959(98)00239-5] [PMID: 10204753]
- [23] Kamei, J.; Ohhashi, Y.; Aoki, T.; Kawasima, N.; Kasuya, Y. Streptozotocin-induced diabetes selectively alters the potency of analgesia produced by mu-opioid agonists, but not by delta- and kappa-opioid agonists. *Brain Res.*, **1992**, *571*(2), 199-203. [http://dx.doi.org/10.1016/0006-8993(92)90655-S] [PMID: 1319265]
- [24] Zurek, J.R.; Nadeson, R.; Goodchild, C.S. Spinal and supraspinal components of opioid antinociception in streptozotocin induced diabetic neuropathy in rats. *Pain*, **2001**, *90*(1-2), 57-63. [http://dx.doi.org/10.1016/S0304-3959(00)00386-9] [PMID: 11166970]
- [25] Chen, S.R.; Pan, H.L. Hypersensitivity of spinothalamic tract neurons associated with diabetic neuropathic pain in rats. *J. Neurophysiol.*, **2002**, *87*(6), 2726-2733. [PMID: 12037174]
- [26] Zhang, X.; Bao, L.; Shi, T.J.; Ju, G.; Elde, R.; Hökfelt, T. Down-regulation of mu-opioid receptors in rat and monkey dorsal root ganglion neurons and spinal cord after peripheral axotomy. *Neuroscience*, **1998**, *82*(1), 223-240. [http://dx.doi.org/10.1016/S0306-4522(97)00240-6] [PMID: 9483516]
- [27] Porreca, F.; Tang, Q.B.; Bian, D.; Riedl, M.; Elde, R.; Lai, J. Spinal opioid mu receptor expression in lumbar spinal cord of rats following nerve injury. *Brain Res.*, **1998**, *795*(1-2), 197-203. [http://dx.doi.org/10.1016/S0006-8993(98)00292-3] [PMID: 9622629]
- [28] Chen, S.R.; Pan, H.L. Antinociceptive effect of morphine, but not mu opioid receptor number, is attenuated in the spinal cord of diabetic rats. *Anesthesiology*, **2003**, *99*(6), 1409-1414. [http://dx.doi.org/10.1097/0000542-200312000-00026] [PMID: 14639157]
- [29] Kohno, T.; Ji, R.R.; Ito, N.; Allchorne, A.J.; Befort, K.; Karchewski, L.A.; Woolf, C.J. Peripheral axonal injury results in reduced mu opioid receptor pre- and post-synaptic action in the

- spinal cord. *Pain*, **2005**, 117(1-2), 77-87. [http://dx.doi.org/10.1016/j.pain.2005.05.035] [PMID: 16098668]
- [30] Kamei, J.; Kasuya, Y. The effects of diabetes on opioid-induced antinociception. In: *Pharmacology of Opioid Peptides*; Tseong, L.F., Ed.; Harwood Academic Publishers, **1995**; pp. 271-286.
- [31] Kamei, J.; Kawashima, N.; Narita, M.; Suzuki, T.; Misawa, M.; Kasuya, Y. Reduction in ATP-sensitive potassium channel-mediated antinociception in diabetic mice. *Psychopharmacology (Berl.)*, **1994**, 113(3-4), 318-321. [http://dx.doi.org/10.1007/BF02245203] [PMID: 7862839]
- [32] van Rijn, R.M.; Brissett, D.I.; Whistler, J.L. Emergence of functional spinal delta opioid receptors after chronic ethanol exposure. *Biol. Psychiatry*, **2012**, 71(3), 232-238. [http://dx.doi.org/10.1016/j.biopsych.2011.07.015] [PMID: 21889123]
- [33] Hull, L.C.; Gabra, B.H.; Bailey, C.P.; Henderson, G.; Dewey, W.L. Reversal of morphine analgesic tolerance by ethanol in the mouse. *J. Pharmacol. Exp. Ther.*, **2013**, 345(3), 512-519. [http://dx.doi.org/10.1124/jpet.112.202184] [PMID: 23528610]
- [34] Cadet, P.; Weeks, B.S.; Bilfinger, T.V.; Manton, K.J.; Casares, F.; Stefano, G.B. HIV gp120 and morphine alter mu opiate receptor expression in human vascular endothelium. *Int. J. Mol. Med.*, **2001**, 8(2), 165-169. [PMID: 11445868]
- [35] Beltran, J.A.; Pallur, A.; Chang, S.L. HIV-1 gp120 up-regulation of the mu opioid receptor in TPA-differentiated HL-60 cells. *Int. Immunopharmacol.*, **2006**, 6(9), 1459-1467. [http://dx.doi.org/10.1016/j.intimp.2006.04.018] [PMID: 16846840]
- [36] Dever, S.M.; Xu, R.; Fitting, S.; Knapp, P.E.; Hauser, K.F. Differential expression and HIV-1 regulation of μ -opioid receptor splice variants across human central nervous system cell types. *J. Neurovirol.*, **2012**, 18(3), 181-190. [http://dx.doi.org/10.1007/s13365-012-0096-z] [PMID: 22528479]
- [37] Gironi, M.; Furlan, R.; Rovaris, M.; Comi, G.; Filippi, M.; Panerai, A.E.; Sacerdote, P. Beta endorphin concentrations in PBMC of patients with different clinical phenotypes of multiple sclerosis. *J. Neurol. Neurosurg. Psychiatry*, **2003**, 74(4), 495-497. [http://dx.doi.org/10.1136/jnnp.74.4.495] [PMID: 12640071]
- [38] Lynch, J.L.; Alley, J.F.; Wellman, L.; Beitz, A.J. Decreased spinal cord opioid receptor mRNA expression and antinociception in a Theiler's murine encephalomyelitis virus model of multiple sclerosis. *Brain Res.*, **2008**, 1191, 180-191. [http://dx.doi.org/10.1016/j.brainres.2007.11.034] [PMID: 18096140]
- [39] Lampe, A.; Doering, S.; Rumpold, G.; Sölder, E.; Krismer, M.; Kantner-Rumplair, W.; Schubert, C.; Söllner, W. Chronic pain syndromes and their relation to childhood abuse and stressful life events. *J. Psychosom. Res.*, **2003**, 54(4), 361-367. [http://dx.doi.org/10.1016/S0022-3999(02)00399-9] [PMID: 12670615]
- [40] Fillingim, R.B.; Edwards, R.R. Is self-reported childhood abuse history associated with pain perception among healthy young women and men? *Clin. J. Pain*, **2005**, 21(5), 387-397. [http://dx.doi.org/10.1097/01.aip.0000149801.46864.39] [PMID: 16093744]
- [41] Barreau, F.; Ferrier, L.; Fioramonti, J.; Bueno, L. New insights in the etiology and pathophysiology of irritable bowel syndrome: contribution of neonatal stress models. *Pediatr. Res.*, **2007**, 62(3), 240-245. [http://dx.doi.org/10.1203/PDR.0b013e3180db2949] [PMID: 17622962]
- [42] Alexander, J.K.; DeVries, A.C.; Kigerl, K.A.; Dahlman, J.M.; Popovich, P.G. Stress exacerbates neuropathic pain via glucocorticoid and NMDA receptor activation. *Brain Behav. Immun.*, **2009**, 23(6), 851-860. [http://dx.doi.org/10.1016/j.bbi.2009.04.001] [PMID: 19361551]
- [43] Low, L.A.; Schweinhardt, P. Early life adversity as a risk factor for fibromyalgia in later life. *Pain Res. Treat.*, **2012**, 2012, 140832. [http://dx.doi.org/10.1155/2012/140832] [PMID: 22110940]
- [44] Afari, N.; Ahumada, S.M.; Wright, L.J.; Mostoufi, S.; Golnari, G.; Reis, V.; Cuneo, J.G. Psychological trauma and functional somatic syndromes: a systematic review and meta-analysis. *Psychosom. Med.*, **2014**, 76(1), 2-11. [http://dx.doi.org/10.1097/PSY.000000000000010] [PMID: 24336429]
- [45] Danese, A.; Pariante, C.M.; Caspi, A.; Taylor, A.; Poulton, R. Childhood maltreatment predicts adult inflammation in a life-course study. *Proc. Natl. Acad. Sci. USA*, **2007**, 104(4), 1319-1324. [http://dx.doi.org/10.1073/pnas.0610362104] [PMID: 17229839]
- [46] Heim, C.; Newport, D.J.; Mletzko, T.; Miller, A.H.; Nemeroff, C.B. The link between childhood trauma and depression: insights from HPA axis studies in humans. *Psychoneuroendocrinology*, **2008**, 33(6), 693-710. [http://dx.doi.org/10.1016/j.psyneuen.2008.03.008] [PMID: 18602762]
- [47] Burke, N.N.; Finn, D.P.; McGuire, B.E.; Roche, M. Psychological stress in early life as a predisposing factor for the development of chronic pain: Clinical and preclinical evidence and neurobiological mechanisms. *J. Neurosci. Res.*, **2016**, Epub a head of print. [http://dx.doi.org/10.1002/jnr.23802] [PMID: 27402412]
- [48] Ploj, K.; Roman, E.; Nylander, I. Long-term effects of short and long periods of maternal separation on brain opioid peptide levels in male Wistar rats. *Neuropeptides*, **2003**, 37(3), 149-156. [http://dx.doi.org/10.1016/S0143-4179(03)00043-X] [PMID: 12860112]
- [49] Weaver, I.C.; Champagne, F.A.; Brown, S.E.; Dymov, S.; Sharma, S.; Meaney, M.J.; Szyf, M. Reversal of maternal programming of stress responses in adult offspring through methyl supplementation: altering epigenetic marking later in life. *J. Neurosci.*, **2005**, 25(47), 11045-11054. [http://dx.doi.org/10.1523/JNEUROSCI.3652-05.2005] [PMID: 16306417]
- [50] Tietjen, G.E.; Peterlin, B.L. Childhood abuse and migraine: epidemiology, sex differences, and potential mechanisms. *Headache*, **2011**, 51(6), 869-879. [http://dx.doi.org/10.1111/j.1526-4610.2011.01906.x] [PMID: 21631473]
- [51] Tietjen, G.E. Childhood maltreatment and headache disorders. *Curr. Pain Headache Rep.*, **2016**, 20(4), 26. [http://dx.doi.org/10.1007/s11916-016-0554-z] [PMID: 26936357]
- [52] Schiavone, S.; Colaianna, M.; Curtis, L. Impact of early life stress on the pathogenesis of mental disorders: relation to brain oxidative stress. *Curr. Pharm. Des.*, **2015**, 21(11), 1404-1412. [http://dx.doi.org/10.2174/1381612821666150105143358] [PMID: 25564385]
- [53] Mhillaj, E.; Morgese, M.G.; Trabace, L. Early life and oxidative stress in psychiatric disorders: what can we learn from animal models? *Curr. Pharm. Des.*, **2015**, 21(11), 1396-1403. [http://dx.doi.org/10.2174/1381612821666150105122422] [PMID: 25564390]
- [54] Pernambuco, A.P.; Schettino, L.P.; Carvalho, L.S.; Reis, D.A. Involvement of Oxidative Stress and Nitric Oxide in Fibromyalgia Pathophysiology: A Relationship to be Elucidated. *Fibrom. Open Access*, **2016**, 1, 105. [http://dx.doi.org/10.4172/foa.1000105]
- [55] Kolberg, C.; Horst, A.; Moraes, M.S.; Duarte, F.C.; Riffel, A.P.; Scheid, T.; Kolberg, A.; Partata, W.A. Peripheral oxidative stress blood markers in patients with chronic back or neck pain treated with high-velocity, low-amplitude manipulation. *J. Manipulative Physiol. Ther.*, **2015**, 38(2), 119-129. [http://dx.doi.org/10.1016/j.jmpt.2014.11.003] [PMID: 25487299]
- [56] Inanir, A.; Sogut, E.; Ayan, M.; Inanir, S. Evaluation of Pain Intensity and Oxidative Stress Levels in Patients with Inflammatory and Non-Inflammatory Back Pain. *Eur. J. Gen. Med. (Los Angel.)*, **2013**, 10(4), 185-190.
- [57] Meeus, M.; Nijs, J.; Hermans, L.; Goubert, D.; Calders, P. The role of mitochondrial dysfunctions due to oxidative and nitrosative stress in the chronic pain or chronic fatigue syndromes and fibromyalgia patients: peripheral and central mechanisms as therapeutic targets? *Expert Opin. Ther. Targets*, **2013**, 17(9), 1081-1089. [http://dx.doi.org/10.1517/14728222.2013.818657] [PMID: 23834645]
- [58] Raut, A.; Igilewski, M.; Ratka, A. Differential effects of impaired mitochondrial energy production on the function of mu and delta opioid receptors in neuronal SK-N-SH cells. *Neurosci. Lett.*, **2006**, 404(1-2), 242-246. [http://dx.doi.org/10.1016/j.neulet.2006.05.055] [PMID: 16808998]
- [59] Raut, A.; Rao, V.R.; Ratka, A. Changes in opioid receptor proteins during mitochondrial impairment in differentiated SK-N-SH cells. *Neurosci. Lett.*, **2007**, 422(3), 187-192. [http://dx.doi.org/10.1016/j.neulet.2007.06.015] [PMID: 17611027]
- [60] Wallace, D.R.; Dodson, S.L.; Nath, A.; Booze, R.M. Delta opioid agonists attenuate TAT(172)-induced oxidative stress in SK-N-SH cells. *Neurotoxicology*, **2006**, 27(1), 101-107. [http://dx.doi.org/10.1016/j.neuro.2005.07.008] [PMID: 16168488]
- [61] Yang, Y.; Xia, X.; Zhang, Y.; Wang, Q.; Li, L.; Luo, G.; Xia, Y. delta-Opioid receptor activation attenuates oxidative injury in the ischemic rat brain. *BMC Biol.*, **2009**, 7, 55. [http://dx.doi.org/10.1186/1741-7007-7-55] [PMID: 19709398]
- [62] Chao, D.; He, X.; Yang, Y.; Bazzi-Asaad, A.; Lazarus, L.H.; Balboni, G.; Kim, D.H.; Xia, Y. DOR activation inhibits anoxic/ischemic Na⁺ influx through Na⁺ channels via PKC mechanisms in the cortex. *Exp. Neurol.*, **2012**, 236(2), 228-239. [http://dx.doi.org/10.1016/j.expneurol.2012.05.006] [PMID: 22609332]

- [63] He, X.; Sandhu, H.K.; Yang, Y.; Hua, F.; Belser, N.; Kim, D.H.; Xia, Y. Neuroprotection against hypoxia/ischemia: δ -opioid receptor-mediated cellular/molecular events. *Cell. Mol. Life Sci.*, **2013**, *70*(13), 2291-2303. [http://dx.doi.org/10.1007/s00018-012-1167-2] [PMID: 23014992]
- [64] Prommer, E.E. Pharmacological Management of Cancer-Related Pain. *Cancer Contr.*, **2015**, *22*(4), 412-425. [PMID: 26678968]
- [65] Cheung, C.W.; Qiu, Q.; Choi, S.W.; Moore, B.; Goucke, R.; Irwin, M. Chronic opioid therapy for chronic non-cancer pain: a review and comparison of treatment guidelines. *Pain Phys.*, **2014**, *17*(5), 401-414. [PMID: 25247898]
- [66] Morrone, L.A.; Rombolà, L.; Amantea, D.; Mizoguchi, H.; Corasaniti, M.T. Contribution of Herbal Medicine to Human Health: A Brief History. In: *Herbal Medicines: Development and Validation of Plant-derived Medicines for Human Health*; , **2012**; pp. 381-411. Chapter XXI CRC Press
- [67] Waldhoer, M.; Bartlett, S.E.; Whistler, J.L. Opioid receptors. *Annu. Rev. Biochem.*, **2004**, *73*, 953-990. [http://dx.doi.org/10.1146/annurev.biochem.73.011303.073940] [PMID: 15189164]
- [68] Snyder, S.H.; Pasternak, G.W. Historical review: Opioid receptors. *Trends Pharmacol. Sci.*, **2003**, *24*(4), 198-205. [http://dx.doi.org/10.1016/S0165-6147(03)00066-X] [PMID: 12707007]
- [69] Fukuda, K.; Kato, S.; Morikawa, H.; Shoda, T.; Mori, K. Functional coupling of the delta-, mu-, and kappa-opioid receptors to mitogen-activated protein kinase and arachidonate release in Chinese hamster ovary cells. *J. Neurochem.*, **1996**, *67*(3), 1309-1316. [http://dx.doi.org/10.1046/j.1471-4159.1996.67031309.x] [PMID: 8752140]
- [70] Gutstein, H.B.; Rubie, E.A.; Mansour, A.; Akil, H.; Woodgett, J.R. Opioid effects on mitogen-activated protein kinase signaling cascades. *Anesthesiology*, **1997**, *87*(5), 1118-1126. [http://dx.doi.org/10.1097/0000542-199711000-00016] [PMID: 9366464]
- [71] Simon, M.I.; Strathmann, M.P.; Gautam, N. Diversity of G proteins in signal transduction. *Science*, **1991**, *252*(5007), 802-808. [http://dx.doi.org/10.1126/science.1902986] [PMID: 1902986]
- [72] Law, P.Y.; Wong, Y.H.; Loh, H.H. Molecular mechanisms and regulation of opioid receptor signaling. *Annu. Rev. Pharmacol. Toxicol.*, **2000**, *40*, 389-430. [http://dx.doi.org/10.1146/annurev.pharmtox.40.1.389] [PMID: 10836142]
- [73] Dhawan, B.N.; Cesselin, F.; Raghurir, R.; Reisine, T.; Bradley, P.B.; Portoghesi, P.S.; Hamon, M. International Union of Pharmacology. XII. Classification of opioid receptors. *Pharmacol. Rev.*, **1996**, *48*(4), 567-592. [PMID: 8981566]
- [74] Hudspeth, M.J.; Siddall, P.J.; Munglani, R. Physiology of pain. In: *Foundations of Anesthesia, Basic sciences for clinical practice by H; Hemmings, B.; Hopkins, P.M., Eds.; Elsevier Mosby*, **2006**; pp. 267-285.
- [75] Negri, L.; Melchiorri, P.; Lattanzi, R. Pharmacology of amphibian opiate peptides. *Peptides*, **2000**, *21*(11), 1639-1647. [http://dx.doi.org/10.1016/S0196-9781(00)00295-3] [PMID: 11090917]
- [76] Yoshikawa, M.; Takahashi, M.; Yang, S. Delta opioid peptides derived from plant proteins. *Curr. Pharm. Des.*, **2003**, *9*(16), 1325-1330. [http://dx.doi.org/10.2174/1381612033454838] [PMID: 12769740]
- [77] Teschemacher, H. Opioid receptor ligands derived from food proteins. *Curr. Pharm. Des.*, **2003**, *9*(16), 1331-1344. [http://dx.doi.org/10.2174/1381612033454856] [PMID: 12769741]
- [78] Davis, M.P.; Pasternak, G.W. Opioid receptors and opioid pharmacodynamics. In: *Opioids in Cancer Pain by M; Davis, P.; Glare, P.A.; Hardy, J.; Quigley, C., Eds.; Oxford University Press*, **2009**; pp. 1-27. [http://dx.doi.org/10.1093/med/9780199236640.003.0001]
- [79] Grond, S.; Meuser, T. Weak opioids an educational substitute for morphine? *Curr. Opin. Anaesthesiol.*, **1998**, *11*(5), 559-565. [http://dx.doi.org/10.1097/00001503-199810000-00019] [PMID: 17013274]
- [80] Marinangeli, F.; Ciccozzi, A.; Leonardi, M.; Aloisio, L.; Mazzei, A.; Paladini, A.; Porzio, G.; Marchetti, P.; Varrassi, G. Use of strong opioids in advanced cancer pain: a randomized trial. *J. Pain Symptom Manage.*, **2004**, *27*(5), 409-416. [http://dx.doi.org/10.1016/j.jpainsymman.2003.10.006] [PMID: 15120769]
- [81] Park, H.J.; Moon, D.E. Pharmacologic management of chronic pain. *Korean J. Pain*, **2010**, *23*(2), 99-108. [http://dx.doi.org/10.3344/kjp.2010.23.2.99] [PMID: 20556211]
- [82] Lewis, K.S.; Han, N.H. Tramadol: a new centrally acting analgesic. *Am. J. Health Syst. Pharm.*, **1997**, *54*(6), 643-652. [PMID: 9075493]
- [83] Christoph, T.; Kögel, B.; Strassburger, W.; Schug, S.A. Tramadol has a better potency ratio relative to morphine in neuropathic than in nociceptive pain models. *Drugs R D.*, **2007**, *8*(1), 51-57. [http://dx.doi.org/10.2165/00126839-200708010-00005] [PMID: 17249849]
- [84] Raffa, R.B.; Buschmann, H.; Christoph, T.; Eichenbaum, G.; Englberger, W.; Flores, C.M.; Hertrampf, T.; Kögel, B.; Schiene, K.; Straßburger, W.; Terlinden, R.; Tzschentke, T.M. Mechanistic and functional differentiation of tapentadol and tramadol. *Expert Opin. Pharmacother.*, **2012**, *13*(10), 1437-1449. [http://dx.doi.org/10.1517/14656566.2012.696097] [PMID: 22698264]
- [85] Schiene, K.; De Vry, J.; Tzschentke, T.M. Antinociceptive and antihyperalgesic effects of tapentadol in animal models of inflammatory pain. *J. Pharmacol. Exp. Ther.*, **2011**, *339*(2), 537-544. [http://dx.doi.org/10.1124/jpet.111.181263] [PMID: 21816956]
- [86] Williams, D.G.; Patel, A.; Howard, R.F. Pharmacogenetics of codeine metabolism in an urban population of children and its implications for analgesic reliability. *Br. J. Anaesth.*, **2002**, *89*(6), 839-845. [http://dx.doi.org/10.1093/bja/aef284] [PMID: 12453926]
- [87] Smith, H.S. Opioids and neuropathic pain. *Pain Phys.*, **2012**, *15*(3) (Suppl.), ES93-ES110. [PMID: 22786465]
- [88] Olkkola, K.T.; Hagelberg, N.M. Oxycodone: new old drug. *Curr. Opin. Anaesthesiol.*, **2009**, *22*(4), 459-462. [http://dx.doi.org/10.1097/ACO.0b013e32832bc818] [PMID: 19369865]
- [89] Davis, M.; Goforth, H.W.; Gamier, P. Oxycodone combined with opioid receptor antagonists: efficacy and safety. *Expert Opin. Drug Saf.*, **2013**, *12*(3), 389-402. [http://dx.doi.org/10.1517/14740338.2013.783564] [PMID: 23534906]
- [90] Schafer, M. Opioids in pain medicine. In: *Guide to Pain Management in Low-Resource Settings by A. Kopf and N; Patel, B., Ed.; IASP: Seattle, USA*, **2010**; pp. 39-45.
- [91] Smith, H. A comprehensive review of rapid-onset opioids for breakthrough pain. *CNS Drugs*, **2012**, *26*(6), 509-535. [http://dx.doi.org/10.2165/11630580-000000000-00000] [PMID: 22668247]
- [92] Clotz, M.A.; Nahata, M.C. Clinical uses of fentanyl, sufentanil, and alfentanil. *Clin. Pharm.*, **1991**, *10*(8), 581-593. [PMID: 1834393]
- [93] Chamorro, C.; Borrillo, J.M.; Romera, M.A.; Silva, J.A.; Balandin, B. Anesthesia and analgesia protocol during therapeutic hypothermia after cardiac arrest: a systematic review. *Anesth. Analg.*, **2010**, *110*(5), 1328-1335. [http://dx.doi.org/10.1213/ANE.0b013e3181d8cacf] [PMID: 20418296]
- [94] Lynch, M.E. The pharmacotherapy of chronic pain. *Rheum. Dis. Clin. North Am.*, **2008**, *34*(2), 369-385. [http://dx.doi.org/10.1016/j.rdc.2008.04.001] [PMID: 18638682]
- [95] Leffler, A.; Frank, G.; Kistner, K.; Niedermirtl, F.; Koppert, W.; Reeh, P.W.; Nau, C. Local anesthetic-like inhibition of voltage-gated Na⁺ channels by the partial μ -opioid receptor agonist buprenorphine. *Anesthesiology*, **2012**, *116*(6), 1335-1346. [http://dx.doi.org/10.1097/ALN.0b013e3182557917] [PMID: 22504149]
- [96] Horan, P.; Tallarida, R.J.; Haaseth, R.C.; Matsunaga, T.O.; Hruby, V.J.; Porreca, F. Antinociceptive interactions of opioid delta receptor agonists with morphine in mice: supra- and sub-additivity. *Life Sci.*, **1992**, *50*(20), 1535-1541. [http://dx.doi.org/10.1016/0024-3205(92)90144-E] [PMID: 1315897]
- [97] Gomes, I.; Gupta, A.; Filipovska, J.; Szeto, H.H.; Pintar, J.E.; Devi, L.A. A role for heterodimerization of mu and delta opiate receptors in enhancing morphine analgesia. *Proc. Natl. Acad. Sci. USA*, **2004**, *101*(14), 5135-5139. [http://dx.doi.org/10.1073/pnas.0307601101] [PMID: 15044695]
- [98] Costantino, C.M.; Gomes, I.; Stockton, S.D.; Lim, M.P.; Devi, L.A. Opioid receptor heteromers in analgesia. *Expert Rev. Mol. Med.*, **2012**, *14*, e9. [http://dx.doi.org/10.1017/erm.2012.5] [PMID: 22490239]
- [99] Yaksh, T.L. Pharmacology and mechanisms of opioid analgesic activity. *Acta Anaesthesiol. Scand.*, **1997**, *41*(1 Pt 2), 94-111. [http://dx.doi.org/10.1111/j.1399-6576.1997.tb04623.x] [PMID: 9061092]
- [100] Dickenson, A.H. Central acute pain mechanisms. *Ann. Med.*, **1995**, *27*(2), 223-227. [http://dx.doi.org/10.3109/07853899509031963] [PMID: 7632418]
- [101] Moolhalla, S.M.; Sawynok, J. Hyperalgesia produced by intrathecal substance P and related peptides: desensitization and cross desensitization. *Br. J. Pharmacol.*, **1984**, *82*(2), 381-388. [http://dx.doi.org/10.1111/j.1476-5381.1984.tb10773.x] [PMID: 6203593]

- [102] Mantyh, P.W.; Rogers, S.D.; Honore, P.; Allen, B.J.; Ghilardi, J.R.; Li, J.; Daughters, R.S.; Lappi, D.A.; Wiley, R.G.; Simone, D.A. Inhibition of hyperalgesia by ablation of lamina I spinal neurons expressing the substance P receptor. *Science*, **1997**, 278(5336), 275-279. [http://dx.doi.org/10.1126/science.278.5336.275] [PMID: 9323204]
- [103] Khasabov, S.G.; Rogers, S.D.; Ghilardi, J.R.; Peters, C.M.; Mantyh, P.W.; Simone, D.A. Spinal neurons that possess the substance P receptor are required for the development of central sensitization. *J. Neurosci.*, **2002**, 22(20), 9086-9098. [PMID: 12388616]
- [104] Endres-Becker, J.; Heppenstall, P.A.; Mousa, S.A.; Labuz, D.; Oksche, A.; Schäfer, M.; Stein, C.; Zöllner, C. Mu-opioid receptor activation modulates transient receptor potential vanilloid 1 (TRPV1) currents in sensory neurons in a model of inflammatory pain. *Mol. Pharmacol.*, **2007**, 71(1), 12-18. [http://dx.doi.org/10.1124/mol.106.026740] [PMID: 17005903]
- [105] Martin, W.R. Pharmacology of opioids. *Pharmacol. Rev.*, **1983**, 35(4), 283-323. [PMID: 6144112]
- [106] Sharp, B.; Yaksh, T. Pain killers of the immune system. *Nat. Med.*, **1997**, 3(8), 831-832. [http://dx.doi.org/10.1038/nm0897-831] [PMID: 9256267]
- [107] Sacerdote, P. Opioid-induced immunosuppression. *Curr. Opin. Support. Palliat. Care*, **2008**, 2(1), 14-18. [http://dx.doi.org/10.1097/SPC.0b013e3282f5272e] [PMID: 18685388]
- [108] Sacerdote, P.; Bianchi, M.; Gaspani, L.; Manfredi, B.; Maucione, A.; Terno, G.; Ammatuna, M.; Panerai, A.E. The effects of tramadol and morphine on immune responses and pain after surgery in cancer patients. *Anesth. Analg.*, **2000**, 90(6), 1411-1414. [http://dx.doi.org/10.1097/00000539-200006000-00028] [PMID: 10825330]
- [109] Nestler, E.J.; Berhow, M.T.; Brodtkin, E.S. Molecular mechanisms of drug addiction: adaptations in signal transduction pathways. *Mol. Psychiatry*, **1996**, 1(3), 190-199. [PMID: 9118343]
- [110] Mizoguchi, H.; Watanabe, C.; Yonezawa, A.; Sakurada, S. New therapy for neuropathic pain. *Int. Rev. Neurobiol.*, **2009**, 85, 249-260. [http://dx.doi.org/10.1016/S0074-7742(09)85019-8] [PMID: 19607975]
- [111] Bagetta, G.; Sakurada, S. Understanding anomalous adaptation in chronic pain for successful development of disease modifying drugs. *Curr. Opin. Pharmacol.*, **2012**, 12(1), 1-3. [http://dx.doi.org/10.1016/j.coph.2011.11.002] [PMID: 22172234]
- [112] Hervera, A.; Negrete, R.; Leáñez, S.; Martín-Campos, J.; Pol, O. The role of nitric oxide in the local antiallodynic and anti-hyperalgesic effects and expression of delta-opioid and cannabinoid-2 receptors during neuropathic pain in mice. *J. Pharmacol. Exp. Ther.*, **2010**, 334(3), 887-896. [http://dx.doi.org/10.1124/jpet.110.167585] [PMID: 20498253]
- [113] Smith, H.S. Variations in opioid responsiveness. *Pain Phys.*, **2008**, 11(2), 237-248. [PMID: 18354715]
- [114] Martini, L.; Whistler, J.L. The role of mu opioid receptor desensitization and endocytosis in morphine tolerance and dependence. *Curr. Opin. Neurobiol.*, **2007**, 17(5), 556-564. [http://dx.doi.org/10.1016/j.conb.2007.10.004] [PMID: 18068348]
- [115] Wong, C.S.; Hsu, M.M.; Chou, Y.Y.; Tao, P.L.; Tung, C.S. Morphine tolerance increases [3H]MK-801 binding affinity and constitutive neuronal nitric oxide synthase expression in rat spinal cord. *Br. J. Anaesth.*, **2000**, 85(4), 587-591. [http://dx.doi.org/10.1093/bja/85.4.587] [PMID: 11064618]
- [116] Mao, J.; Sung, B.; Ji, R.R.; Lim, G. Chronic morphine induces downregulation of spinal glutamate transporters: implications in morphine tolerance and abnormal pain sensitivity. *J. Neurosci.*, **2002**, 22(18), 8312-8323. [PMID: 12223586]
- [117] Gintzler, A.R.; Chakrabarti, S. Opioid tolerance and the emergence of new opioid receptor-coupled signaling. *Mol. Neurobiol.*, **2000**, 21(1-2), 21-33. [http://dx.doi.org/10.1385/MN:21:1-2:021] [PMID: 11327148]
- [118] Whistler, J.L.; von Zastrow, M. Morphine-activated opioid receptors elude desensitization by beta-arrestin. *Proc. Natl. Acad. Sci. USA*, **1998**, 95(17), 9914-9919. [http://dx.doi.org/10.1073/pnas.95.17.9914] [PMID: 9707575]
- [119] Bohn, L.M.; Lefkowitz, R.J.; Gainetdinov, R.R.; Peppel, K.; Caron, M.G.; Lin, F.T. Enhanced morphine analgesia in mice lacking beta-arrestin 2. *Science*, **1999**, 286(5449), 2495-2498. [http://dx.doi.org/10.1126/science.286.5449.2495] [PMID: 10617462]
- [120] Bian, D.; Nichols, M.L.; Ossipov, M.H.; Lai, J.; Porreca, F. Characterization of the antiallodynic efficacy of morphine in a model of neuropathic pain in rats. *Neuroreport*, **1995**, 6(15), 1981-1984. [http://dx.doi.org/10.1097/00001756-199510010-00007] [PMID: 8580422]
- [121] deGroot, J.F.; Coggeshall, R.E.; Carlton, S.M. The reorganization of mu opioid receptors in the rat dorsal horn following peripheral axotomy. *Neurosci. Lett.*, **1997**, 233(2-3), 113-116. [http://dx.doi.org/10.1016/S0304-3940(97)00642-3] [PMID: 9350845]
- [122] Lee, Y.W.; Chaplan, S.R.; Yaksh, T.L. Systemic and supraspinal, but not spinal, opiates suppress allodynia in a rat neuropathic pain model. *Neurosci. Lett.*, **1995**, 199(2), 111-114. [http://dx.doi.org/10.1016/0304-3940(95)12034-2] [PMID: 8584236]
- [123] Zurek, J.R.; Nadeson, R.; Goodchild, C.S. Spinal and supraspinal components of opioid antinociception in streptozotocin induced diabetic neuropathy in rats. *Pain*, **2001**, 90(1-2), 57-63. [http://dx.doi.org/10.1016/S0304-3959(00)00386-9] [PMID: 11166970]
- [124] Porreca, F.; Tang, Q.B.; Bian, D.; Riedl, M.; Elde, R.; Lai, J. Spinal opioid mu receptor expression in lumbar spinal cord of rats following nerve injury. *Brain Res.*, **1998**, 795(1-2), 197-203. [http://dx.doi.org/10.1016/S0006-8993(98)00292-3] [PMID: 9622629]
- [125] Chen, S.R.; Sweigart, K.L.; Lakoski, J.M.; Pan, H.L. Functional mu opioid receptors are reduced in the spinal cord dorsal horn of diabetic rats. *Anesthesiology*, **2002**, 97(6), 1602-1608. [http://dx.doi.org/10.1097/00000542-200212000-00037] [PMID: 12459691]
- [126] Chen, S.R.; Pan, H.L. Antinociceptive effect of morphine, but not mu opioid receptor number, is attenuated in the spinal cord of diabetic rats. *Anesthesiology*, **2003**, 99(6), 1409-1414. [http://dx.doi.org/10.1097/00000542-200312000-00026] [PMID: 14639157]
- [127] Yajima, Y.; Narita, M.; Shimamura, M.; Narita, M.; Kubota, C.; Suzuki, T. Differential involvement of spinal protein kinase C and protein kinase A in neuropathic and inflammatory pain in mice. *Brain Res.*, **2003**, 992(2), 288-293. [http://dx.doi.org/10.1016/j.brainres.2003.08.042] [PMID: 14625068]
- [128] Narita, M.; Oe, K.; Kato, H.; Shibasaki, M.; Narita, M.; Yajima, Y.; Yamazaki, M.; Suzuki, T. Implication of spinal protein kinase C in the suppression of morphine-induced rewarding effect under a neuropathic pain-like state in mice. *Neuroscience*, **2004**, 125(3), 545-551. [http://dx.doi.org/10.1016/j.neuroscience.2004.02.022] [PMID: 15099668]
- [129] Niikura, K.; Narita, M.; Butelman, E.R.; Kreek, M.J.; Suzuki, T. Neuropathic and chronic pain stimuli downregulate central mu-opioid and dopaminergic transmission. *Trends Pharmacol. Sci.*, **2010**, 31(7), 299-305. [http://dx.doi.org/10.1016/j.tips.2010.04.003] [PMID: 20471111]
- [130] Hoot, M.R.; Sim-Selley, L.J.; Selley, D.E.; Scoggins, K.L.; Dewey, W.L. Chronic neuropathic pain in mice reduces μ -opioid receptor-mediated G-protein activity in the thalamus. *Brain Res.*, **2011**, 1406, 1-7. [http://dx.doi.org/10.1016/j.brainres.2011.06.023] [PMID: 21762883]
- [131] Sánchez-Blázquez, P.; Gómez-Serranillos, P.; Garzón, J. Agonists determine the pattern of G-protein activation in mu-opioid receptor-mediated supraspinal analgesia. *Brain Res. Bull.*, **2001**, 54(2), 229-235. [http://dx.doi.org/10.1016/S0361-9230(00)00448-2] [PMID: 11275413]
- [132] Jordan, B.A.; Devi, L.A. G-protein-coupled receptor heterodimerization modulates receptor function. *Nature*, **1999**, 399(6737), 697-700. [http://dx.doi.org/10.1038/21441] [PMID: 10385123]
- [133] Bolan, E.A.; Pan, Y.X.; Pasternak, G.W. Functional analysis of MOR-1 splice variants of the mouse mu opioid receptor gene. *Proc. Natl. Acad. Sci. USA*, **2004**, 101(1), 11-18. [http://dx.doi.org/10.1002/syn.10277] [PMID: 14579421]
- [134] Zukin, R.S.; Eghbali, M.; Olive, D.; Unterwald, E.M.; Tempel, A. Characterization and visualization of rat and guinea pig brain kappa opioid receptors: evidence for kappa 1 and kappa 2 opioid receptors. *Proc. Natl. Acad. Sci. USA*, **1988**, 85(11), 4061-4065. [http://dx.doi.org/10.1073/pnas.85.11.4061] [PMID: 2836869]
- [135] Reisine, T.; Bell, G.I. Molecular biology of opioid receptors. *Trends Neurosci.*, **1993**, 16(12), 506-510. [http://dx.doi.org/10.1016/0166-2236(93)90194-Q] [PMID: 7509520]
- [136] George, S.R.; Fan, T.; Xie, Z.; Tse, R.; Tam, V.; Varghese, G.; Odowd, B.F. Oligomerization of mu- and delta-opioid receptors. Generation of novel functional properties. *J. Biol. Chem.*, **2000**, 275(34), 26128-26135. [http://dx.doi.org/10.1074/jbc.M000345200] [PMID: 10842167]

- [137] Rozenfeld, R.; Devi, L.A. Receptor heterodimerization leads to a switch in signaling: beta-arrestin2-mediated ERK activation by mu-delta opioid receptor heterodimers. *FASEB J.*, **2007**, *21*(10), 2455-2465. [http://dx.doi.org/10.1096/fj.06-7793com] [PMID: 17384143]
- [138] Kabli, N.; Martin, N.; Fan, T.; Nguyen, T.; Hasbi, A.; Balboni, G.; ODowd, B.F.; George, S.R. Agonists at the δ -opioid receptor modify the binding of μ -receptor agonists to the μ - δ receptor hetero-oligomer. *Br. J. Pharmacol.*, **2010**, *161*(5), 1122-1136. [http://dx.doi.org/10.1111/j.1476-5381.2010.00944.x] [PMID: 20977461]
- [139] von Zastrow, M. Role of endocytosis in signalling and regulation of G-protein-coupled receptors. *Biochem. Soc. Trans.*, **2001**, *29*(Pt 4), 500-504. [http://dx.doi.org/10.1042/bst0290500] [PMID: 11498017]
- [140] Sterne-Marr, R.; Benovic, J.L. Regulation of G protein-coupled receptors by receptor kinases and arrestins. *Vitam. Horm.*, **1995**, *51*, 193-234. [http://dx.doi.org/10.1016/S0083-6729(08)61039-0] [PMID: 7483322]
- [141] Rodríguez-Muñoz, M.; Sánchez-Blázquez, P.; Vicente-Sánchez, A.; Berrocoso, E.; Garzón, J. The mu-opioid receptor and the NMDA receptor associate in PAG neurons: implications in pain control. *Neuropsychopharmacology*, **2012**, *37*(2), 338-349. [http://dx.doi.org/10.1038/npp.2011.155] [PMID: 21814188]
- [142] Mayer, D.J.; Mao, J.; Price, D.D. The association of neuropathic pain, morphine tolerance and dependence, and the translocation of protein kinase C. *NIDA Res. Monogr.*, **1995**, *147*, 269-298. [PMID: 8742791]
- [143] Mao, J.; Price, D.D.; Hayes, R.L.; Lu, J.; Mayer, D.J. Differential roles of NMDA and non-NMDA receptor activation in induction and maintenance of thermal hyperalgesia in rats with painful peripheral mononeuropathy. *Brain Res.*, **1992**, *598*(1-2), 271-278. [http://dx.doi.org/10.1016/0006-8993(92)90193-D] [PMID: 1362520]
- [144] Yajima, Y.; Narita, M.; Usui, A.; Kaneko, C.; Miyatake, M.; Narita, M.; Yamaguchi, T.; Tamaki, H.; Wachi, H.; Seyama, Y.; Suzuki, T. Direct evidence for the involvement of brain-derived neurotrophic factor in the development of a neuropathic pain-like state in mice. *J. Neurochem.*, **2005**, *93*(3), 584-594. [http://dx.doi.org/10.1111/j.1471-4159.2005.03045.x] [PMID: 15836617]
- [145] Sánchez-Blázquez, P.; Rodríguez-Muñoz, M.; Berrocoso, E.; Garzón, J. The plasticity of the association between mu-opioid receptor and glutamate ionotropic receptor N in opioid analgesic tolerance and neuropathic pain. *Eur. J. Pharmacol.*, **2013**, pii: S0014-2999(13)00164-7 [http://dx.doi.org/10.1016/j.ejphar.2013.01.066]
- [146] Meller, S.T.; Pechman, P.S.; Gebhart, G.F.; Maves, T.J. Nitric oxide mediates the thermal hyperalgesia produced in a model of neuropathic pain in the rat. *Neuroscience*, **1992**, *50*(1), 7-10. [http://dx.doi.org/10.1016/0306-4522(92)90377-E] [PMID: 1407561]
- [147] Ferreira, S.H.; Duarte, I.D.; Lorenzetti, B.B. The molecular mechanism of action of peripheral morphine analgesia: stimulation of the cGMP system via nitric oxide release. *Eur. J. Pharmacol.*, **1991**, *201*(1), 121-122. [http://dx.doi.org/10.1016/0014-2999(91)90333-L] [PMID: 1665419]
- [148] Hervera, A.; Leáñez, S.; Negrete, R.; Pol, O. The peripheral administration of a nitric oxide donor potentiates the local antinociceptive effects of a DOR agonist during chronic inflammatory pain in mice. *Naunyn Schmiedeberg's Arch. Pharmacol.*, **2009**, *380*(4), 345-352. [http://dx.doi.org/10.1007/s00210-009-0436-6] [PMID: 19636536]
- [149] Leáñez, S.; Hervera, A.; Pol, O. Peripheral antinociceptive effects of mu- and delta-opioid receptor agonists in NOS2 and NOS1 knockout mice during chronic inflammatory pain. *Eur. J. Pharmacol.*, **2009**, *602*(1), 41-49. [http://dx.doi.org/10.1016/j.ejphar.2008.11.019] [PMID: 19041302]
- [150] Park, S.W.; Li, J.; Loh, H.H.; Wei, L.N. A novel signaling pathway of nitric oxide on transcriptional regulation of mouse kappa opioid receptor gene. *J. Neurosci.*, **2002**, *22*(18), 7941-7947. [PMID: 12223547]
- [151] Pol, O.; Sasaki, M.; Jiménez, N.; Dawson, V.L.; Dawson, T.M.; Puig, M.M. The involvement of nitric oxide in the enhanced expression of mu-opioid receptors during intestinal inflammation in mice. *Br. J. Pharmacol.*, **2005**, *145*(6), 758-766. [http://dx.doi.org/10.1038/sj.bjp.0706227] [PMID: 15852037]
- [152] Sánchez-Blázquez, P.; Rodríguez-Muñoz, M.; Garzón, J. Mu-opioid receptors transiently activate the Akt-nNOS pathway to produce sustained potentiation of PKC-mediated NMDAR-CaMKII signaling. *PLoS One*, **2010**, *5*(6), e11278. [http://dx.doi.org/10.1371/journal.pone.0011278] [PMID: 20585660]
- [153] Vanderah, T.W.; Gardell, L.R.; Burgess, S.E.; Ibrahim, M.; Dogrul, A.; Zhong, C.M.; Zhang, E.T.; Malan, T.P., Jr; Ossipov, M.H.; Lai, J.; Porreca, F. Dynorphin promotes abnormal pain and spinal opioid antinociceptive tolerance. *J. Neurosci.*, **2000**, *20*(18), 7074-7079. [PMID: 10995854]
- [154] Goldstein, A.; Tachibana, S.; Lowney, L.I.; Hunkapiller, M.; Hood, L. Dynorphin-(113), an extraordinarily potent opioid peptide. *Proc. Natl. Acad. Sci. USA*, **1979**, *76*(12), 6666-6670. [http://dx.doi.org/10.1073/pnas.76.12.6666] [PMID: 230519]
- [155] Lai, S.L.; Gu, Y.; Huang, L.Y. Dynorphin uses a non-opioid mechanism to potentiate N-methyl-D-aspartate currents in single rat periaqueductal gray neurons. *Neurosci. Lett.*, **1998**, *247*(2-3), 115-118. [http://dx.doi.org/10.1016/S0304-3940(98)00293-6] [PMID: 9655606]
- [156] Hahn, E.T.; Kim, Y.; Lee, J.J.; Cho, Y.W. GABAergic synaptic response and its opioidergic modulation in periaqueductal gray neurons of rats with neuropathic pain. *BMC Neurosci.*, **2011**, *12*, 41. [http://dx.doi.org/10.1186/1471-2202-12-41] [PMID: 21569381]
- [157] Raghavendra, V.; Tanga, F.; Rutkowski, M.D.; DeLeo, J.A. Anti-hyperalgesic and morphine-sparing actions of propentofylline following peripheral nerve injury in rats: mechanistic implications of spinal glia and proinflammatory cytokines. *Pain*, **2003**, *104*(3), 655-664. [http://dx.doi.org/10.1016/S0304-3959(03)00138-6] [PMID: 12927638]
- [158] Narita, M.; Suzuki, M.; Narita, M.; Yajima, Y.; Suzuki, R.; Shioda, S.; Suzuki, T. Neuronal protein kinase C gamma-dependent proliferation and hypertrophy of spinal cord astrocytes following repeated *in vivo* administration of morphine. *Eur. J. Neurosci.*, **2004**, *19*(2), 479-484. [http://dx.doi.org/10.1111/j.0953-816X.2003.03119.x] [PMID: 14725643]
- [159] Tawfik, V.L.; LaCroix-Fralish, M.L.; Nutile-McMenemy, N.; DeLeo, J.A. Transcriptional and translational regulation of glial activation by morphine in a rodent model of neuropathic pain. *J. Pharmacol. Exp. Ther.*, **2005**, *313*(3), 1239-1247. [http://dx.doi.org/10.1124/jpet.104.082420] [PMID: 15743926]
- [160] Mika, J.; Wawrzczak-Bargiela, A.; Osikowicz, M.; Makuch, W.; Przewlocka, B. Attenuation of morphine tolerance by minocycline and pentoxifylline in naive and neuropathic mice. *Brain Behav. Immun.*, **2009**, *23*(1), 75-84. [http://dx.doi.org/10.1016/j.bbi.2008.07.005] [PMID: 18684397]
- [161] Raghavendra, V.; Tanga, F.Y.; DeLeo, J.A. Attenuation of morphine tolerance, withdrawal-induced hyperalgesia, and associated spinal inflammatory immune responses by propentofylline in rats. *Neuropsychopharmacology*, **2004**, *29*(2), 327-334. [http://dx.doi.org/10.1038/sj.npp.1300315] [PMID: 14532913]
- [162] Narita, M.; Suzuki, M.; Narita, M.; Niikura, K.; Nakamura, A.; Miyatake, M.; Yajima, Y.; Suzuki, T. mu-Opioid receptor internalization-dependent and -independent mechanisms of the development of tolerance to mu-opioid receptor agonists: Comparison between etorphine and morphine. *Neuroscience*, **2006**, *138*(2), 609-619. [http://dx.doi.org/10.1016/j.neuroscience.2005.11.046] [PMID: 16417975]
- [163] Habibi-Asl, B.; Hassanzadeh, K.; Charkhpour, M. Central administration of minocycline and riluzole prevents morphine-induced tolerance in rats. *Anesth. Analg.*, **2009**, *109*(3), 936-942. [http://dx.doi.org/10.1213/ane.0b013e318a5f1f13] [PMID: 19690270]
- [164] Due, M.R.; Piekarz, A.D.; Wilson, N.; Feldman, P.; Ripsch, M.S.; Chavez, S.; Yin, H.; Khanna, R.; White, F.A. Neuroexcitatory effects of morphine-3-glucuronide are dependent on Toll-like receptor 4 signaling. *J. Neuroinflammation*, **2012**, *9*, 200. [http://dx.doi.org/10.1186/1742-2094-9-200] [PMID: 22898544]
- [165] Hutchinson, M.R.; Coats, B.D.; Lewis, S.S.; Zhang, Y.; Sprunger, D.B.; Rezvani, N.; Baker, E.M.; Jekich, B.M.; Wieseler, J.L.; Somogyi, A.A.; Martin, D.; Poole, S.; Judd, C.M.; Maier, S.F.; Watkins, L.R. Proinflammatory cytokines oppose opioid-induced acute and chronic analgesia. *Brain Behav. Immun.*, **2008**, *22*(8), 1178-1189. [http://dx.doi.org/10.1016/j.bbi.2008.05.004] [PMID: 18599265]
- [166] Hutchinson, M.R.; Zhang, Y.; Shridhar, M.; Evans, J.H.; Buchanan, M.M.; Zhao, T.X.; Slivka, P.F.; Coats, B.D.; Rezvani, N.; Wieseler, J.; Hughes, T.S.; Landgraf, K.E.; Chan, S.; Fong, S.; Phipps, S.; Falke, J.J.; Leinwand, L.A.; Maier, S.F.; Yin, H.; Rice, K.C.; Watkins, L.R. Evidence that opioids may have toll-like

- receptor 4 and MD-2 effects. *Brain Behav. Immun.*, **2010**, *24*(1), 83-95. [http://dx.doi.org/10.1016/j.bbi.2009.08.004] [PMID: 19679181]
- [167] Fukagawa, H.; Koyama, T.; Kakuyama, M.; Fukuda, K. Microglial activation involved in morphine tolerance is not mediated by toll-like receptor 4. *J. Anesth.*, **2013**, *27*(1), 93-97. [http://dx.doi.org/10.1007/s00540-012-1469-4] [PMID: 22926420]
- [168] Johnston, I.N.; Milligan, E.D.; Wieseler-Frank, J.; Frank, M.G.; Zapata, V.; Campisi, J.; Langer, S.; Martin, D.; Green, P.; Fleshner, M.; Leinwand, L.; Maier, S.F.; Watkins, L.R. A role for proinflammatory cytokines and fractalkine in analgesia, tolerance, and subsequent pain facilitation induced by chronic intrathecal morphine. *J. Neurosci.*, **2004**, *24*(33), 7353-7365. [http://dx.doi.org/10.1523/JNEUROSCI.1850-04.2004] [PMID: 15317861]
- [169] Tai, Y.H.; Wang, Y.H.; Wang, J.J.; Tao, P.L.; Tung, C.S.; Wong, C.S. Amitriptyline suppresses neuroinflammation and up-regulates glutamate transporters in morphine-tolerant rats. *Pain*, **2006**, *124* (1-2), 77-86. [http://dx.doi.org/10.1016/j.pain.2006.03.018] [PMID: 16697108]
- [170] Reeve, A.J.; Patel, S.; Fox, A.; Walker, K.; Urban, L. Intrathecally administered endotoxin or cytokines produce allodynia, hyperalgesia and changes in spinal cord neuronal responses to nociceptive stimuli in the rat. *Eur. J. Pain*, **2000**, *4*(3), 247-257. [http://dx.doi.org/10.1053/eup.2000.0177] [PMID: 10985868]
- [171] Sung, C.S.; Wen, Z.H.; Chang, W.K.; Chan, K.H.; Ho, S.T.; Tsai, S.K.; Chang, Y.C.; Wong, C.S. Inhibition of p38 mitogen-activated protein kinase attenuates interleukin-1 β -induced thermal hyperalgesia and inducible nitric oxide synthase expression in the spinal cord. *J. Neurochem.*, **2005**, *94*(3), 742-752. [http://dx.doi.org/10.1111/j.1471-4159.2005.03226.x] [PMID: 16033422]
- [172] Shavit, Y.; Wolf, G.; Goshen, I.; Livshits, D.; Yirmiya, R. Interleukin-1 antagonizes morphine analgesia and underlies morphine tolerance. *Pain*, **2005**, *115*(1-2), 50-59. [http://dx.doi.org/10.1016/j.pain.2005.02.003] [PMID: 15836969]
- [173] Eichelbaum, M.; Evert, B. Influence of pharmacogenetics on drug disposition and response. *Clin. Exp. Pharmacol. Physiol.*, **1996**, *23*(10-11), 983-985. [http://dx.doi.org/10.1111/j.1440-1681.1996.tb01154.x] [PMID: 8911746]
- [174] Caraco, Y.; Sheller, J.; Wood, A.J. Impact of ethnic origin and quinidine coadministration on codeine disposition and pharmacodynamic effects. *J. Pharmacol. Exp. Ther.*, **1999**, *290*(1), 413-422. [PMID: 10381807]
- [175] Crews, K.R.; Gaedigk, A.; Dunnenberger, H.M.; Klein, T.E.; Shen, D.D.; Callaghan, J.T.; Kharasch, E.D.; Skaar, T.C. Clinical Pharmacogenetics Implementation Consortium (CPIC) guidelines for codeine therapy in the context of cytochrome P450 2D6 (CYP2D6) genotype. *Clin. Pharmacol. Ther.*, **2012**, *91*(2), 321-326. [http://dx.doi.org/10.1038/clpt.2011.287] [PMID: 22205192]
- [176] Galley, H.F.; Mahdy, A.; Lowes, D.A. Pharmacogenetics and anesthesiologists. *Pharmacogenomics*, **2005**, *6*(8), 849-856. [http://dx.doi.org/10.2217/14622416.6.8.849] [PMID: 16296947]
- [177] Samer, C.F.; Daali, Y.; Wagner, M.; Hopfgartner, G.; Eap, C.B.; Rebsamen, M.C.; Rossier, M.F.; Hochstrasser, D.; Dayer, P.; Desmeules, J.A. Genetic polymorphisms and drug interactions modulating CYP2D6 and CYP3A activities have a major effect on oxycodone analgesic efficacy and safety. *Br. J. Pharmacol.*, **2010**, *160*(4), 919-930. [http://dx.doi.org/10.1111/j.1476-5381.2010.00709.x] [PMID: 20590588]
- [178] Zanger, U.M.; Klein, K.; Saussele, T.; Blievernicht, J.; Hofmann, M.H.; Schwab, M. Polymorphic CYP2B6: molecular mechanisms and emerging clinical significance. *Pharmacogenomics*, **2007**, *8*(7), 743-759. [http://dx.doi.org/10.2217/14622416.8.7.743] [PMID: 17638512]
- [179] Wang, S.C.; Ho, I.K.; Tsou, H.H.; Tian, J.N.; Hsiao, C.F.; Chen, C.H.; Tan, H.K.; Lin, L.; Wu, C.S.; Su, L.W.; Huang, C.L.; Yang, Y.H.; Liu, M.L.; Lin, K.M.; Chen, C.Y.; Liu, S.C.; Wu, H.Y.; Chan, H.W.; Tsai, M.H.; Lin, P.S.; Liu, Y.L. CYP2B6 polymorphisms influence the plasma concentration and clearance of the methadone S-enantiomer. *J. Clin. Psychopharmacol.*, **2011**, *31*(4), 463-469. [http://dx.doi.org/10.1097/JCP.0b013e318222b5dd] [PMID: 21694616]
- [180] Yuan, R.; Zhang, X.; Deng, Q.; Wu, Y.; Xiang, G. Impact of CYP3A4*1G polymorphism on metabolism of fentanyl in Chinese patients undergoing lower abdominal surgery. *Clin. Chim. Acta*, **2011**, *412*(9-10), 755-760. [http://dx.doi.org/10.1016/j.cca.2010.12.038] [PMID: 21223952]
- [181] Naito, T.; Takashina, Y.; Yamamoto, K.; Tashiro, M.; Ohnishi, K.; Kagawa, Y.; Kawakami, J. CYP3A5*3 affects plasma disposition of noroxycodone and dose escalation in cancer patients receiving oxycodone. *J. Clin. Pharmacol.*, **2011**, *51*(11), 1529-1538. [http://dx.doi.org/10.1177/0091270010388033] [PMID: 21209234]
- [182] Duguay, Y.; Báár, C.; Skorpén, F.; Guillemette, C. A novel functional polymorphism in the uridine diphosphate-glucuronosyltransferase 2B7 promoter with significant impact on promoter activity. *Clin. Pharmacol. Ther.*, **2004**, *75*(3), 223-233. [http://dx.doi.org/10.1016/j.clpt.2003.10.006] [PMID: 15001974]
- [183] Darbari, D.S.; van Schaik, R.H.; Capparelli, E.V.; Rana, S.; McCarter, R.; van den Anker, J. UGT2B7 promoter variant -840G>A contributes to the variability in hepatic clearance of morphine in patients with sickle cell disease. *Am. J. Hematol.*, **2008**, *83*(3), 200-202. [http://dx.doi.org/10.1002/ajh.21051] [PMID: 17724700]
- [184] Somogyi, A.A.; Barratt, D.T.; Collier, J.K. Pharmacogenetics of opioids. *Clin. Pharmacol. Ther.*, **2007**, *81*(3), 429-444. [http://dx.doi.org/10.1038/sj.clpt.6100095] [PMID: 17339873]
- [185] Thompson, S.J.; Koszdin, K.; Bernards, C.M. Opiate-induced analgesia is increased and prolonged in mice lacking P-glycoprotein. *Anesthesiology*, **2000**, *92*(5), 1392-1399. [http://dx.doi.org/10.1097/00000542-200005000-00030] [PMID: 10781286]
- [186] Drewe, J.; Ball, H.A.; Beglinger, C.; Peng, B.; Kemmler, A.; Schächinger, H.; Haefeli, W.E. Effect of P-glycoprotein modulation on the clinical pharmacokinetics and adverse effects of morphine. *Br. J. Clin. Pharmacol.*, **2000**, *50*(3), 237-246. [http://dx.doi.org/10.1046/j.1365-2125.2000.00226.x] [PMID: 10971308]
- [187] Kharasch, E.D.; Hoffer, C.; Whittington, D. The effect of quinidine, used as a probe for the involvement of P-glycoprotein, on the intestinal absorption and pharmacodynamics of methadone. *Br. J. Clin. Pharmacol.*, **2004**, *57*(5), 600-610. a [http://dx.doi.org/10.1111/j.1365-2125.2003.02053.x] [PMID: 15089813]
- [188] Kharasch, E.D.; Hoffer, C.; Altuntas, T.G.; Whittington, D. Quinidine as a probe for the role of p-glycoprotein in the intestinal absorption and clinical effects of fentanyl. *J. Clin. Pharmacol.*, **2004**, *44*(3), 224-233. b [http://dx.doi.org/10.1177/0091270003262075] [PMID: 14973303]
- [189] Ameyaw, M.M.; Regateiro, F.; Li, T.; Liu, X.; Tariq, M.; Mobarek, A.; Thornton, N.; Folayan, G.O.; Githanga, J.; Indalo, A.; Ofori-Adjei, D.; Price-Evans, D.A.; McLeod, H.L. MDR1 pharmacogenetics: frequency of the C3435T mutation in exon 26 is significantly influenced by ethnicity. *Pharmacogenetics*, **2001**, *11*(3), 217-221. [http://dx.doi.org/10.1097/00008571-200104000-00005] [PMID: 11337937]
- [190] Cascorbi, I. Role of pharmacogenetics of ATP-binding cassette transporters in the pharmacokinetics of drugs. *Pharmacol. Ther.*, **2006**, *112*(2), 457-473. [http://dx.doi.org/10.1016/j.pharmthera.2006.04.009] [PMID: 16766035]
- [191] John, A.; Köpke, K.; Gerloff, T.; Mai, I.; Rietbrock, S.; Meisel, C.; Hoffmeyer, S.; Kerb, R.; Fromm, M.F.; Brinkmann, U.; Eichelbaum, M.; Brockmöller, J.; Cascorbi, I.; Roots, I. Modulation of steady-state kinetics of digoxin by haplotypes of the P-glycoprotein MDR1 gene. *Clin. Pharmacol. Ther.*, **2002**, *72*(5), 584-594. [http://dx.doi.org/10.1067/mcp.2002.129196] [PMID: 12426522]
- [192] Argoff, C.E. Clinical implications of opioid pharmacogenetics. *Clin. J. Pain*, **2010**, *26*(Suppl. 10), S16-S20. [http://dx.doi.org/10.1097/AJP.0b013e3181c49e11] [PMID: 20026961]
- [193] Levran, O.; Awolosi, O.; Linzy, S.; Adelson, M.; Kreek, M.J. Haplotype block structure of the genomic region of the mu opioid receptor gene. *J. Hum. Genet.*, **2011**, *56*(2), 147-155. [http://dx.doi.org/10.1038/jhg.2010.150] [PMID: 21160491]
- [194] Lopez Soto, E.J.; Raingo, J. A118G Mu Opioid Receptor polymorphism increases inhibitory effects on CaV2.2 channels. *Neurosci. Lett.*, **2012**, *523*(2), 190-194. [http://dx.doi.org/10.1016/j.neulet.2012.06.074] [PMID: 22796651]
- [195] Menon, S.; Lea, R.A.; Roy, B.; Hanna, M.; Wee, S.; Haupt, L.M.; Griffiths, L.R. The human μ -opioid receptor gene polymorphism (A118G) is associated with head pain severity in a clinical cohort of female migraine with aura patients. *J. Headache Pain*, **2012**, *13*(7), 513-519. [http://dx.doi.org/10.1007/s10194-012-0468-z] [PMID: 22752568]
- [196] Olsen, M.B.; Jacobsen, L.M.; Schistad, E.I.; Pedersen, L.M.; Rygh, L.J.; Røe, C.; Gjerstad, J. Pain intensity the first year after lumbar disc herniation is associated with the A118G polymorphism in the

- opioid receptor mu 1 gene: evidence of a sex and genotype interaction. *J. Neurosci.*, **2012**, 32(29), 9831-9834. [http://dx.doi.org/10.1523/JNEUROSCI.1742-12.2012] [PMID: 22815498]
- [197] Kim, H.; Mittal, D.P.; Iadarola, M.J.; Dionne, R.A. Genetic predictors for acute experimental cold and heat pain sensitivity in humans. *J. Med. Genet.*, **2006**, 43(8), e40. [http://dx.doi.org/10.1136/jmg.2005.036079] [PMID: 16882734]
- [198] Rakvåg, T.T.; Klepstad, P.; Baar, C.; Kvam, T.M.; Dale, O.; Kaasa, S.; Krokan, H.E.; Skorpén, F. The Val158Met polymorphism of the human catechol-O-methyltransferase (COMT) gene may influence morphine requirements in cancer pain patients. *Pain*, **2005**, 116(1-2), 73-78. [http://dx.doi.org/10.1016/j.pain.2005.03.032] [PMID: 15927391]
- [199] Tammimäki, A.; Männistö, P.T. Catechol-O-methyltransferase gene polymorphism and chronic human pain: a systematic review and meta-analysis. *Pharmacogenet. Genomics*, **2012**, 22(9), 673-691. [http://dx.doi.org/10.1097/FPC.0b013e3283560c46] [PMID: 22722321]
- [200] Reyes-Gibby, C.C.; El Osta, B.; Spitz, M.R.; Parsons, H.; Kurzrock, R.; Wu, X.; Shete, S.; Bruera, E. The influence of tumor necrosis factor- α -308 G/A and IL-6 -174 G/C on pain and analgesia response in lung cancer patients receiving supportive care. *Cancer Epidemiol. Biomarkers Prev.*, **2008**, 17(11), 3262-3267. [http://dx.doi.org/10.1158/1055-9965.EPI-08-0125] [PMID: 18990769]
- [201] Bessler, H.; Shavit, Y.; Mayburd, E.; Smirnov, G.; Beilin, B. Postoperative pain, morphine consumption, and genetic polymorphism of IL-1 β and IL-1 receptor antagonist. *Neurosci. Lett.*, **2006**, 404(1-2), 154-158. [http://dx.doi.org/10.1016/j.neulet.2006.05.030] [PMID: 16777324]
- [202] Berliocchi, L.; Russo, R.; Tassorelli, C.; Morrone, L.A.; Bagetta, G.; Corasaniti, M.T. Death in pain: peripheral nerve injury and spinal neurodegenerative mechanisms. *Curr. Opin. Pharmacol.*, **2012**, 12(1), 49-54. [http://dx.doi.org/10.1016/j.coph.2011.10.021] [PMID: 22088890]
- [203] Ji, R.R.; Kohno, T.; Moore, K.A.; Woolf, C.J. Central sensitization and LTP: do pain and memory share similar mechanisms? *Trends Neurosci.*, **2003**, 26(12), 696-705. [http://dx.doi.org/10.1016/j.tins.2003.09.017] [PMID: 14624855]
- [204] Levine, B.; Kroemer, G. Autophagy in the pathogenesis of disease. *Cell*, **2008**, 132(1), 27-42. [http://dx.doi.org/10.1016/j.cell.2007.12.018] [PMID: 18191218]
- [205] Berliocchi, L.; Russo, R.; Maiarù, M.; Levato, A.; Bagetta, G.; Corasaniti, M.T. Autophagy impairment in a mouse model of neuropathic pain. *Mol. Pain*, **2011**, 7, 83. [http://dx.doi.org/10.1186/1744-8069-7-83] [PMID: 22023914]
- [206] Shi, G.; Shi, J.; Liu, K.; Liu, N.; Wang, Y.; Fu, Z.; Ding, J.; Jia, L.; Yuan, W. Increased miR-195 aggravates neuropathic pain by inhibiting autophagy following peripheral nerve injury. *Glia*, **2013**, 61(4), 504-512. [http://dx.doi.org/10.1002/glia.22451] [PMID: 23361941]



Intrathecal morphine-3-glucuronide-induced nociceptive behavior via *Delta*-2 opioid receptors in the spinal cord

Takaaki Komatsu ^{a,b}, Soh Katsuyama ^c, Hiroshi Nagase ^d, Hirokazu Mizoguchi ^e, Chikai Sakurada ^f, Minoru Tsuzuki ^f, Shinobu Sakurada ^e, Tsukasa Sakurada ^{a,*}

^a Department of Pharmacology, Daiichi University of Pharmacy, 22-1 Tamagawa-cho, Minami-ku, Fukuoka, Fukuoka 815-8511, Japan

^b School of Pharmacy, Duquesne University, 600 Forbes Avenue, Pittsburgh, PA 15282, USA

^c Center for Experiential Pharmacy Practice, Tokyo University of Pharmacy and Life Science, 1432-1 Horinouchi, Hachioji, Tokyo 192-0392, Japan

^d Department of Medicinal Chemistry, Life Science Center of Tsukuba Advanced Research Alliance, University of Tsukuba, 1-1-1 Tennodai, Tsukuba, Ibaraki 305-8577, Japan

^e Department of Physiology and Anatomy, Tohoku Pharmaceutical University, 4-4-1 Komatsushima, Aoba-ku, Sendai 981-8558, Japan

^f Department of Biochemistry, Nihon Pharmaceutical University, 10281 Komuro Ina-Machi Kitaadachi-gun, Saitama 362-0806, Japan

ARTICLE INFO

Article history:

Received 24 January 2015

Received in revised form 11 October 2015

Accepted 13 October 2015

Available online 22 October 2015

Keywords:

Morphine-3-glucuronide (M3G)

Dynorphin

Leucine-enkephalin

δ_2 -opioid receptor

Extracellular signal-regulated kinase (ERK)

Dorsal spinal cord

Mice

ABSTRACT

Intrathecal (i.t.) injection of morphine-3-glucuronide (M3G), a major metabolite of morphine without analgesic actions, produces severe hindlimb scratching followed by biting and licking in mice. The M3G-induced behavioral response was inhibited dose-dependently by pretreatment with an antisera against dynorphin. However, the selective κ -opioid receptor antagonist, nor-BNI did not prevent the M3G-induced behavioral response. Dynorphin is rapidly degraded by a dynorphin-converting enzyme (cystein protease), to leucine-enkephalin (Leu-ENK). The M3G-induced behavioral response was inhibited dose-dependently by pretreatment with the antisera against Leu-ENK. We also showed that M3G co-administered with Leu-ENK-converting enzyme inhibitors, phosphoramidon and bestatin produced much stronger behavioral responses than M3G alone. Furthermore, the M3G-induced behavioral responses were inhibited dose-dependently by i.t. co-administration of the non-selective δ -opioid receptor antagonist, naltrindole or the selective δ_2 -opioid receptor antagonist, naltriben, whereas the selective δ_1 -opioid receptor antagonist, BNTX had no effect. An i.t. injection of M3G also produced a definite activation of ERK in the lumbar dorsal spinal cord. Western blotting analysis revealed that antisera against dynorphin, antisera against Leu-ENK, naltrindole or naltriben resulted in a significant blockade of ERK activation induced by M3G in the spinal cord. Taken together, these results suggest that M3G-induced nociceptive responses and ERK activation may be triggered via δ_2 -opioid receptors activated by Leu-ENK, which is formed from dynorphin in the spinal cord.

© 2015 Elsevier Inc. All rights reserved.

1. Introduction

Morphine, with its potent analgesic property, has been widely used for the treatment of various types of acute pain and for the long-term treatment of severe chronic pain. However, the clinical use of morphine is complicated by unwanted side-effects, including a paradoxical increase in pain sensitivity (i.e., hyperalgesia and allodynia) (Arner et al., 1988; DeConno et al., 1991; Sakurada et al., 2005). These clinical observations have been confirmed in laboratory studies. At doses far higher than those required for antinociception, morphine injected intrathecally (i.t.) into the spinal subarachnoid space of mice produces a spontaneous vocalization/squeaking and agitation as well as hyperalgesia, allodynia and scratching, biting and licking compared with antinociception at low doses (Yaksh et al., 1986; Sakurada et al., 1996, 2005; Komatsu et al., 2007). Previous studies have also demonstrated that these pain-

related behaviors evoked by i.t. high-dose morphine are not an μ opioid receptor-mediated event because behaviors evoked by i.t. high-dose morphine are not reversed by pretreatment with naloxone, an opioid receptor antagonist. Morphine is known to be metabolized by the conjugation of glucuronide to two major metabolites, morphine-3-glucuronide (M3G) and morphine-6-glucuronide (M6G) in humans (Boerner et al., 1975; Christrup, 1997). Most rodents do not form M6G but only form M3G (Handal et al., 2002; Lötsch, 2009). M6G has a high affinity for the μ -opioid receptor and appears to be a more potent opioid agonist than morphine. In contrast, M3G does not bind to μ -, δ -, or κ -opioid receptors, NMDA, GABA_A or glycine receptors and appears to be devoid of analgesic activity. However, despite these apparent lacks of activity, i.t. and intracerebroventricular (i.c.v.) administrations of M3G have been reported to evoke a range of excitatory behaviors in rodents (Smith, 2000; Komatsu et al., 2009a,b, Hemstapat et al., 2009). Despite the increasing amount of evidence for the involvement of M3G in morphine-induced nociceptive responses, very few studies have addressed the underlying signaling mechanism. In the present set of

* Corresponding author.

E-mail address: tsukasa@daiichi-cps.ac.jp (T. Sakurada).

studies, we employed behavioral and biochemical approaches to examine the mechanism of i.t. M3G in morphine-induced nociceptive responses using specific components affecting the signaling pathway.

Elevation in spinal dynorphin content has also been observed in the opioid-induced pain state (Vanderah et al., 2000). Although dynorphin was originally identified as an endogenous κ -opioid receptor agonist and may act as an endogenous antinociceptive peptide under specific conditions, considerable evidence indicates that enhanced expression of spinal dynorphin is pronociceptive. Furthermore, i.t. administration of 15 nmol of dynorphin A(1–17), dynorphin A(2–17), or dynorphin A(2–13) in rats produced evoked allodynia. Similarly, dynorphin A(2–17) (3 nmol, i.t.) in mice also induced allodynia (Laughlin et al., 1997; Vanderah et al., 1996a). Pain-related behavior associated with nerve injury is also blocked by an antiserum to dynorphin (Bian et al., 1999; Malan et al., 2000; Wagner and Deleo, 1996; Wang et al., 2001).

Dynorphin-converting enzymes, belonging to the cysteine protease family, cleave dynorphin A and dynorphin B between Leu⁵–Arg⁶ and Arg⁶–Arg⁷ bonds, thereby generating leucine-enkephalin (Leu-ENK) and Leu-ENK-Arg, which are primarily active in δ -opioid receptors (Silberring et al., 1992). The i.t. administration of dynorphin A(1–17) also produces an anti-analgesic activity against morphine via activation of the δ_2 -opioid receptor by the increased release of Leu-ENK in the spinal cord (Rady et al., 1999, 2001; Tseng et al., 1994). Furthermore, i.t. Leu-ENK in combination with peptidase inhibitors produces nociceptive behavior via activation of the glutamate receptor, which results in the release of nitric oxide via the δ_2 -opioid receptor in the spinal cord (Komatsu et al., 2014). Thus, nociceptive behavior induced by M3G in morphine may potentially occur via δ_2 -opioid receptors activated by Leu-ENK, which is formed from dynorphin in the spinal cord.

Extracellular signaling-regulated kinase (ERK) is activated in the dorsal spinal cord by nociceptive stimuli, including formalin, capsaicin or carrageenan injection (Galan et al., 2002; Ji et al., 1999; Karim et al., 2001). Inhibition of ERK signaling reduces nociceptive behavior after nociceptive stimuli, suggesting that ERK activation contributes to acute nociceptive processing in the spinal cord (Ji et al., 1999; Karim et al., 2001).

The purpose of the present research study was to determine whether δ_2 -opioid receptor activation by Leu-ENK, which is formed from dynorphin, is involved in M3G-induced nociceptive behavior and ERK activation in the spinal cord.

2. Materials and methods

2.1. Animals

Pathogen-free adult male ddY-strain mice weighing an average of 24 g (Shizuoka Laboratory Center, Japan) were used in all experiments. The mice were maintained in a controlled 12 h light–dark cycle with food and water ad libitum. Room temperature and humidity were controlled at 22–24 °C and 50–60%, respectively.

2.2. Intrathecal injections

The i.t. injections were administered by percutaneous lumbar puncture through an intervertebral space at the level of the 5th or 6th vertebrae using the Hylden and Wilcox technique (Hylden and Wilcox, 1980). The drugs were administered i.t. in a volume of 5 μ l with a 50- μ l Hamilton microsyringe. A tail flick was used as an indication that the needle had penetrated the dura.

2.3. Behavioral experiments

Mice were acclimatized initially for 1 h in an individual plastic cage (22.0 \times 15.0 \times 12.5 cm) which also served as the observation chamber. The animals were challenged i.t. with M3G observed for 5 min. The observation of items of the induced behaviors was the total response

time (s) of the following behaviors: hindlimb scratching, biting or licking of the hindpaw.

2.4. Drugs

The following drugs were used: M3G, bestatin, naltrindole, naltriben, *nor*-binaltorphimine dihydrochloride (*nor*-BNI), 7-benzylidenenaltrexone (BNTX), 4-(hydroxymercuri) benzoic acid sodium salt (PHMB) (Sigma Chemical Co., St. Louis, MO, USA), phosphoramidon (Nakalai tesq, Kyoto, Japan), dynorphin A antibody (Phenix Pharmaceutical, Inc., USA), Leucine-enkephalin polyclonal antibody (Millipore Corporation, USA), 1,4-diamino-2,3-dicyano-1,4-bis(2-aminophenylthio) butadiene (U0126) (Calbiochem, Darmstadt, Germany). Monoclonal anti-phospho-p44/42 MAP kinase antibody and anti-p44/42 MAP kinase antibody were obtained from Cell Signaling Technology, Inc. U0126 was initially dissolved in 100% DMSO as stock solution, further diluted by artificial CSF and adjusted to 6.71% DMSO as the final concentration. The other drugs were dissolved in 50% dimethylsulfoxide (DMSO) to prepare the concentrated stock solution and working solutions were then diluted in artificial cerebrospinal fluid (CSF), containing NaCl 7.4 g, KCl 0.19 g, MgCl₂ 0.19 g and CaCl₂ 0.14 g/1000 ml of distilled and sterilized water, in a stepwise fashion. The highest concentrations of drugs used contained 0.9% and 1.4% DMSO, respectively. Low concentrations of DMSO resulted in no substantial effect on M3G-induced behavioral changes.

All antagonists were co-administered i.t. with M3G in a volume of 5 μ l. Antiserum against dynorphin or leucine-enkephalin were injected i.t. 5 min prior to i.t. M3G.

2.5. Sample preparation

At 3 min after i.t. injection, the mice were decapitated and the entire spinal cord was obtained by pressure expulsion with physiological saline. The dorsal part of lumbar spinal cord was dissected quickly on an ice-cooled glass dish for Western blotting analysis.

2.6. Western blotting analysis

Tissue samples were homogenized in 0.1 ml of lysis buffer reagent (150 mM NaCl, 1.0% NP-40, 50 mM Tris–HCl pH 8.0, 1 mM phenylmethylsulfonyl fluoride, 1 mg/ml aprotinin, 1 mM sodium vanadate and 1 mM EDTA pH 8.0) and centrifuged at 15,000 \times g for 30 min at 4 °C. Supernatants were collected and total protein amounts were measured using the Protein Assay (BIO-RAD, Hercules, CA). An equal volume of 2 \times sample buffer (100 mM Tris–HCl pH 6.8, 2.5% SDS, 20% glycerol, 0.006% bromophenol blue and 10% β -mercaptoethanol) was added to 30 μ g of total protein. The samples were boiled, electrophoresed in a 10% SDS-polyacrylamide gel (BIO-RAD, Hercules, CA) and then transferred to a Hybond-P membrane (Amersham Biosciences).

The blotted membrane was then incubated overnight with 5% skim milk (Wako Pure Chemical Industries, LTD, Osaka, Japan) in T-PBS (PBS containing 0.1% v/v Tween 20). All antibody applications were performed in T-PBS. After the membranes were washed, primary antibody incubations were performed for 2 h at room temperature using the appropriate dilutions (anti-phospho-p44/42 MAP kinase 1:1000 and anti-p44/42 MAPK antibody 1:1000). The membranes were extensively washed with T-PBS and incubated for 2 h with the secondary antibody (anti-rabbit or anti-mouse IgG peroxidase-conjugated antibody 1:5000) (Amersham Biosciences). After washing, the proteins were detected using the ECL-Plus Western blotting detection system (Amersham Biosciences) and visualized using the Dolphine-Chemi Image System (Wealtec). MagicMark western protein standard (Invitrogen) was simultaneously resolved on the gel, and the molecular weight of the proteins was estimated.

2.7. Data analyses

Statistical analyses of the results were performed using Dunnett's test for multiple comparison, following analysis of variance (ANOVA). Differences were considered to be significant if $P < 0.05$. All values are expressed as the mean \pm S.E.M.

3. Results

3.1. Effects of antiserum against dynorphin and a selective κ -opioid receptor antagonist on i.t. M3G-induced behavioral response

An i.t. injection of M3G (2.5 nmol) into the spinal lumbar space evoked reciprocal hindlimb scratching toward the flanks in mice. Biting and licking of the hindpaw were also observed after the incidence of scratching. These behavioral characterizations of i.t. M3G confirms previously reported data (Komatsu et al., 2009a). Antiserum against dynorphin, injected i.t. 5 min prior to M3G, inhibited i.t. M3G-induced behavioral responses in a dilution-dependent manner (Fig. 1A). Treatment with nor-BNI, a selective κ -opioid receptor antagonist did not prevent the behavioral responses induced by i.t. M3G (Fig. 1B).

3.2. Effects of antiserum against Leu-ENK and δ -opioid receptor antagonists on i.t. M3G-induced behavioral response

Antiserum against Leu-ENK, injected i.t. 5 min prior to M3G, inhibited i.t. M3G-induced behavioral responses in a dilution-dependent manner (Fig. 2A). Treatment with peptidase inhibitors (Leu-ENK-converting

enzyme inhibitors), phosphoramidon, (an endopeptidase 24.11 inhibitor) (2.0 nmol) and bestatin, (a general amino-peptidase inhibitor) (0.25 nmol), significantly enhanced the efficacy of the i.t. M3G-induced responses (Fig. 2B). The non-selective δ -opioid receptor antagonist, NTI (50–200 pmol) and the selective δ_2 -opioid receptor antagonist, NTB (50–200 pmol) showed a dose-dependent inhibition of i.t. M3G-evoked nociceptive responses (Fig. 2C and D). NTI (200 pmol) and NTB (200 pmol) alone did not induce a significant behavioral response compared to CSF-injected controls. Treatment with BNTX (200 pmol), a selective δ_1 -opioid receptor antagonist, did not prevent an i.t. M3G-evoked nociceptive response (Fig. 2E). The doses of the antagonists used have been previously reported to completely block the antinociception induced by the respective selective opioid agonists (Tseng et al., 1997).

3.3. Effects of the MEK inhibitor on ERK activation in the dorsal spinal cord and on nociceptive responses after i.t. injection of M3G

We further examined whether spinal ERK is activated by i.t. M3G in the lumbar dorsal cord. Activation of ERK in the lumbar dorsal cord was quantified using the Western blotting assay (Fig. 3A). We compared the effect of i.t. M3G (2.5 nmol) with that of the artificial CSF treatment in the lumbar dorsal cord extracted 3 min after i.t. injection. Western blotting analyses revealed that M3G significantly increased phospho-ERK expression (Fig. 3A).

Next, we examined whether upstream effectors of ERK were necessary for the induction of the behavioral responses induced by i.t. M3G. The MEK inhibitor U0126 (5.0 nmol) reduced a significant ERK activation 3 min after i.t. M3G (Fig. 3A). Total spinal ERK expression was unchanged when M3G alone or in combination with U0126 was administered (Fig. 3A). In the behavioral test, i.t. injection of U0126 (2.5–5.0 nmol) caused a dose-dependent inhibition of the nociceptive response induced by i.t. M3G when compared with the artificial CSF-treated controls (Fig. 3B). ERK activation and behavioral characterizations of i.t. M3G confirms previously reported data (Komatsu et al., 2009a).

3.4. Effects of antiserum against dynorphin, antiserum against Leu-ENK and δ -opioid receptor antagonists on M3G-induced ERK activation

To investigate whether the release of dynorphin, Leu-ENK and activation of the δ -opioid receptor is necessary for upstream activators of phospho-ERK, effects of antiserum against dynorphin, antiserum against Leu-ENK, δ -opioid receptor antagonist NTI, selective δ_2 -opioid receptor antagonist NTB and the selective δ_1 -opioid receptor antagonist BNTX were injected i.t. with M3G. Consistent with the behavioral results (Fig. 1A–E), all treatments except BNTX were effective in blocking phospho-ERK activation induced by M3G (Fig. 4A–E).

4. Discussion

The present results demonstrate for the first time that i.t. injection of M3G evoked nociceptive responses and that ERK activation may be triggered via δ_2 -opioid receptors activated by Leu-ENK formed from dynorphin in the spinal cord. Several studies have suggested an important role for spinal dynorphin in abnormal pain. First, blocking the effects of dynorphin with antiserum clearly blocks opioid-induced allodynia and hyperalgesia, and second, continuous intrathecal infusion or subcutaneous administration of the μ -opioid agonist morphine and spinal nerve ligation result in an increase in spinal dynorphin content (Kajander et al., 1990; Draisci et al., 1991; Dubner and Ruda, 1992; Rattan and Tejwani, 1997; Vanderah et al., 2000). In addition, the anti-analgesic activities of i.t. administration of dynorphin were inhibited by naltriben, a δ_2 -opioid receptor antagonist, or by treatment with a δ -opioid receptor antisense oligodeoxynucleotide, which down-regulates spinal δ_2 -opioid receptors (Rady et al., 1999; Tseng et al.,

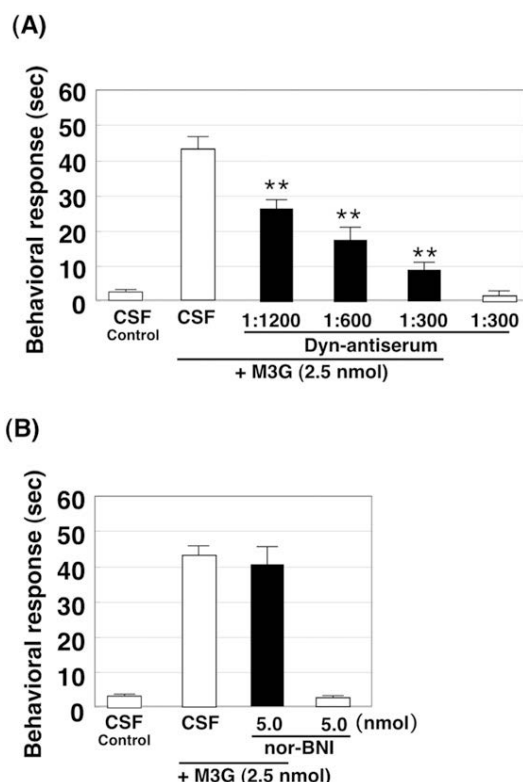


Fig. 1. Effects of antiserum against dynorphin (A) and nor-binaltorphimine dihydrochloride (nor-BNI) (B) on the nociceptive behavior induced by i.t. injection of M3G. Antiserum against dynorphin was pre-injected i.t. 5 min prior to i.t. injection with M3G. The nor-BNI was co-administered i.t. with M3G in a total volume of 5 μ l. The duration of scratching, biting and licking responses induced by M3G was determined over a 5 min period starting immediately after the i.t. injection. Each value represents the mean \pm S.E.M. of ten mice in each group. Statistically significant difference compared with M3G alone is indicated by ** $P < 0.01$, * $P < 0.05$.

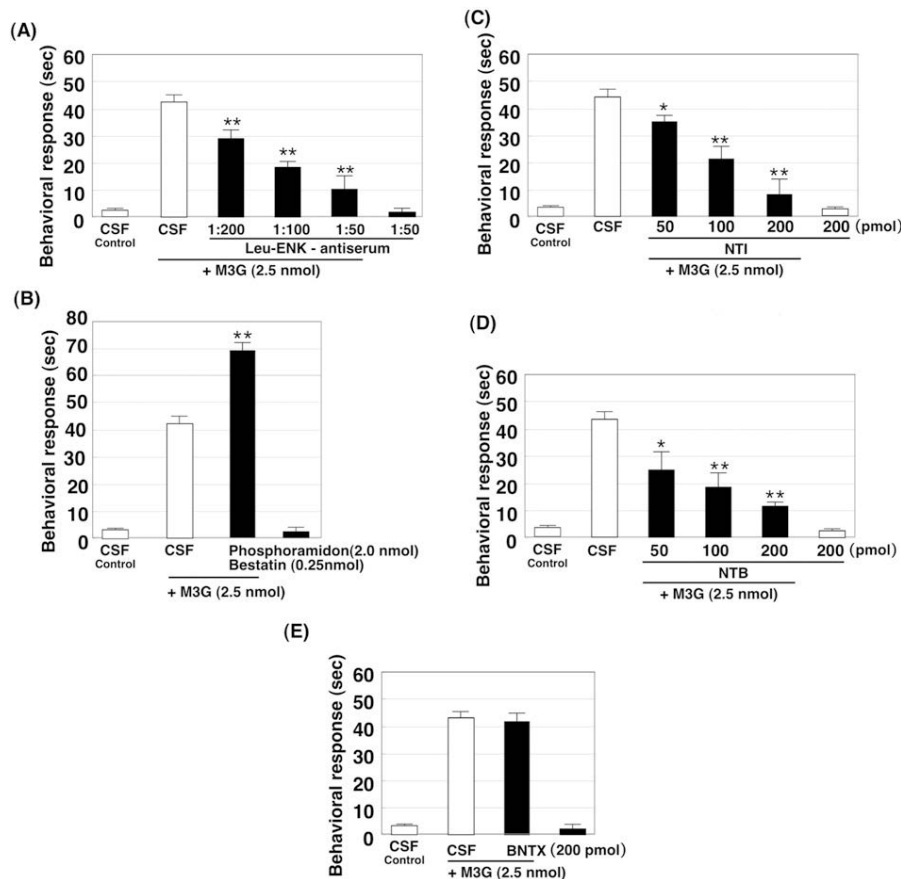


Fig. 2. Effects of antiserum against Leu-ENK(A), Leu-ENK-converting enzyme inhibitors (phosphoramidon and bestatin) (B), naltrindole (NTI) (C), naltriben (NTB) (D) and 7-benzylidenenaltrexone (BNTX) (E) on the nociceptive behavior induced by i.t. injection of M3G. Antiserum against Leu-ENK was pre-injected i.t. 5 min prior to i.t. injection of M3G. Each antagonist was co-administered i.t. with M3G in a total volume of 5 μ l. The duration of scratching, biting and licking responses induced by M3G was determined over a 5 min period starting immediately after i.t. injection. Each value represents the mean \pm S.E.M. of ten mice in each group. Statistically significant difference compared with M3G alone is indicated by ** P < 0.01, * P < 0.05.

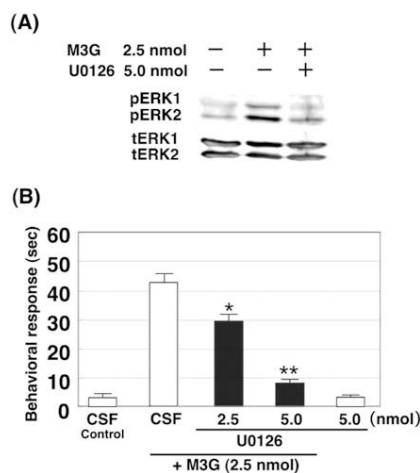


Fig. 3. Effect of U0126, a MEK inhibitor, on spinal ERK activation and nociceptive response induced by i.t. injection of M3G. (A) Western blotting analyses of the dorsal spinal homogenates for pERK and tERK. Dorsal spinal cord samples were obtained 3 min after i.t. injection of M3G. tERK was used as a loading control. U0126 (5.0 nmol) was administered i.t. 5 min prior to i.t. M3G. This Western blot is representative of four independent experiments. (B) Inhibitory effects of i.t. U0126 (2.5–5.0 nmol) on nociceptive behavior induced by i.t. injection of M3G. The duration of scratching, biting and licking responses induced by M3G was determined over a 5 min period starting immediately after the i.t. injection. Each value represents the mean \pm S.E.M. of ten mice in each group. Statistically significant difference compared with M3G is indicated by ** P < 0.01, * P < 0.05.

1994). Leu-ENK antiserum also inhibited i.t. administration of a low dose of Leu-ENK, which produced anti-analgesia activity against morphine-induced antinociception (Rady et al., 2001). Taken together, nociceptive responses evoked by i.t. dynorphin may result from an increasing accumulation of Leu-ENK in the spinal cord. Leu-ENK has a relatively high affinity for the δ -opioid receptor and may act as an endogenous antinociceptive peptide. A genuine effect of enkephalin has not been observed because it is degraded easily by enzymes in the body (Hambrock et al., 1976). Thus, a synthetic inhibitor for enkephalin-degrading enzymes is used. It has been shown that peptidase inhibitors, such as amastatin, captopril, phosphoramidon and spinorphin prevent the degradation of enkephalin, and these peptidase inhibitors enhanced the effects of enkephalin administered at doses required for antinociception (Taguchi et al., 1998; Honda et al., 2001). However, a previous study showed that i.t. injection of a low dose of Leu-ENK, co-administered with peptidase inhibitors, produced behaviors consisting of biting and licking of the hindpaw and tail along with hindlimb scratching directed toward the flank (Komatsu et al., 2014). For this reason, Leu-ENK could act as an inverse agonist to the δ_2 -opioid receptor. This inverse agonist activity was obtained at a low concentration, which is approximately 1/1000 of the amount necessary to produce analgesic synergism with morphine (Vanderah et al., 1996b). Although inverse agonists have been applied to opioid receptor antagonists (Szekeres and Traynor, 1997), they have dual actions, as opioid agonists and antagonists (Crain and Shen, 1990, 1998, 2000a). Low concentrations of opioids (μ , δ , κ opioid peptides) elicit excitatory prolongation of the action potential duration in mouse sensory dorsal root ganglion neurons, whereas

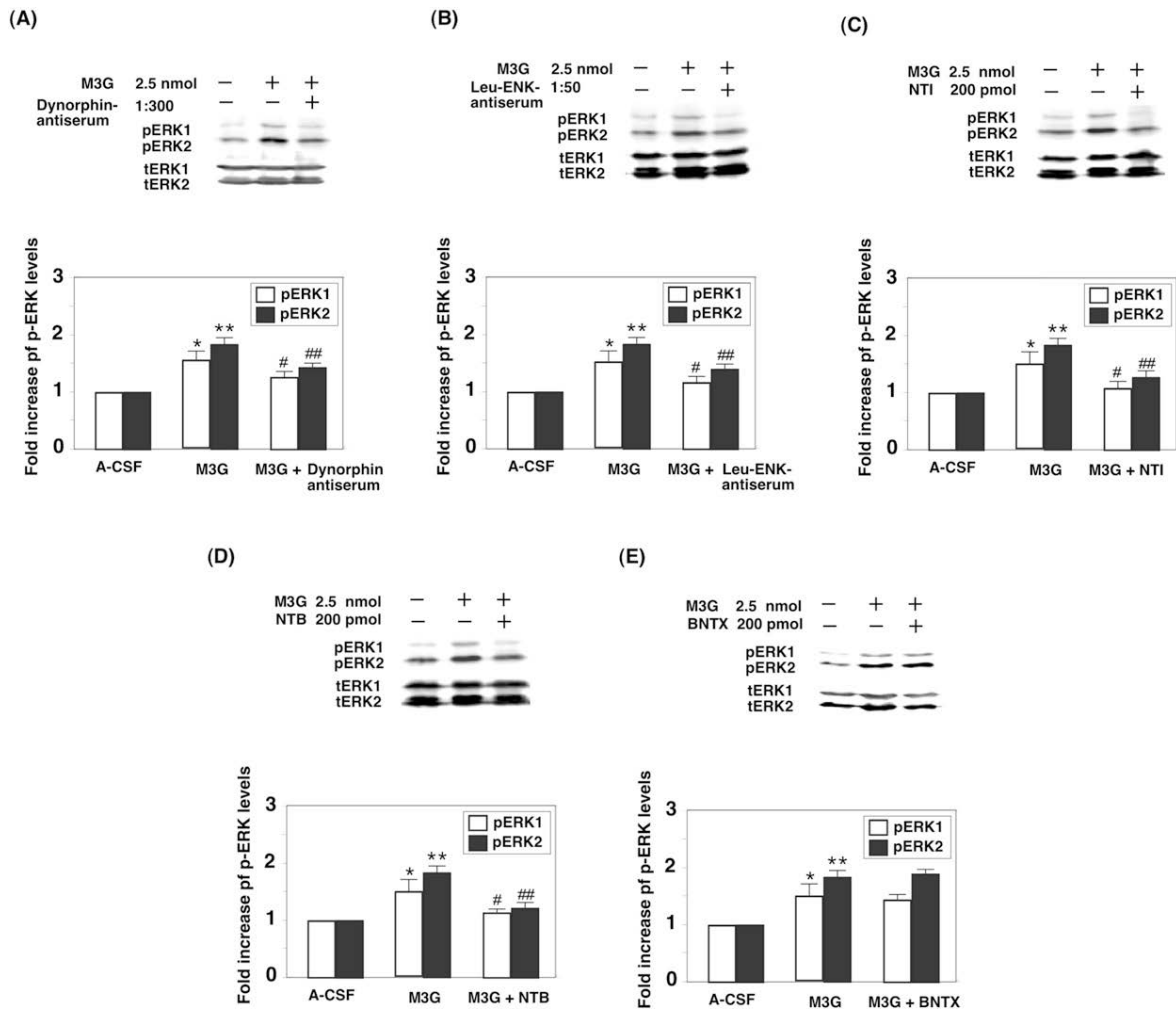


Fig. 4. Effect of antiserum against dynorphin (A), antiserum against Leu-ENK (B), NTL (C), NTB (D) and BNTX (E) on spinal ERK activation induced by i.t. injection of M3G. Western blotting analyses of the dorsal spinal homogenates for pERK and tERK. Representative Western blots are shown on top, and quantification of pERK1 and pERK2 levels are shown in the bar graphs. Dorsal spinal cord samples were obtained 3 min after the i.t. injection of M3G. tERK was used as a loading control. NTL, NTB and BNTX were co-administered i.t. with M3G. Antiserum against dynorphin and antiserum against Leu-ENK were pre-injected i.t. 5 min prior to i.t. injection of M3G. Each value represents the mean \pm S.E.M. of four mice in each group. Statistically significant difference compared with A-CSF controls is indicated by ** $P < 0.01$, * $P < 0.05$, ## $P < 0.01$, # $P < 0.05$ compared to M3G alone.

higher concentrations result in inhibitory shortening of the action potential duration (Shen and Crain, 1994). Shortening of the action potential of primary sensory neurons by opioids has generally been considered to be a useful model of their inhibition of calcium influx and transmitter release at presynaptic terminals in the dorsal spinal cord, thereby accounting for opioid-induced analgesia in vivo (Shen and Crain, 1994). However, the opioid-induced prolongation of action potentials as evidence of the excitatory effects of opioids on sensory neurons, which may result in enhanced calcium influx and transmitter release at presynaptic terminals, may account for some types of hyperalgesia and allodynia elicited by opioids in vivo (Shen and Crain, 1994). These results are consistent with the results of the analgesic activity and the mechanism obtained in the previous study at a low dose (0.5–1.0 fmol) of Leu-ENK in combination with peptidase inhibitors (Komatsu et al., 2014). The nociceptive behavior evoked by i.t. Leu-ENK in combination with peptidase inhibitors was inhibited dose-dependently by co-administration of the non-selective δ -opioid receptor antagonist naltrindole or the selective δ_2 -opioid receptor antagonist naltriben, but not by the selective δ_1 -opioid receptor antagonist BNTX (Komatsu et al., 2014).

Our studies have shown previously that i.t. M3G-evoked nociceptive responses contributes to the activation of spinal ERK signaling in the

NO-cGMP-PKG pathway via the release of a primary afferent neurotransmitter such as glutamate (Komatsu et al., 2009a). Dynorphin-induced allodynia was blocked by MK-801, an NMDA antagonist (Laughlin et al., 1997; Vanderah et al., 1996a,b). The release of excitatory amino acids, such as glutamate and aspartate, increased with i.t. dynorphin and was blocked by MK-801 (Faden, 1992; Skilling et al., 1992). The elimination of morphine-induced antinociception produced by i.t. Leu-ENK may potentially occur by the increased release of glutamate from primary afferent terminals via activation of spinal δ_2 -opioid receptors because i.t. administration of naltriben, a δ_2 -opioid receptor antagonist or MK801, a non-competitive NMDA antagonist inhibited the anti-analgesic action of Leu-ENK (Rady et al., 2001). Furthermore, in an analysis of 129S6/SvEv mice lacking responsiveness to NMDA, i.t. injected Leu-ENK did not inhibit i.t. morphine-induced analgesia (Rady et al., 2001). The anti-analgesic action of dynorphin and Leu-ENK through NMDA receptors suggest that the signaling pathway involved in producing anti-analgesia is different from that for analgesia (Crain and Shen, 1998, 2000b; Fundytus andCoderre, 1999). Previous studies have also indicated that nociceptive behaviors induced by Leu-ENK co-injected with peptidase inhibitors were inhibited by MK-801 (Komatsu et al., 2014). In view of these findings, we speculate that i.t. injection of M3G could release primary afferent neurotransmitters,

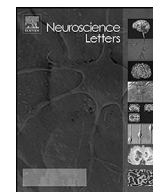
potentially glutamate or activate glutamate receptors, via δ_2 -opioid receptors activated by Leu-ENK formed from dynorphin in the spinal cord. Indeed, i.t. injection of high-doses of morphine in rats evoked a marked increase in glutamate and nitric oxide (NO) release in dorsal spinal cord extracellular fluid (Watanabe et al., 2003). On the basis of our previous results, glutamate released from presynaptic sites in response to i.t. M3G activated NMDA receptors, which triggered a feed-forward mechanism of stimulation of nNOS activity via a mechanism that is largely dependent on calcium. In addition, activation of NMDA receptors can stimulate nNOS activity via a calcium calmodulin-dependent mechanism (Li et al., 1994; Wu et al., 1994). Extracellular calcium also appears essential for noxious stimulation-induced ERK activation (Lever et al., 2003). NMDA receptor functions as a calcium channel and has been widely implicated in ERK activation (Ji et al., 1999; Lever et al., 2003; Kawasaki et al., 2004). Recently, accumulating evidence has suggested that ERK has important roles in the modulation of nociceptive signaling. ERK is activated in the dorsal spinal cord in models of pain, such as formalin, capsaicin or carrageenan injection (Thomas and Hunt, 1993; Ji et al., 1999; Karim et al., 2001; Cruz et al., 2005). Furthermore, inhibition of ERK phosphorylation in the dorsal spinal cord by the MEK inhibitor reduces the pain behavioral response after formalin, capsaicin or carrageenan injection. Western blotting studies had also shown that i.t. M3G evoked a strong activation of spinal phospho-ERK, which is consistent with the nociceptive behaviors induced by i.t. M3G. The MEK inhibitor U0126 in the lumbar spinal cord reveals that the signal transduction pathway through MEK and phospho-ERK can be activated in the lumbar spinal cord after M3G injection (Komatsu et al., 2009a). Importantly, treatment with the non-selective δ opioid receptor antagonist, NTI or the selective δ_2 -opioid receptor antagonist, NTB, could clearly block phospho-ERK, while the selective δ_1 -opioid receptor antagonist BNTX (7-benzylidenenaltrexone), was not effectively blocked. These results support a critical role of ERK activation via the δ_2 -opioid receptor in the establishment of nociception induced by i.t. M3G. Activation of this nociception signaling pathway was observed after M3G injection and supports the heuristic possibility of several independent concepts. Several lines of evidence indicate that the δ -opioid receptor is essential for analgesic tolerance, which could be consistent with the sensitization, resulting in an excitatory action (Kest et al., 1996; Chakrabarti et al., 1998; Zhu et al., 1999; Crain and Shen, 2000a). Indeed, morphine analgesic tolerance does not develop in either δ -opioid receptor or preproenkephalin knock-out mice (Zhu et al., 1999; Joshua et al., 2002). δ -opioid receptor antagonists with morphine reduced analgesic tolerance to morphine and restored morphine analgesic potency. (Abdelhamid et al., 1991; Fundytus et al., 1995; Abul-Husn et al., 2007). More recently, a compound of a μ opioid receptor agonist with a δ opioid antagonist was reported to produce reduced tolerance compared to fentanyl (Mosberg et al., 2014). Moreover, in several studies, blockade of the NMDA receptor-NOS cascade was shown to attenuate the development of tolerance to morphine (Trujillo and Aki, 1991; Kolosnikov et al., 1993; Elliott et al., 1994; Mao et al., 1994; Pasternak et al., 1995; Gonzalez et al., 1997). Subsequent analytical studies of the δ -opioid receptor and preproenkephalin knock-outs mice, and the NMDA receptor-deficient 129S6 inbred mouse strain have supported these hypotheses, implicating the signaling pathway involved in that release of preproenkephalin-derived peptides during chronic morphine exposure, the δ -opioid receptor and the NMDA receptor are necessary for the expression of morphine tolerance (Joshua et al., 2002). Overall, these data suggest that the development of morphine tolerance may result from activation of the NMDA receptor-NOS cascade, via the activation of δ_2 -opioid receptors followed by a continuous release of Leu-ENK during chronic morphine exposure. In conclusion, the current study suggests that nociception and spinal ERK activation evoked by i.t. M3G, major metabolite of morphine may be mediated via δ_2 -opioid receptors activated by Leu-ENK, which is formed from dynorphin in the spinal cord. This finding suggests that inhibitors of δ_2 -opioid receptors can enhance the analgesic response to spinal

morphine, diminishing the development of tolerance to morphine and thus represents a promising lead for the development of opioid analgesics with reduced side effects.

References

- Abdelhamid, E.E., Sultana, M., Portoghese, P.S., Takemori, A.E., 1991. Selective blockage of delta opioid receptor prevents the development of morphine tolerance and dependence in mice. *J. Pharmacol. Exp. Ther.* 258, 299–303.
- Abul-Husn, N.S., Sutak, M., Milne, B., Jhamandas, K., 2007. Augmentation of spinal morphine analgesia and inhibition of tolerance by low doses of μ - and delta-opioid receptor antagonists. *Br. J. Pharmacol.* 151 (6), 877–887.
- Arner, S., Rawal, N., Gustafsson, L.L., 1988. Clinical experience of long-term treatment with epidural opioids a nationwide survey. *Acta Anaesthesiol. Scand.* 32, 253–259.
- Bian, D.S., Ossipov, M.H., Ibrahim, M., Raffa, R.B., Tallarida, R.J., Malan Jr., T.P., Lai, J., Porreca, F., 1999. Loss of anti nociceptive spinal/supraspinal morphine synergy in nerve-injured rats; restoration by MK-801 or dynorphin antiserum. *Brain Res.* 831, 55–63.
- Boerner, U., Abbott, S., Roe, R.L., 1975. The metabolism of morphine and heroin in man. *Drug Metab. Rev.* 4, 39–73.
- Chakrabarti, S., Rivera, M., Yan, S.Z., Tang, W.J., Glintzler, A.R., 1998. Chronic morphine augments Gbg/Gsa stimulation of adenylyl cyclase: relevance to opioid tolerance. *Mol. Pharmacol.* 54, 7655–7662.
- Christrup, L.L., 1997. Morphine metabolites. *Acta Anaesthesiol. Scand.* 116–122.
- Crain, S.M., Shen, K.F., 1990. Opioids can evoke direct receptor-mediated excitatory effects on sensory neurons. *Trends Pharmacol. Sci.* 11, 77–81.
- Crain, S.M., Shen, K.F., 1998. Modulation of opioid analgesia, tolerance and dependence by Gs-coupled, GM1 ganglioside-regulated opioid receptor functions. *Trends Pharmacol. Sci.* 19, 358–365.
- Crain, S.M., Shen, K.F., 2000a. Antagonists of excitatory opioid receptor functions enhance morphine analgesic potency and attenuate opioid tolerance/dependence liability. *Pain* 84, 121–131.
- Crain, S.M., Shen, K.F., 2000b. Enhanced analgesic potency and reduced tolerance of morphine in 129/SvEv mice: evidence for deficiency in GM1 ganglioside-regulated excitatory opioid receptor functions. *Brain Res.* 856, 227–235.
- Cruz, C.D., Neto, F.L., Castro-Lopes, J., McMahon, S.B., Cruz, F., 2005. Inhibition of ERK phosphorylation decreases nociceptive behaviour in monoarthritic rats. *Pain* 116, 411–419.
- DeConno, F., Caraceni, A., Martini, C., Spoldi, E., Salvetti, M., Ventafridda, V., 1991. Hyperalgesia and myoclonus with intrathecal infusion of high-dose morphine. *Pain* 47, 337–339.
- Draisci, G., Kajander, K.C., Dubner, R., Bennett, G.J., Iadarola, M.J., 1991. Up-regulation of opioid gene expression in spinal cord evoked by experimental nerve injuries and inflammation. *Brain Res.* 560 (1–2), 186–192.
- Dubner, R., Ruda, M.A., 1992. Activity-dependent neuronal plasticity following tissue injury and inflammation. *Trends Neurosci.* 15 (3), 96–103.
- Elliott, K., Minami, N., Kolesnikov, Y.A., Pasternak, G.W., Inturrisi, C.E., 1994. The NMDA receptor antagonists, LY274614 and MK-801, and the nitric oxide synthase inhibitor, NG-nitro-L-arginine, attenuate analgesic tolerance to the μ -opioid morphine but not to κ -opioids. *Pain* 56, 69–75.
- Faden, A.L., 1992. Dynorphin increases extracellular levels of excitatory amino acids in the brain through a non-opioid mechanism. *J. Neurosci.* 12, 425–429.
- Fundytus, M.E., Coderre, T.J., 1999. Opioid tolerance and dependence. A new model highlighting the role of metabotropic glutamate receptors. *Pain Forum* 8, 3–13.
- Galan, A., Lopez-Garcia, J.A., Cervero, F., Laird, J.M.A., 2002. Activation of spinal extracellular signaling-regulated kinase-1 and -2 by intraplantar carrageenan in rodents. *Neurosci. Lett.* 322, 37–40.
- Gonzalez, P., Cabello, P., Germany, A., Norris, B., Contreras, E., 1997. Decrease of tolerance to, and physical dependence on morphine by, glutamate receptor antagonists. *Eur. J. Pharmacol.* 332, 257–262.
- Hambrock, J.M., Morgan, B.A., Rance, M.J., Smith, C.F.C., 1976. Mode of deactivation of the enkephalins by rat and human plasma and rat brain homogenates. *Nature* 262, 782–783.
- Handal, M., Grung, M., Skurtveit, S., Ripel, A., Mørland, J., 2002. Pharmacokinetic differences of morphine and morphine-glucuronides are reflected in locomotor activity. *Pharmacol. Biochem. Behav.* 73 (4), 883–892.
- Hemstap, K., Le, L., Edwards, S.R., Smith, M.T., 2009. Comparative studies of the neuro-excitatory behavioural effects of morphine-3-glucuronide and dynorphin a (2–17) following spinal and supraspinal routes of administration. *Pharmacol. Biochem. Behav.* 93 (4), 498–505.
- Honda, M., Okutsu, H., Matsuura, T., Miyagi, T., Yamamoto, Y., Hazato, T., Ono, H., 2001. Spinorphin, an endogenous inhibitor of enkephalin-degrading enzymes, potentiates leu-enkephalin-induced anti-allodynic and antinociceptive effects in mice. *Jpn. J. Pharmacol.* 87, 261–267.
- Hylden, J.L.K., Wilcox, G.L., 1980. Intrathecal morphine in mice: a new technique. *Eur. J. Pharmacol.* 67, 191–194.
- Ji, R.R., Baba, H., Brenner, G.J., Woolf, C.J., 1999. Nociceptive specific activation of ERK in spinal neurons contributes to pain hypersensitivity. *Nat. Neurosci.* 2, 1114–1119.
- Joshua, F.N., Alwin, G.P.S., Michael, A.K., Min, Z., Gavril, W.P., John, E.P., 2002. Genetic dissociation of opiate tolerance and physical dependence in δ -opioid receptor-1 and preproenkephalin knock-out mice. *J. Neurosci.* 22, 10906–10913.
- Kajander, K.C., Sahara, Y., Iadarola, M.J., Bennett, G.J., 1990. Dynorphin increases in the dorsal spinal cord in rats with a painful peripheral neuropathy. *Peptides* 11 (4), 719–728.

- Karim, F., Wang, C.C., Gereau, R.W., 2001. Metabotropic glutamate receptor subtypes 1 and 5 are activators of extracellular signal-regulated kinase signaling required for inflammatory pain in mice. *J. Neurosci.* 21, 3771–3779.
- Kawasaki, Y., Kohno, T., Zhuang, Z.Y., Brenner, G.J., Wang, H., Van, D.M.C., Befort, K., Woolf, C.J., Ji, R.R., 2004. Ionotropic and metabotropic receptors, protein kinase A, protein kinase C, and Src contribute to C-fiber-induced ERK activation and cAMP response element-binding protein phosphorylation in dorsal horn neurons, leading to central sensitization. *J. Neurosci.* 24, 8310–8321.
- Kest, B., Lee, C.E., McLemore, G.L., Inturrisi, C.E., 1996. An antisense oligodeoxynucleotide to the delta opioid receptor (DOR-1) inhibits morphine tolerance and acute dependence in mice. *Brain Res. Bull.* 39, 185–188.
- Kolensnikov, Y.A., Pick, C.G., Ciszewska, G., Pasternak, G.W., 1993. Blockage of tolerance to morphine but not κ opioids by a nitric oxide synthase inhibitor. *Proc. Natl. Acad. Sci. U. S. A.* 90, 5162–5166.
- Komatsu, T., Sakurada, S., Katsuyama, S., Sanai, K., Sakurada, T., 2009b. Mechanism of allodynia evoked by intrathecal morphine-3-glucuronide in mice. *Int. Rev. Neurobiol.* 85, 207–219.
- Komatsu, T., Sakurada, S., Kohno, K., Shiohira, H., Katsuyama, S., Sakurada, C., Tsuzuki, M., Sakurada, T., 2009a. Spinal ERK activation via NO-cGMP pathway contributes to nociceptive behavior induced by morphine-3-glucuronide. *Biochem. Pharmacol.* 78 (8), 1026–1034.
- Komatsu, T., Katsuyama, S., Mizoguchi, H., Sakurada, C., Tsuzuki, M., Sakurada, S., Sakurada, T., 2014. Spinal ERK2 activation through δ 2-opioid receptors contributes to nociceptive behavior induced by intrathecal injection of leucine-enkephalin. *Peptides* 54, 131–139.
- Komatsu, T., Sakurada, C., Sasaki, M., Sanai, K., Tsuzuki, M., Bagetta, G., Sakurada, S., Sakurada, T., 2007. Extracellular signal-regulated kinase (ERK) and nitric oxide synthase mediate intrathecal morphine-induced nociceptive behavior. *Neuropharmacology* 52, 1237–1243.
- Laughlin, T.M., Vanderah, T.W., Lashbrook, J.M., Nichols, M.L., Ossipov, M.H., Porreca, F., Wilcox, G.L., 1997. Spinally administered dynorphin A produces long-lasting allodynia: involvement of NMDA but not opioid receptors. *Pain* 72, 253–260.
- Lever, I.J., Pezet, S., McMahon, S.B., Malcangio, M., 2003. The signaling components of sensory fiber transmission involved in the activation of ERK MAP kinase in the mouse dorsal horn. *Mol. Cell. Neurosci.* 24, 259–270.
- Li, P., Tong, C., Eisenach, J.C., Figueroa, J.P., 1994. NMDA causes release of nitric oxide from rat spinal cord in vitro. *Brain Res.* 637 (1–2), 287–291.
- Lötsch, J., 2009. Pleiotropic effects of morphine-6beta-glucuronide. *Anesthesiology* 110 (6), 1209–1210.
- Malan, T.P., Ossipov, M.H., Gardell, L.R., Ibrahim, M., Bian, D., Lai, J., Porreca, F., 2000. Extrateritorial neuropathic pain correlates with multisegmental elevation of spinal dynorphin in nerve-injured rats. *Pain* 86, 185–194.
- Mao, J., Price, D.D., Mayer, D.J., 1994. Thermal hyperalgesia in association with the development of morphine tolerance in rats: roles of excitatory amino acids receptors and protein kinase C. *J. Neurosci.* 14, 2301–2312.
- Mosberg, H.I., Yeomans, L., Anand, J.P., Porter, V., Sobczyk-Kojiro, K., Traynor, J.R., Jutkiewicz, E.M., 2014. Development of a bioavailable μ opioid receptor (MOPr) agonist, δ opioid receptor (DOPr) antagonist peptide that evokes antinociception without development of acute tolerance. *J. Med. Chem.* 57 (7), 3148–3153.
- Pasternak, G.W., Kolesnikov, Y.A., Babey, A.M., 1995. Perspectives on the N-methyl-D-aspartate/nitric oxide cascade and opioid tolerance. *Neuropsychopharmacology* 13, 309–313.
- Rady, J.J., Holmes, B.B., Fujimoto, J.M., 1999. Antianalgesic action of dynorphine mediated by spinal cholecystokinin. *Proc. Soc. Exp. Biol. Med.* 220, 178–183.
- Rady, J.J., Holmes, B.B., Tseng, H.L., Fujimoto, J.M., 2001. Inverse agonist action of Leu-enkephalin at δ 2-opioid receptor mediates spinal antianalgesia. *J. Pharmacol. Exp. Ther.* 297, 582–589.
- Rattan, A.K., Tejwani, G.A., 1997. Effect of chronic treatment with morphine, midazolam and both together on dynorphin (1–13) levels in the rat. *Brain Res.* 754 (1–2), 239–244.
- Sakurada, T., Komatsu, T., Sakurada, S., 2005. Mechanisms of nociception evoked by intrathecal high-dose morphine. *Neurotoxicology* 26 (5), 801–809.
- Sakurada, T., Wako, K., Sakurada, C., Manome, Y., Tan-No, K., Sakurada, S., Kisara, K., 1996. Spinally-mediated behavioral responses evoked by intrathecal high-dose morphine: possible involvement of substance P in the mouse spinal cord. *Brain Res.* 724, 213–221.
- Shen, K.F., Crain, S.M., 1994. Antagonists at excitatory opioid receptors on sensory neurons in culture increase potency and specificity of opiate analgesics and attenuate development of tolerance/dependence. *Brain Res.* 636, 286–297.
- Silberring, J., Sakurada, T., Nyberg, F., 1992. Dynorphin converting enzyme in the rat spinal cord. Decreased activities during acute phase of adjuvant induced arthritis. *Life Sci.* 50 (12), 839–847.
- Skilling, S.R., Sun, X., Kurtz, H.J., Larson, A.A., 1992. Selective potentiation of NMDA-induced activity and release of excitatory amino acids by dynorphine: possible roles in paralysis and neurotoxicity. *Brain Res.* 575, 272–278.
- Smith, M.T., 2000. Neuroexcitatory effects of morphine and hydromorphone: evidence implicating the 3-glucuronide metabolites. *Clin. Exp. Pharmacol. Physiol.* 27, 524–528.
- Szekeres, P.G., Traynor, J.R., 1997. Delta opioid modulation of the binding of guanosine-5'-O-(35 S)thio)triohisphate to NG108-15 cell membranes: characterization of agonist and inverse agonist effects. *J. Pharmacol. Exp. Ther.* 283, 1276–1284.
- Taguchi, T., Fan, X.-T., Kitamura, K., Oka, T., 1998. Effects of peptidase inhibitors on the enkephalin-induced anti-nociception in rats. *Jpn. J. Pharmacol.* 78, 487–492.
- Thomas, K.A., Hunt, S.P., 1993. The regional distribution of extracellularly regulated kinase-1 and -2. *Neuroscience* 56, 741–757.
- Trujillo, K.A., Aki, H., 1991. Inhibition of morphine tolerance and dependence by the NMDA receptor antagonist MK-801. *Science* 251, 85–87.
- Tseng, L.F., Collins, K.A., Kampine, J.P., 1994. Antisense oligodeoxynucleotide to a δ -opioid receptor selectively blocks the spinal antinociception induced by δ -, but not μ - or κ -opioid receptor agonists in the mouse. *Eur. J. Pharmacol.* 258, R1–R3.
- Tseng, L.F., Narita, M., Mizoguchi, H., Kawai, K., Mizusawa, A., Kamei, J., Suzuki, T., Nagase, H., 1997. Delta-1 opioid receptor-mediated antinociceptive properties of a nonpeptidic delta opioid receptor agonist, (–)TAN-67, in the mouse spinal cord. *J. Pharmacol. Exp. Ther.* 280, 600–605.
- Vanderah, T.W., Bernstein, R.M., Yamamura, H.I., Hruby, V.J., Porreca, F., 1996b. Enhancement of morphine antinociception by CCKB antagonist in mice is mediated via opioid delta receptor. *J. Pharmacol. Exp. Ther.* 278, 212–219.
- Vanderah, T.W., Gardell, L.R., Birge, S.E., Ibrahim, M., Dogrul, A., Zhong, C.M., Zhang, E.T., Malan Jr., T.P., Ossipov, M.H., Lai, J., Porreca, F., 2000. Dynorphine promotes abnormal pain and spinal opioid antinociceptive tolerance. *J. Neurosci.* 20, 7074–7079.
- Vanderah, T.W., Laughlin, T.M., Lashbrook, J.M., Nichols, M.L., Wilcox, G.L., Ossipov, M.H., Malan, T.P., Porreca, F., 1996a. Single intrathecal injections of dynorphin A or des-Tyr-dynorphins produce long-lasting allodynia on rats: blockade by MK-801 but not naloxone. *Pain* 68, 275–281.
- Wagner, R., Deleo, J.A., 1996. Pre-emptive dynorphine and N-methyl-D-aspartate glutamate receptor antagonism alters spinal immunocytochemistry but not allodynia following complete peripheral nerve injury. *Neuroscience* 72, 527–534.
- Wang, Z., Gardell, L.R., Ossipov, M.H., Vanderah, T.W., Brennan, M.B., Hochgeschwender, U., Hruby, V.J., Malan Jr., T.P., Lai, J., Porreca, F., 2001. Pronociceptive actions of dynorphin maintain chronic neuropathic pain. *J. Neurosci.* 21, 1779–1786.
- Watanabe, C., Sakurada, T., Okuda, K., Sakurada, C., Ando, R., Sakurada, S., 2003. The role of spinal nitric oxide and glutamate in nociceptive behaviour evoked by high-dose intrathecal morphine in rats. *Pain* 106, 269–283.
- Wu, W., Liuzzi, F.J., Schinoco, F.P., Depto, A.S., Li, Y., Mong, J.A., Dawson, T., Snyder, S.H., 1994. Neuronal nitric oxide synthase is induced in spinal neurons by traumatic injury. *Neuroscience* 61, 719–726.
- Yaksh, T.L., Harty, G.J., Burton, M., Onofrio, B.M., 1986. High doses of spinal morphine produce a nonopioid receptor-mediated hyperesthesia: clinical and theoretical implications. *Anesthesiology* 64, 590–597.
- Zhu, Y., King, M.A., Schuller, A.G., Nitsche, J.F., Reidl, M., Elde, R.P., Unterwald, E., Pasternak, G.W., Pintar, J.E., 1999. Retention of supraspinal delta-like analgesia and loss morphine tolerance in delta opioid receptor knockout mice. *Neuron* 24, 243–252.



Research paper

Involvement of spinal glutamate in nociceptive behavior induced by intrathecal administration of hemokinin-1 in mice

Chizuko Watanabe^a, Hirokazu Mizoguchi^a, Giacinto Bagetta^b, Shinobu Sakurada^{a,*}^a Department of Physiology and Anatomy, Tohoku Pharmaceutical University, 4-4-1 Komatsushima, Aoba-ku, Sendai 981-8558, Japan^b Department of Pharmacobiology, University of Calabria, Arcavacata di Rende, Cosenza 87036, Italy

HIGHLIGHTS

- Hemokinin-1-induced nociceptive behavior was inhibited by NMDA receptor antagonists.
- Hemokinin-1 produced release of glutamate in the spinal cord.
- Spinal release of glutamate was inhibited by NMDA receptor antagonists.
- The release of glutamate may be involved in the nociceptive behavior of hemokinin-1.

ARTICLE INFO

Article history:

Received 25 December 2015

Received in revised form 10 February 2016

Accepted 14 February 2016

Available online 17 February 2016

Keywords:

Hemokinin-1

Pain

Glutamate

NMDA receptor

Microdialysis

Spinal cord

ABSTRACT

The most recently identified tachykinin, hemokinin-1, was cloned from mouse bone marrow. While several studies indicated that hemokinin-1 is involved in pain and inflammation, the physiological functions of hemokinin-1 are not fully understood. Our previous research demonstrated that the intrathecal (i.t.) administration of hemokinin-1 (0.00625–1.6 nmol) dose-dependently induced nociceptive behaviors, consisting of scratching, biting and licking in mice, which are very similar with the nociceptive behaviors induced by the i.t. administration of substance P. Low-dose (0.0125 nmol) hemokinin-1-induced nociceptive behavior was inhibited by a specific NK₁ receptor antagonist; however, high-dose (0.1 nmol) hemokinin-1-induced nociceptive behavior was not affected.

In the present study, we found that the nociceptive behaviors induced by hemokinin-1 (0.1 nmol) were inhibited by the i.t. co-administration of MK-801 or D-APV, which are NMDA receptor antagonists. Moreover, we measured glutamate in the extracellular fluid of the mouse spinal cord using microdialysis. The i.t. administration of hemokinin-1 produced a significant increase in glutamate in the spinal cord, which was significantly reduced by co-administration with NMDA receptor antagonists. These results suggest that hemokinin-1-induced nociceptive behaviors may be mediated by the NMDA receptor in the spinal cord.

© 2016 Published by Elsevier Ireland Ltd.

1. Introduction

Substance P, neurokinin A, neurokinin B and hemokinin-1 are members of the mammalian tachykinin family. They are derived from distinct preprotachykinin genes: TAC1 encodes substance P and neurokinin A, TAC3 encodes neurokinin B and TAC4 encodes hemokinin-1 [1,2]. Specifically, substance P is mainly distributed in both the peripheral and central nervous systems as a neurotransmitter or neuromodulator in pain processing. Moreover,

substance P is released from small primary afferents and binds to the neurokinin-1 (NK₁) receptor to induce various pharmacological responses. The NK₁ receptor is expressed in the superficial layer of the spinal dorsal horn, which is an important site for pain transmission [3]. Hemokinin-1 is the most recently identified tachykinin peptide, and it resembles substance P in amino acid sequence and has a very high affinity to the NK₁ receptor compared with the NK₂ and NK₃ receptors [4–6]. Hemokinin-1 mRNA is localized in the spinal cord and dorsal root ganglion, as is substance P mRNA [7]. In a previous report, the intrathecal administration of hemokinin-1 induced pain-related behaviors, such as scratching, in rats, and the NK₁ receptor antagonist inhibited pain-related behavior [8]. Interestingly, we demonstrated, in a previous report, that the intrathecal administration of hemokinin-1 induced pain-related responses,

* Corresponding author. Department of Physiology and Anatomy, Tohoku Pharmaceutical University, 4-4-1 Komatsushima, Aoba-ku, Sendai 981-8558, Japan.

E-mail address: s-sakura@tohoku-pharm.ac.jp (S. Sakurada).

consisting of scratching, biting and licking in mice, are very similar with substance P-induced pain behavior; however, the NK₁ receptor antagonist failed to inhibit some of the dose-induced pain-related behaviors [9]. In recent reports, hemokinin-1 is described as a tachykinin with a distinct function compared to substance P in pain and inflammatory processes [8,10–13]. However, these details have not yet been elucidated. On the other hand, glutamate is an important transmitter, as is substance P. Glutamate is the excitatory transmitter that is released from primary afferent synapses in the spinal cord dorsal horn and activates the postsynaptic glutamate receptor. Accordingly, the glutamate receptor in the spinal cord, which is classified into two types, an ionotropic and metabotropic glutamate receptor, plays a crucial role in nociceptive signaling, and both glutamate receptors are also expressed on presynaptic terminals. There are three main classes of ionotropic glutamate receptors, the N-methyl-D-aspartate receptor (NMDAR), the α -amino-3-hydroxy-5-methyl-4-isoxazolepropionic acid receptor (AMPA) and the kainate receptor (KAR) [14,15]. Specifically, the NMDA receptor is suggested to be involved in nociceptive transmission and processing within the spinal cord. Behavior studies indicate that pain-related responses, consisting of scratching, biting and licking, induced by the intrathecal administration of NMDA are inhibited by selective NMDA receptor antagonists [16,17].

In this study, we examined the involvement of the NMDA receptor on the spinally mediated behavioral response induced by hemokinin-1 in mice.

2. Materials and methods

The experiments were performed according to a protocol approved by the Ethics Committee for Animal Experiments in the Tohoku Pharmaceutical University and the National Institutes of Health Guide for the Care and Use of Laboratory Animals. Every effort was made to minimize suffering and the number of animals used.

2.1. Animals

All of the experiments were carried out with male ddY mice weighing 23–25 g (Japan SLC, Hamamatsu, Japan). The mice were maintained in a controlled 12-h light-dark cycle, at a constant temperature of 22–24 °C, at a relative humidity of 55 ± 5%, and had free access to food and water. They were used only once.

2.2. Behavioral observation

The experiments were performed essentially according to the method described by Watanabe et al. [9]. Before drug administration, the mice were adapted to the plastic cage (22.0 cm × 15.0 cm × 12.5 cm) for 60 min, which was used as the observation chamber. The intrathecal administrations (i.t.) were made in conscious mice at the L5 and L6 space in a volume at 5 μ L using the method described by Hylden and Wilcox [18]. The drugs were administered i.t. with a 28-gauge needle attached to a 50- μ L Hamilton syringe. The puncture of the dura was signaled by a slight flick of the tail. Immediately following the i.t. administration, each mouse was returned to its cage and the accumulated time for the nociceptive responses, including scratching, biting and licking, was measured at 5 min intervals.

2.3. Spinal cord microdialysis

Spinal cord microdialysis was conducted according to the modified method of Watanabe et al. [19]. The microdialysis loop-probe consisted of 1.0-cm long microdialysis fibers (active dialysis fibers

of 0.8 cm, with a 0.2-mm inner diameter, a 0.24-mm outer diameter and a 5-kDa molecular weight cut-off). The i.t. catheter was made of a silicon-coated polyethylene tube, which was previously tapered to the appropriate size by heating. Under anesthesia, the microdialysis probe and the i.t. catheter were inserted simultaneously into the mouse spinal cord from L1 to L2, and the tip was placed at L5–L6. After implantation, the dialysis experiment was performed under 1.0% isoflurane anesthesia. The inlet tube of the probe was connected to a syringe pump (EP-800, EICOM, Kyoto, Japan) and was perfused with artificial cerebrospinal fluid (ACSF), containing 126.6 mM NaCl, 2.5 mM KCl, 2.0 mM MgCl₂ and 1.3 mM CaCl₂, at a flow rate of 10 μ L/min, and the dialysate was sampled from the dialysis tube. After the initial 45 min washout period, two samples were collected at 5-min intervals as a control, and the samples were collected at 5-min intervals after treatment with ACSF, hemokinin-1 and the NMDA receptor antagonists with hemokinin-1. Immediately after sample collection, glutamate was analyzed in the dialysate by high-performance liquid chromatography (HPLC: ECD-300, EICOM). The chromatogram was recorded for glutamate on a personal computer using a Data Processor (EPC-500, EICOM).

2.4. Drugs

The following drugs were used: hemokinin-1 (Tocris Cookson, Inc., Bristol, UK); (5S,10R)-(+)-5-Methyl-10,11-dihydro-5H-dibenzo[a,d] cyclohepten-5,10-imine hydrogen maleate (MK-801) and D(-)-2-Amino-5-phosphonopentanoic acid (D-APV) (Sigma-Aldrich, St. Louis, MO, USA). All of the drugs were dissolved in ACSF. MK-801 and D-APV, the NMDA receptor antagonists, were co-administered with hemokinin-1.

2.5. Analyses of data

The total time spent scratching, biting and licking for 5 min is expressed as the mean ± S.E.M. The statistical significance of the differences between the groups was assessed with one-way or two-way analysis of variance (ANOVA) followed by the Bonferroni's test.

3. Results

3.1. Behavioral responses induced by the i.t. administration of hemokinin-1

The i.t. administration of hemokinin-1 produced nociceptive behaviors, consisting of scratching, biting and licking. The time course of the nociceptive responses after the administration of hemokinin-1 peaked at 0–5 min and disappeared within 15 min post-injection. The accumulated nociceptive response time for the 5 min observation following the administration of hemokinin-1 was 58.6 ± 3.7 s. In contrast, the i.t. administration of ACSF did not have an effect (Fig. 1A).

3.2. Antinociceptive effect of the NMDA receptor antagonists

The nociceptive responses elicited by hemokinin-1 were dose-dependently attenuated by the co-administration of MK-801 (2.5–10.0 nmol) or D-APV (0.25–1.0 nmol). The ID₅₀ values of MK-801 and D-APV for the nociceptive responses were 6.10 and 0.72 nmol, respectively (Fig. 2A and B).

3.3. Spinal release of glutamate evoked by the i.t. administration of hemokinin-1

The mean of the baseline samples collected before hemokinin-1 was used for the determination of glutamate in the dorsal spinal

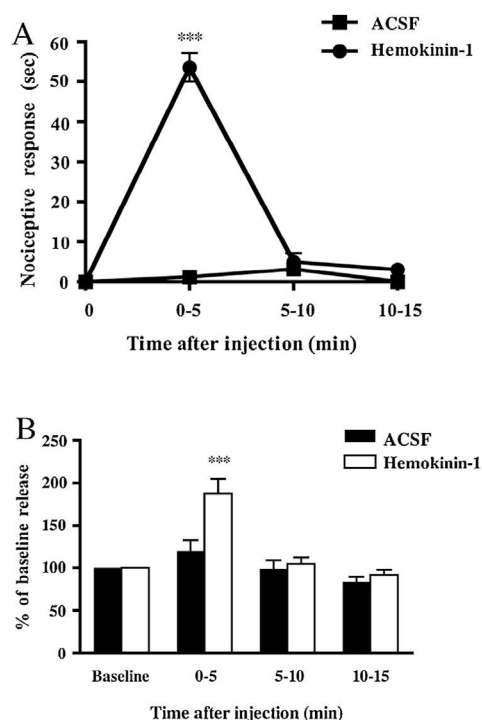


Fig. 1. The time-course of the nociceptive responses (A) and the spinal release of glutamate (B) following the i.t. administration of hemokinin-1. The nociceptive behaviors induced by hemokinin-1 or ACSF are presented as a time-course of the nociceptive response time at 5 min intervals. The concentration of glutamate in the spinal microdialysate is expressed as the percentage change from baseline. Each value represents the mean \pm S.E.M. for 10 or 6 mice. *** P < 0.001 compared with ACSF-treated control group.

cord extracellular fluid. The i.t. administration of hemokinin-1 produced over a 1.5-fold increase of glutamate during the first 5 min compared to ACSF injection. However, the glutamate level during the time interval of 5–15 min was not significantly increased (Fig. 1B).

3.4. Effect of the NMDA receptor antagonists on the spinal release of glutamate

The NMDA receptor antagonists MK-801 (10.0 nmol) and D-APV (1.0 nmol), which completely blocked hemokinin-1-induced the nociceptive responses, when co-administered with the i.t. hemokinin-1, revived the hemokinin-1-evoked increase of glutamate to the control level during the first 5 min (Fig. 3).

4. Discussion

In a previous report, we demonstrated that the intrathecal administration of hemokinin-1 (0.0125–1.6 nmol) dose-dependently produced pain-related responses, which were very similar to substance P-induced pain behaviors. The nociceptive behaviors, after administration of hemokinin-1, peaked at 0–5 min and disappeared within 15 min post-injection. Interestingly, the nociceptive behaviors evoked by a low-dose (0.0125 nmol) of hemokinin-1 were dose-dependently inhibited by the i.t. co-administration of CP-99,994, a non-peptidic NK₁ receptor antagonist, whereas at a high-dose (0.1 nmol), hemokinin-1-induced behaviors were not affected [9]. In the present study, we examined the effects of the NMDA receptor antagonists on the spinally mediated nociceptive behaviors induced by the i.t. administration of high-dose hemokinin-1. Hemokinin-1-induced scratching, biting and licking were dose-dependently inhibited

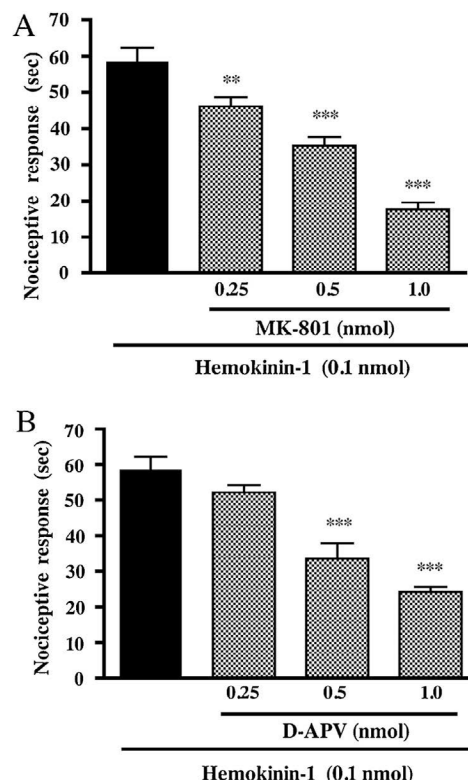


Fig. 2. Effect of MK-801 (A) and D-APV (B) on the behavioral responses induced by the i.t. administration of hemokinin-1. The duration of the nociceptive behaviors induced by hemokinin-1 was measured over a 5-min period starting immediately after administration. MK-801 or D-APV were co-administered i.t. with hemokinin-1. The data represents the mean \pm S.E.M. for 10 mice. *** P < 0.001, ** P < 0.01, compared with the hemokinin-1 alone-treated group.

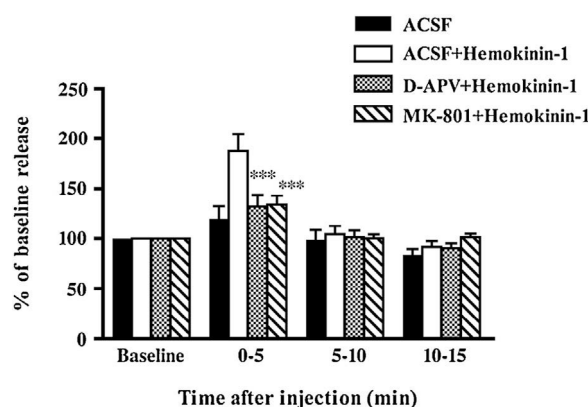


Fig. 3. Effect of MK-801 and D-APV on the increased spinal release of glutamate evoked by the i.t. administration of hemokinin-1. MK-801 or D-APV were co-administered i.t. with hemokinin-1. The concentration of glutamate in the spinal microdialysate is expressed as the percentage change from baseline after hemokinin-1. Each value represents the mean \pm S.E.M. for 6 mice. *** P < 0.001 compared with the hemokinin-1 alone-treated group.

by the co-administration of MK-801 or D-APV, which are the NMDA receptor antagonists. These results suggest that hemokinin-1-induced nociceptive behaviors are mediated through the NMDA receptor. In addition, we measured the release of glutamate using a spinal microdialysis evoked by the i.t. administration of hemokinin-1. As the results indicate, glutamate in the spinal cord was markedly increased in the first 5 min after the i.t. administration of hemokinin-1. The increased release of glutamate in spinal dialysate completely corresponded with the appearance of the nociceptive

responses. Additionally, the co-administration of MK-801 or D-APV completely blocked the increase of glutamate by the i.t. administration of hemokinin-1.

Hemokinin-1 is the newest member of the tachykinin family and was identified in mouse bone marrow in 2000 [20]. The sequence of hemokinin-1 closely resembles substance P, and pharmacological studies demonstrate that substance P and hemokinin-1 are the preferred ligands of the NK₁ receptor. Moreover, hemokinin-1 may also have functions that are similar to those of substance P at the level of the spinal cord [4–6]. On the other hand, several reports, as well as our previous report, suggested that the effects of substance P and hemokinin-1 are slightly different, and the existence of an undefined hemokinin-1 receptor that is not NK₁ receptor has been proposed [8,10]. In the present study, we first demonstrated that hemokinin-1-induced nociceptive behaviors are mediated by the release of glutamate. In other words, hemokinin-1-induced nociceptive behaviors are unrelated to the NK₁ receptor.

Glutamate is the predominant excitatory transmitter in the spinal dorsal horn released from nociceptive primary afferents. The glutamate receptors, both ionotropic and metabotropic, are expressed on the presynaptic and postsynaptic terminals. Although releasing glutamate from nociceptive primary afferents activates the postsynaptic glutamate receptors on the spinal dorsal horn, the presynaptic glutamate receptors in the primary afferent fibers modulate neurotransmitter release. The expression of presynaptic glutamate receptors has been demonstrated in interneurons, particularly on the GABAergic terminus or glycinergic terminus [14,15,21]. In this study, we directly measured the release of glutamate in the spinal dorsal horn evoked by the i.t. administration of hemokinin-1. Interestingly, a significant increase of glutamate in the first 5 min after administration of hemokinin-1 was completely suppressed by the NMDA receptor antagonists as well as in the behavioral study. The present behavioral and microdialysis data indicate that glutamate in the primary afferent fibers is released by hemokinin-1 and activates the postsynaptic glutamate receptor. However, it has not yet been elucidated how hemokinin-1 releases glutamate via the activation of the NMDA receptor in this result.

In conclusion, the present study demonstrated that the nociceptive responses induced by the i.t. administration of hemokinin-1, especially a high-dose of hemokinin-1, may be mediated by the release of glutamate in the spinal dorsal horn. These findings suggest that hemokinin-1 may act an important mediator in spinal pain pathways.

Acknowledgements

This study was supported by JSPS KAKENHI Grant Numbers 23590718 and the MEXT (Ministry of Education, Culture, Sports, Science and Technology)-Supported Program for the Strategic Research Foundation at Private Universities (2015–2019).

References

- [1] T.A. Almeida, J. Rojo, P.M. Nieto, F.M. Pinto, M. Hernandez, J.D. Martin, M.L. Canenas, Tachykinins and tachykinin receptors: structure and activity relationships, *Curr. Med. Chem.* 11 (2004) 2045–2081.
- [2] Y. Zhang, A. Berger, C.D. Milne, C.J. Paige, Tachykinins in the immune system, *Curr. Drug Targets* 7 (2006) 1011–1020.
- [3] T. Hökfelt, J.O. Kellerth, G. Nilsson, B. Pernow, Substance P: localization in the central nervous system and in some primary sensory neurons, *Science* 190 (1975) 889–890.
- [4] F. Bellucci, F. Carini, C. Catalani, P. Cucchi, A. Lecci, S. Meini, R. Patacchini, L. Quartara, R. Ricci, M. Tramontana, S. Giuliani, C.A. Maggi, Pharmacological profile of the novel mammalian tachykinin, hemokinin 1, *Br. J. Pharmacol.* 135 (2002) 266–274.
- [5] M.M. Kurtz, R. Wang, M.K. Clements, M.A. Cascieri, C.P. Austin, B.R. Cunningham, G.G. Chicchi, Q. Liu, Identification, localization and receptor characterization of novel mammalian substance P-like peptides, *Gene* 296 (2002) 205–212.
- [6] O. Morteau, B. Lu, C. Gerard, N.P. Gerard, Hemokinin 1 is a full agonist at the substance P receptor, *Nat. Immunol.* 2 (2001) 1088.
- [7] R.A. Duffy, J.A. Hedrick, G. Randolph, C.A. Morgan, M.E. Cohen-Williams, G. Vassileva, J.E. Lachowicz, M. Lavery, M. Maguire, L.-S. Shan, E. Gustafson, G.B. Varty, Centrally administered hemokinin-1 (HK-1) a neurokinin NK1 receptor agonist, produces substance P-like behavioral effects in mice and gerbils, *Neuropharmacology* 45 (2003) 242–250.
- [8] D. Endo, T. Ikeda, Y. Ishida, D. Yoshioka, T. Nishimori, Effect of intrathecal administration of hemokinin-1 on the withdrawal response to noxious thermal stimulation of the rat hind paw, *Neurosci. Lett.* 392 (2006) 114–117.
- [9] C. Watanabe, H. Mizoguchi, A. Yonezawa, S. Sakurada, Characterization of intrathecally administered hemokinin-1-induced nociceptive behaviours in mice, *Peptides* 31 (2010) 1613–1616.
- [10] R. Naono-Nakayama, N. Sunakawa, T. Ikeda, T. Nishimori, Differential effects of substance P or hemokinin-1 on transient receptor potential channels, TRPV1 TRPA1 and TRPM8, in the rat, *Neuropeptides* 44 (2010) 57–61.
- [11] N. Sunakawa, R. Naono, T. Ikeda, O. Matsushima, S. Sakurada, T. Nishimori, The amino-terminal region of hemokinin-1 regulates the induction of thermal hyperalgesia in rats, *Neuropeptides* 44 (2010) 273–278.
- [12] A. Sakai, K. Takasu, M. Sawada, H. Suzuki, Hemokinin-1 gene expression is upregulated in microglia activated by lipopolysaccharide through NF- κ B and p38 MAPK signaling pathways, *PLoS One* 7 (2012) e32268.
- [13] A. Makino, A. Sasaki, H. Ito, H. Suzuki, Involvement of tachykinins and NK₁ receptor in the joint inflammation with collagen type-II-specific monoclonal antibody-induced arthritis in mice, *J. Nippon. Med. Sch.* 79 (2012) 129–138.
- [14] D.T. Monaghan, R.J. Bridges, C.W. Cotman, The excitatory amino acid receptors: their classes, pharmacology, and distinct properties in the function of the central nervous system, *Annu. Rev. Pharmacol. Toxicol.* 29 (1989) 365–402.
- [15] M. Hollmann, S. Heinemann, Cloned glutamate receptors, *Annu. Rev. Neurosci.* 17 (1994) 31–108.
- [16] L.M. Aanonsen, G.L. Wilcox, Phencyclidine selectively blocks a spinal action of N-methyl-D-aspartate in mice, *Neurosci. Lett.* 67 (1986) 191–197.
- [17] T. Sakurada, Y. Manome, K. Tan-No, S. Sakurada, K. Kisara, The effects of substance P analogues on the scratching, biting and licking response induced by intrathecal injection of N-methyl-D-aspartate in mice, *Br. J. Pharmacol.* 101 (1990) 307–310.
- [18] J.L. Hylden, G.L. Wilcox, Intrathecal morphine in mice: a new technique, *Eur. J. Pharmacol.* 67 (1980) 313–316.
- [19] C. Watanabe, H. Mizoguchi, G. Bagetta, S. Sakurada, The involvement of the spinal release of glutamate and nitric oxide in peripheral noxious stimulation-induced pain-related behaviours-study in mouse spinal microdialysis, *Neurosci. Lett.* 515 (2012) 111–114.
- [20] Y. Zhang, L. Lu, C. Furlonger, G.E. Wu, C.J. Paige, Hemokinin is a hematopoietic-specific tachykinin that regulates B lymphopoiesis, *Nat. Immunol.* 1 (2000) 392–397.
- [21] R. Bardoni, Role of presynaptic glutamate receptors in pain transmission at the spinal cord level, *Curr. Neuropharmacol.* 11 (2013) 477–483.

Note

Analgesic Effects of 1st Generation Anti-histamines in Mice

Mebae Takahashi,^{a,b} Kazuhiro Shima,^a Masahiro Tsuchiya,^c Yoshihiro Hagiwara,^d Hirokazu Mizoguchi,^e Shinobu Sakurada,^e Shunji Sugawara,^a Takuo Fujita,^f Takeshi Tadano,^g Makoto Watanabe,^c Satoshi Fukumoto,^b and Yasuo Endo^{*,a}

^aDivision of Molecular Regulation, Tohoku University Graduate School of Dentistry; Sendai 980–8575, Japan;

^bDivision of Pediatric Dentistry, Tohoku University Graduate School of Dentistry; Sendai 980–8575, Japan; ^cTohoku Fukushi University; Sendai 981–8522, Japan; ^dDepartment of Orthopedic Surgery, Tohoku University Graduate School of Medicine; Sendai 980–8575, Japan; ^eDepartment of Physiology and Anatomy, Tohoku Pharmaceutical University; Sendai 981–8558, Japan; ^fKatsuragi Hospital and Calcium Research Institute; Kishiwada 596–0825, Japan; and ^gDepartment of Health Care Medical Research Venture Business Laboratory, Kanazawa University; Kanazawa 920–1192, Japan.

Received October 4, 2015; accepted December 24, 2015

Pain is sensed, transmitted, and modified by a variety of mediators and receptors. Histamine is a well-known mediator of pain. In addition to their anti-histaminic effects, the classical, or 1st generation, anti-histamines (1st AHs) possess, to various degrees, anti-muscarinic, anti-serotonergic, anti-adrenergic, and other pharmacologic effects. Although there have been attempts to use 1st AHs as analgesics and/or analgesic adjuvants, the advent of non-steroidal anti-inflammatory drugs (NSAIDs) discouraged such trials. We previously reported that in patients with temporomandibular disorders, osteoporosis, and/or osteoarthritis, the analgesic effects of certain 1st AHs (chlorpheniramine and diphenhydramine) are superior to those of the NSAIDs flurbiprofen and indomethacin. Here, we compared analgesic effects among 1st AHs and NSAIDs against responses shown by mice to intraperitoneally injected 0.7% acetic acid. Since 1st AHs are water soluble, we selected water-soluble NSAIDs. For direct comparison, drugs were intravenously injected 30 min before the above tests. Histamine-H1-receptor-deficient (HIR-KO) mice were used for evaluating H1-receptor-independent effects. The tested 1st AHs (especially cyproheptadine) displayed or tended to display analgesic effects comparable to those of NSAIDs in normal and HIR-KO mice. Our data suggest that the anti-serotonergic and/or anti-adrenergic effects of 1st AHs make important contributions to their analgesic effects. Moreover, combination of a 1st AH with an NSAID (cyclooxygenase-1 inhibitor) produced remarkably potent analgesic effects. We propose that a 1st AH, by itself or in combination with a cyclooxygenase-1 inhibitor, should undergo testing to evaluate its usefulness in analgesia.

Key words anti-histamine; analgesic effect; non-steroidal anti-inflammatory drug; cyproheptadine; pain; histamine-H1-receptor

Histamine is a well-known mediator of pain and/or itch.¹⁾ Consequently, many attempts have been made to use classical, or 1st generation, anti-histamines (1st AHs) as analgesics and/or analgesic adjuvants.^{2–4)} However, the advent of various types of non-steroidal anti-inflammatory drugs (NSAIDs), and their rapid spread, seems to have discouraged such efforts to promote 1st AHs as analgesics.

Pain in both masticatory muscles and temporomandibular joints is a major sign of temporomandibular disorders (TMD), which are believed to result from strenuous, improper, or abnormal occlusion, including bruxism and/or prolonged clenching. Interestingly, Watanabe *et al.* noted that the analgesic effect of chlorpheniramine (a 1st AH) is superior to that of flurbiprofen (an NSAID) in patients with TMD.⁵⁾ Bone-joint-muscle pain is commonly experienced by elderly patients with osteoporosis (OP) and/or osteoarthritis (OA). Recently, Fujita *et al.* reported that the analgesic effect of diphenhydramine (a 1st AH) is superior to that of indomethacin (an NSAID) in patients with OP and/or OA.⁶⁾ It is notable that muscle fatigue and pain are common factors among TMD, OP, and OA, and that histamine has been suggested to be causally involved in muscle fatigue and pain.^{7–9)} Collectively, these reports encourage the view that 1st AHs may indeed exert analgesic effects in patients with TMD, OP, and/or OA.

However, pain is transmitted, sensed, and modified *via* a variety of mediators other than histamine and its receptors. These mediators include serotonin, noradrenaline, bradykinin, and prostaglandins. In addition to their antagonistic effects against the histamine-H1-receptor (H1R), 1st AHs possess, to various degrees, anti-muscarinic, anti-serotonergic, anti-adrenergic, and other pharmacologic actions.^{2,10,11)} For example, upon local application, diphenhydramine (a typical 1st AH) is reportedly as effective at pain prevention as the local anesthetic drug lidocaine.¹²⁾ Thus, it is very likely that effects other than antagonism toward H1R are involved in the analgesic effects of 1st AHs.

Here, we examined (i) whether 1st AHs do indeed display analgesic effects, and (ii) how antagonism toward receptors other than H1R might contribute to such analgesic effects. Examining the writhing responses of mice to intraperitoneally injected dilute acetic acid is widely used as a method for evaluating the analgesic or pain-augmenting effects of test materials.^{13,14)} Using this method, we compared analgesic effects among 1st AHs and NSAIDs. Since 1st AHs are water-soluble, we selected water-soluble NSAIDs (diclofenac, indomethacin, and meloxicam). For easy and direct comparison, each drug was intravenously injected 30 min before the writhing test. To evaluate the involvement of antagonism toward receptors other

*To whom correspondence should be addressed. e-mail: endo@dent.tohoku.ac.jp

than H1R, we used mice deficient in H1R (H1R-KO mice).

MATERIALS AND METHODS

Mice BALB/c and C57BL/6 mice were purchased from CREA (Tokyo, Japan), while C3H/HeN and ddY mice were from SLC (Hamamatsu, Japan). H1R-KO mice (C57BL/6 background) were established as previously described,¹⁵⁾ bred in our laboratory, and confirmed by genotyping during this study. The experiments were performed in accordance with International Association for the Study of Pain (IASP) guidelines for the study of pain in animals.¹⁶⁾ All experiments

complied with the Guidelines for Care and Use of Laboratory Animals in Tohoku University and were approved by the Committee on Animal Research of Tohoku University.

Reagents Acetic acid was purchased from Wako Pure Chemical Industries, Ltd. (Osaka, Japan). The drugs used in this study are listed in Table 1. All were dissolved in sterile saline, with the pH of the solutions being adjusted to 7 if necessary with NaOH or HCl, and intravenously injected into mice (0.1 mL/10 g body weight). Experimental protocols and doses are described in the text or the relevant figure legend.

Writhing Test Writhing (abdominal constriction) was induced by intraperitoneal injection of 0.7% (v/v) acetic acid

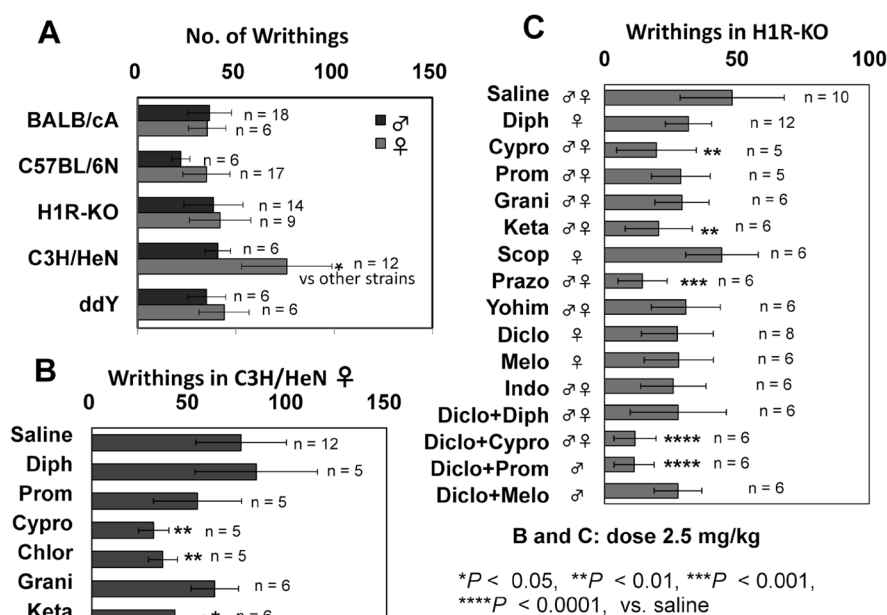


Fig. 1. Writhing Responses in Various Strains of Mice, with Separate Data for Males and Females (A), Together with Analgesic Effects of 1st AHs (and Other Drugs) in Female C3H/HeN (B) and in Male and/or Female H1R-KO (C) Mice

The dose of each tested drug was 2.5 mg/kg (6–8 μ mol/kg), and this was intravenously injected 30 min before the writhing test. The number of mice in each group is shown in the figures. Wherever both genders are shown in C, equal numbers of male and female mice were used. * $p < 0.05$, ** $p < 0.01$, *** $p < 0.001$, and **** $p < 0.0001$ vs. saline group.

Table 1. Drugs Tested in This Study

Name (abbreviation and molecular weight)	Note
1st AHs	
Diphenhydramine hydrochloride (Diph, 291) [§]	An ethanolamine [sedative (relatively strong), anti-motion sickness, local anesthetic, anti-cholinergic]
S-(+)-Chlorpheniramine maleate (Chlor, 391)*	An alkylamine [sedative (relatively weak)]
Promethazine hydrochloride (Prom, 321) [¶]	A phenothiazine [local anesthetic, anti-motion-sickness, anti-cholinergic, anti-adrenergic]
Cyproheptadine hydrochloride (Cypro, 351)*	A piperidine [anti-serotonergic (strong 5HT _{2A} receptor antagonist), anti-motion sickness]
NSAIDs	
Diclofenac sodium (Diclo, 318) [¶]	A phenylacetic acid [cyclooxygenase (Cox)-1 inhibitor]
Meloxicam sodium hydrate (Melo, 373)*	An oxicam [Cox-2 inhibition > Cox-1 inhibition]
Indomethacin (Indo, 358) [¶]	An indoleacetic acid [Cox-1 inhibitor]
Anti-cholinergic drug	
(-)-Scopolamine hydrochloride (Scop, 340)*	Anti-motion sickness; muscarinic acetylcholine receptor antagonist
Anti-serotonergic drugs	
Ketanserin tartrate (Keta, 395)*	5HT _{2A} receptor antagonist
Granisetron hydrochloride (Grani, 348)*	5HT ₃ receptor antagonist
Anti-adrenergic drugs	
Prazosin hydrochloride (Prazo, 420) [¶]	α_1 Receptor antagonist
Yohimbine hydrochloride (Yohim, 391) [¶]	α_2 Receptor antagonist

*From Sigma (St. Louis, MO, U.S.A.), [§]from Kowa Company, Ltd. (Nagoya, Japan), [¶]from Wako Pure Chemical Industries, Ltd. (Osaka, Japan).

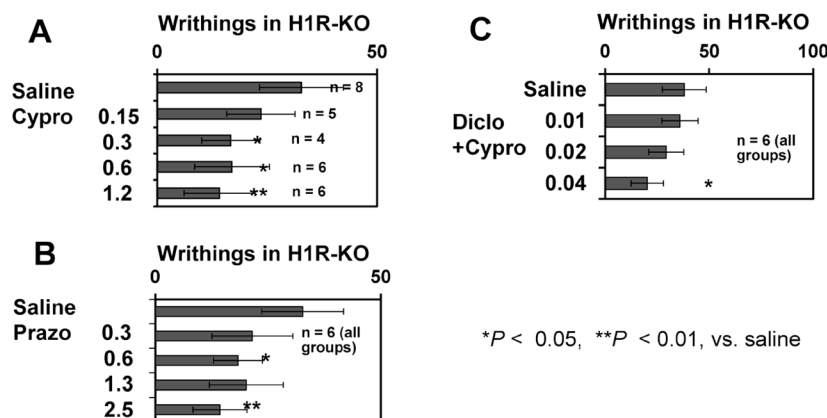


Fig. 2. Dose-Dependency of the Analgesic Effects of Cyproheptadine (A), Prazosin (B), and Diclofenac+Cyproheptadine (C) in the Writhing Test Using H1R-KO

The indicated doses (mg/kg) were intravenously injected 30 min before the writhing test. In experiment C, a mixture of cyproheptadine and diclofenac was injected, with the two drugs being given at equal doses (which are indicated in the figure). In A–C, similar or equal numbers of male and female mice were used, with the total numbers being shown in the figures. * $p < 0.05$ and ** $p < 0.01$ vs. saline group.

(0.1 mL/10 g body weight). The number of writhing movements (“writhings”) was counted in the period from 5 to 30 min after the acetic acid injection.

Data Analysis Experimental values are each given as the mean \pm standard deviation (S.D.). The statistical significance of differences was evaluated using a Bonferroni multiple-comparison test after an ANOVA, p values less than 0.05 being considered significant.

RESULTS

H1R-KO and C3H/HeN Mice Are Useful for the Writhing Test The nociceptive responses of H1R^{-/-} mice are reportedly lower than those of H1R^{+/+} mice in various tests, including the writhing test.¹⁷⁾ However, in the present study, the writhing responses of male and female H1R-KO mice were not different from those shown by male and female C57BL/6N mice (nor from those of male or female BALB or male C3H/HeN mice) (Fig. 1A). We suppose that this may be due to the fact that wild-type C57BL/6 strain used in the present study was commercially obtained, but not derived from the strain used in the original study.¹⁷⁾ In addition, the following factors may also be involved. (i) The sensitivities to nociceptive stimuli and/or to analgesic drugs are reportedly different among strains of mice.¹⁸⁾ (ii) It has also been reported that complete inactivation of a gene may result in altered expressions of related genes or physiologic compensation for the loss of the gene product.¹⁹⁾ Thus, the pain sensitivity of H1R-KO mice might have changed during repeated breeding cycles. In any event, the finding that H1R-KO mice exhibit writhing responses suggests that H1R-KO mice are useful for examining the analgesic effects of 1st AHs that are not mediated *via* H1R. Also note that there was no significant gender difference in H1R-KO mice. Thus, in the following experiments on H1R-KO mice, both males and females were used, these being available to us since they were bred in our laboratory. We confirmed our previous finding²⁰⁾ that the writhing response of female C3H/HeN mice is, or tends to be, greater than those of other strains. Thus, this strain may be convenient for evaluating the analgesic effects of test samples.

Effects of 1st AHs and NSAIDs in C3H/HeN and H1R-

KO Mice The molecular weights of the tested drugs are similar (around 300 to 400) (Table 1). In the experiments shown in Figs. 1B and C, the dose of each drug was 2.5 mg/kg (6–8 μ mol/kg). In female C3H/HeN mice, two of the four 1st AHs tested, namely cyproheptadine and chlorpheniramine, exhibited significant analgesic effects (Fig. 1B). In H1R-KO mice, among the three 1st AHs tested only cyproheptadine exhibited a significant analgesic effect (Fig. 1C), although diphenhydramine and promethazine tended to be analgesic. None of the three NSAIDs tested had significant analgesic effects, although they tended to be analgesic (Fig. 1C). These results indicate that (i) some 1st AHs (especially cyproheptadine) do indeed have analgesic effects, and (ii) such analgesia may involve effect(s) other than H1R-mediated anti-histaminergic effects.

Effects of Anti-serotonergic, Anti-cholinergic, and Anti-adrenergic Drugs Notably, cyproheptadine had a powerful analgesic effect in the writhing test in both C3H/HeN and H1R-KO mice (Figs. 1B, C). In both C3H/HeN and H1R-KO mice, ketanserin significantly reduced the writhing response (Figs. 1B, C), although granisetron only tended to be analgesic in these strains. The α 1-adrenergic antagonist prazosin was effective, too, although there was no α 2-mediated analgesic effect with yohimbine (Fig. 1C). Unlike these antagonists, the muscarinic acetylcholine-receptor antagonist scopolamine was not effective at all (Fig. 1C). These results suggest that anti-serotonergic (especially 5HT2A-blocking) effects and anti-adrenergic (especially α 1-blocking) effects may be involved in the analgesic effects shown by 1st AHs.

Minimum Effective Doses of Cyproheptadine, Ketanserin, and Prazosin in H1R-KO Mice The analgesic effect of cyproheptadine was dose-dependent, and was evident even at 0.3 mg/kg in H1R-KO mice (Fig. 2A). However, ketanserin (which was analgesic at 2.5 mg/kg; see above) was not analgesic at 1.2 mg/kg or less (data not shown). An analgesic effect of prazosin was evident even at 0.6 mg/kg (Fig. 2B). These results suggest that (i) inhibition of 5HT2A receptors and inhibition of α 1-adrenergic receptors are each effective at producing some degree of analgesia, and (ii) inhibition of 5HT2A receptors may contribute to the analgesic effect of cyproheptadine.

Effects of an NSAID+a 1st AH Finally, we examined the effect of a combination of an NSAID plus a 1st AH in HIR-KO mice (Fig. 1C lower portions). Either cyproheptadine (a 1st AH with anti-5HT_{2A} effects) or promethazine (a 1st AH with multiple effects, including anti-adrenergic effects), when combined with the NSAID diclofenac, produced markedly potent analgesic effects, although these effects were not significantly greater than that of cyproheptadine alone. It should be noted that the analgesic effects of diclofenac and promethazine, by themselves, were not significant (Fig. 1C). Cyproheptadine+diclofenac was significantly effective when each was at 0.04 mg/kg (Fig. 2C). However, we observed no augmented effect by combining diclofenac with either diphenhydramine or meloxicam. These results suggest that a combination of cyproheptadine or promethazine with a cyclooxygenase-1 inhibitor induces a very potent analgesic effect.

DISCUSSION

HIRs are distributed widely in a variety of cells, including central nervous system and primary sensory neurons.^{21,22} First AHs have been suggested to have analgesic effects on both somatic and visceral pain.¹⁷ In the present study, 1st AHs exhibited analgesic effects in the writhing test in both C3H/HeN and HIR-KO mice.

As described in Introduction and Table 1, 1st AHs have several pharmacological effects other than anti-histaminic effects. All the 1st AHs used in the present study have some degree of anti-serotonergic activity [strong (cyproheptadine), medium (promethazine and diphenhydramine), or weak (chlorpheniramine)].¹⁰ The 5HT_{2A} antagonist ketanserin exhibited an analgesic effect in both C3H/HeN and HIR-KO mice (Figs. 1B, C). It has been reported that serotonin may mediate mainly pronociceptive effects in the periphery and both antinociceptive and pronociceptive effects within the central nervous system.^{23,24} It is well known that both histamine and serotonin are local mediators of pain and inflammation.¹¹ We suggested previously that histamine is locally involved both in muscle fatigue and in musculoskeletal pain in TMD,^{5,7,9} and serotonin has also been suggested to be involved in TMD as a local pain mediator.²⁵ Our recent clinical study—in which ointments of diphenhydramine and indomethacin were painted over the area where patients with OA and/or OP reported pain sensation—demonstrated an analgesic effect of diphenhydramine that was superior to that of indomethacin.⁶ Moreover, the pain-relieving effect of oral chlorpheniramine in TMD is greater than that of oral flurbiprofen (an NSAID).⁵ Collectively, those observations lead us to suppose that the analgesic effects of 1st AHs may be displayed mainly *via* their local effects, involving blocking effects on peripheral histamine and serotonin receptors.

Adrenergic α 1-receptors have been reported to be involved in various nociceptive responses, including writhing in mice,²⁶ ATP receptor-mediated nociception in rats,²⁷ streptozotocin-induced hyperalgesia in mice,²⁸ and thermal hyperalgesia in humans.²⁹ Indeed, the α 1-antagonist prazosin exhibited a strong analgesic effect in the present writhing test, too. Thus, the anti-adrenergic effects of 1st AHs may also contribute to their analgesic effects.

Interestingly, a combination of a 1st AH (cyproheptadine or promethazine) with the NSAID diclophenac (cyclooxy-

genase-1 inhibitor) had the strongest analgesic effect seen in the present study (Fig. 1C). An analgesic effect of combined cyproheptadine+diclophenac was detected when each was at as low a dose as 0.04 mg/kg (Fig. 2C). It was recently reported that prostaglandin E₂, which is released from epithelial cells in response to various inflammatory stimuli, stimulates mast cells to release histamine, leading to inflammation.³⁰ Moreover, prostaglandin E₂ is released into the peritoneal cavity by dilute acetic acid.³¹ These findings suggest that concomitantly blocking histaminergic, serotonergic, and adrenergic receptors, together with an inhibition of prostaglandin synthesis, may lead to a particularly powerful analgesic effect.

In conclusion, in mice, some 1st AHs displayed potent analgesic effects comparable to or greater than those of NSAIDs. Anti-histaminergic, anti-serotonergic (especially anti-5HT_{2A}), and anti-adrenergic (especially anti- α 1) effects of 1st AHs may be involved in their analgesic effects. We propose that administration of a 1st AH, either by itself or in combination with an NSAID (cyclooxygenase-1 inhibitor), warrants evaluation as a useful analgesic strategy, especially in patients with TMD, OP, and/or OA (see Introduction).

Acknowledgments We are grateful to Dr. R. Timms (Birmingham, U.K.) for editing the manuscript, and to Prof. Kazuhiko Yanai and Dr. Takeo Yoshikawa (Department of Pharmacology, Tohoku University Graduate School of Medicine, Sendai, Japan) for providing HIR-KO mice. This study was supported by Grants from the Japan Society for the Promotion of Science to M. Watanabe (23390439) and M. Tsuchiya (24390429 and 25670813).

Conflict of Interest The authors declare no conflict of interest.

REFERENCES

- 1) Tiligada E, Kyriakidis K, Chazot PL, Passani MB. Histamine pharmacology and new CNS drug targets. *CNS Neurosci. Ther.*, **17**, 620–628 (2011).
- 2) Rumore MM, Schlichting DA. Clinical efficacy of antihistaminics as analgesics. *Pain*, **25**, 7–22 (1986).
- 3) Raffa RB. Antihistamines as analgesics. *J. Clin. Pharm. Ther.*, **26**, 81–85 (2001).
- 4) Farzin D, Asghari L, Nowrouzi M. Rodent antinociception following acute treatment with different histamine receptor agonists and antagonists. *Pharmacol. Biochem. Behav.*, **72**, 751–760 (2002).
- 5) Watanabe M, Tabata T, Huh JI, Inai T, Tsuboi A, Sasaki K, Endo Y. Possible involvement of histamine in muscular fatigue in temporomandibular disorders: animal and human studies. *J. Dent. Res.*, **78**, 769–775 (1999).
- 6) Fujita T, Ohue M, Fujii Y, Jotoku T, Miyauchi A, Takagi Y, Tsuchiya M, Endo Y. Prompt analgesic effect of antihistaminic diphenhydramine ointment on bone-joint-muscle pain, as assessed by skin impedance. *Pharmacology*, **92**, 158–166 (2013).
- 7) Endo Y, Tabata T, Kuroda H, Tadano T, Matsushima K, Watanabe M. Induction of histidine decarboxylase in skeletal muscle in mice by electrical stimulation, prolonged walking and interleukin-1. *J. Physiol.*, **509**, 587–598 (1998).
- 8) Nijima-Yaoita F, Tsuchiya M, Ohtsu H, Yanai K, Sugawara S, Endo Y, Tadano T. Roles of histamine in exercise-induced fatigue: favouring endurance and protecting against exhaustion. *Biol. Pharm. Bull.*, **35**, 91–97 (2012).
- 9) Yoneda H, Nijima-Yaoita F, Tsuchiya M, Kumamoto H, Watanabe

- M, Ohtsu H, Yanai K, Tadano T, Sasaki K, Sugawara S, Endo Y. Roles played by histamine in strenuous or prolonged masseter muscle activity in mice. *Clin. Exp. Pharmacol. Physiol.*, **40**, 848–855 (2013).
- 10) Rumore MM, Schlichting DA. Analgesic effects of antihistaminics. *Life Sci.*, **36**, 403–416 (1985).
 - 11) Garrison JC. Histamine, bradykinin, 5-hydroxytryptamine, and their antagonists. *Goodman and Gilman's the Pharmacological Basis of Therapeutics* (Gilman AG, Rall TW, Nies AS, Taylor P eds.) 8th ed., Pergamon Press, New York, pp. 575–599 (1990).
 - 12) Apiliogullari S, Keles B, Apiliogullari B, Balasar M, Yilmaz H, Duman A. Comparison of diphenhydramine and lidocaine for prevention of pain after injection of propofol: a double-blind, placebo-controlled, randomized study. *Eur. J. Anaesthesiol.*, **24**, 235–238 (2007).
 - 13) Vinegar R, Truax JF, Selph JL, Hohnston PR. Antagonism of pain and hyperalgesia. *Handbook of Experimental Pharmacology*. (Vane JR, Ferreira SH eds.) Vol. 5/II, Springer-Verlag, Berlin, pp. 208–222 (1979).
 - 14) Ueno A, Matsumoto H, Naraba H, Ikeda Y, Ushikubi F, Matsuoka T, Narumiya S, Sugimoto Y, Ichikawa A, Oh-ishi S. Major roles of prostanoïd receptors IP and EP3 in endotoxin-induced enhancement of pain perception. *Biochem. Pharmacol.*, **62**, 157–160 (2001).
 - 15) Inoue I, Yanai K, Kitamura D, Taniuchi I, Kobayashi T, Niimura K, Watanabe T, Watanabe T. Impaired locomotor activity and exploratory behavior in mice lacking histamine H₁ receptors. *Proc. Natl. Acad. Sci. U.S.A.*, **93**, 13316–13320 (1996).
 - 16) Zimmermann M. Ethical guidelines for investigations of experimental pain in conscious animals. *Pain*, **16**, 109–110 (1983).
 - 17) Mobarakeh JI, Sakurada S, Katsuyama S, Kutsuwa M, Kuramasu A, Lin ZY, Watanabe T, Hashimoto Y, Watanabe T, Yanai K. Role of histamine H1 receptor in pain perception: a study of the receptor gene knockout mice. *Eur. J. Pharmacol.*, **391**, 81–89 (2000).
 - 18) Mogil JS. The genetic mediation of individual differences in sensitivity to pain and its inhibition. *Proc. Natl. Acad. Sci. U.S.A.*, **96**, 7744–7751 (1999).
 - 19) Rudmann DG, Durham SK. Utilization of genetically altered animals in the pharmaceutical industry. *Toxicol. Pathol.*, **27**, 111–114 (1999).
 - 20) Kim S, Seiryu M, Okada H, Kuroishi T, Takano-Yamamoto T, Sugawara S, Endo Y. Analgesic effects of the non-nitrogen-containing bisphosphonates etidronate and clodronate, independent of anti-resorptive effects on bone. *Eur. J. Pharmacol.*, **699**, 14–22 (2013).
 - 21) Hill SJ, Ganellin CR, Timmerman H, Schwartz JC, Shankley NP, Young JM, Schunack W, Levi R, Haas HL. International Union of Pharmacology. XIII. Classification of histamine receptors. *Pharmacol. Rev.*, **49**, 253–278 (1997).
 - 22) Kashiba H, Fukui H, Morikawa Y, Senba E. Gene expression of histamine H1 receptor in guinea pig primary sensory neurons: a relationship between H1 receptor mRNA-expressing neurons and peptidergic neurons. *Brain Res. Mol. Brain Res.*, **66**, 24–34 (1999).
 - 23) Bardin L. The complex roles of serotonin and 5-HT receptors in chronic pain. *Behav. Pharmacol.*, **22** (5 and 6), 390–404 (2011).
 - 24) Viguier F, Michot B, Hamon M, Bourgoin S. Multiple roles of serotonin in pain control mechanisms: implications of 5-HT7 and other 5-HT receptor types. *Eur. J. Pharmacol.*, **716**, 8–16 (2013).
 - 25) Gerdle B, Ghafouri B, Ernberg M, Larsson N. Chronic musculoskeletal pain: review of mechanisms and biochemical biomarkers as assessed by the microdialysis technique. *J. Pain Res.*, **7**, 313–326 (2014).
 - 26) Bezerra MM, Lima V, Girão VCC, Teixeira RC, Graça JRV. Antinociceptive activity of sildenafil and adrenergic agents in the writhing test in mice. *Pharmacol. Rep.*, **60**, 339–344 (2008).
 - 27) Meisner JG, Waldron JB, Sawynok J. α 1-Adrenergic receptors augment P2X₃ receptor-mediated nociceptive responses in the uninjured state. *J. Pain*, **8**, 556–562 (2007).
 - 28) Bujalska M, Arażna M, Makulska-Nowak H, Gumulka SW. α 1- and α 2-Adrenoceptor antagonists in streptozotocin- and vincristine-induced hyperalgesia. *Pharmacol. Rep.*, **60**, 499–507 (2008).
 - 29) Drummond PD. α 1-Adrenoceptors augment thermal hyperalgesia in mildly burnt skin. *Eur. J. Pain*, **13**, 273–279 (2009).
 - 30) Morimoto K, Shirata N, Taketomi Y, Tsuchiya S, Segi-Nishida E, Inazumi T, Kabashima K, Tanaka S, Murakami M, Narumiya S, Sugimoto Y. Prostaglandin E₂-EP3 signaling induces inflammatory swelling by mast cell activation. *J. Immunol.*, **192**, 1130–1137 (2014).
 - 31) Murata T, Ushikubi F, Matsuoka T, Hirata M, Yamasaki A, Sugimoto Y, Ichikawa A, Aze Y, Tanaka T, Yoshida N, Ueno A, Oh-ishi S, Narumiya S. Altered pain perception and inflammatory response in mice lacking prostacyclin receptor. *Nature*, **388**, 678–682 (1997).



Contents lists available at ScienceDirect

Allergology International

journal homepage: <http://www.elsevier.com/locate/alit>

Original article

The involvement of central nervous system histamine receptors in psychological stress-induced exacerbation of allergic airway inflammation in mice



Tomomitsu Miyasaka^{a,*}, Kaori Okuyama-Dobashi^{a,c}, Chiaki Masuda^a, Shunya Iwami^a, Miki Sato^a, Hirokazu Mizoguchi^b, Tasuku Kawano^a, Yuichi Ohkawara^a, Shinobu Sakurada^b, Motoaki Takayanagi^a, Isao Ohno^a

^a Department of Pathophysiology, Tohoku Pharmaceutical University, Sendai, Japan

^b Department of Physiology and Anatomy, Tohoku Pharmaceutical University, Sendai, Japan

ARTICLE INFO

Article history:

Received 29 January 2016

Received in revised form
17 May 2016

Accepted 25 May 2016

Available online 11 August 2016

Keywords:

Bronchial asthma

Epinastine

Histamine receptors

Psychological stress

Thiopramide

Abbreviations:

IL, interleukin; HR, histamine receptor; Th2, type 2 T-helper; Th1, type 1 T-helper; FEV₁, forced expiratory volume in 1 s; TNF- α , tumor necrosis factor- α ; CNS, central nervous system; OVA, ovalbumin; RS, restraint stress; FSS, forced swimming stress; PBS, phosphate-buffered saline; ELISA, enzyme-linked immunosorbent assay; BSA, bovine serum albumin; PAS, periodic acid–Schiff; PC₂₀₀, lung resistance to 200% above baseline; SEM, standard error of the mean; HPA, hypothalamic-pituitary-adrenal; CRH, corticotropin-releasing hormone

ABSTRACT

Background: Psychological stress is one of the major risk factors for asthma exacerbation. Although histamine in the brain acts as an excitatory and inhibitory neurotransmitter associated with psychological stress, the contribution of brain histamine to psychological stress-induced exacerbation of asthma remains unclear. The objective of this study was to investigate the role of histamine receptors in the CNS on stress induced asthma aggravation.

Methods: We monitored the numbers of inflammatory cells and interleukin (IL)-13 levels in bronchoalveolar lavage fluid, airway responsiveness to inhaled methacholine, mucus secretion in airway epithelial cells, and antigen-specific IgE contents in sera in a murine model of stress-induced asthma treated with epinastine (an H₁R antagonist), thiopramide (an H_{3/4}R antagonist), or solvent.

Results: All indicators of stress-induced asthma exacerbation were significantly reduced in stressed mice treated with epinastine compared with those treated with solvent, whereas treatment with thiopramide did not reduce the numbers of inflammatory cells in the stressed mice.

Conclusions: These results suggest that H₁R, but not H_{3/4}R, may be involved in stress-induced asthma exacerbations in the central nervous system.

Copyright © 2016, Japanese Society of Allergology. Production and hosting by Elsevier B.V. This is an open access article under the CC BY-NC-ND license (<http://creativecommons.org/licenses/by-nc-nd/4.0/>).

Introduction

Asthma is characterized by chronic airway inflammation in response to various types of inherited and environmental factors, which leads to wheezing, coughing, tightness in the chest, and shortness of breath. Increasing evidence has indicated that asthma is not a disease but a syndrome with heterogeneous pathobiology, clinical course, and therapeutic response to medicines. Therefore, asthma phenotypes based on pathological and clinical features

* Corresponding author. Department of Pathophysiology, Tohoku Pharmaceutical University, 4-4-1 Komatsushima, Aoba-ku, Sendai, Miyagi 981-8558, Japan.

E-mail address: t-miya13@tohoku-mpu.ac.jp (T. Miyasaka).

Peer review under responsibility of Japanese Society of Allergology.

^c Present address: Department of Microbiology, Division of Medicine, Interdisciplinary Graduate School of Medicine and Engineering (Faculty of Medicine), University of Yamanashi, Yamanashi, Japan.

such as types of airway inflammation and risk factors for exacerbations have been proposed to identify more effective asthma therapies specific for each phenotype.¹

In asthma pathophysiology, type 2 T-helper (Th2) cytokines, such as interleukin (IL)-4, IL-5, and IL-13, play pivotal roles in regulating the behavior of inflammatory cells; inducing B cell isotype switching to produce IgE; and promoting the accumulation, activation, and prolonged survival of eosinophils. These events initiate and maintain the cardinal features of asthma, such as asthmatic airway inflammation, thereby accelerating airway responsiveness and epithelial mucus secretion.²

Psychological and psychosocial stressors have been long recognized as important universal risk factors for asthma exacerbations,^{3–9} which are accompanied by aggravation of airway inflammation attributable to further skewing towards a Th2-dominant cytokine profile.^{10–14} The cognitive processes accompanying psychological stress are deeply connected to asthma exacerbations. Activation of the anterior cingulate cortex and insula by psychological stimuli exhibited a greater decrease in forced expiratory volume in 1 s (FEV₁), increased recruitment of eosinophils, and diminished glucocorticoid inhibition of TNF- α production.¹⁵ The intensity of activation in the anterior insula in response to asthma-relevant psychological stimuli is correlated with the severity of airway inflammation evoked by allergen inhalation.¹⁶ Stress-induced brain activation results in the production and release of stress neuropeptides, such as opioid peptides, substance P, and histamine, which bind to membrane receptors in the central nervous system (CNS).^{17,18} However, the molecular mechanism linking psychological stress perceived in the CNS to exacerbations of asthma pathophysiology in airways is not yet fully understood.

Histamine receptors (HRs) are a group of seven-transmembrane G protein-coupled receptors classified to four major subtypes (H₁R, H₂R, H₃R, and H₄R), which are expressed throughout the body including in immune cells, gastric mucosal cells, and neurons.¹⁹ Histamine in the brain is produced by histaminergic neurons comprising the tuberomammillary nucleus in the posterior hypothalamus. Projections from the tuberomammillary nucleus extend to almost all areas in the brain and are implicated in basic homeostatic and higher brain functions such as arousal, cognition, nociception, and responses to perceived stress.^{19–21}

In the present study, we aimed to determine the role of HRs in the CNS in psychological stress-induced asthma exacerbations using a murine model of stress asthma. We found that H₁R in the CNS were required for exacerbation of asthmatic airway responses induced by the stress exposure. In contrast, H_{3/4}R might be irrelevant in this process or function in the negative feedback control of stressor signals in asthma exacerbation.

Methods

Mice and ethical statement

Specific pathogen-free female C57BL/6 mice were purchased from CLEA Japan (Osaka, Japan). All mice were kept under specific pathogen-free conditions at the Institute for Animal Experimentation, Tohoku Pharmaceutical University, Sendai, Japan. Mice were housed under a 12 h/12 h light/dark cycle at a constant temperature (22 \pm 2 °C). Sterilized food and water were available ad libitum. All experimental procedures involving animals were approved by the Committee of Animal Experiments at Tohoku Pharmaceutical University (approval numbers: 13001-cn-a, 14002-cn, and 15001-cn). We took the utmost care to alleviate any pain and suffering on the part of the mice.

Sensitization, antigen challenge, and stress exposure

A schematic of the experimental protocol is shown in Figure 1. Six- to eight-week-old mice were sensitized and made to inhale an aerosolized antigen as previously described.²² Briefly, mice were sensitized by intraperitoneal injections of 8 μ g ovalbumin (OVA; Grade V, Sigma–Aldrich, St. Louis, MO, USA) adsorbed with aluminum hydroxide (Wako Pure Chemical Industries, Osaka, Japan) on days 0 and 5. On days 17 and 24, the mice were challenged with aerosolized OVA (0.5% in saline) for 1 h. Psychological stressors were applied on the following schedule to avoid habituation to psychological stress: 6 h restraint per day from day 17 to day 19, and 3 min forced swim per day from day 20 to day 23. For restraint stress (RS), each mouse was placed in a 50-mL conical centrifuge tube with multiple ventilation holes. For forced swimming stress (FSS), the mice were placed in a plastic tank (19 cm in diameter, 27 cm in height) containing 15 cm water at 32 °C. Non-stressed mice were deprived of food and water, which has been used as a non-stress condition in other rodent experiments that investigated the effect of stress.^{23,24} RS and FSS are category D procedures, as are other types of psychological stress, such as electric foot shock stress, sound stress, and communication box-induced stress, that have been used to investigate the exacerbation of stress-induced allergic airway inflammation by many groups including us. Category D procedures are used in these studies because exposure to stress is required to induce asthma exacerbation, and alternative methods for reducing stress fail to exacerbate the condition.

To test the effects of HR antagonists, 2 μ L epinastine as a selective H₁R antagonist (Tokyo Chemical Industry, Tokyo, Japan),²⁵ ranitidine as a selective H₂R antagonist (Sigma–Aldrich, St. Louis, MO, USA),²⁵ or thioperamide as a selective H_{3/4}R antagonist (Sigma–Aldrich)^{26,27} in calcium- and magnesium-free phosphate-buffered saline (PBS) was intracerebroventricularly administered to selectively block HRs in the CNS 1 h before each stress exposure at the dose indicated. Solvent was used as a negative control. Mice were placed in a stereotaxic device under anesthesia induced by inhalation of 2% isoflurane in oxygen (DS Pharma Animal Health, Tokyo, Japan). A 25G microinjection needle tip was aligned with the bregma and then inserted into the ventricle using the following coordinates from bregma: 1.0 mm anterior and 1.0 mm lateral. Intracerebroventricular injection has been used generally to selectively administer agents to the CNS.²² In our preliminary experiments, the intracerebroventricularly injected solution was not detected outside the CNS within 1 h for volumes below 5 μ L. The doses of HR antagonists used herein were based on those used in previous studies.^{28,29} At the end of the experiments, the mice were euthanized by an overdose of pentobarbital (Somnopentyl; Kyoritsu Seiyaku, Tokyo, Japan).

Preparation of bronchoalveolar lavage (BAL) fluids

BAL samples were collected with 2 \times 0.25 mL chilled PBS through a cannula inserted in the trachea. Total cell numbers recovered from BAL fluid were counted with a hemocytometer. After centrifugation of the BAL fluids, supernatants were stored at –80 °C for cytokine assay. For each sample, 2 \times 10⁵ cells were centrifuged onto a glass slide using a Cytospin 4 (Thermo Scientific, Waltham, MA, USA) and stained with Diff-Quick solution (International Reagents, Kobe, Japan). The fractions of leukocytes were analyzed by counting a minimum of 200 cells under a light microscope.

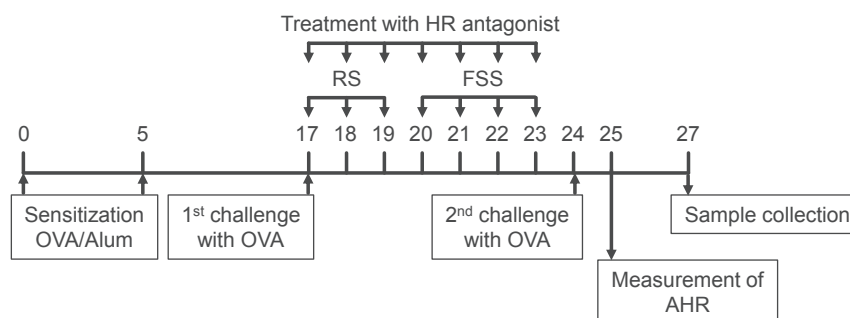


Fig. 1. Schematic of the experimental protocol.

Measurement of airway responsiveness

Lung resistance at the baseline and in response to aerosolized saline and acetyl- β -methylcholine (methacholine; Sigma–Aldrich) were measured for 3 min under each condition.²² To measure airway sensitivity, the concentration of acetyl- β -methylcholine needed to increase lung resistance to 200% above baseline (PC₂₀₀) was calculated by interpolating the log concentration–lung resistance curve from individual mice.

Lung histology

Lungs were isolated from mice 3 days after the last OVA challenge, fixed in 10% buffer formalin, dehydrated, and embedded in paraffin. Sections were cut at 4- μ m-thick and stained with periodic acid–Schiff (PAS). Mucin production was estimated as the proportion of PAS-positive cells in the total airway epithelium of bronchioles in the PAS-stained section. The percentage of PAS-positive cells was calculated in each of five random bronchioles in three lung sections from each mouse.

Measurement of OVA-specific IgE and cytokine

Serum samples were collected 3 days after the last OVA challenge. The quantities of OVA-specific IgE in serum were measured by enzyme-linked immunosorbent assay (ELISA). Briefly, microtiter plates (Nunc A/S, Roskilde, Denmark) were coated with 10 μ g/mL OVA in bicarbonate buffer for 1 h at 37 °C and then blocked with 1% bovine serum albumin (BSA) in PBS at 4 °C overnight. Prior to testing, serum samples were diluted with 1% BSA/PBS. Horseradish peroxidase-conjugated goat anti-mouse IgE antibodies (Bethyl Laboratories, Montgomery, TX, USA) diluted 1:2500 were used for detection. IgE concentrations were determined from the absorbance at 450 nm using that at 650 nm for reference and calculated based on a reference standard of pooled sera from sensitized female mice assigned as 1000 experimental units (EU)/mL. The sensitivity was 1.9×10^{-2} EU/mL for IgE. The concentrations of IL-13 in BAL fluids were measured using an ELISA kit (eBioscience, San Diego, CA, USA) according to the manufacturer's instructions. The limit of detection was 1.5 pg/mL.

Statistical analysis

Statistical analysis was conducted using GraphPad Prism 5 software (GraphPad Software, La Jolla, CA, USA). Differences between the two groups were tested using two-tailed analysis in an unpaired Student's *t*-test. Differences among four or more groups were tested using ANOVA with post hoc analysis (Tukey's multiple comparison test). A *p*-value less than 0.05 was considered significant. Data are expressed as the mean \pm standard error of the mean (SEM).

Results

Effects of HR antagonists on stress-induced exacerbations of airway inflammation

The numbers of total cells, eosinophils, and lymphocytes in BAL fluid were significantly increased by the stress exposure but showed a dose-dependent reduction with epinastine treatment (Fig. 2). Treatment with 3.0×10^{-9} mol epinastine significantly reduced the numbers of inflammatory cells in stressed mice to the levels observed in non-stressed mice treated with the same dose of epinastine and tended to reduce the numbers of total cells, eosinophils, and lymphocytes in BAL fluids of non-stressed mice compared with solvent treatment, although the difference was not statistically significant (Fig. 2). Intracerebroventricular administration of 3.0×10^{-9} mol ranitidine significantly reduced the increased numbers of total cells, eosinophils, and lymphocytes in BAL fluids of stressed mice, whereas treatment with a higher dose (3.0×10^{-8} mol) of ranitidine did not reduce the stress-induced increases (Supplementary Fig. 1). The effects of ranitidine in stressed mice were not dose-dependent but reverse bell-shaped. The maximal suppressive effect was observed at 3.0×10^{-9} mol. In contrast, the effects of ranitidine in non-stressed mice seemed to be dose-dependent but were not statistically significant (Supplementary Fig. 1). Treatment with thioperamide, an H_{3/4}R antagonist, did not significantly reduce the stress-induced increased numbers of inflammatory cells in BAL fluid (Fig. 3), even at a higher dosage (4.9×10^{-8} mol; data not shown).

Effects of an H₁R antagonist, epinastine, on stress-induced exacerbations of asthmatic airway responses

Lung resistance increased dose-dependently in response to inhaled methacholine in all groups of mice. The lung resistance to 200% above baseline (PC₂₀₀) with solvent treatment tended to be lower in stressed mice than in non-stressed mice, although the difference was not significant (Fig. 4). In the stressed mice, epinastine treatment significantly increased the PC₂₀₀ to a level similar to that in the non-stressed mice treated with epinastine. However, in the non-stressed mice, no significant difference in PC₂₀₀ was observed between solvent and epinastine treatments.

Effects of epinastine on stress-induced exacerbations of airway mucus secretion

The number of PAS-positive cells under solvent treatment was significantly higher in the stressed mice than in the non-stressed mice (Fig. 5). In the stressed mice, treatment with epinastine significantly reduced the number of PAS-positive cells to the level

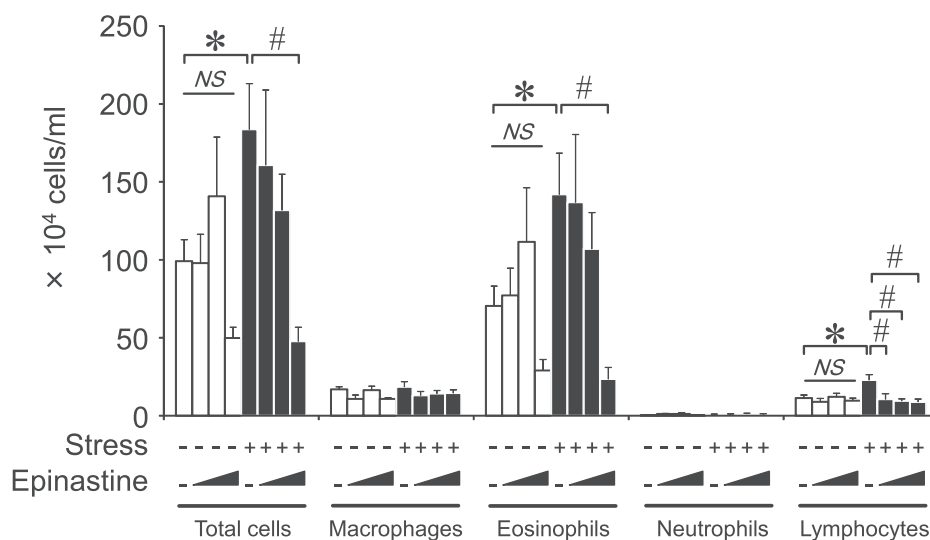


Fig. 2. Effects of epinastine on airway inflammation. Mice were sensitized and challenged with ovalbumin (OVA) in the absence (open bars) or presence (closed bars) of psychological stress. Solvent or 0.3×10^{-9} , 1.0×10^{-9} , or 3.0×10^{-9} mol epinastine was administered intracerebroventricularly before each stress exposure. The numbers of inflammatory cells in bronchoalveolar lavage fluid were counted on day 3 after the last OVA challenge. Each group consisted of 7–17 mice from at least two independent experiments. Data are shown as the mean \pm SEM. * $p < 0.05$ compared with non-stressed mice treated with solvent using an unpaired Student's *t*-test. Differences among the data on the stressed mice or non-stressed mice were tested using ANOVA with Tukey's multiple comparison test. # $p < 0.05$ compared with the stressed mice treated with solvent. NS, not significantly different.

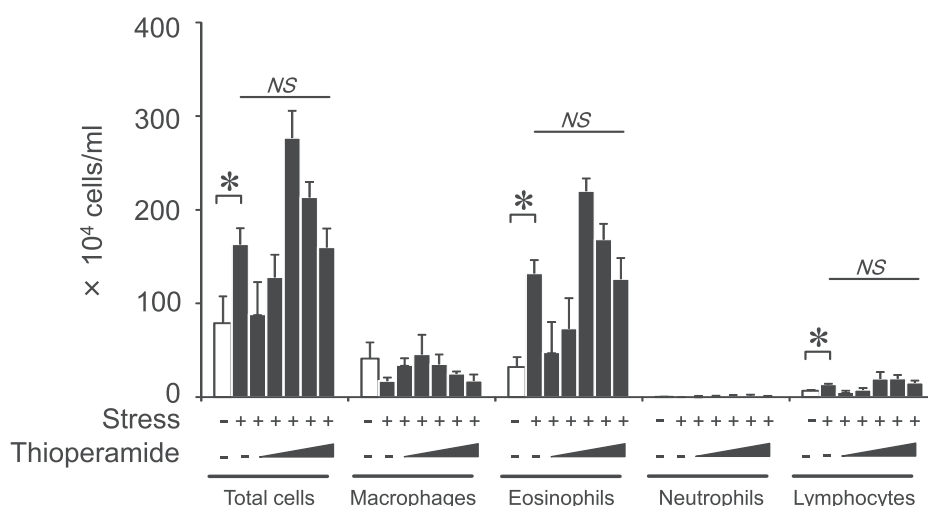


Fig. 3. Effects of thioperamide on airway inflammation. Mice were sensitized and challenged with ovalbumin (OVA) in the absence (open bars) or presence (closed bars) of psychological stress. Solvent or 0.01×10^{-9} , 0.1×10^{-9} , 0.3×10^{-9} , 1.0×10^{-9} , or 3.0×10^{-9} mol thioperamide was administered intracerebroventricularly before each stress exposure. The numbers of inflammatory cells in bronchoalveolar lavage fluid were counted on day 3 after the last OVA challenge. Each group consisted of three to four mice from two independent experiments. Data are shown as the mean \pm SEM. * $p < 0.05$ compared with the non-stressed mice treated with solvent using an unpaired Student's *t*-test. Differences among the data on the stressed mice were tested using ANOVA with Tukey's multiple comparison test. NS, not significantly different.

observed for non-stressed mice treated with epinastine. However, in the non-stressed mice, no significant difference in cell number observed between solvent and epinastine treatments.

Effects of epinastine on the stress-induced increase of IL-13 in BAL fluid

The IL-13 contents in BAL fluids under solvent treatment were significantly higher in the stressed mice than in the non-stressed mice (Fig. 6). In the stressed mice, treatment with epinastine significantly reduced the IL-13 contents to the levels measured for non-stressed mice treated with epinastine. In the non-stressed

mice, there was no significant difference in IL-13 contents between solvent and epinastine treatments.

Effects of epinastine on the stress-induced increase of OVA-specific IgE in sera

OVA-specific IgE concentrations in sera under solvent treatment tended to be higher in the stressed mice than in the non-stressed mice, although the difference was not statistically significant (Fig. 7). In the stressed mice, treatment with epinastine significantly decreased IgE concentrations to the levels of those in the non-stressed mice treated with epinastine. In the non-stressed

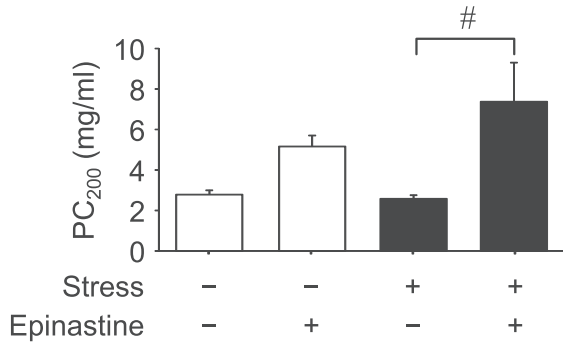


Fig. 4. Effects of epinastine on methacholine-induced airway hyperresponsiveness. Mice were sensitized and challenged with ovalbumin (OVA) in the absence (open bars) or presence (closed bars) of psychological stress. Solvent or 3.0×10^{-9} mol epinastine was administered intracerebroventricularly before each stress exposure. Airway sensitivity was measured 1 day after the last OVA challenge. Each group consisted of six to eight mice from two independent experiments. Data are shown as the mean \pm SEM. # $p < 0.05$ compared with the stressed mice treated with solvent using an unpaired Student's *t*-test.

mice, epinastine treatment yielded no significant difference in IgE concentrations compared with solvent treatment.

Discussion

To our knowledge, this is the first report demonstrating that HRs in the CNS are involved in both the development and psychological stress-induced exacerbations of allergic asthma. Histamine is a neurotransmitter whose release is upregulated in response to perceived stress.¹⁹ Ito *et al.* showed that chronic RS increased histamine turnover in the nucleus accumbens and striatum in Fisher rats.³⁰ In addition, Gadek-Michalska *et al.* showed that intracerebroventricular administration of an H₁R agonist in rats increased the levels of corticosterone, one of the stress hormones released in the neuroendocrine response to psychological stress.³¹ The increase of serum corticosterone after stress exposure was previously observed in this model of stress asthma.²² Therefore, it is likely that histamine was released upon stress exposure in the present study.

Epinastine seemed to increase the PC₂₀₀ (Fig. 4), and reduce the eosinophil counts (Fig. 2), the IL-13 contents in BAL fluid (Fig. 6) and the OVA-specific IgE levels in sera (Fig. 7) of non-stressed mice compared with solvent treatment, although the differences were

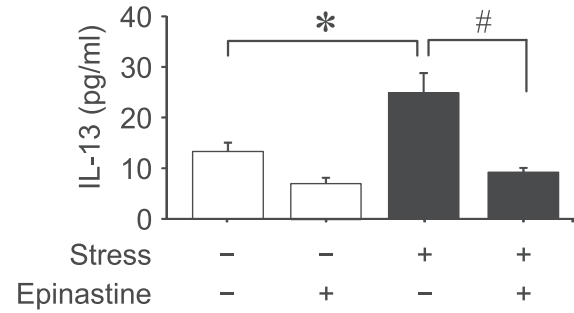


Fig. 6. Effects of epinastine on interleukin (IL)-13 contents in bronchoalveolar lavage (BAL) fluid. Mice were sensitized and challenged with ovalbumin (OVA) in the absence (open bars) or presence (closed bars) of psychological stress. Solvent or 3.0×10^{-9} mol epinastine was administered intracerebroventricularly before each stress exposure. BAL samples were collected on day 3 after the last OVA challenge. The concentration of IL-13 in BAL fluids was measured by enzyme-linked immunosorbent assay. Each group consisted of 4–10 mice from two independent experiments. Data are shown as the mean \pm SEM. * $p < 0.05$ compared with the non-stressed mice treated with solvent; # $p < 0.05$ compared with the stressed mice treated with solvent using an unpaired Student's *t*-test.

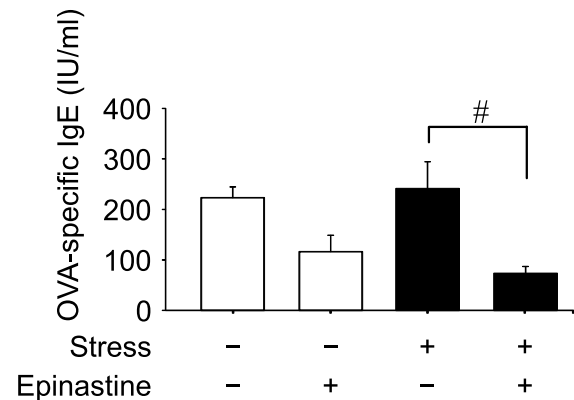


Fig. 7. Effect of epinastine on ovalbumin (OVA)-specific IgE production in serum. Mice were sensitized and challenged with OVA in the absence (open bars) or presence (closed bars) of psychological stress. Solvent or 3.0×10^{-9} mol epinastine was administered intracerebroventricularly before each stress exposure. Serum samples were collected on day 3 after the last OVA challenge. The concentrations of OVA-specific IgE in sera were measured by enzyme-linked immunosorbent assay. Each group consisted of 8–12 mice from two independent experiments. Data are shown as the mean \pm SEM. # $p < 0.05$ compared with the stressed mice treated with solvent using an unpaired Student's *t*-test.

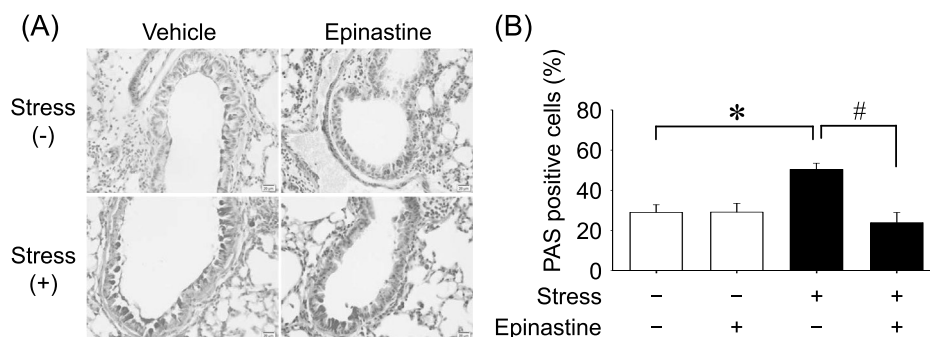


Fig. 5. Effects of epinastine on airway mucus secretion. Mice were sensitized and challenged with ovalbumin (OVA) in the absence (open bars) or presence (closed bars) of psychological stress. Solvent or 3.0×10^{-9} mol epinastine was administered intracerebroventricularly before each stress exposure. Lungs were isolated from mice 3 days after the last OVA challenge. Lung sections were prepared and stained with periodic acid–Schiff (PAS). (A) Representative images of lung sections from the non-stressed and stressed mice treated with solvent or epinastine (scale bar, 20 μ m). (B) The percentage of PAS-positive cells was calculated in each of five random bronchioles in three lung sections from each mouse. Each group consisted of 8–13 mice from two independent experiments. Data are shown as the mean \pm SEM. * $p < 0.05$ compared with the non-stressed mice treated with solvent; # $p < 0.05$ compared with the stressed mice treated with solvent using an unpaired Student's *t*-test.

not statistically significant. In addition, ranitidine tended to dose-dependently reduce the eosinophil counts in non-stressed mice compared with solvent treatment. Previous studies demonstrated that H₁Rs mediated the excitatory CNS functions of brain histamine such as maintenance of wakefulness, acceleration of locomotor activity, enhancement of learning and memory processes, and increased pain perception, and H₂Rs are thought to play similar roles.^{19,32} Therefore, histamine physiologically released in the CNS might be partially involved in the development of allergic airway responses through the activation of H₁Rs and H₂Rs, which could explain the (non-significant) epinastine- and ranitidine-mediated decreases in the development of allergic asthma under stress-free conditions. However, we cannot rule out the possibility that the procedure for intracerebroventricular administration of solvent could induce stress via HR activation in the non-stressed mice. In our previous study investigating the effect of a glucocorticoid receptor antagonist using the same stress model,²² subcutaneous administration of the solvent tended to aggravate allergic airway responses in non-stressed mice compared to untreated non-stressed mice (unpublished data). Thus, epinastine and ranitidine might attenuate the aggravation of asthma-related features caused by stress from handling in non-stressed mice.

Epinastine (3.0×10^{-9} mol) and ranitidine (3.0×10^{-9} mol) significantly attenuated the stress-induced enhancement of asthmatic airway responses and Th2 immune responses to the levels of non-stressed mice treated with the antagonists (Supplementary Fig. 1, Fig. 2,4,5,6,7). These results suggest that the stress exposure exaggerated asthmatic airway responses by increasing histamine release, leading to the further activation of H₁Rs and H₂Rs in the CNS.

On the other hand, the intracerebroventricular administration of an H_{3/4}R antagonist, thioperamide, exhibited no significant effect on the airway inflammation at the same dose (Fig. 3) or at a higher dose (4.9×10^{-8} mol; data not shown). However, within the group receiving thioperamide administration, a bell-shaped enhancement effect was observed, and the maximal effect was observed at 0.3×10^{-9} mol. H₃Rs act as inhibitory auto- and hetero-receptors in the CNS, which inhibit the synthesis and release of histamine^{19,33} and a number of neurotransmitters, including acetylcholine, dopamine, noradrenaline, and serotonin, in a pathway-dependent manner, leading to suppression of convulsion, stress-induced excitation, and feeding behavior.^{20,21} The structure–activity relationships of H₃R and H₄R overlap as G_{i/o} protein-coupled receptors.³⁴ Therefore, the activation H₃Rs and H₄Rs by the stress exposure might play a suppressive role in stress-induced asthma exacerbations.

Taken together, our findings and the physiological properties of each HR subtype suggest that the interaction of histamine with HR subtypes playing distinctive roles in the CNS is associated with the severity of allergic airway responses, particularly in the case of psychological stress-induced exacerbations. Further studies will be required to identify the exact roles of each HR subtype in the CNS and to elucidate how the stressor signal via HRs in the CNS modulates Th2 immune responses in asthmatic pathophysiology. The present study presents a new insight into the global role of the histamine-regulated CNS in allergic asthma, which might lead to the development of more effective strategies for the management of asthmatic patients with the stress-related asthma phenotype.

Acknowledgments

This work was supported in part by a Grant-in-Aid for Scientific Research (No. 25461164) for IO and by the Matching Fund Subsidy for Private Universities from the Ministry of Education, Culture, Sports, Science, and Technology (No. S1511001L) for IO, TK, and TM.

Appendix A. Supplementary data

Supplementary data related to this article can be found at <http://dx.doi.org/10.1016/j.alit.2016.05.015>.

Conflict of interest

The authors have no conflict of interest to declare.

Authors' contributions

Conceived and designed the experiments: IO, TM; performed the experiments: TM, KOD, CM, SI, MS, TK; analyzed the data: TM, IO, KOD; contributed reagents/materials/analysis tools: IO, YO, HM, SS, MT; contributed to the writing of the manuscript: TM, IO, HM.

References

- Haldar P, Pavord ID, Shaw DE, Berry MA, Thomas M, Brightling CE, et al. Cluster analysis and clinical asthma phenotypes. *Am J Respir Crit Care Med* 2008;**178**: 218–24.
- Fahy JV. Type 2 inflammation in asthma—present in most, absent in many. *Nat Rev Immunol* 2015;**15**:57–65.
- Sandberg S, Paton JY, Ahola S, McCann DC, McGuinness D, Hillary CR, et al. The role of acute and chronic stress in asthma attacks in children. *Lancet* 2000;**356**: 982–7.
- Lange NE, Bunyavanich S, Silberg JL, Canino G, Rosner BA, Celedón JC. Parental psychosocial stress and asthma morbidity in Puerto Rican twins. *J Allergy Clin Immunol* 2011;**127**:734–40.
- Dales RE, Choi B, Chen Y, Tang M. Influence of family income on hospital visits for asthma among Canadian school children. *Thorax* 2002;**57**:513–7.
- Cesaroni G, Farchi S, Davoli M, Forastiere F, Perucci CA. Individual and area-based indicators of socioeconomic status and childhood asthma. *Eur Respir J* 2003;**22**:619–24.
- Sandberg S, Järvenpää S, Penttinen A, Paton JY, McCann DC. Asthma exacerbations in children immediately following stressful life events: a Cox's hierarchical regression. *Thorax* 2004;**59**:1046–51.
- Wainwright NW, Surtees PG, Wareham NJ, Harrison BD. Psychosocial factors and incident asthma hospital admissions in the EPIC-Norfolk cohort study. *Allergy* 2007;**62**:554–60.
- Chen E, Chim LS, Strunk RC, Miller GE. The role of the social environment in children and adolescents with asthma. *Am J Respir Crit Care Med* 2007;**176**: 644–9.
- Chen E, Miller GE. Stress and inflammation in exacerbations of asthma. *Brain Behav Immun* 2007;**21**:993–9.
- Liu LY, Coe CL, Swenson CA, Kelly EA, Kita H, Busse WW. School examinations enhance airway inflammation to antigen challenge. *Am J Respir Crit Care Med* 2002;**165**:1062–7.
- Höglund CO, Axén J, Kemi C, Jernelöv S, Grunewald J, Müller-Suur C, et al. Changes in immune regulation in response to examination stress in atopic and healthy individuals. *Clin Exp Allergy* 2006;**36**:982–92.
- Chen E, Hanson MD, Paterson LQ, Griffin MJ, Walker HA, Miller GE. Socioeconomic status and inflammatory processes in childhood asthma: the role of psychological stress. *J Allergy Clin Immunol* 2006;**117**:1014–20.
- Wolf JM, Miller GE, Chen E. Parent psychological states predict changes in inflammatory markers in children with asthma and healthy children. *Brain Behav Immun* 2008;**22**:433–41.
- Rosenkranz MA, Busse WW, Johnstone T, Swenson CA, Crisafi GM, Jackson MM, et al. Neural circuitry underlying the interaction between emotion and asthma symptom exacerbation. *Proc Natl Acad Sci U S A* 2005;**102**:13319–24.
- Rosenkranz MA, Busse WW, Sheridan JF, Crisafi GM, Davidson RJ. Are there neurophenotypes for asthma? Functional brain imaging of the interaction between emotion and inflammation in asthma. *PLoS One* 2012;**7**:e40921.
- Chrousos GP. Stress and disorders of the stress system. *Nat Rev Endocrinol* 2009;**5**:374–81.
- Okuyama K, Ide S, Sakurada S, Sasaki K, Sora I, Tamura G, et al. μ -Opioid receptor-mediated alterations of allergen-induced immune responses of bronchial lymph node cells in a murine model of stress asthma. *Allergol Int* 2012;**61**:245–58.
- Haas HL, Sergeeva OA, Selbach O. Histamine in the nervous system. *Physiol Rev* 2008;**88**:1183–241.
- Tiligada E, Kyriakidis K, Chazot PL, Passani MB. Histamine pharmacology and new CNS drug targets. *CNS Neurosci Ther* 2011;**17**:620–8.
- Passani MB, Blandina P. Histamine receptors in the CNS as targets for therapeutic intervention. *Trends Pharmacol Sci* 2011;**32**:242–9.
- Okuyama K, Dobashi K, Miyasaka T, Yamazaki N, Kikuchi T, Sora I, et al. The involvement of glucocorticoids in psychological stress-induced exacerbations of experimental allergic asthma. *Int Arch Allergy Immunol* 2014;**163**:297–306.
- Mercado AM, Padgett DA, Sheridan JF, Marucha PT. Altered kinetics of IL-1 α , IL-1 β , and KGF-1 gene expression in early wounds of restrained mice. *Brain Behav Immun* 2002;**16**:150–62.
- Ashcraft KA, Hunzeker J, Bonneau RH. Psychological stress impairs the local CD8+ T cell response to mucosal HSV-1 infection and allows for increased

- pathogenicity via a glucocorticoid receptor-mediated mechanism. *Psychoneuroendocrinology* 2008;**33**:951–63.
25. Tripathi T, Khan AA, Shahid M, Khan HM, Siddiqui M, Khan RA, et al. Immunological, biochemical and histopathological evaluation of histamine receptors (H1R, H2R, H3R and H4R)-antagonist in rabbit experimental model: a short term study. *Exp Toxicol Pathol* 2012;**64**:259–66.
 26. Takeshita K, Bacon KB, Gantner F. Critical role of L-selectin and histamine H4 receptor in zymosan-induced neutrophil recruitment from the bone marrow: comparison with carrageenan. *J Pharmacol Exp Ther* 2004;**310**:272–80.
 27. Takeshita K, Sakai K, Bacon KB, Gantner F. Critical role of histamine H4 receptor in leukotriene B4 production and mast cell-dependent neutrophil recruitment induced by zymosan in vivo. *J Pharmacol Exp Ther* 2003;**307**:1072–8.
 28. Kamei J, Hirano S, Miyata S, Saitoh A, Onodera K. Effects of first- and second-generation histamine-H1-receptor antagonists on the pentobarbital-induced loss of the righting reflex in streptozotocin-induced diabetic mice. *J Pharmacol Sci* 2005;**97**:266–72.
 29. Altinbas B, Topuz BB, Ilhan T, Yilmaz MS, Erdost H, Yalcin M. Activation of the central histaminergic system mediates arachidonic-acid-induced cardiovascular effects. *Can J Physiol Pharmacol* 2014;**92**:645–54.
 30. Ito C, Shen H, Toyota H, Kubota Y, Sakurai E, Watanabe T, et al. Effects of the acute and chronic restraint stresses on the central histaminergic neuron system of Fischer rat. *Neurosci Lett* 1999;**262**:143–5.
 31. Gadek-Michalska A, Borycz J, Bugajski J. Effect of social isolation on corticosterone secretion elicited by histaminergic stimulation. *Agents Actions* 1994;41. Spec No: C77-9.
 32. Yanai K, Tashiro M. The physiological and pathophysiological roles of neuronal histamine: an insight from human positron emission tomography studies. *Pharmacol Ther* 2007;**113**:1–15.
 33. Parsons ME, Ganellin CR. Histamine and its receptors. *Br J Pharmacol* 2006;**147**(Suppl 1):S127–35.
 34. Schneider EH, Seifert R. The histamine H4-receptor and the central and peripheral nervous system: a critical analysis of the literature. *Neuropharmacology* 2016;**106**:116–28.

Human CD4⁺ CD8⁺ Invariant Natural Killer T Cells Promote IgG Secretion from B Cells Stimulated by Cross-Linking of Their Antigen Receptors

Tomomitsu Miyasaka^{1*}, Yurie Watanabe¹, Yukiko Akahori^{1*}, Namiko Miyamura¹, Keiko Ishii¹, Yuki Kinjo², Yoshitsugu Miyazaki², Tian-Yi Liu^{3,4}, Yasushi Uemura^{3,5}, Kazuyoshi Kawakami^{1#}

¹Department of Medical Microbiology, Mycology and Immunology, Tohoku University Graduate School of Medicine, Sendai, Japan

²Department of Chemotherapy and Mycoses, National Institute of Infectious Diseases, Tokyo, Japan

³Division of Immunology, Aichi Cancer Center Research Institute (ACCRI), Nagoya, Japan

⁴Key Laboratory of Cancer Center, Chinese PLA General Hospital, Beijing, China

⁵Division of Cancer Immunotherapy, Exploratory Oncology Research & Clinical Trial Center, National Cancer Center (NCC), Kashiwa, Japan

Email: [#]kawakami@med.tohoku.ac.jp

Received 30 January 2016; accepted 9 May 2016; published 12 May 2016

Copyright © 2016 by authors and Scientific Research Publishing Inc.

This work is licensed under the Creative Commons Attribution International License (CC BY).

<http://creativecommons.org/licenses/by/4.0/>



Open Access

Abstract

Immunoglobulin (Ig) M production can be induced by the interaction of thymus-independent type-2 (TI-2) antigen (Ag) with B cell Ag receptors (BCRs) without the involvement of conventional T cells; for IgG production through the same process, however, a second signal is required. Previous studies have reported that invariant natural killer T (iNKT) cells may be responsible for the second signal involved in IgG production. In the present study, we addressed whether human iNKT cells could participate in the production of Ig against TI-2 Ag *in vitro*. Two major distinct subsets of human iNKT cells, CD4⁺ CD8^β⁺ (CD4) and CD4⁺ CD8^β⁺ [double negative (DN)] cells, were generated from peripheral blood monocytes from a healthy volunteer. BCR engagement, triggered by anti-IgM antibody stimulation, examined here as a model of BCR engagement triggered by TI-2 Ag, induced abundant IgM production by B cells. Both CD4 and DN iNKT cells reduced IgM production and conversely enhanced IgG production in a dose-dependent manner. In addition, IgG production by CD19⁺CD27⁺ (naïve) and CD19⁺CD27⁺ (memory) B cells was predominantly promoted by DN

*Present address: Tomomitsu Miyasaka, Department of Pathophysiology, Tohoku Medical and Pharmaceutical University, Sendai, Japan; Yukiko Akahori, Department of Medical Science Technology, International University of Health and Welfare, Narita, Japan.

[#]Corresponding author.

How to cite this paper: Miyasaka, T., Watanabe, Y., Akahori, Y., Miyamura, N., Ishii, K., Kinjo, Y., Miyazaki, Y., Liu, T.-Y., Uemura, Y. and Kawakami, K. (2016) Human CD4⁺ CD8⁺ Invariant Natural Killer T Cells Promote IgG Secretion from B Cells Stimulated by Cross-Linking of Their Antigen Receptors. *World Journal of Vaccines*, 6, 34-41.

<http://dx.doi.org/10.4236/wjv.2016.62005>

iNKT cells rather than CD4 iNKT cells; nevertheless, IgM production by both B cell subsets was similarly reduced by either subset of iNKT cells. These results suggest that the DN iNKT subsets may preferentially promote Ig class switching by B cells upon stimulation with TI-2 Ag.

Keywords

Invariant Natural Killer T Cells, TI-2 Antigen, B Cells, IgM, IgG

1. Introduction

The main causative bacteria of invasive infection, including *Streptococcus pneumoniae* and *Haemophilus influenzae*, possess thick polysaccharide capsules which confer the ability to resist phagocytosis by polymorphonuclear leukocytes [1]. Immunoglobulins specific for these polysaccharide capsules enhances opsonophagocytic killing (OPK) activity, which plays an important role in host protection against infections caused by these encapsulated bacteria [2] [3]. Recently, we reported that immunization with pneumococcal polysaccharide vaccine led to an increase in the serum level of serotype 3-specific IgG3, which facilitates survival after pneumococcal infection in mice [4]. Immunization with pneumococcal polysaccharide vaccine also generates polysaccharide-specific IgG response in humans [5] [6].

Polysaccharide capsule, a thymus-independent type 2 (TI-2) antigen (Ag), has highly repetitive structures with simultaneous cross-linking of B cell receptors (BCRs) and induces B cell proliferation and IgM production [7]. The antibody response induced by TI-2 Ag is smaller than that induced by thymus-dependent (TD) Ag, and consists largely of the production of low-affinity IgM by B cells without the conventionally necessary T cell involvement. In addition, however, IFN- γ induces T cell-independent IgG production in response to TI-2 Ag [8], as this cytokine triggers the secondary stimulatory signals for T cell-independent B cell activation and isotype switching to produce IgG [9] [10].

Human invariant natural killer T (iNKT) cells express only two $\alpha\beta$ T cell Ag receptors, namely, V α 24-J α 18 and V β 11, and have been identified as a unique lymphocyte population playing a critical role in both innate and adaptive immune responses [11] [12]. Although V α 24⁺V β 11⁺ iNKT cells are present only in very small proportions (<0.01% - 1%) in human blood [13], these cells recognize glycolipids from bacteria and/or self in context with CD1d, a nonpolymorphic MHC class I-like molecule, which leads to the production of large quantities of cytokines such as IFN- γ , IL-4, IL-10 and IL-17A [14]. Human V α 24⁺ iNKT cells comprise two distinct major subpopulations, one expressing CD4⁺CD8 β ⁻ (CD4) and the other CD4⁻CD8⁻ [double negative (DN)] [13]. These two subsets of iNKT cells differ in terms of the cytokines they produce to regulate various immune responses [15]. Mice lacking iNKT cells exhibit defective IgG response to pneumococcal polysaccharide Ags, intact response to TD Ags [16] and impaired host defense against pneumococcal infection [17]. These previous observations suggest that iNKT cells may secrete the IFN- γ that triggers isotype switching in TI-2-induced IgG production.

In the present study, we examined the *in-vitro* effect of human iNKT cells on Ig production by human B cells stimulated via cross-linking of their Ag receptors, which mimics BCR engagement by TI-2 Ags. We found that co-culture with iNKT cells reduced IgM production but increased IgG production by B cells stimulated via cross-linking of BCRs, and that this activity was higher in DN iNKT cells than in CD4 iNKT cells. These findings suggest that iNKT cells may contribute to the class-switching from IgM to IgG that occurs upon stimulation with TI-2 Ags.

2. Materials and Methods

2.1. Ethical Statement

All experimental protocols described in this study were reviewed and approved by the Ethics Committee for Human Experimentation at Tohoku University, Sendai, Japan (approval numbers: 2012-1-20, 2013-1-496).

2.2. Ab and Reagents

Alpha-galactosylceramide (α -GalCer; KRN7000) was purchased from Funakoshi (Tokyo, Japan). Recombinant

human (rh) IL-2 was from PeproTech (Rocky Hill, NJ, USA). Polyclonal hIgM and hIgG were from Rockland Immunochemicals (Limerick, PA, USA). Anti-human IgM, anti-human IgG, HRP-conjugated anti-human IgM and HRP-conjugated anti-human IgG for ELISA were from Acris Antibodies (San Diego, CA, USA). Goat F(ab')₂ anti-hIgM and rabbit F(ab')₂ anti-goat IgG for B cell stimulation were from Beckman Coulter (Fullerton, CA, USA). Anti-V α 24J α 18 (Clone; 6B11), anti-V β 11 (C21), isotype-matched control and 7-amino-actinomycin D (7-AAD) were from BD Pharmingen (San Diego, CA, USA). Anti-CD4 (RPA-T4) and anti-CD8 (RPA-T8) were from eBioscience (San Diego, CA, USA). Memory B cell isolation kit was from Miltenyi Biotec (Bergisch Gladbach, Germany).

2.3. Generation of V α 24J α 18⁺ Invariant NKT Cells

Human iNKT cells were separated from peripheral blood mononuclear cells (PBMCs) obtained from peripheral blood of healthy volunteers as described previously [18]. After 15 days of expansion, CD4⁺CD8⁻ (CD4) and CD4⁻CD8⁻ [double negative (DN)] iNKT subsets were sorted using a FACSAria cell sorter (Becton Dickinson, San Diego, CA, USA). The CD4 and DN iNKT cells (2×10^6 cells/well) were stimulated with irradiated allogenic PBMC (1×10^7 cells/well) prepulsed for 5 h with α -GalCer (100 ng/ml) in RPMI 1640 medium supplemented with 10% human serum, 100 U/ml penicillin G, 100 μ g/ml streptomycin, 2 mM L-glutamine, and 25 mM HEPES containing 20 U/ml rhIL-2. From day 3 to day 9, cells were split into two fractions once or twice daily. The cultures were expanded by adding medium containing rhIL-2. On day 11 or 12, expanded cells were collected and used as iNKT cells. The surface phenotypes of expanded iNKT cells were identified by flow cytometry (FACSCant II; BD Biosciences). The presence of dead cells was excluded by running parallel 7-AAD-stained samples. After one or two passages of each primary cell culture, the remaining cells were used in the experiments.

2.4. Human Peripheral Blood B Cells

PBMCs were isolated from heparinized blood of one healthy adult volunteer by standard density gradient concentration over Ficoll-Paque PLUS (GE Healthcare Life Sciences, Piscataway, NJ, USA). Interface PBMCs were pelleted, washed twice, and resuspended in MACS buffer (Miltenyi Biotec). The naïve (CD19⁺CD27⁻) and memory phenotype (CD19⁺CD27⁺) B cells were isolated from PBMCs by a memory B cell isolation kit according to the manufacturer's protocol.

2.5. NKT and B Cell Cultures

The B cells used in the current assays were derived from a single donor. Initially, CD27⁻ and CD27⁺ B cells (2.5×10^4 cells/well) were stimulated with goat F(ab')₂ anti-human IgM (1 μ g/ml) for 15 min on ice. The B cells were washed three times with culture medium, and then co-cultured with rabbit F(ab')₂ anti-goat IgG (3 μ g/ml) in the presence or absence of CD4 or DN iNKT cells (2.5×10^3 - 2.5×10^4 cells/well) for five days. The culture supernatants were stored at -80°C until assayed for immunoglobulins by ELISA.

2.6. Measurement of Total IgG and IgM

The quantities of IgM and IgG in the culture supernatants were measured by enzyme-linked immunosorbent assay (ELISA). Microtiter plates (Nunc A/S, Roskilde, Denmark) were coated with 250 ng/ml of anti-human IgM or 192 ng/ml of anti-human IgG Ab in PBS for 1 h at 37°C, and blocked with 1% FCS PBS at 4°C overnight. Prior to testing, samples were diluted with culture medium supplemented with 0.05% Tween 20. Next, serial two-fold dilution of hIgM or hIgG to 1:1024 was performed arbitrarily; resulting solutions were added to the wells and incubated at room temperature for 2 h. HRP-conjugated anti-human IgM or IgG antibodies diluted with 1:4000 were used as detection Ab. The concentrations of IgM and IgG were determined based on the absorbance at 450 nm. The detection limit was 0.2 ng/ml.

2.7. Statistical Analysis

Data are presented as mean values \pm standard deviation (SD). Differences between the two groups were tested using two-tail analysis in an unpaired Student's *t*-test. Differences among three or more groups were tested using ANOVA with post-hoc analysis (Student-Newman-Keuls test).

3. Results

3.1. Human CD4⁺CD8⁻ (CD4) and CD4⁻CD8⁻ (DN) V α 24 iNKT Cells

To investigate the functional differences between the human iNKT subsets in terms of immunoglobulin production against TI-2 Ags, we initially expanded α -GalCer-specific CD4 and DN iNKT cells separated from healthy individuals. More than 94% - 97% of the cultured iNKT cells, including both CD4 and DN subsets, expressed an invariant TCR, consisting of V α 24J α 18 CDR3 loop and V β 11. The expanded-CD4 iNKT cells were CD4⁺CD8⁻ at 98% - 99% and V α 24J α 18⁺CD4⁺ at 92%. By contrast, 98% - 99% of the DN iNKT cells were negative for expression of CD4 and CD8, whereas 97% of these cells expressed V α 24J α 18 (data not shown).

3.2. iNKT Cell-Induced Enhancement of Immunoglobulin Production by B Cells upon Stimulation with Antigen Receptor-Engagement

To investigate the effect of co-culture with iNKT cells on Ig production by B cells activated via cross-linking of BCRs, B cells were stimulated with anti-IgM Ab in the presence or absence of CD4 or DN iNKT cells, and the production of IgM and IgG in the culture supernatants was analyzed. As shown in **Figure 1(a)**, B cells produced large quantities of IgM under BCR cross-linking alone, whereas the addition of CD4 iNKT cells resulted in the reduction of IgM production in a dose-dependent manner. A similar pattern was observed upon co-culture with DN iNKT cells (**Figure 1(c)**). By contrast, IgG production by B cells was not clearly increased when activated via BCR cross-linking alone (**Figure 1(b)** and **Figure 1(d)**). The synthesis of IgG by B cells stimulated via cross-linking of BCRs was significantly enhanced by co-culture with CD4 and DN iNKT cells in a dose-dependent manner. In addition, this activity was much higher in DN iNKT cells than in CD4 iNKT cells (**Figure 1(b)** and **Figure 1(d)**).

3.3. Role of iNKT Cells in Immunoglobulin Production by Naïve and Memory B Cells upon Stimulation with Antigen Receptor-Engagement

IgM⁺CD27⁺ memory B cells in PBMCs play an important role in anti-pneumococcal polysaccharide IgG pro-

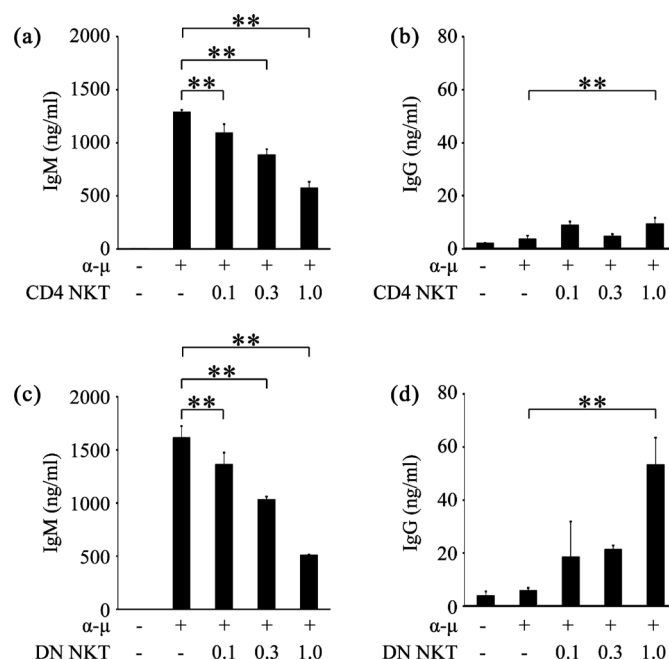


Figure 1. Effect of co-culture with iNKT cells on IgM and IgG production by B cells stimulated with anti-IgM Ab. B cells were stimulated with anti-IgM Ab in the presence or absence of CD4 iNKT cells or DN iNKT cells for five days, and the concentrations of Ig in the culture supernatants were measured. IgM (a) and IgG (b) production by B cells co-cultured with CD4 iNKT cells; IgM (c) and IgG (d) production by B cells co-cultured with DN iNKT cells. Similar results were obtained in two independent experiments. α - μ , anti-IgM Ab. **, $p < 0.01$.

duction in humans [19]. Therefore, to address the effect of co-culture with iNKT cells on Ig production by naïve (CD27⁻) and memory (CD27⁺) B cells, we separated B cells into two subsets according to the expression of CD27 and stimulated each subset with anti-IgM Ab in the presence or absence of CD4 or DN iNKT cells. As shown in **Figure 2(a)** and **Figure 2(c)**, both CD27⁺ and CD27⁻ B cells produced similar levels of IgM upon BCR cross-linking, and IgM production by both subsets was significantly reduced when co-cultured with either CD4 or DN iNKT cells. The cross-linking of BCRs induced low levels of IgG production by naïve and memory B cells in the absence of iNKT cells, and IgG production by CD27⁺ B cells was significantly higher than that by CD27⁻ B cells. In addition, IgG production by naïve and memory B cells was significantly enhanced when they were co-cultured with either CD4 iNKT cells or DN iNKT cells; this enhancement effect was much stronger with DN iNKT cells than with CD4 iNKT cells (**Figure 2(b)** and **Figure 2(d)**).

4. Discussion

In the present study, we evaluated the effect of co-culture with iNKT cells on Ig production by B cells upon stimulation via crosslinking of BCRs. Our data demonstrated that CD4 iNKT cells and DN iNKT cells accelerated the isotype switching from IgM to IgG, as shown by decreased IgM and increased IgG, in both naïve and memory B cells. DN iNKT cells accelerated this response even further than CD4 iNKT cells did. These results suggest that activation of iNKT cells may serve as a potent adjuvant, eliciting TI-2 Ag-induced IgG production in the development of more effective vaccination strategies for prevention of the infectious diseases caused by encapsulated bacteria.

Kobrynski and coworkers [16] demonstrated that TI-2 Ag-specific IgG production was completely abrogated in CD1d- or β 2-microglobulin-deficient mice, suggesting that NKT cells may potentially promote IgG production in response to TI-2 Ags. In addition, we previously reported that activation of iNKT cells by α -GalCer increased IFN- γ -producing NKT cells, and that this increase was correlated with enhanced production of the poly-

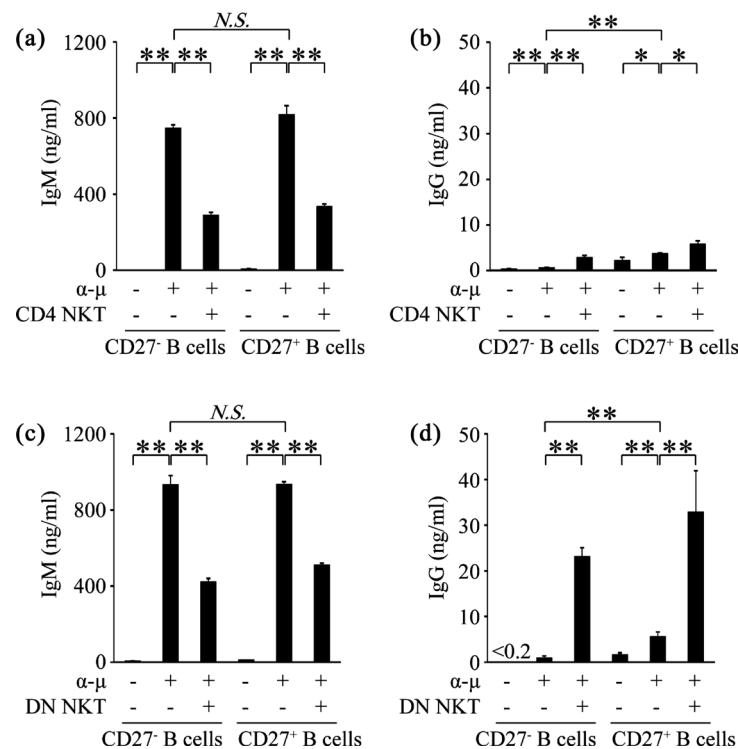


Figure 2. Effect of co-culture of iNKT cells on IgM and IgG production by naïve and memory B cells stimulated with anti-IgM Ab. CD27⁺ or CD27⁻ B cells were stimulated with anti-IgM Ab in the presence or absence of CD4 iNKT cells or DN iNKT cells for five days, and the concentrations of Ig in the culture supernatants were measured. IgM (a) and IgG (b) production by B cells co-cultured with CD4 iNKT cells; IgM (c) and IgG (d) production by B cells co-cultured with DN iNKT cells. Similar results were obtained in two independent experiments. α - μ , anti-IgM Ab. *, $p < 0.05$; **, $p < 0.01$; NS, not significant.

saccharide-specific IgG3 after immunization with pneumococcal polysaccharide vaccine in mice [4]. In our clinical study, immunization with anti-pneumococcal polysaccharide vaccine led to the production of serotype-specific IgG, which was correlated with an increase in DN iNKT cells in peripheral blood [5]. Thus iNKT cells are suggested to play an important role in the production of serotype-specific IgG after immunization with TI-2 Ags.

Co-culture with iNKT cells accelerated the production of IgG by B cells upon stimulation with BCR cross-linking without any exogenously added agonists of iNKT cells. In addition, α -GalCer did not induce any further increase in IgG production promoted by iNKT cells alone (data not shown). In earlier studies by Galli *et al.* [20], iNKT cell-induced promotion of B cell activation was demonstrated to depend on CD1d expressed on a variety of B cell subsets and to be delivered in the absence of α -GalCer [21]. These findings suggest that iNKT cells may recognize some endogenous ligand presented in context with CD1d on B cells, although the responsible molecule remains to be identified.

IgG production by B cells was more dramatically accelerated by DN iNKT cells than by CD4 iNKT cells. While CD4 iNKT cells have the potential to produce large amounts of Th2 cytokines such as IL-4 and IL-13, DN iNKT cells have a Th1-biased profile, enabling increased IFN- γ production and prominent expression of NK lineage receptors [15] [22]–[24]. In addition, chemokine receptors such as CCR6 and CXCR6 are preferentially expressed on DN iNKT cells rather than CD4 iNKT cells [22] [25], though the latter are the more common type among Th1 cells [26]. CD4 co-receptor potentiates the activation of human CD4 iNKT cells by engaging CD1d molecules [24]. Previously, Galli and co-workers [20] demonstrated that, compared to DN iNKT cells, human CD4 iNKT cells induced higher levels of IgM and IgG production in α -GalCer-pulsed B cells. In that study, B cells were considered to receive activation signals during cognate interaction with activated iNKT cells without BCR cross-linking. The current study differed from theirs in terms of the primary B cell activation method. Thus the phenotypic and functional properties of iNKT cells may be associated with IgG production by B cells stimulated with TI-2 Ags, though further investigation is required to define the molecular mechanism mediating the functional difference between CD4 iNKT cells and DN iNKT cells in T cell-independent Ig production.

TI-2 Ags are reported to generate memory B cells, although they do not elicit the Ab booster response or the germinal center formation following secondary immunization [27]. Moens and coworkers [19] reported that CD19⁺CD27⁺ IgM⁺ B cells were predominantly associated with an anti-polysaccharide IgG response after pneumococcal polysaccharide vaccination. In keeping with these previous observations, in the current study, cross-linking of BCRs induced the production of IgG by CD27⁺ (memory type) B cells at a higher level than that by CD27[−] (naïve) B cells in the absence of iNKT cells. Yet iNKT cells promoted IgG production not only by memory B cells but also by naïve B cells. In a previous study by Bai and co-workers [28], iNKT cell activation through cognate interaction with dendritic cells induced isotype switching by B cells and promoted long-term memory response to pneumococcal capsular polysaccharides. In addition, CD4 iNKT cells and DN iNKT cells are reported to promote the proliferation of naïve and memory B cells derived from peripheral blood *in vitro* [20]. Thus, iNKT cells might be involved in the potentiation of IgG production by naïve and memory B cells upon stimulation with TI-2 Ags.

Maddur and coworkers demonstrated that B cells activated via BCR cross-linking enhanced the expression of OX-40L and co-stimulatory molecules such as CD80, CD86 and CD40 on DCs [29] [30]. In our previous study, DCs with increased expression of OX-40L caused NKT cells to produce substantial levels of IFN- γ [31]. Considered collectively, B cells activated by TI-2 Ags may amplify IFN- γ production by iNKT cells through the enhanced Th1 response induced by DCs *in vivo*.

5. Conclusion

In conclusion, we demonstrated that iNKT cells promoted the production of IgG by human CD27⁺ and CD27[−] B cells upon stimulation via cross-linking of BCRs and that IgG production was more strongly promoted by DN iNKT cells than by CD4 iNKT cells. The present study provides important implications for understanding the contribution of iNKT cells to IgG production by TI-2 Ag-stimulated B cells, which is expected to be helpful in the development of more effective vaccination strategies for prevention of pneumococcal infection.

Acknowledgements

This work was supported in part by Grants from the Ministry of Health, Labour and Welfare of Japan (22-

SHINKOU-IPPAN-014 to KK, H25-SHINKOU-WAKATE-005 to YK), a Grant from the Japan Agency for Medical Research and Development, AMED (the Research Program on Emerging and Re-emerging Infectious Diseases), and Aid Funding from the Takeda Science Foundation to YK.

Conflicts of Interest

The authors have no financial conflicts of interest.

References



- [1] De Velasco, E.A., Verheul, A.F., Verhoef, J. and Snippe, H. (1995) *Streptococcus pneumoniae*: Virulence Factors, Pathogenesis, and Vaccines. *Microbiology Reviews*, **59**, 591-603.
- [2] Vitharsson, G., Jónsdóttir, I., Jónsson, S. and Valdimarsson, H. (1994) Opsonization and Antibodies to Apsular and Cell Wall Polysaccharides of *Streptococcus pneumoniae*. *The Journal of Infectious Diseases*, **170**, 592-599. <http://dx.doi.org/10.1093/infdis/170.3.592>
- [3] Hallström, T. and Riesbeck, K. (2010) *Haemophilus influenzae* and the Complement System. *Trends in Microbiology*, **18**, 258-265. <http://dx.doi.org/10.1016/j.tim.2010.03.007>
- [4] Miyasaka, T., Akahori, Y., Toyama, M., Miyamura, N., Ishii, K., Saijo, S., Iwakura, Y., Kinjo, Y., Miyazaki, Y., Oishi, K. and Kawakami K. (2013) Dectin-2-Dependent NKT Cell Activation and Serotype-Specific Antibody Production in Mice Immunized with Pneumococcal Polysaccharide Vaccine. *PLoS One*, **8**, e78611. <http://dx.doi.org/10.1371/journal.pone.0078611>
- [5] Miyasaka, T., Aoyagi, T., Uchiyama, B., Oishi, K., Nakayama, T., Kinjo, Y., Miyazaki, Y., Kunishima, H., Hirakata, Y., Kaku, M. and Kawakami, K. (2012) A Possible Relationship of Natural Killer T Cells with Humoral Immune Response to 23-Valent Pneumococcal Polysaccharide Vaccine in Clinical Settings. *Vaccine*, **30**, 3304-3310. <http://dx.doi.org/10.1016/j.vaccine.2012.03.007>
- [6] Grabenstein, J.D. and Manoff, S.B. (2012) Pneumococcal Polysaccharide 23-Valent Vaccine: Long-Term Persistence of Circulating Antibody and Immunogenicity and Safety after Revaccination in Adults. *Vaccine*, **30**, 4435-4444. <http://dx.doi.org/10.1016/j.vaccine.2012.04.052>
- [7] Mond, J.J., Lees, A. and Snapper, C.M. (1995) T Cell-Independent Antigens Type 2. *Annual Review of Immunology*, **13**, 655-692. <http://dx.doi.org/10.1146/annurev.iv.13.040195.003255>
- [8] Snapper, C.M., Rosas, F., Moorman, M.A., Jin, L., Shanebeck, K., Klinman, D.M., Kehry, M.R., Mond, J.J. and Maliszewski, C.R. (1996) IFN-Gamma Is a Potent Inducer of Ig Secretion by Sort-Purified Murine B Cells Activated through the mIg, but not the CD40, Signaling Pathway. *International Immunology*, **8**, 877-885. <http://dx.doi.org/10.1093/intimm/8.6.877>
- [9] Vos, Q., Lees, A., Wu, Z.Q., Snapper, C.M. and Mond, J.J. (2000) B-Cell Activation by T-Cell-Independent Type 2 Antigens as an Integral Part of the Humoral Immune Response to Pathogenic Microorganisms. *Immunological Reviews*, **176**, 154-170. <http://dx.doi.org/10.1034/j.1600-065X.2000.00607.x>
- [10] Snapper, C.M., McIntyre, T.M., Mandler, R., Pecanha, L.M., Finkelman, F.D., Lees, A. and Mond, J.J. (1992) Induction of IgG3 Secretion by Interferon Gamma: A Model for T Cell-Independent Class Switching in Response to T Cell-Independent Type 2 Antigens. *The Journal of Experimental Medicine*, **175**, 1367-1371. <http://dx.doi.org/10.1084/jem.175.5.1367>
- [11] Kronenberg, M. and Gapin, L. (2002) The Unconventional Lifestyle of NKT Cells. *Nature Reviews Immunology*, **2**, 557-568.
- [12] Godfrey, D.I., MacDonald, H.R., Kronenberg, M., Smyth, M.J. and Van Kaer, L. (2004) NKT Cells: What's in a Name. *Nature Reviews Immunology*, **4**, 231-237. <http://dx.doi.org/10.1038/nri1309>
- [13] Rogers, P.R., Matsumoto, A., Naidenko, O., Kronenberg, M., Mikayama, T. and Kato, S. (2004) Expansion of Human Valpha24⁺ NKT Cells by Repeated Stimulation with KRN7000. *Journal of Immunological Methods*, **285**, 197-214. <http://dx.doi.org/10.1016/j.jim.2003.12.003>
- [14] Van Kaer, L., Parekh, V.V. and Wu, L. (2015) The Response of CD1d-Restricted Invariant NKT Cells to Microbial Pathogens and Their Products. *Frontiers in Immunology*, **6**, 226. <http://dx.doi.org/10.3389/fimmu.2015.00226>
- [15] O'Reilly, V., Zeng, S.G., Bricard, G., Atzberger, A., Hogan, A.E., Jackson, J., Feighery, C., Porcelli, S.A. and Doherty, D.G. (2011) Distinct and Overlapping Effect or Functions of Expanded Human CD4⁺, CD8a⁺ and CD4⁻CD8a⁻ Invariant Natural Killer T Cells. *PLoS One*, **6**, e28648. <http://dx.doi.org/10.1371/journal.pone.0028648>
- [16] Kobrynski, L.J., Sousa, A.O., Nahmias, A.J. and Lee, F.K. (2005) Cutting Edge: Antibody Production to Pneumococcal Polysaccharides Requires CD1 Molecules and CD8⁺ T Cells. *The Journal of Immunology*, **174**, 1787-1790.

<http://dx.doi.org/10.4049/jimmunol.174.4.1787>

- [17] Nakamatsu, M., Yamamoto, N., Hatta, M., Nakasone, C., Kinjo, T., Miyagi, K., Uezu, K., Nakamura, K., Nakayama, T., Taniguchi, M., Iwakura, Y., Kaku, M., Fujita, J. and Kawakami, K. (2007) Role of Interferon-Gamma in Valpha14⁺ Natural Killer T Cell-Mediated Host Defense against *Streptococcus pneumoniae* Infection in Murine Lungs. *Microbes and Infection*, **9** 364-374. <http://dx.doi.org/10.1016/j.micinf.2006.12.003>
- [18] Liu, T.Y., Uemura, Y., Suzuki, M., Narita, Y., Hirata, S., Ohyama, H., Ishihara, O. and Matsushita, S. (2008) Distinct Subsets of Human Invariant NKT Cells Differentially Regulate T Helper Responses via Dendritic Cells. *European Journal of Immunology*, **38**, 1012-1023. <http://dx.doi.org/10.1002/eji.200737838>
- [19] Moens, L., Wuyts, M., Meyts, I., De Boeck, K. and Bossuyt, X. (2008) Human Memory B Lymphocyte Subsets Fulfill Distinct Roles in the Anti-Polysaccharide and Anti-Protein Immune Response. *The Journal of Immunology*, **181**, 5306-5312. <http://dx.doi.org/10.4049/jimmunol.181.8.5306>
- [20] Galli, G., Nuti, S., Tavarini, S., Galli-Stampino, L., De Lalla, C., Casorati, G., Dellabona, P. and Abrignani, S. (2003) CD1d-Restricted Help to B Cells by Human Invariant Natural Killer T Lymphocytes. *The Journal of Experimental Medicine*, **197**, 1051-1057. <http://dx.doi.org/10.1084/jem.20021616>
- [21] Zeng, S.G., Ghnewa, Y.G., O'Reilly, V.P., Lyons, V.G., Atzberger, A., Hogan, A.E., Exley, M.A. and Doherty, D.G. (2013) Human Invariant NKT Cell Subsets Differentially Promote Differentiation, Antibody Production, and T Cell Stimulation by B Cells *In Vitro*. *The Journal of Immunology*, **191**, 1666-1676. <http://dx.doi.org/10.4049/jimmunol.1202223>
- [22] Lee, P.T., Benlagha, K., Teyton, L. and Bendelac, A. (2002) Distinct Functional Lineages of Human Va24 Natural Killer T Cells. *The Journal of Experimental Medicine*, **195**, 637-641. <http://dx.doi.org/10.1084/jem.20011908>
- [23] Gumperz, J.E., Miyake, S., Yamamura, T. and Brenner, M.B. (2002) Functionally Distinct Subsets of CD1d-Restricted natural Killer T Cells Revealed by CD1d Tetramer Staining. *The Journal of Experimental Medicine*, **195**, 625-636. <http://dx.doi.org/10.1084/jem.20011786>
- [24] Thedrez, A., de Lalla, C., Allain, S., Zaccagnino, L., Sidobre, S., Garavaglia, C., Borsellino, G., Dellabona, P., Bonneville, M., Scotet, E. and Casorati, G. (2007) CD4 Engagement by CD1d Potentiates Activation of CD4⁺ Invariant NKT Cells. *Blood*, **110**, 251-258. <http://dx.doi.org/10.1182/blood-2007-01-066217>
- [25] Kim, C.H., Johnston, B. and Butcher, E.C. (2002) Trafficking Machinery of NKT Cells: Shared and Differential Chemokine Receptor Expression among Va24⁺Vβ11⁺ NKT Cell Subsets with Distinct Cytokine-Producing Capacity. *Blood*, **100**, 11-16. <http://dx.doi.org/10.1182/blood-2001-12-0196>
- [26] Kim, C.H., Rott, L., Kunkel, E.J., Genovese, M.C., Andrew, D.P., Wu, L. and Butcher, E.C. (2001) Rules of Chemokine Receptor Association with T Cell Polarization *In Vivo*. *The Journal of Clinical Investigation*, **108**, 1331-1339. <http://dx.doi.org/10.1172/JCI13543>
- [27] Obukhanych, T.V. and Nussenzweig, M.C. (2006) T-Independent Type II Immune Responses Generate Memory B Cells. *The Journal of Experimental Medicine*, **203**, 305-310. <http://dx.doi.org/10.1084/jem.20052036>
- [28] Bai, L., Deng, S., Reboulet, R., Mathew, R., Teyton, L., Savage, P.B. and Bendelac, A. (2013) Natural Killer T (NKT)-B-Cell Interactions Promote Prolonged Antibody Responses and Long-Term Memory to Pneumococcal Capsular Polysaccharides. *Proceedings of the National Academy of Sciences of the United States of America*, **110**, 16097-16102. <http://dx.doi.org/10.1073/pnas.1303218110>
- [29] Maddur, M.S. and Bayry, J. (2015) B Cells Drive Th2 Responses by Instructing Human Dendritic Cell Maturation. *OncoImmunology*, **4**, e1005508. <http://dx.doi.org/10.1080/2162402x.2015.1005508>
- [30] Maddur, M.S., Sharma, M., Hegde, P., Stephen-Victor, E., Pulendran, B., Kaveri, S.V. and Bayry, J. (2014) Human B Cells Induce Dendritic Cell Maturation and Favour Th2 Polarization by Inducing OX-40 Ligand. *Nature Communications*, **9**, No. 4092. <http://dx.doi.org/10.1038/ncomms5092>
- [31] Zaini, J., Andarini, S., Tahara, M., Saijo, Y., Ishii, N., Kawakami, K., Taniguchi, M., Sugamura, K., Nukiwa, T. and Kikuchi, T. (2007) OX40 Ligand Expressed by DCs Costimulates NKT and CD4⁺ Th Cell Antitumor Immunity in Mice. *The Journal of Clinical Investigation*, **117**, 3330-3338. <http://dx.doi.org/10.1172/JCI32693>

RESEARCH ARTICLE

CD8⁺ T Cells Mediate Female-Dominant IL-4 Production and Airway Inflammation in Allergic Asthma

Chihiro Ito¹, Kaori Okuyama-Dobashi¹, Tomomitsu Miyasaka^{1*}, Chiaki Masuda¹, Miki Sato¹, Tasuku Kawano¹, Yuichi Ohkawara¹, Toshiaki Kikuchi², Motoaki Takayanagi¹, Isao Ohno¹

1 Department of Pathophysiology, Tohoku Pharmaceutical University, Miyagi, Japan, **2** Department of Respiratory Medicine and Infectious Diseases, Niigata University Graduate School of Medical and Dental Sciences, Niigata, Japan

 These authors contributed equally to this work.

 Current address: Department of Microbiology, Division of Medicine, Interdisciplinary Graduate School of Medicine and Engineering (Faculty of Medicine), University of Yamanashi, Yamanashi, Japan

* t-miya13@tohoku-pharm.ac.jp



CrossMark
click for updates

OPEN ACCESS

Citation: Ito C, Okuyama-Dobashi K, Miyasaka T, Masuda C, Sato M, Kawano T, et al. (2015) CD8⁺ T Cells Mediate Female-Dominant IL-4 Production and Airway Inflammation in Allergic Asthma. PLoS ONE 10(10): e0140808. doi:10.1371/journal.pone.0140808

Editor: Hiroshi Shiku, Mie University Graduate School of Medicine, JAPAN

Received: May 25, 2015

Accepted: September 29, 2015

Published: October 21, 2015

Copyright: © 2015 Ito et al. This is an open access article distributed under the terms of the [Creative Commons Attribution License](https://creativecommons.org/licenses/by/4.0/), which permits unrestricted use, distribution, and reproduction in any medium, provided the original author and source are credited.

Data Availability Statement: All relevant data are within the paper and its Supporting Information files.

Funding: This work was supported in part by a Grant-in-Aid for Scientific Research (No. 25461164) to I.O. (<https://www.jsps.go.jp/english/index.html>), a Grant-in-Aid for Research Activity Start-up (No. 25893222) to T.M. (<https://www.jsps.go.jp/english/index.html>), the Science Research Promotion Fund from the Promotion and Mutual Aid Corporation for Private Schools of Japan to T. Kawano (http://www.shigaku.go.jp/s_home.htm), and by the Matching Fund Subsidy for Private Universities from the Ministry of Education, Culture, Sports, Science and

Abstract

The prevalence and severity of bronchial asthma are higher in females than in males after puberty. Although antigen-specific CD8⁺ T cells play an important role in the development of asthma through their suppressive effect on cytokine production, the contribution of CD8⁺ T cells to sex differences in asthmatic responses remains unclear. In the present study, we investigated the sex-specific effect of CD8⁺ T cells in the suppression of asthma using an ovalbumin mouse model of asthma. The number of inflammatory cells in bronchoalveolar lavage (BAL) fluid, lung type 2 T-helper cytokine levels, and interleukin-4 (IL-4) production by bronchial lymph node cells were significantly higher in female wild-type (WT) mice compared with male mice, whereas no such sex differences were observed between male and female *cd8α*-disrupted mice. The adoptive transfer of male, but not female, CD8⁺ T cells reduced the number of inflammatory cells in the recovered BAL fluid of male recipient mice, while no such sex difference in the suppressive activity of CD8⁺ T cells was observed in female recipient mice. Male CD8⁺ T cells produced higher levels of IFN-γ than female CD8⁺ T cells did, and this trend was associated with reduced IL-4 production by male, but not female, CD4⁺ T cells. Interestingly, IFN-γ receptor expression on CD4⁺ T cells was significantly lower in female mice than in male mice. These results suggest that female-dominant asthmatic responses are orchestrated by the reduced production of IFN-γ by CD8⁺ T cells and the lower expression of IFN-γ receptor on CD4⁺ T cells in females compared with males.

Technology (MEXT) of Japan to I.O., T.M., and T. Kawano (<http://www.mext.go.jp/english/>). The funders had no role in study design, data collection and analysis, decision to publish, or preparation of the manuscript.

Competing Interests: The authors have declared that no competing interests exist.

Introduction

Bronchial asthma is characterized by chronic airway inflammation in response to inhaled allergens, leading to wheezing, coughing, chest tightness and shortness of breath. Despite advances in both short- and long-term control medications for asthma, the incidence rate of asthma deaths is 1.4 per 10,000 persons with asthma in general population, but can be as high as 5.8 per 10,000 persons with asthma, especially in people aged 65 or over in the USA [1]. In addition, the prevalence of asthma in children aged 0–17 years has increased over the last few years [1].

Gender is an important universal risk factor for severe asthma exacerbations and death [2, 3]. Recent studies have demonstrated that the prevalence and severity of asthma in adults are higher in women than in men [4, 5]. In addition, the rate of relapse after discharge from the emergency department for acute asthma among adults is also higher in women than in men [6], which is likely associated with sex differences in resistance to controller medications such as inhaled corticosteroids [7].

In the development of asthma, allergen-specific CD4⁺ T cells play a pivotal role by facilitating airway inflammation, which is largely mediated by type 2 T-helper (Th2) cytokines such as interleukin 4 (IL-4), IL-5 and IL-13 [8]. IL-4 directly promotes the polarization of naïve CD4⁺ T cell differentiation towards Th2 phenotype, which initiates inflammatory responses and propagates the symptoms of asthma [9, 10]. Furthermore, IL-4 induces higher levels of vascular cell adhesion molecule 1 (VCAM-1) expression on endothelial cells [11], which results in the accumulation of T lymphocytes, monocytes, basophils, and, most prominently, eosinophils to the site of allergic airways. Data from *Il4*-disrupted (knockout) (IL-4KO) mice and CD4-depleted mice revealed the attenuated hallmark signs of asthma, including the accumulation of eosinophils in BAL fluid and airway hyperresponsiveness, indicating that IL-4 production from CD4⁺ T cells is a key factor in the development of asthma [12–14].

Sex-specific differences in Th2 cytokine production have been reported in both asthmatic patients and mice. Recently, Loza et al. demonstrated that greater numbers of IL-13-producing T cells differentiated from anti-CD3/CD28-stimulated peripheral blood lymphocytes taken from atopic asthmatic female subjects compared with male subjects [15]. In our previous studies using murine models of asthma, the recovery of IL-4, IL-5 and IL-13 in bronchoalveolar lavage (BAL) fluid from female mice was significantly higher than that of male mice [16]. Although female-dominant Th2 cytokine production was observed in lung and bronchial lymph node (BLN) cells [16, 17], it is not yet fully understood how these sex differences in Th2 cytokine production are generated in the development of asthma.

CD8⁺ T cells produce Th1- and Th2-associated cytokines and can function as helper T cells under Th2-polarizing conditions [18, 19]. Previous studies revealed that majority of the CD8⁺ T cells in asthma secrete IFN- γ and may act to antagonize a Th2 response [20–22]. Philippe et al. demonstrated that CD8⁺ T cells from the spleens of asthmatic mice produced large amounts of IFN- γ but little IL-4 or IL-5 [18]. The adoptive transfer of antigen-specific CD8⁺ T cells from the cervical lymph nodes increased the number of IFN- γ -producing cells in the lung, which was involved in suppressing late-phase allergic airway responses [23].

Therefore, in the present study, we aimed to determine the role that CD8⁺ T cells play in female-dominant IL-4 production in adult asthma using a mouse model. We found that CD8⁺ T cells were required for the observed sex differences in allergic airway inflammation. The sex differences in IFN- γ production by CD8⁺ T cells and IFN- γ receptor expression on CD4⁺ T cells may be a necessary and sufficient for female-dominant IL-4 production in asthma.

Materials and Methods

Mice

Male and female wild-type (WT) C57BL/6 mice and *cd8α*-disrupted (knockout) CD8KO mice were purchased from CLEA Japan (Osaka, Japan) and the Jackson Laboratory (Bar Harbor, ME, USA), respectively. All mice were kept under specific pathogen-free conditions at the Institute for Animal Experimentation, Tohoku Pharmaceutical University (Sendai, Japan). All experimental procedures involving animals were approved by the Committee of Animal Experiments at Tohoku Pharmaceutical University (approved numbers: 12023-cn, 13001-cn-a and 14002-cn). We took the utmost care to alleviate any pain and suffering on the part of the mice.

Sensitization and antigen challenge

Mice at 6 to 8 weeks of age were sensitized by intraperitoneal injections of 8 μg of ovalbumin (OVA; Grade V, Sigma-Aldrich, St Louis, MO, USA) adsorbed with aluminum hydroxide (Wako Pure Chemical Industries, Osaka, Japan) on days 0 and 5 [24]. On day 30, the mice were challenged with aerosolized OVA (0.5% in saline) for 1 h on two occasions 4 h apart.

Preparation of bronchoalveolar lavage fluids

BAL samples were collected with 2 x 0.25 ml of chilled PBS through a cannula inserted in the trachea. Total cell numbers recovered from the BAL fluid were counted with a hemocytometer. Then, 2×10^5 cells were centrifuged onto a glass slide using a Cytospin 4 (Shandon, Runcorn, UK) and then stained with Diff-Quick solution (International Reagents Corp., Kobe, Japan). Cell differential percentages were determined by counting a minimum of 200 cells under light microscopy.

Preparation of lung homogenates

The lung were excised one day after OVA challenge from WT and CD8KO mice and homogenized in chilled 0.1% Triton-X PBS with 1% protease inhibitor (Sigma-Aldrich). After centrifugation at $15,000 \times g$ for 15 min at 4°C, the supernatants were stored at -80°C for subsequent cytokine assays.

Cell preparation and stimulation

BLN cells were prepared from WT and CD8KO mice (5 to 14 mice for one experiment) one day after OVA challenge as previously described [17]. BLN cells (4×10^5 cells/well) were cultured in the presence of OVA for 3 days. Lipopolysaccharide (LPS) prepared from *Escherichia coli* O-111 (Sigma-Aldrich) was used as a control. CD4⁺ T cells and CD8⁺ T cells in BLN, and CD11c⁺ cells in spleen of sensitized and challenged male and female WT mice were purified by positive selection on an autoMACS Separator (Miltenyi Biotec, Bergish Gladbach, Germany) using anti-mouse CD4 (L3T4), anti-mouse CD8α (Ly-2) and anti-mouse CD11c MicroBeads (Miltenyi Biotec), respectively. CD4⁺ T cells were co-cultured with male or female CD8⁺ T cells and CD11c⁺ cells in the presence of OVA for 3 days. CD11c⁺ cells were prepared as a mixture of male and female CD11c⁺ cells at ratio of 1:1. Because we previously reported the functional difference in CD11c⁺ cells from BLN between male and female mice [25], it is possible that the function of splenic CD11c⁺ cells were different between the sexes. Therefore, in order to exclude the influence of sex differences in the antigen presenting cells, the mixture of CD11c⁺ cells was used in this study. A 10 μg/ml of anti-IFN-γ neutralizing antibody (Ab) (PeproTech, Inc., Rocky Hill, New Jersey, USA) was used to block the effects of IFN-γ. In another experiment, CD4⁺ T cells and CD11c⁺ cells were cultured with 10 ng/ml of recombinant (r)IFN-γ

(PeproTech) [26]. Naïve CD4⁺ T cells were isolated from spleen of male and female WT mice using autoMACS Separator and cultured with rIFN- γ (10 ng/ml) for 72 h. The concentration of IFN- γ (10 ng/ml) [26] used in the current study was about 1,000 times higher than that, the levels of pg/ml, in BAL fluids and lung homogenates in mice models of allergic asthma [27]. However, the concentration at the site of inflammation would be higher than the concentration in samples such as BAL fluids and lung homogenates in consideration of the sampling procedures.

Flow cytometric analysis

The BAL cells were preincubated with anti-FcR2 and III mAb on ice for 15 min in PBS containing 1% fetal calf serum (FCS) and 0.1% sodium azide, and stained with APC-conjugated anti-CD3 (Clone 145-2C11; BioLegend, San Diego, CA, USA), FITC-conjugated anti-CD4 (clone GK1.5; BioLegend) and peridinin-chlorophyll protein complex (PerCP)-conjugated anti-CD8 (Clone 53-6.7; BioLegend). For intracellular staining of IL-4 and IFN- γ on T cells, BLN cells were isolated from WT mice one day after challenge, and cultured at 2×10^5 cells with 5 ng/ml of phorbol 12-myristate 13-acetate, 500 ng/ml of ionomycin and 2 μ M of monensin (Sigma-Aldrich) for 4 hours at 37°C before the cell surface was stained. Then, Fc receptors on cell surface were blocked, and cells were stained with PerCP-conjugated anti-CD3 (Clone 145-2C11; BioLegend) and FITC-conjugated anti-CD4 (BioLegend) or FITC-conjugated anti-CD8 mAbs (clone 53-6.7; BD Biosciences Pharmingen, San Diego, CA, USA). The isotype-matched control IgG for each Ab was used as a reference. Cells were then incubated in the presence of cytofix/cytoperm (BD Biosciences Pharmingen), washed twice in BD perm/wash solution and stained with phycoerythrin (PE)-conjugated anti-IL-4 (clone 11B11; Biolegend), PE-conjugated anti-IFN- γ mAbs (clone XMG1.2; eBiosciences) or control rat IgG. For evaluation of IFN- γ receptor expression on CD4⁺ T cells, BLN cells obtained from asthmatic WT mice and splenic CD4⁺ T cells from naïve WT mice were stained with PE-conjugated anti-mouse CD119 (anti-IFN- γ receptor α , clone 2E2; eBioscience) or anti-IFN- γ receptor β chain (clone MOB-47; BioLegend). The stained cells were analyzed using a BD FACSCalibur flow cytometer (BD Biosciences, San Jose, CA, USA) or BD AriaII flow cytometer (BD Biosciences). Data were collected from 30,000 individual cells using parameters of forward scatter (FSC) and side scatter (SSC) to limit the lymphocyte population. The number of CD4⁺ and CD8⁺ T cells was estimated by multiplying the lymphocyte number, calculated as mentioned above, by the proportion of each subset.

Quantitative real-time RT-PCR analysis

Total RNA was extracted from the CD8⁺ T cells using an RNeasy Micro Kit (QIAGEN, Valencia, CA, USA), and the first-strand cDNA was synthesized using PrimeScript RT reagent kit with gDNA Eraser (TaKaRa Bio Inc., Otsu, Japan). Quantitative real-time reverse transcription (RT)-PCR was performed using gene-specific primer and Power SYBR Green PCR Master Mix (Applied Biosystems, Foster City, CA, USA) in a StepOnePlus Real-Time PCR System (Applied Biosystems). The primer sequences used for amplification are shown in Table 1. The expression levels of target genes and hypoxanthine-guanine phosphoribosyltransferase (*Hprt*) as a reference were calculated for each sample using the reaction efficiency determined using standard amplifications.

Measurement of cytokine concentration

The levels of IL-2, IL-4 and IFN- γ in lung homogenates and culture supernatants were assayed using an ELISA kits (eBioscience, San Diego, CA, USA). The detection limits were 2 pg/ml for

Table 1. Primer sequences for quantitative real-time RT-PCR.

	Forward (5'-3')	Reverse (5'-3')
IFN- γ	ATCTGGAGGAAGTGGCAAAGGATG	ATGACGCTTATGTTGTTGCTGATGG
T-bet	CACTAAGCAAGGACGGCGAATG	GTCCACCAAGACCACATCCACAA
GATA-3	TCTGGAGGAGGAACGCTAATGGG	TTCGGGTCTGGATGCCTTCTTTC
IL-10	GCACTACCAAAGCCACAAGGCA	CAGTAAGAGCAGGCAGCATAGCA
TGF- β_1	TGATACGCCTGAGTGGCTGTC	CCTGTATTCCGCTCTCCTTGGTTCA
Perforin	ACTACGGCTGGGATGATGACCTT	GTGAGATGGGGCAGACACTTGG
Fas ligand	TTCTGGTGGCTCTGGTTGGAATG	ACTGGGGTTGGCTATTTGCTTTTC
HPRT	TTGGGCTTACCTCACTGCTTTCC	ATCATCGCTAATCACGACGCTGG

HPRT: hypoxanthine-guanine phosphoribosyltransferase.

doi:10.1371/journal.pone.0140808.t001

IL-2, 4 pg/ml for IL-4 and 15 pg/ml for IFN- γ . The contents of IL-5 and IL-13 in the lung homogenates were measured using an ELISA kits (R&D systems, Minneapolis, MN, USA). The limits of detection were 7 and 1.5 pg/ml, respectively. Total protein levels of lung homogenates were measured using a detergent-compatible protein assay kit (Bio-Rad Laboratory, Hercules, CA, USA). The cytokine concentration was adjusted for the protein level of each lung.

Adaptive transfer of CD8⁺ T cells

CD8⁺ T cells (4×10^5 cells/mouse) were transferred into OVA-sensitized CD8KO mice via the tail vein. Three days later, mice were challenged with aerosolized OVA.

Statistical analysis

Statistical analysis was conducted using GraphPad Prism 5 software (GraphPad Software, La Jolla, CA, USA). Differences between the two groups were tested using two-tail analysis in an unpaired Student's *t*-test. Differences among three groups or more were tested using ANOVA with post hoc analysis (Student-Newman-Keuls test). A *p*-value of less than 0.05 was considered significant.

Results

Involvement of CD8⁺ T cells in sex differences in asthma features

To clarify the sex differences in prototypical asthma-related features in WT mice, we initially compared the development of airway inflammation between male and female WT mice. As shown in Fig 1A, the numbers of total cells, eosinophils and lymphocytes in the BAL fluid of female WT mice were significantly higher than those in male WT mice. Furthermore, the number of CD4⁺ T cells in BAL fluids of WT mice was significantly higher in female mice than in male mice, whereas CD8⁺ T cell counts in BAL fluids were not different between male and female mice (Fig 1C). By contrast, the sex differences in differential cell counts and the number of CD4⁺ T cells in BAL fluids were abrogated in CD8KO mice (Fig 1B and 1D). Furthermore, the production of Th2 cytokines such as IL-4, IL-5 and IL-13 in the lung were significantly increased in female WT mice compared to male WT mice (Fig 2A), although there was no apparent difference between male and female CD8KO mice (Fig 2B). In the case of Th1 cytokine production, the sex differences in IL-2 and IFN- γ contents in the lung were not observed between male and female WT mice, whereas those cytokines were significantly higher in female CD8KO mice than male CD8KO mice (Fig 2A and 2B). These data indicate that CD8⁺ T cells

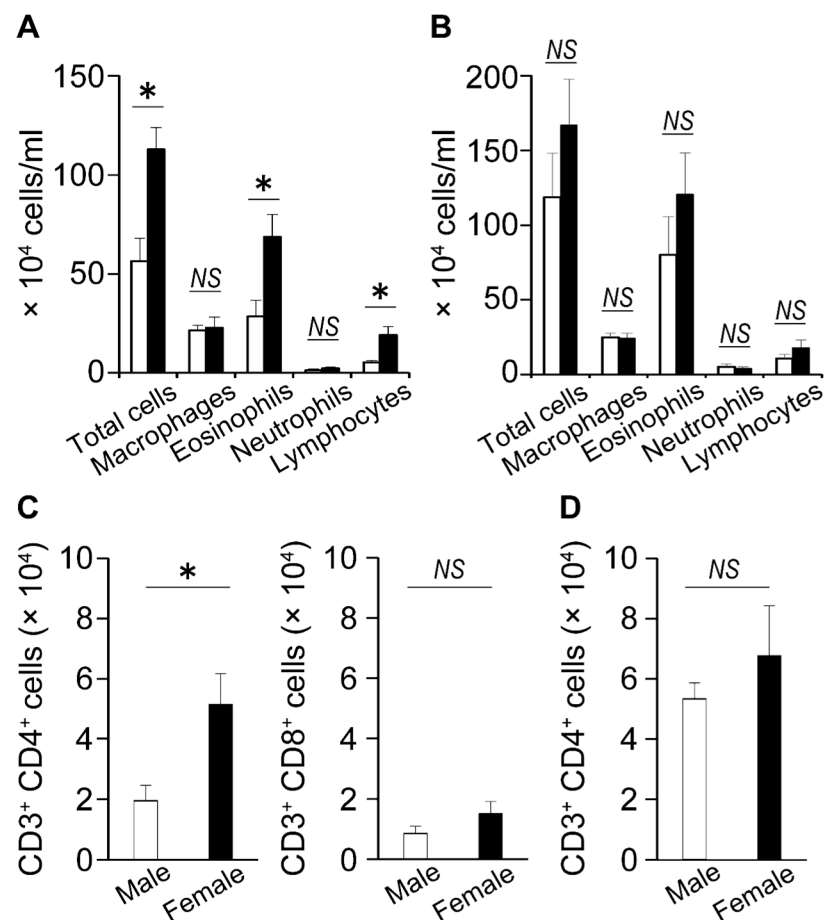


Fig 1. Sex differences in inflammatory cell infiltration in BAL fluid. Male and female WT mice (A) and CD8KO mice (B) were sensitized and challenged. The number of inflammatory cells in BAL fluids were counted on day 5 after OVA challenge. Data are shown as the mean \pm SEM from at least three independent experiments ($n = 12-16$). (C and D) The number of CD4⁺ and CD8⁺ T cells in BAL fluids of WT mice (C) and CD8KO mice (D) on day 5 after OVA challenge is shown. Each column represents the mean \pm SEM of four to five mice. Open bars, male mice; closed bars, female mice. *, $P < 0.05$; NS, not significant.

doi:10.1371/journal.pone.0140808.g001

may be involved in the development of the sex differences in asthmatic responses, including Th1 and Th2 cytokine production, and eosinophil and lymphocyte infiltration in the lungs.

Involvement of CD8⁺ T cells in female-dominant IL-4 production by bronchial lymph node cells

The pathogenesis of asthma is directed by allergen-specific Th2 cells generated in the secondary lymphoid organs such as the BLN, and the migration of Th2 cells into lung plays an important role in mobilization of eosinophils via the secretion of IL-4 and IL-5 [28]. Therefore, to address the role of CD8⁺ T cells in sex differences in cellular responses to inhaled allergen, we examined how the lack of CD8⁺ T cells affected the production of IL-4 by BLN cells upon stimulation with OVA. As shown in Fig 3A, the production of IL-4 by BLN cells upon stimulation with OVA was significantly higher in female WT mice than in males. A similar pattern was observed when T cells were non-specifically activated via LPS. In contrast, female-dominant IL-4 production by BLN cells upon stimulation was not observed in CD8KO mice (Fig 3B).

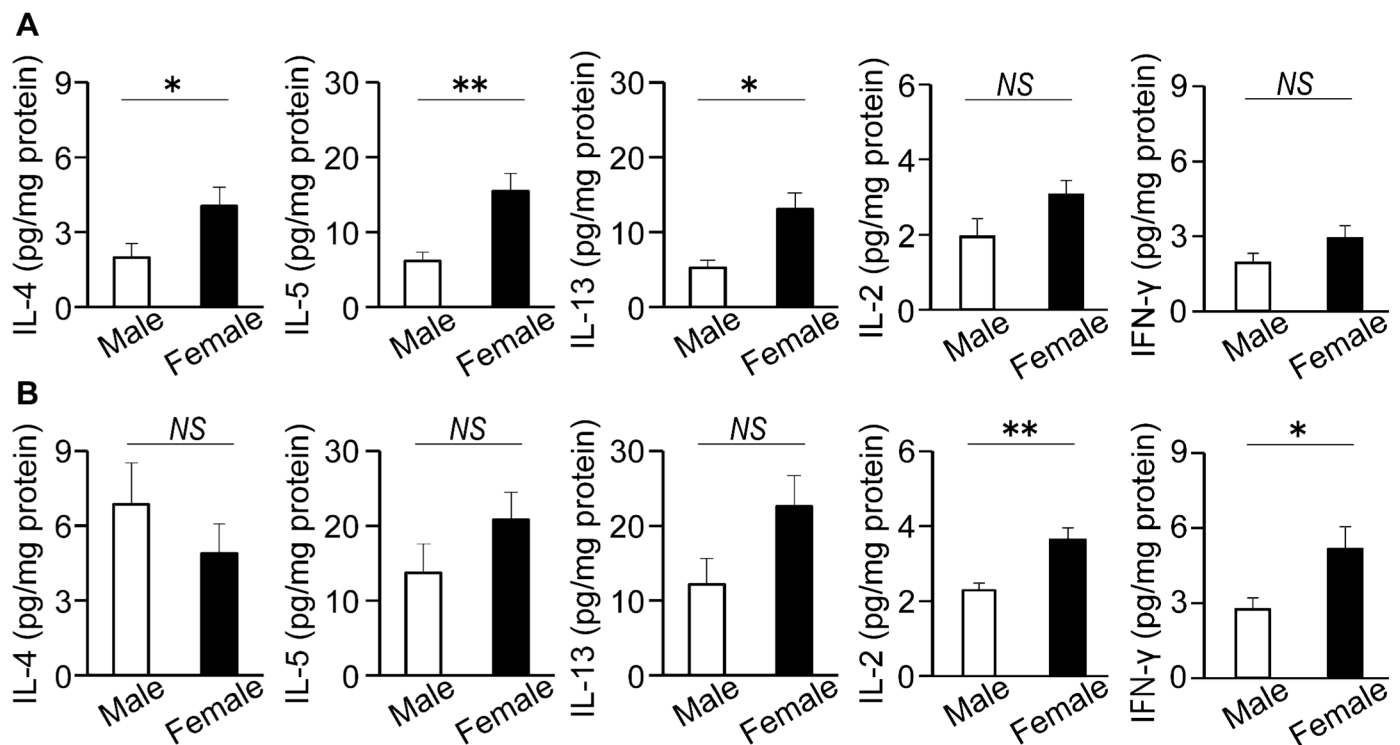


Fig 2. Sex differences in cytokine production in lung. Male and female WT mice (A) and CD8KO mice (B) were sensitized and challenged. IL-2, IL-4, IL-5, IL-13 and IFN-γ levels in the lung were measured by ELISA one day after OVA challenge. Data are shown as the mean ± SEM from at least three independent experiments (n = 8–11). Open bars, male mice; closed bars, female mice. *, P < 0.05; **, P < 0.01; NS, not significant.

doi:10.1371/journal.pone.0140808.g002

Male CD8⁺ T cells show reduced IL-4 production by male CD4⁺ T cells

CD8⁺ T cells attenuate allergic inflammation and play a central role in moderating Th2 polarization within the lymph nodes during allergic sensitization [29]. Therefore, to address the sex difference in suppressive effects of CD8⁺ T cells on IL-4 production by CD4⁺ T cells, male or female CD4⁺ T cells derived from BLN were cultured with male or female CD8⁺ T cells isolated

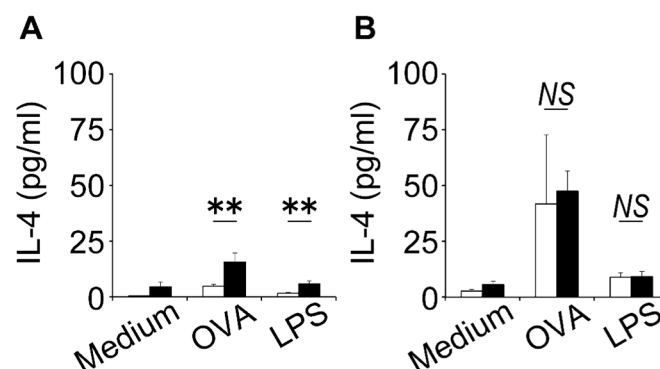


Fig 3. Sex differences in IL-4 production from BLN cells. BLN cells from WT mice (A) and CD8KO (B) mice were prepared one day after OVA inhalation and cultured with 3 μg/ml of OVA or 1 μg/ml of LPS for 72 h. The concentration of IL-4 in the culture supernatants was measured by ELISA. Data are shown as the mean ± SD of triplicate cultures. Experiment were repeated twice with similar results. Open bars, BLN cells from male mice; closed bars, BLN cells from female mice. **, P < 0.01; NS, not significant.

doi:10.1371/journal.pone.0140808.g003

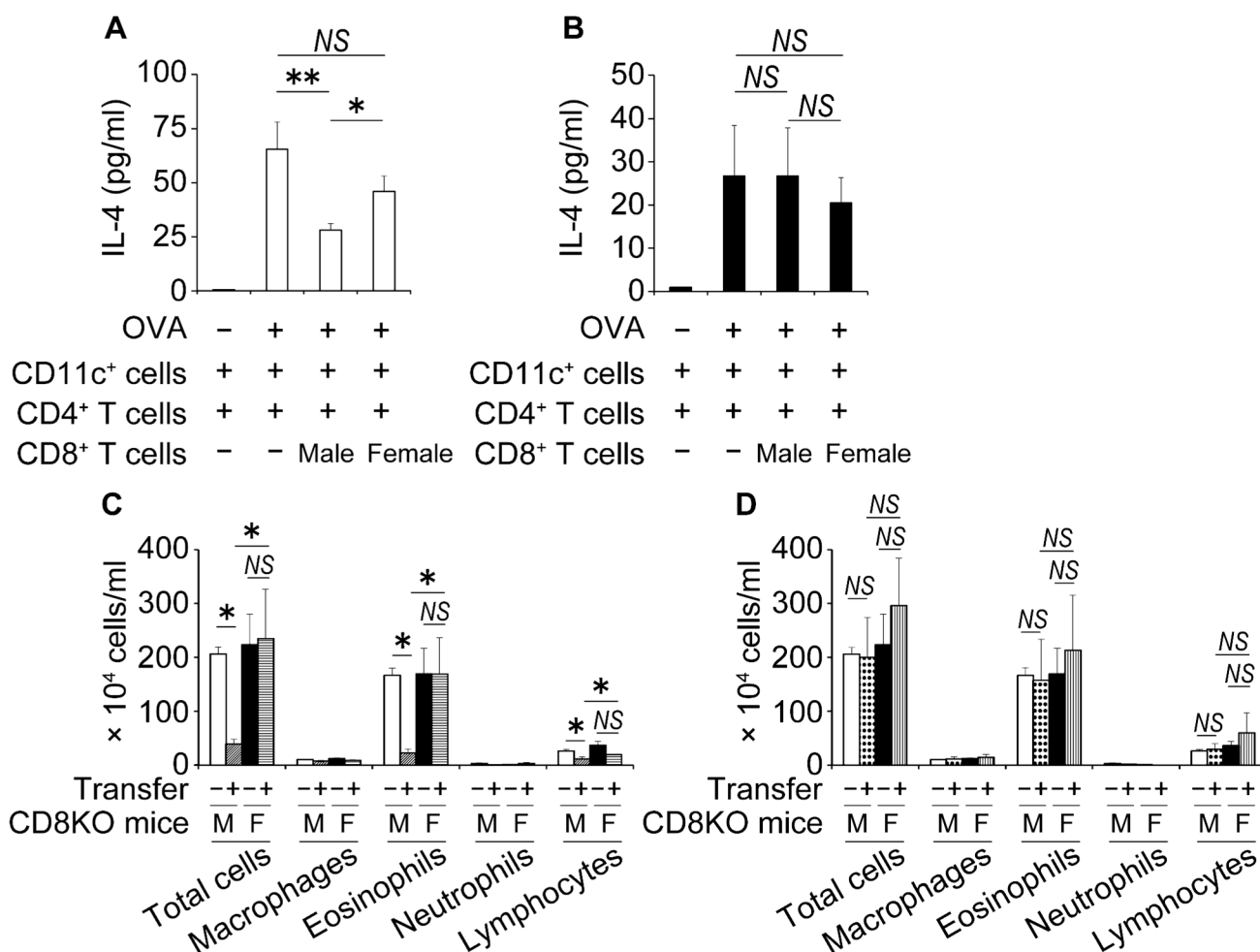


Fig 4. Sex differences in the inhibitory effect of BLN CD8⁺ T cells. Male (A) or female (B) CD4⁺ T cells (2×10^5 cells/well) were cultured with CD8⁺ T cells (2×10^5 cells/well) and splenic CD11c⁺ cells (2×10^5 cells/well) in the presence of OVA (50 μ g/ml) for 72 h. Concentration of IL-4 in the culture supernatants was measured by ELISA. Data are shown as the mean \pm SD of triplicate cultures. Experiment were repeated twice with similar results. (C and D) Sensitized male or female CD8KO mice were adoptively transferred with CD8⁺ T cells from BLN of sensitized and challenged male (C) or female (D) WT mice. Saline was used as control of the transfer. Three days later, recipient CD8KO mice were challenged with OVA aerosol, and then sacrificed on day 5 post-OVA challenge. The numbers of inflammatory cells in BAL fluids were counted. Data are shown as the mean \pm SEM from two independent experiments ($n = 4-9$). Open bars, male mice transferred with saline; closed bars, female mice transferred with saline; hatched bars, male mice transferred with male CD8⁺ T cells; horizontal line bars, female mice transferred with male CD8⁺ T cells; dotted bars, male mice transferred with female CD8⁺ T cells; vertical line bars, female mice transferred with female CD8⁺ T cells. -, mice transferred with saline; +, mice transferred with CD8⁺ T cells; *, $P < 0.05$; **, $P < 0.01$; NS, not significant.

doi:10.1371/journal.pone.0140808.g004

from BLN cells of WT mice in the presence of CD11c⁺ cells as antigen-presenting cells with OVA. As shown in Fig 4A, the amount of IL-4 in the cultures of male CD4⁺ T cells were significantly reduced in the presence of male CD8⁺ T cells, but not in the presence of female CD8⁺ T cells, compared with the amount recovered in the absence of CD8⁺ T cells. In contrast, the amount of IL-4 in the cultures of female CD4⁺ T cells was not reduced in the presence of either male or female CD8⁺ T cells, compared with the amount in the absence of CD8⁺ T cells (Fig 4B). These results suggest that the attenuation of CD8⁺ T cell-mediated suppression may play a role in the elevated IL-4 production in the BLN of female mice.

Male CD8⁺ T cells contribute to the suppression of inflammatory cell infiltration in the BAL fluid of male mice

We next examined the functional relevance of the suppressive effect of CD8⁺ T cells on the infiltration of inflammatory cells into the lung. BLN CD8⁺ T cells from male or female WT mice were transferred intravenously into sensitized CD8KO mice that then inhaled OVA on day 3 after the cell transfer. As shown in Fig 4C, the transfer of male CD8⁺ T cells into male CD8KO mice significantly reduced the numbers of total cells, eosinophils and lymphocytes in BAL fluids compared with saline transfer. The transfer of male CD8⁺ T cells into female CD8KO mice, however, did not have this effect. In contrast, the transfer of female CD8⁺ T cells to neither male nor female CD8KO mice significantly reduced the numbers of inflammatory cells in BAL fluid compared with saline transfer (Fig 4D).

The involvement of IFN- γ in the suppressive effect of male CD8⁺ T cells

It has been established that IFN- γ plays an important role in suppressing the development of Th2 cells as well as Th2 cytokine production [30]. Therefore, we first compared the expression of IFN- γ in male and female CD8⁺ T cells isolated from BLN one day after OVA challenge. As shown in Fig 5A, IFN- γ production in CD8⁺ T cells was significantly higher in male WT mice than female WT mice, although IL-4 production did not differ between male and female CD8⁺ T cells. In line with these data, the expression of *Ifng* mRNA in CD8⁺ T cells was also higher in male WT mice than in female WT mice (Fig 5B). These results suggest that the induction of type-1-cytokine-producing CD8⁺ T cell responses may be facilitated in the BLN of male WT mice under allergic asthma conditions. This possibility was supported by the finding that *Tbet* expression levels were significantly higher in male CD8⁺ T cells than in female CD8⁺ T cells, whereas *Gata3* expression levels did not differ between male and female CD8⁺ T cells (Fig 5C). In addition, we sought to establish whether the addition of an anti-IFN- γ monoclonal (m)Ab would alter the observed sex difference in the suppressive effect of CD8⁺ T cells on IL-4 production by male CD4⁺ T cells. As shown in Fig 5D, this treatment completely abrogated the sex difference in the suppressive activity of CD8⁺ T cells on IL-4 production from male CD4⁺ T cells, whereas the addition of control rat IgG did not.

The expression of the IFN- γ receptor on CD4⁺ T cells is implicated in the sex differences in CD8⁺ T cell-mediated suppression

In Fig 4, the suppressive effects of male CD8⁺ T cells on IL-4 production were observed in the cultures of male CD4⁺ T cells but not female CD4⁺ T cells. Furthermore, those effects of male CD8⁺ T cells on the accumulation of inflammatory cells into the airway were observed in CD8KO male, but not female, mice. These results suggest that the sex difference in asthmatic responses may be due to both sex-specific functional differences in CD8⁺ T cells in terms of IFN- γ production and CD4⁺ T cells in terms of the sensitivity to suppressive stimuli such as IFN- γ . To address this possibility, we examined sex differences in the susceptibility of CD4⁺ T cells to the inhibitory activity of CD8⁺ T cells. As shown in Fig 6, IL-4 production from male CD4⁺ T cells was reduced by adding rIFN- γ , whereas this effect was not observed in female CD4⁺ T cells. Furthermore, the amount of IL-4 produced by female CD4⁺ T cells was significantly higher than male CD4⁺ T cells in the presence of IFN- γ , whereas the amount of IL-4 produced by CD4⁺ T cells did not differ between male and female mice in the absence of IFN- γ . These results suggest that sex differences in the susceptibility of CD4⁺ T cells to IFN- γ are implicated in the sex differences in IL-4 production by CD4⁺ T cells. In agreement with these

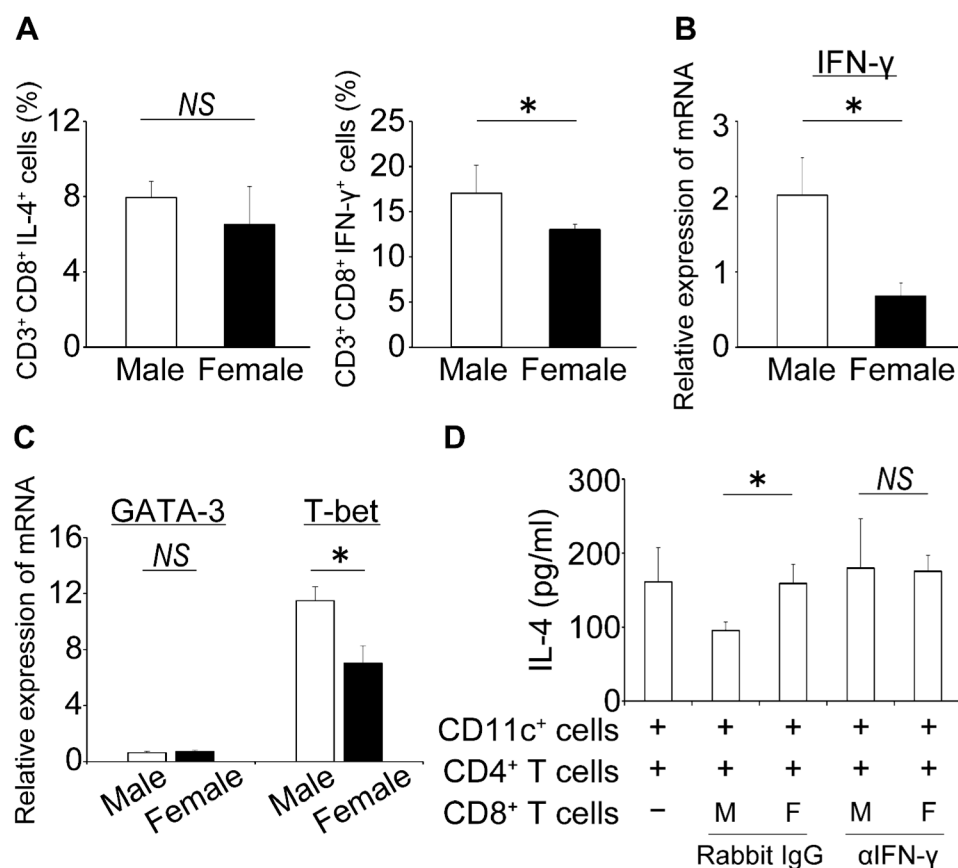


Fig 5. Involvement of IFN-γ in sex differences in the inhibitory effect of BLN CD8⁺ T cells. (A) Intracellular cytokine expression by CD8⁺ T cells was analyzed using a flow cytometer. Data are shown as the mean ± SD of four mice. The expression of *Ifng* (B), *Gata3* and *Tbet* (C) in CD8⁺ T cells were measured by quantitative real-time RT-PCR. Data are shown as the mean ± SEM of four to eight mice. (D) Male CD4⁺ T cells (2×10^5 cells/well), CD11c⁺ cells (2×10^5 cells/well) and CD8⁺ T cells (0.66×10^5 cells/well) were cultured with 50 μg/ml of OVA in presence of an anti-IFN-γ mAb (10 μg/ml) or control IgG for 72 h. The concentration of IL-4 in the culture supernatants was measured by ELISA. Data are shown as the mean ± SD of triplicate cultures. Experiment were repeated twice with similar results. *, $P < 0.05$; NS, not significant.

doi:10.1371/journal.pone.0140808.g005

data, the expression of the IFN-γ receptor α (Fig 7A and 7B) and β chain (Fig 7A and 7C) on CD4⁺ T cells was strikingly lower in female mice compared with male mice.

The involvement of IFN-γ in the sex differences in IFN-γ receptor expression on CD4⁺ T cells

To further address the mechanisms that regulate sex differences in the expression of IFN-γ receptors on CD4⁺ T cells, we examined the effect of IFN-γ on IFN-γ receptor α and β expression on WT naïve CD4⁺ T cells. As shown in Fig 7D and 7E, the proportion of IFN-γ receptor α⁺ CD4⁺ T cells was significantly increased in both male and female mice, although the proportion of IFN-γ receptor β⁺ CD4⁺ T cells was significantly reduced in both male and female mice. In addition, there was a significant difference in the proportion of IFN-γ receptor α⁺ CD4⁺ and receptor β⁺ CD4⁺ T cells between male and female mice after the treatment.

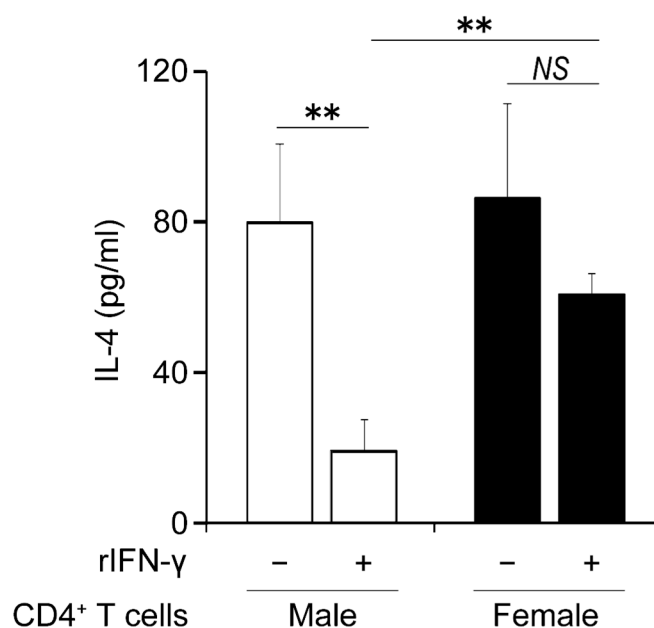


Fig 6. IFN- γ attenuates IL-4 production from BLN male CD4⁺ T cells. Male or female CD4⁺ T cells (2×10^5 cells/well) and CD11c⁺ cells (2×10^5 cells/well) were cultured with 50 μ g/ml of OVA in presence of rIFN- γ (10 ng/ml) or vehicle for 72 h. Data are shown as the mean \pm SD of triplicate cultures. Experiments were repeated twice with similar results. Open bars, male CD4⁺ T cells; closed bars, female CD4⁺ T cells. **, $P < 0.01$; NS, not significant.

doi:10.1371/journal.pone.0140808.g006

Discussion

This is the first report demonstrating that CD8⁺ T cells play an important role in the development of sex difference in allergic airway inflammation, indicated by the following findings that

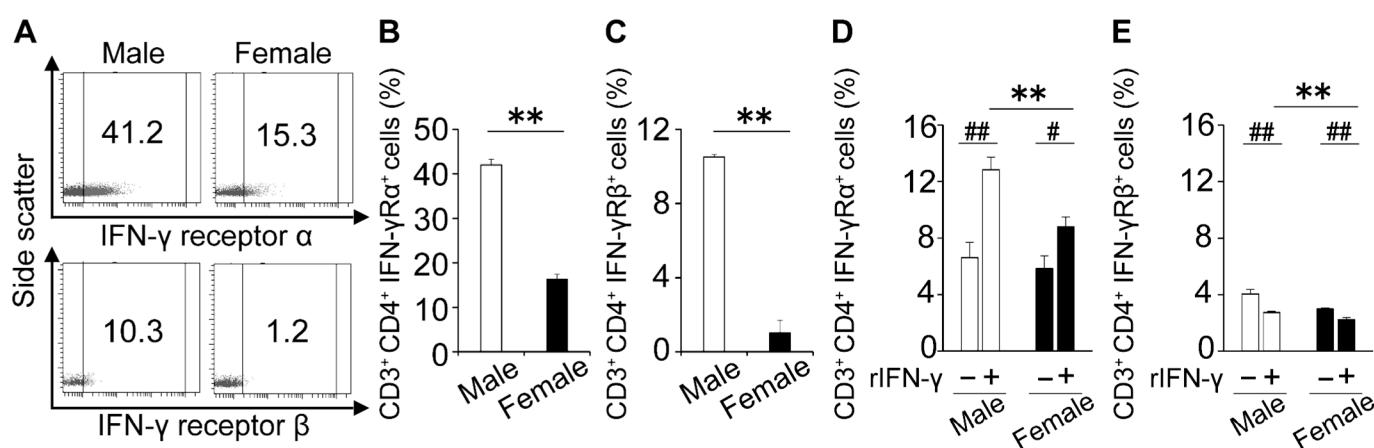


Fig 7. Sex differences in IFN- γ receptor expression on CD4⁺ T cells from WT mice. (A) Representative profiles of IFN- γ receptor expression on CD4⁺ T cells in BLN of male and female mice are shown. Cut-off lines were determined on the basis of an IgG isotype-matched control profile. The percentages of IFN- γ receptor α ⁺ population (B) and IFN- γ receptor β ⁺ population (C) in CD4⁺ T cells were analyzed in each group. Data are shown as the mean \pm SD of three to five mice. Experiment were repeated twice with similar results. (D and E) CD4⁺ T cells obtained from naïve WT mice were cultured with rIFN- γ (10 ng/ml) for 72 h. The percentage of IFN- γ receptor α ⁺ population (D) and IFN- γ receptor β ⁺ population (E) in CD4⁺ T cells were analyzed before and after the culture. Data are shown as the mean \pm SD of triplicate cultures. Experiments were repeated twice with similar results. **, $P < 0.01$ compared with male mice; #, $P < 0.05$; ##, $P < 0.01$ compared to vehicle pretreatments.

doi:10.1371/journal.pone.0140808.g007

i) the number of eosinophils, lymphocytes and CD4⁺ cells in BAL fluid (Fig 1A and 1C) and the levels of recovered Th2 cytokines in the lung (Fig 2A) were greater in female WT mice than male WT mice; ii) this female-dominant allergic inflammation was not observed in CD8KO mice (Figs 1B, 1D and 2B); and iii) the adoptive transfer of male CD8⁺ T cells significantly reduced the infiltration of inflammatory cells in the BAL fluid of male but not female CD8KO mice leading to female-dominant airway inflammation, whereas that of female CD8⁺ T cells did not (Fig 4C and 4D). By comparison of WT mice with CD8KO mice in each sex, the sex differences in allergic airway inflammation were likely to depend on higher suppression by CD8⁺ T cells in male than female mice, confirmed by the CD8⁺ T cell transfer experiments. The inhibitory role of CD8⁺ T cells in the regulation of allergic inflammatory responses has been extensively investigated, although the sex-related function of CD8⁺ T cells in the regulation of allergic asthma has never been investigated. Tang and coworkers reported that antigen-specific effector CD8⁺ T cells attenuated allergic pulmonary inflammation by enhancing IFN- γ production and altering the ability of pulmonary dendritic cells (DCs) to polarize OVA-specific CD4⁺ T cells toward a Th1 phenotype [31]. The depletion of CD8⁺ T cells increased the circulating levels of antigen-specific IgE and IgG1, and airway reactivity and remodeling [18, 32]. Wells et al. reported that the transfer of CD8⁺ T cells from OT-I transgenic mice resulted in a marked suppression of airway eosinophilia and Th2 lung cytokine responses at least partly through the stimulation of IL-12 in the lung, reflecting their bias toward the cytotoxic type 1 (Tc1) phenotype [33].

We previously demonstrated the involvement of immune cells in the sex-related allergic airway inflammation in the study of the adoptive transfer of splenocytes from sensitized mice to naïve mice in which the most severe airway inflammation was observed in female mice transferred with female splenocytes [16]. The increased number of macrophages in airways of female mice has been reported to contribute to the sex difference in allergic airway inflammation in mice [34]. Furthermore, we have reported differential function of CD11c⁺ cells from BLN in the activation of CD4⁺ cells [25]. Accordingly, various types of cells involved in Th2 immune responses such as dendritic cells and NKT cells would be promising targets in investigating mechanisms for the sex difference in asthma pathophysiology.

CD8⁺ T cells could contribute to the development of the sex differences mainly by the induction of female-dominant Th2 differentiation, suggested by current findings that IL-4 production by BLN cells stimulated with OVA was greater in female WT mice than male WT mice (Fig 3A), whereas this female-dominant IL-4 production was not observed in CD8KO mice (Fig 3B). Female-dominant Th2 differentiation is supported by our previous findings that Th2 cells identified as T₁/ST₂⁺ CD4⁺ T cells were increased in female BLN cells stimulated with OVA compared to male BLN cells [17]. Interestingly, IL-4 production by CD4⁺ T cells either after the culture with OVA and APCs (Fig 6) or after the stimulation with PMA/Ionomycin (S1 Fig) was not different between the sexes. However, in the case of male CD4⁺ T cells, the presence of male, but not female, CD8⁺ T cells decreased IL-4 production after the culture with OVA and APCs (Fig 4A), while neither male nor female CD8⁺ T cells did in the case of female CD4⁺ T cells (Fig 4B). These findings suggest that male-dominant Th2-suppression by CD8⁺ T cells might result in female-dominant Th2 differentiation, leading to higher suppression of allergic airway inflammation by CD8⁺ T cells in male than female mice as discussed above.

As one of underlying mechanisms for male-dominant Th2-suppression by CD8⁺ T cells, the interaction of IFN- γ with its receptors was suggested by the following findings that i) the production of IFN- γ from male CD8⁺ T cells was significantly higher than female CD8⁺ T cells associated with higher expression of Tc1-oriented transcription factor, T-bet, in male CD8⁺ T cells (Fig 5A, 5B and 5C); ii) the addition of an anti-IFN- γ Ab abrogated the inhibitory effect of male CD8⁺ T cells (Fig 5D); iii) rIFN- γ significantly reduced IL-4 production by male CD4⁺ T

cells, but not by female CD4⁺ T cells (Fig 6); and iv) IFN- γ receptor expression was significantly higher in male CD4⁺ T cells than female CD4⁺ T cells (Fig 7A, 7B and 7C). Together with these results, higher production of IFN- γ by male CD8⁺ T cells and higher expression of IFN- γ receptors on male CD4⁺ T cells seem to induce male-dominant Th2 suppression, alternatively female-dominant Th2 differentiation, resulting in female-dominant allergic airway inflammation. The higher expression of immune regulatory molecules such as IL-10, TGF- β ₁ and perforin was observed in male than female CD8⁺ T cells (S2 Fig). The contribution of these molecules to the sex differences would need to be further investigated.

Unexpectedly, there was no sex difference in the levels of Th1 cytokines such as IL-2 and IFN- γ in the lung from WT mice (Fig 2A), even though male CD8⁺ T cells produced more IFN- γ (Fig 5A and 5B). These observations in the lung were consistent with that there were sex differences neither in the percentages of IFN- γ producing cells in CD4⁺ T cells from BLN (S1 Fig) nor in IFN- γ production by BLN cells cultured with OVA (data not shown). On the other hand, the levels of these cytokines in the lung were significantly higher (Fig 2B) and IFN- γ production by BLN cells cultured with OVA showed a tendency to be higher (data not shown) in female than male CD8KO mice. By comparison of the levels in WT mice with those in CD8KO mice in each sex, it is supposed that IFN- γ production by cells other than CD8⁺ T cells was suppressed by the presence of CD8⁺ T cells, especially in female mice. These data suggest that CD8⁺ T cells contribute to the development of the sex differences in allergic airway inflammation through the regulation of, in addition to IL-4 production by CD4⁺ T cells, Th1-related cytokine production.

Several studies have reported the suppressive activity to allergic inflammatory responses of CD8⁺ T cells is mediated by their production of IFN- γ [35–37]. However, the sex difference in IFN- γ production by CD8⁺ T cells has never been reported. Although the precise mechanisms by which male CD8⁺ T cells produce more IFN- γ were not determined in the current study, female hormone is possible to play a role in lower production of IFN- γ in female mice as reported in a previous study in which 17 β -estradiol treatment down-regulated IFN- γ expression by draining lymph node cells in the delayed-type hypersensitivity response [38].

To our knowledge, it has not been reported that IFN- γ receptor expression on CD4⁺ T cells was higher in male than female mice (Fig 7A, 7B and 7C). Several studies have reported that IFN- γ receptor expression was up-regulated by IL-1 β [39], TNF- α , IL-6 [40] and prostaglandin E2 [41]. In this study, we demonstrated for the first time that IFN- γ has a potential to up-regulate the expression of IFN- γ receptor α in the both sexes (Fig 7D). Mechanisms for the up-regulation by IFN- γ remain to be determined, although IFN- γ has been reported to up-regulate the expression of receptors for IL-1 β and TNF- α , which are able to increase the receptor [39, 40]. Therefore, the sex difference in IFN- γ receptor α expression on CD4⁺ T cells might be attributable to the sex difference in synergistic and/or additive effect(s) of several types of cytokines, such as IFN- γ , IL-1 β , IL-6 and TNF- α , *in vivo*. In contrast to the case of IFN- γ receptor α , IFN- γ down-regulated the expression of IFN- γ receptor β in the both sexes (Fig 7E). The down-regulation of IFN- γ receptor β expression in CD4⁺ T cells might be due to the ligand-induced auto-regulation, which is supported by Bach and coworkers' study demonstrating ligand-induced down-regulation of IFN- γ receptor in helper T cells [42]. Therefore, one of the possible reasons for the sex difference in the expression of IFN- γ receptor β could be the difference between the sexes in mechanisms for ligand-induced down-regulation of this receptor, although the precise mechanisms were not determined in this study.

In summary, we demonstrated, as a possible mechanism for the sex differences in allergic airway inflammation, the induction of female-dominant Th2 immune responses resulting from, at least, male-dominant Th2 suppression evoked by the interaction of IFN- γ produced by CD8⁺ T cells with IFN- γ receptors expressed on CD4⁺ T cells which does not effectively

work in female mice. To understand how and why sex differences in functional capacity of CD8⁺ T cells and CD4⁺ T cells are established, further studies to clarify the male-dominant Th2 suppression will be required. The present study would provide important implications for understanding the pathophysiological role of gender in asthma phenotyping, which may lead to the development of more effective management strategies for immune diseases from which mainly female patients suffer such as asthma and autoimmune diseases.

Supporting Information

S1 Fig. Sex differences in cytokine production by CD4⁺ T cells in BLN. Intracellular cytokine expression in CD4⁺ T cells was analyzed using a flow cytometer. Data are shown as the mean \pm SD of four mice. Experiments were repeated twice with similar results. NS, not significant. (TIF)

S2 Fig. Gene expression of regulatory molecules in CD8⁺ T cells in BLN from male and female WT mice. The expression of *Il10*, *Tgfb1*, *Prf1* and *Fas1* in CD8⁺ T cells were measured by quantitative real-time RT-PCR. Data are shown as the mean \pm SEM from at least two independent experiments (n = 7–9). *, P < 0.05; **, P < 0.01; NS, not significant. (TIF)

Author Contributions

Conceived and designed the experiments: IO TM. Performed the experiments: CI TM CM MS KO-D. Analyzed the data: TM IO CI CM KO-D MS T. Kawano YO T. Kikuchi MT. Contributed reagents/materials/analysis tools: IO T. Kikuchi YO MT. Wrote the paper: TM IO.

References

1. Moorman JE, Akinbami LJ, Bailey CM, Zahran HS, King ME, Johnson CA, et al. National surveillance of asthma: United States, 2001–2010. *Vital Health Stat* 3. 2012; 35: 1–67.
2. Pérez-Perdomo R, Pérez-Cardona C, Disdier-Flores O, Cintrón Y. Prevalence and correlates of asthma in the Puerto Rican population: Behavioral Risk Factor Surveillance System, 2000. *J Asthma*. 2003; 40: 465–474. PMID: 14529096
3. Akinbami LJ, Moorman JE, Bailey C, Zahran HS, King M, Johnson CA, et al. Trends in asthma prevalence, health care use, and mortality in the United States, 2001–2010. *NCHS Data Brief*. 2012; 94: 1–8. PMID: 22617340
4. Moorman JE, Person CJ, Zahran HS; Centers for Disease Control and Prevention (CDC). Asthma attacks among persons with current asthma—United States, 2001–2010. *MMWR Surveill Summ*. 2013; 62: 93–98. PMID: 24264497
5. Follenweider LM, Lambertino A. Epidemiology of asthma in the United States. *Nurs Clin North Am*. 2013; 48: 1–10. doi: 10.1016/j.cnur.2012.12.008 PMID: 23465442
6. Rowe BH, Villa-Roel C, Sivilotti ML, Lang E, Borgundvaag B, Worster A, et al. Relapse after emergency department discharge for acute asthma. *Acad Emerg Med* 2008; 15: 709–717. doi: 10.1111/j.1553-2712.2008.00176.x PMID: 18637082
7. Camargo CA; for the MARC Investigators. Randomized trial of medium-dose fluticasone vs placebo after an emergency department visit for acute asthma [abstract]. *J Allergy Clin Immunol*. 2000; 105: S262.
8. Robinson D, Hamid Q, Bentley A, Ying S, Kay AB, Durham SR. Activation of CD4⁺ T cells, increased TH2-type cytokine mRNA expression, and eosinophil recruitment in bronchoalveolar lavage after allergen inhalation challenge in patients with atopic asthma. *J Allergy Clin Immunol*. 1993; 92: 313–324. PMID: 8349942
9. Schipf A, Heilmann A, Boue L, Mossmann H, Brocker T, Röcken M. Th2 cells shape the differentiation of developing T cell responses during interactions with dendritic cells *in vivo*. *Eur J Immunol*. 2003; 33: 1697–1706. PMID: 12778488

10. Choi P, Reiser H. IL-4: role in disease and regulation of production. *Clin Exp Immunol*. 1998; 113: 317–319. PMID: [9737656](#)
11. Steinke JW, Borish L. Th2 cytokines and asthma. Interleukin-4: its role in the pathogenesis of asthma, and targeting it for asthma treatment with interleukin-4 receptor antagonists. *Respir Res*. 2001; 2: 66–70. PMID: [11686867](#)
12. Gavett SH, Chen X, Finkelman F, Wills-Karp M. Depletion of murine CD4⁺ T lymphocytes prevents antigen-induced airway hyperreactivity and pulmonary eosinophilia. *Am J Respir Cell Mol Biol*. 1994; 10: 587–593. PMID: [8003337](#)
13. Brusselle G, Kips J, Joos G, Bluethmann H, Pauwels R. Allergen-induced airway inflammation and bronchial responsiveness in wild-type and interleukin-4-deficient mice. *Am J Respir Cell Mol Biol*. 1995; 12: 254–259. PMID: [7873190](#)
14. Komai M, Tanaka H, Masuda T, Nagao K, Ishizaki M, Sawada M, et al. Role of Th2 responses in the development of allergen-induced airway remodelling in a murine model of allergic asthma. *Br J Pharmacol*. 2003; 138: 912–920. PMID: [12642393](#)
15. Loza MJ, Foster S, Bleecker ER, Peters SP, Penn RB. Asthma and gender impact accumulation of T cell subtypes. *Respir Res*. 2010 Jul 28; 11: 103. doi: [10.1186/1465-9921-11-103](#) PMID: [20667106](#)
16. Okuyama K, Wada K, Chihara J, Takayanagi M, Ohno I. Sex-related splenocyte function in a murine model of allergic asthma. *Clin Exp Allergy*. 2008; 38: 1212–1219. doi: [10.1111/j.1365-2222.2008.03015.x](#) PMID: [18498415](#)
17. Wada K, Okuyama K, Ohkawara Y, Takayanagi M, Ohno I. Gender differences in transcriptional regulation of IL-5 expression by bronchial lymph node cells in a mouse model of asthma. *Respirology*. 2010; 15: 629–635. doi: [10.1111/j.1440-1843.2010.01721.x](#) PMID: [20337994](#)
18. Stock P, Kallinich T, Akbari O, Quarcoo D, Gerhold K, Wahn U, et al. CD8(+) T cells regulate immune responses in a murine model of allergen-induced sensitization and airway inflammation. *Eur J Immunol*. 2004; 34: 1817–1827. PMID: [15214030](#)
19. Ying S, Humbert M, Barkans J, Corrigan CJ, Pfister R, Menz G, et al. Expression of IL-4 and IL-5 mRNA and protein product by CD4⁺ and CD8⁺ T cells, eosinophils, and mast cells in bronchial biopsies obtained from atopic and nonatopic (intrinsic) asthmatics. *J Immunol*. 1997; 158: 3539–3544. PMID: [9120316](#)
20. McMenamin C, Holt PG. The natural immune response to inhaled soluble protein antigens involves major histocompatibility complex (MHC) class I-restricted CD8⁺ T cell-mediated but MHC class II-restricted CD4⁺ T cell-dependent immune deviation resulting in selective suppression of immunoglobulin E production. *J Exp Med*. 1993; 178: 889–899. PMID: [8102390](#)
21. Renz H, Lack G, Saloga J, Schwinzer R, Bradley K, Loader J, et al. Inhibition of IgE production and normalization of airways responsiveness by sensitized CD8 T cells in a mouse model of allergen-induced sensitization. *J Immunol*. 1994; 152: 351–360. PMID: [8254203](#)
22. Maestrelli P, Del Prete GF, De Carli M, D'Elios MM, Saetta M, Di Stefano A, et al. CD8 T-cell clones producing interleukin-5 and interferon-gamma in bronchial mucosa of patients with asthma induced by toluene diisocyanate. *Scand J Work Environ Health*. 1994; 20: 376–381. PMID: [7863302](#)
23. Suzuki M, Taha R, Ihaku D, Hamid Q, Martin JG. CD8⁺ T cells modulate late allergic airway responses in Brown Norway rats. *J Immunol*. 1999; 163: 5574–5581. PMID: [10553086](#)
24. Nagafuku M, Okuyama K, Onimaru Y, Suzuki A, Odagiri Y, Yamashita T, et al. CD4 and CD8 T cells require different membrane gangliosides for activation. *Proc Natl Acad Sci U S A*. 2012; 109: E336–E342. doi: [10.1073/pnas.1114965109](#) PMID: [22308377](#)
25. Okuyama K, Suenaga M, Furuki S, Kawano T, Ohkawara Y, Takayanagi M, et al. Contribution of CD4⁺ T cells and dendritic cells to female-dominant antigen-induced T helper type 2 cytokine production by bronchial lymph node cells. *Int Arch Allergy Immunol*. 2013; 161 Suppl 2: 58–65. doi: [10.1159/000350426](#) PMID: [23711855](#)
26. Hansen G, Berry G, DeKruyff RH, Umetsu DT. Allergen-specific Th1 cells fail to counterbalance Th2 cell-induced airway hyperreactivity but cause severe airway inflammation. *J Clin Invest*. 1999; 103: 175–83. PMID: [9916129](#)
27. Mac Sharry J, Shalaby KH, Marchica C, Farahnak S, Chieh-Li T, Laphorne S, et al. Concomitant exposure to ovalbumin and endotoxin augments airway inflammation but not airway hyperresponsiveness in a murine model of asthma. *PLoS One*. 2014 Jun 26; 9(6): e98648. doi: [10.1371/journal.pone.0098648](#) PMID: [24968337](#)
28. Lloyd CM, Gonzalo JA, Coyle AJ, Gutierrez-Ramos JC. Mouse models of allergic airway disease. *Adv Immunol*. 2001; 77: 263–295. PMID: [11293118](#)
29. Betts RJ, Kemeny DM. CD8⁺ T cells in asthma: friend or foe? *Pharmacol Ther*. 2009; 121: 123–131. doi: [10.1016/j.pharmthera.2008.09.001](#) PMID: [18940198](#)

30. Cohn L, Homer RJ, Niu N, Bottomly K. T helper 1 cells and interferon gamma regulate allergic airway inflammation and mucus production. *J Exp Med*. 1999; 190: 1309–1318. PMID: [10544202](#)
31. Tang Y, Guan SP, Chua BY, Zhou Q, Ho AW, Wong KH, et al. Antigen-specific effector CD8 T cells regulate allergic responses via IFN- γ and dendritic cell function. *J Allergy Clin Immunol*. 2012; 129: 1611–1620. doi: [10.1016/j.jaci.2011.12.976](#) PMID: [22385629](#)
32. Tsuchiya K, Isogai S, Tamaoka M, Inase N, Akashi T, Martin JG, et al. Depletion of CD8⁺ T cells enhances airway remodelling in a rodent model of asthma. *Immunology*. 2009; 126: 45–54. doi: [10.1111/j.1365-2567.2008.02876.x](#) PMID: [18564065](#)
33. Wells JW, Cowled CJ, Giorgini A, Kemeny DM, Noble A. Regulation of allergic airway inflammation by class I-restricted allergen presentation and CD8 T-cell infiltration. *J Allergy Clin Immunol*. 2007; 119: 226–34. PMID: [17208606](#)
34. Melgert BN, Oriss TB, Qi Z, Dixon-McCarthy B, Geerlings M, Hylkema MN, et al. Macrophages: regulators of sex differences in asthma? *Am J Respir Cell Mol Biol*. 2010; 42: 595–603. doi: [10.1165/rcmb.2009-0016OC](#) PMID: [19574533](#)
35. Takeda K, Dow SW, Miyahara N, Kodama T, Koya T, Taube C, et al. Vaccine-induced CD8⁺ T cell-dependent suppression of airway hyperresponsiveness and inflammation. *J Immunol*. 2009; 183: 181–190. doi: [10.4049/jimmunol.0803967](#) PMID: [19542429](#)
36. Marsland BJ, Harris NL, Camberis M, Kopf M, Hook SM, Le Gros G. Bystander suppression of allergic airway inflammation by lung resident memory CD8⁺ T cells. *Proc Natl Acad Sci U S A*. 2004; 101: 6116–6121. PMID: [15079067](#)
37. Suzuki M, Maghni K, Molet S, Shimbara A, Hamid QA, Martin JG. IFN-gamma secretion by CD8T cells inhibits allergen-induced airway eosinophilia but not late airway responses. *J Allergy Clin Immunol*. 2002; 109: 803–809. PMID: [11994704](#)
38. Salem ML, Matsuzaki G, Kishihara K, Madkour GA, Nomoto K. beta-estradiol suppresses T cell-mediated delayed-type hypersensitivity through suppression of antigen-presenting cell function and Th1 induction. *Int Arch Allergy Immunol*. 2000; 121: 161–169. PMID: [10705227](#)
39. Shirey KA, Jung JY, Maeder GS, Carlin JM. Upregulation of IFN-gamma receptor expression by proinflammatory cytokines influences IDO activation in epithelial cells. *J Interferon Cytokine Res*. 2006; 26: 53–62. PMID: [16426148](#)
40. Sanceau J, Merlin G, Wietzerbin J. Tumor necrosis factor-alpha and IL-6 up-regulate IFN-gamma receptor gene expression in human monocytic THP-1 cells by transcriptional and post-transcriptional mechanisms. *J Immunol*. 1992; 149: 1671–1675. PMID: [1387149](#)
41. elMasry MN, Rich RR. Prostaglandin E2 selectively increases interferon gamma receptor expression on human CD8⁺ lymphocytes. *J Clin Invest*. 1989; 83: 1436–1440. PMID: [2522938](#)
42. Bach EA, Szabo SJ, Dighe AS, Ashkenazi A, Aguet M, Murphy KM, et al. Ligand-induced autoregulation of IFN-gamma receptor beta chain expression in T helper cell subsets. *Science*. 1995; 270: 1215–1218. PMID: [7502050](#)

平成27年度～平成31年度私立大学戦略的研究基盤形成支援事業研究成果報告書

令和2年5月発行

編集 私立大学戦略的研究基盤形成支援事業（創薬研究）運営委員会

発行 東北医科薬科大学

〒981-8558 仙台市青葉区小松島4-4-1

TEL 022-234-4181

印刷 株式会社東北プリント
